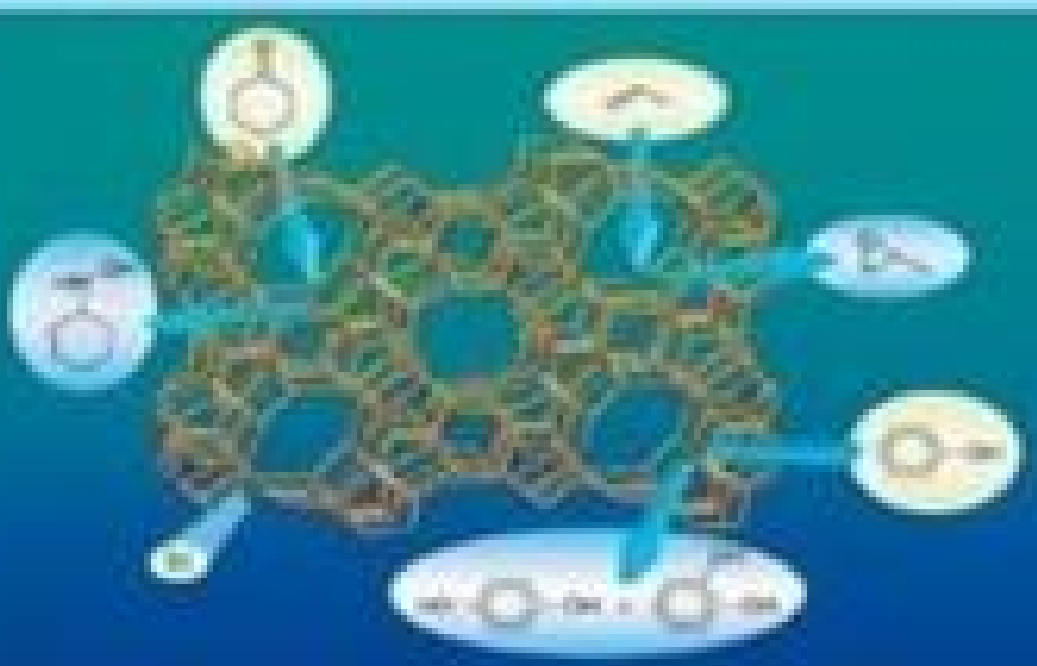
Liquid Phase Oxidation via Heterogeneous Catalysis

Organic Synthesis and Industrial Applications

Edited by
Mario G. Clerici and Oxana A. Kholdeeva



WILEY

LIQUID PHASE OXIDATION VIA HETEROGENEOUS CATALYSIS

LIQUID PHASE OXIDATION VIA HETEROGENEOUS CATALYSIS

Organic Synthesis and Industrial Applications

Edited by

MARIO G. CLERICI
Formerly with Enitecnologie (ENI Group)
San Donato Milanese, Italy

OXANA A. KHOLDEEVA
Boreskov Institute of Catalysis
Novosibirsk, Russia

WILEY

Copyright © 2013 by John Wiley & Sons, Inc. All rights reserved

Published by John Wiley & Sons, Inc., Hoboken, New Jersey
Published simultaneously in Canada

No part of this publication may be reproduced, stored in a retrieval system, or transmitted in any form or by any means, electronic, mechanical, photocopying, recording, scanning, or otherwise, except as permitted under Section 107 or 108 of the 1976 United States Copyright Act, without either the prior written permission of the Publisher, or authorization through payment of the appropriate per-copy fee to the Copyright Clearance Center, Inc., 222 Rosewood Drive, Danvers, MA 01923, (978) 750-8400, fax (978) 750-4470, or on the web at www.copyright.com. Requests to the Publisher for permission should be addressed to the Permissions Department, John Wiley & Sons, Inc., 111 River Street, Hoboken, NJ 07030, (201) 748-6011, fax (201) 748-6008, or online at http://www.wiley.com/go/permission.

Limit of Liability/Disclaimer of Warranty: While the publisher and author have used their best efforts in preparing this book, they make no representations or warranties with respect to the accuracy or completeness of the contents of this book and specifically disclaim any implied warranties of merchantability or fitness for a particular purpose. No warranty may be created or extended by sales representatives or written sales materials. The advice and strategies contained herein may not be suitable for your situation. You should consult with a professional where appropriate. Neither the publisher nor author shall be liable for any loss of profit or any other commercial damages, including but not limited to special, incidental, consequential, or other damages.

For general information on our other products and services or for technical support, please contact our Customer Care Department within the United States at (800) 762-2974, outside the United States at (317) 572-3993 or fax (317) 572-4002.

Wiley also publishes its books in a variety of electronic formats. Some content that appears in print may not be available in electronic formats. For more information about Wiley products, visit our web site at www.wiley.com.

Library of Congress Cataloging-in-Publication Data:

Liquid phase oxidation via heterogeneous catalysis : organic synthesis and industrial applications / edited by Mario G. Clerici, formerly with Enitecnologie (ENI Group) ; San Donato Milanese, Italy, Oxana A. Kholdeeva, Boreskov Institute of Catalysis, Novosibirsk, Russia.
pages cm
Includes index.
ISBN 978-0-470-91552-3 (cloth)
1. Oxidation. 2. Oxidation–Industrial applications. 3. Heterogeneous catalysis. 4. Heterogeneous catalysis–Industrial applications. I. Clerici, Mario G. II. Kholdeeva, Oxana A.
QD281.O9L57 2013
541′.393–dc23
2012047247

Printed in the United States of America

ISBN: 9780470915523

10 9 8 7 6 5 4 3 2 1

CONTENTS

Preface **xi**

Contributors **xiii**

Abbreviations **xv**

1 Environmentally Benign Oxidants **1**
Giorgio Strukul and Alessandro Scarso

1.1 Introduction 1
1.2 Oxygen (Air) 3
1.3 Alkylhydroperoxides 5
1.4 Hydrogen Peroxide 9
1.5 Conclusions 16
References 17

2 Oxidation Reactions Catalyzed by Transition-Metal-Substituted Zeolites **21**
Mario G. Clerici and Marcelo E. Domine

2.1 Introduction 21
2.2 Synthesis and Characterization of Zeolites 22
2.2.1 Isomorphous Metal Substitution 23
2.2.2 Synthesis of Titanium Silicalite-1 (TS-1) 24
2.2.3 Characterization of Titanium Silicalite-1 (TS-1) 26
2.2.4 Ti-Beta, Synthesis and Characterization 30

2.2.5 Other Ti Zeolites 32
2.2.6 Other Metal Zeolites 33
2.3 Catalytic Properties 34
2.3.1 Hydroxylation of Alkanes 34
2.3.2 Hydroxylation of Aromatic Compounds 40
2.3.3 Oxidation of Olefinic Compounds 47
2.3.4 Oxidation of Alcohol and Ether Compounds 59
2.3.5 Reactions of Carbonyl Compounds 60
2.3.6 Oxidation of N-Compounds 63
2.3.7 Oxidation of S-Compounds 65
2.4 Mechanistic Aspects 66
2.4.1 The Nature of Active Species 66
2.4.2 Hydroxylation 69
2.4.3 Epoxidation 71
2.4.4 Oxidation of Alcohols 72
2.4.5 Ammoximation 73
2.4.6 Decomposition of Hydrogen Peroxide 74
2.4.7 Active Species, Adsorption and Catalytic Activity 74
2.5 Stability of Metal-Substituted Zeolites to Reaction Conditions 77
2.6 Conclusions 78
References 80

3 Selective Catalytic Oxidation over Ordered Nanoporous Metallo-Aluminophosphates 95
Parasuraman Selvam and Ayyamperumal Sakthivel

3.1 Introduction 95
3.2 Synthesis 100
3.2.1 Microporous Aluminophosphates 100
3.2.2 Mesoporous Aluminophosphates 102
3.3 Characterization 103
3.4 Catalytic Properties 106
3.4.1 Oxidation of Hydrocarbons 106
3.4.2 Oxidation of Olefins 110
3.4.3 Oxidation of Alcohols 111
3.4.4 Oxidation of Phenols 113
3.4.5 Ammoximation and Ammoxidation 114
3.4.6 Baeyer–Villiger Oxidation 116
3.4.7 Oxidation of Heterocycles 116
3.5 Mechanistic Aspects 116
3.6 Catalysts Stability 118
3.7 Conclusion 119
References 120

4 Selective Oxidations Catalyzed by Mesoporous Metal Silicates 127
Oxana A. Kholdeeva

4.1 Introduction 127
4.2 Synthesis and Characterization 128
4.2.1 General Synthetic Approaches 128
4.2.2 Characterization Techniques 129
4.2.3 Sol-Gel Synthesis of Amorphous Mixed Oxides 132
4.2.4 Thermolytic Molecular Precursor Method 136
4.2.5 Templated Synthesis of Ordered Metal Silicates 136
4.2.6 Postsynthesis Modifications 156
4.2.7 Organic–Inorganic Hybrid Materials 162
4.3 Catalytic Properties 163
4.3.1 Oxidation of Alkanes 163
4.3.2 Oxidation of Aromatic Compounds 167
4.3.3 Oxidation of Olefins 172
4.3.4 Oxidation of Alcohols 182
4.3.5 Oxidation of Ketones and Aldehydes 183
4.3.6 Oxidation of S-compounds 185
4.3.7 Oxidation of Amines 188
4.4 Mechanistic Aspects 189
4.5 Stability 194
4.5.1 Mechanisms of Deactivation 194
4.5.2 Solving Problem of Hydrothermal Stability 197
4.5.3 Hydrothermally Stable Catalysts: Scope and Limitations 199
4.6 Conclusions and Outlook 200
References 201

5 Liquid Phase Oxidation of Organic Compounds by Supported Metal-Based Catalysts with a Focus on Gold 221
Cristina Della Pina, Ermelinda Falletta, and Michele Rossi

5.1 Introduction 221
5.2 Catalyst Preparation and Characterization 222
5.3 Catalytic Properties 224
5.3.1 Oxidation of Hydrocarbons 224
5.3.2 Oxidation of Alcohols and Phenols 228
5.3.3 Oxidation of Carbohydrates: The Case of Glucose 241
5.3.4 Oxidation of Amines and Aminoalcohols 244
5.3.5 Oxidative Polymerization of Aniline and Pyrrole 245
5.4 Reaction Mechanisms 250
5.5 Catalyst Stability 254
5.6 Conclusions 256
References 256

6 Selective Liquid Phase Oxidations in the Presence of Supported Polyoxometalates **263**
Craig L. Hill and Oxana A. Kholdeeva

6.1 Introduction 263
6.2 Synthesis and Characterization 266
6.2.1 Choice of POM 266
6.2.2 Embedding POM into Silica and Other Matrixes 267
6.2.3 Adsorption on Active Carbon 271
6.2.4 Electrostatic Attachment 273
6.2.5 Dative and Covalent Binding 283
6.3 Catalytic Properties 287
6.3.1 Oxidation of Alkanes 287
6.3.2 Oxidation of Aromatic Compounds 288
6.3.3 Oxidation of Olefins 288
6.3.4 Oxidation of Alcohols 297
6.3.5 Oxidation of Aldehydes 298
6.3.6 Co-Oxidation of Alkenes and Aldehydes 299
6.3.7 Oxidation of S-containing Compounds 301
6.4 Mechanistic Aspects 304
6.5 Stability 307
6.6 Conclusions 309
References 311

7 Selective Oxidations Catalyzed by Supported Metal Complexes **321**
Alexander B. Sorokin

7.1 Introduction 321
7.2 Synthesis and Characterization 323
7.2.1 General Synthetic Strategies 324
7.2.2 Metal Porphyrins 329
7.2.3 Metal Phthalocyanines 331
7.2.4 Complexes with Other Macrocyclic Ligands 336
7.2.5 Chiral Complexes 337
7.3 Catalytic Properties and Stability 338
7.3.1 Oxidation of Alkanes 339
7.3.2 Oxidation of Olefins 344
7.3.3 Oxidation of Aromatic Hydrocarbons 352
7.3.4 Oxidation of Substituted Phenols 353
7.3.5 Oxidation of Alcohols 356
7.3.6 Miscellaneous Oxidations 359
7.4 General Remarks on Stability 362
7.5 Conclusion and Perspectives 364
References 365

8 Liquid Phase Oxidation of Organic Compounds by Metal-Organic Frameworks 371
Young Kyu Hwang, Gérard Férey, U-Hwang Lee, and Jong-San Chang

8.1 Introduction 371
8.2 Characteristics and Structures 372
8.2.1 Characteristics 372
8.2.2 Structures 374
8.2.3 Syntheses 378
8.2.4 Active Sites 380
8.3 Catalytic Properties 388
8.3.1 Oxidation of Cycloalkanes 388
8.3.2 Oxidation of Aromatic Compounds 389
8.3.3 Oxidation of Olefins 393
8.3.4 Oxidation of Alcohols and Phenols 398
8.3.5 Oxidation of Sulfides 399
8.4 Mechanistic Aspects 400
8.5 Stability 402
8.5.1 Thermal and Chemical Stability 402
8.5.2 Leaching of Active Metal Components 404
8.6 Conclusion 405
References 405

9 Heterogeneous Photocatalysis for Selective Oxidations with Molecular Oxygen 411
Andrea Maldotti, Rossano Amadelli, and Alessandra Molinari

9.1 Introduction 411
9.2 Catalysts Preparation and Mechanistic Aspects 413
9.2.1 Titanium Dioxide 413
9.2.2 Highly Dispersed Oxides 416
9.2.3 Polyoxotungstates 418
9.3 Catalytic Properties 422
9.3.1 Oxidation of Alkanes 422
9.3.2 Oxidation of Aromatic Compounds 427
9.3.3 Oxidation of Alcohols 430
9.3.4 Oxidation of Olefins 436
9.4 Stability 438
9.5 Conclusions 443
References 444

10 Industrial Applications 451
10.1 The Hydroxylation of Phenol to Hydroquinone and Catechol 451
Ugo Romano and Marco Ricci

10.1.1 The Discovery of TS-1 451

10.1.2 The Hydroxylation of Phenol 452
10.1.3 The Industrial Process 456
10.1.4 Other Processes Exploiting TS-1 460
References 461
10.2 The Greening of Nylon: The Ammoximation Process 462
Franco Rivetti and Roberto Buzzoni
10.2.1 Nylon-6 and ε-Caprolactam, Outlook and Industrial Production 462
10.2.2 TS-1 Catalyzed Ammoximation 466
10.2.3 Eni Cyclohexanone Ammoximation Process 467
10.2.4 Salt-Free Caprolactam Production 470
10.2.5 Other TS-1-Catalyzed Ammoximation Reactions and Related Processes of Industrial Relevance 470
10.2.6 Conclusion 471
References 472
10.3 Production of Propylene Oxide 474
Anna Forlin, Massimo Bergamo, and Joerg Lindner
10.3.1 Propylene Oxide Production *via* Ethylbenzene Hydroperoxide Route 476
10.3.2 Propylene Oxide Production *via* Cumene Hydroperoxide Route 480
10.3.3 Propylene Oxide Production *via* Hydrogen Peroxide Route 483
10.3.4 Conclusions 487
References 494
10.4 Engineering Aspects of Liquid Phase Oxidations 496
Bruce D. Hook
10.4.1 Heterogeneous Liquid Phase Systems 496
10.4.2 Temperature-Control Requirements 499
10.4.3 Packed-Bed Reactors 500
10.4.4 Three-Phase Systems – Gas, Liquid, Solid 501
10.4.5 Oxidant Selection 503
10.4.6 Summary 505
References 506

Index **507**

PREFACE

Liquid phase oxidation finds widespread application in the chemical industry for the manufacture of a variety of chemicals ranging from the commodities to fine chemical specialties. About half of the overall capacity of oxidation processes, in fact, are liquid phase ones. Until not long ago, however, heterogeneous catalysis did not play a major role in this area, if compared to homogeneous catalysis. The prospects started to change at the beginning of the 1980s with the synthesis of Titanium Silicalite-1 (TS-1), even though the new processes based on it had to wait until the 2000s. Actually, the need to use hydrogen peroxide was initially felt to be a serious obstacle to the development of large volume processes for which TS-1 appeared to be suited. On the other hand, research activities, both in academia and industry, received a great stimulus with papers and patents growing exponentially on the synthesis, characterization and application of a large variety of new metal-substituted molecular sieves, catalytically active for oxidation reactions. At the same time, other families of catalysts, namely supported transition-metal complexes, noble metal nanoparticles and photoactive materials benefited from major development. On the whole, the area of catalysis related to liquid phase oxidations has experienced an impressive progress in the last two to three decades, from both a scientific and industrial perspective.

Books and journal reviews of excellent quality dealing with the above-mentioned catalysts are available. Liquid phase oxidation, however, is in most cases covered by single chapters, inevitably providing a partial picture of a multifaceted topic. The second aspect is that the point of view and the needs of chemists looking for novel synthetic routes generally remain in the background. This new book has the aim to overcome these limitations, giving a comprehensive picture of promising materials, privileging their application to organic synthesis and illustrating industrial

realizations. Sections on synthesis and characterization provide essential information on the different classes of materials. Stability under reaction conditions and reusability are specifically stressed in each chapter.

The book is mainly oriented to an audience composed of faculty members, researchers of both academia and industry, and R&D managers directly or indirectly involved in organic synthesis and catalysis. To facilitate the desired approach, all chapters are organized in a similar fashion, with the exception of the first and last ones. Trying to adhere to the style of organic chemistry textbooks, catalytic properties are organized per class of compounds.

Typical oxidants, illustrated in the first chapter, are molecular oxygen, organic hydroperoxides and, especially, hydrogen peroxide, while oxidants more or less distant from "green chemistry" are extraneous to the book. Inorganic molecular sieve catalysts, namely, transition-metal-substituted zeolites, aluminophosphates and mesoporous silicates are the subjects of the next three chapters. Supported catalysts of gold, polyoxometalates and metal complexes are dealt with in chapters five through seven and are followed by a novel class of functional materials, metal-organic frameworks, and by heterogeneous photocatalysts. Industrial applications in the last chapter, from early POSM process to recent ones for the hydroxylation of phenol, production of caprolactam and of propylene oxide, are contributed by authors directly involved in their development. A section on engineering aspects of liquid phase oxidations dealing with issues that could facilitate subsequent scale up of lab results closes the last chapter. Each chapter contains an extensive bibliography covering most of the recent literature up to the beginning of 2012.

We would like to thank the authors that accepted to contribute to the book for their nice work and their adhering to a uniform style. Finally, we thank Jonathan T. Rose, Senior Editor of Wiley for his help and assistance from the initial preparation of the book project through to its realization.

MARIO G. CLERICI
OXANA A. KHOLDEEVA

October 2012
Milan and Novosibirsk

CONTRIBUTORS

Rossano Amadelli, CNR-ISOF, U.O.S, c/o Dipartimento di Chimica Università di Ferrara, Ferrara, Italy.

Massimo Bergamo, Dow Deutschland Anlagengesellschaft mbH, Stade, Federal Republic of Germany.

Roberto Buzzoni, Eni S.p.A., Green Chemistry - Research Center Novara, Catalysis, Novara, Italy.

Jong-San Chang, Research Group for Nanocatalyst and Biorefinery Research Group, Korea Research Institute of Chemical Technology (KRICT), Daejeon, Republic of Korea.

Mario G. Clerici, formerly with ENI Group, San Donato Milanese, Italy.

Cristina Della Pina, Università degli Studi di Milano, Dipartimento di Chimica e ISTM-CNR, Milano, Italy.

Marcelo E. Domine, Instituto de Tecnología Química, ITQ (UPV - CSIC), Valencia, Spain.

Ermelinda Falletta, Università degli Studi di Milano, Dipartimento di Chimica e ISTM-CNR, Milano, Italy.

Gérard Férey, Université de Versailles Saint-Quentin-en-Yvelines, Institut Lavoisier (UMR CNRS 8180), Versailles cedex, France.

Anna Forlin, Dow Italia S.r.L., Correggio (Reggio Emilia), Italy.

Craig L. Hill, Emory University, Department of Chemistry, Atlanta - GA, USA.

Bruce D. Hook, The Dow Chemical Company, Performance Materials R&D, Freeport - TX, USA.

Young Kyu Hwang, Research Group for Nanocatalyst and Biorefinery Research Group, Korea Research Institute of Chemical Technology (KRICT), Daejeon, Republic of Korea.

Oxana A. Kholdeeva, Boreskov Institute of Catalysis, Novosibirsk, Russia.

U-Hwang Lee, Research Group for Nanocatalyst and Biorefinery Research Group, Korea Research Institute of Chemical Technology (KRICT), Daejeon, Republic of Korea.

Joerg Lindner, Dow Deutschland Anlagengesellschaft mbH, Stade, Federal Republic of Germany.

Andrea Maldotti, Dipartimento di Chimica Università di Ferrara, Ferrara, Italy.

Alessandra Molinari, Dipartimento di Chimica Università di Ferrara, Ferrara, Italy.

Marco Ricci, Eni S.p.A., Centro Ricerche per le Energie non Convenzionali - Istituto Eni Donegani, Novara, Italy.

Franco Rivetti, formerly with ENI Group, Milano, Italy.

Ugo Romano, FEEM - Fondazione Eni Enrico Mattei, Milano, Italy.

Michele Rossi, Università degli Studi di Milano, Dipartimento di Chimica e ISTM-CNR, Milano, Italy.

Ayyamperumal Sakthivel, University of Delhi, Department of Chemistry, Delhi, India.

Alessandro Scarso, Università Ca' Foscari, Dipartimento di Scienze Molecolari e Nanosistemi, Venezia, Italy.

Parasuraman Selvam, Indian Institute of Technology - Madras, National Centre for Catalysis Research and Department of Chemistry, Chennai, India.

Alexander B. Sorokin, Institut de Recherches sur la Catalyse et l'Environnement de Lyon, IRCELYON, UMR 5256, CNRS, Université Lyon 1, Villeurbanne, France.

Giorgio Strukul, Università Ca' Foscari, Dipartimento di Scienze Molecolari e Nanosistemi, Venezia, Italy.

ABBREVIATIONS

$(FePctBu_4)_2N$	N-bridged di-iron phthalocyanine complex
2,6-AQDS	anthraquinone-2,6-disulfonate
$2,6Cl_2pyNO$	2,6-dichloropyridine-*N*-oxide
2-pymo	2-hydroxypyrimidinolate
2R, RR-L	(R,R)-(-)-1,2-cyclohexanediamino-N,N'-bis(3-*tert*-butyl-5-(4-pyridyl)salicylidene)
2S, SS-L	(S,S)-(-)-1,2-cyclohexanediamino-N,N'-bis(3-*tert*-butyl-5-(4-pyridyl)salicylidene)
ACP	acetophenone
AO	anthraquinone process
APO	aluminophosphate
AZY	azoxybenzene
AZO	azobenzene
BDC	1,4-benzenedicarboxylate
BDPB	1,4-bis[(3,5-dimethyl)pyrazol-4-yl]-benzene
BIPY	2,2'-bipyridine
bpdc	biphenyldicarboxylate
BPED	meso-1,2-bis(4-pyridyl)-1,2-ethanediol
bpy	4,4'-bipyridine
BQ	benzoquinone
BT	benzothiophene
btb	1,3,5-benzene-tri-benzoic acid

BTC	1,3,5-benzenetricarboxylate
BTEC	1,2,4,5-benzenetetracarboxylic acid
BV	Baeyer–Villiger (oxidation reaction)
CD	colloidal dispersion
CHP	cumyl hydroperoxide
CHPO	chlorohydrin process
CMOF	isoreticular chiral metal-organic framework
CSTR	continuous stirred-tank reactior
CT	charge transfer
CUM	coordinatively unsaturated metal
CVD	chemical vapor deposition
DBT	dibenzothiophene
DEF	diethylformamide
DFT	density functional theory
DHBDC	2,5-dihydroxybenzenedicarboxylate
DHTP	dihydroxyterephtalate
DMDBT	4,6-dimethyl dibenzothiophene
DMF	N,N'-dimethylformamide
DOPO	direct oxidation of propylene with oxygen
DP	deposition-precipitation
DPM	diphenylmethane
DR UV-vis	diffuse reflectance UV-vis
DTBP	2,6-di-*tert*-butylphenol
EB	ethylbenzene
EBHP	ethylbenzene hydroperoxide
ES-40	ethyl silicate 40
EXAFS	extended X-ray absorption fine structure
FAMEs	fatty acid methyl esters
FDMS	1,1′-ferrocenediyl-dimethylsilane
FePcS	iron tetrasulfophthalocyanine
$FePc^tBu_4$	iron tetra-*tert*-butylphthalocyanine
GA	glutaraldehyde
H_2tea	triethanolamine
H_2TMPyP	5,10,15,20-tetrakis(1-methyl-4-pyridinio)porphyrin
HDS	hydrodesulfurization
Hmdea	N-methyldiethanolamine
HMDS	hexamethyldisilazane
HOPO	hydro-oxidation of propylene with oxygen and hydrogen

HP/HPPO	HPPO with H_2O_2 from direct synthesis
HPPO	hydrogen peroxide to propylene oxide (PO process)
Hpz	pyrazole
HQ	hydroquinone
HR TEM	high-resolution transmission electron microscopy
IBA	isobutyraldehyde
Im	imidazole
IWI	incipient wetness impregnation
KIE	kinetic isotope effect
L1 and L2	1,2,4,5-tetrakis(4-carboxyphenyl) benzene and 5,15-dipyridyl-10,20-bis(pentafluorophenyl)-porphyrin
LDH	layered double hydroxide
L-lac	L-lactic acid
MAPO	metal-substituted APO
MAS NMR	magic-angle spinning nuclear magnetic resonance
MBA	methylbenzylalcohol
MIL	Materials of Institut Lavoisier
MIL-101	mesoporous chromium terephthalate, abbreviation derives from "Matériau de l'Institut Lavoisier"
MMO	methane mono-oxygenase
MN	2-methylnaphthalene
Mn(acac)	Mn(II) acetylacetonate complex
MNQ	2-methyl-1,4-naphthoquinone
MOF(s)	metal-organic framework(s)
MPc	metal phthalocyanine complex
$MPc(NO_2)_4$	metal tetranitrophthalocyanine complex
$MPcCl_{16}$	metal hexadecachlorophthalocyanine complex
$MPcF_{16}$	metal phthalocyanine perflorinated complexes (M = Fe, Ru).
MPcS	metal tetrasulfophthalocyanine complex
MPS	methyl phenyl sulfide
MTBE	methyl-*tert*-butyl ether
MTDCPP	metal 5,10,15,20-tetra(2,6-dichlorophenyl)porphyrin complex
MTMP	metal tetamesytilporphyrin complex
MTMPyP	metal tetra(4-N-methylpyridyl)porphyrin complex
MW	microwave
NDS	naphthalene disulfonate
NHPI	N-hydroxyphthalimide
NP(s)	nano-particle(s)
NSB	nitrosobenzene

ODS	oxidative desulfurization
PANI	polyaniline
PDMS	polydimethylsiloxane membrane
PILC	pillared clay
PMO	periodic mesoporous organosilicas
PO	propylene oxide
POM	polyoxometalate
POSM	propylene oxide – styrene monomer (PO process)
POSS	polyhedral oligomeric silsesquioxane
PSD	pore-size distribution
PVA	polyvinylalcohol
PVDF	polyvinylidene fluoride
PVP	polyvinylpyrrolidone
Py	pyridine
PYZ	pyrazine
PZ	pyrazole
PZDC	pyrazine-2,3-dicarboxylate
RPM(s)	robust porphyrinic material(s)
SAPO	silicoaluminophosphate
SAXS/SANS	small-angle X-ray/neutron scattering
SBU(s)	secondary building unit(s)
SCD	supercritical drying
SEM	scanning electron microscopy
SDA	structure-directing agent
TBAOH	tetrabutylammonium hydroxide
TEAOH	tetraethylammonium hydroxide
TBHP	*tert*-butyl hydroperoxide
TBOT	tetra-*n*-butyl orthotitanate
TBSIB	2-(*tert*-butylsulfonyl)iodosylbenzene
TCPP	tetra(4-carboxyphenyl)porphyrin
TDCPP	5,10,15,20-tetra(2,6-dichlorophenyl)porphyrin
TEMPO	2,2,6,6-tetramethylpiperidyl-1-oxyl
TEOS	tetraethyl orthosilicate
TEOT	tetraethyl orthotitanate
TIE	template ion exchange
TMA	trimethylacetaldehyde
TMOS	tetramethyl orthosilicate
TMBQ	2,3,5-trimethylbenzoquinone

TMP	2,3,6-trimethylphenol
tmtacn	1,4,7-trimethyl-1,4,7-triazacyclononane ligand
TOF	turnover frequencies
TON(s)	turnover number(s)
TPAOH	tetrapropylammonium hydroxide
TPABr	tetrapropylammonium bromide
TPD	temperature-programmed desorption
TPM	triphenylmethane
TS-1	titanium silicalite-1
UHP	urea hydroperoxide
XANES	X-ray absorption near-edge structure
XPS	X-ray photoelectron spectroscopy
XRD	X-ray diffraction
ZMOF(s)	zeolite-like metal-organic framework(s)

1

ENVIRONMENTALLY BENIGN OXIDANTS

GIORGIO STRUKUL* AND ALESSANDRO SCARSO

1.1 INTRODUCTION

The arsenal of possible oxidants available to the organic chemist to carry out oxidation reactions is very wide. It ranges from the simplest one, naturally occurring, air (oxygen) to other common synthetic ones like, e.g., hydrogen peroxide and bleach, to more sophisticated ones, often requiring relatively complex synthetic procedures, e.g., organic peroxides and hydroperoxides, peroxy acids, iodoso benzenes, and dioxiranes. At variance with other catalytic reactions involving simple molecules like hydrogenation or hydroformylation, oxygen activation and transfer is a much more complex, more difficult to control process and has not witnessed similar extreme degrees of efficiency in terms of activity and selectivity. In fact, while the synthesis of sophisticated complex molecules, like some fine or chiral chemicals involved in pharmaceutical or natural product synthesis is still dominated by the use of homogeneous catalysts, often with the use of toxic oxidants, generating large amounts of waste, implying complex process procedures for the separation of products from unreacted reagents and catalysts, in oxidation even some large industrial processes (e.g., the Wacker and Oxirane processes, the synthesis of adipic and terephthalic acids) still rely on the use of soluble catalysts.

Nowadays, sustainability issues are also becoming important economic factors so, even this area is being strongly influenced by the implementation of the current binding twelve principles of Green Chemistry [1]. Replacement of

*Corresponding author

Liquid Phase Oxidation via Heterogeneous Catalysis: Organic Synthesis and Industrial Applications, First Edition. Edited by Mario G. Clerici and Oxana A. Kholdeeva.
© 2013 John Wiley & Sons, Inc. Published 2013 by John Wiley & Sons, Inc.

technologies based on soluble catalysts with heterogeneous ones is intrinsically more likely to lead to important technical improvements in terms of catalyst design, process simplification, milder or more sustainable reaction conditions, use of cheaper or more environmentally friendly oxidants. In the overall process the latter represents a key issue.

Going green implies an evaluation of the properties of common oxidants. Table 1.1 reports an analysis of the byproduct formed, the atom efficiency and the cost for a series of them [2, 3]. Two oxidants stand out in terms of environmental acceptability: oxygen (air) and hydrogen peroxide giving either no byproduct or water as byproduct and an atom efficiency close to or above 50%. An analysis of their E-factor leads to similar conclusions (Table 1.1) [4, 5]. Although the E-factor refers to a specific reaction, it is strongly influenced by the choice of the oxidant. As an example, in Table 1.1 the E-factor is calculated for the epoxidation of propene with different oxidants. As shown, water is not considered a waste and its E-factor is assumed to be zero. For all the other oxidants reported, the amount of waste compares to and in some cases largely exceeds the amount of useful product. A third class can be included in this restricted list of environmentally benign oxidants, i.e. alkylhydroperoxides, even if the justification of this choice is not related to their intrinsic properties but relies on different grounds, as will be clear in the foregoing. In the next sections the general properties, methods of production, environmental impact and some considerations related to the use of oxygen, alkyl hydroperoxides and hydrogen peroxide will be critically presented with the aim of providing some general guidelines for their use in catalytic oxidation reactions.

TABLE 1.1 Comparison between Different Terminal Oxidants in Terms of Green Character

Oxidant	Byproduct[a]	Atom efficiency (%)[a]	E-factor[b]	Cost (€/kg) or (€/l)[c]
O_2	H_2O (none)	50 (100)	0	35
H_2O_2	H_2O	47	0	63
$CH_3C(O)OOH$	$CH_3C(O)OH$	27	1.03	390
t-BuOOH	*t*-BuOH	22	1.27	150
NaClO	NaCl	21	1.01	16
Pyridine-*N*-oxide	Pyridine	17	1.36	450
CumOOH	CumOH	12	2.34	110
$KMnO_4$	$MnO_2 + H_2O$	10	1.50	89
$2KHSO_5 + KHSO_4 + K_2SO_4$ (Oxone®)	$3\ KHSO_4 + K_2SO_4$	10[d]	10.03	73
m-CPBA	*m*-CBA	9	2.70	460
PhIO	PhI	7	3.52	[e]

[a]One O atom transfer, in parentheses two O atoms transfer.
[b]Calculated for the epoxidation of propene.
[c]Data from www.sigmaaldrich.com for the most concentrated sold version of the oxidant, May 2012.
[d]Two O atoms are transferred to products.
[e]Not sold.

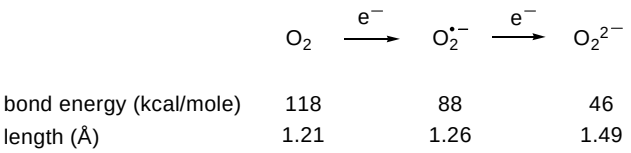
1.2 OXYGEN (AIR)

Air is the cheapest possible oxidant and the most desired for large industrial catalytic operations. However, in most cases for an effective catalytic reaction pure oxygen is preferred. The reasons are many: (i) faster reactions and greater reactor productivity; (ii) improved yield and better energy efficiency by avoiding dilution of reaction gases with nitrogen; (iii) smaller, lower capital cost plants; (iv) lower energy consumption; (v) environmental improvements due to significant reduction in the amount of purge gas. This implies a separation process from the other air components generally accomplished *via* fractional distillation of liquid air.

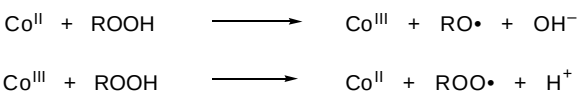
Air is first condensed through a series of compression/expansion cycles and subsequently separated in a double distillation column. The original Hampson–Linde process exploiting the Joule–Thomson effect has been modified and improved several times over the years in order to increase the efficiency and reduce energy consumption [6]. Even with these improvements the process remains quite energy intensive and the optimum economic balance requires that oxygen is manufactured on very large scale plants and then distributed to users as piped gas, as liquid oxygen in road tankers or as compressed gas in cylinders [6]. Distribution costs are very high in relation to the fairly low ex-factory cost of oxygen so that the price per unit can vary more than one order of magnitude depending on distribution facility. The consequence is that the cost of oxygen as oxidant for laboratory or small scale organic syntheses (gas cylinders used) is not much lower than other common oxidants (Table 1.1).

By contrast with many other simple diatomic molecules such as N_2 or H_2, the oxygen molecule (or dioxygen) is paramagnetic as it has two unpaired electrons in the ground state. The highest occupied molecular orbitals (HOMOs) are a pair of π^* orbitals of identical energy, so that the two highest energy electrons have no reason to spin-pair [7]. The diradical nature of the oxygen molecule is very useful in understanding its chemistry. In fact, most of its reactions proceed in one-electron steps: electrons added to the O_2 molecule populate antibonding (π^*) orbitals and weaken the O−O bond (Scheme 1.1) [8]. This effect is evident in both the O−O bond length and its dissociation energy making the resulting superoxo ($O_2^{\bullet -}$) and peroxo (O_2^{2-}) species more reactive and kinetically more easy to control.

As rationalized by Sheldon and Kochi [9], metal catalyzed oxidations can be conveniently divided into two types: homolytic and heterolytic. Homolytic oxidations involve free-radical intermediates and, in solution, are catalyzed by first-row transition metals characterized by one-electron redox steps (e.g., Co^{II}/Co^{III},



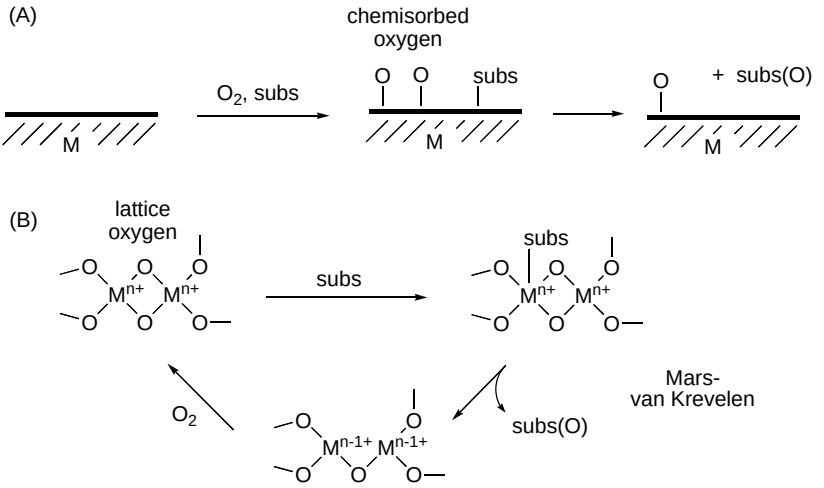
SCHEME 1.1 Basic data on the dioxygen molecule and the superoxo and peroxo anions.



SCHEME 1.2 Cobalt-catalyzed decomposition of hydroperoxides (Haber-Weiss mechanism).

Mn^{II}/Mn^{III}, Cu^{I}/Cu^{II}). In homolytic reactions the hydrocarbon to be oxidized is generally not coordinated to the metal and is oxidized outside the coordination sphere *via* a radical chain. The main role of the metal is generally to decompose organic hydroperoxides, formed in solution either spontaneously or by action of an initiator, generating radicals to sustain the radical chain. This behavior is also known as the Haber–Weiss mechanism (Scheme 1.2). These radical processes are common and constitute the basis for several very important industrial applications (e.g., the synthesis of adipic [10] and terephthalic [11] acids). However, radical chains are difficult to control, they do not often preserve the configuration of the substrate and typically lead to the formation of a wide variety of products as a consequence of a series of consecutive reactions because the reaction product is generally more easily oxidizeable than the reactant itself. It should be pointed out that the triggering of radical chains is not an exclusive property of certain metal ions in solution but can be effected also by the surface of a heterogeneous catalyst, especially when reactions are carried out in the liquid phase. The general consequence is that reactions involving one-electron processes with dioxygen as the oxidant are generally carried out at low conversion per pass and normally show only moderate to low selectivities towards the desired product.

In the activation of dioxygen on the surface of a heterogeneous catalyst (particularly in gas phase reactions) the formation of surface oxo species is generally invoked. Oxygen is chemisorbed on Group 8–10 metals in this way, even at relatively low temperatures. Indeed these surface oxo species are often represented as single bonded to the surface (Scheme 1.3**A**) to indicate their high reactivity once adsorbed on defective, coordinatively unsaturated surface sites. This chemisorbed oxygen can be exploited for the oxidation of, e.g., ethylene to ethylene oxide [12–14], CO to CO_2 [15, 16] or in catalytic combustion [17–20], i.e. in reactions where selectivity is either not a problem or poor selectivity can be economically tolerated. In the same way, metal-oxide or mixed-metal-oxide catalysts generally employ their already existing surface oxo species (lattice oxygen) for the high temperature oxidation of hydrocarbons. This is typical for n-type semiconductor oxides (e.g., Ti, V, and Mo) where a lower oxidation state is easily accessible to the central metal atom (Scheme 1.3**B**). Oxygen vacancies are subsequently replenished by dioxygen. This two-step process is known as the Mars–Van Krevelen mechanism [21]. Because lattice oxygen is more tightly bound than chemisorbed oxygen, it can be delivered in a more controlled fashion opening the way to selective oxidation and this mechanism is involved in processes like, e.g., the synthesis of acrolein or acrylonitrile [22–24].



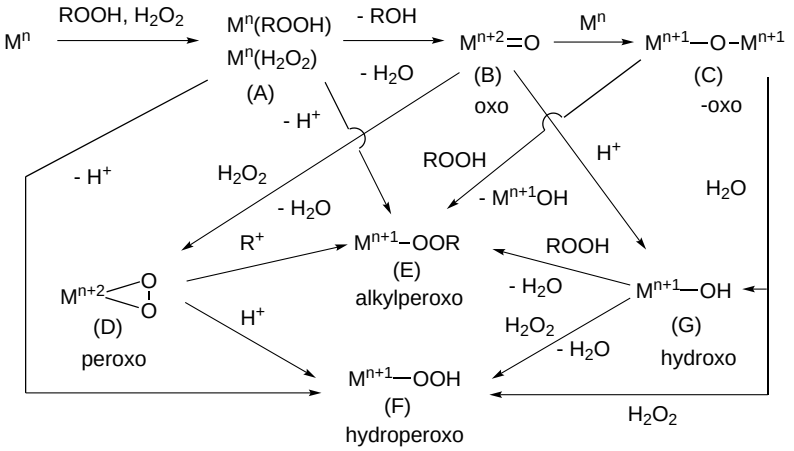
SCHEME 1.3 Oxygen activation on the surface of heterogeneous catalysts. (A) Through chemisorption; (B) by replenishing consumed lattice oxygen.

For the reasons described above the use of oxygen as oxidant in heterogeneously catalyzed organic reactions is always associated, to a variable extent, with substrate total oxidation and/or with the formation of byproducts. Therefore, one of the main efforts in catalyst design is to keep these problems to a minimum, because the advantage of using a cheap and environmentally benign oxidant can be outweighed by loss of starting reagent and the need to dispose significant amounts of unwanted byproducts. Moreover, oxygen is a gas and its use for reactions in the liquid phase generally requires medium to high pressures to increase the solubility in the reaction medium. It forms explosive gas mixtures with the vast majority of volatile organic compounds requiring adequate safety control in the apparatus to stay out of the explosion limits (extra capital investment). In other words, despite oxygen being a very cheap and practical oxidant, its environmental sustainability may become a questionable concept that should be evaluated only *a posteriori.*

1.3 ALKYLHYDROPEROXIDES

Hydroperoxides represent a reduced and easier to control form of dioxygen. As is clear from Scheme 1.1, in peroxides the O−O bond is longer and its energy lower than in free dioxygen. Therefore, it is easier to deliver one of the oxygen atoms of hydroperoxides in a controlled manner under mild conditions.

They can easily react with suitable transition-metal precursors to give a variety of species (some of which are stable enough to be isolated) involved in oxygen transfer to hydrocarbons. The different oxygenated species that are liable to play a



SCHEME 1.4 Schematic network connecting the metal-oxo and -peroxo species involved in metal-promoted oxidations.

role in oxidation processes are schematically represented in Scheme 1.4. The first step consists of the formation of a hydroperoxide adduct from which all other species can form in a cascade of reactions. Among the different species shown in the scheme, only hydroxo (**G**) are not directly involved as the oxidizing species in oxygen transfer processes. With the exception of oxo species, where hydroperoxides operate as mono-oxygen donors to the metal, in the other cases the O−O moiety remains intact. In all cases, only one of the peroxy oxygens is utilized in oxygen transfer, the other one is used to make alcohols (water).

Their behavior in oxidation is largely dependent on the type of metal used as catalyst. With one-electron redox systems homolytic oxidation prevails and hydroperoxides are simply decomposed in the catalytic system to generate radical species according to the Haber–Weiss mechanism (Scheme 1.2).

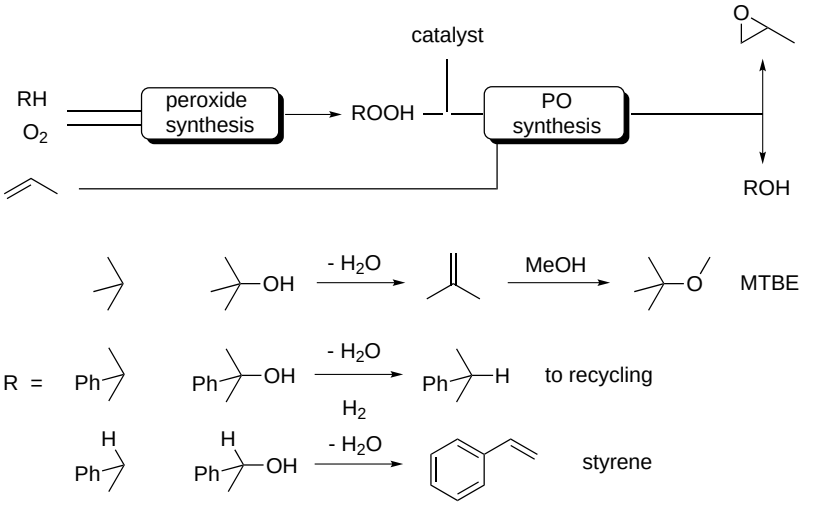
With two-electron redox systems heterolytic oxidations are generally involved and the metal can selectively transfer one oxygen atom to a suitable substrate. This is the basis for a wide variety of catalytic oxidation reactions, some of which have found applications in industry like, e.g., the Halcon and Shell processes for the production of propylene oxide [25, 26] or the synthesis of Esomeprazole [27, 28] and Indinavir [29, 30] in the pharmaceutical industry that are based on enantioselective sulfoxidation and epoxidation respectively.

Alkylhydroperoxides can be prepared in many different ways [31], however, only the most stable ones have been used in practice as oxidants for organic transformations. Bulk hydroperoxides are intrinsically unsafe materials as they can decompose violently by homolytic or heterolytic fission hence proper care must be taken to handle them safely. Their stability follows the well-known order, tertiary > secondary > primary, that also parallels the ease with which they can form from the corresponding hydrocarbons *via* radical autoxidation.

Stable alkylhydroperoxides that have been extensively used in catalytic oxidations are *t*-butyl hydroperoxide (TBHP), cumyl hydroperoxide (CHP) and ethylbenzene hydroperoxide (EBHP). Their major application is in the synthesis of propene oxide (PO) according to different technologies. They are produced by the autoxidation of the corresponding hydrocarbons containing a tertiary or a benzylic C−H bond. In the industrial practice their synthesis is carried out in one section of the plant.

The use of hydroperoxides implies that one molecule of alcohol is released per molecule of propylene oxide in the epoxidation stage. Indeed, much more alcohol is coproduced, owing to the less than 100% selectivity in both the autoxidation and epoxidation reactions. The choice of the peroxide is dictated also by the economics of the process that is strongly bound to the possibility to convert the large amounts of the alcohol coproduct into commercially valuable chemicals. Generally, ethylbenzene or isobutane are used, and the corresponding 1-phenyl ethanol and *t*-butanol are transformed into polymer-grade styrene or isobutene for octane enhancers in gasoline (MTBE, ETBE) [26]. The end of pipe recycling or commercialization of the coproduct is a key issue to justify the environmental acceptability of processes based on alkylhydroperoxides. Nonetheless, the presence of a coproduct implies that the value of propylene oxide is significantly affected by the demand/pricing of the coproduct and difficulties can arise in balancing two different markets that may occasionally experience diverging dynamics of growth.

In all cases the alkylhydroperoxide oxidant is produced on site and the synthesis unit is integrated in the main PO process. A simplified view of the main integrated process operations is shown in Scheme 1.5.



SCHEME 1.5 A simplified view of the operations taking place in the different propene oxide technologies, including the transformation of the alcohol coproducts into valuable chemicals.

The process originally developed by Halcon/ARCO, with a current market share of *ca*. 13%, is based on the use of TBHP as the oxidant. Isobutane is oxidized with air at *ca*. 120–140 °C and 25–35 bar in a typical autoxidation reaction yielding comparable quantities of TBHP and *t*-butyl alcohol (TBA) with conversions around 40%. The epoxidation of propylene is a liquid phase homogeneous reaction carried out in TBA as the solvent at 110–120 °C, under pressure (*ca*. 40 bar), in the presence of a soluble Mo^{VI} catalyst. Yields on propylene are *ca*. 90% at 10% conversion. The ratio of the coproduced TBA to propylene oxide is in the range 2.4 to 2.7. TBA is mostly dehydrated to isobutene and etherified with methanol or ethanol for the production of octane boosters [32].

Alternatively, EBHP is used in two other processes, developed by Halcon/ARCO and by Shell, with a whole market share of *ca*. 35%. EBHP is produced by the autoxidation of ethylbenzene at 140–160 °C, limiting the conversion to somewhat below 15% to minimize the decomposition of the hydroperoxide. The selectivity to EBHP is in the range 80–85%, with the balance being a mixture of 1-phenylethanol and acetophenone. The epoxidation of propylene, catalyzed in the Shell process by Ti^{IV} supported on silica (Ti/SiO_2) and by a soluble organic salt of Mo^{VI} in the Halcon/ARCO process, is operated in the liquid phase at *ca*. 100–120 °C. In both cases, the 1-phenylethanol coproduct is dehydrated to styrene. The yields of propylene oxide are 91–92%, with a styrene to propylene oxide ratio close to 2.2 [32].

An advanced version of the hydroperoxide process, in which the alcohol is transformed back into the starting hydrocarbon, was commercialized by Sumitomo in 2003 (market share *ca*. 4%). As the end use of the coproduct is no longer a discriminating issue for the choice of oxidant, the preference was for CHP over other hydroperoxides, on the grounds of its higher stability and superior performance in the epoxidation stage. Cumene is regenerated at the end of the process by the dehydration–hydrogenation of cumyl alcohol and recycled to the autoxidation reactor. In practice, hydrogen and oxygen are consumed to yield equimolar amounts of epoxide and water; in this aspect the process resembles the monooxygenase type of reactions [32].

The above examples clearly show that despite unfavorable atom efficiency and E-factor the sustainable use of alkylhydroperoxides as oxidants is possible, although it strongly depends on the profitable conversion of the corresponding alcohol. This is possible in large scale plants where process integration is easy to practice, it does not constitute a problem for small applications in fine chemistry because the amount of hydroperoxide necessary can be easily bought on the market and the alcohol disposed of, but it becomes complicated in medium scale operations where neither of the above conditions apply (easy hydroperoxide supply and alcohol conversion), posing economic constraints that may suggest other oxidant systems. This is why, as reported above, commercial applications of alkylhydroperoxides other than propylene oxide are mainly in the synthesis of pharmaceuticals where the large added value of the final product compensates for the cost of disposal of all the byproducts produced along the complex synthetic procedure.

TBHP is commercialized on a large scale by Lyondell-Basell with a total capacity of 27,000 ton/y and plants located in Texas and The Netherlands [33]. It is sold as a 70% aqueous solution and it is one of only two organic peroxides that the US Department of Transportation certifies for tank truck shipment. Its largest application is in the synthesis of peroxy derivatives such as tertiary-butyl peresters, perketals, and dialkylperoxides. Other uses are as free radical polymerization initiator, in epoxidation and other oxidation reactions, in sulfur removal from petroleum or as additive to lubricants. Other peroxides are sold on the market in moderate amounts by a variety of chemical companies.

1.4 HYDROGEN PEROXIDE

As shown in Table 1.1 hydrogen peroxide is, along with oxygen, the only oxidant giving virtually no waste. It is also a powerful oxidant and a major chemical commodity. Its total production in 2005 was 3.52 Mt/y (as 100% H_2O_2) with an expected growth of 3–5% per year [34]. The global hydrogen peroxide market is expected to reach 4.67 Mt by 2017 [35]. It is sold as aqueous solutions with 35, 50 and 70% by weight (although the latter is no longer available from chemical retailers), and the major industrial segments employing hydrogen peroxide are summarized in Figure 1.1. As can be seen, the fraction going into the production of chemicals is about one fifth of the hydrogen peroxide market, while the vast majority is consumed by unselective oxidations like the bleaching of textiles, pulp and paper, and in the treatment of wastewaters before they are released into the environment (2008 data).

Substantial increase in production is expected in the near future driven mainly by the continuing replacement of chlorine compounds with hydrogen peroxide in the pulp and paper industry and in environmental remediation. Moreover, the new HPPO technology developed and commercialized jointly by BASF and Dow, utilizes large quantities of hydrogen peroxide for production of PO without the release

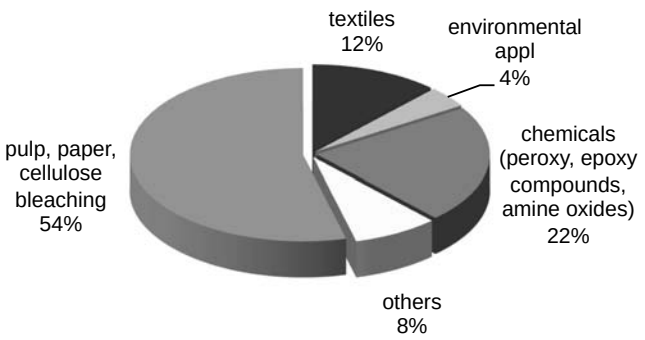
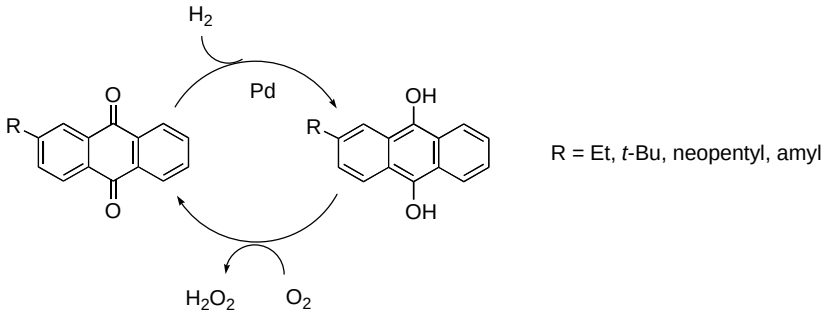


FIGURE 1.1 Use of hydrogen peroxide divided by industrial segments.

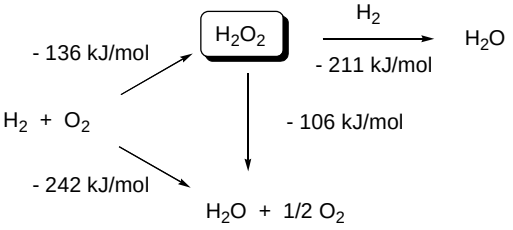


SCHEME 1.6 Essential features of the anthraquinone process.

of any byproducts in the process [36]. Environmental regulations and laws have played a vital role in popularizing the use of hydrogen peroxide over other chemicals, by virtue of the chemical being emission-free and ecofriendly in nature. Hydrogen peroxide's robust growth over the past few years could be traced back to the overwhelming support of the environmental protection authorities and tightening effluent regulations in almost every application area. These arguments and the easy availability of hydrogen peroxide, albeit at a relatively high price, also make it the ideal oxidant for a variety of small to medium to relatively large size catalytic applications, especially in synthetic organic chemistry.

Nowadays virtually all hydrogen peroxide production is based on the so-called Riedl–Pfleiderer [37] or Anthraquinone Process (AO), a small fraction being made by electrochemical oxidation of dilute NaOH solutions [38]. The anthraquinone process consists in the hydrogenation of a substituted anthraquinone to the corresponding anthrahydroquinone using a Pd or Ni catalyst and the oxidation of latter with air back to anthraquinone with production of hydrogen peroxide (Scheme 1.6) [39–41].

A solvent mixture is generally required to dissolve both the anthraquinone and the anthrahydroquinone that have different solubilities. The solvent mixture must also be inert to hydrogenation and oxidation and immiscible with water used for efficient hydrogen peroxide extraction. Examples of solvent mixtures reported in the patent literature are substituted benzenes, toluene, and naphthalenes mixed with phosphonic and phosphoric esters, nonyl alcohols, etc. [39]. Major limitations of this process are the following: (i) a substrate loss at each catalytic cycle (1%) because of overreduction leading to hydroquinones that are difficult to reoxidize in the next step, these products must be removed or regenerated; (ii) low conversion during the hydrogenation step in order to minimize secondary reactions; (iii) high H_2O_2 purification and concentration costs because the crude aqueous H_2O_2 from the extractor has a concentration in the 15–30% range ad is contaminated by organics; (iv) toxic organic wastes disposal (benzene, C_9–C_{11} aromatics, C_7–C_9 alcohols); (v) difficulties in the complete recovery of the hydrogenation catalyst; (vi) need of large plants to compensate for high operating costs. These issues have



SCHEME 1.7 The different reactions taking place with $H_2/O_2/H_2O_2$ mixtures.

led to a situation in which the anthraquinone process is practiced by a few large producers (Arkema, Chang Chun Petrochemical, Evonik Degussa, Nippon Peroxide, Mitsubishi Gas Chemicals and Solvay, among others) that dominate the market with significant economic consequences.

The direct synthesis of hydrogen peroxide from hydrogen and oxygen is an obvious and attractive green technology to replace the current anthraquinone process since it is the most atom-efficient approach by which hydrogen peroxide can be prepared. The study of the direct synthesis of hydrogen peroxide is about one century old. The first patent was issued in 1914 using Pd as catalyst [42], with little progress until the 1980s when the interest was renewed, driven by the strong demand for H_2O_2 [e.g., 43–48] but once again hampered by the severe practical difficulties posed by safety issues. Nevertheless, the direct synthesis of hydrogen peroxide remains a challenging opportunity. A schematic network connecting the different reactions taking place among hydrogen, oxygen and hydrogen peroxide is reported in Scheme 1.7.

The problems to be overcome are the following: (i) water is by far the most thermodynamically favored product; (ii) the decomposition rate of H_2O_2 can be very high especially in the presence of dispersed metals; (iii) The explosion range of H_2/O_2 mixtures is very wide (4% to 96% of H_2 in O_2 at 20 °C and 1 bar [49]) implying very stringent safety conditions; (iv) all reactions are catalyzed by Pd, i.e. the catalyst of choice for H_2O_2 direct synthesis. Hence, tuning the catalyst activity, selectivity and stability with time to maximize hydrogen peroxide productivity is like tightrope walking.

In the past 10–15 years the system has also been thoroughly investigated by academia, elucidating some of the key issues governing the activity and selectivity of the catalysts. However, in spite of several published patents [43–48], recent literature [50–57] and economic appeal, no process for the direct synthesis of hydrogen peroxide has yet been marketed. The field has been thoroughly reviewed [58–60]. Common features of the vast majority of systems reported are the following: (i) the use of Pd supported catalysts, either as Pd alone or as Pd/X alloys (X = Pt, Ag, Au) dispersed on a variety of supports ranging from carbon to SiO_2 or Al_2O_3 to other less common ones like Fe_2O_3, ZrO_2 or CeO_2; (ii) the use of acidic solutions (e.g., H_2SO_4, HCl) and the presence of promoters (e.g., Br^-, Cl^-) to improve the activity and selectivity; (iii) batchwise reactions carried out either at atmospheric or high

pressure (up to 100 bar) and low temperature (10–25 °C); (iv) the need to operate with O_2/H_2 mixtures often in the explosion range to maximize the activity. The latter is a particularly stringent limitation. For example Pd/SiO_2 catalysts have been extensively studied by Lunsford and coworkers with useful results in terms of overall hydrogen peroxide productivity [61–68]. H_2O_2 concentrations up to 1.8% with > 90% selectivity were observed using 10^{-1} mol L^{-1} HCl and 10^{-2} mol L^{-1} Br^- to promote the reaction but only operating inside the explosive regime. Still open challenges are therefore the need to operate under intrinsically safe conditions with both an adequate selectivity towards the desired reaction and a hydrogen peroxide productivity that could be of practical significance (at least 1–2% solutions).

In this respect an important role is played by the support and its capacity to impart the appropriate metal morphology. To illustrate this crucial point some papers that recently appeared in the literature will be considered. The group of Hutchings has recently reported a comparison [69] among different Pd and Pd-Au catalysts deposited on supports such as Al_2O_3, Fe_2O_3, C, TiO_2, CeO_2 based on extensive work carried out by these authors in this area [70–74], all tested at 2 °C outside the explosion regime at 30 bar total pressure and using CO_2 as active gases diluent (Figure 1.2).

In general, bimetallic Pd-Au catalysts provide better performance with respect to monometallic ones, the best catalyst being Pd-Au deposited on HNO_3 or HOAc washed carbon [70]. Acid pretreatment was of foremost importance in stopping

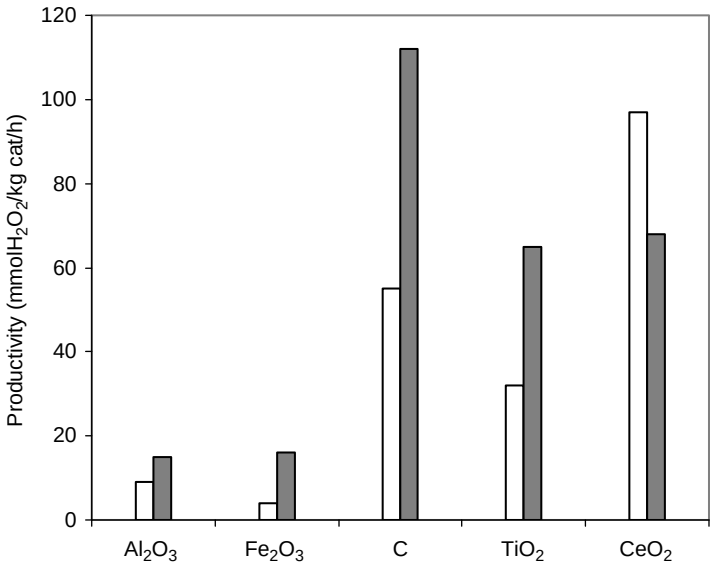


FIGURE 1.2 H_2O_2 productivity in the direct synthesis from hydrogen and oxygen using Pd (white) and Pd-Au (gray) catalysts on different supports according to ref. 69.

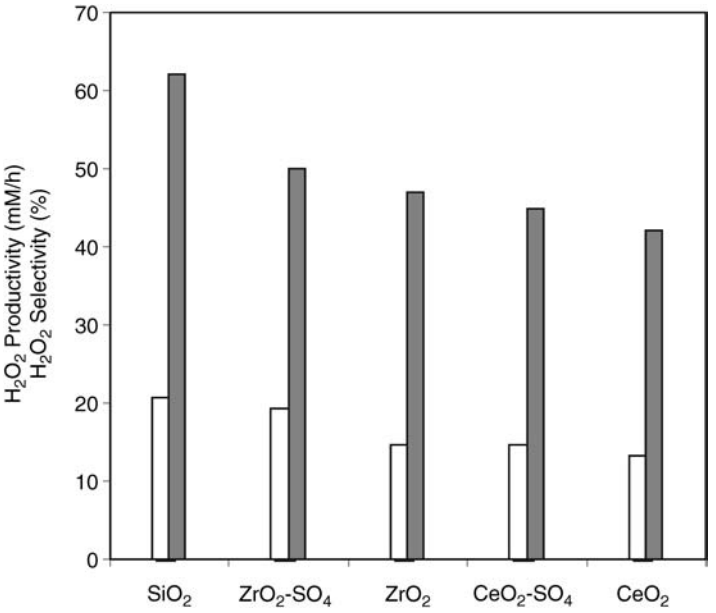
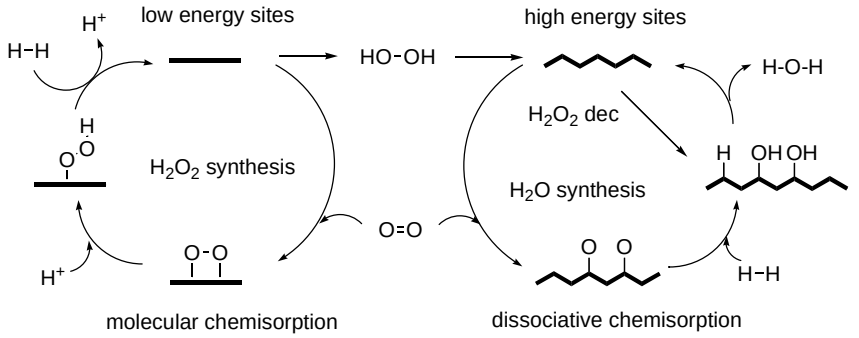


FIGURE 1.3 H_2O_2 productivity (white) and selectivity (gray) in the direct synthesis from hydrogen and oxygen using a series of Pd catalysts on different supports according to ref. 75.

H_2O_2 hydrogenation (Scheme 1.7), maximizing selectivity ($>98\%$), improving productivity (1.1% H_2O_2 in methanol was obtained building up on 5 consecutive experiments) and imparting significant catalyst stability (30 min tests were repeated up to 5 times without appreciable loss of productivity) [70]. The second best support was CeO_2, even if in this case the monometallic catalyst was more productive than the bimetallic one and the selectivity was much lower (43%).

A similar comparison has been recently reported by Menegazzo et al. [75] also based on new and previous work in the area [76–79]. Figure 1.3 reports the activity and selectivity for a series of monometallic Pd catalysts tested at room temperature and 1 bar outside the explosion regime. Even here, acid doping (H_2SO_4) of the support exerts a beneficial effect on the performance of the catalysts although the influence is not dramatic.

With all the catalysts reported in Figure 1.3 hydrogen peroxide hydrogenation/decomposition has a negligible influence on selectivity, this being determined mainly by H_2O_2 *vs.* H_2O direct formation (Scheme 1.7). The best catalyst appears to be Pd/SiO_2 without the addition of any acid or halide promoter, its productivity and selectivity remain the same after 10 h time on stream and the productivity increases more than 10 times increasing the total pressure to 10 bar, even upon dilution with CO_2 yielding $<1\%$ methanolic solutions [75]. These properties make this catalyst a potential candidate for practical applications. At variance with the previous

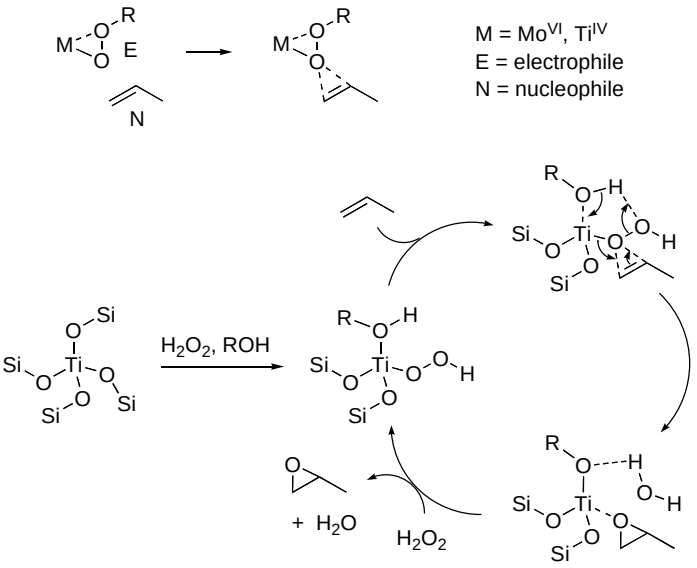


SCHEME 1.8 Proposal of the role of metal surface morphology in H_2O_2 synthesis *vs.* decomposition and water formation.

examples reported by Hutchings, in this case ceria yields the less appealing catalysts. This observation emphasizes the crucial role of synthetic procedures and parameters in determining the morphological properties of the active phase. While it is generally accepted that a high metal dispersion increases the overall catalyst activity, it also increases the rate of the undesired reactions at the expense of selectivity. A key feature maximizing selectivity is the presence of relatively large, nondefective Pd clusters [75] a condition that was suggested to promote H_2O_2 formation over the other reactions because O_2 (and H_2O_2) chemisorption on Pd is more likely to occur without dissociation (Scheme 1.8) [80].

Like all hydroperoxides, H_2O_2 can be activated homolytically and heterolytically and, at variance with oxygen, its reactivity in oxidation reactions can be more easily controlled, thus minimizing side reactions and increasing selectivity. The different species that can form between transition metals and hydrogen peroxide by heterolytic activation are summarized in Scheme 1.4. When the intermediates responsible for oxygen transfer are oxo species **B**, **C** then the behavior of hydrogen peroxide as oxidant does not differ from alkylhydroperoxides, except for the rate with which oxo species are formed. However, in the case of the simple adduct **A** or hydroperoxo species **F** the reactivity of hydrogen peroxide is influenced by the nature of the metal ion to which it is coordinated.

The concept of electrophilic and nucleophilic activation of hydrogen peroxide has been proposed many years ago [81], it exploits the amphoteric nature of hydrogen peroxide and reflects the change in the electronic properties of the peroxy oxygen that is transferred to the substrate depending on the metal ion carrying out the catalytic transformation. Electrophilic activation occurs with Lewis-acidic transition-metal centers in their highest oxidation state (e.g., Ti^{IV}, V^{V}, Mo^{VI}) and it is very common especially with classical heterogeneous metal oxide catalysts. Nucleophilic activation has been identified mainly with soluble complexes of low-valent, electron-rich metals (e.g., Co^{II}, Pd^{II}, Pt^{II}) and also applies to their heterogenized congeners. This distinction has important

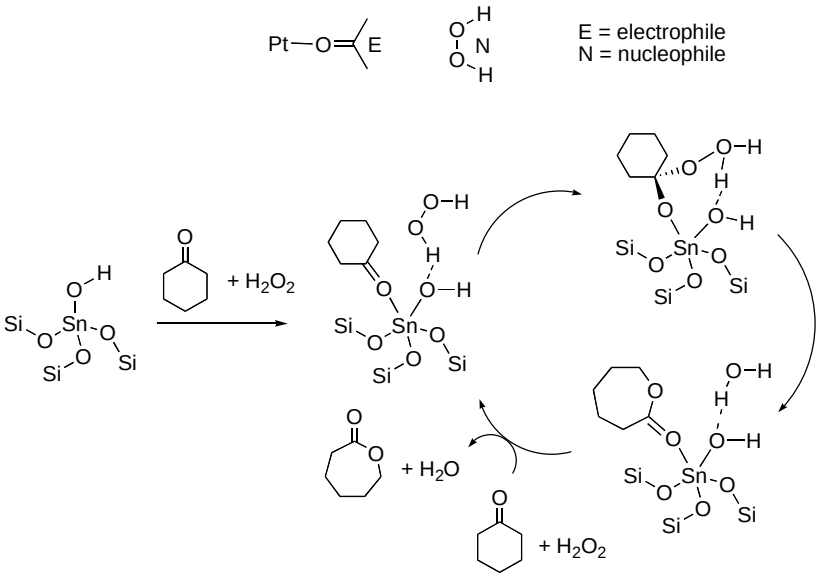


SCHEME 1.9 The principle of electrophilic activation and its application in the epoxidation of propene with the TS-1/H_2O_2 system.

practical implications as an electron-poor peroxy oxygen will be more easily delivered to an electron-rich substrate (e.g., internal and suitably substituted olefins, and sulfides) while an electron-rich peroxy oxygen to an electron-poor substrate (aldehydes, ketones, terminal olefins, etc.).

To illustrate this principle two examples are cited. Scheme 1.9 shows the electrophilic activation of the oxidant that occurs in the Halcon and Shell processes for the epoxidation of propene, where the electron poor, Lewis-acidic metal-center coordinates an alkylhydroperoxide generating an electrophilic peroxygen that is delivered to a noncoordinated nucleophilic propene [82, 83]. A known consequence is that these systems work even better with more electron-rich substrates such as highly substituted alkenes and allylic alcohols. Scheme 1.9 also shows the same principle applied to the epoxidation of propene with hydrogen peroxide catalyzed by TS-1 as demonstrated by Clerici et al. [84, 85] where the essential features are identical except for the ancillary role of the alcohol solvent that favors the leaving of water.

The amphoteric nature of hydrogen peroxide also makes possible nucleophilic activation. Scheme 1.10 shows the principle originally suggested for the Baeyer–Villiger oxidation of ketones, where a soluble Pt^{II} complex now activates the ketone substrate, increasing its electrophilicity and making it susceptible to nucleophilic attack by free hydrogen peroxide [86–91]. Sn-beta catalysts follow the same principle as was demonstrated by Corma and coworkers by mechanistic studies and also by DFT calculations [92–97].



SCHEME 1.10 The principle of nucleophilic activation of hydrogen peroxide and its application in the Baeyer–Villiger oxidation of cyclohexanone with Sn-beta.

1.5 CONCLUSIONS

In this brief overview we have tried to discuss the basic properties, industrial synthetic procedures and activation principles of the topmost environmentally acceptable oxidants, i.e. oxygen, alkylhydroperoxides and hydrogen peroxide. A critical evaluation clearly suggests that the green character of these oxidants depends on their intrinsic properties only in part. Popular parameters like atom economy or E-factor are always calculated assuming 100% conversion and 100% selectivity, conditions that are hardly achieved in practice. So, for a given reaction, the final word in this contest can be said only *a posteriori* considering the real case that includes also other variables like reaction conditions (temperature, pressure), conversion, selectivity, ease of product separation, number and nature of byproducts. Additional economic issues are oxidant market price and ease of supply.

All together the oxidant that seems to emerge as the most promising is hydrogen peroxide that couples the advantage of zero waste to the possibility of easily yielding (generally) high selectivity in the reactions where it is employed, albeit at the expense of a relatively high price. If the new direct synthesis from hydrogen and oxygen does become an industrial reality this problem will probably be solved and a push toward a widespread use of hydrogen peroxide in catalytic oxidation will be experienced. The future will tell.

REFERENCES

1. Anastas P.T., Warner J.C. *Green Chemistry: Theory and Practice*. Oxford University Press, New York, 1998.
2. Trost B.M. (1991). *Science* 254, 1471–1477.
3. Trost B.M. (1995). *Angew. Chem. Int. Ed.* 34, 259–281.
4. Sheldon R.A. (2007). *Green Chem.* 9, 1273–1283.
5. Sheldon R.A. (2008). *Chem. Commun.*, 3352–3365.
6. Grant W.J., Redfearn S.L. In: *The Modern Inorganic Chemical Industry*. Thompson R., ed. The Chemical Society, London, 1977, pp. 273–284.
7. Huheey J.E. *Inorganic Chemistry*, 3rd ed. Harper & Row, New York, 1983.
8. Parshall G.W. *Homogeneous Catalysis*. Wiley, New York, 1980, p. 188.
9. Sheldon R.A., Kochi, J.K. *Metal Catalyzed Oxidations of Organic Compounds*. Academic Press, New York, 1981.
10. Musser M.T. In: *Ullmann's Encyclopedia of Industrial Chemistry*, Vol. A8, 5th edn. Wiley-VCH, Weinheim, 1995, pp. 217–226.
11. Sheehan R.J. In: *Ullmann's Encyclopedia of Industrial Chemistry*, Vol. A26, 5th edn. Wiley-VCH, Weinheim, 1995, pp. 193–204.
12. Weissermel K, Arpe H.J. *Industrial Organic Chemistry*, 4th edn. Wiley-VCH, Weinheim, 2003, p. 148.
13. Van Santen R.A., Kuipers H. P. C. E. In: *Advances in Catalysis*, Vol. 35. Eley D.D., Pines H., Weisz P.B., eds. Academic Press, San Diego, 1987, pp. 265–321.
14. Waugh K.C., Hague M. In: *Mechanisms in Homogeneous and Heterogeneous Epoxidation Catalysis*. Oyama S.T., ed. Elsevier, Amsterdam, 2008, pp. 233–281.
15. Lox E.S.J., Engler B.H. In: *Handbook of Heterogeneous Catalysis*, Vol. 4. Ertl G., Knoetzinger H., Weitkamp J., eds. VCH, Weinheim, 1997, pp. 1559–1633.
16. Kummer J. In: *Catalysts for the Control of Automotive Pollutants*. McAvoy J., ed. ACS Series 143. American Chemical Society, Washington, DC, 1975, pp. 178–192.
17. Forzatti P., Groppi G. (1999). *Catal. Today* 54, 165–180.
18. Dalla Betta R.A. (1997). *Catal. Today* 35, 129–135.
19. Zwinkels M.F.M., Jaras S.G., Menon P.G., Griffin T.A. (1993). *Catal. Rev.-Sci. Eng.* 35, 319–358.
20. Prasad R., Kennedy L.A., Ruckenstein E. (1984). *Catal. Rev.-Sci. Eng.* 26, 1–58.
21. Hagen, J. *Industrial Catalysis*. Wiley-VCH, Weinheim, 1999, p. 148.
22. Burrington J.D., Kartisek C.T., Grasselli R.K. (1984). *J. Catal.* 87, 363–380.
23. Grasselli R.K. In: *Handbook of Heterogeneous Catalysis*. Ertl, G., Knötzinger, H., Weitkamp, J., eds. VCH, Weinheim, 1997, pp. 2302–2326.
24. Grasselli R.K., Burrington J.D. In: *Advances in Catalysis*, Vol. 30. Eley D.D., Pines H., Weisz P.B., eds. Academic Press, San Diego, 1981, pp. 133–163.
25. Clerici M.G., Ricci M., Strukul G. In: *Metal Catalysis in Industrial Organic Processes*. Chiusoli G.P., Maitlis P.M., eds. The Royal Society of Chemistry, Cambridge, 2006, pp. 23–78.
26. Kahlich D., Wiechern U., Lindner J. In: *Ullmann's Encyclopedia of Industrial Chemistry*, Vol. A22, 5th edn. Wiley-VCH, Weinheim1995, pp. 239–260.

27. Federsel H.–J., Larsson M. In: *Asymmetric Catalysis on Industrial Scale. Challenges, Approaches and Solutions*. Blaser H.U., Schmidt E., eds. Wiley-VCH, Weinheim, 2004, pp. 413–436.
28. Cotton H., Elebring T., Larsson M., Li L., Sörenson H., von Unge S. (2000). *Tetrahedron: Asymm*. 11, 3819–3821.
29. Senanayake C.H., Smith G.B., Ryan K.M., Fredenburgh L.E., Liu J., Roberts F.E., Hughes D.L., Larsen R.D., Verhoeven T.R., Reider P.J. (1996). *Tetrahedron Lett*. 37, 3271–3274.
30. Senanayake C.H., Roberts F.E., Di Michele L.M., Ryan K.M., Liu J., Fredenburgh L., Foster B.S., Douglas A.W., Larsen R.D., Verhoeven T.R., Reider P.J. (1995). *Tetrahedron Lett*. 36, 3993–3996.
31. Scarso A., Strukul G. In: *Science of Synthesis. Vol. 38, Peroxides*. Berkessel A., ed. Georg Thieme, Stuttgart, 2009, pp 9–72.
32. Clerici M. G., Ricci M., Strukul G. In: *Metal Catalysis in Industrial Organic Processes*. Chiusoli G.P., Maitlis P.M., eds. The Royal Society of Chemistry, Cambridge, 2006, p. 42.
33. http://www.lyondellbasell.com/techlit/techlit/2644.pdf
34. *Chem. Week* (2005). 167, 36.
35. http://www.prweb.com/releases/hydrogen_peroxide/bleaching_pulp_paper/prweb9268178.htm
36. http://www.basf.com/group/pressrelease/P-09-154
37. Riedl H., Pfleiderer G., inventors; I. G. Farbenindustrie, assignee. U.S. Patent 2,158,525. 1936.
38. http://www.chemsystems.com/about/cs/news/items/PERP%200708_3_Hydrogen%20Peroxide.cfm#content
39. Goor G. In: *Catalytic Oxidations with Hydrogen Peroxide as Oxidant*. Strukul G., ed. Kluwer, Dordrecht, 1992, p. 13–15.
40. Jones C.W. *Applications of Hydrogen Peroxide and Derivatives*. The Royal Society of Chemistry, Cambridge, 1999, p. 3–7.
41. Weigert, W.M., Delle H., Kaebisch G. In: *Wasserstoffperoxid und seine Derivate*. Weigert W.M., ed. Huethig, Heidelberg, 1978, p. 9–15.
42. Henkel H., Weber W., inventors; Henkel, assignee. US Patent 1,108,752. 1914.
43. Gosser L.W., inventor; E.I. DuPont de Nemours, assignee. US Patent 4,681,751. 1987.
44. Gosser L.W., Schwartz J.T., inventors; E.I. DuPont de Nemours, assignee. US Patent 4,772,458. 1988.
45. Van Weynbergh J., Schoebrechts J.-P., Colery J.-C., inventors; Solvay Interox, assignee. US Patent 5,447,706. 1995.
46. Bertsch-Frank B., Hemme I., Von Hoppel L., Katusic S., Rollmann J., inventors; Degussa-Hüls, assignee. US Patent 6,387,346. 2002.
47. Paparatto G., D'Aloisio R., De Alberti G., Buzzoni R., inventors; Eni and Enichem, assignees. US Patent 6,630,118. 2003.
48. Chuang K.T., Zhou B., inventors; EKA Nobel, assignee. US Patent 5,925,588. 1999.
49. Lewis B., von Elbe G. *Combustion, Flames and Explosion of Gases*. Academic Press, New York and London, 1961.
50. Burch R., Ellis P.R. (2003). *Appl. Catal., B - Environ.* 42, 203–211.

51. Choudhary V.R., Jana P. (2007). *J. Catal.* 246, 434–439.
52. Samanta C., Choudhary V.R. (2007). *Catal. Commun.* 8, 2222–2228.
53. Herzing A., Carley A.F., Edwards J.K., Hutchings G.J., Kiely C.J. (2008). *Chem. Mater.* 20, 1492–1501.
54. Edwards J.K., Thomas A., Solsona B., Landon P., Carley A.F., Hutchings G.J. (2007). *Catal. Today* 122, 397–402.
55. Hancu D., Beckman E.J. (2001). *Green Chem.* 3, 80–86.
56. Park S., Choi J.H., Kim T.J., Chung Y., Oh S., Song I. (2012). *J. Mol. Catal. A: Chemical* 353, 37–43.
57. Rueda T.M., Serna J.G., Cocero M.J. (2012). *J. Supercrit. Fluids* 61, 119–125.
58. Campos-Martin J.M., Blanco-Brieva G., Fierro J.L.G. (2006). *Angew. Chem. Int. Ed.* 45, 6962–6984.
59. Samanta C. (2008). *Appl. Catal. A: General* 350, 133–149.
60. Edwards J.K., Hutchings G.J. (2008). *Angew. Chem. Int. Ed.* 47, 9192–9198.
61. Liu Q., Bauer J.C., Schaak R.E., Lunsford J.H. (2008). *Appl. Catal. A: General* 339, 130–136.
62. Liu Q., Lunsford J.H. (2006). *J. Catal.* 239, 237–243.
63. Liu Q., Lunsford J.H. (2006). *Appl. Catal. A: General* 314, 94–100.
64. Han Y., Lunsford J.H. (2005). *J. Catal.* 230, 313–316.
65. Chinta S., Lunsford J.H. (2004). *J. Catal.* 225, 249–255.
66. Dissanayake D.P., Lunsford J.H. (2003). *J. Catal.* 214, 113–120.
67. Lunsford J.H. (2003). *J. Catal.* 216, 455–460.
68. Dissanayake D.P., Lunsford J.H. (2002). *J. Catal.* 206, 173–176.
69. Ntainjua E.N., Piccinini M., Pritchard J.C., Edwards J.K., Carley A.F., Kiely C.J., Hutchings G.J. (2011). *Catal. Today* 178, 47–50.
70. Edwards J.K., Solsona B.E., Ntainjua E.N., Carley A.F., Herzing A.A., Kiely C.J., Hutchings G.J. (2009). *Science* 323, 1037–1041.
71. Edwards J.K., Solsona B.E., Landon P., Carley A.F., Herzing A.A., Kiely C.J., Hutchings G.J. (2005). *J. Catal.* 236, 69–79.
72. Edwards J.K., Ntainjua E.N., Carley A.F., Herzing A.A., Kiely C.J., Hutchings G.J. (2009). *Angew. Chem. Int. Ed.* 48, 8512–8015.
73. Solsona B.E., Edwards J.K., Landon P., Carley A.F., Herzing A.A., Kiely C.J., Hutchings G.J. (2006). *Chem. Mater.* 18, 2689–2695.
74. Edwards J.K., Solsona B.E., Landon P., Carley A. F, Herzing A.A., Watanabe M., Kiely C.J., Hutchings G.J. (2005). *J. Mater. Chem.* 15, 4595–4600.
75. Menegazzo F., Signoretto M., Frison G., Pinna F., Strukul G., Manzoli M., Boccuzzi F. (2012). *J. Catal.* 290, 143–150.
76. Ghedini E., Menegazzo F., Signoretto M., Manzoli M., Pinna F., Strukul G. (2010). *J. Catal.* 273, 266–273.
77. Menegazzo F., Signoretto M., Manzoli M., Boccuzzi F., Cruciani G., Pinna F., Strukul G. (2009). *J. Catal.* 268, 122–130.
78. Menegazzo F., Burti P., Signoretto M., Manzoli M., Vankova S., Boccuzzi F., Pinna F., Strukul G. (2008). *J. Catal.* 257, 369–381.
79. Melada S., Rioda R., Menegazzo F., Pinna F., Strukul G. (2006). *J. Catal.* 239, 422–430.

80. Abate S., Centi G., Melada S., Perathoner S., Pinna F., Strukul G. (2005). *Catal. Today* 104, 323–328.
81. Strukul G. In: *Catalytic Oxidations with Hydrogen Peroxide as Oxidant*. Strukul G., ed. Kluwer, Dordrecht, 1992, pp. 177–221.
82. Chong A.O., Sharpless K.B. (1977). *J. Org. Chem.* 42, 1587–1590.
83. Parshall G.W., *Homogeneous Catalysis*. Wiley-Interscience, New York, 1980, p. 117.
84. Clerici M.G., Ingallina P. (1993). *J. Catal.* 140, 71–83.
85. Clerici M.G., Bellussi G., Romano U. (1991). *J. Catal.* 129, 159–167, and references therein.
86. Del Todesco Frisone M., Pinna F., Strukul G. (1993). *Organometallics* 12, 148–156.
87. Gusso A., Baccin C., Pinna F., Strukul G. (1994). *Organometallics* 13, 3442–3451.
88. Gavagnin R., Cataldo M., Pinna F., Strukul G. (1998). *Organometallics* 17, 661–667.
89. Paneghetti C., Gavagnin R., Pinna F., Strukul G. (1999). *Organometallics* 18, 5057–5065.
90. Cavarzan A., Bianchini G., Sgarbossa P., Lefort L., Gladiali S., Scarso A., Strukul G. (2009). *Chem. Eur. J.* 15, 7930–7939.
91. Michelin R.A., Sgarbossa P., Scarso A., Strukul G. (2010). *Coord. Chem. Rev.* 254, 646–660.
92. Corma A., Nemeth L.T., Renz M., Valencia S. (2001). *Nature* 412, 423–425.
93. Renz M., Blasco T., Corma A., Fornes V., Jensen R., Nemeth L.T. (2002). *Chem. Eur. J.* 8, 4708–4717.
94. Corma A., Navarro M.T., Nemeth L., Renz M. (2001). *Chem. Commun.*, 2190–2191.
95. Corma A., Navarro M.T., Renz M. (2003). *J. Catal.* 219, 242–246.
96. Boronat M., Corma A., Renz M., Sastre G., Viruela P.M. (2005). *Chem. Eur. J.* 11, 6905–6915.
97. Boronat M., Concepcion P., Corma A., Renz M. (2007). *Catal. Today* 121, 39–44.

2

OXIDATION REACTIONS CATALYZED BY TRANSITION-METAL-SUBSTITUTED ZEOLITES

MARIO G. CLERICI* AND MARCELO E. DOMINE

2.1 INTRODUCTION

The recognition in the late 1980s of the potentialities of Titanium Silicalite-1 (TS-1) prompted an intensive research activity on the new catalyst and a search of other metal-substituted molecular sieves, particularly with larger porosity [1–7]. Rapid progress on TS-1 and the discovery of Ti-Beta and several other metal zeolites were the scientific fruits, whereas applications did not advance beyond a demonstration unit for ammoximation and the plant for the hydroxylation of phenol. Ratnasamy et al. could observe, still at the beginning of the 2000s, that not only was no comparison possible for TS-1 with aluminosilicate zeolites, but the hypothesis of applications in petrochemical area was in contrast with the necessity of using hydrogen peroxide, believed to be compatible only with high value products worth at least 2$/kg [7]. However, large plants for the production of propylene oxide (PO) and cyclohexanone oxime were just around the corner, in an advanced phase of implementation to become operative in the first decade of the 2000s (Chapter 10). In a parallel trend, R&D activities intensified on TS-1 while shifting from Ti-Beta to Ti-MWW and, maybe, Ti-MOR, with increasing interest for applicative issues related to PO and cyclohexanone oxime production, such as the generation of mesoporosity, methods of synthesis by cheaper reagents and the application of

*Corresponding author

Liquid Phase Oxidation via Heterogeneous Catalysis: Organic Synthesis and Industrial Applications, First Edition. Edited by Mario G. Clerici and Oxana A. Kholdeeva.
© 2013 John Wiley & Sons, Inc. Published 2013 by John Wiley & Sons, Inc.

continuous reactors. Certain directions of research also imply an interest for other petrochemical applications, including the hydroxylation of benzene.

Several reviews cover the advances in the area of metal zeolites, often privileging synthetic and characterization aspects. It is the scope of this review to focus instead on catalytic applications and reaction mechanisms, further extending the scope of an earlier review with a similar approach [6]. Synthesis and characterization are dealt with the purpose of general information on the catalyst offered to the organic chemist with, however, pertinent references for full details.

2.2 SYNTHESIS AND CHARACTERIZATION OF ZEOLITES

Zeolites are porous crystalline aluminosilicates of the tectosilicates group possessing channels and cavities of molecular dimensions (0.2–1.2 nm) [8]. They can be obtained in a wide range of Si/Al atomic ratios (from 1 to ∞), i.e. they can contain both Si and Al or be purely siliceous. Other elements, mainly transition metals can also be incorporated in their structure. Zeolite nomenclature consists of the name given by the authors and of a three-letter code assigned after structure validation by the International Zeolite Association (IZA). Thus, the faujasite has the code FAU, ZSM-5 zeolite the code MFI, Beta zeolite the code BEA, etc.

Zeolites are synthesized either in nature or in the laboratory under hydrothermal conditions, namely, in aqueous medium and at temperatures between 50 and 400 °C. Water acts as mineralizing agent and solvent, favoring species transport and reaction in liquid phase. In addition to water, other reactants commonly used in the process are the sources of Si, sources of Al and other metals, inorganic and/or organic cations, and hydroxyl or fluoride anions behaving also as mineralizing agents.

The first laboratory syntheses were performed in moderately basic media, using alkaline cations to favor Si and metal species solubility. Such conditions led to A and X zeolites with the maximum possible Al content (Si/Al ratio of 1), and high exchange and adsorption capacity [9]. Low Si/Al zeolites (e.g., Y, MOR and L zeolites, Si/Al = 1.5–5) were obtained by increasing the concentration of alkaline cations, the pH (>10) and the temperature. The employment of organic cations allowed synthesizing a range of zeolites (i.e. Beta, ZSM-5, and ZSM-11) with high Si/Al ratio, characterized by superior thermal and hydrothermal stability, stronger acid sites, and greater hydrophobicity than the low Si/Al zeolites [10]. Finally, purely siliceous and highly hydrophobic zeolites were synthesized, such as silicalite-1 (S-1, MFI structure) [11].

Silicalite-1 was also the first zeolite obtained by replacing OH^- anions with F^- anions, working at pH close to neutrality or even slightly acid. Afterwards, the F^- medium method was extended to the synthesis of a wide range of zeolites [12]. Typical of this route is the retention of fluoride species inside the small cages of zeolitic structures, with a stabilizing effect of the structure. In general, zeolites with larger crystal size are obtained than from the OH^- medium. A second important difference is the higher hydrophobicity thanks to fewer structural defects, i.e. of less hydrophilic Si–O^- groups on the surface.

Silicoaluminates are used as cationic exchangers and adsorbents, as well as heterogeneous catalysts in a wide range of chemical reactions. The incorporation of transition metals (e.g., Ti, V, Cr, Fe, Sn) in MFI, MEL, BEA, and other zeolitic structures makes possible their utilization as catalysts in liquid phase oxidation processes.

2.2.1 Isomorphous Metal Substitution

Two main routes exist for the introduction of heteroatoms into zeolites. The first one encompasses simple procedures, such as cation exchange, encapsulation of metal complexes within cavities, metal dispersion. The second route, of interest to this review, consists in the isomorphous substitution for Si (or Al), leading to metal-substituted zeolites with novel physical and chemical properties. Such a metal insertion in the lattice has been reported for a wide range of atoms, such as Ti, V, Sn, Fe, Cr, Co, Zn, Be, Ge, B, and Zr, but not unambiguously demonstrated in all the cases. Heteroatoms, actually, should possess tetrahedral (T) coordination and maintain almost unaltered the main zeolitic structure. The R_T/R_O ratio, defined as the ratio of the ionic radium of heteroatom in its corresponding oxidation state over that of O^{2-} anion, was taken as determining criterion (so called Pauling criterion) and isomorphous substitution reputed possible when R_T/R_O ratio was comprised between 0.225 and 0.414 [13]. Nevertheless, this criterion is not generally valid and should be considered with certain flexibility. In fact, isomorphous substitution has been established also for atoms that do not fall in the above range, as indeed for Ti, despite its R_T/R_O ratio of *ca.* 0.47.

In general, the introduction in the zeolitic network of T heteroatoms with different atomic sizes than Si (or Al) modifies lattice parameters. For larger-sized ones, the T−O bond distance exceeds that of the Si−O bond, thus producing an expansion of the unit-cell parameters, as in the case of the substitution of tetrahedral Ti^{4+} ($r_{Ti4+} = 42$ pm) for Si^{4+} ($r_{Si4+} = 26$ pm) (*vide infra*) [2]. Heteroatoms with smaller atomic sizes lead to a contraction or decrease of the unit-cell volume due to the shorter T−O bond, as observed for B-containing zeolites. However, the presence of a T element with a different T−O bond length does not necessarily imply a clear variation of unit-cell parameters because these also depend on the relative orientation of tetrahedra and the Si–O−T angles that, in general, vary with substitution.

The synthesis of metal-containing zeolites is generally carried out hydrothermally (direct synthesis), following a quite similar procedure to that of related aluminosilicates, however, modified by the introduction of a heteroatom source, in appropriate concentration to avoid its segregation outside the zeolite structure. In this sense, the number of heteroatoms incorporated in the framework will strictly depend on the solubility and specific chemical properties of its precursors in the synthesis mixture.

Metal zeolites are prepared also by secondary synthesis, usually performed by the reaction of preformed zeolites, generally dealuminated, with metal halides, such as BCl_3 and $TiCl_4$ [14].

2.2.2 Synthesis of Titanium Silicalite-1 (TS-1)

The most important case of isomorphous substitution is that of Si atoms replaced by Ti, owing to the catalytic versatility of Ti-containing zeolites. Titanium Silicalite-1 (TS-1), synthesized by Taramasso et al. at the end of the 1970s, was the first Ti zeolite [1]. Its catalytic novelty and success opened the way to other Ti-containing zeolites as well as mesoporous materials. Comprehensive reviews on their synthesis, characterization, and catalytic activity can be found in the literature [6, 7, 15–17].

TS-1 (MFI structure) possesses a tridirectional (3D) pore system with straight channels (0.53×0.56 nm) along *[010]* intersecting slightly more elliptical sinusoidal channels (0.51×0.55 nm) along *[100]*, formed by rings of 10 SiO_4 and TiO_4 tetrahedra (10MR) [18]. Since Ti has the same oxidation state as Si, no framework charge is created by the substitution and, thus, no extraframework cations are required in the pores.

The synthesis of TS-1 is commonly performed hydrothermally by two methods differing for the preparation of crystallization gel [1]. In the most used "mixed alkoxide method", the gel is obtained by the controlled hydrolysis of tetraethyl orthotitanate (TEOT), $Ti(OC_2H_5)_4$, and tetraethyl orthosilicate (TEOS), $Si(OC_2H_5)_4$, in the presence of tetrapropylammonium hydroxide (TPAOH) [19]. It is crucial to prevent segregation of Ti phases by the correct procedure and control of the conditions. As indicated in the original patent, the absence of alkali-metal ions in the synthesis mixture is critical for the incorporation of Ti in the lattice. Their presence as impurities in commercial samples of TPAOH was not recognized in several studies, particularly in early ones, with the result that TS-1 could be not phase pure, also containing TiO_2 particles and amorphous Ti silicates [15]. Sometimes, however, alkali metals and other impurities can be present as a consequence of the deliberate use of cheaper sources of Si and tetrapropylammonium hydroxide, in an attempt to decrease the costs of production (*vide infra*). Their removal, but not that of segregated TiO_2 phases, is possible by exchange with acid or NH_4^+ solutions, followed by calcination.

The second method of preparation entails peroxytitanates, which are stable species in strongly basic solutions [1]. In this case, tetraethyl orthotitanate is hydrolyzed by slow addition of water to yield a gel that, after consecutive addition of 30 wt% H_2O_2 and aqueous TPAOH, generates a tetrapropylammonium peroxytitanate. The latter as a titanium source is used in admixture with Ludox colloidal SiO_2 to prepare TS-1 hydrothermally. The maximum amount of Ti that can be accommodated in the framework by both routes, expressed as the atomic ratio $Ti/(Ti + Si)$, is believed to be limited to *ca.* 0.025 [20], while that in excess to this value segregates at extraframework positions [15].

Continuous efforts have been performed in past years for finding ways to increase the content of lattice Ti beyond the 0.025 limit. A key issue appears to be the harmonization of the rates of (i) hydrolysis of both Ti and Si alkoxides, (ii) polymerization of Ti^{4+} and/or Si^{4+} species, (iii) nucleation, and (iv) crystal growth, to prevent the growth of TiO_2 and other extraframework species. A first example of

Ti-reach TS-1 was that of Thangaraj and Sivasanker claiming the incorporation of 8 Ti atoms per unit cell (Ti/(Ti + Si) *ca*. 0.1), by the use of tetra-*n*-butyl orthotitanate (TBOT), $Ti(OC_4H_9)_4$, dissolved in 2-propanol before its addition to the aqueous solution of hydrolyzed TEOS [21]. Reportedly, the precipitation of TiO_2 was prevented by the slower hydrolysis rate of TBOT than TEOT. Nevertheless, this result could not be reproduced by others [22]. A method for the synthesis of a Ti-reach silicalite-1 (YNU) was also claimed by Tatsumi and coworkers by using $(NH_4)_2CO_3$ as a crystallization-mediating agent [23]. The so-prepared catalyst had a Si/Ti ratio of 34, apparently without the formation of extraframework Ti species, a lower content of defects sites and higher hydrophobicity. Other ammonium salts, such as $(NH_4)_2SO_4$ and $(NH_4)_2PO_4$, reportedly favored the inclusion of Ti in the framework [24]. Sulfate salts, however, could have affected positively the catalyst by a different mechanism, namely, the inactivation of extraframework Ti−O−Ti species that may contaminate TS-1 [25].

The synthesis of TS-1 by more economical and faster routes is the subject of growing research, justified by its relevance for industrial applications. As the preparation of alkali-free TPAOH solutions is quite expensive, alternative syntheses of TS-1 envisage lower amounts of TPAOH and even its replacement by other organic templates or template systems. The first option comprises the addition in the synthesis gel of nonionic surfactants [26, 27]. The additive compensates for the lower concentration of TPAOH, maintaining fast the crystallization rate and low the crystal size, while preventing the deposition of TiO_2. TPAOH was also partially replaced by tetrahethylammonium hydroxide (TEAOH) or NH_4OH with, however, the same need as before of a pure base and the obtention of a larger-sized TS-1 [28]. The second option was initially pursued by the complete substitution of TPAOH with mixtures of tetrabutylammonium hydroxide (TBAOH) and TEAOH [29]. More recent works envisage the use of TPABr, as less expensive and usually alkali-free template. Müller and coworkers first reported the synthesis of TS-1 by its use, at the cost, however, of a high consumption of ammonia needed for the alkalinity of the medium [30]. Afterwards, a range of template systems combining TPABr with organic amines (i.e. methylamine, *n*-butylamine, diethylamine, ethylenediamine, hexanediamine and triethanolamine) or with TBAOH and TEAOH were investigated [31–33]. While TPABr and TBAOH act as templates, the role of organic amines is mostly that of basicity regulators [29, 33]. A comparison of the templating effectiveness showed the order, $TPA^+ > TBA^+ > TEA^+ \gg$ organic amine. The addition of preformed seeds was claimed to assist the template efficiency of amines and even to render usable NaOH for the alkalinity of the medium [34, 35]. As general rule, alternative template systems produce much larger TS-1 crystals (>1 μm) than TPAOH, to detriment of catalytic performances. Normally, TEOT and TBOT are the Ti sources, though $TiCl_3$ [36] and other Ti compounds, including TiO_2, have also been explored.

Combining the use of TPABr to that of amorphous SiO_2 as silicon source allows a further reduction of synthesis costs with, however, the drawback of crystal sizes in the range 2–10 μm and the segregation of titania phases [37]. Other routes envisage syntheses by wetness impregnation of a SiO_2-TiO_2 cogel

and Ti insertion into a preformed MFI framework by gas phase reaction with $TiCl_4$ [38, 39].

2.2.2.1 Mesoporous TS-1 The generation of mesopores, either by modifications of hydrothermal synthesis or by post-treatments, is increasingly studied to solve diffusion limitations of large crystals. The first approach comprises the addition in the synthesis medium of either organic particles that, occluded in the crystals, will leave voids on calcination or organics that inhibit their regular growth. Schmidt et al. first used carbon black (average diameter 18 nm), functioning as hard template to obtain mesoporous TS-1 [40]. They estimated a single crystal could incorporate an interconnected porous network built from more than 1500 primary carbon particles. Various kinds of hard templates and methods were then employed for both TS-1 and TS-2 [41–43]. The silanization of zeolitic seeds, either *ex situ* or *in situ*, produced nanocrystalline TS-1 with hierarchical porosity [44, 45]. With the use of amphiphilic organosilanes, however, the expected diffusional advantages provided by mesoporosity were offset by the highly hydrophilic character of silanol-rich surface [45]. Triethanolamine and macromolecules, like soluble starch and carboxymethyl cellulose, were also reported to create mesopores [46, 47]. Recently, the use of diquaternary $[R(CH_3)_2N^+\text{-}C_6H_{12}\text{-}N^+(CH_3)_2C_6H_{13}](OH^-)_2$ ammonium templates ($R = C_{16}H_{33,}\ C_{22}H_{45}$), as structure-directing agents, has allowed the synthesis of TS-1 in the form of nanosheets with very short diffusion paths (down to 2 nm along the *b*-axis), organized in disordered assemblies with high intersheet mesopore volume [48, 49]. Several composite materials, consisting of TS-1 domains dispersed within mesoporous structures, have also been prepared (Chapter 4).

Postsynthesis methods consist in the selective leaching of zeolitic crystallites with basic solutions, during which the framework undergoes a partial dissolution, with the creation in the crystals of new voids and pores in the mesoporous range [50–52]. The kind of porosity obtained in TS-1, as well as the effectiveness of the method, varies with the nature of the base. Specific to the use of TPAOH, first applied by Tuel and coworkers to obtain hollow crystals, is, besides dissolution, a parallel reconstruction of the framework [51]. A sequential treatment with NaOH and TPAOH was reported to create mesoporosity with improved properties for hydroxylation [53].

2.2.3 Characterization of Titanium Silicalite-1 (TS-1)

The incorporation of Ti in TS-1 and other Ti zeolites is demonstrated by a multiplicity of methods and spectroscopic techniques, with the most effective ones summarized in the following.

2.2.3.1 X-ray Diffraction (XRD) X-ray diffraction is a powerful technique to determine the identity, degree of purity, and crystallinity of zeolites because each crystalline phase presents a characteristic X-ray diffraction pattern. For TS-1 materials, XRD shows the presence of MFI-type structure by a single diffraction peak at 2θ of *ca.* 24.45°, instead of the common multiple-peak pattern observed for parent

silicalite-1 in this region of the spectrum, indicating a change from monoclinic (S-1) to orthorhombic symmetry (TS-1) [1, 2].

The formal substitution of Si^{4+} by larger-sized Ti^{4+} results in an expansion of the unit-cell volume, in a linear trend with the content of Ti up to a limiting value of *ca*. 0.025 for Ti/(Ti + Si) atomic ratio. Such a structural modification is generally accepted proof of Ti incorporation in the framework and, according to Perego, Millini and coworkers, the determination of unit-cell parameters is the most reliable method, and probably the only one, to determine the true content of lattice Ti [2, 20]. Actually, the linearity of calibration curves, within a set of identically prepared samples differing only in the Si/Ti ratios of their frameworks, is often observed and the calculation of Ti contents from unit-cell volumes of TS-1 is thus possible, but the method is not exempt from some controversy. Höft et al. noted that the unit-cell volumes of TS-1 crystallites with identical Si/Ti ratios could differ depending on the synthesis route [54]. In fact, lattice parameters can also vary for such factors, as the presence of organic or inorganic species in the channels, the degree of hydration, the presence of defect sites, etc. In this sense, lattice-parameter changes observed by XRD measurements are an effective tool that, however, cannot be used as unique proof of Ti incorporation in MFI-structure.

The application of neutron powder diffraction to TS-1 has recently provided evidence of the nonuniform distribution of Ti over the 12 independent crystallographic T sites of the unit cell [55–57]. The low amount of Ti and the presence of silicon vacancies, however, make their identification quite controversial [57, 58].

2.2.3.2 FT-IR and Raman Spectroscopy FT-IR spectroscopy allows information about the structure, the surface and acid-basic sites of zeolites to be obtained. The medium region of IR spectrum (4000–250 cm^{-1}) is conveniently divided into three zones, providing different and complementary information: 1300–250 cm^{-1}, 2500–1300 cm^{-1}, 4000–2500 cm^{-1}.

The skeletal region of the spectrum, 1300–250 cm^{-1}, informs on the structural and compositional changes of the zeolitic framework, by: (i) internal vibrations of tetrahedral TO_4 sites (insensitive to structure variations) and (ii) external vibrations between tetrahedra (sensitive to framework topology) [59]. In general, TO_4 vibrations are not specific to Si, Al, and other T atoms, but some changes in number, position, and intensity of bands can occur as a function of the heteroatom present in the framework. In the case of TS-1, a typical IR band, normally taken as fingerprint of framework Ti, usually appears at near 960 cm^{-1} [2]. Its assignment, however, is not free of controversy, having been attributed to the stretching vibration of: (i) Si−O bonds of Si−O−Ti bridges, (ii) Si−O−Si bonds next to Ti, (iii) Ti=O titanyl groups, (iv) local modes of TiO_4 tetrahedra, (v) Si−O bonds of internal Si−OH nests, and (vi) Si−O bonds of $Si-O^-$ defect groups associated with TPA^+ cations [60–65]. This signal also appears in zeolites substituted with others heteroatoms, e.g., V, Sn, Cr, as well as in materials with a high density of structural defects. It is generally believed that the presence of the 960 cm^{-1} band is necessary but not sufficient to confirm Ti incorporation, on consideration that, while Ti=O groups are excluded by UV-vis and template molecules are not present in calcined TS-1, a

range of other attributions is still possible. Other and more complex signals in the skeletal region comprise a relatively strong band centered at 500–550 cm^{-1}, not shown by amorphous silica and considered as a crystallinity band [63]. It could be overlapped by a broader spectrum developing from TiO_2 impurities [66].

The absorptions in the range 2500–1300 cm^{-1} correspond to deformation vibrations of adsorbed organic molecules, e.g., pyridine and ammonia used to obtain information on the nature, number and strength of acid sites, while those in the region 4000–2500 cm^{-1} correspond to O−H bond stretching vibrations of different Si−OH groups present in defective sites mostly localized within the pores [67]. Both IR regions are also informative on other issues than Ti incorporation. The bands at 3395, 3295 and 1608 cm^{-1}, detected on ammonia physisorption, are specific to TS-1 samples, while those at near 3400 and at 1635 cm^{-1} are observed with both TS-1 and S-1. The former modes are typically shown, shifted to lower frequencies, by ammonia coordinated on Lewis-acid sites, e.g., on TiO_2, and were ascribed to the presence of Ti sites [66]. Ti−OH groups cannot be evidenced, due to the intrinsic weakness of their IR bands and poor Ti content.

Raman signals arise from changes in the polarizability of molecules due to Raman frequency irradiation. Normally, symmetric vibrations, active in Raman, are inactive in IR and *vice versa* for asymmetric ones, making Raman and IR spectroscopies complementary techniques. Raman spectroscopy, however, being much more sensitive to both anatase and rutile phases of crystalline TiO_2 even at very low concentrations, is a powerful tool for the detection of extraframework Ti in TS-1 samples [68]. Since anatase (four main peaks at 144 cm^{-1}, 638 cm^{-1}, 396 cm^{-1}, and 517 cm^{-1}, in approximate order of decreasing intensity) begins to transform into rutile only above 700 °C, rutile signals are commonly not observed in TS-1 samples. Zecchina et al. established that the minimum TiO_2 content detectable in TS-1 by Raman spectroscopy is approximately 0.5 wt%, which, however, is at least one order of magnitude larger than for UV-vis spectroscopic measures [68]. The intensity of the Raman band near 960 cm^{-1}, normalized to that of 800 cm^{-1} peak, could be used for a qualitative estimate of Ti incorporation [69].

The development by Li et al. of the resonance Raman spectroscopy allowed the diverse Ti species that may be present in TS-1 samples to be distinguished unambiguously [61]. This is based on the selective enhancement of Raman peaks associated with a specific Ti species, when this is excited by a laser source of energy close to the $O^{2-} \rightarrow Ti^{4+}$ charge-transfer transition, while the rest of the Raman spectrum remains unchanged. Irradiation of TS-1 at 244 nm frequency, lying on the low-energy tail of 210 nm UV absorption, enhanced the Raman peaks of lattice Ti sites (T_d symmetry) at 490, 530, and 1125 cm^{-1}. Raman spectra of impure TS-1, excited at 325 and 488 nm, showed the enhancement of typical bands of TiO_2 (anatase) at 144, 390, and 637 cm^{-1}. The use of 244 and 442 nm excitation frequencies, close to the 385 nm absorption of TS-1/H_2O_2, allowed the identification a Ti peroxo species with Raman absorption at 618 cm^{-1} (875 cm^{-1} for physisorbed H_2O_2) [70].

2.2.3.3 Diffuse Reflectance UV-Visible Spectroscopy Ti-containing zeolites, such as TS-1, present bands of charge-transfer transition from oxygen to

Ti ($O^{2-} \rightarrow Ti^{4+}$) assigned to Ti in different surrounds: isolated tetrahedral Ti (*ca.* 205 nm), isolated pentacoordinated Ti (*ca.* 212 nm), isolated octahedral Ti (*ca.* 225 nm), and oligomeric octahedral Ti−O−Ti (*ca.* 260 nm) [25, 60, 67]. Ideally, the DR UV-vis spectrum of a well-prepared TS-1 should present a strong band centered at 205–215 nm, characteristic of tetrahedrally coordinated Ti species. Shoulders, sometimes visible at higher wavelengths, reveal the presence of penta- and octa-coordinated Ti species. The broadening of the absorption and the shift of the maximum to lower energies reflect the expansion of Ti coordination above four, as on adsorption of polar molecules. A broad band at *ca.* 385 nm that appears on addition of H_2O_2 to TS-1 was assigned to a Ti peroxide [71, 72].

More than Raman spectroscopy, DR UV-vis is sensitive to extraframework Ti, and a band in the range 300–350 nm, attributed to $O^{2-} \rightarrow Ti^{4+}$ charge-transfer transition, indicates the presence of anatase TiO_2 in ill-prepared TS-1 samples (lower limit of detection, *ca.* 0.03 wt%) [68].

2.2.3.4 X-ray Absorption Spectroscopy (XANES-EXAFS) This technique is based on the sharp increase of X-ray absorption coefficient of a material when the photon energy of the incident radiation surpasses the bonding energy of internal electrons of the absorbing atom. Edges K, L, M, ... corresponding to the energy levels ($n = 1, 2, 3, \ldots$) of electrons abandoning the atom are distinguished. For isolated atoms, the absorption coefficient decreases monotonically beyond the absorption edge, but if it is part of molecules or solids the absorption spectrum is more complex, presenting a set of peaks and modulations, depending on the atom environment. For Ti zeolites, X-ray absorption spectra are commonly measured at the K-edge of Ti (4965 eV), using synchrotron-generated radiation. The spectra normally divide into three well-defined regions: (i) a pre-edge absorption region (from 50 to 4965 eV for Ti), (ii) a XANES region (from the K-edge up to *ca.* 50 eV beyond the absorption jump), (iii) a EXAFS region (*ca.* 1000–1500 eV beyond the K-edge, i.e. from *ca.* 5020 to 6000–6500 eV for Ti). The XANES region provides qualitative information about the electronic structure and coordination geometry of Ti, while the EXAFS region provides structural information on nearest neighbors of Ti atom, e.g., their number and bond distances.

Early XANES and EXAFS studies published in the 1990s definitely confirmed Ti siting in silicalite-1 framework, in a T_d-like configuration, and the reversible structural changes it undergoes on adsorption of polar molecules [73–75]. A narrow and intense pre-edge peak at 4967 eV, due to the $1s \rightarrow 3d$ electronic transition typical of tetrahedrally coordinated Ti, characterize XANES spectra of carefully dehydrated TS-1 samples. Rehydration or adsorption of other polar molecules, leading to an increase of Ti coordination number to 5 and 6, makes the electronic transition symmetry-forbidden and consequently pre-edge peak much less intense. Structural information extracted from EXAFS data shows also that four oxygen ligands surround Ti, with a Ti−O bond length of *ca.* 1.80 Å, in excellent agreement with XRD data, while 1.61 Å is the length of Si−O [58]. Such a difference probably makes the local structure around Ti seriously distorted and explains some of the difficulties encountered for Ti inclusion in the framework during TS-1 synthesis.

EXAFS also shows that two kinds of Ti sites are present in calcined and fully dehydrated TS-1, namely, closed-shell $Ti(OSi)_4$ sites and defective $Ti(OSi)_3OH$ sites, both in a T_d-like environment [58, 76].

2.2.3.5 Other Spectroscopic Techniques Other spectroscopic techniques and methods used for the characterization of TS-1, not specific, however, for the determination of Ti siting, are the following. X-ray photoelectron spectroscopy (XPS) provides information about the state and composition (and even Ti coordination) of the outer layer of zeolitic crystals, penetrating only to a depth of 4–5 nm. Nuclear magnetic resonance spectroscopy (^{29}Si MAS NMR) informs on T−O−T angle variation after isomorphous substitution, as well as on the presence of hydrolyzed Ti−O−Si bonds and connectivity defects. Nitrogen adsorption isotherms allow surface area, pore size distribution, micropore volume, the presence of mesopores, etc. to be estimated. Scanning electron microscopy (SEM) reveals crystal morphologies and sizes, while transmission electron microscopy (TEM) is useful for crystal structures and the detection of mesopores. TEM and SEM, also detect the presence of other phases, such as occluded amorphous matter undetectable by XRD.

The final and important proof of Ti isomorphous substitution in TS-1 samples consists in the catalytic performances with H_2O_2, particularly in phenol oxidation, most sensitive to Ti siting [4, 77].

2.2.4 Ti-Beta, Synthesis and Characterization

The relatively small pore diameter of TS-1 (*ca*. 0.55 nm), little suited to voluminous reagents, was the main driving force to develop larger pore Ti zeolites. The first of this kind to be discovered was Ti,Al-Beta (BEA structure), characterized by a tridirectional system of channels with two different pore diameters, 0.76×0.63 and 0.55×0.55 nm, respectively [78]. It is formed by the intergrowing of at least two polymorphs (A and B), and, possibly, of third polymorph (C), while the existence of a fourth one has not been ruled out completely.

2.2.4.1 Synthesis Ti,Al-Beta is commonly synthesized in alkaline medium with tetraethylammonium hydroxide (TEAOH) as the structure-directing agent (SDA), using titanium alkoxides, aluminum nitrate and amorphous silica as Ti, Al and Si sources, respectively. As for TS-1, it is crucial to prevent TiO_2 precipitation during the preparation of the gel, since its redissolution is practically impossible. Preferably, alkali metals should be avoided, though a certain tolerance exists up to a (Na + K)/Ti molar ratio of *ca*. 0.03 [79]. Competition for framework incorporation between Ti and Al is generally observed.

The presence of Al, besides that of internal and external Si–OH groups resulting from the intergrowth of different polymorphs, confers to Ti,Al-Beta a rather hydrophilic character and a significantly different catalytic behavior with respect to TS-1. There was, therefore, a strong incentive for the preparation of Ti-Beta with low or, even better, no Al content by new synthetic routes, namely, the seeding methods, the use of seeds and special SDA, the fluoride method, and dry gel conversion [80–84].

Deboronated B-Beta and dealuminated Al-Beta seeds allowed the preparation of Al-free Ti-Beta, as well as purely siliceous Beta [80, 81]. The synthesis of Al-free Ti-Beta through spontaneous nucleation (without seeding) was obtained by employing 4,4′-trimethylene-bis(N-benzyl-N-methyl piperidinium)$^{2+}$ cation as SDA [85]. Ti-Beta obtained by these methods was much more effective for oxidations with H_2O_2.

The synthesis of Ti-Beta with TEAOH in fluoride medium, first reported by Corma's group, produces a more hydrophobic material, relatively free of framework Al and silanol defects, but with crystallites significantly larger than those of Ti-Beta(OH^-) [86]. Al-free Ti-Beta(F^-), used by Blasco et al. for the epoxidation of bulky alkenes, showed conversions and turnover numbers comparable to those of Ti-Beta(OH^-) with, however, higher epoxide selectivities [83]. Residual fluorine, forming with the lattice a five-coordinate $(SiO_4)SiF^-$ species, is believed to be harmful to catalytic activity. Actually, its reduction by the treatment with a quaternary ammonium basic solution, followed by calcination, led to an enhancement of epoxidation activity [16]. Subsequently, the fluoride method was extended to Ti-Beta preparations with other SDAs than TEAOH, such as organic cations and amines, and to the synthesis of other zeolites [87].

Ti can be introduced into the framework of Beta zeolite by postsynthesis treatments, e.g., with concentrated solutions of perchloric and nitric acid, performed in the presence of dissolved Ti compounds [88]. Both Al extraction from the framework and Ti incorporation occur simultaneously, yielding an almost Al-free Ti-Beta.

2.2.4.2 Characterization Ti-Beta does not differ significantly from TS-1 for the characterization and use of a combination of physicochemical techniques and catalytic tests to ascertain Ti incorporation [83, 89]. Most applied is X-ray powder diffraction for the identification and the determination of crystallinity and phase purity of the material. Although the incorporation of Ti in the framework is, in principle, expected to cause a linear increase of unit-cell parameters, the intergrowth of different polymorphs seriously limits the effectiveness of the method for Ti-Beta. Nevertheless, a linear increase of the unit-cell volume of polymorph A with Ti content was observed for Al-free Ti-Beta(F^-) samples up to a Ti/(Ti + Si) mole fraction of 0.037 (2.3 Ti/uc) [83]. Beyond this value, no further increase of the unit cell occurred and anatase started to appear as revealed by DR UV and Raman spectra. Normally, Ti-Beta samples show a sharp absorption in the 205–220 nm ultraviolet region, for Ti/(Ti + Si) molar fractions below 0.037, beyond which, the 330 nm absorption of anatase is detected in Ti-Beta(F^-) materials, while it is not in Ti-Beta (OH^-) samples even at high Ti contents.

Al-free Ti-Beta shows three clear absorption bands in the 950–980 cm^{-1} region of the infrared and Raman spectra, generally attributed to the presence of Ti in the framework. The Raman spectrum shows its usefulness for the detection of anatase (characterized by a strong absorption at *ca.* 144 cm^{-1}), normally negative when the Ti molar fraction is below the upper limit mentioned earlier.

The presence of tetrahedrally coordinated Ti, with a Ti−O bond length of *ca.* 1.80 Å, was demonstrated by XANES and EXAFS spectroscopic measurements on

calcined and dehydrated samples [83, 89]. Upon hydration, changes in the XANES and EXAFS spectra occurred, consistently with an increase of Ti coordination that, depending on the composition and synthesis route of the material, ranged from a 5-fold coordination in Al-free Ti-Beta(F^-) to a highly distorted 6-fold coordination in Ti,Al-Beta(OH^-).

Other characterization techniques reveal the differences of connectivity defects and adsorption properties in Ti-Beta samples obtained by different routes. ^{29}Si MAS NMR, $^{1}H \rightarrow {}^{29}Si$ CP MAS NMR, and IR spectroscopies showed that no hydrolysis of Si−O−Ti bonds (i.e. absence of Si−OH and Ti−OH groups) occurs in Ti-Beta(F^-) zeolites upon contact with ambient humidity, while this is a major drawback of the Ti-Beta(OH^-) samples [83]. Adsorption microcalorimetry experiments showed the highly hydrophobic nature of purely siliceous Beta(F^-) zeolite, slightly decreased by Ti incorporation in the framework due to the relatively strong adsorption of one H_2O molecule per Ti site [83]. On the contrary, the Ti-Beta(OH^-) zeolites showed an enhanced hydrophilicity due to the presence of large amounts of connectivity defects.

2.2.5 Other Ti Zeolites

Several other Ti zeolites have been prepared during last two decades. Medium pore TS-2, with MEL-type structure and intersecting tridirectional straight channels (10MR, 0.53×0.54 nm) is most similar to TS-1 for structure and catalytic properties [90]. It was obtained by direct synthesis under hydrothermal conditions. Ti-FER, namely, Ti-ferrierite (FER structure), with intersecting 10MR (0.43×0.55 nm) and 8MR (0.34×0.48 nm) channels was similarly prepared [91]. Direct synthesis allowed the preparation also of Ti-ZSM-48 (not-intersecting unidirectional pores), Ti-STT (a bidirectional pore system composed of 9MR and 7MR channels) and Ti-CHA (a tridirectional pore structure) comprising an elongated cage with 8MR 0.38 nm windows [92–94].

Besides Ti-Beta, other catalytically relevant large pore zeolites are Ti-MWW and Ti-MOR. The synthesis of the former (MWW structure), also called Ti-MCM-22, had been a challenge until it was prepared for the first time from a synthesis gel composed of boric acid, a Ti source, fumed silica and a cyclic amine as SDA (hexamethyleneimine or piperidine) [95]. Ti incorporation in the MWW lattice was highly efficient and its tetrahedral coordination demonstrated by XRD and UV-vis analyses. However, boron was also incorporated in a Si to B ratio in the range 11–13. Direct synthesis of B-free Ti-MWW continues to be a challenge, whereas an indirect route, consisting in the acid leaching of B-MWW (Si to B ratio > 500), followed by treatment with $Ti(OBu)_4$ in the presence of an amine SDA, had some success [16].

The synthesis of Ti-MOR [96, 97], characterized by nonintersecting unidirectional pores (0.65×0.70 nm), Ti-FAU [88, 98], containing large supergages with pore windows of 0.75 nm, and Ti-MCM-68 (MSE topology) [99] was performed by postsynthesis incorporation of Ti in partially dealuminated parent Al-zeolites. Ti-MAZ, Ti-LTL, Ti-SSZ-42, and Ti-SSZ-33, almost unused in

catalysis, were prepared by a similar method. Direct synthesis could be applied for Ti-ZSM-12 (12MR, 0.55×0.59 nm) [100], Ti-ITQ-7 (tridirectional large pore system) [101, 102] and extra-large pore Ti-UTD-1 (14MR, 0.75×1.0 nm) [103]. It should be noticed that the structure-directing agent for latter one is bis(pentamethylcyclopentadienyl)cobalt(III) hydroxide and Co oxide impurities can remain dispersed on the catalyst after calcination, with negative consequences for the stability of hydrogen peroxide.

A third kind of Ti catalyst, characterized by much larger porous capacity, consists of delaminated zeolites. These are high surface area materials with reduced microporosity, which try to combine the stability of zeolites with the accessibility of mesoporous materials. Ti-ITQ-6 ($>600\,m^2/g$) was prepared by the delamination of Ti-FER layered precursor [104, 105]. Materials with expanded porosity, deriving from lamellar MWW precursors, are Del-Ti-MWW (full delamination), Ti-MCM-56 (partial delamination), Ti-MCM-36 (interlayer pillaring with silica), IEZ-Ti-MWW (interlayer silylation and calcination), Ti-YNU-1 (acid leaching) [106–110]. Ti-ITQ-2 was obtained by the reaction of dichlorotitanocene with the silanols of siliceous ITQ-2 material, followed by calcination [111, 112]. ITQ-2, obtained in turn from the delamination of parent MCM-22 (MWW), ideally contains up to a single layer of MWW sheets.

2.2.6 Other Metal Zeolites

The attractiveness of metal zeolites with novel catalytic properties prompted numerous studies on the isomorphous substitution of several other transition metals [15, 16]. V silicalites, VS-1 (MFI structure) and VS-2 (MEL structure), were the first to be prepared and applied to catalytic oxidations, followed by V-NCL-1, V-ZSM-48 and V-Beta [113–117]. In general, V incorporation is relatively low, as in VS-1 with maximum V content of *ca.* 1% [118]. Vanadium sites differ from Ti sites for the reversible oxidation that V^{IV} undergoes to V^{V}, during calcination, and for the bonds formed with the framework, through silanols of structural defects. None of the proposed sites, "framework satellite", represents a true isomorphous substitution [15].

Fe and Cr zeolites were prepared but scarcely used as liquid phase catalysts [119]. They share with V zeolites the variation of oxidation state during calcination and the tendency to leaching, particularly in protic solutions of hydrogen peroxide (Section 2.5). Worthy of mention is a gas phase process catalyzed by Fe-ZSM-5 for the hydroxylation of benzene [120].

Tin substitution was reported for various zeolitic structures, such as S-1, S-2, ZSM-12 and Beta [121–124]. As for Cr and V, Sn tends to localize in structural defects of the framework. Its coordination in Al-free Sn-Beta, synthesized by Corma's group in fluoride medium, was proven to be tetrahedral by ^{119}Sn MAS NMR spectroscopy [125–127]. The Lewis acidity of tin is responsible for the catalytic activity observed in the Baeyer–Villiger and other reactions.

TABLE 2.1 Summary of Structural and Spectroscopic Properties of Selected Metal Zeolites

Name	Structure type code [18]	Channel dimensions (nm) [18]	Pore system	UV-vis	IR, Raman
TS-1	MFI	0.53×0.56 *[010]* 0.51×0.55 *[100]*	Tridirectional, intersecting	205–215 nm [66]	$\approx 960\ cm^{-1}$ [68]
TS-2	MEL	0.53×0.54 *[100]*			
Ti-MOR	MOR	0.65×0.70 *[001]* 0.26×0.57 *[001]* [a]	Unidirectional	220 nm [97]	$963\ cm^{-1}$ [97]
Ti-MWW (Ti-MCM-22)	MWW	0.40×0.55 *[001]* 0.41×0.51 *[001]*	Two channel systems[b]	220 and 260 nm [16, 95]	$\approx 960\ cm^{-1}$ [95]
Ti-Beta	BEA	0.76×0.63 *[010]* 0.55×0.55 *[100]*	Tridirectional, intersecting	205–220 nm [66, 83]	$950–980\ cm^{-1}$ [83]
Sn-Beta	BEA	0.76×0.63 *[010]* 0.55×0.55 *[100]*	Tridirectional, intersecting	205 nm (weak)	$\approx 960\ cm^{-1}$ [124]
VS-1	MFI	0.53×0.56 *[010]* 0.51×0.55 *[100]*	Tridirectional, intersecting	230–280 nm [118]	$\approx 960\ cm^{-1}$ [114]
VS-2	MEL	0.53×0.54 *[100]*			

[a] Too small for catalysis.
[b] Supercages $0.7 \times 0.7 \times 1.8$ nm and, at the crystal exterior, pockets formed by half-supercages (0.7×0.7 nm).

Table 2.1 summarizes the relevant features of catalytically significant metal zeolites.

2.3 CATALYTIC PROPERTIES

2.3.1 Hydroxylation of Alkanes

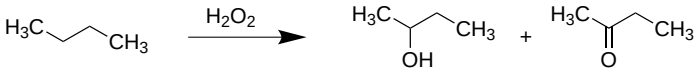
The cleavage of saturated C−H bonds under mild conditions is not a rare event. Not considering free radical systems, it occurs on metal surfaces and on metal complexes smoothly, even though in most cases consists in a reversible splitting, only detectable by isotopic labeling, and in the cyclometalation of coordinated ligands [128]. Functionalization, i.e. C−H activation followed by the formation of a C-heteroatom bond, is observed in a relatively few cases, rarely occurring catalytically. Actually, the search of such a catalyst active and selective under mild conditions could be compared to that of the Holy Grail [129].

A range of systems, including electrophilic and nucleophilic late transition metal compounds, grafted organometallic species, metal complexes mimicking P450 and methane mono-oxygenase (MMO) type of enzymes, allowed to gather valuable information on the factors that promote C−H splitting [128, 130]. It became

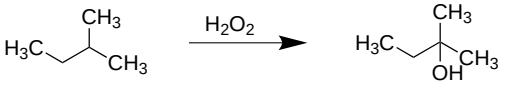
apparent that the large bond strength was not the only impediment and probably not the principal one. For instance, the effectiveness of high valent metal-oxo species is strictly related to the microenvironment in which they operate. The catalytic performances of metal sites in enzymes are unrivalled *in vivo* and often good even *in vitro* conditions, whereas are relatively poor or nil in their organometallic analogs, merely able to mimic active species but not their surrounds. Actually, the high activity of MMO enzymes is never replicated by biomimetic systems.

Titanium zeolites, with their inorganic and relatively simple structure, are most distant from enzymes and their sophisticated architecture. Active species too are different, since it is iron and not titanium that is commonly met in biological systems. However, TS-1 and other Ti zeolites share with them a major feature, namely, a relatively hydrophobic environment, which makes the oxidant species able to functionalize C−H bonds at near room temperature [6].

2.3.1.1 Titanium Silicalite-1 and Titanium Silicalite-2 The oxidation of paraffins is easily performed by TS-1 and dilute hydrogen peroxide, under mild conditions (Eqs. 2.1–2.2) [131–133]. TS-2 and Al-TS-1 behave alike, not unexpectedly if the similarities of pores and active sites are recalled [133, 134]. Catalytic activity and lattice Ti are linearly related, as already shown by early studies on TS-1 [132].



(2.1)



(2.2)

Linear alkanes yield a mixture of secondary alcohol isomers and, by consecutive oxidation, corresponding ketones. Regio and product selectivity are largely dependent on reaction conditions, particularly on the solvent. It is remarkable, however, that alcohol products could be subject to the competition of parent alkane, showing comparable or even slower kinetics (Figure 2.1). Branched alkanes are preferentially hydroxylated at tertiary C−H bonds and negligibly or nil at the secondary carbons that may be present [133]. Methyl groups, including those at benzylic positions, are completely inert. Major side reactions are the dismutation of hydrogen peroxide and, to a lesser extent, the oxidation of the solvent. Their incidence grows with the bulkiness of the paraffin, becoming predominant for molecular sizes comparable to that of the pores.

An organic solvent may be used to increase the mutual miscibility of the aqueous and the organic phases, such as methanol, generally preferable for TS-1 and TS-2, *t*-butanol, acetonitrile, acetone, 2-butanone and N,N-dimethylformamide [133–135]. Depending on the mass ratios of the three liquid components, i.e. solvent, hydrocarbon and aqueous oxidant, the reaction medium can consist of one single phase or of two distinct ones. The first option implies necessarily low concentrations of

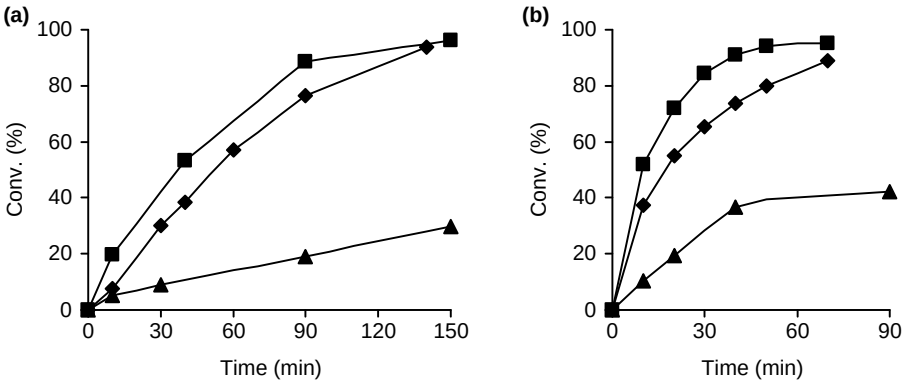


FIGURE 2.1 Oxidation of hexane (◆), 2-hexanol (■) and 3-hexanol (▲), in methanol (**a**) and *t*-butanol (**b**). Substrate 0.6 mol L^{-1}, H_2O_2 0.5 mol L^{-1}, TS-1 15.7 g L^{-1}, T 55 °C.

both the alkane and hydrogen peroxide, typically in the range 0.6–1.3 and 0.2–0.6 mol L^{-1}, respectively, with the alkane normally used in excess over the oxidant [133]. Since the early studies, it was apparent that the choice of the solvent influenced the catalytic performances. Initial conversions in the oxidation of *n*-hexane on TS-1 decreased in the order, *t*-butanol > *t*-butanol/water > methanol ≈ acetonitrile (≈water). Hydrogen peroxide efficiency showed a similar trend (max. *ca.* 90%).

In the second option, the solvent only has the function of raising the mutual solubility of hydrogen peroxide and the alkane, particularly in the mainly aqueous phase, it being this one that wets the catalyst particles and is relevant for adsorption equilibria, with the organic phase just functioning as a reservoir of the alkane. The upper limit for the concentration of hydrogen peroxide in the mainly aqueous phase can be much higher now, as in a series of papers on the oxyfunctionalization of *n*-hexane on TS-1 and TS-2, in which it varied in the range 9–2 mol L^{-1}, depending on the amount of solvent added to 30 wt% H_2O_2 [136–140]. Conversely, the concentration of *n*-hexane, albeit improved by the addition of the solvent, never surpassed the limit of *ca.* 0.1 mol L^{-1}. Under such conditions, favorable to the adsorption of the oxidant, the hydrogen peroxide efficiency was much lower (max. 70%). Contrasting results were reported for the effect of the solvent on kinetics. In the early paper, the rate decreased in the order, methanol > acetone > acetonitrile > water, not dissimilarly to oxidations performed in a single liquid phase. In subsequent studies, based on a different approach for kinetic modeling of the multiphase system, rate constants were reportedly independent of the solvent added, whose only function was therefore to increase the solubility of *n*-hexane in the aqueous phase.

Regioselectivity varies with the solvent. In methanol, *t*-butanol and acetone, C−H hydroxylation decreased on moving from the outer methylene group to inner ones in the alkyl chain, i.e. with the increase of steric restrictions at the site of attack

[133, 134]. The 2- to 3-product ratio was typically close to two under most reaction conditions. On the contrary, acetonitrile, 2-butanone and N,N-dimethylformamide promoted hydroxylation at inner methylene groups. In water and acetone it was reported to occur almost randomly [132].

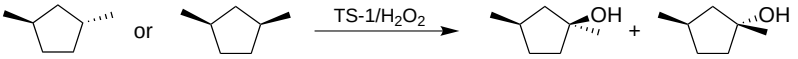
The rather odd reactivity order of linear alkanes, measured at 50% H_2O_2 conversion, hexane > heptane ≈ octane > butane > pentane > propane is, in all likelihood, the combined result of different effects of electronic, steric and adsorptive nature [133]. Actually, the alkane length influences kinetics positively through adsorption and inductive effects, while negatively through diffusivity and steric hindrance [6, 141, 142]. Considering the competition between hydroxylation and side reactions, it is not surprising that the yields based on hydrogen peroxide increased up to a maximum for C_5–C_7 *n*-alkanes to then decrease for higher alkanes.

The oxidation of cyclohexane to cyclohexanol and cyclohexanone is exceedingly slow at near room temperature and, consequently, little selective on the oxidant. Owing to its industrial potential, the reaction was investigated in a wide range of experimental conditions [143–145]. The best turnover numbers, yet not much higher than 100, were observed in acetone solvent between 100–150 °C, with hydrogen peroxide efficiency never surpassing 40% [143]. As expected, mesoporous TS-1 obtained by TPAOH post-treatment was more active and H_2O_2 selective (*ca.* 60% yield at 80 °C) [145].

Mechanistic Investigations C−H hydroxylation, like other oxidations, is most sensitive to acid, base and alkali salt additives, with the former behaving as promoters and the latter two as inhibitors [85, 133, 146]. The degree of inhibition increases with their amount and basic strength, up to complete deactivation. For instance, lithium acetate, loaded in a comparable amount to Ti sites, poisoned TS-1 completely. Its neutralization by *ca.* one equivalent trifluoroacetic acid fully restored initial activity. With a similar amount of lithium chloride most activity was retained, while one-tenth equivalent acid was sufficient to obtain full recovery.

The presence of electron-withdrawing groups in the alkyl chain, as in 2- and 3-alkanols, 1-chlorohexane and methyl heptanoate, strongly decreases hydroxylation while orienting the attack on remote methylene groups [133]. Accordingly, dihydroxylation was not observed on relatively short alkanes, while was negligible on C_8–C_{12} *n*-paraffins, even at high conversion. On arylalkanes, the oxidation concerned both the aromatic ring and the side chain, with a preference for the latter one. Consistently, the competitive hydroxylation of benzene and *n*-hexane or cyclohexane mainly occurred on the alkane. The apparent activation energy for *n*-hexane was 14.0 kcal mol^{-1} (30–50 °C).

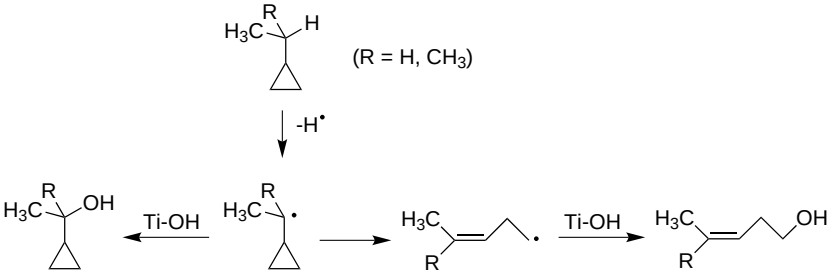
The predilection for aliphatic C−Hs, the greater reactivity at tertiary than at secondary carbons and the effects of acids, bases and electron-attracting substituents suggest a radical mechanism of electrophilic nature, in which the mildly acidic Ti−OOH hydroperoxide is the precursor of active species. To test the consistency of the homolytic hypothesis, *cis*- and *trans*-1,3-dimethylcyclopentane and ethyl- and 2-propylcyclopropane, were used as substrate probes [135]. In the



SCHEME 2.1 Hydroxylation of *cis*- and *trans*-1,3-dimethylcyclopentane on TS-1.

hydroxylation of the first two, a concerted heterolytic mechanism by Ti−OOH species would predict either the retention or the inversion of configuration at the chiral center. Conversely, the stereochemistry of a radical mechanism would be determined by the competition between the epimerization of the transient tertiary carbon radical and C−O formation (Scheme 2.1). On the second type of molecules (radical clocks), hydrogen-atom abstraction leads to a cyclopropylcarbinyl radical that can either rearrange to ultimately form the ring-opened unsaturated olefin or rebound to yield corresponding alcohol product directly, with intact cyclopropyl group (Scheme 2.2). What discriminates between the two routes is the lifetime of intermediate radical. With TS-1, nearly equal amounts of *trans*- and *cis*-1,3-dimethylcyclopentanol were obtained from each cyclopentane probe, while no rearranged products were observed for cyclopropyl ones. These results suggest that the putative radical intermediate is very short lived to allow opening of the cyclopropyl ring, but not short enough to prevent the racemization of tertiary carbon radical on the cyclopentane ring. Incidentally, it was estimated that the epimerization of 1,3-dimethylcyclopentanes and the rearrangement of cyclopropyl ring have first-order rate constants of *ca.* 10^9 and $10^8\ s^{-1}$, respectively [135, 147]. It can be argued that a mechanism passing through a carbocation would lead to analogous stereochemical results. However, such an intermediate is hardly conceivable in the hydroxylation of alkanes on TS-1, as its formation on heterogeneous catalysts generally implies very different conditions, namely, strongly acidic sites and/or high operating temperatures.

The addition of radical quenchers (kinetic diameters within brackets), namely, 2,6-ditertbutyl-4-methylphenol (BHT) (>0.6 nm), carbon tetrachloride (0.52 nm), chloroform (0.46 nm) and dichloromethane (0.40 nm), neither modified the time course of hydroxylation nor produced chlorinated derivatives, thus excluding radical chain mechanisms in the liquid phase while confirming the absence of



SCHEME 2.2 Competitive pathways in the oxidation of ethyl- and 2-propyl-cyclopropane.

long-lived alkyl radicals in the pores. Measured kinetic isotope effects for the hydroxylation of cyclohexane and cyclohexane-d_{12} were 4.1 in methanol and 4.7 in *t*-butanol [133]. A k_H/k_D of this magnitude is consistent with substantial C−H bond cleavage in the transition state, while is not compatible with a radical chain oxidation initiated by hydroxyl radicals ($k_H/k_D = 1–2$).

The kinetics of *n*-hexane oxidation was repeatedly studied under the conditions of partial miscibility (see above). Different rate expressions were obtained, with the final one showing partial and second-order dependence on the alkane and hydrogen peroxide, respectively [136, 140]. The adsorption of two moles of hydrogen peroxide on Ti, predicted as the rate-limiting step, is quite at odds with other experimental and theoretical evidences, including the primary kinetic isotopic effect just mentioned.

2.3.1.2 Other Ti Silicates with MFI Structure The patent literature is rich in synthetic methodologies claimed to yield Ti silicates with MFI structure, having different and/or more Ti sites than TS-1, with improved catalytic properties. One such a material, characterized by hydrophilicity and a variety of Ti species, was applied to the oxidation of *n*-hexane, with selectivities on hydrogen peroxide reportedly as high as 99% in the temperature range 40–60 °C [148]. Unfortunately, generic reference to a patent makes duplication difficult.

2.3.1.3 Large Pore Ti Zeolites Ti,Al-β is moderately active for C−H hydroxylation [79, 149, 150]. Predictably enough, the range of alkanes is broader than for TS-1 and the oxidation of cycloalkanes more effective than that of linear ones. Cyclohexane, needing high temperatures on TS-1, could be oxidized at 60 °C. Dimethyl-substituted cyclohexane, cycloheptane and cyclooctane compounds yielded corresponding tertiary alcohols and a mixture of secondary alcohols and ketones under analogous conditions. The other side of the medal, in the comparison with TS-1, is represented by the lower yields and the greater incidence of side reactions, as revealed by comparative oxidations of freely diffusing alkanes. Actually, the best hydrogen peroxide utilization was around 50%, with the remainder undergoing dismutation to water and molecular oxygen. The reason is likely to be the more hydrophilic intraporous volume, more favorable to the adsorption of hydrogen peroxide.

Regio- and stereoselectivity of dimethyl cyclohexanes is strictly related to the availability of equatorial *t*-C−H bonds in their most stable configurations, as in *trans*-1,3- and *cis*-1,2-dimethylcyclohexane [150]. Apparently, the steric hindrance of axial *t*-C−Hs, available in the *cis*-1,3- and *trans*-1,2-isomers, is high enough to make their hydroxylation comparable to or even slower than that of methylene groups. Accordingly, the former two alkanes produced tertiary alcohols with 82% and 72% selectivity, respectively, whereas the latter ones yielded a mixture of secondary alcohols and ketones.

The oxidation of *n*-hexane and cyclohexane was briefly reported for Ti,Al-MOR [96]. Hydroxylation, however, was just a minor reaction with respect to the dismutation of hydrogen peroxide.

2.3.1.4 V Silicates VS-2 differs from Ti zeolites in a major catalytic feature, i.e. the ability to also hydroxylate methyl groups, albeit at slower rate than methylene ones: *s*-C−H > *p*-C−H (no information on *t*-C−H) [151]. In the oxidation of linear C_6–C_8 alkanes, a complex mixture of primary and secondary alcohols, carbonyl compounds, lactones and other overoxidation products was obtained, with hydrogen peroxide selectivity to monofunctional products generally lower than 67%. The larger production of over oxidized products, in the range 20–25%, and of aldehyde and ketones over alcohols point to a higher activity of V over Ti [152]. Its regioselectivity too was different, with a preference for the oxidation of central methylene groups.

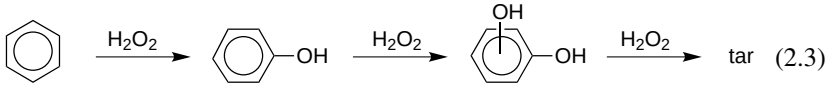
Similar yields and product distribution were reported for V-NCL-1 (*ca.* 0.7 nm) with the same substrates [153]. Larger pores also made possible the oxidation of mono-, di- and trimethylbenzenes, both at benzylic and nuclear positions. Tests for V-leaching, however, were not performed for either kind of catalyst.

2.3.2 Hydroxylation of Aromatic Compounds

The hydroxylation of phenol became, in the wake of the first industrial success of TS-1, a favorite topic of early research. Though the attention on this reaction is still alive, it is the hydroxylation of benzene, a long-sought objective of homogeneous and heterogeneous catalysis, that is gaining momentum in a parallel trend with the weakening of the old belief on the incompatibility of hydrogen peroxide with petrochemical applications. Phenolic ethers and alkylbenzenes are the subject of a few studies, mostly carried out with TS-1. Other metal-substituted zeolites, such as large pore Ti zeolites and V-substituted ones, are little considered [154].

2.3.2.1 Hydroxylation of Benzene The first mention was in a 1990 overview of oxidations on TS-1 [4]. Other brief accounts, in those years, dealt with the use of Al-TS-1 and Pd/TS-1, whereas the first detailed studies had to wait for the 2000s [154–157]. Recent studies, paying attention to side reactions and means to reduce the cost of the catalyst and add mesoporosity in it, possibly anticipate new research directions implying an industrial objective [46, 158, 159]. Studies on large pore Ti zeolites are substantially limited to a few accounts with Ti-MOR [96, 160]. Its lower activity is a likely consequence of the hydrophilicity generated by residual Al.

The hydroxylation of benzene is, probably, the reaction catalyzed by TS-1 most susceptible to overoxidation. With ordinary solvents, low hydrogen peroxide to benzene ratios and small sized TS-1, the selectivity to phenol fell below 50% at already 3–4% benzene conversion, while hydrogen peroxide efficiency hardly surpassed 20% [155, 156]. Overoxidation products comprised diphenols (*ca.* 30%), benzoquinone (< 4%) and a relevant quantity of tars (25–35%) (Eq. 2.3).



(2.3)

TABLE 2.2 Effects of the Solvent on the Hydroxylation of Benzene[a]

Solvent	Benzene conv. (%)	H_2O_2 conv. (%)	Selectivity to phenol	
			based on benzene (%)	based on H_2O_2 (%)
Acetone	4.2	90	41	19
Acetonitrile	4.6	93	43	21
t-Butanol	4.1	90	44	20
Sulfolane	7.8	97	83	67
Sulfolane/TS-1B	8.6	97	94	83

Source: Adapted from Ref. [155]. Copyright 2003, with permission of Wiley-VCH.
[a] H_2O_2/benzene = 0.1 molar ratio, $T = 100\,^{\circ}C$.

Dimethyl and tetramethylene sulfones, however, proved to be singularly effective solvents, increasing selectivity to phenol and hydrogen peroxide efficiency up to 83% and 67%, respectively, moreover at nearly doubled benzene conversions (Table 2.2). A second and major pace forward consisted in the post-treatment of TS-1 with a solution of $(NH_4)HF_2$ and H_2O_2, under controlled conditions [155]. The modified catalyst, called TS-1B by the inventors, raised further the selectivities to phenol and hydrogen peroxide to 94% and 83%, respectively, with negligible production of tars.

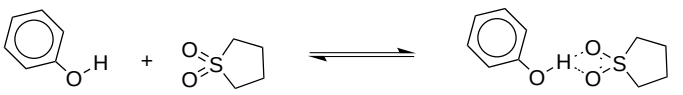
It should be noted that the cumene process consists of three consecutive steps (alkylation of benzene, autoxidation of cumene, decomposition of cumyl hydroperoxide) with an overall per pass yield that does not exceed 8–9% (*ca*. 99% after recycles). The combined use of TS-1B and tetramethylene sulfone (sulfolane) improves direct hydroxylation of benzene close to this target, being susceptible to further increase by the selective hydrogenation to phenol of byproduct diphenols [161]. The penalty for the relatively high cost of hydrogen peroxide could find, in principle, compensation in a simpler process scheme. In this perspective, the oxidation of benzene was carried out continuously, in a stirred-tank reactor (CSTR) for over 100 h onstream successfully [155, 161]. However, if the use of sulfolane pushes up the yields, its boiling point (bp: 285 °C) complicates the separation of products and byproducts, particularly that of hydroquinone and catechol for which a basic extraction, with consequent production of saline byproducts, becomes necessary. Considering also the hydrogenation step, a process that in principle could have been a single-step process, turns out to be again a multistep one.

Incomparably better yields and without the need for any organic cosolvent, such as 78% efficiency at 87% benzene conversion, were claimed under triphase conditions (aqueous H_2O_2, benzene, TS-1) [162]. As for other oxidations on Ti zeolites, a solvent indeed is not indispensable for the hydroxylation of benzene to occur, but no other group was able to reproduce such results [156, 157, 163]. Good yields were claimed also for the relatively hydrophilic titanosilicate, prepared by Halasz et al. (Section 2.3.1.2) [148, 163].

Mechanistic Investigations The post-treatment of TS-1 with $(NH_4)HF_2$ extracted up to 75% Ti, as $(NH_4)_3Ti(O_2)F_5$ peroxide, and only 1% silica [156]. $(NH_4)F$, HF and other protonic acids could remove Ti from TS-1 without, however, any benefit for catalytic performances. Both morphology and MFI structure remained the same in TS-1B, as revealed by XRD and TEM. Residual Ti, however, changed for a large part into species absorbing at near 250 nm in the UV-vis spectrum, with the remainder retaining the original tetrahedral state. Other evidences also seemed to indicate an increase of hydrophobicity and porosity.

It is not clear whether the improved performances of TS-1B stem from Ti species absorbing at 250 nm or from surface modifications. In principle, a catalytic role could be conceivable for the new Ti sites, even though it would be the first time for Ti in a different state in zeolites to be more effective than tetrahedral one. As an alternative, it is possible that the residual amount of unmodified Ti is still the source of catalytic activity and the improvement of performances arises from enhanced hydrophobicity. Such a phenomenon, though unprecedented for TS-1, is not rare for acid zeolites. For instance, the yields in the acetylation of anisole improved by one order of magnitude by a post-treatment of H-Y catalyst, in which the Si/Al ratio increased by a factor of twelve [164]. A similar behavior was observed for the hydration of phenyl acetylene and the hydroxymethylation of furfuryl alcohol, catalyzed by H-MOR [165]. In these and other examples, the greater hydrophobicity of the surface prevails and is at a premium over the decrease of active sites.

The second question concerns the function of sulfolane. Balducci et al. argued, with the support of spectroscopic and kinetic evidences, for the formation of a hydrogen-bonded bulky adduct of phenol with the solvent, which would favor its desorption and permanence in the liquid phase, away from oxidant sites (Eq. 2.4) [155].



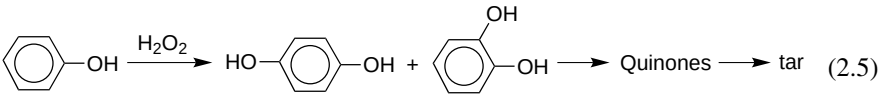
(2.4)

Considering also the enhanced adsorption of benzene promoted by the polarity of the medium, the properties of sulfolane would have the overall effect of narrowing the kinetic gap between phenol and benzene. Actually, their turnover frequencies on TS-1 changed from $190\,h^{-1}$ and $19\,h^{-1}$, respectively, in acetone to $51\,h^{-1}$ and $31\,h^{-1}$ in sulfolane. Using TS-1B instead of TS-1, the rates of phenol ($81\,h^{-1}$) and benzene ($80\,h^{-1}$) became practically the same [156].

The explanation offered by Balducci and colleagues implies that the hydroxylation occurs inside the pores, consistently with several other evidences (Section 2.3.2.2) [155]. According to Barbera et al., instead, the hydroxylation of benzene occurs by two kinetically parallel pathways, one leading to benzoquinone by fast consecutive oxidation in the intraporous volume and the other to phenol on the exterior surface [157]. Catechol and hydroquinone would be secondary products of phenol on external Ti sites and, possibly, by the attack of $^{\bullet}OH$ radicals in the liquid phase. The concomitance of radical chain processes, detrimental to phenol

selectivity, was specifically addressed by a study with thermally generated •OH radicals and their incidence shown to depend on reaction conditions, being contrasted by such inhibitors as sulfolane, acetonitrile and phosphate salts [158]. It should be noticed, however, that the choice of the temperature, 100 °C for Balducci and colleagues [155] and only 60 °C for the other two groups [157, 158], could be relevant for the competition of Ti-centered species and liquid phase •OH radicals, making the conclusions drawn at 60 °C misleading when extrapolated to higher temperature conditions. It can be noted that acetonitrile, too small for bulky complexes with phenol, while at 60 °C was as good inhibitor as sulfolane of side reactions, at 100 °C it was as ineffective as methanol and acetone.

2.3.2.2 Hydroxylation of Phenol The hydroxylation of phenol on Ti zeolites yields catechol, hydroquinone and, often, 1,4-benzoquinone, in accordance with the rules of an electrophilic mechanism. 1,2-Benzoquinone is normally too reactive for isolation. Further oxidation of the aromatic ring eventually leads to carboxylic acids, tarry compounds and carbon dioxide (Eq. 2.5). High selectivity is normally achieved by operating with an excess of phenol over hydrogen peroxide.



(2.5)

Titanium Silicalites TS-1 and TS-2 The hydroxylation of phenol was first reaction catalyzed by TS-1 to be discovered and applied commercially. TS-2 is similarly active [4, 90, 166]. Their yields depend on different factors, among which the phenol to hydrogen peroxide ratio, the contents of lattice and extralattice titanium, the concentration of the catalyst, the temperature and the solvent are the most relevant ones (Section 10.1).

Huybrechts et al. showed that the activity of TS-1 was linearly proportional to overall Ti content up to *ca.* 2 wt% (as TiO_2), a threshold beyond which the activity grew slower to eventually level off [62]. Actually, the upper limit for the linearity of relationship had to be *ca.* 2.8%, i.e. the maximum content of lattice Ti in well-behaved materials, before segregation to TiO_2 anatase and/or amorphous Ti silicates start to be relevant. Both kinds of impurities were shown, in fact, to catalyze readily the decomposition of hydrogen peroxide and the formation of tars [135, 167]. It is worthy of mention that the hydroxylation of phenol, owing to its sensitivity to extra-framework Ti species, was proposed and really used in early years to asses the phase purity of TS-1 samples [77, 168].

The yields also increase with the concentration of TS-1 and the temperature, up to a plateau in a trend that probably reflects the competition of radical chains in the bulk solution. On a qualitative basis, the behavior of TS-2 is similar [168]. Acetone and methanol solvents proved by far preferable to *t*-butanol, acetonitrile and 2-butanone for both TS-1 and TS-2 [4, 168–170]. In both media, the selectivity to dihydroxybenzenes could be as high as 90–95%,

for phenol conversions of 25–30% [4, 77, 90, 168]. Water promoted faster kinetics than any organic solvent, in agreement with the larger partition coefficient (33 in water and *ca.* 1 in acetone or methanol) [171–173]. However, the deposition of tars was also faster and their amount larger, with the consequence of faster decay of initially better activity [171].

Product selectivity is also solvent dependent, with acetone favoring the production of catechol and methanol that of hydroquinone, in a ratio spanning from 1.3 to 0.5 [4, 77, 168]. Edge values were normally observed in dilute solutions, whereas, when phenol was the main component of reaction medium, catechol was obtained in only a small excess over hydroquinone [4, 77, 168]. Selectivity variations claimed to occur with the reactants ratio could be only apparent and due to faster kinetics of catechol oxidation to tar [174]. 1,4-Benzoquinone and, sometimes, its 1,2-isomer were reportedly major products on Ti-rich TS-1 and TS-2 in, however, abnormally lengthy hydroxylation reactions (6 h and 30 h, respectively) [169, 170].

Intracrystalline diffusion is important for hydroxylation, owing to the molecular sizes of phenol and dihydroxybenzenes comparable to pore diameters [90, 171, 175]. Estimates based on the Weisz theory led to the conclusion that catalyst efficiency can approach unity only for crystallites smaller than 0.3 μm, becoming just one tenth for those of 5 μm [175]. The creation of additional porosity, by the addition of carbon black acting as hard template during hydrothermal synthesis or by post-treatments, compensates for diffusion deficiencies of large crystal catalysts [47, 51–53]. Worthy of note, Tsai et al. reported yields for post-treated 5 μm crystallites not so far from those with untreated 0.05 μm ones [53]. TS-1B allowed higher hydrogen peroxide efficiency and *p*-selectivity than parent TS-1 [156].

Continuous-flow hydroxylation is the subject of recent papers. In a fixed-bed, deactivation resulted to be relatively fast, with the conversion almost halving by *ca.* 50 h onstream, in parallel with the growth of H_2O_2 dismutation and benzoquinone production [176, 177]. Hydrogen peroxide efficiency was relatively low even initially (*ca.* 75%), in line with the kind of impurities of diatomite binder ($Fe_2O_3 \leq 1.5\%$) and of TS-1 (anatase). A catalyst prepared from amorphous SiO_2 and TPABr template showed poorer activity and efficiency, consistently with the large size of crystals and TiO_2 impurities [37]. Lu et al., in turn, studied hydroxylation in a CSTR reactor fitted with a submerged ceramic membrane, on which a cake layer of TS-1 particles functioned as filter [178]. The conversion (at a phenol to oxidant ratio of 2.7) decreased relatively fast to less than 20% within 20 h onstream. Selectivity to dihydroxybenzenes was close to 90%, with a productivity claimed to be higher than that by fixed-bed operation above ($2.47\ g_{prod}\ h^{-1}\ g_{cat}{}^{-1}$). In a recent study hydrogen peroxide too is fed through a tubular ceramic membrane, immersed in the CSTR, to intensify the micromixing and reduce consecutive oxidations (95% selectivity) [179]. Hydroxylation was also studied by unconventional systems, e.g., miniature reactors (0.8–2 mm) [180].

Fixed-bed operation also served to derive one of three kinetic laws. Liu et al. found that a kinetic expression, of Eley–Rideal type, fitted well the hydroxylation rates experimentally determined (Eq. 2.6), whereas the Langmuir–Hinshelwood (L−H) approach was unsatisfactory (r, C_i and K_i are hydroxylation rate,

concentrations and adsorption equilibrium constants, respectively) [177]. The rate-determining step appeared to be the reaction of physisorbed phenol with chemisorbed hydrogen peroxide. Klaewkla et al., on the other hand, with tests carried out batchwise using both TS-1 and SnTS-1, claimed that a L–H rate law shows the best fitting (Eq. 2.7, where r_{Ph} is the rate of consumption of phenol) [181]. Both kinetic models differ from early one of Wilkenhöner et al., for which the conversion of phenol fitted well in a simple second-order kinetic expression: $r_{Ph} = -kC_{Ph}C_{H2O2}$ [171].

$$r = \frac{kK_1C_{H_2O_2}C_{Ph}}{1 + K_1C_{H_2O_2} + K_2C_{Ph} + K_3C_{Prod}} \tag{2.6}$$

$$r_{Ph} = -\frac{k_{Ph}C_{H_2O_2}C_{Ph}}{(1 + K_1C_{H_2O_2} + K_2C_{Ph})^2} \tag{2.7}$$

The reasons why such different rate expressions could be obtained can be various and not easy to assess, though the absence of an adsorption term for hydrogen peroxide in the simplest rate expression and the markedly low selectivity to dihydroxybenzenes in experimental tests used for the kinetic law of Eley–Rideal type are apparent. More interesting might be dwelling upon the structural implications of the Langmuir–Hinshelwood approach. The dual-site model, in fact, implies that Ti can assemble in pairs of adjoining or sufficiently close lattice sites, e.g., of the type -O−Ti−O−Ti−O- or -Ti−O−Si−O−Ti-, despite its low content (somewhat less than 2.5 T sites over 98 of the unit cell are occupied by Ti). Recent neutron diffraction studies, indeed, support a nonrandom distribution of Ti, with three over twelve crystallographically distinct T sites preferentially substituted, albeit disagreeing on their identity [55–57]. With even half of the Ti content distributed over T8 sites [57], however, the frequency of vicinal Ti pairs, their reciprocal distance and the geometrical requisites for the oxidant species on one Ti can attack phenol adsorbed on the other with the observed *o*- and *p*-selectivity, remain unresolved questions. On the other hand, the single-site L−H model is even more problematic, since it could be hardly coherent with *p*-hydroxylation (Figure 2.2) [171].

Different also are the explanations given for the relative roles of internal and external sites in product selectivity. According to Tuel et al., the geometrical constraints of the pores orient hydroxylation on *p*-position, while *o*-attack is

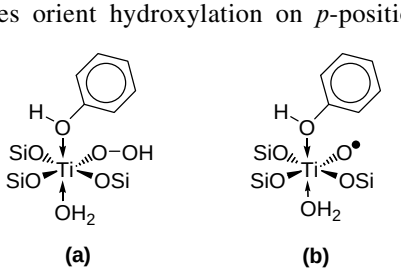


FIGURE 2.2 Phenol adsorption on possible oxidant species. For the species (**a**) and (**b**), see section 2.4.2.

statistically favored on external unhindered sites, with selectivity merely reflecting their different propensity to fouling in different solvents [168]. Evidences were the fast aging and almost exclusive production of catechol (>95%) on as-synthesized TS-1, i.e. with the pores still filled by the template, and the time profile of selectivity of calcined TS-1 in methanol and acetone. In the former, a bad solvent of tars, catechol selectivity decreased from initial 80% to *ca.* 50% in a few minutes time, to gradually stabilize on the standard value of 35%, owing, it was argued, to faster fouling of external sites. In acetone, a good solvent for tars, catechol was constantly the main product from the beginning to the end. Wilkenönher et al., by decoupling overall rate constants into specific contributions of internal and external sites, confirmed that *p*-hydroxylation prevails within the pores while *o*-hydroxylation on external sites was faster in acetone only [171]. A third view is that of Barbera et al. reported in Section 2.3.2.1 [157].

Large Pore Ti Zeolites The literature consisted of brief accounts, until the publication of a recent study on Ti-β. In early report, Ti,Al-β was moderately active with an *ortho* to *para* ratio of *ca.* 1 [182]. A subsequent study evidenced the higher conversion obtainable on Ti-β (19.5%) than on TS-1(6%), when diffusional path lengths were comparable, and the rather low catechol to hydroquinone ratio (0.5) [171]. In both studies, hydrogen peroxide efficiency was rather modest (*ca.* 63%). Subsequently, Ti-MCM-68 was reported to be superior to early catalysts: Ti-MCM-68 > Ti-MWW > TS-1 > Ti-β [99]. Hydrogen peroxide efficiency was, however, relatively high only for Ti-MCM-68 (up to 85%), whereas it was peculiarly low for the other terms of comparison. Its *o*-selectivity, with an *ortho* to *para* ratio of *ca.* 4, is unprecedented. The activity of Ti-SSZ-42 is relatively low [183].

V and Sn Zeolites VS-2, V-ZSM-48 and V,Al-β, with a hydrogen peroxide efficiency generally lower than 60%, proved to be poor hydroxylation catalysts [184–186]. Contradictory results were reported for VS-2 and VS-1, apparently showing in methanol nil and good activity, respectively [184, 185]. Tests on V-leaching are either missing or unsatisfactory.

The hydroxylation of phenol on SnS-1 was, in early report, relatively slow, with hydrogen peroxide efficiency modest (<70%) and the *ortho* to *para* ratio close to 1.6 [187]. Recently, tin for Si/Sn molar ratios ≥ 100 has been claimed to improve kinetics of TS-1, even though Ti incorporation and crystal size also varied with its addition [172, 181]. Reportedly, both hydroxylation of phenol and consecutive oxidation of the products, with the exception of that of catechol, fitted well in rate expressions of the Langmuir–Hinshelwood type.

2.3.2.3 Oxidation of Alkylbenzenes Alkyl substitution produces opposite effects on aromatic hydroxylation, with steric hindrance prevailing over electron donation in TS-1, even for toluene shown to react at a similar rate to that of benzene [4]. More generally, the nuclear reactivity trend in TS-1 and TS-2 is in the order, toluene > *p*-xylene ≥ ethylbenzene > *p*-methylethylbenzene, with no hydroxylation occurring on cumene [133, 135, 188]. Size effects also manifest in large pore Ti-MOR,

toluene > benzene > ethylbenzene > cumene, though to a lesser degree [97, 160]. Actually, the rate of hydroxylation of xylene isomers increased as expected for an electrophilic attack, *para* < *ortho* < *meta*, in contrast to the sterically controlled one, *ortho* < *meta* ≪ *para*, of TS-1. It is worth mentioning that the least hindered *p*-xylene exhibited the same reactivity on either catalyst. Not unexpectedly, the introduction of mesoporosity increased activity significantly, as in the hydroxylation of toluene and 2,3,6-trimethylphenol. For the former, the TON increased in the order, TS-1 ≤ Ti-MOR < meso-Ti-MOR [189]. 2,3,5-Trimethyl-*p*-benzoquinone, a key intermediate in the production of Vitamin E, could be obtained even on TS-1, once it had been made mesoporous [190].

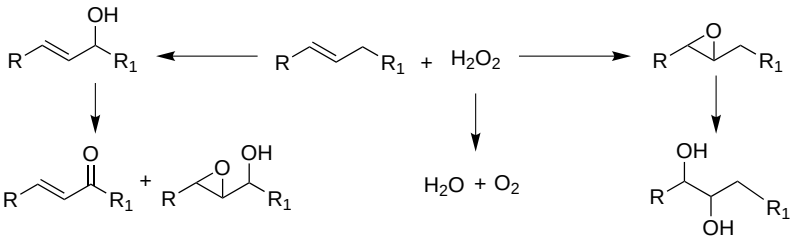
The oxidation of alkyl side chain produces secondary alcohols and ketones, in often-larger yields over phenolic products [133, 135, 188]. No reaction occurs at benzylic methyls, tertiary carbons, and β-CH_2 of both 1-propyl and 1-butyl groups. Others, by contrast, reported negligible oxidation of side chains for both TS-1 and Ti-MOR [97, 160]. Benzyl chloride and benzyl alcohol produced benzaldehyde, benzoic acid and phenolic derivatives in a ratio determined by reaction conditions [162].

With medium pore VS-2, toluene afforded benzyl alcohol (8%) and benzaldehyde (52%), in addition to *o*- (20%) and *p*-cresols (17%) [152]. Large pore V-NCL-1 also catalyzed the oxidation of bulkier molecules, e.g., xylenes and trimethylbenzenes, mostly at one methyl group [153]. Acetophenone was the main product of ethylbenzene oxidation on SnS-1 [191]. No test was carried out on the stability of lattice V and Sn.

2.3.2.4 Miscellanea of Aromatic Oxidations Electron-poor chlorobenzene, nitrobenzene, benzonitrile, benzaldehyde, and benzoic acid are stable to ring hydroxylation [4]. Anisole produced on TS-1 *o*- (30%) and *p*-methoxyphenol (70%) [4, 192]. Biphenyl ether, 2,3-dihydrobenzofuran and 1,4-dimethoxybenzene were also hydroxylated on TS-1 and TS-1B, whereas 1,2- and 1,3-dimethoxybenzene were inert [193]. Phthalan (1,3-dihydro-isobenzofuran) and 1,3-benzodioxole were preferentially oxidized at the activated methylene group to phthalide (3H-isobenzofuran-1-one) and catechol, respectively [193]. 2-Methyl-1,4-naphthoquinone (menadione, vitamin K_3) was obtained by the oxidation of 2-methylnaphthalene on Ti- and Fe-β and on Ti-NCL-1 [194]. Naphthalene afforded on large pore V-NCL-1 a mixture of phthalic anhydride and minor amounts of naphthols and 1,4-naphthoquinone [153].

2.3.3 Oxidation of Olefinic Compounds

The oxidation of simple olefins can interest the double bond and the allylic C−H, to yield corresponding epoxides and allyl alcohols. With aqueous hydrogen peroxide and conventional Group IV–VI metal-oxide catalysts, both oxidations occur together with other reactions, such as the dismutation of the oxidant and the hydrolytic opening of the oxirane ring (Scheme 2.3) [195]. Actually, the need for relatively high temperatures, to circumvent the inhibition of water, and the acidic



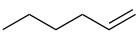
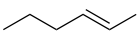
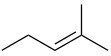
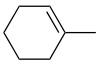
SCHEME 2.3 Catalytic oxidation of olefins with aqueous hydrogen peroxide: possible pathways.

properties of metal oxides favor the products of side reactions, unless the epoxidation zone is maintained water free by the continuous distillation of water, by operating under phase-transfer conditions, or by the use of hydrophobic catalysts, e.g., Ti zeolites [6]. The key feature of the latter, indeed, is the organophilic environment that acts as a barrier against the adsorption of water and protects, from one side, the active site from inhibition and, from the other, the epoxide and the oxidant from side reactions (Section 2.4.7).

2.3.3.1 Epoxidation of Simple Olefins on TS-1 and TS-2 Most studies on TS-1 and TS-2 concern the epoxidation of olefins, probably for its smoothness and economic value. Not dissimilarly to the oxidation of alkanes, distinctive features of the reaction are fast kinetics in dilute solutions of aqueous hydrogen peroxide and the preference for protic and polar media, particularly for methanol [19, 196]. With freely diffusing olefins, the oxidation of the double bond is practically quantitative, with no allylic attack detected and negligible incidence of hydrogen peroxide decomposition and methanol oxidation. Epoxide selectivity varies with operative conditions and can be higher than 90%. However, as the kinetic diameter of the olefin approaches *ca.* 0.60 nm, epoxidation becomes increasingly slower and the yields lesser, to the advantage of competing side reactions [196, 197]. Principal byproducts are corresponding glycol and its mono ether derivatives. Sterically pure *cis*- and *trans*-butenes produce corresponding epoxides with full retention of configuration [196].

The reactivity of the olefin is the result of electronic and steric factors, inherent to the molecule, and of adsorption and deactivation phenomena related to microporosity [142, 196]. The incidence of electron donation is evident in reactivity orders predicted by the nucleophilicity of the double bond: propylene $\gg$ ethylene, 1-butene $>$ allyl chloride $>$ allyl alcohol, and 2-methyl-2-butene $>$ 2-methyl-1-butene $>$ 3-methyl-1-butene [196]. Steric impediments, however, either to the diffusion of the olefin in the pores (reactant shape selectivity) or to the attack of the double bond on the active species (transition-state shape selectivity) normally offset electronic factors, leading to unprecedented orderings. The first can alone explain the epoxidation of cyclohexene, found at near room temperature to be slower than

TABLE 2.3 Relative Epoxidation Rates of C_6 Olefins

Olefin						Ref.
TS-1	1.0	2.3	0.29	—	—	[198]
Ti,Al-β	1.0	1.1	1.6	1.6	1.2	[198]
CH_3CO_3H	1.0	20–24	(*ca.* 240)	27	(≥240)	[199]

that of 1-hexene by almost two orders of magnitude [196]. The second is apparent in the relative rates of freely diffusing olefins, which are not of the expected magnitude or even appear reversed (Table 2.3) [196, 198, 199]. Physisorption is an excellent explanation for the increase, within a homologous series of olefins, of initial epoxidation rates with the chain length, in a parallel trend with partition coefficients [141, 142]. The different behavior observed at longer times onstream is attributable to deactivation phenomena, which increase with chain length, thus masking the true epoxidation ordering. A discussion of internal and external factors and of their effects on epoxidation is in earlier reviews [6, 200].

The solvent employed to dissolve the reagents has an impressive effect on catalytic performances. An early study showed an increase of conversion in the order, *t*-butanol < acetonitrile < methyl acetate < ethanol < methanol [19]. Other studies considered 2-propanol, acetone, 2-butanone and tetrahydrofuran, these also less effective than methanol [146, 201, 202]. Initial rates in pure water were seemingly faster than in methanol with, however, the drawback of an even faster deactivation of the catalyst. Reduced amounts of acetonitrile, acetone or 2-butanone apparently improved epoxidation in methanol [202]. In the oxidation of cyclopentene and styrene, *t*-butanol and acetonitrile, respectively, were reported to be superior to methanol [203, 204].

The high activity of TS-1 in protic and polar media is, since early studies, a most debated question with two different interpretations generally given, one based on the coadsorption of a protic molecule on active species and the other on the partition of the olefin between the pores and external solution (Section 2.4.7). A third hypothesis on a relationship between solvent and olefin diffusivity, seemingly supported by the decrease of the latter in a similar trend as kinetics, methanol > acetonitrile > acetone, was excluded by estimates for the Weisz modulus. These indicated that the epoxidation of 1-hexene could become diffusion limited only for crystal sizes of TS-1 greater than 38 μm [205]. Unfortunately, the use by the authors of silicalite-1 instead of TS-1 and the absence of hydrogen peroxide in the solutions used for the measurements of diffusion may cast doubts on the conclusions drawn. Wu et al., actually, showed that the diffusivity of aromatics was greatly dependent on both the content of lattice Ti and the presence of hydrogen peroxide [160].

The main side reaction is normally the solvolysis of the product by uncatalyzed and acid catalyzed reactions. The former pathway is slow and its contribution quite negligible under ordinary conditions [19]. As to the reasons for the second one, the acid activity of TS-1 proved just slightly greater than that, substantially negligible, of S-1 [206]. Claims to the contrary in the literature are possibly

explained by trace lattice Al, coming from the use of impure silica sources. Actually, Al-free TS-1 develops appreciable acidity, measurable by titration or by the solvolysis of the oxirane ring, only in the presence of hydrogen peroxide [206, 207]. On its addition, the solvolysis of 2,3-epoxybutanes on TS-1 became faster by about two orders of magnitude, proving faster than that by a 0.1 mol L^{-1} solution of formic acid. The absence of any such effect on silicalite-1, the increase of solvolysis with the concentration of hydrogen peroxide and the inertness of *t*-butyl hydroperoxide are of further support to the identification of the acid species in TS-1·H_2O_2 complex [135, 196, 208]. Its solvolytic activity varied with the kind of solvent, decreasing in the order, methanol > ethanol > water [196].

On these grounds, the TS-1·H_2O_2 system can be reputed as an ion-exchange material and its acidity moderated accordingly. Thus, the addition of small amounts of basic compounds, either directly into the epoxidation medium or by the pretreatment of the catalyst, leads to a drastic reduction of solvolysis [19, 146, 209–211]. Amounts in the ppm range are normally sufficient with Al-free TS-1 for epoxide selectivities up to 98%, without significant penalization of activity, with the residual 2% solvolysis attributable to the uncatalyzed route [19]. Further increasing the base decreases the activity progressively up to complete inhibition, because of the formation of anionic peroxides catalytically inert [19, 212].

Epoxidation kinetics is the subject of three papers [213–215]. Two of them deal with the epoxidation of propene, reaching opposite conclusions on the kinetic model. Liang et al. found that a rate expression of the Eley–Rideal type, with the oxygen transfer as limiting step, fitted well experimentally determined rates, whereas a Langmuir–Hinshelwood one did not [213]. For Shin and Chadwick, initial rates could be fitted best by dual-site L−H type of equation, with the single-site one being statistically less significant [214]. In a third study, with 1-hexene as the substrate, the Eley–Rideal approach was again preferred [215]. The reasons for such dissonances are not so clear, though the dual-site L−H approach is liable to the same objections raised in Section 2.3.2.2, in relation to Ti distribution in TS-1. In addition, it predicts the adsorption of the olefin on oxophilic Ti in a competition with adsorbates like water, methanol and the epoxide, despite the absence of any evidence in support and several arguments to the contrary. In a recent study, the chemisorption of 1-hexene on Ti sites was specifically addressed and could be ruled out [205].

A number of studies deal with modified TS-1 catalysts. Ion-exchanging Al-TS-1 with heavier alkali metals resulted in a significant enhancement of epoxidation activity [216]. Both theoretical calculations and IR evidences, together with the absence of any such effect for C−H hydroxylation, led the authors to propose a π-interaction of the cation with the olefin, leading to better catalytic performances by the improvement of olefin diffusivity. Sulfate deposition on TS-1 was reported to be positive for catalysis, while that of phosphates had a negative impact (phosphates are common stabilizers of hydrogen peroxide against metal impurities) [25, 217, 218]. Post-treatments with Zn salts or with ammonia, the latter at high temperature, improved epoxide selectivity by the likely formation of Ti−O−Zn and Ti−NH−Si bonds [219, 220]. The introduction of mesoporosity in TS-1 facilitated the diffusion

of the reagents to the active sites, favoring the epoxidation of bulky olefins and even the use of *t*-butyl hydroperoxide as oxidant [42, 44, 48, 49, 221–223]. A stacked morphology, in the straight channels direction, significantly improved the epoxidation of linear olefins [224].

The use of continuous-flow reactors is the subject of several studies, mostly dealing with the synthesis of propene oxide (Section 2.3.3.3). One refers to the epoxidation of 1-pentene in a microstructured reactor etched onto a silicon wafer, carrying a coating of TS-1 crystals directly grown on the walls [225]. Ti leaching was reportedly one of the causes of deactivation.

2.3.3.2 Epoxidation of Olefins on Large Pore Ti Zeolites The interest in this class of catalysts, applied to the epoxidation of olefins, has grown significantly since the first study with Ti,Al-β was published in 1992 [78, 149, 150, 198, 226–230], focusing afterwards on Ti-β [202, 231–236] and Ti-MWW [202, 237–241]. Ti-Y [98], Ti-SSZ-33 [242] and other materials, obtained by grafting Ti on delaminated MWW (Ti-ITQ-2) [111, 112], interlayer expansion of Ti-MWW precursor (Ti-MCM-56, Ti-MCM-36, IEZ-Ti-MWW, Ti-YNU-1) [107–110, 243, 244] and by the delamination of Ti-FER (Ti-ITQ-6) [105] have also been studied in some detail. Ti-MWW is included in this section for the presence in the structure of large supercages and external cups, in addition to medium pore inter- and intralayer channel systems.

Preferable oxidant is again hydrogen peroxide, though *t*-butyl hydroperoxide is also viable thanks to the spaciousness of pores [107, 111, 198, 226, 229, 237]. For the same reason relatively bulky olefins, such as substituted cyclohexene, 1-methylcyclopentene, cyclododecene, norbornene, camphene, limonene, are easily epoxidized under mild conditions [198, 234, 236, 244]. Steric factors, however, are still important, as shown by the epoxidation order of linear olefins (Table 2.3), and by the regioselectivity of cyclic olefins with unsaturations localized in both the ring and the side group [236].

It is a widespread belief that active sites and epoxidation mechanisms are substantially the same of TS-1. Both structures and properties of Ti sites together with the epoxidation behavior of different olefins support, indeed, the presence of the same electrophilic Ti−OOH species, though the proximity of Al sites and the different framework topology might affect somewhat its activity. Because of the more hydrophilic surface, however, large pore Ti zeolites are intrinsically less active than TS-1, as evidenced by the oxidation of linear olefins carried out under optimal conditions for either catalyst. Occasional reports to the contrary, claiming the superiority of Ti-MWW or Ti-β, suffer from the use of acetonitrile solvent, known to be a handicap for TS-1, or from insufficient detail on the catalyst used, e.g., on crystal size and phase purity. Epoxide selectivity too decreases in large pore zeolites, owing to the greater incidence of solvolysis, even in the absence of framework Al, as in Ti-β. Ion exchange with basic compounds or just their addition in the reaction medium, the use of mildly basic acetonitrile as solvent and of *t*-butyl hydroperoxide as oxidant limit the losses of the product efficiently [198, 226, 237]. Allylic byproducts and hydrogen peroxide dismutation, normally larger than with TS-1, are

indicative of a catalytic environment favorable to the competition of radical side reactions (Section 2.4.7).

A second difference with TS-1 is in the solvent and its effects on kinetics and selectivity. The choice is again restricted to alcohols, acetone and acetonitrile, but the latter is now preferable to methanol for higher conversions and less solvolysis [202, 226, 228, 233]. In protic media, glycols are normally far from being negligible, even with Al-free Ti-β. As a general rule, methanol is the best solvent for oxidations catalyzed by TS-1, whereas acetonitrile should be preferred for large pore zeolites. Deviations from the rule were reported for the epoxidation of specific olefins and, in one instance, for trifluorethanol solvent that was said to be the best one for Ti,Al-β [227].

Discordant reports and different experimental approaches are an obstacle to a clear ordering of large pore zeolites as per activity, though Ti-β looks more active than Ti,Al-β, while Ti MWW is emerging as superior to Beta ones. Their performances can be improved by appropriate methods of synthesis or post-treatments. For instance, the fluoride method produced a hydrophobic Ti-β, more effective for the epoxidation of alkenes [83, 232]. Post-treatments with piperidine or hexamethyleneimine led to an increase in the hydrophobicity of Ti-MWW and its activity [241].

Ti-MWW zeolites, for the singularity of their porous system, deserve a few more words. The siting of Ti in different porous environments, i.e. in sinusoidal 10MR channels, in external 12MR cups and in supercages with 10MR entrance windows, leads to active species liable to different diffusional and steric constraints [95]. Thus, the epoxidation of bulky olefins can occur exclusively in external pockets, whereas the linear ones are less subject to site limitations. Delamination, pillaring and expansion of the interlayer distance allow the preparation of Ti-MWW-type catalysts with more accessible intraporous volume. Normally, their performances were significantly better than for the original Ti-MWW [107, 109, 243]. Moderate to negligible improvement, however, was observed for the epoxidation of 1-hexene and propylene, consistent with their ability to diffuse already to any Ti site of original material [108, 109]. Ti-MWW is also unusual as a catalyst in the epoxidation of *cis*- and *trans*-olefins. At odds with TS-1 and Ti-Beta zeolites, *trans*-stereo isomers were epoxidized faster than their *cis* analogs [238]. A better fitting of *trans* configuration to the tortuosity of 10MR channels was suggested as an explanation.

2.3.3.3 Synthesis of Propylene Oxide The epoxidation of propene on TS-1 is the subject of numerous studies, often related to cheaper synthetic routes for the catalyst, the improvement of its porosity, means to reduce the incidence of hydrogen peroxide costs and the use of continuous reactors. TS-2, on the contrary, has been the subject of just one paper [245].

TEOS and alkali-free TPAOH allow the preparation of both phase-pure and small crystal TS-1 with optimal catalytic performances, however, at the expense of a relatively high production cost. With the growing prospects for high volume processes, implying far greater catalyst inventories than early hydroxylation of phenol, synthetic methodologies based on less expensive reagents could become attractive. Most studies have focused on the use of TPABr template, in association with

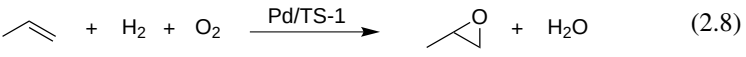
ammonia or other nitrogen bases, and colloidal silica as the Si source [33, 159, 201, 211, 246–249]. Ti insertion by the treatment of MFI and MEL zeolites with gaseous $TiCl_4$ has also been reinvestigated [159, 245].

Normally, TS-1 materials obtained by TPABr and colloidal silica differ from canonical TS-1 for some acidic Al sites, extraframework Ti phases and relatively large crystallites, all detrimental to catalytic performances. A somewhat lower hydrogen peroxide efficiency seems unavoidable, for the lack of effective strategies to the removal of extraframework Ti from the catalyst [159, 247]. The acidity, however, can be moderated by feeding a basic stream [247] while the lower activity and faster deactivation [196], typical of larger-sized crystallites, can find an antidote in the creation of additional porosity [250, 251].

The epoxidation of propylene carried out continuously, either in slurry [146, 252] or, preferably, in fixed-bed reactors [211, 246, 248, 249, 253–256], is the subject of numerous papers. The catalyst for the former setup was shaped by the spray drying of a dispersion of TS-1 in admixture with 10 wt% silica, to obtain micrometer-sized particles rich in the active phase, whereas those for fixed-bed operation were normally obtained by extrusion with a binder, such as alumina, silica, diatomite and clays. Adventitious acidic species, possibly introduced in the catalyst by the binder, are neutralized by the same basic side stream normally fed to control the acidity of Ti–OOH and Al sites [211, 257].

As a third alternative, TS-1 was supported as a thin layer on small ceramic balls for a better control of heat and mass transfer [248]. With a catalyst of this kind loaded in a relatively large fixed-bed reactor (2.5 kg capacity), the epoxidation of propylene endured about one thousand hour operation, with little deactivation (conversion of $H_2O_2 = 96$–98%, utilization of $H_2O_2 = 98\%$, PO selectivity $= 90$–95%) [257]. Its regeneration, after 1200 h onstream, could be carried out thermally under oxidizing conditions. Cofeeding water vapor with air allowed epoxidation to be restarted with high initial selectivity to epoxide, otherwise relatively low for a catalyst regenerated in a dry stream. In other studies, with either fixed-bed reactors and extruded catalysts or with continuous slurry reactors, deactivation was observed at much shorter times onstream.

Alternatives to commercial hydrogen peroxide and its relatively high cost consist in *in situ* generation and in process integration. The first option, possessing also the advantage of rendering the epoxidation process independent from external supplies, is of two types [258, 259]. The first one requires that TS-1 is converted into a bifunctional catalyst by the deposition of a metal species able to catalyze the direct synthesis of H_2O_2 from the elements [251, 260, 261]. The high activity of TS-1 in very dilute solutions of hydrogen peroxide favors its fast consumption in the epoxidation reaction and minimizes decomposition on metal particles (Eq. 2.8).

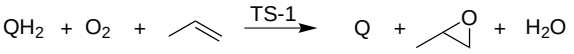


(2.8)

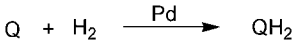
Normally, the hydrogenation of the olefin is a major side reaction, so that in early studies, performed batchwise on Pd-Pt/TS-1, the best yield was *ca.* 12%, with 54%

of propene being lost as propane [260]. The use of supercritical carbon dioxide was reported to decrease both PO solvolysis and propene hydrogenation [262]. The best yields (23%) and selectivities (82% to PO and 10% to propane) were obtained by the addition of small amounts of methanol and ammonium acetate in the supercritical medium [263]. In a continuous fixed-bed reactor, both activity and selectivity were initially high (99% selectivity at 3.5% conversion), to decay rapidly in a few hours [261].

The second approach envisages the autoxidation of an alkylanthrahydroquinone compound or other organic carriers (QH_2), performed in the presence of propylene and TS-1 (Eqs. 2.9 and 2.10) [258, 259, 264]. The major limitation is the solvent that has to comply with two requirements, namely, good solubility of the oxidized and the hydrogenated forms of the aromatic carrier and no negative impact on TS-1 activity. Normally, these conditions are met by the use of a mixture of the bulky solvents commonly used in the anthraquinone oxidation process (AO), with the addition of methanol to promote the activity of TS-1.



(2.9)



(2.10)

Epoxidation tests on propene, with a 2-alkylanthrahydroquinone (alkyl = ethyl, *t*-butyl) as the carrier, proved the feasibility of the concept, with yields in the range 62–78% [259]. Beyond a certain concentration, however, methanol causes separation of two liquid phases, one richer in methanol/water and the other in the working solution, with serious limitations for mass transfer between the four different phases present [264]. The use of a gas-lift recirculated reactor (Section 10.4), proved to be effective for operation under such conditions, allowing 82% yield. A different approach claimed in patents, to reduce the complexity of the working solution drastically, envisages organic carriers soluble in aqueous methanol, such as secondary alcohols and anthraquinone compounds carrying hydrophilic substituent groups.

Basically, process integration consists in the simplification of AO final steps, i.e. H_2O_2 extraction, purification, concentration and stabilization, which also implies the use for epoxidation of a relatively impure hydrogen peroxide solution. The tolerability of a limited content of impurities was verified successfully by the use of a technical-grade solution still containing a few hundreds ppm of organics [258]. Process integration was simulated by the use for the extraction of hydrogen peroxide of the same water–methanol medium of the epoxidation step. Tests carried out at the laboratory scale showed the tolerability of the small amounts of methanol and organics transported from one process to the other, respectively, and the compatibility of the hydrogen peroxide solution so obtained [258, 264]. Risks for the activity of the catalyst could result, however, from inorganic additives that may be required in the AO process and are extracted together with hydrogen peroxide [264]. Other carriers studied for process integration were 2-propanol, once used industrially for the production of hydrogen peroxide, and 1-phenylethanol [85, 213].

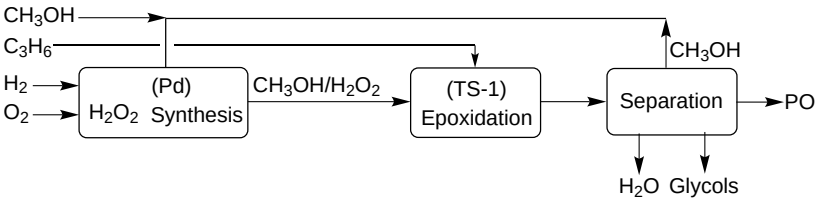


FIGURE 2.3 Synthesis of propylene oxide with hydrogen peroxide produced by direct synthesis.

Most innovative integration, however, would consist of the synthesis of hydrogen peroxide from the elements directly in aqueous methanol, thus obtaining a solution to be fed into the epoxidation reactor, as obtained or after an intermediate purification from possible additives. In this embodiment of process integration, aqueous methanol is at the same time the solvent of both processes and the physical carrier of hydrogen peroxide (Figure 2.3).

2.3.3.4 Oxidation of Substituted Olefins Following an early report on the epoxidation of allyl alcohol and allyl chloride on TS-1 [196], numerous papers appeared in subsequent years focusing on both the synthetic and mechanistic aspects. The range of catalysts extended to comprise TS-2, Ti,Al-β, Ti-β and Ti-MWW, and that of the substrates to a series of allyl and other substituted olefins.

Epoxidation of Allyl Alcohols In principle, allyl alcohols may undergo oxidation at the double bond or the alcohol group. In the absence of steric constraints, Ti zeolites catalyze epoxidation selectively, with the oxidation to carbonyl products growing in parallel with the steric hindrance on the double bond [265–267]. Triols and related monoethers also form, depending on the acidity of the catalyst, the kind of solvent employed and reaction conditions, to the point that in aqueous methanol or ethanol and with the least reactive substrates, these can be the main and even the sole products. The precaution of using acidity moderators, aprotic solvents, the hydrogen peroxide adduct with urea and *t*-butyl hydroperoxide reduces the solvolysis of the epoxide greatly [267–271]. C*is*-allyl alcohols resulted to be far more reactive than corresponding *trans*-isomers [267].

As for other oxidations, the highest activity was observed in methanol and ethanol for TS-1 and TS-2 and in acetonitrile for Ti-Beta and Ti-MWW zeolites. Worthy of note are the yields, up to 94%, shown by Ti-MWW in the epoxidation of allyl alcohol in water, a result of potential interest for a greener production of glycidol [270]. The same study emphasizes its superiority over TS-1 and Ti-β, in decreasing order. Selective poisoning tests showed that epoxidation on Ti-MWW occurred for the most part in the intralayer 10MR channels of crystallites [270].

Ti leaching is, to a variable degree, a quite common risk in the epoxidation of allyl alcohols. Davies et al. showed its dependence on the nature of the catalyst, the

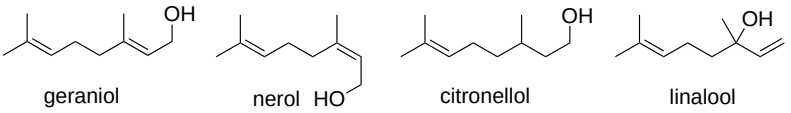


FIGURE 2.4 Chemical structures of unsaturated alcohols.

presence of hydrogen peroxide and the formation of strongly chelating ligands, namely, vicinal triols [269, 272]. Ti leaching, in fact, was noticeable in the epoxidation of geraniol with hydrogen peroxide, but not in that of citronellol with a distant hydroxy group (Figure 2.4) or in the use of *t*-butyl hydroperoxide [267, 272]. In the oxidation of crotyl alcohol (1-but-2-enol), it decreased in the expected order based on the known stability of the catalysts, Ti,Al-β > Ti-β ≫ TS-1 [269, 272]. Actually, for Ti leaching to occur in TS-1, the combined action of hydrogen peroxide and a vicinal triol proved necessary, while for Ti-Beta catalysts hydrogen peroxide alone could be sufficient. Leached Ti species, in turn, contribute to a homogeneous catalytic pathway that can be as significant as the heterogeneously catalyzed one. Actually, the oxidation of crotyl alcohol and geraniol with Ti,Al-β in methanol became, after an induction period necessary to the release of Ti, an essentially homogeneous process. In general, the use of TBHP strongly reduced Ti leaching. At that time, Ti-MWW was little studied, whereas afterwards a similar indepth investigation on stability has not been carried out, though acetonitrile in which it is generally used minimizes the harmful formation of triols. A significant leaching of B was, however, noticed from Ti-MWW [270].

The epoxidation of geraniol and nerol on TS-1, in acetone solution, was reported by Kumar et al. to occur on vicinal double bond selectively [266]. Somewhat at odds, Schofield et al. observed epoxidation at either the double bond of geraniol, with a ratio of *ca.* 2 : 1 in favor of the nonallylic one, and no oxidation of nerol [267]. Methanol solvent by competition or bulky substituents close to the alcohol group, as in linalool, inhibited the allylic double bond completely while orienting epoxidation at the most nucleophilic distant one, thus suggesting OH-coordination on Ti in the allylic epoxidation step. The mechanism was definitely proved by the stereo- and regioselectivity observed in the epoxidation of cyclic and chiral allyl alcohols [273]. The *cis*-epoxides obtained from the former and the kind of diastereomers from the latter can only be explained by the preference in the oxygen-transfer step for one of the two enantiofaces, resulting from the coordination of the alcohol group on the oxidant site.

Epoxidation of Allyl and Methallyl Chloride The epoxidation of allyl and methallyl chlorides with hydrogen peroxide occurs readily on TS-1 and Ti-MWW, whereas it is less viable on Ti-β and Ti-MOR [36, 196, 208, 271, 274–276]. Again, the best solvent is methanol for TS-1 and TS-2 and acetonitrile for the other catalysts. On most studied zeolites, namely, TS-1 and Ti-MWW, the solvolysis of epichlorohydrin is relatively slow, with a selectivity that can exceed 90% even for

conversions around 90%. It is remarkable that a similar performance was observed for Ti-MWW in water without the need for acidity moderators [276]. Ti-leaching was negligible for both TS-1 and Ti-MWW, whereas that of B was significant from the latter.

A new process based on hydrogen peroxide and a Ti zeolite would represent a cleaner alternative to current production of epichlorohydrin by chlorine-water. Fixed-bed operation is the subject of two studies, one focusing on the catalyst, consisting of TS-1 grown on a stainless steel net as the support, and the other on the development of an industrial-scale packed-bed reactor [277, 278]. For the mathematical model, the latter authors found that an Eley–Rideal-type rate expression was appropriate, in accordance with an early kinetic study carried out by Gao et al. with TS-1 [208]. Two studies seem to address the same issue with the *in situ* production of the oxidant, either on Pd/TS-1 or through the autoxidation of an organic carrier [275, 279]. In the second option, the addition of methanol to a working solution, composed by 2-ethylanthrahydroquinone, C_9 aromatic hydrocarbons and trioctyl phosphate, was needed for the activity of TS-1, in accordance with earlier findings. Drawbacks could lie in the inherent complexity of overall system and in the kinetics, alleged elsewhere to be slow [276].

Epoxidation of Other Substituted Olefins TS-1 and Ti-MWW, the former in methanol and the latter in acetonitrile and acetone, are effective catalysts for the epoxidation of diallyl ether to monoglycidyl and diglycidyl derivatives [4, 280, 281]. Monoepoxidation could be made selective by keeping conversion at below 30%. Allyl carbonate and allyl methacrylate produced on TS-1 corresponding monoglycidyl derivatives [4].

In a comparative study of allyl- and vinyl-substituted olefins, carried out with Ti-MWW, the conversion of allyl acetate and allyl ethyl ether was much greater than that of their vinyl analogs [281]. The reactivity of other olefins decreased in the order, allyl alcohol > allyl chloride > vinyl acetate > ethyl acrylate ≫ acrylic acid, in parallel with the decrease of nucleophilicity. TS-1 was briefly mentioned and reported to be a less effective catalyst.

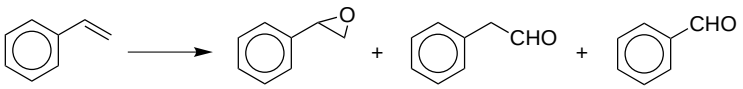
Epoxides and minor amounts of glycols were obtained from the oxidation of α,β-unsaturated ketones on TS-1, Ti-YNU-1 and Ti-Beta, whereas carboxylic acids formed from unsaturated aldehydes [244, 282]. Methyl substitution on the double bond reduced or suppressed epoxidation. α,β-Unsaturated acids and esters were inert under analogous reaction conditions. Ti leaching was observed to occur from Ti-β.

Butadiene produced 3,4-epoxy-1-butene selectively at 25 °C and, at higher temperatures, increasing amounts of rearranged byproduct 2-butyn-1-ol together with the diepoxide [4, 283].

2.3.3.5 Oxidation of Olefins to Glycols and Rearranged Products Some acid activity, due to chemisorption of hydrogen peroxide on Ti or to trivalent metals, is a constant in the use of Ti zeolites. Strong acidity characterize Ti,Al-β, Ti-MOR and Al-, Ga-, and Fe-TS-1, while that of Al-free Ti zeolites, which necessitates the

presence of hydrogen peroxide to manifest itself, is milder even though significant. Relatively weak is the acidity of boron-substituted zeolites, like B-TS-1 and Ti-MWW. Even though in most epoxidations this is an undesirable property to be moderated with basic additives, in some instances combined redox/acid catalysis might be useful for the one-pot synthesis of products such as β-phenylacetaldehyde and certain glycol ethers.

The oxidation of styrene on TS-1 and other Ti zeolites produces β-phenylacetaldehyde, 1,2-styrene oxide, glycol ethers and benzaldehyde in variable ratios, depending on the catalyst and reaction conditions (Eq. 2.11).



(2.11)

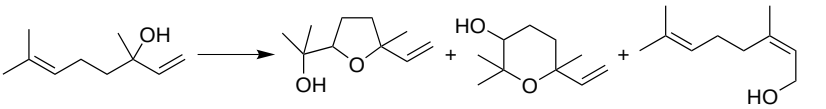
The reaction has been the subject of numerous studies, probably for the value of the aldehyde in fine chemistry and the interest in a seemingly odd mechanism [42, 159, 204, 210, 284–290]. The proper choice of the solvent, the alternative between aqueous H_2O_2 and the urea·H_2O_2 adduct, the optimization of the catalyst are all important for the desired selectivity. Up to 85% 1,2-styrene oxide was obtained by the use of urea·H_2O_2 as the oxidant [287]. Conversely, β-phenylacetaldehyde was favored by aqueous hydrogen peroxide and acidity, with selectivities up to 78% on B-TS-2 and Al-impure TS-1, and by the optimization of the catalyst (up to 90%) [159, 285, 290]. The positive role of urea for epoxide yield, noted also in other epoxidations, was a likely consequence of the neutralization of acidity [210].

On the mechanism the authors divided, with most being in favor of the theory of β-phenylacetaldehyde merely formed by a consecutive acid-catalyzed rearrangement of intermediate 1,2-styrene oxide and others, instead, favoring a parallel oxidation pathway, independent from epoxidation, involving both Ti–$O_2^{\bullet}$ superoxide and acid sites in a synergic catalytic role [288, 289]. Support for the first thesis comes from the time evolution of products [284] and from the ability of strongly and mildly acidic catalysts, like ZSM-5 and B-TS-1, to catalyze the aforesaid rearrangement [285, 291], despite an allegation to the contrary of Zhuang et al. [288]. The evidence in favor of the rival theory appears to be less solid, having been obtained from *in situ* NMR studies performed, however, on TS-1 materials with acid sites of unspecified nature [288, 289]. It is also questionable that the oxidant used, urea·H_2O_2, could be compatible with surface acidity, claimed to be crucial for a surface intermediate to decompose to β-phenylacetaldehyde.

Derouane et al. exploited the dual catalytic function and the spaciousness of pores of Ti,Al-β to prepare directly, by the oxidation of cyclohexene and cyclopentene in methanol and ethanol, corresponding *trans*-2-alkoxycycloalkanols, of interest as pharmaceutical intermediates [292]. The use of aqueous hydrogen peroxide and TS-1 under triphase conditions promoted the oxidation of unsaturated alcohols and halides to corresponding triols and diols, whereas epoxides formed in acetone solvent [293]. Similarly, tetralkyl-substituted olefins produced pinacols

(tetralkyl-substituted glycols) in water and epoxides in acetonitrile, with Ti-β reported to be best catalyst among various Ti zeolites [294].

In the oxidation of 3- and 4-unsaturated linear alcohols on TS-1 and Ti,Al-β, intramolecular cyclization to furano products, by internal attack of the hydroxy group on intermediate oxirane ring, prevailed over that to pyrano derivatives and over triols [295]. Cyclization was observed also in the oxidation of linalool to furano and pyrano products, in a ratio depending on the catalyst (TS-1, Ti,Al-β), the oxidant used (H_2O_2, urea·H_2O_2, TBHP) and reaction time (Eq. 2.13) [257, 296].



(2.12)

Unsaturated cyclic alcohols (Figure 2.5), namely, isopulegol (**a**), α-terpineol (**b**) and *trans-p*-menth-6-ene-2,8-diol (**c**) produced corresponding bicyclic derivatives, by a similar epoxidation/cyclization pathway, with high selectivity [295].

2.3.4 Oxidation of Alcohol and Ether Compounds

The oxidation of primary and secondary alcohols occurs readily on TS-1 and Ti,Al-β, to form corresponding aldehydes and ketones, together with emiacetals, acetals, carboxylic acids and esters as byproducts (Eq. 2.13) [4, 139, 228, 297–301]. *t*-Butanol forms *t*-butyl hydroperoxide.



(2.13)

Methanol, *t*-butanol, acetone and water, from one side, and acetonitrile, from the other, have been used as solvents for TS-1 and Ti,Al-β. The addition of water in acetonitrile was shown to retard the oxidation of cyclohexanol on Ti,Al-β and the effect was attributed to a water–alcohol competition for the active site [228]. Primary alcohols react slower than secondary ones while, within a homologous series, kinetics improves with the chain length, consistently with both an electrophilic mechanism and increasingly stronger adsorption. Methanol is the least reactive of unhindered alcohols and its relative inertness can explain its use as solvent for other oxidations, including that of alcohols. Shape selectivity is apparent in

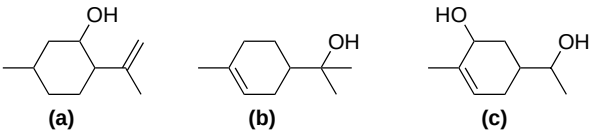


FIGURE 2.5 Chemical structures of cyclic unsaturated alcohols.

the lower reactivity of alcohols having the hydroxy group at more internal positions (α-alcohol ≫ β-alcohol ≥ γ-alcohol) or with vicinal methyl groups [297–299].

Oxidation kinetics is the subject of significant interest [139, 298, 299, 301]. Early studies, with TS-1 and Ti,Al-β as the catalysts, were performed under conditions of complete miscibility, with the reagents dissolved in methanol or other solvents. Equation 2.14, of the Langmuir–Hinshelwood type, illustrates the rate expression that best fitted the experimental data for both catalysts (k and K_i are the rate and equilibrium adsorption constants, $[Ti_0]$ is the initial concentration of active sites, [ROH], $[H_2O_2]$, [Solv] are the concentrations of substrate, oxidant and solvent) [298, 299]. It is consistent with spectroscopic evidences on the adsorption of protic molecules and hydrogen peroxide on Ti sites and can explain the inhibition of water. The rate-limiting step is the oxidation of alcohol adsorbed on Ti–OOH.

$$r = \frac{kK_2K_4[Ti_0][ROH][H_2O_2]}{1 + K_1[Solv] + K_2[ROH] + [H_2O_2]\{K_3K_1[Solv] + K_4K_2[ROH]\}} \qquad (2.14)$$

Gallot et al., on the other hand, studied the oxidation of 2- and 3-hexanol, in a two-liquid phase reaction medium (Section 2.3.1). The rate expression, with second-order dependence on hydrogen peroxide, requires the generation of Ti–OOH species to be rate controlling, as in the oxidation of alkanes [139].

The one-step synthesis of isoamyl butyrate from isoamyl alcohol and *n*-butyraldehyde at first glance might appear a quite odd oxidation for TS-1, since the oxidant was molecular oxygen [302]. The apparent contradiction could be settled, however, by the hypothesis of an *in situ* autoxidation of *n*-butyraldehyde to *n*-butyl hydroperoxide, with the latter functioning as the true oxidant by virtue of its compatibility with the pores of TS-1.

Glycols undergo oxidation at the secondary alcohol group preferentially [303]. Thus, propylene glycol and 2-phenylethane-1,2-diol afforded hydroxyacetone and β-hydroxyacetophenone, respectively. The oxidation of 2,3-butandiol was solvent dependent, with the production of acetoin in water and methanol, and that of butan-1,2-dione in acetone. Ethylene glycol yielded glycolic acid and small amounts of glyoxylic acid. The cleavage of the C(OH)−C(OH) bond was sometimes observed.

The oxidation of tetrahydrofuran and tetrahydropyran produced γ-butyrolactone and δ-valerolactone in 40% and 55% yield, respectively, whereas linear ethers yielded corresponding acids, presumably through the oxidation of a α-methylene group and subsequent *in situ* hydrolysis of intermediate esters [304].

2.3.5 Reactions of Carbonyl Compounds

Strictly speaking, this section should have comprised only the oxidation of carbonyl groups, namely, the Baeyer–Villiger oxidation and that of α,β-unsaturated aldehydes (Section 2.3.3.4). However, ammoximation is also included here, despite the fact that the oxidation process does not concern the carbonyl group specifically, according to the mostly accepted mechanism.

2.3.5.1 Ammoximation The word ammoximation defines the reaction of a carbonyl group with ammonia, under oxidative conditions, to yield the corresponding oxime. After early catalysts, which were too poorly selective, the prospects changed with the discovery of TS-1, shown by Roffia et al. to be an excellent ammoximation catalyst with hydrogen peroxide as oxidant, in contrast to amorphous Ti/SiO_2 (Table 2.4) [305]. Selectivities to oxime as high as 99% on cyclohexanone and 95% on hydrogen peroxide, at almost complete conversion of the ketone, were reported at 80 °C in aqueous *t*-butanol as solvent. Good results were also claimed in the absence of a cosolvent [306]. The yield increases with the concentration of the catalyst and proportionally to the content of lattice Ti [305, 307]. Major side reactions consist of the oxidation of ammonia to N_2, N_2O, nitrites and nitrates, in the decomposition of H_2O_2 to molecular O_2 and in the formation of a range of organic byproducts [308, 309]. Details can be found in Section 10.2.

TS-1, in sharp contrast to its proven stability in other oxidations, undergoes a slow dissolution of the siliceous matrix by the basic medium, with consequent aggregation of isolated Ti sites into discrete TiO_2 particles, while crystallinity remains fairly constant [310, 311]. The activity declines in a parallel trend, eventually approaching that of supported Ti [310]. Deactivation by coke deposition and a decrease of adsorption capacity with time onstream were also observed in the recovered catalysts [310, 312].

The ammoximation reaction holds general validity and, in addition to cyclohexanone oxime, provides an efficient route to many other oximes [313–317]. Acetone, butanone, C_5–C_8 cyclic ketones, methyl- and dimethyl-substituted cyclohexanones, acetophenone and its *o*- and *p*-hydroxy derivatives yielded corresponding oximes with generally high conversion and selectivity. Steric restrictions of dimethylcyclohexanones decreased, with reference to the position of second methyl group, in the order: β-equatorial > α-equatorial > β-axial > α-axial [314]. The ammoximation also of cyclododecanone and 4-butylcyclohexanone, which are unable to diffuse in TS-1, occurred with relatively high yields.

Other zeolite catalysts are TS-2, Ti-ZSM-48, Ti,Al-β, Ti-MOR and Ti-MWW, normally studied under similar conditions to those for TS-1 [189, 315, 318–322]. Ti,Al-β and Ti-ZSM-48 were applied to the ammoximation of *p*-hydroxyacetophenone, to obtain with fairly good selectivities a key intermediate in the industrial synthesis of 4-acetaminophenol (the analgesic Paracetamol) [315]. Ti-MOR was active in the ammoximation of a series of ketones and aromatic

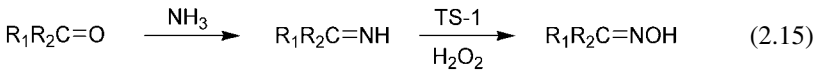
TABLE 2.4 Ammoximation of Cyclohexanone on Titanium Silicates

	Conv. $C_6H_{10}O$ (%)	Selectivity based on $C_6H_{10}O$ (%)	Yield based on H_2O_2 (%)
Ti/SiO_2	49.3	9.3	4.4
TS-1	99.9	98.2	93.2

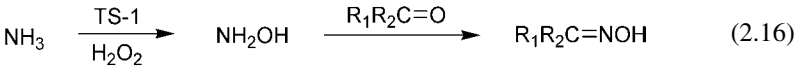
T 80 °C; solvent *t*-butanol/water; cyclohexanone:NH_3:H_2O_2 1.0 : 2.0 : 1.1 molar ratios; time 1.5 h; Ti content of the catalysts 1.5 wt%.

aldehydes, with selectivities up to 99%. Both activity and selectivity were influenced negatively by a higher content of lattice Al [319]. Ti-MWW has been the subject of detailed studies, particularly for the ammoximation of cyclohexanone and methyl ethyl ketone [320–322]. Reportedly, its catalytic performances were superior to those of other catalysts, namely, Ti-MWW $\geq$ TS-1 > Ti-MOR > Ti-β, with a 99% selectivity at 99% conversion of the ketone claimed under optimum conditions.

Two ammoximation routes were proposed for TS-1, one passing through the formation of cyclohexanone imine and the other of hydroxylamine as key intermediates (Eqs. 2.15 and 2.16).



(2.15)



(2.16)

The high yields obtained with cyclododecanone and 4-butylcyclohexanone, both hindered to diffuse inside the pores of TS-1, are only consistent with a mechanism in which the hydroxylamine produced by the oxidation of ammonia on Ti sites is then captured by the ketone in the bulk medium [313, 317]. Based on similar evidences and arguments, the hydroxylamine route was also extended to Ti-MOR and Ti-MWW catalysts [319, 320]. Mantegazza and colleagues showed its consistency, proving the fast oxidation of ammonia to hydroxylamine under ammoximation conditions and the feasibility of subsequent uncatalyzed oximation in the liquid phase [323, 324], confirmed by others to be ten times faster [325]. In the absence of a carbonyl acceptor, hydroxylamine undergoes consecutive oxidation to N_2, N_2O, nitrites and nitrates [309, 323]. On these grounds, the ammoximation reaction can be seen as a competitive process with *in situ* production of hydroxylamine. The relative rates of condensation and consecutive oxidation of hydroxylamine determine the selectivity based on ammonia. A recent kinetic study supports the preliminary formation of hydroxylamine by the attack of ammonia on Ti peroxide, according to an Eley–Rideal mechanism [326].

IR evidences, on the other hand, have suggested to Liu et al. a completely different third mechanism, in which a Ti peroxide oxidizes cyclohexanone to its dioxirane derivative and this in turn forms cyclohexanone oxime by the reaction with ammonia [327].

Numerous studies deal, directly or indirectly, with topics related to process development. Nanocrystalline TS-1 was grown on carbon granules or within the layers of bentonite clay, in an attempt to combine the better diffusion of small-sized crystals with the easier recovery of larger particles [326, 328, 329]. The separation step was tackled by innovative engineering approaches, such as by membrane modules, either of the side-stream or submerged type, and by a tubular membrane reactor [330–332]. The gradual dissolution of the catalyst led to a preference for continuous-flow slurry reactors (CSTR) for either TS-1, Ti-MWW and Ti-MOR [189, 319, 322, 328, 332]. Under comparable conditions, the lifetime of Ti-MWW

was reportedly longer than that of TS-1 (214 h *vs.* 124 h) and could be extended further by the addition of a source of silica in the reactor to counter the dissolution of the catalyst (see also Section 10.2) [321, 322]. Ti-MOR, particularly in its mesoporous modification, was also claimed to be superior to TS-1 [189].

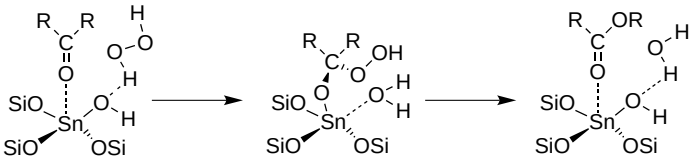
Integration with the hydrogen peroxide process is the subject of two studies, one considering the autoxidation of isopropyl alcohol, once practiced industrially, and the other, most detailed, the AO process [333, 334]. In the former, the solution from the autoxidation reactor was concentrated and fed as such, whereas in the latter one, aqueous methanol was used as the extractant. In both cases, the impurities fed into the reactor with hydrogen peroxide did not influence conversion and selectivity in ammoximation.

2.3.5.2 Baeyer–Villiger Oxidation The Baeyer–Villiger oxidation of cyclohexanone and acetophenone with TS-1/H_2O_2, under triphase conditions, proved to be poorly selective with the formation of a variety of products [335]. Sn-β/H_2O_2 on the contrary, showed excellent selectivity in the oxidation of several cyclic ketones to corresponding lactones [125, 336, 337]. An even better activity was reported for the catalyst obtained by the post-treatment of dealuminated Beta with $SnCl_4$ [338]. Aromatic aldehydes produced a mixture of phenols, formate esters and carboxylic acids, with selectivity depending on the solvent, the nature of the substrate and the amount of hydrogen peroxide [336]. The highest selectivity to phenol was observed with electron-rich aldehydes and in aqueous acetonitrile. Sn-β was stable to leaching and could be used repeatedly [125].

Noteworthy is the different chemoselectivity of Ti-β and Sn-β in the oxidation of unsaturated carbonyl compounds, leading selectively to corresponding epoxides and lactones/phenols, respectively [125, 336]. Corma and coworkers argued that, while Ti adsorbs hydrogen peroxide to form a peroxo species, the Lewis acidity of Sn favors instead the adsorption of the carbonyl group and its activation for external attack by hydrogen peroxide (Scheme 2.4). Such a Criegee-like mechanism was fully consistent with the results of a kinetic study [337].

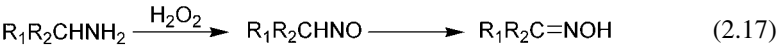
2.3.6 Oxidation of N-Compounds

Primary amines, having at least one α-C−H bond, form unstable alkylnitroso intermediates, which can further isomerize to corresponding oximes, dimerize to nitroso dimers, condense with a parent amine to hydrazone and oxidize to nitro compounds, with a selectivity that depends on the oxidant system and reaction conditions. TS-1,

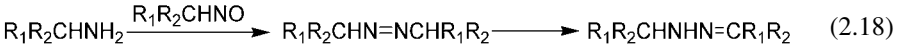


SCHEME 2.4 Oxidation of carbonyl compounds on Sn-β.

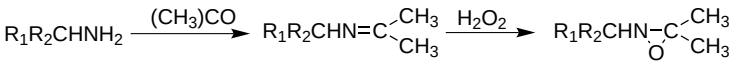
TS-2 and Ti,Al-β with hydrogen peroxide as the oxidant allow a high selectivity to oxime, with hydrazones as secondary products (Eqs. 2.17 and 2.18) [339–341]. Catalytic performances decrease with increasing chain length of the alkyl group. Methanol and *t*-butanol are suitable solvents, while acetone converts the amines to corresponding N,N′-dimethyl imines, which then undergo oxidation to aziridines (Eq. 2.19).



(2.17)

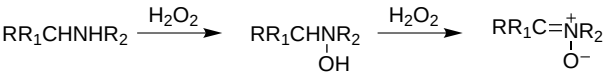


(2.18)



(2.19)

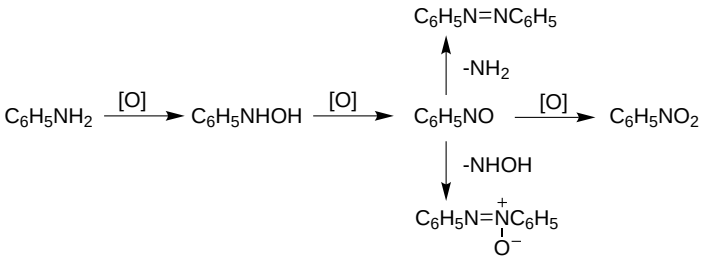
Secondary amines produce a mixture of hydroxylamines and nitrones (Eq. 2.20) [342, 343]. A high selectivity to N,N′-diethyl hydroxylamine was obtained on TS-1 and TS-2, at the amine to H_2O_2 molar ratio of two.



(2.20)

The oxidation of aniline can lead to different products, among which nitroso- and azoxybenzene are the most desirable (Scheme 2.5). With TS-1, TS-2, Ti-ZSM-48 and Ti,Al-β as the catalysts, azoxybenzene forms selectively at low hydrogen peroxide to aniline molar ratios, with the best yields obtained on Ti,Al-β (up to 95%) [344–346]. The use of a multichannel membrane microreactor was reported to be beneficial to selectivity [347]. At relatively lower temperatures, nitrosobenzene was the main product [348].

Several other arylamines, with either electron-donating or -withdrawing groups, and 1-naphtylamine undergo a similar oxidation to azoxybenzene on TS-1 [340, 344]. Oxidations claimed to occur with CrS-2 and bulky TBHP were probably catalyzed by leached Cr species [340].



SCHEME 2.5 Different products obtainable in the oxidation of aniline.

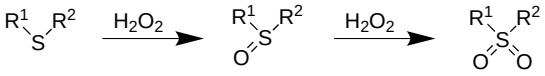
The oxidation of aromatic and aliphatic oximes and of tosylhydrazones on TS-1 and excess H_2O_2 regenerates corresponding aldehydes [349, 350]. These can be also obtained by the one-pot oxidation of primary amines with a large excess of hydrogen peroxide [340].

The oxidation of pyridine, picolines and other substituted pyridines to corresponding N-oxides on TS-1, reported to occur with generally high yields, met with the reservations of others [351–353]. In a recent paper, Ti-MWW showed higher activity and selectivity than TS-1, Ti-β and Ti-MOR, in the decreasing order, for the oxidation of pyridine and 3- and 4-picoline [354].

Hydrazine was produced by the oxidation of ammonia with hydrogen peroxide on TS-1, VS-1, B-TS-1 and V-TS-1, in the presence of 4-heptanone [355]. It is possible that the reaction proceeds through an intermediate imine and its oxidative dimerization to the corresponding azine, then followed by hydrolysis.

2.3.7 Oxidation of S-Compounds

The oxidation of thioethers on Ti-containing zeolites produces corresponding sulfoxides and, by consecutive oxidation, sulfones more slowly (Eq. 2.21):



(2.21)

Early studies envisaged TS-1, TS-2 and Ti-β as catalysts, hydrogen peroxide as the oxidant and a large variety of thioethers [356–361]. An uncatalyzed pathway normally contributes to the first step, whereas the second one to sulfone is fully catalytic. The selectivity depends on reaction conditions and steric restrictions [358, 361]. Experimental rates, in the oxidation of dibutylsulfoxide on Ti-β, fitted well the second-order rate expression $r = k[R_2SO][cat]$, with a zero-order dependence on hydrogen peroxide [360]. A heterolytic mechanism, consisting in the nucleophilic attack of external sulfur on Ti−OOH for both the oxidation to sulfoxide and subsequent one to sulfone, was suggested [360, 362]. Allyl thioethers were oxidized selectively on sulfur, with no reaction of the double bond [357, 361].

The oxidation of thioethers bears implications with the development of an oxidative process for the desulfurization of oil fractions (ODS), characterized by low temperature (*ca.* 50 °C) and atmospheric pressure of operation, potentially alternative to the high temperature (300–450 °C), high pressure (200–350 atm) and hydrogen-consuming hydrodesulfurization (HDS) [363]. ODS envisages a two-stage process with sulfides oxidized first to corresponding sulfones and then extracted from the oil with a solvent or adsorbed on an inert material. The reason for the preliminary oxidation is the higher polarity of sulfones that facilitates subsequent removal procedures. Ti molecular sieves are just one of several systems investigated to this end.

The first paper mentioning ODS explicitly appeared in 2001, with several more following in subsequent years [364–372]. Normally, the studies consider model

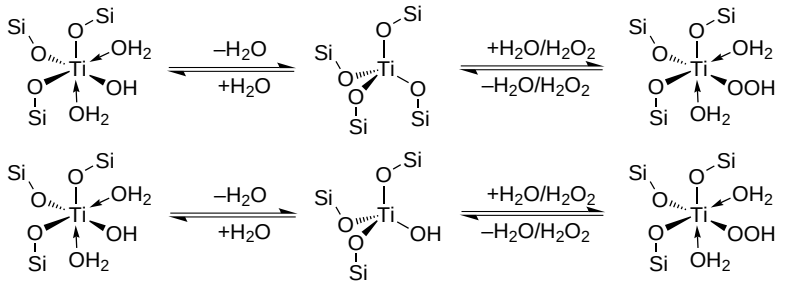
molecules of fuel oils contaminants, namely, thiophene, benzothiophene and dibenzothiophene. Hydrogen peroxide or *t*-butyl hydroperoxide is the oxidant with the second one favored by its solubility in oil fractions. Ti-Beta, for its larger pore size, was shown by early studies to be more suited than TS-1 [364, 366]. The introduction of mesoporosity, however, can reverse the relationship, as shown by a kinetic study with benzothiophene, in which catalytic performances decreased in the order, TS-1 (mesoporous) > Ti-β > TS-1 [372]. Peculiarly enough, the conversion of sulfur compounds on mesoporous TS-1 increased as: thiophene < benzothiophene < dibenzothiophene, i.e. to the reverse of usual trend of conventional desulfurization. Experimental data fitted an empirical rate expression first order on both benzothiophene and hydrogen peroxide, while a dual-site Langmuir–Hishelwood model had to be ruled out.

2.4 MECHANISTIC ASPECTS

A key question is why Ti inserted in a zeolitic structure is so effective with aqueous hydrogen peroxide, whereas Ti on amorphous silica and in soluble complexes is not or, from a different perspective, why polar solvents promote the activity of Ti zeolites, whereas they inhibit conventional Ti catalysts. The increase of the partition coefficients of apolar reagents, i.e. of their concentrations in the pores of TS-1, with solvent polarity and, in turn, of kinetics with partition coefficients seems to suggest the right answer [142]. While, however, such a sequential correlation proves the existence of a primary role of adsorption, it does not prove that adsorption is the sole explanation of solvent effects. On the other hand, the relationship between kinetics and partition coefficients only holds within a homogeneous series of solvents, whereas it fails when no distinction is made between protic and aprotic ones and the entire set of solvents is considered [6, 200, 373]. It is worthy of note that the epoxidation of 1-hexene on Ti,Al-β and the hydroxylation of *n*-hexane on TS-1 are faster in acetonitrile and *t*-butanol, respectively, despite partitions coefficients indicating methanol [133, 200, 228]. An explanation entirely based on the partitioning of the substrate between bulk and intraporous phases is also incompatible with the results of a recent kinetic study [215]. According to the early view, indeed, the solvent could affect catalysis not only by the adsorption of the substrate but also by other means, e.g., through the participation in the reaction mechanism [19, 133, 196].

2.4.1 The Nature of Active Species

The strain caused in the lattice by the substitution of Ti^{+4} for Si^{+4}, coupled with the Lewis acidic character and the tendency of tetrahedral Ti to expand coordination above four, represent favorable conditions for the hydrolysis of one Ti−OSi bond of [$Ti(OSi)_4$] site. Bellussi et al. proved it to occur in a reversible mode at ambient conditions, without any apparent structural damage, by the use of ^{16}O and ^{17}O labeled water (Scheme 2.6) [206]. According to To et al., most Ti sites, in the



SCHEME 2.6 Adsorption of water and hydrogen peroxide on Ti sites.

presence of water, adopt the tripodal state of $[Ti(OSi)_3OH]$. Their formation occurs with inversion of configuration at the Ti center, relief of lattice strain and stabilization of structure [374]. A variety of spectroscopic and chemical evidences showed that hydrogen peroxide behaves similarly, producing a Ti peroxo species [70, 72]. The same peroxide forms by the reaction of H_2O_2 with the titanol of $[Ti(OSi)_3OH]$ site. Ti−OOH hydroperoxide, instead of $Ti(\eta^2\text{–}O_2)$, was originally suggested to best represent it, on account of its acidic properties and chemical similarities with organic and inorganic oxidants having X−OOH structure (X is an electronegative group) [133, 196].

With the growing support of chemical evidences and theoretical studies, an active species based on Ti−OOH became over the years a widely accepted concept, extended also to hold for other Ti molecular sieves. Its fine structure, however, remains a matter of debate. Is the hydroperoxo group side-on (η^2) bonding on Ti? Is the coadsorption of a protic molecule relevant for its stability and activity? In the early proposal, Ti−OOH had end-on (η^1) coordination and was stabilized in a five-membered ring by a hydrogen-bonded protic adsorbate, typically methanol or water, based on the above arguments (Figure 2.6**b**) [133, 196]. On the other hand, theoretical studies typically predict side-on coordination and just a spectator role, if any, for protic adsorbates (Figure 2.6**c**,**d**) [375–380]. In species **(c)**, computed by Sinclair and Catlow [376], the physisorption of ROH just completes the hexacoordination preferred by Ti, while in variant **(d)** it is prevented by steric crowding. Wells et al. [380], in a comparative study of different active species, at the same

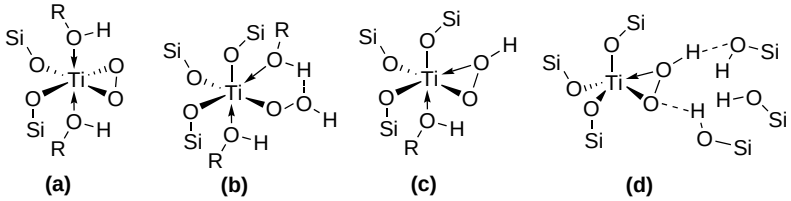


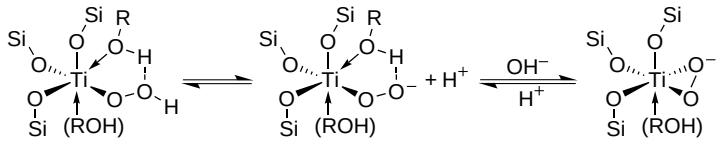
FIGURE 2.6 Proposed structures for Ti peroxo species formed by TS-1/H_2O_2.

level of theory and based on relatively larger cluster models (6–8 T-sites), computed the lowest energy of formation for species **(d)**, stabilized by both η^2-coordination and hydrogen bonding with a vicinal silanol nest.

In rare instances, theoretical studies support species **(b)**, as in early study by Neurock and Manzer and more recently by Barker et al., or just estimate that both species (**b**) and (**c**) have comparable energetics and probability of existence in TS-1 [377, 381–384]. However, they also envisage a series of other active species, e.g., physisorbed hydrogen peroxide, either on Ti or silanols, and framework-embedded SiOOTi peroxide, all incompatible with the chemical properties of Ti zeolites [385–387]. Such a variety of predictions merely reflects the variety of approaches. These may differ in the assumptions and simplifications about the environment of Ti sites, the cluster model, the level of theory and the computational method applied. Actually, the formation of five-membered species **(b)** could be highly endothermic, at more than 90 kJ mol^{-1} in an early study, and exothermic at −41 kJ mol^{-1} in a recent one [382, 385]. On one issue, theoretical studies are unanimous, namely, the unlikelihood of active species **(a)**.

Where hydroperoxide **(b)** receives substantial support is in experimental evidences. Actually, spectroscopic studies show that water, unavoidable in the use of hydrogen peroxide, and methanol, a common solvent of oxidations with TS-1, readily adsorb on Ti [60]. The acidity of Ti−OOH is solvent dependent, in accordance with structure **(b)** [206]. Several kinetic expressions require a methanol or water adsorbate carried by the oxidant species. Albeit these evidences could be inadequate to inform on the structural details of Ti−OOH, its cyclic form is consistent with the oxidation mechanism of alcohols on TS-1 and Ti,Al-β and with the opposite kinetic dependence of the oxidations of 1-hexene and cyclohexanol on the concentration of water [228, 298, 299]. In the former, water promotes the formation of active species, whereas in the latter water competes with the alcohol for Ti, thus hampering its oxidation. The formation of a bulky species protruding in the pores, identified by Wu et al. in the cyclic hydroperoxide **(b)**, is an excellent explanation for the decrease of diffusivity and adsorption capacity of aromatic compounds in TS-1 and Ti-MOR, which is caused by the contemporary presence of water and hydrogen peroxide and is linearly proportional to the content of Ti [160]. A more detailed discussion of these and other issues concerning active species **(a)–(c)** of Figure 2.6 is in an earlier review [6].

Besides Ti−OOH, whatever its structure might be, the chemistry of soluble metal peroxides suggests that other Ti peroxides with a different catalytic activity would exist in an equilibrium sensitive to acid and basic adsorbates [133, 196]. Actually, the gradual addition of basic compounds initially moderates the acidity of Ti−OOH, with a reduction of solvolysis during epoxidation, then produces increasing inhibition and eventually complete deactivation, by the formation of catalytically inert anionic peroxides (ammoximation is an exception) (Scheme 2.7). Owing to the equilibrium nature of their formation, any attempt to prepare in a pure state anionic TS-1 peroxides failed. Obtained in an impure form, they were catalytically inert, becoming stoichiometric oxidants and active catalysts again on neutralization of basicity with protonic acids [212].

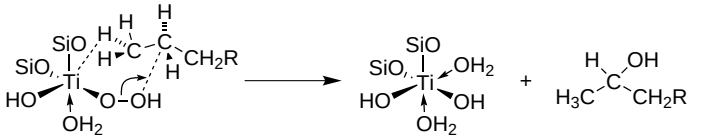


SCHEME 2.7 Acid–base equilibria of Ti−OOH species.

2.4.2 Hydroxylation

There are four mechanistic proposals, each one differing from the others for the active species and the mode of C−H activation. The first one, envisaging H-abstraction by diradical $Ti^{(III)}-OO^{\bullet}$, falls short for depending on $Ti(\eta^2-O_2)$ as the active species and the cleavage of the Ti−O bond in the latter instead of the weaker peroxidic one [132]. Also homolytic is the mechanism proposed by Khouw et al., entailing the anionic form of Ti−OOH for the hydroxylation step. This is in contrast with the inhibition of basic additives, while the link between the anionic nature of $Ti-OO^{-}$ and homolytic H-abstraction is not immediately clear [135].

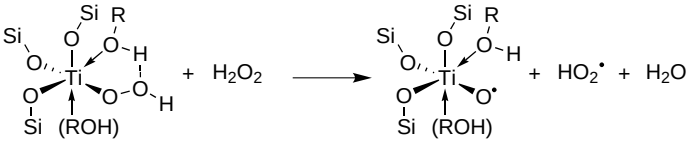
The concerted mechanism of Gallot et al. develops upon an agostic bond (a three-center M···H−C bond) that would anchor the alkane to Ti, through a terminal C−H, in a cyclic transition state ending with the hydroxylation of a methylene group (Scheme 2.8) [137, 139]. The frequent examples of internal agostic bonds in metal alkyl and other organometallic complexes seems to support such a concerted mechanism, particularly if the relatively high concentration of alkane molecules in the pore of TS-1 and the host–guest interactions therein that might force methyl groups close to Ti are also considered. However, this kind of metal-hydrogen bond with free alkanes, lacking in the entropic advantage of being tethered to a strongly bonded ligand, has very limited stability, having rarely been detected and with genuine examples still missing in isolated crystalline complexes [388–390]. Moreover, under the conditions selected by the authors for their tests, the alcohol products in the aqueous phase, which is in contact with the catalyst, can have an even larger concentration than the parent alkane, so as to compete favorably with it for adsorption in the pores and then even more, through the OH-group, on oxophilic Ti [137]. Based on kinetic and theoretical evidences, coordination on Ti site could be excluded, indeed, even for the olefins with their better donating double bond [205, 376].



SCHEME 2.8 Hydroxylation of saturated C−H bonds assisted by a Ti···H−C agostic bond.

Direct experimental evidences (Section 2.3.1.1) and several points of contact with biomimetic and mono-oxygenase catalysts inspired a fourth mechanistic proposal. This entails $Ti^{IV}-O^{\bullet}$ as the active species, after $Fe^{III}-O^{\bullet}$ of aprotic $Fe^{II}/H_2O_2/CH_3CN$ system and $Fe^{IV}-O^{\bullet}$ of P450 and MMO types of enzymes and biomimetic systems [6, 200, 373]. Such an atypical $Ti^{IV}-O^{\bullet}$ radical had no precedents for Ti, but could find support in the $V^{V}-O^{\bullet}$ radical, reputed by Bonchio et al. to be the true hydroxylation species of benzene by $VO(\eta^2-O_2)(H_2O)_2L$, (L = picolinic acid) [391].

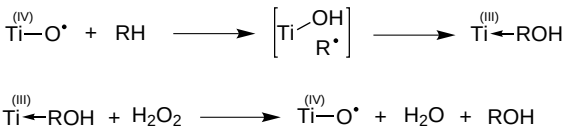
In the proposed mechanism, $Ti^{IV}-O^{\bullet}$ is generated by the one-electron reduction of Ti−OOH by a second H_2O_2 molecule, either physisorbed in the pores or coordinated on Ti (Eq. 2.22). The alternative between η^1 and η^2 Ti hydroperoxides is a question that does not change the spirit of the proposal.



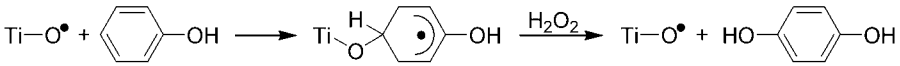
(2.22)

Hydroxylation occurs by an oxygen-rebound mechanism, after that originally proposed by Groves and van der Puy for hydroxylations with Fe^{II}/H_2O_2 in CH_3CN (Scheme 2.9. Only bonds and species participating in the process are shown in these and the following structures). The primary isotope effect in the range 4.1–4.7 suggests that H-abstraction is the rate-determining step, followed by the fast recombination of $R^{\bullet}$ radical finally introducing the hydroxy group in the alkyl chain. The chemisorption of hydrogen peroxide on Ti^{III}, following desorption of the product, re-forms the active species. The generation of a Ti-bound radical, namely $Ti^{IV}-O^{\bullet}$, instead of Ti^{IV} and free $^{\bullet}OH$ as normally observed for the one-electron oxidation of low valent metal ions with H_2O_2 in water, corresponds to the generation of $Fe^{III}-O^{\bullet}$ from Fe^{II}/H_2O_2 in aprotic media [147, 392, 393]. A parallel is apparent between the intraporous volume of TS-1 and $Fe^{II}/H_2O_2/CH_3CN$, both characterized by the reduced presence of protic species. Similarities exist also with MMO, whose active species $Fe^{IV}-O^{\bullet}$ forms in a hydrophobic pocket of the enzyme [130].

The mechanism is able to explain the effect of basic additives, as far as a Ti−OOH hydroperoxide is the precursor of $Ti^{IV}-O^{\bullet}$, the behavior of radical quenchers (too short a lifetime of $R^{\bullet}$ radical), and that of probe molecules



SCHEME 2.9 Hydroxylation of saturated C−H bond by a rebound mechanism based on $Ti^{IV}-O^{\bullet}$.



SCHEME 2.10 Hydroxylation of phenol involving $Ti^{IV}-O^{\bullet}$ as active species.

(Section 2.3.1.1). $Ti^{IV}-O^{\bullet}$ active species also fully accounts for the competition of hydrogen peroxide dismutation, an inseparable companion of hydroxylation. Recent theoretical studies on Ti-substituted polyoxometalates and molecular sieves support the existence of $Ti^{IV}-O^{\bullet}$ species and the energetically feasibility of its formation by the reaction of Ti−OOH with a H_2O_2 molecule (Eq. 2.22) [384, 394].

$Ti-O_2^{\bullet}$ superoxide has been sometimes proposed for C−H hydroxylation [7]. To early arguments, once opposed to such a mechanism [6], a recent EPR study adds with clear experimental evidences showing that the decay rate of $Ti-O_2^{\bullet}$ remains unaffected by the presence of propane [395]. This study also enables ruling out any $Ti-O_2^{\bullet}$/TiOOH interconversion claimed in the past [7].

Aromatic C−H hydroxylation has not been the subject of detailed studies, although Wilkenhöner et al. proposed for phenol concerted mechanisms based on Ti−OOH, with *o*- and *p*-hydroxylation occurring by substantially different routes [171]. $Ti^{IV}-O^{\bullet}$ offers the opportunity of an alternative mechanistic hypothesis, of homolytic nature as shown by Scheme 2.10 for the *p*-hydroxylation of phenol [6, 373]. The mechanism for *o*-positions and for benzene would be similar.

2.4.3 Epoxidation

Distinctive features of TS-1, such as the quantitative yields (including glycols), the absence of allylic products and the retention of configuration of *cis*- and *trans*-olefins, are only consistent with a heterolytic mechanism. Quite similar evidences lead to the same conclusion for large pore Ti zeolites. Proposing $Ti^{IV}-O^{\bullet}$ and even more superoxide $Ti-O_2^{\bullet}$ is unrealistic and the conclusion to draw is that different active species, one operating homolytically and the other heterolytically, are active in the oxidation of alkanes and olefins, respectively. Allylic products, sometimes detectable when epoxidation is so slow to become comparable to side reactions, imply a different explanation (see Section 2.4.7).

Ti−OOH, after the original proposal of the early 1990s, has been generally recognized as the active species [133, 196]. However, different epoxidation mechanisms exist in the literature, reflecting the disagreement on its fine structure. Most credited ones bear similarities with those of peracids and of organic hydroperoxides (Figure 2.7).

The first mechanism pivots upon the cyclic hydroperoxide of Figure 2.6**b**, formed by the reversible adsorption of both hydrogen peroxide and a water or alcohol molecule on Ti [6, 196]. The nucleophilic attack of the double bond on the peroxo oxygen vicinal to Ti leads to the irreversible formation of epoxide, alkoxide and water products, adsorbed on Ti. The desorption of the epoxide and the reaction

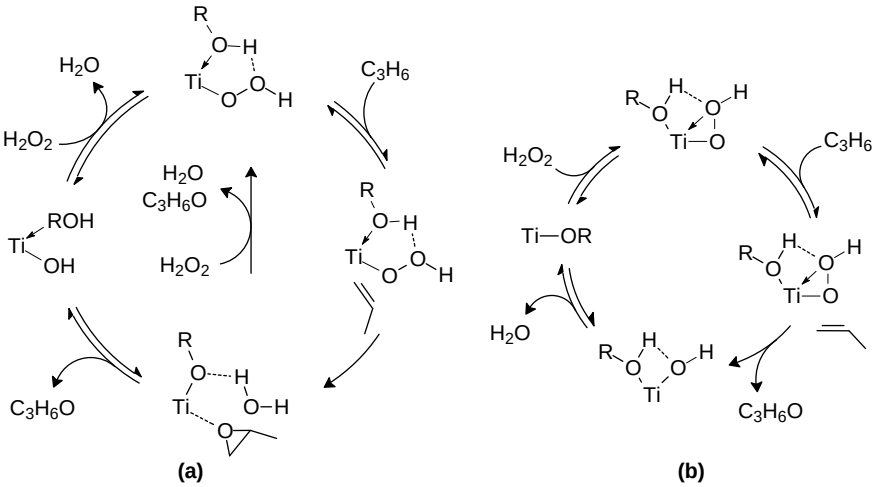


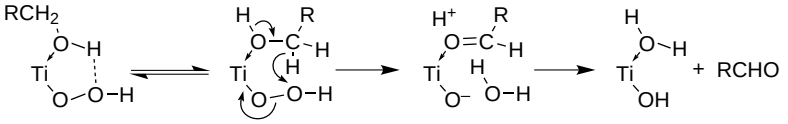
FIGURE 2.7 Epoxidation mechanisms centered on species **(b)** and **(c)** of Figure 2.6.

of Ti alkoxide with water remove an inhibitor and restore the initial Ti site, respectively, completing the catalytic cycle. As an alternative, H_2O_2 could chemisorb on Ti alkoxide to regenerate the oxidant species directly. The peracid-like mechanism, initially proposed in two options on chemical grounds, achieved its definitive profile by the contribution of early DFT calculations [381].

The second mechanism, based on Ti(η^2−OOH), has its point of strength in the distal OH being already coordinated on Ti, so that little atom motion is required in the epoxidation step (Figure 2.7**b**) [376]. Variants of this mechanism, albeit based on the same η^2-bonded hydroperoxide, can differ significantly in the energetics and the details of the epoxidation process [375, 378, 379]. Assistance of a vicinal silanol nest to the oxygen transfer is envisaged, for instance, in a recent proposal with species **d** of Figure 2.6, which, however, predicts the formation of the active species as the slow step of epoxidation, quite in contrast to experimental evidences [380].

2.4.4 Oxidation of Alcohols

The oxidation mechanism, originally proposed by Maspero and Romano based on kinetic evidences, envisages a concerted mechanism in which a α-C−H bond undergoes H-abstraction by distal oxygen of Ti−OOH (Scheme 2.11) [139, 298, 299].



SCHEME 2.11 Oxidation mechanism proposed for alcohols.

The preliminary step is the rearrangement of cyclic hydroperoxide, pushing the C−H bond vicinal to the OH group. Protic compounds, including water, compete with the alcohol substrate for adsorption on active sites, so that different Ti(η^1−OOH)(ROH) species may exist in equilibrium. Such a competitive adsorption accounts nicely for the inhibition shown by water in the oxidation of cyclohexanol in acetonitrile solvent [228].

2.4.5 Ammoximation

Central to the ammoximation mechanism is the generation of hydroxylamine, whereas subsequent condensation with the carbonyl group occurs by a conventional pathway (Eq. 2.16). Particularly useful, to this end, were spectroscopic studies carried out *in situ* by the Zecchina group on TS-1 [324]. The same mechanism is believed to hold also for Ti-MWW and Ti-MOR, owing to a similar catalytic behavior [319, 320].

The basicity of the medium drives the chemisorption of hydrogen peroxide towards the formation of anionic Ti(η^2−O_2)$^-$ species, with two molecules of water and ammonia completing the coordination sphere of Ti (Figure 2.8). An important issue that spectroscopic studies do not help to solve is whether hydroxylamine forms by an intramolecular reaction between chemisorbed species or by an external attack of physisorbed ammonia. According to a recent kinetic study, the second pathway appears to be more likely [326]. A further issue concerns the nature of the active species, whether this is Ti−OOH or Ti(η^2−O_2)$^-$ anion. The basic medium, indeed, should shift the acid–base equilibrium towards the formation of Ti(η^2−O_2)$^-$, but the presence of a minor fraction of Ti−OOH cannot be *a priori* ruled out and its greater electrophilicity could compensate for a lower site population.

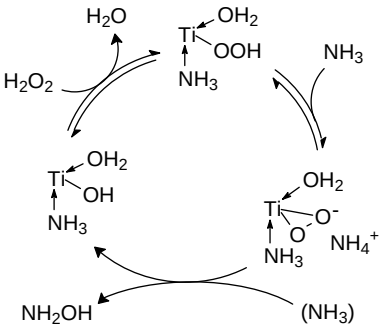


FIGURE 2.8 Ammoximation mechanism.

2.4.6 Decomposition of Hydrogen Peroxide

The mode in which hydrogen peroxide decomposes has not attracted so much interest, except for a kinetic study and occasional tests that did not persist later [138]. A mechanism, however, was inspired by the proposal of $Ti^{IV}-O^{\bullet}$ species and, according to this, dismutation initiates with the oxidation of hydrogen peroxide by Ti−OOH hydroperoxide to $HO_2^{\bullet}$ (Eq. 2.22) [6, 373]. This can evolve to molecular oxygen by different pathways, e.g., by the interaction with surface species, including same $Ti^{IV}-O^{\bullet}$ (Eq. 2.23). $Ti^{IV}-O^{\bullet}$ in turn may further contribute to dismutation by the attack of hydrogen peroxide, a reaction that enters into competition with C−H hydroxylation if an alkane is present (Eq. 2.24 and Scheme 2.9) [6, 396]. The decomposition mechanism initiated by Eq. 2.22 has been recently extended by Yoon et al. to Ti-SBA-15 and shown to be energetically feasible [384].

$$Ti-O^{\bullet} + HO_2^{\bullet} \longrightarrow Ti-OH + O_2 \qquad (2.23)$$

$$Ti-O^{\bullet} + H_2O_2 \longrightarrow Ti-OH + HO_2^{\bullet} \qquad (2.24)$$

$$Ti-OH + HO_2^{\bullet} \longrightarrow Ti-O_2^{\bullet} + H_2O \qquad (2.25)$$

$Ti-O_2^{\bullet}$ superoxide, normally detected on addition of hydrogen peroxide to TS-1, could be a side product of hydrogen peroxide decomposition, through the reaction of lattice titanols with mildly acidic $HO_2^{\bullet}$ radical (Eq. 2.25) [373, 397]. A recent study supports such a pathway, in that it shows the production of $Ti-O_2^{\bullet}$ is reduced to *ca.* one third by the addition of propane [395]. Actually, the competition of the alkane for $Ti^{IV}-O^{\bullet}$ also implies a reduction of $HO_2^{\bullet}$ production (Scheme 2.9 and Eqs. 2.24 and 2.25).

2.4.7 Active Species, Adsorption and Catalytic Activity

Different active species and different mechanisms appear to be operative in Ti zeolites, though interrelated through a common Ti−OOH hydroperoxide. This is the oxidant species of olefins, alcohols and hydrogen peroxide and is the acidic catalyst responsible for solvolysis during epoxidation by Al-free TS-1. It is also the precursor of a radical species, probably Ti^{IV}–$O^{\bullet}$, active in the hydroxylation of C−H bonds and the decomposition of hydrogen peroxide, and of the anion $Ti(\eta^2-O_2)^-$ involved in the oxidation of ammonia to hydroxylamine. Descending all active species from a common origin, it is a reasonable hypothesis that a network of competing oxidations operates in Ti zeolites and that factors such as the kind of substrate, the kind of solvent, reaction conditions and surface properties, determine the relative weight of one reaction path over others. In fact, any oxidation on Ti zeolites is accompanied, to a variable degree, by other reactions that become negligible only under favorable conditions. A notable case is the epoxidation of olefins, which in most cases is so fast as to hide any other competitor. Figure 2.9 is a summary, in a simplified form, of active species and oxidation pathways, based upon the cyclic Ti η^1-hydroperoxide. Analogous schemes can be developed upon other Ti−OOH structures.

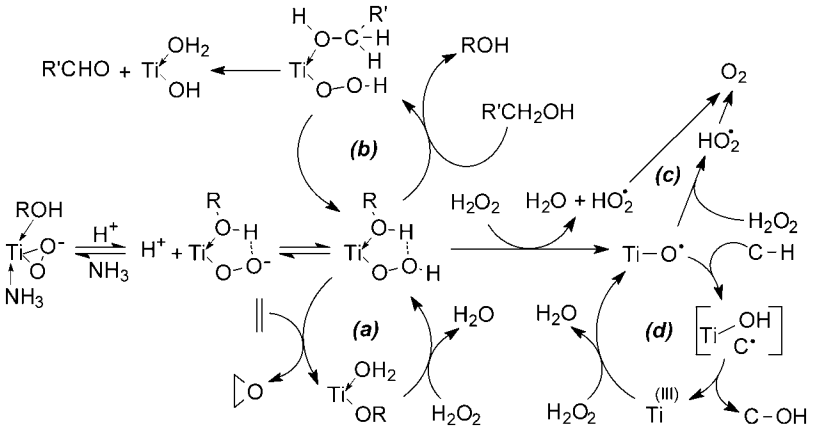


FIGURE 2.9 Summary of active species and competing oxidation pathways on Ti sites.

Unhindered olefins are the most active substrates, undergoing fast epoxidation by Ti−OOH species even at temperatures below room temperature (path ***a***). Alcohols and hydrogen peroxide appear to react much slower and, if methanol is the solvent and TS-1 the catalyst, the epoxidation yield (including glycols) is practically quantitative. The oxidation of the solvent, however, becomes no longer negligible if less inert alcohols, like ethanol and isopropanol, are used and even with methanol methyl formate may be noticeable in the epoxidation of propylene. The acid–base equilibrium of Ti−OOH is controlled by the addition of basic compounds, to minimize solvolysis. With TS-1, the oxidation of allylic C−H is untraceable and the decomposition of hydrogen peroxide is negligible, since the competition of the olefin for Ti−OOH prevails over that of hydrogen peroxide leading to $Ti^{IV}-O^{\bullet}$ species.

With sterically hindered olefins or less active Ti zeolites, necessitating higher temperatures and longer contact times, the competition of methanol (path ***b***) and hydrogen peroxide for Ti−OOH can grow significantly. Oxygen evolution and allylic products (paths ***c*** and ***d***) can be no longer negligible, to the point that with the least reactive olefins these prevail over epoxidation. Several examples are apparent in the literature, even with TS-1.

Analogous arguments as for olefins hold for alcohol substrates. Their oxidation still prevails over that of hydrogen peroxide, but to a lesser degree than in epoxidation as shown by lower hydrogen peroxide efficiencies. With the increase of steric hindrance around the alcohol group or with less active catalysts, competing oxidations increase similarly as for the olefins.

In the absence of an organic substrate or when the latter is an alkane, which are most inert to Ti−OOH, the only feasible reaction is that with hydrogen peroxide. The new oxidant species, $Ti^{IV}-O^{\bullet}$, is able to hydroxylate C−H bonds and promote the decomposition of hydrogen peroxide homolytically, with kinetics of comparable magnitude. In fact, H_2O_2 decomposition is constantly present in the

hydroxylation of alkanes, being significant even in the fastest one observed on TS-1, namely, the hydroxylation of *n*-hexane. With the least reactive alkanes, e.g., with bulky ones, the decomposition of H_2O_2 is normally the main or sole reaction.

However, the relative weight of oxidation pathways of Figure 2.9 is not only related to the nature of reagents but also to their partition coefficients or, in more general terms, not only to the relative reactivity of substrates but also to their relative concentration in the pores. Thus, a factor even more relevant for the direction of oxidation is adsorption, governed in turn by the properties of both the surface and the solvent. For instance, at a fixed composition of the external medium, both the H_2O_2 to organic substrate and the H_2O to organic substrate ratios increase with the hydrophilicity of surface in the order, TS-1 < Ti-β < Ti,Al-β ≪ Ti-MCM-41, and in a similar trend should also increase the competition of H_2O_2 for Ti−OOH, leading to the generation of $Ti^{IV}-O^{\bullet}$ radical species. Allylic oxidation of olefins (path ***d***) and H_2O_2 decomposition (path ***c***) increase accordingly, at the expense of the selectivity of epoxidation or alcohol oxidation (paths ***a, b***). Actually, epoxidation is generally slower and less selective on relatively hydrophilic Ti-Beta than on TS-1 and, within Ti-Beta materials, on Ti,Al-β and Ti-β(OH^-) than on Ti-β(F^-), becoming negligible on mesoporous Ti silicates. The faster kinetics and selectivities of Ti zeolites with hydrogen peroxide in polar media and of Ti/SiO_2 with organic hydroperoxides in apolar ones have a similar explanation, being the result of the synergic role of surface and solvent on adsorption. Actually, the relative affinity of the olefin for the pores and the solvent determines its partition between the two phases, with polar solvents favoring the adsorption in hydrophobic pores and the opposite occurring with apolar ones. Less investigated is the adsorption–solvent relationship for Ti-MWW, but the decomposition of hydrogen peroxide is often significant in its epoxidations.

Analogous considerations, for the effect of surface and solvent, apply even more to the slower C−H hydroxylation. Actually, only a few alkanes are oxidized with relatively good selectivity on TS-1, while their hydroxylation on large pore zeolites is merely an exception. At odds with the above rule on solvent polarity are the performances observed in *t*-butanol for the hydroxylation of *n*-hexane on TS-1, which is significantly better than in methanol. This observation could be a prelude to a further effect of the solvent, such as an interaction with oxidation intermediates [373].

Experimental procedures also influence the relative incidence of oxidation pathways, in that they affect the adsorption extent of the reagents. Normally, an excess of substrate over the oxidant and the gradual addition of the latter, in a procedure that maximizes their ratio in the pores, augments the selectivity.

The above discussion links the different performances of Ti zeolites with a surface effect on the adsorption of the reagents, with the implicit assumption of a substantially similar activity of active sites. Actually, the evidences from characterization and theoretical studies lead to the conclusion that such an assumption is largely correct, since some differences in the structure of Ti sites may exist, but not to the point to modify significantly their catalytic activity. The hydrolytic opening of one Ti−OSi bond probably tends to reduce under reaction conditions structural dissimilarities.

2.5 STABILITY OF METAL-SUBSTITUTED ZEOLITES TO REACTION CONDITIONS

The decay of catalytic activity in metal zeolites is normally due to three reasons: pore plugging, metal leaching and structural degradation. The first kind of deactivation can be relatively fast, owing to molecular dimensions of pores and relatively low temperatures, both favoring the retention of the products with their further transformation. Generally, the answer is in the use of nanosized catalysts and continuous-flow operation. Specific to epoxidation is the feeding of a basic additive to moderate the acidity of Ti−OOH and of adventitious Al sites that, besides causing a loss of the product, also catalyze the formation of polyether compounds [19, 85, 146, 248, 257]. With a side stream of ammonia solution, the epoxidation of propylene could be operated uninterruptedly for several hundred hours with negligible deactivation, while a few tens of hours could be sufficient for a drop of activity in the absence of basic additives [146, 248, 257]. The use of alkali-metal salts is also an option though less effective than ammonia or sodium acetate [85, 146].

Thermal regeneration in an oxidizing atmosphere is the usual way to restore the initial activity of spent catalysts. Alternative methods, proposed for the epoxidation of propylene, envisage milder treatments with either a dilute solution of hydrogen peroxide or just with methanol at around 100 °C, and with steam at 300 °C [19, 257]. The optimum regeneration was claimed by a first treatment with air or hydrogen peroxide, followed by a second one with steam. Reportedly, steaming prevented the selectivity of the regenerated catalyst from being initially low [257].

Metal leaching is a potential drawback of most metal-oxide catalysts used in liquid phase oxidation. Though metal zeolites are no exception in this regard, the possibility of leaching is underestimated or merely ignored in most studies. Its incidence depends on different factors, e.g., the kind of metal and zeolite, the presence of hydrogen peroxide, and the formation of chelating products. Normally, Ti siting is stable in MFI and other zeolitic structures, under most conditions. A negligible leaching, probably of loosely bonded species, could be observed at the very beginning of oxidations carried out continuously [212]. It becomes, however, a major problem for other metal zeolites, e.g., Cr, V, Fe, and Sn zeolites, with the chance that homogeneous catalytic pathways overlap and even prevail over heterogeneous ones [398]. Detailed studies carried out on Cr-substituted molecular sieves showed that the tiny fraction of leached metal species, corresponding to 1–2 ppm Cr in the solution, was sufficient to account for the observed catalytic performances. Oxidations also with bulky *t*-butyl hydroperoxide attributed to VS-1 and VS-2 were likely the fruit of homogeneous V species.

There are substances, such as hydrogen peroxide and chelating products, which favor the instability of metal siting in the lattice. Actually, the only example known of Ti leaching from TS-1, namely, in the epoxidation of crotyl alcohol, was determined by the combination of both factors, whereas each one alone was harmless [269]. Apparently, the chelating strength of 1,2,3-trihydroxy butane, combined with the formation of soluble Ti peroxides, could prevail over the usual stability of Ti–OSi bonds in MFI lattice. Leaching in the same oxidation was much greater for

other Ti catalysts, increasing in the order TS-1 < Ti,Al-β < Ti-MCM-41 < Ti-xerogel, with a clear correlation between leaching and surface defectivity. For Ti, Al-β the presence of hydrogen peroxide alone was sufficient for Ti leaching to occur. The loss of Ti was more pronounced under continuous-flow operation, suggesting a reversible exchange of species between surface and solution. A special case is that of Ti-MWW, from which the leaching of B can occur, albeit this is irrelevant for oxidation activity [237, 280].

Sheldon showed that the usual method of repeated catalytic tests with the recycled solid to verify the loss of activity is inadequate to exclude metal leaching and assess the heterogeneity of catalysis [398]. The best approach to the problem is interrupting the reaction at a significant stage of advancement, filtrating the solution while still hot and continuing oxidation with the filtered solution alone to test its activity. Hot filtration was indispensable to avoid the readsorption of solubilized Cr species on cooling. It also prevented the reduction of the metal to a lower oxidation state during cooling and consequent misinterpretation of a possible induction period due to reoxidation in a subsequent control test.

Lattice degradation, by aggressive reagents, is the third cause of instability. It is paradigmatic that there is lattice dissolution during ammoximation, originally observed for TS-1 and subsequently for Ti-MWW and Ti-MOR as well [189, 310, 322]. The silica framework slowly dissolves in the basic medium, while Ti tends to aggregate into TiO_2 particles dispersed on residual crystallites. The addition of a silica source in the ammoximation medium has been claimed to slow the phenomenon and increase the lifetime of the catalyst [321, 322]. A partial regeneration of the structure was envisaged for Ti-MWW by the treatment of the spent catalyst with the structure-directing agent piperidine [322].

A partial degradation of the framework was observed for Ti,Al-Beta and Ti-Beta (OH^-) put in contact with aqueous hydrogen peroxide [399]. It is likely that this kind of structural instability is associated with the presence of connectivity defects and, as such, indirectly related to the kind of synthesis (Section 2.2.4). It is known that the fluoride method allows production of less defective and, presumably, more stable materials.

2.6 CONCLUSIONS

Three decades of intense activity by experimental and theoretical studies have produced enormous progress in the knowledge of TS-1 and other metal zeolites. The basic principles, like the isomorphous substitution of Ti, the formation of Ti−OOH species on chemisorption of hydrogen peroxide, its better oxidizing power than Ti(η^2-O_2) peroxide and the heterolytic nature of epoxidation mechanism are now widely recognized. Even early structural disagreement seems to be settling, on consideration of recent computational studies showing little energetic differences between side-on Ti(η^2-OOH) and cyclic end-on-bonded Ti(η^1-OOH)(ROH) peroxy species. New ideas are emerging, like the nonrandom siting of Ti in TS-1, evidenced by neutron diffraction studies, the generation of mesoporosity and the

synthesis of TS-1 in the form of nanosheets. Reaction mechanisms, on the other hand, are substantially the same as those of the 1990s, with a partial exception for recent evidences in support of $Ti^{IV}-O^{\bullet}$ species, which is active in C−H hydroxylation and hydrogen peroxide decomposition.

The search for alternatives to TS-1 seems to focus on Ti-MWW and related materials and, maybe, on Ti-MOR. Other metal zeolites generally prove less effective for catalytic oxidations and/or less stable to leaching, with the notable exception of Sn-Beta zeolite that was shown to be effective for Baeyer–Villiger oxidations. Currently, however, metal zeolites that could challenge the primacy of TS-1 are not in view. Actually, TS-1 is unique in that combines at best a series of favorable factors, i.e. the effectiveness of active species, the framework stability of Ti, the hydrophobicity of the surface and the size of the pores in the range of molecular dimensions. Thanks to the last two properties, the heats of adsorption of linear hydrocarbons are high enough to make their oxidation feasible at near temperature, even with water present in the reaction medium. The little or no activity of other titanium zeolites in the hydroxylation of alkanes actually finds its first explanation in a reduced efficacy of the pores for the adsorption of apolar molecules.

Where the achievements are most impressive is in the area of industrial applications in which several processes have become operative in last decade, going well beyond initial hopes aroused by the first discovery. In effect, the catalytic performances of TS-1 appeared immediately to be outstanding for several oxidations of potential interest to the chemical industry, but their dependency on hydrogen peroxide was felt as a major obstacle on the way to commercialization. Currently, a large fraction of world capacity of propylene oxide (*ca.* 8%) and a significant portion of cyclohexanone oxime relies on TS-1 and hydrogen peroxide, not to mention the relatively modest production of hydroquinone and catechol operative from the early years. Moreover, the interest for both cheaper methods of synthesis of the catalyst and the generation of mesoporosity in the large crystals so obtained, together with the efforts to develop direct routes to hydrogen peroxide, may be a prelude to further developments. It is worthy of note, in this regard, that other Ti zeolites, namely Ti-MWW and Ti-MOR, apparently attract a certain interest particularly for the ammoximation of cyclohexanone. It is possible that other industrial processes, based on current research efforts worldwide, will add to the hydroxylation of phenol, the ammoximation of cyclohexanone and the epoxidation of propylene in the foreseeable future.

ACKNOWLEDGMENTS

The authors are most grateful to collaborators and colleagues whose names appear in the references. M.G.C. whishes to thank Mr. G. Piccoli (epoxidation, hydroxylation), Mr. B. Anfossi (epoxidation) and Mr. A. D'Alfonso (continuous-flow epoxidation) for their skilled assistance over several years. M.E.D. also thanks Ms. S. Valencia (Beta zeolites synthesis) for her valuable assistance.

REFERENCES

1. Taramasso M., Perego G., Notari B. inventors; Snamprogetti S.p.A. assignee. US Patent 4,410,501. 1983.
2. Perego G., Bellussi G., Corno C., Taramasso M., Buonomo F., Esposito A. In: *New Developments in Zeolite Science and Technology. Proceed. 7th Zeol. Conf*. Murakami Y., Iijima A., Ward J.M. eds. Kodansha, Tokyo, 1986, pp. 129–136.
3. Notari B. (1988). *Stud. Surf. Sci. Catal.* 37, 413–425.
4. Romano U., Esposito A., Maspero F., Neri C., Clerici M.G. (1990). *Stud. Surf. Sci. Catal.* 55, 33–41; and *Chim. Ind. (Milan)* 72, 610–616.
5. Notari B. In: *Advances in Catalysis*, Vol. 41. Eley D.D., Haag W.O., Gates B.C., eds. Academic Press, San Diego, 1996, pp. 253–334.
6. Clerici M.G. In: *Metal Oxide Catalysis*, Vol. 2. Jackson S.D., Hargreaves J.S.J., eds. Wiley-VCH, Weinheim, 2009, pp. 705–749.
7. Ratnasamy P., Srinivas D., Knözinger P. In: *Advances in Catalysis*, Vol. 48. Gates B.C., Knözinger H., eds. Elsevier - Academic Press, Amsterdam, 2004, pp. 1–169.
8. Barrer R.M. *Hydrothermal Chemistry of Zeolites*. Academic Press, London, 1982.
9. Rabo J.A., Schoonover M.W. (2001). *Appl. Catal. A: General* 222, 261–275.
10. Burton A.W., Zones S.I. (2007). *Stud. Surf. Sci. Catal.* 168, 137–179.
11. Flanigen E.M., Bennett J.M., Grose R.W., Cohen J.P., Patton R.L., Kirchner R.M., Smith J.V. (1978). *Nature* 271, 512–516.
12. Guth J.L., Kessler H., Higel J.M., Lamblin J.M., Patarin J., Seive A., Chezeau J.M., Wey R. In: *Zeolites Synthesis*. Occelli M.L., Robson H.E., eds. ACS Symp. Series 398. American Chemical Society, Washington, DC, 1989, pp. 176–195.
13. Guth J.L., Caullet P. (1986). *J. Chim. Phys.* 83, 155–175.
14. Chen C.-Y., Zones S. I. In: *Zeolites and Catalysis. Synthesis, Reactions and Applications*, Vol. 1. Čějka J., Corma A., Zones S., eds. Elsevier, Amsterdam, 2010, pp. 155–170.
15. Perego G., Millini R., Bellussi G., In: *Molecular Sieves - Science and Technology*, Vol. I. Karge H.G., Weitkamp J., eds. Springer-Verlag, Heidelberg, 1998, pp. 187–228.
16. Tatsumi T. In: *Zeolites and Catalysis. Synthesis, Reactions and Applications*. Vol. 2 Čějka J., Corma A., Zones S., eds. Elsevier, Amsterdam, 2010, pp. 713–743.
17. Bordiga S., Damin A., Bonino F., Lamberti C. In: *Surface and Interfacial Organometallic Chemistry and Catalysis*. Topics Organomet. Chem., Vol. 16. Copéret C., Chaudret B., eds. Springer-Verlag, Heidelberg, 2005, pp. 37–68.
18. Baerlocher Ch., McCusker L.B., Olson D.H. *Atlas of Zeolite Framework Types*, 6th edn. Elsevier, Amsterdam, 2007.
19. Clerici M.G., Bellussi G., Romano U. (1991). *J. Catal.* 129, 159–167.
20. Millini R., Previde Massara E., Perego G., Bellussi G. (1992). *J. Catal.* 137, 497–503.
21. Thangaraj A., Sivasanker S. (1992). *J. Chem. Soc., Chem. Commun.*, 123–124.
22. Schuchardt U., Pastore H.O. Spinacé E.V. (1994). *Stud. Surf. Sci. Catal.* 84, 1877–1882.
23. Fan W., Duan R.G., Yokoi T., Wu P., Kubota Y., Tatsumi T. (2008). *J. Am. Chem. Soc.* 130, 10150–10164.

24. Fan W., Fan B., Shen X., Li J., Wu P., Kubota Y., Tatsumi T. (2009). *Micropor. Mesopor. Mater.* 122, 301–308.
25. Su J., Xiong G., Zhou J., Liu W., Zhou D., Wang G., Wang X., Guo H. (2012). *J. Catal.* 288, 1–7.
26. Khomane R.B., Kulkarni B.D., Paraskar A., Sainkar S.R. (2002). *Mater. Chem. Phys.* 76, 99–103.
27. Liu H., Lu G., Hu H. (2006). *Mater. Chem. Phys.* 100, 162–167.
28. Tuel A., Ben Taarit Y. (1993). *Micropor. Mater.* 1, 179–189.
29. Tuel A., Ben Taarit Y., Naccache C. (1993). *Zeolites* 13, 454–461.
30. Müller U., Steck W. (1994). *Stud. Surf. Sci. Catal.* 84, 203–210.
31. Tuel A. (1996). *Zeolites* 16, 108–117.
32. Shibata M., Gabelica Z. (1997). *Zeolites* 19, 246–252.
33. Li G., Guo X., Wang X., Qi Z., Bao X., Han X., Lin L. (1999). *Appl. Catal. A: General* 185, 11–18.
34. Zhang H.J., Liu Y.M., Jiao Z., He M.Y., Wu P. (2009). *Ind. Eng. Chem. Res.* 48, 4334–4339.
35. Vasile A., Busuioc-Tomoiaga A.M. (2012). *Mater. Res. Bull.* 47, 35–41.
36. Gao H., Suo J., Li S. (1995). *J. Chem. Soc., Chem. Commun.*, 835–836.
37. Liu H., Lu G.Z., Guo Y.L., Guo Y. (2005). *Appl. Catal. A: General* 293, 153–161.
38. Uguina M.A., Ovejero G., Van Grieken R., Serrano D.P., Camacho M. (1994). *J. Chem. Soc., Chem. Commun.*, 27–28.
39. Kraushaar-Czarnetzki B., van Hoof J.H.C. (1998). *Catal. Lett.* 1, 81–84.
40. Schmidt I., Krogh A., Wienberg K., Carlsson A., Brorson M., Jacobsen C.J.H. (2000). *Chem. Commun.*, 2157–2158.
41. Janssen A.H., Schmidt I., Jacobsen C.J.H., Koster A.J., de Jong K.P. (2003). *Micropor. Mesopor. Mater.* 65, 59–75.
42. Kustova M.Y., Hasselriis P., Christensen C.H. (2004). *Catal. Lett.* 96, 205–211.
43. Xin H.C., Zhao J., Xu S.T, Li J.P., Zhang W.P., Guo X.W., Hensen E.J.M, Yang Q.H., Li C. (2010). *J. Phys. Chem. C* 114, 6553–6559.
44. Serrano D., Sanz R., Pizarro P., Moreno I. (2009). *Chem. Commun.*, 1407–1409.
45. Cheneviere Y., Chieux F., Caps V., Tuel A. (2010). *J. Catal.* 269, 161–168.
46. Ke X.B, Xu L., Zeng C.F, Zhang L.X., Xu N.P. (2007). *Micropor. Mesopor. Mater.* 106, 68–75.
47. Tao H., Li C., Ren J., Wang Y., Lu G. (2011). *J. Solid State Chem.* 184, 1820–1827.
48. Na K., Changbum Jo C., Kim J., Ahn W.-S., Ryoo R. (2011). *ACS Catal.* 1, 901–907.
49. Wang J., Xu L., Zhang K., Peng H., Wu H., Jiang J., Liu Y., Wu P. (2012). *J. Catal.* 288, 16–23.
50. Hua Z.L., Zhou J., Shi J.L. (2011). *Chem. Commun.* 47, 10536–10547.
51. Wang Y., Lin M., Tuel A. (2007). *Micropor. Mesopor. Mater.* 102, 80–85.
52. Chao P.-Y., Tsai S.-T., Tsai T.-C., Mao J., Guo X.-W. (2009). *Top. Catal.* 52, 185–192.
53. Tsai S.-T., Chao P.-Y., Tsai T.-C., Wang I., Liu X., Guo X.-W. (2009). *Catal. Today* 148, 174–178.
54. Höft E., Kosslick H., Fricke R., Hamann H.J. (1996). *J. Prakt. Chem.* 338, 1–15.

55. Lamberti C., Bordiga S., Zecchina A., Artioli G., Marra G.L., Spanò G. (2001). *J. Am. Chem. Soc.* 123, 2204–2212.
56. Hijar C.A., Jacubinas R.M., Eckert J., Henson N.J., Hay P.J., Ott K.C. (2000). *J. Phys. Chem. B* 104, 12157–12164.
57. Henry P.F., Weller M.T., Wilson C.C. (2001). *J. Phys. Chem. B* 105, 7452–7458.
58. Bordiga S., Bonino F., Damin A., Lamberti C. (2007). *Phys. Chem. Chem. Phys.* 9, 4854–4878.
59. Flanigen E.M. In: *Zeolite Chemistry and Catalysis*. Rabo J.A., ed. ACS Monograph, Vol. 171. Washington, DC, 1976, pp. 80–117.
60. Boccuti M.R., Rao K.M., Zecchina A., Leofanti G., Petrini G. (1989). *Stud. Surf. Sci. Catal.* 48, 133–144.
61. Li C., Xiong G., Liu J.K., Ying P.L., Xin Q., Feng Z.C. (2001). *J. Phys. Chem. B* 105, 2993–2997.
62. Huybretchs D.R.C., Buskens P.L., Jacobs P.A. (1992). *J. Mol. Catal.* 71, 129–147.
63. Zecchina A., Spoto G., Bordiga S., Padovan M., Leofanti G., Petrini G. (1991). *Stud. Surf. Sci. Catal.* 65, 671–680.
64. Scarano D., Zecchina A., Bordiga S., Geobaldo F., Spoto G., Petrini G., Leofanti G., Padovan M., Tozzola G. (1993). *J. Chem. Soc., Faraday Trans. I* 89, 4123–4130.
65. Camblor M.A., Corma A., Perez-Pariente J. (1993). *J. Chem. Soc., Chem. Commun.*, 557–559.
66. Astorino E., Peri J.B., Willey R.J., Busca G. (1995). *J. Catal.* 157, 482–500.
67. Zecchina A., Bordiga S., Spoto G., Marchese L., Petrini G., Leofanti G., Padovan M. (1992). *J. Phys. Chem.* 96, 4991–4997.
68. Zecchina A., Spoto G., Bordiga S., Ferrero A., Petrini G., Leofanti G., Padovan M. (1991). *Stud. Surf. Sci. Catal.* 69, 251–258.
69. Bellussi G., Carati A., Clerici M.G., Esposito A. (1991). *Stud. Surf. Sci. Catal.* 63, 421–429.
70. Bordiga S., Damin A., Bonino F., Ricchiardi G., Zecchina A., Tagliapietra R., Lamberti C. (2003). *Phys. Chem. Chem. Phys.* 5, 4390–4393.
71. Huybrechts D.R.C., Vaesen I., Li H.X., Jacobs P.A. (1991). *Catal. Lett.* 8, 237–244.
72. Geobaldo F., Bordiga S., Zecchina A., Giamello E., Leofanti G., Petrini G. (1993). *Catal. Lett.* 16, 109–115.
73. Pei S., Zajac G.W., Kaduk J.A., Faber J., Boyanov B.I., Duck D., Fazzini D., Morrison T.I., Yang D.S. (1993). *Catal. Lett.* 21, 333–344.
74. Lopez A., Tuilier M.H., Guth J.L., Delmotte L., Popa J.M. (1993). *J. Solid State Chem.* 102, 480–491.
75. Bordiga S., Coluccia S., Lamberti S., Marchese L., Zecchina A., Boscherini F., Buffa F., Genoni F., Leofanti G., Petrini G., Vlaic G. (1994). *J. Phys. Chem.* 98, 4125–4132.
76. Gleeson D., Sankar G., Catlow C.R.A, Thomas J.M., Spanò G., Bordiga S., Zecchina A., Lamberti C. (2000). *Phys. Chem. Chem. Phys.* 2, 4812–4817.
77. Martens J.A., Buskens P.L., Jacobs P.A., van der Pol A., van Hooff J.H.C., Ferrini C., Kouwenhoven H.W., Kooyman P.J., van Bekkum H. (1993). *Appl. Catal. A: General* 99, 71–84.

78. Camblor M.A., Corma A., Martínez A., Pérez-Pariente J. (1992). *Chem. Commun.*, 589–590.
79. Camblor M.A., Corma A., Martínez A., Pérez-Pariente J. (1993). *Zeolites* 13, 82–87.
80. Van der Waal J.C., Rigutto M.S., van Bekkum H. (1994). *J. Chem. Soc., Chem. Commun.*, 1241–1242.
81. Camblor M.A., Constantini M., Corma A., Gilbert L., Esteve P., Martínez A., Valencia S. (1996). *Chem. Commun.*, 1339–1340.
82. Van der Waal J.C., Kooyman P.J., Jansen J.C., van Bekkum H. (1998). *Micropor. Mesopor. Mater.* 25, 43–57.
83. Blasco T., Camblor M.A., Corma A., Esteve P., Guil J.M., Martínez A., Perdigón-Melón J.A., Valencia S. (1998). *J. Phys. Chem. B* 102, 75–88.
84. Tatsumi T., Jappar N. (1998). *J. Phys. Chem. B* 102, 7126–7131.
85. Saxton R.J. (1999). *Top. Catal.* 9, 43–57.
86. Camblor M.A., Corma A., Valencia S. (1996). *Chem. Commun.*, 2365–2366.
87. Sasidharan M., Bhaumik A. (2011). *Phys. Chem. Chem. Phys.* 13, 16282–16294.
88. Di Renzo F., Gomez S., Teissier R., Fajula F. (2000). *Stud. Surf. Sci. Catal.* 130B, 1631–1636.
89. Blasco T., Camblor M.A., Corma A., Pérez-Pariente J. (1993). *J. Am. Chem. Soc.* 115, 11806–11813.
90. Reddy J.S., Kumar R. (1991). *J. Catal.* 130, 440–446.
91. Aehedi R.K., Kotasthane A.N. (1998). *J. Mater. Chem.* 8, 1685–1686.
92. Reddy K.M., Kaliaguine S., Sayari A. (1994). *Catal. Lett.* 23, 169–173.
93. Eilertsen E.A., Giordanino F., Lamberti C., Bordiga S., Damin A., Bonino F., Olsbye U., Lillerud K.P. (2011). *Chem. Commun.* 47, 11867–11869.
94. Eilertsen E.A., Bordiga S., Lamberti C., Damin A., Bonino F., Arstad B., Svelle S., Olsbye U., Lillerud K.P. (2011). *ChemCatChem* 3, 1869–1871.
95. Wu P., Tatsumi T., Komatsu T., Yashima T. (2001). *J. Phys. Chem. B* 105, 2897–2905.
96. Kim G.J., Cho B.R., Kim J.H. (1992). *Catal. Lett.* 22, 259–270.
97. Wu P., Komatsu T., Yashima T. (1997). *Stud. Surf. Sci. Catal.* 105, 663–670.
98. Oumi Y., Manabe T., Sasaki H., Inuzuka T., Sano T. (2010). *Appl. Catal. A: General* 388, 256–261.
99. Kubota Y., Koyama Y., Yamada T., Inagaki S., Tatsumi T. (2008). *Chem. Commun.*, 6224–6226.
100. Tuel A. (1995). *Zeolites* 15, 236–242.
101. Díaz-Cabañas M.J., Camblor M.A., Villaescusa L. (2000). *Chem. Commun.*, 761–762.
102. Corma A., Díaz-Cabañas M.J., Domine M.E., Rey F. (2000). *Chem. Commun.*, 1725–1726.
103. Balkus K.J., Gabrielov A.G., Zones S.I. (1995). *Stud. Surf. Sci. Catal.* 97, 519–525.
104. Corma A., Díaz U., Domine M.E., Fornés V. (2000). *J. Am. Chem. Soc.* 122, 2804–2809.
105. Corma A., Díaz U., Domine M.E., Fornés V. (2000). *Chem. Commun.*, 137–138.
106. Wu P., Nuntasri D., Ruan J., Liu Y., He M., Fan W., Terasaki O., Tatsumi T. (2004). *J. Phys. Chem. B* 108, 19126–19131.

107. Wang L.L., Wang Y., Liu Y.M., Chen L., Cheng S.F., Gao G.H., He M.Y., Wu P. (2008). *Micropor. Mesopor. Mater.* 113, 435–444.
108. Kim S.-Y., Ban H.-J., Ahn W.-S. (2007). *Catal. Lett.* 113, 160–164.
109. Wang L.L., Wang Y., Liu Y.M., Wu H.H., Li X.H., He M.Y., Wu P. (2009). *J. Mater. Chem.* 19, 8594–8602.
110. Fan W.B., Wu P., Namba S., Tatsumi T. (2006). *J. Catal.* 243, 183–191.
111. Corma A., Díaz U., Fornés V., Jordá J.L., Domine M.E., Rey F. (1999). *Chem. Commun.*, 779–780.
112. Adam W., Corma A., García H., Weinchold O. (2000). *J. Catal.* 196, 339–344.
113. Rigutto M.S., van Bekkum H. (1991). *Appl. Catal.* 68, L1–L7.
114. Hari Prasad Rao P.R., Kumar R., Ramaswamy A.V., Ratnasamy P. (1993). *Zeolites* 13, 663–670.
115. Reddy K.R., Ramaswamy A.V., Ratnasamy P. (1992). *J. Chem. Soc., Chem. Commun.*, 1613–1615.
116. Tuel A., Ben Taarit Y. (1994). *Zeolites* 14, 18–24.
117. Sen T., Chatterjee M., Sivasanker S. (1995). *J. Chem. Soc., Chem. Commun.*, 207–208.
118. Guo B., Zhu L., Hu X., Zhang Q., Tong D., Li G., Hu C. (2011). *Catal. Sci. Technol.* 1, 1060–1067.
119. Arends I.W.C.E., Sheldon R.A. (2001). *Appl. Catal. A: General* 212, 175–187.
120. Panov G.I., Uriarte A.K., Rodkin M.K., Sobolev V.I. (1998). *Catal. Today* 41, 365–385.
121. Mal N.K., Ramaswamy A.V., Ganapathy S., Ramaswamy V. (1994). *J. Chem. Soc., Chem. Commun.*, 1933–1934.
122. Mal N.K., Ramaswamy V., Ganapathy S., Ramaswamy A.V. (1995). *Appl. Catal. A: General*, 125, 233–245.
123. Mal N.K., Bhaumik A., Kumar R., Ramaswamy A.V. (1995). *Catal. Lett.* 33, 387–394.
124. Mal N.K., Ramaswamy A.V. (1997). *Chem. Commun.*, 425–426.
125. Corma A., Nemeth L.T., Renz M., Valencia S. (2001). *Nature* 412, 423–425.
126. Corma A., Domine M.E., Valencia S. (2003). *J. Catal.* 215, 294–304.
127. Boronat M., Corma A., Renz M., Sastre G., Valencia S. (2005). *Chem. Eur. J.* 11, 6905–6915.
128. Shilov A.E., Shul'pin G.B. (1997). *Chem. Rev.* 97, 2879–2932.
129. Arndtsen B.A., Bergman R.G., Mobley T.A., Peterson T.S. (1995). *Acc. Chem. Res.* 28, 154–162.
130. Baik Mu-H., Newcomb M., Friesner R.A., Lippard S.J. (2003). *Chem. Rev.* 103, 2385–2419.
131. Tatsumi, T., Nakamura M., Negishi S., Tominaga H. (1990). *J. Chem. Soc., Chem. Commun.*, 1990, 476–477.
132. Huybrechts D.R.C., De Bruycker L., Jacobs P.A. (1990). *Nature* 345, 240–242.
133. Clerici M.G. (1991). *Appl. Catal.* 68, 249–261.
134. Sudhakar Reddy J., Sivansaker S., Ratnasamy P. (1991). *Appl. Catal.* 70, 335–342.
135. Khouw C.B., Dartt C.B., Labinger J.A., Davis M.E. (1994). *J. Catal.* 149, 195–205.
136. Fu H., Kaliaguine S. (1994). *J. Catal.* 148, 540–549.
137. Gallot J.E., Fu H., Kapoor M.P., Kaliaguine S. (1996). *J. Catal.* 161, 798–809.

138. Gallot J.E., Trong On D., Kapoor M.P., Kaliaguine S. (1997). *Ind. Eng. Chem. Res.* 36, 3458–3467.
139. Gallot J.E., Fu H., Kapoor M.P., Kaliaguine S. (1998). *AIChE J*. 44, 1438–1454.
140. Gallot J.E., Kaliaguine S. (1998). *Can. J. Chem. Eng.* 76, 833–852.
141. Derouane E.G. (1998). *J. Mol. Catal. A: Chemical* 134, 29–45.
142. Langhendries G., De Vos D.E., Baron G.V., Jacobs P.A. (1999). *J. Catal.* 187, 453–463.
143. Spinacé E.V., Pastore E.O., Schuchardt U. (1995). *J. Catal.* 157, 631–635.
144. Tao J., Tang D., Li Q., Yu Z., Min E. (2001). *J. Nat. Gas Chem.* 10, 295–307.
145. Shi C.F., Zhu B., Lin M., Long J., Wang R.W. (2011). *Catal. Today* 175, 398–403.
146. Thiele G.F., Roland E. (1997). *J. Mol. Catal. A: Chemical* 117, 351–356.
147. Costas M., Chen K., Que Jr., L. (2000). *Coord. Chem. Rev.* 200–202, 517–544.
148. Halasz I., Agarwal M., Senderov E., Marcus B., (2003). *Appl. Catal. A: General* 241, 167–184.
149. Corma A., Camblor M.A., Esteve P., Martínez A., Pérez-Pariente J. (1994). *J. Catal.* 145, 151–158.
150. Jappar N., Xia Q., Tatsumi T. (1998). *J. Catal.* 180, 132–141.
151. Hari Prasad Rao P.R., Ramaswamy A.V., Ratnasamy P. (1993). *J. Catal.* 141, 604–611.
152. Ramaswamy A.V., Sivasanker S., Ratnasamy P. (1994). *Micropor. Mater.* 2, 451–458.
153. Ramesh Reddy K., Ramaswamy A.V., Ratnasamy P. (1993). *J. Catal.* 143, 275–285.
154. Clerici M.G. In: *Fine Chemicals through Heterogeneous Catalysis*. Sheldon R.A., van Bekkum H., eds. Wiley-VCH, Weinheim, 2001, pp. 538–551.
155. Balducci L., Bianchi D., Bortolo R., D'Aloisio R., Ricci M., Tassinari R., Ungarelli R. (2003). *Angew. Chem. Int. Ed.* 42, 4937–940.
156. Bianchi D., Balducci L., Bortolo R., D'Aloisio R., Ricci M., Spanò G., Tassinari R., Tonini C., Ungarelli R. (2007). *Adv. Synth. Catal.* 349, 979–986.
157. Barbera D., Cavani F., D'Alessandro T., Fornasari G., Guidetti S., Aloise A., Giordano G., Piumetti M., Bonelli B., Zanzottera C. (2010). *J. Catal.* 275, 158–169.
158. Neidig M.L., Hirsekorn K.F. (2011). *Catal. Commun.* 12, 480–484.
159. Wang X.S., Guo X.W. (1999). *Catal. Today* 51, 177–186.
160. Wu P., Komatsu T., Yashima T. (1998). *J. Phys. Chem. B* 102, 9297–9303.
161. Clerici, M.G., Ricci, M., Rivetti, F. In: *Encyclopaedia of Hydrocarbons*. Vol. 2. Beccari M., Romano U., eds. Eni & Istituto dell'Enciclopedia Italiana G. Treccani, Rome, 2006, pp. 661–686.
162. Kumar R., Bhaumik A. (1998). *Micropor. Mesopor. Mater.* 21, 497–504.
163. Chammingkwan P., Hoelderich W.F., Mongkhonsi T., Kanchanawanichakul P. (2009). *App. Catal. A: General* 352, 1–9.
164. Gaare, K., Akporiaye D. (1996). *J. Mol. Catal. A: Chemical* 109, 177–187.
165. Finiels A., Geneste P., Lecomte J., Marichez F., Moreau C., Moreau P. (1999). *J. Mol. Catal. A: Chemical* 148, 165–172.
166. Tuel A., Ben Taarit Y. (1993). *Appl. Catal. A: General* 102, 69–77.
167. Kraushaar-Czarnetzki A., van Hooff, J.H.C. (1989). *Catal. Lett.* 2, 43–48.
168. Tuel A., Moussa-Khouzami S., Ben Taarit Y., Naccache (1991). *J. Mol. Catal.* 68, 45–52.

169. Sudhakar Reddy J., Sivasanker S., Ratnasamy P. (1992). *J. Mol. Catal.* 71, 373–381.
170. Thangaraj A., Kumar R., Ratnasamy P. (1991). *J. Catal.* 131, 294–297.
171. Wilkenhöner U., Langhendries G., van Laar F., Baron G.V., Gammon D.W., Jacobs P.A., van Steen E. (2001). *J. Catal.* 203, 201–212.
172. Klaewkla R., Kulprathipanja S., Rangsunvigit P., Rirksomboon T., Nemeth L. (2003). *Chem. Commun.*, 1500–1501.
173. Atoguchi T., Yao S. (2001). *J. Mol. Catal. A: Chemical* 176, 173–178.
174. Callanan L.H., Burton R.M., Mullineux J., Engelbrecht J.M.M., Rau R. (2012). *Chem. Eng. J.* 180, 255–262.
175. Van der Pol A.J.H.P., Verduyn A.J., van Hooff J.H.C. (1992). *Appl. Catal. A: General* 92, 113–130.
176. Liu H., Lu G.Z., Guo Y.L., Guo Y., Wang J.S. (2005). *Chem. Eng. J.* 108, 187–192.
177. Liu H., Lu G.Z., Guo Y.L., Guo Y., Wang J.S. (2006). *Chem. Eng. J.* 116, 179–186.
178. Lu C.J., Chen R.Z., Xing W.H., Jin W.Q., Xu N.P. (2008). *AIChE J.* 54, 1842–1849.
179. Jiang H., Meng L., Chen R.Z., Jin W.Q., Xing W.H., Xu N.P. (2011). *Ind. Eng. Chem. Res.* 50, 10458–10464.
180. Yube K., Furuta M., Mae K. (2007). *Catal. Today* 125, 56–63.
181. Klaewkla R., Kulprathipanja S., Rangsunvigit P., Rirksomboon T., Rathbun W., Nemeth L. (2007). *Chem. Eng. J.* 129, 21–30.
182. Camblor M.A., Costantini M., Corma A., Esteve P., Gilbert L., Martinez A., Valencia S., (1995). *Appl. Catal. A: General* 133, L185–L189.
183. Hamoudi S., Larachi F., Sayari A. (2001). *Catal. Lett.* 77, 227–231.
184. Hari Prasad Rao P.R., Ramaswamy A.V. (1993). *Appl. Catal. A: General* 93, 123–130.
185. Tuel A., Ben Taârit Y. (1993). *Appl. Catal. A: General* 102, 201–214.
186. Du H.B., Fang M., Liu Y.L., Qiu S.L., Pang W.Q. (1997). *Zeolites* 18, 334–339.
187. Mal N.K., Ramaswamy A.V. (1996). *J. Mol. Catal. A: Chemical* 105, 149–158.
188. Vayssilov G.N., Popova Z., Bratinova S., Tuel A. (1997). *Stud. Surf. Sci. Catal.* 110, 909–918.
189. Xu H., Zhang Y.T., Wu H.H., Liu Y.M., Li X.H., Jiang J.G., He M.Y., Peng W. (2011). *J. Catal.* 281, 263–272.
190. Zhou J., Hua Z., Cui X.Z., Ye Z.Q., Cui F.M., Shi J.L. (2010). *Chem. Commun.* 46, 4994–4996.
191. Mal N.K., Ramaswamy A.V. (1996). *Appl. Catal. A: General* 143, 75–85.
192. Vayssilov G.N., Popova Z., Tuel A. (1997). *Chem. Eng. Technol.* 20, 333–337.
193. Bianchi B., D'Aloisio R., Bortolo R., Ricci M. (2007). *Appl. Catal. A: General* 327, 295–299.
194. Anunziata O.A., Pierella L.B., Beltramone A-R. (1999). *J. Mol. Catal. A: Chemical* 149, 255–261.
195. Mugdan M., Young D.P. (1949). *J. Chem. Soc.*, 2988–3000.
196. Clerici M.G., Ingallina P. (1993). *J. Catal.* 140, 71–83.
197. Tatsumi T., Nakamura M., Yuasa K., Tominaga H. (1990). *Chem. Lett.*, 297–298.
198. Corma A., Esteve P., Martínez A., Valencia S. (1995). *J. Catal.* 152, 18–24.
199. Swern, D. (1947). *J. Am. Chem. Soc.* 69, 1692–1698.

200. Clerici M.G. (2006). *Oil Gas - Europ. Magazine* 32, 77–87.
201. Liu X.W., Wang X.S., Guo X.W., Li G. (2004). *Catal. Today* 93–95, 505–509.
202. Fan W.B., Wu P., Tatsumi T. (2008). *J. Catal.* 256, 62–73.
203. Hulea V., Dumitriu E., Patcas F., Ropot R., Graffin P., Moreau P. (1998). *Appl. Catal. A: General* 170, 169–175.
204. Hulea V., Dumitriu E. (2004). *Appl. Catal. A: General* 277, 99–106.
205. Ramachandran C.E., Zhao Q., Zikanova A., Kocirik M., Broadbelt L.J., Snurr R.Q. (2006). *Catal. Commun.*, 936–940.
206. Bellussi G., Carati A., Clerici M.G., Maddinelli G., Millini R. (1992). *J. Catal.* 133, 220–230.
207. Bonino F., Damin A., Ricchiardi G., Ricci M., Spanò G., D'Aloisio R., Zecchina A., Lamberti C., Prestipino C., Bordiga S. (2004). *J. Phys. Chem. B* 108, 3573–3583.
208. Gao H.X., Lu G.X., Suo J.H., Li S.B. (1996). *Appl. Catal. A: General* 138, 27–38.
209. Capel-Sanchez M.C., Campos-Martin J.M., Fierro J.L.G. (2003). *Appl. Catal. A: General* 246, 69–77.
210. Choudhary V.R., Patil N.S., Bhargava S.K. (2003). *Catal. Lett.* 89, 55–62.
211. Li G., Wang X.S., Yan H.S., Chen Y.Y., Su Q.S. (2001). *Appl. Catal. A: General* 218, 31–38.
212. Clerici M.G., Ingallina P., Millini R. In: *Proc. 9th Int. Zeol. Conf., Montreal, 1992*. von Ballmoos R., Higgins J.B., Treacy M.M.J., eds. Butterworth-Heinemann, Boston, MA, 1993, 445–452.
213. Liang X.H., Mi Z.T., Wu Y.L., Li Wang L., Xing E.H. (2003). *React. Kinet. Catal. Lett.* 80, 207–215.
214. Shin S.B., Chadwick D. (2010). *Ind. Eng. Chem. Res.* 49, 8125–8134.
215. Ramachandran C.E., Du H.W., Kim Y.J., Kung M.C., Broadbelt L.J., Snurr R.Q. (2008). *J. Catal.* 253, 148–158.
216. Kuwahara Y., Nishizawa K., Nakajima T., Kamegawa T., Mori K., Yamashita H. (2011). *J. Am. Chem. Soc.* 133, 12462–12465.
217. Nur H., Prasetyoko D., Ramli Z., Endud S. (2004). *Catal. Commun.*, 725–728.
218. Duprey E., Maquet J., Man P.P., Manoli J.-M., Delamar M., Brégeault J.-M. (1995). *Appl. Catal. A: General* 128, 89–96.
219. Arca V., Boscolo Boscoletto A., Fracasso N., Meda L., Ranghino G. (2006). *J. Mol. Catal. A: Chemical* 243, 264–277.
220. Li H., Lei Q., Zhang X.M., Suo J.S. (2012). *Micropor. Mesopor. Mater.* 147, 110–116.
221. Lin K., Lebedev O.I., van Tendeloo G., Jacobs P.A., Pescarmona P.P. (2010). *Chem. Eur. J.* 16, 13509–13518.
222. Chen L., Wang Y.M., He M.Y. (2011). *Mater. Res. Bull.* 46, 698–701.
223. Ok D.-Y., Jiang N., Prasetyanto E.A., Jin H., Park S.-E. (2011). *Micropor. Mesopor. Mater.* 141, 2–7.
224. Jin H., Jiang N., Oh S.-M., Park S.-E. (2009). *Top. Catal.* 52, 169–177.
225. Wan Y.S.S., Chau J.L.H., Yeung K.L., Gavriilidis A. (2004). *J. Catal.* 223, 241–249.
226. Sato T., Dakka J., Sheldon R.A. (1994). *J. Chem. Soc., Chem. Commun.*, 1887–1888.
227. Sato T., Dakka J., Sheldon R.A. *Stud. Surf. Sci. Catal.* 84, 1853–1860.

228. Corma A., Esteve P., Martínez A. (1996). *J. Catal.* 161, 11–19.
229. Xia Q.-H., Chen X., Tatsumi T. (2001). *J. Mol. Catal. A: Chemical* 176, 179–193.
230. Goa Y., Wu P., Tatsumi T. (2004). *J. Phys. Chem. B* 108, 8401–8411.
231. Blasco T., Camblor M.A., Corma A., Esteve P., Martínez A., Prieto C., Valencia S. (1996). *Chem Commun*. 2367–2368.
232. Camblor M.A., Corma A., Esteve P., Martínez A., Valencia S. (1997). *Chem. Commun.*, 795–796.
233. van der Waal J.C., van Bekkum H. (1997). *J. Mol. Catal. A: Chemical* 124, 137–146.
234. van der Waal J.C., Rigutto M.S., van Bekkum H., (1998). *Appl. Catal. A: General* 167, 331–338.
235. Ogura M., Nakata S., Kikuchi E., Matsukata M. (2001). *J. Catal.* 199, 41–47.
236. Sasidharan M., Bhaumik A. (2010). *J. Mol. Catal. A: Chemical* 328, 60–67.
237. Wu P., Tatsumi T., Komatsu T., Yashima T. (2001). *J. Catal.* 202, 245–255.
238. Wu P., Tatsumi T. (2001). *Chem. Commun.*, 897–898.
239. Wu P., Nuntasri D, Liu Y.M., Wu H.H., Jiang Y.W. (2006). *Catal. Today* 117, 199–205.
240. Wu H.H., Liu Y.M., Wang L.L., Zhang H.J., He M.Y., Wu P. (2007). *Appl. Catal. A: General* 320, 173–180.
241. Wang L.L., Liu Y.M., Xie W., Wu H.H., Li X.H., He M.Y., Wu P. (2008). *J. Phys. Chem. C* 112, 6132–6138.
242. Christopher B., Dartt C.B., Davis M.E. (1996). *Appl. Catal. A: General* 143, 53–73.
243. Fan W.B., Wu P., Namba S., Tatsumi T. (2004). *Angew. Chem. Int. Ed.* 43, 236–240.
244. Shen X.H., Fan W.B., He Y., Wu P., Wang J.G., Tatsumi T. (2011). *App. Catal. A: General* 401, 37–45.
245. Zhang F.Z., Guo X.W., Wang X.S., Li G.Y., Zhao Q., Bao, X.H. Han X.W., Lin L.W. (2000). *Appl. Catal. A: General* 192, 157–163.
246. Wang X.S., Guo X.W., Li G. (2002). *Catal. Today* 74, 65–75.
247. Guo X.W., Wang X.S., Liu M., Li G., Chen Y.Y., Xiu J.H., Zhuang J.Q., Zhang W.P., Bao X.H. (2002). *Catal. Lett.* 81, 125–130.
248. Li G., Wang X.S., Yan H.S., Liu Y. H, Liu X.W. (2002). *Appl. Catal. A: General* 236, 1–7.
249. Zhao J., Shen B., Xiao W., Zhang C., Wang L. (2009). *Energy Sources, Part A* 31, 108–117.
250. Liu N., Guo H.C., Wang X.S., Chen L.X., Zou L.J. (2006). *React. Kinet. Catal. Lett.* 87, 77–83.
251. Shi C.F., Zhu B., Lin M., Long J. (2009). *Eur. J. Inorg. Chem.*, 4433–4440.
252. Wang Q.F., Wang L., Chen J.X., Wu Y.L., Mi Z.T. (2007). *J. Mol. Catal. A: Chemical* 273, 73–80.
253. Cheng W.G., Wang X.S., Li G., Guo X.W., Du B.J. (2004). *Catal. Lett.* 95, 185–190.
254. Cheng W.G., Wang X.S., Li G., Guo X.W., Lin Q.S. (2005). *Chin. Chem. Lett.* 16, 103–106.
255. Zhao J.L., Zhou J.C., Su J., Guo H.C., Wang X.S., Gong W.M. (2007). *AIChE J.* 53, 3204–3209.
256. Serrano D.P., Sanz R., Pizarro P., Moreno I., de Frutos P., Blázquez S. (2009). *Catal. Today* 143, 151–157.

257. Liu X.W., Wang X.S., Guo X.W., Li G., Yan H.S. (2004). *Catal. Lett.* 97, 223–229.
258. Clerici M.G., Ingallina P. In: *Green Chemistry. Designing Chemistry for the Environment*. Anastas P.T., Williamson T.C., eds. ACS Symp. Series 626. American Chemical Society, Washington, DC, 1996, pp. 59–68.
259. Clerici M.G., Ingallina P., (1988). *Catal. Today* 41, 351–364.
260. Meiers R., Dingerdissen U., Hölderich W.F. (1998). *J. Catal.* 176, 376–386.
261. Jenzer G., Mallat T., Maciejewski M., Eigenmann F., Baiker A. (2001). *Appl. Catal. A: General* 208, 125–133.
262. Danciu T., Beckman E.J., Hancu D., Cochran R.N., Grey R., Hajnik D.M., Jewson J., (2003). *Angew. Chem. Int. Ed.* 42, 1140–1142.
263. Chen Q.L., Beckman E.J. (2008). *Green Chem.* 10, 934–938.
264. Wang C.Y., Wang B.G., Meng X.K., Mi Z.T. (2002). *Catal. Today* 74, 15–21.
265. Tatsumi T., Yako M., Nakamura M., Yuhara Y. (1993). *J. Mol. Catal.* 78, L41–L45.
266. Kumar R., Pais G.C.G., Pandey B., Kumar P. (1995). *J. Chem. Soc., Chem. Commun.*, 1315–1316.
267. Schofield L.J., Kerton O.J., McMorn P., Bethell D., Ellwood S. *J. Chem. Soc., Perkin Trans.* 2, 1475–1481.
268. Hutchings G.J., Lee D.F. (1994). *J. Chem. Soc., Chem. Commun.*, 1095–1096.
269. Davies L.J., McMorn P., Bethell D., Bulman Page P.C., King F., Hancock F.E., Hutchings G.J. (2001). *J. Catal.* 198, 319–327.
270. Wu P., Tatsumi T. (2003). *J. Catal.* 214, 317–326.
271. Wróblewska A. (2005). *J. Mol. Catal. A: Chemical* 229, 207–210.
272. Davies L.J., McMorn P., Bethell D., Bulman Page P.C., King F., Hancock F.E., Hutchings G.J. (2001). *J. Mol. Catal. A: Chemical* 165, 243–247.
273. Adam W., Corma A., Reddy T.I., Renz M. (1997). *J. Org. Chem.* 62, 3631–3637.
274. Pandey R.K., Kumar R. (2007). *Catal. Commun.* 8, 379–382.
275. Wang Q.F., Mi Z.T., Wang Y.Q., Wang L. (2005). *J. Mol. Catal. A: Chemical* 229, 71–75.
276. Wang L.L., Liu Y.M., Xie W., Zhang H.J., Wu H.H., Jiang Y.W., He M.Y., Wu P. (2007). *J. Catal.* 246, 205–214.
277. Zheng Y., Zhang Y., Wang Z., Liu Y., He M., Wu P. (2011). *Ind. Eng. Chem. Res.* 50, 9587–9593.
278. Kim W., Yun C., Kim Y., Park J., Park S., Jung K.T., Lee Y.H., Kim S.H. (2011). *Ind. Eng. Chem. Res.* 50, 1187–1195.
279. Wang Q.F., Wang L., Mi Z.T. (2005). *Catal. Lett.* 103, 161–164.
280. Wu P., Liu Y.M., He M.Y., Tatsumi T. (2004). *J. Catal.* 228, 183–191.
281. Li N.N., Liu Y.M., Wu H.H., Li X.H., Xie W., Zhao ZL., Wu P., He M.Y. (2008). *Chin. J. Catal.* 29, 102–104.
282. Sasidharan M., Wu P., Tatsumi T. (2002). *J. Catal.* 205, 332–338.
283. Zhang X.M., Zhang Z.R., Suo J.S., Li S.B. (2000). *Catal. Lett.* 66, 175–179.
284. Kumar S.B., Mirajkar S.P., Pais G.C.G., Kumar P., Kumar R. (1995). *J. Catal.* 156, 163–166.
285. Fu Z., Yin D., Yin D., Li Q., Zhang L., Zhang Y. (1999). *Micropor. Mesopor. Mater.* 29, 351–359.

286. Uguina M.A., Serrano D.P., Sanz R., Fierro J.L.G., López-Granados M., Mariscal R. (2000). *Catal. Today* 61, 263–270.
287. Laha S.C., Kumar R. (2001). *J. Catal.* 204, 64–70.
288. Zhuang J.Q., Yang G., Ma D., Lan X.J., Liu X.M., Han X.W., Bao X.H., Müller U. (2004). *Angew. Chem. Int. Ed.* 43, 6377–6381.
289. Zhuang J.Q., Han X.W., Bao X.H., Müller U. (2009). *J. Catal.* 267, 177–180.
290. Wang X.B., Zhang X.F., Wang Y., Liu H.O., Qiu J.S., Wang J.Q., Han W., Yeung K.L. (2011). *ACS Catal.* 1, 437–445.
291. Smith K., Al-Shamali M. In: *Proc. 12th Int. Zeolite Conf., July 5–10, 1998, Baltimore*. Bei E., Treacy M.M.J., Marcus B.K., Bisher M.E., Higgins J.B., eds. Material Research Society, Warrendale, PA, *1999*, pp. 1129–1132.
292. Derouane E.G., Hutchings G.J., Mbafor W.F., Roberts S.M. (1998). *New J. Chem.*, 797–799.
293. Bhaumik A., Tatsumi T. (1998). *J. Catal.* 176, 305–309.
294. Sasidharan M., Wu P., Tatsumi T. (2002). *J. Catal.* 209, 260–265.
295. Bhaumik A. Tatsumi T. (1999). *J. Catal.* 182, 349–356.
296. Corma A., Iglesia M., Sánchez F. (1995). *J. Chem. Soc., Chem. Commun.*, 1635–1636.
297. van der Pol A.J.H., Hoof J.H.C. (1993). *Appl. Catal. A: General* 106, 97–113.
298. Maspero F., Romano U. (1994). *J. Catal.* 146, 476–482.
299. Corma A., Esteve P., Martínez A. (1996). *Appl. Catal. A: General* 143, 87–100.
300. Hayashi H., Kikawa K., Murai Y., Shigemoto N., Sugiyama S., Kawashioro, K. (1996). *Catal. Lett.* 36, 99–102.
301. Danov S.M., Sulimov A.V., Fedosov A.E. (2007). *Russ. J. App. Chem.* 80, 2111–2112.
302. Zhao R., Ding Y., Peng Z.G., Wang X.L., Suo J. (2003). *Catal. Lett.* 87, 81–83.
303. Sheldon R.A., Dakka J. (1993). *Erdöl Erdgas Kohle* 109, 520–522.
304. Sasidharan M., Suresh S., Sudalai A. (1995). *Tetrahedron Lett*. 36, 9071–9072.
305. Roffia P., Leofanti G., Cesana A., Mantegazza M., Padovan M., Petrini G., Tonti S., Gervasutti P. (1990). *Stud. Surf. Sci. Catal.* 55, 43–52; and *Chim. Ind. (Milan)* 72, 598–603.
306. Thangaraj A., Sivasanker S., Ratnasamy P. (1991). *J. Catal.* 131, 394–400.
307. Mantegazza M.A., Petrini G., Spanò G., Bagatin R., Rivetti F. (1999). *J. Mol. Catal. A: Chemical* 146, 223–228.
308. Cesana A., Mantegazza M.A., Pastori M. (1997). *J. Mol. Catal. A: Chemical* 117, 367–373.
309. Dal Pozzo L., Fornasari G., Monti T. (2002). *Catal. Commun.*, 369–375.
310. Petrini G., Cesana A., de Alberti G., Genoni F., Leofanti G., Padovan M., Paparatto G., Roffia P. (1991). *Stud. Surf. Sci. Catal.* 68, 761–766.
311. Wu C.T., Wang Y.Q., Mi Z.T., Xue L., Wu W., Min E.Z., Han S., He F., Fu S.B. (2002). *React. Kinet. Catal. Lett*. 77, 73–81.
312. Zhang X.J., Wang Y., Xin F. (2006). *App. Catal. A: General* 307, 222–230.
313. Zecchina A., Spoto G., Bordiga S., Geobaldo F., Petrini G., Leofanti G., Padovan M., Mantegazza M., Roffia P. (1993). *Stud. Surf. Sci. Catal* 75, 719–729.
314. Tatsumi T., Jappar N. (1996). *J. Catal.* 161, 570–576.

315. Le Bars J., Dakka J., Sheldon R.A. (1996). *Appl. Catal. A: General* 136, 69–80.
316. Liang X.H., Mi Z.T., Wang Y.Q., Li W., Zhang X.W., (2004). *React. Kinet. Catal. Lett.* 82, 333–337.
317. Zhang Y.J., Wang Y.Q., Bu Y.F., Wang L., Mi Z.T., Wu W., Min E.Z., Fu S.B., Zhu Z.H. (2006). *React. Kinet. Catal. Lett.* 87, 25–32.
318. Sudhakar Reddy J., Sivasanker S., Ratnasamy P. (1991). *J. Mol. Catal.* 69, 383–392.
319. Wu P., Komatsu P., Yashima T. (1997). *J. Catal.* 168, 400–411.
320. Song F., Liu Y.M., Wu H.H., He M.Y., Wu P., Tatsumi T. (2006). *J. Catal.* 237, 359–367.
321. Song F., Liu Y.M., Wang L.L., Zhang H.J., He M.Y., Wu P. (2007). *Appl. Catal. A: General* 327, 22–31.
322. Zhao S., Xie W., Yang J.X., Liu Y.M., Zhang Y.T., Xu B.L., Jiang J.-G., He M.Y., Wu P. (2011). *Appl. Catal. A: General* 394, 1–8.
323. Mantegazza M., Leofanti G., Petrini G., Padovan M., Zecchina A., Bordiga S. (1994). *Stud. Surf. Sci. Catal.* 82, 541–550.
324. Zecchina A., Bordiga S., Lamberti C., Ricchiardi G., Scarano D., Petrini G., Leofanti G., Mantegazza M. (1996). *Catal. Today* 32, 97–106.
325. Kul'kova N., Kotova V.G., Kvyathovskaya M.Yu., Murzin D.Yu. (1997). *Chem. Eng. Technol.* 20, 43–46.
326. Yip A.C.K., Hu X. (2011). *Ind. Eng. Chem. Res.* 50, 13703–13710.
327. Liu H., Liu P., You K., Luo H. (2010). *Cat. Commun.* 11, 887–891.
328. Birke P., Kraak P., Pester R., Schödel R., Vogt F. (1994). *Stud. Surf. Sci. Catal.* 83, 425–432.
329. Yip A.C.K., Hu X. (2009). *Ind. Eng. Chem. Res.* 48, 8441–8450.
330. Zhong Z.X., Xing W.H., Liu X., Jin W.Q., Xu N.P. (2007). *J. Membr. Sci.*, 301, 67–75.
331. Chen R.Z., Bu Z., Li Z.H., Zhong Z.X., Jin W.Q., Xing W.H. (2010). *Chem. Eng. J.* 156, 418–422.
332. Li Z.H., Chen R.Z., Xing W.H., Jin W.Q., Xu N.P. (2010). *Ind. Eng. Chem. Res.* 49, 6309–6316.
333. Liang X.H., Mi Z.T., Wang Y.Q., Li W., Zhang X.W., Liu T.F., (2004). *Chem. Eng. Technol.* 27, 176–189.
334. Liu T.F., Meng X.K., Wang Y.Q., Liang X.H., Mi Z.T., Qi X.J., Li S.Y., Wu W., Min E. Z., Fu S.B. (2004). *Ind. Eng. Chem. Res.* 43, 166–172.
335. Bhaumik A., Kumar P., Kumar R. (1996). *Catal. Lett.* 40, 47–50.
336. Corma A., Fornés V., Iborra S., Mifsud M., Renz M. (2004). *J. Catal.* 221, 67–76.
337. Boronat M., Concepción P., Corma A., Renz M. (2007). *Catal. Today* 121, 39–44.
338. Li P., Liu G.Q., Wu H.H., Liu Y.M., Jiang J.-G., Wu P. (2011). *J. Phys. Chem. C* 115, 3663–3670.
339. Sudhakar Reddy J., Jacobs P.A. (1993). *J. Chem Soc., Perkin Trans* 1, 2665–2666.
340. Suresh S., Joseph R., Jayachandran B., Pol A.V., Vinod M.P., Sudalai A., Sonawane H. R., Ravindranathan T. (1995). *Tetrahedron* 41, 11305–11318.
341. Sudhakar Reddy J., Sayari A. (1995). *Appl. Catal. A: General* 128, 231–242.
342. Joseph R., Sudalai A., Ravindranathan T. (1995). *Synlett*, 1177–1178.

343. Sudhakar Reddy J., Jacobs P.A. (1996). *Catal. Lett.* 37, 213–216.
344. Sonawane H.R., Pol A.V., Moghe P.P., Biswas S.S., Sudalai A. (1994). *J. Chem. Soc., Chem. Commun.*, 1215–1216.
345. Gontier S., Tuel A. (1994). *Appl. Catal. A: General* 118, 173–186.
346. Gontier S., Tuel A. (1995). *J. Catal.* 157, 124–132.
347. Wan Y.S.S., Yeung K.L., Gavriilidis A. (2005). *Appl. Catal. A: General* 281, 285–293.
348. Selvam T., Ramaswamy A.V. (1996). *Chem. Commun.*, 1215–1216.
349. Kumar P., Hegde V.R., Pandey B., Ravindranathan T. (1993). *J. Chem. Soc., Chem. Commun.*, 1553–1554.
350. Joseph R., Sudalai A., Ravindranathan T. (1994). *Tetrahedron Lett*. 35, 5493–5496.
351. Ramakrishna Prasad M., Kamalakar G., Madhavi G., Kulkarni S.J., Raghavan K.V. (2000). *Chem. Commun.*, 1577–1578.
352. Ramakrishna Prasad M., Kamalakar G., Madhavi G., Kulkarni S.J., Raghavan K.V. (2002). *J. Mol. Catal. A: Chemical* 186, 109–120.
353. Robinson D.J., McMorn P., Bethell D., Bulman-Page P.C., Slyd C., King F., Hancock F. E., Hutchings G.J. (2001). *Catal. Lett.* 72, 233–234.
354. Xie W., Zheng Y.T., Zhao S., Yang J.X., Liu Y.M., Wu P. (2010). *Catal. Today* 157, 114–118.
355. Kapoor M.P., Gallot J.E., Raj A., Kaliaguine S. (1995). *J. Chem. Soc., Chem. Commun.*, 2281–2282.
356. Reddy R.S., Sudhakar Reddy J., Kumar R., Kumar P. (1993). *J. Chem. Soc., Chem. Commun.*, 84–85.
357. Hulea V., Moreau P., Di Renzo F. (1996). *J. Mol. Catal. A: Chemical* 111, 325–332.
358. Hulea V., Moreau P. (1996). *J. Mol. Catal. A: Chemical* 113, 499–505.
359. Corma A., Iglesias M., Sánchez S. (1996). *Catal. Lett.* 39, 153–156.
360. Moreau P., Hulea V., Gomez S., Brunel D., Di Renzo F. (1997). *Appl. Catal. A: General* 155, 253–263.
361. Robinson D.J., Davies L., McGuire N., Lee D.F., McMorn P., Willock D.J., Watson G. W., Bulman Page P.C., Bethell D., Hutchings G.J. (2000). *Phys. Chem. Chem. Phys.* 2, 1523–1529.
362. Adam W., Mitchell C.M., Saha-Möller C.R., Selvam T., Weichold O. (2000). *J. Mol. Catal. A: Chemical* 154, 251–255.
363. Srivastava V.C. (2012). *RSC Adv*. 2, 759–783.
364. Hulea V., Fajula F., Bousquet J. (2001). *J. Catal.* 198, 179–186.
365. Kong L.Y., Li G., Wang X.S. (2004). *Catal. Today* 93–95, 341–345.
366. Chica A., Corma A., Dómine M.E. (2006). *J. Catal.* 242, 299–308.
367. Fang Y.M., Hu H.Q. (2007). *Catal. Commun.*, 817–820.
368. Jia Y.H., Li G., Ning G.L., Jin C.Z. (2009). *Catal. Today* 140, 192–196.
369. Napanang T., Sooknoi T. (2009). *Catal. Commun.*, 1–6.
370. Zhang J., Zhao D.S., Yang L.Y., Li Y.B. (2010). *Chem. Eng. J.* 156, 528–531.
371. Wang X.X., Li G., Wang W.H., Jin C.Z., Chen Y.Y. (2011). *Micropor. Mesopor. Mater.* 142, 494–502.

372. Sengupta A., Kamble P.D., Basu J.K., Sengupta S. (2012). *Ind. Eng. Chem. Res.* 51, 147–157.
373. Clerici M.G. (2001). *Top. Catal.* 15, 257–263.
374. To J., Sokol A.A., French S.A., Catlow C.R.A., Sherwood P., van Dam H.J.J. (2006). *Angew. Chem. Int. Ed.* 45, 1633–1638.
375. Karlsen E., Schijffel K. (1996). *Catal. Today* 32, 107–114.
376. Sinclair P.E., Catlow C.R.A. (1999). *J. Phys. Chem. B* 103, 1084–1095.
377. Sever R.R., Root T.W. (2003). *J. Phys. Chem. B* 107, 4080–4089.
378. Sever R.R., Root T.W. (2003). *J. Phys. Chem. B* 107, 4090–4099.
379. Limtrakul J., Inntam C., Truong T.N. (2004). *J. Mol. Catal. A: Chemical* 207, 137–146.
380. Wells D.H., Joshi A.M., Delgass W.N., Thomson K.T.A. (2006). *J. Phys. Chem. B* 110, 14627–14639.
381. Neurock M., Manzer L.M. (1996). *Chem. Commun.*, 1133–1134.
382. Barker C.M., Gleeson D., Kaltsoyannis N., Catlow C.R.A., Sankar G., Thomas J.M. (2002). *Phys. Chem. Chem. Phys.* 4, 1228–1240.
383. To J., Sokol A.A., French S.A., Catlow C.R.A. (2008). *J. Phys. Chem. C* 112, 7173–7185.
384. Yoon C.W., Hirsekorn K.F., Neidig M.L., Yang X.Z., Tilley T.D. (2011). *ACS Catal.* 1, 1665–1678.
385. Vayssilov G.N., van Santen R.A. (1998). *J. Catal.* 175, 170–174.
386. Lundin A., Panas I., Ahlberg E. (2007). *Phys. Chem. Chem. Phys.* 9, 5997–6003.
387. Munakata H., Oumi Y., Miyamoto A. (2001). *J. Phys. Chem. B* 105, 3493–3501.
388. Brookhart M., Green M.L.H., Parkin G. (2007). *PNAS* 104, 6908–6914.
389. Evans D.R., Drovetskaya T., Bau R., Reed C.A., Boyd P.D.W. (1997). *J. Am. Chem. Soc.* 119, 3633–3634.
390. Castro-Rodriguez I., Nakai H., Gantzel P., Zakharov L.N., Rheingold A.L., Meyer K. (2003). *J. Am. Chem. Soc.* 125, 15734–15735.
391. Bonchio M., Conte V., Di Furia F., Modena G. (1989). *J. Org. Chem.* 54, 4368–4371.
392. Groves J.T., van der Puy M. (1974). *J. Am. Chem. Soc.* 96, 5274–5275.
393. Groves J.T., McClusky G.A. (1976). *J. Am. Chem. Soc.* 98, 859–861.
394. Antonova N.S., Carbó J.J., Kortz U., Kholdeeva O.A., Poblet J.M. (2010). *J. Am. Chem. Soc.* 132, 7488–7497.
395. Heinrich S., Plettig M., Klemm E. (2011). *Catal. Lett.* 141, 251–258.
396. Zalomaeva O.V., Trukhan N.N., Ivanchikova I.D., Panchenko A.A., Roduner E., Talsi E.T., Sorokin A.B., Rogov V.A., Kholdeeva O.A. (2007). *J. Mol. Catal. A: Chemical* 277, 185–192.
397. Bonoldi L., Busetto C., Congiu A., Marra G., Ranghino G., Salvalaggio M., Spanò G., Giamello E. (2002). *Spectrochim. Acta, Part A* 58, 1143–1154.
398. Sheldon R.A., Wallau M., Arends I.W.C.E., Schuchardt U., (1998). *Acc. Chem. Res.* 31, 485–493.
399. Carati A., Flego C., Previde Massara E., Millini R., Carluccio L., Parker Jr. W.O., Bellussi G. (1999). *Micropor. Mesopor. Mater.* 30, 137–144.

3

SELECTIVE CATALYTIC OXIDATION OVER ORDERED NANOPOROUS METALLO-ALUMINOPHOSPHATES

PARASURAMAN SELVAM* AND AYYAMPERUMAL SAKTHIVEL

Dedicated to Professor B. Viswanathan on the occasion of his 70th Birthday.

3.1 INTRODUCTION

The aluminophosphate molecular sieves, known as $AlPO_4$-*n* (also referred as APO-*n* or AlPO-*n*), where *n* denotes to a distinct structure type, are built of strictly alternating [AlO_4] and [PO_4] tetrahedral units with a general formula: $(AlO_2)_x(PO_2)_x \cdot yH_2O$. They form a new class of microporous crystalline materials comparable to the well-known zeolites [1–9]. Further, unlike most zeolites, the aluminophosphate molecular sieves are ordered with an Al/P ratio of unity. The first successful synthesis of aluminophosphate molecular sieve, henceforth designated as APO-*n*, was reported in 1982 by Wilson et al. [6, 7] and addition of silicon to the aluminophosphate molecular sieves resulting in the silicoaluminophosphates (SAPO-*n*) was reported in 1984 [8, 9]. Among the various structures of APO-*n*, some are zeolite analogs but there are also novel, unique, and neutral open-framework structures. Apart from their structural similarity, the crystal chemistry of aluminophosphates and zeolites differs considerably. For example, the aluminophosphate framework is neutral in contrast to the negatively charged aluminosilicates.

*Corresponding author

Liquid Phase Oxidation via Heterogeneous Catalysis: Organic Synthesis and Industrial Applications, First Edition. Edited by Mario G. Clerici and Oxana A. Kholdeeva.
© 2013 John Wiley & Sons, Inc. Published 2013 by John Wiley & Sons, Inc.

In addition, the aluminum ions in the aluminosilicate framework are always tetrahedrally coordinated in contrast to four-, five- or six-coordinated aluminum ions in the aluminophosphate framework. These facts illustrate the structural diversity of APO-*n* molecular sieves. A summary of the channel systems and ring structures along with the structure codes is presented in Table 3.1. The aluminophosphate molecular sieves exhibit not only structural but also compositional diversity as the frameworks can be modified by other elements.

The framework of trivalent aluminium and/or pentavalent phosphorous ions can partially be replaced by silicon and/or other cations that create catalytically active centers [4, 5, 10]. For example, the incorporation of silicon results in silico-

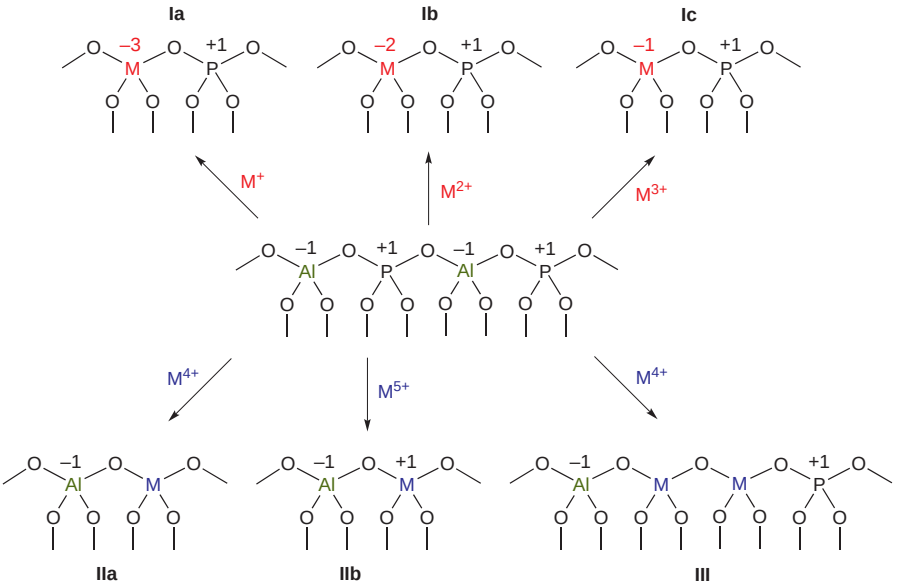
TABLE 3.1 Typical Framework Structures of APO-*n* Molecular Sieves[a]

Material	Structure code	Channel opening	Channel dimension (*nm*)
Very large pore			
VPI-5	VFI	18-ring	1.21
APO-8	AET	14-ring	0.79×0.87
Large pore			
APO-5	AFI	12-ring	0.73
SAPO-40	AFR	12/8-ring	$0.67 \times 0.69/0.37$
APO-31	ATO	12-ring	0.54
MAPO-36	ATS	12-ring	0.65×0.75
SAPO-37	FAU	12-ring	0.74
MAPO-50	AFY	12/8-ring	$0.61/0.40 \times 0.43$
Intermediate pore			
APO-11	AEL	10-ring	0.39×0.63
APO-41	AFO	10-ring	0.43×0.70
Small pore			
APO-18	AEI	8-ring	0.38
APO-22	AWW	8-ring	0.42×0.46; 0.38
APO-25	ATV	8-ring	0.39
APO-33	ATT	8-ring	0.30×0.49
APO-34	CHA	8-ring	0.38
APO-35	LEV	8-ring	0.36×0.48
APO-39	ATN	8-ring	0.40
APO-42	LTA	8-ring	0.41
APO-43	GIS	8-ring	0.31×0.45; 0.28×0.48
APO-52	AFT	8-ring	0.28×0.44
SAPO-56	AFX	8-ring	0.34×0.36
Very small pore			
APO-16	AST	6-ring	0.3
APO-20	SOD	6-ring	0.3

[a]Adapted from Ref. [154]. The acronym used in this monograph for pure aluminophosphates is APO-*n* instead of $AlPO_4$-*n* or AlPO-*n*. All these acronyms are interchangeably used in the published literature.

aluminophosphates (SAPO-*n*), while the isomorphous substitution of metal ions (M) yields analogous metallo-aluminophosphates (MAPO-*n*) or metallo-silico-aluminophosphates (MSAPO-*n*). The MAPO-*n* and MSAPO-*n* materials encompass the characteristics of both zeolites and aluminophosphates, which results in their unique catalytic, ion-exchange and adsorption properties. In this regard, isomorphous substitution, i.e. the replacement of trivalent aluminium ion and/or pentavalent phosphorous ion by a tetrahedrally coordinated metal ion has been reported for a number of elements. Hence, the incorporation of transition-metal ions in the APO-*n* framework is of considerable interest. However, the integration of these metal ions into the matrix is a big challenge as they can be either incorporated in framework sites, anchored in defect sites as extraframework cations, or present as isolated clusters in the matrix [11]. The substitution of trivalent aluminium ions by divalent metal ions generates Brønsted acid sites as well as Lewis acid sites in the aluminophosphates. On the other hand, the incorporation of a transition-metal ion, which can easily change its oxidation state, creates a redox active site. Thus, the coupling of acidic with redox properties opens up routes towards shape-selective bifunctional catalysis and to the design of novel catalysts. Table 3.2 summarizes the different transition-metal ions incorporation into various APO frameworks.

The different types of isomorphic substitutions according to various substitution mechanisms are elaborated [11] in Scheme 3.1.

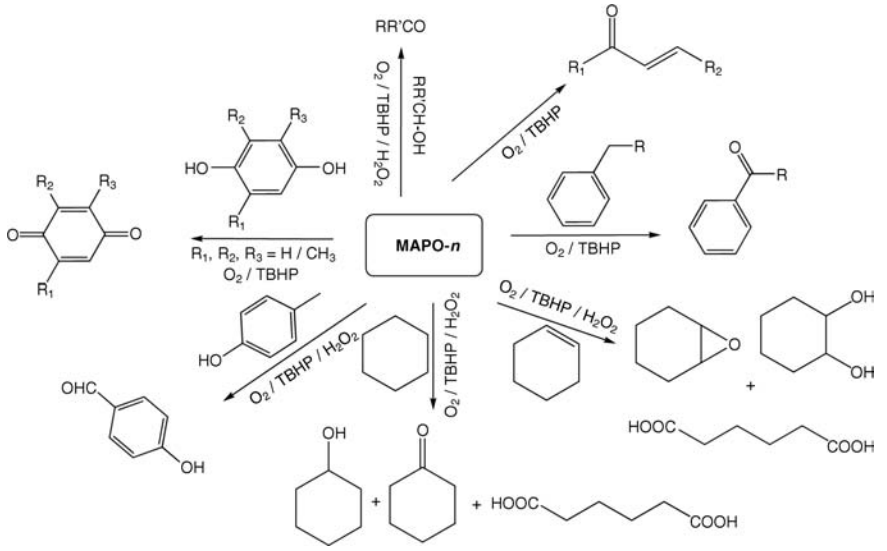


SCHEME 3.1 Isomorphous substitution of aliovalent metal ions in aluminophosphate framework structure. Reproduced with permission from Ref. [11], © Elsevier.

TABLE 3.2 Transition-Metal Ions Incorporated in Microporous Aluminophosphates

	M *in* MAPO-*n*/MSAPO-*n*									
Material	Ti	V	Cr	Mn	Fe	Co	Ni	Cu	Zn	Cd
MAPO-5	√	√	√	√	√	√	√	√	√	√
MSAPO-5	√	√	√	√			√			
MAPO-11	√	√	√	√	√	√	√		√	
MSAPO-11		√	√	√		√	√		√	
MAPO-14						√				
MAPO-16						√				
MAPO-17						√				
MAPO-18				√		√	√		√	
MSAPO-18						√	√			
MAPO-20				√		√	√			
MAPO-25						√				
MAPO-31	√	√		√				√		√
MSAPO-31				√						
MAPO-34				√		√	√		√	
MSAPO-34			√	√		√	√			
MAPO-35										
MAPO-36	√			√		√			√	
MSAPO-36						√				
MAPO-37						√			√	
MSAPO-37	√		√	√	√	√			√	
MAPO-39						√				
MAPO-40						√			√	
MSAPO-40						√			√	
MAPO-41				√		√				
MSAPO-41				√		√	√			
MAPO-42				√		√				
MAPO-44				√		√				
MSAPO-44		√		√		√			√	
MAPO-46				√		√	√		√	
MAPO-47						√				
MSAPO-47						√				
MAPO-50				√		√			√	
MSAPO-50						√			√	

Accordingly: i) isomorphic substitution of monovalent (**Ia**), divalent (**Ib**) and trivalent (**Ic**) metal ions for the trivalent aluminum sites in the APO-*n* framework results in M−O−P bonds; ii) isomorphous substitution of tetravalent (**IIa**) and pentavalent (**IIb**) metal ions for pentavalent phosphorous ions results in M−O−Al bonds; iii) the simultaneous substitution of tetravalent ion pairs (**III**) for adjacent metal ions results in Al−O−M, M−O−M and M−O−P bonds. The desired structures with predefined pore structures, building units and compositions can be designed based on constrained assembly of ions or automated assembly of secondary building units [12] in a similar way to that of zeolites [13].

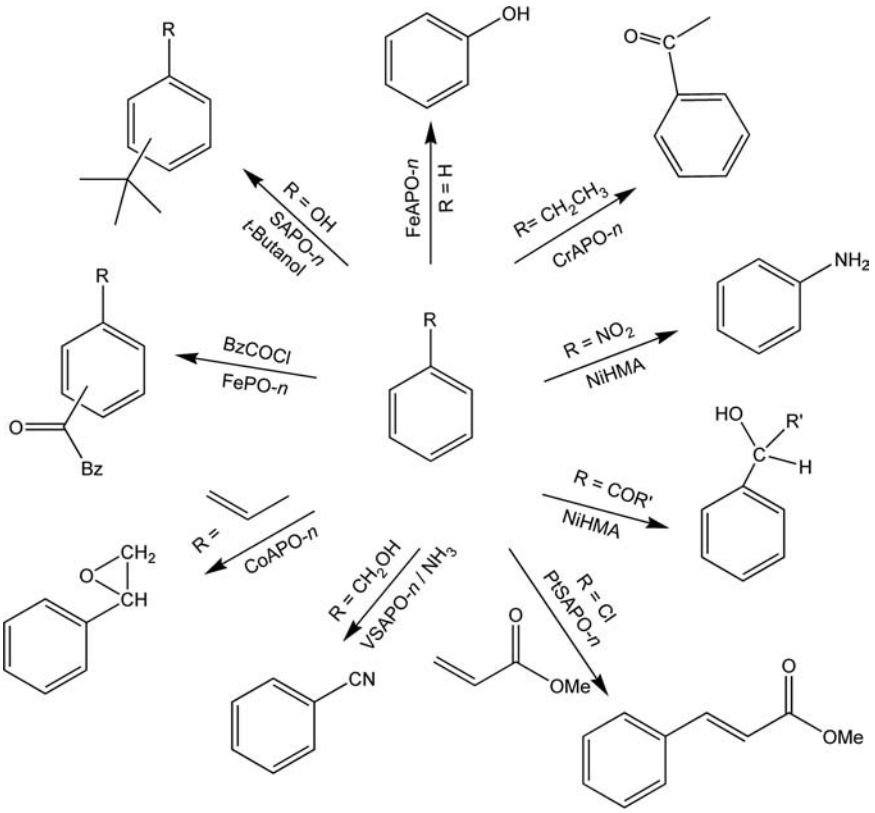


SCHEME 3.2 Versatility of transition metal-containing microporous aluminophosphates for oxidation reactions.

As with zeolites, open-framework structures of aluminophosphates are made up of Al−O−P bonds that obey Löwenstein's rule [14] with an avoidance of Al−O−Al bonds (only one exceptional case was reported for a layered APO containing Al−O−Al linkage). The P−O−P bonds do not appear to be stable in these structures. The APO framework structures exhibit lattice flexibility, which favored the isomorphous substitution of a large number of transition-metal ions. Hence, these materials are of great interest for development of oxidation catalysts as well as bifunctional (both acid–base and redox behavior) catalysts [15–25]. In particular, the transition-metal-containing microporous aluminophosphates were promising for many industrially important oxidations (Scheme 3.2) as well as various other organic transformations (Scheme 3.3).

One of the important applications of APOs is the facile of aerial oxidation of linear and cyclic hydrocarbons [15, 16]. Another important area of progress is in the conversion of methanol-to-gasoline (MTG) and methanol-to-olefins (MTO) processes [18–20]. Likewise, they have also been identified as potential catalysts for isomerization of *n*-paraffins [21, 22], olefins [23], aromatic transformations [24], and cracking of n-alkanes [25]. Despite numerous advantages, the microporous aluminophosphates are inadequate for the conversion of bulkier molecules owing to pore limitations. Therefore, attempts were made for the synthesis of molecular sieves with much larger (meso) pore dimensions.

The successful synthesis of mesoporous aluminophosphate molecular sieves has opened up further new prospects and excellent opportunities in the area of heterogeneous catalysis [17, 26–36]. However, in the present chapter, we restrict ourselves



SCHEME 3.3 Versatility of aluminophosphates for various organic transformations.

to focus on the industrially important liquid phase oxidation reactions employing metal-substituted/incorporated microporous and mesoporous aluminophosphate molecular sieve materials. Before going into details about the catalysts ability, we briefly discuss the synthesis methodology of both microporous and mesoporous aluminophosphates and their characterization. This chapter also covers the regenerability of the catalysts as well as the leaching of metal ions from framework structure. The emphasis is made on the reaction mechanism and the key role of substituted metal ion in the matrix.

3.2 SYNTHESIS

3.2.1 Microporous Aluminophosphates

The discovery of aluminophosphate molecular sieves, APO-*n*, was reported in 1982 [6, 7] followed by the silicon-substituted variant, namely, SAPO-*n* [8, 9], in 1984

and metal incorporated aluminophosphates (MAPO-*n*) in 1986 [37]. Subsequently, researchers developed a variety of structure types and framework compositions based on APO-*n* framework. Although structurally zeolites and aluminophosphates are similar in nature, the chemistry behind the formation of these materials is very different [2, 3], and the former is formed mostly in alkaline media, while the latter is formed either in neutral or acid medium. The introduction of tetravalent silicon in the aluminophosphate matrix leads to the formation of Brønsted acid sites and was found to be useful for a number of organic transformations including methanol to olefin [19, 20, 38], hydrocracking of alkane [39], etc. The introduction of transition-metal ions in the framework of APO-*n* and SAPO-*n* structures also showed interesting catalytic properties [2, 3].

In general, microporous APO-*n* materials are synthesized by hydrothermal or solvothermal methods in which crystallization of aluminophosphate gels occurs in the presence of an organic base as the template [2, 3, 12]. Several APO-*n* framework structures can be synthesized using a particular template only by tuning the synthesis conditions. For example, the use of di-*n*-propylamine can yield various framework APO-*n* structures, such as APO-11, APO-31, APO-39, APO-41, APO-43, APO-46, APO-47, APO-50, H-3, MCM-1, etc. Likewise, some structures, e.g., APO-5, can readily be formed from different templates [12]. Normally, APO-*n* and SAPO-*n* crystallize at higher temperatures as compared to MAPO-*n* materials. However, apart from the temperature and time, the type of structure formed depends on the control of a number of variables, including the reactant gel composition, the type of templates, the individual characteristics of reactants, pH, etc. Typically, the synthesis of APO-*n* involves the use of an aqueous reaction mixture containing an aluminum source, a phosphate source and an organic amine and/or a quaternary ammonium salt as a template molecule. In particular, the template molecules exhibit a critical structure-directing role in the synthesis. In the absence of templates, no crystalline phase forms. Further, the structure-directing specificity varies widely. For example, a number of templates lead to the formation of APO-5 structure, while several organic amines are known to produce different framework structures by slightly changing the synthesis variables. On the other hand, the aluminum source is typically aluminum isopropoxide or pseudo-boehmite, while orthophosphoric acid is a frequently used source for the phosphorus component. In the case of SAPO-*n*, MAPO-*n* and MAPSO-*n*, silica sol and/or a solution of the corresponding metal salts (often acetate or sulphate) are employed in the reaction mixture. In the case of solvothermal synthesis, the template and solvent molecules may form complexes that are capable of doing specific functions in the final framework structure [2, 3].

The microporous APO-*n* structure can also be synthesized in the presence of fluoride ions [40–42]. For example, the crystallization of APO-*n* with ZON structure type needs the presence of anions that compensate the charge of cationic template [41]. The fluoride ion is known to be an excellent mineralizing agent in the preparation of various microporous materials [42]. It solubilizes aluminum in the reaction mixture leading to a slower nucleation, and as a consequence yielding crystals of larger size with fewer defects. The fluoride ions can also behave as bidentate ligands

connecting two aluminum ions and a protonated organic amine as counterion. Indeed, APO-34, SAPO-34 and MAPO-*n* have been prepared from a fluoride-containing reaction medium. In the as-synthesized samples, the fluoride ions interact with the framework causing deformation, however, the fluoride ions are completely removed during the calcination [40–42].

Another important synthesis technique for the production of APO-*n* framework is the dry-gel conversion method in which a dry gel was prepared by mixing appropriate amounts of aluminium, phosphorous, and silicon sources with deionized water, and the resulting wet gel was subsequently heated to form a dry gel. The crystallization of dry gel was carried out in the presence of small amount of water vapor and/or volatile organics [43–45]. Recently, ionic liquids were used for the preparation of APO-*n* wherein ionic-liquid acts as a solvent as well as a template cation [46]. Such a method of preparation of zeo-type materials is referred to as ionothermal synthesis. Typically, 1-methyl-3-ethyl imidazolium bromide and choline chloride with urea mixture are used to prepare a number of microporous aluminophosphates, namely, SIZ-1, SIZ-2, SIZ-3, SIZ-4 and SIZ-5 [2, 3]. Further, APO-*n* structures, e.g., APO-5 and APO-11, were also prepared *via* ionothermal method, and the properties were compared with those of the samples synthesized employing conventional method [47]. In a similar way, a number of APO-*n* structures, e.g., UiO-7, APO-17, APO-22, APO-5 and SIZ-10 were also reported [48].

The microwave-assisted synthesis of molecular sieves is a new area of research. Accordingly, combining a hydrothermal technique and microwave heating, APO-*n* framework structure was prepared successfully [2, 3]. The main advantage of this method is that the crystallization time is considerably reduced owing to the fact that microwaves destroy the hydrogen bridges between water molecules causing fast gel dissolution and the formation of Al−O−P building blocks. In this way, several structures, including APO-5, MnAPO-*n* and MnAPSO-*n* ($n = 5$, 44) were reported [2, 3]. Moreover, microwaves also influence considerably the ionothermal solvent-based molecular sieve synthesis.

3.2.2 Mesoporous Aluminophosphates

Mesoporous aluminophosphate molecular sieve was first prepared using neutral surfactant leading to lamellar structure [28] followed by mesoporous silicoaluminophosphates [30]. Tetramethylammonium cations play an important role in the synthesis of mesoporous aluminophosphates such as (i) to adjust the pH of the mixture and (ii) participate in modifying the strength of the electrostatic interaction between APO species and cationic surfactants [31, 32, 49]. The nature of mesostructured APO-*n* formation depends on various synthetic conditions such as pH, synthesis temperature and Al/P ratio. The synthesis of mesoporous APO-*n* using a low Al/P molar ratio under high hydrothermal synthesis conditions results in lamellar structure [31]. The reduction of hydrothermal synthesis conditions, such as temperature, pressure, and surfactant concentration, favored formation of hexagonal mesoporous aluminophosphate structure [31, 50]. It was also reported that fluoride favors a facile synthesis of mesoporous aluminophosphates with hexagonal and

lamellar structure. However, upon calcination, the formation of a dense aluminophosphate phase with β-cristobalite has been noted [33, 44]. More details on recent progress on controlled synthesis of mesoporous aluminophosphate materials can be found in a review article [51]. A novel approach has been applied to the synthesis of thermally stable mesoporous APO from a preformed precursor of microporous aluminophosphate by a two-step procedure [52]. The triblock copolymers P123 and F127 have been used to prepare a highly ordered large pore (12 nm) mesoporous aluminophosphate based on an "acid–base" pair route [53]. The utilization of F127 as a structure-directing agent with different aluminium and phosphorous precursors such as $AlCl_3/H_3PO_4$, $AlCl_3/OP(OCH_3)_3$, and $Al(OC_4H_9)_3/PCl_3$ under nonaqueous (alcoholic) conditions leads to hexagonal mesoporous aluminophosphates, designated as HMA.

To retain the stability of mesoporous aluminophosphate materials, attempts were made to prepare mesoporous silico-aluminophosphate materials of MCM-41 type, using the gel mixture containing amorphous mesoporous aluminosilicate and aluminophosphate phases as precursor by a two-step procedure [54, 55]. High surface area mesoporous aluminum-phosphorus oxide-based derivatives have been synthesized through an S^+I^- surfactant-assisted cooperative mechanism by means of a one-pot preparative procedure using a water–alcohol reaction medium with the starting materials of aluminum atrane complexes and phosphoric and/or phosphorous acids [56]. The presence of triethanol amine originated from inert alumatrane proved the effectiveness of harmonizing the rate of hydrolytic reaction and the self-assembling process [56]. A series of aluminophosphate and iron-containing aluminophosphate was synthesized with the use of semifluorinated surfactant, which results in highly stable worm-like mesoporous aluminophosphate materials having very good thermal stability [57]. Table 3.3 summarizes mesoporous APO-*n*, developed by several researchers using surfactant template synthetic strategies and their structural information [26].

3.3 CHARACTERIZATION

The APO-*n* framework structure discussed so far includes an extensive range of microporous/mesoporous compositions. A large number of experimental techniques have routinely been used to characterize the framework structure that include diffraction, spectroscopy, thermal and imaging methods. In this section, we cover briefly the various methods employed for characterization of these materials. X-ray diffraction (XRD) is a very important and vital technique to characterize microporous and mesoporous aluminophosphates [72, 73]. The replacement of trivalent aluminium or pentavalent phosphorous by heteroions leads to an increase or decrease in unit-cell volume provided the symmetry of the materials remains intact [74]. This method is also useful to distinguish different phase formation under similar conditions [66]. On the other hand, small-angle X-ray scattering (SAXS) under different temperature and time intervals is a valuable technique for monitoring phase formation under the synthesis conditions, e.g.,

TABLE 3.3 Synthetic Conditions for the Preparation of Mesoporous Aluminophosphates[a]

Research Group	Surfactant (S)	Composition of starting mixture	Temp., time
Lamellar structure			
Kraushaar-Czarnetzki et al. [58]	$H_2N(CH_2)_nNH_2$	$0.5Al_2O_3$:$1.0P_2O_5$:1.0S:$80H_2O$	120°C; 24 h
Fyfe et al. [49]	$H_2N(CH_2)_nNH_2$	$1.0Al_2O_3$:$1.4P_2O_5$:0.7S:$50H_2O$	180°C; 16 h
	C_nTMABr	$0.3Al_2O_3$:$1.0P_2O_5$:1.0S:1.6TMAOH:$15H_2O$	150°C; 5 d
Kimura et al. [34]	C_nTMACl	$0.5Al_2O_3$:$1.0P_2O_5$:1.0S:2.0TMAOH:$65H_2O$	150°C; 5 d
Oliver et al. [59, 60]	$C_nH_{2n+1}NH_2$	$0.9Al_2O_3$:$1.8P_2O_5$:3.0S:2.$5H_2O$:14TEG	180°C; 3 d
Sayari et al. [28]	$C_nH_{2n+1}NH_2$	$1.0Al_2O_3$:$1.0P_2O_5$:1.0S:$60H_2O$	100°C, 24 h
Gao et al. [61, 62]	$C_nH_{2n+1}NH_2$	$0.5Al_2O_3$:$0.9P_2O_5$:3.4S:$1.7H_2O$:3.4n-C_mH_{2m+1}OH:13.8EG	180°C; 8 d
Khimyak and Klinowski [63, 64]	C_nTMACl	$0.83Al_2O_3$:$1.0P_2O_5$:0.8S:1.1TMAOH:$190H_2O$	130°C; 2 d
Yuan et al. [65]	C_nPBr/C_nTMACl	$1.0Al_2O_3$:$1.8P_2O_5$:1.0S:4.0TMAOH:$335H_2O$	100°C; 2 d
Feng et al. [33]	$H_2N(CH_2)_nNH_2$	$0.5Al_2O_3$:$1.0P_2O_5$:0.32S:$0.95H_2O$:13.5EG	180°C; 4 d
2-D Hexagonal (or disordered) structure			
Kimura et al. [34]	C_nTMACl	$1.0Al_2O_3$:$1.0P_2O_5$:1.0S:2.0TMAOH:$65H_2O$	< 130°C
Chakraborty et al. [30, 67]	C_nTMABr	$0.38Al_2O_3$:$1.0P_2O_5$:$0.014SiO_2$:$0.44S$:$85.4H_2O$	110°C; 12 h
Feng et al. [33]	C_nTMABr	$1.0Al_2O_3$:$1.3P_2O_5$:0.26S:1.7TMAOH:0.8HF:$117H_2O$:8.2EtOH	< 70°C
Zhao and coworkers [31, 50]	C_nTMACl	$1.24Al_2O_3$:$1.0P_2O_5$:1.0S:1.3TMAOH:$196H_2O$	RT
Tiemann et al. [67]	$C_nH_{2n+1}NH_2$	$1.0Al_2O_3$:$1.0P_2O_5$:1.0S:64EtOH:$6H_2O$	90°C; 2 d
Tiemann et al. [67]	$C_nH_{2n+1}NH_2$	$1.0Al_2O_3$:$1.0P_2O_5$:0.5S:32EtOH	90°C; 2 d
Yuan [65]	C_nTMABr	$1.0Al_2O_3$:$1.0P_2O_5$:0.35S:2.0-4.0TMAOH:$335H_2O$	RT, 24 h
Zhao and Lu [68]	C_nTMABr	$0.5Al_2O_3$:$0.75P_2O_5$:$0.2SiO_2$:1.0S:1.4TMAOH:8.0EtOH:$138H_2O$	70°C; 2 d
Kriesel et al. [69]	$EO_{106}PO_{70}EO_{106}$; $EO_{20}PO_{70}EO_{20}$	Using a molecular precursor such as $[Al(O^iPr)_2O_2P(O^tBu_2)]_4$	135°C; 12 h
Wang et al. [53]	$EO_{106}PO_{70}EO_{106}$; $EO_{20}PO_{70}EO_{20}$	Using inorganic acid–base pair sources such as $AlCl_3$ and H_3PO_4	RT
Mesoporous Thin Film			
Mazaj et al. [70]	$EO_{106}PO_{70}EO_{106}$	$1Al_2O_3$:12 H_2O:$2P_2O_5$:$0.4SiO_2$:001 S:100EtOH:(0.02-0.1) MnO_x:$8H_2O$	60°C; 24 h
Cecowski et al. [71]			130°C; 24 h

[a]Partially reproduced with permission from Ref. [26], © Elsevier.

the formation of lamellar mesoporous aluminophosphate/surfactant composite system can easily be monitored [66].

The nature of aluminum species and its coordination in aluminophosphate matrix can be studied using either conventional magic-angle spinning nuclear magnetic resonance (MASNMR) spectroscopy or with double rotation (DOR) and quadrupole nutation with fast MAS [75–81]. The ^{27}Al MASNMR spectra of aluminophosphates resulted in asymmetric multiple resonance maxima in the range -19 to 45 ppm with reference to $Al(H_2O)_6^{3+}$. The peak maxima at about 39 ppm are assigned to tetrahedral framework aluminum, and the remaining peak perceived in the range of -7 to -21 ppm corresponds to octahedral aluminum in nonframework location [75–81]. The use of DOR and dynamic-angle-spinning (DAS) techniques helps to remove first-order broadening effects such as chemical-shift anisotropy as well as second-order quadrupolar interactions [80]. The quadrupole nutation spectrum helps in orientation of sample, which enables identification of different kinds of tetrahedral species in aluminophosphate molecular sieves. For example, it is possible to distinguish two tetrahedral framework aluminium sites in VPI-5 [80]. In contrast, ^{31}P MASNMR spectra yield symmetrical lines in the chemical-shift range of -19 to -30 ppm with reference to phosphoric acid, H_3PO_4 [75–81]. Importantly, the chemical-shift values for ^{31}P MASNMR are structurally specific. For example, SAPO-37 of Faujasite-type structure yielded one signal at -26.1 ppm due to uniform distribution of phosphorous in the double six-membered (D6R) secondary building unit. In turn, SAPO-5 having secondary building units of double six-membered (D6R) and single six-membered ring (S6R) showed two resonances at -27.4 and -32.8 ppm, representing the phosphorous in D6R and S6R sites [75, 76].

The nature of transition-metal ions in the framework, their coordination environment and oxidation state are normally characterized using several spectroscopic techniques, such as FT-IR, diffuse reflectance UV-Vis (DR UV-Vis), and ESR. FT-IR spectra of aluminophosphate give important information in three regions, which are: (i) the 940–1200 cm^{-1} region features the stretching vibrations of T$-$O$-$T and T$-$O$-$M, where T stands for the central atom in the primary units as TO_4 tetrahedra; (2) the 750–950 cm^{-1} region, in which the bending of X-OH (where X = any atom other than O and H) occurs; and (3) the region $< 600\ cm^{-1}$, where the bending vibrations of T$-$O$-$T and T$-$O$-$M appear [82]. DR UV-Vis spectroscopy is an authoritative technique to distinguish the presence of framework and extraframework transition-metal ions in aluminophosphate molecular sieves [3, 4, 74, 82–85]. For example, DR UV-Vis spectra of titanium-containing molecular sieves normally show a single peak centered around 230 nm that corresponds to framework Ti(IV) species, and the absence of a shoulder around 300 nm represents the absence of bulk TiO_2 phase [3, 4, 74, 82, 84, 86]. Similarly, the DR UV-Vis spectra of cobalt (Co^{II} ions) containing aluminophosphate framework exhibit an absorption band in the region of 500–600 nm characteristic of tetrahedral species [3, 4, 74, 82, 85]. The DR UV-vis spectra of as-synthesized chromium-containing aluminophosphate show distinctive absorption bands at 642, 445 and 290 nm, typical of Cr^{III} ions in octahedral

(framework/extraframework/nonframework) coordination, which become upon calcination a strong charge-transfer band at 375 nm and a weak shoulder at 445 nm assigned to chromate and polychromate species, respectively [87–90].

The ESR spectroscopic technique is another useful tool to interpret the nature of transition-metal ion in the framework of aluminophosphate molecular sieves. ESR spectra of as-synthesized vanadium-containing aluminophosphate show well-resolved hyperfine splitting corresponding to tetravalent vanadium bonded strongly to oxygen ions in the matrix. The $g_{||}$ values are 2.0221 and 2.0046 and $g_{\perp}$ values are 2.0440 and 2.0380 for VAPSO and VAPO catalysts, respectively [82, 91–94]. However, the calcined samples exhibit a relatively low intensity peak, which indicates the oxidation of the framework tetravalent vanadium to the ESR silent pentavalent vanadium species. The ESR spectrum of manganese-containing aluminophosphate shows an intense and large signal at $g_{\text{eff}} = 2$ and a very broad and weak line at $g_{\text{eff}} = 4.2$, characteristics of Mn^{II} ions in extraframework octahedral and framework tetrahedral species, respectively [32, 82, 95]. Similarly, the ESR study on iron-containing aluminophosphate molecular sieves allow distorted and isolated trivalent iron species to be distinguished based on the strong signal at $g_{\text{eff}} = 4.3$ and the weak signal at $g_{\text{eff}} = 2$, respectively [36]. The nature of transition-metal ions in the framework of aluminophosphate can be elaborated with the help of various spectroscopic techniques.

The nature of acidic sites and the kind of acidity of silica-substituted and metal-substituted aluminophosphates are commonly studied by diffuse reflectance IR Fourier transform (DRIFT) spectroscopy in the OH-stretching vibration region and by the adsorption of probe molecules (NH_3 and CO), calorimetric measurements of the differential molar heat of ammonia (NH_3) and temperature-programmed desorption (TPD) of ammonia [96, 97]. The materials having mild acidity were studied using the weakly interacting probe molecules such as CO, H_2, and N_2 [98, 99]. The recent development on *in situ* and high throughput techniques might help to understand catalytic active species under reaction conditions [82, 92]. In the next section we will be covering the liquid phase oxidation of various organic substrates using aluminophosphate molecular sieves.

3.4 CATALYTIC PROPERTIES

3.4.1 Oxidation of Hydrocarbons

The activation of carbon–hydrogen (C−H) bonds of saturated hydrocarbons and aromatic compounds over heterogeneous catalysts is an important topic for both basic and applied chemistry. In this regard, APO-5/APO-34 structures containing framework cobalt species were shown to be promising catalysts for activation of methane [100] and propane [101] by partial oxidation at elevated temperature. Likewise, vanadium- and cobalt-containing APO-5 materials were found to be potential catalysts for oxydehydrogenation of alkanes such as ethane and propane [102, 103]. In this section, we present certain important

applications of aluminophosphate molecular sieves as catalysts for various hydrocarbon oxidation reactions.

3.4.1.1 Linear Alkanes The oxidation products of linear alkanes are a source of important feedstock for the fine chemicals, polymer and pharmaceutical industries. On the other hand, the oxygenation of linear alkanes is one of the major challenges of modern catalysis. Aluminophosphate molecular sieves having framework transition-metal ions serve as efficient catalysts for regioselective oxidation of linear alkanes [104]. Trivalent cobalt containing APO-18 framework structure favors regioselective oxidative attack of *n*-hexane at both ends [105] and leads to the formation of terminally oxidized products such as hexanol, hexanal and hexanoic acid.

3.4.1.2 Cycloalkanes The oxidation of cyclohexane in liquid phase using heterogeneous catalysts is an important area of research. In this regard, metalloaluminophosphates MAPO-*n* (M = V, Cr, Mn, Fe, Co, Cu) are promising catalysts [106]. Among the various APO-*n* structures, APO-5, APO-18, APO-36, and APO-VFI frameworks have been identified as a suitable matrix for the oxidation of cyclohexane based on the kinetic diameter of the reactant and product molecules [107]. CrAPO-5 [87], MnAPO-5 [108, 109] and CoAPO-5 [110] showed potential as catalysts for autoxidation of cyclohexane. CrAPO-5 and MnAPO-5 produced a mixture of cyclohexanol and cyclohexanone as the major products as a result of selective decomposition of cyclohexyl hydroperoxide [87]. On the other hand, quenching studies over CrAPO-5 reveal considerable leaching of active (chromium) species under the reaction conditions, which accounts for the observed activity. Interestingly, CoAPO-5 yields adipic acid with a selectivity of 45%. The redox properties of the catalyst were related to the presence of the framework cobalt ions in two different oxidation states [110]. Similarly, MAPO-VFI (M = Ti, V, Cr, Mn, Fe, Co) in the presence of *tert*-butyl hydroperoxide (TBHP) oxidize selectively cyclohexane to cyclohexanone [111]. The catalysts VAPO-VFI and CrAPO-VFI show better activity; however, leaching of the active metal species occurs. On the one hand, the use of small pore FeAPO-31 increased adipic acid selectivity compared to FeAPO-5 [104]. This was rationalized in terms of limited diffusion of cyclohexane and cyclic intermediates within the FeAPO-31 channel system, which facilitates further oxidation of the cyclic intermediates into linear products. The use of acetylperoxyborate (APB) as oxidant in conjunction with MAPO-*n* catalyst containing redox centers, namely, FeAPO-31, FeAPO-5 and MnAPO-5, enables conversion of cyclohexane with high efficiency (*ca.* 88%) and exceptionally high selectivity (*ca.* 81%) to adipic acid [112]. The key feature of this reaction is that up on dissolving APB, peroxy acetic acid forms and releases active oxygen.

Metal-substituted hexagonal mesoporous aluminophosphates (MHMA; M = V, Cr, Fe, Co) were studied for oxidation of cycloalkanes in the presence of methyl ethyl ketone (MEK) as initiator and H_2O_2 as oxidant in acetic acid medium [35, 36, 85, 90, 94]. Among the materials studied, VHMA and CrHMA show superior performance [90, 94]. Unlike many other chromium-based silicate matrixes [113–116], the mesoporous aluminophosphates stabilize the active site, possibly, in the

TABLE 3.4 Oxidation of Cycloalkanes over Various Cobalt Catalysts[a]

Catalyst	Substrate	Conversion[b,c] (wt%)	Product Selectivity (wt%)[b,c]		
			-ol	-one	Others
CoHMA	Cyclohexane	90.7 (86.8)	93.4 (88.9)	4.8 (9.4)	1.8 (1.7)
	Cyclooctane	92.4 (90.8)	85.0 (81.5)	11.5 (14.8)	3.5 (3.7)
	Cyclododecane	89.8 (86.0)	77.0 (75.5)	17.1 (20.0)	5.9 (4.5)
Co/MCM-41[d]	Cyclohexane	68.7 (40.7)	87.1 (86.7)	8.7 (10.8)	4.2 (2.5)
CoAPO-5	Cyclohexane	78.9 (50.8)	81.6 (8.2)	17.3 (15.1)	6.1 (4.7)
Co/S-1[d]	Cyclohexane	41.2	85.7	6.7	7.6

Reaction conditions: substrate: oxidant (H_2O_2) = 1 : 1; catalyst, 50 mg (3.3 wt%); solvent, acetic acid (10 ml); MEK 5 mmol; temperature 373 K; time 12 h.

[a]Reproduced with permission from Ref. [35], © Elsevier.

[b]First run.

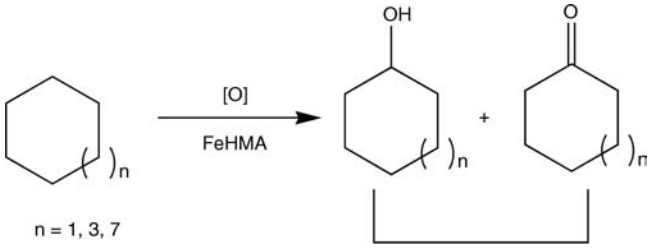
[c]Values in parenthesis indicate for the fourth run.

[d]Nonframework cobalt ion.

framework. Further, the higher catalytic activity was explained based on the pentavalent/hexavalent chromium in a tetrahedral environment present in the matrix, which may interact with the oxidant (hydrogen peroxide) to form a catalytically active peroxo complex. The reaction was also carried out over Co/MCM-41, CoAPO-5 and Co/S-1, and the activity followed the trend: CoHMA > CoAPO-5 > Co/MCM-41 > Co/S-1 [17, 35]. In the case of silicate matrix, i.e. CoS-1 and CoMCM-41, the metal oxides generally decompose hydrogen peroxide, which thus decreases the efficiency of the oxidant, and this may be the cause of the lower activity. The activity also decreased with recycling, with a considerable amount of cobalt leached into the reaction mixture (Table 3.4).

However, CoHMA [85] and FeHMA [36, 117] showed relatively low cyclohexane conversion compared to the corresponding chromium and vanadium analogs. The catalytic activity was practically unaffected by recycling experiments [85, 118]. It was also demonstrated that FeHMA is an efficient catalyst (Scheme 3.4) for the oxidation of cycloalkanes with molecular oxygen or air [117]. In all these cases, the HMA structure remained intact even after several recycle exercises and the catalyst showed better activity than many other catalytic systems reported so far.

3.4.1.3 Aromatics The development of catalysts for liquid phase oxidation of aromatics into valuable products such as phenol, benzaldehyde, benzoic acid, and terephthalic acid, is an important area of research. FeAPO-5 is a promising catalyst for oxidation of benzene to phenol in vapor phase; however, the activity is reduced drastically after 6 h of reaction time owing to coke formation [57]. On the other hand, CuAPO-11 shows potential for hydroxylation of benzene into phenol in the presence of H_2O_2 in liquid phase [118], and the observed catalytic activity is



SCHEME 3.4 Oxidation of cycloalkanes over FeHMA. Reproduced with permission from Ref. [117], © The Chemical Society of Japan.

attributed to framework copper species without any leaching of the active species. It is also observed during the reaction that the evolution of molecular O_2 suggests the presence of hydroxyl radicals (•OH) and hydroperoxide radicals (•OOH), both of which are generated upon the interaction of the framework copper ions with H_2O_2. The use of a radical quencher such as ethanol alters the benzene conversion, which confirms that the above reaction proceeds *via* a free-radical mechanism [118].

3.4.1.4 Alkyl Aromatics CoAPO-11 and CoAPO-5 are effective, stable and recyclable heterogeneous catalysts for oxidation of *p*-cresol to *p*-hydroxybenzaldehyde (*p*-HBA) using molecular O_2 as oxidant with a conversion and selectivity of $\sim 90\%$ [119, 120]. The superior performance of CoAPO-*n* molecular sieves in comparison with homogeneous cobalt-based catalysts can be explained on the basis that the formation of μ-hydroxo-bridged cobalt dimer, which has a detrimental effect in the said transformation, is prevented in the confined environment of the APO catalyst [119]. However, the use of methanolic sodium hydroxide results in leaching of cobalt species, thus suggesting that the reaction occurs in the homogeneous phase [120]. The catalysts CoAPO-5, CoAPO-11, and CoAPO-31 were also screened for the oxidation of ethylbenzene (EB) using TBHP as oxidant [121]. Acetophenone, benzaldehyde and ethylbenzene tertiary butyl hydroperoxide (EBTBHP) were obtained as the reaction products. It was elaborated that the reaction proceeds through a free-radical mechanism that involves first formation of EBTBHP intermediate on the active sites. Then the intermediate is converted to final products, namely, acetophenone and benzaldehyde [121]. A similar kind of study was also carried out over CrAPO-5, which showed a complete conversion of EB and over 84% conversion of tetralin [122]. As expected, the catalysts revealed considerable leaching of chromium ions from the framework structure. VHMA was also evaluated for oxidation of EB and benzyl alcohol with TBHP as oxidant [123]. The high activity of the catalyst was explained based on the framework vanadium ions in the mesoporous matrix [123]. Mesoporous chromium-containing aluminophosphate was found to be active in vapor phase oxidation of toluene with molecular oxygen [124]. Many catalysts, including FeHMA, CoHMA and CrHMA as well as

the corresponding APO-5 structures, were studied for liquid phase oxidation of tetralin using TBHP as oxidizing agent [125]. In general, the chromium containing catalysts showed higher catalytic activity; the chromium-containing MCM-41 displayed better results, except for the fact that it suffered from leaching of active chromium species much higher than the aluminophosphate matrix [126].

3.4.2 Oxidation of Olefins

The use of metallo-aluminophosphates (MAPO-*n*) as epoxidation catalysts has attracted considerable interest for various industrially important olefins. Microporous TiAPO-5, TiAPO-11 and TiAPO-36 catalyze oxidation of olefins with H_2O_2 in liquid phase; however, the conversion is lower than over the corresponding silicates, namely, TS-1 [86]. In the case of APO-*n*, the low conversion is attributed to the presence of titanium, mostly, in extraframework sites. On the other hand, TiAPO-5 was also found to be an effective catalyst for the production of adipic acid from cyclohexene in the absence of an organic solvent [127]. Likewise, mesoporous titanosilicates, e.g., Ti-HMS, were used for the conversion of α-pinene to campholenic aldehyde *via a* direct epoxidation route in the absence of radicals [128].

MnAPO-36 and CoAPO-36 convert cyclohexene, pinene, limonene and styrene in the presence of benzaldehyde to their corresponding epoxides and diols under aerobic (dry air) conditions [129] *via* the radical route where a large amount of allylic oxidation products is formed. Benzaldehyde, used as a sacrificial reductant, interacts with active sites and generates $PhCO^{\bullet}$ radicals followed by interaction with O_2 to yield $PhCOOO^{\bullet}$ radical that subsequently reacts with olefin to produce epoxides [129]. The higher activity of MAPO-36 could be attributed to the presence of a greater fraction of trivalent manganese or cobalt ions in the framework structure. However, the presence of divalent manganese in the APO-5 framework structure favors epoxidation of cyclohexene and methylcyclohexene (Table 3.5) in the presence of APB [130].

The simultaneous presence of titanium and cobalt in the APO-5 framework results in a highly efficient catalyst for epoxidation of cyclohexene with APB (see

TABLE 3.5 Selective Oxidation of Alkenes over Various MAPO-*n* in Presence of APB[a]

Substrate	Catalyst	Conversion (mol%)	Selectivity (mol%)	
Cyclohexene			Epoxide	Diols
	MnAPO-5	32.3	31.9	0.5
	TiAPO-5	35.0	99.0	—
	CoAPO-5	12.0	99.0	—
	TiCoAPO-5	82.0	99.0	—
			Epoxide	Others
1-Methyl-1-cyclohexene	MnAPO-5	32.6	31.0	1.5

[a]Reproduced with permission from Ref. [130], © Royal Society of Chemistry.

TABLE 3.6 Epoxidation of Various Olefins over VHMA in the Presence of H_2O_2[a]

Substrate	Product	Conversion (%)	Selectivity (%)
Styrene	Styrene oxide	75.2 (74.0)[b]	99.2 (98.3)[b]
α-Pinene	Pinene oxide	56.7	97.3
Limonene	Limonene oxide	51.2	96.7
Norbornene	exo-Norbornene oxide	68.4	99.1

[a]Reproduced with permission from Ref. [123], © Elsevier.
[b]Recycling results (after 2 runs).

Table 3.5) [131]. The bimetallic (TiCoAPO-5) catalyst gives a significantly higher level of cyclohexene conversion (82%) as compared to its monometallic analogs, namely, CoAPO-5 (12%) and TiAPO-5 (35%). The higher activity of the former may be explained based on the synergistic effect of the different metal ions present in the microporous matrix. That is, the cobalt centers help in the initiation and generation of free-radical intermediates [131], while titanium acts as an oxophilic center that participates in concomitant interaction with the olefin during the reaction.

In the case of VAPO-*n*, the catalysts show pore-size-dependent activity for the epoxidation of cyclopentene in presence of APB [132]. The large pore VAPO-5 (7.3 Å) affords relative ease of access of the substrate and oxidant to the active sites located in the channels compared to small pores (4.0 × 6.5 Å) of the VAPO-11 channel that significantly retards the diffusion, thus limiting the turnover frequency values [132]. Interestingly, mesoporous VHMA [123] shows promise for epoxidation of various alkenes with H_2O_2 as oxidant (Table 3.6). The catalyst can also be recycled without much loss in activity, and the framework structure remains intact throughout the process.

Chromium-containing APO-5 and APO-11 catalysts are also promising for allylic oxidation of α-pinene to verbenone using TBHP as oxidant [133]. The stability of chromium, in general, in the APO-*n* framework structure was evaluated by filtering experiments under the reaction conditions. It was inferred that crystal size plays a significant role in metal leaching, and more importantly, leaching of trace amounts of chromium species from the matrix is sufficient for the observed catalytic activity.

3.4.3 Oxidation of Alcohols

Oxidation of alcohols into aldehydes, ketones, and corresponding acids is an important reaction in organic synthesis, normally carried out using salts or oxides of transition metals. MnAPO-5 and CrAPO-5 catalysts in the presence of dissolved APB selectively oxidize primary, secondary, benzylic and other alcohols under mild reaction conditions [130]. Table 3.7 presents the results of the oxidation of various aromatic, aliphatic and unsaturated alcohols.

TABLE 3.7 Selective Oxidation of Alcohols over Various MAPO-*n* in the Presence of APB[a]

Substrate	Catalyst	Conversion (mol%)	Selectivity (mol%)		
1-Octanol			Octanal	Octanoic acid	
	CrAPO-5	12.6	12.4	0.3	
2-Octanol			2-Octanone	Others	
	MnAPO-5	21.9	21.5	0.5	
	CrAPO-5	45.4	44.5	1.2	
Benzyl alcohol			Benzaldehyde	Benzoic acid	Others
	MnAPO-5	28.7	25.6	1.0	1.3
	CrAPO-5	11.9	11.7	–	–
Cyclohexanol			Cyclohexanone	ε-Caprolactone	Others
	MnAPO-5	86.3	44.1	30.0	12.0
	CrAPO-5	71.2	32.0	36.5	2.3
4-Hydroxytoluene			4-Hydroxy-benzaldehyde	4-Hydroxy-benzoic acid	4-Methyl catechol
	MnAPO-5	9.2	2.6	6.7	–

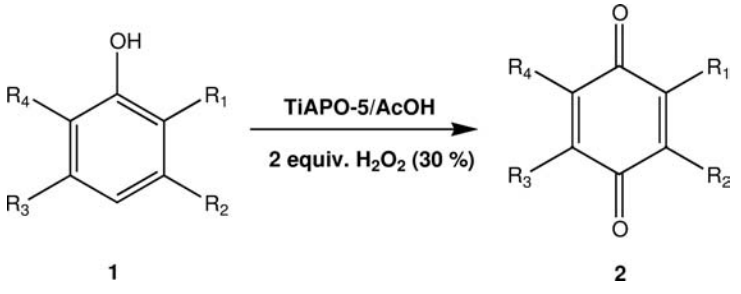
[a]Reproduced with permission from Ref. [130], © Royal Society of Chemistry.

The liquid phase oxidation of glycerol using various transition-metal-containing APO-5 and silicalite-1 (S-1) matrixes was studied in the temperature range of 20–80 °C using H_2O_2 as oxidant [134]. Formic acid and mono-formate ester of glycerol were found to be the major products together with a complex mixture of acetals. Among the various catalysts studied, vanadium- and chromium-containing silicalite and aluminophosphate materials show higher activity even at low (20 °C) temperature. The higher activity is attributed to considerable leaching of the active metal ions from the framework, while the titanium-containing materials are quite stable under the reaction conditions.

3.4.4 Oxidation of Phenols

A series of metal-substituted APO-11 framework structures was studied for hydroxylation of phenol using H_2O_2 as oxidant at 80 °C. Among the transition-metal-containing catalysts, FeAPO-11 and CoAPO-11 revealed comparable performance to TS-1 [135]. The CoAPO-*n* matrices having different pore sizes were also evaluated for the title reaction. The observed order of activity is as follows: CoAPO-11 ≫ CoAPO-50 > CoAPO-36 = CoAPO-5. On the other hand, TiAPO-5 having a large pore size (7.3 Å) facilitates the oxidation of substituted phenols (2,3,5-trimethylphenol, TMP) to the corresponding quinones (2,3,5-trimethylbenzoquinone, TMBQ) with nearly a complete conversion and excellent selectivity [136]. The reaction was supposed to proceed through hydroxylation of TMP to give trimethylhydroquinone (TMHQ) followed by the oxidative dehydrogenation to yield TMBQ. The catalyst was also employed for the transformation of several other substituted phenols (Scheme 3.5) and the results are summarized in Table 3.8. The presence of methyl group at the *ortho*- and *para*- positions favored higher activity compared to substitution at the *meta* positions as well as unsubstituted phenol owing to inductive effect of alkyl groups [136].

In a similar way, mesoporous TiHMA was found to be a potential catalyst for oxidation of phenol with the conversion level of 18.5%, which is slightly low compared with TS-1 (27%). However, TiHMA showed remarkable *para*-isomer selectivity with a *para*-to-*ortho* ratio of 1.7 and the reaction also proceeded at a



SCHEME 3.5 Oxidation of substituted phenols over TiAPO-5. Reproduced with permission from Ref. [136], © The Chemical Society of Japan.

TABLE 3.8 Oxidation of Substituted Phenols over TiAPO-5[a]

Substrate[b]	R_1	R_2	R_3	R_4	Product	Conversion (wt%)	Yield (wt%)
1a	Me	H	H	Me	**2a**	49.2	19.4
1b	H	Me	Me	H	**2b**	99.0	71.3
1c	Me	H	H	H	**2c**	48.1	14.2
1d	H	Me	H	H	**2d**	51.4	25.3
1e	H	H	H	H	**2e**	7.0	traces

[a]Reproduced with permission from Ref. [136], © The Chemical Society of Japan.
[b]See Scheme 3.5.

lower temperature [84]. Importantly, the leaching study at the reaction temperature indicated no evidence of leaching of titanium from HMA framework structure, in addition to the activity that was retained over several recycle runs [84]. The oxidation of bulkier molecules such as 2,6-di-*tert*-butyl phenol (2,6-DTBP) into corresponding quinone (2,6-DTBQ) over this catalyst showed 42% conversion, whereas the corresponding microporous analogs, namely, TiAPO-5 and TS-1, produced only 5% conversion [137]. The observed lower conversion in the latter case is attributed to smaller pore opening that possibly hinders the diffusion of bulk molecules. Iron-substituted mesoporous aluminophosphate FeHMA catalyzed phenol hydroxylation using a phenol-to-peroxide ratio of 3:1 and water as solvent [138].

3.4.5 Ammoximation and Ammoxidation

The conversion of cyclohexanone to oxime and its subsequent Beckmann rearrangement to ε-caprolactam is imperative as the products are key intermediates in the manufacture of nylon-6 (Scheme 3.6).

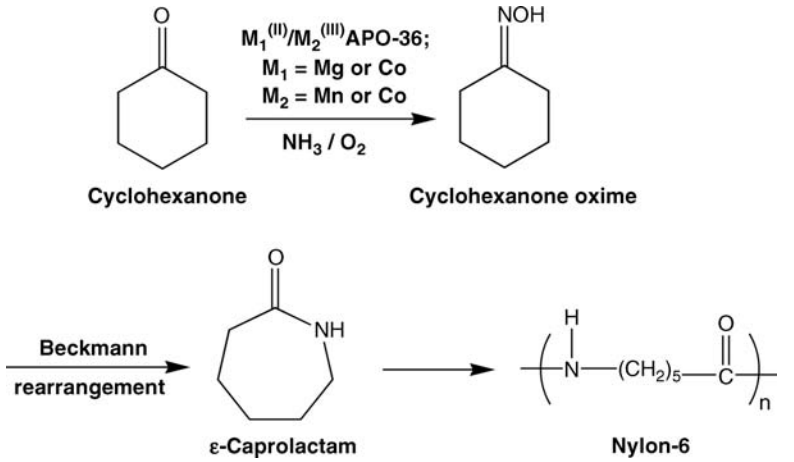
Aluminophosphates having bifunctionality, e.g., $M_1^{II}M_2^{III}$APO-36 ($M_1 = $ Mg or Co and $M_2 = $ Co or Mn), with both redox and acidic sites, effectively convert cyclohexanone to ε-caprolactam *via* cyclohexanone oxime [139]. In the framework of $M_1^{II}M_2^{III}$APO-36, M^{II} ions create Brønsted acid sites, while M^{III} ions function as redox sites. The pore dimensions of MAPO-36 (see Table 3.1) are sufficiently large for penetration of the reactant as well as the product molecules. Thus, the reaction proceeds elegantly over $Mg^{II}M_2^{III}$APO-36 ($M_2 = $ Mn or Co) as the trivalent redox site in the framework structure, in the presence of ammonia and molecular oxygen, generates hydroxylamine (NH_2OH) *in situ* [104, 139] that reacts with cyclohexanone to form cyclohexanone oxime that, in turn, isomerizes to ε-caprolactum at Brønsted acid sites. Among the different oxidants, molecular O_2 yields NH_2OH more efficiently than H_2O_2 or TBHP over these catalysts (Table 3.9). In the case of analogous ($Mg^{II}Co^{III}$)APO-18, the pore diameter is considerably smaller and hence the reaction does not proceed well [139].

TABLE 3.9 Solvent-Free Ammoximation of Cyclohexanone over MAPO-*n*[a]

Catalyst	Oxidant	Conversion (%)	TON	Selectivity (%)		
				Oxime	ε-Caprolactam	Others
Co^{II}APO-36	O_2	1.9	28	28.4	–	72.3
$Co^{II}Co^{III}$APO-36	O_2	20.2	322	54.2	21.1	24.5
	H_2O_2	12.9	215	36.4	14.7	55.3
	TBHP	17.9	289	76.7	10.0	13.3
$Mn^{II}Mn^{III}$APO-36	O_2	23.6	381	57.0	20.2	22.8
	H_2O_2	15.8	254	41.1	18.4	40.6
	TBHP	19.0	308	65.4	18.2	15.9
$Mg^{II}Co^{III}$APO-36	O_2	21.5	212	33.9	42.9	22.7
$Mg^{II}Mn^{III}$APO-36	O_2	23.0	262	36.2	45.2	18.0
$Mg^{II}Co^{II}$APO-36	O_2	2.2	15	26.9	–	73.0
Co^{III}APO-18	O_2	32.4	550	86.5	–	13.7
$Mg^{II}Co^{III}$APO-18	O_2	31.7	412	87.5	–	12.3

[a]Reprinted with permission from Ref. [139]. Copyright (2001) American Chemical Society.

Ammoxidation of C−H bonds located in the allylic/benzylic position of unsaturated hydrocarbons is an important industrial process for the production of nitriles using ammonia and oxygen. Vanadium-containing VSAPO-37 show promise as mild and selective ammoxidation catalysts in vapor phase [140].



SCHEME 3.6 Ammoximation of cyclohexanone over MAPO-36. Reprinted with permission from Ref. [139]. Copyright (2001) American Chemical Society.

3.4.6 Baeyer–Villiger Oxidation

The oxidation of ketones into corresponding lactones is one of the main transformations in organic synthesis. A series of aluminophosphate catalysts, e.g., CoAPO-5, CoAPO-36, MnAPO-36, and MnAPO-5, was used for such conversion, and the trivalent cobalt and manganese sites have been identified as the active centers [104, 141]. These catalysts are highly efficient in the presence of molecular oxygen and benzaldehyde as sacrificial reductant. The large pore APO-36 and APO-5 molecular sieves having cobalt and manganese ions oxidized varieties of ketones, including adamantan-2-one, to lactones with a very high selectivity [104, 141]. Percarboxylic acid formed *in situ* from the sacrificial aldehyde and dioxygen acts as an oxygen donor to convert cyclic ketones into the corresponding lactones [142].

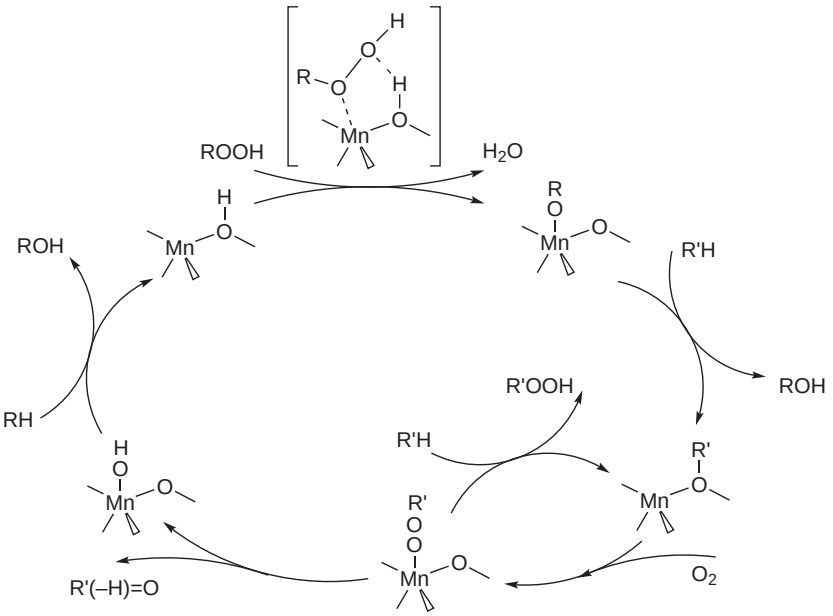
3.4.7 Oxidation of Heterocycles

The microporous MnAPO-5 catalyst was used for selective oxidation of heterocyclic compounds such as picolines, pyrazines and pyridazines to the related carboxylic acid with APB as oxidant [143]. The conversion of 4-picoline into isonicotnic acid was achieved up to 70% with a remarkable selectivity of 90%. The reaction was also studied in the presence of peroxyacetic acid and nearly the same conversion was obtained; however, the selectivity for isonicotinic acid was reduced drastically [143]. The reaction was also studied in the presence of borate component such as Neobor$^{@}$(borax pentahydrate), which helps in dissolution of APB in reaction media and favors high activities [143].

3.5 MECHANISTIC ASPECTS

In order to understand the catalytic behavior for any set of reaction, it is important to know the mechanistic pathway. Transition-metal-containing aluminophosphates MAPO-*n* are promising catalysts for oxidation of several organic substrates with the help of oxidants such as H_2O_2, ROOH, and O_2. The oxidation using the above catalysts can proceed *via* homolytic routes that involve free-radical ($HO^{\bullet}$, $HOO^{\bullet}$, $RO^{\bullet}$, $ROO^{\bullet}$) intermediates and/or heterolytic oxygen transfer through the formation of oxometal or peroxometal species [145]. Transition-metal ions in their highest oxidation state with d^0 configurations such as Ti^{IV}, Mo^{VI} and W^{VI} favor peroxometal route due to the Lewis acid character of the metal ions, and their oxidation state does not change during the pathway [110, 114, 115, 145, 147]. On the other hand, strong (one-electron) oxidants, e.g. later and/or first-row transition elements such as Cr^{III}, Mn^{III}, Co^{III} and Fe^{III}, operate either through the oxometal route or homolytic decomposition of ROOH [110, 145–148].

It is widely accepted that the oxidation of hydrocarbons with molecular O_2 proceeds *via* a classical free-radical mechanism with the formation of ROOH intermediates [15, 16, 110, 145]. The role of free radicals in oxidation of alkanes using Co- and Mn-containing APO-36 was confirmed using radical scavengers [15, 16].



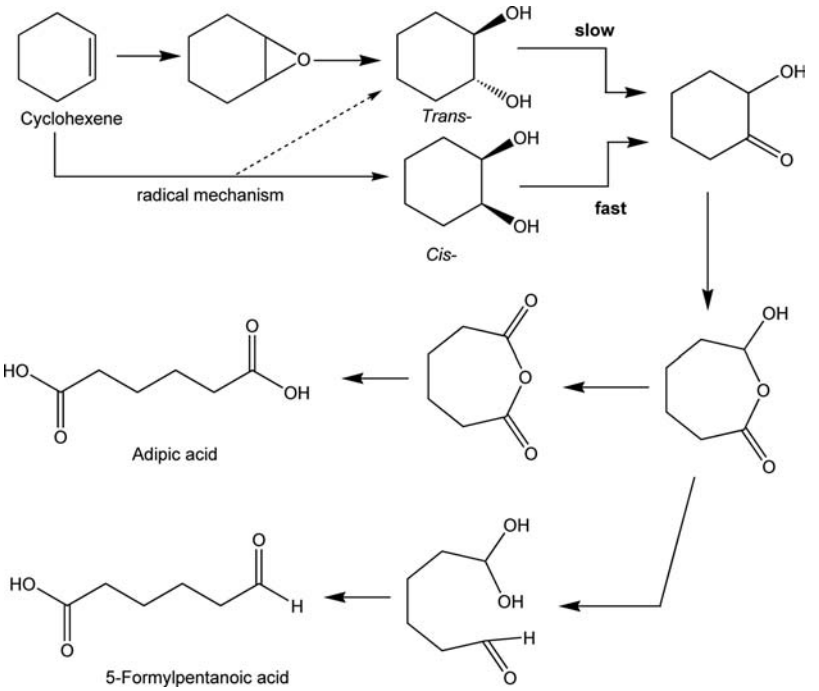
SCHEME 3.7 Mechanistic pathways for the oxidation of cyclohexane catalyzed by MnAPO-5. Reproduced with permission from Ref. [146], © Elsevier.

An induction period observed for the oxidation of alkanes was reduced by the addition of traces of a free-radical initiator such as TBHP. On the other hand, kinetic and isotopic studies on the oxidation of cyclohexane on MnAPO-5 catalysts with O_2 as oxidant allowed the authors to propose an alternate set of elementary steps that avoids free-radical intermediates and instead includes bound radical-like species that form ROH and R(−H)=O in a stepwise fashion (Scheme 3.7).

A detailed mechanism for the oxidation of cyclohexene to adipic acid using aqueous hydrogen peroxide and TiAPO-5 was established by parallel ^{13}C NMR, ^{1}H NMR and GC-MS techniques [127]. The proposed reaction pathway is shown in Scheme 3.8. In general, the oxidation of cyclohexene to adipic acid involves a multistep process, where the formation of only *cis*-diol proceeds *via* a free-radical mechanism while other steps do not involve free-radical intermediates.

The oxidation of benzene with H_2O_2 on CuAPO-11 and CuAPO-5 follows similar to Fenton's chemistry [118]. The reaction mechanism involves the formation of $^{\bullet}OOH$ and $^{\bullet}OH$ radicals through interaction of the oxidant with framework Cu^{2+} and Cu^{+} species, respectively, and subsequent hydroxylation of benzene with hydroxyl radicals. The conversion of benzene is hindered by addition of ethanol as a free-radical quencher [118].

The oxidation of *p*-cresol into *p*-hydroxy benzaldehyde over cobalt-containing APO shows much better yield than the corresponding homogeneous cobalt salt. In a homogeneous medium, cobalt forms μ-oxo bridged complex that reduces the



SCHEME 3.8 Mechanistic pathways for the oxidation of cylcohexene with H_2O_2 catalyzed by TiAPO-5. Reproduced with permission from Ref. [127], © John Wiley and Sons.

conversion, whereas in heterogeneous catalyst, the absence of μ-oxo bridged complex formation effectively helps to increase the conversion of *p*-cresol into *p*-hydroxy benzaldehyde [120].

3.6 CATALYSTS STABILITY

Heterogeneous catalysts should possess structural stability for long catalytic runs. Although many studies focus on catalytic activity of MAPO-*n* for a variety of catalytic transformations, only a few concern the structural stability and catalyst reusability. The liquid phase oxidation reactions carried out over transition-metal-ion containing MAPO-*n* under acidic or basic conditions normally affect either structure stability and/or transition-metal ions stability in the framework [120, 141–150]. For example, the dissolution of APO-*n* material has been noticed during the catalytic oxidation of *p*-cresol process over CoAPO-11 [120]. Although CoAPO-*n* show constant activity for epoxidation of cycloalkenes as well as

oxidation of 2-nonanol, a totally new situation emerges on the structural stability [151]. That is, the structure remains intact under the conditions of epoxidation, but it collapses during the oxidation of 2-nonanol reaction. Similarly, in the case of VAPO-5, the framework crystallinity decreases with increasing vanadium loading and a complete collapse of the framework structure is noticed with the formation of dense tridymite phase for the aerial oxidation of *n*-hexane to adipic acid [104]. However, in most cases, the MAPO-*n* structures having transition-metal ions isomorphically substituted in place of trivalent aluminum ions show good resistivity against leaching as well as excellent thermal stability [16, 17, 123, 126, 132, 136].

To check the reusability of the mesoporous aluminophosphate catalysts, recycling and washing experiments were normally carried out. In the case of CoHMA [35], only a small loss in activity was observed even after the fourth run. This clearly indicates that most of the cobalt ions are intact in the framework, which was confirmed by ICP-AES analysis of the filtrate. Moreover, the reaction was also performed on the filtrate and the quenched solution, which showed only a meager activity, thus suggesting CoHMA to be a truly heterogeneous catalyst. This is well supported by the DR UV-Vis studies of the treated catalysts, and further confirmed by performing the reaction over ammonium-acetate-washed catalyst, where comparable activity was observed. Importantly, CoHMA shows strong stability during several treatments such as ammonium-acetate washing, recalcination or even several catalytic runs [35]. A similar observation was made for several other catalysts, namely, TiHMA [84], VHMA [94], CrHMA [90, 113], and FeHMA [36, 117, 152] wherein the materials retained their structure even when they were subjected to catalytic transformation in acetic acid medium. In contrast, the mesoporous materials accompanied with the nonregular alternation of four-, five- or six-coordinated AlO_x polyhedra and PO_4 tetrahedra demonstrate a lower hydrothermal stability compared to microporous APO-*n* materials [26, 34, 66, 68, 153].

3.7 CONCLUSION

The aluminophosphate molecular sieves having both micropores and mesopores are revolutionary new materials among the numerous heterogeneous catalysts. The remarkable diversity in structure and porosity offers broader adsorptive and catalytic applicability. The organic templates, surfactants, and synthesis conditions play a major role in the formation of these ordered open-framework structures. Transition-metal-ion substituted materials have fascinating properties and are the subject of research in various oxidation processes. Although they show promising results, a better understanding of their framework textural properties, active sites and their interaction with guest molecules needs to be addressed. More advanced synthesis procedures have to be developed that selectively increases the amount of framework transition-metal ions in the matrix. Similarly, the reproducible synthesis methodology is required to establish stable mesoporous aluminophosphate framework preparation.

ACKNOWLEDGMENTS

This work is partially supported by a grant-in-aid for the scientific research by the Council of Scientific and Industrial Research, New Delhi under the New Millennium Indian Technology Leadership Initiative programme (No. 5/258/52/2006-NMITLI). We also thank the Department of Science and Technology, New Delhi for funding the National Centre for Catalysis Research, IIT-Madras, Chennai. One of the authors (A.S.) would like to thank Delhi University, Delhi for the financial support (R & D grant 2012/917).

REFERENCES

1. Flanigen E.M., Lok B.M., Patton R.L., Wilson S.T. (1986). *Pure Appl. Chem.* 58, 1351–1358.
2. Pastore H.O., Coluccia S., Marchese L. (2005). *Annu. Rev. Mater. Sci.* 35, 351–395.
3. Rajić N. (2005). *J. Serb. Chem. Soc.* 70, 371–391.
4. Hartmann M., Kevan L. (1999). *Chem. Rev.* 99, 635–663.
5. Hartmann M., Kevan L. (2002). *Res. Chem. Intermed.* 28, 625–695.
6. Wilson S.T., Lok B.M., Flanigen E.M., inventors; Union Carbide Corporation, assignee. US Patent 4,310,440. 1982.
7. Wilson S.T., Lok B.M., Messina C.A., Cannan T.R., Flanigen E.M. (1982). *J. Am. Chem. Soc.* 104, 1146–1147.
8. Lok B.M., Messina C.A., Patton R.L., Gajek R.T., Cannan T.R., Flanigen E.M., inventors; Union Carbide Corporation, assignee. US Patent 4,440,871. 1984.
9. Lok B.M., Messina C.A., Patton R.L., Gajek R.T., Cannan T.R., Flanigen E.M. (1984). *J. Am. Chem. Soc.* 106, 6092–6093.
10. Flanigen E.M., Patton R.L., Wilson S.T. (1988). *Stud. Surf. Sci. Catal.* 37, 13–27.
11. Martens J.A., Jacobs P.A. (1994). *Stud. Surf. Sci. Catal.* 85, 653–685.
12. Yu J., Xu R. (2006). *Chem. Soc. Rev.* 35, 593–604.
13. Yang Y.M., Walawalkar G., Pinkas J., Roesky H.W., Schmidt H.G. (1998). *Angew. Chem. Int. Ed.* 37, 96–98.
14. Löwenstein W. (1954). *Am. Mineral.* 39, 92–96.
15. Thomas J.M., Raja R., Sankar G., Bell R.G. (1999). *Nature* 398, 227–230.
16. Thomas J.M., Raja R., Sankar G., Bell R.G. (2001). *Acc. Chem. Res.* 34, 191–200.
17. Mohapatra S.K. (2005). *Ph.D. Thesis*, IIT-Bombay.
18. Stöcker M. (1999). *Microporous and Mesoporous Mater*. 29, 3–48.
19. Inui T., Matsuda H., Okaniwa H., Miyamoto A. (1990). *Appl. Catal. A: General* 58, 155–163.
20. Thomas J.M., Xu Y., Catlow C.R.A., Couves J.W. (1991). *Chem. Mater.* 3, 667–672.
21. Weitkamp J. (1982). *Ind. Eng. Chem., Proc. Res. Dev.* 21, 550–558.
22. Liu Y., Liu C., Liu C., Tian Z., Lin L. (2004). *Energy and Fuels* 18, 1266–1271.
23. Rastelli H., Lok B.M., Duisman J.A., Earls D.E., Mullhaupt J.T. (1982). *Can. J. Chem. Eng.* 40, 44–49.

24. Elangovan S.P., Kannan C., Arabindoo B., Murugesan V. (1988). *Appl. Catal. A: General* 174, 213–219.
25. Rabo J.A., In: *Zeolite Microporous Solids: Synthesis, Structure and Reactivity*, Vol. 352. NATO ASI Series, Kluwer, London, 1992, pp. 531–554.
26. Kimura T. (2005). *Micropor. Mesopor. Mater.* 77, 97–107, and references cited therein.
27. Oliver S., Kuperman A., Coombs N., Louth A., Ozin G.A. (1995). *Nature* 378, 47–50.
28. Sayari A., Karra V.R., Reddy J.S., Moudrakovski I.L. (1996). *Chem. Commun.*, 411–412.
29. Sayari A., Moudrakovski I.L., Reddy J.S. (1996). *Chem. Mater.* 8, 2080–2088.
30. Chakraborty B., Pulikottil A.C., Das S., Viswanathan B. (1997). *Chem. Commun.*, 911–912.
31. Zhao D., Luan Z., Kevan L. (1997). *Chem. Commun.*, 1009–1010.
32. Zhao D., Luan Z., Kevan L. (1997). *J. Phys. Chem. B* 101, 6943–6948.
33. Feng P., Xia Y., Feng J., Bu X., Stucky G.D. (1997). *Chem. Commun.*, 949–950.
34. Kimura T., Sugahara Y., Kuroda K. (1999). *Chem. Mater.* 11, 508–518.
35. Selvam P., Mohapatra S.K. (2005). *J. Catal.* 233, 276–287.
36. Selvam P., Mohapatra S.K. (2006). *J. Catal.* 238, 88–99.
37. Wilson S.T., Flanigen E.M., inventors; Union Carbide Corporation, assignee. US Patent 4,567,029. 1986.
38. Zhu Z.D., Hartmann M., Kevan L. (2000). *Chem. Mater.* 12, 2781–2787.
39. Martens J.A., Grobet P.J., Jacobs P.A. (1990). *J. Catal.* 126, 299–305.
40. Marchese L., Frache A., Coluccia E., Martra G., Causá M., Coluccia S. (1999). *Micropor. Mesopor. Mater.* 30, 145–153.
41. Sierra L., Patarin J., Guth J.L. (2000). *Micropor. Mesopor. Mater.* 38, 123–133.
42. Wheatley P.S., Morris R.E. (2002). *J. Solid State Chem.* 167, 267–273.
43. Zhang L., Gavalas G.R. (1999). *Chem. Commun.*, 97–98.
44. Zhang L., Yao J., Zeng C., Xu N. (2003). *Chem. Commun.*, 2232–2233.
45. Bandyopadhyay R., Bandyopadhyay M., Kubota Y., Sugi Y. (2002). *J. Porous Mater.* 9, 83–95.
46. Cooper E.R., Andrews C.D., Wheatley P.S., Webb P.B., Wormald P., Morris R. (2004). *Nature* 430, 1012–1016.
47. Parnham E.R., Morris R.E. (2007). *Acc. Chem. Res.* 40, 1005–1013.
48. Liu L., Li X., Xu H., Li J., Lin Z., Dong J. (2009). *J. Chem. Soc., Dalton Trans.*, 10418–10421.
49. Fyfe C.A., Schwieger W., Fu G., Kokoailo G.T., Grondey H. In: *Symposium on Zeolites, Layered Compounds and Other Microporous Solids. American Chemical Society, 209th National Meeting*, Anaheim, CA, USA, 1995, pp. 266.
50. Luan Z., Zhao D., He H., Kilnowski J., Kevan L. (1998). *J. Phys. Chem. B* 102, 1250–1259.
51. Perez J.O., Borade R.B., Clearfield A. (1998). *J. Mol. Struct.* 470, 221–228.
52. Zhou Z., Liu G., Zhang W.X., Liao X.Z., Hou Y.Z., Jia M.Z. (2005). *Mater. Lett.* 59, 3503–3506.

53. Wang L., Tian B., Fen J., Liu X., Yang H., Yu C., Tu B., Zhao D. (2004). *Micropor. Mesopor. Mater.* 67, 123–133.
54. Conesa T.D., Mokaya R., Campelo J.M., Romero A.A. (2006). *Chem. Commun.*, 1839–1841.
55. Conesa T.D., Mokaya R., Yang Z., Luque R., Campelo J.M., Romero A.A. (2007). *Micropor. Mesopor. Mater.* 252, 1–10.
56. Haskouri J.E., Cabero M.P., Guillem C., Latorre J., Beltràn A., Beltràn D., Amorós P. (2009). *J. Solid State Chem.* 182, 2122–2199.
57. Shiju N.R., Fiddy S., Sonntag O., Stockenhuber M., Sankar G. (2006). *Chem. Commun.*, 4955–4957.
58. Kraushaar-Czarnetzki B., Stork W.H.J., Dogterom R.J. (1993). *Inorg. Chem.* 32, 5029–5033.
59. Oliver S., Kuperman A., Coombs N., Lough A., Ozin G.A. (1995). *Nature* 378, 47–51.
60. Oliver S., Coombs N., Ozin G.A. (1995). *Adv. Mater.* 7, 931–935.
61. Gao Q., Xu R., Chen J., Li R, Li S., Qiu S., Yue Y. (1996). *J. Chem. Soc., Dalton Trans.*, 3303–3307.
62. Gao Q., Chen J., Xu R., Yue Y. (1997). *Chem. Mater.* 9, 457–462.
63. Khimyak Y.Z., Klinowski J. (1998). *Chem. Mater.* 10, 2258–2265.
64. Khimyak Y.Z., Klinowski J. (1998). *J. Chem. Soc., Faraday Trans.* 94, 2241–2247.
65. Yuan Z.-Y., Chen T.-H., Wang J.-Z., Li H.-X. (2001). *Mater. Chem. Phys.* 68, 110–118.
66. Chakraborty B., Pulikottil A. C, Viswanathan B. (1998). *Appl. Catal. A: General* 167, 173–181.
67. Tiemann M., Fröba M., Rapp G., Funari S.S. (2009). *Stud. Surf. Sci. Catal.* 129, 559–566.
68. Zhao X.S., Lu G.Q. (2001). *Micropor. Mesopor. Mater.* 44–45, 185–194.
69. Kriesel J.W., Sander M.S., Tilley T.D. (2001). *Adv. Mater.* 13, 331–335.
70. Mazaj M., Costacurta S., Logar N.Z., Mali G., Tušar N.N., Innocenzi P., Malfatti L., Thibault-Starzyk F., Amenitsch H., Kaučič V., Soler-Illia G.J.A.A. (2009). *Langmuir* 24, 6220–6225.
71. Cecowski S., Tušar N.N., Rangus M., Mali G., Soler-Illia G.J.A.A., Kaučič V. (2010). *Micropor. Mesopor. Mater.* 135, 161–169.
72. Richardson J.J.W., Pluth J.J., Smith J.V. (1988). *Acta Crystallogr.* B44, 367–373.
73. Davis M.E., Saldarriaga C., Montes C., Garces J.M., Crowder C. (1988). *Nature* 331, 698–699.
74. Weckhuysen B.M., Rao R.R., Martens J.A., Schoonheydt R.A. (1999). *Eur. J. Inorg. Chem.*, 565–577.
75. Blackwell C.S., Patton R.L. (1984). *J. Phys. Chem.* 88, 6135–6139.
76. Blackwell C.S., Patton R.L. (1988). *J. Phys. Chem.* 92, 3965–3970.
77. Wu Y., Chmelka B.F., Pines A., Davis M.E., Grobet P.J., Jacobs P.A. (1990). *Nature* 346, 550–552.
78. Barrie P.J., Smith M.E., Klinowski J. (1991). *Chem. Phys. Lett.* 180, 6–12.
79. Jelinek R., Chmelka B.F., Wu Y., Grandinetti P.J., Pines A., Barrie P.J., Klinowski J. (1991). *J. Am. Chem. Soc.* 113, 4097–4101.

80. Rocha J., Klinowski J., Barrie P.J., Jelinek R., Pines A. (1992). *Solid State Nucl. Magn. Reson.* 1, 217–225.
81. Mali G., Rangus M., Soler-Illia G.J.A.A., Kaučič V. (2008). *Stud. Surf. Sci. Catal.* 174, 949–952.
82. Frunza L., Pelgrims J., Leeman H., Van Der Voort P., Vansant E.F., Schoonheydt R.A., Weckhuysen B.M. (2001). *J. Phys. Chem. B* 105, 2677–2686.
83. Ashtekar S., Chilukuri S.V.V., Prakash A.M., Harendranath C.S., Chakrabarty D.K. (1995). *J. Phys. Chem.* 99, 6937–6943.
84. Mohapatra S.K., Hussian F., Selvam P. (2003). *Catal. Commun.* 4, 57–62.
85. Mohapatra S.K., Selvam P. (2003). *Top. Catal.* 22, 17–21.
86. Zahedi-Niaki M.H., Kapoor M.P., Kaliaguine S. (1998). *J. Catal.* 177, 231–239.
87. Chen J.D., Sheldon R.A. (1995). *J. Catal.* 153, 1–8.
88. Weckhuysen B.M., Verberckmoes A.A., De Baets A.R., *Schoonheydt R. A.* (1997). *J. Catal.* 166, 160–171.
89. Zhu Z., Chang Z., Kevan L. (1999). *J. Phys. Chem. B* 103, 2680–2688.
90. Mohapatra S.K., Hussian F., Selvam P. (2003). *Catal. Lett.* 85, 217–222.
91. Kulkarni S.J., Rao R.R., Subrahmanyam M., Farsinavis S., Rao P.K., Rao R.A.V. (1995). *Stud. Surf. Sci. Catal.* 98, 161–165.
92. Weckhuysen B.M., Vannijvel I.P., Schoonheydt R.A. (1995). *Zeolites* 15, 482–489.
93. Frunza L., Van Der Voort P., Vansant E.F., Schoonheydt R.A., Weckhuysen B.M. (2000). *Micropor. Mesopor. Mater.* 39, 493–507.
94. Mohapatra S.K., Selvam P. (2004). *Catal. Lett.* 93, 47–53.
95. Sinha A.K., Satyanarayana C.V.V., Srinivas D., Sivasanker S., Ratnasamy P. (2000). *Micropor. Mesopor. Mater.* 35–36, 471–481.
96. Lohse U., Bertram R., Jancke K., Kurzawaski I., Parlitz B., Löffler E., Schreier E. (1995). *J. Chem. Soc., Faraday Trans.* 91, 1155–1161.
97. Akolekar D.B. (1995). *J. Mol. Catal. A: Chemical* 104, 95–102.
98. Coluccia S., Marchese L., Martra G. (1999). *Micropor. Mesopor. Mater.* 30, 43–56.
99. Knözinger H., Huber S. (1998). *J. Chem. Soc., Faraday Trans.* 94, 2047–2059.
100. Maroni V.A., Williams K.A., Nguyen H., Iton L.E. In: *ACS Symposium on Fuels Chemistry 35*, 1990, pp. 584–591.
101. Sasidharan M., Kiyozumi Y., Bhaumik A. (2011). *Catal. Sci. Technol.* 1, 255–259.
102. Blasco T., Concepción P., López-Nieto J.M., Pérez-Pariente J. (1995). *J. Catal.* 152, 1–17.
103. Concepción A., Corma A., López-Nieto J.M. Pérez-Pariente J. (1996). *Appl. Catal. A: General* 143, 17–28.
104. Raja R., Sankar G., Thomas J.M. (2000). *Angew. Chem. Int. Ed.* 39, 2310–2313.
105. Raja R., Thomas J.M. (2002). *J. Mol. Catal. A: Chemical* 181, 3–14.
106. Schuchardt U., Cardoso D., Sercheli R., Pereira R., Da Cruz R.S., Guerreiro M.C., Mandelli D., Spinacé E.V., Pires E.L. (2001). *Appl. Catal. A: General* 211, 1–17.
107. Sankar G., Raja R., Thomas J.M. (1998). *Catal. Lett.* 55, 15–23.
108. Dugal M., Sankar G., Raja R., Thomas J.M. (2000). *Angew. Chem. Int. Ed.* 39, 2310–2313.

109. Hou Z., Han B., Gao L., Liu Z., Yang G. (2002). *Green Chem*. 4, 426–430.
110. Lin S.S., Weng H.S. (1993). *Appl. Catal. A: General* 105, 289–308.
111. Luna F.J., Ukawa S.E., Wallau M., Schuchardt U. (1997). *J. Mol. Catal. A: Chemical* 117, 405–411.
112. Raja R., Thomas J.M., Xu M., Harris K.D.M., Greenhill-Hooper M., Quill K. (2006). *Chem. Commun.*, 448–450.
113. Sakthivel A., Selvam P. (2002). *J. Catal.* 211, 134–143.
114. Sakthivel A., Dapurkar S.E., Selvam P. (2003). *Appl. Catal. A: General* 246, 283–293.
115. Dapurkar S.E., Sakthivel A., Selvam P. (2003). *New J. Chem.* 27, 1184–1190.
116. Sakthivel A., Arunkumar N., Selvam P. (2002). *Bull. Chem. Soc. Ind.* 1, 136–141.
117. Mohapatra S.K., Selvam P. (2004). *Chem. Lett.* 33, 198–199.
118. Qi X., Li J., Ji T., Wang Y., Feng L., Zhu Y., Fan X., Zhang C. (2009). *Micropor. Mesopor. Mater.* 122, 36–41.
119. Sheldon R.A., De Heij N. In: *The Role of Oxygen in Chemistry and Biochemistry*. Ando W., Mora-oka Y. eds. Elsevier, Amsterdam, 1988, pp. 243–256.
120. Peeters M.P.J., Busio M., Leijten P. (1994). *Appl. Catal. A: General* 118, 51–62.
121. Venkatathiri N., Kumar G.P.A. (2004). *Ind. J. Chem. Technol.* 11, 843–847.
122. Vidya K., Mahalingam R.J., Selvam P. (2002). *Bull. Catal. Soc. Ind.* 1, 142–148.
123. Venkatathri N., Srivastava R. (2005). *Catal. Commun.* 6, 177–183.
124. Subrahmanyam Ch., Louis B., Rainone F., Viswanathan B., Renken A., Varadarajan T.K. (2003). *Appl. Catal. A: General* 241, 205–215.
125. Shaikh R.A., Chandrasekar G., Biswas K., Choi J.S., Son W.J., Jeong S.Y., Ahn W.S. (2008). *Catal. Today* 132, 52–57.
126. Sakthivel A., Badamali S.K., Selvam P. (2002). *Catal. Lett.* 80, 73–76.
127. Lee S.O., Raja R., Harris K.D.M., Thomas J.M., Johnson B.F.G., Sankar G. (2003). *Angew. Chem. Int. Ed.* 42, 1520–1523.
128. Suh Y.W., Kim N.K., Ahn W.S., Rhee H.K. (2003). *J. Mol. Catal. A: Chemical* 198, 309–316.
129. Raja R., Sankar G., Thomas J.M. (1999). *Chem. Commun.*, 829–830.
130. Raja R., Thomas J.M., Hooper M.G., Doukova V. (2007). *Chem. Commun.*, 1924–1926.
131. Paterson J., Potter M., Gianotti E., Raja R. (2011). *Chem. Commun.*, 517–519.
132. Vishnuvarthan M., Paterson A.J., Raja R., Piovano A., Bonino F., Gianotti E., Berlier G. (2011). *Micropor. Mesopor. Mater.* 138, 167–175.
133. Lempers H.E.B., Sheldon R.A. (1998). *J. Catal.* 175, 62–69.
134. McMorn P., Roberts G., Hutchings G.J. (1999). *Catal. Lett.* 63, 193–197.
135. Dai P.E., Petty R.H., Ingram C.W., Szostak R. (1996). *Appl. Catal. A: General* 143, 101–110.
136. Mahalingam R.J., Selvam P. (1999). *Chem. Lett.*455–456.
137. Tanev P.T., Chibwe M., Pinnavaia T.J. (1994). *Nature* 368, 321–323.
138. Du Y., Yang Y., Liu S., Xiao N., Zhang Y., Xiao F.S. (2008). *Micropor. Mesopor. Mater.* 114, 250–256.
139. Raja R., Sankar G., Thomas J.M. (2001). *J. Am. Chem. Soc.* 123, 8153–8154.

140. Kulkarni S.J., Rao R.R., Subrahmanyam M., Rao A.V.R., Sarkany A., Guzi L. (1996). *Appl. Catal. A: General* 139, 59–74.
141. Raja R., Thomas J.M., Sankar G. (1999). *Chem. Commun.*, 525–526.
142. Thomas J.M., Raja R., Sankar G., Johnson B.F.G., Lewis D.W. (2001). *Chem. Eur. J.* 7, 2973–2978.
143. Raja R., Thomas J.M., Greenhill-Hooper M., Ley S.V., Almeida-Paz F.A. (2008). *Chem. Eur. J.* 14, 2340–2348.
144. Vanoppen D.L., De Vos D.E., Genet M.J., Rouxhet P.G., Jacobs P.A. (1995). *Angew. Chem. Int. Ed.* 34, 560–563.
145. Sheldon R.A., Arends I.W.C.E., Lempers H.E.P. (1998). *Catal. Today* 41, 387–407.
146. Modén B., Bi-Zeng Z., Dakka J., Santiesteban J.G., Iglesia E. (2006). *J. Catal.* 239, 390–401.
147. Sheldon R.A., Arends I.W.C.E., Dijksman A. (2000). *Catal. Today* 57, 157–166.
148. Gómez-Hortigüel L., Corà F., Catlow C.R.A. (2011). *ACS Catalysis* 1, 945–955.
149. Lempers H.E.B., Sheldon R.A. (1997). *Stud. Surf. Sci. Catal.* 105, 1061–1068.
150. Haanepen M.J., van Hooff J.H.C. (1997). *Appl. Catal. A: General* 152, 183–201.
151. Van Breukelen H.F.W.J., Gerritsen M.E., Ummels V.M., Broens J.S., van Hooff J.H.C. (1997). *Stud. Surf. Sci. Catal.* 105, 1029–1035.
152. Selvam P., Mohapatra S.K. (2002). *Chem. Commun.*, 1466–1467.
153. Rajic N., Kaucic V., Logar N.Z. *Molecular Sieves: Aluminophosphates. Encyclopedia of Catalysis*, Wiley, 2011, DOI: 10.1002/0471227617.eoc151.pub2.
154. Meier W.M., Olson D.H., Baerlocher Ch., *Atlas of Zeolite Structure Types*, 4th revised edn, Elsevier, New York, 1996

4

SELECTIVE OXIDATIONS CATALYZED BY MESOPOROUS METAL SILICATES

OXANA A. KHOLDEEVA

4.1 INTRODUCTION

At the end of the 20th century and at the dawn of the 21st one, a large scientific effort was made on the elaboration of methods for the synthesis and characterization of a wide variety of mesoporous materials [1, 2]. The great interest in such materials in the catalytic community was caused by their potential advantage in transformations of large molecules that meets the demands of the fine chemicals industry [3, 4], refining of heavy petroleum components [5], and transformation of biomass to fuels [6]. Indeed, microporous zeolites are efficient catalysts for transformations of small molecules (propene, phenol, benzene, etc.) but they become unsuitable when reactants with sizes comparable with the dimensions of the pores have to be involved into the catalytic process. The rational approach to overcome mass-transfer limitations would be to increase the diameter of pores, bringing them into the mesoporous region (according to the IUPAC definition, these are materials with pore diameters in the range of 20–500 Å).

Several methodologies have been suggested for elaboration of mesoporous materials containing catalytically active transition-metal ions (M) as a part of the solid structure. Synthesis of hierarchical zeolites that comprise both micro- and mesopores has received significant attention [2, 7]. Such materials are discussed in Chapter 2 of this book. The sol-gel technique was widely applied for the preparation

Liquid Phase Oxidation via Heterogeneous Catalysis: Organic Synthesis and Industrial Applications, First Edition. Edited by Mario G. Clerici and Oxana A. Kholdeeva.
© 2013 John Wiley & Sons, Inc. Published 2013 by John Wiley & Sons, Inc.

of amorphous mixed oxides comprising catalytically active MO_n species dispersed at the molecular level within the main silicon oxide matrix. The synthesis, characterization, and catalytic applications of MO_n–SiO_2 mixed oxides have been reflected to varying degrees in a few review articles and book chapters [8–17]. Since the discovery of the M41S family of molecular sieves by researchers at Mobil Oil Corporation in the early 1990s [18–20] the surfactant-templating strategy has been widely used for the preparation of ordered materials, including transition-metal-containing mesoporous silicates*. Various aspects of such materials, particularly synthetic routes, formation mechanisms, surface modification, characterization, and applications, have been covered by the extensive review literature [21–43].

Following the critical target of creating a mesoporous analog of the titanium silicalite TS-1, a great deal of research work was devoted to the synthesis of mesoporous titanium silicates and assessment of their catalytic performance, which has been reflected in numerous reviews [11–13, 21–29, 32, 34–37]. Significant progress has been also achieved in the inclusion of other metals (M = Zr, Ce, V, Nb, Cr, Mo, W, Mn, Fe, Co, etc.) into mesoporous silicates. Here, we review the current state of the mesoporous metal silicates research after more than fifteen years of intense activity in the field. Research articles published until the end of 2011 have been surveyed from the standpoint of their relevance to heterogeneous liquid phase oxidation catalysis. Our aim was to summarize the main achievements in the preparation of both ordered and nonordered transition-metal-containing mesoporous silicates and to analyze critically their applications as catalysts, providing a guideline for the correct evaluation of the large amount of data available in the literature. This chapter will not cover mesoporous catalysts prepared by tethering, anchoring, and ship-in-bottle techniques that will be covered in Chapters 6 and 7.

The chapter starts with a brief description of the general approaches for the synthesis of mesoporous metal silicates and the most commonly used characterization techniques. Advantages and disadvantages of different synthetic methodologies related to catalysis are addressed. After discussion of the major synthetic routes, liquid phase oxidation processes over mesoporous metal silicates are surveyed, with particular emphasis on the structure/activity/selectivity relationships and critical analysis of the catalyst stability and reusability. Discussion on the scope and limitations of such catalysts in liquid phase oxidation processes closes the chapter.

4.2 SYNTHESIS AND CHARACTERIZATION

4.2.1 General Synthetic Approaches

The majority of known mesoporous metal silicates can be divided into two fundamentally different classes, namely, nonordered materials and ordered ones. The first class includes mixed oxides of silicon and transition metals (aerogels and xerogels).

* The terms “silica” and “silicate” are interchangeably used in the literature related to mesoporous materials.

Such materials are most often obtained by the conventional sol-gel methodology [8–15, 17, 44], although some other techniques can be applied [16, 45, 46]. Miller and Ko [47] have defined mixed oxides as materials that approach homogeneity throughout the bulk on a molecular scale.

The second class comprises mesostructured materials that are prepared by the so-called templated synthesis [18–43, 48]. Their structure is characterized by an ordered arrangement of uniform mesopores-channels, while the silica walls separating the channels are amorphous. The peculiarity of such structure is reflected in the terms "mesophase" and "mesostructure" which imply existence of long-range ordering and lack of short-range ordering (at the atomic level). This structural feature distinguishes mesostructured materials from zeolites, crystalline materials that possess both types of ordering. Hence, mesostructured materials occupy an intermediate position between zeolites and amorphous oxides. A combination of different synthetic strategies can be applied to prepare composite materials comprising different structural elements [7, 49].

Catalytically active metal ions can be introduced into a silica matrix directly during its synthesis or alternatively deposited onto the surface of a silica support following various postsynthesis methodologies [16, 25, 34, 36, 45, 50–52]. Chemical design of catalysts with site-isolated active centers was the focus of catalytic research since the early 1970s, and the first catalysts of this type appeared in the field of catalytic polymerization [51, 52]. Then the concept of site isolation has received significant development in the works of Basset [51, 53], Ermakov [54], Thomas [50, 55, 56], Don Tilley [16, 45, 57], and other groups [58]. Thomas defined *single-site heterogeneous catalysts* (SSHC) as catalysts that possess spatially isolated and uniform in composition and distribution accessible active sites strongly bound to the surface, thus ensuring constant energetic interaction between each metal center and the reactants. SSHC differ from supported nanodispersed oxides where surface metal-oxide phases can be identified by modern spectroscopic techniques. The latter materials find applications in gas phase processes but their use in liquid phase is restricted by propensity to metal leaching. Hence, SSHC are in the focus of this chapter.

4.2.2 Characterization Techniques

Physicochemical techniques used for characterization of mesoporous materials, in particular, metal silicates, have been covered by extensive review literature [11–14, 21–28, 30, 33, 34, 36, 38–43]. Here, we aim to provide just a brief summary on the main characterization methods, which could be useful for readers who are not directly involved in the mesoporous materials research.

Scanning electron microscopy (SEM) is used to investigate surface topography and morphology of mesoporous materials, including the size and shape of particles. High-resolution transmission electron microscopy (HR TEM) provides direct structural information at the nanometer scale. Low-temperature (77 K) nitrogen adsorption allows surface area determination and pore-size analysis. Both mesostructured silicates and aerogels reveal adsorption isotherms of type IV in the IUPAC

classification, typical of mesoporous materials. With increasing P/P_0, a liquid-like adsorbate film is formed on the pore walls and, at a certain pressure, capillary condensation takes place, filling mesopores with condensed adsorbate. The narrow interval of $\Delta(P/P_0)$, within which the nitrogen capillary condensation occurs, is a manifestation of a narrow pore-size distribution (PSD), characteristic of ordered materials. The standard Brunauer–Emmett–Teller (BET) analysis is widely used to evaluate mesopore surface areas (the relative pressure range of 0.05–0.3 or 0.04–0.2). The Barrett–Joyner–Halenda (BJH) method is frequently used to determine PSD but it may underestimate the size of mesopores. For more precise calculation of PSD, new advanced methods are employed [27, 30, 33, 43, 59–64]. The primary mesopore volume, external surface area and micropore volume are determined by comparative methods (t-plot and α-plot) [40, 59].

Low-angle X-ray diffraction (XRD) is conventionally used to recognize the formation of a mesostructured material [18, 23, 26, 27, 30, 40, 41, 43]. Each type of mesostructure reveals a specific XRD pattern in the range of low angles and no high angle distinctive peaks, indicating the amorphous nature of the silica wall and the absence of impurity MO_n phase (for metal silicates). Electron diffraction (ED) and small-angle X-ray/neutron scattering (SAXS/SANS) are complementary techniques for structural characterization. A combination of XRD, N_2 adsorption and HR TEM is most frequently used to identify the formation of a specific mesostructure. Generally, it is expected that the unit-cell parameter a_0 will be enlarged after incorporation of metals with ionic radius larger than that of Si^{4+}. The thickness of the silicate walls h_W can be evaluated as a difference between the value of a_0 determined by XRD and the pore-size diameter D evaluated from N_2 adsorption data. Since different methods are used for calculation of D [59, 62, 64], the reported h_W values can vary significantly (up to 1.5–2 times) for the same type of material.

The ^{29}Si nuclear magnetic resonance spectroscopy with line narrowing by the magic-angle spinning (^{29}Si MAS NMR) provides important supplementary information on the structure of silica walls [11, 14, 17, 19, 23, 27, 38, 43]. Despite some ambiguities in the deconvolution of overlapping signals in the spectra, this technique makes it possible to estimate the number of sites with specific coordination, i.e. $Si(OSi)_n(OH)_{4-n}$ (Q_n, $n = 2$–4). Materials with a more intensive Q_4 peak (*ca.* –110 ppm) compared to Q_3 (–100 ppm) and Q_2 (–90 ppm) peaks have more crosslinked silica network and, hence, are more hydrophobic. Incorporation of transition metals M often promotes a further crosslinking of silica framework, which is manifested by the increasing relative intensity of the Q_4 peak. The ^{29}Si MAS NMR technique is widely used to quantify the degree of surface silylation after postsynthesis modifications. Additionally, the surface concentration of silanol groups can be evaluated by FT-IR, mass spectrometry, thermogravimetric analysis (TGA) or titration with specific reagents [38, 44].

The crucial information for understanding the catalytic performance on the state (oxidation degree, coordination geometry, nuclearity) of metals in silica matrix is gained by spectroscopic techniques, such as FT-IR, Raman, UV-vis, EPR, X-ray absorption spectroscopy (EXAFS/XANES), X-ray photoelectron spectroscopy (XPS), photoluminescence, and some others [11, 13, 21, 23, 28, 34, 36, 56]. Each

technique provides unique and complementary information that can be combined to get a fairly complete description of the active sites.

Bulk characterization techniques. UV-vis spectroscopy in a diffuse reflectance mode (DRS UV-vis) is a simple and very useful technique that often allows conclusions to be drawn about the oxidation degree and coordination of M ions inserted in silica network [11, 13, 23, 28]. Oxometal species give absorption bands in the UV-vis region due to ligand-to-metal ($O^{2-} \rightarrow M^{n+}$) charge transfer (CT). The position of this electronic transition depends on the ligand-field symmetry surrounding the M center. For oxygen ligands, a higher-energy transition is expected for tetrahedral M^{n+} than for octahedral one. The appearance of dimeric, oligomeric and polymeric metal-oxide species is manifested by a progressive long-wave shift of the DRS UV band and its broadening. Extended X-ray Absorption Fine Structure (EXAFS) analysis affords useful information about the first and second coordination shell of a heteroelement in silicate matrix, including interatomic distances [11, 13, 23, 34, 56]. EXAFS seems to be the most suitable method for direct verification of framework incorporation, by identifying silicon as the backscatterer in the second shell. The position, shape and intensity of X-ray absorption near-edge structure (XANES) peak allow conclusions to be drawn about the local structure of M ions (Ti, Fe, Cr, Co, etc.). Through careful EXAFS/XANES analyses, it is possible sometimes to identify and distinguish between surface-bound and framework-incorporated transition metals. Raman spectroscopy enables detection of early stages of the emergence of metal-oxide microcrystallites [21, 23]. For paramagnetic ions, EPR is a complimentary technique for drawing conclusions about the electronic and coordination state [21, 23, 28]. Solid-state nuclear magnetic resonance (NMR ^{17}O, ^{27}Al, ^{51}V, ^{119}Sn, etc.) gives additional information about the structure of active centers [21, 23, 27, 28].

Surface characterization techniques. Characterization of surface of metal silicates is necessary for understanding catalytic performance. Information about the composition of the surface layer (4–5 nm) and the electronic structure of the elements can be acquired from XPS studies [11, 13]. This technique is widely employed in combination with bulk elemental analysis methods (ICP–AES, EDX, etc.) to verify whether all M ions are homogeneously distributed within a silica particle (silicate wall) or there is a surface enrichment or, oppositely, deficiency. Surface-sensitive information, particularly, surface acidity, can be derived from FT-IR techniques using molecular adsorbates [65–67]. Weak (CO, N_2), intermediate (CH_3CN, CD_3CN), or strong (NH_3, pyridine) bases are used as probe molecules; however, weak and intermediate bases are preferable because they are much more specific than strong ones. In metal silicates, Brønsted sites are typically surface OH groups and aprotonic Lewis sites are framework M at the surface. A basic probe molecule interacts with hydroxyl groups *via* hydrogen-bonding, resulting in weakening of the O–H bond and in a shift ($\Delta\nu_{OH}$) of the O–H stretching frequency to lower values. The larger the $|\Delta\nu_{OH}|$ the higher the acidic strength of the Brønsted sites. Adsorption of a base on aprotonic Lewis sites leads to the formation of a Lewis acid–base adduct. The higher the Lewis acidity the larger is the shift of adsorbed molecules stretching frequencies. Presently, there are no direct methods

to strictly quantify the accessibility of active metal centers; however, this important parameter can be estimated by FT-IR spectroscopy using probe molecules (CO, CH_3CN) [66, 67].

4.2.3 Sol-Gel Synthesis of Amorphous Mixed Oxides

Fundamentals of the sol-gel processing have been comprehensively described in a few monographs and book chapters [17, 44, 68, 69]. Traditionally, sol-gel synthesis is carried out in an alcohol solvent with a small addition of water; however, non-hydrolytic routes have also received significant attention [9, 46, 69]. The sol-gel technique allows control of the molecular-scale mixing of reactants, promoting formation of Si–O–M bonds. The goodness of mixing strongly affects the catalytic properties of mixed oxides [8–17, 47, 70–79]. Reactivities of silicon and transition metal alkoxides in hydrolysis/condensation reactions differ significantly, and special measures are needed to avoid the formation of M–O–M bonds and segregation of active metal into a metal-oxide phase. Different strategies can be applied for adjusting the relative precursor reactivity. Among them are prehydrolysis of tetraethyl orthosilicate (TEOS) [11, 12, 47, 70, 72–75, 77], use of a more reactive silicon precursor, namely tetramethyl orthosilicate (TMOS) [12, 47, 71, 76, 78, 79] and/or modification of metal alkoxides with complexing agents to adjust the hydrolysis rate [71–77, 80]. Meanwhile, the upper limit for the amount of a foreign metal oxide that can be introduced with a good homogeneity into a silica matrix (without appearance of MO_n microcrystallites) typically does not exceed 20 mol%.

The alcogel drying procedure is crucial for the textural properties of the resulting material. Xerogels are produced by a conventional evaporative drying when high capillary pore forces operate, resulting in a substantial collapse of the gel network and a several-fold decrease of the initial gel volume. The production of aerogels is based on the supercritical drying (SCD) technique that has the advantage of eliminating the "liquid/vapor" interface and allows considerable structural modifications of the alkogel to be avoided. Consequently, aerogels reveal very large specific surface areas (700–1000 $m^2\ g^{-1}$) and pore volumes (1–3.7 $cm^3\ g^{-1}$). SCD can be accomplished in a high-temperature (HT) mode with alcohols used as solvents and a low-temperature (LT) mode when, prior to drying, solvent is exchanged by liquid CO_2 that has a low SC temperature – 304 K [8, 10, 12, 15, 17, 71–75]. LT aerogels generally exhibit a better M dispersion and mesoporosity than HT aerogels.

Both acid and base catalysts are employed to accelerate the hydrolysis and polycondensation steps. The use of bases gives rise to gels composed of large particles with wide pores between them, whereas finely structured gels composed of small particles separated by narrow pores are formed under the conditions of acid catalysis. The structure of alcogels prepared under acidic conditions is extremely fragile and breaks down significantly even upon drying in supercritical CO_2. The polysilicate primary particles formed under basic conditions are not only larger but also more crosslinked than those formed under acidic conditions. Brinker et al. [81] suggested controlling the structure of silica gels using a two-step sol-gel procedure with subsequent utilization of acid and base (amine) catalysts. Rey et al. [82]

reported a fluoride-catalyzed route for the synthesis of nonordered mesoporous silica-based materials. This method allows control of both the textural properties and the different hydrolysis rate of silicon and metal alkoxides, leading to highly homogeneous metal-containing silicas with a good mesoporosity.

The porosity of sol-gel-derived oxides can be tuned not only through manipulation of processing conditions but also through manipulation of precursor composition and geometry. The use of $[Si_8O_{12}](OCH_3)_8$ as the structurally rigid cubic precursor instead of TMOS led to xerogels with a higher surface area (919 vs. $510\,m^2 \cdot g^{-1}$) and more uniformly sized silica structures [14]. Mixed oxides synthesized using ethyl silicate 40 (ES-40, the commercially available form of ethoxypolysiloxane [68]) revealed pores and pore volumes notably larger than the materials synthesized using TEOS alone [83].

Major advantages of aerogels are their high specific surface area and mesoporosity, which makes it possible to increase the number of active sites per gram of material and to use the internal surface without diffusion limitation. However, small particles and the low density of aerogels cause difficulties with their handling and separation from reaction mixtures. Low hydrothermal stability is another serious shortcoming. By contrast, xerogels suffer from diffusion limitations but are more resistant to crumbling and water. Various approaches have been suggested to create materials that would combine the benefits of both aerogels and xerogels but would not display their shortcomings (see Sections 4.2.5 and 4.5.2).

4.2.3.1 Titania–Silica Mixed Oxides Baiker and coworkers studied extensively effects of sol-gel parameters (hydrolysis route, catalyst amount, Ti content, drying and aging conditions, calcinations temperature) on the structure and catalytic performance of TiO_2–SiO_2 mixed oxides [12, 71–76]. The optimum parameters derived from this study were 20 wt% nominal TiO_2, modification of Ti(*i*OPr)$_4$ with acetylacetone (1 : 1), a molar ratio of water/alkoxide/acid of 5/1/0.09, no prehydrolysis of TMOS, and an aging period of 240 h [76]. Aerogels combining high dispersion of Ti and mesoporosity could be prepared only by LT SCD. Anatase segregation was observed for HT SCD aerogels.

Large pore volume titania–silica aerogels have been obtained using the two-step, acid–base synthesis sequence, with TMOS as silica precursor and trihexylamine as catalyst [78, 79]. These aerogels showed good Ti dispersion and mesopore volume of *ca.* $2\,cm^3\,g^{-1}$. Aerogels featuring an open structure and high nanoscale homogeneity have been prepared using a similar procedure combined with a replacement of traditional silicon alkoxides by less expensive ES-40. This procedure enabled the preparation of aerogels with mesopore volume of $2.4–3.7\,cm^3\,g^{-1}$ [83, 84]. ^{29}Si MAS NMR study revealed that the use of ES-40 favored increasing the degree of silicon self-condensation [83].

Numerous studies showed that the degree of titanium dispersion in silica matrix depends on both the Ti content and synthesis conditions. Prehydrolysis of TEOS [11, 12, 17, 47, 85] and the use of TMOS [12, 47, 71, 78, 79], the addition of chelate ligands [71, 74, 75, 80, 83], and application of NH_4F as catalyst [82] allow for matching the hydrolysis rates of silicon and titanium precursors and result in a

better Ti–O–Si heteroconnectivity. Studies by ^{29}Si and ^{17}O MAS NMR, EXAFS, and FT-IR techniques confirmed that the use of acetylacetone significantly increases the amount of Ti–O–Si bonding in xerogels; however, the upper limit for solubility of TiO_2 in SiO_2 remains below 15 mol% [83, 86].

Mesoporous TiO_2–SiO_2 xerogels have been prepared by the nonhydrolytic sol-gel synthesis [46, 87–90]. The reaction of $SiCl_4$ and $TiCl_4$ with diisopropyl ether in CH_2Cl_2 under solvothermal conditions (110–150 °C) offers a simple and efficient route to xerogels with homogeneous distribution of titanium [90]. This process is based on the etherolysis and condensation reactions (Eqs. 4.1 and 4.2; M = Si or Ti):

$$M - Cl + iPr_2O \rightarrow M - OiPr + iPrCl \tag{4.1}$$

$$M - Cl + M - OiPr \rightarrow M - O - M + iPrCl \tag{4.2}$$

The high degree of condensation of nonhydrolytic gels prevents complete pore collapse during the evaporation of solvent. Xerogels containing 6–9 mol% of Ti prepared at 150 °C exhibited truly outstanding textures, with pore volumes up to 2.5 $cm^3\,g^{-1}$, usually associated with aerogels.

The state of Ti. Since the state of titanium in silica matrix is crucial for the catalytic performance, it was the focus of numerous studies by spectroscopic techniques (FT-IR, Raman, DRS UV, XANES, EXAFS, photoluminescence, XPS, ^{17}O NMR, etc.) [11–13, 21, 23, 28, 91–94]. DR UV-vis spectroscopy is a readily available technique to characterize local geometry and bonding environment of Ti atoms in silica matrixes. Bands at 208–210 nm are attributed to oxygen–to–metal CT at isolated tetrahedrally coordinated Ti^{IV} centers, similar to the centers present in TS-1 [11, 13, 21, 23, 91–93]. Absorptions in the range of 220–260 nm are often assigned to isolated 5/6-coordinated Ti^{IV} [21, 23, 28, 91, 93, 95, 96]. The propriety of such an assignment is confirmed if a blue shift of the band is observed upon sample dehydration (Figure 4.1).

At the same time, DR UV bands at 220–230 nm can be due to distorted tetrahedral Ti^{IV} [93, 95] while broad absorptions centered at 240–260 nm may belong to 6-coordinated Ti^{IV} dimers and small oligomers [95–98]. These species can be distinguished from the hydrated 5/6-coordinated Ti species by invariability of the band position upon dehydration. A further long-wave shift to 260–290 nm is usually interpreted as an indication of a gradual increase in the degree of Ti oligomerization and formation of subnanometric TiO_2 clusters [13, 79, 83, 99, 100]. Anatase microcrystallites are manifested by a characteristic absorption at 330 nm [91–93].

X-ray absorption spectroscopy (EXAFS/XANES) is a complementary valuable technique for probing local structure around Ti atoms [11, 13, 23, 34, 83, 85, 91–93]. Using EXAFS/XANES it is possible to identify isolated Ti, dimeric/oligomeric species, and anatase microcrystallites embedded into silica. Furthermore, accurate measurements of the height and position of the pre-edge peak in Ti K-edge XANES may differentiate 4-, 5-, and 6-fold coordination of isolated Ti species [11, 13, 23, 101]. The Ti K-edge XANES spectra of calcined and dehydrated samples of mesoporous

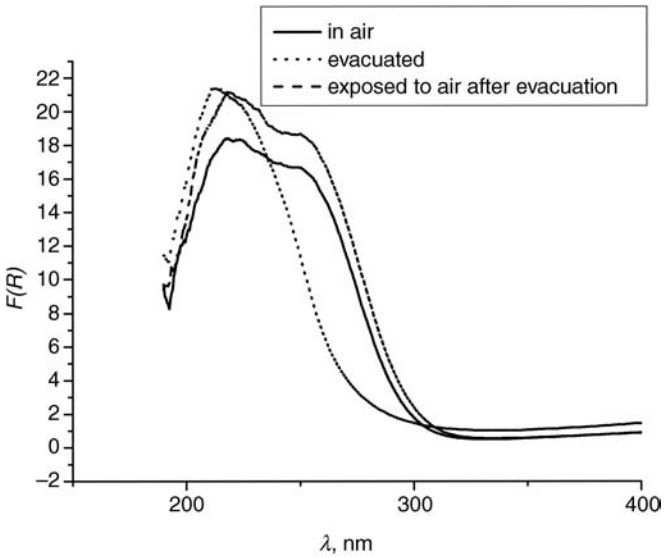


FIGURE 4.1 DR UV-vis spectra of TiO_2–SiO_2 aerogel (1.68 wt.% Ti).

titanium silicates are similar to the spectrum of TS-1 and completely different from that of anatase; the intensity of the Ti pre-edge peak is *ca.* 75%, while it reduces to 30–33% in air due to coordination of water molecules and extension of Ti coordination sphere.

Raman spectroscopy enables detection of the early stages of the emergence of TiO_2 anatase microcrystallites (a characteristic band at 140–145 cm^{-1}) [13, 23, 91, 99, 100, 102–104]. The IR absorption band at 960 cm^{-1}, often attributed to Si–O–Ti stretching vibrations and used to confirm incorporation of Ti in zeolites [91–93], can be also due to Si–OH groups present on the mesoporous silica surface and, hence, can not serve as unambiguous prove for Ti insertion into hydrophilic silica framework [11, 23].

4.2.3.2 Other Mixed Oxides Besides titania–silica, other binary oxides with prevailing silica content were reported. ZrO_2–SiO_2 mixed oxides were prepared using both the classic sol-gel procedure [47, 77, 105, 106] and its modification that involved hydrothermal treating of the gels [107]. The latter technique led to xerogels with narrow pore-size distributions and pore diameters in the region of mesopores (*ca.* 4 nm). Ce-containing (5.9 wt%) amorphous silicas with average pore diameters of about 3.3 nm and surface areas around 170 $m^2\,g^{-1}$ have been prepared by an acid-catalyzed sol-gel procedure [108]. Baiker and coworkers [109] synthesized vanadia–silica LT aerogels using acid catalysis together with prehydrolysis in order to achieve matching of the reactivities of vanadium(V) oxide triisopropoxide and TEOS. Strukul and coworkers [110, 111] reported the preparation of niobia–silica aerogels and xerogels under both acidic and basic conditions. The same group

prepared mesoporous WO_3–SiO_2 mixed oxides (xerogel and aerogel with 1 wt% W) under basic conditions [112].

4.2.4 Thermolytic Molecular Precursor Method

An alternative to the sol-gel method is based on the use of single-source molecular precursors that possess a defined ratio of elements to be incorporated into the target material and provide a low-temperature, kinetically controlled pathway to homogeneous, mixed-metal-oxide materials [16, 45]. Don Tilley's group prepared a number of transition-metal tris(*tert*-butoxy)siloxy complexes of the type $M[OSi(O^tBu)_3]_n$, where M = Ti [57], Ta [113], Fe [114], Cr [115], and other metals. Upon heating (usually 100–150 °C either in solution or in solid state) these oxygen-rich molecular precursors eliminate isobutylene and water to give homogeneous, mixed-element-oxide materials with well-defined stoichiometries, e.g., according to Eq. (4.3):

$$M[OSi(O^tBu)_3]_4 \xrightarrow{\Delta} MO_2 \cdot 4\,SiO_2 + 12\,CH_2 = CMe_2 + 6\,H_2O \qquad (4.3)$$

The dimeric molecular precursor $[(^tBuO)_2Ti\{\mu\text{-}O_2Si[OSi(O^tBu)_3]_2\}]_2$ was synthesized by silanolysis of $Ti(O^tBu)_4$ with $(HO)_2Si[OSi(O^tBu)_3]_2$ and used for the preparation of titania–silica ($TiO_2{\cdot}3SiO_2$) [116]. The solution phase thermolysis of $(^iPrO)_2Ta[OSi(O^tBu)_3]_3$ acquired *via* silanolysis of $Ta(O^iPr)_5$ with $(^tBuO)_3$-SiOH in nonpolar media afforded xerogels $Ta_2O_5{\cdot}6SiO_2$ [113]. A more silica-rich material ($Ta_2O_5{\cdot}18SiO_2$) was prepared with the same Ta molecular precursor and $HOSi(O^tBu)_3$. Since the latter cleanly converts to SiO_2 *via* the stoichiometric elimination of isobutylene and water, the formation of incompletely condensed alkoxy groups is avoided, unlike the case with TEOS.

4.2.5 Templated Synthesis of Ordered Metal Silicates

The era of mesostructured silicates started at the early 1990s when Mobil researchers introduced a new concept in the materials synthesis that is based on the use of supramolecular assemblies of surfactants as templates for inorganic precursors [18–20] instead of the use of single molecules as structure-directing agents (the case of zeolites). Surfactant molecules aggregate in solution due to their amphiphilic nature. The mechanisms leading to mesostructures – liquid crystal templating and cooperative self-assembly – have long been discussed in the literature [22, 23, 26, 27, 30, 31, 33, 36, 38, 39, 41, 43, 48, 117, 118] and are beyond the scope of this chapter. A simplified representation of a self-assembly process is shown in Figure 4.2.

Mesopores emerging after removal of templates by calcination or extraction have calibrated sizes in the nanometer range and form a system of channels. The surface areas of mesopores attain 600–1400 $m^2\,g^{-1}$, while pore volumes are usually in the range of 0.6–2.5 $cm^3\,g^{-1}$. The size and shape of the pore channels depend on

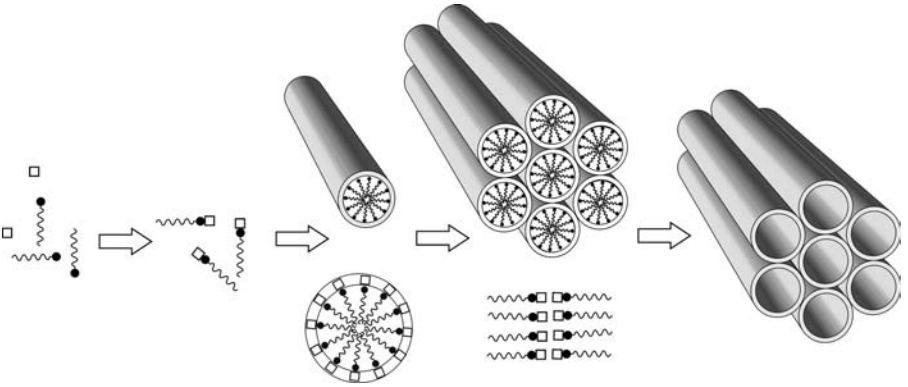


FIGURE 4.2 Schematic illustration of self-assembly route leading to hexagonal mesostructure.

the size and nature of the surfactant and the synthesis conditions. A description of various templates can be found in the literature [22, 23, 26, 27, 31–33, 36, 38].

A number of review papers devoted to the synthesis of ordered mesoporous silicates are available [26, 27, 32, 38–43]. Cool and coworkers [40] surveyed verified receipts for the synthesis of selected relevant materials of the MCM, SBA, MSU, and other families. For each material, a basic set of characteristics (N_2 sorption, XRD, TEM, SEM, NMR, etc.) is reported. Alternative synthesis setups and their combinations (reflux, autoclaves, microwaves, etc.) are also discussed [40].

The use of expensive organosilicas limits synthesis of mesostructured materials on a large, industrial scale, and procedures based on less expensive and more available inorganic precursors such as water-soluble sodium silicates [119–125], colloidal and fumed silicas [40, 43, 123, 124, 126] have been developed. Materials such as FSM-16 [127] and PHC [128] have been prepared from layered silicates, kanemite and saponite, respectively.

Silica condensation can occur under acidic, alkaline or neutral conditions. The type of interaction between inorganic component (I) and surfactant (S) depends on both the pH conditions and the nature of the template and is a crucial factor that governs the formation of a specific mesostructure. Four main assembly pathways have been proposed in the literature. Pathway 1 is based on direct electrostatic interactions and involves cocondensation of cationic surfactant S^+ with anionic inorganic species I^- to produce assembled ion pairs (S^+I^-) [18, 19, 129]. Pathway 2 involves indirect electrostatic interaction between surfactant and inorganic species of the same charge mediated by counterion X^- ($S^+X^-I^+$) [48, 129]. Pathway 3 is based on weak hydrogen-bonding interactions between neutral surfactant and neutral inorganic precursors (S^0I^0) [129–132]. Finally, pathway 4 engages a combination of electrostatic and hydrogen-bonding interactions ($S^0H^+X^-I^+$) [133, 134].

The pathway S^+I^- is realized in the synthesis of the M41S family in alkaline media using alkyltrimethylammonium salts or hydroxides with the general formula

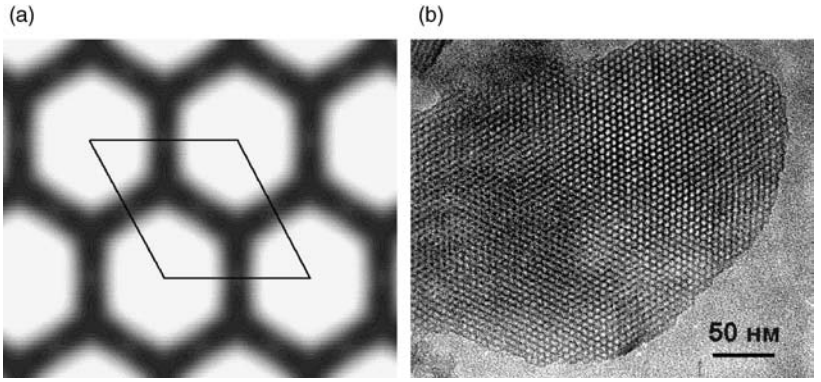


FIGURE 4.3 Electron-density map (a) and TEM micrograph (b) for MCM-41 type material (adapted from ref. [137] with permission of Elsevier, copyright 2001).

$C_nH_{2n+1}(CH_3)_3NX$ ($n = 6$–22; $X = Cl^-$, Br^-, OH^-, etc.) as templates under hydrothermal conditions [18–20, 129, 135–137]. Cetyltrimethylammonium bromide ($n = 16$, CTAB) is most frequently used giving rise to mesopores of 3–4 nm. TEM studies [63] and X-ray structural modeling [137] revealed that mesopores in well-ordered MCM-41 may have a true hexagonal shape (Figure 4.3) and the effective silica wall thickness is 0.8–1 nm, which corresponds to 2–2.5 SiO_4 tetrahedra [44].

The shape of pores, channels and particles strongly depends on the synthesis conditions [38–40, 43]. Increasing the temperature and the ratio of surfactant/Si results in transformation of mesophase from 2D hexagonal MCM-41 through cubic MCM-48 to lamellar MCM-50 [18, 19, 26, 27, 138]. The M41S family is presented in Figure 4.4.

Cubic MCM-48 can be easily prepared at room temperature by using gemini surfactants $[C_nH_{2n+1}(CH_3)_2N–(CH_2)_s–N(CH_3)_2\text{-}C_mH_{2m+1}]Br_2$ ($n = m = 12$, 14, 16, 18, 20, 22; $s = 2$–12) [138]. The addition of sodium ethylenediaminetetraacetate, adipic acid, or benzenedisulfonic acid during hydrothermal synthesis of MCM-41 resulted in a new mesoporous material, KIT-1, having short worm-like channels with uniform widths that are interconnected in a three-dimensional, fully disordered way [125].

Tanev et al. [130, 131] first reported the use of nonionic amine surfactants to produce HMS mesostructures at pH close to 7 through the S^0I^0 pathway. As judged from TEM images, the mesopores-channels in HMS are arranged in a hexagonal-like fashion but reveal a much shorter range of ordering than MCM-41 [139]. Such a wormhole-like structure is manifested by a higher width of the low-angle XRD reflections and broader interval of the relative pressure $\Delta(P/P_0)$ within which the capillary condensation occurs [129]. The S^0I^0 pathway offers the advantage of facile template recovery by solvent extraction. Neutral templating may result in materials with more crosslinked frameworks, thicker silica walls and improved textural mesoporosities [129–131, 139].

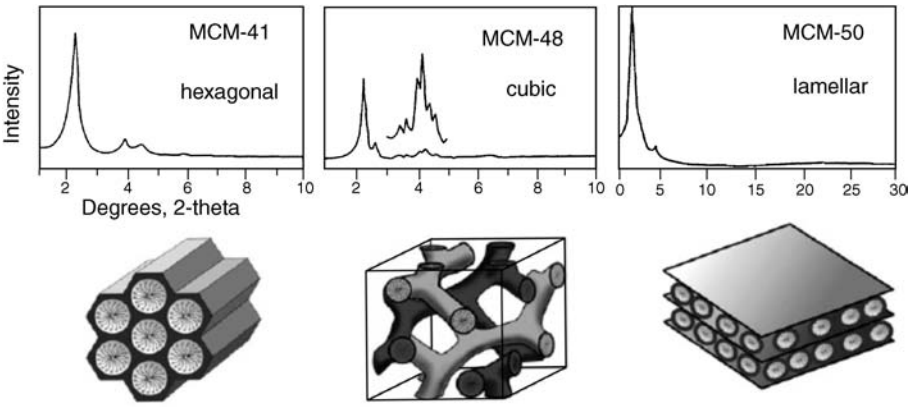


FIGURE 4.4 Mesoporous M41S family: Schematic representation of mesostructures and the corresponding XRD patterns. Elaborated from ref. [329] by permission of John Wiley & Sons.

Bagshaw et al. [132] suggested synthesis of mesoporous silicates, denoted MSU-X, through the S^0I^0 pathway using low-cost, nontoxic, and biodegradable polyethylene oxide (PEO) polymers as nonionic surfactants. For example, MSU-1 is made with alkyl–PEO alcohols like Tergitol, MSU-2 with alkyl–aryl–PEO surfactants like Triton-X, etc. Very large pore hexagonal and cellular foam-like silicas (MSU-H and MSU-F, respectively) with well crosslinked framework walls have been prepared from water-soluble silicate precursors [121]. Materials denoted MSU-G with vesiclelike hierarchical structure and high hydrothermal stability have been obtained through a supramolecular assembly pathway that relies on hydrogen-bonding between gemini surfactants $C_nH_{2n+1}NH(CH_2)_2NH_2$ and silica precursors derived from TEOS [140, 141].

Near neutral pH, silica condensation is fast and can be completed within a few minutes at room temperature [42, 142]. Maschmeyer et al. [143, 144] developed a new templating method based on the use of inexpensive nonsurfactant chemical, triethanolamine (TEA), to prepare hydrothermally stable foam-like material TUD-1.

Well-ordered mesoporous silicates can be synthesized in strongly acidic media at pH < 1.5 [48, 120, 129, 133, 134, 138, 139] through the reaction pathway $S^+X^-I^+$ or $(S^0H^+)X^-I^+$. Alkylammonium salts, gemini surfactants, oligomeric alkylpolyethylene oxides with the general formula $C_nH_{2n+1}EO_m$ ($n = 11$–18; $m = 9$–25) or triblock copolymers poly(ethylene oxide)–poly(propylene oxide)–poly(ethylene oxide), $EO_nPO_mEO_p$ ($0 < n < 100$, $5 < m < 150$, $0 \leq p < 100$; trade name Pluronics) are used as templates. The SBA-15 materials prepared using cheap nonionic triblock copolymers (Pluronic P123, $EO_{20}PO_{70}EO_{20}$, is most often used) are characterized by pore volumes up to 2.5 $cm^3\,g^{-1}$ and thick silica walls (3–6 nm) [120, 133, 134]. An important feature of SBA-15 is the presence of microporosity in the

silica walls. For the same template, higher temperatures and longer reaction times result in larger pore sizes and thinner silica walls [133]. The pore size can be further increased by the addition of a swelling agent, e.g., mesitylene, during the synthesis. Similarly, mesostructured cellular foam (MCF), the material with two PSD maxima, can be obtained [145]. The main types of mesostructured silicates and some important characteristics are summarized in Table 4.1.

Incorporation of transition-metal ions into the framework of mesostructured silicates can be accomplished by the addition of a metal source to the synthesis gel. As in the case of mixed oxides, the reactivity of the metal precursor is often tuned using chelate ligands to suppress M segregation into MO_n phase and to enhance incorporation of M into the silica network. The incorporation level strongly depends on the synthesis route and the nature of metal precursor [21, 23, 26–28]. Substitution of M^{IV} for Si^{IV} occurs more efficiently than insertion of other metal ions for which compensation of excessive positive or negative charge is required. Incorporation of metal ions with radii close to that of Si^{IV} is more favorable than incorporation of larger ions. Inclusion of metals like Cr^{VI}, Mo^{VI} and W^{VI} in silica framework is additionally complicated by their polynuclear anionic nature preserved in a wide range of pH.

In contrast to the syntheses performed under basic and neutral conditions, incorporation of transition metals into SBA silica matrixes is difficult because the formation of M–O–Si bonds is disfavored at high acidity [102, 129, 147–149]. For most transition metals, a pH range of 2.5 to 4 is optimal to reach a sufficient level of M hydrolysis [150], but namely in this range, which is near the isoelectric point of silica, the formation of mesostructures is disfavored [32, 119]. A great amount of research was devoted to the development of procedures for the synthesis of mesoporous metal silicates under week acidic conditions [104, 151–162]. Romannikov and coworkers [104, 152] suggested a methodology that involves a two-step change of pH during the synthesis. In the first step (pH 0.5–1.5) a silica mesophase is basically formed *via* the $S^+A^-I^+$ (or $S^0H^+X^-I^+$) route upon interaction of surfactant with a silica sol containing M source. In the second step, pH is increased to 2.5–3.5 by the addition of a basic solution of sodium silicate, resulting in hydrolysis of the metal ions and their condensation with the formation of M–O–Si bonds. The materials thus obtained combine a well-ordered structure with a sufficient level of metal incorporation and possess hydrothermal stability. Well-ordered mesoporous silicate materials with Al [153], Ti [152, 156, 163], and Fe [159] ions have been prepared using this method. The groups of Xiao [35, 154] and Li [155, 164] reported similar "pH-adjusting" methods for the synthesis of SBA-15 substituted with Al [154, 155], Ti [154], and Fe [164]. The metal source was added into the initial reaction mixture in strongly acidic media; when the mesostructure was basically formed, the pH value was adjusted from strong acidic to near neutral, followed by hydrothermal treatment. This procedure was adapted for the synthesis of SBA-15 containing Co [160], Cr [157], Sn [165], Nb [166], and Mn [167] ions.

In the following sections, we address the synthesis and characterization of the main types of mesostructured metal silicates reported so far in the literature. Since the state of metal M is crucial for catalysis, significant attention is given to

TABLE 4.1 Main Types of Mesostructured Silicates Prepared by Template Synthesis

Material	Pathway	Medium	Template	Silica source	Structure	D^a (h_W),[b] nm	Q_4/Q_3[c]	Key refs.
MCM-41	S^+I^-	Basic	Alkyltrimethylammonium salts[d]	Sodium silicate Fumed silica Colloidal silica TEOS, TMOS	Hexagonal	2–4 (1–1.2)	0.7–1.5	18, 19, 40 40 129 40, 139
MCM-48	S^+I^-	Basic	Alkyltrimethylammonium salts Gemini surfactants[e]	TEOS, TMOS Fumed silica	Cubic	2–4 (1)	1.1	18, 138 40, 126
FSM-16	S^+I^-	Basic	Alkyltrimethylammonium salts	Layered silicate ($NaHSi_2O_5$)	Hexagonal	2–3 (1)		127
PCH		Basic	Alkyltrimethylammonium salts + Alkylamines	Layered silicate + TEOS	Lamellar	1.4–2.2		128
KIT-1	S^+I^-	Basic	Alkyltrimethylammonium salts + sodium salts of organic acids	Sodium silicate	Wormhole	3–4 (1.1–1.3)	1.6	125
HMS	S^0I^0	Neutral	Primary amines C_8-C_{18}	TEOS	Hexagonal or wormhole	2–4 (1.1–2.7)	2.7–3.1	130, 131
MSU-X	S^0I^0	Neutral	Poly(ethylene oxides)[f]	TEOS, TMOS	Wormhole	2–6 (1–2.5)		132
MSU-H			$EO_{20}PO_{70}EO_{20}$	Sodium silicate	Hexagonal	8–11	4.5	121
MSU-G			Neutral gemini surfactants[g]	TEOS	Vesicle-like	2.7–4 (2–3)	6.2–7.1	140, 141

(*continued*)

TABLE 4.1 *(Continued)*

Material	Pathway	Medium	Template	Silica source	Structure	D^a (h_W),[b] nm	Q_4/Q_3[c]	Key refs.
COK-12	S^0I^0	Near neutr.[h]	$EO_{20}PO_{70}EO_{20}$	Sodium silicate	Hexagonal	4.5–6.5 (4–5)	1.8	42, 142
TUD-1		Neutral	$(HOCH_2CH_2)_3N$	TEOS	Foam-like	2.5–25		143, 144
SBA-1	$S^+X^-I^+$	Acidic	Alkyltrimethylammonium salts Gemini surfactants[c]	TEOS	Cubic	2–4		48, 138
SBA-3	$S^+X^-I^+$	Acidic	Alkyltrimethylammonium salts	TEOS	Hexagonal	2–4 (1–1.3)	1.0–1.2	48, 138
SBA-15	(S^0H^+) X^-I^+	Acidic	Triblok copolymers $EO_nPO_mEO_p$[i]	TEOS, TMOS Sodium silicate	Hexagonal	4–12 (3–6)	1.3–1.7	133, 134 40, 120
SBA-16	(S^0H^+) X^-I^+	Acidic	$C_{12}H_{25}EO_{23}$ or $EO_{106}PO_{70}EO_{106}$	TEOS Sodium silicate	Cubic	4.5–6.5		40, 134 120
MCF	(S^0H^+) X^-I^+	Acidic	$EO_{20}PO_{70}EO_{20}$ + swelling agent[j]	TEOS	Cellular foam-like	20–30[k]		40, 145
FDU-5		Acidic	$EO_{20}PO_{70}EO_{20}$ + additives[l]	TEOS	Cubic	4.5–9.5	3.8	146

[a]Mesopore diameter; [b]silica wall thickness; [c]the ratio of tetrapodal and tripodal Si atoms determined from ^{29}Si MAS NMR spectra; [d]$(C_nH_{2n+1}(CH_3)_3NX$, where X = Cl, Br, OH/Cl and $n = 8$–18; [e]$[C_mH_{2m+1}(CH_3)_2N$–C_sH_{2s}–$N(CH_3)_2C_nH_{2n+1}]_2Br$, where m and $n = 16$–18 and $s = 2$–12; [f]$C_nH_{2n+1}EO_m$, $n = 11$–18, $m = 9$–25; [g]$C_nH_{2n+1}NH(CH_2)_2NH_2$, $n = 10$–14; [h]citric acid – citrate buffer pH 5–6.5; [i]$0 < n < 100$, $5 < m < 150$, $0 \le p < 100$; [j]mesitylene (1,3,5-trimethylbenzene) most commonly used; [k]size of cages (BJH, adsorption branch), entrances are 10–15 nm (desorption branch); [l]3-mercaptopropyltrimethoxysilane, benzene, or a benzene derivative.

the spectroscopic characterization that allow isolated, oligomerized and phase-agglomerated states of the heterometal to be distinguished.

4.2.5.1 Mesostructured Titanium Silicates The first syntheses of mesostructured titanium silicates Ti-MCM-41 and Ti-HMS were realized in 1994 by Corma's [168] and Pinnavaia's [130] groups, respectively, followed by physicochemical studies on these materials [124, 129, 169, 170]. Since that time, different synthesis procedures have been developed, leading to a wide variety of catalytic materials, such as Ti-MCM-48 [102, 135, 136], Ti-MSU-1(2) [132, 171], Ti-SBA-15 [102–104, 147–149, 154, 172], Ti-SBA-1 [173], Ti-TUD-1 [143, 144, 174], Ti-MMM [175, 176], Ti-MMM-2 [152, 156, 163], Ti-MMM-1 [177], Ti-MMS [178], Ti-MSU-G [179], MTS-9 [180], and some others. The main characteristics of these materials are presented in Table 4.2.

While inclusion of Ti^{IV} into silica framework readily occurs under basic and neutral conditions, its incorporation in strongly acidic media (e.g., syntheses of Ti-MCM-41, Ti-SBA-1 and Ti-SBA-15) requires a large excess of titanium because of its poor ability to form Ti–O–Si bonds under such conditions [129, 147, 149, 173]. Increasing pH of the synthesis allows an increase in the level of Ti incorporation but another problem, namely oligomerization of titanium, arrises [104, 124, 154, 172]. A compromise between the level of Ti incorporation and its isolation has been achieved in the synthesis of Ti-MMM-2 (MMM stands for mesoporous mesophase material) using the following two-step procedure [152, 156]. In the first step, Ti source is added to a preliminary prepared silica sol (pH *ca*. 1.0) followed by mixing with an acidic solution of surfactant (CTAB). A mixture of CTAB and Pluronic P123 (5/95) can also be used [163]. In the second step, a basic solution of sodium silicate is added to increase and maintain pH *ca*. 3.0 followed by hydrothermal treatment. Calcined Ti-MMM-2 has a well-ordered structure of hexagonally packed mesopores-channels and possesses hydrothermal stability.

Ti-MMM-1 (here, MMM stands for microporous mesoporous material), a mixed-phase material with a Si/Ti ratio of 100 has been synthesized by a procedure involving the addition of two templates, CTAB and TPABr (TPA = tetrapropylammonium), at staggered times and the temperature manipulation on a single reaction mixture [177]. Xiao and coworkers [35, 180] prepared hydrothermally stable MTS-9 in strong acidic media by a two-step procedure where preformed TS-1 nanoclusters were used to assemble with Pluronic P123.

Prehydrolysis of TEOS [136] and complexing agents (H_2O_2, acetylacetone, aminoalcohols, fluoride, etc.) [102, 147, 149, 171] were employed to favor the formation of isolated Ti species. In the synthesis of Ti-TUD-1, triethanolamine not only played the role of a mesopore template and a director of positioning of Ti species onto the internal mesopore surface but also stabilized the Ti source, ensuring the prevalence of isolated tetrahedrally coordinated Ti sites [143, 174]. Oligo(ethylene oxide) alkyl ether surfactant Brij56 played a similar role in preparation of mesostructured titania–silica thin films with a high titanium loading [181].

Sophisticated catalysts of the so-called core–shell morphology, consisting of a silica core and ordered mesoporous titanium silicate shell, have been prepared using

TABLE 4.2 Mesostructured Titanium Silicate Catalysts Prepared by Direct Synthesis

Catalyst	Surfactant	Metal source	Silica source	pH[a]	D^b (h_W)[c] nm	S^d $m^2\ g^{-1}$	V^e $cm^3\ g^{-1}$	Si/Ti[f]	λ_{max} DR-UV nm	Ref.
Ti-MCM-41	$C_{16}H_{33}(CH_3)_3NBr$	$Ti(OEt)_4$	Fumed silica		3.1–3.5 (1.0)	990	0.6	60	210–230	168, 169
		$Ti(^iPrO)_4$	Colloidal silica	12	2.9 (1.5)	859	0.7	44	220, 260	129
			TEOS	1.5[g]	2.7 (1.5)	1354	0.9	40	220, 260	129
	$C_{16}H_{33}(CH_3)_3NCl$	$Ti(^nBuO)_4$	TEOS	11–12	2.7	1070		100	220	124
			Colloidal silica						220, 270	
			Sodium silicate						220, 270, 300	
Ti-MCM-48	$C_{16}H_{33}(CH_3)_3NCl$	$Ti(^nBuO)_4$	TEOS	11–12	2.5	1000		70–100	213–220	135, 136
	Gemini 18-12-18	Ti-TEA[h]	TEOS		2.7	1300	1.0	25–30	210–213, 270	102
Ti-MMM	$C_{16}H_{33}(CH_3)_3NBr$	$TiOSO_4/H_2SO_4$	Sodium silicate	9	3.4-3.8 (1.0)	990	0.8	49–166	225–230	175, 176
Ti-MMS	$C_{16}H_{33}(CH_3)_3NBr$	$Ti(^iPrO)_4$	H_2SiF_6	7.3–8.0	3.1 (1.0)	900	1.1	22–89	220	178
Ti-HMS	$C_nH_{2n+1}NH_2$ [i]	$Ti(^iPrO)_4$	TEOS	Neutral	2.5–2.9 (1.5)	990	0.6	30–85	215–220	129, 130
Ti-MSU-1	$C_{11-15}(EO)_{12}$	$Ti(OR)_4$	TEOS	Neutral	3.0	950				132
Ti-MSU-2	$C_{10}Ph(EO)_{10}$	Ti-bis[j]	TEOS	Neutral	2.1–2.7	1020	1.0	38–75	245	171
Ti-MSU-G	$C_{10}H_{21}NH(CH_2)_2NH_2$	$Ti(^nBuO)_4$	TEOS	Neutral	2.5	530	n.d.	31–69	220	179
Ti-TUD-1	$(HOCH_2CH_2)_3N$	$Ti(OR)_4$	TEOS	Neutral	4.5–5.7 (3.2)	820	1.0	50	225	143, 174
Ti-SBA-1	$C_{16}H_{33}(CH_3)_3NBr$	$Ti(^nBuO)_4$	TEOS	< 1	2.0	1200	0.7	30–93	210	173

TABLE 4.2 ***(Continued)***

Catalyst	Surfactant	Metal source	Silica source	pH[a]	D^b (h_W)[c] nm	S^d $m^2\ g^{-1}$	V^e $cm^3\ g^{-1}$	Si/Ti[f]	λ_{max} DR-UV nm	Ref.
Ti-SBA-15	Pluronic P123	$Ti(^iPrO)_4$	TMOS	1.0	10	1000	1.2	100–200	210	147
		$TiOSO_4/H_2SO_4$	Sodium silicate	2.7–3.2	11 (1.6)	570	1.2	10–38	250–270, 300	104
		$TiCl_4$	TEOS	< 1	7–8 (3.1)	820	0.9	n.d.	210, 290	103
		$TiCl_3$	TEOS	1.8	4.3–5.5	670	0.6	60–120	213	148
		Cp_2TiCl_2	TEOS	0.3	9–14	800	1.1	94–120	210	149
		$TiCl_4$	TEOS	7.5	9	800	n.d.	22–71	225–240, 270	154
		$Ti(^iPrO)_4$	TEOS	>2	8.8 (3.1–3.7)	970	1.1	19–89	245–260, 300	172
	Pluronic P123 + $C_{16}H_{33}(CH_3)_3NBr$	$TiOSO_4/H_2SO_4$	Sodium silicate	3.0	4.5–6.7 (4.0)	520	0.6	40	210	163
Ti-MMM-2	$C_{16}H_{33}(CH_3)_3NBr$	$TiOSO_4/H_2SO_4$	Sodium silicate	3.0	3.2 (1.0)	1120	0.7	35–46	205–210	156, 163
Ti-MMM-1	$C_{16}H_{33}(CH_3)_3NBr$ + TPABr[k]	$Ti(O^nBu)_4$/ H_2O_2	TEOS	Basic	*ca.* 4[l]	480	0.43[l]	100		177
MTS-9	Pluronic P123	TS-1 nanoclusters		< 0	8.0 (4.8)	980	*ca.*1[m]	30	215	180

[a]pH of the synthesis gel at the final stage; [b]mesopore diameter range; [c]silica wall thickness; [d]average surface area; [e]average mesopore volume; [f]Si/Ti molar ratio in calcined samples determined by elemental analysis; [g]SBA-3 analog; [h]titanium isopropoxy(triethanolaminato), Ti(IV)-Dupont-TEA; [i]$n = 10$–16; [j]Ti(IV)bis(ethy1 acetoacetato)diisopropoxide; [k]tetrapropylammonium bromide (template for the synthesis of TS-1); [l]estimated from N_2 adsorption isotherm reported in [177]; [m]micropore volume 0.13 $cm^3 \cdot g^{-1}$.

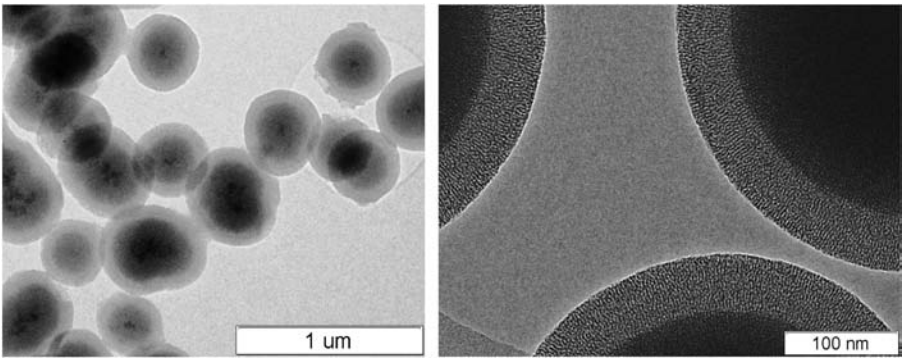


FIGURE 4.5 TEM images of magnetic Ti-SMCMS catalysts. Reproduced from ref. [184] by permission of The Royal Society of Chemistry.

a combination of different synthetic approaches [182–184]. A composite Fe*x*O*y*@Ti-HMS was synthesized *via* coating of as-synthesized iron oxide nanoparticles with an amorphous silica layer followed by the sol-gel polymerization using TEOS, Ti(^{i}PrO)$_4$, and dodecylamine as surfactant [182]. Physicochemical characterization revealed that superparamagnetic iron-oxide nanoparticles were irregularly dispersed within the silica matrix. Barmatova et al. [184] prepared Ti-SMCMS (solid magnetic core–mesoporous shell) materials with quasispherical particles consisting of a nonporous magnetic silica core and a mesoporous titanium silicate shell (*ca*. 45 nm) with quasiparallel channels oriented perpendicularly to the core surface (Figure 4.5).

The local elemental analysis by EDX confirmed that superparamagnetic nanoparticles are embedded into the core and are completely protected from the reaction medium [184]. XRD and N_2 adsorption studies confirmed MCM-41 structure of the shell while DRS UV-vis identified isolated Ti centers [183, 184].

4.2.5.2 Zr, Sn and Ce Silicates *Zirconium silicates*. Incorporation of zirconium in HMS [28, 185], MSU-1 [132], MCM-41 [186–188], and MCM-48 [189] has been accomplished using Zr(^{i}PrO)$_4$ [132, 185, 187, 189], $ZrO(NO_3)_2{\cdot}2H_2O$ [186], $Zr(SO_4)_2{\cdot}4H_2O$, and $ZrOCl_2{\cdot}8H_2O$ [188] as Zr source. All zirconium introduced into the synthesis gel was incorporated in HMS up to Si/Zr = 15 [185]. A Si/Zr molar ratio of 20 was achieved for Zr-MCM-41 [186]. The extent of Zr incorporation under acidic conditions strongly depended on the synthesis pH and the nature of the Zr precursor [188]. To increase the efficiency of Zr incorporation, Newalkar et al. [190] suggested using microwave (MW) hydrothermal conditions to accelerate heterocondensation polymerization; however, another group [191] revealed that both classical hydrothermal synthesis and a MW-assisted one produce a similar efficiency in Zr insertion, though MW treatment favors the formation of thicker pore walls.

They determined a Si/Zr ratio of 20 as the upper limit of Zr incorporation into SBA-15. Materials with Si/Zr ratio > 20 revealed a DRS UV band at 205–210 nm associated with isolated Zr^{IV} [190]. Chen et al. [192] carried out a direct synthesis of Zr-SBA-15 using $ZrOCl_2 \cdot 8H_2O$ without addition of a mineral acid. The main strategy was to utilize the acidity self-generated in the aqueous solutions of the zirconium precursor as the catalyst for TEOS hydrolysis. As the Zr content was increased from Zr/Si = 0.01 to 0.1, pH of the solution decreased from 2.25 to 1.23. The amount of Zr incorporated in SBA-15 prepared under such mild conditions was greater than that of materials synthesized in strong acidic media (Si/Zr = 10 *vs* Si/Zr = 20 in 2 M HCl); however, the state of Zr in such Zr-rich samples was not addressed. Zirconium-doped MSU-type silicas were prepared using sodium silicate, zirconyl chloride, and Triton X100 as template [193]. Zr-TUD-1 was synthesized with TEA as both complexing and templating agent [194]. FT-IR, XPS and DR UV-vis studies showed that all Zr^{IV} was tetrahedrally incorporated into the silica framework at Si/Zr ratios of 25 and higher.

Tin silicates. Synthesis of Sn-MCM-41 was first reported in 1995 [195] followed by synthesis of Sn-HMS [196]. Fumed silica in combination with TMOS [195, 197], TEOS [196], and Aerosil [198] were used as silica source while $SnCl_4 \cdot 5H_2O$ [195, 197, 198] and $Sn(^iPrO)_4$ [196] were employed as tin precursors. Sn-MCM-41 with Si/Sn > 40 were characterized by DR UV, FT-IR, ^{29}Si MAS NMR, ^{119}Sn MAS NMR, and Mössbauer spectroscopic techniques [197]. It was concluded that tetrahedrally coordinated Sn^{IV} is manifested by a DRS UV band at *ca.* 210 nm, while 6-coordinated Sn^{IV} species show a band near 230 nm. A broad absorption centered at 280 nm, which appears at high tin loadings, is associated with polymeric Sn–O–Sn species [197]. Direct hydrothermal syntheses of Sn-SBA-15 have been accomplished [158, 165, 199]. The Si/Sn molar ratio up to 13.5 was reached at H_2O/HCl molar ratio of 295 (pH *ca.* 2.4). DRS UV-vis revealed the presence of isolated Sn^{VI} in tetrahedral coordination [165].

Cerium silicates. While incorporation of Ce in crystalline microporous zeolite framework is problematic because of size incompatibility between lanthanides and Si^{IV}, causing longer Si–O–Ce bonds and more strained bond angles, inclusion of Ce into amorphous silica network of mesostructured materials was expected to be easier due to the greater flexibility of the network. Indeed, cerium was incorporated into Ce-MCM-41 [200, 201], Ce-SBA-15 [202, 203], and Ce-TUD-1 [204]. Lanthanide (La, Ce, and Nd) containing SBA-15 with a molar ratio of Si/Ln = 5–100 were prepared *via* direct synthesis under weak acidic conditions (pH 1.5–3.0) [161]. Materials with Si/Ce > 25 revealed a strong DR UV-vis band centered at 265–300 nm that was assigned to the presence of isolated, conceivably, tetra-coordinated cerium ions incorporated in the silica network [200, 202, 203]. Absorptions at *ca.* 265 and 300 nm were assigned to CT transitions of $O^{2-} \rightarrow Ce^{3+}$ and $O^{2-} \rightarrow Ce^{4+}$, respectively [202]. The absorption at *ca.* 400 nm observed for samples with high Ce loading belongs to extraframework cerium-oxide species [200]. SBA-15 synthesized by a two-step procedure at a final pH 6.0 contained mostly Ce^{3+} ions (EPR isotropic peak at $g = 2.375$), but at higher pH values Ce^{4+} predominated [202].

4.2.5.3 V and Nb Silicates *Vanadium silicates*. A great amount of research work was devoted to the synthesis and characterization of V-containing silicates because high redox potential of V^V makes such materials potentially interesting for the selective oxidation of hydrocarbons. In 1994, Reddy et al. [205] reported inclusion of vanadium in the framework of MCM-41 and then two research groups reported the preparation of V-HMS [206, 207]. Since that time, many papers have been published on the synthesis and characterization of V-containing MCM-41 and HMS-type materials [208–216]. Incorporation of vanadium in V-HMS occurs readily, and samples with Si/V molar ratio of *ca*. 30 can be prepared at room temperature [28, 207]. For V-MCM-41, the level of vanadium incorporation is lower [205, 209–212, 214]. A higher level of vanadium inclusion was established for V^{IV} precursors, $VOSO_4{\cdot}5H_2O$ and $VO(acac)_2$ [214]. The maximum Si/V ratio of 35 (*ca*. 1.23 wt% of V) was attained at Si/V = 25 in the synthesis gel. Other authors deduced from different characterization techniques (XRD, FT-IR, ^{29}Si MAS NMR, DR UV-vis, EPR, ^{51}V MAS NMR, and Raman) that, regardless of the silica source, *ca*. 1 wt% of V is incorporated into the MCM-41 framework and thereby increases the structural ordering, silica crosslinking, and wall thickness of the material [215]. Zhang and Pinnavaia [135] prepared V-MCM-48 using CTAB as surfactant. Mathieu et al. [217] optimized the synthesis procedure using gemini 16-12-16 surfactant as the structure-directing agent. The unit-cell parameter and the pore wall thickness increased as a function of the V loading. When the vanadium content was higher than 3.5 wt%, a fraction of polymerized VO_x species was observed by spectroscopic techniques. Optimum synthesis conditions yielded V-MCM-48 material with a maximum of 1 wt% fully incorporated V species and 2.5 wt% surface species [217]. Nonframework vanadium-oxide species can be removed by washing calcined V-MCM-48 with ammonium acetate solution [218]. A noticeably large amount of vanadium (Si/V = 14–20) was incorporated into the cubic SBA-1 mesophase under strongly acidic conditions [219]. Adjusting pH in the range of 1.3–3.0, V-SBA-15 was synthesized by a direct hydrothermal method using NH_4VO_3 [220] or $VOSO_4{\cdot}5H_2O$ [221] and Pluronic P123. The maximal Si/V atomic ratio in the calcined material was 12–15 at Si/V = 5–10 in the synthesis gel [220, 221].

A considerable effort was made to characterize the V state in mesoporous vanadium silicates by means of spectroscopic techniques, such as DR UV-vis, EPR, ^{51}V solid-state NMR, Raman, X-ray absorption, etc. [21, 28, 207–210, 212–221]. Calcined samples are usually EPR silent and do not exhibit *d–d* transitions in the region 600–800 nm, indicating that all vanadium is present in the form of V^V. A typical solid-state ^{51}V NMR spectrum of calcined vanadium silicates shows a single peak or two signals in the range of $-(506-576)$ ppm, characteristic of V^V in T_d environment [21, 28, 135, 206–209, 212–215, 218, 221, 222]. The presence of tetrahedral V^V species with different local coordination (perfect or distorted T_d) is most likely responsible for the multiple peak positions after -500 ppm. Based on the ^{51}V NMR study of model compounds, the resonance at *ca*. -420 ppm was assigned to octahedral V^V [222]. The signal intensity is strongly enhanced upon sample hydration [207]. The lack of peaks around -300 ppm indicates that the material is free of V_2O_5.

Well-prepared freshly calcined V-MCM-41 samples are white, but after contact with humid air may turn pale yellow. The presence or appearance of an intensive yellow color is an indication of the formation of extraframework six-coordinated vanadium species that are highly prone to leaching [175, 210, 217]. DR UV-vis spectroscopy usually reveals two intense absorption bands with maxima centered in the range of 255 – 285 and 360 – 400 nm in calcined materials [207, 208, 210, 212–215, 218–221]. Dehydrated samples may show a broad band centered at 285 – 300 nm that can be deconvoluted into two main absorptions at 250 and 320 nm [175, 217]. All these bands are attributed to $O^{2-} \rightarrow V^{5+}$ CT transitions. The higher-energy band at 250 – 275 nm is consistent with V^V in tetrahedral environment and is often treated as an indicator for incorporation of V^V species in the silica framework [207, 209, 217]. The absorption at *ca.* 340 nm is usually assigned to V^V in distorted tetrahedral coordination, e.g., with one V=O double bond and three V–O single bonds [207, 208, 212]. A long-wave shift and broadening of this band suggest that distorted tetrahedral V^V species attracted by water molecules transform into penta or octahedral V^V species [207–209, 212, 215, 217, 218, 221]. In turn, the intensity of absorption around 400 nm may decrease upon sample dehydration [28, 207, 209, 215, 221], corroborating reversible transitions between V^V species in different coordination environment. On the other hand, disappearance of this band also occurs after sample washing and is explained by removal of vanadium-oxide nonframework species [218].

The formation of extraframework V^V species upon sample hydration can be avoided if vanadium loading is low and synthesis conditions ensure its high dispersion in the silica matrix. Wei et al. [212] prepared V-MCM-41 with Si/V = 210 and higher, systematically varying the pore size using C_8–C_{16} cationic surfactants. Studies by UV Raman, DR UV-vis, ^{51}V solid-state NMR, and X-ray absorption spectroscopies implicated that V^V is incorporated into the silica framework of both hydrated and dehydrated samples, mostly occupying isolated tetrahedrally coordinated sites. A small number of octahedral sites was observed in samples with larger pore size, presumably, due to their higher hydrophilicity [212].

Niobium silicates. In 1997, two groups reported synthesis of Nb-MCM-41 [223, 224]. The molecular structure of niobium in Nb-MCM-41 (3.5 wt% Nb) was investigated by *in situ* Raman and DR UV-vis-NIR spectroscopies and compared with a supported Nb_2O_5/SiO_2 catalyst containing 1 wt% of Nb [225]. The spectroscopic results revealed that under dehydrated conditions, Nb cations in both Nb-MCM-41 and Nb_2O_5/SiO_2 are predominantly composed of isolated NbO_4 units. Ziolek's group used different Nb^V precursors (chloride, oxalate, ammonium–oxalate complex) and TEOS or sodium silicate as Si source to prepare Nb-containing MCM-41, SBA-3 and SBA-15 materials [226–231]. A higher Nb content in the final material was reached with $NbCl_5$. The use of traditional synthesis methods did not allow elimination of extraframework niobium species in SBA-15 when the Si/Nb ratio was lower than 128. Similarly to Zr-SBA-15 [192], a relatively well-ordered Nb-SBA-15 material was prepared *via* the HCl-free synthesis route when the acidity of the solution was controlled by the amount of $NbCl_5$ [231]. The lack of absorption at *ca.* 300 nm confirmed the absence of extraframework niobium species for samples

with Si/Nb = 15. Selvaraj et al. [166] prepared Nb-SBA-15 in weak acidic medium. Studies by ICP–AES, TEM–EDX and XPS showed that samples with a Si/Nb ratio up to 6.7 can be prepared at pH 2.2. Nb-containing MSU-X silicas were prepared using TEOS, ammonium trisoxalate niobium(V) and nonionic surfactant under strong acidic, acidic or near neutral conditions [232].

4.2.5.4 Cr, Mo and W Silicates *Chromium silicates*. The first syntheses of Cr-containing mesostructured silicates are dated to 1996 when Ulagappan and Rao reported the preparation of Cr-MCM-41 under basic conditions using Cr $(NO_3)_3{\cdot}9H_2O$ or CrO_3 as chromium sources [233], while Pinnavaia's group reported synthesis of Cr-HMS and Cr-MCM-41 with CrO_3 under neutral and acidic conditions, respectively, [211] and synthesis of Cr-MCM-48 with $CrC1_3{\cdot}6H_2O$ under basic conditions [135]. The value of the unit-cell parameter a_0 enlarged with increasing Cr amount [233], suggesting chromium incorporation in the silica framework. DRS UV − vis and EPR studies revealed that Cr^{III} species predominate in the as-synthesized samples (bands at 440 and 620 nm) but calcination leads to the appearance of Cr^{VI} (370 nm). Kevan's group prepared a series of Cr-MCM-41 with variable Si/Cr ratios using $CrCl_3{\cdot}6H_2O$ [234]. The materials were characterized by XRD, electron probe microanalysis (EMPA), N_2 adsorption, FT-IR, DRS UV-vis, EPR, and Raman techniques. In contrast to what was observed by other authors [233], a decrease of the unit-cell parameter was found with increasing Cr content. However, based on the results of ^{29}Si MAS NMR study it was suggested that at least some of the Cr is incorporated in the MCM-41 structure. DR UV-vis spectra of calcined, dehydrated Cr-MCM-41 were dominated by two intense bands around 259 and 350 nm assigned to $O^{2-} \rightarrow Cr^{6+}$ CT of a monochromate species, while no absorption around 440 nm characteristic of Cr^{VI} polychromate species was observed, which agreed with the results of the Raman study. It was concluded that the as-synthesized Cr-MCM-41 contained atomically dispersed Cr^{III}, while tetrahedrally coordinated Cr^{VI} monochromate CrO_4^{2-} and not higher chromates existed in the calcined samples.

Sakthivel and Selvam prepared a series of Cr-MCM-41 samples using a Si/Cr ratio of 25–200 in the synthesis gel [235]. XRD showed no appreciable incorporation of Cr into the silica matrix. ^{29}Si MAS NMR studies revealed that the number of Q_3 sites is considerably reduced for Cr-MCM-41 compared to siliceous MCM-41, which supports the stabilization of chromium ions *via* silanol groups. Calcined samples contained a certain number of loosely bound polychromate clusters that could be removed by treatment with 1 M ammonium acetate solution [235, 236]. The yellow color of the calcined sample changed to white after washing, indicating successful removal of the polychromate species. The washed sample contained *ca.* 0.77 wt% of Cr and was stable toward further leaching.

Wang et al. [237] prepared Cr-MCM-41 by both direct hydrothermal synthesis and template-ion exchange (TIE). It was inferred from DR UV, XANES/EXAFS, and UV-Raman spectroscopic data that monochromate species mainly exist in the samples prepared by the hydrothermal method, while both monochromates and polychromates coexist in the samples prepared by the TIE method. Bhaumik and coworkers [238] introduced 4.6 wt% of Cr in MCM-41 by a procedure that involved

slow hydrolysis of TEOS in the presence of CTAB by very mild acidic solution of chromium sulfate followed by addition of a base, favoring condensation of silica and chromium species. Again, DR UV-vis spectra showed the presence of both monochromate and polychromate species in the calcined materials.

Finally, Selvaraj et al. [157, 239, 240] synthesized Cr-SBA-15 by the NH_4F acidic method and by the pH-adjusting method; the latter gave a higher amount of Cr incorporation (Si/Cr = 9–10). The state of Cr was probed by EPR and DRS UV-vis [240]. After washing, the intensity of the band around 455 nm attributed to Cr^{VI} polychromate species reduced significantly as compared to the absorption around 275 and 365 nm, indicating the predominance of tetrahedrally coordinated monochromate species.

Molybdenum silicates. While the rigid structure of microporous zeolites limits its incorporation of large Mo^{VI} ions into the framework, a more flexible structure of mesoporous silicas makes it possible, although synthesis of molybdenum silicates remains tricky because Mo^{VI} exists in aqueous solutions mostly in anionic forms with predominance of isopolyanions in acidic media (Eqs. 4.4 and 4.5) [241, 242].

$$7[MoO_4]^{2-} + 8H^+ \rightleftharpoons [Mo_7O_{24}]^{6-} + 4H_2O \tag{4.4}$$

$$[Mo_7O_{24}]^{6-} + 3H^+ + [HMoO_4]^- \rightleftharpoons [Mo_8O_{26}]^{4-} + 2H_2O \tag{4.5}$$

Under basic conditions silicate species are negatively charged and cause a repulsion of molybdenum oxoanions, thus limiting the insertion of Mo into the silica framework. Indeed, the amount of Mo in Mo-MCM-41 and Mo-MCM-48 prepared under conventional basic conditions was very low (0.1 wt% MoO_3) [243]. DRS UV-vis bands at 242 and 277 nm indicated the presence of two types of Mo^{VI} species.

Synthesis under acidic conditions is more favorable for the incorporation of Mo. Cations $[MoO_2(H_2O)_4]^{2+}$ predominate in 6 M HCl while in the range of $[H^+]$ from 3 to 0.2 M they are in equilibrium with dimer $[Mo_2O_4(\mu\text{-}OH)(H_2O)_6]^{3+}$ [241, 242]. Morey et al. [244] synthesized Mo-SBA-1 under strongly acidic conditions using $MoCl_5$ (aq) as Mo source. However, metal loading has not reached a level of interest because of the high solubility of the precursor in strong acidic medium. Tatsumi's group optimized synthesis conditions by adjusting the H_2O/HCl and Si/Mo molar ratios of starting gels to introduce a higher percentage of Mo into SBA-1 [245]. A Si/Mo molar ratio as low as 23 was achieved. However, at such high Mo loading a part of it existed in the form of octahedrally coordinated polymeric species (absorbance at 320 nm) while at Si/Mo ratios beyond 68 only bands centered at 230 and 278 nm were present, indicating tetrahedrally and octahedrally coordinated monomeric Mo^{VI} species. In the presence of moisture, the tetrahedral Mo sites were partially converted to octahedral monomeric and polymeric species.

Higashimoto et al. [246] prepared a series of Mo-MCM-41 samples with a Mo content in the range of 0.5–4 wt% under acidic conditions (pH 0.5) at room temperature. The progressive increase in a_0 with increasing Mo loading was revealed by XRD, suggesting incorporation of Mo into the silica framework. The local structure

of the Mo sites was probed by XRD, UV-vis, photoluminescence, and XAFS techniques. The presence of three types of Mo species has been supposed, namely tetra-coordinated monomeric molybdate, tetra-coordinated dimeric and/or oligomeric molybdate, and hexa-coordinated polymeric molybdate, the ratio between them being dependent on the Mo content.

Tungsten silicates. Zhang et al. [247] first reported incorporation of tungsten in MCM-41 silica using TEOS and ammonium tungstate in the presence of CTAB in a strongly acidic medium. The maximum achieved incorporation level was 7.8 wt % W (Si/W = 35); both XRD and Raman techniques identified the presence of extraframework WO_3 phase at such W loading. A DRS UV-vis study allowed suggesting that, starting from Si/W = 50 and higher, most of the W was present in the form of isolated tetrahedral species (absorption at *ca*. 215 nm). No extraframework WO_3 was found until Si/W reached 31 if the synthesis was performed in the presence of H_2O_2, which favors the formation of low nuclearity oxoperoxotungstates [248]. Dai et al. [249] reported synthesis of highly ordered W-MCM-41 (Si/W = 32) under mild acidic conditions using Na_2SiO_3 and $Na_2WO_4{\cdot}2H_2O$ as precursors in the presence of ethyl acetate. The state of W was not addressed. Klepel et al. [250] accomplished incorporation of W in MCM-41 under basic conditions (pH = 10.5) using TMOS, CTAB and ammonium metatungstate. The use of a high amount of tungsten in the starting gel (40 wt%) and a washing procedure prior to calcination led to a material with Si/W = 17 and almost no extraframework WO_3.

Yang et al. [251] prepared W-MCM-48 from TEOS, CTAB and $Na_2WO_4{\cdot}2H_2O$ using pH adjustment. First, the reactants were subjected to hydrothermal treatment under basic conditions and then pH of the gel was adjusted to *ca*. 2 by HCl followed by additional hydrothermal treatment. Raman and DRS UV-vis spectra revealed the presence of WO_3 in the samples with W loading higher than 10 wt%. A broad band with a maximum at 300 nm present in the samples with lower W content was attributed to small tungsten-oxide oligomeric species. The same team reported synthesis of W-HMS [252] and W-SBA-15 [253] as well as W-MCF [254]. Treatment of the calcined materials with 1 M solution of NH_4OAc at 80 °C for 6 h resulted in a significant decrease of the amount of tungsten in the material. DRS UV-vis showed that crystallites of WO_3 (430 nm) were removed first, followed by the polymeric WO_3 species (290 nm). After three washing procedures, the amount of W in the samples remained constant (*ca*. 0.7 wt%) and the increased intensity of the DRS UV band at 230 nm indicated that a significant part of it was present in an isolated form that was stable to leaching. Tungsten-containing MCM-48 was synthesized using a rapid and facile room-temperature procedure with tungsten(VI) chloride as precursor [255]. No crystalline WO_3 was observed for W-MCM-48 with a Si/W ratio of 45 (the minimal ratio achieved) as revealed by DRS UV-vis, Raman, and XRD analysis. Finally, W-HMS (4.3 wt% of W) was prepared through the condensation of TEOS templated by amphiphilic diblock copolymers modified with tungsten isocyanide complexes [256]. The results of TEM and XPS study were consistent with the presence of well-dispersed tungsten-oxide species.

4.2.5.5 Fe, Mn, Co and Cu Silicates *Iron silicates*. In 1995, Yuan et al. [257] reported synthesis of Fe-MCM-41 and, based on the results of the EPR study (signal with $g = 4.2$) supposed Fe incorporation in the silica framework. He at al. [258] prepared Fe-MCM-41 and characterized the iron state by EPR and Mössbauer spectroscopies. Calcination led to disappearance of the EPR signal at $g = 4.3$, suggesting removal of Fe^{3+} species from the framework. A series of Fe-HMS samples with Si/Fe from 100 to 15 was prepared by Tuel and Gontier [28, 259]. Calcination produced no significant changes in the EPR spectra, indicating no formation of extraframework iron species, which was in agreement with the results of Mössbauer spectroscopy.

Wang et al. [260] synthesized Fe-MCM-41 using both direct hydrothermal and TIE methods. All as-synthesized Fe-MCM-41 samples prepared by hydrothermal synthesis exhibited a white color, suggesting that no bulk iron oxide was present. The white color was kept after calcination for the samples with Fe content lower than 0.9 wt%. As Fe content exceeded this level, the calcined sample became off-white in color, most likely, due to appearance of extraframework iron-oxide species. The characterization by DRS UV-vis, EPR, and EXAFS suggested that the iron cations were highly dispersed and tetrahedrally coordinated with oxygen at low iron content (< 0.9–1.1 wt%). As in the case of Cr-substituted MCM-41 [237], samples prepared by TIE contained mainly small iron-oxide clusters.

Up to 8.2 wt% of Fe (Si/Fe = 10) were inserted in MCM-41 using a method that involved slow hydrolysis of TEOS in the presence of CTAB and acidic solution of $FeCl_3$ followed by addition of aq. NaOH and hydrothermal treatment at pH 8–8.5 [261]. DR UV-vis, EPR, and Mössbauer spectroscopic studies indicated that iron was present mostly as tetrahedrally coordinated Fe^{3+} species in samples with Si/Fe = 23. Direct synthesis of well-ordered Fe-SBA-15 at pH *ca*. 2.2 was reported by Vinu et al. [262]. Samples with a Si/Fe molar ratio as high as 21 were obtained at Si/Fe = 5 in the gel. When the pH was below 2.0, no incorporation of iron occurred. The characterization by DRS UV-vis, EPR, and XANES suggested that the iron atoms are highly dispersed and mostly occupy isolated tetrahedral sites, the number of which decreases with decreasing Si/Fe molar ratio. The same group synthesized Fe-SBA-1 where the amount of Fe incorporation was controlled by adjustment of the HCl/Si molar ratio and achieved Si/Fe = 36 at Si/Fe = 20 in the gel and HCl/Si = 10 [263]. Fe-SBA-15 containing highly isolated framework iron species has been prepared by direct hydrothermal method at pH 1.5–5.6 [164]. The level of Fe incorporation strongly increased on increasing the pH of the synthesis gel. The Si/Fe molar ratio achieved 100 at pH 5.6, while at pH 1.5 it was only 450 at Si/Fe = 50 in the gel. DR UV-vis study showed that samples with Fe < 0.2 wt% synthesized at pH 1.5 contained mostly isolated iron in tetrahedral coordination (absorption at 220–250 nm). At higher Fe content, the samples were brown owing to the presence of iron oxide phase.

Fe-MMM-2 was synthesized under mild acidic conditions by a two-step procedure [159] similar to that employed for the synthesis of Ti-MMM-2 [152, 156]. Samples prepared at pH 1.0 and 2.0 revealed two DRS UV-vis bands at 222 and 252 nm. The absorption above 350 nm due to the presence of nonframework

iron-oxide species appeared for samples synthesized at pH > 2.0 and/or samples with Fe content > 1.8 wt% [159].

DR UV-vis spectroscopy was extensively used to characterize the nature and coordination of Fe^{3+} ions in iron silicates, but the spectra interpretation is still a matter of discussion. Typical DR UV-vis spectra show two strong absorption bands with maxima at *ca.* 220 and 255 nm (sometimes, only the latter is observed) [159, 164, 260, 261]. These bands can be assigned to the $t_1 \rightarrow t_2$ and $t_1 \rightarrow e$ transitions involving Fe^{3+} in the [FeO_4] tetrahedron; however, octahedral complexes of Fe^{3+} are also characterized by two strong bands in the same energy range [264]. Indeed, Selvam et al. [265] found an absorption at *ca.* 250 nm for MCM-41 supported iron oxide nanoparticles. Therefore, DRS UV-vis bands in the 220–260 nm range can be interpreted as the presence of both framework and nonframework Fe^{3+} species and caution should be taken in making conclusions on the nature of iron on the basis of DRS UV-vis only, although the absence of absorption above 320 nm (brown color) certainly indicates the absence of aggregated phases of Fe_2O_3 or Fe_3O_4.

Mesoporous Fe-containing silicate materials usually reveal two main EPR signals, at $g = 2.0$ and $g = 4.3$ [28, 260–265]. The signal at $g = 4.3$ is due to distorted tetrahedral Fe^{3+} species, whilst the signal at $g = 2.0$ is assigned by different authors to undistorted tetrahedral or octahedral Fe^{3+} sites [260, 264, 266]. Raman [164], XPS [263], X-ray absorption [260, 262, 267], and Mössbauer spectroscopies [28, 261, 265] as well as magnetic susceptibility measurements [268] are complementary methods for the elucidation of the local environment of iron in Fe-containing materials.

Manganese silicates. Zhao and Goldfarb [269] prepared Mn-modified MCM-41 and MCM-48 by direct synthesis in both acidic and basic media using $MnCl_2$ and TEOS or sodium silicate. In calcined samples, Mn^{2+} species were not incorporated into the silica walls but located within mesopores. Zhang et al. [270] prepared Mn-MCM-41 materials by both direct hydrothermal (Si/Mn = 47–359) and TIE (Si/Mn = 33–214) methods and studied them using EPR, XANES, DRS UV-vis, UV–Raman, and XPS. Kevan's group [271] characterized Mn-containing MCM-48 and AlMCM-48 (Si/Mn = 1000) prepared by both direct synthesis and ion-exchange methods by means of EPR and electron spin-echo modulation (ESEM) spectroscopy. Five types of Mn^{2+} species have been identified, including two framework-substituted sites and three extraframework species.

Mn incorporation into MCM-41 under acidic conditions has been studied by Zhang and Goldfarb [272]. At [Si]/[H^+] = 0.1 and 0.4 only 4% and 9%, respectively, of the total Mn added to the synthesis gel were incorporated into the final product. Two Mn^{2+} sites were distinguished using high field pulsed EPR and electron-nuclear double resonance (ENDOR) spectroscopies. One site was attributed to a hexa-coordinated Mn^{2+} with water ligands attached to the internal pore surface of the silica either by one coordination site or through hydrogen bond(s), while the second site was assigned to Mn^{2+} in a distorted tetrahedral coordination, located within the first few layers of the silica wall. When the water content in the final products increased, the characteristics of the second site became close to the characteristics of the first one, suggesting that the silica wall is "soft". NMR and *in situ*

EPR measurements showed that incomplete TEOS hydrolysis and slow silica polymerization, which occur for $[Si]/[H^+] > 0.1$, assist the formation of the octahedral Mn^{2+}, whereas complete hydrolysis and fast polymerization favor the formation of the distorted tetrahedral Mn^{2+} species [272].

Inclusion of Mn into SBA-15 was realized by adjusting the molar ratio of water to HCl under direct hydrothermal conditions [167]. A Si/Mn ratio as high as 2.2 was achieved at $H_2O/HCl = 295$. EPR studies suggested that the majority of the Mn ions in this material existed in a distorted octahedral coordination environment. A series of Mn-TUD-1 with manganese content 1–11 wt% was prepared and characterized by FT-IR, DR UV-vis, and EPR spectroscopies [273]. The fraction of Mn^{2+} was below 1% in the as-prepared samples and dropped to zero upon calcination. Temperature-dependent EPR spectroscopy revealed the antiferromagnetic coupling of up to 75% of the detectable manganese atoms. The uncoupled, that is isolated, framework-incorporated Mn species played a major role in catalysis by Mn-TUD-1. When Mn content exceeded 3.8 wt%, a separate phase, probably, Mn_2O_3 was detected by both XRD and HR TEM.

Cobalt silicates. Lercher and coworkers [274] prepared Co-containing MCM-41 by adding $CoC1_2{\cdot}6H_2O$ to the synthesis gel ($Si/Co = 59$). EXAFS study showed that Co atoms were surrounded by oxygen atoms ($N_{Co-O} = 3.6$) in the first and by Co atoms ($N_{Co-Co} = 5.7$) in the second coordination shell, indicating that the Co atoms are not incorporated in the silica framework positions but present mostly as finely dispersed small Co oxide clusters (5-6 atoms). Subsequent reports claimed incorporation of Co into the framework of mesoporous silicas [275–279]. Haller and coworkers [279] reported the synthesis of highly ordered Co-MCM-41 with $Si/Co = 100$ (*ca.* 1 wt% Co). Vrålstad et al. [278] prepared Co-MCM-48 and Co-MCM-41 with up to 2.5 wt% of Co. It was demonstrated that EXAFS is the most suitable method for direct verification of framework incorporation, by identifying silicon as the backscatterer in the second shell [277]. From EXAFS analyses, it is possible to distinguish between surface-bound and framework-incorporated cobalt. Information about the coordination symmetry of Co may be obtained by both XANES and DR UV-vis techniques.

Co-SBA-1 was synthesized under acidic conditions using CTAB, TEOS and Co(II)acetate tetrahydrate [275]. The amount of cobalt in the calcined samples was in the range of 0.15–0.8 wt%. A reduction of the HCl/TEOS and HCl/CTAB molar ratios in the starting gel resulted in a higher degree of structural ordering and a higher amount of incorporated cobalt. Based on the results of DRS UV-vis–NIR studies, the authors assumed that the cobalt ions in dehydrated samples of Co-SBA-1 are not tetrahedrally coordinated but possess a trigonal pyramidal symmetry [275]. Well-ordered Co-SBA-15 materials were synthesized using the pH-adjusting approach [160]. The level of Co loading strongly increased with increasing pH from 0.5 to 5.5–7 and then tended to decrease. The optimal pH value that allowed the high surface area and mesopore volume to be combined with a reasonable level of cobalt incorporation (0.27 wt%) was found to be 3.0.

Co-TUD-1 materials with Si/Co ratios in the range of 10–100 were synthesized using TEOS, $CoSO_4{\cdot}7H_2O$ and TEAOH [276]. Studies by XRD, ^{29}Si MAS NMR,

DR UV-vis, and Raman spectroscopies showed that, at Si/Co = 50–100, cobalt is incorporated into the framework of TUD-1 as isolated, most likely, tetrahedrally coordinated Co^{II} atoms, whereas at higher loadings, clusters Co_3O_4, along with a small amount of cobalt oxide nanoparticles, predominate. DR UV-vis spectra of the calcined samples with Co content below 0.5 wt% exhibit three bands at 520, 580 and 655 nm that can be assigned to Co^{II} in tetrahedral configuration ($^4A_2 \rightarrow {}^4T_1(P)$ energy transition that causes the blue color of the samples). Higher Co loadings result in the appearance of broad absorptions at 410 and 710 nm, similar to those of Co_3O_4, indicating octahedrally coordinated, most likely, clusterized Co^{III} ions.

Copper silicates. The significant difference in the size and charge of Cu and Si raises doubts about the possibility of copper incorporation in the silica framework. Indeed, reports on the direct synthesis of mesostructured copper silicates are relatively scarce. Tsai et al. [280] prepared MCM-41 samples containing Cu^{II} and Al^{III} by a hydrothermal method using $Cu(NO_3)_2$ as copper source and characterized them by XRD, N_2 adsorption, XANES, EPR, and ^{27}Al solid state NMR. The state of Cu differed from that in the samples where Cu^{2+} was introduced *via* ion exchange; however, no unambiguous evidence for copper incorporation in the silica framework was obtained. Cu,Al-MCM-41 and Cu,Nb-MCM-41 with various Si/Cu ratios were prepared at room temperature by direct synthesis [281]. Cu-SBA-15 was synthesized using TEOS and $Cu(CH_3COO)_2{\cdot}H_2O$ as silicon and copper sources, Pluronic P123 as surfactant, and $Al(NO_3)_3{\cdot}9H_2O$ as a mineralizing agent [282]. Without the latter, the synthesis was not possible, although no aluminum was found in the final material.

4.2.6 Postsynthesis Modifications

Alternatively to incorporation of metal ions into silica *via* direct synthesis, active sites can be created on the silica surface by various postsynthesis techniques [13, 16, 23, 25, 26, 28, 31, 50–58]. Good thermal and chemical stability, ease of handling, quite rigid structure, noncompressibility and stability with respect to swelling in solvents as well as abundance of exposed silanol groups make silica a support of choice for construction of single-site heterogeneous catalysts. Here, we consider methodologies that may result in the formation of direct M–O–Si bonds on the silica surface (the so-called grafting), leading to totally inorganic materials after calcination. Techniques that basically preserve the organic ligands surrounding of the metal-ion precursor, namely anchoring, tethering and encapsulation, will be described in Chapter 7.

4.2.6.1 Mesoporous Silicates as Supports The surface of silica is hydrophilic due to the presence of numerous silanol groups [38, 44, 51, 52]. IR spectra reveal a sharp band at 3740–3745 cm^{-1} attributed to isolated SiOH groups and a broad band at *ca*. 3550 cm^{-1} due to hydrogen-bonded silanols. The nature and density of surface silanols can be controlled by thermal treatment. The surface concentration of silanols in ordered mesoporous materials is generally lower compared to conventional hydroxylated silicas (2–3 SiOH/nm^2 *vs*. 4–6 SiOH/nm^2 [36, 97, 283]).

However, to avoid hydrolysis, polymerization and deactivation of the metal precursor, most postsynthesis techniques operate under anhydrous conditions and employ partially dehydrated silicas (pretreatment at 200–300 °C in vacuum) with silanol populations in the range of 1.5–2.5 SiOH/nm^2 [52].

Mesostructured silicates are considered as feasible supports due to their spatially ordered architecture with tunable pore sizes and narrow pore-size distributions [22–28, 31, 36, 45, 50, 52, 56, 58]. Their high surface areas and pore volumes would allow a higher accommodation capacity of metal precursors with respect to conventional silicas. Keeping in mind the attractive features of ordered silicates, one should remember that commercial amorphous silicas are by far cheaper and more available, usually possess higher thermal and mechanical stabilities and, as will be shown in Section 4.3, often allow the preparation of catalysts with the catalytic performance comparable or even superior to that of ordered materials. Therefore, the choice of the silica support depends on the intended objectives and the specific catalytic reaction.

4.2.6.2 Postsynthesis Techniques *Template ion exchange* (TIE) method, where as-synthesized materials containing an ionic template within mesopores are subjected to the ion-exchange procedure, occupies an intermediate position between direct and postsynthesis methods. Mesostructured silicates modified with Cr^{3+} [237], Fe^{3+} [260, 284, 285], Mn^{2+} [270, 286], and other metal ions were prepared by exchanging the surfactant cations with cationic forms of the metal precursors. Suib and coworkers [287] suggested incorporating transition metals through ion exchange of the surfactant anions located in the channels with high-valence metal precursor anions, e.g., MnO_4^-, VO_4^{3-}, or CrO_4^{2-}. The decrease in surface area and pore volume of thus-prepared M-MCM-48 with respect to the parent silicate are consistent with the inclusion of MO_x species within the pores. Spectroscopic studies [237, 260, 287] showed that the TIE approach produces mainly small metal-oxide clusters on the silica surface while direct synthesis often allows obtaining site-isolated M centers at comparable metal loadings. Removal of the organic template by calcination may result in true grafting, i.e. formation of M–O–Si bonds, in the materials prepared by the TIE method [284].

In the late 1960s, Shell Oil Co. developed the TiO_2-on-SiO_2 catalyst, which still remains the heart of the styrene monomer–propylene oxide (SMPO or POSM) process (see Chapter 10). This catalyst is prepared in a multistep gas phase process by deposition of a Ti precursor ($TiCl_4$ or an organotitanium compound) onto silica, calcination in inert atmosphere, followed by steam treatment and silylation [288–291]. It is now generally believed [291] that reaction of $TiC1_4$ with silica involves three Si-OH groups (Eq. 4.6):

$$\equiv \mathrm{Si-OH})_3 + \mathrm{TiCl_4} \rightarrow \equiv \mathrm{Si-O})_3 - \mathrm{TiCl} + 3\,\mathrm{HCl} \qquad (4.6)$$

Hence, the Shell catalyst can be considered as the first example of titanium grafting onto silica. The low Ti content (*ca.* 2 wt% TiO_2) and the synthesis conditions

ensure the formation of Ti species well dispersed on the solid support. The Lewis acidity of the Ti^{IV} centers is increased compared to homogeneous Ti complexes due to the electron-withdrawing effect of the siloxy ligands [288].

An exponential evolution of the Shell approach can be found in the synthesis of numerous Ti/silica catalysts by grafting $TiCl_4$ [100, 292–297] or $Ti(OiPr)_4$ [28, 99, 102, 283, 298–303], or $Ti(OBu)_4$ [304], onto the surface of ordered (MCM-41, MCM-48, SBA-15, MSU-X, KIT-1, FSM-16, etc.) or amorphous silicas. Grafting can be performed either from the gas phase or liquid phase.

Chemical vapor deposition (CVD) is a useful postsynthesis technique, provided the precursors are volatile reagents (e.g., metal chloride, carbonyl, cyclopentadienyl, metallocene) [13, 36, 292–296, 305]. Deposition under controlled gas–solid phase conditions usually preserves the high surface area of the silica support. The maximum achievable number of grafted metal species is related to the number of silanols present on the surface and not by the geometrical surface, which has a higher capacity [305]. Chiker et al. [292, 294] found that both the temperature and deposition time affect dispersion of titanium inside pores of SBA-15. A gas phase *molecular designed dispersion* (MDD) method was employed to anchor $VO(acac)_2$ on the partially silylated surface of MCM-48 [306]. This method allowed creation of V-centers that were almost exclusively present as isolated, tetrahedral Si–O–V $(O)(OH)_2$ species with enhanced stability to leaching.

Incipient-wetness impregnation (IWI) of silica is commonly used for the preparation of molecularly dispersed silica-supported oxides [13, 36]. Nonaqueous solutions of alkoxides are most often used for impregnation [99, 102, 189, 298, 299, 301–304] although solutions of inorganic salts or metal complexes are also employed [100, 307]. The dispersion capacity is closely related to the surface concentration of silanols and the preparation technique, specifically, the pretreatment temperature, impregnation time, reactivity and molecular size of the precursor [13]. The maximal loading of around 1.4 Ti/nm^2 is widely accepted as the upper limit for mesoporous silica [303]. Both CVD and IWI techniques produce materials that reveal different types of M species, ranging from isolated to oligo/polymeric MO_x and even bulk MO_n oxides. Only at low metal loadings (Si/M = 80 and higher), can isolated metal centers be the predominant species [99, 302].

Ion-beam implantation allowed preparation of a Ti/SiO_2 catalyst (0.28 wt% Ti) with highly isolated Ti centers directly from Ti metal [308]. The Ti atoms were ionized first and the ionized Ti beam was accelerated under high voltage to be implanted at high speed onto silica. The implanted Ti ions are highly isolated since the ion density in the beam is low and the ions are repelled from each other.

Special postsynthesis techniques were developed to increase metal loading but maintain its isolated state. The impregnation of SBA-15 or MCM-41 with a mixture of quaternary ammonium hydroxide and partially hydrolyzed $Ti(OBu)_4$ followed by filtration, washing and calcination gave anatase-free mesoporous titanosilicates with Si/Ti ratios between 116 and 16 [309]. At Si/Ti ratios higher than 50, the Ti species were mainly isolated and tetrahedrally coordinated. The role of the organic ammonium hydroxides is, most likely, to promote a better Ti dispersion *via* complexation. Hua et al. [49] coated channels of SBA-15 by

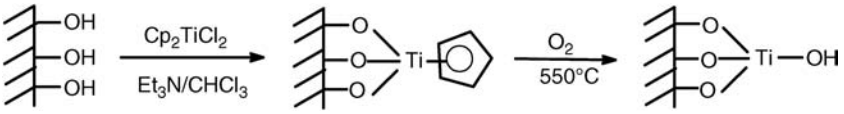
TiO_2–SiO_2 mixed oxide. The resulting materials showed a high portion of isolated Ti species up to Si/Ti = 10.

Great attention was given to the development of rational, molecular-engineering approaches for construction of spatially isolated metal centers on the silica surface using tools of *surface organometallic chemistry* [16, 25, 34, 50–54, 56–58]. Systematic studies of the reactivity of organometallic complexes or coordination compounds with the silica surface have led to the conclusion that the surface can be considered as a rigid polydentate ligand [51]. Grafting of a mononuclear metal precursor $M(L)_n$ can result in the formation of monopodal $(\equiv Si–O)–M–(L)_{n-1}$, bipodal $(\equiv Si–O)_2–M–(L)_{n-2}$, or tripodal $(\equiv Si–O)_3–M–(L)_{n-3}$ species [51, 52]. The type of bonding (podality) depends not only on the surface density of silanols, but also on the surface curvature, which is related to the pore diameter, as well as on the nature of the metal precursor. During calcination, the mobility of bi- and monopodally bound M species may lead to metal oligomerization [57]. In the case of highly oxophilic metals, such as Ti^{IV} or V^{V} tripodal bonding can be the favored, most stable configuration, provided a sufficient amount of silanols is available on the support [56, 305]. Surface silanols can react with a titanium alkoxide precursor according to Eq. 4.7

$$\equiv Si - OH)_3 + Ti(OR)_4 \rightarrow \equiv Si - O)_3 - Ti(OR) \qquad (4.7)$$

Although being the most inexpensive precursors for grafting, metal alkoxides reveal several disadvantages, such as incomplete surface silanol consumption, release of strongly surface-coordinating alcohols, and di(oligo)merization of alkoxide species on the surface [52, 300]. It was supposed that utilization of organometallic precursors with bulky ligands may enhance the formation of isolated metal sites on the surface [50–52, 310]. One of the first examples of the deposition of active metal sites through the fixation of a bulky organometallic complex was reported by Maschmeyer et al. [50]. Treatment of MCM-41 with a chloroform solution of titanocene dichloride in the presence of NEt_3 led to grafting of the titanocene complex through oxygen atoms onto the pore surface (Scheme 4.1). The evolved HCl was scavengered by the amine, thereby rendering its harmless. According to EXAFS studies, this grafting produces tripodal $(\equiv Si–O)_3TiCp$ as the predominant surface sites, while calcination under a stream of oxygen removes the Cp ligand and generates isolated, structurally well-defined active $\equiv TiOH$ sites [101].

The atomic nature of thus-prepared Ti/MCM-41 materials was probed by a range of experimental and computational techniques [50, 95, 97, 101]. It was found that



SCHEME 4.1 Metallocene route to grafted Ti/silica catalysts.

samples prepared in dry Ar and containing less than 2 wt% of Ti possess mostly tetrahedral Ti^{IV} sites that absorb at 210–230 nm in DR UV-vis spectra and exhibit an emission at 430 and 490 nm when excited with a 250 nm light [97]. Samples with greater than 4 wt% loading contain TiO_2-like microclusters absorbing at $\lambda > 250$ nm in DRS UV-vis and emitting very weakly in the 500–600 nm region. The catalysts prepared in air, in the presence of atmospheric water revealed incipient formation of dimeric or small oligomeric Ti species even at the lowest Ti loading (<0.5%).

Guidotti et al. [311, 312] adapted and optimized the titanocene-based grafting procedure for amorphous silicas. Although the bulky Cp ligand limits the coalescence of the Ti species on the surface, agglomeration of the metal species evidently occurs at high Ti loadings [67, 313]. Isolated Ti species predominate at low Ti density (<0.2 Ti/nm^2) while dimeric and small oligomeric species prevail in the range of 0.4–1.1 Ti/nm^2 [313]. Clearly, for the same Ti content in the sample, the surface concentration of Ti species and, hence, Ti dispersion depends on the specific surface area of the support. Thus Ti/MCM-41 (970 $m^2 g^{-1}$) with 2 wt% of Ti contains mostly site-isolated Ti centers whereas di(oligo)merized Ti species predominate on the surface of Ti/SiO_2 (290 $m^2 g^{-1}$) as verified by DRS UV-vis technique (Figure 4.6) [313].

Catalysts with dimeric or small oligomeric Ti centers can be constructed using di(poly)nuclear Ti precursors. Nanometric titanium oxide particles have been dispersed on the surface of SBA-15 by solution grafting of the hexanuclear cluster $[Ti_6(\mu_3\text{-}O)_6(\mu\text{-}O_2CC_6H_4OPh)_6(OEt)_6]$ [314]. A catalyst containing Ti oxide dimers was prepared by simple impregnation and thermal decomposition of $(NH_4)_8[Ti_2(C_6H_4O_7)_2(O_2)_2]_2 \cdot 8H_2O$ [313, 315]. The dimeric structure of the Ti centers in the sample containing 2 wt% Ti was confirmed by EXAFS analysis [315].

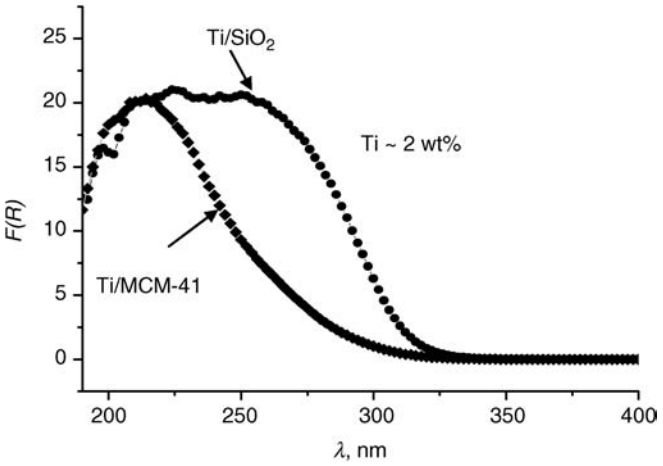


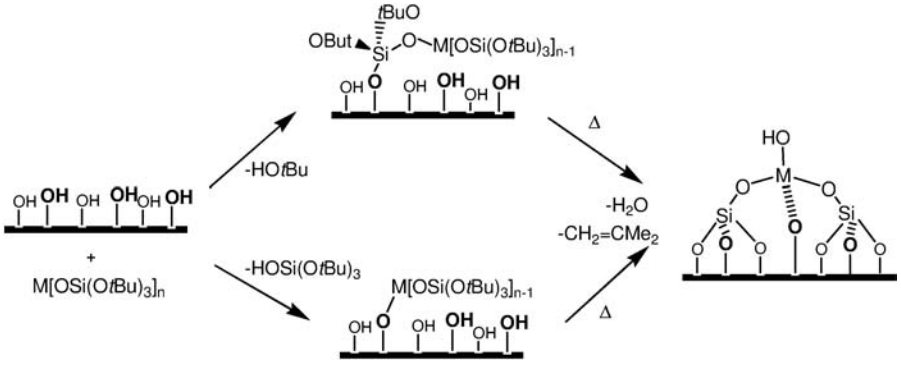
FIGURE 4.6 DR UV-vis spectra of Ti/MCM-41 and Ti/SiO_2 with similar Ti content prepared by grafting Cp_2TiCl_2 [313].

Transition metals other than titanium (Zr^{IV}, Hf^{IV}, V^{IV}, and Mo^{VI}) were grafted onto silica *via* the metallocene route [34, 316–319]. Tetraneopentylzirconium was used to prepare silica-bound $(\equiv SiO)ZrNp_3$ species that could be further transformed by hydrolysis or hydrogenolysis to $(\equiv SiO)Zr(OH)_3$ or $(\equiv SiO)_3ZrOH$, respectively [320]. Metalorganic precursors of Sn^{IV} [321–323] and Ta^{V} [113, 324, 325] were grafted onto the silica surface. The nature of reagents used for grafting can strongly affect the properties of the resulting materials. It was demonstrated for Sn/MCM-41 that tin reagents R_nSnCl_{4-n} with $n = 1$ or 2 produce best incorporation (up to 2.9 wt% SnO_2) and avoided the formation of inactive polymeric tin-oxo species [321, 322]. Alternatively, Sn/MCM-41 materials were prepared by reaction of $SnBu_4$ with surface silanols [323]. DR UV spectra of samples with $Si/Sn = 14$ were mainly composed of an intense absorption at 220 nm, in agreement with 4-coordinated tin, while for higher loadings, a small shoulder near 260 nm, characteristic of 6-coordinated tin, appeared.

Supported Ta(V) oxide catalysts were prepared by grafting calixarene–Ta(V) and TaX_5 complexes on SiO_2 at coverages less than 0.25 Ta/nm^2 [325]. Thermogravimetric and elemental analyses and DRS UV-vis indicated that catalysts consist of isolated, 1:1 Ta : ligand surface sites, producing $(\equiv SiO)_3Ta{=}O$ species after calcination.

The thermolytic molecular precursor method is an efficient technique to produce single-site metal (Ti, Cr, Fe, Ta, V, etc.) centers on the silica surface [16, 45, 57, 113–116]. Typically, a molecular precursor of the general formula $M[OSi(O^tBu)_3]_n$ is first grafted onto high surface area silica, to form a molecular species monopodally bound to the surface, which then undergoes facile thermolytic elimination of isobutene and water to give a stable inorganic "single site" (Scheme 4.2).

A clear advantage of metal silicates prepared by postsynthesis techniques is high accessibility of metal centers, which may result in a higher catalytic activity compared to their analogs prepared by direct synthesis. However, the higher exposure to reactants often results in a poorer stability of the active centers toward metal leaching.



SCHEME 4.2 Illustration of thermolytic molecular precursor method (adapted from [114]).

4.2.7 Organic–Inorganic Hybrid Materials

Considerable efforts were made to incorporate organic moieties within inorganic metal-silica frameworks to tune the surface properties and the catalytic performance. Synthetic methodologies leading to hybrid organic–inorganic materials have been comprehensively reviewed [39, 41, 69, 326–330]. Like metal species, an organic functionality can be introduced by direct synthesis or postsynthesis. Since the hydrophilic nature of mesoporous silicates is often detrimental for liquid phase oxidations, in particular, when hydrophobic substrates are involved, surface hydrophobization with silylating reagents is conventionally applied [52, 326, 328, 329]. Hexamethyldisilazane (HMDS) and trimethylchlorosilane are the most frequently used silylating agents [19, 290, 309, 331–335].

Alternatively to postsynthesis, an organic functionality can be introduced during the direct sol-gel synthesis *via* cocondensation of TEOS (TMOS) and organotrialkoxy silanes, $RSi(OEt)_3$ [9, 14, 15, 69, 78, 336–339]. The incorporation of nonpolar (R = alkyl, phenyl, benzyl) or polar (acetoxypropyl, aminopropyl) organic groups may dramatically improve catalytic performance, depending on the specific reaction. The nonhydrolytic sol-gel route [87] allows preparation of mesoporous hybrid titania–silica xerogels with a Si/Ti molar ratio of 10 using low cost precursors ($TiCl_4$, $SiCl_4$ and $MeSiCl_3$) and routine evaporative drying technique [340].

Stein et al. [326] comprehensively reviewed hybrid mesostructured materials prepared by cocondensation through S^+I^-, $S^+X^-I^+$, and S^0I^0 pathways. Highly ordered organically functionalized Ti-MCM-41 materials were synthesized employing a mixture of two silicon sources, TEOS and $RSi(OEt)_3$ (R = methyl, vinyl, allyl, 3-chloropropyl, pentyl, and phenyl), and $Ti(OBu)_4$ as titanium source [341]. Methyl-functionalized Ti-MCM-41 nanoparticles with a size of 80 to 160 nm were prepared *via* a dilute solution route by the cocondensation of TEOS and methylalkoxysilanes at room temperature [342]. Organically modified Ti-SBA-15 with high dispersion of Ti and enhanced hydrophobic behavior were synthesized through cocondensation of TEOS, $RSi(OEt)_3$ and titanocene dichloride in the presence of Pluronic 123 under acidic conditions [343]. Cr-containing organosilicas were prepared by cocondensation of TEOS, chromium nitrate and organotrialkoxysilanes (chloropropyl, vinyl, methyl) in the presence of CTAB [344]. Bifunctionalized silica, CoPh-HMS, was synthesized using TEOS, $PhSi(OEt)_3$ and $Co(OAc)_2{\cdot}4H_2O$ in the presence of hexadecylamine as template [345].

Vinyltrimethoxysilane was polymerized under nonaqueous conditions through radical initiation, and the resulting polymer was used as precursor under mild basic conditions in the presence of CTAB to obtain a mesoporous organic–inorganic hybrid polyvinylsiloxane HPVS-1 [346]. The addition of $Ti(^nBuO)_4$ in the synthesis gels led to a titanium analog, Ti-HPVS-1. XRD, TEM and N_2 sorption measurements indicated highly porous wormhole-like disordered structure. Solid-state ^{29}Si MAS NMR, UV-vis, and FT-IR studies suggested the incorporation of isolated tetrahedral Ti sites in the hybrid silica framework for samples with Si/Ti = 25 and higher.

Organic–inorganic hybrid materials having organic moieties as molecularly bridging ligands in the framework position referred to by the name *periodic mesoporous organosilicas* (PMO) are obtained from the hydrolysis and condensation of silsesquioxane precursors $(OR)_3Si–R_1–Si(OR)_3$ ($R_1 = –CH_2–$, $–(CH_2)_2–$, $–C_6H_5–$, etc.) in the presence of various surfactants [326–329, 347–349]. Transition metals can be incorporated within the framework of such PMO materials [350–353]. Ti-containing (*ca.* 2 wt%) ethane-bridged hybrid mesoporous materials Ti-HMM were synthesized using 1,2-bis(trimethoxysilyl)ethane or 1,2-bis(triethoxysilyl)ethane (BTESE), TEOS, $Ti(^nBuO)_4$ and cationic surfactants under basic conditions [350, 351]. XRD, TEM and N_2 adsorption studies revealed uniform hexagonal arrangement of 2.7–2.9 mn mesopores with 1.3–1.5 wall thickness. Another Ti-containing PMO was prepared using TEOS, BTESE, $TiCl_3$, and Pluronic P123 in acidic media [352]. The maximum level of Ti incorporation was about 0.34 wt% regardless of the initial Si/Ti ratio. Cr-PMO (Cr 1.8–2.7 wt%) with hexagonal arrangement of mesopores was synthesized from BTESE, TEOS, chromium nitrate and alkyltrimethyl ammonium salts (C_{16} and C_{18}) as surfactants [353]. FT-Raman, DR UV-vis and XPS indicated a highly dispersed state of chromium in this material.

4.3 CATALYTIC PROPERTIES

Since the first syntheses of mesoporous metal silicates at the early 1990s a huge number of research papers devoted to evaluation of their catalytic properties in liquid phase oxidations has been published. Unfortunately, many of them (especially, early publications) did not touch upon the questions of catalyst recycling, metal leaching and the nature of catalysis (true heterogeneous vs. homogeneous due to leached active species) although these issues are crucial for assessment of the potential utility of solid catalysts in liquid phase processes [4, 354]. In this section, we aimed at considering, first, the catalytic systems, for which the nature of catalysis was investigated following the methodology suggested by Sheldon and coworkers that involves *filtering the catalysts at the reaction temperature before completion of the reaction and testing the filtrate for activity* [354].

4.3.1 Oxidation of Alkanes

Alkanes are among the most abundant naturally occurring organic substrates but they are also among the most difficult molecules to functionalize in a controllable manner. The selective catalytic oxidation of alkanes is a demanding task because the oxidation products are desirable potential feedstocks for the chemical industry. The oxidation of cyclohexane (CH) into a mixture of cyclohexanone (K) and cyclohexanol (A), the so-called K-A oil, has particular significance for the manufacture of Nylon-6 and Nylon-6,6. Currently, K-A oil is produced *via* auto-oxidation of CH using homogeneous cobalt or manganese catalysts [355]. Since both A and K are substantially more reactive than CH, high selectivities to K-A can be achieved only at low (<5%) substrate conversions. The creation of heterogeneous catalysts for the

selective oxidation of CH to K-A oil or direct oxidation of CH (or *n*-hexane) to adipic acid (AA), an important building block for polyamides and urethanes, is a challenging goal [356].

In 2001, Schuchardt et al. [357] reviewed the catalytic systems used for the oxidation of CH with particular attention to the issue of metal leaching from solid catalysts. The lower activity and H_2O_2 efficiency of Ti-MCM-41 relative to TS-1 was attributed to the hydrophilic environment of Ti active centers, which disfavors CH adsorption within pores and, oppositely, favors unproductive decomposition of the oxidant. Organofunctionalized Fe-MCM-41 showed an improved activity relative to ordinary Fe-MCM-41. Besides Ti-MCM-41, all metal silicates suffered leaching of the metal, and the observed catalytic activity was mainly due to homogeneous species.

A significant progress in the selective heterogeneous oxidation of CH has been achieved in the first decade of the 21st century. Co-TUD-1 was shown to be an active and selective catalyst for the aerobic oxidation of CH using traces of cyclohexyl hydroperoxide (CHHP) as initiator [358]. The catalyst with Si/Co = 100 containing isolated Co atoms displayed the highest activity. Under continuous semibatch reactor conditions, CH conversion after 6 h attained 5–6% and the selectivity to the mono-oxygenated products (mostly A and K) was 87%, which compares well with the homogeneous industrial process [355]. The decomposition of CHHP was independently studied over Co-TUD-1, and complete conversion of CHHP with excellent selectivity toward A and K and stable activity over a period of one week was found. Although some acids were formed, no cobalt leaching was found (the detection limit for Co in solution was 0.1 ppm). Slow deactivation of Co-TUD-1 was possibly due to the rather crude feed [358]. For comparison, Co/SiO_2 catalyst synthesized by flame-spray pyrolysis produced 4% CH conversion after 4 h, 30 and 60% of A and K, respectively, and 10% of acids [359]. About 11% conversion of CH and 79% total selectivity to K and A was found for Co-HMS [360]. Over hybrid CoPh-HMS, a conversion of 9–10% was attained with the selectivity to K + A *ca.* 74% [345]. The main byproducts were acids and ethers.

Over periodic mesoporous organosilicas Cr-PMO, the conversion of CH was 7% and the selectivity to K + A achieved 94% (K/A = 2.6) [353, 361]. The catalyst was recyclable with a slight change in the selectivity. The main byproducts were CHHP and adipic acid. Similar results in conversion and selectivity were obtained with Cr-MCM-48 [361] and another Cr-containing organic–inorganic hybrid material [344]. For the latter, hot filtration experiments performed by removing the catalyst after 2 and 6 h showed that catalysis was mostly heterogeneous at low conversions but then became homogeneous due to the formation of acids that accelerate leaching of the active species, as usually observed with acetic acid as solvent.

Among M-HMS catalysts, Al-HMS revealed the best performance, behaved as a true heterogeneous catalyst, did not suffer from leaching and showed stable catalytic properties for 5 reuses [360]. Surprisingly, Bi-MCM-41 was found to be an efficient catalyst for the oxidation of CH with molecular oxygen [362]. Hot filtration experiments corroborated the true heterogeneous nature of catalysis. A short

TABLE 4.3 Oxidation of Cyclohexane with O_2 over Mesoporous Metal Silicates

Catalyst	P (bar)	T (°C)	Time (h)	Conv. (%)	Select. K + A (%)	Leaching	K/A	Ref.
Co-TUD-1	15[a]	120	6	5-6	87	<0.1 ppm	0.64	[358]
Co/SiO_2[b]	27.6	130	4	4	90	no	2.0	[359]
Co-HMS	5	140	4	11	79	[c]	1.5	[360]
Al-HMS	5	140	4	10	92	no	1.8	[360]
CoPh-HMS	10	120	6	9–10	74	[c]	1.5	[345]
Bi-MCM-41	10	140	4	12–17	91–94	no	3.5[d]	[362]
Cr-PMO	27	120	6	7	94	[c]	2.6	[361]
Cr-MCM-48	27	120	6	7	93	[c]	2.9	[361]
Hybrid Cr-Si	27	120	6	8	92	no/yes[e]	2.1	[344]

[a] 5% O_2, 95% N_2.
[b] Nonporous material.
[c] No elemental analysis data and no hot filtration test were reported.
[d] Strongly affected by metal content.
[e] Depended on the conversion.

summary of the results reported so far for the selective oxidation of CH with molecular oxygen over mesoporous metal silicates is presented in Table 4.3.

Although the most sustainable (both clean and economically sound) approach to CH oxidation is based on the use of molecular oxygen, oxidations with alkylhydroperoxides and hydrogen peroxide are widely explored [356]. Amorphous mesoporous cerium silicates were found to be efficient catalysts for CH oxidation with *tert*-butyl hydroperoxide (TBHP) [108]. CH conversions up to 12% were obtained in acetone as solvent; the only identified products were K, A and CHHP. A hot filtration test indicated the heterogeneous nature of catalysis. Among the family of M-TUD-1 sponge-like materials (M = Ti, Co, Fe, Cr, and Cu; Si/M = 100) the highest CH conversions (10–14%) were achieved with M = Co, Cr and Cu; however, only for Co-TUD-1, catalysis was true heterogeneous and no metal leaching occurred [276, 363, 364]. In the filtrate of Co-TUD-1, the conversion of TBHP almost stopped and the rate of CH oxidation dramatically slowed down (some residual activity was attributed to the radicals still present in the reaction mixture). The overall $K + A$ selectivity was 92% ($K/A = 6$) at *ca.* 10% substrate conversion.

Cr-MCM-41 showed excellent catalytic activity and high selectivity in the oxidation of cyclohexane and cyclooctane with dilute aqueous H_2O_2 or TBHP as oxidant in acetonitrile as solvent at 80 °C [238]. Ketones were the principal reaction products. Cr-PMO exhibited higher catalytic activities and selectivities than conventional Cr-MCM-41 in the CH oxidation with aqueous H_2O_2 and nonaqueous TBHP [353]. Hot catalyst filtration tests revealed a substantial chromium leaching and homogeneous nature of catalysis in the case of H_2O_2, while catalysis was principally heterogeneous, at least at the initial stage of the reaction, with nonaqueous TBHP. Stability with respect to leaching was higher for Cr-PMO than for Cr-MCM-41. The major products of the CH oxidation with TBHP over Cr-PMO

were K and A with trace amounts of CHHP and cyclohexyl-*tert*-butylperether. The conversion of CH was 4% in the absence of solvent and increased to 12% in acetone (70 °C, 5 h, [CH]/[TBHP] = 1). The K/A ratios were high (> 5 after 5 h) [353]. The higher catalytic activity and stability of Cr-PMO were attributed to the improved hydrophobicity of this material and to the complementary textural and structural features that facilitate adsorption of the reactants close to the active Cr sites.

A few papers claimed high (> 90%) selectivities to cyclohexanol or K-A at 85–95% conversions of CH over Cr-MCM-41 [235], V-MCM-41 [214, 365], V-MCM-48 [218], Ce-MCM-41 [201], and Ce-SBA-15 [203] with H_2O_2 as oxidant in acetic acid as solvent. In other solvents (methanol, dioxane, or acetone) CH conversion was much lower. Typically, the activity of these catalysts decreased after first recycle(s), owing to leaching of nonframework metal ions, but then it remained nearly the same for several reuses [203, 214, 235, 365]. After removal of the nonframework metal species by washing (e.g., with ammonium acetate), the washed catalyst showed activity similar to that of the recycled catalyst [214, 235, 365]. Based on the so-called quenching tests [366] (similar to hot filtration test), it was concluded that the recycled and washed catalysts are truly heterogeneous.

Unfortunately, comparison of catalytic systems reported for the CH oxidation is often difficult (if possible) not only because different reaction conditions and setups are employed. So far, determination of CH conversions and $K + A$ selectivities remains the area of some confusion. Evaporation losses of CH upon pressure release at the end of a catalytic run may prevent a complete mass balance in GC analysis, and conversions of CH are often overestimated [358]. In addition, CHHP cannot be identified by GC because it rapidly decomposes in the injector to produce A and K. Furthermore, its decomposition affects the A to K ratio on the chromatogram. To make analysis of products formed during the liquid phase oxidation of hydrocarbons more reliable, a simple method based on the comparison and quantification of chromatograms of the reaction samples before and after reduction of hydroperoxide, e.g. with triphenylphosphine, should be employed [359, 360, 367]. Coupled with independent iodometric titration of the hydroperoxide [345, 360, 368], this method allows correct evaluation of the CHHP, A and K yields. Acidic byproducts, including 6-hydroxyhexanoic, 6-hydroperoxyhexanoic, adipic, glutaric and other acids, can be identified by GC only in the form of ethers, i.e. after derivatization (methylation, silylation, etc.). Several low boiling byproducts (valeric acid, methanol, 1-butanol, 1-pentanol, etc.) as well as CO and CO_2 can be found, especially at high conversions, if both the liquid and the gas phase is thoroughly analyzed [359].

Oxidations of acyclic alkanes over mesoporous metal silicates are scarce. Tatsumi et al. [331] demonstrated that trimethylsilylation of Ti-MCM-41 and Ti-MCM-48 improves both the catalytic activity and H_2O_2 efficiency in the solvent-free oxidation of hexane, but the achieved level of conversion remained very low (< 0.2%). The mixed-phase catalyst Ti-MMM-1 was found to be more active and selective than either Ti-MCM-41 or TS-1 in the oxidation of cyclohexane and *n*-octane with H_2O_2 [177]. Comparison of the catalytic performances is shown in

TABLE 4.4 Catalytic Performances of Ti-MMM-1, Ti-MCM-41 and TS-1 in Oxidation of Alkanes with H_2O_2

Alkane	Catalyst	Conversion (%)	Ketone(s) (%)	Alcohol(s) (%)
Cyclohexane	TS-1	4	26	28
	Ti-MCM-41	2	10	17
	Ti-MMM-1	9	35	55
n-Octane	TS-1	13	10	80
	Ti-MCM-41	3	22	53
	Ti-MMM-1	20	15	81

Reaction conditions: alkane 1 g, acetone 5 g, H_2O_2 (30 wt%, moles of alkane/moles of $H_2O_2 = 3$), catalyst 0.1 g, 95 °C, 8 h. Adapted from ref. [177] with permission of Elsevier, Copyright 2002.

Table 4.4. Unfortunately, no catalyst recycling and leaching tests were provided for the Ti-MMM-1 catalyst.

Hydrothermally stable Ti-MMM-2 catalyzed the oxidation of a range of alkanes (cyclooctane, *n*-heptane, *n*-octane, *iso*-octane, methylcyclohexane, *cis*- and *trans*-1,2-dimethylcyclohexane) by H_2O_2 in acetonitrile [369]. The reaction stopped completely after removal of the catalyst by hot filtration. Cyclododecane was oxidized with H_2O_2 over V-MCM-41 [205] and V-SBA-15 [221] to produce cyclododecanone. The recycling behavior and washing tests suggested that extraframework V species leached during the first run but then it could stop [221].

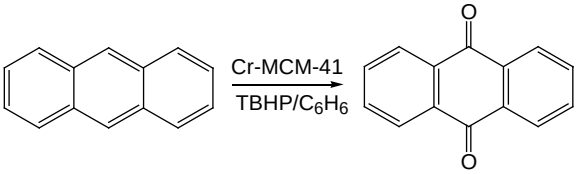
4.3.2 Oxidation of Aromatic Compounds

4.3.2.1 Arenes *Oxidation of aromatic ring*. In 1996, Pinnavaia and coworkers [211] reported H_2O_2-based hydroxylation of benzene to phenol in the absence of solvent catalyzed by M-MCM-41 and M-HMS (M = Ti, V, Cr, Mn, and Mo). At conversions below 10%, the selectivity to phenol was *ca*. 100%. Ti-, V- and Mn-MCM-41 showed the highest activity (TON = 150–200 after 24 h at 72 °C) but the nature of catalysis was not addressed. The oxidation of benzene to phenol over Ti-HMS and Ti-MCM-41 in acetone, the solvent normally used for benzene hydroxylation with TS-1, was also reported [130]. Later, it was found that both Ti-HMS and Ti-MCM-41, unlike TS-1, catalyze the oxidation of acetone at rates competitive with benzene oxidation [211].

The formation of phenol was highly selective (*ca*. 100% at 42% conversion of hydrogen peroxide and 7.5% conversion of benzene) over Fe/SBA-15 (0.5 wt% Fe) prepared by the thermolytic molecular precursor method [114]. The solvent-free hydroxylation of benzene with H_2O_2 (molar ratio benzene/$H_2O_2 = 3$) over V-MCM-41 produced phenol as the only identified product at the oxidant conversion 97% and H_2O_2 selectivity 79% [213]. V-containing MCM-41 synthesized by direct hydrothermal method (V-MCM-41) and grafting (V/MCM-41) catalyzed hydroxylation of biphenyl with aqueous H_2O_2 [370]. Hot filtration tests revealed a significant contribution of homogeneous catalysis by leached vanadium species for

both catalysts; V/MCM-41 was less stable than V-MCM-41. Similar results were obtained for oxidation of naphthalene over V-MCM-41 and V/MCM-41 [307].

The oxidation of anthracene with TBHP in benzene as a solvent was studied using various M-MCM-41 catalysts [371]. Cr-MCM-41 (0.46 wt% Cr) revealed the best catalytic performance and produced 9,10-anthraquinone (AQ) with *ca*. 98% selectivity at 79% conversion after 20 h at 80 °C.



Benzene was quite inert under these conditions. The yields of AQ were nearly constant during four reuses, and hot filtration tests proved the heterogeneous nature of catalysis [371]. A 90% yield of AQ was reported for the anthracene oxidation with TBHP over Ti-HMS (Si/Ti = 30) [372].

The catalytic oxidation of 2-methylnaphthalene (MN) to 2-methyl-1,4-naphthoquinone (MNQ, menadione or vitamin K_3) with environmentally benign oxidants is a demanding task as MNQ is currently produced in industry *via* the stoichiometric oxidation of MN by carcinogenic chromium(VI) oxide. The selectivity to MNQ as high as 90% at 66% substrate conversion was claimed for the MN oxidation with H_2O_2 over Ti-MCM-41 [373]. The major byproducts were 1-hydroxy-2-methyl naphthalene and 1,4-dihydroxy-2-methyl naphthalene. Surprisingly, 6-MNQ was not found among the oxidation products.

Oxidation of side chain in alkylaromatics. In contrast to microporous TS-1 and TS-2, which produce mostly *o*- and *p*-cresols in the oxidation of toluene, oxyfunctionalization of the side chain predominates over aromatic ring hydroxylation in the case of mesoporous titanium silicates [93]. The difference in the catalytic performance of V-MCM-41 and VS-2 is not so dramatic: the oxidation of toluene in MeCN over both catalysts produces benzaldehyde along with *o*- and *p*-cresols as the major products [213]. VO_x/MCM-48 prepared by grafting vanadium onto the partially silylated surface showed 12% conversion of toluene to benzaldehyde with TBHP as oxidant and demonstrated enhanced stability to V leaching as compared to its nonsilylated analog [306]. Fe/SBA-15 catalyzed oxidation of toluene with H_2O_2 in acetonitrile to a mixture of benzaldehyde and *o*- and *p*-cresols [114]. Very little change in TOF (turnover frequency) was found on increasing the iron coverage in the range of 0.05–0.24 Fe/nm^2, consistent with the presence of isolated Fe^{III} sites over this range of loadings. The heterogeneous nature of catalysis was demonstrated convincingly, but some decrease of the activity was observed in the second reuse.

Ti-containing HMS and MCM-41 catalyzed the oxidation of 4-*tert*-butyltoluene to 4-*tert*-butylbenzaldehyde using TBHP or H_2O_2 in acetonitrile [374]. Maximal 22–24% conversions of the substrate with >99% selectivity were achieved over catalysts containing an optimal amount of Ti (4.8%) using nonaqueous TBHP.

Substantially lower conversions were obtained with aqueous H_2O_2 due to clusterization of Ti^{IV} centers under reaction conditions and enhanced dismutation of H_2O_2. Grafted Ti/HMS was more active than Ti-HMS prepared by direct synthesis, suggesting that postsynthesis ensures optimal access to Ti sites at the silica surface [374]. However, the higher activity of the grafted catalyst could also be due to better Ti dispersion in the Ti/HMS, which was indicated by the position of the DRS UV-vis band (215–225 nm for Ti/HMS vs. 236 nm for Ti-HMS).

Cr-MCM-41 washed with 1 M ammonium acetate catalyzed a number of benzylic oxidations using a two-fold excess of 50% H_2O_2 [236]. Ethylbenzene (EB) and tetraline produced acetophenone and tetralone, respectively, with *ca.* 100% selectivity at 85–87% conversion. The oxidation of diphenylmethane gave exclusively benzophenone at 54% conversion, while toluene yielded solely benzaldehyde at 28% conversion. Only 3–6% conversion of EB was found in the filtrate after removal of the catalyst, implying that the contribution of homogeneous catalysis to the overall activity is minor. ICP–AES analysis of the filtrates detected no chromium.

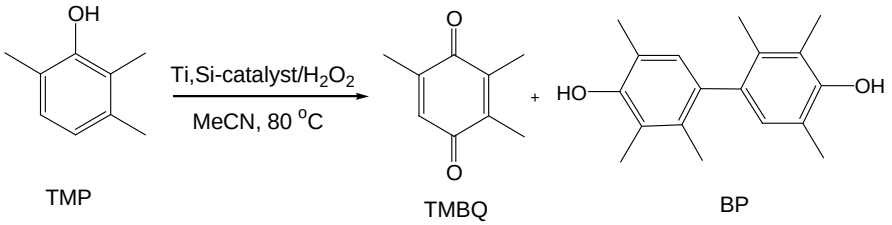
4.3.2.2 Phenols and Naphthols The selective oxidation of phenols plays a central role in organic synthesis and many biological systems. Various metal-containing mesoporous silicates were tested in the hydroxylation of phenol with H_2O_2 [180, 195, 206, 208, 282]. V-HMS produced 58% of catechol (CAT) and 42% of hydroquinone (HQ) at 13% phenol conversion in water solvent [208]. With Sn-MCM-41, CAT was the major product formed along with HQ and *p*-benzoquinone [195]. Over mesoporous titanium silicates, phenol conversions and oxidant efficiencies were lower than with TS-1. Meanwhile, the results comparable with TS-1 (phenol conversion 26%, CAT 51% and HQ 47.8%, H_2O_2 efficiency 80%) were achieved using micro/mesoporous MTS-9 prepared from TS-1 preformed clusters [35, 180]. Attempts at using Fe- and Cu-containing mesoporous molecular sieves in the H_2O_2-based phenol hydroxylation and oxidation of bulky phenols were reported [280, 281, 375]; however, few authors addressed the stability issue.

MCM-41 and HMS materials substituted with Ti-, Zr-, Ce-, Sn- and V-catalyzed oxidation of 1-naphthol with H_2O_2 (or TBHP) to produce 1,4-naphthoquinone [195, 200, 205, 208], but again the nature of catalysis was not always clear. TS-1-coated mesoporous cellular foams (TS-1/MCF) revealed a higher activity than TS-1 and Ti-MCF alone in this reaction [376]. An additional activity enhancement was induced by silylation with HMDS. No Ti leaching was observed for silylated TS-1/MCF.

The oxidation of alkylated phenols was one of the first reactions accomplished using mesoporous titanium silicate catalysts. Pinnavaia's group [129, 130] first reported the oxidation of 2,6-di-*tert*-butylphenol (DTBP) to a mixture of *p*-benzoquinone (*p*-BQ) and diphenoquinone (DPQ) with aqueous H_2O_2 over Ti-HMS and Ti-MCM-41. Catalysts prepared by grafting metal precursors on to the surface of MCM-41, KIT-1, MCM-48 or HMS [304, 318, 319], Ti-MMS [178], and Zr-HMS [185] were also active in the H_2O_2-based oxidation of DTBP. Metal leaching was detected for all grafted HMS catalysts: V/HMS (22 wt%) $\gg$ Zr/HMS

(3 wt%) > Ti/HMS (2 wt%). A significant contribution of homogeneous catalysis was established for V/HMS and Zr/HMS [319]. Leaching of V was found for directly synthesized V-HMS in DTBP oxidation with both H_2O_2 and TBHP [208].

Two groups independently discovered the oxidation of 2,3,6-trimethylphenol (TMP) to trimethyl-*p*-benzoquinone (TMBQ, vitamin E key intermediate) with H_2O_2 as oxidant and a mesoporous titanium silicate as catalyst [377–379].



The yields of TMBQ attained 77–82%; the major byproduct was 2,2′,3,3′,5,5′-hexamethyl-4,4′-biphenol (BP). When Ti^{IV} was replaced by V^{V} or TBHP was used instead of H_2O_2, the yield of TMBQ was significantly lower [378]. In contrast to Ti-MMM, a substantial leaching of vanadium and contribution of homogeneous catalysis to the overall oxidation process were observed for V-MMM (Figure 4.7).

Surprisingly, TiO_2–SiO_2 aerogels appeared to be very selective catalysts for the TMP oxidation with H_2O_2: TMBQ yield attained 95–98% for samples containing

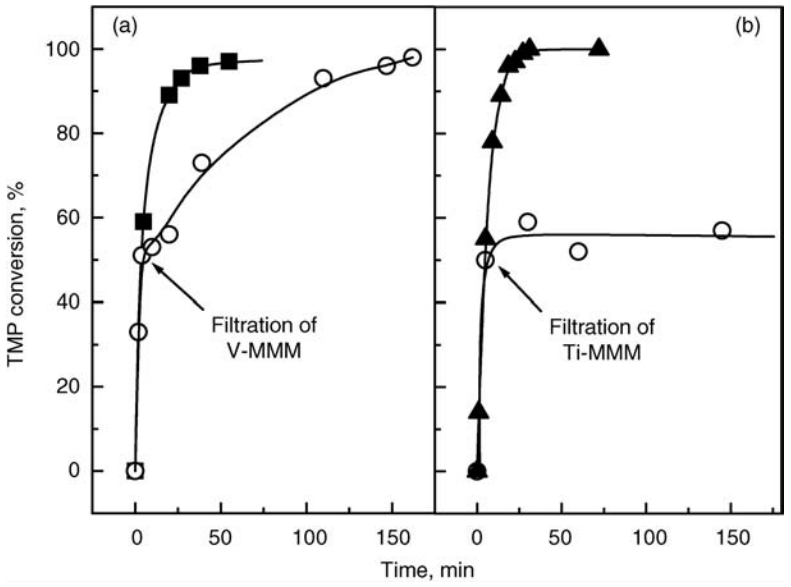


FIGURE 4.7 Hot filtration test for TMP oxidation with (a) TBHP over V-MMM and (b) H_2O_2 over Ti-MMM. Reproduced from ref. [378] with permission of Elsevier, copyright 2001.

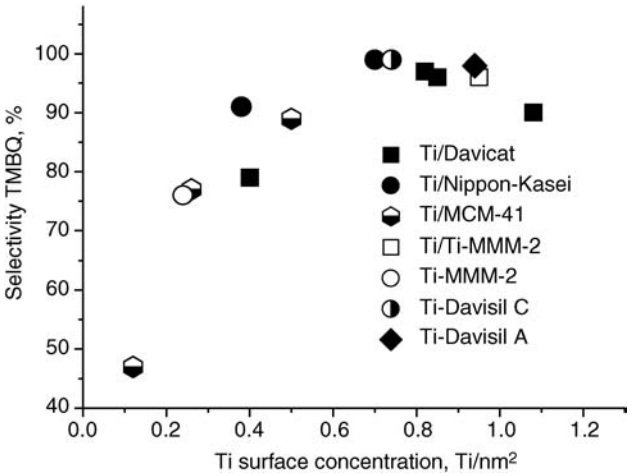


FIGURE 4.8 TMBQ selectivity *versus* Ti surface concentration for silica-grafted Ti catalysts [313]. Reaction conditions TMP 0.1 M, H_2O_2 0.35 M, Ti 0.006 mmol, CH_3CN 1 mL, 80 °C.

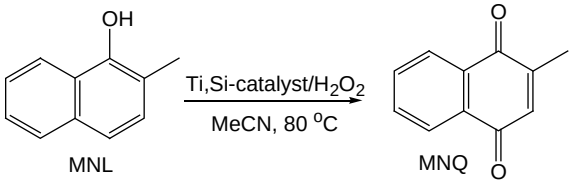
4–7 wt% Ti [83, 84]. Selectivities in TMBQ up to 98% were reported for TiO_2 nanoparticles monodispersed on SBA-15 [314]. Finally, a nearly quantitative yield of TMBQ was achieved using Ti(IV) grafted on commercial mesoporous silicas [313, 380]. No titanium leaching was detected, and catalysis was true heterogeneous.

Kholdeeva et al. [381] deduced the factors that lead to high yields of TMBQ: use of MeCN as solvent, elevated temperature (80 °C), low phenol concentration (0.1 M), high H_2O_2/substrate molar ratio (*ca.* 3.5 vs. 2.0 required by stoichiometry), and low phenol/Ti ratio (10–20). While a hydrophilic surface is not favorable for the oxidation of nonpolar substrates, oppositely, it shows advantages in the oxidative transformations of phenols. Indeed, surface silylation led to reduction of both TMP conversion and selectivity to TMBQ [381]. A similar deterioration effect was produced by the use of concentrated H_2O_2 in this reaction [378]. A correlation between TMBQ selectivity and Ti surface concentration has been hypothesized [381]. The existence of such correlation was confirmed using a series of grafted Ti catalysts (Figure 4.8) [313].

Mesoporous silicas with Ti surface concentration in the range of 0.7–1.0 Ti/nm^2 were identified as optimal catalysts for the selective transformation of alkylphenols to *p*-benzoquinones [313, 381]. Catalysts with Ti coverage <0.6 Ti/nm^2 (isolated Ti sites) produced a mixture of TMBQ and BP. Conversely, when di-/tetranuclear titanium precursors were used in the synthesis, a reduction of the general Ti surface concentration had no influence on TMBQ selectivity, which remained as high as 96–99%. It was concluded that the key point to achieve the high selectivity is the presence of Ti dimers or subnanometer-size clusters homogeneously distributed within silica mesopores. Such species show characteristic broad DRS UV bands centered around 240–270 nm (see Figure 4.6). The absence of anatase-like

microcrystallites in the catalyst is crucial for the selectivity and should be checked carefully by the Raman technique [104]. Although the nature of mesoporous silica has little effect on the catalytic performance, mesoporosity itself is crucial: with Ti grafted onto nonporous Aerosil, TMBQ selectivity was only 47% in spite of the optimal density of Ti centers (0.85 Ti/nm^2) [381]. While microporous TS-1 showed very little activity in the TMP oxidation (only 7% conversion and 4% TMBQ yield [156]), a large increase in mesopore diameter from 2.6 nm (Ti/MCM-41) to 15.4 nm (Ti/SiO_2 Davicat) produced no effect on the reaction rate, indicating that diffusion limitations do not play a primary role in the oxidation of TMP over catalysts with mesopores larger than 2.6 nm.

The oxidation of 2-methylnaphthol (MNL) to MNQ was accomplished using 30% H_2O_2 and Ti-MMM-2 catalyst [163, 382].



The yield of the target quinone achieved 78%, which is significantly higher than the yields obtained starting from 2-methylnaphthalene [382]. The main byproducts were C–C coupling dimers, dinaphthol and dinaphthoquinone [383]. The catalyst could be reused several times without loss of the activity. Ti-SBA-15 [172] and Nb_2O_5–SiO_2 mixed oxides [384] were also applied as catalysts for this reaction.

The oxidation of 2-allylphenol and phenols bearing alcohol functional groups over Ti-MMM-2 produced *p*-BQ with good to moderate yields keeping the other oxidizable sites intact [385]. For example, 2-hydroxybenzyl alcohol, which could be alternatively converted to salicylaldehyde, gave 2-hydroxymethyl-*p*-BQ in a 74% yield.

4.3.3 Oxidation of Olefins

4.3.3.1 Epoxidation Epoxides are key intermediates in the manufacture of a wide variety of valuable products. The Shell TiO_2-on-SiO_2 catalyst forms the basis of the commercial POSM process for propylene epoxidation with ethylbenzene hydroperoxide (EBHP) [288–291, 386, 387]. Using this catalyst, in fixed-bed operation, propylene oxide (PO) is obtained in more than 95% selectivity based on EBHP at 96% conversion of the oxidant (for more details see Chapter 10).

The Shell catalyst is rapidly deactivated by water, which renders it unsuitable for oxidations with H_2O_2. This limitation has been overcome by the creation of hydrophobic TS-1. However, small pores of TS-1 allow efficient transformations of linier alkenes but not of cyclic and branched olefins [91]. In 1994, Corma et al. [168] applied Ti-MCM-41 for epoxidation of alkenes. Its activity to epoxidize small linear molecules with H_2O_2 was lower than the activity of TS-1 (9% *vs.* 49% conversion of hexene-1) [169]. Conversely, the advantage of Ti-MCM-41 was

TABLE 4.5 Catalytic Performance of Ti,Si-Catalysts in Propene Epoxidation with Alkylhydroperoxides

Catalyst	Method	Oxidant	Reaction time (h)	Oxidant conversion (%)	PO selectivity (%)	Ref.
TS-1		EBHP	1.0	32.2	75.6	[389]
Ti-MCM-41[a]	Direct synth.	EBHP	0.5	99.2	89.2	[389]
Ti/SiO_2 [a]	Impregnation	EBHP	1.0	94.9	89.2	[389]
Ti/MCM-41[b]	CVD (800)[c]	EBHP		96.9	97.3	[295]
Ti/MCM-41[b]	CVD (800)[c]	TBHP		98.0	91.8	[295]
Ti/SiO_2 [d]	CVD (900)[c]	TBHP	1.0	98.0	96.3	[297]
Ti/SBA-15[e]	CVD (700)[c]	CHP[f]		87.3	96.4	[296]

[a]Silylated using HMDS.
[b]1.8 wt% Ti.
[c]Optimal CVD temperature.
[d]1.07 wt% Ti.
[e]4.6 wt% Ti.
[f]Cumyl hydroperoxide.

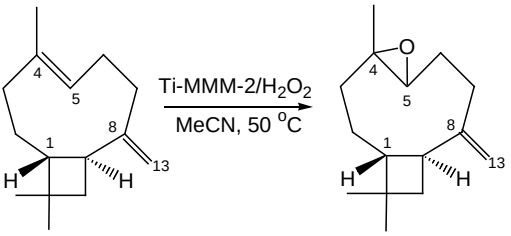
manifested by its ability to epoxidize large molecules, e.g., α-terpineol and norbornene, as well as to use organic hydroperoxides as oxidants. Likewise, mesoporous titanium silicates were almost inactive compared to TS-1 in the epoxidation of propene with aqueous H_2O_2 [388] but demonstrated superior activity with bulky alkylhydroperoxides [295–297, 389]. The data on the propene epoxidation with alkylhydroperoxides are summarized in Table 4.5.

It was reported that a new "PO-only" Sumitomo process (see Chapter 10) employs a mesoporous catalyst obtained by grafting titanium onto silica [387]; no other information about this catalyst is available in the literature.

Numerous studies demonstrated that mesoporous titanium silicates are more active catalysts than TS-1 in the oxidation of cyclic alkenes with H_2O_2 [28, 124, 136, 156, 176, 178, 301, 331, 390–392]. For substrates containing reactive H atoms in the allylic position (cyclohexene, cyclopentene, α-pinene, limonene, etc.) the epoxide selectivity is usually poor. However, a controlled drop-wise addition of H_2O_2 allows excellent selectivity (>98%) and fairly good yields (44–63%) of cyclohexene epoxide to be obtained [303, 393]. The slow addition of H_2O_2 is crucial to avoid, or at least minimize, unproductive decomposition of the oxidant and to keep the local concentration of water as low as possible. The formation of allylic oxidation products (2-cyclohexene-1-ol and 2-cyclohexene-1-one) and hydrolysis of epoxide to diol are thus suppressed.

On the other hand, H_2O_2 can be a suitable oxidant for epoxidation of cyclic alkenes that are not prone to allylic oxidation. The oxidation of cyclododecene (*cis*/*trans* = 75/25) over Ti-MCM-48 produced selectively cyclododecene oxide (*cis*/*trans* = 58/42) with higher turnovers than Ti-MCM-41, which was attributed to

the three-dimensional structure of Ti-MCM-48 [136, 331]. (–)-Caryophyllene, a component of glove oil, was oxidized with H_2O_2 over Ti-MMM [176] and Ti-MMM-2 [156] to give 4,5-monoepoxide with 70–80% selectivity.



With TS-1, negligible conversion of this substrate was observed. Ti-MMM-2 showed stable catalytic performance for, at least, several reuses [156].

Irrespective of the alkene nature, high epoxide yields are reached over mesoporous titanium silicates using alkylhydroperoxides as oxidants [169, 174, 179, 292–294, 392]. (*R*)-limonene and α-pinene produced epoxides with 97 and 91% yields and 93 and 96% hydroperoxide efficiencies, respectively [293]. With both TBHP and CHP, no leaching of titanium and very little change of catalytic activity was observed after four successive reaction cycles. Grafted Ti/MCM-41 demonstrated high selectivity in epoxidation of cyclohexene and pinene with TBHP [50]. When the TOF values were compared with Ti-MCM-41 [50] or Ti-TUD-1 [143, 174], the activities were similar. The Ti/MCM-41 catalyst was deactivated after 90 min, but it could be regenerated by calcination. Nearly quantitative yield of cyclohexene epoxide was obtained in 2 h at 80 °C in MeCN using CHP and Ti/SBA-15 prepared by CVD [294]. The reaction performed in the absence of any solvent and at a substrate to oxidant molar ratio of 100/11 led to an epoxide yield $> 90\%$.

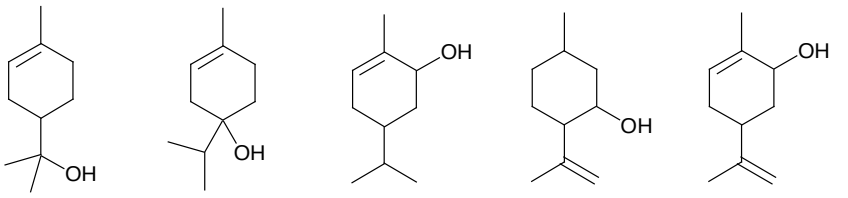
The potential of mixed TiO_2–SiO_2 oxides as catalysts for alkene epoxidation has been studied intensively [8, 11, 12, 71, 73, 74, 76, 78, 79, 87, 340]. The rate of cyclohexene epoxidation with CHP increased monotonically with increasing Ti content in TiO_2–SiO_2 aerogels until it reached *ca.* 20 wt% TiO_2 [73]. The catalyst with 20 wt% TiO_2 allowed epoxidation of a variety of cyclic alkenes with 87–100% selectivity and 79–92% oxidant efficiency. A comparison of the catalytic performance of TiO_2–SiO_2 aerogels with other titanium silicate catalysts can be found in the review of Baiker and coworkers [76]. In general, the catalytic behavior of mixed oxides resembles that of the Shell catalyst. The advantage of aerogels is the possibility of the higher titanium loading with good Ti dispersion, which may ensure higher catalyst productivity.

A few studies demonstrated that the catalytic performances of ordered titanium silicates are often fully comparable to those of Ti-containing amorphous silicas, provided the pore size is large enough to ensure diffusion of the reactants and titanium active sites are evenly dispersed and accessible [283, 312, 394]. A similar conclusion was made for Nb-containing silicates [111].

Epoxidation of functionalized alkenes. An overview of the literature up to 2000 on the epoxidation of functionalized olefines can be found in ref. [395]. The

selectivity of the epoxidation of unsaturated alcohols with TBHP in the presence of TiO_2–SiO_2 aerogel could be substantially improved by the catalyst modification with amine and 3-acetoxypropyl groups or by adding a base into the reaction mixture to neutralize acid sites that cause ring opening of acid-sensitive epoxides [79, 337, 339].

Unsaturated alcoholic terpenes, α-terpineol, terpinen-4-ol, carvotanacetol, isopulegol, and carveol, were epoxidized with TBHP over both ordered and nonordered Ti-containing mesoporous silica catalysts [311, 396]. High conversions (up to 90%) and good selectivity to epoxides (60–80%) were achieved in polar aprotic solvents (acetonitrile, ethyl acetate) under reflux conditions.



α-terpineol terpinen-4-ol carvotanacetol isopulegol carveol

A complete diastereoselective epoxidation (100% *d.e.*) was obtained on homoallylic and bishomoallylic substrates, α-terpineol and terpinen-4-ol, respectively, due to the role of the OH-function in directing the oxygen transfer from the oxidant to one specific side of the six-membered ring of the substrate. When OH-group in α-terpineol was replaced by acetyl moiety (α-terpinylacetate), *d.e.* decreased from 100% down to 66% [311]. The rate of α-terpineol epoxidation was *ca.* 10 times higher over grafted Ti/MCM-41 than over in-framework Ti-MCM-41, which was attributed to a better accessibility of Ti centers in the former catalyst [396]. However, another reason for the higher activity could be a better dispersion of Ti in the Ti/MCM-41 sample.

Grafted Ti-containing silicas showed promising results in the TBHP-based epoxidation of C_{18} unsaturated fatty acid methyl esters (FAMEs) and their mixtures obtained from high-oleic sunflower, castor, coriander, and soy-bean oils [397, 398]. Epoxidation proceeds stereoselectively: only *cis*-epoxide was obtained from (*Z*)-isomer (methyl oleate) and *trans*-epoxide from (*E*)-isomer (methyl elaidate). In the presence of nonporous Ti/SiO_2, (*Z*)-isomer reacted four times faster than (*E*)-isomer but the difference in the epoxidation rates decreased over mesoporous Ti/SiO_2 and especially Ti/MCM-41, suggesting that (*E*)-isomer could fit inside the channels of Ti-MCM-41 more easily than (*Z*)-isomer. High yields (95–96%) of epoxidized methyl linoleate and castor oil methyl ester were achieved with a relatively small excess (10 mol.%) of TBHP over Ti-MCM-41 [399]. Recent studies demonstrated a comparable behavior of Ti/MCM-41, Ti/MCM-48 and Ti/SiO_2, in terms of conversion and selectivity, in epoxidation of methyl oleate with H_2O_2, notwithstanding the morphology and textural properties of the silica support [400]. A slow addition of H_2O_2 under optimal

TABLE 4.6 Effects of Surface Hydrophobization on the Epoxidation of Cyclohexene

Catalyst	Oxidant	Cyclohexene conversion (%)	Epoxide selectivity[a] (%)	Ref.
TiO_2–SiO_2 aerogel	TBHP	18	80	[338]
Hydrophobic TiO_2–SiO_2[b]	TBHP	33	94	[338]
Ti-MCM-41	TBHP	63	91	[332]
Hydrophobic Ti-MCM-41[c]	TBHP	87	99	[332]
Ti-MCM-41	H_2O_2	0.7	0	[331]
Hydrophobic Ti-MCM-41[d]	H_2O_2	13	14	[331]
Ti-SBA-15	TBHP	1.9	84	[309]
Hydrophobic Ti-SBA-15[c]	TBHP	21	97	[309]

[a]Based on substrate.
[b]Modified with Ph groups during sol-gel synthesis.
[c]Silylated using HMDS.
[d]Silylated using $(CH_3)_3SiCl$.

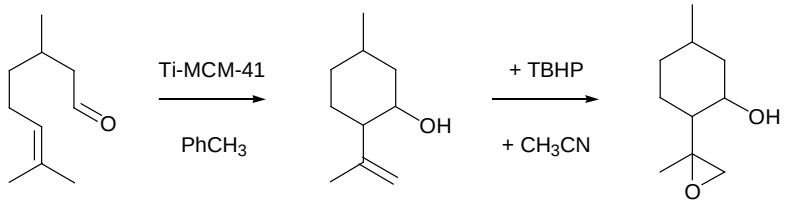
reaction conditions led to 91% epoxide yield with a high stereoselectivity (80%) towards *cis*-epoxide.

Effect of surface hydrophobization. Surface hydrophobization can improve significantly the catalytic performance of titanium silicates in alkene epoxidation. Some examples for oxidation of cyclohexene are given in Table 4.6.

Silylated Ti-TUD-1 was significantly more selective in epoxidation of 1-octene with CHP than unsilylated one [335]. Moreover, it was quite active even with electron-poor olefins, e.g., *p-tert*-butylphenylallyl ether gave epoxide with 87% selectivity. Organically modified Ti-SBA-15 revealed a correlation between the catalytic activity in epoxidation of 1-octene with TBHP and the length of the alkyl chain [343]. An improved efficiency in the use of the oxidant was observed, and reutilization tests indicated the high stability of the catalysts. Mesoporous hybrid titania–silica xerogels prepared by the nonhydrolytic sol-gel route showed practically complete conversion (>98%) of cyclohexene to its epoxide after only 30 min at 90 °C with CHP as oxidant [340]. The high activity was explained by a large amount of incorporated hydrophobic methyl groups (6 CH_3 for 10 Si atoms). Hot filtration test proved the true heterogeneous nature of catalysis. Incorporation of Ti-MCM-41 in a hydrophobic polydimethylsiloxane membrane enabled the oxidation of *cis*-cyclooctene by TBHP with high conversion (72% vs. 14% for the parent Ti-MCM-41), epoxide selectivity (75%), and oxidant efficiency (95%) under solvent-free reaction conditions [401]. Organic–inorganic hybrid polyvinylsiloxane Ti-HPVS-1 showed superior catalytic activity and selectivity in the epoxidation of R-(–)-carvone with H_2O_2: after 10 h, the epoxide yield was 49% *vs.* 28% for Ti-MCM-41 [346]. Ethane-bridged hybrid Ti-HMM gave α-pinene epoxide with more than 99% selectivity at 23% substrate conversion and displayed up to 50% hydrogen peroxide efficiency [350]. After removal of the catalyst by hot filtration, the reaction stopped completely.

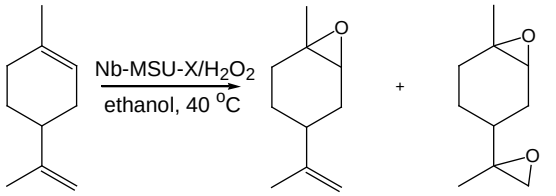
While surface hydrophobization normally has a positive effect on the oxidation of nonpolar or low polar molecules, a hydrophilic environment may offer advantages for substrates with intermediate polarity and bearing functional groups that are able to interact with the catalyst surface. Thus, silylated Ti-MCM-41 was more active in epoxidation of limonene, but epoxidation of α-terpineol occurred more readily over nonsilylated Ti-MCM-41 [402]. In the epoxidation of methyl linoleate, the interaction of the already formed epoxides with the hydrophilic catalyst surface favored the transformation of methyl epoxyoleate into methyl diepoxystearate. A correlation between the surface density of silanols and the selectivity to diepoxides was found in the epoxidation of the soy-bean oil FAME mixture [397].

Grafting of Ti(IV) species onto mesoporous silica can give rise to a bifunctional acid and oxidation catalyst. Isopulegol epoxide (a compound with fungicidal and insect-repellent activity) was synthesized over Ti/MCM-41 under one-pot two-step conditions with a 68% yield [403].



citronellal isopulegol isopulegol epoxide

A few highly selective and true heterogeneous epoxidations were reported for mesoporous silicates containing metals other than titanium [232, 254, 273, 325, 404]. Niobium-containing MSU-X efficiently catalyzed the selective oxidation of several terpenes and terpenoids (geraniol, limonene, α-terpineol) with 1 equiv. of H_2O_2 [232]. In the oxidation of limonene, the selectivity for 1,2-epoxide was *ca.* 100% at the beginning of the reaction but then dropped to 70% due to the formation of diepoxide.



limonene 1,2-epoxylimonene diepoxide

The oxidation was not stereoselective and gave a nearly 1:1 mixture of *cis*- and *trans*-limonene oxides. No allylic oxidation products, carveol and carvone, formed, indicating heterolytic oxidation mechanism. The oxidation of geraniol produced 6,7-epoxygeraniol (98%) and practically no 2,3-epoxygeraniol and 2,3:6,7-diepoxygeraniol, thus discriminating the role of the OH group in the

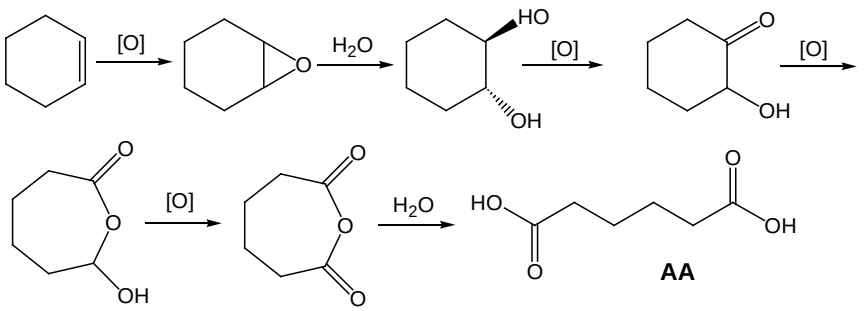
epoxidation reaction. Interestingly, epoxidation of the 2,3 double bond was reported for oxidation of geraniol with H_2O_2 over Nb_2O_5–SiO_2 [110] and WO_3–SiO_2 [112] mixed oxides.

In the epoxidation of cycloocta-1,5-diene with 50% H_2O_2, W-MCF revealed a greater selectivity to monoepoxide (93–96%) and TOF values compared with W-containing SBA-15 and MCM-41, demonstrating advantages of the ultralarge pores and the unique 3D cell-window structure of the MCF materials [254]. No appreciable loss of the activity and selectivity was observed for five reuses, and no tungsten was determined in the filtrate. The H_2O_2 utility was close to 50% for both the fresh and recycled 10%WO_3-MCF. The activity of this catalyst was several times higher than that of 10%WO_3/MCF prepared by impregnation.

Silica-grafted calixarene–Ta(V) complexes catalyzed cyclohexene and cyclooctene oxidation with H_2O_2 in acetonitrile [325]. The selectivity to cyclohexene epoxide and diol achieved 90–95% at 10% substrate conversion. The catalysts revealed TOF values of 2.3 min^{-1}, unaffected by surface density until 0.25 Ta/nm^2, demonstrating the single-site character of the active centers. Even higher activity was found for grafted Ta/SBA-15 catalysts prepared by thermolytic molecular precursor method, while tantala–silica mixed oxides appeared to be less active [113].

Co-TUD-1 showed high conversion (92% after 10 h) and selectivity (91%) toward *trans*-stilbene oxide in the oxidation of *trans*-stilbene with molecular oxygen (1 atm) in dimethylformamide [404]. The conversion and selectivity were similar for fresh and recycled catalyst. A microwave-assisted reaction reduced the reaction time from 10 to 2 h, keeping high selectivity. The catalytic activity of Mn-TUD-1 in epoxidation of styrene or *trans*-stilbene with TBHP strongly depended on the fraction of isolated Mn^{3+} sites in the framework [273]. With acetonitrile as solvent, Mn-TUD-1 (Si/Mn = 100) produced epoxides with 61–66% selectivity at 54–77% conversion and TOF 555–880 min^{-1}. Benzaldehyde was the main byproduct. The Mn-TUD-1 catalyst was significantly more active than Mn-MCM-41 [270] or Mn-SBA-15 [167] and revealed high stability toward manganese leaching.

4.3.3.2 Oxidative Cleavage The catalytic systems for the direct oxidation of cyclohexene to AA have been recently reviewed [356].



Bonardet and coworkers [405] found that introduction of Al^{III} into SBA-15 by direct synthesis or postsynthesis with subsequent Ti deposition enables deep cyclohexene oxidation to AA in a 80% yield at 100% substrate conversion using TBHP as oxidant and MeCN as solvent. The major byproducts were *trans*-1,2-cyclohexandiol, 2-hydroxycyclohexanone, glutaric and succinic acids. The diol was identified as a long-lived intermediate product. In the absence of Al^{III}, practically no AA formed. Recycling and reuse of the catalysts showed no loss of activity, and the absence of metal leaching was confirmed by elemental analysis.

The catalytic properties of Ti-MMM-2 and Ce-SBA-15 were explored in the oxidative cleavage of cyclohexene with aqueous H_2O_2 under solvent-free conditions [406]. The yield of AA was 10–15%, but stepwise addition of the oxidant allowed it to be increased to 33 and 18% for Ti-MMM-2 and Ce-SBA-15, respectively. The AA yield acquired over Ti-MMM-2 was close to that reported for TAPO-5 [407]. The activity of both Ti-MMM-2 and Ce-SBA-15 decreased in the second run. W-SBA-15 washed with 1 M aqueous ammonium acetate to remove loosely bound tungsten species (the remaining amount of W was just 0.058 wt%) oxidized effectively cyclohexene with 30% H_2O_2 to produce AA in a 30% yield under solvent-free conditions [408]. The recycled catalyst revealed some drop of activity (TOF 354 h^{-1} vs. 404 h^{-1}) but the final yield of AA was even higher (46% after 30 h). The structure of W-SBA-15 was completely preserved after multiple reuses. No tungsten was found in the filtrate. A short summary on the cyclohexene oxidations to AA is given in Table 4.7.

The oxidation of cyclopentene with 50% H_2O_2 in *tert*-butanol over tungsten-containing MCM-41 [249], MCM-48 [251], and HMS [252] produced glutaraldehyde (GA) with 67–76% yields and oxidant efficiencies 60–77%. Trace amounts of leached W species ($<$ 1 ppm) had almost no contribution into the reaction [251]. Surprisingly, very little input of homogeneous catalysis was found for WO_3/SBA-15 (Si/W =40) prepared by IWI using $WO_3 \cdot H_2O$, dissolved in an aqueous solution of oxalic acid [409]. Over this catalyst, 85% yield of GA was obtained (81% in the second run). The highest yield of GA (91%) was acquired using anhydrous H_2O_2-tributyl phosphate system and W-SBA-15 [253]. Tungsten leaching was below 1 ppm and the high catalytic activity was almost kept after six catalyst reuses.

TABLE 4.7 Oxidation of Cyclohexene to Adipic Acid over Metal Silicate Catalysts

Catalyst	Oxidant (equiv.)	Time (h)	T (°C)	Conversion (%)	Selectivity (%)	Ref.
Ti,Al-SBA-15	TBHP[a] (4)	48	80	100	80	[405]
Ti-MMM-2	H_2O_2 (4.2)	72	80	100	33	[406]
TiAPO-5	H_2O_2 (3.5)	72	80	100	30	[407]
Ce-SBA-15	H_2O_2 (3.6)	72	80	100	18	[406]
W-SBA-15	H_2O_2 (4.7)	13 (30)[b]	85	100	30 (46)[b]	[408]

[a]Reaction in MeCN solvent.
[b]Second reuse.

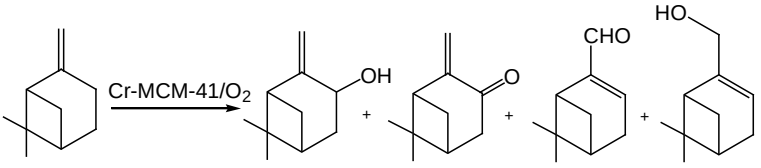
4.3.3.3 Allylic Oxidation Allylic oxyfunctionalization of cyclic olefins produces α,β-unsaturated ketones and alcohols, which are valuable intermediates for the fine chemicals industry [410, 411]. The ketonic products are often more desirable due to the presence of the carbonyl group that is very reactive toward addition reactions. Chromium catalysts are well known for the selective oxidation of cyclic alkenes to α,β-unsaturated ketones using TBHP as oxidant. Allylic oxidation of cyclohexene with 70% TBHP over Cr-MCM-41 and Cr-MCM-48 in chlorobenzene gave 2-cyclohexen-1-one as the major product [366, 412]. The activity of Cr-MCM-48 was higher compared to Cr-MCM-41. After the initial loss of nonframework chromium species in the first catalytic run, no further leaching was noted. Catalyst washing with successive portions of acidified ferrous sulfate solution resulted in the material with the amount of Cr similar to that determined in the recycled catalyst (0.76 and 0.98 wt% in MCM-41 and MCM-48, respectively). The filtrate obtained from the calcined catalyst after 2 h of the reaction showed a considerable activity (*ca.* 12–15%), indicating that homogeneous catalysis could take place owing to the presence of chromium in solution. On the other hand, the filtrate obtained from the washed catalyst revealed no chromium and showed negligible activity, suggesting the heterogeneous nature of catalysis. Cr-MCM-41 in combination with 50% H_2O_2 was found to be highly active and selective for the allylic and benzylic oxidation of alkenes to enones with *ca.* 100% selectivity at reasonable conversions (e.g., 47% for cyclohexene) [236]. Hot filtration tests demonstrated the true heterogeneous nature of catalysis for Cr-MCM-41 preliminary washed with 1 M ammonium acetate solution.

The oxidation of C5–C7 cycloolefins to α,β-unsaturated ketones was effectively fulfilled with 1 atm of dioxygen under mild (70 °C) solvent-free conditions using Cr-MCM-41 [413]. Cyclohexene was converted to cyclohexenone with 71% selectivity at 52% conversion, which is comparable with the results acquired over Cr-MCM-41 with 70% TBHP in chlorobenzene [412]. The other reaction products were cyclohexenyl hydroperoxide (14%), 2-cyclohexen-1-ol (11%) and epoxide (3%). Some gradual decrease in the conversion was observed after catalyst recycling, which was attributed to leaching of loosely bound chromium species. Elemental analysis determined loss of *ca.* 0.3–0.4 wt% of Cr in the recycled catalyst. In the subsequent reuses, leaching of chromium stopped, according to ICP–AES, and catalysis was supposed to be heterogeneous based on filtration and quenching experiments.

The allylic oxidation of terpenes, which are low cost renewable feedstock for a wide variety of flavors, fragrances, medicines and agrochemicals, has attracted great attention. Hutchings and coworkers [414] reported allylic oxidation of α-pinene with TBHP (80% in di-*tert*-butyl ether) over a commercial silica–titania cogel catalyst EP350 (containing 0.98 wt% Cr added by impregnation) to yield verbenone with 63% selectivity at 32% conversion. A complex range of byproducts were observed but none was formed with selectivity $> 2\%$. The catalyst without Cr showed results similar to the blank reaction, indicating that the observed catalytic activity was due to chromium rather than titanium. The nature of catalysis over the EP350 catalyst and the possibility of recycling were not addressed. Cr-SBA-15 was used for the oxidation of α-pinene with a 5-fold excess of TBHP in chlorobenzene as solvent [240]. A 92% substrate conversion was achieved after 24 h

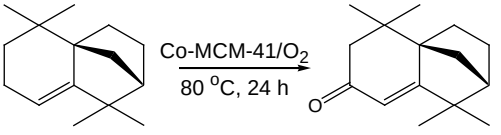
at 85 °C, and verbenone selectivity was 88%; however, leaching of chromium was substantial. The activity of the washed catalyst (Si/Cr = 12.3) was similar to that of the initial Cr-SBA-15 (Si/Cr = 9.9) observed in the third run. ICP-AES analysis confirmed that Cr leaching from Cr-SBA-15 practically stopped after the third run. A similar selectivity was reported for CrAPO-5 [410].

Gusevskaya and coworkers [415] studied the aerobic oxidation of monoterpenic alkenes over chromium silicate catalysts under mild solvent-free conditions. Various oxygenated monoterpenoids relevant for the flavor and fragrance industry were obtained with combined selectivities of 75–92% at 30–40% substrate conversions. Although several major products are formed from each substrate, their separation is often not necessary as the mixtures themselves show interesting organoleptic properties and can be used directly in fragrance compositions. Moreover, separation of the unreacted substrate from the products is often not necessary because the oils enriched in oxygenated compounds find various applications. The oxidation of β-pinene led almost exclusively to allylic mono-oxygenated derivatives with a total selectivity of 92% [415]. A silica–chromia catalyst prepared by the conventional sol-gel method showed activity comparable with that of Cr-MCM-41 but the selectivity was much lower.



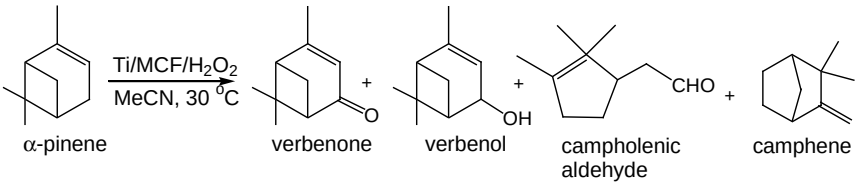
In the presence of chromium silicate catalysts, both limonene and α-pinene demonstrated a stronger preference to allylic oxidation over epoxidation [415]. To control metal leaching, Cr-MCM-41 was removed at the reaction temperature after 0.5 h and the solution was allowed to react further. Only trace amounts of products were detected in the filtrate, suggesting the heterogeneous nature of catalysis, at least, at the initial stage of the reaction. The catalyst could be easily recovered and reused (TON = 222 after three cycles) without no need for a special regeneration.

An efficient process for the aerobic oxidation of isolongifolene, one of the most available sesquiterpenes, has been developed using Co-MCM-41 [416]. Under mild solvent-free conditions, isolongifolen-9-one, a compound that occupies a vintage place in the modern perfume industry, was produced with 81% yield.



A hot filtration test performed after 2 h indicated the true heterogeneous nature of catalysis. The catalyst was reused without loss of activity and selectivity.

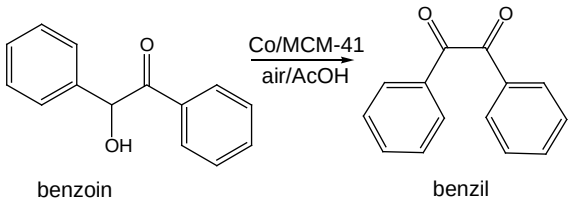
Catalytic properties of various silica materials containing Ti^{IV}, Zr^{IV} and Fe^{III} were assessed in the allylic oxidation of α-pinene with 30% H_2O_2 [301]. The activity decreased in the order Ti/MCF > Ti-MMM-2 > Zr/MCF > TiO_2–SiO_2 > Fe-MMM-2. The major oxidation products were verbenol, verbenone and campholenic aldehyde. The product of α-pinene rearrangement, camphene, was also identified.



Under optimized conditions (MeCN, 30 °C) the selectivity to verbenol/verbenone reached the maximal value of 80–82% at 8–15% conversion and then decreased due to overoxidation/polymerization processes. The oxidation was a true heterogeneous process, as verified by hot filtration tests. Some loss of activity was observed for Ti/MCF after recycling but calcination of the catalyst or its evacuation at 200 °C allowed the catalytic properties to be completely restored, indicating reversibility of the deactivation process.

4.3.4 Oxidation of Alcohols

Analysis of the review literature shows that oxidations of alcohols over mesoporous metal silicate catalysts are relatively scarce [21, 23, 36, 37, 208, 417]. The oxidation of cyclododecanol with both H_2O_2 and TBHP over V-HMS produced cyclododecanone with 92–94% selectivity; however, V leaching was significant [208]. Benzyl alcohol was oxidized by H_2O_2 at a 5.6-fold excess of the substrate to give benzaldehyde with *ca.* 100% selectivity using Fe/SBA-15 [114]. Tin-modified MCM-48 catalyzed oxidation of benzyl alcohol to benzaldehyde with 70% TBHP [418]. Samples with lower tin loadings were more active, most likely, owing to higher dispersion of Sn species. At a substrate to oxidant ratio of 2:1, the selectivity to benzaldehyde reached 93% at 59% substrate conversion over catalysts with Si/Sn = 60. FT-IR study of pyridine adsorption/desorption revealed a correlation between the catalytic activity and the strong Lewis acidity generated by the presence of tin. The activity of the reused samples was maintained within 5–10% after two cycles. The oxidation of benzoin in acetic acid using air as oxidant and Co/MCM-41 as catalyst produced nearly 81% yield of benzil [419].

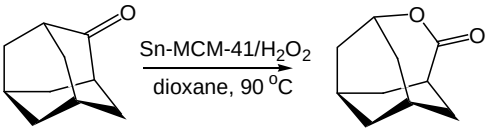


The catalyst demonstrated a good recyclability. Surprisingly, a hot filtration test revealed the heterogeneous nature of catalysis, which one could hardly expect for acetic acid solvent. A negligible amount of cobalt was detected in the filtrate by ICP–AES.

4.3.5 Oxidation of Ketones and Aldehydes

4.3.5.1 Baeyer–Villiger Oxidation The Baeyer–Villiger (BV) reaction is one of the most important transformations in synthetic organic chemistry [420]. Solid catalysts can be used to promote *in situ* formation of peracids from sacrificial aldehydes and molecular oxygen. Fe-MCM-41 exhibited high activity in the BV oxidation of cyclic ketones to corresponding lactones using O_2 and benzaldehyde [285]. Thus, 85% conversion of cyclohexanone to ε-caprolactone was achieved with 78% selectivity without appreciable loss in activity and selectivity for four cycles. Unlike Fe/MCM-41 prepared by TIE method, no Fe leaching was detected and a hot filtration test verified the true heterogeneous nature of catalysis. Under identical experimental conditions, the catalytic activity of Fe-MCM-48 was superior to that of Fe-MCM-41, which was attributed to the three-dimensional mesopore system of MCM-48 [421]. No iron leaching was detected for samples with Fe loadings below 1 wt%, and the catalysts showed good reusability.

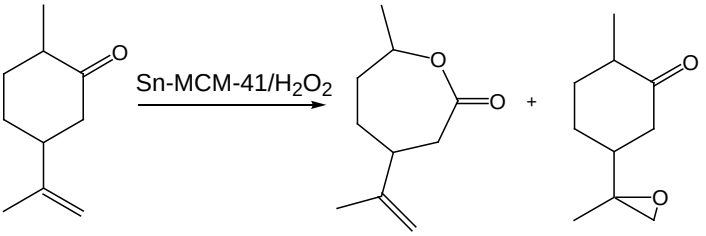
Since the use of sacrificial aldehyde leads to the formation of a carboxylic acid byproduct in a stoichiometric amount, the aldehyde/O_2 system is less attractive for industry than systems based on the use of "clean" oxidants, such as H_2O_2 that produces water as the sole byproduct. Following the success of zeolite Sn-Beta in the BV oxidations [422, 423], mesoporous catalysts Sn-MCM-41 [198] and Sn/MCM-41 [321] have been tested in BV oxidations with H_2O_2. In the oxidation of cyclohexanone, the molecule of which is small enough to penetrate into the channels of zeolite Beta, both types of mesoporous tin-containing MCM-41 were intrinsically less active than Sn-Beta. The activity of Sn-MCM-41 strongly depended on the Sn loading (TOF 23 and 13 h^{-1} for samples with 1 and 2% SnO_2). Irrespective of the metal content, the selectivity to lactone attained 94–97% [198]. The activity of Sn-SBA-15 in the BV oxidation of cyclohexanone with TBHP was comparable with that of Sn-MCM-41 and *ca.* three times lower than the activity of Sn-Beta zeolite [199]. With a more bulky substrate, adamantanone, both Sn-MCM-41 and Sn/MCM-41 showed activities comparable to that of Sn-Beta (TOF 140 and 160 h^{-1} vs. 165 h^{-1}) [322]. The oxidation of adamantanone over Sn-MCM-41 showed complete substrate conversion after 6 h in dioxane and produced lactone as the only product (>99% selectivity) with H_2O_2 efficiency of more than 90% [198].



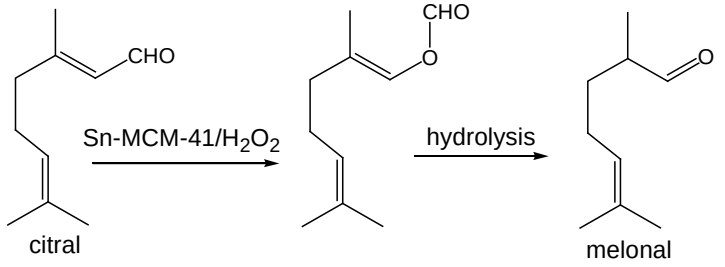
To check a possible contribution of the homogeneous reaction, Sn-MCM-41 was removed from the reaction mixture at *ca.* 70% conversion and the solution was

heated further [198]. The reaction in the filtrate did not proceed, corroborating the view that the active species was present on the catalyst surface. Furthermore, it was shown that homogeneous Sn species is about one order of magnitude less active than Sn incorporated into MCM-41. Nevertheless, some loss of activity was observed for Sn-MCM-41, most likely, due to lactone remaining adsorbed inside the catalyst pores. The catalyst activity was recovered after extraction with methanol or calcination.

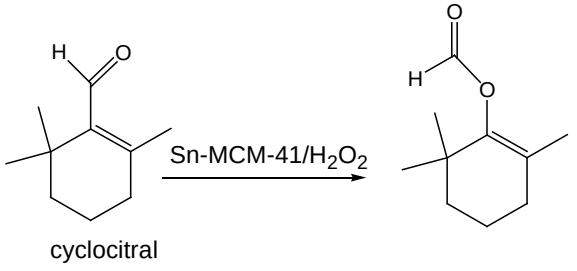
Unsaturated ketones can be oxidized with good chemoselectivity to unsaturated lactones using Sn-MCM-41 that, in contrast to peracids and Ti-containing catalysts, is practically inactive in the epoxidation reaction [198, 321]. Thus, dihydrocarvone gave 68% of lactone, just 18% of epoxide, and no epoxylactone at 22% conversion.



Citral (3,7-dimethyl-6-octen-1-al), a common compound in the fragrance industry, was oxidized chemoselectively with 50% H_2O_2 over Sn-Beta or Sn-MCM-41 as catalysts to produce, after hydrolysis, the fragrance melonal [424].



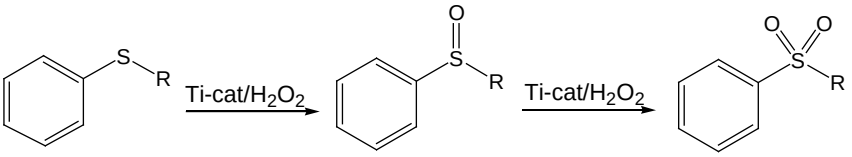
Sn-Beta was more active than Sn-MCM-41. On the contrary, with cyclocitral as substrate, Sn-Beta showed only 43% conversion and 36% selectivity while Sn-MCM-41 converted 90% of cyclocitral into the formate ester with 100% selectivity.



4.3.5.2 Ammoximation The ammoximation of ketones is very important industrially for the production of caprolactam [425] (see also Chapter 10). While hybrid mesoporous material Ti-HMM revealed a lower activity in the ammoximation of cyclohexanone with aqueous H_2O_2 relative to conventional TS-1, with more bulky cyclododecanone, its catalytic performance was superior to that of TS-1 or Ti-MCM-41 [351]. Calcination increased the activity of Ti-HMM but did not affect the selectivity. Although the ethane fragment was completely decomposed at 550 °C, the hydrophobic features remained in the structure and, coupled with large pore size, this led to the improved catalytic activity. The higher hydrophobicity of the calcined Ti-HMM compared with Ti-MCM-41 was confirmed by water adsorption measurements at 298 K [351].

4.3.6 Oxidation of S-compounds

4.3.6.1 Thioethers The oxidation of thioethers over mesoporous titanium silicates was first described by Corma et al. [426].



While zeolite Ti-Beta was more active than Ti-MCM-41 in the oxidation of methyl phenyl sulfide (MPS) with both H_2O_2 and TBHP, an opposite trend was observed for a more bulky substrate, isopentyl phenyl sulfide.

Ti-MMM was highly active in MPS oxidation with H_2O_2 at room temperature [175, 176]. The substrate conversion achieved 98–99% after 15 min, and the selectivity to sulfoxide was 76% in both MeCN and MeOH. In acetone, the molar ratio of products changed (39% sulfoxide and 58% sulfone). Likewise for TS-1 and Ti-Beta, the oxidation rate decreased in the order: MeOH > MeCN > $(CH_3)_2O$ [175]. In the range of Ti loadings 1–2.5 wt% the value of TOF was constant, indicating the uniformity of Ti active centers in the catalyst. The oxidant efficiency achieved 90%. A progressive decay of the activity occurred in the consecutive reuses because of low hydrothermal stability of Ti-MMM. Hydrothermally stable Ti-MMM-2 revealed the activity and selectivity similar to Ti-MMM but demonstrated an excellent recycling behavior [156]. The Ti-SMCMS catalyst with magnetic core and Ti-containing mesoporous shell could be separated from the reaction mixture using an external magnet [184]. A comparison of the catalytic properties of various titanium silicate catalysts in the MPS oxidation with hydrogen peroxide is given in Table 4.8.

Vanadium-containing MMM showed 98% conversion of MPS after 4 min and 82% selectivity to sulfoxide, but practically all vanadium species leached into solution [175]. With nonaqueous TBHP as oxidant, no metal leaching was detected but the reaction was much slower and the selectivity to sulfoxide was poor.

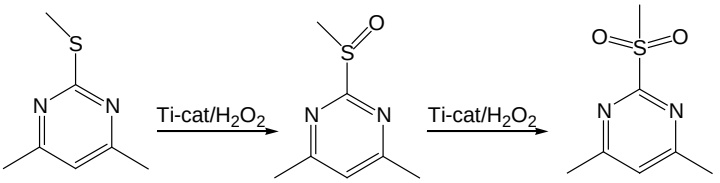
TABLE 4.8 Oxidation of Methyl Phenyl Sulfide with H_2O_2 over Titanium Silicates[a]

Catalyst (wt% Ti)	Sulfide conversion (%)	TOF[b] (h^{-1})	Sulfoxide selectivity[c] (%)	Reference
TS-1 (2.54)	29[d]	25	79	[104]
Ti-HMS (2.60)	98	60	75	[176]
Ti-MMM (1.89)	99	85	76	[156, 176]
Ti-MMM-2 (1.67)	98	100	75	[156]
Ti-SMCMS (0.6)[e]	100	100	76	[184]

[a]Reaction conditions: MPS 0.1 M, MPS/H_2O_2 = 1/1.2, catalyst 15 mg (Ti 6×10^{-3} mmol), 20 °C, MeCN 3 mL, 35 min.
[b]$TOF_{av.}$ = (moles of MPS consumed)/(moles Ti × h).
[c]GC yield based on substrate consumed, sulfone was the only byproduct.
[d]After 1 h.
[e]1 mL MeCN.

Ti-containing MCM-41 prepared by the TIE method catalyzed asymmetric oxidation of sulfides with H_2O_2 in the presence of optically active tartaric acid [427]. The chemical and optical yields of methyl 4-methylphenyl sulfoxide reached 54% and 30% *ee*, respectively, in dichloromethane at a tartaric acid/titanium ratio of 2 at 0 °C and 72 h reaction time. The enantiomeric excess gradually increased during the reaction course due to contribution of kinetic resolution in the subsequent oxidation of sulfoxide to sulfone. The titanium content in the filtrate after the reaction was below the detection limit (ppb order).

Sulfoxidation of 4,6-dimethyl-2-methylthiopyrimidine with H_2O_2 was accomplished using Ti-SBA-15 and Ti-Ge-MCM-41 (Si/Ti = 44–66) in dioxane, ethanol and ionic liquids, 1-ethyl-3-methylimidazolium tetrafluoroborate ([emim][BF4]) and triflate ([emim][OTf]) [428].

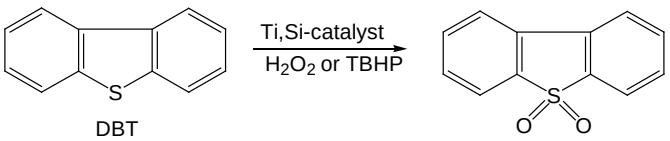


The reactions in ionic liquids showed superior selectivity of sulfoxidation (83–93% at 100% substrate conversion) compared with the molecular solvents (58–75% selectivity). A significant increase in the catalyst stability was found in the ionic liquids both in terms of recycling activity and titanium leaching. Ti-SBA-15 was notably more stable than Ti-Ge-MCM-41 [428].

4.3.6.2 Thiophenes Sulfur in transportation fuels is a major source of air pollution. Environmental regulations have been introduced in many countries to reduce the sulfur content in gasoline and diesel fuel to ultralow levels (10 ppm). Existing hydrodesulfurization (HDS) processes for reducing sulfur in fuel require severe

processing conditions to remove the last 100 ppm which are constituted mainly from bulky benzothiophenic compounds. The oxidative desulfurization (ODS) is not cost competitive with HDS, but it may be useful to remove the last ppm of sulfur until the levels fixed by environmental legislations.

Hulea et al. [429] compared the catalytic activity of TS-1, Ti-Beta and Ti-HMS in the oxidation of thiophene derivatives with hydrogen peroxide. While TS-1 was inactive in the oxidation of bulky polyaromatic compounds like benzothiophene (BT) and dibenzothiophene (DBT) due to restricted access of the reactants into the micropores, the polyaromatic substrates could be readily oxidized at 60 °C over Ti-Beta and Ti-HMS. In the case of BT, the activity of Ti-Beta was higher than the activity of Ti-HMS. On the contrary, with DBT, a bulky and weakly reactive molecule, Ti-Beta was slightly less active that Ti-HMS. The oxidation of kerosene (1310 ppm sulfur) with H_2O_2 was investigated at 70 °C. The peroxide efficiency was *ca*. 90% for Ti-Beta and 80% for Ti-HMS. The best results were obtained using MeCN as solvent: the removal of sulfur achieved 94 and 85.5% for Ti-Beta and Ti-HMS, respectively [429].



The catalytic performance of metal-containing molecular sieves, including Ti-MCM-41, has been evaluated in the oxidative desulfurization of model sulfur-containing compounds dissolved in *n*-heptane using TBHP as oxidant [430]. The best catalysts were then studied for the ODS of simulated and industrial diesels (40–300 ppm of sulfur) in a continuous fixed-bed reactor. Calcined Ti-MCM-41 was more active, did not leach Ti, and deactivated more slowly than other catalysts. Even the most difficult S-compound, 4,6-dimethyl dibenzothiophene (DMDBT), was fully oxidized to sulfone. The amount of adsorbed sulfone was strongly reduced by decreasing the polarity of Ti-MCM-41 by silylation, with the corresponding increase in catalyst activity and lifetime. Deactivated catalysts could be regenerated by washing with methanol.

Efficient removal of BT, DBT and DMDBT has been achieved *via* oxidation with 70% H_2O_2 using an amorphous Ti/SiO_2 catalyst prepared by grafting [431]. Both BT and DBT were easily oxidized to sulfones; however, the reaction with DMDBT was slow, presumably, because of the steric hindrance of the alkyl groups. The catalysts were reused four times in the reaction with DBT without loss of activity. The H_2O_2 efficiency was *ca*. 80%. The oxidation of S-containing compounds present in a commercial kerosene fraction (1291 ppm S) was carried out by applying the optimal conditions that had been established using DBT (0.25 g Ti/SiO_2, 90 g of fuel, H_2O_2/S molar ratio of 2.5/1, 20 mL of acetonitrile, 60 °C). After 5 min, the remaining sulfur concentration in the kerosene was below 250 ppm, and after 15 min it was below 10 ppm (sulfur removal >99%) [431].

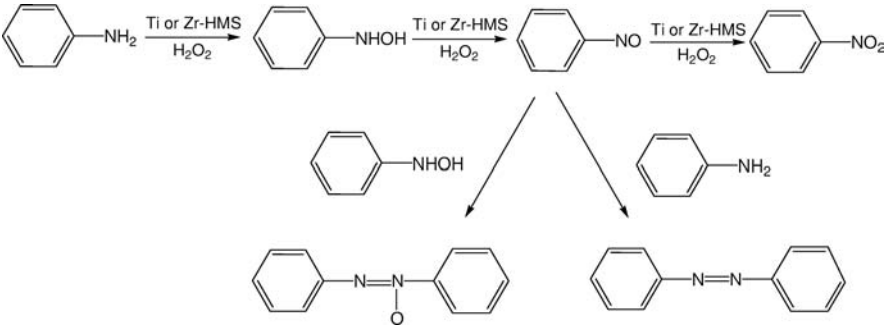
Mesoporous TiO_2–SiO_2 xerogels prepared by the nonhydrolytic sol-gel method showed excellent catalytic performances in the oxidation of bulky sulfides and thiophenes with H_2O_2 [89, 90]. Even DMDBT, the less reactive molecule, could be effectively oxidized. In all cases, H_2O_2 efficiency was more than 98%. Anhydrous TBHP (5.5 M in decane) and 70% aqueous TBHP produced results similar to those acquired with H_2O_2. The catalysts were stable under the operating conditions. Only a very small increase in DBT conversion (37% vs. 35%) was observed in the hot filtration test performed at 35% conversion.

4.3.7 Oxidation of Amines

Mesoporous titanium silicates show very little activity in the oxidation of primary aliphatic amines [432]. While TS-1, TS-2, and Ti-Beta produced 21–25% conversions after 2 h with 64–84% selectivity in the H_2O_2-based oxidation of *n*-propylamine to propionaldehyde oxime, Ti-MCM-41, Ti-HMS, and TiO_2–SiO_2 were almost inactive. Practically no activity was observed with TBHP as well. In contrast to alkylamines, the oxidation of arylamines, specifically aniline, proceeds efficiently over mesoporous metal silicates, such as Ti-, Zr- and V-containing HMS, Ti-MCM-41, and Ti-SBA-15, using H_2O_2 or TBHP as oxidant [28, 314, 390, 433, 434]. The catalytic activity of Ti-HMS in the oxidation of aniline was found to be close to that of Zr-HMS, Ti-MCM-41, Ti-SBA-15, and Ti-Beta and a little higher than the activity of TS-1. At low oxidant/substrate ratios and relatively high temperature (70 °C), azoxybenzene (AZY) was the major product but some amounts of azobenzene (AZO) and nitrosobenzene (NSB) were also detected. The selectivity in AZY was higher with H_2O_2 than with TBHP and achieved 90–95% at *ca.* 100% H_2O_2 conversion [434]. Phenylhydroxylamine (PHA) and nitrobenzene (NB) were never observed under these reaction conditions. NB appeared among the oxidation products when more than 6-fold excess of the oxidant was used. NSB was detected at the early stages of the reaction and then slowly disappeared, while the amount of AZY increased continuously. In fact, NSB was already formed at 0 °C, whereas significant amounts of AZY were only observed at 40 °C [434]. Such evolution is consistent with a reaction scheme where consecutive and bimolecular condensation reactions between products and/or unreacted aniline occur (Scheme 4.3).

Advantages of mesoporous Ti- and Zr-HMS over TS-1 were manifested in the oxidation of substituted anilines. At 70 °C, the corresponding azoxy product was formed within 30 min with 95–97% selectivity and 95–99% H_2O_2 efficiency while TS-1 gave very few of oxygenated products even after 3 h. Decreasing the reaction temperature to 0 °C modified the product selectivity and nitroso derivative was the main product formed [390, 434].

The course of aniline oxidation was completely different when TBHP was used as oxidant instead of H_2O_2 [434]. The reaction did not occur with TS-1 because the oxidant is too large to penetrate the channels of the MFI structure. On the other hand, Ti-Beta, Ti-, Zr- and V-HMS were active catalysts and produced AZY and AZO at temperatures above 50 °C. The nature of the catalyst had a strong impact on the product distribution: the selectivity to AZY was 90–92% for Ti- or Zr-HMS and



SCHEME 4.3 Oxidation of aniline with H_2O_2 over Ti- and Zr-HMS (elaborated from [390, 434]).

only 40% for Ti-Beta at comparable conversions. V-HMS was only active when TBHP was used as oxidant and led to the formation of NB with *ca*. 100% selectivity [433]. However, a reaction performed after removal of the catalyst showed a similar conversion, suggesting the presence of active vanadium species in solution [390]. The oxidation of aniline with 50% H_2O_2 over Cr-MCM-41 produced NB with 92% selectivity at 42% substrate conversion [236].

4.4 MECHANISTIC ASPECTS

Active sites and intermediates in titanium silicates have been addressed by several authors [56, 91, 93, 101, 386, 435, 436]. Clerici was the first who suggested that titanium hydroperoxo species (TiOOH) are the active oxygen-donating intermediates that operate in TS-1 (see Chapter 2 and references therein). Mesoporous titanium silicates with comparable Ti loadings have similar spectral parameters regardless of the preparation technique, and the values of these parameters stand between TS-1 and anatase (Table 4.9). Similar spectroscopic characteristics imply a similar structure of active centers and allow expecting a comparable catalytic behavior, on the stipulation that surrounding of the active centers does not differ significantly. Indeed, several examples given in Section 4.3 support this suggestion.

The oxidation mechanisms over hydrophobic mesoporous titanium silicates are expected to be similar to those of TS-1, with the main difference that mesopores do not afford shape selectivity. The hydrophilic environment around Ti centers disfavors adsorption of nonpolar substrates within pores but favors adsorption of H_2O_2. As a result, hydroxyl radicals formed during unproductive decomposition of the oxidant act as strong H-atom abstraction agents, decreasing the reaction selectivity and H_2O_2 efficiency relative to TS-1 and other hydrophobic materials. Unlike TS-1 and TS-2, oxyfunctionalization of the side chain in toluene predominates over aromatic ring hydroxylation with mesoporous catalysts, indicating a predominance of a

TABLE 4.9 Spectroscopic Characteristics of Representative Titanium Silicates (Ti *ca.* 2 wt%) and Anatase

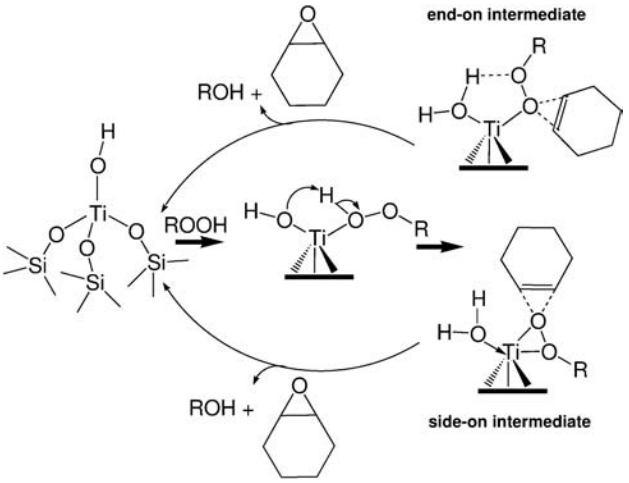
Method / Parameter)	TS-1 [91]	TiO_2–SiO_2 [11, 13, 83]	Ti/MCM-41 [50, 97, 101]	Ti-MCM-41 [23, 129]	Ti-MMM-2 [156, 163]	Anatase [91]
DRS UV-vis / Maximum of CT band (nm)	205–208	220–230	220–230	210–230	205–210	330
XANES / Intensity of pre-edge peak (%)	75	32 (58–75)[a]	50–65	33 (77)[a]	30	<5%
EXAFS / Average length of Ti–O bond (Å)	1.79–1.81	1.81–1.82	1.81	1.81	1.81	1.94
XPS / Ti($2p_{3/2}$), bond energy (eV)	460.2	460.0	459.8	459.9	460.1	458.4

[a]For samples dehydrated by evacuation.

conventional radical oxidation mechanism [93]. The selectivity parameters C(1):C(2):C(3):C(4), which reflect the relative reactivities of hydrogen atoms at carbons 1, 2, 3 and 4 of the *n*-heptane or *n*-octane chain, differ significantly for Ti-MMM-2 and TS-1 (1:5.2:4.5:4.4 *vs.* 1:80:62:59 for *n*-octane) [369]. The bond-selectivity parameters 1°:2° in the oxidation of 2,2,4-trimetylpentane and methylcyclohexane by the H_2O_2/Ti-MMM-2 system are close to the parameters found for homogeneous systems that oxidize alkanes with the participation of hydroxyl radicals. The oxidation of *cis*- and *trans*-1,2-dimethylcyclohexanes proceeds nonstereoselectively to give a mixture of *cis*- and *trans*-isomeric alcohols.

The basic order of reactivity for PO production with H_2O_2 (TS-1 > Ti-Beta > [Ti,Al]-Beta > Ti-MCM-41) matches the decrease in hydrophobicity in the same order [435]. Competition between epoxide production and decomposition of peroxide depends on the relative rates of these reactions. When the olefin is relatively inert, unselective decomposition of the oxidant dominates, as observed for propylene [388] or *p-tert*-butylphenylallyl ether [335]. If radical species are generated, allylic oxidation (homolytic pathway) and epoxidation (heterolytic pathway) compete with each other for alkenes possessing reactive H atoms in the allylic position (cyclohexene, terminal olefins, etc.). For cyclic olefins, epoxidation becomes the predominant reaction as the olefin ring size increases (*cis*-cyclooctene, cyclododecene, caryophyllene, etc.).

Surface acidity may strongly affect the oxidation pathways. Surface hydroxyls in mesoporous titanium silicates possess weak Brønsted acidity, close to the acidity of TS-1 [66]. To suppress ring opening in acid-sensitive epoxides, basic additives are used; however, similarly to TS-1, they produce a retarding effect on the oxidation rate [93, 435]. By contrast, to favor epoxide ring opening and subsequent oxidative cleavage, strong acidic centers are created on the silica surface through insertion of trivalent elements [405].



SCHEME 4.4 Tentative mechanism of Ti-catalyzed alkene epoxidation with alkylhydroperoxides (adapted from [437]).

The mechanism of alkene epoxidation with alkylhydroperoxides over mesoporous titanium silicates was probed using both experimental and theoretical methods [50, 56, 79, 93, 101, 334, 386, 437]. The most active species are believed to be the four-coordinated isolated Ti^{IV} centers tripodally bound to silica, which represent a compromise between the accessibility of the Ti center and its electrophilicity that seems to increase with the number of siloxy substituents. On the basis of XAFS analysis and DFT computations, Thomas et al. [56, 101, 437] concluded that the coordination shell of the original four-coordinated Ti^{IV} expands to six due to formation of an alkylperoxo intermediate. As in the case of TS-1 and H_2O_2 [435, 438, 439], the question of whether the η^1 (end-on) or η^2 (side-on) coordination mode of the peroxo species is preferred remains open. Both η^2 and η^1 intermediates provide equally good fits to the EXAFS data [437]. The following reaction scheme has been proposed for alkene epoxidation (Scheme 4.4).

Buijink et al. [386] trended towards Ti(η^2-OOR) intermediate that is generated from the active sites (or rather, precursor sites) *via* reaction with ROOH that involves proton transfer to one of the siloxy ligands and forms a neutral coordinated silanol group together with the titanium alkylperoxo group. The Ti–O–Si moieties acting as a "proton parking place" are thus seriously weakened.

Polyhedral oligomeric silsesquioxane derivatives (POSS) containing tetrahedrally coordinated Ti^{IV} and other metals can mimic the surface of silica and serve as molecular models to probe the oxidation mechanisms [51, 440–444]. Using a range of techniques, including pre- and near-edge X-ray absorption spectroscopy [101], molecular dynamics calculations [442], and DR UV-vis [441], it was concluded that the nature of the Ti^{IV} active center in heterogeneous titanium silicate

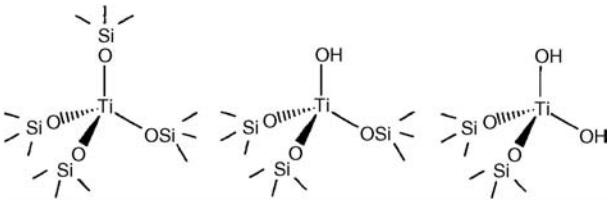


FIGURE 4.9 Possible Ti sites in titanium silicates and Ti-POSS.

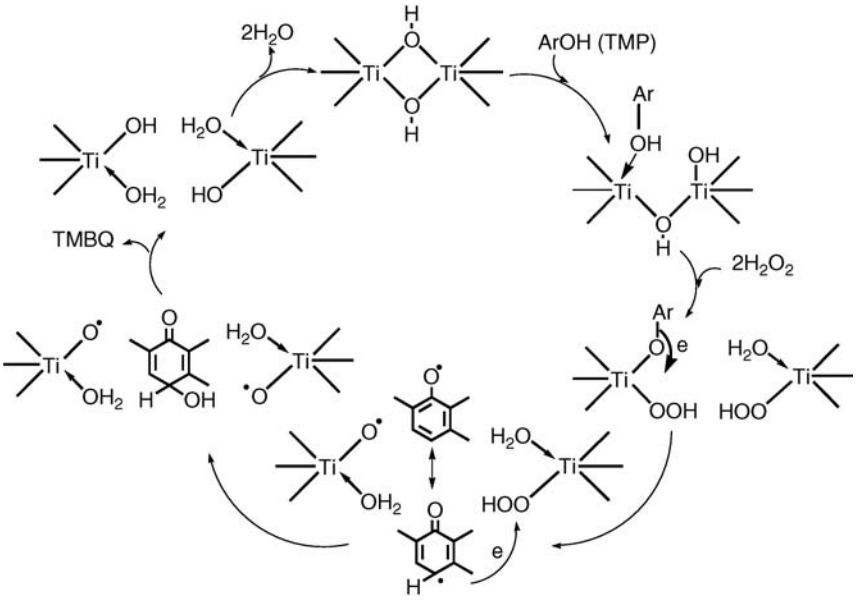
catalysts is nearly the same as that of Ti^{IV} bound to soluble silsesquioxane ligands. Possible types of Ti sites are shown in Figure 4.9.

Model studies implemented on Ti-POSS confirmed that the four-coordinated Ti sites with tripodal geometry display better activities and selectivities in alkene epoxidation with ROOH than the corresponding bipodal or tetrapodal ones [440–444].

Kholdeeva and Maksimovskaya [445, 446] found that Ti- and Zr-substituted polyoxometalates (POM) mimic the catalytic action of hydrophilic Ti- and Zr-silicates and suggested using Ti- and Zr-POMs as molecular models for studying mechanisms of H_2O_2-based oxidations over hexacoordinated Ti- and Zr-centers. It was demonstrated that such centers can activate H_2O_2 *via* homolytic routes and are able to catalyze allylic oxidation of alkenes along with oxidation of phenols and thioethers but can not perform selective epoxidation that requires heterolytic activation of the oxidant. It is possible to switch the oxidation mechanism from homolytic to heterolytic either by increasing the protonation state of POM [447, 448] or by changing the coordination geometry of Ti [449]. A polyoxotungstate containing TiOH groups with Ti atom in a 5-coordinated square-pyramidal environment revealed high activity and selectivity in alkene epoxidation with H_2O_2 [449, 450]. Several authors pointed out the importance of hydrogen bonding in the activation of H_2O_2 over Ti centers based on the results acquired by experimental and theoretical methods [438, 439, 450–453].

A few authors suggested that complete site isolation is not a necessary requirement for effective alkene epoxidation [79, 300, 315, 386, 454]. Buijink et al. [386] proposed that "the active site" of the POSM titania-on-silica catalyst is actually a continuum of silica-supported unsaturated mono- and polynuclear Ti species. Interestingly, a thermally robust polyoxotitanate, $[(c\text{-}C_7H_{13})_7Si_6O_{11}]_3[TiOH]_4$, appeared to be an efficient catalyst for alkene epoxidation with H_2O_2 [443]. To accomplish the selective transformation of alkylated phenols to benzoquinones, the presence of at least two close Ti centers is required to favor interaction between the phenolic molecule and two contiguous TiOOH groups that ensure fast oxidation of intermediate aryloxyl radicals, preventing their coupling to dimeric byproduct [313, 381]. A tentative reaction mechanism is shown in Scheme 4.5.

The mechanism of the Baeyer–Villiger oxidation over tin silicates was intensively studied by Corma's group [321, 322]. They suggested that Sn sites selectively



SCHEME 4.5 Oxidation of alkylphenols to quinones with H_2O_2 over dimeric Ti(IV) centers [313, 381].

activate ketone rather than oxidant. In this way, the positive charge on the C atom of the carbonyl group is increased, facilitating the nucleophilic attack by H_2O_2 (see Scheme 1.10 in Chapter 1). On the other hand, side reactions such as epoxidation, which require activation of the oxidant, are largely avoided [198, 321]. The ability of calcined Sn/MCM-41 to activate the carbonyl bond was confirmed by *in situ* IR spectroscopic study [321]. Two main types of Sn^{IV} centers have been detected by means of IR spectroscopy of probe molecules (MeCN) and modeled by DFT calculations [322, 455]: inactive fully coordinated Sn atoms in framework positions, Sn $(–Si–O–)_4$, that weakly interact with Lewis bases and highly active strong Lewis-acid sites associated with Sn centers with one or two hydrolyzed Sn–O–Si bonds, $(–Si–O–)_3Sn–OH$ or $(–Si–O–)_2Sn–(OH)_2$, respectively.

Possible reaction mechanisms for tin-catalyzed BV oxidation with H_2O_2 have been studied by the DFT method [456]. It was concluded that the reaction most likely proceeds through a Criegee intermediate that contains a five-membered chelate ring with the tin center. Rearrangement of this intermediate is the rate-determining step for the overall reaction. DFT was also used to compare model epoxidation and BV reaction mechanisms for Ti(IV)-H_2O_2 and Sn(IV)-H_2O_2 systems [457]. It was found that activation of H_2O_2 *via* formation of a metal hydroperoxo intermediate proceeds with similar energetics over titanium and tin; the overall reaction kinetics for alkene epoxidation were also similar. However, the intrinsic reaction rate for BV oxidation of either acetone or 2-methyl-3-pentanone was approximately five orders of magnitude higher with Sn(IV) than with Ti(IV). It was

concluded that the greater Lewis acidity of tin relative to titanium enhances adsorption of the ketone substrate on the metal active site and reduces the rate-determining activation barrier for Baeyer–Villiger rearrangement of the chelated Criegee intermediate [457].

4.5 STABILITY

In the field of fine chemicals, where the high added value of the final products may account for the use of valuable and costly reactants, a solid catalyst is often considered as a consumable reagent and is thus disposed of and substituted by a fresh one [458, 459]. However, the ever-increasing attention towards the economical and environmental sustainability is prompting the scientific community to develop stable solid catalysts that can be recycled and reused [4, 460].

4.5.1 Mechanisms of Deactivation

Deactivation of metal silicates can be caused by mechanical, thermal and hydrothermal treatments as well as by detrimental interaction with the reaction mixture that, in turn, may result in poisoning or fouling and/or induce irreversible transformations of active sites, such as their agglomeration on the surface and leaching into solution. Only poisoning and fouling belong to deactivation processes that could be, in principle, reversible, i.e. the catalyst activity can be partially or totally restored by various treatments such as calcination, extraction, and washing.

Poisoning can be caused by chemisorption of impurities derived from feed components or reaction products that possess a strong affinity to the catalytic site and hinder adsorption of reactants. For example, in alkene epoxidation over titanium silicates with TBHP, glycol byproducts poison Ti active sites, and only calcination allows removal of them from the catalyst surface and the catalytic properties to be restored [334, 393, 396]. *Fouling* implies the phenomena where the catalyst surface is covered by species that block the connection between the active sites and the reaction mixture [458]. Contrary to poisoning, fouling is not selective. Although the effects of fouling are less pronounced for mesoporous silicates than for microporous zeolites, they can take place in the case of materials with one-dimensional channel systems (MCM-41, HMS) where even minimal amounts of carbonaceous compounds deposited at pore openings can block the access to the entire pore. If this occurs, the use of materials with open three-dimensional ordered (MCM-48, SBA-1, SBA-16), disordered worm-like (KIT-1, MSU-X) or foam-like (TUD-1, MCF) structures may be advantageous. Catalyst regeneration by calcination is possible, provided it has a sufficient thermal stability.

Mechanical degradation includes phenomena, such as crushing, attrition, friction and/or erosion of the catalyst particles, which shorten the catalyst lifetime and may affect negatively its performance. Mechanical stability is an important issue for materials that have to be shaped into beads or pellets for use in a catalytic reactor. Stability to mechanical treatments usually decreases in the following order:

silicagels (xerogels) > mesostructured silicas > aerogels. Di Renzo and coworkers [38, 461] came to the conclusion that the mesoporous silicates with a lower initial pore volume and thicker walls are generally more stable. The loss of pore volume upon a compressive stress of 100 MPa varied from 5 to 50% for different samples and occurred without any significant decrease of the pore size for both cubic MCM-48 and hexagonal MCM-41. Mechanical stabilities of a wide range of mesoporous materials (MCM-41, MCM-48, HMS, FSM-16, KIT-1, PCH, and SBA-15) were studied using XRD and nitrogen sorption [64]. All materials collapsed at a maximum pelletizing pressure of 450 MPa. Ball milling caused destruction of Ti-MCM-41 accompanied by blocking of the channels, but did not affect the local environment around Ti centers [462]. The presence of moisture decreases the resistance to mechanical degradation. A 2–3-fold improvement of the mechanical stability of MCM-48 was observed after silylation [306, 333]. Although the mechanical stability of mesostructured silicas is inferior to that of alumina, silica gels and zeolites, it is more than sufficient to withstand typical treatments such as pressing and molding.

Thermal degradation implies processes induced by high temperatures in dry air that lead to a decrease in surface area and a partial or even total collapse of the porous structure that, in turn, may result in sintering of the active component, its entrapment inside the reorganized support and loss of accessibility. Thermal degradation can occur during the catalyst activation, pretreatment or regeneration steps. Thermal stabilities of mesostructured silicas, MCM-41, MCM-48, HMS, FSM-16, KIT-1, PCH, and SBA-15, have been studied by many research groups [32, 38, 64, 127, 461–463]. It was concluded that this property strongly depends on both the wall thickness of the material and the silica precursor used in the synthesis. By comparing hexagonal mesostructures with similar wall thicknesses, the following stability trend was observed: KIT-1 (colloid silica), MCM-41 (fumed silica) > FSM16 (layered silicate) > MCM-41 (TEOS), HMS (TEOS) [64]. The M41S materials prepared from fumed silica were stable to at least 850 °C, whereas materials prepared with TEOS completely collapsed at 750 °C. Although SBA-15 is also synthesized using TEOS, it shows a much higher stability than TEOS-derived HMS and MCM-41 due to the much thicker pore walls (See Table 4.1). The thermal stability of Ti-MCM-41 was practically independent of the metal content ($5 \leq Si/Ti \leq 100$) [463]. The complete collapse of the ordered structure occurred only at 1100 °C, while for the pure silica MCM-41 it started at 1000 °C. Tetracoordinated titanium incorporated in the walls remained stable up to 873 °C. In general, the thermal stability of mesoporous metal silicate catalysts is sufficient, at least, for fine chemicals synthesis, as most materials can resist temperatures up to 700 °C, which is more than enough for catalysts activation and regeneration by calcinations.

A weak point of most known mesoporous silicate materials is *hydrothermal stability* (the resistance to the combined effect of water/steam and temperature) [22, 23, 29–36, 38, 40, 64, 125, 137, 464–469]. Full collapse of MCM-41 structure occurred when a sample was left in air for three months [465]. Cassiers et al. [64] subjected mesostructured silicates to a mild hydrothermal treatment at 400 °C with 25% steam at 1 atm pressure and revealed that the hydrothermal stability follows a different trend from the thermal stability: KIT-1 > SBA-15 > MCM-48 (fumed

silica and TEOS), PCH > FSM-16, MCM-41 (fumed silica and TEOS), HMS. Whereas SBA-15 and KIT-1 could even withstand a more severe test under autogenous pressure, the structure of the other materials was completely destroyed under the rather mild steaming conditions. For materials with comparable wall thicknesses, the structural degradation was lower for cubic MCM-48 than for hexagonal mesostructures HMS, MCM-41, and FSM-16 [64]. Increasing the thickness of silica walls and the degree of silica polymerization enhanced the hydrothermal stability. Similar conclusions were made by other authors [214, 468]. Preorganized silica precursors, such as fumed, layered or colloidal silica, produced more stable structures than molecular precursors (TEOS). Meanwhile, a direct correlation between the degree of silica polymerization (Q_4/Q_3 in ^{29}Si MAS NMR spectra) and the hydrothermal stability was not always found [469, 470]. Some materials, e.g., COK-11 [471], COK-12 [42, 142], and MMM-2 [156, 162], revealed a fairly good hydrothermal stability although they have a moderate degree of silica polymerization ($Q_4/Q_3 = 1.5$–1.8) and thin silica walls (COK-11, MMM-2). A few authors assumed that the main reason for the low hydrothermal stability of most ordered mesoporous silicates is a high ratio of strained siloxane bonds in the amorphous silica walls as compared to crystalline walls of zeolites [464–467, 472, 473]. These strained bonds are first subjected to hydrolysis followed by the formation of local defects during calcinations. In general, hydrothermal stability does not correlate to the degree of long range order present in the material [472], but the higher local order might be important [469]. Strategies that allow for increasing the hydrothermal stability of mesoporous silicates will be discussed in Section 4.5.2.

Interaction with the reaction mixture can produce a stong deactivation effect on mesoporous metal silicate catalysts. Silica materials are relatively stable under acidic conditions, whereas they degrade readily in basic media [44]. Their hydrophilic surface easily adsorbs water that causes not only hydrolysis of ≡Si–O–Si≡ bonds and collapse of the porous structure (the process described above) but may also hydrolyze ≡Si–O–M≡ bonds, inducing movement of the metal to extraframework positions followed by leaching into solution and/or agglomeration to MO_x domains on the catalyst surface. The combination of water and peroxide is particularly detrimental [67, 84, 378, 392, 462]. In methanol, H_2O_2-based oxidations are usually accompanied by titanium leaching [72, 73, 392]. With acetonitrile as solvent, Ti leaching may not occur but irreversible deactivation caused by oligomerization of Ti centers on the silica surface takes place [67, 84, 374, 378, 462]. Similar processes were observed for Ti-Beta [96] and mesoporous silicates containing Fe [159] and Ce [406]. The gradual aggregation of isolated tetrahedral Ti centers into ultrafine titania clusters under operation conditions has been established for the Shell catalyst [386]. Agglomeration and leaching of active metal can be minimized to ensure a good catalyst reusability if H_2O_2 is added drop-wise to the reaction mixture [303, 393] or 30% H_2O_2 is replaced with a more concentrated one [313, 378] or with anhydrous alkylhydroperoxide [67, 73, 174, 179, 392, 474].

Leaching is a serious problem of solid catalysts in liquid phase oxidation and is attributed to the strong complexing and solvolytic properties of oxidants and/or polar products bearing –OH, –NH_2 or –COOH groups, especially, in a chelate

form (polyols, dicarboxylic acids, etc.) [354]. In the epoxidation of crotyl alcohol over titanium silicates, gradual Ti leaching is caused by the reaction byproduct, 1,2,3-butanetriol [475]. Cr-containing catalysts start to lose the active metal as cyclohexane conversion increases and carboxylic acids appear among the oxidation products [344]. Along with experimental conditions and the nature of reactants/products, structural and geometrical factors as well as the nature and state of active metal may strongly affect stability of catalysts to leaching. For amorphous MO_x–SiO_2 mixed oxides, leaching is a typical drawback [109–111]. Generally, metal cations incorporated in the silica framework are more resistant to leaching than grafted species, which are more exposed to reactants, or extraframework metal-oxide clusters. The inclination to form polynuclear species makes metals, like V, Cr, Mo, and W, especially disposed to leaching. The weakness of ≡Cr–O–Si≡ bonds is believed to be a major hurdle toward leaching-resistant Cr-containing molecular sieves.

If the species leached is a poor homogeneous catalyst (typical of Ti and Sn) catalysis has a true heterogeneous nature, but after a limited number of reuses the catalyst loses its activity as no active metal remains. By contrast, the leached species can possess a high activity in solution (typical of Co, Mn, Fe, V, Cr, W, Mo, Cu), leading to a parallel homogeneous pathway that may be responsible for a reduction of selectivity and cause product contamination with transition metals. For this reason, the nature of catalysis should be checked by hot filtration test [354] that was described in Section 4.3. Taking into account that products may cause leaching, filtration tests must be carried out in the presence of all reactants (not only solvent or oxidant as sometimes can be found in the literature) and not at the initial stage of the reaction when leaching can be still minor. In the case of autoxidation processes, interpretation of the hot filtration test is not always easy because some residual activity of the filtrate can be due to thermal reaction induced by the primary oxidation products, hydroperoxides [358, 359]. Determination of the metal concentration in the filtrate helps to draw a proper conclusion about the nature of catalysis.

4.5.2 Solving Problem of Hydrothermal Stability

Bearing in mind that hydrothermal stability is one of the main critical parameters for potential applications of mesoporous silicates, enormous efforts have been made to improve it either by adjusting the synthesis procedure or by postsynthesis manipulations. All these methods were directed to increase the silica wall thickness, degree of its polymerization or local order within the silica walls. Ryoo and Kim [464] found that pH adjustment of a S^+I^- reaction mixture with acetic acid to keep pH *ca.* 11 leads to MCM-41 materials stable up to 700 °C in humid air. Edler and White [472] revealed that resistance to degradation is favored by long aging of the dry template containing MCM-41 materials prior to calcination. Increasing crystallization temperature and adding small amounts of fluoride ions allowed a considerable improvement in the hydrothermal stability of MCM-48 [476]. Besides, stability could be increased by the addition of inorganic salts or organic additives during the synthesis [125, 470, 477]. Hydrothermal stability of MCM-41 and MCM-48 was

enhanced by postsynthesis restructuring through additional hydrothermal treatments of the material before removal of the surfactant [469, 478, 479]. Mokaya [473] suggested restructuring *via* a route that involves the use of calcined MCM-41 as a "silica source" for secondary synthesis. The remarkable stability observed was rationalized by a combination of thicker pore walls, higher silica condensation, and a less-strained silica framework.

A breakthrough in solving the problem of hydrothermal stability is related to the synthesis of SBA-15, the material with extremely thick silica walls (3–6 nm) [133, 134]. Zhao and coworkers [480] suggested that microporosity of SBA-15 is also an important factor that ensures good hydrothermal stability. No structural degradation of SBA-15 was observed after treatment in boiling water for 48 h [134]. However, after 10 days of a similar treatment, a significant loss of the structural ordering was observed for SBA-15 and SBA-16 [481]. A carbon-propping thermal treatment improved stability of SBA-15 *via* enhancing polymerization of the silica walls.

Ultrastable mesostructured material MSU-G resisted calcination at 1000 °C and hydrothermal treatment with boiling water at 100 °C for 150 h while other mesostructured silicas with benchmarked hydrothermal stabilities such as KIT-1 and SBA-15 became X-ray amorphous and lost mesoporosity in 50 h when subjected to equivalent treatments [140, 141]. The high hydrothermal stability of MSU-G is explained by the thick walls (2.5 nm) and the unusually high degree of silica polymerization ($Q_4/Q_3 = 6.2$–7.1). The specific hierarchical structure of MSU-G with wormhole-like mesopores arranged between undulated silica sheets of the multilamellar vesicles may also account for the unprecedentedly high stability.

Incorporation of a metal heteroatom in the silicate framework often allows enhancement of the hydrothermal stability. This was established by several groups for Al-containing mesostructured materials [482–485]. Studies by ^{29}Si MAS NMR revealed that titanium incorporation promotes crosslinking of the SBA-15 framework [147]. Similar results were documented for metal-substituted MCM-41 systems [129, 170, 213]. On the other hand, a lower stability of Ti-MCM-41 [124] and Ti-MSU-G [179] against water compared to pure silica materials was also precedented. The effect of the heterometal on the catalyst resistance to water may strongly depend on the specific Si/M ratio [484–486]. Thus, stability of Cr-MCM-48 in boiling water was improved with increasing the Cr content to achieve a maximum at Si/Cr = 50 (the catalyst maintained its mesoporous structure after refluxing in boiling water for 36 h) and then tended to decrease [486].

Since the poor stability of mesoporous materials is widely attributed to the amorphous nature of their walls, a number of strategies have been advanced toward zeolitization of the walls. Partial recrystallization of the amorphous walls into zeolitic domains was induced by impregnation of MCM-41 with TPAOH followed by a hydrothermal treatment [487]. Composite micro/mesoporous materials have been prepared by a mixed-template approach that involves a simultaneous crystallization of ZSM-5 and MCM-41 phases [488]. An approach that seems to be the most useful for the preparation of metal silicate catalysts involves the assembly of zeolite seeds or protozeolite clusters in mesoporous frameworks [489, 490]. A few composite micro/mesoporous materials have been prepared using presynthesized TS-1 as a

component for the subsequent step in the synthesis of a mesoporous material [177, 180, 391, 485, 491–493]. Sometimes, however, the existence of a micropore system is not evident in the pore-size distributions, which is ascribed to the extremely small dimensions of the microporous building units forming pore walls [494]. Alternatively, the walls of mesoporous silica can be coated with zeolitic nanoclusters/nanoparticles [376, 495–497].

Incorporation of nonpolar organic groups either during synthesis or *via* postsynthesis silylation is widely used to improve hydrothermal stability of mesoporous catalysts. Such techniques have been described in Section 4.2.7. Whereas the structure of Ti-MCM-41 was almost completely destroyed upon exposure to moisture over saturated aqueous solution of NH_4Cl for 3 days, silylated Ti-MCM-41 and Ti-MCM-48 kept their structures intact for 30 days [331]. Kisler et al. [498] compared silylation methods with regards to improvement of the stability of MCM-41 in aqueous solutions and found that the hydrophobic coating created using HMDS persists on the surface after storing in water for up to 7 days, unlike the coating obtained using trichloromethylsilane. Mesoporous organosilicas PMO-SBA-15 and PMO-SBA-16 exhibited unprecedented hydrothermal stability for as long as 60 days without any loss of structural integrity, as verified by SAXS, nitrogen adsorption, TEM, SEM, and ^{29}Si MAS NMR techniques [481]. The superior hydrothermal stability of the hybrid PMO materials as compared to SBA-15 and SBA-16 was attributed to a blend of thick pore walls, enhanced polymerization degree of siloxane bonds and highly hydrophobic nature of the organosilica framework. In spite of the low decomposition temperature of the organic moiety, thermal treatment seems to induce further condensation of the silica walls, thus increasing hydrothermal stability.

4.5.3 Hydrothermally Stable Catalysts: Scope and Limitations

Thus far, not all catalytic materials that had been claimed as hydrothermally stable have been tested in liquid phase oxidations. For some materials, the catalytic activity in the first run only was reported and compared with conventional catalysts, like TS-1 and Ti-MCM-41, while neither recycling behavior nor leaching tests were provided. Therefore, a reliable conclusion on their utility for liquid phase oxidation catalysis seems to be premature.

Although hydrothermal stability of the silica matrix does not give a 100% guarantee that no catalyst deactivation would occur due to a synergistic attack at M–O–Si bonds by H_2O_2 and H_2O molecules, the hydrothermally stable catalysts, such as Ti-containing MSU-G [179], SBA-15 [104, 309], MCF [301], TUD-1 [174], and MMM-2 [156], are certainly less prone to the deactivation processes than catalysts with low hydrothermal stability. Indeed, Ti-SBA-15 demonstrated much better resistance against titanium leaching than Ti-MCM-41 [309]. Although no loss of active metal occurred for Ti-MSU-G, the isolated Ti centers were more stable toward clusterization with TBHP than with aqueous H_2O_2 [179]. While TiO_2–SiO_2 aerogels [84] and mesostructured Ti-MMM [378] lost their activity already after the first run, Ti-MMM-2 revealed fairly good recyclability in H_2O_2-based oxidations [156, 163].

After treatment with 30% H_2O_2 in MeCN solution followed by drying and calcination, the position of the DR UV-vis maximum (205–210 nm) of Ti-MMM-2 remained practically unchanged, indicating a relative stability of the tetrahedrally coordinated Ti centers toward clusterization. Meanwhile, in the oxidation of cyclohexene to adipic acid, where higher concentrations of hydrogen peroxide were employed, a gradual transformation of the isolated Ti centers to oligomerized TiO_2-like species led to irreversible catalyst deactivation [406]. Furthermore, titanium leaching into solution happened at high conversions due to interaction of the Ti sites with adipic acid. Hence, high concentrations of H_2O_2 and formation of highly polar products, in particular, dicarboxylic acids is a serious limitation for catalytic applications of even hydrothermally stable metal silicates, let alone unstable ones.

4.6 CONCLUSIONS AND OUTLOOK

Twenty years have passed since the first syntheses of mesoporous metal silicates were accomplished. During these years the synthetic methodologies have been greatly expanded and improved, and a wide range of transition-metal ions have been successfully incorporated into the silica frameworks. In this chapter we tried to show the evolution from the first, relatively simple strategies for incorporation of transition metals into mesoporous silica matrixes to the more sophisticated methods that have led to the highly active and selective, true heterogeneous, and recyclable catalysts.

From the very beginning, mesoporous metal silicates were expected to show advantages relative to microporous zeolites in the oxidation of sterically demanding substrates, and the examples given in Section 4.3 have clearly demonstrated the success of this concept. In the oxidation of small molecules, however, mesoporous catalysts revealed intrinsically lower activities than TS-1 or Ti-Beta, most likely due to the presence of a large number of silanol groups that promote adsorption of water at the expense of nonpolar substrates. Some reactions easily realizable over TS-1 with H_2O_2 (propylene epoxidation, oxidation of linear alkanes and primary amines) are virtually impossible over hydrophilic mesoporous Ti,Si-catalysts. On the contrary, numerous oxidations with bulky alkylhydroperoxides have become possible due to mesoporous metal silicates.

Catalysis by titanium incorporated into silica matrix remains the most developed area although many interesting catalytic applications have been found for mesoporous silicates containing other metals, such as V, Nb, Cr, Co, Fe, Mn, Ce, and Sn. A great progress has been achieved in solving the problem of metal leaching and in the development of materials with high hydrothermal stability, which significantly broadens the application of mesoporous metal silicates in liquid phase processes, including those employing aqueous H_2O_2 as oxidant. However, some restrictions still exist with regards to the operation conditions and specific oxidation reactions. Even hydrothermally stable catalysts should be used

with a caution, because the formation of highly polar products or an improper choice of solvent, oxidant concentration or other parameters can be potentially detrimental for the catalysts.

At the moment, it is not always easy to conclude which types of catalysts are superior in terms of activity, selectivity and stability because direct comparative studies are still a rare case, while the reaction conditions used by different authors may differ significantly. An exchange of samples within the scientific community would favor further progress in the development of new efficient catalytic materials and their diversification. In addition, more contacts between "synthetic" and "catalytic" groups would gain benefits for both of them and would facilitate finding new solutions and the discovery of new approaches.

The present state-of-the-art of the field suggests that synthesis of fine chemicals remains the most suitable area for application of mesoporous metal silicate catalysts that could form a basis for new advanced oxidation technologies. In the future, such clean technologies using environmentally benign oxidants should replace the existing stoichiometric processes that employ hazardous reactants and produce a huge amount of waste. The beneficial use of mesoporous metal silicates in liquid phase oxidation catalysis will mainly depend on the progress made in both tailoring the surface chemistry of these materials and overcoming the operation and economical obstacles, such as the cost of catalyst relatively to the cost of products, catalyst lifetime, and the possibility of regeneration.

ACKNOWLEDGMENTS

The author thanks all coauthors of the joint papers published on catalysis by mesoporous metal silicates. The help of Dr. M. Guidotti in the preparation of Sections 4.2.6.2, 4.3.3.1 and 4.5.1 as well as discussions of Dr. M. Melgunov on hydrothermal stability are highly appreciated. Partial financial support from the Russian Foundation for Basic Research (grants 01-03-32852 and 05-03-34760) is acknowledged.

REFERENCES

1. *Zeolites and Mesoporous Materials at the Dawn of the 21 st Century*. Galarneau A., Di Renzo F., Fajula F., Vedrine J., eds. *Stud. Surf. Sci. Catal.* Vol. 135. Elsevier, Amsterdam, 2001.
2. *Nanotechnology in Mesostructured Materials*, Park S.-E., Ryoo R., Ahn W.-S., Lee C.W., Chang J.-S., eds. *Stud. Surf. Sci. Catal*. Vol. 146. Elsevier, Amsterdam, 2003.
3. *Catalysts for Fine Chemical Synthesis*, Vol. 4: Micro and Mesoporous Solid Catalysts. Derouane E., Roberts S.M., eds. Wiley-VCH Verlag, Weinheim, 2006.
4. *Fine Chemicals through Heterogeneous Catalysis*. Sheldon R.A., van Bekkum H., eds. Wiley-VCH, Weinheim, 2001.

5. Angevine P.J., Gaffney A.M., Shan Z., Yeh C.Y. In: *Innovations in Industrial and Engineering Chemistry*. ACS Symposium Series, Vol. 1000. Flank W.H., Abraham M.A., Matthews M.A., eds. American Chemical Society, Washington, DC, 2009, pp. 335–363.
6. Perego C., Bosetti A. (2011). *Micropor. Mesopor. Mater.* 144, 28–39.
7. Holm M.S., Taarning E., Egeblad K., Christensen C.H. (2011). *Catal. Today* 168, 3–16.
8. Schneider M., Baiker A. (1995). *Catal. Rev.-Sci. Eng.* 37, 515–556.
9. Corriu R.J.P., Leclercq D. (1996). *Angew. Chem. Int. Ed. Engl.* 35, 1420–1436.
10. Pajonk G.M. (1997). *Catal. Today* 35, 319–337.
11. Davis R.J., Liu Z. (1997). *Chem. Mater.* 9, 2311–2324.
12. Schneider M., Baiker A. (1997). *Catal. Today* 35, 339–365.
13. Gao X., Wachs I.E. (1999). *Catal. Today* 51, 233–254.
14. Barton T.J., Bull L.M., Klemperer W.G., Loy D.A., McEnaney B., Misono M., Monson P. A., Pez G., Scherer G.W., Vartuli J.C., Yaghi O.M. (1999). *Chem. Mater.* 11, 2633–2656.
15. Pierre A.C., Pajonk G.M. (2002) *Chem. Rev.* 102, 4243–4265.
16. Fujdala K.L., Don Tilley T. (2003) *J. Catal.* 216, 265–275.
17. Landau M.V. In: *Handbook of Heterogeneous Catalysis*. Ertl G., Knözinger H, Schüth F, Weitkamp J., eds. Wiley-VCH, Weinheim, 2008, pp. 119–160.
18. Kresge C.T., Leonowicz M.E., Roth W.J., Vartuli J.C., Beck J.S. (1992). *Nature* 359, 710–712.
19. Beck J.S., Vartuli J.C., Roth W.J., Leonowicz M.E., Kresge C.T., Schmitt K.D., Chu C.T., Olson D.H., Sheppard E.W., McCullen S.B., Higgens B., Schlenker J.L. (1992). *J. Amer. Chem. Soc.* 114, 10834–10843.
20. Kresge C.T., Leonowicz M.E., Roth W.J., Vartuli J.C., inventors; Mobil Oil Corp., assignee. US Patent 5,098,684. 1992.
21. Sayari A. (1996). *Chem. Mater.* 8, 1840–1852.
22. Zhao X.S., Lu G.Q., Millar G.J. (1996). *Ind. Eng. Chem. Res.* 35, 2075–2090.
23. Corma A. (1997). *Chem. Rev.* 97, 2373–2419.
24. Corma A. (1997). *Topics Catal.* 4, 249–260.
25. Maschmeyer T. (1998). *Curr. Opin. Solid State Mater. Sci.* 1, 71–78.
26. Ying J.Y., Mehnert C.P., Wong M.S. (1999). *Angew. Chem. Int. Ed.* 38, 56–77.
27. Biz S., Occelli M.L. (1998). *Catal. Rev.-Sci. Eng.* 40, 329–407.
28. Tuel A. (1999). *Micropor. Mesopor. Mater.* 27, 151–169.
29. Trong On D., Desplantier-Giscard D., Danumah C., Kaliaguine S. (2001). *Appl. Catal. A: General* 222, 299–357.
30. Selvam P., Bhatia S.K., Sonwane C.G. (2001). *Ind. Eng. Chem. Res.* 40, 3237–3261.
31. Soler-Illia G.J. de A.A., Sanchez C., Lebeau B., Patarin J. (2002). *Chem. Rev.* 102, 4093–4138.
32. Linssen T., Cassiers K., Cool P., Vansant E.F. (2003). *Adv. Colloid Interface Sci.* 103, 121–147.
33. Polarz S. In: *Encyclopedia of Nanoscience and Nanotechnology*, Vol. 8. Nalwa H.S., ed. American Scientific Publishers, Electronic edition, www.aspbs.com/enn, 2004, pp. 239–258.

34. Thomas J.M., Raja R. (2004). *Stud. Surf. Sci. Catal.* 148, 163–211.
35. Xiao F.-S. (2005). *Topics Catal.* 35, 9–24.
36. Taguchi A., Schüth F. (2005). *Micropor. Mesopor. Mater.* 77, 1–45.
37. Viswanathan B., Jacob B. (2005). *Catal. Rev. Sci. Eng.* 47, 1–82.
38. Di Renzo F., Galarneau A., Trens P., Fajula F. In: *Handbook of Porous Solids*, Vol. 3. Schüth F., Sing K.S.W., Weitkamp J., eds. Wiley-VCH, Weinheim, 2002, pp. 1311–1395.
39. Kleitz F. In: *Handbook of Heterogeneous Catalysis*, Vol. 1. Ertl G., Knözinger H, Schüth F, Weitkamp J., eds. Wiley-VCH, Weinheim, 2008, pp. 178–219.
40. Meynen V., Cool P., Vansant E.F. (2009). *Micropor. Mesopor. Mater.* 125, 170–223.
41. Wan Y., Zhao D. In: *Synthesis of Solid Catalysts*. de Jong K.P., ed. Wiley-VCH, Weinheim, 2009, pp. 277–300.
42. Martens J.A., Jammaer J., Bajpe S., Aerts A., Lorgouilloux Y., Kirschhock C.E.A. (2011). *Microp. Mesop. Mater.* 140, 2–8.
43. Edler K.J. In: *Porous Materials*. Bruce D.W., O'Hare D., Walton R.I., eds. Wiley, Chichester, 2011, pp. 69–146.
44. Iler R.K. *The Chemistry of Silica*, Vol. 2. Wiley-Interscience, New York, 1979, pp. 421–1120.
45. Don Tilley T. (2002). *J. Mol. Catal.* 182–183, 17–24.
46. Mutin P.H., Vioux A. (2009). *Chem. Mater.* 21, 582–596.
47. Miller J.B., Ko E.I. (1997). *Catal. Today* 35, 269–292.
48. Huo Q., Margolese D. I., Ciesla U., Feng P., Sieger P., Leon R., Petroff P., Schuth F., Stucky G.D. (1994). *Nature* 368, 317–321.
49. Hua Z., Bu W., Lian Y., Chen H., Li L., Zhang L., Li C., Shi J. (2005). *J. Mater. Chem.* 15, 661–665.
50. Maschmeyer T., Rey F., Sanker G., Thomas J.M. (1995). *Nature* 378, 159–162.
51. Coperet C., Chabanas M., Saint-Arroman M.P., Basset J.M. (2003). *Angew. Chem. Int. Ed.* 42, 156–181.
52. Anwander R. (2001). *Chem. Mater.* 13, 4419–4438.
53. Basset J.-M, Choplin A. (1983). *J. Mol. Catal.* 21, 95–108.
54. Ermakov Yu.I. (1983). *J. Mol. Catal.* 21, 35–55.
55. Thomas J.M. (1988). *Angew. Chem. Int. Ed.* 27, 1673–1691.
56. Thomas J.M. *Design and Applications of Single-site Heterogeneous Catalysts: Contributions to Green Chemistry, Clean Technology and Sustainability*. Imperial College Press, London, UK, 2012.
57. Jarupatrakorn J., Don Tilley T. (2002). *J. Am. Chem. Soc.* 124, 8380–8388.
58. *Proc. R. Soc. A* 468 (2012). *Special issue on Recent Advances in Single-site Heterogeneous Catalysts*. Thomas J.M., ed
59. Kruk M., Jaroniec M., Ko C.H., Ryoo R. (2000). *Chem. Mater.* 12, 1961–1968.
60. Kruk M., Jaroniec M., Sayari A. (1997). *Langmuir* 13, 6267–6273.
61. Ravikovitch P.I., Wei D., Chueh W.T., Haller G. L., Neimark A.V. (1997). *J. Phys. Chem. B* 101, 3671–3679.
62. Fenelonov V.B., Romannikov V.N., Derevyankin A.Y. (1999). *Micropor. Mesopor. Mater.* 28, 57–72.

63. Kruk M., Jaroniec M., Sakamoto Y., Terasaki O., Ryoo R., Ko C.H. (2000). *J. Phys. Chem. B* 104, 292–301.
64. Cassiers K., Linssen T., Mathieu M., Benjelloun M., Schrijnemakers K., Van Der Voort P., Cool P., Vansant E.F. (2002). *Chem. Mater.* 14, 2317–2324.
65. Busca G. In: *Metal Oxide Catalysis*, Vol. 1. Jackson S.D., Hargreaves J.S.J., eds. Wiley-VCH, Weinheim, 2009, pp. 95–176.
66. Trukhan N.N., Panchenko A.A., Roduner E., Melgunov M.S., Kholdeeva O.A., Mrowiec-Białoń J., Jarzębski A.B. (2005). *Langmuir* 21, 10545–10554.
67. Gianotti E., Bisio C., Marchese L., Guidotti M., Ravasio N., Psaro R., Coluccia S. (2007). *J. Phys. Chem. C* 111, 5083–5089.
68. Brinker C.J., Scherer G.W. *Sol-Gel Science – the Physics and Chemistry of Sol-gel Processing*. Academic Press, New York, 1990.
69. Corriu R., Anh N.T. *Molecular Chemistry of Sol-Gel Derived Nanomaterials*. Wiley, Chichester, 2009.
70. Miller J.B., Johnston S.T., Ko E.I. (1994). *J. Catal.* 150, 311–320.
71. Hutter R., Dutoit D.C.M., Mallat T., Schneider M., Baiker A. (1995). *J. Chem. Soc., Chem. Commun.*, 163–164.
72. Dutoit D.C.M., Schneider M., Baiker A. (1995). *J. Catal.* 153, 165–176.
73. Hutter R., Mallat T., Baiker A. (1995). *J. Catal.* 153, 177–189.
74. Dutoit D.C., Schneider M., Hutter R., Baiker A. (1996). *J. Catal.* 161, 651–658.
75. Dutoit D.C., Göbel U., Schneider M., Baiker A. (1996). *J. Catal.* 164, 433–439.
76. Hutter R., Mallat T., Dutoit D., Baiker A. (1996). *Topics Catal.* 3, 421–436.
77. Miller J.B., Rankin S.E., Ko E.I. (1994). *J. Catal.* 148, 673–682.
78. Müller C.A., Schneider M., Mallat T., Baiker A. (2000). *J. Catal.* 192, 448–451.
79. Beck C., Mallat T., Bürgi T., Baiker A. (2001). *J. Catal.* 204, 428–439.
80. Schubert U. (2005). *J. Mater. Chem.* 15, 3701–3715.
81. Brinker C.J., Keefer K.D., Schaefer D.W., Ashley C.S. (1982). *J. Non-Cryst. Solids* 48, 47–64.
82. Reale E., Leyva A., Corma A., Martınez C., Garcıa H., Rey F. (2005). *J. Mater. Chem.* 15, 1742–1754.
83. Mrowiec-Białoń J., Jarzębski A.B., Kholdeeva O.A., Trukhan N.N., Zaikovskii V.I., Kriventsov V.V., Olejniczak Z. (2004). *Appl. Catal. A: General* 273, 47–53.
84. Kholdeeva O.A., Trukhan N.N., Vanina M.P., Romannikov V.N., Parmon V.N., Mrowiec-Bialon J., Jarzebski A.B. (2002). *Catal. Today* 75, 203–209.
85. Mountjoy G., Pickup D.M., Wallidge G.W., Anderson R., Cole J.M., Newport R.J., Smith M.E. (1999). *Chem. Mater.* 11, 1253–1258.
86. Pickup D.M., Mountjoy G., Wallidge G.W., Anderson R., Cole J.M., Newporta R.J., Smith M.E. (1999). *J. Mater. Chem.* 9, 1299–1305.
87. Lafond V., Mutin P.H., Vioux A. (2002). *J. Mol. Catal. A: Chemical* 182–183, 81–88.
88. Lafond V., Mutin P.H., Vioux A. (2004). *Chem. Mater.* 16, 5380–5386.
89. Cojocariu A.M., Mutin P.H., Dumitriu E., Fajula F., Vioux A., Hulea V. (2008). *Chem. Commun.*, 5357–5359.
90. Cojocariu A.M., Mutin P.H., Dumitriu E., Aboulaich A., Vioux A., Fajula F., Hulea V. (2010). *Catal. Today* 157, 270–274.

91. Notari B. In: *Advances in Catalysis*, Vol. 41. Eley D.D., Haag W.O., Gates B.C., eds. Academic Press, San Diego, 1996, pp. 253–334.
92. Vayssilov G.N. (1997). *Catal. Rev. Sci. Eng.* 39, 209–251.
93. Ratnasamy P., Srinivas D., Knozinger H. (2004). *Adv. Catal.* 48, 1–169.
94. Kholdeeva O.A., Trukhan N.N. (2006). *Russ. Chem. Rev.* 75, 411–432.
95. Marchese L., Maschmeyer T., Gianotti E., Coluccia S., Thomas J.M. (1997). *J. Phys. Chem. B* 101, 8836–8838.
96. Carati A., Flego C., Previde Massara E., Millini R., Carluccio L., Bellussi G. (1999). *Micropor. Mesopor. Mater.* 30, 137–144.
97. Marchese L., Gianotti E., Dellarocca V., Maschmeyer T., Rey F., Coluccia S., Thomas J.M. (1999). *Phys. Chem. Chem. Phys.* 1, 585–592.
98. Gianotti E., Frache A., Coluccia S., Thomas J.M., Maschmeyer T., Marchese L. (2003). *J. Mol. Catal. A: Chemical* 204–205, 483–489.
99. Luan Z., Maes E.M., van der Heide P.A., Zhao D., Czernuszewicz R.S., Kevan L. (1999). *Chem. Mater.* 11, 3680–3686.
100. Aronson B.J., Blanford C.F., Stein A. (1997). *Chem. Mater.* 9, 2842–2851.
101. Thomas J.M., Sankar G. (2001). *Acc. Chem. Res.* 34, 571–581.
102. Morey M.S., O'Brien S., Schwarz S., Stucky G.D. (2000). *Chem. Mater.* 12, 898–911.
103. Newalkar B.L., Olanrewaju J., Komarneni S. (2001). *Chem. Mater.* 13, 552–557.
104. Trukhan N.N., Romannikov V.N., Shmakov A.N., Vanina M.P., Paukshtis E.A., Bukhtiyarov V.I., Kriventsov V.V., Danilov I.Yu., Kholdeeva O.A. (2003). *Micropor. Mesopor. Mater.* 59, 73–84.
105. Palazzi C., Oliva L., Signoretto M., Strukul G. (2000). *J. Catal.* 194, 286–293.
106. Morandin M., Gavagnin R., Pinna F., Strukul G. (2002). *J. Catal.* 212, 193–200.
107. Avendano R.G.R., De Los Reyes J.A., Viveros T., De La Fuente J.A.M. (2009). *Catal. Today* 148, 12–18.
108. Pires E.L., Arnold U., Schuchardt U. (2001). *J. Mol. Catal. A: Chemical* 169, 157–161.
109. Dutoit D.C.M., Schneider M., Fabrizioli P., Baiker A. (1996). *Chem. Mater.* 8, 734–743.
110. Somma F., Canton P., Strukul G. (2005). *J. Catal.* 229, 490–498.
111. Somma F., Strukul G. (2006). *Catal. Lett.* 107, 73–81.
112. Somma F., Strukul G. (2004). *J. Catal.* 227, 344–351.
113. Brutchey R.L., Lugmair C.G., Schebaum L.O., Don Tilley T. (2005). *J. Catal.* 229, 72–81.
114. Nozaki C., Lugmair C.G., Bell A.T., Don Tilley T. (2002). *J. Am. Chem. Soc.* 124, 13194–13203.
115. Fujdala K.L., Don Tilley T. (2001). *Chem. Mater.* 13, 1817–1827.
116. Brutchey R.L., Mork B.V., Sirbuly D.J., Yang P., Don Tilley T. (2005). *J. Mol. Catal. A: Chemical* 238, 1–12.
117. Monnier A., Schüth F., Huo Q., Kumar D., Magnolese D., Maxwell R.S., Stucky G.D., Krishnamurty M., Petroff P., Firouzi A., Janicke M., Chmelka B.F. (1993). *Science* 261, 1299–1303.
118. Firouzi A., Kumar D., Bull L.M., Besier T., Sieger P., Huo Q., Walker S.A., Zasadzinski J.A., Glinka C., Nicol J., Magnolese D., Stucky G.D., Chmelka B.F. (1995). *Science* 267, 1138–1143.

119. Sierra L., Guth J.-L. (1999). *Micropor. Mesopor. Mater.* 27, 243–253.
120. Kim J.M., Stucky G.D. (2000). *Chem. Commun.*, 1159–1160.
121. Kim S.-S., Pauly T.R., Pinnavaia T.J. (2000). *Chem. Commun.*, 1661–1662.
122. Pinnavaia T.J., Pauly T.R., Kim S.-S., inventors; Michigan State University, assignee. US Patent 6,607,705. 2003.
123. Boissiere C., Larbot A., Prouzet E. (2000). *Chem. Mater.* 12, 1937–1940.
124. Koyano K.A., Tatsumi T. (1997). *Micropor. Mater.* 10, 259–271.
125. Ryoo R., Kim J. M., Ko C.H., Shin C.H. (1996). *J. Phys. Chem.* 100, 17718–17721.
126. Collart O., Van Der Voort P., Vansant E.F., Desplantier-Gescard D., Galarneau A., Di Renzo F., Fajula F. (2001). *J. Phys. Chem. B* 105, 12771–12777.
127. Inagaki S., Fukushima Y., Kuroda K. (1993). *J. Chem. Soc., Chem. Commun.*, 680–682.
128. Galarneau A., Barodawalla A., Pinnavaia T.J. (1995). *Nature* 374, 529–531.
129. Zhang W., Fröba M., Wang J., Tanev P.T., Wong J., Pinnavaia T. (1996). *J. Am. Chem. Soc.* 118, 9164–9171.
130. Tanev P.T., Chibwe M., Pinnavaia T. (1994). *Nature* 368, 321–323.
131. Tanev P.T., Pinnavaia T.J. (1995). *Science* 267, 865–867.
132. Bagshaw S.A., Pouzet E., Pinnavaia T.J. (1995). *Science* 269, 1242–1244.
133. Zhao D., Feng J., Huo Q., Melosh N., Fredrickson G.H., Chmelka B.F., Stucky G.D. (1998). *Science* 279, 548–552.
134. Zhao D., Huo Q., Feng J., Chmelka B.F., Stucky G.D. (1998). *J. Am. Chem. Soc.* 120, 6024–6036.
135. Zhang W., Pinnavaia T.J. (1996). *Catal. Lett.* 38, 261–265.
136. Koyano K.A., Tatsumi T. (1996). *Chem. Commun.*, 145–146.
137. Solovyov L.A., Kirik S.D., Shmakov A.N., Romannikov V.N. (2001). *Micropor. Mesopor. Mater.* 44–45, 17–23.
138. Huo Q.S., Margolese D.I., Stucky G.D. (1996). *Chem. Mater.* 8, 1147–1160.
139. Tanev P.T., Pinnavaia T.J. (1996). *Chem. Mater.* 8, 2068–2079.
140. Kim S.S., Zhang W., Pinnavaia T.J. (1998). *Science* 282, 1302–1305.
141. Kim S.S., Liu Y., Pinnavaia T.J. (2001). *Micropor. Mesopor Mater.* 44, 489–498.
142. Jammaer J., Aerts A., D'Haen J., Seo J.W., Martens J.A. (2009). *J. Mater. Chem.* 19, 8290–8293.
143. Shan Z., Gianotti E., Jansen J.C., Peters J.A., Marchese L., Maschmeyer T. (2001). *Chem. Eur. J.* 7, 1437–1443.
144. Jansen J.C., Shan Z., Marchese L., Zhou W., Puil N. v. d., Th. Maschmeyer (2001). *Chem. Commun.*, 713–714.
145. Schmidt-Winkel P., Lukens W.W., Jr., Zhao D., Yang P., Chmelka B.F., Stucky G.D. (1999). *J. Am. Chem. Soc.* 121, 254–255.
146. Liu X., Tian B., Yu C., Gao F., Xie S., Tu B., Che R., Peng L.-M., Zhao D. (2002). *Angew. Chem. Int. Ed.* 41, 3876–3878.
147. Zhang W., Lu J., Han B., Li M., Xiu J., Ying P., Li C. (2002). *Chem. Mater.* 14, 3413–3421.
148. Chen Y., Huang Y., Xiu J., Han X., Bao X. (2004). *Appl. Catal. A: General* 273, 185–191.

149. Melero J.A., Arsuaga J.M., de Frutos P., Iglesias J., Sainz J., Blázquez S. (2005). *Micropor. Mesopor. Mater.* 86, 364–373.
150. Baes C.F., Mesmer R.E. *The Hydrolysis of Cations*. Wiley, New York, 1976.
151. Choi D.-G., Yang S.-M. (2003) *J. Colloid Interface Sci.* 261, 127–132.
152. Kholdeeva O.A., Mel'gunov M.S., Shmakov A.N., Trukhan N.N., Malishev M.E., Fenelonov V.B., Parmon V.N., Romannikov V.N., inventors; Boreskov Institute of Catalysis, assignee. RU Patent 2229930. 2003.
153. Mel'gunov M.S., Mel'gunova E.A., Shmakov A.N., Zaikovskii V.I. (2003). *Stud. Surf. Sci. Catal.* 146, 543–546.
154. Wu S., Han Y., Zou Y.C., Song J.W., Zhao L., Di Y., Liu S.Z., Xiao F.S. (2004). *Chem. Mater.* 16, 486–492.
155. Li Y., Zhang W.H., Zhang L., Wei Z., Yang Q., Feng Z., Li C. (2004). *J. Phys. Chem. B* 108, 9739–9744.
156. Kholdeeva O.A., Melgunov M.S., Shmakov A.N., Trukhan N.N., Kriventsov V.V, Zaikovskii V.I., Malyshev M.E., Romannikov V.N. (2004). *Catal. Today* 91–92, 205–209.
157. Selvaraj M., Kawi S. (2007). *Chem. Mater.* 19, 509–519.
158. Shah P., Ramaswamy A.V., Lazar K., Ramaswamy V. (2007). *Micropor. Mesopor. Mater.* 100, 210–226.
159. Timofeeva M.N., Mel'gunov M.S., Kholdeeva O.A., Malyshev M.E., Shmakov A.N., Fenelonov V.B. (2007). *Appl. Catal. B: Environ.* 75, 290–297.
160. Lou Z., Wang R., Sun H., Chen Y., Yang Y. (2008). *Micropor. Mesopor. Mater.* 110, 347–354.
161. Mu Z., Li J.J., Hao Z.P., Qiao S.Z. (2008). *Micropor. Mesopor. Mater.* 113, 72–80.
162. Romannikov V.N., Mel'gunov M.S., Shmakov A.N., Malyshev M.E., Vodennikov A.N., Fenelonov V.B. (2008). *Rus. Chem. Bull., Int. Ed.* 57, 29–35.
163. Kholdeeva O.A., Zalomaeva O.V., Melgunov M.S., Sorokin A.B. (2005). *J. Catal.* 236, 62–68.
164. Li Y., Feng Z., Lian Y., Sun K., Zhang L., Jia G., Yang Q., Li C. (2005). *Micropor. Mesopor. Mater.* 84, 41–49.
165. Selvaraj M., Kawi S. (2007). *J. Mater. Chem.* 17, 3610–3621.
166. Selvaraj M., Kawi S., Park D.-W., Ha C.S. (2009). *J. Phys. Chem. C* 113, 7743–7749.
167. Selvaraj M., Lee T.G. (2006). *J. Phys. Chem. B* 110, 21793–21802.
168. Corma A., Navarro M.T., Perez-Pariente J. (1994). *J. Chem. Soc., Chem. Commun.*, 147–148.
169. Blasco T., Corma A., Navarro M.T., Pérez-Pariente J. (1995). *J. Catal.* 156, 65–74.
170. Alba M.D., Luan Z., Klinowski J. (1996). *J. Phys. Chem.* 100, 2178–2182.
171. Bagshaw S.A., Di Renzo F., Fajula F. (1996). *Chem. Commun.*, 2209–2210.
172. Selvaraj M., Kandaswamy M., Park D.W., Ha C.S. (2010). *Catal. Today* 158, 377–384.
173. Ji D., Ren T., Yan L., Suo J. (2003). *Mater. Lett.* 57, 4474–4477.
174. Shan Z., Jansen J.C., Marchese L., Maschmeyer T. (2001). *Micropor. Mesopor. Mater.* 48, 181–187.
175. Trukhan N.N., Derevyankin A.Yu., Shmakov A.N., Paukshtis E.A., Kholdeeva O.A., Romannikov V.N. (2001). *Micropor. Mesopor. Mater.* 44–45, 603–608.

176. Kholdeeva O.A., Derevyankin A.Yu., Shmakov A.N., Trukhan N.N., Paukshtis E.A., Tuel A., Romannikov V.N. (2000). *J. Mol. Catal. A: Chemical* 158, 417–421.
177. Poladi R.H.P.R., Landry C.C. (2002). *Micropor. Mesopor. Mater.* 52, 11–18.
178. Ahn W.-S., Kim N.-K., Jeong S.-Y. (2001). *Catal. Today* 68, 83–88.
179. Wu P., Sugiyama H., Tatsumi T. (2003). *Stud. Surf. Sci. Catal.* 146, 613–616.
180. Han Y., Xiao F.-S., Wu S., Sun Y., Meng X., Li D., Lin S., Deng F., Ai X. (2001). *J. Phys. Chem. B* 105, 7963–7966.
181. Hüsing N., Launay B., Doshi D., Kickelbick G. (2002). *Chem. Mater.* 14, 2429–2432.
182. Mori K., Kondo Y., Morimoto S., Yamashita H. (2008). *J. Phys. Chem. C* 112, 397–404.
183. Barmatova M.V., Ivanchikova I.D., Kholdeeva O.A., Zaikovskii V.I., Shmakov A.N., Mel'gunov M.S. (2009). *Catal. Lett.* 127, 75–82.
184. Barmatova M.V., Ivanchikova I.D., Kholdeeva O.A., Shmakov A.N., Zaikovskii V.I., Mel'gunov M.S. (2009). *J. Mater. Chem.* 19, 7332–7339.
185. Gontier S., Tuel A. (1996). *Appl. Catal. A: General* 143, 125–135.
186. Wang X.X., Lefebvre F., Patarin J., Basset J.-M. (2001). *Micropor. Mesopor. Mater.* 42, 269–276.
187. Jones D.J., Jiménez-Jiménez J., Jiménez-López A., Maireles-Torres P., Olivera-Pastor P., Rodríguez-Castellón E., Rozière J. (1997). *J. Chem. Soc., Chem. Commun.*, 431–432.
188. Wong M.S., Huang H.C., Ying J.Y. (2002). *Chem. Mater.* 14, 1961–1973.
189. Morey M.S., Stucky G.D., Schwarz S., Fröba M. (1999). *J. Phys. Chem. B* 103, 2037–2041.
190. Newalkar B.L., Olanrewaju J., Komarneni S. (2001). *J. Phys. Chem. B* 105, 8356–8360.
191. Szczodrowski K., Prélot B., Lantenois S., Zajac J., Lindheimer M., Jones D., Julbe A., van der Lee A. (2008). *Micropor. Mesopor. Mater.* 110, 111–118.
192. Chen S.-Y., Jang L.-Y., Cheng S. (2004). *Chem. Mater.* 16, 4174–4180.
193. Infantes-Molina A., Mérida-Robles J., Maireles-Torres P., Finocchio E., Busca G., Rodríguez-Castellón E., Fierro J.L.G., Jiménez-López A. (2004). *Micropor. Mesopor. Mater.* 75, 23–32.
194. Ramanathan A., Villalobos M.C.C., Kwakernaak C., Telalovic S., Hanefeld U. (2008). *Chem. Eur. J.* 14, 961–972.
195. Das T.K., Chaudhari K., Chandwadkar A.J., Sivasanker S. (1995). *J. Chem. Soc., Chem. Commun.*, 2495–2496.
196. Abdel-Fattah T.M., Pinnavaia T.J. (1996). *Chem. Commun.*, 665–666.
197. Chaudhari K., Das T.K., Rajmohanan P.R., Lazar K. (1999). *J. Catal.* 183, 281–291.
198. Corma A., Navarro M.T., Nemeth L., Renz M. (2001). *Chem. Commun.*, 2190–2191.
199. Sasidharan M., Kiyozumi Y., Mal N.K., Paul M., Rajamohanan P.R., Bhaumik A. (2009). *Micropor. Mesopor. Mater.* 126, 234–244.
200. Laha S.C., Mukherjee P., Sainkar S.R., Kumar R. (2002). *J. Catal.* 207, 213–223.
201. Yao W., Chen Y., Min L., Fang H., Yan Z., Wang H., Wang J. (2006). *J. Mol. Catal. A: Chemical* 246, 162–166.
202. Dai Q., Wang X., Chen G., Zheng Y., Lu G. (2007). *Micropor. Mesopor. Mater.* 100, 268–275.
203. Selvaraj M., Park D.-W., Ha C.S. (2011). *Micropor. Mesopor. Mater.* 138, 94–101.

204. van de Water L.G.A., Bulcock S., Masters A.F., Maschmeyer T. (2007). *Ind. Eng. Chem. Res.* 46, 4221–4225.
205. Reddy K.M., Moudrakovski I., Sayari A. (1994). *J. Chem. Soc., Chem. Commun.*, 1059–1060.
206. Reddy J.S., Sayari A. (1995). *J. Chem. Soc., Chem. Commun.*, 2231–2232.
207. Gontier S., Tuel A. (1995). *Micropor. Mater.* 5, 161–171.
208. Reddy S.J., Ping L., Sayari A. (1996). *Appl. Catal. A: General* 148, 7–21.
209. Luan Z., Xu J., He H., Klinowski J., Kevan L. (1996). *J. Phys. Chem.* 100, 19595–19602.
210. Chao K.J., Wu C.N., Chang H., Lee L.J., Hu S. (1997). *J. Phys. Chem. B* 101, 6341–6349.
211. Zhang W., Wang J., Tanev P.T., Pinnavaia T.J. (1996). *Chem. Commun.*, 979–980.
212. Wei D., Wang H., Feng X., Chueh W.-T., Ravikovitch P., Lyubovsky M., Li C., Takeguchi T., Haller G.L. (1999). *J. Phys. Chem. B* 103, 2113–2121.
213. Chatterjee M., Iwasaki T., Hayashi H., Onodera Y., Ebina T., Nagase T. (1999). *Chem. Mater.* 11, 1368–1375.
214. Selvam P., Dapurkar S.E. (2005). *J. Catal.* 229, 64–71.
215. Shylesh S., Singh A.P. (2005). *J. Catal.* 233, 359–371.
216. Shiraishi Y., Morishita M., Teshima Y., Hirai T. (2006). *J. Phys. Chem. B* 110, 6587–6594.
217. Mathieu M., Van Der Voort P., Weckhuysen B.M., Rao R.R., Catana G., Schoonheydt R.A., Vansant E.F. (2001). *J. Phys. Chem. B* 105, 3393–3399.
218. Selvam P. Dapurkar S.E. (2004). *Appl. Catal. A: General* 276, 257–265.
219. Dai L.-X., Tabata K., Suzuki E., Tatsumi T. (2001). *Chem. Mater.* 13, 208–212.
220. Gao F., Zhang Y., Wan H., Kong Y., Wu X., Dong L., Li B., Chen Y. (2008). *Micropor. Mesopor. Mater.* 110, 508–516.
221. Selvaraj M., Park D.W. (2010). *Appl. Catal. A: General* 388, 22–30.
222. Eckert H., Wachs I.E. (1989). *J. Phys. Chem.* 93, 6796–6805.
223. Zhang L., Ying J.Y. (1997). *AIChE J.* 43, 2793–2801.
224. Ziolek M., Nowak I. (1997). *Zeolites* 18, 356–360.
225. Gao X., Wachs I.E., Wong M.S., Ying J.Y. (2001). *J. Catal.* 203, 18–24.
226. Ziolek M., Sobczak I., Lewandowska A., Nowak I., Decyk P., Renn M., Jankowska B. (2001). *Catal. Today* 70, 169–181.
227. Ziolek M. (2003). *Catal. Today* 78, 47–64.
228. Nowak I., Kilos B., Ziolek M., Lewandowska A. (2003). *Catal. Today* 78, 487–498.
229. Kilos B., Aouine M., Nowak I., Ziolek M., Volta J.C. (2004). *J. Catal.* 224, 314–325.
230. Kilos B., Tuel A., Ziolek M., Volta J.C. (2006). *Catal. Today* 118, 416–424.
231. Trejda M., Tuel A., Kujawa J., Kilos B., Ziolek M. (2008). *Micropor. Mesopor. Mater.* 110, 271–278.
232. Feliczak-Guzik A., Nowak I. (2009) *Catal. Today* 142, 288–292.
233. Ulagappan N., Rao C.N.R. (1996). *Chem. Commun*, 1047–1048.
234. Zhu Z., Chang Z., Kevan L. (1999). *J. Phys. Chem. B* 103, 2680–2688.
235. Sakthivel A., Selvam P. (2002). *J. Catal.* 211, 134–143.

236. Mohapatra S.K., Selvam P. (2007). *J. Catal.* 249, 394–396.
237. Wang Y., Ohishi Y., Shishido T., Zhang Q., Yang W., Guo Q., Wan H., Takehira K. (2003). *J. Catal.* 220, 347–357.
238. Samanta S., Mal N.K., Bhaumik A. (2005). *J. Mol. Catal. A: Chemical* 236, 7–11.
239. Selvaraj M., Kawi S. (2007). *Micropor. Mesopor. Mater.* 101, 240–249.
240. Selvaraj M., Kandaswamy M., Park D.W., Ha C.S. (2010). *Catal. Today* 158, 286–295.
241. Richens D.T. *The Chemistry of Aqua Ions: Synthesis, Structure and Reactivity: A Tour Through the Periodic Table of the Elements*. Wiley-VCH, New York, 1997, pp. 323–327.
242. Maksimovskaya R.I., Maksimov G.M. (2007). *Inorg. Chem.* 46, 3688–3695.
243. Rana R.K., Viswanathan B. (1998). *Catal. Lett.* 52, 25–29.
244. Morey M.S., Davidson A., Stucky G.D. (1998). *J. Porous Mater.* 5, 195–204.
245. Che S., Sakamoto Y., Yoshitake H., Terasaki O., Tatsumi T. (2001). *J. Phys. Chem. B* 105, 10565–10572.
246. Higashimoto S., Hua Y., Tsumura R., Iino K., Matsuoka M., Yamashita H., Shul Y.G., Che M., Anpo M. (2005). *J. Catal.* 235, 272–278.
247. Zhang Z., Suo J., Zhang X., Li S. (1998). *Chem. Commun.*, 241–242.
248. Briot E., Piquemal J.-Y., Vennat M., Bregeault J.-M., Chottard G., Manoli J.-M. (2000). *J. Mater. Chem.* 10, 953–958.
249. Dai W.-L., Chen H., Cao Y., Li H., Xie S., Fan K. (2003). *Chem. Commun.*, 892–893.
250. Klepel O., Böhlmann W., Ivanov E.B., Riede V., Papp H. (2004). *Micropor. Mesopor. Mater.* 76, 105–112.
251. Yang X.-L., Dai W.-L., Gao R., Chen H., Li H., Cao Y., Fan K. (2005). *J. Mol. Catal. A: Chemical* 241, 205–214.
252. Yang X.-L., Dai W.-L., Chen H., Xu J.-H., Cao Y., Li H., Fan K. (2005). *Appl. Catal. A: General* 283, 1–8.
253. Yang X.-L., Dai W.-L., Chen H., Xu J.-H., Cao Y., Li H., He H., Fan K. (2005). *J. Catal.* 229, 259–263.
254. Gao R., Yang X., Dai W.-L., Le Y., Li H., Fan K. (2008). *J. Catal.* 256, 259–267.
255. Zhao D., Rodriguez A., Dimitrijevic N.M., Rajh T., Koodali R.T. (2010). *J. Phys. Chem. C* 114, 15728–15734.
256. Ke I.-S., Liu S.-T. (2007). *Appl. Catal. A: General* 317, 91–96.
257. Yuan Z.Y., Liu S.H., Chen T.H., Wang J.Z., Li H.X. (1995). *J. Chem. Soc., Chem. Commun.*, 973–974.
258. He N.-Y., Bao S.-L., Xu Q.-H. (1998). *Stud. Surf. Sci. Catal.* 105, 85–92.
259. Tuel A., Gontier S. (1996). *Chem. Mater.* 8, 114–122.
260. Wang Y., Zhang Q., Shishido T., Takehira K. (2002). *J. Catal.* 209, 186–196.
261. Samanta S., Giri S., Sastry P.U., Mal N.K., Manna A., Bhaumik A. (2003). *Ind. Eng. Chem. Res.* 42, 3012–3018.
262. Vinu A., Sawant D.P., Ariga K., Hossain K.Z., Halligudi S.B., Hartmann M., Nomura M. (2005). *Chem. Mater.* 17, 5339–5345.
263. Vinu A., Krithiga T., Balasubramanian V.V., Asthana A., Srinivasu P., Mori T., Ariga K., Ramanath G., Ganesan P.G. (2006). *J. Phys. Chem. B* 110, 11924–11931.

264. Bordiga S., Buzzoni R., Geobaldo F., Lamberti C., Giamello E., Zecchina A., Leofanti G., Petrini G., Tozzola G. (1996). *J. Catal.* 158, 486–501.

265. Selvam P., Dapurkar S.E., Badamali S.K., Murugasan M., Kuwano H. (2001). *Catal. Today* 68, 69–74.

266. Goldfarb D., Bernard M., Strohmainer K.G., Vaughan D.E.W., Thomann H. (1994). *J. Am. Chem. Soc.* 116, 6344–6353.

267. Berlier G., Pourny M., Bordiga S., Spoto G., Zecchina A., Lamberti C. (2005). *J. Catal.* 229, 45–54.

268. Badamali S.K., Selvam P. (2009). *Catal. Today* 141, 103–108.

269. Zhao D., Goldfarb D. (1995). *J. Chem. Soc., Chem. Commun.*, 875–876.

270. Zhang Q., Wang Y., Itsuki S., Shishido T., Takehira K. (2002). *J. Mol. Catal. A: Chemical* 188, 189–200.

271. Xu J., Luan Z., Hartman M., Kevan L. (1999). *Chem. Mater.* 11, 2928–2936.

272. Zhang J., Goldfarb D. (2000). *J. Am. Chem. Soc.122*, 7034–7041.

273. Ramanathan A., Archipov T., Maheswari R., Hanefeld U., Roduner E., Gla1ser R. (2008). *J. Phys. Chem. C* 112, 7468–7476.

274. Jentys A., Pham N.H., Vinek H., Englisch M., Lercher J.A. (1996). *Micropor. Mater.* 6, 13–17.

275. Vinu A., Dedecek J., Murugesan V., Hartmann M. (2002). *Chem. Mater.* 14, 2433–2435.

276. Hamdy M.S., Ramanathan A., Maschmeyer T., Hanefeld U., Jansen J.C. (2006). *Chem. Eur. J.* 12, 1782–1789.

277. Vrålstad T., Glomm W.R., Rønning M., Dathe H., Jentys A., Lercher J.A., Øye G., Stöcker M., Sjöblom J. (2006). *J. Phys. Chem. B* 110, 5386–5394.

278. Vrålstad T., Øye G., Stöcker M., Sjöblom J. (2007). *Micropor. Mesopor. Mater.* 104, 10–17.

279. Lim S., Ciuparu D., Yang Y., Du G., Pfefferle L.D., Haller G.L. (2007). *Micropor. Mesopor. Mater.* 101, 200–206.

280. Tsai C.-L., Chou B., Cheng S., Lee J.-F. (2001). *Appl. Catal. A: General* 208, 279–289.

281. Sobczak I., Ziolek M., Renn M., Decyk P., Nowak I., Daturi M., Lavalley J.-C. (2004). *Micropor. Mesopor. Mater.* 74, 23–36.

282. Wang L., Kong A., Chen B., Ding H., Shan Y., He M. (2005). *J. Mol. Catal. A: Chemical* 230, 143–150.

283. Fraile J.M., Garcia J.I., Moyoral J.A., Vispe E., Brown D.R., Naderi M. (2001). *Chem. Commun.*, 1510–1511.

284. Bourlinos A.B., Karakassides M.A., Petridis D. (2000). *J. Phys. Chem. B* 104, 4375–4380.

285. Kawabata T., Ohishi Y., Itsuki S., Fujisaki N., Shishido T., Takaki K., Zhang Q., Wang Y., Takehira K. (2005). *J. Mol. Catalysis A: Chemical* 236, 99–106.

286. Yonemitsu M., Tanaka Y., Iwamoto M. (1998). *J. Catal.* 178, 207–213.

287. Gómez S., Giraldo O., Garcés L.J., Villegas J., Suib S.L. (2004). *Chem. Mater.* 16, 2411–2417.

288. Sheldon R.A. (1980). *J. Mol. Catal.* 7, 107–126.

289. Wulff H.P., Wattimena F., inventors; Shell Oil Co., assignee. US Patent 4,021,454. 1977.
290. Buijink J.K.F., VanVlaanderen J.J.M., Crocker M., Niele F.G.M. (2004). *Catal. Today* 93–95, 199–204.
291. Sheldon R.A., van Vliet M.C.A. In: *Fine Chemicals through Heterogeneous Catalysis*. Sheldon R.A., van Bekkum H., eds. Wiley-VCH, Weinheim, 2001, pp. 473–490.
292. Chiker F., Nogier J.Ph., Launay F., Bonardet J.L. (2003). *Appl. Catal. A: General* 243, 309–321.
293. Chiker F., Launay F., Nogier J.P., Bonardet J.L. (2003). *Green Chem*. 5, 318–322.
294. Chiker F., Nogier J.P., Launay F., Bonardet J.L. (2004). *Appl. Catal. A: General* 259, 153–162.
295. Li K.T., Lin C.C. (2004). *Catal. Today* 97, 257–261.
296. Yao J., Zhan W., Liu X., Guo Y., Wang Y., Guo Y., Lu G. (2012). *Micropor. Mesopor. Mater.* 148, 131–136.
297. Li K.T., Chen I.C. (2002). *Ind. Eng. Chem. Res.* 41, 4028–4034.
298. Srinivasan S., Datye A.K., Smith M.H., Peden C.H.F. (1994). *J. Catal.* 145, 565–573.
299. Fraile J.M., Garcia J.I., Mayoral J.A., de Menorval L.C., Rachdi F. (1995). *J. Chem. Soc., Chem. Commun.*, 539–540.
300. Bouh A.O., Rice G.L., Scott S.L. (1999). *J. Am. Chem. Soc.* 121, 7201–7210.
301. Maksimchuk N.V., Melgunov M.S., Mrowiec-Białoń J., Jarzębski A.B., Kholdeeva O.A. (2005). *J. Catal.* 235, 175–183.
302. Capel-Sanchez M.C., Campos-Martin J.M., Fierro J.L.G. (2003). *J. Catal.* 217, 195–202.
303. Fraile J.M., Garcia J.I., Mayoral J.A., Vispe E. (2003). *Appl. Catal. A General* 245, 363–376.
304. Ahn W.S., Lee D.H., Kim J.H., Seo G., Ryoo R. (1999). *Appl. Catal. A: General* 181, 39–49.
305. Van der Voort P., Morey M., Stucky G.D., Mathieu M., Vansant E.F. (1998). *J. Phys. Chem. B* 102, 585–590.
306. Van Der Voort P., Baltes M., Vansant E.F. (2001). *Catal. Today* 68, 119–128.
307. Shylesh S., Singh A.P. (2004). *J. Catal.* 228, 333–346.
308. Yang Q., Li C., Yuan S., Li J., Ying P., Xin Q., Shi W. (1999). *J. Catal.* 183, 128–130.
309. Wu P., Tatsumi T., Komatsu T., Yashima T. (2002). *Chem. Mater.* 14, 1657–1664.
310. Capel-Sanchez M.C., Blanco-Brieva G., Campos-Martin J.M., de Frutos M.P., Wen W., Rodriguez J.A., Fierro J.L.G. (2009). *Langmuir* 25, 7148–7155.
311. Guidotti M., Conti L., Fusi A., Ravasio N., Psaro R. (2002). *J. Mol. Catal. A Chemical* 182–183, 151–156.
312. Guidotti M., Ravasio N., Psaro R., Ferraris G., Moretti G. (2003). *J. Catal.* 214, 242–250.
313. Kholdeeva O.A., Ivanchikova I.D., Guidotti M., Pirovano C., Ravasio N., Barmatova M.V., Chesalov Y.A. (2009). *Adv. Synth. Catal.* 351, 1877–1889.
314. Tuel A., Hubert-Pfalzgraf L.G. (2003). *J. Catal.* 217, 343–353.
315. Mimura N., Tsubota S., Murata K., Bando K.K., Bravo-Suárez J.J., Haruta M., Oyama S.T. (2006). *Catal. Lett.* 110, 47–51.

316. Shannon I.J., Maschmeyer T., Oldroyd R.D., Sankar G., Thomas J.M., Pernot H., Balikdjian J.P., Che M. (1998). *J. Chem. Soc., Faraday Trans.* 94, 1495–1499.
317. Oldroyd R.D., Sankar G., Thomas J.M., Hunnius M., Maier W.F. (1998). *J. Chem. Soc., Faraday Trans.* 94, 3177–3182.
318. Kang K.K., Ahn W.S. (2000). *J. Mol. Catal. A: Chemical* 159, 403–410.
319. Kim N.K., Kim G.J., Ahn W.S. (2000). *React. Kinet. Catal. Lett.* 71, 273–279.
320. Quignard F., Choplin A., Teissier R. (1997). *J. Mol. Catal. A: Chemical* 120, L27–L31.
321. Corma A., Navarro M.T., Renz M. (2003). *J. Catal.* 219, 242–246.
322. Boronat M., Concepcion P., Corma A., Navarro M.T., Renz M., Valencia S. (2009). *Phys. Chem. Chem. Phys.* 11, 2876–2884.
323. Wang X., Xua H., Fua X., Liu P., Lefebvre F., Basset J.-M. (2005). *J. Mol. Catal. A: Chemical* 238, 185–191.
324. Petroff Saint-Arroman R., Didillon B., de Mallmann A., Basset J.M., Lefebvre F. (2008). *Appl. Catal. A: General* 337, 78–85.
325. Morlanes N., Notestein J.M. (2010). *J. Catal.* 275, 191–201.
326. Stein A., Melde B.J., Schroden R.C. (2000). *Adv. Mater.* 12, 1403–1419.
327. Sayari A., Hamoudi S. (2001). *Chem. Mater.13*, 3151–3168.
328. Wight A.P., Davis M.E. (2002). *Chem. Rev.* 102, 3589–3614.
329. Hoffmann F., Cornelius M., Morell J., Fröba M. (2006). *Angew. Chem. Int. Ed.* 45, 3216–3251.
330. Hüsing N. In: *Hybrid Materials: Synthesis, Characterization, and Applications*. Kickelbick G., ed. Wiley-VCH, Weinheim, 2007, pp. 175–223.
331. Tatsumi T., Koyano K.A., Igarashi N. (1998). *Chem. Commun.*, 325–326.
332. Corma A., Domine M., Gaona J.A., Jorda J.L., Navarro M.T., Rey F., Perez-Pariente J., Tsuji J., McCulloch B., Neneth L.T. (1998). *Chem. Commun.*, 2211–2212.
333. Koyano K.A., Tatsumi T., Tanaka Y., Nakata S. (1997). *J. Phys. Chem. B* 101, 9436–9440.
334. Pena M.L., Dellarocca V., Rey F., Corma A., Coluccia S., Marchese L. (2001). *Micropor. Mesopor. Mater.* 44–45, 345–356.
335. Prasad M.R., Hamdy M.S., Mul G., Bouwman E., Drent E. (2008). *J. Catal.* 260, 288–294.
336. Kochkar H., Figueras F. (1997). *J. Catal.* 171, 420–430.
337. Müller C.A., Maciejewski M., Mallat T., Baiker A. (1999). *J. Catal.* 184, 280–293.
338. Müller C.A., Deck R., Mallat T., Baiker A. (2000). *Topics Catal.* 11/12369–378.
339. Dusi M., Mallat T., Baiker A. (1999). *J. Catal.* 187, 191–201.
340. Lorret O., Lafond V., Mutin P.H., Vioux A. (2006). *Chem. Mater.* 18, 4707–4709.
341. Bhaumik A., Tatsumi T. (2000). *J. Catal.* 189, 31–39.
342. Lin K., Pescarmona P.P., Houthoofd K., Liangb D., Van Tendeloo G., Jacobs P.A. (2009). *J. Catal.* 263, 75–82.
343. Iglesias J., Melero J.A., Sainz-Pardo J. (2008). *J. Mol. Catal. A: Chemical* 291, 75–84.
344. Shylesh S., Samuel P.P., Singh A.P. (2007). *Appl. Catal. A: General* 318, 128–136.
345. Chen C., Xu J., Zhang Q., Ma H., Miao H., Zhou L. (2009). *J. Phys. Chem. C* 113, 2855–2860.

346. Chandra D., Laha S.C., Bhaumik A. (2008). *Appl. Catal. A: General* 342, 29–34.
347. Asefa T., MacLachlan M.J., Coombs N., Ozin G.A. (1999). *Nature* 402, 867–871.
348. Inagaki S., Guan S., Fukushima Y., Ohsuna T., Terasaki O. (1999). *J. Am. Chem. Soc.* 121, 9611–9614.
349. Inagaki S., Guan S., Ohsuna T., Terasaki O. (2002). *Nature* 416, 304–307.
350. Kapoor M.P., Bhaumik A., Inagaki S., Kuraoka K., Yazawa T. (2002). *J. Mater. Chem.* 12, 3078–3083.
351. Bhaumik A., Kapoor M.P., Inagaki S. (2003). *Chem. Commun.*, 470–471.
352. Chu H., Wana Y., Zhao D. (2009). *Catal. Today* 148, 19–27.
353. Shylesh S., Srilakshmi Ch., Singh A.P., Anderson B.G. (2007). *Micropor. Mesopor. Mater.* 99, 334–344.
354. Sheldon R.A., Wallau M., Arends I.W.C.E., Schuchardt U. (1998). *Acc. Chem. Res.* 31, 485–493.
355. Musser M.T. Cyclohexanol and Cyclohexanone. In: *Ullmann's Encyclopedia of Industrial Chemistry*, electronic edition, Wiley-VCH, Weinheim, 2011.
356. Cavani F., Alini S. In: *Sustainable Industrial Processes*. Cavani F., Centi G., Perathoner S., Trifiro F., eds. Wiley-VCH, Weinheim, 2009, pp. 331–391.
357. Schuchardt U., Cardoso D., Sercheli R., Pereira R., da Cruz R.S., Guerreiro M.C., Mandelli D., Spinacé E.V., Pires E.L. (2001). *Appl. Catal. A: General* 211, 1–17.
358. Ramanathan A., Hamdy M.S., Parton R., Maschmeyer T., Jansen J.C., Hanefeld U. (2009). *Appl. Catal. A: General* 355, 78–82.
359. Turrà N., Acuña A.B., Schimmöller B., Mayr-Schmölzer B., Mania P., Hermans I. (2011). *Topics Catal*. 54, 737–745.
360. Li J., Shi Y., Xu L., Lu G. (2010). *Ind. Eng. Chem. Res.* 49, 5392–5399.
361. Singh A.P., Torita N., Shylesh S., Iwasa N., Arai M. (2009). *Catal. Lett.* 132, 492–499.
362. Qian G., Ji D., Lu G.-M., Zhao R., Qi Y.-X., Suo J.-S. (2005). *J. Catal.* 232, 378–385.
363. Hamdy M.S., Mul G., Wei W., Anand R., Hanefeld U., Jansen J.C., Moulijn J.A. (2005). *Catal. Today* 110, 264–271.
364. Anand R., Hamdy M.S., Gkourgkoulas P., Maschmeyer T., Jansen J.C., Hanefeld U. (2006). *Catal. Today* 117, 279–283.
365. Dapurkar S.E., Sakthivel A., Selvam P. (2004). *J. Mol. Catal. A: Chemical* 223, 241–250.
366. Dapurkar S.E., Sakthivel A., Selvam P. (2003). *New J. Chem.* 27, 1184–1190.
367. Shul'pin G.B. (2002). *J. Mol. Catal. A: Chemical* 189, 39–66.
368. Chen J.D., Sheldon R.A. (1995). *J. Catal.* 153, 1–8.
369. Bonon A.J., Mandelli D., Kholdeeva O.A., Barmatova M.V., Kozlov Y.N., Shul'pin G.B. (2009). *Appl. Catal. A: General* 365, 96–104.
370. George J., Shylesh S., Singh A.P. (2005). *Appl. Catal. A: General* 290, 148–158.
371. Srinivas N., Radha Rani V., Kulkarni S.J., Raghavan K.V. (2002). *J. Mol. Catal. A: Chemical* 179, 221–231.
372. Araújo R.S., Azevedo D.C.S., Rodrúguez-Castellón E., Jiménez-López A., Cavalcante C.L. Jr. (2008). *J. Mol. Catal. A: Chemical* 281, 154–163.
373. Anunziata O.S., Beltramone A.R., Cussa J. (2004). *Appl. Catal. A: General* 270, 77–85.

374. Yu W., Zhang Z., Wang H., Ge Z., Pinnavaia T.J. (2007). *Micropor. Mesopor. Mater.* 104, 151–158.

375. Navalon S., Alvaro M., Garcia H. (2010). *Appl. Catal. B: Environmental* 99, 1–26.

376. Ungureanu A., Trong On D., Dumitriu E., Kaliaguine S. (2003). *Appl. Catal. A: General* 254, 203–223.

377. Kholdeeva O.A., Romannikov V.N., Trukhan N.N., Parmon V.N., inventors; Boreskov Institute of Catalysis, assignee. RU Patent 2164510. 2000.

378. Trukhan N.N., Romannikov V.N., Paukshtis E.A., Shmakov A.N., Kholdeeva O.A. (2001). *J. Catal.* 202, 110–117.

379. Sorokin A., Tuel A. (2000). *Catal. Today* 57, 45–59.

380. Kholdeeva O.A., Ivanchikova I.D., Guidotti M., Ravasio N. (2007). *Green Chem.* 9, 731–733.

381. Kholdeeva O.A., Ivanchikova I.D., Guidotti M., Ravasio N., Sgobba M., Barmatova M. (2009). *Catal. Today* 141, 330–336.

382. Kholdeeva O.A., Zalomaeva O.V., Sorokin A.B., Ivanchikova I.D., Della Pina C., Rossi M. (2007). *Catal. Today* 121, 58–64.

383. Zalomaeva O.V., Trukhan N.N., Ivanchikova I.D., Panchenko A.A., Roduner E., Talsi E.P., Sorokin A.B., Rogov V.A., Kholdeeva O.A. (2007). *J. Mol. Catal. A: Chemical* 277, 185–192.

384. Strukul G., Somma F., Ballarini N., Cavani F., Frattini A., Guidetti S., Morselli D. (2009). *Appl. Catal. A: General* 356, 162–166.

385. Zalomaeva O.V., Kholdeeva O.A., Sorokin A.B. (2006). *Green Chem.* 8, 883–886.

386. Buijink J.K.F., Lange J.-P., Bos A.N.R., Horton A.D., Niele F.G.M. In: *Mechanisms in Homogeneous and Heterogeneous Epoxidation Catalysis.* Oyama S.T., ed. Elsevier, Amsterdam, 2008, pp. 356–371.

387. Cavani F., Gaffney A.M. In: *Sustainable Industrial Processes*. Cavani F., Centi G., Perathoner S., Trifiro F., eds. Wiley-VCH, 2009, pp. 287–337.

388. Chen L.Y., Chuah G.K., Jaenicke S. (1998). *J. Mol. Catal. A: Chemical* 132, 281–292.

389. Tsuji J., Yamamoto J., Corma A., Rey F.G., inventors; Sumitomo Chemical Company. US Patent 6,211,388. 2001.

390. Tuel A. (1998). *Stud. Surf. Sci. Catal.* 117, 159–170.

391. Eimer G.A., Díaz I., Sastre E., Casuscelli S.G., Crivello M.E., Herrero E.R., Perez-Pariente J. (2008). *Appl. Catal. A: General* 343, 77–86.

392. Chen L.Y., Chuah G.K., Jaenicke S. (1998). *Catal. Lett.* 50, 107–114.

393. Guidotti M., Pirovano C., Ravasio N., Lázaro B., Fraile J.M., Mayoral J.A., Coq B., Galarneau A. (2009). *Green Chem.* 11, 1421–1427.

394. Berlini C., Ferraris G., Guidotti M., Moretti G., Psaro R., Ravasio N. (2001). *Micropor. Mesopor. Mater.* 44–45, 595–602.

395. Dusi M., Mallat T., Baiker A. (2000). *Cat. Rev. -Sci. Eng.* 42, 213–278.

396. Berlini C., Guidotti M., Moretti G., Psaro R., Ravasio N. (2000). *Catal. Today* 60, 219–225.

397. Guidotti M., Ravasio N., Psaro R., Gianotti E., Marchese L., Coluccia S. (2006). *J. Mol. Catal. A: Chemical* 250, 218–225.

398. Guidotti M., Ravasio N., Psaro R., Gianotti E., Marchese L., Coluccia S. (2003). *Green Chem.* 5, 421–424.
399. Guidotti M., Psaro R., Ravasio N., Sgobba M., Gianotti E., Grinberg S. (2008). *Catal. Lett.* 122, 53–56.
400. Guidotti M., Gavrilova E., Galarneau A., Coq B., Psaro R., Ravasio N. (2011). *Green Chem.* 13, 1806–1811.
401. Vankelecom I., Vercruysse K., Moens N., Parton R., Reddy J.S., Jacobs P.A. (1997). *J. Chem. Soc., Chem. Commun.*, 137–138.
402. Guidotti M., Batonneau-Gener I., Gianotti E., Marchese L., Mignard S., Psaro R., Sgobba M., Ravasio N. (2008). *Micropor. Mesopor. Mater.* 111, 39–47.
403. Guidotti M., Moretti G., Psaro R., Ravasio N. (2000). *Chem. Commun.*, 1789–1790.
404. Quek X.-Y., Tang Q., Hu S., Yang Y. (2009). *Appl. Catal. A: General* 361, 130–136.
405. Lapisardi G., Chiker F., Launay F., Nogier J.-P., Bonardet J.-L. (2005). *Micropor. Mesopor. Mater.* 78, 289–295.
406. Timofeeva M.N., Kholdeeva O.A., Jhung S.H., Chang J.-S. (2008). *Appl. Catal. A: General* 345, 195–200.
407. Lee S.O., Raja R., Harris K.D.M., Tomas J.M., Johnson B.F.J., Sankar G. (2003). *Angew. Chem. Int. Ed.* 42, 1520–1523.
408. Cheng C.Y., Lin K.J., Prasad M.R., Fu S.J., Chang S.Y., Shyu S.G., Sheu H.S., Chen C.H., Chuang C.H., Lin M.T. (2007). *Catal. Commun.* 8, 1060–1064.
409. Yang X.-L., Gao R., Dai W.-L., Fan K. (2008). *J. Phys. Chem. C* 112, 3819–3826.
410. Sheldon R.A. In: *Fine Chemicals through Heterogeneous Catalysis.* Sheldon R.A., van Bekkum H., eds. Wiley-VCH, Weinheim, 2001, pp. 519–526.
411. Murphy E.F., Mallat T., Baiker A. (2000). *Catal. Today* 57, 115–126.
412. Sakthivel A., Dapurkar S.E., Selvam P. (2003). *Appl. Catal. A: General* 246, 283–293.
413. Dapurkar S.E., Kawanami H., Komura K., Yokoyama T., Ikushima Y. (2008). *Appl. Catal. A: General* 346, 112–116.
414. McMorn P., Roberts G., Hutchings G.J. (2000). *Catal. Lett.* 67, 203–206.
415. Robles-Dutenhefner P.A., Brandao B.B.N.S., de Sousa L.F., Gusevskaya E.V. (2011). *Appl. Catal. A: General* 399, 172–178.
416. Robles-Dutenhefner P.A., da Silva Rocha K.A., Sousa E.M.B., Gusevskaya E.V. (2009). *J. Catal.* 265, 72–79.
417. Mallat T., Baiker A. (2004). *Chem. Rev.* 104, 3037–3058.
418. Endud S., Wong K.-L. (2007). *Micropor. Mesopor. Mater.* 101, 256–263.
419. Li B., Wang J., Fu J., Wang J., Zou C. (2008). *Catal. Commun.* 9, 2000–2002.
420. ten Brink G.-J., Arends I.W.C.E., Sheldon R.A. (2004). *Chem. Rev.* 104, 4105–4123.
421. Subramanian H., Nettleton E.G., Budhi S., Koodali R.T. (2010). *J. Mol. Catal. A: Chemical* 330, 66–72.
422. Corma A., Nemeth L.T., Renz M., Valencia S. (2001). *Nature* 412, 423–425.
423. Corma A., Iborra S., Mifsud M., Renz M., Susarte M. (2004). *Adv. Synth. Catal.* 346, 257–262.
424. Corma A., Iborra S., Mifsud M., Renz M. (2005). *J. Catal.* 234, 96–100.

425. Clerici M.G. In: *Metal Oxide Catalysis*, Vol. 2. Jackson S.D., Hargreaves J.S.J., eds. Wiley-VCH, Weinheim, 2009, pp. 705–754.
426. Corma A., Iglesias M., Sanchez F. (1996). *Catal. Lett.* 39, 153–156.
427. Iwamoto M., Tanaka Y., Hirosumu J., Kita M., Triwahyono S. (2001). *Micropor. Mesopor. Mater.* 48, 271–277.
428. Cimpeanu V., Hardacre C., Parvulescu V.I., Thompson J.M. (2005). *Green Chem.* 7, 326–332.
429. Hulea V., Fajula F., Bousquet J. (2001). *J. Catal.* 198, 179–186.
430. Chica A., Corma A., Dómine M.E. (2006). *J. Catal.* 242, 299–308.
431. Capel-Sanchez M.C., Campos-Martin J.M., Fierro J.L.G. (2010). *Energy Environ. Sci.* 3, 328–333.
432. Reddy J.S., Sayari A. (1995). *Appl. Catal. A General* 128, 231–242.
433. Gontier S., Tuel A. (1995). *J. Catal.* 157, 124–132.
434. Besson M., Bonnet M.C., Gallezot P., Tkatchenko I., Tuel A. (1999). *Catal. Today* 51, 547–560.
435. Clerici M.G. In: *Proceedings of the DGMK/SCI Conference "Oxidation and Functionalisation: Classical and Alternative Routes and Sources"* October 12–142005, Milan, Italy, pp. 165–176.
436. Bordiga S., Bonino F., Damin A., Lamberti C. (2007). *Phys. Chem. Chem. Phys.* 9, 4854–4878.
437. Thomas J.M., Catlow R.C.A., Sankar G. (2002). *Chem. Commun.*, 2921–2925.
438. Sever R.R., Root T.W. (2003). *J. Phys. Chem. B* 107, 4080–4089.
439. Wells D.H., Jr., Delgass W.N., Thomson K.T. (2004). *J. Am. Chem. Soc.* 126, 2956–2962.
440. Maschmeyer T., Klunduk M.C., Martin C.M., Shephard D.S., Thomas J.M., Johnson B.F.G. (1997). *Chem. Commun.*, 1847–1848.
441. Crocker M., Herold R.H.M., Orpen A.G., Overgaag M.T.A. (1999). *J. Chem. Soc., Dalton Trans.*, 3791–3804.
442. Thomas J.M., Sankar G., Klunduk M.C., Attfield M.P., Maschmeyer T., Johnson B.F.G., Bell R.G. (1999). *J. Phys. Chem. B* 103, 8809–8813.
443. Abbenhuis H.C.L. (2000). *Chem. Eur. J.* 6, 25–32.
444. Quadrelli E.A., Basset J.-M. (2010). *Coord. Chem. Rev.* 254, 707–728.
445. Kholdeeva O.A. (2006). *Topics Catal.* 40, 229–243.
446. Kholdeeva O.A., Maksimovskaya R.I. (2007). *J. Mol. Catal. A: Chemical* 262, 7–24.
447. Kholdeeva O.A., Trubitsina T.A., Timofeeva M.N., Maksimov G.M., Maksimovskaya R.I., Rogov V.A. (2005). *J. Mol. Catal. A: Chemical* 232, 173–178.
448. Jiménez-Lozano P., Ivanchikova I.D., Kholdeeva O.A., Poblet J.M., Carbó J.J. (2012). *Chem. Commun.* 48, 9266–9268.
449. Kholdeeva O.A., Donoeva B.G., Trubitsina T.A., Al-Kadamany G., Kortz U. (2009). *Eur. J. Inorg. Chem*, 5134–5141.
450. Antonova N.S., Carbó J.J., Kortz U., Kholdeeva O., Poblet J.M. (2010). *J. Am. Chem. Soc.* 132, 7488–7497.
451. Kholdeeva O.A., Trubitsina T.A., Maksimovskaya R.I., Golovin A.V., Neiwert W.A., Kolesov B.A., López X., Poblet J.M. (2004). *Inorg. Chem.* 43, 2284–2292.

452. Berkessel A., Brandenburg M., Leitterstorf E., Frey J., Lex J., Schäfer M. A. (2007). *Adv. Synth. Catal.* 349, 2385–2391.
453. Cordeiro P.J., Don Tilley T. (2011). *ACS Catal.* 1, 455–467.
454. Viotti O., Seisenbaeva G.A., Kessler V.G. (2009). *Inorg. Chem.* 48, 9063–9065.
455. Boronat M., Concepción P., Corma A., Renz M., Valencia S. (2005). *J. Catal.* 234, 111–118.
456. Sever R.R., Root T.W. (2003). *J. Phys. Chem. B* 107, 10848–10862.
457. Sever R.R., Root T.W. (2003). *J. Phys. Chem. B* 107, 10521–10530.
458. Guisnet M., Guidotti M. In: *Catalysts for Fine Chemical Synthesis*. Vol. 4. *Micro and Mesoporous Solid Catalysts*. Derouane E., Roberts S.M., eds. Wiley-VCH Verlag, Weinheim, 2006, pp. 39–67.
459. Trimm D.L. (2001). *Appl. Catal. A: General* 212, 153–160.
460. *Recoverable and Recyclable Catalysts*. Benaglia M., ed. Wiley, Chichester, UK, 2009.
461. Galarneau A., Desplantier-Giscard D., di Renzo F., Fajula F. (2001). *Catal. Today* 68, 191–200.
462. Hagen A., Schueler K., Roessner F. (2002). *Micropor. Mesopor. Mater.* 51, 23–33.
463. Galacho C., Carrott M.M.L.R., Carrott P.J.M. (2008). *Micropor. Mesopor. Mater.* 108, 283–293.
464. Ryoo R., Kim J.M. (1995). *J. Chem. Soc., Chem. Commun.*, 711–712.
465. Zhao X.Z., Audsley F., Lu G.Q. (1998). *J. Phys. Chem. B* 102, 4143–4146.
466. Landau M.V., Varkey S.P., Herskowitz M., Regev O., Pevzner S., Sen T., Luz Z. (1999). *Micropor. Mesopor. Mater.* 33, 149–163.
467. Davidson A. (2002). *Curr. Opin. Colloid Interf. Sci.* 7, 92–106.
468. Igarashi N., Koyano K.A., Tanaka Y., Nakata S., Hashimoto K., Tatsumi T. (2003). *Micropor. Mesopor. Mater.* 59, 43–52.
469. Galarneau A., Driole M.-F., Petitto C., Chiche B., Bonelli B., Armandi M., Onida B., Garrone E., di Renzo F., Fajula F. (2005). *Micropor. Mesopor Mater.* 83, 172–180.
470. Kim J.M., Jun S., Ryoo R. (1999). *J. Phys. Chem. B* 103, 6200–6205.
471. Verlooy P., Aerts A., Lebedev O.I., Van Tendeloo G., Kirschhock C., Martens J.A. (2009). *Chem. Commun.*, 4287–4289.
472. Edler K.J., White J.W. (1999). *J. Mater. Chem.* 9, 2611–2615.
473. Mokaya R. (2001). *Chem. Commun.*, 933–934.
474. Deng Y., Lettmann C., Maier W.F. (2001). *Appl. Catal. A: General.* 214, 31–45.
475. Davies L.J., McMorn P., Bethell D., Bulman Page P.C., King F., Hancock F.E., Hutchings G.J. (2001). *J. Catal.* 198, 319–327.
476. Wang L., Zhang J., Chen F. (2009). *Micropor. Mesopor. Mater.* 122, 229–233.
477. Das D., Tsai C.M., Cheng S. (1999). *Chem. Commun.*, 473–474.
478. Chen L., Horiuchi T., Mori T., Maeda K. (1999). *J. Phys. Chem. B* 103, 1216–1222.
479. Kruk M., Jaroniec M., Sayari A. (1999). *Micropor. Mesopor. Mater.* 27, 217–229.
480. Zhang F., Yan Y., Yang H., Meng Y., Yu C., Tu B., Zhao D. (2005). *J. Phys. Chem. B* 109, 8723–8732.
481. Guo W.P., Li X., Zhao X.S. (2006). *Micropor. Mesopor. Mater.* 93, 285–293.
482. Shen S.C., Kawi S. (1999). *J. Phys. Chem. B* 103, 8870–8876.

483. Mokaya R. (2000). *J. Phys. Chem. B* 104, 8279–8286.
484. Kodenev E.G., Shmakov A.N., Derevyankin A.Yu., Lapina O.B., Romannikov V.N. (2000). *J. Mol. Catal. A: Chemical* 158, 349–354.
485. Han Y., Li N., Zhao L., Li D., Xu X., Wu S., Di Y., Li C., Zou Y., Yu Y., Xiao F.S. (2003). *J. Phys. Chem. B* 107, 7551–7556.
486. Shao Y., Wang L., Zhang J., Anpo M. (2008). *Micropor. Mesopor. Mater.* 109, 271–277.
487. Verhoef M.J., Kooyman P.J., van der Waal J.C., Rigutto M.S., Peters J.A., van Bekkum H. (2001). *Chem. Mater.* 13, 683–687.
488. Karlsson A., Stacker M., Schmidt R. (1999). *Microp. Mesop. Mater.* 27, 181–192.
489. Zhang Z., Han Y., Xiao F.S., Qiu S., Zhu L., Wang R., Yu Y., Zhang Z., Zou B., Wang Y., Sun H., Zhao D., Wei Y. (2001). *J. Am. Chem. Soc.* 123, 5014–5021.
490. Liu Y., Pinnavaia T.J. (2002). *Chem. Mater.* 14, 3–5.
491. Xiao F.S., Han Y., Yu Y., Meng X., Yang M., Wu S. (2002). *J. Am. Chem. Soc.* 124, 888–889.
492. Jin C., Li G., Wang X., Zhao L., Liu L., Liu H. (2007). *Chem. Mater.* 19, 1664–1670.
493. Jin C., Li G., Wang X., Wang Y., Zhao L., Sun D. (2008). *Micropor. Mesopor. Mater.* 111, 236–242.
494. M. Reichinger, W. Schmidt, M.W.E. van den Berg, A. Aerts, J.A. Martens, C.E.A. Kirschhock, H. Gies, W. Grünert (2010). *J. Catal.* 269, 367–375.
495. Trong On D., Kaliaguine S. (2002). *Angew. Chem. Int. Ed.* 41, 1036–1040.
496. Trong On D., Ungureanu A., Kaliaguine S. (2003). *Phys. Chem. Chem. Phys.* 5, 3534–3538.
497. Zamani S., Chiesa M., Meynen V., Xiao Y., Prélot B., Zajac J., Verpoort F., Cool P., Van Doorslaer S. (2010). *J. Phys. Chem. C* 114, 12966–12975.
498. Kisler J.M., Gee M.L., Stevens G.W., O'Connor A.J. (2003). *Chem. Mater.* 15, 619–624.

5

LIQUID PHASE OXIDATION OF ORGANIC COMPOUNDS BY SUPPORTED METAL-BASED CATALYSTS WITH A FOCUS ON GOLD

CRISTINA DELLA PINA,* ERMELINDA FALLETTA, AND MICHELE ROSSI

5.1 INTRODUCTION

Many years have gone by since the first reports on CO oxidation and liquid phase oxidation of diols by gold catalysis were published [1–5]. What could appear to be just a promise is now reality, as presently several protocols for catalytic oxidation are available, which take advantage of the properties of gold in terms of activity, selectivity, reusability and resistance to poisons [6–12]. Green oxidations, of potential interest to fine chemicals, pharmaceuticals and food industry areas, see more and more gold – alone or alloyed with other metals – as the catalyst. Biocompatibility, catalytic effectiveness and ability to select among different functional groups are sufficient reasons for the growing number of papers and patents on the use of the "yellow metal" in the oxidation and other transformations of organic substrates. Besides the low temperature CO oxidation [1–17], H_2O_2 synthesis from the elements [18–20], water gas shift [21, 22], C−C coupling reactions [23–25], synthesis of N- and O- heterocycles [26], conversion of carbohydrates and alcohols to the corresponding carbonylic and carboxylic compounds [5, 11, 27–50] are some of the most successful applications.

*Corresponding author

Liquid Phase Oxidation via Heterogeneous Catalysis: Organic Synthesis and Industrial Applications, First Edition. Edited by Mario G. Clerici and Oxana A. Kholdeeva.
© 2013 John Wiley & Sons, Inc. Published 2013 by John Wiley & Sons, Inc.

The catalytic breakthrough was determined by the availability of metal particles on the nanometric scale, as physical-chemical characteristics of nanogold mutate significantly with respect to bulk gold, to the point that catalytic inertness changes into remarkable effectiveness. Such a behavior has been underpinned by a series of kinetic studies showing how the activity is dependent on the size of metallic gold particles. Actually, many investigations on liquid phase oxidation of alcohols and carbohydrates showed that only sufficiently small gold particles displayed good catalytic activity [7, 28]. Currently, oxidation by gold has become of relevant interest in organic chemistry, potentially providing green processes based on environmentally friendly oxidants air, pure O_2, and H_2O_2.

Other heterogeneous catalysts, namely supported Pd and Pt, had long been studied before the introduction of nanometric gold for the same kind of oxidations. Actually, catalytic oxidations by Pd, Pt and Au share several common features, while many gold catalysts benefit by the doping with platinum or palladium. Excellent reviews have been published, examining the literature from different perspectives [6–11, 15]. In this chapter we present an overview, mostly dealing with applications of gold to liquid phase oxidations, thus trying to meet the needs of organic chemists. Other metal catalysts and some gas phase processes worthy of mention will be occasionally included when pertinent.

5.2 CATALYST PREPARATION AND CHARACTERIZATION

Several methods are available for preparing supported gold-based catalysts, among which impregnation to incipient wetness, deposition–precipitation and deposition/immobilization of colloidal gold onto supports are the most commonly used [1–11].

In the impregnation technique, the pores of the support are filled with a solution of the metal precursor up to incipient wetness. The metal dispersion ultimately obtained strictly depends on the conditions of drying. This method has long been considered unsuitable for gold catalysts, because it usually leads to gold particles larger than 5 nm, and little active. Recently, modified methods have been developed, in which the key issue is impregnation with hydrogen tetrachloroaurate followed by an additional step of ion exchange of chlorides with the hydroxyls of a base. The resulting material is dried and then activated, not by calcination, but rather by reduction with hydrogen gas, in a method that is simple and suitable for the production of effective gold catalysts. These displayed high activity, selectivity and also long-term stability in the liquid phase oxidation of glucose to gluconic acid [43, 44].

In the deposition–precipitation (DP) procedure, the hydroxide or hydrated oxide is deposited on the surface of the support by the gradual increase of the pH of a solution of metal precursor in which the support is suspended. The precipitate may be nucleated by surface functional groups, thus allowing the active phase to be more firmly attached to the support. Hydrogen tetrachloroaurate is again the gold precursor. In aqueous media, hydrogen tetrachloroaurate(III) hydrolyzes to yield various species with different amounts of chloride, water and hydroxyl (e.g., $[AuCl_4]^-$, $[AuCl_3(H_2O)]$, $[AuCl_3OH]^-$, $[AuCl_2(OH)_2]^-$, $[AuCl(OH)_3]^-$, $[Au(OH)_4]^-$), their

composition depending on pH and chloride concentration. Typical precipitating agents are either sodium hydroxide (DP NaOH) or urea (DP urea). Baatz and Pruesse showed that the deposition–precipitation method leads to quite active and long-term stable catalysts for glucose oxidation, but they noted marked differences in the reproducibility and a loss of gold remaining dissolved in solution [44]. It was not possible to adjust a definite gold content using DP by NaOH method and, during the preparation, a gold loss up to 70% was observed. Conversely, the DP urea method was found to be very suitable for the preparation of catalysts with definite gold content and reduced losses of gold. A comparative study of the catalysts prepared by impregnation and DP led to the conclusion that the former still remains preferable for higher reproducibility.

A particular focus deserves the immobilization of a preformed gold colloidal dispersion (sol) on activated carbons and various oxides. This method, in fact, presents great advantages with respect to other methods, especially concerning the nanoparticles size control and metal dispersion. The type and amount of protecting agent (mainly, polyvinylalcohol PVA, polyvinylpyrrolidone PVP, but also polyhydroxylated compounds like D-glucose), the reducing agent ($NaBH_4$), pH value, gold sol concentration and gold loading on the support deeply affect the final catalytic performance. The classical generation of a protected gold sol involves the reduction of a Au(III) salt (e.g., $HAuCl_4$) to Au (0) by $NaBH_4$ addition, in the presence of the protecting agent at room temperature [5, 28]. Typical reagent compositions, yielding a brown-tea colloidal dispersion of 3–5 nm particles, are Au: PVA from 1.5 to 50 or Au: glucose from 30 to 3000 and Au: $NaBH_4 = 1 : 1$ (wt:wt ratios). The preparation of bimetallic systems (e.g., Au–Pd, Au–Pt, Au–Cu) follows the same protocol, with the addition to gold of a second metal precursor (generally, $PdCl_2$, $KPtCl_4$, $CuCl_2$). Within a few seconds from metal colloid generation, the sol is immobilized by adding under vigorous stirring the support, typically carbon or metal oxides such as Al_2O_3, SiO_2, TiO_2, Fe_2O_3, ZrO_2, CeO_2, after adjusting the pH at the isoelectric point of the supporting material. After a time of 15–30 min, depending on the support, the slurry is filtered, the catalyst washed thoroughly with warm distilled water, until chloride and protecting agent residues are no longer detected, and finally dried overnight or calcined.

The nature of the supporting material can determine the final catalytic performance, as will be shown for alcohols oxidation (Section 5.3.2). Interestingly, gold supported on various carbons displayed differences in the same reaction, induced by the nature of the carbon, as well as by the preparation method [52]. The most relevant parameter for the choice of a support seems to be the type and distribution of surface groups, as these can favor or inhibit the grafting of the nanoparticles. Hence, acidic or basic treatments of supporting materials are often required in order to "activate" the surface before depositing the metal, to optimize catalytic performances in terms of activity, selectivity and durability. For instance, the metal dispersion of a platinum catalyst (Pt/C), employed for the aerobic oxidation of benzyl alcohol to acid, was found to depend on the pretreatment of the carbon, besides the method of preparation. Thus, the platinum catalyst prepared by impregnation of CO_2-activated carbon showed the best activity and selectivity compared to platinum catalysts prepared on air-activated carbon or by cationic exchange [53].

Many examples throughout this chapter will show how alloying with a second metal, particularly Pt, Pd and Cu, enhances the catalytic performance of gold owing to a synergistic effect between the metals, resulting also in novel catalytic properties [18, 19, 42, 46–48, 54–59]. In particular, the improved stability of the bimetallic catalyst with respect to the corresponding monometallic will be considered in Section 5.5.

A thorough catalyst characterization requires a combination of analytical techniques. Inductively coupled plasma-atomic emission spectroscopy (ICP-AES) allows the determination of the actual metal content, while a combination of X-ray powder diffraction (XRPD) and transmission electron microscopy (TEM) leads to the average value and statistic distribution of metal particle diameters. The STEM-HAADF (scanning transmission electron microscopy–high angle annular dark field) and STEM-XEDS (scanning transmission electron microscopy–X ray energy dispersive spectroscopy) represent the advanced evolution of such techniques. X-ray photoelectron spectroscopy (XPS) is a powerful tool for obtaining the elemental composition of the surface (1–10 nm depth) and the electronic state of each element. The temperature-programmed reduction (TPR) turns out to be useful for monitoring the presence of different types of gold species, as significantly different reduction temperatures are a clear indication for different metal species on an identical support or for different interactions of the same species with different supports.

5.3 CATALYTIC PROPERTIES

5.3.1 Oxidation of Hydrocarbons

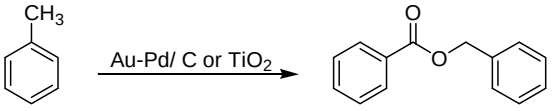
The application of gold to liquid phase oxidation of hydrocarbons is not as developed as that of other substrates, e.g., hydroxylated compounds. A sufficient number of studies, however, are available to give an outline of the catalytic behavior of gold in this area of catalysis. Notable examples are the oxidation of cyclohexane to cyclohexanol–cyclohexanone mixture (KA oil), the recent selective oxidation of the primary carbon–hydrogen bond in toluene and lower alkanes and that of other molecules of interest like, α-pinene, phenol and styrene. The gas phase oxidations of propene to propene oxide (PO) and ethene to vinyl acetate monomer (VAM) will be briefly mentioned for their relevance. A comparison of gold with platinum and palladium will be occasionally presented.

5.3.1.1 Oxidation of Cyclohexane The cyclohexanone–cyclohexanol mixture (KA oil), obtained from cyclohexane oxidation, is particularly appealing for the chemical industry, being the starting material for the production of ε-caprolactam and adipic acid, used in nylon-6 and nylon-6,6 manufacture. The first research group employing gold catalysis in this oxidation was Zhao's. They showed that Au/ZSM-5 and Au/MCM-41 allow a selectivity around 90% at 10–15% conversion and $T = 150\,^{\circ}\mathrm{C}$ [60, 61]. The major obstacle to any applicative development was a loss of both activity and selectivity on recycling. Other studies tried to reach a

satisfactory one-pot oxidation of cyclohexane [62–65]. Au/graphite, without the use of any solvent but with a halogenated benzene as an additive, led to 92% selectivity (cyclohexanone + cyclohexanol) even though at a very modest conversion (1%) [63]. As far as the liquid phase oxidation of other alkanes is concerned, this has been poorly investigated, despite the interest for petrochemical and natural gas conversion [11].

5.3.1.2 Oxidation of Methane, Ethane, and Propane Worthy of note, even though performed in homogeneous phase, is the basic research of Shilov and coworkers on the role of bioinorganic catalysis in the aerobic oxidation of the simplest alkane, methane [66, 67]. The authors employed gold (I) complexes with the bioflavonoid rutin ligand in the presence of NADH as a reducing agent, to catalyze the oxidation of methane to methanol with air, under mild conditions (aqueous solution, atmospheric pressure and room temperature). The reaction was extended to ethane and propane, yielding ethanol and 2-propanol respectively. Even though TONs (mole of product per mole of metal catalyst: $0.6\,h^{-1}$ for methane, $4.2\,h^{-1}$ for ethane and $4.6\,h^{-1}$ for propane) are modest, these findings can help to gain an insight into the catalytic mechanism of alkane oxidation.

5.3.1.3 Oxidation of Toluene and Indane The selective oxidation of toluene represents a rather appealing goal, benzyl alcohol and benzaldehyde being valuable chemicals for industry. The applications of benzyl alcohol range from being a solvent for inks, paints, lacquers and epoxy-resin coatings to being a precursor for a variety of esters, used in the soap, perfume and flavor industries. Regarding benzaldehyde, this is chiefly employed to confer almond flavor, but it is also used as a precursor to other organic compounds, ranging from pharmaceuticals to plastic additives. Other metal catalysts were known for this oxidation, but either possessed low activity and/or selectivity or required activated oxygen donors. For instance, iron, manganese [68–70], cobalt [71], and chromium [72] catalysts displayed poor turnover numbers of less than 100, even at temperatures above 190 °C, leaving room enough for the development of alternative heterogeneous catalysts. Hutchings and coworkers reported that supported Au–Pd nanoparticles on carbon or TiO_2 were active and selective (around 90% at 83% conversion) for the aerobic oxidation of methyl group in toluene and related molecules, yielding benzyl benzoate, under solvent-free conditions, at $T = 160\,°C$ and 1 atm oxygen pressure (Eq. 5.1) [54].



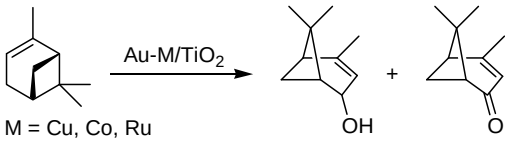
(5.1)

They rationalized the differences of catalytic activity of Au–Pd nanoparticles, in terms of the particle–support interaction and the availability of exposed corner/edge sites. By itself, Au was little active for this reaction, but the addition of Pd significantly enhanced the conversion, demonstrating a clear synergistic effect in

bimetallic Au–Pd catalysts. This was underpinned by physically mixing Au/C and Pd/C catalysts: in this case no enhancement was, in fact, registered, thus showing the molecular-scale nature of the synergy. The latter is likely due to both electronic and morphological features, in accord with transmission electron microscopy (TEM), showing that the mean particle size of the nanoparticles decreased somewhat on addition of Pd to Au.

Other benzylic compounds were converted to the corresponding aromatic ketones. In particular, supporting gold on titania and working at $T = 100\,^{\circ}\mathrm{C}$, $pO_2 =$ 1 atm under solvent-free conditions, indane was oxidized to 1-indanone with 90% selectivity at 46% conversion [73]. The aromatic ring was inert to oxidation.

5.3.1.4 Oxidation of α-Pinene Verbenol and verbenone are employed as intermediates for fragrances and flavors, as well as for a number of therapeutic agents [74]. Owing to the high commercial demand, the oxidation of α-pinene as an alternative to the natural route represents an important target. A limit to be overcome, however, regards the relative complexity of this molecule, which makes selectivity to the desired product difficult to achieve. After a number of attempts with both heterogeneous and homogeneous catalysis, gold applied to α-pinene oxidation has finally resulted to be of some interest, particularly under bimetallic formulation (Eq. 5.2) [75].



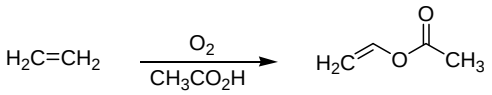
(5.2)

Gold alloyed with Cu, Co and Ru supported on TiO_2, prepared *via* the deposition–precipitation method, followed the order of catalytic efficiency: $AuCu/TiO_2 >$ $AuCo/TiO_2 > Cu/TiO_2 > Au/TiO_2 > AuRu/TiO_2$. Even though the products of interest (verbenone, verbenol, α-pinene oxide and alkyl-pinene peroxide) were always detected after reaction, selectivity to one product only did not exceed 50% at 70–94% conversion, thus indicating the need for further optimization of the catalytic process. The role of the catalyst in promoting both activity and selectivity was confirmed by comparative kinetic studies with the uncatalyzed reaction.

5.3.1.5 Oxidation of Ethene and Propene The epoxidation of alkenes by gold-based catalysis is normally studied under gas phase conditions. Owing to the importance of ethene and propene oxidation products, a brief outline of some recent developments will be presented here, to stimulate the interest of the reader.

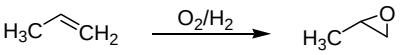
The acetoxylation of ethene to vinylacetate (VA) is an industrially important transformation, in which gold plays a role as an active component of the catalyst (Eq. 5.3) [76]. The interest in VA is related to the production of polyvinylacetate (PVAc) and the system $Au–Pd/SiO_2$ promoted by potassium acetate is the well-known system presently applied for its production [11]. Vinyl acetate monomer still

goes on drawing both academic and industrial attention due to its high added value. Consequently, many patents have reported novel preparation methods of the catalyst trying to improve the commercially applied protocol and research at Celanese International Corporation has resulted to be particularly fruitful [77].



(5.3)

Since Haruta's first paper on the gas phase oxidation of propene to propene oxide (PO) by gold catalysis in the mid-1990s, the necessity of using sacrificial hydrogen for oxygen activation, to generate the active hydroperoxide species, has been an issue (Eq. 5.4) [3].



(5.4)

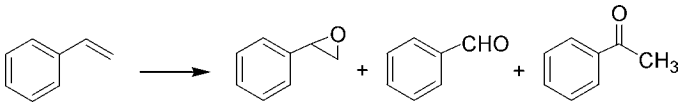
Recent studies envisage routes to PO that avoid, or limit, the need for H_2 in the oxidation. According to Lee et al., subnanometric gold clusters (Au_6–Au_{10}) catalyze the epoxidation of propene in the presence of water vapor, replacing the less manageable molecular hydrogen [78]. Water as a substitute of H_2 seems to favor the hydroxy equilibrium at the surface of the support, required for O_2 activation. Such research also underlines the positive role of alumina as the support of gold, whereas previous studies considered titania to be an essential aid for assisting the formation of peroxidic species.

Ojeda and Iglesia also carried out the epoxidation of propene in the absence of sacrificial hydrogen, using Au/TiO_2 as the catalyst in the presence of water vapor [79]. In this case too, the crucial step of the reaction seems to be the formation of hydroperoxide species coming from H_2O–O_2 interaction at the surface of nanometric gold particles. Even though penalized from a kinetic point of view with respect to $O_2 + H_2$, the system $H_2O + O_2$ is, however, safer and avoids significant losses of the costly H_2 coreactant *via* the unproductive pathway to H_2O. Haruta et al. recently came back on this topic, demonstrating that the reaction can be performed without major amounts of H_2 [80]. Their patent considers the use of oxygen in the presence of water and a catalytic amount of hydrogen. The gas phase process occurs with gold nanoparticles supported on an alkali-treated titanosilicalite or mesoporous titanosilicate, with a much higher rate with respect to the two above H_2-free methods [78, 79].

5.3.1.6 Oxidation of Higher Alkenes Hydrogen as a sacrificial reductant and acetic acid as an acetylating reagent, respectively, are not fundamental in the aerobic oxidation of higher alkenes in the liquid phase, using supported gold catalysts [62, 81, 82]. In this case, alkene oxidation is achieved by adding a catalytic amount of peroxides (either hydrogen peroxide or *t*-butylhydroperoxide) as oxygen chain initiator. The papers highlight how selectivity and conversion are dependent on substrate, catalyst and experimental conditions: with a proper tuning, an effective

oxidation of cyclohexene, styrene, stilbene and cyclooctene could be carried out. The most active catalytic systems were gold supported on carbon, alumina, and titania, which were compared to World Gold Council reference catalysts [83].

Regarding cyclohexene oxidation, Au/C led to the best performance in terms of selectivity to epoxide (50%) and ketone (26%) at 30% conversion in 1,2,3,5-tetramethylbenzene solvent [62]. The same catalyst turned out to be active also for the epoxidation of styrene, even though with lower performances (29% selectivity). In this case a mixture of 1,2,4,5-tetramethylbenzene and 1,4-dimethylbenzene or hexafluorobenzene as a solvent was used. The main oxidation product was benzaldehyde with selectivity around 46% for both solvents, besides small amounts of acetophenone (Eq. 5.5) [62].



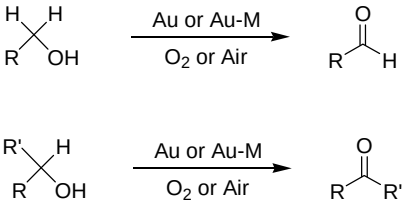
(5.5)

A recent study describes a new route to acetophenone by supported Pd-Au, with H_2O_2 as the oxidant [55]. The high conversion of styrene and the good selectivity to acetophenone were shown to be due to the use of supercritical CO_2 as the solvent. Also, the type of support strongly affects the catalytic performance. In particular, Al_2O_3 allowed the best performance, as 87% selectivity at 68% conversion was reached at 90 atm and 120 °C. Further studies on modified substrates (substituted styrenes) and catalysts (gold nanoparticles with selectively poisoned sites) were performed to derive useful models able to make this reaction of general synthetic interest [84]. Recently, very small sized gold (particle diameter around 1.4 nm), obtained from $Au_{55}(PPh_3)_{12}C_{l6}$ cluster supported on inert materials, allowed the aerobic oxidation of styrene in toluene without any peroxidic species. The performance was modest, both in terms of activity (TOF *ca.* $0.02\,s^{-1}$) and selectivity towards styrene epoxide (14%) being benzaldehyde (82%) the main product, but this study highlights the marked role of gold particles dimension and peroxidic species [85]. The authors found a size threshold in the catalytic activity, by comparing gold nanoparticles of increasing diameters: $d > 2$ nm led to the total inactivity, thus suggesting that oxygen activation is connected to the altered electronic structure typical of small gold nanoparticles.

Hutchings and coworkers applied a gold-based catalyst (Au/graphite) for the aerobic oxidation of *cis*-stilbene to corresponding epoxide in *i*-propylbenzene as a solvent, obtaining the *trans*-product (74% selectivity, at 48% conversion) [62]. In the oxidation of *cis*-cyclooctene, the best result was observed with Au/C as the catalyst in 1,2,3,5-TMB (94% epoxide selectivity, at 28% conversion).

5.3.2 Oxidation of Alcohols and Phenols

Alcohol compounds represent key substrates in organic chemistry owing to wide diffusion, easy availability from renewable sources and the value of their derivatives



SCHEME 5.1 Aerobic oxidation of alcohols by gold-based catalysts.

as chemicals. Their oxidation, performed selectively with molecular oxygen in the presence of a catalytic system is highly desirable for its low environmental impact, especially if compared to stoichiometric oxidations. Actually, the growing interest in efficient catalysts has led to a competition among platinum, palladium, ruthenium and gold catalysts as the literature well documents [7, 9–11, 34, 35, 53, 73, 86–96]. In this broad research area, we will focus our attention on gold compared to other metals as the catalysts, aiming at deriving general rules, if possible, on how the choice of different parameters can influence the selectivity towards a given product.

Gold, alone or alloyed with other metals, displays much of its catalytic potential in the aerobic oxidation of alcohols to carbonylic and carboxylic compounds (Scheme 5.1) [7, 10, 11, 15, 31].

Different methodologies are available, since it can be chosen if performing the oxidation by homogeneous or heterogeneous catalysis, gaseous or liquid phase, with ordinary solvents, supercritical CO_2 or solventless. Following different catalyst preparations leads to different products, while pressure, temperature and catalyst to substrate ratio affect yield and productivity. Such a variety of choices, however, makes it difficult to draw general conclusions from the comparison of different literature data, normally performed under a variety of conditions.

Among the notable achievements reached in this topic, Rossi's, Hutchings' and Corma's deserve particular attention. Rossi and coworkers first discovered the catalytic effectiveness of gold for liquid phase oxidation of the C–OH functional group [11, 31]: they found that, while the gas phase oxidation of alcohols produces mainly carbonylic derivatives, carboxylic acids or esters can be prepared under liquid phase and mild conditions, in the presence of alkali. Corma and coworkers reported on the marked synergistic effect between gold nanoparticles and the support (namely, nanometric CeO_2) in the absence of solvent [97]. Hutchings and coworkers employing bimetallic Au–Pd catalysts, focused on the synergistic effect between the two metals [98]. A very innovative method, probably the first example of this kind, has been recently proposed by Kobayashi and coworkers [99]. They have engineered a gold-immobilized microchannel flow reactor allowing the oxidation of various alcohols towards corresponding aldehydes and ketones with good to excellent yields. The absence of leaching and steady catalytic activity for four days make this method promising.

Thermally stable alcohols can be oxidized in gaseous phase over gold-based catalysts to aldehydes. Au on SiO_2 resulted to be effective in the selective oxidation of C_3–C_5 alcohols. Carrying out the reactions in the temperature range of 250–300 °C, the activity followed the order $C_4 > C_5 > C_3$. Secondary alcohols were oxidized to corresponding ketones under milder temperatures (100–150 °C) (Scheme 5.1) [27]. Under condensed conditions (liquid phase, batch reactions) different approaches have been investigated.

The borderline between homogeneous and heterogeneous systems is represented by unsupported metal nanoparticles. Although this chapter is intended to focus on supported catalysts, a short account on unsupported ones is important to gain an insight into the intrinsic role of the metal. Actually, gold nanoparticles (AuNPs), which have always drawn attention for their beautiful color, recently have become the subject of an interest directed to scientific applications, particularly the catalytic ones [28, 38, 100, 101].

Since the first paper on the oxidation of glucose catalyzed by AuNPs [28], several studies considered the oxidation of monohydric alcohols, focusing on the stability of metallic colloids (sol) during reaction. In benzyl alcohol oxidation, under basic conditions and at room temperature, AuNPs was stabilized by polyvinylpyrrolidone and maintained good catalytic activity over a long time, producing benzoic acid in almost quantitative yield [101]. Catalytic performances changed by changing the substituents on the aromatic ring and varying the kind of nanoparticles, as highlighted by kinetic studies. An *ortho* or *para* OH group decreased the catalyst activity while enhancing the selectivity to aldehyde, even under basic conditions. Similarly sized PdNPs and AuNPs were compared under the same reaction conditions: gold with respect to palladium displayed a better activity, while it was subjected to a stronger influence of particle size, thus suggesting different oxidation mechanisms for the two kinds of catalysts.

PVA-protected AuNPs were reported to be effective in catalyzing diols conversion to the corresponding hydroxyacids using membrane filtrations for catalyst recovery [102]. The authors investigated various solvents besides water (*t*-BuOH, 2-propanol and methanol), showing that a shift from water to alcohols led to an activity drop, while the choice of the membrane depended on the solvent. However, it should be emphasized that only the use of organic solvents allows oxidization of long chain diols, otherwise scarcely soluble in water [103].

A key point in the gold-catalyzed conversion of alcohols is the role of alkali: no conversion was ever observed in the absence of a base and this has been a matter of study since alkali was found to be compulsory, in general, for hydroxyl and carbonyl groups oxidation. As will be discussed in Section 5.4, the base reasonably appears to be involved in the first step of the oxidative process for the creation of the alkoxide anion. Concerning the use of the traditional protecting agents (i.e. PVP and PVA), whereas they guarantee a long lifetime of metal nanoparticles avoiding agglomeration and leaching during reaction, their shielding effect also decreases the metal–substrate interaction, thus worsening the catalytic activity [33].

Despite the interest in colloidal or colloid-like systems, supported metal nanoparticles represent the catalyst of choice for organic compounds oxidation, owing

to durability, easy handling and easy recovery after use. Numerous studies deal with their preparation and application to the oxidation of different alcohols.

Similarly sized supported (Au/C) and unsupported AuNPs (microgel-stabilized nanoparticles) were directly compared in an aqueous medium [104]. The unsupported gold particles were grown inside a polymer structure that provided both size control and stabilization of the NPs under the reaction conditions. Testing the two catalytic systems in the oxidation of aliphatic alcohols, namely, *n*-butanol and *n*-octanol, the unsupported NPs showed enhanced activity with respect to the supported on carbon. Conversely, carbon-supported catalysts turned out to be more effective when polyhydroxylated compounds were used as the substrates, thus underlining the importance of the relative affinity of substrate and support for aqueous media.

Since methanol is rather inert to aerobic oxidation, it could be advantageously used as solvent/reactant in the production of methyl glycolate from ethandiol [7, 105]. At 90 °C, Au supported on Al_2O_3 was found to be more active and selective with respect to Pd and Ru, showing 83% selectivity to methyl glycolate at 63% conversion. Methyl formate deriving from methanol oxidation was present only in very low amount. Au on TiO_2 and ZrO_2 were similarly used to achieve *n*-propyl propionate and *n*-butyl butanoate respectively, with a selectivity of 81% and 79% at comparable conversion. The same catalytic system, Au/TiO_2, was also employed to synthesize the corresponding methylesters from *n*-hexanol, benzyl and cinnamyl alcohols at 130 °C but, under these conditions, methanol was partly oxidized to formic acid, methyl formate and CO_2 [106]. The authors found that the presence of a base ($NaOCH_3$) increased the reaction rate. On the contrary, the selectivity was improved by increasing the excess of methanol most likely favoring the formation of methyl hemiacetal with respect to hexyl hemiacetal. Corma and coworkers [107] suggested a possible reaction pathway for 3-phenyl-1-propanol oxidation, where a hemi-acetal intermediate is formed in the absence of water, which then undergoes oxidization to the corresponding ester in a similar way as the aldehyde hydrate is oxidized to the carboxylic acid [88, 33].

Ester formation was fruitfully used for lactone synthesis. Hence, 1,4-butanediol gave γ-butyrolactone in *t*-butylphosphate as the solvent, under moderate conditions ($T = 120$–140 °C, $P_{air} = 12.5$ atm) and using Au/TiO_2 as the catalyst [108]. The XPS technique allowed the Au(0)/Au(III) ratio to be followed, showing that the reaction rate increased with the Au(0) content. In fact, no reaction was observed below 50% Au(0).

Gold-catalyzed oxidation of alcohols is generally limited by slow kinetics (TOF is often in the range of dozens or hundreds h^{-1}). The contribution of a second metal, particularly palladium and platinum, was often shown to be effective to overcome the intrinsic low activity of gold. Accordingly, benzylic alcohol under solventless conditions could be oxidized to aldehyde five times faster with Au–Pd/TiO_2 than with Au/TiO_2 at 100 °C and $p_{O2} = 2$ atm, with selectivity to aldehyde over 90% at 75% conversion [98]. STEM and XPS helped to visualize the bimetallic catalyst structure: Au–Pd/TiO_2 prepared according to impregnation protocol, followed by calcination at 400 °C, had a Pd-rich shell and Au-rich core design. Other supports,

such as Al_2O_3 or Fe_2O_3, did not give catalysts as active, selective and stable as Au–Pd/TiO_2. The effect of Au/Pd ratio on the products distribution was particularly evident under forced reaction conditions (160 °C and 10 atm). In this case, the most active catalyst was 2.5%Au-2.5%Pd (wt:wt), whereas monometallic Au/TiO_2 turned out to be the most selective to aldehyde. Therefore, palladium enhances activity, while slightly depressing selectivity to aldehyde [109].

The role of the support in the Au–Pd catalytic system was investigated by using nanosized CeO_2, instead of TiO_2, in a comparative study with the gold monometallic catalyst (Au/CeO_2) [110]. In allylic alcohols oxidation conducted at 120 °C and atmospheric pressure, nanoceria as the support led to a more active and selective catalyst with monometallic Au than with Au–Pd, which in turn was better than Au–Pd/TiO_2. Conversely, Pd on nano-CeO_2 was found to be less selective producing a higher amount of isomerized product. The higher selectivity of Au on CeO_2 could be due to the fast oxidation of intermediate metal-hydrides that, on the contrary, are not oxidized rapidly enough on Pd, thus favoring double bond isomerization and reduction. In any case, nano-CeO_2 acts as an activity enhancer.

In benzyl alcohol oxidation at 100 °C and 2 atm of O_2 without any solvent, other supports were investigated for Au and Au–Pd [111]: zeolites (ZMS-5, β, Y) were used and compared to TS-1 and TiO_2. Acidic zeolites, except for ZMS-5, produced larger amounts of benzyl benzoate, dibenzyl acetal and dibenzylether, while Au on zeolite β was shown to be more active than Au on TiO_2. By adding Pd to Au, the activity slightly improved without significantly affecting selectivity.

The reactions herein presented have been partly performed in the presence of a solvent and partly under solvent-free conditions. This is an important point in catalysis: finding a proper solvent that enhances catalytic performances and fulfils ecological restrictions is not always an easy choice, whereas under solventless conditions – which generally represent an ecofriendly route – drawbacks can occur principally correlated to the physical state of the substrate and its thermal stability. However, solventless conditions often emphasize the action of the base, so important in gold-catalyzed alcohols oxidation. For instance, in the solvent-free oxidation of benzyl alcohol conducted at moderate temperature (80 °C) by Au/TiO_2 catalysis and addition of K_2CO_3 (0.2% with respect to alcohol), a marked effect of the base was evident as TOF reached the value of 7851 h^{-1}, much higher than TOF = 19 h^{-1} achieved without any alkaline promoter [112]. By changing the type of base, some differences were registered: sodium carbonate and acetate improved the oxidation, whereas stronger bases did not have the same prominent effect. The solvent, in its turn, can deeply influence the catalytic performance, as shown by the oxidation of benzyl alcohol on Au/U_2O_3, in which the addition of solvents like toluene, *p*-xylene, DMF and DMSO caused activity and selectivity drop [113]. The reason could be ascribed to a competitive adsorption of solvent and alcohol on the active sites of the catalyst.

A large number of primary and secondary alcohols were oxidized to carbonylic derivatives using mesitylene as the solvent at 90 °C and gold on $CuMg_xAl_yO_z$ as the catalyst, thus achieving almost total selectivity ($\geq$ 98%) [114]. TOFs were not particularly high (20–1300 h^{-1}) especially with aliphatic primary alcohols ($<$100 h^{-1}),

but the activity could be tuned on the composition of the support. Regarding this, the ratio Cu:Mg:Al = 5 : 1 : 2 was found to favor the highest activity. The oxidation of benzyl alcohol on Au/TiO_2 at 100 °C, under supercritical CO_2, led to an almost total selectivity to aldehyde. The activity was similar to that obtained under solventless conditions [115].

Among the various parameters affecting gold-catalyzed oxidation of alcohols, the key role of the solvent on activity and selectivity is a fact. The ideal medium would be water, which is ecofriendly, cheap and easy to handle, but unfortunately its use depends on the hydrophobic/hydrophilic properties of both substrate and catalytic system. However, water represents the solvent of choice for an extended category of substrates, such as polyhydroxylated compounds, while solventless conditions, when possible, can provide a valid solution for water-insoluble compounds.

Gold appears to be the catalyst of choice in water because, compared to more traditional catalysts like palladium or platinum, it does not suffer from deactivation when employed in the presence of molecular oxygen, moreover it is highly chemoselective [5]. Regarding the support, activated carbon and graphite are the most investigated materials for aqueous phase oxidation by gold due to both high performance under mild conditions and economical reasons: these materials are, in fact, cheap and allow an easy recovery of the precious metal by burning off the support [7]. However, hydrophilic supports are preferable when water is the solvent, because the dependency on a basic promoter is reduced, as in the case of ethanol oxidation to acetic acid catalyzed by $Au/MgAl_2O_4$ [116]. This reaction, conducted under forced conditions (3.5 atm of air, $T = 150$–180 °C) up to the notable 92% yield in acetic acid, represents the first example of a gold-catalyzed oxidation proceeding in water in the absence of a base. Actually, a peculiarity of gold-catalyzed oxidations of alcohols and aldehydes in water is, indeed, the need for basic conditions even if aldehydes can be smoothly oxidized under neutral conditions [33]. Hence, the basic strength of the alcoholic group is crucial [117]. Moreover, the presence of a base promotes the desorption of the products from the surface, thus prolonging the catalyst life.

Two ways can be chosen for providing the reaction system with a basic environment: a continuous addition of alkali (pH-controlled conditions) or an excess of base added at the beginning of the reaction. These conditions favor the formation of intermediate aldehyde, which, however, is more easily oxidized to carboxylate than parent alcohol [7, 9–11, 27]. In some cases, the aldehyde can be isolated in high yield (90%) even in the presence of alkali, as in *o*-hydroxybenzyl oxidation catalyzed by Au/Fe_2O_3 carried out at 50 °C, atmospheric pressure and Na_2CO_3 [118].

Hydrogen peroxide represents an efficient alternative to air or molecular oxygen for performing environmentally friendly oxidations of organic compounds. For instance, Kholdeeva et al. developed new clean and efficient methods for the production of 2-methyl-1,4-naphthoquinone (MNQ, menadione, Vitamin K_3) based on the oxidation of 2-methyl-1-naphthol (MNL) with cheap and environmentally benign oxidants, aqueous hydrogen peroxide, *t*-butyl hydroperoxide and molecular oxygen, using three types of heterogeneous catalysts, namely, mesoporous titanium silicate Ti-MMM-2, silica supported iron phthalocyanine and supported gold

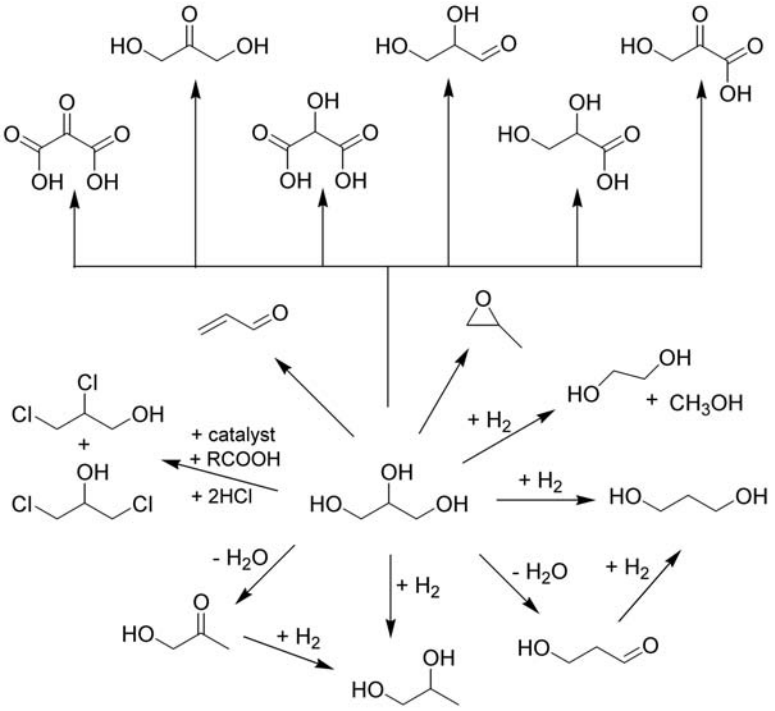
nanoparticles [50]. The oxidation proceeded easily with aqueous H_2O_2 over Ti-MMM-2, a truly heterogeneous and recyclable catalyst, with good selectivity, even though with low volume yield, whereas, FePcS/SiO_2/TBHP and Au/C/O_2 systems provided MNQ with moderate selectivity and yield. Interestingly, it was also found that this reaction fairly proceeds at $p_{O2} = 3$ atm in nonpolar solvents without any catalyst.

Caps and coworkers deposited gold nanoparticles on inorganic supports and used them for the oxidation of substituted phenols (2,6-di-tert-butyl phenol and 2,3,6-trimethyl phenol) with aqueous hydrogen peroxide [51]. By contrast to other catalysts, such as Ti-containing mesoporous silicas, which convert phenols to the corresponding benzoquinones, gold nanoparticles were very selective to biaryl compounds (3,3,5,5-tetra-tert-butyl diphenoquinone and 2,2,3,3,5,5-hexamethyl-4,4-biphenol, respectively). Product yield and selectivity depended on the solvent used, the best results being obtained in methanol with yield >98%. Therefore, gold offered the possibility to completely change the selectivity, directing the oxidation of substituted phenols to C−C coupling products. This has been explained by the low stability of Au–H_2O_2 adducts as compared to Ti–OOH species, favoring the formation of phenoxy radicals. Gold is, therefore, complementary to Ti-silicas and could be a promising catalyst for the clean synthesis of biaryl compounds (low temperature, no byproducts, green oxidant).

Going back to oxidations conducted with molecular oxygen as the oxidant, platinum displays some limits related to overoxidation and poisoning phenomena as in the case of phenol aerobic oxidation [90]. Pt/graphite, Pt/TiO_2, Pt/Al_2O_3 and Pt/active carbon were studied in a continuous slurry reactor (CSTR). Three model reactions, namely, phenol, maleic acid and malonic acid deep oxidations, were investigated in the temperature range from 120 to 170 °C, at a total reactor pressure of 17 atm. Platinum on graphite was found to be the most suitable catalyst, with complete conversion for both phenol and maleic acid oxidations to CO_2, at $T =$ 150 °C. Deactivation due to overoxidation was progressive for 5.3% Pt/graphite as compared to 15.3% Pt/TiO_2, 19.5% Pt/Al_2O_3 and 19.0% Pt/C. Deactivation by fouling or blocking of active sites is one of the consequences of overoxidation, particularly during phenol oxidation whereby *p*-benzoquinone and polymer precursors are formed. It was further found that in the presence of Pt/graphite catalyst and oxygen, malonic acid reactions comprised noncatalyzed decarboxylation, catalytic decarboxylation to CO_2 and acetic acid and catalytic oxidation to CO_2 and H_2O.

In the wide spectrum of alcohols so far examined, glycerol and benzyl alcohol represent the most intensively investigated with the number of papers, reviews and patents definitely confirming supported gold to be a valid alternative to early Pt- and Pd-based catalysts. Their application to such reactions, in fact, has hugely improved the performances in terms of selectivity, conversion and recycling of the catalyst.

5.3.2.1 Oxidation of Glycerol The development of proper alternatives to fossil-fuel derivatives is causing a growing overproduction of glycerol - the main byproduct of biodiesel synthesis - with the result of stimulating research to find new ways for changing it into valuable chemicals (Scheme 5.2) [34, 35].



SCHEME 5.2 Schematic representation of potential pathways in the catalytic conversion of glycerol.

Currently, two research teams, namely, Hutchings's and Prati's, are mainly involved in the application of gold-catalyzed oxidation to glycerol. In both cases, gold has not failed to meet expectations especially in terms of selectivity, which is so important in the entangled net of the possible products. Hutchings et al. have shown that, using graphite as a support in aqueous solution at 100 °C and in the presence of NaOH, 100% selectivity to sodium glycerate could be easily obtained at 50–60% conversion [119]. In the same paper, they reported on the strategic transformation of glycerol to lactate *via* preliminary reduction to 1,2-propandiol followed by oxidation of the primary alcohol group to carboxylate. Catalysts based on a gold–palladium alloy were superior to the monometallic gold catalyst when applied to the oxidative step to lactate [56]. The addition of palladium to gold significantly enhanced the activity while retaining the high selectivity to lactate (up to 96% selectivity at 94% conversion). Two supports, TiO_2 and carbon, and two preparation methods, wet impregnation and sol-immobilization, were compared. The use of the sol-immobilization method led to catalysts with the highest activity for lactate formation. An interesting comparison inside C3 alcohols showed that the reactivity decreased in the order glycerol > 1,2-propanediol > 1,3-propanediol > 1-propanol > 2-propanol.

Prati et al. have evaluated gold nanoparticles, either unsupported or supported on carbon and on TiO_2, in terms of selectivity and activity, as well as the role of the base and of hydrogen peroxide formed during the oxidation to glycerate [120]. It has been derived that the selectivity is lowered by the C−C bond fission of glycerol, which grows with the reaction time and partially with the rate of degradation of the byproduct H_2O_2. The authors have also thoroughly studied supported gold alloyed with a second metal (Pt and Pd) thus underlining some important points: the activity can be improved by using the bimetallic Au–Pt and Au–Pd systems, whereas the selectivity to the desired product can be affected by the composition and texture of the catalyst (particle size, kind of support and alloyed phases) and experimental conditions [57, 58, 120]. A wise use of the second metal tuned up the selectivity. Accordingly, pure gold favored glyceric acid formation, Pd addition led to further transformation to tartronic acid and Pt addition allowed carbon–carbon bond fission towards glycolic acid. An important parameter, together with the small particle size, is the atomic ratio of the metals in Au_xPd_y catalysts, which deeply influenced activity and selectivity, as well as the supporting materials (carbon, graphite, TiO_2, Ti/SiO_2, SiO_2).

A marked progress has been reached by eliminating the need for a base, while maintaining valuable performances: 80% glyceric acid selectivity at full conversion [58]. As already mentioned, the pH of the reaction medium and the type of the catalyst (Pt-, Pd- and Au-based catalysts) significantly affect glycerol oxidation reaction. This is usually carried out in acidic or basic conditions when using platinum or palladium, while on the contrary the activity of gold is almost exclusively limited to basic media. One of the main advantages for working in acidic media is, of course, the prevention of salt formation, whose disposal cost is always an issue in the design of industrial processes.

In order to better evaluate the different catalytic behavior of palladium, platinum and gold induced by pH during glycerol oxidation, we will intentionally avoid the bimetallic catalysts for which the synergistic effect between the metals is strong, so it would be difficult to specifically decouple the pH effect on the various metals. We will focus, instead, on monometallic supported catalysts (Pd, Pt and Au/C). Most of these studies have been carried out employing Pd/C catalysts [46, 57, 58, 91, 93, 96]. In many cases, the experiments were performed at pH = 11 in order to increase the activity of the catalysts. The main oxidation product was always glyceric acid resulting from the activation of the primary hydroxyl group of glycerol. Some authors also found the formation of tartronic acid and oxalic acid in lower quantities.

Gallezot and coworkers systematically studied the impact of the pH on the catalytic activity, using 5%Pd/C as a catalyst [93]. The catalytic activity increased with the pH of the reaction medium. At pH 11, glycerol full conversion was reached after around 4 h reaction, whereas lower pH values resulted in incomplete conversion even after a doubled reaction time. Concerning selectivity at pH 11, they found glyceric acid to be the main product, but, when conversion reached 100%, the selectivity to this product reached a plateau at 67% owing to oxalic acid formation. Since the selectivity of the coproduced tartronic acid and dihydroxy acetone remained constant even at high conversion, the only explanation for the formation of oxalic

acid is the decomposition of glyceric acid by a decarboxylation mechanism. The formation of C_1 products was recently reported by Prati et al. who used carbon-supported palladium (1%Pd/C) under acidic conditions (pH 5) [46]. The activity was rather low (5% conversion of glycerol after 2 h) but it is worth mentioning that the observed main products were C_1 compounds, probably formed by C−C bond cleavage induced by hydrogen peroxide, a known byproduct under these reaction conditions.

Also, platinum can be used either in acidic or basic conditions. In the middle of the 1990s, Gallezot and coworkers examined the catalytic activity of carbon-supported platinum catalysts at pH 6 and 11 [93, 121, 122]. Their activity was significantly lower when employed in acidic conditions, as shown by the initial specific rates (40 mol h^{-1} mol^{-1} at pH 6 and 110 mol h^{-1} mol^{-1} at pH 11). Unfortunately, the authors did not mention the selectivity of the different products, but the overall yield of the identified products (glyceric acid, dihydroxy acetone and tartronic acid) was 35% under acidic conditions and 70% under basic ones. To clarify the impact of the pH, the authors studied in detail 5%Pt/C as the catalyst, showing that the initial rate of glycerol oxidation was pH dependent, passing through a maximum (375 mmol h^{-1} $mmol^{-1}$) in neutral media [93]. As in the case of palladium catalysts, the principal product was glyceric acid, albeit with a lower yield (from 70 to 55%), whereas that of dihydroxy acetone increased (from 8 to 12%). No explanation was formulated for such selectivities. The increase of platinum loading (7 wt% Pt/C) favored the yield of tartronic acid, while dihydroxy acetone formation was limited to neutral or acid conditions, which is in line with previous works [122].

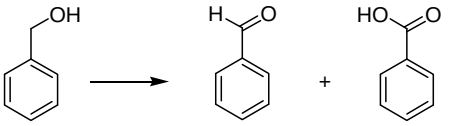
The oxidation of glycerol using carbon-supported platinum in acidic media was also studied by Kimura et al. [92, 94], Liang et al. [95] and Prati and coworkers [46, 58]. While Kimura et al. reported low activity for this catalyst, Liang et al. claimed a 50% conversion and Prati and coworkers even 78%. A clear crossevaluation of such results is impossible due to the different reaction conditions, however all authors reported an important selectivity to C_1 compounds, namely carbon dioxide and formic acid. In turn, Hutchings and coworkers showed that, with 5 wt% Pt/C at 60 °C, glycerol conversion after 3 h reaction increased from 27% to 56% by increasing the NaOH/glycerol molar ratio from 0 to 2 [96]. At the same time, the selectivity to glyceric acid and glyceraldehyde passed from 28% and 0% to 69% and 30%, respectively. Oxalic acid was detected only in the absence of sodium hydroxide. Catalyst activity changed significantly with the nature of metal hydroxides used. In fact, glycerol conversion under the same reaction conditions decreased in the sequence: NaOH (63%) > CsOH (52%) > LiOH (49%) > RbOH (37%) > KOH (35%). On the other hand, a correlation with selectivity was not so obvious, as the highest (87%) and the lowest (14%) selectivities to glyceric acid were found for KOH and RbOH, respectively, while tartronic acid was produced only in the presence of NaOH. Nevertheless, a systematic study of the pH impact on the catalytic activity and selectivity of platinum-based catalysts is still missing.

As previously mentioned, the use of gold limits oxidation conditions to basic media, where sodium hydroxide is generally the first choice. The basicity is thought to favor the first step of the oxidation mechanism, i.e. the hydrogen abstraction from

the hydroxyl groups, believed to be impossible for gold catalysts in the absence of a base [58, 119]. Thus, the main product is always the sodium salt of glyceric acid with yields depending on NaOH/glycerol ratio: an increased ratio, in fact, leads to a decreased formation of tartronic acid in favor of glyceric acid.

A systematic study of pH effects using carbon-supported gold catalysts was carried out also by Demirel et al. [123]. They found that the catalytic activity was directly correlated to the pH of the reaction medium, the highest initial reaction rate being reached for a NaOH/glycerol ratio of 4. They confirmed also the results of Hutchings and coworkers regarding the dependency of glyceric acid and tartronic acid formation on the amount of base. We have already mentioned Prati's work on glycerol oxidation using gold-based catalysts in a base-free medium [58].

5.3.2.2 Oxidation of Benzyl Alcohol The interest in benzyl alcohol oxidation is related to the high added value of the corresponding products, benzaldehyde *in primis*, being the artificial bitter-almond aroma employed in food and cosmetic industry (Eq. 5.6). Actually, such a chlorine-free route to benzaldehyde represents a real interest for industry [11]. Moreover, it is often taken as a model reaction for gold catalysis, both in liquid and gas phase, and for studies of the effect of ring substitution.



(5.6)

The liquid phase oxidation of benzyl alcohol occurs smoothly by several transition-metal catalysts, owing to the activating effect of the aromatic ring. Even though the important role of the supports in favoring gold catalysis is a well-known *leit motiv* for this kind of oxidations, indeed, better catalytic performances for gold and gold–palladium systems can be reached by their optimization. Carbon nanotubes and nanofibers, for instance, used as an alternative to activated carbon, led to a selectivity towards benzaldehyde of 96% at 90% conversion after a careful dispersion of bimetallic Au and Pd nanoparticles on their surface [87]. Palladium nanoparticles supported on carbon nanotubes (CNTs) allowed a higher selectivity to benzaldehyde than Pd nanoparticles supported on activated carbon. Under solventless conditions, a significant improvement in selectivity was observed for the former, whereas using the latter a considerable overoxidation of benzaldehyde was detected. Transmission electron microscopy analysis visualized differences in metal dispersion between Pd/C and Pd/CNTs, since active carbon and carbon nanotubes are indeed different from the textural, chemical and physical points of view. Activated carbon allowed an easier metal dispersion and this could be the reason for the higher activity of Pd/C catalyst. However, Pd/CNTs resulted to be more stable on recycling than Pd/C as to Pd leaching and particle coalescence: after 7 reaction runs, an activity loss of 50% was registered when using carbon nanotubes as a support, whereas activated carbon led to an activity loss of 70%. By alloying Pd to Au,

the catalyst life was markedly increased. The prolific application of polymeric materials employed as supports for gold catalysis also includes the use of a porous polyimide membrane [100, 101]. Mertens et al. stabilized gold–palladium clusters with polyvinylpyrrolidone without loss of nanodispersion [124]. The resulting catalytic membrane was highly active in the solvent-free oxidation of benzylic (TOF 22 500 h^{-1} for benzyl alcohol and 59 000 h^{-1} for 1-phenylethanol) and allylic alcohols with total selectivity to the carbonylic compounds. Such a kind of catalytic membrane can actively contribute to the progress of green chemistry, owing to the high performance and easy recycling.

Another innovative support, namely, ceria prepared under supercritical conditions, has been recently proposed [125]. Its use allowed the synthesis of effective catalysts for the aerobic oxidation of benzyl alcohol under solvent-free conditions, i.e. the monometallic Au/scCeO_2 and Pd/scCeO_2 and bimetallic Au–Pd/scCeO_2. These, evaluated at 140 °C with O_2 in the absence of solvent, appeared to be selective to benzaldehyde (*ca.* 91% selectivity, obtained at the modest conversion of 2%). The other products were mainly benzyl benzoate (3%), benzoic acid (2%) and toluene (3%). The Au–Pd supported on supercritical CeO_2 catalyst was approximately 4 times more active than Au–Pd supported on conventional CeO_2.

Christensen and coworkers dedicated a study to the mechanism of aerobic oxidation of alcohols using a series of *p*-substituted benzyl alcohols (Hammett methodology), showing that the activation of the alcohol involves the breakage of the C–H (D) bond in the benzylic position, thus leaving behind a partial positive charge [88].

Besides gold and palladium, platinum has also been successfully employed as a catalyst for the oxidation of benzyl alcohol by molecular oxygen and of a series of primary alcohols [53, 89, 90]. Pt/ZrO_2, using *n*-heptane as the solvent, was very active and 100% selective to benzaldehyde at total conversion [89]. The catalyst could be separated by filtration and reused after an almost complete conversion and selectivity (2.5 h reaction). No leaching of Pt or Zr into the solution was observed. Kinetic data obtained were fitted into Langmuir–Hinshelwood, and Eley–Rideal models of rate expressions, with Langmuir–Hinshelwood one showing the best fitting.

Gallezot and coworkers presented carbon-supported platinum catalysts as highly efficient heterogeneous catalysts for the selective oxidation of various types of primary alcohols to the corresponding aldehydes and carboxylic acids, using a low pressure of air and a temperature of 100 °C [53]. In particular, alcohols could be oxidized to afford the corresponding aldehyde in high yields in dioxane, whereas carboxylic acid was selectively produced in dioxane/aqueous solution mixtures and dioxane/alkaline aqueous solution mixtures. The dispersion of the platinum catalyst depended on the carbon activation treatment and on the method of preparation and it influenced significantly the activity and the resulting selectivity, in particular in benzyl alcohol oxidation. The addition of sodium hydroxide promoted the formation of the acid. Reaction selectivity was over 99% at total conversion in most cases.

5.3.2.3 Oxidation of Allyl Alcohol One of most interesting building blocks in organic synthesis is 3-hydroxypropionic acid (3-HP), which is particularly

TABLE 5.1 Allyl Alcohol Oxidation in the Presence of 0.3% Au/C Catalyst[a]

			Yield (%)			
NaOH/Allyl alcohol[b]	T (°C)	Conv. (%)	3-HP	Acrylate	Acrylate	Glycerol
1	25	98	19	15	38	traces
3	25	100	16	30	5	0
1	50	98	42	13	33	traces
3	50	100	79	9	11	0
3	80	100	74	18	6	0

[a]Reaction conditions: allyl alcohol 1 mol L^{-1}, $p_{O2} = 3$ bar, allyl alcohol/metal = 4000 (molar ratio), $t = 24$ h. Yields by HPLC analysis on the crude reaction product.
[b]Molar ratio.

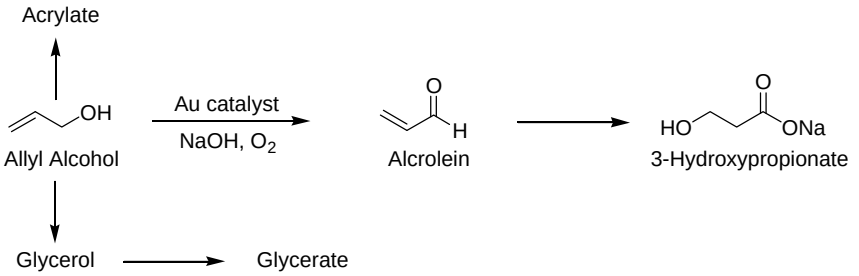
important for the manufacture of high performance polymers. Despite all the efforts addressed to find effective biological and chemical routes, no large scale process for manufacturing 3-HP is now industrially applied. One potential starting material could be represented by allyl alcohol, in principle obtainable from glycerol, thereby mirroring a biorenewable pathway. Schüth and coworkers realized the first step using iron oxide as a catalyst to convert glycerol to allyl alcohol through dehydration and consecutive hydrogen transfer [126]. Rossi and coworkers recently found an innovative route to 3-hydroxypropionic acid by oxidizing allyl alcohol in the presence of a gold catalyst [49]. Actually, on reacting allyl alcohol in aqueous alkali solution with O_2, a slow oxidation takes place, leading to 3-hydroxypropionate, together with acrylate and glycerate. Nanometric gold dispersed on activated carbon was shown to be better than Au/TiO_2 for activity, while selectivity could be controlled by regulating the amount of alkali and temperature. A high selectivity (79% at full conversion after 24 h) to the desired 3-hydroxypropionic acid was obtained with NaOH in excess (3 : 1) at 50 °C (Tables 5.1 and 5.2).

The authors suggested a possible mechanism where acrolein, primarily formed, undergoes a Michael-type addition of water, leading eventually to 3-hydroxypropionic acid (Scheme 5.3, see also Section 5.4).

TABLE 5.2 Allyl Alcohol Oxidation in the Presence of 1.5% Au/TiO_2 Catalyst[a]

			Yield (%)			
NaOH/Allyl alcohol[b]	T (°C)	Conv. (%)	3-HP	Acrylate	Acrylate	Glycerol
1	25	37	8	23	0	0
3	25	25	7	18	0	0
1	50	94	50	37	8	0
3	50	97	53	32	12	0
3	80	97	11	21	6	0

[a]Experimental conditions as in Table 5.1.
[b]Molar ratio.



SCHEME 5.3 Proposed pathway to 3-hydroxypropionic acid from allyl alcohol oxidation by gold catalysis.

The catalytic transformation of allyl alcohol to 3-hydroxypropionic acid still reserves interesting challenges in catalyst design, related to the control of selectivity, because acrylic acid, acrolein and glyceric acid can also be obtained.

Another major issue is catalyst recycling: Au/C catalyst, in fact, was not stable as the selectivity to 3-HP decreased after the second reaction cycle, therefore casting doubts on the viability of this new route. In order to overcome the problem of selectivity, Rossi and coworkers [59] prepared and tested a series of bimetallic Au–M nanoparticles (M = Pt, Pd, Cu or Ag) supported on carbon, as alloying gold with a second metal has been shown to be often effective in enhancing gold performances [11]. In Section 5.5 the strategy adopted for outweighing the limit of the short catalyst life will be discussed.

5.3.3 Oxidation of Carbohydrates: The Case of Glucose

The last decade has witnessed the rapid rise of interest for the valorization of renewable feedstocks, including the oxidation of glucose and other carbohydrates to valuable chemicals [11]. In this area, many studies focused on catalytic questions and process feasibility.

Pioneering works by Rossi and coworkers [31, 32] allowed a general trend of reactivity in the aerobic oxidation of aliphatic oxygenated compounds on supported gold to be established: aldehydes > primary alcohols > secondary alcohols. Tertiary alcohols and carboxylic acids are almost inert under moderate conditions (up to $T = 60\,^{\circ}\mathrm{C}$ and $p_{O2} = 3$ atm). In particular, the aerobic oxidation of aldehydes can be performed using water, organic solvents and solvent-free conditions, also in the absence of alkali. Gold is a fairly good catalyst for this oxidation in aqueous solution and, differently from Pt, without any deactivation on recycling. According to the expected trend, aldose oxidation occurs at the aldehydic group leading to carboxylic acid or carboxylates.

The attractiveness of gluconic acid and gluconates is related to their use as industrial intermediates largely employed in food chemistry, surfactants and cleansing agents. Therefore, finding a catalytic route to glucose oxidation as a valid alternative to the present industrial route – *via* fermentation by enzyme (*aspergillus niger*

mould) – still remains an ambitious aim. Pt-based catalysts fulfill the requirements only partially because, even if allowing high conversion and good selectivity, they undergo a fast deactivation. The problem of leaching, self-poisoning and overoxidation could be partly overcome by using bi- and trimetallic catalysts and by Bi doping [127, 128], but it is with gold catalysis that a notable progress was achieved.

Since the first report, it was evident the superiority of the "yellow metal" over the traditional Pd and Pt [129]. A comparison under the same conditions, $T = 50\,^{\circ}C$ and atmospheric pressure, demonstrated the outstanding peculiarity of gold: whereas palladium and platinum catalysts led to gluconate with selectivity $< 95\%$, gold resulted in a selectivity close to 100% at total conversion. Further optimization allowed the initial TOFs of a few hundred h^{-1} units to be improved to the exceptional value close to sixty thousand units, thus shortening the distance between gold catalysts and enzymes [28]. A subsequent paper confirmed the results: the authors compared *Hyderase* (from Amano Enzyme Co., UK), a biological preparation containing *glucose oxidase* and *catalase* as active components and flavine-adenine dinucleotide (FAD) as the rate controlling factor (1.3×10^{-6} mol g^{-1}), with their most efficient gold catalyst, 0.5% Au/C, prepared by metal colloid (sol) deposition on the support (particles of 3.6 nm) [36]. A proper tuning of reaction parameters such as pH, temperature, glucose concentration and stirring speed led to the results illustrated in Table 5.3.

The superior productivity finally achieved with the inorganic catalyst can be explained by also taking into account the relatively low FAD concentration in the enzymatic extract and the possibility given by gold to start with a three-fold higher glucose concentration. On the other hand, considering the molecular efficiency of the active FAD sites, a turnover frequency of 600 000 h^{-1} was reached, a markedly better value than the efficiency of active external gold atoms in the inorganic catalyst, calculated as 90 000 h^{-1}.

As recently reported by Haruta and coworkers, the solid grinding method offers an efficient and easy protocol for preparing well dispersed catalysts, successfully applied also in glucose oxidation [130]. In particular, Au/ZrO_2 catalyst displayed the highest catalytic activity allowing a turnover frequency of 45 mol glucose (mol surface Au)$^{-1}$ s^{-1} at 50 °C and pH 9. This value is superior to any TOF per surface Au atom reported before. Comparing the TOFs of various catalysts, the authors confirmed a well-known peculiarity of nanoparticles: TOF increases with the decrease of gold particles size, a *leit motiv* that, however, a recent paper by Guczi and coworkers has questioned [131]. These authors have evaluated a series of gold catalysts

TABLE 5.3 Comparison between the Inorganic Catalyst (0.5% Au/C) and the Enzymatic Catalyst (Hyderase) in the Aerobic Oxidation of Glucose

Catalyst	Glucose (mol L^{-1})	Catalyst/ Glucose (g kg^{-1})	pH	Stirring speed (rpm)	T (°C)	Specific Activity (h^{-1})	Productivity (kg m^{-3} h^{-1})
Au/C	3	5	9.5	39 000	50	218	514
Hyderase	1	6	5–7	900	30	145	122

supported on TiO_2, SiO_2, and CeO_2, prepared by colloidal gold deposition and stabilized by polyvinylalcohol (PVA) or tannic acid-citrate, thus leading to particles size of 5–7 nm and 7–13 nm, respectively. Surprisingly, they found that the largest sized gold was more active than the smallest one, particularly with the SiO_2 support. According to the authors, the effect of the support could be more significant than that of the gold particle size.

Pruesse's research group has successfully extended the application of gold catalysis to a broad series of carbohydrates [11, 43, 44].

Yin et al. studied the activity of innovative nanoporous bulk gold catalyst, synthesized by selective leaching of Ag/Au alloy, in the oxidation of glucose to gluconic acid under mild conditions, as function of pH, temperature and porous size [132]. Such a catalytic system does not match the performances of traditional catalysts containing Au nanoparticles, but it is advantageous in terms of easy preparation, recycling and recovery. It can also be employed as a component for innovative membrane reactors due to its structural continuity and excellent electric conductivity.

Even though oxygen and air still remain the "greenest" oxidants, hydrogen peroxide is drawing attention due to its biocompatibility and usefulness for mechanistic studies [40]. In fact, the oxidation of glucose by H_2O_2 has been recently reinvestigated by Haruta and coworkers, using gold nanoparticles deposited directly from an aqueous solution of diethylenediaminegold(III) onto commercially available polymer beads, such as poly(methyl methacrylate) (PMMA), polystyrene (PS) and polyaniline (PANI) [133]. The reduction of Au(III) to Au(0) was possible by dropwise addition of $NaBH_4$, which allowed small Au(0) nanoparticles with a narrow size distribution to be obtained. The kinetics turned out to be influenced by the kind of supports (PMMA > PS > PANI), rather than by the size of Au particles.

The patent literature has not kept up with the scientific progress in the last few years, a clear sign that further improvement is required for a concrete feasibility of the process [134].

A first contribution to an insight into glucose aerobic oxidation was provided by the detailed kinetic studies carried out by Claus in Germany and Rossi in Italy. These kinetic investigations were performed using carbon-supported gold particles [37] or unsupported colloidal gold particles [38] as the catalysts, leading to two different mechanistic models. It is worth noting the detection by Rossi and coworkers of hydrogen peroxide, instead of water, as the reduction product of O_2 [38, 40]. The same authors also carried out a further kinetic investigation for a comparison between enzymatic and gold catalysis [39]. Both catalytic systems resulted in the oxidation of glucose being carried out by same initial process, namely, by a 2-electron reduction of molecular oxygen yielding hydrogen peroxide as a transient byproduct. Nevertheless, enzymatic and inorganic catalysis follow different oxidation pathways: a) in the enzymatic system, the rate-determining step is the oxidation of the substrate by the enzyme, with zero-order dependence of the rate on dioxygen; b) the oxidation of glucose by dioxygen represents the rate-limiting step of the gold catalytic process, with the dependence of the rate on pO_2 being first order. On this basis, a mechanism of glucose oxidation on a gold nanoparticle could be suggested, in which the promoting role of alkali and the detection of H_2O_2 as a byproduct are also considered (Section 5.4) [40].

5.3.4 Oxidation of Amines and Aminoalcohols

Up to a few years ago, catalytic methods for amines oxidation were almost unknown in organic synthesis, owing to the inhibition by the amino group of traditional metal catalysts [11, 32, 135], but over the last three years a number of papers have flourished on this topic [73]. Rossi and coworkers first found gold to be an exception, if compared to palladium and platinum under similar conditions, displaying notable and stable catalytic performances in the aerobic oxidation of aminoalcohols and tertiary amines [32, 135]. Of all possible products, ranging from corresponding aminoacid to the N-oxide derivatives, depending on the nature of the nitrogen substituents, experimental conditions and catalytic system, the selectivity to N-oxidation products was remarkably high. The authors also showed, by reacting different kinds of aminoalcohols at $T = 70\,^{\circ}C$, with O_2 under slight pressure ($p_{O2} =$ 3 atm) and substrate/NaOH=1 molar ratio, that the alkali increased the oxidation rate and alumina was a better supporting material than carbon [32].

From tertiary amines, mono- and bimetallic catalysts (Au/C, Pt/C, Rh/C, Au–Pt/C, Au–Rh/C, Au/Al_2O_3, Au/TiO_2) favored the formation of corresponding N-oxides under "green" conditions, that is working in aqueous solution with molecular oxygen under mild conditions [135]. 100% yields were achieved with triethylamine and pyridine using Au/C as a catalyst under appropriate conditions. In the case of N-substituted aminoalcohols, the oxidation took place exclusively at the nitrogen atom, thus leading to the corresponding N-oxide, while no aminoacid was formed. Hence, from 3-dimethylamino-1-propanol, the corresponding N-oxide formed with 100% regioselectivity. In principle, the oxidation of the amino group is possible both in the absence and in the presence of alkali: without any alkali, 100% selectivity was observed with different metal catalysts, but only gold-containing catalysts allowed 100% conversion, while Pt/C was inert and Rh/C led to only 20% conversion towards unidentified compounds (Table 5.4).

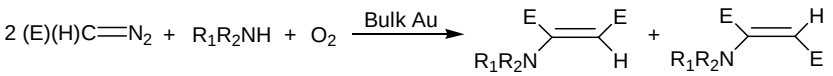
Angelici and coworkers discovered the remarkable activity of large gold particles (*ca.* 1000 nm) in the reactions of carbon monoxide or isocyanides, with primary amines and molecular oxygen under mild conditions, yielding ureas or carbodiimides, respectively [136–140]. They also showed that bulk gold is effective in the

TABLE 5.4 Oxidation of 3-dimethylamino-1-propanol by Molecular O_2 on Different Catalysts[a]

Catalyst	Conversion (%)	Selectivity to N-oxide (%)
1% Au/C	100	100
1% Au/Al_2O_3	100	100
1% Au/TiO_2	95	100
1% Rh/C	20	0
1% Pt/C	0	0
0.5%Au-0.5%Rh/C	33	100
0.5%Au-0.5%Pt/C	40	100

[a]Substrate $= 0.4\ mol\ L^{-1}$, substrate/metal = 1000, $p_{O2} = 2$ atm, $T = 90\,^{\circ}C$, $t = 24$ h.

oxidative dehydrogenation of secondary amines to imines. The discovery of a novel aerobic reaction catalyzed by bulk gold, able to transform diazoalkanes and amines into enamines (Eq. 5.7), is ascribed to the same research team: this is the first report on such a catalytic reaction and the process is simple and effective, allowing high yields (58–94%) [140].



(5.7)

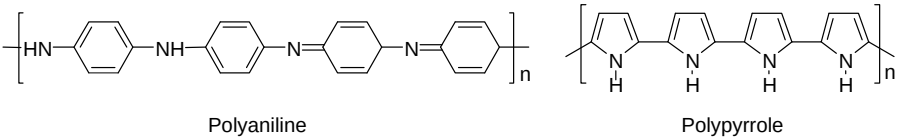
Mullins and coworkers have also shown that bulk gold can be an active catalyst, as in the case of the oxidation of propylamine with oxygen to proprionitrile and propionaldehyde [141]. However, these are just a few exceptions emerging from a two-decade-long research activity, during which the superiority of nanometric gold over bulk *status*, has been generally underpinned in numerous oxidation reactions. Corma's group has recently confirmed this by successfully applying supported gold nanoparticles to the aerobic oxidation of amines [142]. After a broad and thorough investigation on various substrates, they concluded that the oxidation of amines to benzylidene amines on gold is a structure-sensitive reaction that requires small crystallites. Gold supported on carbon catalyzed full oxidative cross condensation of benzylamines and amines selectively, while gold supported on titania favored the formation of secondary benzylamines through a one-pot two-step reaction that involves one oxidative crosscondensation step followed by hydrogenation.

The catalytic effectiveness of nanogold on titania in the aerobic oxidation of amines was also shown by Christensen and coworkers [143, 144]. They reported on gold's ability in promoting the oxidation of *n*-hexyl amine and 1,6-hexanediamine with high selectivity into the corresponding amides, *N*-hexyl hexanoic amide and caprolactam, respectively.

Finally, Baiker and coworkers recent work describing a novel generation of gold catalysts for amines oxidation is note worthy, showing how it is possible to synthesize an efficient catalyst without using any dedicated step for the creation of supported gold nanoparticles [145–147]. They started from $Au(OAc)_3$ precursor and an oxidic support (CeO_2, TiO_2, SiO_2, Al_2O_3), which were simply added to the reaction mixture to form *in situ* supported gold nanoparticles, without any reduction or calcination step. They then progressively improved the catalyst preparation protocol and extended the kind of substrates, always demonstrating the catalyst to be truly heterogeneous and reusable, as well as active in the aerobic oxidation of amines. Among the examined substrates, benzylamine, dibenzylamine and indoline were converted to the corresponding imines in 89–100% yield. By comparison, bulk powder gold did not show any detectable catalytic activity under similar conditions.

5.3.5 Oxidative Polymerization of Aniline and Pyrrole

Conducting polymers are appealing materials due to their eclectic peculiarities: they display the typical electronic properties of both metals and semiconductors,



Polyaniline Polypyrrole

FIGURE 5.1 Polyaniline and polypyrrole structures.

associated with the mechanical properties of organic macromolecules. Since the end of the 1970s, when the first highly conducting polyacetylene (PA) was synthesized, a progressive interest has emerged in the synthesis of other organic conducting polymers, mainly polyaniline and polypyrrole (PPy) (Figure 5.1).

These efforts have led to their applications in many devices combining optical, electrochemical and conducting properties, where polyaniline and polypyrrole are particularly appealing owing to their stability in air and tuneable conductivity [148]. PANI conductivity is related to the degree of acid doping (pH) and the oxidation state of the material: equal numbers of oxidized and reduced units (emeraldine form), with one proton doping every two units, guarantee optimum conductivity of the polymer [149, 150].

Another fundamental factor influencing the characteristics and performance of the material is the morphology of the conducting polymers. Various geometries such as films, hollow spheres and nanoparticles allow these materials to be widely employed as OLED (organic light-emitting diodes), drug delivery, and materials for absorption and separation. Different synthetic methods are available for addressing the final shape of the material [148, 151]. The following section reports a brief overview of the present catalytic protocols based on gold for the preparation of polyaniline and polypyrrole.

5.3.5.1 Oxidative Polymerization of Aniline Aniline polymerization is traditionally performed through oxidative coupling of aniline or its dimer, *N*-(4-aminophenyl) aniline, using oxidants such as ammonium peroxydisulfate, $K_2Cr_2O_7$, KIO_3. When aniline is oxidized in an acidic aqueous medium with ammonium peroxydisulfate, a PANI precipitate is produced. During the polymerization the initially formed blue *pernigraniline* converts into the green protonated *emeraldine*. The reaction is exothermic and leads, besides PANI, to sulfuric acid as a byproduct. It is possible to monitor the polymerization progress by recording either the temperature or the pH. Even though the whole mechanism has not yet been elucidated, it is known that aniline oxidation with ammonium peroxydisulfate in aqueous solution of strong (sulfuric) or weak (acetic) acids occurs by substantially different pathways: while in sulfuric acid solution a granular PANI can be produced, in acetic acid solution PANI nanotubes can be obtained. Moreover, when ammonium peroxydisulfate is used as an oxidant, aniline polymerization proceeds well in water even without any added acid, because sulfuric acid produced by the decomposition of peroxydisulfate already provides the necessary acidity [148]. However, the advantage given by the ease of such a synthesis protocol is not accompanied by notable conductive properties of the derived polyaniline. Moreover, the presence of inorganic byproducts represents a

further drawback due to their disposal, while employing other reagents, such as metals in a high oxidation state, does not always offer a better solution [152–157]. The use of gold and copper as the catalysts for polyaniline synthesis has opened up a potentially green route to this conducting material [158, 159].

The aniline/emeraldine emichlorohydrate redox potential is quite high (*ca.* 1.46 V), thus causing a thermodynamic barrier to the aerobic oxidation of aniline (E° $O_2/H_2O = 1.23$ V), but a favorable situation exists with the other eco-friendly oxidant H_2O_2 ($E^\circ = 1.78$ V). However, aniline, even if dissolved in aqueous HCl, is inert towards oxidation with H_2O_2 without a suitable catalyst. Rossi and coworkers have recently found that the addition of a gold catalyst allows the insoluble green polymer "emeraldine" to be obtained, then purified by extraction with 1-methyl-2-pirrolidone and evaporation of the solvent under vacuum [148, 158]. Different gold-based catalytic systems were tested (colloidal gold, gold supported on carbon and gold supported on titania), with Au/TiO_2 displaying the best performance, especially in terms of yield to PANI. Only a scarce catalytic effect (typically 4–5% yield) was detected when a small amount of colloidal gold (Au: aniline = 0.001, molar ratio) was employed in the presence of H_2O_2. No product was isolated without any catalyst and no benefit was observed from using H_2O_2 in excess, but the PANI yield could be improved by increasing the gold amount in the range Au:Aniline = 0.001–0.004 (molar ratio), thus reaching the asymptotic value of 27% after a 1-day reaction (Table 5.5). With oxygen as the oxidizing reagent, no oxidative polymerization of aniline was observed, even using different catalytic systems under a slight oxygen pressure (3 atm) at room temperature.

The well-known short catalytic life of "naked" gold particles in oxidation reactions [28] could explain the modest conversion of aniline to PANI. In order to support such a hypothesis, the oxidative polymerization of aniline was also carried out in the presence of supported gold catalysts (0.5% Au/C, 1% Au/TiO_2), actually allowing improved performances (Table 5.6).

In particular, the superior performance of Au/TiO_2 with respect to Au/C can be ascribed to a synergistic effect of the supporting material titania with gold. In fact, differently from carbon support, which was inert in aniline polymerization by H_2O_2, P25 titania itself catalyzed the partial oxidation of aniline to soluble dark oligomers. However, without any gold loading, no long-chain polymer could be formed.

TABLE 5.5 Oxidative Polymerization of Aniline with H_2O_2 by Colloidal Gold Catalysis[a]

Au: Aniline (molar ratio)	H_2O_2: Aniline (molar ratio)	Yield (%)
0	1	0
0.001	1	4.8
0.001	2	4.8
0.001	4	4.0

[a]Aniline 0.05 mol L^{-1}, HCl 0.025 mol L^{-1}, solvent water, $T = 20\,^\circ$C, $t = 24$ h, nitrogen atmosphere.

TABLE 5.6 Oxidative Polymerization of Aniline with Gold Supported Catalysts in the Presence of H_2O_2[a]

H_2O_2: Aniline[b]	Au: Aniline[b]	Catalyst	Yield (%)
1	1 : 1000	0.5% Au/C	12
1	1 : 1000	1% Au/TiO_2	70

[a]Aniline 0.05 mol L^{-1}, HCl 0.025 mol L^{-1}, solvent water, $T = 20\,^{\circ}C$, $t = 24$ h, N_2 atmosphere.
[b]Molar ratio.

The products obtained in all the preparations were identified as ES (*emeraldine* salt) according to the FT-IR, UV-vis and XRD spectra, while the morphology of the products was analyzed by transmission electron microscopy (TEM) and scanning electron microscopy (SEM). Emeraldine mainly forms as nanospheres of 44–160 nm with both Au/C and Au/TiO_2 catalysts (Figure 5.2).

The conductivity of the polymer obtained in the high-yield route with Au/TiO_2 catalyst (Table 5.6) reached the value of 1.5×10^{-1} S/cm, as determined by a

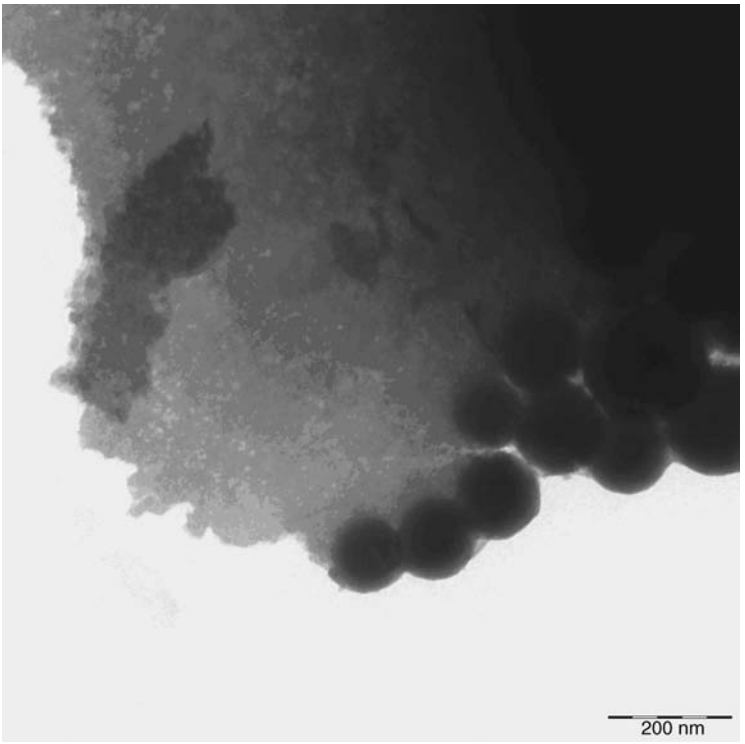
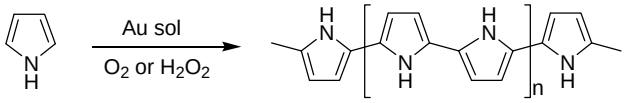


FIGURE 5.2 TEM picture of polyaniline nanospheres obtained during aniline oxidative polymerization by H_2O_2 and Au/TiO_2.



SCHEME 5.4 Oxidative polymerization of pyrrole by gold catalysis.

standard conductivity cell (CON-H Material Mates), and this value is similar to those obtained through other polymerization methods [158].

5.3.5.2 Oxidative Polymerization of Pyrrole The metal-assisted oxidative polymerization of pyrrole (Py) has drawn minor attention if compared to aniline, but the results reported by Rossi and coworkers demonstrate the effectiveness of such a route. The authors reported the first example catalyzed by colloidal gold in aqueous solution and mild conditions, using O_2 and H_2O_2 as oxidants (Scheme 5.4) [160].

Blank tests were conducted with air or oxygen and with hydrogen peroxide as the oxidizing reagents: by stirring the aqueous solution of pyrrole hydrochloride at room temperature for several days, under air and in the absence of gold nanoparticles, no insoluble product was collected from the dark solution, meaning that only short-chain oligomers could form by spontaneous auto-oxidation. Using pure dioxygen under pressure (3 atm) led to a modest yield of insoluble polymer (12%) after 3 days. On the other hand, with hydrogen peroxide as the oxidant, a notable pyrrole polymerization was achieved even in the absence of any catalyst, yielding 57% of the polymeric material after 1 day. The addition of gold, in the form of colloidal nanoparticles, to an acidic (HCl) aqueous solution of pyrrole, under oxygen ($pO_2 = 3$ atm) at room temperature, allowed a slow oxidative polymerization. The observed yields of polypyrrole, up to 75% after 1 day and almost 100% after 3 days, depended on the total gold amount ranging in the interval Py:Au = 1000–10 000 molar ratio (Figure 5.3). A significant improvement could be achieved employing H_2O_2, instead of O_2, as the oxidizing agent [160]. Yields as high as 99% were obtained after 24 h, as against 57% observed in the absence of any catalyst.

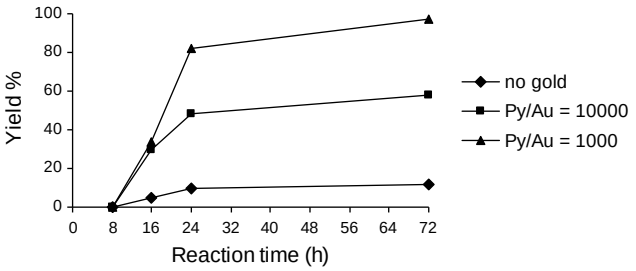


FIGURE 5.3 Oxidative polymerization of pyrrole with oxygen, with and without gold. Reaction conditions: pyrrole (Py) 0.15 mol L^{-1}, HCl 0.15 mol L^{-1}, water, $p_{O2} = 3$ atm, $T = 20\,^{\circ}C$.

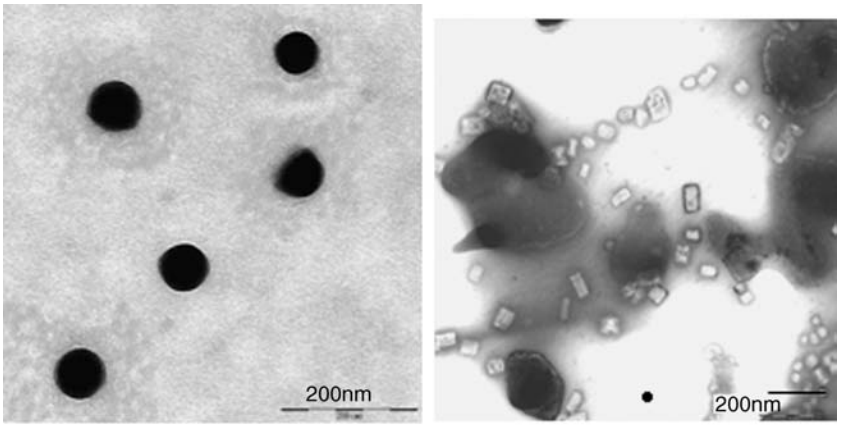


FIGURE 5.4 TEM images of polypyrrole obtained by aerobic polymerization. a) uncatalyzed erobic reaction; b) catalyzed aerobic reaction.

As far as morphology is concerned, a concert of different analytical techniques allowed the characterization of the obtained polypyrrole structures. These, independently from the synthetic method, displayed a similar IR spectrum, clearly showing stretching absorptions of C=C (1560 and 1471 cm^{-1}) and C−N (1385 and 1311 cm^{-1}) bonds, and bipolaron bands (1196 and 923 cm^{-1}). Typical X-ray diffraction patterns, further confirmed their identity [148].

TEM analyses pictured different morphologies for different experimental protocols. The low-yield, noncatalyzed polymerization with gaseous oxygen produced more ordered structures, made up of 40–80 nm spheres, whereas a large amount of peculiar thin squares (20–60 nm) were observed in the high yield polymerization catalyzed by gold (Figure 5.4). Using H_2O_2, the uncatalyzed polymerization led to a partly reticulated structure, whereas catalysis by gold produced an amorphous material. The latter structure is unusual, also in the context of conventional polymerizations of pyrrole, and could be of interest for composite special applications.

The conductivity correlated to the bulk resistance of the synthesized polypyrrole materials ranged from 2.7×10^{-4} to 5×10^{-3} S cm^{-1}. As already observed in the case of polyaniline, also these values are in line with the typical conductivity registered using conventional preparation methods with stoichiometric reagents, but much lower than the values generally found in electrochemical film deposition [148].

5.4 REACTION MECHANISMS

The activity of gold particles for a number of oxidations and hydrogenations starts to increase dramatically as the size falls below 3 nm. This is accompanied by an increased propensity to chemisorption, especially of oxygen and hydrogen.

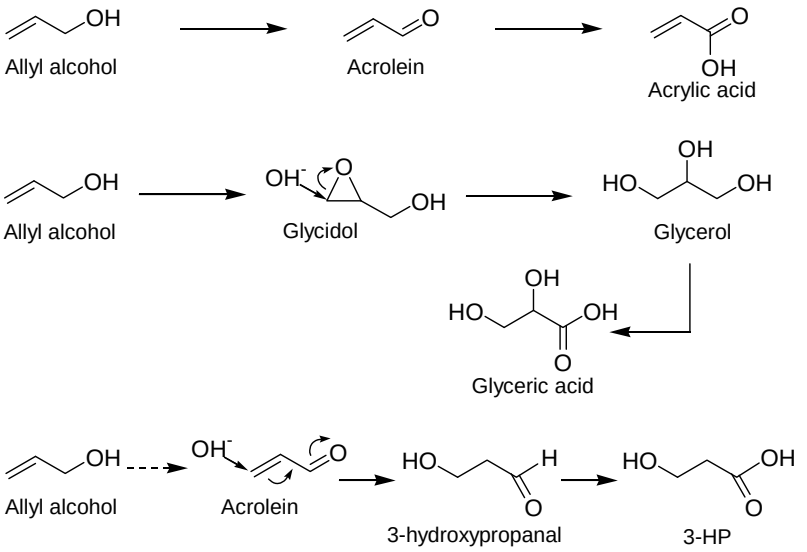
One explanation puts into relation the catalytic activity with the strength and extent of chemisorption of the reactants, the latter depending in turn on the electronic structure of the gold atoms constituting the active center. Examination of the electronic changes points to a loss of metallic character at about 3 nm, as energy bands are replaced by levels and a bandgap appears, but the definite reason for this is still a matter for debate and it continues to be a fertile area for theoreticians [7]. It is also natural to look at the changing surface/volume ratio, and consideration of static models of various crystal forms immediately suggests that the proportion of atoms of low coordination number occurring at edges and corners, often identified as the locus of the activity, increases rapidly as the particle size gets smaller and smaller [161]. Theoretical studies also indicate a different electronic structure for atoms close to the surface [162].

The mechanisms of liquid phase oxidations on gold are less investigated and understood than for certain gas phase oxidations, probably because proper kinetic measurements are hard to obtain. However, what has been found regarding the interaction of oxygen with gold is that O_2 may be involved in one of four ways: a) by becoming adsorbed on the support in an activated form adjacent to a gold particle to which the other reactant is attached; b) by directly reacting with that reactant *via* a Eley-Rideal mechanism without prior chemisorption; c) by extracting electrons from gold atoms with the formation of an ionic bond such as Au^{+}–O_2^{-}; d) by dissociative chemisorption into atoms on the same kind of surface sites.

A specific feature of liquid phase oxidations is their better performances with bimetallic catalysts, as has been frequently shown throughout this chapter. There appears to be little understanding of why bimetallic catalysts are preferable and even their physical structure is generally unknown. Unfortunately, systematic mechanistic studies on bimetallic catalysts are not yet available.

Relatively more information is available on certain oxidations. The currently widely accepted mechanism for alcohols was proposed in analogy to that of Pd and Pt catalysts. Accordingly, the first step consists in the formation of a metal alcoholate by reaction of positively charged gold atoms, acting as Lewis-acid sites, with the free alcohol or the alcoholate in solution. Alternately, the alcohol or the alcoholate can interact with other Lewis-acid sites present on the support next to gold atoms. In this case the support cooperates in the reaction mechanism, favoring the adsorption of the substrate. Alcoholates, due to their higher basicity, interact more strongly with such sites than corresponding neutral alcohols. Taking into account that water competes with the alcohol for the Lewis sites, for those reactions carried out in aqueous media the presence of strong alkali conditions is usually necessary to promote the oxidation by giving rise to a sufficient concentration of alcoholate. After the metal alcoholate is formed, hydride transfer from O−C−H to the metal atom occurs, with the formation of a metal hydride and a ketone still adsorbed on the gold. This is apparently the rate-determining step of the process. After its formation, the ketone is desorbed and the metal hydride restored to the initial metal site by oxygen forming water.

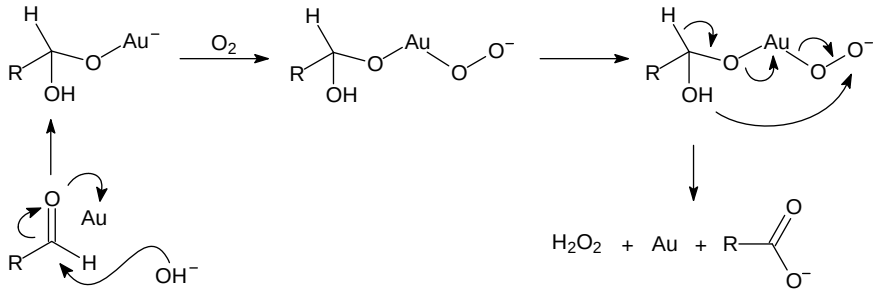
Kinetic studies on the oxidation of glycerol catalyzed by Au/C confirmed the need for basic conditions, with the rate dependent on glycerolate concentration



SCHEME 5.5 Allyl alcohol oxidation by gold catalysis: possible routes to the products.

(Section 5.3.2.1). Nonetheless, bimetallic Au–Pd nanoparticles, prepared by the immobilization of Au sol onto activated carbon followed by immobilization of Pd(0), showed superior activity compared to monometallic Pd or Au nanoparticles on the same support [46]. Their use allowed elimination of the need for a base while maintaining high the activity and selectivity [58]. By selecting a proper alloy of metals, namely Au–Pt, and supporting material, particularly H-mordenite, it became possible to prepare an active and durable catalyst, highly selective towards the formation of oxidized C_3 molecules from glycerol under acidic conditions. Again, the reason why proper bimetallic formulations markedly change the catalytic performance of the corresponding monometallic systems still needs to be disentangled.

The reaction mechanism for allyl alcohol oxidation with O_2 leading to the observed products, namely, 3-hydroxypropionate, glycerate and acrylate (Section 5.3.2.3), has been difficult to develop (Scheme 5.5) [49]. In fact, during the initial transformation of the reagent, besides acrylic acid, glyceric acid and trace amounts of glycerol (<1%) no transient precursors of 3-hydroxypropionate could be detected, despite very frequent sampling. Specific tests showed that glycerol could transform into glyceric acid under reaction conditions but neither acrylic acid, nor glyceric acid and 3-hydroxypropene oxide (glycidol) could lead to 3-hydroxypropionic acid in detectable amounts, thus suggesting different parallel routes for the different kind of products. On using acrolein in progressive small additions as the starting reagent, instead of allyl alcohol, 3-hydroxypropionate formed in 10% yield after a 24-h reaction. This experiment suggested acrolein as a possible non detectable intermediate undergoing a base-catalyzed Michael addition of water to give



SCHEME 5.6 Electron-rich gold and dioxogold species suggested as intermediates in the mechanism of glucose oxidation.

3-hydroxypropanal. The observed 3-hydroxypropionate would derive by a fast oxidation of the aldehyde.

Detailed kinetic studies carried out by Claus in Germany and Rossi in Italy (Section 5.3.3), were crucial to the elaboration of the reaction mechanism of aerobic oxidation of glucose by gold catalysts4 [37, 38, 40]. The fundamental step was shown to be the formation of the electron-rich gold species, by the chemisorption of hydrated glucose anion on gold. This species is supposed to activate oxygen by nucleophilic attack and the derived dioxogold intermediate can then behave as a bridge for the two-electron transfer from glucose to dioxygen (Scheme 5.6).

A geometrical model for describing the electronic properties of two catalysts made of carbon-supported gold particles, prepared according to colloidal gold deposition and having an average size of 3.30 nm and 7.89 nm, respectively, has been derived at Milan University [41]. The tests were conducted by progressively poisoning these catalysts with thiocyanate, cyanide, cysteine and thiourea during the aerobic oxidation of glucose: the observed deactivation trend followed the order thiocyanate$>$ cyanide$\approx$cysteine $>$ thiourea. The kinetics of deactivation led to the supposition of a long range poison-catalyst interaction influencing the entire metal particle, as a contribution of electronic factors that overlap the space shielding of active sites. The evaluation of the kind of molecules causing a detectable poisoning effect, as well as the promoting effect of OH^-, allowed the conclusion to be drawn that the dioxygen reduction step is differently influenced by soft and hard nucleophiles. Whereas a hard nucleophile prevents backdonation from the metal to the Lewis base, thus leaving in the reacting solution the original or a higher catalytic effect, as in the case of OH^-, a soft nucleophile, showing π backbonding ability, can withdraw the electron density from the metal, thus inhibiting dioxygen reduction and decreasing the catalytic property of the entire gold particle.

Kinetic studies led to the conclusion that PVP-stabilized AuNPs and PdNPs operate by different mechanisms in benzylic alcohol oxidation (Section 5.3.2.2). The most relevant difference is that in the case of AuNPs the rate-determining step involves the H-atom abstraction by a superoxo-like oxygen species adsorbed on Au. This superoxo species, evolving to hydrogen peroxide, was also invoked on the

basis of kinetic studies for glucose and benzylic alcohol oxidation by gold [88]. Regarding PdNPs, the rate-determining step is represented by the transfer of H atom of the β-carbon of the adsorbed alkoxide to form the aldehyde and a Pd–hydride species.

A study on the aerobic oxidation of alcohols employing a series of *p*-substituted benzyl alcohols (Hammett methodology), clearly showed that the rate-determining step of the reaction is the generation of a partial positive charge at the benzylic position (i.e. hydride abstraction) [88]. The use of an alcohol substrate deuterated at this position confirmed the result: a kinetic isotope effect ($k_H/k_D = 1.41$) was in fact determined. The authors suggested the existence of a special gold site, which stabilizes the formation of a cation, and a neighboring gold site responsible for "hosting" the reactive oxo-moiety. According to their kinetic studies, the activation of the alcohol indeed involves the cleavage of the C–H(D) bond at benzylic position, thus leaving behind a partial positive charge.

5.5 CATALYST STABILITY

The activity and selectivity of heterogeneous catalysts normally decay during reaction, due to various reasons. Active sites may become poisoned by the adsorption of impurities in the feed stream. The fouling of the surface and blockage of pores by heavy organics, may limit the access to active sites. The loss of surface area and the changes in the electronic state by crystal growth and agglomeration, often as a consequence of thermal degradation, as well as the loss of catalytic species due to metal leaching or chemical transformations, may also contribute to activity decline. The adsorption of poisons may not only block active sites, but also change the electronic and/or geometric structure of the surface, thus making it difficult to restore the original performance of gold once poisoned. Coke deposits can be easily removed by oxidation–reduction cycles at high temperature, however, at the risk of sintering, particularly harmful for activity. As such a transformation is irreversible, no restoring of initial activity would be generally possible for sintered particles.

Leaching control is extremely important for liquid phase oxidations with heterogeneous catalysts. Frequently, leached metal species are responsible for catalytic activity observed in some reactions, erroneously considered to be heterogeneous, which are in fact homogeneous. To answer this question, Sheldon et al. suggested a practical method consisting in separating the catalyst from the reaction mixture before cooling and continuing the reaction in its absence [163]. For a truly heterogeneous oxidation, the activity of the clear solution in a subsequent catalytic test should be negligible. Unfortunately, the leaching of gold nanoparticles from some kinds of support is still quite serious. One possible solution is to "activate" the supporting material in order to allow metal nanoparticles to be better bound and stabilized on the surface. This can be carried out by both chemical and physical pretreatments of the support.

Carbon, commonly used as a support of noble metals, possesses oxygenated functionalities on its surface (e.g., carboxylic, phenolic, lactone and ether groups)

that are responsible for both acid/base and redox properties. Its chemical activation by oxidative treatment increases the density of surface acidic sites, while it destroys basic ones. Such a treatment can be performed by different oxidants: HNO_3, H_2O_2, O_2. The final effect is the improvement of metal dispersion and stability, promoted by the oxygenated groups created on the support. Another means of chemical activation consists in the functionalization of the surface. Functional groups, originally present, can be boosted by binding different ligands. This enables the metal nanoparticles to be better grafted at the surface. Some easy and site-selective chemical modification methods, such as Schiff base formation, N-acylation and reduction, are available. Particular attention has been addressed to sulfur-containing covalent and noncovalent linkers (i.e. -SH). Indeed, due to the soft character of the -SH group leading to a high affinity for gold, thiol groups can be successfully employed as linkers for anchoring gold nanoparticles to the support.

Regarding the physical activation, it consists of a thermal treatment of carbon performed under an inert atmosphere at 800–1100 °C or in air steam at 400–500 °C, with the aim to remove the impurities and increase the surface area. Other supports are also normally subjected to suitable pretreatments.

The progressive optimization of the synthetic techniques has led to gold-based catalysts that generally display good stability on recycling and no metal leaching. The breakthrough occurred with the discovery of the improved catalytic performances and better stability achieved by gold when alloyed with a second metal, particularly Pt, Pd and Cu [18, 19, 42, 46–48, 54–59]. Among various examples present in the literature and throughout this chapter, toluene oxidation to benzyl benzoate, benzyl alcohol oxidation to benzaldehyde and allyl alcohol oxidation to 3-hydroxypropionic acid represent fitting cases. As to the oxidation of toluene, Hutchings and coworkers investigated the stability of Au–Pd/TiO_2 and Au–Pd/C. With both catalysts, the reaction was stopped at partial conversion and the catalysts were allowed to settle. The liquid phase was then carefully removed by decantation and fresh toluene was added. While for Au–Pd/TiO_2 only a catalytic test was carried out on recycled solid, showing no decay of activity, for Au–Pd/C both the recovered catalyst and the clear solution were subjected to analytic and catalytic control. No metal species was detected in the liquid phase nor showed any catalytic activity. The reaction profile of recovered solid in three further oxidation tests of toluene matched that of the fresh catalyst. When the Au–Pd/C system was used over an extended reaction period repeatedly, detailed STEM characterization showed there was minimal particle growth and morphology change. It is clear that any sintering or structural modification of this highly active catalyst is minimal, thus making it stable and reusable. By itself, Au was not active for this reaction, but the addition of Pd significantly enhanced the conversion, demonstrating a clear synergistic effect for the Au–Pd catalysts as compared with the monometallic species [54].

Prati and coworkers compared the stability of Pd nanoparticles supported on activated carbon and carbon nanotubes (CNTs), used for liquid phase oxidation of benzyl alcohol (Section 5.3.2.2) [87]. The high Pd leaching detected (28% and 25%, for Pd/C and Pd/CNTs, respectively) prompted the authors to look for a solution, eventually reached by modifying the monometallic palladium with gold. Au–Pd

supported on CNTs showed limited Pd leaching and stable catalytic performances over 8 reaction cycles, whereas Au–Pd on carbon was less stable.

Regarding allyl alcohol oxidation (Section 5.3.2.3), since Au/C turned out to be unstable as shown by the selectivity drop to 3-hydroxypropionic acid (3-HP) in the second reaction cycle (leaching could be excluded as a possible cause), Rossi and coworkers prepared and tested a series of bimetallic Au–M nanoparticles (M = Pt, Pd, Cu and Ag) supported on carbon. The conversion, selectivity and lifetime of the bimetallic catalysts could be tuned and markedly improved by optimizing the preparation protocols, as well as the experimental conditions, thus leading to notable performances also after 4 reaction cycles, especially for the 0.3% $Au_{99}Cu_1$/C system. Accordingly, the selectivity to 3-HP changed from 95% (1st cycle) to 78% (4th cycle), retaining the same conversion (around 98%). The stabilization of the catalytic activity due to the presence of the dilute second metal was likely due to electronic modifications in the gold nanoparticle. A significant particle size effect, in this case, was reputed to be unlikely, as STEM analyses showed clear signs of metal particles sintering. Most probably, the low redox potential of copper could be implicated in the sustained high performance, thus outweighing the negative effect of particle growth during recycling [59].

5.6 CONCLUSIONS

The discovery of the catalytic power of gold has signaled a breakthrough in the selective oxidation of organic compounds, thus favoring novel "green" ways towards a wide number of important chemicals. The keystone is represented by the nanometric scale: only when gold could be obtained as nanoparticles of diameter below *ca.* 15 nm, did its peculiar catalytic activity emerge. Owing to a progressive improvement of both catalyst design and experimental conditions, including the bimetallic formulations where gold is alloyed to a second metal, some processes seem now to be close to an industrial development. In particular, the liquid phase oxidation of glucose by gold catalysis is approaching as good performances as the industrially applied biochemical route.

Another important achievement is the gold-catalyzed oxidation of amines that has developed over the last three years, giving rise to a novel chapter in the organic chemistry of nitrogen compounds. A novel scenario is now emerging: the application of gold in material science, particularly promising in the facile polymerization of aniline and pyrrole *via* ecofriendly protocols. Although methods and techniques need further refinement, the versatility and effectiveness of gold catalysis provide a powerful tool for making green processes a more widespread reality.

REFERENCES

1. Haruta M., Kobayashi T., Sano H., Yamada N. (1987) *Chem. Lett.* 16, 405–408.
2. Haruta M., Yamada N., Kobayashi T., Iijima S. (1989). *J. Catal.* 115, 301–309.

3. Haruta M. (1997). *Catal. Today* 36, 153–166.
4. Haruta M. (1997). *Stud. Surf. Sci. Catal.* 110, 123–134.
5. Prati L., Rossi M. (1998). *J. Catal.* 176, 552–560.
6. Sheldon R.A., Kochi J.K. *Metal-Catalyzed Oxidations of Organic Compounds*. Academic Press, New York, 1981.
7. Bond G.C., Louis C., Thompson D.T. *Catalysis by Gold*. Catalytic Science Series, Vol. 6. Imperial College Press, London, 2006.
8. Daniel M.C., Astruc D. (2004). *Chem. Rev.* 104, 293–346.
9. Hashmi A.S.K., Hutchings G.J. (2006). *Angew. Chem. Int. Ed.* 45, 7896–7936.
10. Hashmi A.S.K. (2007). *Chem. Rev.* 107, 3180–3211.
11. Della Pina C., Falletta E., Prati L., Rossi M. (2008). *Chem. Soc. Rev.* 37, 2077–2095.
12. Carrettin S., Concepcion P., Corma A., López-Nieto J.M., Puntes V.F. (2004) *Angew. Chem. Int. Ed.* 43, 2538–2540.
13. Bond G.C., Thomson D.T. (2000). *Gold Bull*. 33, 41–50.
14. Chen M.S., Goodman D.W. (2004). *Science* 306, 252–255.
15. Hutchings G.J. (2005). *Catal. Today* 100, 55–61.
16. Weiher N., Beesley A.M., Tsapatsaris N., Delannoy L., Louis C., van Bokhoven J.A., Schroeder S.L.M. (2007). *J. Am. Chem. Soc.* 129, 2240–2241.
17. Janssens T.V.W., Clausen B.S., Hvolbaek B., Falsig H., Christensen C.H., Bligaardand T., Nørskov J.K. (2007). *Top. Catal.* 44, 15–26.
18. Hutchings G.J. (2008). *Chem. Commun.*, 1148–1164.
19. Edwards J.K., Carley A.F., Herzing A.A., Kiely C.J., Hutchings G.J. (2008). *Faraday Discuss*. 138, 225–239.
20. Edwards J.K., Solsona B., Edwin N.N., Carley A.F., Herzing A.A., Kiely C.J., Hutchings G.J. (2009). *Science* 323, 1037–1041.
21. Fu Q., Saltsburg H., Flytzani-Stephanopoulos M. (2003). *Science* 301, 935–938.
22. Fu Q., Kudriavtseva S., Saltsburg H., Fltzani-Stephanopoulos M. (2003). *Chem. Eng. J.* 93, 41–53.
23. Hashmi A.S.K., Weyrauch J.P., Rudolph M., Kurpejovic E. (2004). *Angew. Chem. Int. Ed.* 43, 6545–6547.
24. Xie J., Li H., Zhou J., Cheng Y., Zhu C. (2012). *Angew. Chem. Int. Ed.* 51, 1252–1255.
25. González-Arellano C., Abad A., Corma A., García H., Iglesias M., Sánchez F. (2007). *Angew. Chem. Int. Ed.* 46, 1536–1538.
26. Hashmi A.S.K. (2010). *Pure Appl. Chem.* 82, 1517–1528.
27. Biella S., Rossi M. (2003). *Chem. Commun.*, 378–379.
28. Comotti M., Della Pina C., Matarrese R., Rossi M. (2004). *Angew. Chem. Int. Ed.* 43, 5812–5815.
29. Pollington S.D., Enache D.I., Landon P., Meenakshisundaram S., Dimitratos N., Wagland A., Hutchings G.J., Stitt E.H. (2009). *Catal. Today* 145, 169–175.
30. Lanfranchi M., Prati L., Rossi M., Tiripicchio A. (1993). *Chem. Commun.*, 1698–1699.
31. Prati L., Rossi M. (1997). *Stud. Surf. Sci. Catal.* 110, 509–515.
32. Biella S., Castiglioni G., Fumagalli C., Prati L., Rossi M. (2002). *Catal. Today* 72, 43–49.
33. Biella S., Prati L., Rossi M. (2003). *J. Catal.* 197, 207–212.

34. Pagliaro M., Rossi M. *The Future of Glycerol: New Usages for a Versatile Raw Material*. RSC Green Chemistry Book Series, RSC Publishing, Cambridge, UK, 2008.
35. Pagliaro M., Ciriminna R., Kimura H., Rossi M., Della Pina C. (2007). *Angew. Chem. Int. Ed.* 46, 4434–4440.
36. Comotti M., Della Pina C., Falletta E., Rossi M. (2006). *J. Catal.* 244, 122–125.
37. Önal Y., Schimpf S., Claus P. (2004). *J. Catal* 223, 122–133.
38. Beltrame P., Comotti M., Della Pina C., Rossi M. (2006). *Appl. Catal. A: General* 297, 1–7.
39. Beltrame P., Comotti M., Della Pina C., Rossi M. (2004). *J. Catal.* 228, 282–287.
40. Comotti M., Della Pina C., Falletta E., Rossi M. (2006). *Adv. Synth. Catal.* 348, 313–316.
41. Della Pina C., Falletta E., Rossi M., Sacco A. (2009). *J. Catal.* 263, 92–97.
42. Comotti M., Della Pina C., Rossi M. (2006). *J. Mol. Catal. A: Chemical* 251, 89–92.
43. Baatz C., Decker N., Pruesse U. (2008). *J. Catal.* 258, 165–169.
44. Baatz C., Pruesse U. (2007). *J. Catal.* 249, 34–40.
45. Porta F., Prati L. (2004). *J. Catal.* 224, 397–403.
46. Bianchi C., Canton P., Dimitratos N., Porta F., Prati L. (2005). *Catal. Today* 102, 203–212.
47. Dimitratos N., Porta F., Prati L., Villa A. (2005). *Catal. Lett.* 99, 181–185.
48. Villa A., Wang D., Spontoni P., Arrigo R., Sub D., Prati L. (2010). *Catal. Today* 157, 89–93.
49. Della Pina C., Falletta E., Rossi M. (2009). *Chem. Sus. Chem.* 2, 57–58.
50. Kholdeeva O.A., Zalomaeva O.V., Sorokin A.B., Ivanchikova I.D., Della Pina C., Rossi M. (2007). *Catal. Today* 121, 58–64.
51. Cheneviere Y., Caps V., Tuel A. (2010). *Appl. Catal. A: General* 387, 129–134.
52. Prati L., Porta F. (2005). *Appl. Catal. A: General* 291, 199–203.
53. Korovchenko P., Donze C., Gallezot P., Besson M. (2007). *Catal. Today* 121, 13–21.
54. Kesavan L., Tiruvalam R., Ab Rahim M.H., Izham bin Saiman M., Enache D.I., Jenkins R.L., Dimitratos N., Lopez-Sanchez J.A., Taylor S.H., Knight D.W., Kiely C.J., Hutchings G.J. (2011). *Science* 331, 195–199.
55. Wang X., Venkataramanan N.S., Kawanami H., Ikushima Y. (2007). *Green Chem.* 9, 1352–1355.
56. Dimitratos N., Lopez-Sanchez J.A., Meenakshisundaram S., Anthonykutty J.M., Brett G., Carley A.F., Taylor S.H., Knight D.W., Hutchings G.J. (2009). *Green Chem.* 11, 1209–1216.
57. Wang B., Villa A., Porta F., Prati L., Su D. (2008). *J. Phys. Chem. C* 112, 8617–8622.
58. Villa A., Gaiassi A., Veith M., Prati L. (2010). *Angew. Chem. Int. Ed.* 49, 4499–4502.
59. Falletta E., Della Pina C., Rossi M., He Q., Kiely C.J., Hutchings G.J. (2011). *Faraday Discuss.* 152, 367–379.
60. Zhao R., Ji D., Lu G., Qian G., Yan L., Wang X., Suo J. (2004). *Chem. Commun.*, 904–905.
61. Lü G., Zhao R., Qian G., Qi Y., Wang X., Suo J. (2004). *Catal. Lett.* 97, 115–118.
62. Hughes M.D., Xu Y.-J., Jenkins P., McMorn P., Landon P., Enache D.I., Carley A.F., Attard G.A., Hutchings G.J., King F., Stitt E.H., Johnston P., Griffin K., Kiely C.J. (2005). *Nature* 437, 1132–1135.

63. Xu Y.-J., Landon P., Enache D.I., Carley A.F., Roberts M.W., Hutchings G.J. (2005). *Catal. Lett.* 101, 175–179.
64. Zhu K.K., Hu J.C., Richards R. (2005). *Catal. Lett.* 100, 195–199.
65. Xu L.-X., He C.-H., Zhu M.-Q., Wu K.-J., Lai Y.-L. (2007). *Catal. Lett.* 118, 248–253.
66. Levchenco L.A., Sadkov A.P., Larionsteva N.V., Koldasheva E.M., Shilova A.K., Shilov A.E. (2001). *Dokl. Biochem. Biophys.* 377, 123–124.
67. Levchenco L.A., Lobanova N.G., Martinenko V.M., Sadkov A.P., Shestakov A.F., Shilova A.K., Shilov A.E. (2010). *Dokl. Chem.* 430, 50–53.
68. Li X., Xu J., Zhou L., Wang F., Gao J., Chen C., Ning J., Ma H. (2006). *Catal. Lett.* 110, 149–154.
69. Wang F., Xu J., Li X., Gao J., Zhou L., Ohnishi R. (2005). *Adv. Synth. Catal.* 347, 1987–1992.
70. Gao J., Tong X., Li X., Miao H., Xu J. (2007). *J. Chem. Technol. Biotechnol.* 82, 620–625.
71. Brutchey R.L., Drake I.J., Bell A.T., Tilley D.T. (2005). *Chem. Commun.*, 3736–3738.
72. Singh A.P., Selvam T. (1996). *J. Mol. Catal. A: Chemical* 113, 489–497.
73. Dapurkar S.E., Yokoyama Z., Toshirou Y., Kawanami H. (2009). *Catal. Lett.* 130, 42–47.
74. Della Pina C., Falletta E., Rossi M. (2012). *Chem. Soc. Rev.* 41, 350–369.
75. Ajaikumar S., Ahlkvist J., Larsson W., Shchukarev A., Leino A.-R., Kordas K., Mikkola J.-P. (2011). *Appl. Catal. A: General* 392, 11–18.
76. Weissermel K., Arpe H.-J. *Industrial Organic Chemistry*. 3rd ed. Wiley-VCH, Weinheim, 1997, pp. 144–150.
77. Herzog B., Mark M., Stein R., Wang T. inventors; Celanese Chemicals assignee. Ger. Offen. DE10030039. 2002.
78. Lee S., Molina L.M., López M.J., Alonso J.A., Hammer B., Lee B., Seifert S., Winans R.E., Elam J.W., Pellin M.J., Vajda S. (2009). *Angew. Chem. Int. Ed.* 48, 1467–1471.
79. Ojeda M., Iglesia E. (2009). *Chem. Commun.*, 352–354.
80. Haruta M., Huang J., Takei T., Akita T. inventors; Tokyo Metropolitan University assignee. US Patent Appl. 20100234623. 2010.
81. Patil N.S., Jha R., Uphade B.S., Bhargava S.K., Choudhary V.R. (2004). *Appl. Catal. A: General* 275, 87–93.
82. Patil N.S., Uphade B.S., McCulloh D.G., Bhargava S.K., Choudhary V.R. (2004). *Catal. Commun.*, 681–685.
83. http://www.gold.org/
84. Pei Y., Shao N., Gao Y., Zeng X.C. (2010). *ACS Nano 4*, 2009–2020.
85. Turner M., Golovko V.B., Vaughan O.P., Abdulkin P., Berenguer-Marcia A., Tikhov M.S. (2008). *Nature* 454, 981–983.
86. Mallat T., Baiker A. (2004). *Chem. Rev.* 104, 3037–3058.
87. Villa A., Wang D., Dimitratos N., Su D., Trevisan V., Prati L. (2010). *Catal. Today* 150, 8–15.
88. Fristrup P., Bahn Johansen L., Christensen C.H. (2008). *Catal. Lett.* 120, 184–190.
89. Ilyas M., Sadiq M. (2007). *Chem. Eng. Technol.* 30, 1391–1397.

90. Masende Z.P.G., Kustera B.F.M., Ptasinski K.J., Janssen F.J.J.G., Katima J.H.Y., Schouten J.C. (2005). *Top. Catal.* 33, 87–99.
91. Katryniok B., Kimura H., Skrzyńska E., Girardon J.-S., Fongarland P., Capron M. (2011). *Green Chem*. 13, 1960–1979.
92. Kimura H., Tsuto K. (1993). *Appl. Catal. A: General* 96, 217–228.
93. Garcia R., Besson M., Gallezot P. (1995). *Appl. Catal. A: General* 127, 165–176.
94. Kimura H. (1993). *Appl. Catal. A: General* 105, 147–158.
95. Liang D., Gao J., Wang J., Chen P., Hou Z., Zheng X. (2009). *Catal. Commun.*, 1586–1590.
96. Carrettin S., McMorn P., Johnston P., Griffin K., Kiely C. J, Hutchings G.J. (2003). *Phys. Chem. Chem. Phys.* 5, 1329–1336.
97. Abad A., Conception P., Corma A., Garcia H. (2005). *Angew. Chem. Int. Ed.* 44, 4066–4069.
98. Enache D.I., Edwards J.K., Landon P., Solsona-Espriu B., Carley A.F., Herzing A.A., Watanabe M., Kiely C.J., Knight D.W., Hutchings G.J. (2006). *Science* 311, 362–365.
99. Wang N., Matsumoto T., Ueno M., Miyamura H., Kobayashi S.A. (2009). *Angew. Chem.* 121, 4838–4840.
100. Shan J., Tenhu H. (2007). *Chem. Commun.*, 4580–4598.
101. Tsunoyama H., Sakurai H., Negishi Y., Tsukuda T. (2005). *J. Am. Chem. Soc.* 127, 9374–9375.
102. Mertens P.G.N., Bulut M., Gevers L.E.M., Vankelecom I.F.J., Jacobs P.A., De Vos D.E. (2005). *Catal. Lett.* 102, 57–61.
103. Mertens P.G.N., Vankelecom I.F.J., Jacobs P.A., De Vos D.E. (2005). *Gold Bull*. 38, 157–162.
104. Biffis A., Cunial S., Spontoni P., Prati L. (2007). *J. Catal.* 251, 1–6.
105. Hayashi T., Inagaki T., Itayama N., Baba H. (2006). *Catal. Today* 117, 210–213.
106. Nielsen I.S., Taarning E., Egeblad K., Madsen R., Christensen C.H. (2007). *Catal. Lett.* 116, 35–40.
107. Abad A., Amela C., Corma A., Garcia H. (2006). *Tetrahedron* 62, 6666–6672.
108. Huang J., Dai W.-L., Li H., Fan K. (2007). *J. Catal.* 252, 69–76.
109. Enache D.I., Barker D., Edwards J.K., Taylor S.H., Knight D.W., Carley A.F., Hutchings G.J. (2007). *Catal. Today* 122, 407–411.
110. Abad A., Amela C., Corma A., Garcia H. (2006). *Chem. Commun.*, 3178–3180.
111. Li G., Enache D.I., Edwards J.K., Carley A.F., Knight D.W., Hutchings G.J. (2006). *Catal. Lett.* 110, 7–13.
112. Zheng N., Stucky G.D. (2007). *Chem. Commun.*, 3862–3864.
113. Choudhary V., Jha R., Jana P. (2007). *Green. Chem.* 9, 267–272.
114. Haider P., Baiker A. (2007). *J. Catal.* 248, 175–187.
115. Kimmerle B., Grunwaldt J.-D., Baiker A. (2007). *Top. Catal.* 44, 285–292.
116. Christensen C.H., Jorgensen B., Rass-Hansen J., Egeblad K., Madsen R., Klitgaard S.K., Hansen S.M., Hansen M.R., Andersen H.C., Riisager A. (2006). *Angew. Chem. Int. Ed.* 45, 4648–4651.
117. Ketchie W.C., Murayama M., Davis R.J. (2007). *Top. Catal.* 44, 307–317.

118. Milone C., Ingoglia R., Neri G., Galvagno S. (2001). *Appl. Catal. A: General* 211, 251–257.
119. Carrettin S., McMorn P., Johnston P, Griffin K, Hutchings G.J. (2002). *Chem. Commun.*, 696–697.
120. Prati L., Spontoni P., Gaiassi A. (2009). *Top. Catal.* 52, 288–296.
121. Gallezot P. (1997). *Catal. Today* 37, 405–418.
122. Fordham P., Besson M., Gallezot P. (1997). *Catal. Lett.* 46, 195–199.
123. Demirel S., Kern P., Lucas M., Claus P. (2007). *Catal. Today* 122, 292–300.
124. Mertens P.G.N., Vendezande P., Ye X., Poelman H., De Vos D.E., Vankelecom I.F.J. (2008). *Adv. Synth. Catal.* 350, 1241–1247.
125. Miedziak P.J., Tang Z., Davies T.E., Enache D.I., Bartley J.K., Carley A.F., Herzing A.A., Kiely C.J., Taylor S.H., Hutchings G.J. (2009). *J. Mater. Chem.* 19, 8619–8627.
126. Liu Y., Tüysüz H., Jia C.-J., Schwickardi M., Rinaldi R., Lu A.-H., Schmidt W., Schüth F. (2010). *Chem. Commun.* 46, 1238–1240.
127. Besson M., Lahmer F., Gallezot P., Fuertes P., Fleche G. (1995). *J. Catal.* 152, 116–121.
128. Besson M., Gallezot P. (2000). *Catal. Today* 57, 127–141.
129. Biella S., Prati L., Rossi M. (2002). *J. Catal.* 206, 242–247.
130. Ishida T., Kinoshita N., Okatsu H., Akita T., Takei T., Haruta M. (2008). *Angew. Chem. Int. Ed.* 47, 9265–9268.
131. Benkóa T., Beck A., Geszti O., Katona R., Tungler A., Frey K., Guczi L., Schay Z. (2010). *Appl. Catal. A: General* 388, 31–36.
132. Yin H., Zhou C., Xu C., Liu P., Xu X., Ding Y. (2008). *J. Phys. Chem. C* 112, 9673–9678.
133. Ishida T., Kuroda K., Kinoshita N., Minagawa W., Haruta M. (2008). *J. Colloid Interf. Sci.* 323, 105–111.
134. Kowalczyk J., Begli A.H., Prüsse U. Berndt H., Haji A., Pitsch I., inventors; Südzucker AG assignee. Eur. Pat. 2332900. 2011.
135. Della Pina C., Falletta E., Rossi M. (2007). *Top. Catal.* 44, 325–329.
136. Lazar M., Angelici R.J. (2006). *J. Am. Chem. Soc.* 128, 10613–10620.
137. Zhu B., Angelici R.J. (2006). *J. Am. Chem. Soc.* 128, 14460–14461.
138. Zhu B., Angelici R.J. (2007). *Chem. Commun.*, 2157–2159.
139. Zhu B., Lazar M., Trewyn B.G., Angelici R.J. (2008). *J. Catal.* 260, 1–6.
140. Zhou Y., Angelici R.J., Woo L.K. (2010). *Catal. Lett.* 137, 8–15.
141. Gong J., Yan T., Mullins C.B. (2009). *Chem. Commun.*, 761–763.
142. Grirrane A., Corma A., Garcia H. (2009). *J. Catal.* 264, 138–144.
143. Klitgaard S.K., Egeblad K., Mentzel U.V., Popov A.G., Jensen T., Taarning E., Nielsen I.S., Christensen C.H. (2008). *Green Chem.* 10, 419–423.
144. Kegnæs S., Mielby J., Mentzel U.V., Christensen C.H., Riisager A. (2010). *Green Chem.* 12, 1437–1441.
145. Aschwanden L., Mallat T., Krumeich F., Baiker A. (2009). *J. Mol. Catal. A: Chemical* 309, 57–62.
146. Aschwanden L., Mallat T., Maciejewski M., Krumeich F., Baiker A. (2010). *ChemCatChem* 2, 666–673.

147. Aschwanden L., Panella B., Rossbach P., Keller B., Baiker A. (2009). *ChemCatChem* 1, 111–115.
148. Della Pina C., Falletta E., Rossi M. (2011). *Catal. Today* 160, 11–27.
149. Mallick K., Witcomb M.J., Dinsmore A., Scurrell M.S. (2005). *Rapid Commun*. 232–235.
150. Mallick K., Witcomb M.J., Dinsmore A., Scurrell M.S. (2006). *J. Polym. Res.* 13, 397–401.
151. Sapurina I., Riede A., Strejskal J. (2001). *Synth. Met.* 123, 503–507.
152. Feng X., Mao C., Yang G., Hou W., Zhu J. (2006). *Langmuir* 22, 4384–4389.
153. Mallick K., Witcomb M.J., Dinsmore A., Scurrell M.S. (2005). *Langmuir* 21, 7964–7967.
154. Wang Y., Liu Z., Han B., Sun Z., Huang Y., Yang G. (2005). *Langmuir* 21, 833–836.
155. Sun Z., Geng Y., Li J., Wang X., Jing X., Wang F. (1999). *J. Appl. Polym. Sci.* 72, 1077–1084.
156. Sarma T.K., Chowdhury D., Paul A., Chattopadhyay A. (2002). *Chem. Commun.*, 1048–1049.
157. Moon D.K., Osokada K., Maruyama T., Yamamoto T. (1992). *Macromol. Chem.* 193, 1723–1728.
158. Chen Z., Della Pina C., Falletta E., Lo Faro M., Pasta M., Rossi M., Santo N. (2008). *J. Catal.* 259, 1–4.
159. Chen Z., Della Pina C., Falletta E., Rossi M. (2009). *J. Catal.* 267, 93–96.
160. Della Pina C., Falletta E., Lo Faro M., Pasta M., Rossi M. (2009). *Gold Bull*. 42, 27–33.
161. Bond G.C. (2011). *Faraday Discuss*. 152, 277–291.
162. Liu Z.-P., Hu P., Alavi A. (2002). *J. Am. Chem. Soc.* 124, 14770–14779.
163. Sheldon R.A., Wallau M., Arends I.W.C.E., Schuchardt U. (1998). *Acc. Chem. Res.* 31, 485–493.

6

SELECTIVE LIQUID PHASE OXIDATIONS IN THE PRESENCE OF SUPPORTED POLYOXOMETALATES

Craig L. Hill* and Oxana A. Kholdeeva*

6.1 INTRODUCTION

The selective catalytic oxidation of organic compounds with environmentally benign, cheap and readily available oxidants is the most economic and ecological route to a wide variety of valuable oxygen-containing products and intermediates [1–6]. Although heterogeneous catalysis offers the clear advantages of facile catalyst separation and recycling and thus better meets the requirements of sustainable chemistry, which has become one of the greatest scientific challenges of our time [7–9], many bulk chemicals and a few fine and specialty chemicals are produced using homogeneous catalysts [1, 5, 10–12]. Moreover, most fine chemical manufactures still employ conventional stoichiometric processes that use hazardous reagents and produce a huge amount of inorganic waste [2]. In the past decades, the replacement of stoichiometric and homogeneous oxidation processes by environmentally friendly technologies, which employ heterogeneous catalysts and "green" oxidants – O_2 and H_2O_2 – has become a widely accepted strategy [2, 6, 7, 13]. However, progress in this direction is obstructed by the limited availability of efficient and stable heterogeneous catalysts for selective oxidations in the liquid phase [2, 12–16]. The development of new leaching-tolerant solid catalysts would have a major impact in industrial applications as well as in scientific research.

*Corresponding authors

Liquid Phase Oxidation via Heterogeneous Catalysis: Organic Synthesis and Industrial Applications, First Edition. Edited by Mario G. Clerici and Oxana A. Kholdeeva.
© 2013 John Wiley & Sons, Inc. Published 2013 by John Wiley & Sons, Inc.

In recent years, much attention was focused on the elaboration of different approaches that allow constructing on a surface or within pores of solid supports spatially well-separated active centers, uniform in composition and distribution. Such catalysts, which have received the name "single-site heterogeneous catalysts" (SSHC) [17–20], are believed to combine the advantages of both homogeneous catalysts (activity and selectivity) and heterogeneous ones (simplicity of separation and recycling). The key strategies to their design involve introduction of an active center (it can be either mononuclear or polynuclear) into an inert matrix using different methodologies, such as framework substitution, grafting, tethering, encapsulation, intercalation, and some others [17–25].

It is well-known that conventional transition-metal complexes, homogeneous or heterogenized by means of different techniques, are disposed to destruction owing to thermodynamically favorable oxidation of organic ligands. Although several techniques have been developed to improve the stability of such catalysts, fully inorganic systems have more scope for practical applications than those containing organic ligands or supports [15]. These facts have greatly increased interest in a large family of early transition-metal oxygen-anion nanosize clusters or polyoxometalates (POMs), which have completely inorganic, metal oxide-like structure and are, therefore, thermodynamically stable to oxidation. POMs have a general formula $[X_xM_mO_y]^{q-}$ $(x \leq m)$ where X is defined as the heteroatom and M are the addenda atoms. The latter are usually either Mo^{VI} or W^{VI}, while the heteroatom can be ether a transition-metal or main-group element (the most common heteroatoms are P^V and Si^{IV}). An extensive review literature on different aspects of POM chemistry, including catalysis, is available [26–47].

POMs have several advantages as oxidation catalysts: (i) their redox and acid–base properties as well as solubility can be controlled by changing the chemical composition and/or structure, (ii) they are not prone to oxidative and thermal degradation in comparison with organometallic complexes (generally POM are stable to at least 350–450 °C in the presence of molecular oxygen), and (iii) most POMs possess good hydrolytic stability over a wide pH range. Some structural types of POMs that will be discussed in this chapter in context with their oxidation catalysis are shown in Figure 6.1.

A large variety of POMs can be obtained by linking metal–oxygen building units either as existing or virtual species [33, 37, 48]. The apparent structural analogy of POMs and metal oxide surfaces allows viewing POMs as discrete, soluble

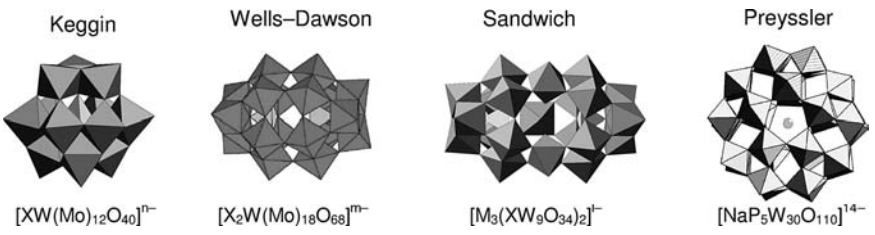


FIGURE 6.1 Polyhedral drawings of some structural types of polyoxometalates.

fragments of extended metal-oxide lattices [42, 49–53]. Significantly, POMs can be designed and characterized at the atomic/molecular level, both structurally and mechanistically, which makes them good objects for studying the structure–activity relationships and mechanisms of catalysis.

In view of the numerous advantages of POMs, the development of strategies for converting them to solid catalysts that could be easily separated from reaction mixtures and reused is of primary interest. First, catalytically active POMs can be heterogenized in the form of insoluble salts using Cs^+, Ag^+, K^+, NH_4^+ and some organic polycations [54–62]. Such salts possess micro/mesoporous texture and their surface area is typically in the range of 10–150 $m^2\,g^{-1}$. The second general approach involves dispersion or immobilization of POMs on a suitable carrier material and/or entrapping them within inert matrices. A combination of both approaches is also possible [63–65]. Solidification of POMs through the use of appropriate cations and their application in catalysis have been extensively reviewed [27, 31–34, 39, 43, 54–57] and is outside the scope of this chapter that deals with the second approach, i.e. supported POM catalysts. A recent review of Mizuno et al. [39] covers a considerable part of the literature related to POM heterogenization until 2005, but comparison with the state-of-the-art at the beginning of 2012 shows that this field has rapidly expanded in recent years.

The first attempts to prepare supported POM catalysts employed conventional techniques, like wet impregnation or nonspecific adsorption. A great deal of work was aimed at depositing POMs on various inorganic supports, such as silica, active carbon, alumina, titania, zirconia, magnesia, etc., and testing them as catalysts in liquid phase processes. Silica and active carbon were among the most frequently used carriers because of their weak acidic or neutral surface properties that facilitate POM deposition without POM destruction. Strongly basic supports such as Al_2O_3 or MgO frequently led to POM degradation. A few monographs and review papers summarized the early research in this area [27, 34, 39, 43, 54–57]. Subsequent studies demonstrated that catalysts prepared by the impregnation technique suffer from several drawbacks, such as nonhomogeneous dispersion of POM units and pores blocked by POM aggregates as well as susceptibility to POM leaching in polar reaction media.

To overcome these limitations, several concepts of POMs immobilization on solid supports through the formation of chemical (ionic, dative or covalent) bonds and/or entrapment within carrier materials have been elaborated during the past two decades [43, 66–75]. In this chapter, we survey recent achievements in the field of POM immobilization and their application in liquid phase selective oxidation. Heterogeneous POM-based composite photocatalysts have been comprehensively reviewed by Maldotti and coworkers in Chapter 9 of this book and, hence, will not be considered here.

Following the general thrust of this book, we pay special attention to analysis of the frequently success-limiting issues of the effect of support on catalytic activity and reaction selectivity, POM leaching under the conditions of liquid phase oxidation, catalyst reusability, and the nature of catalysis.

6.2 SYNTHESIS AND CHARACTERIZATION

6.2.1 Choice of POM

Research papers published over the past two decades have firmly established the significant potential of POMs as homogeneous oxidation catalysts. The existing literature in this area has been comprehensively reviewed by Hill [28, 38], Neumann [30, 35, 36], and Mizuno et al. [43]. Keeping this in mind, we just briefly summarize below the most studied systems that have attracted great attention as objects for immobilization.

The ability of the mixed-addenda heteropoly anions of the Keggin structure and general formula $[PV_nMo_{12-n}O_{40}]^{(3+n)-}$ (shortly, PV_nMo_{12-n} or HPA-n; $n = 1$–6) to oxidize organic substrates and then to be restored to the initial state through reoxidation of V^{IV} to V^{V} with molecular oxygen was discovered by Matveev in the late 1970s [76]. Subsequently many groups have further studied such systems [28–30, 32, 34–36, 38, 41, 43, 45, 77]. The history of this field has been recently reviewed by Neumann and Khenkin [40].

In the mid-1980s, the groups of Venturello [78, 79] and Ishii [80–82] developed independently highly effective systems for a range of selective oxidations based on the use of the peroxometalate $\{PO_4[WO(O_2)_2]\}^{3-}$ (PW_4, the so-called Venturello complex) and $[PW_{12}O_{40}]^{3-}$ (PW_{12}), respectively, or their molybdenum analogs as catalysts for aqueous hydrogen peroxide-based oxidations. Peroxometalates with central atoms other than P (e.g. As, S, Se) were also found to be active catalysts [43]. Considerable research was devoted to immobilization of both PW_4 and PW_{12} and the application of these materials as heterogeneous catalysts for alkene epoxidation, and the oxidation of alcohols, diols, and thioethers.

In 1986, Hill and Brown first revealed that some *d*-electron-transition-metal-monosubstituted POMs (M-POM, $M = Mn^{II}$ and Co^{II}) are remarkably effective catalysts for oxygen-atom transfer from typical single oxygen donors, such as iodosylarenes and aniline *N*-oxide, to alkenes [83]. Katsoulis and Pope demonstrated similar properties of Cr-POM [84]. These findings have allowed the authors to call M-POMs "oxidatively resistant inorganic analogs of metalloporphyrins" and many subsequent studies developed such systems and some of their immobilized forms. The structure of the widely used M-POM of the Keggin structural class, $[XW_{11}M(L)O_{39}]^{n-}$ ($XW_{11}M$), is shown in Figure 6.2.

One can see that such M-POM comprise an active center, M, isolated in the tungsten-oxide matrix that strongly binds it through multiple M−O−W and M−O−X bridges. This multidentate ligation by the lacunary (defect) POM prevents the active metal from hydrolyzing and facilitating oligomerization. These attributes of M-POMs enable them to be potential building blocks for designing and studying single-site heterogeneous catalysts [18, 85, 86]. The synthesis of POMs of various structures (Keggin, Dawson, sandwich) having more than one tungsten atom in the heteropoly anion substituted with another transition metal(s) is possible starting from multidefect POM species, e.g. *A*-$[XW_9O_{34}]^{n-}$, *B*-$[XW_9O_{34}]^{n-}$, $[X_2W_{15}O_{56}]^{n-}$ or $[\gamma\text{-}SiW_{10}O_{36}]^{8-}$ [26, 37].

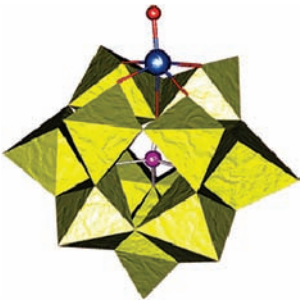


FIGURE 6.2 Monosubstituted Keggin-type heteropoly anion $[XW_{11}M(L)O_{39}]^{n-}$.

Co-substituted POMs appeared to be efficient catalysts for homogeneous aerobic oxidations [87–89] and even the oxidation of water [90, 91], which stimulated the development of methods for construction of solid Co-POM-containing catalysts [92–99]. Thus, various Co-POMs were deposited on cotton cloth [93] and silica [99], datively [94] or electrostatically [95, 96] bonded to NH_2-modified silica surfaces as well as intercalated in layered double hydroxides (LDHs) [92, 97, 98]. The resulting materials were used for the aerobic oxidation of aldehydes, alkenes, alkanes, alcohols and some other organic substrates.

The γ-isomer Keggin-type silicodecatungstate $[\gamma\text{-}SiW_{10}O_{36}]^{8-}$ has been used as a structural platform for dimetal-substituted POMs with bis-μ-oxo(or hydroxo)-dimetal cores, $[\gamma\text{-}SiW_{10}\{Fe(OH_2)\}_2O_{38}]^{6-}$ and $[SiW_{10}O_{38}V_2(\mu\text{-}OH)_2]^{4-}$, which catalyze epoxidation of various alkenes using H_2O_2 with a high epoxide yield and high H_2O_2 utilization efficiency under very mild reaction conditions [43].

An important class of catalytically active POMs is the so-called "sandwiches" that contain various transition metals (3 or 4 atoms) in the belt sandwiched between two lacunary POM species. For example, $\{[(WZnM_2(H_2O)_2][(ZnW_9O_{34})_2]\}^{q-}$ (M = Mn, Rh, Zn, etc.) exhibit superior catalytic activity and stability in a number of selective oxidations using hydrogen peroxide as oxidant [35, 36, 100]. Iron-containing POMs of the "sandwich" structure show remarkable activity in alkene epoxidation practically without nonproductive decomposition of H_2O_2 [101].

These and many other POMs were subjected to immobilization by various techniques that will be described in the following subsections. To verify retention of the POM structure after immobilization spectroscopic methods are used, such as FT-IR, Raman, diffuse reflectance (DR) UV-vis, ^{31}P NMR MAS, EDX, etc. The dimension of POM aggregates on the support surface and homogeneity of their distribution are evaluated by high-resolution transmission electron microscopy (HR TEM).

6.2.2 Embedding POM into Silica and Other Matrixes

A promising approach to the fabrication of heterogeneous POM-based catalysts involves embedding a catalytically active POM in silica or other inert

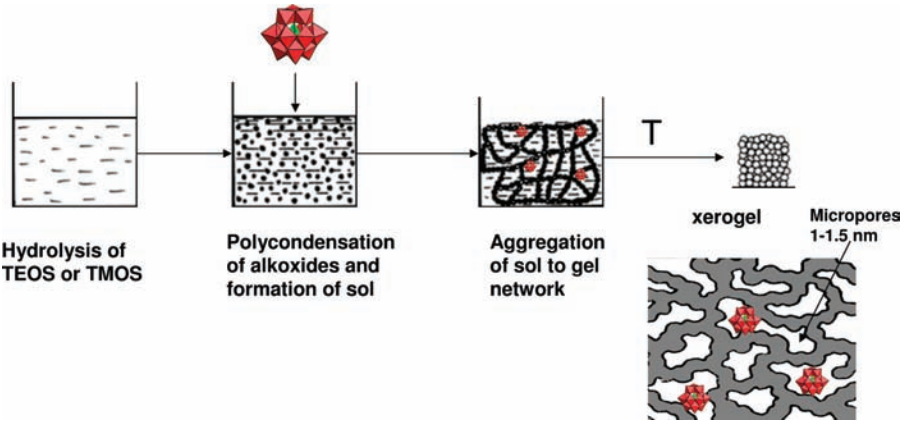


FIGURE 6.3 Embedding POMs into a microporous silica matrix by the sol-gel method.

matrices during synthesis of the matrix by sol-gel and some related techniques. A schematic representation of the POM immobilization process is shown in Figure 6.3.

Izumi and coworkers were the first to embed a catalytically active POM, $Cs_{2.5}H_{0.5}PW_{12}O_{40}$, into silica by means of sol-gel technology using tetraethyl orthosilicate (TEOS) as a silica source [54 and references therein]. A composite mesoporous material with a surface area 364 m^2/g has been prepared and used as acid solid catalyst in liquid phase. Subsequently, a preparative method for silica-encapsulated PW_{12} was developed by alteration of the sol-gel procedure, initially by increasing the silica content to make the matrix denser and thus to prevent POM leaching [54]. Jarzebski and coworkers found that TEOS can be replaced by ethyl-silicate 40 (ES-40, a commercial form of ethoxypolysiloxane) to produce POM/SiO_2 ($POM = PW_{12}$ or PMo_{12}) composite materials with high surface areas and improved adsorption properties [102].

Two composite materials, $Co\text{-}POM/SiO_2$ [95, 96] and $Ti\text{-}POM/SiO_2$ [103], have been prepared by the sol-gel method using $Na_5PW_{11}CoO_{39}$ and $H_5PW_{11}TiO_{40}$, respectively, and tetramethyl orthosilicate (TMOS) as the silica precursor. The molar ratio of reagents was as follows: $Si : H_2O : MeOH : HCl = 1 : 9\text{-}12 : 6\text{-}9 : 0.0016$. First, TMOS was prehydrolyzed using $^1/_2$ the total amount of methanol, a 0.2 M solution of HCl and 2 moles of water per 1 mole of Si at 50 °C for 1 h. Then, the solution containing the remaining half of the methanol, the rest of water and M-POM (10 wt%) was added to the first solution under vigorous stirring. After gelation and aging for 7 days at room temperature (Co-POM) or 50 °C (Ti-POM), the resulting materials were dried in vacuum, ground, washed several times with water, and dried again. The Co- and $Ti\text{-}POM/SiO_2$ composites were characterized by elemental analysis, FT-IR, DR UV-vis and N_2 adsorption. The textural properties of some POM/SiO_2 composite materials obtained by the sol-gel method along with elemental analysis data are presented in Table 6.1.

TABLE 6.1 Physicochemical Characteristics of POM/SiO_2 Sol-Gel Composites

POM	S^a (m^2/g)	V^b (cm^3/g)	D^c (nm)	M-POM (wt%)
$H_3PW_{12}O_{40}$ [54]	554	0.20	1.4	11
$H_3PW_{12}O_{40}$ [102]	325	0.16	1.4	8
$H_3PMo_{12}O_{40}$ [102]	363	0.18	1.5	8
$Na_5PW_{11}CoO_{39}$ [95]	442	0.17	1.5	4
$H_5PW_{11}TiO_{40}$ [103]	$<0.5^d$	-	-	9

[a]Specific surface area.
[b]Micropore volume.
[c]Average pore size.
[d]Nonporous material.

The Co-POM/SiO_2 material was microporous with textural properties being similar to those found for the silica-included PW_{12} and PMo_{12} [54, 102], while Ti-POM/SiO_2 appeared to be effectively nonporous. The DR UV-vis spectrum of Co-POM/SiO_2 was very similar to that of $Na_5[PW_{11}Co(H_2O)O_{39}]$ in aqueous solution [104], which confirmed preservation of the $PW_{11}Co$ structure and ligand environment in the sol-gel composite.

POM/SiO_2 nanocomposites (POM = α-$[PW_{11}Fe^{III}(H_2O)O_{39}]^{4-}$ or B-α-$[(PW_9O_{34})_2Fe^{III}_4(H_2O)_2]^{6-}$) were obtained by alkaline hydrolysis of TEOS using a reverse micelle and sol-gel technique [105]. Two microemulsions were prepared. The first one contained Triton X-100, 1-octanol, cyclohexane, TEOS and the K-salt of POM dissolved in water while the second one contained Triton X-100, 1-octanol, cyclohexane and aqueous 25 wt% NH_3. After vigorous stirring for 30 min, the two microemulsions were mixed and the resulting mixture was stirred at room temperature for 48 h. Acetone was then added and a precipitate was obtained. After separation, washing and drying under vacuum silica nanoparticles containing 44 wt% of K-$PW_{11}Fe$ or 41 wt.% of K-$(PW_9)_2Fe_4$ were obtained. The spectroscopic studies (FT-IR, Raman) suggested that the POMs were successfully immobilized on the silica nanoparticles. TEM images of the two silica materials revealed that these nanoparticles have a spherical form and similar diameters (25–35 nm).

The discovery and growing development of mesostructured materials (a comprehensive review on these materials is presented in Chapter 4 of this book) prompted researchers to attempt the incorporation of POMs into (onto) the walls of ordered mesoporous silica materials by encapsulating POM during the silica synthesis [70, 106–110]. Yang et al. [106] incorporated PW_{12} into SBA-15 matrix by adding the heteropoly acid to the SBA-15 synthesis mixture. A similar approach was used to introduce PW_{12} into MSU-type silica [110]. Shi et al. obtained SBA-15-supported PW_{12} (or PMo_{12}) catalysts by adding P and W (or Mo) sources, Na_2HPO_4 and Na_2WO_4 (or Na_2MoO_4) into the synthesis gel during hydrolysis of TEOS to form the Keggin-type POM *in situ* [111, 112].

Stable and reactive POM-modified mesoporous hybrid materials have been obtained by one-pot synthesis in the presence of POM and two templates, ionic

cetyltrimethylammonium bromide (CTAB) and nonionic Pluronic P123 ($EO_{20}PO_{70}EO_{20}$), together [70]. Template removal by calcination–extraction sequence was essential to yield stable materials with intact Keggin unit. It has been proposed that when POM is introduced, it takes up a position at the periphery of the micelle creating surface microporosity by molecular imprinting. Thus, after polymerization of TEOS, some of the POM is at the center of micropores in the interior walls of the as-made material. If extraction with methanol is performed at this stage, this leads to total elimination of POM from the micropores. In turn, calcination leads to some restructuring of the surface, which inhibits extraction. Probably, calcination reduces the size of the entrance of the micropore host of the POM moiety, which is now thermally degraded. When treatment with methanol of the calcined material is performed, the part of the degraded POM, which was located on the silica wall surface, is eliminated into solution. However, the surface restructuring prevents the extraction of POM inside the micropores, and methanol-mediated reformation of the Keggin structure takes place there. Thus, the final material contains trapped, structurally intact and accessible POM moieties at the surface of the channels of the mesoporous silica [70].

To enhance POM dispersion within mesoporous silica matrix, Martens and coworkers [109] prepared SBA-15 mesoporous silica materials containing up to 40 wt% of PW_{12} *via* an original method that involves the addition of the heteropoly acid to an acidified solution of Pluronic P123 triblock copolymer prior to the addition of the silica source. The model for the synthesis is presented in Figure 6.4. Heteropoly anions can partially substitute Cl^- anions in the shell surrounding the P123 micelle. The long time allowed for this equilibrium to be established (24 h), ensured that most of the HPAs are attached and molecularly dispersed on the micelle. When TEOS is finally added, it hydrolyzes and transforms into the protonated monomers due to the very low pH value. The $H_5SiO_4^+$ cations interact with the anionic shell surrounding the P123 micelle, thus trapping both Cl^- and heteropoly anions between the P123 and the silica. Thus, the HPAs are expected to be present at the interface between the silica and the P123 polymer. During the hydrothermal treatment the silica layer is polymerized. Washing and drying steps do not remove the HPAs since they are trapped inside the SBA-15 particles. In the calcination step, the P123 template is eliminated from the pores but the PW_{12} molecules stay fixed onto the pore walls. The catalysts showed a homogeneous dispersion of the HPAs even at loadings as high as 30 wt%. Characterization by

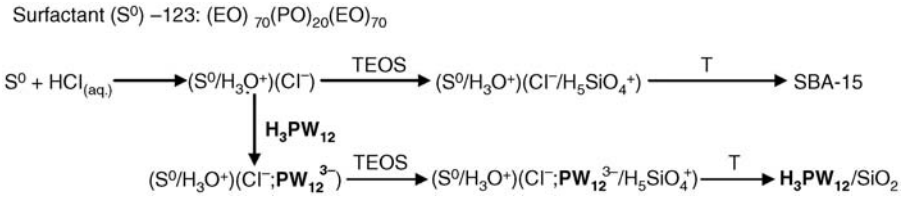


FIGURE 6.4 Proposed mechanism for POM incorporation within SBA-15. Adapted from ref. [109] with permission of Elsevier, copyright 2009.

XRD, ^{31}P NMR MAS, NH_3-TPD, and N_2 adsorption showed that even after calcination, PW_{12} in the directly synthesized samples was better dispersed than in the samples obtained by impregnation. ^{31}P NMR MAS spectroscopy was used to determine the amount of occluded PW_{12} molecules and characterize their stability during calcination of the PW_{12}/SBA-15 samples.

During the last two decades the sol-gel approach has been significantly developed by material chemists to insert POMs into various inorganic matrices. Silica sources (TEOS, TMOS) can be replaced by Zr(IV) or Ti(IV) alkoxides to give materials where POM is entrapped within ZrO_2 [113, 114] or TiO_2 [115], respectively, while application of templates leads to ordered mesoporous materials [114, 115]. A series of well-ordered mesoporous POM/ZrO_2 nanocomposites has been prepared through a surfactant-assisted sol-gel copolymerization route [114]. The synthetic procedure involved controlled crosslinking copolymerization of zirconium oxo-hydroxide species and $[PMo_{12}O_{40}]^{3-}$ anions in the presence of nonionic block copolymer Pluronic F127. Small angle X-ray scattering, HR TEM and N_2 physisorption measurements suggested that the resulting materials possess a well-ordered hexagonal mesostructure with large pores (*ca.* 4–6 nm), BET surface areas 60–103 $m^2\,g^{-1}$ and pore volume 0.04–0.07 $cm^3\,g^{-1}$. The pore walls are constituted by nanocrystalline ZrO_2 and Keggin PMo_{12} components with POM loading in the range of 12–37 wt%. The framework wall thickness increases from 3.3 to 5.4 nm with increasing POM content. The structure of the incorporated POMs is intact according to EDX, FT-IR and DR UV-vis/NIR spectroscopy.

Although a large variety of sol-gel POM composites have been reported [116–119], the number of their applications in liquid phase oxidation catalysis is still not as large as one might have anticipated based on the advantages that POMs offer in the ease of incorporation into sol-gel matrixes and their unique blend of properties. One of possible reasons is the lack of information on the stability of the composite materials toward POM leaching in polar media.

6.2.3 Adsorption on Active Carbon

Active carbons have long been used to support catalytically active POMs [32, 34, 39, 43, 56, 74, 93, 108, 120–128]. Izumi and Urabe [120] first found that POMs can be entrapped strongly on active carbon and that, in contrast to other supports, carbon-supported POMs do not leach out. Van Bekkum and coworkers [122] studied in detail the controlled adsorption and desorption of two heteropoly acids, PW_{12} and SiW_{12}, onto well-characterized activated carbon supports. It was shown that the surface structure and origin of the carbon, as well as the mode of activation have a strong impact on strength and amount of HPA adsorption. Specifically, a combination of the number and the nature of the active groups, size of basal planes, surface area and pore volume determine the amount of POM adsorbed. Subsequent studies revealed that the nature of the POM species supported on activated carbon depends on the concentration of the impregnating solutions, the solvent used, the pH of the solution, and other parameters [34, 123]. When Keggin HPAs were supported from concentrated aqueous solutions, they retained their structure and formed finely

dispersed species without formation of an HPA crystal phase even at an HPA loading as high as 45 wt%. A significant broadening of the ^{31}P, ^{29}Si and ^{17}O NMR MAS signals indicated a strong interaction between POM anions and the carbon support. Meanwhile, partial decomposition of the Keggin HPA was observed at low concentration of the impregnating solution and low POM loading levels (*ca.* 5 wt%), as suggested from signal splitting in the FT-IR and ^{31}P NMR MAS spectra [123].

The heteropoly acid $H_5PV_2Mo_{10}O_{40}$ (PV_2Mo_{10}) has been adsorbed on porous carbons, such as Ambersorbs 563 (hydrophobic) and 572 (hydrophilic), Calgon, Maxsorb, etc., and various carbon-fiber materials to create selective and recoverable heterogeneous catalysts for detoxification of organic pollutants like thioethers, thiophenes and aldehydes [93, 124, 125]. It was found that none (<1%) of the POM was lost when PV_2Mo_{10}/PPAN (PPAN = pyrolyzed polyacrylonitrile) or PV_2Mo_{10}-/Ambersorb 572 was washed in water or acetonitrile solvent, even after 12 h at 40 °C [125]. A prototype material for the sustained catalytic decontamination of mustard analogs with the goal being the fabrication of self-decontaminating clothing has been elaborated.

Wu et al. [126] deposited a range of Keggin-type heteropoly acids on six sorts of active carbons, including coconut shell carbon, hawnut nucleon carbon, nickory nut necleon carbon, coal-based carbon, and fiber carbon. The basic coal carbon exhibited the highest adsorbed amount of HPA while the acidic fiber carbon exhibited the least. The heteropoly acid PMo_{12} was supported on four activated carbons in order to analyze the influence of the textural properties of carbon on the adsorption capacity [128]. It was found that the HPA is preferably adsorbed in supermicropores as a consequence of the POM size (1.2 nm for Keggin structure), which limits the entrance into the smaller micropores. XRD indicated that POM is highly dispersed within the carbon support and does not develop any crystalline phase.

Timofeeva et al. [129] reported adsorption of PW_{12} from water and organic solvents on mesoporous carbon materials, Sibunit and fluorinated Sibunit (the chemical composition of F-Sibunit corresponds to the general formula $CF_{1.25}$). Subunit revealed a high adsorption capacity (40, 36 and 26 wt% from water, acetone and acetonitrile, respectively); furthermore, 6–10 wt% of HPA could not be desorbed even in boiling water and methanol. The maximal adsorption of HPA on F-Sibunit, an inert surface support, was much lower and decreased in the inverse order: MeCN (9%) > Me_2CO (1.3%) > H_2O (0%). Only 1 wt% of HPA was adsorbed irreversibly and only in the case of MeCN. HR TEM data showed that sample 8%HPA/F-Sibunit contained the HPA in two main forms: isolated molecules less than 20 Å in size and clusters of *ca.* 35–50 Å. HPA aggregates larger than 100–150 Å were not observed, which was explained by the pronounced hydrophobic properties of the F-Sibunit surface, which prevents the formation of large hydrophilic aggregates. The same group used filamentous carbons as supports for a few HPAs [130]. The maximal amount of HPA adsorbed decreased in the series: $H_3PW_{12}O_{40} > H_6P_2W_{21}O_{71}(H_2O)_3 > H_6P_2W_{18}O_{69} \geq H_6As_2W_{21}O_{69}(H_2O)$. However, it is not possible to know the amount of irreversibly adsorbed HPA from the data reported.

Adsorption of several redox active Keggin-type POMs ($PW_{11}M$, M = Co, Ti, Zr) on two commercial active carbons, microporous L2701 (S 1240 m^2/g) and

mesoporous Sibunit (S 670 m^2/g) has been accomplished from aqueous solutions of the POMs (10 wt%) at 25 °C for 3 days [74]. Retention of POM structure after immobilization was confirmed by FT-IR spectroscopy. Depending on the nature of POM and carbon, irreversible adsorption of 7–17 wt% of POM occurred. The maximum Co-POM loading was twice higher for L2701 compared to Sibunit. The interaction between POM and carbon appeared to be so strong that even after prolonged extraction of the carbon-supported catalysts with hot ethanol, and even acetic acid in a Soxhlet apparatus, the POM loading remained unchanged.

Recently, an iron-containing sandwich-type POM, $Na_6((CH_3)_4N)_4$ $[Fe_4(H_2O)_2(FeW_9O_{34})_2]\cdot 45H_2O$, was supported on carbon nanotubes [131]. Raman and cyclic voltammetry studies confirmed that the individual POM molecules maintained their chemical integrity. HR TEM imaging showed the presence of bundles of nanotubes decorated by dark spots that had the size expected (1.6×1 nm) for the individual POM molecules; no assemblies with larger sizes were detected.

Thus far, the mechanism of POM adsorption on active carbons is not completely clear. The acid strength of supported $H_3PW_{12}O_{40}$ is ranked as $SiO_2 > Al_2O_3 > C$, assuming a stronger interaction between HPA and carbon as compared to silica and alumina [34]. One could expect that oxygen-containing groups present on the surface would play an important role in the adsorption. It is well known that heteropoly acids form complexes with diethyl ether that are believed to contain protonated ether as a counterion to the heteropoly anion [26]. Van Bekkum and coworkers [122] assumed that the interaction between HPA and carbon comes from electrostatic attraction caused by proton transfer to the carbon functional groups (carboxylic, hydroxyl, diol, lactone, ether, or quinone moieties). The type of surface group is therefore important, as the different oxygen functions span a large range of acidities. Nevertheless, later it was demonstrated that treatment of Sibunit-supported POM catalysts with 1 M Bu_4NClO_4 did not allow solution recovery of the POM, indicating that interactions other than electrostatic ones might contribute to retention of the POM on the carbon support [74].

6.2.4 Electrostatic Attachment

The first examples of electrostatic attachment of POM on solid supports are dated to the mid-1980s. Baba et al. [132] reported immobilization of heteropoly acids on the anion-exchange resin Amberlist-15. This type of support was successfully used by Jacob's group to immobilize the Venturello complex $\{PO_4[WO(O_2)_2]_4\}^{3-}$ [133–135].

Electrostatic attachment to supports modified with cationic groups (sometimes such groups are generated *in situ* by protonation of a basic, e.g. amine, function) was widely used for POM immobilization *via* anion exchange or ion pairing [136–147]. Heteropoly acids PW_{12} and PMo_{12} were incorporated in polyaniline [136] and polyimine [137] through protonation of the basic sites of the polymer matrices. The polymer-supported HPAs revealed a decreasing acidity function but enhancing thermal stability and redox activity. Yamada [148] introduced a concept known as "*molecular convolution*", where a soluble linear polymer having multiple ligand groups is convoluted (noncovalently crosslinked) with transition metals *via*

coordinative or ionic complexation. A convoluted polymeric tungstate catalyst, (isopropylacrylamide)polymer-supported PW_{12}, was used for the oxidation of alcohols; however, the catalytic activity was insufficient and the heterogeneous catalyst became emulsive during the reaction, presumably due to its physical fragility, which resulted in poor recyclability [149]. To overcome these drawbacks, the same group developed tightly convoluted polypyridinium–phosphotungstate catalysts that showed high catalytic activity and good recyclability in liquid phase reactions [150].

Many research groups used for immobilization inorganic (frequently, silica) supports functionalized with appropriate spacer ligands containing quaternary ammonium cations [134, 138, 143, 147] or amine groups [94–96, 139–142, 144, 145]. Such ligands can be easily grafted onto silica surfaces, and their covalent attachment ensures stability of the resulting materials [151].

Heteropoly acids $H_{3+n}PMo_{12-n}V_nO_{40}$ ($n = 1$–3) were supported on amine-functionalized MCM-41 [139] and SBA-15 silicas [142, 152, 153]. Small angle X-ray scattering (SAXS) analysis and SEM provided evidence for the structural integrity of the immobilized catalysts. DR UV-vis, ^{31}P NMR and FT-IR data confirmed incorporation of the intact HPA onto the silica walls.

Immobilization of the cobalt- and cerium-monosubstituted Keggin heteropoly anions, $[PW_{11}CoO_{39}]^{5-}$ [95, 96] and $[SiW_{11}CeO_{39}]^{4-}$ [154] on amine-modified amorphous silica (NH_2-xerogel) [95, 154] and well-ordered hydrothermally stable mesostructured silicate materials NH_2-SBA-15 and NH_2-MCF [96] has been accomplished and comprehensively studied. Two tetra-butylammonium (TBA) salts, $TBA_4H[PW_{11}CoO_{39}]$ and $TBA_5[PW_{11}CoO_{39}]$, have been prepared [95] and used for immobilization and catalytic studies. The effect of protonation of the amine-modified silica surface on the Co-POM loading, activity and stability of the solid catalyst was investigated.

To realize attachment of the Co-POM to the surface, two different approaches were explored, namely, anion exchange and ion pairing. The first one involved treatment of the support with an acid solution followed by the anion exchange process (Eqs. 6.1 and 6.2)

$$\text{X-NH}_2 + \text{HClO}_4 \rightleftharpoons \text{X-NH}_3{}^+\text{ClO}_4{}^- \tag{6.1}$$

$$n\text{X-NH}_3{}^+\text{ClO}_4{}^- + \text{TBA}_5\text{PW}_{11}\text{CoO}_{39} \rightleftharpoons (\text{X-NH}_3{}^+)_n\text{TBA}_{5-n}[\text{PW}_{11}\text{CoO}_{39}] + n\text{TBAClO}_4 \tag{6.2}$$

The Co-POM loading increased with increasing amount of H^+ added in the first step. Samples with 13 and 32 wt% of Co-POM were obtained for $n = 1$ and 5, respectively [95]. The higher the number of $NH_3{}^+$ groups on the support, the stronger electrostatic binding between the POM and the support is expected. This approach can be employed for other monosubstituted Keggin anions $[XW_{11}MO_{39}]^{n-}$ with M = M(II) or M(III) which, in contrast to heteropoly anions with M(IV) and M(V), are not stable in acidic solutions.

In the second approach, M-POMs containing protons as counterions were used to fulfill electrostatic attachment to the support in one stage *via* the formation of

TABLE 6.2 Physicochemical Properties of NH_2-Silica Supported $TBA_4H[PW_{11}CoO_{39}]$

NH_2-Support/Catalyst	S^a m^2/g	V^b cm^3/g	d^c nm	NH_2 mmol/g	POM wt.%	NH_2/POM mol/mol
xerogel	540	1.2	12–16[d]	1.15		
Co-POM/xerogel	510 (520)[e]	0.9 (1.0)[e]	12–16[d]		20 (5)[e]	21
SBA-15	623	1.3	13	0.64		
Co-POM/SBA-15	418 (420)[e]	1.2 (1.1)[e]	13 (13)[e]		15 (7)[e]	16
MCF	625	2.8	15	2.59		
Co-POM/MCF	440 (400)[e]	1.4 (1.4)[e]	15 (14)[e]		32 (18)[e]	30

[a]Mesopore surface area.
[b]Mesopore volume.
[c]Average mesopore diameter.
[d]Broad mesopore distribution.
[e]Inside parentheses, the values after five catalytic cycles of α-pinene and IBA co-oxidation [96].

anion–cation pairs (Eqs. 6.3 and 6.4).

$$X\text{-}NH_2 + TBA_4[HPW_{11}CoO_{39}] \rightleftharpoons (X\text{-}NH_3{}^+)TBA_4[PW_{11}CoO_{39}] \tag{6.3}$$

$$3X\text{-}NH_2 + NaH_3[SiW_{11}Ce(H_2O)_nO_{39}] \rightleftharpoons (X\text{-}NH_3{}^+)_3Na[SiW_{11}Ce(H_2O)_nO_{39}] \tag{6.4}$$

The supported POM catalysts were characterized by N_2 adsorption measurements, XRD (for ordered supports), elemental analysis, DR UV-vis and FT-IR spectroscopy. Textural and elemental analysis data for the supported Co-POM catalysts prepared *via* Eq. 6.3 (X = xerogel, SBA-15 or MSF) are given in Table 6.2. The textural properties of the initial, POM-free supports are shown for comparison.

The Co-POM loading depended on the concentration of NH_2-groups on the support. Both the surface area and pore volume decreased upon Co-POM deposition. FT-IR studies revealed that no damage of the Co-POM structure occurred when TBA-salts dissolved in MeCN were used for immobilization. As one can judge from Figure 6.5, the IR spectra after subtraction of the peaks due to support exhibited the principal stretching modes of the Keggin Co-POM unit.

On the contrary, the use of an aqueous solution of a sodium salt resulted in a partial destruction of the Co-POM structure during deposition. A similar observation was made by Johnson and Stein [94]. Since the Keggin Ce-POM is more stable than the Co-POM, both an aqueous solution of $NaH_3SiW_{11}CeO_{39}$ and a MeCN solution of $TBA_3HSiW_{11}CeO_{39}$ could be successfully used for the immobilization process.

The ionic character of the binding between Co-POM and the support was confirmed by DR UV-vis spectroscopy. The spectra of the NH_2-silica-supported Co-POM catalysts prepared *via* two-step and one-step procedures are very similar and resemble the spectrum of $Na_5[PW_{11}Co(H_2O)O_{39}]$ in water [104] or in SiO_2 matrix (Figure 6.6) as well as that of $TBA_4H[PW_{11}Co(H_2O)O_{39}]$ in MeCN [96]. Importantly, these spectra differ from the spectra published for Co-POM datively

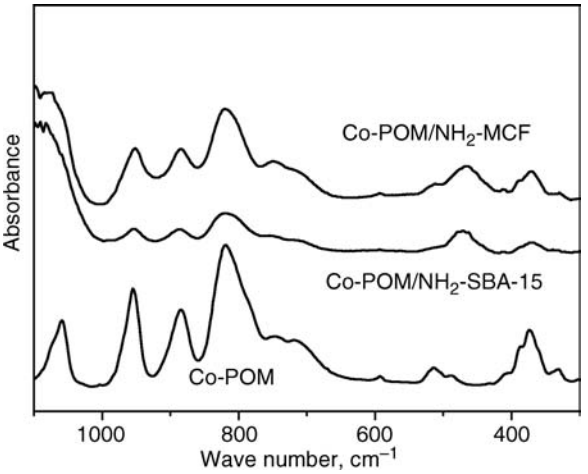


FIGURE 6.5 FT-IR spectra of bulk $TBA_4H[PW_{11}CoO_{39}]$ and the Co-POM supported on NH_2-modified SBA-15 and MSF (the spectra of supports are subtracted).

linked to NH_2-silica *via* a ligand-exchange process in the cobalt coordination sphere [94]. Indeed, no peaks or shoulders were observed in the range of 628–640 nm, indicating no formation of dative bonds between NH_2 groups and cobalt.

Another argument in favor of the electrostatic nature of the interaction between Co-POM and NH_2 groups of the support was obtained from anion-exchange experiments [96]. The color of the supported catalyst (pale pink) became completely colorless after treatment with a 1 M solution of $TBAClO_4$ in MeCN. Additionally, the

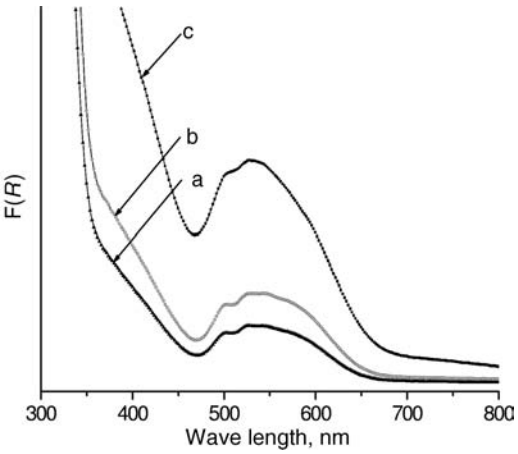


FIGURE 6.6 DR UV-vis spectra of (a) NH_2-silica-supported $TBA_4H[PW_{11}Co(H_2O)O_{39}]$, (b) NH_3^+-silica-supported $TBA_5[PW_{11}Co(H_2O)O_{39}]$ and (c) $Na_5[PW_{11}Co(H_2O)O_{39}]/SiO_2$ composite.

elemental analysis data confirmed elimination of Co-POM from the solid into solution after such treatment.

Another research group immobilized $TBA_4H[PW_{11}CoO_{39}]$ on NH_2–$(CH_2)_x$–SiO_2 supports with $x = 0$, 2 and 3 [155]. DR UV-vis spectroscopic data indicated that the type of interaction between Co-POM and support depends on the number and type of functional groups on the silica surface. The increase in the number of NH_2-groups and the distance between NH_2-function and the surface (the latter depends on x) favors electrostatic binding between NH_3^+ and the heteropoly anion.

The polyoxometalate, $[(Eu_2PW_{10}O_{38})_4(W_3O_8(H_2O)_2(OH)_4)]^{22-}$, was inserted inside the channels of NH_2-MCM-41 and characterized by XRD, UV-vis absorption, emission, Raman excitation, Raman, IR, and ^{31}P solid-state NMR measurements [156]. Rare-earth-metal sandwiched Keggin-type POMs, $K_{11}[RE(PW_{11}O_{39})_2]$ (RE = La, Ce, Pr, Nd, Sm, Eu, Dy and Y), were anchored onto aminosilylated SBA-15 and the resulting materials were characterized by ICP, FT-IR, XRD, N_2 adsorption, ^{31}P NMR MAS and TEM [157]. The POM clusters preserved their structure after immobilization. The tetrairon(III)-substituted polyoxotungstates $[Fe_4(H_2O)_{10}(\beta\text{-}XW_9O_{33})_2]^{n-}$ ($n = 6$, $X = As^{III}$, Sb^{III}; $n = 4$, $X = Se^{IV}$, Te^{IV}) were immobilized on SBA-15 functionalized with (3-aminopropyl)triethoxysilane [145]. Iron and manganese monosubstituted Keggin-type POMs, $[XM^{III}(H_2O)W_{11}O_{39}]^{n-}$ (X = P, M = Fe or Mn; X = Si or B, M = Fe) were supported on modified amorphous silica prepared from 3-bromopropylsilica and triethylamine, $N(Et)_3$ [158]. FT-IR, Raman and DR UV-vis spectroscopic techniques confirmed preservation of the POM structure after immobilization.

Wells–Dawson $[P_2W_{18}O_{62}]^{6-}$ (P_2) and Preyssler $[NaP_5W_{30}O_{110}]^{14-}$ (P_5) polyoxometalates (the structures are shown in Figure 6.1) were supported on MCM-48, SBA-3, SBA-15 and NH_3^+-functionalized SBA-15 [159]. The amount of POM deposited onto the surface of SBA-15 increased significantly (22 wt% *versus* 14 wt%) after silica functionalization with NH_3^+ groups. The structural maintenance of the silica supports after POM immobilization was confirmed by XRD, although incorporation of POM guests reduced the order of the mesostructured systems. The results of N_2 adsorption measurements indicated a decrease in both surface area and pore volume due to inclusion of the POM species within the pores and channels of the silica supports. The reduction was more significant for the Preyssler POM as a result of its larger size compared to the Wells–Dawson complex.

In 1995, Neumann and Miller suggested a strategy for designing supported POM catalysts, capable of effective transformation of nonpolar substrates with aqueous H_2O_2 [138]. They accomplished immobilization of $\{PO_4[WO(O_2)_2]_4\}^{3-}$ and $[ZnWMn_2(H_2O)_2(ZnW_9O_{34})_2]^{12-}$ on silica xerogel modified with phenyl groups and quaternary ammonium cations, prepared by copolymerization of $Si(OEt)_4$, $PhSi(OEt)_3$ and quaternary ammonium salts of substituted siloxanes of the general formula $(R^3O)_3SiR^1N^+R^2Me_2C1^-$ using the sol-gel technique followed by addition of POM to the gel and evaporation of the solvent. The same group electrostatically bound these POMs to quaternary ammonium sites of the alkylated polyethylenimine (Alk-PEI) [160]. The new Alk-PEI/POM materials also had hydrophobic

regions enabling the solubilization or adsorption of hydrophobic substrates and were active catalysts for selective oxidations in water.

Inumaru et al. [69] prepared water-tolerant, highly active solid acid catalysts composed of PW_{12} immobilized in hydrophobic nanospaces of organomodified mesoporous silica. Two kinds of organic groups, *n*-octyl and 3-aminopropyl, were grafted onto the pore walls of SBA-15. The aminopropyl groups electrostatically immobilized POM anions on the pore walls, leaving some of the acidic protons on the anions, while the octyl groups formed hydrophobic regions around the polyanions. Infrared spectra and ICP analysis confirmed that the Keggin POM structure was maintained in the catalysts while X-ray diffraction corroborated maintenance of the SBA-15 mesostructure. The N_2 adsorption measurements demonstrated that the parent SBA-15 and the PW_{12}/SBA-15 solids had mesopores with diameters of 7.5 and 5.5 nm, respectively, thus indicating deposition of POM anions within channels of SBA-15. The PW_{12}/SBA-15 catalyst showed high stability during reactions in water.

Mizuno and coworkers synthesized an organic–inorganic hybrid support by covalently anchoring *N*-octyldihydroimidazolium cation fragment onto SiO_2 [146]. This support acted as a good anion exchanger, and the catalytically active polyoxometalate anion, $[\gamma\text{-}1,2\text{-}H_2SiV_2W_{10}O_{40}]^{4-}$ was immobilized with stoichiometric anion exchange. The POM structure was preserved after the anion exchange as verified by IR and ^{51}V NMR spectroscopy. The same team reported immobilization of peroxotungstate $[W_2O_3(O_2)_4(H_2O)_2]^{2-}$ on dihydroimidazolium-based ionic-liquid-modified SiO_2 [161].

A Chinese group immobilized peroxotungstates on both a monolayered ionic-liquid-modified silica [162] and a multilayered one (referred to as "ionic-liquid brushes") [163]. The latter had the advantage of the higher number of cationic imidazolium groups on the carrier and, hence, a higher number of catalytic active sites. In addition, the coral-like brushes provided an ionic-liquid microenvironment for substrates, reactants and active species. A supported ionic-liquid strategy has been also applied for immobilization of $H_5PMo_{10}V_2O_{40}$ onto SBA-15 [164]. Up to 40% of the HPA has been loaded. Retention of the silica structure after the immobilization procedure was confirmed by XRD.

Halligudi and coworkers [165] supported PW_{12} heteropoly acid on ZrO_2 nanoparticles that were initially embedded inside channels of SBA-15. The effects of grafting alumina species on the surface of silica support on the PW_{12} immobilization capacity were studied for conventional silica gel and mesostructured silica SBA-15 [166]. It was demonstrated that grafting on silica small alumina clusters at partial to full surface coverage produced isolated basic sites of comparable strength as at the surface of pure alumina and these sites anchored the molecular PW_{12}, retaining the polyanion structure. Hill and coworkers attached $[V_{10}O_{28}]^{6-}$, $[PV_2Mo_{10}O_{40}]^{5-}$ and $[(Fe^{III}(OH_2)_2)_3(A\text{-}\alpha\text{-}PW_9O_{34})_2]^{9-}$ on cationic silica nanoparticles (Figure 6.7) covered with alumina $(Si/AlO_2)^{n+}$ [167, 168]. The POMs formed an approximately single layer of monoanions on the surface (*ca.* 58 POM molecules per nanoparticle).

$H_5PMo_{10}V_2O_{40}$ was immobilized electrostatically on nitrogen-containing macroporous carbon [169] and spherical carbon particles with a diameter of *ca.* 12 μm

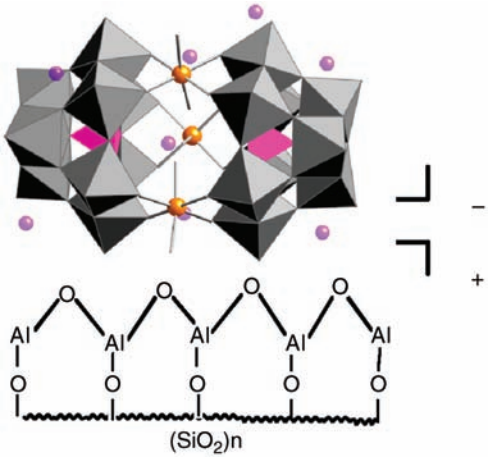


FIGURE 6.7 Electrostatic immobilization of POM on the surface of $(Si/AlO_2)^{n+}$ particles. Reprinted with permission from [167]. Copyright (2003) American Chemical Society.

synthesized by a hydrothermal method using a melamine–formaldehyde resin as a carbon precursor [170]. $H_3PW_{12}O_{40}$ and $H_3PMo_{12}O_{40}$ were supported on graphite oxide modified by a polymer containing cationic groups [171].

Transition-metal polyoxoanions can be intercalated in hydrotalcite-like anionic clays or layered double hydroxides (LDHs, $[M(II)_{1-x}M(III)_x(OH)_2](A^{n-})_{x/n}\cdot zH_2O$, where M(II) = Mg, Zn, Co, Ni, Cu . . . , M(III) = Al, Cr, Fe . . . and $A^{n-} = CO_3$, SO_4, NO_3, OH, Cl . . .) by anion exchange and some direct synthesis methods [92, 97, 172–179]. The POM-LDHs materials typically possess a surface area of about 90–200 $m^2\,g^{-1}$. The structural, thermal and textural properties of the LDH-POM intercalates were comprehensively studied by XRD, FT-IR, TEM, EDX, and N_2 adsorption techniques. A gallery height of about 10 Å was observed for the LDH intercalated by the symmetrical Keggin POM, whereas two different gallery heights were found for the cylindrical Dawson (14.5 and 12.8 Å) and Finke (13.3 and 12.6 Å) anions, depending on the preparation temperature [92]. The differences in POM orientations were rationalized in terms of different electrostatic and hydrogen-bonding interactions between the POM pillars and the LDH layers. Because of the strong basicity of LDHs, which may cause decomposition of some POMs, a special strategy to control the pillaring reactions is necessary for successful intercalation of POM anions between hydrotalcite layers [175].

Several monographs and review papers have addressed the synthesis, properties and applications in catalysis of POM-LDHs materials [180–185]. So, we only address here some recent results that demonstrate the high interest in these materials for liquid phase oxidations.

Co-substituted Keggin-type POMs, α-$\{SiW_9O_{37}\{Co(H_2O)\}_3]^{10-}$ and $[Co^{II}M_{11}Co^{II}(H_2O)O_{39}]^{8-}$ (M = W or Mo), were inserted between the layers of basic

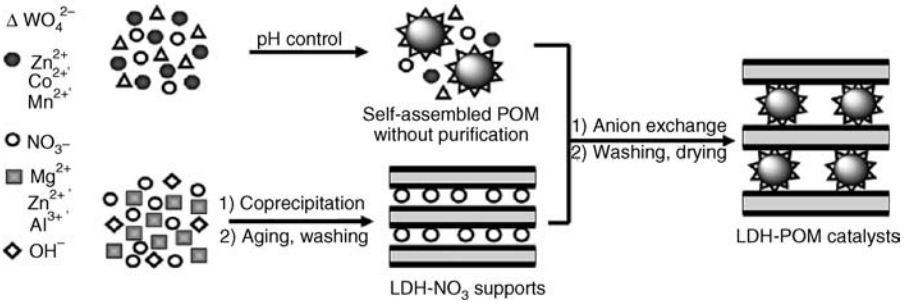


FIGURE 6.8 Schematic representation for the synthesis of LDH–POM catalysts using self-assembled POM solutions. Reprinted from ref. [188] with permission of Elsevier, copyright 2009.

Mg_3Al-hydrotalcite and used for the aerobic oxidation of hydrocarbons [97]. A new type of LDH intercalated by peroxo-polyoxometalates was synthesized by treating PdMAl-$[PW_{11}O_{39}]$ ($M = Mg^{2+}$ or Zn^{2+}) with 30% H_2O_2 [186]. XRD, FT-IR, and ^{31}P NMR MAS studies revealed that the interlayer anion $[PW_{11}O_{39}]^{7-}$ was converted mainly to $\{PO_4[WO(O_2)_2]_4\}^{3-}$ and $[W_2O_3(O_2)_4(H_2O)_2]^{2-}$. ^{27}Al NMR MAS showed that the brucite-like layers did not collapse during the synthesis. Li and coworkers [187, 188] suggested a method for the fabrication of LDH–POM catalysts that directly uses a self-assembled polyoxometalate solution without isolation and purification (Figure 6.8). A series of self-assembled POMs, including sandwich-type $[WZn_3(ZnW_9O_{34})_2]^{12-}$, $[WCo_3(CoW_9O_{34})_2]^{12-}$ and $[WZnMn_2(ZnW_9O_{34})_2]^{12-}$ and lacunary $[PW_{11}O_{39}]^{7-}$ were thus immobilized. The sandwich-type POM species were found to be more suitable than the Keggin-type POM for the direct immobilization process, because strict pH control is not needed for the former and the LDH host can be kept intact. The material thus obtained exhibits high dispersion of POMs and good hydrothermal stability.

In the past decade, a new class of materials, namely metal-organic frameworks (MOFs) or porous coordination polymers, appeared and immediately attracted the attention of the catalytic community [189]. A number of organic–inorganic ionic hybrid materials containing POM anions have been reported [72]. Coordination polymer networks with POMs immobilized through host–guest interactions have been recently reviewed [71]. In most of these materials the pores are totally blocked by the bulky POM anions. However, a few of them do not have this problem and are thus promising candidates for catalytic applications. The $[Cu^{II}_2(btc)_4/_3(H_2O)_2]_6[H_nXM_{12}O_{40}]\cdot(TMA)_2$ (btc = benzenetricarboxylate; TMA = tetramethylammonium; X = Si, Ge, P, As; M = W, Mo) coordination polymers were obtained from the simple one-step hydrothermal reaction of copper nitrate, btc, and Keggin POMs [190]. These materials possess high surface areas ($460\,m^2\,g^{-1}$) and two kinds of pores, one of which is occupied by POMs, while the other is partially filled with water molecules and TMA^+

cations. X-ray crystallographic analyses, TG, FT-IR, UV-vis, N_2 adsorption studies, and acid–base titration demonstrated high stability and tolerance for thermal and acid–base conditions. These well-defined, crystalline MOF-supported POMs behave as true heterogeneous acid catalysts. No POM leaching or framework decomposition was observed. The unique attributes of the MOF and well-dispersed POMs prohibited conglomeration and deactivation of polyanions.

In 2005, Férey and coworkers demonstrated the successful incorporation of a Keggin-type heteropolytungstate within the cages of the metal-organic framework MIL-101, the chromium terephthalate that possesses a rigid zeotype (MTN) crystal structure consisting of quasispherical cages of two modes (2.9 and 3.4 nm) accessible through windows of *ca.* 1.2 and 1.6 nm [191]. Cr-MIL-101 is resistant to air, water, common solvents and thermal treatment (up to 300 °C). To probe the presence of the polyanion within the pores of MIL-101, the resulting solid was analyzed by thermal gravimetric analysis (TGA), N_2 sorption measurement, XRD, ^{31}P solid-state NMR, and IR spectroscopy. All of these techniques confirmed the presence of a large number of POM ions within the pores. A theoretical estimation gave the value of ~5 Keggin anions per nanocage.

A range of hybrid materials based on the MIL-101 matrix and redox active heteropoly anions, $[PW_{11}CoO_{39}]^{5-}$, $[PW_{11}TiO_{40}]^{5-}$ [192], $[PMo_{10}V_2O_{40}]^{5-}$ [75], $[PW_{12}O_{40}]^{3-}$ and $\{PO_4[WO(O_2)_2]_4\}^{3-}$ [193] were prepared by adsorption of the corresponding Na- or TBA-salts from aqueous or acetonitrile solutions at room temperature. Adsorption studies revealed irreversible character of the sorption of about 10 wt% POM (~1 POM anion per MIL-101 cage, Figure 6.9), which indicated a

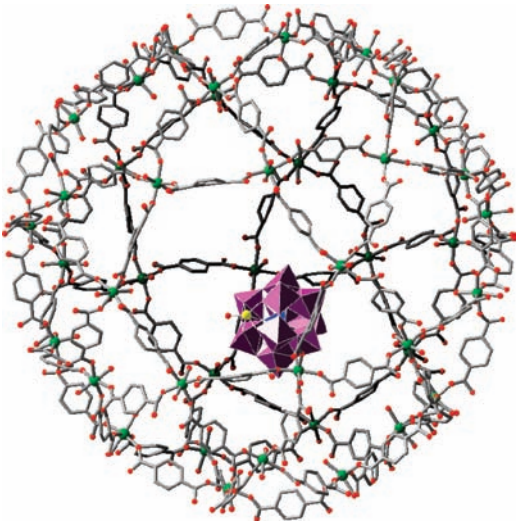


FIGURE 6.9 Immobilization of Keggin-type POM within nanocage of MIL-101. Reprinted from ref. [192] with permission of Elsevier, copyright 2008.

strong interaction between the POM and the MOF. Importantly, the major part of the immobilized POM can be re-extracted using a solution of a perchlorate or nitrate salt, thus pointing to the electrostatic character of POM binding to the positively charged surface of MIL-101. The ^{31}P NMR spectrum of the wash-out solution revealed the presence of the intact Keggin unit [193].

It was established that POM incorporation within Cr-MIL-101 occurs *via* exchange with nitrates according to Eq. 6.5 [75].

$$^{n}\Big/_{0.2}\left[Cr_3O(bdc)_3(H_2O)_2F_{0.8}(NO_3)_{0.2}\right] + POM^{n-} \rightarrow [Cr_3O(bdc)_3(H_2O)_2F_{0.8}]_{n/0.2} \cdot POM + nNO_3^- \quad (6.5)$$

Nitrate was determined quantitatively in the supernatant solution after immobilization of POMs. After immobilization of heteropoly acids in MIL-101, no change of pH was observed, which implies that protons remain in the mother solution and the POM, most likely, inserts into the MOF as the cluster-anion alone.

The MIL-supported POM catalysts were characterized by elemental analysis, XRD, N_2 adsorption, FT-IR, Raman, and ^{31}P NMR MAS spectroscopic techniques that confirm that both MIL and POM structures remain structurally intact after immobilization. Both the positions and width of the X-ray reflections remain unchanged but some redistribution of the reflection intensities is observed compared to the initial MIL-101, which could be attributed to strong interaction between the polyanions and the MIL-101 surface [75, 191, 192]. According to the N_2 adsorption data, both specific surface area and pore volume decrease after POM insertion, indicating that POM anions are incorporated mostly within cages and not on the external surface of the MIL-101 particles.

The addition of heteropoly acid PW_{12} to the synthesis mixture of MIL-101 results in the direct encapsulation of POM inside the MOF structure with a good distribution over the MIL-101 crystals [194]. DRIFT, Raman, and UV-vis techniques reveal a partial substitution of tungsten in PW_{12} by Cr^{III} to form $PW_{11}Cr$. This one-pot procedure affords POM/MIL-101 composite materials with the small cavities occupied by POM units that are bigger than the pentagonal windows of the cage and, hence, cannot leach into solution.

Complexation of Keggin-type heteropoly anions, $[\alpha\text{-}PW_{12}O_{40}]^{3-}$, $[\alpha\text{-}SiW_{12}O_{40}]^{4-}$, and $[\gamma\text{-}SiV_2W_{10}O_{38}(OH)_2]^{4-}$ with cationic transition-metal complexes having a triazacyclononane ligand, $[M(tacn)_2]^{n+}$ ($M = Co^{III}$ and Ni^{II}; tacn = 1,4,7-triazacyclononane), yields inorganic–organic composite materials. The strong electrostatic interaction between the highly negatively charged HPAs and the positively charged $[M(tacn)_2]^{n+}$ as well as the hydrophobicity of the latter result in the formation of the water-insoluble binary composites [195].

The Cu-containing POM, $[CuPW_{11}O_{39}]^{5-}$, was inserted in the pores of a Cu-containing MOF (HKUST-1, MOF-199) [196]. The electrostatic interaction between Cu–POM molecules and the MOF structural unit resulted in a substantial synergistic stabilization of both the MOF and the POM in the hybrid catalytic material $[Cu_3(C_9H_3O_6)_2]_4$ $[\{(CH_3)_4N\}_4CuPW_{11}O_{39}H]$.

6.2.5 Dative and Covalent Binding

Examples of dative binding of catalytically active POMs to produce heterogeneous POM-based catalysts are rare in the literature compared to the examples of electrostatic attachment discussed in the previous section. Johnson and Stein [94] reported anchoring of transition-metal-substituted POMs, $[PW_{11}M^{II}(H_2O)O_{39}]^{5-}$ (M = Co, Zn) and $[SiW_9O_{37}\{Co^{II}(H_2O)\}_3]^{10-}$ (Co_3-POM), to NH_2-modified macroporous (400 nm pores), mesoporous (2.8 nm pores), and amorphous fumed silica surfaces. The materials were characterized by solid-state ^{31}P NMR MAS, UV-vis, FT-IR spectroscopy, and N_2 adsorption measurements to verify cluster attachment and the structure of the POM on the support. The integrity of the $[PW_{11}CoO_{39}]^{5-}$ anion was maintained for nonaqueous impregnation with $TBA_5[PW_{11}CoO_{39}]$, while partial degradation of the cluster occurred when it was impregnated from aqueous solution using the corresponding K-salt. DRS UV-vis study revealed splitting of the $^4T_{1g_{1g}}$ band of the Co^{II} absorbance and the appearance of a shoulder at 628–640 nm, indicating the formation of a donor–acceptor bond between cobalt and the surface-anchored NH_2-ligand *via* substitution of H_2O in the coordination sphere of cobalt in $[PW_{11}Co^{II}(H_2O)O_{39}]^{5-}$ [94] (Figure 6.10).

When the Co-POM was impregnated by incipient wetness onto unmodified silica [94], embedded in a silica matrix or attached electrostatically to NH_3^+-silica [95, 96], no splitting of the absorption band occurred (Figure 6.6). Recently, the formation of a coordination bond was found for the sandwich-type polyanion, $[(PW_9O_{34})_2Co_4^{II}(H_2O)_2]^{10-}$, supported on NH_2-silica [197]. Using DR UV-vis spectroscopy the authors also confirmed the coordination of cobalt centers in the monosubstituted $[SiW_{11}Co^{II}(H_2O)O_{39}]^{6-}$ with the nitrogen atom of amine groups of NH_2-modified silica at pH $\geq$ 5.5 or the electrostatic bonding between the polyoxoanion and protonated $C_3H_6NH_3^+$-group at pH = 3.5 [197]. These results are consistent with the conclusions on the type of Co-POM attachment on NH_2-silica made by Stein and other groups.

Neumann and Cohen introduced a concept of "solvent-anchored supported liquid phase catalysis" [198, 199]. Using the sol-gel method they prepared silicates with surfaces containing various combinations of hydrophilic polyethylene oxide (PEO) and hydrophobic polypropylene oxide (PPO). These functionalized silicates were coupled with polyanions to produce catalytically active assembles, in which PEO and PPO acted as a solvent and/or complexing agent for POMs (Figure 6.11). Introducing cationic quaternary ammonium groups additionally to the PEO and PPO units allowed electrostatic binding of the POM to the support.

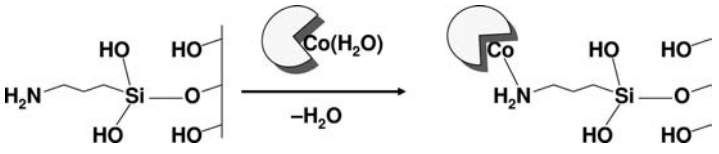


FIGURE 6.10 Dative binding of $[PW_{11}CoO_{39}]^{5-}$ to NH_2-modified silica (adapted from [94]).

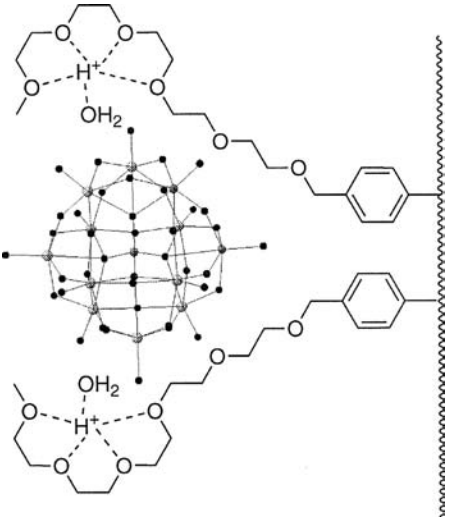


FIGURE 6.11 An illustration of $H_5PV_2Mo_{10}O_{40}$ complexed by PEO–SiO_2. Reprinted from ref. [199] with permission of Elsevier, copyright 1999.

Various supports containing phosphorylated ligands were synthesized and used to form covalent bonds with peroxotungstate species [25, 134, 200, 201]. Jacobs and coworkers developed an original route to support a peroxo–tungstate complex (Figure 6.12), in which the formation of P−O−W bonds is performed directly on the inner wall of MCM-41 [134]. First, a phosphoramide-grafted MCM material was prepared by functionalization of the surface silanols of MCM-41 *via* reaction with alkoxysilyl amino compounds followed by the reaction with $POCl_3$ in order to generate P−N covalent bonds. Finally, this material was treated with H_2O_2 and H_2WO_4. ^{31}P NMR data confirmed that the immobilized $–PO_3H_2$ groups react with the peroxo complexes by formation of P−O−W bonds. IR and Raman spectroscopy gave clear evidence for the existence of peroxo–tungstate species in the material, which is capable of epoxidizing olefins with H_2O_2 in a heterogeneous way.

Using a similar approach, $[HPO_4\{W(O)(O_2)_2\}_2]^{2-}$ (PW_2) was synthesized on the surface of another mesoporous silicate, HMS (see Chapter 4 for details), by reacting HMS–$(CH_2)_3NH(PO_3H_2)$ with peroxo tungstate $[W_2O_3(O_2)_4(H_2O)_2]^{2-}$ [202]. Then, palladium ions were exchanged into the channels of HMS to form a hybrid catalyst that appeared to be active in the epoxidation of propene with molecular oxygen.

Organically functionalized POMs are useful hybrid building blocks for the synthesis of hybrid organic–inorganic structures [42, 203]. The preparation of solids with covalently attached POM complexes is a serious and worthwhile research goal because such materials could well be quite resistant to POM leaching in solution. Many new materials of this type have been reported in the literature [25, 39, 66, 68, 71, 118, 133, 204–211]; however, catalytic studies on covalently bound POMs are in their infancy.

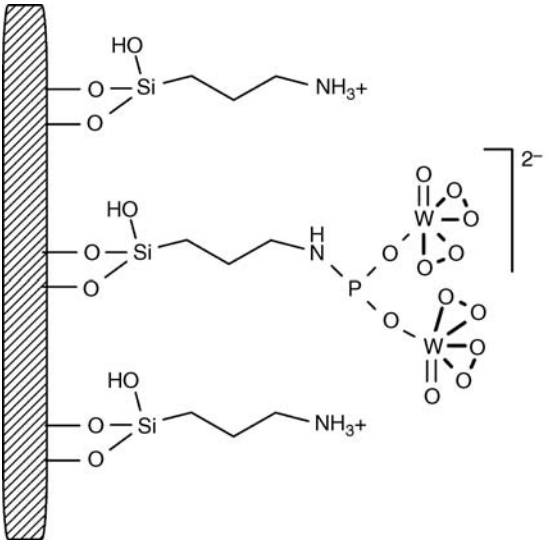


FIGURE 6.12 Schematic representation of peroxo–tungstate complex covalently anchored to silica. Reprinted from ref. [134] with permission of Elsevier, copyright 2000.

In 1992, Judeinstein reported the first POM–polymer hybrid where a lacunary Keggin POM cluster was covalently linked to polystyrene or polymethacrylate backbone through Si−O bonds [204]. The lacunary $[SiW_{11}O_{39}]^{8-}$ reacted with trichloro or trialkoxysilanes to produce $[SiW_{11}O_{40}(SiR)_2]^{4-}$ (R = vinyl, allyl, methacryl, styryl) that were then polymerized in the presence of a radical initiator to yield hybrid polymers. A similar approach was applied for di- and trivacant polyoxotungstates $[\gamma\text{-}SiW_{10}O_{36}]^{8-}$ and $\alpha\text{-}A\text{-}[SiW_9O_{34}]^{10-}$ [205, 206].

An example of well-defined covalent attachment of a POM to a surface is that of a thiol-functionalized POM on gold nanoparticles [209]. Functionalization of $\gamma\text{-}[SiW_{10}O_{36}]^{8-}$ with the sulfonylalkylsilane $HSC_3H_6Si(OMe)_3$ afforded difunctionalized $\gamma\text{-}[SiW_{10}O_{36}(HSC_6H_3Si)_2O]^{4-}$, which upon addition to colloidal solutions of gold nanoparticles (4–12 nm) formed a novel hybrid nanosystem. Errington and coworkers reported immobilization of the Linquist-type polyoxometalate $[(OMe)TiW_5O_{18}]^{3-}$ on alkanol-derivatized silicon surfaces through the formation of covalent M−O−C alkoxide bonds by alcoholysis of the Ti−OR bond in the POM [210]. Samples of single-crystal and porous silicon were functionalized with ω-hydroxyundecyl monolayers and then treated with acetonitrile solutions of $(TBA)_3[(MeO)TiW_5O_{18}]$ at 85 °C.

Xu et al. [208] elaborated a method for the selective synthesis of bifunctionalized organoimido hexamolybdates, which allows facile introduction of two functional groups to a hexamolybdate cluster and thus paves the way for the synthesis of main-chain–POM-containing hybrid polymers. Hill and coworkers [66, 211]

reported synthesis of three-dimensional coordination polymers *via* linking a catalytically active POM-based structural unit containing two juxtaposed organic groups $[V_6O_{13}\{(OCH_2)_3C(NHCH_2C_6H_4\text{-}4\text{-}CO_2)\}_2]^{4-}$ with lanthanide ions. In this material, the organic groups in the linking unit are covalently attached to the POM moiety (formally $[V_6O_{19}]^{8-}$) by triester groups that are quite robust (thermally stable to 100 °C and hydrolytically stable even in water).

Lacunary polyanions $XW_{11}O_{39}^{n-}$ (X = P, Si, Ge, B) were incorporated into the wall structure of macroporous silica resulting in hybrid XW_{11}–SiO_2 composites through the chemical grafting of organosilanol groups from the silica network onto the surface oxygen atoms at vacancies of XW_{11} clusters [118]. POM-functionalized mesoporous hybrid silicas, XW_{11}/MHS (X = P, Si), were synthesized by a cocondensation route by employing monovacant SiW_{11} or PW_{11} as POM precursors in the presence of Pluronic P123 under acidic conditions [68, 212]. This synthesis allows the bulky inorganic metal–oxygen clusters to be grafted directly on the surface of the SBA-15 silica. The XW_{11}/MHS samples were characterized by FT-IR, DRS UV-vis, ^{29}Si CP MAS NMR, XRD, TEM, N_2 adsorption measurements and elemental analysis. These materials possess not only hexagonal mesoscopic order and homogeneous pore sizes, but also intact Keggin units immobilized in channels by covalent linkages with the mesopore walls. The covalent bond results from the reaction of TEOS with XW_{11}, in which Si species are inserted into the vacancy of the lacunary POM to form Si−O−W bonds and an intermediate $XW_{11}O_{39}[O(SiOH)_2]^{n-}$ ($XW_{11}Si_2$), by which the POM is bound onto the framework of mesoporous silica. The introduced SiW_{11} is not only bound on the primary mesopore wall surfaces, but also entrapped in the complementary pores on the walls. The content of SiW_{11} in the hybrid material can reach 26–27 wt%. A higher SiW_{11} concentration can enhance the loading of POM to a certain extent, but may also lead to a disordered structure. The presence of chemical linkage(s) between the POM and the surface of mesoporous silica ensures the higher stability of the hybrid materials in water-leaching experiments compared to the impregnated samples. Another mesoporous hybrid, $Bu_4NPW_{11}Si_2$/MHS, was prepared by a postsynthesis route, in which $(Bu_4N)_3PW_{11}O_{40}(SiOH)_2$ was covalently bonded onto the mesopore walls of SBA-15 [212].

Wu and coworkers [73] suggested a new strategy for the preparation of POM-based heterogeneous catalysts through immobilization of supramolecular aggregates of a surfactant-encapsulated POM (SEP). First, the counterions of POM are replaced by quaternary ammonium cations, e.g. di(11-hydroxyundecyl)dimethylammonium. Through sol-gel condensation with TEOS, SEPs with hydroxyl groups at the periphery can be covalently anchored within a silica gel matrix [213]. The immobilized supramolecular POM aggregates possess a defined hydrophobic environment, similar to that of a reverse micelle system, which favors capturing of apolar organic substrates, and thus enhances the catalytic efficiency. The BET surface area of such hybrid catalysts is *ca.* 400 $m^2 g^{-1}$ with a total pore volume of 1.0 $cm^3 g^{-1}$ [73]. Catalysts of this type with entrapped $[PW_{12}O_{40}]^{3-}$ catalyze the efficient oxidation of alcohols, alkenes, and sulfides with H_2O_2 as the oxidant and can be conveniently recovered and reused.

6.3 CATALYTIC PROPERTIES

6.3.1 Oxidation of Alkanes

Kaleta and Nowińska used $H_6PMo_9V_3O_{40}$ supported on amino-silylated MCM-41 for cyclohexane oxidation with *tert*-butyl hydroperoxide (TBHP) as oxidant and acetonitrile as solvent [141]. The substrate conversion and turnover number (TON) achieved over a catalyst containing 10 wt% of the POM were similar to those observed for homogeneous PMo_9V_3. Increasing the POM content to 30 wt% led to decreasing activity, most likely due to a poorer dispersion of the POM on the silica surface resulting in inferior accessibility of the active sites. Leaching of the POM was minor in the polar reaction medium (*ca.* 1.5 wt%) and the catalyst showed very little decrease of catalytic activity in the second run.

Corma et al. [97] have patented a process of oxidizing cycloalkane with molecular oxygen to produce cycloalkanol and/or cycloalkanone in the presence of hydrotalcite-intercalated heteropoly anion $[Co^{II}M_{11}Co^{II}(H_2O)O_{39}]^{8-}$ (M = W or Mo), which contain one cobalt as the central atom and another substituting for a W=O fragment in the Keggin structure. At 130 °C and 0.5 MPa of O_2, 64 and 24% selectivity to cyclohexanone and cyclohexanol, respectively, was achieved at a cyclohexane conversion about 5%. No information about catalyst reusability and possible leaching of POM was reported.

Iron- and manganese-monosubstituted polyoxotungstates immobilized on triethylpropylammonium-functionalized silica were tested in the oxidation of cyclooctane at 80 °C using hydrogen peroxide as oxidant and acetonitrile as solvent [158]. Cyclooctane conversions as high as 71–74% were achieved, with moderate selectivity for cyclooctane hydroperoxide, cyclooctanone and cyclooctanol, together with minor amounts of 1,2-epoxycyclooctane. The product distribution was somewhat different from that obtained in the corresponding homogeneous system. Some of these supported catalysts could be reused several times without appreciable loss of catalytic activity.

The tetrairon(III)-substituted polyoxotungstates $[Fe_4(H_2O)_{10}(\beta\text{-}XW_9O_{33})_2]^{n-}$ ($n = 6$, $X = As^{III}$, Sb^{III}; $n = 4$, $X = Se^{IV}$, Te^{IV}) immobilized on (3-aminopropyl)triethoxysilane-modified SBA-15 showed fairly good catalytic performance for solvent-free aerobic oxidation of long-chain *n*-alkanes using air as oxidant under ambient conditions [145]. The catalysts maintained the high catalytic activity even after four cycles of catalyst reuse. Moreover, hot catalyst filtration experiments [14] indicated that there was no contribution from leached, homogeneous, catalytically active POM species.

Heteropolyacids $H_{3+n}PMo_{12}V_nO_{40}$ ($n = 1$–3) attached to amine-functionalized SBA-15 catalyzed oxyfunctionalisation of adamantane with 30% aqueous H_2O_2 (1 equiv.) in butyronitrile solvent [153]. Adamantanol was the main oxidation product formed with 76–81% selectivity at 49–65% substrate conversion after 12 h at 85 °C. The catalysts revealed fairly good recyclability in four consecutive runs, and the heterogeneous nature of catalysis was proved by a hot filtration test.

6.3.2 Oxidation of Aromatic Compounds

The heteropoly acid, PV_2Mo_{10}, complexed to 25% PEO–SiO_2 was employed as a recyclable catalyst in oxydehydrogenation of dihydroanthracene with TBHP as oxidant, showing improved activity and selectivity compared to the nonsupported POM [199]. Anthracene (AN) was produced in 96% yield. The same heteropoly acid immobilized on amine-functionalized SBA-15 was examined in the liquid phase oxidation of AN with 70% aqueous TBHP in benzene as solvent [152]. The catalyst operated with the turnover frequency (TOF) of 21 mole AN converted per mole of catalyst per hour and produced 9,10-anthraquinone in 100% selectivity. Leaching studies indicated the absence of POM leaching into the reaction medium, and the hot filtration experiment at 25% conversion provided convincing evidence of the heterogeneous nature of the catalysis.

Supported PV_nMo_{12-n} ($n = 1$–6) were used as catalysts for oxidation of alkylphenols to quinones [56, 63, 64]. Ishii and coworkers [63] studied the oxidation of a range of organic compounds, including phenols, with molecular oxygen catalyzed by $(NH_4)_5H_6PMo_4V_8O_{40}$ supported on carbon. In the case of reactions in polar media, a significant leaching of POM from the support was observed. Specifically, in the oxidation of 2,3,6-trimethylphenol to trimethyl-*p*-benzoquinone in AcOH-H_2O, 7% of the POM leached into the reaction medium, which could give rise to the homogeneously catalyzed reaction. Although the recycled catalyst showed almost the same activity as the fresh one, this experimental evidence is not sufficient to exclude the homogeneous reaction [14]. In the oxidation of 2,6-dimethylphenol over 40% $Cs_3HPMo_{11}VO_{40}$ supported on commercial silica, a catalyst filtration test revealed the mostly heterogeneous nature of the catalysis [64].

6.3.3 Oxidation of Olefins

6.3.3.1 Epoxidation The heteropoly acid $H_6PMo_9V_3O_{40}$ attached to NH_2-MCM-41 was used for cyclohexene oxidation with TBHP in MeCN [139]. The catalyst with 10 wt% POM loading revealed almost the same activity as homogeneous PMo_9V_3 and was significantly more stable to leaching in polar solvent medium compared to the catalyst supported on NH_2-free MCM-41. In the oxidation of a range of alkenes (norbornene, cyclooctene, cyclohexene, and styrene) with aqueous H_2O_2, the catalytic activity of $PMo_{11}V$ supported on amine-functionalized SBA-15 was, in general, lower than that of the homogeneous $PMo_{11}V$ heteropoly acid but the selectivity was higher in the former case [142]. The immobilized catalyst demonstrated fairly good reusability and stability to leaching (*ca.* 1% of POM was found in the filtrate). The filtration experiment confirmed that the catalysis was mostly heterogeneous in nature.

The supported Venturello complex obtained *via* anion exchange with Amberlite IRA-900 showed excellent selectivity in the epoxidation of acid-sensitive natural terpenes and allylic alcohols with aqueous H_2O_2 [133–135]. Selectivities as high as 93 and 97% were attained for limonene and 3-carene at 84 and 55% conversions, respectively, after 24 h at 38 °C. The catalytic activity of the reused catalyst was

TABLE 6.3 Epoxidation of *cis*-Cyclooctene with H_2O_2 over PW_4 Supported Catalysts (MeCN, 50 °C)

Catalyst	Time (h)	Alkene conversion (%)	Epoxide select.[a] (%)	Oxidant efficiency[b] (%)	Leaching[c]
Amberlite/PW_4	16	85	>95	95	no
MCM-N^+/PW_4	16	20	>95	90	<1 ppm W
MCM-NH(PO_3H_2)-W-peroxo	12	70	>95	>90	<2 ppm W

Elaborated from Ref. [134].

[a]Byproduct was diol.

[b]Mole of epoxide produced per mole of H_2O_2 consumed.

[c]Measured by ICP analysis and checked by filtration experiments.

completely maintained after several catalytic cycles, and the filtrate was catalytically inactive [135]. It was found that epoxide product deactivates the catalyst and the reaction practically stops when the amount of epoxide added is equivalent to about 160 turnovers [214]. Nevertheless, the catalyst could be reactivated by washing with acetone. PW_4 attached to $N^+(Et)_3$-modified MCM-41 was less active than the corresponding Amberlite-supported catalyst, while covalently attached to a silica tungsten peroxo complex (presumably, PW_2) revealed a fairly good activity and oxidant efficiency (Table 6.3). Tungsten leaching was limited to less than 2 ppm [134].

Two polyanions, $\{PO_4[WO(O_2)_2]_4\}^{3-}$ and $[ZnWMn_2(H_2O)_2\ (ZnW_9O_{34})_2]^{12-}$, immobilized on xerogels modified with phenyl groups and quaternary ammonium cations were employed for heterogeneous alkene oxidation using aqueous H_2O_2 in a solvent-free system [138]. The presence of the two types of functional groups on the catalyst surface produced a synergistic effect on the catalytic activity. The careful control of surface hydrophobicity allowed the achievement of essentially the same reactivity as in the biphasic liquid–liquid reaction medium where the catalyst is dissolved in a chlorohydrocarbon organic phase.

The PEO/PPO–SiO_2-anchored PW_4 catalyzed selectively (99%) cyclooctene epoxidation with 30% H_2O_2 without organic solvent at room temperature [198]. The proper balance of polyethers was critical for the catalytic activity: a mixture of 10% PEO and 10% of PPO was established as optimal for the solubility of both cyclooctene and hydrogen peroxide in the polyether-bound phase. The solvent-anchored catalyst was recycled five times without loss of the catalytic activity. No catalytic species and no catalytic activity were found in the filtrate. The sandwich heteropoly anion $[ZnWMn_2(ZnW_9O_{34})_2]^{12-}$ bound by a Q^+ moiety to the silicate surface also modified with polyethers formed a catalytically active assembly that had excellent recyclability with respect to alkene epoxidation by aqueous 30% H_2O_2 [199]. Again, the catalyst with a hydrophobic (PPO)/hydrophilic (PEO) balance showed the highest activity due to optimal mutual contact of the apolar hydrocarbon and the polar oxidant.

The catalyst prepared by noncovalent fixing of R_3PW_{12} ($R = \pi\text{-}C_5H_5N^+(CH_2)_{15}CH_3$) on hydrophobic mesoporous silica gel modified with Ph_3SiOEt and

$Me_3NCH(OCH_2Ph)_2$ groups produced epoxides from different alkenes in yields up to 97% using aqueous 15% H_2O_2 without an organic solvent [215]. The high hydrophobicity of both the silica gel surface and the POM countercation favored an easy access of hydrophobic alkenes to the catalytic centers. No data on the catalysts stability, recyclability, metal leaching and the nature of catalysis were reported for this system.

The peroxotungstate $[W_2O_3(O_2)_4(H_2O)_2]^{2-}$ immobilized on dihydroimidazolium-based ionic-liquid-modified silica was employed for alkene and allylic alcohol epoxidation [161]. The activity and selectivity of the immobilized complex were comparable to those of the homogeneous complex. The regioselective epoxidation of geraniol occurred at the electron-deficient 2,3-allylic double bond to afford 2,3-epoxy alcohol in high yield. The epoxidation of *cis*- and *trans*-alkenes proceeded stereospecifically. The catalyst could be easily recovered by filtration and reused at least three times without loss of catalytic activity and selectivity. The oxidation process was terminated completely after catalyst removal, and no tungsten species were detected in the filtrate, suggesting no contribution to the observed catalysis from homogeneous tungsten species that might have leached into the reaction solution.

Hydrotalcites intercalated with $[Mo_7O_{24}]^{6-}$ and $[H_2W_{12}O_{42}]^{10-}$ showed catalytic activities for the shape-selective epoxidation of alkenes with H_2O_2 [175]. Heptamolybdate, $[Mo_7O_{24}]^{6-}$, supported on hydrotalcites was evaluated in the oxidation of norbornadiene, benzonorbornadiene and cyclohexene using hydrogen peroxide as oxidant and dioxane or dioxane–butyl maleate mixture as solvents [179]. The selectivity to epoxides depended on the hydrotalcite composition and on the solvent. Recycling tests over six successive runs indicated that the catalysts retained all their activity and selectivity. However, elemental analysis of the liquor indicated some loss of the active component (about 1.2%); no convinced proof of the true heterogeneous catalysis was provided.

The catalysts, prepared *via* immobilization of self-assembled POMs including $[WZn_3(ZnW_9O_{34})_2]^{12-}$ (ZnWO) onto layered double hydroxides, were evaluated in the epoxidation of allylic alcohols with aqueous H_2O_2 [187, 188]. The LDH–ZnWO catalyst exhibited excellent activity (TOF in the range of 1030–18000 h^{-1} at 50 °C in acetonitrile solvent) and could be readily recycled (six reuses) with no apparent loss of performance [187]. The FT-IR spectrum of the recovered LDH-ZnWO catalyst confirmed retention of the original ZnWO structure, and ICP–AES analysis of the filtrate indicated no leaching of W and Zn species during oxidation. After the catalyst was removed at about 50% conversion of (*E*)-2-hexen-1-ol, no further reaction was detected in the filtrate after 3 h when additional H_2O_2 was added, which confirms that LDH-ZnWO acts as a true heterogeneous catalyst. The catalytic performance of the LDH–POM catalysts in solvent-free epoxidation with H_2O_2 strongly depended on the type of POM, the surface basicity of LDH, the pH value of aqueous H_2O_2, and the hydrophilicity of substrate [188]. The MgAl–ZnWO catalyst exhibited up to 99% epoxide selectivity, 95% H_2O_2 utilization efficiency and 37 200 h^{-1} TOF with no need of base additives or control of pH. The LDH-supported catalyst showed much higher epoxide selectivity than the

corresponding homogeneous Na salt of the POM, which has been attributed to the beneficial effect of basic LDH host on suppression of the acid-catalyzed epoxide ring opening. The MgAl-type LDH host with higher surface basicity was more effective than the ZnAl-type LDH in improving the epoxide selectivity.

Heteropoly anion $[\gamma\text{-}1,2\text{-}H_2SiV_2W_{10}O_{40}]^{4-}$ electrostatically bound to silica was capable of oxidizing heterogeneously a broad range of olefins with high selectivity to the desired products [146]. The unique stereospecificity, diastereoselectivity, and regioselectivity of the catalyst were very close to those of the homogeneous analog under the same reaction conditions, showing heterogenization without loss of the intrinsic POM properties. In the competitive epoxidation of *cis*- and *trans*-2-octenes, the oxidation rate of the *cis*-isomer was much higher than that of the *trans*-isomer. More-accessible, but less-nucleophilic double bonds in nonconjugated dienes were epoxidized with high regioselectivity. The activity of the supported catalyst was about half that of the homogeneous analog. Oxidation was immediately stopped by removal of the solid catalyst, and vanadium and tungsten species could hardly be found in the filtrate after removal of the catalyst. These results rule out any contribution to the observed catalysis from vanadium and tungsten species that leached into the reaction solution and suggest that the observed catalysis was truly heterogeneous in nature. In addition, the catalyst was reused without loss of the catalytic performance. The same group also demonstrated that fine particles of the hybrid ionic composites formed by $[\gamma\text{-}SiV_2W_{10}O_{38}(OH)_2]^{4-}$ and cationic hydrophobic transition-metal complexes $[Ni(tacn)_2]^{2+}$ (tacn = triazacyclononane) catalyze, heterogeneously, the epoxidation of olefins with H_2O_2 [195].

The catalytic activity of the rare-earth-metal sandwiched Keggin-type polyoxometalates, $K_{11}[RE(PW_{11}O_{39})_2]$ (RE = La, Ce, Pr, Nd, Sm, Eu, Dy and Y), electrostatically attached to aminosilylated mesoporous silica SBA-15 was tested in the oxidation of cyclohexene by H_2O_2 [157]. The presence of amine groups on the silica support prevented POM leaching during the reaction. After 2 h in which the cyclohexene conversion reached *ca.* 41%, the reaction mixture was filtered and then the mother liquor was allowed to react for another 8 h under the same reaction conditions. No significant activity was observed, demonstrating that the active species are not homogeneous species leached from the support.

The catalytic activity of $PW_{11}Fe/SiO_2$ and $(PW_9)_2Fe_4/SiO_2$ composites was studied in the epoxidation of geraniol using H_2O_2 as the oxidizing agent and CH_3CN as solvent [105]. The highest catalytic activity was obtained in the presence of $PW_{11}Fe/SiO_2$ (96% conversion after 3 h *versus* 81% conversion after 5 h attained with $(PW_9)_2Fe_4/SiO_2$); the selectivity to 2,3-epoxygeraniol was 88% and 91%, respectively. Similar activities were observed for the corresponding TBA salts of the POMs, which are soluble in the reaction medium. The addition of a radical scavenger, 2,6-di-*tert*-butyl-4-methylphenol (BHT), did not affect the product formation, suggesting a nonradical reaction mechanism. The composite catalysts could be easily separated and reused. The spectroscopic studies suggested that the POM in the silica nanocomposites was not destroyed. After catalyst removal at *ca.* 25% conversion, the reaction in the filtrate was very slow, indicating that the observed catalysis had mostly heterogeneous nature.

Mesoporous PMo_{12}/ZrO_2 nanocomposites prepared by the evaporation-induced cooperative assembly method were found to be active in the oxidation of various alkenes using hydrogen peroxide in acetonitrile as solvent [114]. The catalyst containing 37 wt% of POM demonstrated activity comparable to that of homogeneous $H_3PMo_{12}O_{40}$ (TOF = 9–50 h^{-1} depending on the nature of the alkene), suggesting that the zirconia matrix embeds the HPA without affecting its catalytic performance. The epoxide selectivity was 47, 81 and 100% for cyclohexene, 2-methylcyclohexene and cyclooctene, respectively. Styrene gave predominantly benzaldehyde. In contrast to the catalyst obtained by simple impregnation of mesoporous ZrO_2 with PMo_{12}, the nanocomposite revealed fairly good reusability in the oxidation reaction. The IR spectrum of the four-times-reused catalyst showed the presence of the principal Keggin POM bands, while EDX microanalysis confirmed that the amount of POM in the reused catalyst remained nearly the same as before catalysis. However, the lack of a hot filtration test does not allow unambiguous conclusions about the nature of catalysis to be drawn.

The hybrid materials PW_x/MIL-101 ($x = 4$ or 12) containing 5–10 wt% of polyoxotungstate demonstrated fairly good catalytic activities and selectivities in the epoxidation of various alkenes (3-carene, limonene, α-pinene, cyclohexene, cyclooctene, 1-octene) with aqueous H_2O_2 in MeCN solvent [193]. A simple one-pot procedure that involves both the catalyst preparation and oxidation reaction was used to achieve high yields of epoxides. Both the TOF values and alkene conversions were close to the corresponding parameters achieved with homogeneous PW_x. For the oxidation of substrates with aromatic groups (styrene, *cis*- and *trans*-stilbenes), a higher level of olefin conversion was attained with PW_{12}/MIL-101 than with homogeneous PW_{12}. The catalytic performance of PW_{12} immobilized on different supports in the H_2O_2-based epoxidation of cyclohexene is shown in Table 6.4 in comparison with the homogeneous HPA.

In contrast to the homogeneous system, with PW_{12}/MIL-101 the use of a higher H_2O_2/alkene molar ratio allows increasing simultaneously both the alkene conversion and epoxide selectivity despite the increasing amount of water in the system

TABLE 6.4 Cyclohexene Epoxidation with H_2O_2 over Supported PW_{12} Catalysts[a] [74]

Catalyst	Cyclohexene conversion (%)	TOF[b] (min^{-1})	Epoxide selectivity[c] (%)
PW_{12}[d]	72	0.41	78
PW_{12}/NH_2-SBA-15	48	0.19	17
PW_{12}/Sibunit	65	0.18	62
PW_{12}/MIL-101	84	0.40	80

[a]Reaction conditions: cyclohexene, 0.1 mmol; H_2O_2, 0.2 mmol; catalyst, 6×10^{-3} mmol W; MeCN, 1 mL; 50 °C, 3 h.
[b]TOF = (moles of substrate consumed)·(moles of W)$^{-1}$ time^{-1}; determined by GC from the initial rates.
[c]GC yield based on alkene consumed.
[d]Homogeneous catalyst (6×10^{-3} mmol W).

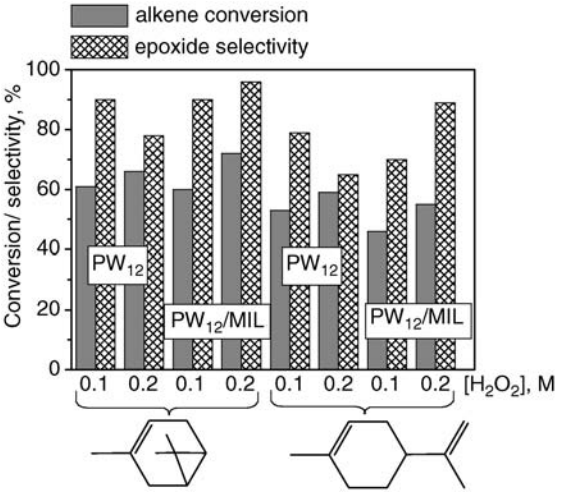
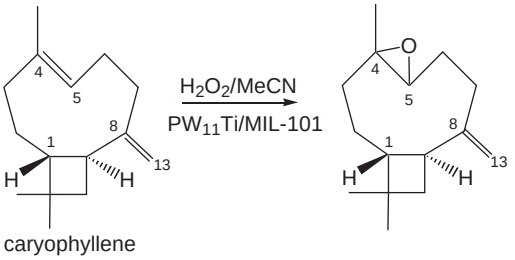


FIGURE 6.13 Opposite effects of H_2O_2 concentration on epoxide selectivity in the presence of PW_{12} and PW_{12}/MIL-101. Reaction conditions: 0.1 M alkene, 28 mg catalyst (5.8×10^{-3} mmol W), 1 mL MeCN, 50 °C, 3 h.

(Figure 6.13). Such atypical behavior, most likely, results from the specific sorption properties of the MIL-101 coordination polymer.

A similar effect was observed for epoxidation of caryophyllene with H_2O_2 over PW_{11}Ti/MIL-101 [192].



Importantly, the selectivity to caryophyllene epoxide was significantly higher for MIL-supported Ti-POM than for homogeneous $H_5PW_{11}TiO_{40}$ (80% *versus* 52% under the same reaction conditions). This could result from deprotonation of the Ti-POM anion upon immobilization on MIL-101 *via* anion exchange (*vide supra*), which protects the acid-sensitive epoxide from ring opening.

The PW_x/MIL-101 and PW_{11}Ti/MIL-101 composite materials are stable to POM and chromium leaching, behave as true heterogeneous catalysts, are easily recovered by filtration and are reused several times with maintenance of the catalytic performance [192, 193]. While PW_{12}/MIL-101 retained its activity and selectivity

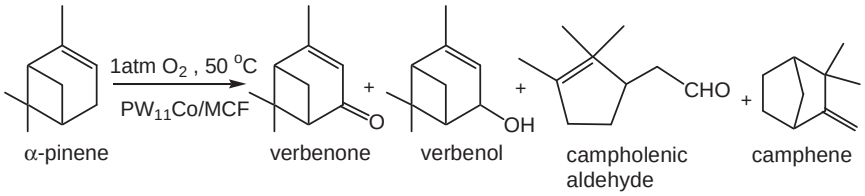
during four catalytic cycles of cyclohexene epoxidation (600 TON), $PW_{11}Ti$/MIL-101 showed stable catalytic performance for at least five reuse procedures (1840 TON).

Although a few POM-based catalytic systems produced high yields of epoxides using H_2O_2 as the green oxidant, selective epoxidation of terminal and some cyclic alkenes with molecular oxygen without addition of a sacrificial reducing agent (e.g. aldehyde) still remains rare. Silver and ruthenium colloids stabilized with $H_5PV_2Mo_{10}O_{40}$ to give 3–5 nm particles and then supported on alumina yielded catalysts that were highly selective for epoxidation of a range of alkenes with molecular oxygen [40, 216]. For a series of terminal alkenes such as 1-octene, epoxidation reactions catalyzed by Ag^0– or Ru^0–PV_2Mo_{10}/α-Al_2O_3 yielded 90% epoxide at 10–15% conversion after 0.5–1 h. Cyclohexene produced 41–50% of the epoxide at 20–25% conversion with both catalysts while 1-methylcyclohexene gave up to 90% of epoxide at 54% conversion using Ru^0–PV_2Mo_{10}/α-Al_2O_3. Longer reaction times resulted in a linear increase in the conversion but a significant decrease in the epoxide selectivity most likely due to competing autoxidation processes, which were inhibited only at the initial period of the reaction. IR spectra after the reaction did not show the typical absorption peaks of the POM, thus indicating POM decomposition on the alumina surface. Although no POM was found in solution, a recycled catalyst did not show the same activity and selectivity as the fresh one.

The solid hybrid catalyst Pd–HMS-PrNH–PW_2 was found to be active in the oxidation of propylene in methanol using O_2 as oxidant to produce propylene oxide in 83% selectivity at 34% conversion [202]. The actual epoxidation catalyst is suggested to be the HMS-bound peroxo species PW_2, regenerated by H_2O_2, which is likely produced by the reaction of methanol and O_2 over the palladium catalyst. The active components, palladium and tungsten, did not leach into the reaction medium, and the catalyst could be reused. The selectivity for propylene oxide over the solid catalyst was similar to that over a homogeneous catalyst containing $[(C_6H_{13})_4N]_2\{HPO_4[W(O)(O_2)_2]_2\}$ and $Pd(OAc)_2$ although the propylene conversion over the solid catalyst was lower than that with the homogeneous catalyst. An increase in the amount of the solid catalyst increased substrate conversion.

The hydrotalcite-supported catalyst PdMgAl–[$PW_4 + W_2$] showed 91.5% selectivity for propene oxide at 47.5% conversion during propene epoxidation by O_2 in methanol at 80 °C for 10 h [186]. The catalytic activity was attributed to the presence of highly active Pd particles in the brucite-like layers that generate H_2O_2 *in situ*, the strong epoxidation ability of interlayer peroxo-polyoxometalates with dilute H_2O_2, and the promotion effect of the basic MgAl-type brucite-like layers on alkene epoxidation. The catalyst was separated by filtration and reused without leaching of the active components.

6.3.3.2 Allylic Oxidation The catalytic properties of Co-monosubstituted Keggin-type POM immobilized on the hydrothermally stable mesostructured silicates SBA-15 and MCF modified with amino groups were assessed in α-pinene oxidation with molecular oxygen [96].



At low conversions, the oxidation produced mainly the allylic oxidation products, verbenol and verbenone, along with some campholenic aldehyde and the isomerization product, camphene. With increasing conversion the selectivity to the allylic oxidation products decreased due to overoxidation processes. Thus, the verbenol/verbenone selectivity attained 70 and 40% at 20 and 46% conversion of α-pinene, respectively. The activity of the supported Co-POM catalysts was as high as that of homogeneous $TBA_4H[PW_{11}CoO_{39}]$. The supported catalysts could be used repeatedly without loss of activity and selectivity during several catalytic runs and catalysis was truly heterogeneous, as confirmed by a hot catalyst filtration test [96].

The composite materials $PW_{11}Co$/silica [96] and $PW_{11}Ti$/silica [103] prepared by the sol-gel technique catalyzed α-pinene oxidation to verbenol/verbenone using molecular oxygen and aqueous H_2O_2, respectively, as oxidants in MeCN as solvent. Both composite catalysts revealed similar selectivities to the allylic oxidation products at similar substrate conversions. The activity of $PW_{11}Co/SiO_2$ expressed in TOF values was higher than the activity of homogeneous $TBA_4H[PW_{11}CoO_{39}]$. Interestingly, $PW_{11}Ti/SiO_2$, despite its nonporous structure revealed the same activity as homogeneous $H_5PW_{11}TiO_{40}$; furthermore, a remarkable increase of selectivity to verbenol/verbenone was observed for the sol-gel composite. The considerable differences in the catalytic activities and selectivities, which are observed for POM/SiO_2 composite materials *versus* homogeneous POMs, can be rationalized by several arguments. Previously, it was suggested that POM is entrapped in the silica network as a highly concentrated aqueous solution [54], which might account for the increased catalytic activity. The microporous structure of the matrix may enhance the reaction selectivity by suppressing overoxidation and polymerization processes. However, it is well documented that the acidity of heteropoly acids is reduced by silica supports [55, 56]. This may also lead to enhanced selectivity in some reactions, especially those accompanying by acid-catalyzed rearrangements of substrate and/or target product. Both composite catalysts revealed good recyclability and heterogeneous nature of catalysis. Figure 6.14 demonstrates recycling behavior and hot filtration test for the $PW_{11}Ti/SiO_2$ catalyst.

The $PW_{11}Co$/MIL-101 and $PW_{11}Ti$/MIL-101 hybrid materials demonstrated fairly good catalytic performance in α-pinene allylic oxidation (81–84% verbenol/verbenone selectivity at 15–25% substrate conversion) with O_2 and H_2O_2, respectively [192]. Comparison of the catalytic performance of $PW_{11}Co$ and $PW_{11}Ti$ supported on various solid carriers in α-pinene allylic oxidation has been reported [74].

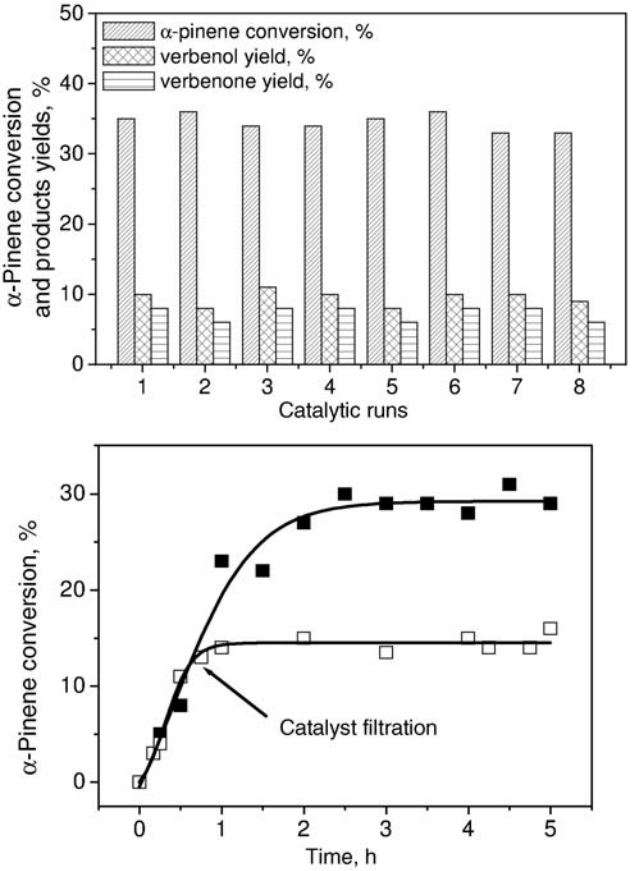


FIGURE 6.14 Oxidation of α-pinene with 30% H_2O_2 over sol-gel $H_5PW_{11}TiO_{40}/SiO_2$ composite: catalyst recycling (top) and hot catalyst filtration test (bottom). Reaction conditions: α-pinene, 0.1 mmol, H_2O_2, 0.12 mmol, catalyst, 14 mg, MeCN, 1 mL, 30 °C. Elaborated from ref. [103].

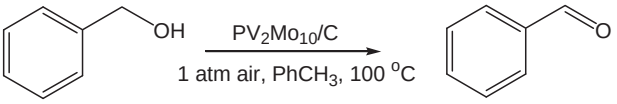
It is worth noting that the activity of the M-POM/MIL catalysts expressed in TOF values was close to the activity of the corresponding homogeneous POMs, indicating successful immobilization. Interestingly, the MIL-supported POMs appeared to be more selective in α-pinene allylic oxidation than the NH_2-silica-supported Co-POM [96], probably, due to the zeotype porous structure and smaller pore diameter of MIL-101, which may prevent the allylic oxidation products from oxidatively polymerizing.

The Co-POM/MIL-101 catalyst could be used repeatedly without suffering a loss of the activity and selectivity in the oxidations with molecular oxygen. However, when H_2O_2 was used as the oxidant, the reaction conditions had a strong

impact on the Ti-POM/MIL-101 catalyst stability. Under rather mild conditions ($< 50\,^{\circ}C$, $[H_2O_2] < 0.2\,M$), the Ti-POM/MIL-101 composite was rather stable according to FT-IR, elemental analysis, N_2 adsorption and XRD measurements, behaved as a true heterogeneous catalyst, did not undergo POM leaching, and could be reused without loss of catalytic properties. At higher H_2O_2 concentrations and higher temperatures, however, the MIL-101 matrix was destroyed and the POM/MIL-101 catalyst underwent deactivation and leaching.

6.3.4 Oxidation of Alcohols

Neumann and Levin [121] reported the liquid phase oxidative dehydrogenation of benzylic alcohols catalyzed by carbon-supported HPA-*n* in toluene at 100 °C with 94–100% yields to benzaldehydes, without overoxidation to carboxylic acids.



Carbon-supported $(NH_4)_5H_6PMo_4V_8O_{40}$ showed high catalytic activity for the oxidative dehydrogenation of benzylic and allylic alcohols to the corresponding aldehydes and ketones (46–92% yield) in toluene [63]. The catalyst could be recycled without loss of activity. In contrast, the parent NH_4^+ salt, which is insoluble in the reaction mixture, was inactive. The enhancement of catalytic activity after immobilization of the POM on active carbon was rationalized in terms of the higher concentration of substrates and oxygen due to their adsorption close to the active site. In addition, the active carbon can be a good mediator of the electron-transfer steps involved in the catalytic process. Another reason for the higher activity could be a larger surface area of the supported POM compared to the bulk POM.

The heteropoly acid $H_5PMo_{10}V_2O_{40}$, immobilized on an ionic-liquid-modified mesoporous silica SBA-15 demonstrated high activity in the aerobic oxidation of primary and secondary alcohols to aldehydes and ketones, respectively [164]. A broad range of benzylic, allylic, and aliphatic alcohols were oxidized under mild conditions with a high degree of chemoselectivity; no overoxidation of the primary alcohols to carboxylic acids was observed. Secondary alcohols were chemoselectively oxidized to ketones in the presence of primary alcohol, heteroatom, and allyl groups. The activities and product selectivities were comparable to those of the homogeneous analog, demonstrating successful heterogenization of the latter. The supported POM catalyst could be recycled five times without obvious loss of activity. ICP–AES analysis confirmed that no vanadium or molybdenum species were present in the solution.

The catalytic performance of MIL-supported $[PMo_{10}V_2O_{40}]^{5-}$ was assessed in the oxidation of two representative alcohols, cyclohexanol and carveol to the corresponding ketones [75]. The $PMo_{10}V_2$/MIL-101 material exhibited catalytic activity close to that of homogeneous POM coupled with excellent selectivity. Interestingly,

the selectivity to ketones was higher for the supported POM as compared to its homogeneous analog. The MIL-supported catalyst demonstrated good recyclability and true heterogeneous catalysis.

The Co-trisubstituted POM α-$[SiW_9O_{37}\{Co(H_2O)\}_3]^{10-}$ intercalated between the layers of basic Mg_3Al-hydrotalcite showed high catalytic activity and reusability in the liquid phase oxidation of cyclohexanol to cyclohexanone using 1 atm of molecular oxygen under mild reaction conditions [98]. The pillared catalyst exhibited similar XRD and FT-IR patterns before and after the oxidation reaction and its surface area did not change significantly, suggesting stability of the POM-based supported catalyst under turnover conditions. Elemental analysis confirmed the presence of trace amounts (at the ppb level) of cobalt species in the solution, but a hot catalyst filtration experiment pointed out the true heterogeneous nature of catalysis [98].

The activity of $TBA_4H[PW_{11}CoO_{39}]$ immobilized on amine-modified silica (NH_2–$(CH_2)_x$–SiO_2, $x = 0$, 2, 3) was tested in the oxidation of benzyl alcohol with molecular oxygen in CH_3CN medium [155]. Benzaldehyde formed with *ca.* 100% selectivity at substrate conversion of 8–20%, which was comparable or higher than the conversion achieved using the Co-POM as homogeneous catalyst. The higher substrate conversions were attained for supports containing higher numbers of amine functional groups with $x = 3$. These catalysts also revealed higher stability with respect to POM leaching.

$Cs_{2.5}H_{0.5}PW_{12}O_{40}$/SBA-15 materials prepared by subsequent impregnation of SBA-15 with Cs_2CO_3 and PW_{12} to form the highly dispersed insoluble Cs salt of the POM efficiently catalyzed the direct production of glutaric acid with the yield as high as 88% in the selective oxidation of cyclopentane-1,2-diol by aqueous hydrogen peroxide [63]. Over $Cs_{2.5}H_{0.5}PW_{12}O_{40}$ itself, the yield of glutaric acid was only 31%. The catalyst containing 40 wt% of the Cs salt was found to be optimal; at higher loadings, leaching of the active POM was serious. The catalyst could be easily recycled after the reaction, regenerated by simple calcinations in air and reused six times with only a slight decrease in activity. The structure of the $Cs_{2.5}H_{0.5}PW_{12}O_{40}$/SBA-15 catalysts was retained after the reaction, as determined by XRD, Raman, FT-IR and ^{31}P MAS NMR techniques.

Polymeric phosphotungstate catalyst bearing a poly(ethylene oxide-pyridinium) matrix catalyzed oxidation of a variety of alcohols, including sterically demanding neopentyl alcohol, with H_2O_2 to afford the corresponding carbonyl compounds in up to quantitative yields [150]. The chemoselective oxidation of sterically hindered secondary alcohols in the presence of primary alcohols was achieved. The catalyst could be reused four times without loss of activity.

6.3.5 Oxidation of Aldehydes

The catalytic performance of the NH_2-silica-supported Co-POM catalysts was examined in aerobic oxidation of isobutyraldehyde (IBA) [95]. The activity of the catalyst containing 13 wt% of Co-POM was as high as the activity of homogeneous $TBA_4H[PW_{11}CoO_{39}]$ (TOF = 31 h^{-1}). However, some loss of activity was already observed after 3 catalytic cycles because of Co-POM leaching during the oxidation process, as

determined by both elemental analysis and FT-IR spectroscopy [95]. An increase in the Co-POM loading up to 32 wt% was accompanied by a reduction of the catalytic activity (TOF = 13 h^{-1}). The composite material Co-POM/SiO_2 prepared by the sol-gel method revealed high activity (TOF = 31 h^{-1}) and superior selectivity in the oxidation of IBA (selectivity to isobutyric acid was 98% at 93% conversion after 6 h at room temperature) [95]. While the activity of the composite catalyst was close to that of the homogeneous Co-POM, the selectivity of the latter was much lower (just 57%). In contrast to Co-POM supported on NH_2-silica, the silica-entrapped Co-POM could be used repeatedly without suffering a loss in the catalytic activity and selectivity [95]. No Co-POM leaching was determined by elemental analysis. The superior stability of Co-POM/SiO_2 is, most likely, due to its microporous structure, which may prevent leaching caused by the carboxylic acid product.

Co- and Ce-monosubstituted Keggin-type POMs have been identified as active and selective catalysts in homogeneous aerobic oxidation of formaldehyde to formic acid under mild reaction conditions (25–40 °C, 1 atm of air) [95, 217]. The catalytic performance of both Co- and Ce-POM supported on NH_2-functionalized mesoporous silica was assessed in the aerobic oxidation of formaldehyde in water [95, 154]. While the Co-POM-based catalyst underwent rapid deactivation, the supported Ce-POM catalyst could be used repeatedly without significant loss of the activity [154].

Hill and coworkers used heteropoly acid PV_2Mo_{10} supported on fiber and fabric carbon materials for O_2-based oxidations of acetaldehyde and 1-propanethiols [93]. Kinetics, radical scavenging, and other experiments were consistent with the PV_2Mo_{10} fabric functioning primarily as a radical chain initiator. Surface area measurements and scanning electron microscopy before and after catalysis indicated that the fibers are not demonstrably altered and that the PV_2Mo_{10} fabric catalysts are not significantly deactivated by use. Cobalt-containing POMs, $Na_8Co_2W_{11}O_{39}$, $K_8SiCoVW_{10}O_{39}$, and $K_7SiCoVW_{10}O_{39}$ were even more active than $H_5PV_2Mo_{10}O_{40}$. Cotton-supported Co_2W_{11} produced acetic acid with 66% yield and *ca.* 1000 TON in chlorobenzene solvent [93]. The same group demonstrated application of $[V_{10}O_{28}]^{6-}$, $[PV_2Mo_{10}O_{40}]^{5-}$ and $[(Fe^{III}(OH_2)_2)_3(A\text{-}\alpha\text{-}PW_9O_{34})_2]^{9-}$ bound to cationic silica nanoparticles as heterogeneous catalysts for efficient autoxidation of acetaldehyde to acetic acid under ambient conditions [167]. Association of the POMs with the cationic surfaces of the $(Si/AlO_2)^{n+}$ nanoparticles dramatically increased the catalytic activity of the POMs, in particular the iron sandwich POM. The number of turnovers for all three POMs was enhanced by electrostatic immobilization on the nanoparticles. The recovered solid catalysts were almost as active as in the initial reaction, and the filtrate was completely inactive. This strongly supports the fact that the solid is the actual active catalyst and these new catalytic materials are quite stable.

6.3.6 Co-Oxidation of Alkenes and Aldehydes

Co-oxidation of alkenes with branched aldehydes (isobutyraldehyde, pivalaldehyde, etc.) produces epoxides along with corresponding carboxylic acids using various catalysts, including POMs [87–89]. This reaction proceeds *via* a conventional

radical-chain mechanism but allows achieving excellent yields of epoxides due to high selectivity of acylperoxy radical that is the main epoxidizing species in the system [88, 139].

Khenkin et al. [139] used $PMo_{10}V_2$ supported on MCM-41 and NH_2-MCM-41 for aerobic oxidation of hydrocarbons, including alkenes, in the presence of IBA. The presence of an amine function increased resistance of the material toward leaching of POM but decreased the catalytic activity. Stability to leaching strongly depended on the concentration of aldehyde used.

Johnson and Stein [94] tested the catalytic performance of Co-POMs datively bound to NH_2-modified silicas in the epoxidation of cyclohexene to cyclohexene oxide in the presence of IBA. The conversion of the substrate and the amount of product formed per unit time were similar for Co-POM supported on three representative silica supports with different textural properties, but slightly lower than for the purely homogeneous reaction. This could arise from the occupation of the sixth position in the cobalt coordination sphere by NH_2-ligand, which reduces the accessibility of the active center. Significantly, the trisubstituted polyanion $[SiW_9O_{37}\{Co^{II}(H_2O)\}_3]^{10-}$ with three available cobalt centers exhibits higher catalytic activity with nearly identical performance on a silica support or in homogeneous solution. In the case of the monosubstituted Co-POM, a small fraction of the POM leached into solution during the reaction, but the immobilized Co_3-POM was stable, thus showing a clear advantage of binding to the support *via* three (or possibly, two) cobalt centers.

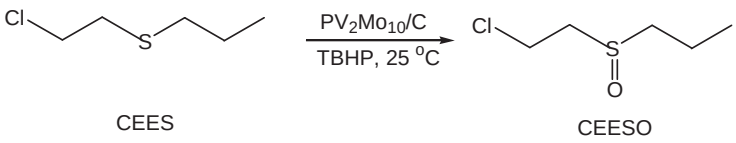
α-Pinene co-oxidation with IBA in the presence of monosubstituted Co-POM supported on hydrothermally stable mesostructured silicates SBA-15 and MCF modified with amino groups gave selectively α-pinene epoxide and isobutyric acid [96]. In contrast to the datively bound Co-POM [94], the activity of the electrostatically attached Co-POM catalysts was comparable to the activity of the homogeneous Co-POM. The selectivity of the co-oxidation process could be altered by varying the number of NH_2-groups on the support. Thus, for Co-POM supported on NH_2-MCF and NH_2-SBA-15 (NH_2/Co-POM = 30 and 16 mol/mol, respectively), the α-pinene epoxide selectivity attained 94 and 76%, respectively, at 96% of substrate conversion. This may be rationalized if we take into account that the excessive surface NH_2-groups may partially neutralize carboxylic acid formed during the co-oxidation process and thus improve the epoxide selectivity. The activity of the supported catalysts remained constant during few catalytic cycles and then tended to decrease regardless of the nature of the support. FT-IR data revealed that the Co-POM structure was retained after several reuses of the catalyst, while the nitrogen adsorption data confirmed retention of the support texture properties. Meanwhile, a DR UV-vis study pointed out some changes in the position and intensity of *d–d* transition bands in the spectra of the supported Co-POM after α-pinene/IBA co-oxidation (similar changes were observed after the catalyst treatment with isobutyric acid), indicating that the catalyst deactivation may arise from the chemisorption of the polar reaction product on the external position of the cobalt catalytic center [95, 96]. Indeed, both the catalytic activity and selectivity remained constant during several catalytic cycles when catalyst regeneration by evacuation was performed to remove the adsorbed carboxylic acid [96].

In contrast to α-pinene autoxidation that produced products of rather low polarity, the reaction rate in the filtrate of α-pinene/IBA co-oxidation after catalyst separation was significantly higher than that in the blank experiment. This indicated that Co-POM leaching from the solid catalyst into the solution occurred in the co-oxidation process and that catalysis had, at least partially, proceeded homogeneously. Indeed, the elemental analysis data confirmed substantial leaching of Co-POM after several operation cycles of α-pinene/IBA co-oxidation. Meanwhile, both the substrate conversion and the product yields remained unchanged during several consecutive runs of the α-pinene/IBA co-oxidation, provided the catalyst was exposed to regeneration before reuse. This seeming contradiction between the recycling and filtration experiments may be explained by a bell-shaped dependence of the oxidation rate *vs.* catalyst concentration, which is typical of chain-radical reactions in the presence of Co-containing catalysts [88, 89]. As a result, the observed catalytic activity is maintained over a wide range of cobalt concentration. Hence, the pinene/IBA co-oxidation reaction in the presence of the supported Co-POM catalysts can serve as an excellent example demonstrating that good catalyst recyclability itself can be a proof of neither the absence of leaching nor the heterogeneous nature of catalysis.

Co-POM/SiO_2 sol-gel composite was even more active than NH_2-silica-supported Co–POM in α-pinene/IBA co-oxidation and produced the corresponding epoxide with nearly quantitative yield [74, 96]. Both the epoxide selectivity and alkene conversion were superior to those acquired using homogeneous Co-POM. Under the same conditions, carbon-supported Co-POM catalysts, 6.5% Co-POM/Sibunit and 12% Co-POM/L2701, showed nearly 100% epoxide selectivity at 100% substrate conversion and 75% selectivity at only 12% conversion after 1 h, respectively [74]. Hot catalyst filtration tests revealed that, in contrast to silica-supported POMs, catalysis over Co-POM/Sibunite is truly heterogeneous, even if carboxylic acids form in the reaction. This agrees with the irreversible character of POM sorption on the active carbon. However, catalyst regeneration and recycling could be a problem for carbon-supported POMs because of strong, irreversible adsorption of the reaction products.

6.3.7 Oxidation of S-containing Compounds

Hill and coworkers [124, 125] used PV_2Mo_{10} heteropoly acid supported on porous carbons and carbon fiber materials for oxidation of the highly toxic mustard gas simulant 2-chloroethyl ethyl sulfide (CEES) to the corresponding sulfoxide (CEESO) using TBHP as oxidant.



CEES CEESO

Both selectivities (95 to 99% for sulfoxide) and rates (∼20%) varied with the carbon support at parity of all other parameters. The catalyst containing 10 wt% of PV_2Mo_{10} on Rohm and Haas Ambersorb produced CEESO with over 99% selectivity at even 75% conversion of the sulfide [124]. High selectivity to the corresponding sulfoxide is extremely important for this reaction because the sulfoxide is much less toxic than the sulfone. Washing for 125 h in toluene resulted in no significant loss in catalytic activity and a recovery and reusability study at high turnover also indicated that the catalysts are very stable. Cationic silica nanoparticles coated with the anionic multi-iron polyoxometalates, when suspended in a solution of $CuNO_3$ or CuOTf, favored aerobic oxidation of CEES to CEESO with effectively quantitative selectivity under ambient conditions [168].

The oxidation of tetrahydrothiophene (THT) to tetrahydrothiophene oxide (THTO) by TBHP readily occurred in the presence of PV_2Mo_{10}/Ambersorb and was found to be first order in substrate and oxidant and proportional to the concentration of active sites on the support [124]. The oxidation products, THTO and *tert*-butyl alcohol, inhibit the reaction at high conversions; however, the catalytic activity can be restored by heating in a vacuum at 80 °C [125]. The reactivity for oxidation of four different thioethers by TBHP catalyzed by PV_2Mo_{10} supported on hydrophobic (Ambersorb 563) and hydrophilic (Ambersorb 572) carbon powders indicated that while the steric and electronic characteristics of the thioether substrates are a factor in reactivity, the hydrophobicity of the carbon support is not.

Electrostatically bound to silica $[\gamma\text{-}1,2\text{-}H_2SiV_2W_{10}O_{40}]^{4-}$ was capable of heterogeneously oxidizing a broad range of organic sulfides to sulfoxides with high selectivity (90–96%) at 92–95% conversion [146]. Successful recovery of the catalyst could be achieved by simple decantation (or filtration). The recovered catalyst could be reused without any loss of catalytic performance. Silica-attached decatungstate $[W_{10}O_{32}]^{4-}$ also demonstrated fairly good catalytic activity, selectivity and reusability in H_2O_2-based sulfoxidation of various thioethers, including allyl phenyl sulfide and dibenzyl sulfide [147]. Turnover numbers as high as 960 were achieved. The heterogeneous nature of catalysis was demonstrated convincingly by carrying out a hot filtration test.

Peroxotungstates immobilized on ionic-liquid-modified silicas were employed for heterogeneous oxidation of thioethers to sulfoxides with 30% aqueous H_2O_2 [162]. The catalyst showed quite good recyclability, but SEM–EDX analysis performed on the recovered catalyst after six runs revealed some decrease in tungsten content. The same group reported selective oxidation of sulfides with H_2O_2 under mild conditions using peroxotungstates immobilized on multilayer ionic-liquid brushes-modified silica [163]. The catalytic activities depended on the number of supported ionic liquid layers and N-end-capped alkyl group on the imidazole ring. The sulfides were selectively oxidized to sulfoxides in high yields with traces of sulfones upon using 1.1 equivalents of the oxidant. At 2.5 equivalents of H_2O_2 the sulfones were the main products. The catalyst demonstrated high chemoselectivity towards sulfur groups with substrates containing unsaturated double bonds even though an excess of hydrogen peroxide was used. No apparent loss of catalytic efficiency was observed during seven reuses. ICP–MS analysis of the reaction solution

after filtration of the brushes showed the presence of 0.58 mg/L of tungsten. Since the question on the activity of the filtrate was not addressed [162, 163], the nature of catalysis in these systems remained unclear.

Dawson $[P_2W_{18}O_{62}]^{6-}$ and Preyssler $[NaP_5W_{30}O_{110}]^{14-}$ polyoxometalates immobilized within MCM-48, SBA-3, SBA-15 and NH_3^+-functionalized mesoporous silicas were studied as catalysts for oxidation of a range of thioethers [159]. The selectivity to sulfoxide attained 90–98% at 90–100% substrate conversion, depending on the specific thioethers and catalyst. The immobilized Preyssler complex was slightly more active than the Dawson POM. The textural and chemical properties of the silica framework had a pronounced effect on the oxidation efficiency, stability, and reusability of the catalysts. Catalysts with larger pores were more effective in the oxidation of relatively large thioethers, and functionalization with NH_3^+ improved further the catalytic properties. The [SBA-15-NH_3^+]/P_5 catalyst could be recovered for at least four runs without loss in activity. The catalysts were filtered after 30 min of the reaction and the filtrate was allowed to react further. In case of [SBA-15/NH_3^+]/P_5, the liquor did not react further. A negligible change in the reaction coordinate was found for SBA-15/P_5 and MCM-48/P_5 while in the SBA-3/P_5 system, the reaction proceeded with a very slow rate after the catalyst removal, indicating some minor leaching of the active POM.

The POM-containing open-framework materials prepared in the Hill group catalyzed peroxide-based sulfoxidation, but significantly more noteworthy, one of them, the 3D coordination network $\{Tb(bpdo)_2[V_6O_{13}\{(OCH_2)_3C(NHCH_2C_6H_4\text{-}4\text{-}CO_2)\}_2]\}$ (bpdo = 4,4′-bis(pyridine-*N*-oxide)), Tb-POM, catalyzed O_2-based oxidations and did so at ambient or nearly ambient temperature [66, 211]. A case in point is the oxidation of thiols, a common odorant in human environments and a mildly toxic class of compounds, to disulfides that have almost no odor and are less toxic. The stoichiometry for oxidation of a representative substrate, *n*-propane thiol, was established to be that in Eq. 6.6.

$$2\,PrSH + 0.5\,O_2 \rightarrow PrSSPr + H_2O \tag{6.6}$$

After 30 days at 45 °C, the Tb-POM material produced *ca.* 19 turnovers of disulfide product based on the bis(trisester)V_6 groups in the open-framework structure, using only ambient air as the oxidant.

Insertion of $[CuPW_{11}O_{39}]^{5-}$ in the pores of the Cu-containing MOF, $\{[Cu_3(C_9H_3O_6)_2]_4\}_n$, dramatically increased the catalytic activity of the Cu–POM for air-based oxidations [196]. The hybrid material efficiently catalyzed the chemo- and shape-selective oxidation of thiols to disulfides at room temperature, and facilitated the sustained removal of toxic H_2S (4000 turnovers in $<$20 h) by using only atmospheric oxygen. The POM activation by encapsulation in the MOF likely involves electrostatic interactions between the two components resulting in a higher reduction potential of the POM.

Surfactant-encapsulated polyoxometalates covalently bound to silica efficiently catalyze the oxidation of sulfides with H_2O_2 [73]. Diphenylsulfide, methyl phenyl sulfide, and dimethylsulfide were oxidized with 100% selectivity either to the

corresponding sulfoxides or sulfones, depending on the oxidant to substrate molar ratio. Dibenzothiophene (DBT) was quantitatively converted to the corresponding sulfone using 2.5 equiv. of H_2O_2. The supramolecular synergy between substrate adsorption, reaction, and product desorption during the oxidation process has been found to have an obvious influence on the reaction kinetics, with the activity of the catalyst being greatly improved. Substrates of low polarity such as DBT, dissolved in a polar solvent (MeCN), tend to adsorb at the more hydrophobic region composed of the alkyl chains of surfactants surrounding the POMs. Besides its high activity and selectivity, the SEP catalyst also demonstrated a high efficiency of H_2O_2 usage, which is important for practical applications. The SEP catalyst could be easily recovered by simple filtration and reused. The catalytic activity was well retained for at least five recycles. Stability of the POM structure in the recovered catalyst was confirmed by IR, ^{31}P NMR and XPS techniques. Yet, the W/C and W/Si elemental mass ratios were almost the same as those in the freshly prepared catalyst, suggesting that the SEP complexes were firmly bonded within the silica matrix and that no POMs had leached into the reaction solution.

6.4 MECHANISTIC ASPECTS

Mechanisms of catalytic action of various types of POMs in homogeneous liquid phase oxidations have been extensively studied, as has been reflected in several review papers [28, 30, 35, 36, 38, 40, 45, 85, 86]. Generally, the mechanisms of catalysis by homogeneous and supported POMs do not differ if the structure of POM remains intact after immobilization.

Catalytic reactions with oxidants other that dioxygen usually involve interaction of an oxygen donor with POM to form an activated intermediate capable of oxidizing an organic substrate (Eqs. 6.7 and 6.8).

$$\text{Oxidant} + \text{POM} \rightarrow [\text{POM} - \text{Ox}] \tag{6.7}$$

$$[\text{POM} - \text{Ox}] + \text{Substrate} \rightarrow \text{POM} + \text{Product} \tag{6.8}$$

The main pathways of activation of oxygen donors by metal centers that may be present in POM-based catalysts are shown in Figure 6.15.

The presence in POMs of high valent d^0-metal atoms makes them potential candidates for activation of hydrogen peroxide *via* formation of peroxo complexes. While POMs are thermodynamically stable to oxidation, $[PW_{12}O_{40}]^{3-}$ and $[PMo_{12}O_{40}]^{3-}$, as well as the corresponding lacunary heteropoly anions (e.g. $[PW_{11}O_{39}]^{7-}$) are prone to solvolytic destruction in the presence of aqueous H_2O_2, which leads to the formation of low nuclearity peroxotungstate (molybdate) species of varying catalytic activity [218–221]. It was found that the main active species operating in the $PW_{12}/H_2O_2/H_2O$ system is the Venturello complex, PW_4, formed *in situ*. The use of an organic medium increases the solvolytic stability of PW_{12} and leads to incomplete and reversible transformations [222]. In general, the higher the

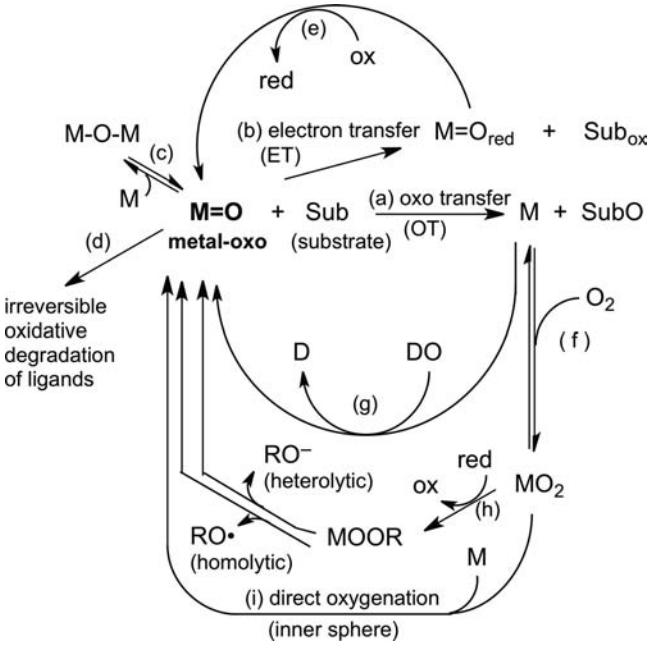


FIGURE 6.15 Pathways for activation of various oxidants by metal centers in POMs and other soluble oxidation catalysts. The metal-oxo (also frequently written "oxo-metal") species, (center left in bold), typically reacts in four frequently competing ways: by (a) direct oxo transfer oxidation of the substrate (Sub); (b) electron transfer from the substrate; (c) with another metal center (frequently the starting complex in its nonoxidized form, "M") forming a μ–oxo dimer, which is frequently a reversible process; or (d) oxidation of nonsubstrate organic species (ligands and sometimes solvent), which is always an irreversible process. The metal-oxo species can be regenerated by reaction with O_2 (oxygenation, path f) followed by reaction with a reductant (path i) or with M (path h), directly by back oxo transfer from an oxo donor molecule, DO (path g), or occasionally by another route. The metallo-alkylperoxide, MOOR, intermediates can undergo either hemolytic or heterolytic decomposition depending on the reaction conditions.

negative charge of POM, the higher is the solvolytic stability. Thus, $[SiW_{12}O_{40}]^{4-}$ or Keggin phosphotungstates substituted with Ti^{IV}, V^V, or Nb^V are intrinsically more stable towards the hydrolytic conditions of aqueous H_2O_2 relative to PW_{12}. For bulky sandwich-type POMs, the turnover number may reach tens of thousands without any noticeable destruction [28, 30, 35, 38]. In any case, it is necessary to analyze carefully by spectroscopic techniques the POM structure after interaction with excess of H_2O_2 and to perform structure–activity studies to identify the true oxidizing species in the catalytic system.

The reactivity and the mechanism of interaction between the peroxo species and an organic substrate depend on both the structure of the peroxo complex and the nature of the organic substrate. While the Venturello complex, PW_4, is highly active in the selective oxidation of a range of organic substrates, including alkenes, the

belt and cap tungsten atoms in sandwich $[P_2W_{21}O_{71}(H_2O)_3]^{6-}$ (P_2W_{21}) and Keggin PW_{12} are capable of catalyzing selective oxidation of thioethers and alcohols with H_2O_2 but are not able to accomplish epoxidation reactions [223]. Ti-monosubstituted Keggin-type polyoxotungstate $TBA_4[PTi(OH)W_{11}O_{39}]$, which forms upon interaction with aqueous H_2O_2 a monoprotonated peroxo complex $TBA_4[HPTi(O_2)W_{11}O_{39}]$ [224], is an active catalyst in H_2O_2-based oxidations of thioethers and alkylphenols and operates through homolytic pathways [85, 86]. However, this Ti-POM and other Ti-POMs with hexa-coordinated Ti^{IV} centers are not active in alkene epoxidation, which requires a heterolytic mechanism [225]. At the same time, the recently discovered 19-tungstodiarsenate(III) $[Ti_2(OH)_2As_2W_{19}O_{67}(H_2O)]^{8-}$ containing TiOH groups where the Ti atom has a 5-coordinated square-pyramidal geometry exhibits high activity and selectivity in alkene epoxidation with H_2O_2 *via* an electrophilic oxygen-transfer mechanism [225, 226]. In some cases, the reactivity and oxidation mechanism can be affected by the composition of POM countercations (the degree of POM protonation). For example, the catalytic activity of the heteropoly acid P_2W_{21} in the thioether oxidation was several times higher than the activity of its TBA salt. On the contrary, the heteropoly acid was completely inactive in the oxidation of cyclohexanol, while the TBA salt did this effectively [223]. In turn, increasing the number of protons facilitates a heterolytic oxidation mechanism with Ti-monosubstituted Keggin POMs [85, 86, 227].

Homolytic decomposition of H_2O_2 to produce O_2 and H_2O may occur parallel to the main oxidation process, decreasing the efficiency of oxidant utilization. The contribution of nonproductive decomposition of the oxidant is usually higher for catalysts containing metals with a high redox potential, like Co, Fe, Mn, V, etc.; however, their structural inclusion into a POM may have a strong impact on the redox properties and, hence, H_2O_2 utilization efficiency [43, 101]. Tuning the surface properties of the support *via* hydrophobization [138, 160, 199] or designing a hydrophobic supramolecular shell around the POM [73] enables control over the oxidation pathways through a proper regulation of reactant adsorption/association.

Oxidation with alkylhydroperoxides usually involves the formation of alkylperoxo complexes and their subsequent transformations (Figure 6.15). Predominance of the homolytic or heterolytic mechanism depends on the nature of the heterometal in POM along with other factors [36, 38].

The activation of O_2 *via* reaction sequence (6.7)–(6.8) is a fairly rare phenomenon but one found to be operable for a Ru-containing POM [228]. In effect, the composition of the POM has a strong impact on the mechanism of molecular oxygen activation. POMs containing transition metals like Co, Fe, Mn, etc. usually act as initiators of a chain-radical oxidation process and may also participate in chain branching *via* homolytic decomposition of intermediate hydroperoxides. At high concentrations, they may participate in chain termination *via* capturing of active radicals [88, 89].

The mechanisms of catalytic action of heteropoly acids (or acid salts) with polyanion of the general formula $[PV_nMo_{12-n}O_{40}]^{(3+n)-}$ ($n = 2$–6) have been addressed in a few review papers [36, 38, 40, 45, 56]. The oxidation mechanism depends on the nature of substrate to be oxidized as well as on the reaction conditions. Oxydehydrogenation through proton-coupled electron-transfer (PCET) steps followed

by reoxidation of V^{IV} to V^{V} with molecular oxygen (Eqs. 6.9 and 6.10) is the most common mechanism.

$$SH_2(\text{Substrate}) + [PMo_{10}V^{V}{}_2O_{40}]^{5-} \rightarrow S\ (\text{Product}) + H_2[PMo_{10}V^{IV}{}_2O_{40}]^{5-} \quad (6.9)$$

$$H_2[PMo_{10}V^{IV}{}_2O_{40}]^{5-} + 1/2O_2 \rightarrow [PMo_{10}V^{V}{}_2O_{40}]^{5-} + H_2O \quad (6.10)$$

Meanwhile, oxygenation of condensed arenes and alkylarenes through an electron-transfer–oxygen-transfer (ET–OT) mechanism (Eqs. 6.11–6.13), a homogeneous analog of the Mars–van Krevelen mechanism, which is common in gas phase oxidations over metal-oxide catalysts but normally does not occur in liquid phase, is also possible [40, 45].

$$SH_2 + M^{n+}{=}O \rightarrow S + 2H^+ + M^{(n-2)+}{=}O \quad (6.11)$$

$$M^{(n-2)+}{=}O + S \rightarrow M^{(n-2)+} + SO \quad (6.12)$$

$$M^{(n-2)+} + O_2 + 2H^+ \rightarrow M^{n+}{=}O + H_2O \quad (6.13)$$

Normally, the support itself is inert and participates only in the adsorption/desorption steps of the oxidation process. The exception seems to be active carbon that may be directly involved in the redox catalysis, as indicated by the superior activity of some carbon-supported POM catalysts compared to silica- and alumina-supported ones. A study from the Neumann group led to the formulation that quinones, likely formed on the active carbon surface through the presence of the polyoxometalate and oxygen, might play a role as an intermediate oxidant [229]. Thus, a catalytic cycle may be considered, whereby a surface quinone oxidizes the alcohol to the aldehyde and is reduced to a hydroquinone, which is then reoxidized in the presence of the catalyst and O_2.

6.5 STABILITY

The issue of stability of supported POM-based catalysts, in effect, involves three main concerns: 1) stability of the structure of active component (POM itself) towards the reaction medium; 2) stability of the solid catalyst towards leaching of POM into solution, and 3) stability of the textural and structural properties of the support under liquid phase conditions. The first concern is related mainly to catalytic systems that use aqueous hydrogen peroxide as oxidant and was already discussed in Section 6.4. Immobilization on a solid support may enhance stability of POM. Thus, incorporation within the MIL-101 matrix leads to greatly increased stability of PW_{12} towards solvolytic destruction in the presence of H_2O_2 [193]. In cyclohexene epoxidation with H_2O_2, 770 TON was achieved without POM destruction *versus* 155 TON for homogeneous PW_{12} under the same conditions.

The stability of solid catalysts towards leaching of the active species is a serious problem in liquid phase oxidation processes [14, 22]. Many solid catalysts have

been claimed to be heterogeneous; however, the nature of catalysis has not been investigated in most cases. Wet impregnation techniques can produce solids containing up to 50 wt% of POM on a mesoporous silica support, e.g. MCM-41 [230]; however, such catalysts undergo rapid POM leaching and catalyst deactivation in polar reaction media. For example, PW_{12} is quantitatively removed from MCM-41 and SBA-15 silica supports (the initial amount of POM on the support was *ca.* 30 wt%) after washing in water at 50 °C for 2 h [231]. In general, silica-supported POM catalysts obtained by simple impregnation are not stable to leaching in polar reaction medium and behave as homogeneous rather than heterogeneous catalysts. However, in a few cases, a careful control of the POM loading, the solvent used for impregnation as well as the textural and surface properties of the support enabled solid catalysts to be prepared that are relatively stable to leaching, provided the reaction mixture polarity is also under control [120, 121, 124, 139]. The mechanism of the strong adsorption of POMs on some silica at low loadings is not fully understood yet. ^{1}H and ^{31}P NMR MAS studies indicate a chemical interaction between the heteropoly anion and the support. Indeed, a significant broadening of the ^{31}P NMR MAS signal is observed for POMs deposited on Aerosil [232] and MCM-41 [139]. The formation of $(SiOH_2^+)(H_2PW_{12}O_{40}^-)$ species on the silica surface was supposed [232, 233]. Hence, it seems very likely that electrostatic interaction may contribute significantly in binding POMs to the surface of some silicate materials. However, one should remember that strong interaction with a support surface may result in polyanion destruction [234], so careful documentation of the POM structure after immobilization using a range of spectroscopic techniques is warranted.

Leaching of POM from ordered mesoporous silica in polar reaction media can be prevented by surface modification of the support. MCM-41 and SBA-15 coated with submonolayer quantities of alumina, titania or zirconia keep a heteropoly acid on the support more efficiently than uncoated silicas [231]. Functionalization with amino groups allows POM attachment to the silica surface by ionic or dative bonds, producing catalysts that are rather stable to leaching in polar medium. Thus, only 0.8 wt% of PMo_9V_3 anchored to amine-modified MCM-41 was removed after 2 h extraction with boiling methanol, while 95 wt% of the HPA was removed from the unmodified support when treated with methanol at room temperature [141]. However, if carboxylic acids are the reaction products, POM leaching and significant contribution of homogeneous catalysis is typically observed [74]. Interestingly, despite the gradual POM leaching, good catalyst recyclability can be observed during several reuses, producing an illusion of exclusive heterogeneous catalysis. Only hot catalyst filtration test allows one to draw an unambiguous conclusion about the true nature of catalysis in such systems [14, 22, 74].

The composite POM/SiO_2 materials obtained by the sol-gel technique are fairly stable to POM leaching, behave as true heterogeneous catalysts and can be used repeatedly without sustaining a loss of activity and selectivity in oxidations with O_2 and H_2O_2 under mild reaction conditions [74, 103, 192]. The protonation of surface silanols under the acidic sol-gel conditions to form cationic $Si-OH_2^+$ groups, which may act as countercations for POM anions, has been suggested [232, 233]. Hence, in addition to the occluding effect, electrostatic binding between $Si-OH_2^+$

groups and polyanions might be expected to contribute to the high stability of the composite POM/SiO_2 materials.

The stability of carbon-supported POMs to leaching strongly depends on the type of carbon, POM loading and reaction conditions [120–122, 125]. The possibility of the POM being leached from the support becomes more serious when the solvent is better suited as a counterion in protonated form, with the formation of lower energy ion associations with the heteropoly anion or, perhaps when the solvent strongly adsorbs onto the carbon support [122]. Water may be easily protonated but since the hydronium ion does not form ion associations with the polyanion moiety it is not a good extracting solvent, and leaching at the temperature of adsorption is minimal. With ethanol the picture is already changing; both in column extraction and Soxhlet experiments, ethanol extracts HPA far better than water does. This effect is also seen in the adsorption isotherms of phosphotungstic acid onto activated carbon from several alcohols. Because of this the usefulness of the catalyst is limited in solvents like the lower alcohols, ethers, esters and their mixtures with water. However, in apolar solvents such as alkanes, chlorinated alkanes, aromatic hydrocarbons or higher aliphatic alcohols the leaching is negligible, enabling the use as a truly heterogeneous catalyst. Evaluation of the desorption of PV_2Mo_{10} from six carbon supports indicates that pyrolyzed polyacrylonitrile and Ambersorb 572 materials are highly effective at retaining the immobilized PV_2Mo_{10} even under catalytic conditions (oxidation of tetrahydrothiophene by TBHP) [125]. POMs adsorbed on mesoporous carbon Sibunit revealed unprecedented stability towards leaching even in the presence of carboxylic acids [74].

The stability of a solid support under the reaction conditions strongly depends on its fundamental bonding and acid–base properties. Ordered mesoporous silicates, like MCM-41, suffer from low hydrothermal stability. This matter was addressed in detail in Chapter 4 of this book and will not be considered here. Hydrothermally stable silicates, like SBA-15 and MCF, are therefore preferable for POM immobilization. Organic–inorganic materials have a limited thermal stability and can be subject to oxidative destruction; hence, caution should be exercised not to exceed their stability limits. The study of the resistance of the coordination polymer MIL-101 to aqueous H_2O_2 demonstrated that it is stable under rather mild conditions ($T < 50\,^{\circ}C$, $[H_2O_2] < 0.2\,M$) but at higher peroxide concentrations and/or temperatures, the matrix is destroyed, and the POM/MIL-101 catalyst undergoes deactivation [192].

6.6 CONCLUSIONS

Polyoxometalates undoubtedly have enormous catalytic potential in the liquid phase selective oxidation of organic compounds. Various strategies for immobilization of POMs on solid matrices have been developed during the past two decades and these efforts have opened up new opportunities for practical applications. The most developed and widely used technique is electrostatic attachment of polyanions to positively charged supports, such as anion resins, hydrotalcite-like materials, cation-modified silica and other materials, including some sophisticated

coordination polymers. The number of materials, where POM is bound *via* dative or covalent bonding, remains low but these families are also growing rapidly because many material and synthetic chemists are working in this field. There are many POM-based materials, for which different types of interactions may contribute to the immobilization process and one can hardly classify these materials in terms of chemical binding. Synthetic chemists certainly outnumber catalytic researchers, and the catalytic potential of many new POM-based materials still remains unstudied. Collaborative efforts of specialists from different fields of chemical science would lead to a rapid advancement in this area.

The problem of decreasing catalytic activity upon immobilization of POMs seems to be solved to a considerable degree by using high surface area supports and employing methods that allow creation on the surface of spatially well-separated active centers, while keeping the POM structure intact. The catalytic activity of electrostatically immobilized POMs is often as high as that of the corresponding homogeneous POM, because the ligand environment of the active-site metal remains unchanged after immobilization. However, strong interaction with the surface (especially, when it is not mediated by a spacer ligand) may result in destruction of the POM. Hence, the maintenance of the POM structure after immobilization has to be carefully monitored by the use of suitably informative spectroscopic techniques, particularly FT-IR, DR UV-vis and ^{31}P NMR MAS.

As illustrated by the examples given in this chapter, the catalytic properties of POMs may benefit from association with the matrix, and in some cases both enhanced activity and selectivity result from immobilization. That is often the case of POMs embedding in silica matrix and may be attributed to a "constrained environment effect". However, it is still very difficult to predict the catalytic performance after immobilization, and only experiments can clarify this matter. Meanwhile, a rational modification of acid–base and/or hydrophobic–hydrophilic properties of a support is possible in some cases and can tune the catalytic properties.

Many supported POMs demonstrate fairly good recyclability in liquid phase oxidations. The use of hydrothermally stable supports, such as SBA-15, MCF, etc., ensures stability of textural properties of the supported catalysts. However, good recyclability does not mean that no leaching of the active POM occurs and that catalysis is truly heterogeneous rather than partially or wholly attributable to leached, homogeneous species. Indeed, some electrostatically attached and silica-embedded POMs are quite stable in reaction media of a medium polarity, but leaching still remains a serious problem when highly polar products, such as carboxylic acids, are formed during the oxidation process. Such products may induce POM leaching *via* anion-exchange or ligand-substitution mechanisms, the latter being expected for datively bound POMs. In turn, covalently attached POMs are anticipated to be stable with respect to anion exchange or ligand substitution, but one has to remember that hydrolysis of covalent bonds, e.g. M−O−Si or Si−O−Si, is another process that might be responsible for leaching, particularly, when aqueous hydrogen peroxide is used as oxidant. It should be noted, however, that the number of catalytic studies on datively and covalently attached POMs is still too limited to make general conclusions about their stability. POM destruction during

immobilization or catalysis is another process that may account for leaching of the active species from supported POM catalysts. Sometimes, immobilization allows increasing stability of the POM structure with respect to solvolytic destruction that may occur in the presence of hydrogen peroxide. This is the case for the frequently investigated PW_{12}: it easily transforms in polar solutions to lower nuclearity species, including the Venturello complex PW_4, but its initial structure may be restored if it is supported. In general, the stability of POMs with respect to H_2O_2 increases with increasing negative charge on the polyanion. Again, however, the retention of POM structure after several cycles of the supported catalyst use must be verified by spectroscopic techniques.

At the end of the 1990s and the beginning of the 2000s very little research addressed the crucial issue of POM leaching under the reaction conditions and the nature of catalysis following the methodology suggested Sheldon and coworkers [14]. However, one must acknowledge that most papers in the area of liquid phase oxidations over supported POM catalysts published in 2004–2011 provided the required experiments and discussions on this matter. Although many supported catalysts still remain "Trojan Horses" in liquid phase oxidation processes, a considerable number of novel catalytic materials do behave as efficient and true heterogeneous catalysts. Even if they are not "Philosophers' Stones" yet, the prospect for development of highly effective (fast, selective and stable) heterogeneous catalysts for liquid phase selective oxidations today is far more positive than 15 years ago. Progress in this field is to a great extent related to the creation of new families of immobilized POM catalysts. It is apparent, however, that a great number of opportunities, challenges, and applications are yet to come in the near future.

ACKNOWLEDGMENTS

The authors thank the U.S. Civilian Research and Development Foundation for the financial support of the joint research on supported POMs (CRDF grant RC1-2371-NO-02). CLH thanks the NSF (grant CHE-0911610) for support.

REFERENCES

1. Sheldon R.A., Kochi J.K. *Metal-Catalyzed Oxidations of Organic Compounds*. Academic Press, New York, 1981.
2. *Fine Chemicals through Heterogeneous Catalysis*. Sheldon R.A., van Bekkum H., eds. Wiley-VCH, Weinheim, 2001.
3. Centi G., Cavani F., Trifiro F. *Selective Oxidation by Heterogeneous Catalysis*. Kluwer Academic/Plenum Publishers, New York, 2001.
4. Centi G., Perathoner S. In: *Encyclopedia of Catalysis*, Vol. 6. Horvath I. T., ed. Wiley-Interscience, New Jersey, 2003, p. 239.
5. Brink G.-J., Arends I.W.C.E., Sheldon R.A. In: *Encyclopedia of Catalysis*, Vol. 6. Horvath I. T., ed. Wiley-Interscience, New Jersey, 2003, p. 189.

6. *Modern Heterogeneous Oxidation Catalysis: Design, Reactions and Characterization*. Mizuno N., ed. Wiley-VCH, Weinheim, 2009.
7. *Sustainable Industrial Processes*. Cavani F., Centi G., Perathoner S., Trifiro F., eds. Wiley-VCH, Weinheim, 2009.
8. Cavani F., Teles J.H. (2009). *Chem. Sus. Chem.* 2, 508–534.
9. *Chem. Soc. Rev.* 41 (2012). *Green Chemistry Themed Issue*. Li C.-J., Anastas P., eds.
10. *Ulmann's Encyclopedia of Industrial Chemistry*; 5th edn, Elvers B., Hawkins S., Shulz G., eds.; Vol. A(18), Wiley-VCH, Weinheim, 1991.
11. Parshall G.W., Ittel S.D. *Homogeneous Catalysis: The Applications and Chemistry of Catalysis by Soluble Transition Metal Complexes*; 2nd edn, Wiley-Interscience, New York, 1992.
12. Sheldon R., Arends I.W.C.E., Hanefeld U. *Green Chemistry and Catalysis*. Wiley-VCH, Weinheim, 2007.
13. *Catal. Sci. Technol.* 1 (2011). *Special issue on Heterogeneous Catalysis for Fine Chemicals*. Pagliaro M., Hutchings G., guest editors.
14. Sheldon R.A., Wallau M., Arends I.W.C.E., Schuchardt U. (1998). *Acc. Chem. Res.* 31, 485–493.
15. Sanderson W.R. (2000). *Pure Appl. Chem.* 72, 1289–1304.
16. Clark J.H., Rhodes C.N. *Clean Syntheses Using Porous Inorganic Solid Catalysts and Supported Reagents*. Royal Society of Chemistry, Cambridge, UK, 2000.
17. Thomas J.M. (1988). *Angew. Chem. Int. Ed.* 27, 1673–1691.
18. Thomas J.M., Raja R. (2006). *Top. Catal.* 40, 3–17.
19. *Proc. R. Soc. A* 468 (2012). *Special issue on Recent Advances in Single-site Heterogeneous Catalysts*. Thomas J.M., guest editor.
20. Thomas J.M. *Design and Applications of Single-site Heterogeneous Catalysts: Contributions to Green Chemistry, Clean Technology and Sustainability*. Imperial College Press, London, UK, 2012.
21. Ermakov Yu.I. (1983). *J. Mol. Catal.* 21, 35–55.
22. Sheldon R.A., Arends I.W.C.E., Lempers H.E.B. (1998). *Catal. Today* 41, 387–407.
23. Coperet C., Chabanas M., Saint-Arroman M.P., Basset J.M. (2003). *Angew. Chem. Int. Ed.* 42, 156–181.
24. Don Tilley T. (2002). *J. Mol. Catal.* 182–183, 17–24.
25. De Vos D.E., Dams M., Sels B.F., Jacobs P.A. (2002). *Chem. Rev.* 102, 3615–3640.
26. Pope M.T. *Heteropoly and Isopoly Oxometalates*. Springer, Berlin, 1983.
27. Moffat J.B. *Metal-Oxygen Clusters: The Surface and Catalytic Properties of Heteropoly Oxometalates*. Kluwer/Plenum, New York, 2001.
28. Hill C.L., Prosser-McCartha C.M. (1995). *Coord. Chem. Rev.* 143, 407–455.
29. *Chem. Rev.* 98 (1998). *Special issue on POMs*. Hill C.L., guest editor.
30. Neumann R. (1998). *Prog. Inorg. Chem.* 47, 317–370.
31. *Polyoxometalate Chemistry for Nanocomposite design*. Yamase T., Pope M.T., eds. Kluwer Academic/Plenum Publishes, 2002, pp. 1–235.
32. Okuhara T., Mizuno N., Misono M. (2001). *Appl. Catal. A: General* 222, 63–77.
33. *Polyoxometalate Chemistry: From Topology via Self-Assembly to Applications*. Pope M.T., Müller A. eds. Kluwer, Dordrecht, The Netherlands, 2001.

34. Kozhevnikov I.V. *Catalysis by Polyoxometalates*, In: *Catalysts for Fine Chemical Synthesis*, Vol. 2. Roberts S.N., Kozhevnikov I.V., Derouane E., eds. Wiley, Chichester, 2002.
35. Neumann R. In: *Transition Metals for Organic Synthesis*; 2nd edn, Vol. 2. Beller M., Bolm C., eds. Wiley-VCH, Weinheim, 2004, pp. 415–426.
36. Neumann R. In: *Modern Oxidation Methods*, Baeckvall J.-E., ed. Wiley-VCH, Weinheim, 2004, pp. 223–251.
37. Pope M.T. In: *Comprehensive Coordination Chemistry II*, Vol. 4. Wedd A.G., ed. Elsevier Science, New York, 2004, pp. 635–678.
38. Hill C.L. In: *Comprehensive Coordination Chemistry II*; Vol. 4. Wedd A.G., ed. Elsevier Science, New York, 2004, pp. 679–759.
39. Mizuno N., Kamata K., Yamaguchi K. In: *Surface and Nanomolecular Catalysis*. Richards R., ed. CRC Press LLC, Boca Raton, Fla, 2006, pp. 463–492.
40. Neumann R., Khenkin A.M. (2006). *Chem. Commun.*, 2529–2538.
41. *J. Mol. Catal. A: Chem.* 262 (2007). *Special issue on Polyoxometalates in Catalysis*. Hill, C.L., guest editor.
42. Proust A., Thouvenot R., Gouzerh P. (2008). *Chem. Commun.*, 1837–1852.
43. Mizuno N., Kamata K., Uchida S., Yamaguchi K. In: *Modern Heterogeneous Oxidation Catalysis: Design, Reactions and Characterization*. Mizuno N., ed. Wiley-VCH, Weinheim, 2009, pp. 185–217.
44. *Eur. J. Inorg. Chem.* 34 (2009). *Special Issue on Polyoxometalates*. Kortz U., guest editor.
45. Neumann R. (2010). *Inorg. Chem.* 49, 3594–3601.
46. Putaj P., Lefebvre F. (2011). *Coord. Chem. Rev.* 255, 1642–1685.
47. *Israel J. Chem. 51, issue 2* (2011). *Special Issue on Frontiers in Metal Oxide Cluster Science*. Weinstock I.A., guest editor.
48. Schäffer C., Todea A.M., Gouzerh P., Müller A. (2012). *Chem. Commun.* 48, 350–352.
49. Baiker L.C.W. In: *Advances in the Chemistry of Coordination Compounds*. Kirschner S., ed. Macmillan, New York, 1961.
50. Day V.W., Klemperer W.G. (1985). *Science* 228, 533–541.
51. Finke R.G., Droege M.W. (1984). *J. Am. Chem. Soc.* 106, 7274–7277.
52. Fournier M., Louis C., Che M., Chaquin P., Masure D. (1989). *J. Catal.* 119, 400–414; 415–425.
53. Chen Q., Zubieta J. (1992). *Coord. Chem. Rev.* 114, 107–167.
54. Izumi Y. (1998). *Res. Chem. Intermed.* 24, 461–471.
55. Mizuno N., Misono M. (1998). *Chem. Rev.* 98, 199–217.
56. Kozhevnikov I.V. (1998). *Chem. Rev.* 98, 171–198.
57. Okuhara T. (2002). *Chem. Rev.* 102, 3641–3666.
58. Rhule J.T., Neiwert W.A., Hardcastle K.I., Do B.T., Hill C.L. (2001). *J. Am. Chem. Soc.*, 123, 12101–12102.
59. Yamaguchi K., Mizuno N. (2002). *New J. Chem.* 26, 972–974.
60. Vasylyev M.V., Neumann R. (2004). *J. Am. Chem. Soc.* 126, 884–890.
61. Plault L., Hauseler A., Nlate S., Astruc D., Ruiz J., Gatard S., Neumann R. (2004). *Angew. Chem., Int. Ed.* 43, 2924–2928.

62. Vazylyev M., Sloboda-Rozner D., Haimov A., Maayan G., Neumann R. (2005). *Topics Catal*. 34, 93–99.
63. Fujibayashi S., Nakayama K., Hamamoto M., Sakaguchi S., Nishiyama Y., Ishii Y. (1996). *J. Mol. Catal. A* 110, 105–117.
64. Villabrille P., Romanelli G., Vázquez P., Cáceres C. (2008). *Appl. Catal. A: General* 334, 374–380.
65. Gao R., Chen H., Le Y., Dai W.-L., Fan K. (2009). *Appl. Catal. A: General* 352, 61–65.
66. Cao R., Han J.W., Anderson T.M., Hillesheim D.A., Hardcastle K.I., Slonkina E., Hedman B., Hodgson K.O., Kirk M.L., Musaev D.G., Morokuma K., Geletii Y.V., Hill C.L. In: *Advances in Inorganic Chemistry*, Vol. 60, van Eldik R., ed. Academic Press, The Netherlands, 2008, pp. 245–272.
67. Kholdeeva O.A. In: *Heterogeneous Catalysis Research Progress*. Gunther M.B., ed. Nova Science Publ., New York, NY, 2008, pp. 267–297.
68. Zhang R., Yang C. (2008). *J. Mater. Chem.* 18, 2691–2703.
69. Inumaru K., Ishihara T., Kamiya Y., Okuhara T., Yamanaka S. (2007). *Angew. Chem. Int. Ed.* 46, 7625–7628.
70. Dufaud V., Lefebvre F., Niccolaic G.P., Aouine M. (2009). *J. Mater. Chem.* 19, 1142–1150.
71. Yu R., Kuang X.-F., Wu X.-Y., Lu C.-Z., Donahue J.P. (2009). *Coord. Chem. Rev.* 253, 2872–2890.
72. Dolbecq A., Dumas E., Mayer C.R., Mialane P. (2010). *Chem. Rev.* 110, 6009–6048.
73. Qi W., Wang Y., Li W., Wu L. (2010). *Chem. Eur. J.* 16, 1068–1078.
74. Kholdeeva O.A., Maksimchuk N.V., Maksimov G.M. (2010). *Catal. Today* 157, 107–113.
75. Maksimchuk N.V., Kholdeeva O.A., Kovalenko K.A., Fedin V.P. (2011). *Israel J. Chem.* 2, 281–289.
76. Matveev K.I. (1977). *Kinet. Catal.* 18, 716–729.
77. Grate J.H. (1996). *J. Mol. Catal. A: Chem.* 114, 93–101.
78. Venturello C., D'Aloisio R., Bart J.C.J., Ricci M. (1985). *J. Mol. Catal.* 32, 107–110.
79. Venturello C., D'Aloisio R. (1988). *J. Org. Chem.* 53, 1553–1557.
80. Matoba Y., Inoue H., Akagi J., Okabayashi T., Ishii Y., Ogawa M. (1984). *Synth. Commun.* 14, 865–873.
81. Ishii Y., Yamawaki K., Yoshida T., Ura T., Ogawa M. (1987). *J. Org. Chem.* 52, 1868–1870.
82. Ishii Y., Yamawaki K., Ura T., Yamada H., Yoshida T., Ogawa M. (1988). *J. Org. Chem.* 53, 3587–3593.
83. Hill C.L., Brown R.B. (1986). *J. Am. Chem. Soc.* 108, 536–539.
84. Katsoulis D.E., Pope M.T. (1986). *J. Chem. Soc., Chem. Commun.*, 1186–1187.
85. Kholdeeva O.A. (2006). *Topics Catal*. 40, 229–243.
86. Kholdeeva O.A., Maksimovskaya R.I. (2007). *J. Mol. Catal. A: Chem.* 262, 7–24.
87. Mizuno N., Hirose T., Tateishi M., Iwamoto M. (1993). *Chem. Lett*. 22, 1839–1842.
88. Kholdeeva O.A., Grigoriev V.A., Maksimov G.M., Fedotov M.A., Golovin A.V., Zamaraev K.I. (1996). *J. Mol. Catal. A: Chem.* 114, 123–130.
89. Kholdeeva O.A., Khavrutskii I.V., Romannikov V.N., Tkachev A.V., Zamaraev K.I. (1997). *Stud. Surf. Sci. Catal.* 110, 947–955.

90. Yin Q., Tan J.M., Besson C., Geletii Y.V., Musaev D.G., Kuznetsov A.E., Luo Z., Hardcastle K.I., Hill C.L. (2010). *Science* 238, 342–345.
91. Huang Z., Luo Z., Geletii Y.V., Vickers J., Yin Q., Wu D., Hou Y., Ding Y., Musaev D.G., Hill C.L., Lian T. (2011). *J. Am. Chem. Soc.* 133, 2068–2071.
92. Yun S.K., Pinnavaia T.J. (1996). *Inorg. Chem.* 35, 6853–6860.
93. Xu L., Boring E., Hill C.L. (2000). *J. Catal.* 195, 394–405.
94. Johnson B.J.S., Stein A. (2001). *Inorg. Chem.* 40, 801–808.
95. Kholdeeva O.A., Vanina M.P., Timofeeva M.N., Maksimovskaya R.I., Trubitsina T.A., Melgunov M.S., Burgina E.B., Mrowiec-Bialon J., Jarzebski A.B., Hill C.L. (2004). *J. Catal.* 226, 363–371.
96. Maksimchuk N.V., Melgunov M.S., Mrowiec-Białoń J., Jarzębski A.B., Chesalov Yu.A., Kholdeeva O.A. (2007). *J. Catal.* 246, 241–248.
97. Corma A., Lopez Nieto J.M., Domine M.E., inventors; Sumitomo Chemical Company, assignee. European Patent 1707553. 2006.
98. Jana S.K., Kubota Y., Tatsumi T. (2008). *J. Catal.* 255, 40–47.
99. Kharat A.N., Pendleton P., Badalyan A., Abedini M., Amini M.M. (2001). *J. Mol. Catal. A: Chem.* 175, 277–283.
100. Neumann R., Gara M. (1995). *J. Am. Chem. Soc.* 117, 5066–5074.
101. Zhang X., Anderson T.M., Chen Q., Hill C.L. (2001). *Inorg. Chem.* 40, 418–419.
102. Mrowiec-Bialon J., Turek W., Jarzebski A.B. (2002). *React. Kinet. Catal. Lett.* 76, 213–219.
103. Maksimchuk N.V., Melgunov M.S., Mrowiec-Bialon J., Jarzebski A.B., Kholdeeva O.A. (2005). *J. Catal.* 235, 175–183.
104. Weakley T.J.R. (1973). *J. Chem. Soc. Dalton Trans.*, 341–346.
105. Sousa J.L.C., Santos I.C.M.S., Simões M.M.Q., Cavaleiro J.A.S., Nogueira H.I.S., Cavaleiro A.M.V. (2011). *Catal. Commun.* 12, 459–463.
106. Yang L., Qi Y., Yuan X., Shen J., Kim J. (2005). *J. Mol. Catal. A: Chem.* 229, 199–205.
107. He N.-Y., Woo C.-S., Kim H.-G., Lee H.-I. (2005). *Appl. Catal. A: General* 281, 167–178.
108. Lapkin A., Bozkaya B., Mays T., Borello L., Edler K., Crittenden B. (2003). *Catal. Today* 81, 611–621.
109. Gagea B.C., Lorgouilloux Y., Altintas Y., Jacobs P.A., Martens J.A. (2009). *J. Catal.* 265, 99–108.
110. Toufaily J., Soulard M., Guth J.-L., Patarin J., Delmotte L., Hamieh T., Kodeih M., Naoufal D., Hamad H. (2008). *Colloid Surf. A: Physicochem. Eng. Aspects* 316, 285–291.
111. Shi C., Wang R., Zhu G., Qiu S., Long J. (2005). *Eur. J. Inorg. Chem.*, 4801–4807.
112. Shi C., Wang R., Zhu G., Qiu S., Long J. (2006). *Eur. J. Inorg. Chem.*, 3054–3060.
113. Farhadi S., Zaidi M. (2009). *Appl. Catal. A: General* 354, 119–126.
114. Armatas G.S., Bilis G., Louloudi M. (2011). *J. Mater. Chem.* 21, 2997–3005.
115. Fuchs V., Méndez L., Blanco M., Pizzio L. (2009). *Appl. Catal. A: General* 358, 73–78.
116. Guo Y.-H., Hu C.-W. (2007). *J. Mol. Catal. A: Chem.* 262, 136–148.
117. Katsoulis D.E. (1998). *Chem. Rev.* 98, 359–387.
118. Guo Y., Yang Y., Hu C., Guo C., Wang E., Zou Y., Feng S. (2002). *J. Mater. Chem.* 12, 3046–3052.

119. Wu Q. (2002). *Mater. Chem. Phys.* 77, 204–208.
120. Izumi Y., Urabe K. (1981). *Chem. Lett.*, 663–664.
121. Neumann R., Levin M. (1991). *J. Org. Chem.* 56, 5707–5710.
122. Schwegler M.A., Vinke P., van der Eijk M., van Bekkum H. (1992). *Appl. Catal.* 80, 41–57.
123. Kozhevnikov I.V., Sinnema A., Jansen R.J.J., van Bekkum H. (1994). *Catal. Lett.* 27, 187–197.
124. Gall R.D., Hill C.L., Walker J.E. (1996). *J. Catal.* 159, 473–478.
125. Gall R.D., Hill C.L., Walker J.E. (1996). *Chem. Mater.* 8, 2523–2527.
126. Wu Y., Ye X., Yang X., Wang X., Chu W., Hu Y. (1996). *Ind. Eng. Chem. Res.* 35, 2546–2560.
127. Pizzio L.R., Caceres C.V., Blanco M.N. (1998). *Appl. Catal. A: General* 167, 283–294.
128. Alcañiz-Monge J., Trautwein G., Parres-Esclapez S., Maciá-Agulló J.A. (2008). *Micropor. Mesopor. Mater.* 115, 440–446.
129. Timofeeva M.N., Ayupov A.B., Mitkin V.N., Volodin A.V., Burgina E.B., Chuvilin A.L., Echevsky G.V. (2004). *J. Mol. Catal. A: Chem.* 217, 155–160.
130. Timofeeva M.N., Matrosova M.M., Reshetenko T.V., Avdeeva L.B., Budneva A.A., Ayupov A.B., Paukshtis E.A., Chuvilin A.L., Volodin A.V., Likholobov V.A. (2004). *J. Mol. Catal. A: Chem.* 211, 131–137.
131. Giusti A., Charron G., Mazerat S., Compain J.-D., Mialane P., Dolbecq A., Riviere E., Wernsdorfer W., Biboum R.N., Keita B., Nadjo L., Filoramo A., Bourgoin J.-P., Mallah T. (2009). *Angew. Chem. Int. Ed.* 48, 4949–4952.
132. Baba T., Ono Y., Ishimoto T., Morikawa S., Tanooka S. (1985). *Bull. Chem. Soc. Jpn.* 58, 2155–2156.
133. De Villa P.A.L., Sels B.F., De Vos D.E., Jacobs P. A. (1999). *J. Org. Chem.* 64, 7267–7270.
134. Hoegaerts D.H., Sels B.F., De Vos D.E., Verpoort F., Jacobs P. A. (2000). *Catal. Today* 60, 209–218.
135. Sels B.F., de Villa P.A.L., Hoegaerts D.H., De Vos D.E., Jacobs P.A. (2000). *Topics Catal.* 13, 223–229.
136. Hasik M., Turek W., Stochmal E., Lapkowski M., Pron A. (1994). *J. Catal.* 147, 544–551.
137. Stochmal-Pomarzanska E., Hasik M., Turek W., Pron A. (1996). *J. Mol. Catal. A: Chem.* 114, 267–275.
138. Neumann R., Miller H. (1995). *J. Chem. Soc., Chem. Commun.*, 2277–2278.
139. Khenkin A.M., Neumann R., Sorokin A.B., Tuel A. (1999). *Catal. Lett.* 63, 189–192.
140. Li W., Li L., Wang Z., Cui A., Sun C., Zhao J. (2001). *Mater. Lett.* 49, 228–234.
141. Kaleta W., Nowinska K. (2001). *Chem. Commun.*, 535–536.
142. Kala Raj N.K., Deshpande S.S., Ingle R.H., Raja T., Manikandan P. (2004). *Catal. Lett.* 98, 217–223.
143. Kumar D., Landry C.C. (2007). *Micropor. Mesopor. Mater.* 98, 309–316.
144. Zhou Y., Bao R., Yue B., Gu M., Pei S., He H. (2007). *J. Mol. Catal. A: Chem.* 270, 50–55.
145. Chen L., Zhu K., Bi L.-H., Suchopar A., Reicke M., Mathys G., Jaensch H., Kortz U., Richards R.M. (2007). *Inorg. Chem.* 46, 8457–8459.

146. Kasai J., Nakagawa Y., Uchida S., Yamaguchi K., Mizuno N. (2006). *Chem. Eur. J.* 12, 4176–4184.
147. Bigi F., Corradini A., Quarantelli C., Sartori G. (2007). *J. Catal.* 250, 222–230.
148. See for review: Yamada Y.M.A. (2005). *Chem. Pharm. Bull.* 53, 723–729.
149. Yamada Y.M.A., Ichinohe M., Takahashi H., Ikegami S. (2001). *Org. Lett.* 3, 1837–1840.
150. Yamada Y.M.A., Jin C.K., Uozumi Y. (2010). *Org. Lett.* 12, 4540–4543.
151. Wight A.P., Davis M.E. (2002). *Chem. Rev.* 102, 3589–3614.
152. Bordoloi A., Lefebvre F., Halligudi S.B. (2007). *J. Catal.* 247, 166–175.
153. Bordoloi A., Vinu A., Halligudi S.B. (2007). *Appl. Catal. A: General* 333, 143–152.
154. Kholdeeva O.A., Timofeeva M.N., Maksimov G.M., Maksimovskaya R.I., Rodionova A.A., Hill C.L. *Catalysis of Organic Reactions*. In: Sowa J.R., Jr., ed. Taylor & Francis Group, Boca Raton, 2005, pp. 429–433.
155. Panchenko V.N., Borbáth I., Timofeeva M.N., Gőbölös S. (2010). *J. Mol. Catal. A: Chem.* 319, 119–125.
156. Zhang X., Zhang C., Guo H., Huang W., Polenova T., Francesconi L.C., Akins D.L. (2005). *J. Phys. Chem. B* 109, 19156–19160.
157. Zhou Y., Bao R., Yue B., Gu M., Pei S., He H. (2007). *J. Mol. Catal. A: Chem.* 270, 50–55.
158. Estrada A.C., Santos I.C.M.S., Simoes M.M.Q., Neves M.G.P.M.S., Cavaleiro J.A.S., Cavaleiro A.M.V. (2011). *Appl. Catal. A: General* 392, 28–35.
159. Karimi Z., Mahjoub A.R. (2011). *Catal. Commun.* 12, 984–988.
160. Haimov A., Cohen H., Neumann R. (2004). *J. Am. Chem. Soc.* 126, 11762–11763.
161. Yamaguchi K., Yoshida C., Uchida S., Mizuno N. (2005). *J. Am. Chem. Soc.* 127, 530–531.
162. Shi X.-Y., Wei J.-F. (2008). *J. Mol. Catal. A: Chem.* 280, 142–147.
163. Shi X., Han X., Ma W., Wei J., Li J., Zhang Q., Chen Z. (2011). *J. Mol. Catal. A: Chem.* 341, 57–62.
164. Bordoloi A., Sahoo S., Lefebvre F., Halligudi S.B. (2008). *J. Catal.* 259, 232–239.
165. Sawant D.P., Vinu A., Jacob N.E., Lefebvre F., Halligudi S.B. (2005). *J. Catal.* 235, 341–352.
166. Rao P.M., Wolfson A., Kababya S., Vegac S., Landau M.V. (2005). *J. Catal.* 232, 210–225.
167. Okun N.M., Anderson T.M., Hill C.L. (2003). *J. Am. Chem. Soc.* 125, 3194–3195.
168. Okun N.M., Anderson T.M., Hill C.L. (2003). *J. Mol. Catal. A: Chem.* 197, 283–290.
169. Lee J., Kim H., La K.W., Park D.R., Jung J.C., Lee S.H., Song I.K. (2008). *Catal. Lett.* 123, 90–95.
170. Hong U.G., Park D.R., Park S., Seo J.G., Bang Y., Hwang S., Youn M.H., Song I.K. (2009). *Catal. Lett.* 132, 377–382.
171. Petit C., Bandosz T.J. (2009). *J. Phys. Chem. C* 113, 3800–3809.
172. Kwon T., Tsigdinos G.A., Pinnavaia T.J. (1988). *J. Am. Chem. Soc.* 110, 3653–3654.
173. Drezdzon M. (1988). *Inorg. Chem.* 27, 4628–4632.
174. Kwon T., Pinnavaia T.J. (1992). *J. Mol. Catal.* 74, 23–33.

175. Tatsumi T., Yamamoto K., Tajima H., Tominaga H. (1992). *Chem. Lett.*, 815–816.
176. Evans J., Pillinger M., Zhang J. (1996). *J. Chem. Soc. Dalton Trans.*, 2963–2974.
177. Gardner E., Pinnavaia T.J. (1998). *Appl. Catal. A: General* 167, 65–74.
178. Hu C., Zhang X., Xu L., Mu B., Zu W., Wang E. (1998). *Appl. Clay Sci.* 13, 495–511.
179. Carriazo D., Martin C., Rives V., Popescu A., Cojocaru B., Mandache I., Parvulesku V.I. (2006). *Micropor. Mesopor. Mater.* 95, 39–47.
180. Izumi Y., Urabe K., Onaka A. *Zeolite, Clay, and Heteropolyacids in Organic Reactions*. Kodansha, Tokio-VCH, Weinheim, 1992, pp. 1–106.
181. Cavani F., Trifiro F., Vaccari A. (1991). *Catal. Today* 11, 173–301.
182. Vaccari A. (1998). *Catal. Today* 41, 53–71.
183. Rives V., Ulibarri M.A. (1999). *Coord. Chem. Rev.* 181, 61–120.
184. Sels B.F., De Vos D.E., Jacobs P. A. (2001). *Catal. Rev. Sci. Eng.* 43, 443–488.
185. Centi G., Perathoner S. (2008). *Micropor. Mesopor. Mater.* 107, 3–15.
186. Liu Y., Murata K., Hanaoka T., Inaba M., Sakanishi K. (2007). *J. Catal.* 248, 277–287.
187. Liu P., Wang H., Feng Z., Ying P., Li C. (2008). *J. Catal.* 256, 345–348.
188. Liu P., Wang C., Li C. (2009). *J. Catal.* 262, 159–168.
189. Corma A., García H., Llabrés i Xamena F.X. (2010). *Chem. Rev.* 110, 4606–4655.
190. Sun C.-Y., Liu S.-X., Liang D.-D., Shao K.-Z., Ren Y.-H., Su Z.-M. (2009). *J. Am. Chem. Soc.* 131, 1883–1888.
191. Férey G., Mellot-Draznieks C., Serre C., Millange F., Dutour J., Surble S., Margiolaki I. (2005). *Science* 309, 2040–2042.
192. Maksimchuk N.V., Timofeeva M.N., Melgunov M.S., Shmakov A.N., Chesalov Yu.A., Dybtsev D.N., Fedin V.P., Kholdeeva O.A. (2008). *J. Catal.* 257, 315–323.
193. Maksimchuk N.V., Kovalenko K.A., Arzumanov S.S., Chesalov Yu.A., Stepanov A.G., Fedin V.P., Kholdeeva O.A. (2010). *Inorg. Chem.* 49, 2920–2930.
194. Juan-Alcañiz J., Ramos-Fernandez E.V., Lafont U., Gascon J., Kapteijn F. (2010). *J. Catal.* 269, 229–241.
195. Uchida S., Hikichi S., Akatsuka T., Tanaka T., Kawamoto R., Lesbani A., Nakagawa Y., Uehara K., Mizuno N. (2007). *Chem. Mater.* 19, 4694–4701.
196. Song J., Luo Z., Britt D., Furukawa H., Yaghi O.M., Hill C.L. (2011). *J. Am. Chem. Soc.* 133, 16839–16846.
197. Gamelas J.A.F., Evtuguin D.V., Esculcas A.P. (2007). *Transit. Metal. Chem.* 32, 1061–1067.
198. Neumann R., Cohen M. (1997). *Angew. Chem. Int. Ed. Engl.* 36, 1738–1740.
199. Neumann R., Cohen M. (1999). *J. Mol. Catal. A: Chem.* 146, 291–298.
200. Gelbard G., Breton F., Quenard M., Sherrington D.C. (2000). *J. Mol. Catal. A: Chem.* 153, 7–18.
201. Gelbard G., Gauducheau T., Vidal E., Parvulescu V.I., Crosmanb A., Pop V.M. (2002). *J. Mol. Catal. A: Chem.* 182–183, 257–266.
202. Liu Y., Murata K., Inaba M. (2004). *Green Chem.* 6, 510–515.
203. Gouzerh P., Proust A. (1998). *Chem. Rev.* 98, 77–111.
204. Judeinstein P. (1992). *Chem. Mater.* 4, 4–7.

205. Mazeaud A., Ammari N., Robert F., Thouvenot R. (1996). *Angew. Chem. Int. Ed.* 35, 1961–1964.
206. Mayer R.C., Thouvenot R. (2000). *Chem. Mater.* 12, 257–260.
207. Sanchez C., Lebeau B., Ribot F. (2000). *J. Sol-gel Sci. Technol.* 19, 31–38.
208. Xu L., Lu M., Xu B., Wei Y., Peng Z., Powell D.R. (2002). *Angew. Chem. Int. Ed.* 41, 4129–4132.
209. Mayer C.R., Neveu S., Cabuil V.A. (2002). *Angew. Chem. Int. Ed.* 41, 501–503.
210. Errington R.J., Petkar S.S., Horrocks B.R., Houlton A., Lie L.H., Patole S.N. (2005). *Angew. Chem. Int. Ed.* 44, 1254–1257.
211. Han J.W., Hill C.L. (2007). *J. Am. Chem. Soc.* 129, 15094–15095.
212. Luo X., Yang C. (2011). *Phys. Chem. Chem. Phys.* 13, 7892–7902.
213. Qi W., Li H., Wu L. (2007). *Adv. Mater.* 19, 1983–1987.
214. Aída Luz Villa de P., Farlán Taborda A., Consuelo Montes de Correa, (2002). *J. Mol. Catal. A: Chem.* 185, 269–277.
215. Sakamoto T., Pac C. (2000). *Tetrahedron Lett*. 41, 10009–10012.
216. Maayan G., Neumann R. (2005). *Chem. Commun.*, 4595–4597.
217. Kholdeeva O.A., Timofeeva M.N., Maksimov G.M., Maksimovskaya R.I., Neiwert W.A., Hill C.L. (2005). *Inorg. Chem.* 44, 666–672.
218. Dengel A.C., Griffith W.P., Parkin B.C. (1993). *J. Chem. Soc., Dalton Trans.*, 2683–2688.
219. Salles L., Aubry C., Thouvenot R., Robert F., Doremieux-Morin C., Chottard G., Ledon H., Jeannin Y., Brégeault J.-M. (1994). *Inorg. Chem.* 33, 871–878.
220. Duncan D.C., Chambers R.C., Hecht E., Hill C.L. (1995). *J. Am. Chem. Soc.* 117, 681–691.
221. Ding Y., Gao Q., Li G., Zhang H., Wang J., Yan L., Suo J. (2004). *J. Mol. Catal. A: Chem.* 218, 161–170.
222. Zhang S., Zhao G., Gao S., Xi Z., Xu J. (2008). *J. Mol. Catal. A: Chem.* 289, 22–27.
223. Trubitsina T.A., Donoeva B.G., Maksimov G.I., Maksimovskaya R.I., Kholdeeva O.A. (2009). *Eur. J. Inorg. Chem.*, 5142–5147.
224. Kholdeeva O.A., Trubitsina T.A., Maksimovskaya R.I., Golovin A.V., Neiwert W.A., Kolesov B.A., López X., Poblet J.M. (2004). *Inorg. Chem.* 43, 2284–2292.
225. Hussain F., Bassil B.S., Kortz U., Kholdeeva O.A., Timofeeva M.N., de Oliveira P., Keita B., Nadjo L. (2007). *Chem. Eur. J.* 13, 4733–4742.
226. Kholdeeva O.A., Donoeva B.G., Trubitsina T.A., Al-Kadamany G., Kortz U. (2009). *Eur. J. Inorg. Chem.*, 5134–5141.
227. Kholdeeva O.A., Trubitsina T.A., Timofeeva M.N., Maksimov G.M., Maksimovskaya R.I., Rogov V.A. (2005). *J. Mol. Catal. A: Chem.* 232, 173–178.
228. Neumann R., Dahan M. (1997). *Nature* 388, 353–355.
229. Neumann R., Khenkin A.M., Vigdergauz I. (2000). *Chem. Eur. J.* 6, 875–882.
230. Kozhevnikov I.V., Sinnema A., Jansen R.J.J., Pamin K., Van Bekkum H. (1994). *Catal. Lett.* 30, 241–252.
231. Herrera J.E., Kwak J.H., Hu J.Z., Wang Y., Peden C.H.F. (2008). *Top. Catal.* 49, 259–267.
232. Lefebvre F. (1992) *J. Chem. Soc., Chem. Commun.*, 756–757.
233. Guo Y.-H., Hu C.-W. (2003). *J. Cluster Sci.* 14, 505–526.
234. Brückman K., Che M., Haber J., Tatibouet J.M. (1994). *Catal. Lett.* 25, 225–240.

7

SELECTIVE OXIDATIONS CATALYZED BY SUPPORTED METAL COMPLEXES

ALEXANDER B. SOROKIN

7.1 INTRODUCTION

Catalysis is an essential component of the green chemistry concept [1]. The most skillful green chemist is Nature that provides countless examples of difficult chemical processes performed at ambient temperature and pressure in aqueous medium with high chemo-, regio- and stereoselectivity. Many important processes catalyzed by enzymes, e.g. photosynthesis, activation of dinitrogen, mild oxidation of methane, are still open challenges for chemistry. In the search for clean processes it is tempting to mimic enzymatic systems in order to create efficient chemical catalysts able to function in clean media including water. Another important benefit is the possibility to create energy-efficient processes working at ambient or near-ambient conditions of temperature and pressure. Thus, enzyme mimicking represents an important way toward environmentally friendly sustainable processes.

Such a bioinspired approach can be directed to model the structures of active sites of enzymes performing key chemical steps. However, the most fruitful approach to achieve efficiency and selectivity is probably to create chemical systems functioning according to mechanisms adopted by enzymes, not necessarily copying the structural details of the prosthetic groups and their protein surroundings. In this context, organometallic and coordination chemistry provide a variety of transition-metal complexes as a basis for searching and designing the efficient

Liquid Phase Oxidation via Heterogeneous Catalysis: Organic Synthesis and Industrial Applications, First Edition. Edited by Mario G. Clerici and Oxana A. Kholdeeva.
© 2013 John Wiley & Sons, Inc. Published 2013 by John Wiley & Sons, Inc.

catalysts. In addition, enzymes employ abundant and nontoxic metals (Fe, Mn, etc.) and successful modeling can allow replacing noble and toxic metal catalysts.

A vast majority of oxidation reactions in biochemistry is mediated by iron-containing enzymes. Mono-oxygenase and dioxygenase natural catalysts are capable of performing various oxidations including very difficult reactions in very selective way under very mild (physiological) conditions. Cytochromes P-450 [2] and methane mono-oxygenases [3] are the most representative examples of enzymes able to oxidize strong C−H bonds. Mimicking active sites of these enzymes in order to reproduce their catalytic performance is therefore a possible strategy for development of green catalysts that could operate under mild conditions. To approach this goal, numerous porphyrin [4], phthlocyanine [5] and nonheme complexes [6] were prepared and tested in homogeneous oxidation. Accessibility of the catalysts in terms of their cost and availability at a large scale are important issues for economical viability of the processes. The resistance of the complex ligand to oxidative destruction is another prerequisite for the successful application. The important point is also to find a compromise between accessibility from the preparation point of view and structural elaboration to provide the necessary properties (activity, stability, etc.). In this context, available, cheap and stable phthalocyanine metal complexes are very attractive candidates as catalysts for oxidation.

Once a successful homogeneous catalyst is found the next step should be its immobilization onto a suitable solid support. In the ideal case, this procedure should be simple, efficient and general to provide a stable heterogeneous catalyst showing high activity and selectivity with no leaching of the active sites. In practice, the combination of all these properties is not easy to achieve. The most challenging in the oxidation field is to reach a high chemical stability of the catalyst since an organic ligand of the complex is susceptible to oxidation. However, if the catalyst exhibits a high selectivity, environmental and economical benefits might be more significant than the catalyst lifetime due to more efficient use of raw materials and lower waste-disposal costs. In this context, we believe that it is appropriate to discuss in detail the catalyst stability issues along with the catalytic properties of the supported metal complexes.

The topic of this chapter is the preparation of truly heterogeneous catalysts by immobilization of bioinspired metal complexes onto solid supports and applications of these catalysts in oxidation reactions to achieve high conversions of substrates, high product yields and high turnover numbers with these readily separable heterogeneous catalysts. In view of rational application including recycling and reuse of the elaborated metallocomplex catalysts, it is highly desirable to apply the optimal strategy for their fixation onto solid supports. Different approaches have been developed for immobilization of the metal complexes using a variety of supports [7–9]. Application of high area supports allows high loading of catalytic sites to be obtained. Stability as well as polarity (or hydrophobicity) of support should be taken into account during preparation of heterogeneous catalysts.

The nature of the active sites in heterogenized metal complexes is essentially the same as in homogeneous conditions. However, when several forms of the complex can exist in solution, selective immobilization of the active form of the complex can

provide improved catalysts. Immobilization of the complexes can also improve their stability since a self-degradation *via* bimolecular reactions becomes impossible. In general, supported metal complexes operate *via* the same mechanisms as their homogeneous counterparts. Specific properties of the supported metal complexes that differentiate them from the corresponding homogeneous systems can originate from the influence of support. These surface effects as well as mechanistic features responsible for high performance of the supported catalysts will be discussed along with their general catalytic properties in Section 7.3. Thus, there is no separate section on the mechanistic aspects of the oxidation reactions.

Traditionally, supported metallocomplex catalysts are applied in batch reactors. Continuous processing is very attractive on the industrial scale. An excellent review on the challenges and opportunities for implementation of continuous-flow processes with organometallic catalysts is available [10].

7.2 SYNTHESIS AND CHARACTERIZATION

The main motivation for immobilization of the catalytically active complexes is an easy separation of a catalyst from the reaction mixture. In principal, this goal can be achieved with reusable homogeneous catalytic systems based on supercritical fluids [11], perfluorinated solvents [12] or ionic liquids [13]. Another approach is the attachment of the complex onto macromolecular supports soluble in organic solvents. These catalysts can be separated from the reaction mixture by nanofiltration. The scope and limitations of multiphase systems for the recycling are discussed in the recent reviews [14, 15] and will not be treated here.

Different synthetic strategies have been developed for the preparation of supported transition-metal complexes. The most simple and straightforward approach to supported catalysts without the need for modifying any reagents is the physical adsorption of the complex from solution onto the support surface. In the case of strong affinity of the complex to the surface the supported catalyst can be isolated by filtration. Otherwise, after stirring of the reaction mixture for several hours, the solvent can be slowly removed using a rotor evaporator. However, impregnated materials may contain catalytic sites that are not well defined, especially when very high complex loadings are used that leads to the adsorption of several complex layers and a significant part of the metal complex becomes unavailable for the reaction with the terminal oxidant and substrate. Obviously, the physically adsorbed solid catalysts cannot be used in the solvents in which the complex is soluble because of its possible leaching. Despite the limitations, these readily available catalysts can successfully be used, taking into account the aforementioned considerations.

The covalent and electrostatic fixation approaches often need a preliminary modification of the complex and/or the support. If the modification of the complex is necessary, it should be done at a peripheral position to avoid disturbing the catalytic activity. In some cases the support is noninnocent in catalysis and its properties can play an important role. For example, its polarity, or more precisely the hydrophobicity or hydrophilicity, can influence the local concentration of the substrate near the

supported catalytic site, thus changing the reaction rate. The support properties can be tuned by appropriate modification of the support surface to achieve optimal hydrophilic/hydrophobic profile for efficient mass transfer of reagents. There are numerous successful examples when immobilized catalysts exhibit a higher reaction rate compared to their homogeneous counterparts. In the case of porous systems, the porosity of supports provides a possibility to discriminate substrates according the size. Due to steric hindrance exerted by the support, a supported catalyst site is often less accessible than in homogeneous solution. This can result in a decrease of the reaction rate.

Detailed characterization and understanding of parameters influencing the catalytic properties of supported complexes is the important goal. IR, NMR, EPR and UV-vis spectroscopies are commonly used for the investigation of catalytically active sites in solid catalysts and the reactants interacting with these sites [16]. Along with techniques typical for heterogeneous catalysis in general, e.g. X-ray diffraction and determination of textural parameters by the nitrogen adsorption method, spectroscopic characterization of the state of the supported complexes can provide valuable information. Loading of the complex, the key parameter for the catalytic tests, can be determined by metal analysis using ICP. The supported catalysts can also be characterized by X-ray absorption spectroscopy (EXAFS, XANES), X-ray emission spectroscopy (XES) [17], X-ray photoemission spectroscopy (XPS), Raman spectroscopy, etc. Selected examples of spectroscopic studies providing important mechanistic insights will be described below.

7.2.1 General Synthetic Strategies

Synthetic strategies used for immobilization of metal complexes can be divided in two main groups [8, 9]: (i) ionic binding *via* electrostatic interaction and chemical covalent fixation of the complexes onto support (grafting and anchoring) and (ii) physical encapsulation or entrapment of complexes within porous support matrix (Figure 7.1).

To chose an optimal support the following factors should be considered: (i) stability of the support under reaction conditions; (ii) possible involvement to

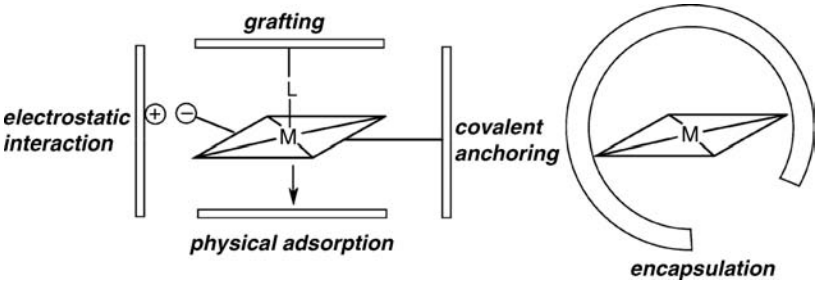


FIGURE 7.1 Schematic representation of different immobilization strategies.

reaction; (iii) capacity to readily introduce functionality for covalent anchoring; (iv) degree of functionalization; and (v) availability and cost of the support.
Both organic polymers and inorganic materials can be used as supports. However, more robust inorganic solids are more suitable for oxidation reactions. From practical considerations, accessible and stable to oxidation inorganic supports should be preferred, although organic polymers can sometimes be used. Accessible amorphous silica is most frequently applied; other oxides like alumina or zirconia have a limited use. Porous materials with high surface area, e.g. zeolites, mesoporous silicas, and layered structures (clay minerals, pillared clays and layered double hydroxides) provide a high catalyst loading and a possibility to use confinement effects. In this case a relation between pore dimensions and substrate size is an important factor. Many reviews covering different aspects of ordered mesoporous materials are available [18–20].

7.2.1.1 Grafting The catalyst can be covalently linked to support *via* grafting or anchoring. In the grafting procedure the complex is immobilized *via* direct coordination of metal with support. Thus, the coordination sphere of the complex differs from that of a homogeneous complex. This modification can influence the catalytic properties of the complex. In general, this approach is not suitable for fixation of chiral complexes because modification of the stereogenic center can disturb the chiral induction. Alternatively, the complex can be anchored to the support surface *via* a linker or tether using a periphery of the ligand. In this case the active metal site retains the structure of the homogeneous counterpart.

The grafting concept is particularly developed for organometallic surface species [21] and Ti-silica materials [22]. The grafting capacity of amorphous and mesoporous silicas is determined by the amount of silanols onto its surface. Silanols can be isolated, geminal or hydrogen bound. The amount and the nature of Si–OH are determined by the treatment conditions of starting silicas [20]. The modification of the silica surface to introduce a grafting site can conveniently be performed with a variety of commercially available silylating agents carrying the coordination site. Coordination bonding of this site (typically nitrogen) to metal complex provides heterogeneous catalysts with modified catalytic properties. Resting after catalyst grafting free silanol groups can be in turn modified to confer the surface desired hydrophilic/hydrophobic properties.

7.2.1.2 Tethering, Anchoring Modification of the silica surface by silylation procedure to introduce anchors is the preliminary step for tethering the complexes, which should also contain an appropriate functionality. Thus, the common point of the grafting and tethering methods is the modification of the support to provide coordination bonding in the former case and covalent tether with complex ligand in the latter case. The most frequently used are amino-modified silicas (3-aminopropyltriethoxysilane) and chloro-modified silicas (3-chloropropyltrimethoxysilane). Other functional mono- and oligosilanes can be used to provide ligand sites containing diamine, thiols, pyridines, imidazole, cyanopropyl and epoxide groups for metal-ion adsorption leading to grafted metal sites in the ligand environment

provided by the modified support itself [23]. However, in contrast to anchored complexes, leaching of metal from such materials is often an issue.

Along with a postsynthetic approach, a direct cocondensation route to hybrid materials has been developed [19, 23, 24]. Simultaneous condensation reactions of inorganic tetraalkoxysilane precursors $(RO)_4Si$ (R = methyl or ethyl group) with $(RO)_3SiR'$ silica compounds modified with organic groups (R′) result in hybrid materials with the organic groups incorporated into the pore walls of the silica network [24]. This approach can be used for the direct incorporation of the functionalities needed for further grafting or anchoring metal complexes. Alternatively, cocondensation of the silica precursors and metal complexes (or ligands) having alkoxysilane substituents directly leads to supported materials. For instance, the solid prepared from cyclam-functionalized silica contained almost all cyclam ligands localized on the pore surface that were readily accessible to complexation by Co(II) and Cu(II) ions [25]. Nevertheless, the cocondensation method has some drawbacks. The degree of ordering in the solid materials decreases with increasing concentration of the component having organic functionality. Increased loading of the incorporated organic groups can also lead to a reduction in the pore diameter, pore volume and surface area. Thus, the loading of the organic component should not exceed 40 mol% [24]. In addition, the proportion of organic groups incorporated into the pore walls is usually lower than it should be on the basis of their concentration in the initial reaction mixture. Finally, particular care should be taken to the removal of the surfactant in order not to destroy the introduced organic functionality: extraction methods should be preferred to calcination that should be avoided in most cases.

Two strategies can be applied using a support modified with an appropriate group: (i) first, anchoring ligand and then introduction of a metal and (ii) direct anchoring of the metal complex. Alternatively, the complex (or ligand) can be modified by introduction of tether followed by anchoring onto an unmodified support. Complexes having acidic functions on the periphery of the ligand can readily be anchored onto an amino-modified surface *via* formation of covalent bonds or ionic interaction. For example, tetrasulfonated metallophthalocyanines in sulfochloride form are conveniently fixed *via* strong sulfamide bonds [26, 27]. Alternatively, anchoring can be accomplished *via* electrostatic (ionic) interaction.

7.2.1.3 Encapsulation The encapsulation approach is often associated with "ship-in-a-bottle" constructions. Romanovsky and coworkers prepared metallophthalocyanines (MPc) inside the supercages of zeolite NaY for the first time using a "ship-in-a-bottle" method [28]. In this method, a metal complex is constructed inside the zeolite pores from template metal ions and *o*-dicyanobenzene. The formed phthalocyanine molecules are believed to be sterically entrapped inside the pores because the size of MPc exceeds the pore-entrance dimensions.

Encapsulated "ship-in-a-bottle" materials can be prepared by the flexible ligand method, the template synthesis method and the zeolite synthesis method. The scope and limitations of these methods are discussed in the literature [29]. In the first method, a flexible ligand is capable of diffusing through zeolite pores, but upon

complexation with a metal ion the complex becomes too bulky and rigid to escape the zeolite cages. This approach is especially suitable for metal(salen) complexes. Mesoporous cage-like silicas SBA-16 with different pore entrance (4.9, 5.4 and 5.9 nm) were used to encapsulate chiral Co(salen) complex [30]. The entrance size of SBA-16 was further tailored by the treatment with phenyltrimethoxysilane. The flexible salen ligand can diffuse in the SBA-16 cages through entrances that fit to its size. After coordination with Co ions the rigid Co(salen) complex will be encapsulated if its molecular size is larger than the pore-entrance size. Only SBA-16 (4.9 nm) and SBA-16(5.4)-Ph materials provided successful trapping of Co(salen) complex inside the cages.

This approach was extended to encapsulation of chiral Co(salen) complex in SBA-16 followed by the treatment with alkoxysilanes with different length of the alkoxy chain ($C_1 - C_{12}$) [31]. The pore-entrance size can be diminished due to silylation and complexes would be entrapped inside the pores if the appropriate size of alkyl chain is used. Reactants and products can freely diffuse through the entrance cage and a confined catalyst can catalyze the reaction like in a homogeneous process. The evident advantage of this approach is that the complex efficient in homogeneous conditions can directly be used without the need for modification. Importantly, this methodology can allow encapsulating several molecules in the same cage to perform reactions with cooperative activation effects [32]. This effect is difficult or impossible to achieve with site-isolated heterogeneous catalysts prepared by other methods. The cages of a mesoporous support represent nanoreactors containing confined metal complexes with a high local concentration [33]. This approach is especially beneficial for reactions involving cooperative activation by separate catalytic centers or second-order kinetics on the local catalyst concentration.

When the synthesis of the complex is performed directly inside the pores, it can result in the incomplete formation of complex. Such materials may contain precursor molecules and free nonmetalated ligands. To remove these impurities compromising the catalytic activity an extensive Soxhlet washing is necessary. During "ship-in-a-bottle" synthesis the relative amount of free nonmetallated ligand depends on the bulkiness of the complex. In the limiting case, the formation of bulky tetraphenyl- and tetramethylporphyrin by condensation of pyrrole and aldehyde was not observed within zeolite Y and MCM-41 pores [34]. While the material adsorbed inside the pores consisted of porphyrinogen precursors, the target porphyrins were only formed in the solution, although preparation of porphyrins absorbed on faujasites has been reported. However, even in the case of less sterically demanding Mn salen complex, the salen/Mn(III) ratio was determined to be 1.3 indicating a slight excess of the uncomplexed ligand [35]. The presence of uncomplexed metal ion and nonmetallated ligand inside the zeolite bulk might complicate characterization and reactivity study [29].

Other synthetic strategies can be used for the preparation of encapsulated complexes. A metal complex can be added during crystallization of the zeolite host as a possible template agent. Faujasite zeolites have been modified with $CoPcF_{16}$ and $CuPcF_{16}$ by synthesizing NaX around the complexes [36]. Alternatively, the same

complexes were prepared by template synthesis inside NaY zeolites ion exchanged with Co^{2+} and Cu^{2+}. Zeolite synthesis approach provides better defined materials since there are no free metal ions or ligand left in the zeolite that could complicate characterization or reactivity. Although ordered mesoporous silicas are porous materials suitable for encapsulation, covalent anchoring of the complexes onto their surface is the principal approach.

7.2.1.4 Other Methods The recent development of metal-organic frameworks (MOF) possessing large surface areas and adjustable pore sizes has attracted great attention to their use in catalytic oxidation as catalysts and as catalyst supports [37, 38]. This rapidly developing area is reviewed in another chapter of this book [39]. Only several examples related to metal complexes will be considered here. In particular, a 3D pore system of MIL-101 with calibrated cavities of 2.9 nm and 3.4 nm is a prospective support for immobilization of metal complexes. These cages are accessible through windows of *ca.* 1.2 nm and 1.6 nm. FePcS has been rapidly and irreversibly inserted into nanocages of MIL-101 though its size ($\sim 1.7 \times 1.7$ nm) slightly exceeds the dimensions of the aperture [40]. FePcS could not be extracted from the material by intensive washing and ion exchange. XPS analysis revealed that the surface [Fe]/[Cr] atomic ratio was close to the bulk value found by ICP-AES elemental analysis and practically did not change after argon-ion sputtering. The local elemental analyses in different particle places performed by EDX also showed a homogeneous Fe distribution in the MIL-101 material. These results suggest that FePcS molecules can be located inside MIL-101 cages. The size of MPc strongly influenced on the location of the complex in MIL-101. The MPc-MIL-101 materials were prepared by wet infiltration of MPc solutions in acetone or CH_2Cl_2 into MIL-101 [41]. While $FePcF_{16}$ and $RuPcF_{16}$ were incorporated inside MIL-101 pores, a bulkier μ-nitrido di-iron phthalocyanine $(FePc^tBu_4)_2N$ was strongly absorbed at the outer surface of the MIL-101 crystallites. The different organization of these materials had an effect on the catalytic properties.

Another attractive approach is to construct a framework consisting of a catalytically competent complex with salen, porphyrin or phthalocyanine ligands. A key issue for successful application of such materials is the stability of the structure. Of more than 70 reported porphyrinic coordination polymer frameworks, only a few have been shown to be both permanently microporous and contain internally accessible sites for catalysis [42]. Although a limited number of "proof-of-concept" catalytic applications has yet been published [42, 43], one can expect that further development will show the utility of these materials for the preparation of fine chemicals and chiral compounds. Since MOFs enable uniform catalytic sites to be created with identical environments near them throughout the material, they maintain promise for asymmetric catalysis [44].

Polymeric membranes can be used for encapsulation of homogeneous catalysts conferring an advantage of selective sorption of substrates and products, especially in the case of immiscible reagents phases. However, catalyst leaching to solution can be a problem. The complexes can be incorporated in sol-gel materials during sol-gel processing. Complexes bearing negatively charged groups (typically

sulfonates) are suitable for incorporation by ion exchange using layered inorganic supports consisting of positively charged layers separated by exchangeable anions.

7.2.2 Metal Porphyrins

Since active sites of many enzymes involved in the bio-oxidation reactions contain iron protoporphyrin IX, it is quite logical to use metal porphyrin complexes as catalysts. Pioneering studies by Groves and coworkers on cytochrome P-450 mimics [45] have initiated the development of metalloporphyrin systems for oxidation [46–49]. This research was mainly directed at the mechanistic issues and these systems have not often been used for synthetic purposes until recently. Along with the high cost of porphyrin complexes, the stability of porphyrin ligand to oxidative destruction is an important problem. For this reason, a tetraphenylporphyrin scaffold is usually preferred to protoporphyrin IX and other naturally occurring ligands (Figure 7.2).

In order to increase the stability of the porphyrin core to oxidative degradation, bulky or electron-withdrawing substituents are introduced in phenyl groups, especially in *ortho*-positions. Further modification of β-pyrrolic positions with halogen substituents strongly influences on catalytic properties and stability of the

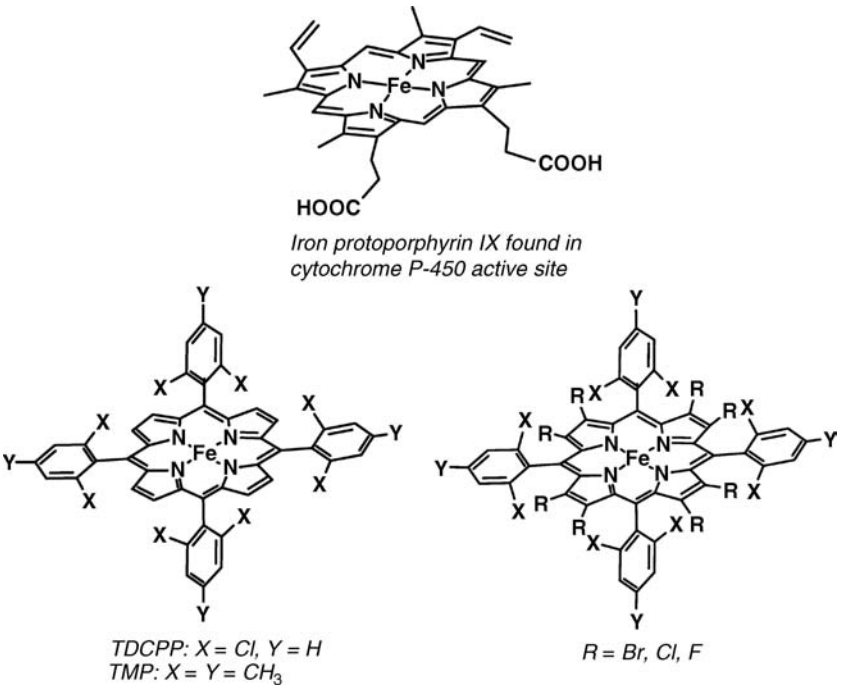


FIGURE 7.2 Structure of the natural iron protoporphyrin IX and synthetic porphyrin complexes frequently used as oxidation catalysts.

complexes. The most frequently used 5,10,15,20-tetra(2,6-dichlorophenyl)porphyrin (TDCPP), tetramesytilporphyrin (TMP) can be prepared by condensation of pyrrole and aldehyde with 27–30% yields.

Metalloporphyrins can be immobilized using different strategies including coordinative binding *via* metal, covalent binding *via* porphyrin ligand, ionic interactions, intercalation and encapsulation. Several factors should be taken into account: the strength of the attachment to the support, ease of preparation, general applicability to different porphyrin structures and stability. Manganese and iron porphyrin complexes were grafted to silicas and polymers modified with imidazole or pyridine [50, 51]. These studies showed significant limitations for grafting complexes *via* coordination of metal to nitrogen group of support. This method can not be routinely applied to all Fe and Mn porphyrins. However, by careful selection of complex, solvent and support, stable catalysts can be prepared.

Cationic tetra(4-N-methylpyridyl)porphyrin manganese complex (MnTMPyP) can be immobilized by electrostatic interaction onto montmorillonite clay, sulfonated polymers and even onto slightly negative surface of SiO_2 [52]. In turn, anionic tetra(4-carboxyphenyl)porphyrin and tetra(4-sulfonatophenyl)porphyrin manganese complexes were similarly supported onto alumina and magnesia. This very simple preparation afforded supported catalysts that completely retained the adsorbed complexes even after stirring in CH_2Cl_2 or CH_3CN for several days. Noteworthy, the nature of the support influenced the catalytic properties of the supported catalysts. Although the origin of the support effect was not investigated, silica-supported catalyst was more efficient in oxidation of cyclooctene and alkanes by PhIO.

Porphyrins bearing $(RO)_3Si$ groups were used for preparation of "bridged porphyrylpolysilsesquioxanes" and a sol-gel material with isolated porphyrin sites by cocondensation with $Si(OEt)_4$ (Figure 7.3) [53].

The latter materials exhibited higher specific surface areas (690–770 $m^2\,g^{-1}$), but the catalytic properties of both materials in oxidation of alkanes by PhIO were similar. In addition to Fe and Mn porphyrins, homogeneous Ru porphyrins as well as immobilized onto insoluble supports and covalently attached to soluble supports were shown to catalyze the selective oxidation of a variety of substrates (olefins, α,β-unsaturated ketones, steroids, alkylarenes and arenes) with 2,6-dichloropyridine-N-oxide ($2,6Cl_2pyNO$) in up to 99% yields and with TON of up to 30 000 [54]. The serious drawback of the metalloporphyrin catalysts is the necessity of using PhIO, $2,6Cl_2pyNO$ and other expensive oxidants noncompatible with the green-chemistry concept. Unfortunately, H_2O_2 and O_2 oxidants can rarely be used in combination with porphyrin-based catalysts for heterogeneous oxidation. When hydrogen peroxide is used, the concurrent catalase reaction producing O_2 can occur. In addition, initially formed in the presence of H_2O_2 homogeneous porphyrin Fe(III)−OOH tends to undergo a homolytic O−O bond cleavage to form PFe(IV) = O (sluggish oxidant) and hydroxyl radical provoking degradation of the porphyrin ligand. To avoid these undesirable side reactions more sophisticated approaches should be applied [55]. Heterogeneous metalloporphyrin catalysts for the efficient oxidation by H_2O_2 are still to be developed. Halogenated metalloporphyrin complexes were shown to be particularly active in the homogeneous oxidation of the

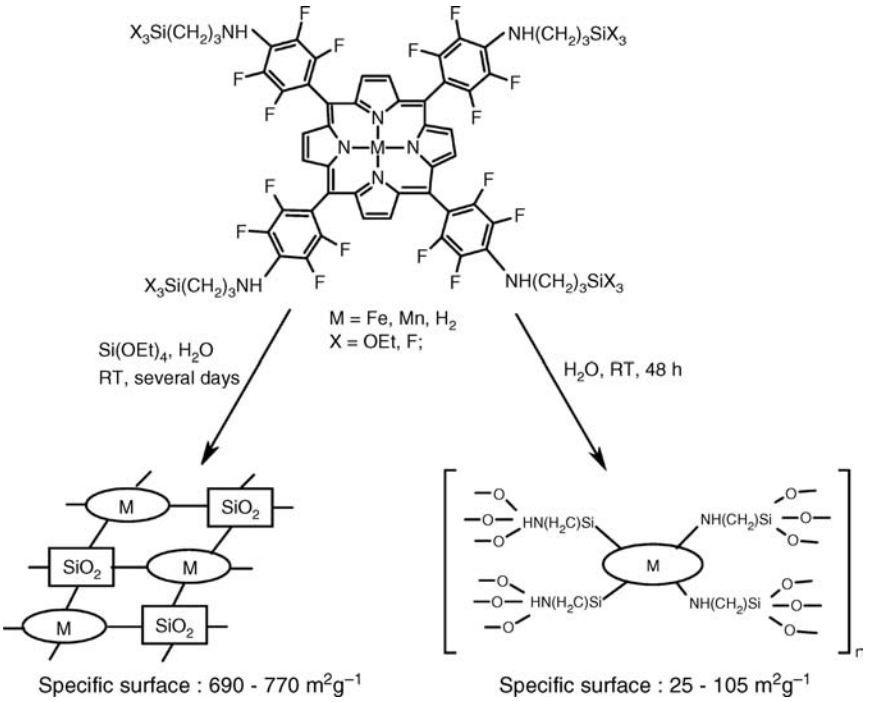


FIGURE 7.3 Preparation of hybrid porphyrinosilicas and porphyrylpolysilsesquioxanes.

alkanes by molecular oxygen *via* a catalytic pathway that very efficiently generates alkyl and alkoxy radicals at low temperatures [56]. A heterogeneous version of this catalytic system has not been published.

7.2.3 Metal Phthalocyanines

Phthalocyanine metal complexes are widely used as versatile catalysts for selective oxidation and bleaching reactions. The resemblance of their macrocyclic structure with that of porphyrins employed by Nature in the active sites of numerous oxygenase enzymes, their rather cheap and facile preparation on a large scale as well as their chemical and thermal stability are the principal reasons for widespread catalytic applications. Indeed, the worldwide annual production of phthalocyanines exceeds 80 000 t/y. Cobalt sulfonated phthalocyanine is industrially applied in the large scale Merox process for the initial chemical treatment of petroleum for removal of mercaptans [57]. Among different phthalocyanine ligands the most useful for catalytic applications are tetrasulfo-, hexadecachloro-, and hexadecafluoro derivatives (Figure 7.4).

Their heterogenization is an important goal toward their use in catalysis including possible industrial applications. A variety of methods can be used. Metal tetrasulfophthalocyanines (MPcS, M = Fe, Mn) were strongly fixed onto ion-exchange

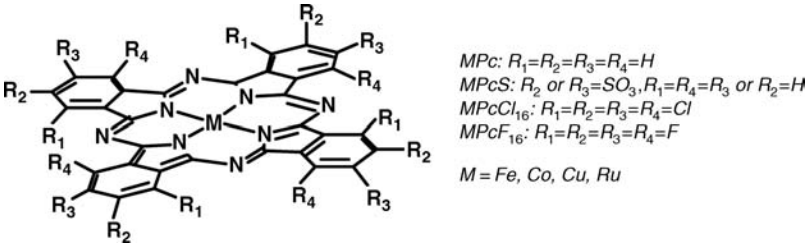


FIGURE 7.4 General structure of phthalocyanine complexes mostly used in oxidation catalysis.

resins containing quaternary ammonium residues (Amberlite IRA 900) or pyridinium groups *via* electrostatic interaction with negatively charged sulfonate groups of the complex (Figure 7.5) [58].

Uncharged poly(vinylpyridine)resin can be used for coordinative fixation [58]. After methylation of the free pyridine groups an additional electrostatic interaction reinforces the complex fixation. The resulting MPcS-polymer materials are very stable to leaching in water or common organic solvents. They are efficient catalysts for the oxidation of chlorinated phenols that are recalcitrant priority pollutants. This method can be applied to other complexes bearing sufonate groups. MPcS can be anchored onto the acrylic copolymers Met-Expansin-NH_2 and Met-Expansin-Piperazine *via* covalent sulfamide bond between the amine groups of the resin and $-SO_2Cl$ groups of the phthalocyanine ligand [59]. The length of the linker influenced on the catalytic properties of these materials. The immobilization of MPc on chitosan aerogel microspheres (polysaccharide with amine groups derived from chitin obtained by removing most of the acetyl groups) afforded oxidation catalysts

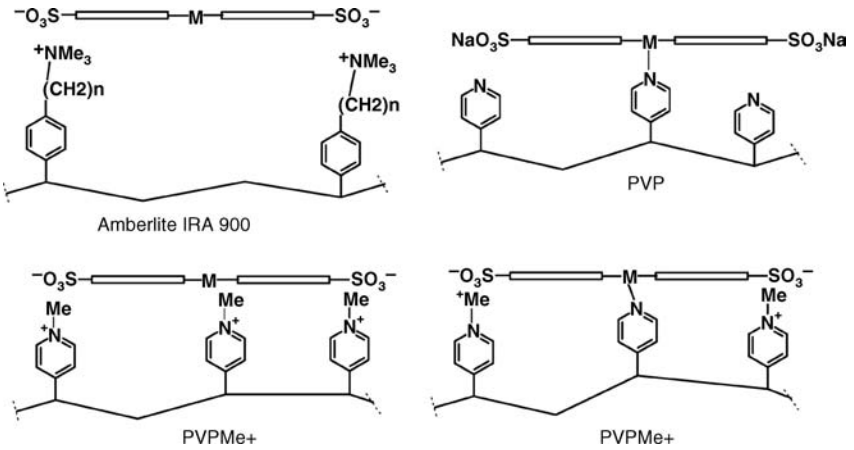


FIGURE 7.5 Supporting of FePcS onto positively charged ion-exchange resins by donating and electrostatic interaction.

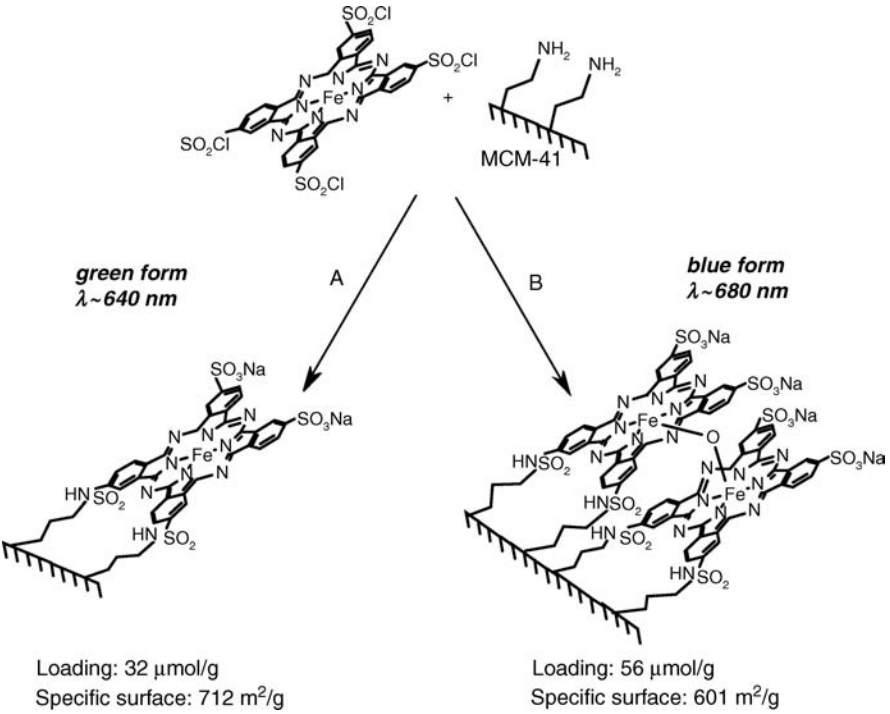


FIGURE 7.6 Monomeric and dimeric FePcS catalysts supported onto amino-modified silicas. Protocol A: 18 h incubation of $FePc(SO_2Cl)_4$ in Py, slow addition to a suspension of NH_2-MCM-41 in Py, stirring at 80 °C for 24 h. Protocol B: rapid addition of $FePc(SO_2Cl)_4$ in Py to a suspension of NH_2-MCM-41 in Py, stirring at 20 °C for 24 h.

containing in addition to the oxidation sites of the complex the basic sites of the chitosan support that could be advantageous for some reactions, e.g. aerobic oxidation of isophorone [60].

A covalent anchoring of MPcS onto amino-modified MCM-41 or amorphous silicas was shown to occur either in monomeric or in μ-oxo dimeric form depending on the reaction conditions (Figure 7.6) [26, 27, 61]. Perhalogenated $MPcF_{16}$ and $MPcCl_{16}$ complexes are also amenable for covalent anchoring onto amino-modified silicas *via* nucleophilic substitution.

Complexes containing free acid residues can be anchored in mesoporous titania by a one-pot hydrolytic process using a titanium alkoxide preliminary modified as shown in Figure 7.7 [62]. The loading of the complex in the hybrid material can be easily modulated by adding various amounts of $Ti(OPr^i)_4$ additive during the hydrolysis. Very high complex loadings can be easily reached (in the case of FePcS 214 μmol g^{-1} or 19.2 wt%).

This catalyst containing two different catalytic sites (iron phthalocyanine and titanium oxide sites) exhibited superior results in heterogeneous aerobic oxidation

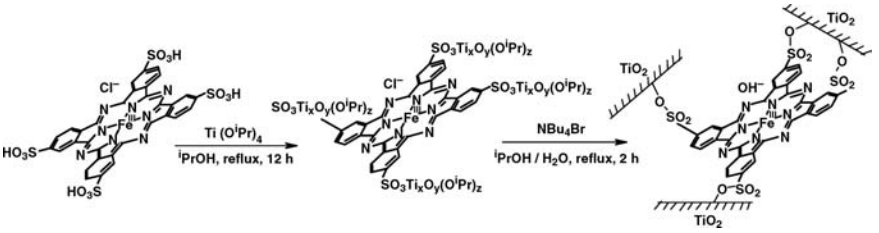


FIGURE 7.7 Preparation of FePcS-TiO_2 from iron phthalocyanine modified titanium alkoxide.

of cyclic olefins exemplified by β-isophorone compared with the same catalyst fixed onto SiO_2.

FePcS was directly incorporated in sol-gel materials during the synthesis of hydrophobic or hydrophilic sol-gel materials [63]. However, the incorporation of FePcS occurred in aggregated form that resulted in lower conversion and selectivities of aromatic oxidations compared to catalysts prepared by covalent anchoring of FePcS onto silicas. A more elaborate approach is necessary to avoid aggregation phenomena and to access to separated single catalytic sites. Following a pioneering study by Romanovsky and coworkers [28] the encapsulation of MPc into zeolites and molecular sieves was further developed. Encapsulation of CuPc into mesoporous channels of Cu-exchanged MCM-41 was achieved by chemical vapor deposition using 1,2-dicyanobenzene [64]. Application of microwave irradiation for assembling MPc within MCM-41 allows shortening the reaction time [65]. The zeolite surface was proposed to catalyze the redox and acid–base reactions involved in the synthesis of the phthalocyanine moiety [66]. In order to obtain MPc, cation-exchanged zeolites are typically used. However, the chelation of the exchanged metal ion by Pc is incomplete and metal ions left in zeolite pores can compromise a catalytic activity by side reactions, for example by decomposition of peroxide oxidant. Using ferrocene as the iron source has enabled a complete chelation of all iron by phthalocyanine molecules resulting in the particularly active catalyst for alkane oxidation by ^{t}BuOOH [67].

The precise location of phthalocyanine complexes in zeolites has been a matter of debate. The aperture of the main channels of zeolite Y is 7.4 Å and the diameter of cage is about 12 Å. The diameter of the planar MPc molecule is estimated to be 13 Å. Consequently, entrapment of MPc in a zeolite Y cage requires deformation of the complex or of the cage (Figure 7.8) [68].

The red shift of the Q band of $FePcF_{16}$ to 644 nm compared to 622 nm for the outer surface-physisorbed complex and to 616 nm for solution in acetone has been ascribed to a slight distortion of the macrocycle inside the supercage, although it may also arise from other interactions between the complex and the zeolite lattice. The formation of local defects in the zeolite structure was suggested on the basis of electron microscopy results [69]. Extensive Soxhlet extraction with several solvents can give an indication on the MPc location. When $FePc(NO_2)_4$ was used, its loading

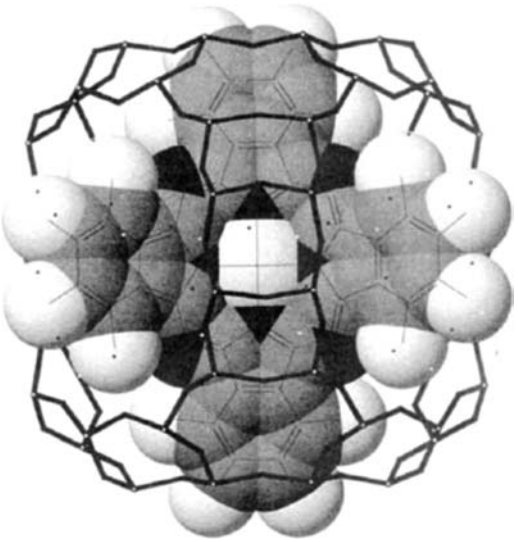


FIGURE 7.8 Schematic representation of $RuPcF_{16}$ and a NaY supercage containing $RuPcF_{16}$. Reprinted with permission from [68]. Copyright (1995) American Chemical Society.

was lower than for unsubstituted FePc [70]. $FePc(NO_2)_4$-Y material was subjected to the extensive extraction procedure and all the phthalocyanine molecules were removed from the zeolite, clearly indicating that the complex was not formed inside the zeolite cages. On the contrary, it was impossible to remove all the complex from unsubstituted FePc-Y by the same procedure that could be compatible with encapsulation. These "ship-in-a-bottle" materials have been investigated using different physicochemical and spectroscopic techniques (N_2 adsorption, FTIR, XRD, EPR, SEM, etc.) but some aspects are still obscure and not all questions have been adequately addressed [29, 69].

An interesting approach was proposed by Jacobs and coworkers [71]. Iron phthalocyanine encapsulated in the supercages of zeolite Y was embedded in a polydimethylsiloxane membrane (PDMS). Such a hierarchical structure resembles the structural organization of the enzymatic systems where active cytochrome P-450 is situated in a phospholipid membrane. Occlusion of MPc in PDMS membrane led to increased catalytic activity in the oxidation of cyclohexane.

Binuclear iron complexes with macrocyclic porphyrin-like ligands have been recently proposed as catalysts for oxidation of strong C−H bonds [5, 72]. This concept was inspired by biochemical precedents of difficult oxidation reactions performed by soluble MMO and cytochrome P-450 enzymes containing di-iron nonheme and iron porphyrin sites, respectively. Combining the structural features of two enzyme families two iron atoms connected *via* a μ-nitrido bridge have been put into a macrocyclic ligand environment (Figure 7.9). These μ-nitrido di-iron phthalocyanines were supported onto silica by impregnation.

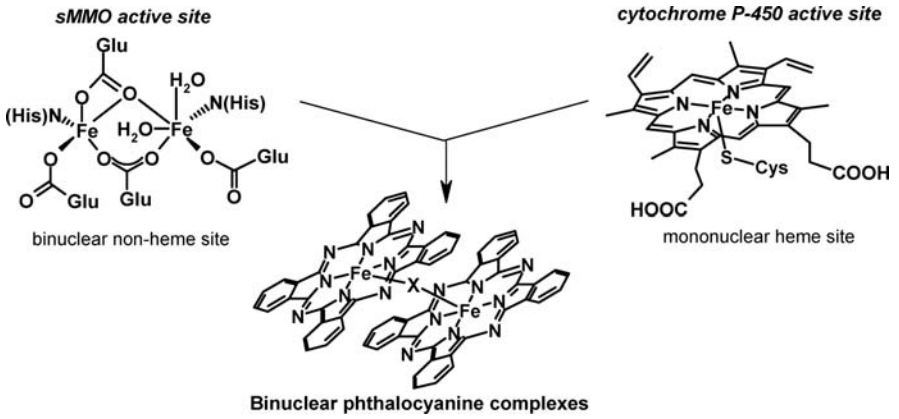


FIGURE 7.9 Concept for binuclear phthalocyanine complexes as catalysts for oxidation.

7.2.4 Complexes with Other Macrocyclic Ligands

The interest in nonplanar complexes stems from the variety of mononuclear [73] and binuclear [74] nonheme oxygenase enzymes performing a number of difficult oxidation reactions in mild conditions. Despite significant efforts concentrated on the development of homogeneous biomimetic systems, heterogeneous oxidation catalysts issued from this area are still to be developed. At present, the most successful examples of nonplanar complexes are based on salen [75] and related ligands [76] as well as on triazacyclononane [66] (Figure 7.10).

Salen-type ligands are among the most widely studied and applied in chemistry. Relatively simple structure and straightforward synthetic access with good yields using accessible diamines and aromatic aldehydes with different substituents are important from the practical point of view, which contributes to their numerous applications. Easy access to chiral complexes with stereogenic substituents close to metal site makes salen complexes especially useful for asymmetric catalysis. Details on their preparation, properties and applications can be found in recent comprehensive reviews [77, 78]. The principal interest of heterogenization of salen

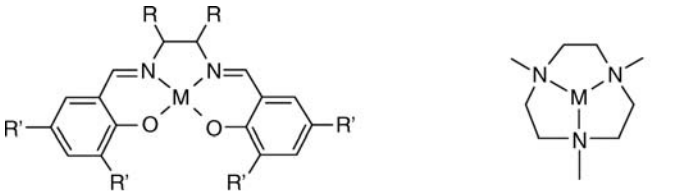


FIGURE 7.10 General structures of salen and triazacyclononane complexes.

complexes deals with Jacobsen's epoxidation catalyst, Mn(salen) chiral complex with bulky substituents. This topic was intensively studied and many excellent reviews are available [79, 80]. The influence of different factors to optimize the performance of supported salen complexes was carefully studied by Corma and Garcia [81]. The activity of the salen complexes varies with the type of Schiff base ligand and transition-metal ions. Possible use of different metal ions makes these complexes very versatile. The nature of the support is important for the catalytic performance.

Manganese mononuclear and dimeric complexes with cyclic triamine 1,4,7-trimethyl-1,4,7-triazacyclononane (tmtacn) are another accessible platform for oxidation catalysis. De Vos and coworkers have explored several approaches to heterogenization of these complexes [82]. Dimanganese (IV,IV) tmtacn complex catalyzes oxidation of olefins by H_2O_2 in the presence of carboxylic acids, which suppress the catalase activity of the complex. An original method of preparation of active heterogeneous catalyst was developed [83]. It consists of grafting of dimeric Mn(tmtacn) complex onto carboxylic acid-modified silica (CA-S) serving as surface-assembling construction and cocatalyst (Figure 7.11). Supporting of Mn (tmtacn) complexes in mononuclear or binuclear forms lead to catalysts with different catalytic activity.

7.2.5 Chiral Complexes

Enantioselective reactions involving chiral complexes attract much attention in current chemistry and industry. Since chiral complexes are in general more expensive

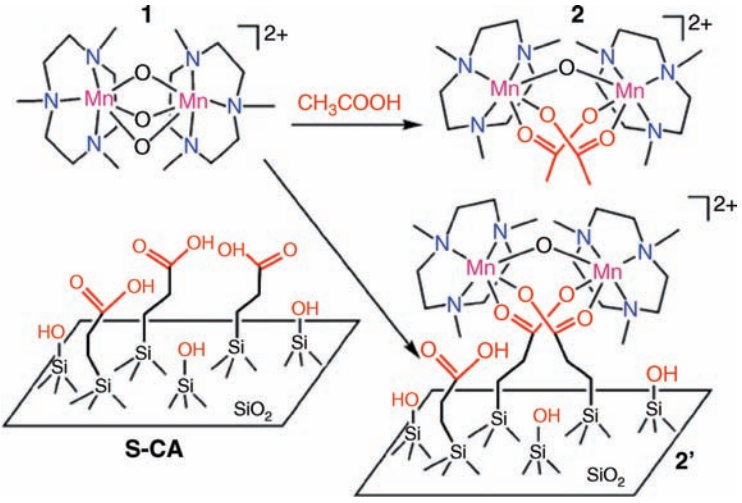


FIGURE 7.11 Schematic representation of grafting of a Mn(tmtacn) complex onto carboxylic acid-modified silica. Reproduced from [83] by permission of The Royal Society of Chemistry.

and more difficult to prepare there is a strong impetus to recover and to recycle them to improve their applicability. Recovering of chiral catalyst is especially important because of the large amounts often applied (7–10 mol%) to achieve both high product yields and enantioselectivities. Although different approaches have been used for the synthesis of chiral solid catalysts, heterogeneous catalysts often show lower enantioselectivity than their homogeneous analogs. Immobilization of chiral catalysts onto supports may also result in significant changes of the catalytic activity. Their performance can be diminished but sometimes it can be enhanced. The different aspects of this problem have been discussed [84]. Since the environment near the active site can strongly influence the approach and hence the orientation of the substrate with respect to the catalytic site, it can affect the stereoselectivity of the reaction. The strong influence of the tether length on the *ee* of epoxidation of olefins catalyzed by covalently supported salen complexes was shown. A preferential approach is to place the catalyst using a long linker to simulate the behavior of the complex in the solution. Alternatively, a chiral complex can be confined within the pores of the organized support in the hope that support effects can be used to improve enantiomeric excess of the reaction carried out in a confined space. However, this approach is not yet well developed and only a limited number of examples is available. Compared to grafting/anchoring methods, no special modification of the chiral complex is required for the encapsulation method. It is of great importance for asymmetric catalysis because the best in terms of activity and enantioselectivity complex can be directly used. Application of chiral porphyrin and salen complexes mainly for olefin epoxidation will be discussed below.

7.3 CATALYTIC PROPERTIES AND STABILITY

Along with catalytic activity and selectivity, the essential characteristics of supported catalysts are stability under reaction conditions, deactivation pathways, and the possibility of regeneration and recycling. These important issues are often underestimated in the literature on the application of supported catalysts. A critical analysis of this problem can be found in ref. [85]. It should be noted that achieving stability of catalyst for oxidation is much more challenging compared to other reactions. Careful indepth investigations of the catalyst stability and reuse issues have not yet been frequently published. Along with description of the catalytic properties these points will be addressed in detail below using the most representative examples of these studies. It would be very instructive to immobilize the same complex by several methods described above and compare the catalytic properties of this series of the catalysts in the same test reaction. However, such experiments are difficult to find in the literature.

The emphasis will be placed on the use of accessible and environmentally benign oxidants, like H_2O_2 and organic peroxides. Reactions involving sophisticated organic oxidants (PhIO, 2,6-dichloropyridine N-oxide) will be discussed only when significant mechanistic or other advances have been achieved. Reactions performed using a very large substrate excess and small amount of oxidant will not be

considered here. These conditions, for example catalyst:oxidant:substrate ratios of 1: 10–20: 1000–10 000, are frequently used in biomimetic studies, typically with nonheme complexes to protect the complex from degradation by the huge substrate excess (substrate protection). Such studies might provide mechanistic insights but have low practical significance. The next important point is the efficiency of the oxidant utilization, in other words the selectivity on the oxidant. The excess of the oxidant should not be very high. Evidently, the closer the oxidant/substrate molar ratio is to unity the more efficient the catalytic system.

In general, several variable parameters can be tuned in order to obtain the best yield and, in certain cases, to change a selectivity. The most important variables are the nature and amount of oxidant, the nature and amount of the catalyst, the properties of the support, the reaction temperature, and the solvent. One of the main problems with zeolite-based catalysts is their limited pore size and consequently severe diffusion restrictions and tendency to pore blockage by reaction products.

7.3.1 Oxidation of Alkanes

Selective oxidation of alkanes under mild conditions is still an open challenge in heterogeneous catalysis, although much effort has been devoted to develop different approaches. Supported metallophthalocyanine and metalloporphyrin complexes seem to provide promising results. The first MPc-zeolite materials suffered from problems with preparation of well-defined materials containing no free metal ions and nonmetallated organic ligand as well as severe diffusion problems [29]. Although both FePc$(NO_2)_4$-Y and FePc-Y materials contained a significant proportion of free phthalocyanines TON for oxidation of cyclohexane by ^{t}BuOOH to a $\sim$2.5 : 1 mixture of cyclohexanone and cyclohexanol were 400 and 4500 in the presence of FePc-Y and FePc$(NO_2)_4$-Y, respectively [70]. Catalyst containing only FePc molecules within zeolite with no residual iron ions was particularly active for alkane oxidation by ^{t}BuOOH [67]. While corresponding homogeneous catalysts were deactivated by bimolecular oxidative self-destruction after a few turnovers, the site isolation in the protective zeolite matrix led to a TON of 6000 in the oxidation of cyclohexane. Zeolite- and MCM-41-encapsulated CoPc, $CoPcF_{16}$, CuPc complexes were also applied for the oxidation of cyclohexane by ^{t}BuOOH and H_2O_2 with about 1 : 1 alcohol/ketone selectivity [86]. Alternatively, FePc was supported onto activated carbon black by impregnation [87]. This material was more efficient in the oxidation of cyclohexane by ^{t}BuOOH at 25 °C than zeolite encapsulated complex. This was attributed to the increased hydrophobicity of the carbon surface that favorably changed the adsorption behaviour of the components in the reaction mixture toward substrate. Using 0.5 g of catalyst, 50 mmol of C_6H_{12} and 100 mmol of ^{t}BuOOH $\sim$34% and $\sim$14% conversions were achieved after 24 h with FePc–carbon black and FePc–zeolite Y catalyst, respectively. No data on the product composition were given. The release of the FePc from the carbon support to the solution followed by oxidative degradation of the complex was observed [87].

The significant breakthrough was made by Jacobs and coworkers who incorporated FePc-zeolite Y in the polydimethylsiloxane membrane [71]. The catalyst

showed a turnover rate of 3.3 min^{-1} in the oxidation of cyclohexane by ^{t}BuOOH at room temperature. On the basis of (i) the absence of bicyclohexyl, *t*-butylperoxocyclohexane, *t*-butylcyclohexylether products typical for the radical oxidation; (ii) kinetic isotope effect of 9.0 obtained in the concurrent C_6H_{12}/C_6D_{12} oxidation; (iii) regioselectivity in adamantane oxidation, a heterolytic nonradical oxidation mechanism was proposed. Using 0.32 g of FePc-zeolite Y/PDMS (0.096 g of FePc-zeoilte Y, the amount of FePc was not indicated), 40 mmol of ^{t}BuOOH (7% aqueous solution) and 300 mmol of cyclohexane in a countercurrent membrane reactor a TON of 1000 was achieved after 5 h [71]. The increase of catalytic activity can be attributed to the better balanced concentration of substrate, peroxide and ligand around the catalytic site [88]. Lowered mobility of the axial ligand in the membrane can also contribute to the 20-fold increase of catalytic activity. Although no recycling study was published this catalytic system seems particularly promising. However, the further development of this approach has only been briefly published [89]. Some deactivation of the catalyst was observed that was attributed to an increased sorption of polar compounds in the zeolite as the reaction proceeded. Regeneration of the membrane by treating at 150 °C under vacuum was published to be sufficient to re-establish the original catalytic activity. It is noteworthy that when FePc was directly occluded in PDMS without zeolite matrix the material underwent very rapid degradation.

Balkus and coworkers have prepared $FePcF_{16}$ and $RuPcF_{16}$ zeolite entrapped materials by a zeolite-synthesis method around $MPcF_{16}$ [68]. While $FePcF_{16}$ intrazeolite material was not sufficiently stable in the presence of high concentration of peroxide oxidant, a Ru-based catalyst with loading of ∼1 complex per 125 NaX supercages showed improved catalytic properties and stability. This low loading is essential in maintaining diffusion pathways during catalysis. Room-temperature oxidation of cyclohexane (0.66 mL, 6 mmol) was performed in the presence of ^{t}BuOOH (0.3 mL, 2.4 mmol) and $RuPcF_{16}$-zeolite (100 mg, 0.0002 mmol) in 1.5 mL acetone (substrate:oxidant:catalyst = 30 000 : 12 000 : 1). Homogeneous $RuPcF_{16}$ (0.0044 mmol) showed a slow oxidation rate of ∼250 cycles per day with no signs of deactivation after one week. Encapsulated catalyst was much more active, providing about 3000 turnovers/day with no sign of deactivation after > 20 000 turnovers, corresponding to ∼70% cyclohexane conversion. Incorporation of the $RuPcF_{16}$ in zeolite increased the selectivity to cyclohexanone (98.4% vs. 67% for homogeneous reaction, conversion was not mentioned in [68]). The $RuPcF_{16}$ zeolite exhibited a substrate-size selectivity providing further evidence for the location of the active sites. Homogeneous oxidation occurred with comparable rates for cyclododecane and cyclohexane: 243 and 258 turnovers/day, respectively. $RuPcF_{16}$ zeolite catalyst was much more active in the oxidation of cyclohexane, 2933 vs. 295 turnovers/day, in accordance with the steric constraints exerted by zeolite matrix [68].

A positive effect of encapsulating of $FePcF_{16}$ and $RuPcF_{16}$ in MIL-101 metal-organic framework by wet infiltration was demonstrated in the aerobic oxidation of tetralin [41]. The complex loading was 2.1 wt% and 3.6 wt% for $FePcF_{16}$ and $RuPcF_{16}$, corresponding to ∼0.8 and ∼1.2 complex molecules per large cage,

TABLE 7.1 Aerobic Oxidation of Tetraline to 1-Tetralone Catalyzed by Homogeneous and MIL-101 Encapsulated $FePcF_{16}$ and $RuPcF_{16}$ [41]

Catalyst	TON after 6 h	TON after 24 h	Selectivity to 1-tetralone after 6 h (24 h), %
MIL-101	0	—	—
$FePcF_{16}$	3400	6300	68
$FePcF_{16}$@MIL-101	24 200	48 200	80 (80)
$RuPcF_{16}$	5200	n.d.	70
$RuPcF_{16}$@MIL-101	30 900	46 300	62 (74)

respectively. The homogeneous distribution of complexes inside of MIL-101 material was confirmed by EDX analysis. The catalytic experiments performed with a substrate:catalyst molar ratio of 147 000 : 1 for $FePcF_{16}$@MIL-101 and 92 000/1 for $RuPcF_{16}$@MIL-101 showed a very efficient aerobic oxidation of tetraline (Table 7.1) [41]. Turnovers obtained in heterogeneous catalysis were much higher (6–8 times) compared to those for unsupported complexes. $FePcF_{16}$@MIL-101 provided a better selectivity (up to 80%) to the desired 1-tetralone, a diesel fuel additive and an intermediate for the synthesis of agricultural chemicals. The occurrence of an induction period and low values of the kinetic isotope effect ($KIE_{Fe} = 1.99$, $KIE_{Ru} = 1.76$) in the oxidation of the adamantane-d_2 probe are consistent with a free-radical mechanism. Although no leaching of the complexes was detected by a UV-vis method, the catalytic activity of the heterogeneous catalyst decreased on reuse, presumably because of the blocking of the pores by side overoxidation products.

The oxidation of *n*-octane and *n*-heptane by ^{t}BuOOH in the presence of Mn (salen)-PDMS was slightly favored at position 2 compared with homogeneous Mn (salen) [90]. However, no change of regioselectivity was observed in the oxidation of n-hexane and n-pentane.

Oxidation of methane is particularly difficult compared to other alkanes because the methane C−H bond has the highest dissociation energy (435 kJ mol^{-1}). Current approaches to utilization of methane involve mainly high temperature processes. A direct low-temperature conversion of CH_4 to valuable products continues to be a major challenge in catalysis both from fundamental and practical point of view. For a long time this approach was associated with activation of CH_4 itself at transition-metal centers like Pt, Pd, Ir, and Hg [91]. Relatively high temperatures (100–220 °C) and strong concentrated acids (oleum, CF_3COOH) are generally needed for activation of methane by this approach. A homogeneous (bipyrimidine)$Pt^{II}Cl_2$ complex [92] and a heterogeneous triazine-based framework providing similar Pt coordination in the solid polymer [93] convert CH_4 to CH_3OSO_3H in 9–30% oleum at 217–220 °C with TON ∼200–500. In Nature, methane mono-oxygenase enzymes (MMO) transform CH_4 to CH_3OH under extremely mild conditions (water, ambient temperatures) *via* a different mechanism. They activate O_2 to generate a powerful oxidant able to attack the C−H bond of CH_4. A chemical system, capable of

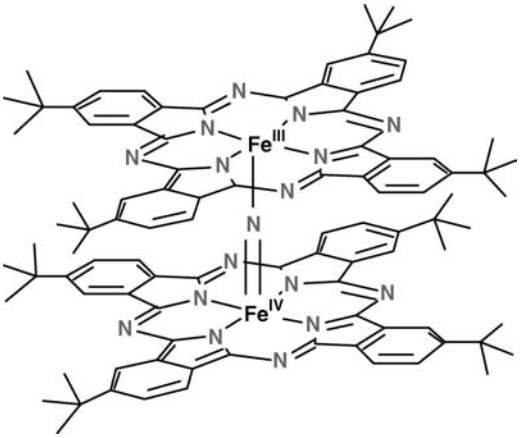


FIGURE 7.12 Structure of μ-nitrido bridged di-iron tetra-*tert*-butylphthalocyanine.

oxidizing CH_4 under ambient conditions like MMO does, would be a significant achievement. However, chemical analogs for such a process are unknown, despite considerable efforts [6]. An essential feature of MMO is an active site with two iron centers in a nonheme environment. We have proposed to use binuclear iron complexes with *macrocyclic porphyrin-like ligands* as catalysts for oxidation [94]. Although these and similar complexes have often been considered as inert in catalysis, we have shown that μ-nitrido di-iron phthalocyanine complexes ($(FePc)_2N$, Figure 7.12) possess remarkable catalytic properties, in particular, in mild oxidation of methane by hydrogen peroxide.

The distinctive feature of $(FePc)_2N$ is its high stability which is an important requirement for the development of an oxidation catalyst. The stability of the binuclear structure is provided by the bridging nitrogen atom as follows from 1s N XPS and ESI-MS data. UV-vis and EPR data indicated a slow reaction between $(FePc)_2N$ and H_2O_2 to form hydroperoxo $(Pc)Fe^{IV}=N–Fe^{III}(Pc)–OOH$ complex. This complex undergoes heterolytic O−O cleavage to generate a high valent di-iron oxo complex $(Pc)Fe^{IV}=N–Fe^{IV}(Pc^{+\cdot})=O$ as directly evidenced by ESI-MS experiments with labelled $H_2{}^{18}O_2$ (Figure 7.13).

Low temperature UV-vis, EPR, Mössbauer, EXAFS and XANES data were also consistent with involvement of $(Pc)Fe^{IV}=N–Fe^{IV}(Pc^{+\cdot})=O$ operating *via* oxo-transfer chemistry [95]. Such a highly electrophilic species should be a very powerful oxidant that was further demonstrated in oxidation of CH_4. Indeed, a $(FePc)_2N$ (0.1 mM) – H_2O_2 (67 mM) homogeneous system catalyzes the oxidation of CH_4 in acetonitrile at near-ambient temperatures (25–60 °C) with a TON of 41 [94, 96]. Formic acid was the major product of this oxidation and formaldehyde and methanol were minor products. Isotope labeling studies indicated a parallel oxidation of acetonitrile solvent, which is not surprising in the presence of the species capable of oxidizing methane. This side

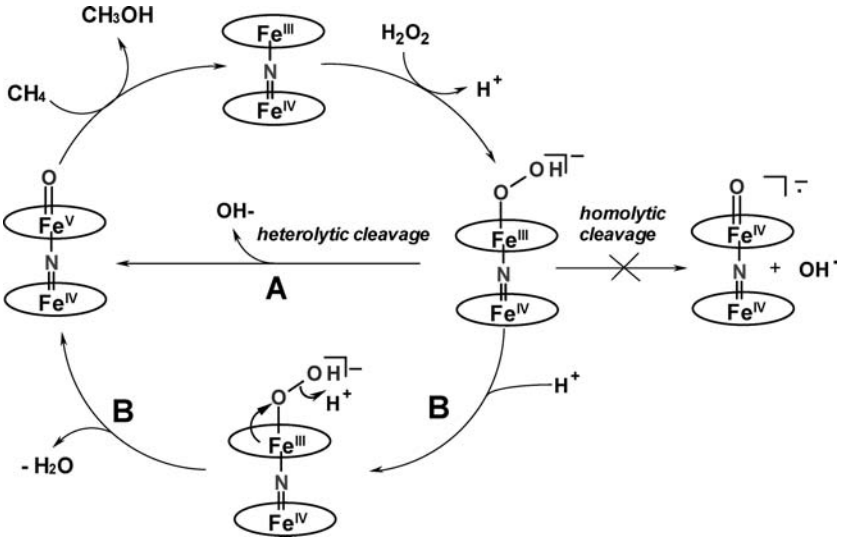


FIGURE 7.13 Proposed mechanism of H_2O_2 activation and formation of $(Pc)Fe^{IV}=N–Fe^{IV}(Pc^{+\cdot})=O$ active species.

oxidation of organic solvent is inevitable, thus masking the reaction and probably decreasing the performance of the catalytic system.

To circumvent this problem and to explore the possibility of recycling $(FePc)_2N$ was supported onto silica aerogel by impregnation. The oxidation of CH_4 was performed in water to avoid a parallel oxidation of organic solvent. In this context, water is not only a stable but also a clean solvent. Using the $(FePc)_2N$-SiO_2-supported catalyst, CH_4 was oxidized even at 25 °C in pure water although with a moderate TON of 13. The optimal reaction temperature was 40–60 °C to obtain a TON $\sim$ 26–29. A key step for the formation of $(Pc)Fe^{IV}=N–Fe^{IV}(Pc^{+\cdot})=O$ proposed active species is the heterolytic cleavage of O−O bond in the hydroperoxo complex (Figure 7.13, pathway A). This step should be favored by protonation of peroxide oxygen and release of H_2O, a better leaving group (Figure 7.13, pathway B). Indeed, in the presence of diluted H_2SO_4 the catalytic activity was strongly increased (Figure 7.14).

The maximal catalytic activity with 223 turnovers was obtained in 0.075 M H_2SO_4. Upon further increase of the acid concentration the catalytic performance decreased. The blue color of $(FePc)_2N$ catalyst almost disappeared when the 20 h oxidation reaction was performed in pure water, indicating its degradation under very strong oxidizing conditions that are necessary for methane oxidation. In the presence of diluted acid the stability of $(FePc)_2N$ was significantly higher. After completing the first reaction, a new portion of H_2O_2 was added directly to the reaction mixture. The catalytic system retained practically the same catalytic activity in the second cycle, indicating a high stability of the catalyst and even the possibility of recycling.

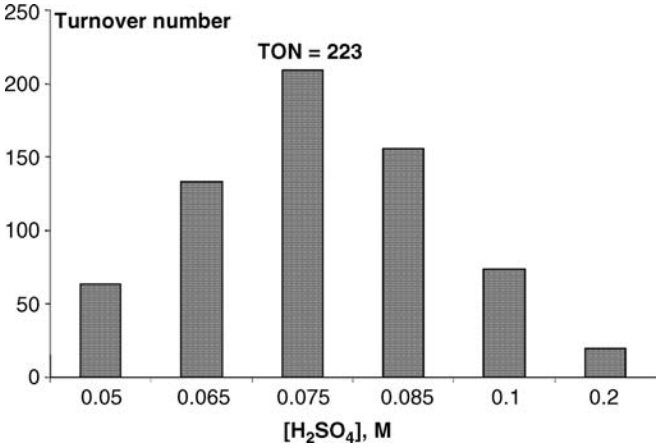


FIGURE 7.14 Dependence of the efficiency of methane oxidation on the acid concentration. Conditions: 32 bar methane, 2 mL diluted acid solution, supported $(FePc^{t}Bu_4)_2N\text{-}SiO_2$ (1 μmol), 678 μmol H_2O_2, T = 60 °C, reaction time – 20 h.

7.3.2 Oxidation of Olefins

Iron and manganese TDCPP complexes coordinatively fixed onto imidazole- and pyridine-modified silicas showed the high activity and stability in the oxidation of olefins by PhIO in CH_2Cl_2 or CH_3CN solvents. In order to obtain the optimal selectivity the oxidant should be added in small portions because a relatively small PhIO current concentration should be used to avoid side oxidation of the solvent and disproportionation of PhIO to PhI and $PhIO_2$. Although heterogeneous oxidations were markedly slower than homogeneous ones (by a factor of 10), SiO_2-Im/FeTDCPP and SiO_2-Im/MnTDCPP were used in 8 and 28 repetitive epoxidations of *(Z)*-cyclooctene by PhIO achieving 7900 and 24 700 turnovers, respectively [50]. Similar results were obtained using SiO_2-Py/FeTDCPP catalysts and no appreciate difference between SiO_2-Im and SiO_2-Py silica supports was detected [51]. After achieving 7900 turnovers the catalyst was partially destroyed, resulting in >50% reduction in activity. The formation of minor quantities of benzaldehydes along with major epoxides was observed in the course of oxidation of styrenes. A small catalyst leaching (<3%) was detected during oxidation of styrenes [51].

Efficient epoxidation systems based on Ru porphyrins have been developed by Che and Huang [54]. Anchoring of Ru porphyrins onto MCM-41 [97, 98] and Merrifield's peptide resin [99] provided more efficient and stable epoxidation catalysts. Low loaded RuPorphyrin-MCM-41 catalyst (0.1 mass% Ru) showed high turnover numbers in oxidation of olefins by ^{t}BuOOH that were 20–40 times superior to those for homogeneous complex (Table 7.2).

Although recycling data were not available, the supported catalyst didn't appreciably change the catalytic activity after 48 h. Aromatic and aliphatic alkenes

TABLE 7.2 Oxidation of Olefins by ^{t}BuOOH Catalyzed by Ru(II) *Meso*-tetrakis(4-chlorophenyl)porphyrin-MCM-41

Substrate	Product	TON	Yield, %
Norbornene	*exo*-norbornene oxide	9003 (230)[a]	52.6
cis-Cyclooctene	cyclooctene oxide	2044 (69)	11.9
Cyclohexene	cyclohexene oxide	377 (20)	2.2
	cyclohex-2-en-1-ol	1219 (26)	7.1
	cyclohex-2-en-1-one	2100 (38)	12.3
Styrene	styrene oxide	1878 (52)	11.0
	benzaldehyde	4545 (121)	26.5
cis-Stilbene	c*is*-stilbene oxide	245 (35)	1.4
	trans-stilbene oxide	1468 (37)	8.6
	benzaldehyde	161 (3)	0.9
trans-Stilbene	c*is*-stilbene oxide	31 (1)	0.2
	trans-stilbene oxide	1595 (85)	19.9
	benzaldehyde	59 (traces)	0.3

Reaction conditions: CH_2Cl_2 2 mL, olefin 0.2 g, ^{t}BuOOH 0.1 g, catalyst 50 mg (5.84×10^{-5} mmol), nitrogen, room temperature, 24 h.

[a]In parentheses, comparison with homogeneous conditions.

Adapted from [97] by permission of The Royal Society of Chemistry.

(1 mmol) have been converted to the epoxides in good yields and selectivities in the presence of RuTDCPP (0.195 μmol, 5130 : 1 substrate/catalyst ratio) grafted onto amino-modified MCM-41 and 2,6-dichloropyridine N-oxide (2,6-Cl2pyNO) oxidant (1.1 mmol) [98]. Efficient oxidation of styrene (98% conversion, 91% selectivity, 4550 turnovers), *cis*-stilbene (76%, 98%, 3819), cyclohexene (84%, 61%, 2628), norbornene (81%, 94%, 3905), cyclooctene (89%, 91%, 3762) and octene-1 (80%, 92%, 3774) indicated the large scope of this catalytic system. The steric constraints exerted by mesoporous material lead to unusual selectivity. In particular, the disubstituted exocyclic double bond in limonene is preferred over the endocyclic trisubstituted bond, though the more substituted bond should be epoxidized first because of electronic effects. The RuTDCPP-MCM-41 catalyst was reused three times and 67% of its initial activity was retained after 11 700 turnovers. Analysis of recovered after 1st run catalyst showed a 5% loss of Ru attributed to the catalyst degradation and leaching [98].

In order to improve catalyst recycling, Ru(II) 5,10,17-(tris(4-R-phenyl)-20-(4-hydroxyphenyl)porphyrins (R = Cl, Me) were covalently attached to Merrifield's peptide resin (MPR) with loading of 8.3 wt% [99]. MPR is chloromethylated styrene – divinylbenzene copolymer showing good solvatation and swelling in common organic solvents. A wide variety of alkenes, including aromatic and aliphatic terminal olefins, c*is*- and *trans*-stilbenes, cycloalkenes, α,β-unsaturated ketones, conjugated enynes, glycal, and protected α-amino alkenes (18 examples) were selectively epoxidized with 56–98% yields (on consumed oxidant) after 24 h reaction at room temperature using a catalyst:oxidant:substrate molar ratio of

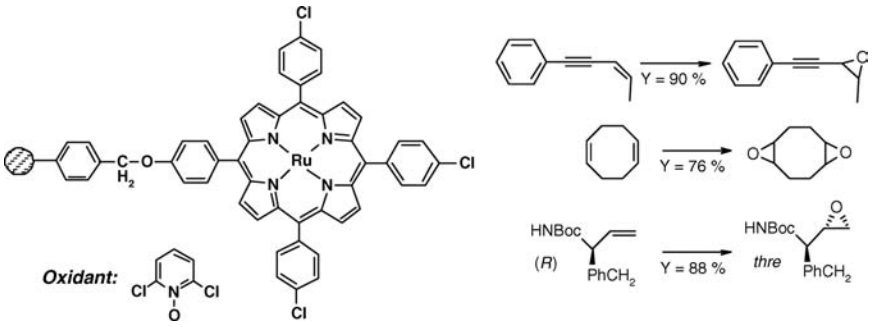


FIGURE 7.15 Epoxidation of selected olefins by 2,6-dichloropyridine N-oxide mediated by Ru(II)porphyrins anchored on Merrifield's peptide resin [99].

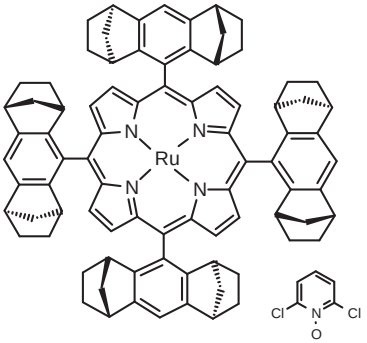
1 : 1400 : 1600. It was noteworthy that unusual selectivity was obtained for several olefins (Figure 7.15).

Under the above conditions the catalyst was reused four times in the epoxidation of styrene without detectable leaching (Ru analysis) or appreciate loss of epoxide yield (96, 93, 90, 92, 91%, respectively). Low loaded catalyst (0.17 wt% Ru porphyrin) exhibited 65–88% epoxide yields (8 examples) and very high TONs (2300–18 000). The high stability of the catalyst was confirmed by a recycling study. After a drop of epoxide yield in the second run the styrene epoxide yield was fairly stable for seven consecutive oxidations without detectable Ru leaching.

The scope of this system was extended to asymmetric epoxidation of olefins, which is the important procedure providing versatile building blocks for organic synthesis. In this case chiral porphyrin complexes with bulky chiral auxiliaries should be used [100]. Because of the tedious preparation and high cost of these elaborated complexes their recycling is especially important. Chiral D_4-symmetric Ru porphyrin immobilized in sol-gel silica showed high epoxidation activity with very small loading of the catalyst (5 mg, 0.02 μmol for 0.5 mmol olefin, 1 : 25 000 catalyst/substrate ratio) using 2,6-dichloropyridine N-oxide as an oxidant (Figure 7.16).

Compared to homogeneous conditions, a much longer reaction time was required because of diffusion problems and a very low catalyst loading. The observed *ee* values were similar to those obtained in homogeneous conditions and very high TONs were achieved. The reuse of the catalyst was studied with a 6-fold higher loading in the oxidation of styrene in benzene for 24 h. A gradual decrease of the catalytic activity was observed during 3 successive runs (Table 7.3).

The catalyst did not show the catalytic activity in the fourth cycle mainly owing to leaching of the complex to solution and its oxidative deactivation. However, a total TON of over 6000 turnovers was obtained that largely exceeded the catalyst productivity under homogeneous conditions [100]. A crucial role of support was demonstrated when this Ru porphyrin was grafted on amino-modified MCM-41



Catalyst : Substrate : Oxidant

1 25000 27500
(1) (1000) (1100)

0.02 µmol 0.5 mmol 0.55 mmol
(0.5 µmol) (0.5 mmol) (0.55 mmol)

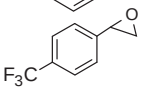
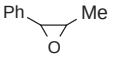
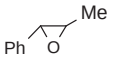
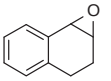
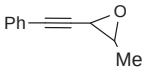
Epoxide	t, h	conv. %	sel, %	TON	ee, %
	48 (1.5)	60 (100)	75 (84)	10800 (875)	70 (69)
	48 (-)	23 (-)	96 (-)	6100 (-)	71 (-)
 *cis*-substrate	48 (3)	32 (100)	98 (98)	8480 (990)	66 (68)
 *trans*-substrate	48 (16)	20 (21)	96 (98)	5580 (270)	26 (30)
	48 (3)	52 (100)	65 (78)	4300 (890)	72 (80)
	48 (2)	24 (90)	85 (86)	6300 (700)	72 (70)

FIGURE 7.16 Heterogeneous asymmetric olefin epoxidations catalyzed by Ru porphyrin entrapped in sol-gel silica (5 mg) at room temperature. In parentheses – comparison with homogeneous conditions [100].

(one-dimensional channel system), MCM-48 (three-dimensional network) and amorphous silica, and the sol-gel catalyst was compared with these materials in the asymmetric epoxidation of styrene (Table 7.4) [101]. The use of a three-dimensional MCM-48 support providing a large surface area for high accessibility of reactants to active sites within the porous network, the highest conversion, TON

TABLE 7.3 Reuse of the Supported onto Silica Ru Porphyrin Catalyst in the Oxidation of Styrene by Cl_2pyNO [100]

	Cycle 1	Cycle 2	Cycle 3
Conversion, %	90	51	12
Selectivity, %	82	82	80
TON	3360	2180	600
ee, %	70	69	69

Reaction conditions: substrate 0.5 mmol, oxidant 0.55 mmol, catalyst 30 mg, benzene solvent, room temperature, 24 h. The solid catalyst was recycled by filtration and washed with benzene before reuse.

and *ee* were obtained. The catalyst supported on amorphous silica underwent significant Ru leaching. A sol-gel encapsulated catalyst showed low activity owing to slow diffusion of reagents. Recycling experiments were performed using 2 mmol substrate, 2.2 mmol oxidant and 0.1 μmol catalyst (20 000 : 22 000 : 1 molar ratio). When total turnovers reached to 26 000 after 2 reuses, the reactivity was almost unchanged, but *ee* decreased to 66% [101].

A coordination polymer consisting of Pd porphyrin units connected *via* Cd(II) nodes (Figure 7.17) and possessing two kinds of channels with dimensions of 4.61×12.55 Å^2 and 8.27×9.32 Å^2 exhibited a superior activity in the oxidation of styrene and selectivity to methylphenylketone compared to homogeneous Pd tetra (carboxyphenyl)porphyrin, Pd-carbon-supported catalyst and simple Pd salts (Table 7.5) [43].

A hot filtration test showed a truly heterogeneous reaction and no porphyrin complex was found in the solution by ^{1}H NMR. A coordination polymer catalyst recovered by simple filtration without any additional treatment retained the same catalytic properties in 6 successive reuses [43].

The selectivity of the MPc-mediated oxidation of olefins can be changed depending on the oxidant used. For example, when O_2 was used as oxidant in combination with isobutyric aldehyde, epoxides of cyclooctene, cyclohexene and styrene were obtained in 90%, 78% and 74% yields, respectively [27]. In the presence of

TABLE 7.4 Asymmetric Epoxidation of Styrene by 2,6-Cl_2pyNO Catalyzed by Grafted D_4-Symmetric Ru Porphyrin (see Figure 7.16 for the Structure)

Support	Conversion, %	Selectivity, %	TON	*ee*, %
MCM-48	84	86	3610	75
MCM-41	79	86	3390	72
Amorphous silica	42	79	1650	43
Sol-gel	10	68	340	66

Reaction conditions: 0.2 μmol catalyst, 1 mmol substrate, 1.1 mmol oxidant, benzene solvent, room temperature, 24 h.

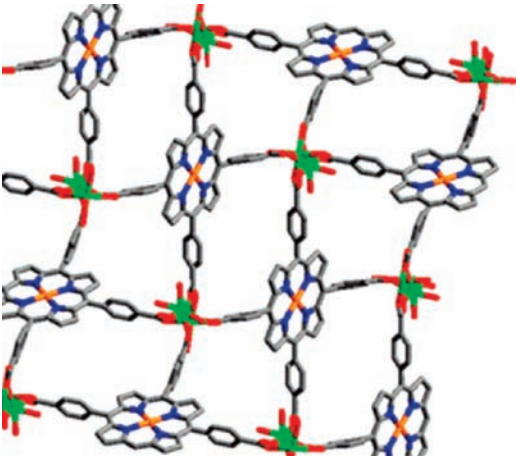
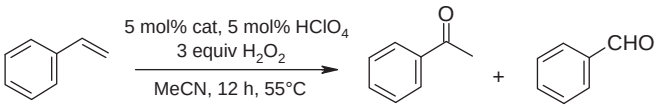


FIGURE 7.17 Structure of palladium porphyrin coordination polymer. Reproduced from [43] by permission of The Royal Society of Chemistry.

^{t}BuOOH, 2-cyclohexen-1-one was obtained in the oxidation of cyclohexene with 57% yield along with only a trace amount of epoxide.

The influence of the support was shown in the aerobic oxidation of β-isophorone (β-IP) to ketoisophorone (KIP), which is an important intermediate for the preparation of flavours and fragrances (Table 7.6) [60, 62]. A regular FePcS-SiO_2 catalyst provided a 38% yield of KIP while the same FePcS complex grafted onto TiO_2 was more efficient giving a 57% KIP yield (+ 21% yield of the corresponding allylic

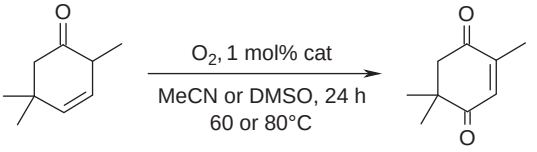
TABLE 7.5 Oxidation of Styrene Catalyzed by Palladium Porphyrin Coordination Polymer



Catalyst	Conversion, %	Selectivity, %	
		ketone	aldehyde
$PdCl_2$	0	0	0
$Pd(OAc)_2$	100	57	7
Pd/C	35	49	51
Pd porphyrin	90	78	22
Pd porphyrin - MOF	100	91	9
6th use	100	89	11

Adapted from [43] by permission of The Royal Society of Chemistry.

TABLE 7.6 Aerobic Oxidation of β-Isophorone (β-IP) to Ketoisophorone (KIP) Catalyzed by Grafted Phthalocyanine Complexes



Catalyst	Conversion, %	Yield, %
FePcS-SiO_2	92	38
FePcS-TiO_2	99	57
FePcS-chitosan	48	17
CoPcS-chitosan	85	39

alcohol) at 99% conversion [62]. It should be noted that TiO_2 was not an innocent support in this case. Although the mechanism of this cooperative effect is not yet clear, the combination of two catalytic sites in FePcS-TiO_2 resulted in more selective oxidation of β-IP to KIP. On reuse, a gradual decrease of the catalytic activity was observed (77 and 64% conversion in runs 2 and 3, respectively) because of the leaching of 9.9% of fixed FePcS to the reaction mixture per run. Materials combining oxidation and basic sites were prepared by supporting MPc onto chitosan, a polysaccharide containing free amino groups [60]. In this case CoPcS-chitosan exhibited better catalytic properties in the oxidation of β-IP to KIP than FePcS-chitosan catalyst. On reuse, a 10–20% decrease of the catalytic activity was observed between runs, but the KIP selectivity remained fairly constant for successive runs.

Mn(tmtacn) complex can be silica supported in monomeric or dimeric form [102]. Mononuclear active sites are good epoxidation catalysts with hydrogen peroxide but *cis*-diols are also obtained in direct one-step incorporation of two oxygen atoms with about 35% selectivity rather than by epoxide hydrolysis affording *trans*-diols. This system represents a rare example of a *cis*-dihydroxylation catalyzed by a first-row transition metal. Formation of the dimeric Mn(tmtacn) catalyst on the SiO_2 surface *in situ* afforded a much more active catalyst. Combined Mn(tmtacn)-CA-S catalyst (CA-S – carboxylic acid modified silica) showed an increased by factor ~10 TON in the oxidation of cyclooctene compared with a homogeneous Mn(tmtacn) complex alone or in the presence of unfunctionalized SiO_2 or Al_2O_3. Carboxylic acid surface density and CA to Mn molar ratio are important parameters for catalytic productivity. The catalytic performance of Mn(tmtacn)-CA-S is given in Table 7.7. No data on the stability and recycling of this catalyst was given.

The most developed approach based on the manganese salen complexes was introduced by Jacobsen [103] and Katsuki [104]. Epoxidation of conjugated *cis*-olefins, tri- and tetrasubstituted alkenes provides epoxides with $ee > 95\%$ in the presence of 2.5–5 mol% catalyst. Chiral Mn(salen) complexes suffer from instability and TONs of about 100 can typically be obtained. The initial approach to their immobilization was based on the covalent attachment to organic polymers. These

TABLE 7.7 Oxidation of Olefins by H_2O_2 Catalyzed by Mn(tmtacn)-CA-S

Substrate	Total TON	% epoxide : % diol : % other
cis-Cyclooctene	465	61 : 39 : 0
Cyclohexene	835	63 : 6 : 31
Norbornene	585	91 : 3 : 6
Cyclohexenone	238	75 : 15 : 10
1-Octene	609	90 : 3 : 7
Styrene	544	92 : 3 : 5
α-Methylstyrene	824	83 : 16 : 1
trans-β-Methylstyrene	248	79 : 11 : 10
cis-Stilbene	213	41 : 55 : 4

Reaction conditions: MeCN, CA:Mn = 10 : 1, [catalyst]:[substrate]:[H_2O_2] = 0.13 mM:0.17 M:0.64 M, 0 °C, 3 h.
Adapted from [83] by permission of The Royal Society of Chemistry.

materials often showed lower enantioselectivity because of interactions between the polymer backbone and the complex. Microporous and mesoporous organized materials are more suitable for development of supported salen catalysts. Three chiral Mn(salen) complexes were grafted in mesopores of MCM-41 (1.6 and 2.7 nm), SBA-15 (7.6 nm) and activated silica with sharp pore-size distribution (9.7 nm) using an anchored phenyl sulfonate group (Figure 7.18) [105]. Positive effect of the

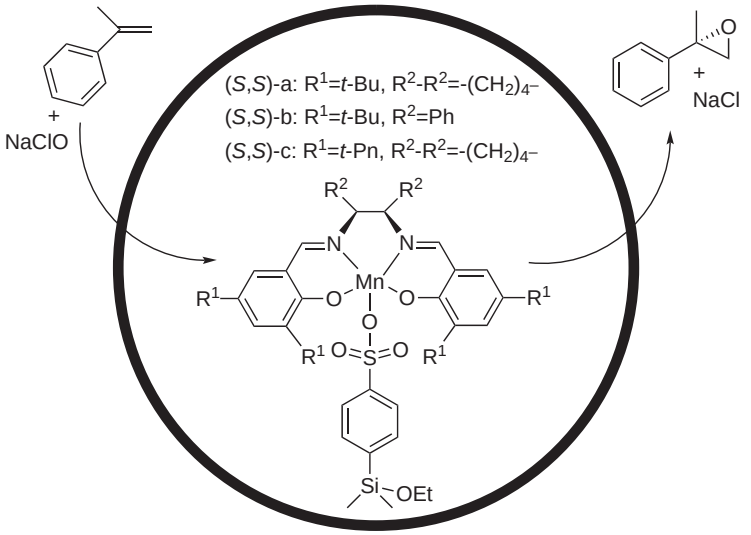


FIGURE 7.18 Schematic illustration of asymmetric epoxidation by chiral Mn(salen) complexes grafted in mesopores of silica supports. Reproduced from [105] by permission of The Royal Society of Chemistry.

TABLE 7.8 Asymmetric Epoxidation of Olefins by NaOCl Catalyzed by Mn(salen) Complexes Grafted in the Siliceous Mesopores

	α-methylstyrene epoxide		*cis/trans*-epoxides of *cis*-β-methylstyrene		
Catalyst	yield, %	*ee*, %	yield, %	*ee*, %	*cis/trans*
Mn(salen-a)Cl	100	55	28/73	55/100	0.38
Mn(salen-a)MCM(1.6)[a]	87	78	66/4	95/76	17.6
Mn(salen-a)MCM(2.7)	78	66	—	—	—
Mn(salen-a)SBA(7.6)	66	74	36/3	95/76	12.8
Mn(salen-a)SiO_2(9.7)	64	76	21/1	94/100	16.2

[a]In parentheses, average pore size of the support in nm.
Adapted from [105] by permission of The Royal Society of Chemistry.

catalyst confinement was observed in the epoxidation of α-methylstyrene and especially *cis*-β-methylstyrene. Enantiomeric excesses improved from 55% for homogeneous conditions to 78 and 95%, respectively, for heterogeneous epoxidation (Table 7.8).

A pronounced confinement effect on *cis/trans* selectivity was observed in epoxidation of *cis*-β-methylstyrene due to restricted rotation of the radical intermediated in the pore confined space. Surprisingly, olefin conversions decreased with increase of pore size and no clear relationship between pore size and enantioselectivity was observed. The nature of the axial tether group did not influence the *ee* values. More detailed studies showed the limitation of the scope. While heterogenization was beneficial for the above two substrates, other olefins did not show improvement in enantioselectivity [106]. Noteworthy, Mn(salen-a)SiO_2(9.7 nm) provided high enantioselectivity in epoxidation of α-methylstyrene during 8 successive runs: 65, 63, 68, 66, 67, 69, 75, 74%, although the product yield progressively decreased: 82, 85, 80, 75, 70, 65, 55 and 44%. After 8 runs the total TON of heterogeneous catalyst was 371 compared with 63 obtained with homogeneous complex until its destruction.

7.3.3 Oxidation of Aromatic Hydrocarbons

Oxidation of aromatic compounds to quinones is an important synthetic transformation for the preparation of vitamins and drugs. Particularly difficult oxidation of 2-methylnaphthalene (MN) to 2-methyl-1,4-naphthoquinone (MNQ, vitamin K_3) is still performed in industry by $CrO_3 - H_2SO_4$ with 40–50% yields. Numerous oxidation products are usually obtained, thus explaining moderate yields of the target MNQ [26, 27]. In the search for cleaner methods of the MN oxidation different homogeneous catalysts [107] were tested. Heterogeneous aromatic oxidation is less explored. Phthalocyanines of iron, manganese and cobalt anchored onto the surface of mesoporous and amorphous SiO_2 were compared in the oxidation of 2-methylnaphthalene by ^{t}BuOOH [26]. FePcS-SiO_2 catalyst supported in μ-oxo dimer form showed superior catalytic properties compared to homogeneous and monomeric

supported catalysts providing a 34% vitamin K_3 yield. The same catalyst anchored onto MCM-41 exhibited lower conversion and selectivity. This can be explained by the increased residence time of the substrate in the MCM-41 porous system that should favor the overoxidation reaction and limit conversion. Less demanding aromatic oxidation of anthracene and xanthene resulted in 90% and 99% yields of anthraquinone and xanthone, respectively.

Efficient oxidation of toluene to benzaldehyde with 98% selectivity was achieved in Mn(salen)-PDMS – ^{t}BuOOH system with TON = 1290 compared to 90% selectivity and TON = 1660 in the case of homogeneous system [90]. Supported Co(II) bipyridine complex prepared by anchoring (4,4′-di-^{t}Bu-bipy)Co[OSi(O^tBu)$_3$]$_2$ onto SBA-15 silica catalyzed heterogeneous benzylic oxidation of alkylaromatic compounds to the corresponding ketones without leaching of Co(II) [108]. High turnover frequencies were obtained in the oxidation of ethylbenzene ($582\,h^{-1}$), 4-ethylnitrobenzene ($252\,h^{-1}$), 4-bromoethylbenzene ($338\,h^{-1}$), 1,4-diethylbenzene ($335\,h^{-1}$), 4-ethylmethoxybenzene ($349\,h^{-1}$), toluene ($103\,h^{-1}$) and cumene (2-phenyl-2-propanol, $759\,h^{-1}$) with 80–100% selectivity.

7.3.4 Oxidation of Substituted Phenols

Two different cases can be considered. Halogenated phenols are among the priority pollutants and much research was devoted to their oxidative destruction. Supported FePcS was very efficient for oxidative degradation of 2,4,6-trichlorophenol resulting in (i) the cleavage of the aromatic cycle to form chloromaleic, chlorofumaric, maleic, fumaric and oxalic acids, (ii) the release of more than 2 Cl^- anions per trichlorophenol molecule and (iii) the formation of CO_2 and CO with 14% total yield. Detailed studies of this system can be found elsewhere [109] and will not be considered here.

The second direction is the selective oxidation of phenols to obtain corresponding quinones. This oxidation is the key step in the preparation of many vitamins and valuable synthetic precursors for drugs [110, 111]. The oxidation of 2,3,6-trimethylphenol (TMP) to 2,3,5-trimethylbenzoquinone (TMBQ), precursor of vitamin E was performed in the presence of supported phthalocyanine complexes (Table 7.9) [27].

TABLE 7.9 Oxidations of 2,3,6-Trimethylphenol to 2,3,5-Trimethylbenzoquinone Mediated by Heterogeneous MPc Catalysts

Catalyst	Substrate conversion, %	Product yield, %
Homogeneous FePcS	96	47
d-FePcS-MCM-41	98	24
m-FePcS-MCM-41	98	21
d-FePcS-SiO_2	96	77
d-FePcS-SiO_2	95	42
MnPcS-SiO_2	65	22
MnPcS-MCM-41	94	47

Reaction conditions: ^{t}BuOOH, CH_2ClCH_2Cl, 30 °C, 2 h.

The catalytic activity of MPc covalently supported onto mesoporous MCM-41 and amorphous Degussa Aerosil 200 silicas was almost the same, but the selectivity to TMBQ was notably higher in the latter case. The possible reason is easier over-oxidation of TMBQ inside mesopores. However, manganese-supported catalysts showed the opposite behaviour: MnPcS-MCM-41 provided 47% yield of TMBQ vs 22% in the case of MnPc-SiO_2 catalyst. Supported iron dimeric catalyst was more selective than homogeneous FePcS and monomeric supported catalyst affording 77% TMBQ yield compared with 47% and 42%, respectively. The stability of the d-FePcS-SiO_2 was studied in the repetitive TMP oxidation without any regeneration procedure. The catalytic activity remained the same in three cycles (96, 97 and 93% conversions) but the TMBQ yield was gradually decreasing: 77, 59 and 51% [27]. UV-vis study of the catalyst recovered after 3rd run showed a gradual transformation of μ-oxo dimer to monomeric FePcS, resulting in a decrease of the oxidation selectivity. This lack of stability of the μ-oxo di-iron site under reaction conditions is the principal inactivation pathway [26]. The stabilization of the supported dimer by covalent linking of two adjacent phthalocyanine molecules using a diamine spacer provided a more selective and stable catalyst: TMBQ was obtained with 87% yield at 97% TMP conversion [27].

Selective oxidation of only one group in compounds having several oxidizable functions keeping other sites intact is a significant synthetic challenge. A case example is the oxidation of functionalized phenols to quinones bearing different functional groups. They are powerful intermediates in organic synthesis and show biological activity since quinone fragments often occur within the molecular frameworks of natural products. Although functionalized quinones can be prepared using multistep synthetic strategies, the selective aromatic oxidation of readily available phenols is the most direct approach [5]. FePcS-SiO_2 catalyst in combination with ^{t}BuOOH was found to be quite selective in the aromatic oxidation of phenols containing easily oxidizable groups such as alcohol groups, double and triple bonds, benzylic positions (Table 7.10) with no need for protection/deprotection additional

TABLE 7.10 Oxidations of Functionalized Phenols Mediated by Heterogeneous FePcS-SiO_2 Catalyst [5]

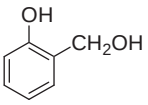
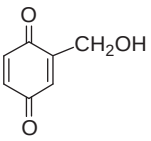
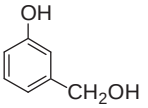
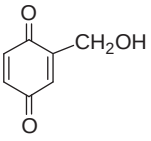
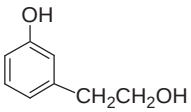
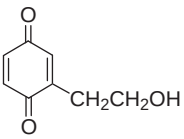
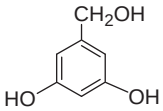
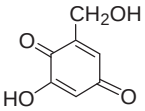
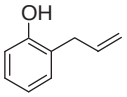
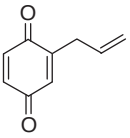
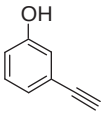
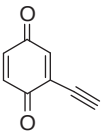
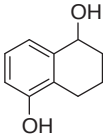
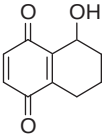
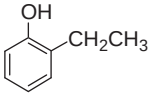
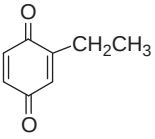
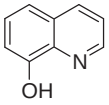
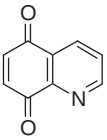
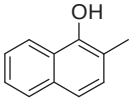
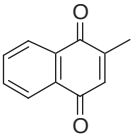
Entry	Substrate	Product	Conversion, % (reaction time, h)	Yield, %
1[a]			91 (2)	52
2[a]			100 (2.5)	53

TABLE 7.10 (Continued)

Entry	Substrate	Product	Conversion, % (reaction time, h)	Yield, %
3[a]			100 (1.5)	56
4[a]			84 (2)	46
5[b]			98 (2)	47
6[a]			32 (2)	17
7[a]			100 (0.5)	40
8[a]			92 (2)	43
9[a]			84 (2)	61
10[c]			96 (1)	57

[a]Conditions: FePcS-SiO_2, ^{t}BuOOH, acetone, 30 °C.
[b]The same conditions, but in MeCN.
[c]Dichloroethane, 80 °C.

procedures. The presence of additional functionalities enhances the versatility of the quinone building blocks for the synthesis of elaborated structures. Catalyst loading is generally 0.5–1 mol% and the product yields are in the range of 40–60%. The quinones bearing double and triple bonds have been obtained for the first time.

The preparation of quinoline-5,8-dione by direct oxidation of 8-hydroxyquinoline with 61% yield [112] is another important example since metal catalysts can often be inactivated by this substrate because of coordination of the metal site with a quinoline nitrogen atom. The observed high selectivity of aromatic oxidation *versus* oxidation of substituents can be explained by the coordination of a phenolic group to iron phthalocyanine followed by interaction with ^{t}BuOOH and by two successive one electron oxidations (Figure 7.19).

Such a mechanism was proposed for oxidation of alkyl-substituted phenols and naphthols on the basis of $^{18}O_2$ labelling experiments, EPR spectroscopy with spin traps, kinetic studies and complete analysis of all reaction products [113]. It should be noted that in order to get the optimal yield of quinones the solvent dependence should be studied since the selectivity of phenol oxidation depends on the solvent nature. In practice, acetonitrile, acetone and dichloroethane are among the best solvents for these reactions.

The aforementioned examples illustrate how the appropriate change of the structure of the supported catalyst and reaction conditions leads to tuning the catalytic activity. A detailed study of these variables was performed in the ^{t}BuOOH oxidation of 8-hydroxyquinoline to quinoline-5,8-dione, valuable drug precursor [112]. The catalytic oxidation showed high turnover frequency values: 217–3570 h^{-1} depending on the catalyst structure. The crucial factors affecting the product yield were the supporting procedure, the solvent nature, the catalyst amount, the substrate concentration and the oxidant/substrate ratio. Under optimal conditions, the selectivity to quinone was 70% at a 94% substrate conversion. Hot catalyst filtration experiments showed a truly heterogeneous oxidation, but the conversion and selectivity decreased in the second cycle to 66% and 41%, respectively. According to UV-vis data the possible reason was the oxidative degradation of phthalocyanine ligand. The improvement of the stability of the ligand by structural modification might lead to the catalysts being more amenable to recycling.

7.3.5 Oxidation of Alcohols

Application of supported metal complexes for the oxidation of primary and secondary alcohols to aldehydes or carboxylic acids and ketones is less developed compared with using supported metal Au, Pd and Ru catalysts [114]. The latter are especially suitable to perform these oxidations with O_2. Che and coworkers have supported Ru(III)(tmtacn) complex onto silica by impregnation and studied its catalytic properties in oxidation of primary and secondary benzyl, allylic and propargylic alcohols [115]. A variety of alcohols were oxidized by ^{t}BuOOH to the corresponding aldehydes and ketones with good yields (Table 7.11).

No appreciate oxidation of C=C and C≡C was observed for the allylic and propargylic alcohol oxidations, indicating a good chemoselectivity of this catalytic

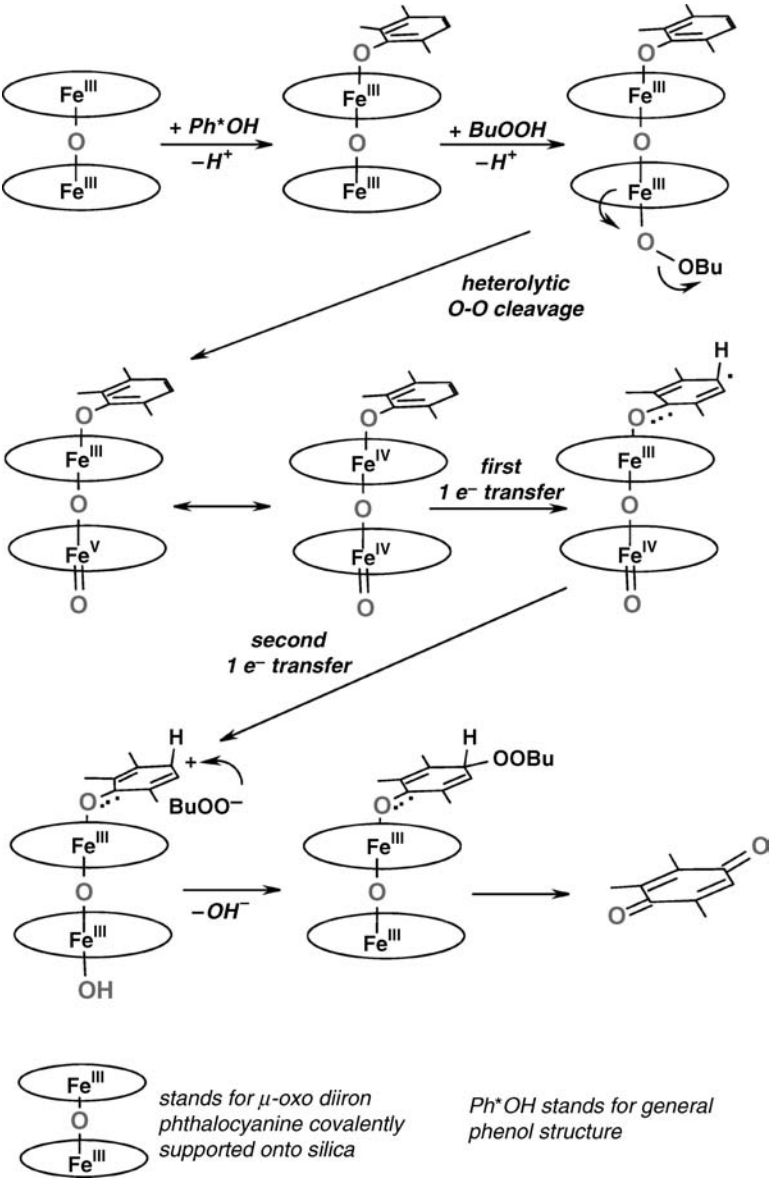
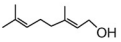
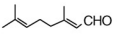
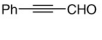
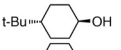
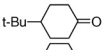
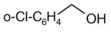
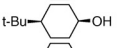
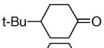
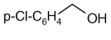
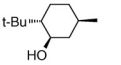
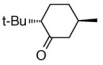


FIGURE 7.19 Proposed mechanism of oxidation of phenols by ^{t}BuOOH mediated by FePcS-SiO_2.

system. The Ru(tmtacn)-SiO_2 catalyst was subjected to eight reuses in the oxidation of 1-phenyl-1-propanol (40–45 °C, 14 h). The regeneration procedure consisted in the separation of solid by decantation and washing with CH_2Cl_2. Interestingly, while in CH_2Cl_2 the conversion and selectivity decreased from 76% to 57% and

TABLE 7.11 Oxidation of Alcohols by ^{t}BuOOH in the Presence of a Silica-Supported Ru(III)(tmtacn) Complex [115]

Substrate	Product	Conv., % (Select., %)	Substrate	Product	Conv., % (Select., %)
		99 (94)			85 (87)
		93 (99)			74 (89)
		95 (89)			77 (91)
		67 (99)			51 (90)
	PhCHO	81 (86)			90 (99)
	o-Cl-C_6H_4CHO	81 (77)			96 (99)
	p-Cl-C_6H_4CHO	93 (76)			11 (79)
		81 (70)			41 (86)

Conditions: a mixture of alcohol (1 mmol), supported catalyst (0.94 wt%, 600 mg), ^{t}BuOOH (2.3 mmol) in 5 mL hexane was stirred at 45 °C for 12–16 h.

from 97% to 85%, respectively, the catalyst retained the same catalytic activity (93–96% conversion) and selectivity (99%) during 8 runs in *n*-hexane solvent. After 8 reuses the catalyst contained the same 0.94% w/w Ru content (ICP analysis) indicating no complex leaching. Over 9000 turnovers have been attained for the oxidation of 1-phenyl-1-propanol to 1-phenyl-1-propanone.

The successful use of heterogeneous versions of 2,2,6,6-tetramethylpiperidyl-1-oxyl (TEMPO) for oxidation of alcohols with NaOCl in bromide-free and chlorinated-solvent-free systems is worth mentioning [116]. The development of the increasingly applied TEMPO oxidation method allowed the use of cocatalyst NaBr (10 mol%) and chlorinated solvents to be avoided, which are drawbacks of the standard process. In particular, a commercially available chimassorb 944, an oligomeric, sterically hindered amine (MW$\sim$3000) generated a recyclable oligomeric TEMPO with catalytic amounts of $Na_2WO_4{\cdot}2H_2O$. The use of polymer-immobilized piperidinyl oxyl (1 mol%) in combination with 1.25 equiv. of 0.35 M NaOCl provided the efficient solvent-free oxidation of octan-1-ol (90% conversion, 50% selectivity), octane-2-ol (99%, $>$ 99%), cyclooctanol (100%, $>$ 99%), benzyl alcohol (100%, $>$ 99%), 1-phenylethanol (100%, $>$ 99%) and butylproxitol (89%, $>$ 99%) within 30–60 min at 0 °C. Under these environmentally friendly conditions this system was superior to the homogeneous TEMPO and silica, MCM-41 and sol-gel supported TEMPO. The problem of low selectivity in the oxidation of primary alcohols could be overcome by using *n*-hexane as the solvent. The use of homogeneous $RuCl_2(PPh_3)_3$/TEMPO system allowed replacement of NaOCl with O_2, thus improving the green character of the process. However, the attempts to use the heterogeneous version of the system were unsuccessful [116].

In the current green-chemistry context, glycerol is an emerging sustainable raw material issued from biodiesel production. Oxidation of glycerol can give a number of high value products, e.g. dihydroxyacetone, glyceric, and tartronic acids [117]. The critical point is to achieve a good selectivity in target product which is challenging task. At present, this area is dominated by using metal (Au, Pd, Pt, Bi) supported catalysts [118]. Heterogenized TEMPO, Ru(tmtacn) or Pd 1,10-phenantroline [119] complexes might be prospective candidates for heterogeneous transformation of glycerol.

7.3.6 Miscellaneous Oxidations

α,β-Acetylenic ketones are very useful building blocks for enantioselective total synthesis and for the preparation of heterocyclic compounds, nucleosides, nonproteinogenic amino-acids, pheromones and drugs. Conjugated ynones are usually prepared by acylation of metal acetylenides and by multistep syntheses and only a few methods have been reported using direct stoichiometric α-oxidation of alkynes. The heterogeneous catalysts FePcS-SiO_2 and $FePcCl_{16}$-SiO_2 were used for selective oxidation of alkynes and propargylic alcohols to α,β–acetylenic ketones (Table 7.12) [120]. Three successive oxidations of 1-phenyl-1-butyne showed that the catalytic activity of $FePcCl_{16}/SiO_2$ remained high, the conversions and selectivities being 86, 84, 73% and 93, 100, 95%, respectively. The catalyst recycled after

TABLE 7.12 Oxidation of Alkynes by TBHP Catalyzed by Supported Metallo-Phthalocyanines [120]

Catalyst	Substrate	Product	Conv., %	Selectivity, %
FePcS-SiO_2	$C_3H_7C{\equiv}CC_3H_7$	$C_3H_7C{\equiv}CC(O)C_2H_5$	80	89
FePcS-SiO_2	$PhC{\equiv}CC_2H_5$	$PhC{\equiv}CC(O)CH_3$	75	83
FePcS-SiO_2	$HC{\equiv}CC_6H_{13}$	$HC{\equiv}CC(O)C_5H_{11}$	38	38
FePcS-SiO_2	$HC{\equiv}CC(OH)C_5H_{11}$	$HC{\equiv}CC(O)C_5H_{11}$	84	100
FePcS-SiO_2	$CH_3C{\equiv}CC_5H_{11}$	$CH_3C{\equiv}CC(O)C_4H_9$	64	47
$FePcCl_{16}$-SiO_2	$C_3H_7C{\equiv}CC_3H_7$	$C_3H_7C{\equiv}CC(O)C_2H_5$	79	88
$FePcCl_{16}$-SiO_2	$PhC{\equiv}CC_2H_5$	$PhC{\equiv}CC(O)CH_3$	86	93

Reaction conditions: 40 °C, 24 h, catalyst/alkyne/oxidant = 1/50/200.

3 oxidations exhibited the same DR UV-vis spectrum as that of the initial supported catalyst.

FePcS-SiO_2 was more efficient than Fe-pillared clays in Baeyer–Villiger oxidation of cyclohexanone to caprolactone by O_2 in the presence of 2 equiv. PhCHO at 25 °C [121]. The product yield of 61%, selectivity above 95% and TON = 4300 were achieved using a small amount of the heterogeneous catalyst (1.4 μmol FePcS for 10 mmol substrate). ICP analysis showed no iron leaching.

The microenvironment of mesoporous silica cages containing an encapsulated complex can be finely tuned using silylation reagents with various organic groups [122]. Li and coworkers showed a strong influence of the pore surface properties on the asymmetric oxidation of sulfides by H_2O_2 catalyzed by entrapped Fe(salan) complex (Figure 7.20).

Upon encapsulation and silylation procedures the surface area, pore volume and cage size of the materials decreased. Hydrophobic/hydrophilic properties of the catalysts were evaluated in gas adsorption experiments using benzene and water probes. Depending on the silylation reagent used solid catalysts with hydrophilic, hydrophobic and amphiphilic properties can be obtained. This approach provides a possibility of entrapment of the complex without modification of its structure and fine tuning of textural and polarity properties. This useful strategy can allow improvement in the partition of the reactants and products during the catalytic process, which strongly influences on the catalytic properties. Thus, Fe(salan) encapsulated in the amphiphilic cage exhibited much higher enantioselectivity and activity compared with the same complex situated in hydrophilic or hydrophobic environment (Table 7.13).

Fe(salan)TBNBr catalyst has amphiphilic surface properties and can absorb both hydrophilic H_2O_2 and hydrophobic thioanisole, thus allowing the fast diffusion of both reactants in the cages of the solid catalyst. Quite remarkably, the conversion and the initial oxidation rate in porous solid were even higher than those of the homogeneous complex. This is a rare example because owing to a diffusion limitation the reaction rate in porous system is usually significantly lower than that in homogeneous conditions. However, the enantioselectivity of heterogeneous

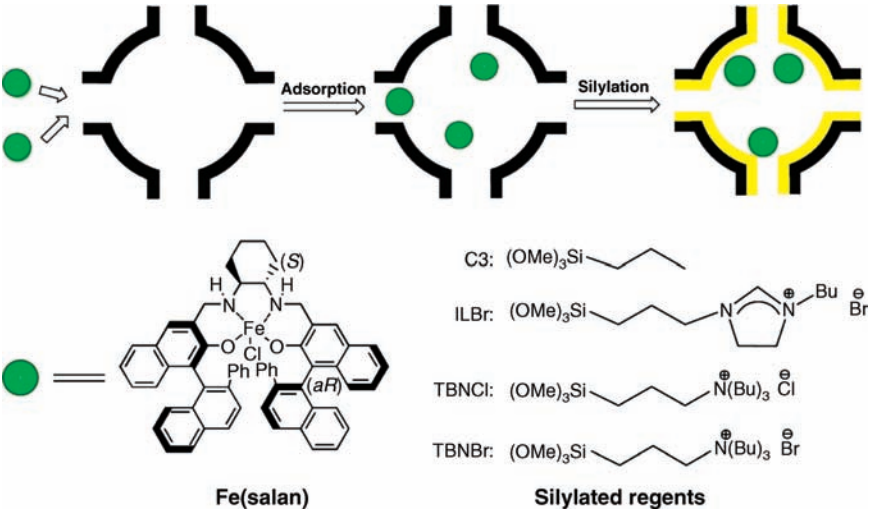
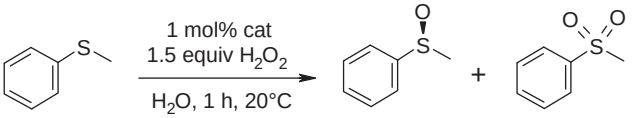


FIGURE 7.20 Encapsulation of Fe(salan) complex in the SBA-16 nanocages followed by silylation of the surface. Reproduced from [122] by permission of the PCCP Owner Societies.

catalysts was in general lower, Fe(salan)/TBNBr being the best with 74% *ee* vs 87% *ee* for homogeneous complex. It should be noted that even the change of anion from Br^- to Cl^- significantly modified the catalytic properties, indicating the sensitivity of such a construction to structural organization. Sheldon's test showed the heterogeneous character of the reaction, no leaching of Fe(salan) was detected in the filtrate. The recycling experiments showed a gradual decrease of catalytic

TABLE 7.13 Asymmetric Oxidation of Thioanisole Catalyzed by Fe(salan) Entrapped in SBA-16 of Different Surface Polarity. For the Structures of Catalysts see Figure 7.20.



Catalyst	Conversion, %	Sulfoxide selectivity, %	*ee*, %	TOF, h^{-1}
Fe(salan)	95	94	87	112
Fe(salan)/C3	55	97	57	88
Fe(salan)/ILBr	70	96	68	96
Fe(salan)/TBNCl	52	98	52	72
Fe(salan)/TBNBr	98	96	74	180

TOF (turnover frequency) was calculated for the initial 15 min.
Adapted from [122] by permission of the PCCP Owner Societies.

activity and enantioselectivity in 5 successive oxidations: 98, 94, 92, 85, 75% and 74, 70, 66, 60, 56%, respectively. The microenvironment characterization of Fe(salan)/TBNBr after the 5th recycling by benzene–water gas absorption experiments showed the hydrophilic character of the material. This indicates that TBNBr group was not stable and Fe(salan)/TBNBr gradually lost its amphiphilicity during the repetitive oxidations. The Fe(salan)/TBNBr catalyst exhibited the similar activity and enantioselectivity compared to homogeneous complex in the oxidation of several sulfides [122].

Li and coworkers nicely showed the cooperative activation of Co(salen) complexes *via* adjusting the loading of freely moving catalyst in confined space of porous SBA-16 solid [33]. After introducing 1.2, 1.9, 3.4 and 4.9 Co(salen) molecules per cage, the pore-entrance size was reduced by silylation with propyltrimethoxysilane. In addition, this silylating agent with moderate hydrophobicity allowed modification of the inner surface of SBA-16 thereby optimizing the diffusion rates and partition of reagents. These materials showed a very high performance in hydrolytic kinetic resolution of epoxides, in particular propylene epoxide. Though it is not an oxidation reaction, it involves epoxides that are important oxidation products. Hydrolysis of epoxides performing by two Co(salen) molecules occurs, with higher rate and higher enantioselectivity compared to monomolecular reaction. For Co(salen)/SBA-16 with 1.2 Co(salen) molecules per cage, a monomolecular pathway occurs resulting in low conversion of propylene epoxide (8%) and lower *ee* (93%). The increase of Co(salen) loading to 1.9, 3.4 and 4.9 molecules per SBA-16 cage leads to much higher performance (49% conversion with 98% *ee* of the diol) [33].

Another advantage of this encapsulated catalyst is the constant "volume active site density", i.e. local concentration of the complex per cage volume. To achieve such a concentration in the homogeneous solution a very large amount of the complex should be employed. In contrast, small amounts of the encapsulated catalyst can be used without decrease of "volume active site density" to provide a high catalytic activity. With 12 000 : 1 substrate/catalyst ratio homogeneous catalyst provided 7% conversion with TOF of $35\,h^{-1}$ to afford 7% *ee* epoxide and 89% *ee* diol. The performance of Co(salen)/SBA-16 under the same condition was remarkable: 50% conversion with TOF of $250\,h^{-1}$ (more than 7 times higher compared to the homogeneous system) with excellent resolution: 98% *ee* epoxide and 98% *ee* diol. A TON of 6000 was achieved with heterogeneous catalyst. Co(salen)/SBA-16 retained the same catalytic performance (43–45% diol yield and 97–98% diol *ee*) during 8 consecutive runs and Co content in the filtrate was below the detection limit of ICP-AES analysis [33].

7.4 GENERAL REMARKS ON STABILITY

For economy and greenness of processes the recovery and reuse of catalysts are of the primary importance. Hence, the stability of the heterogeneous metal-complex catalysts is an important issue. In order to show the potential of any particular

catalyst in terms of its efficiency and possible application, the stability and recycling aspects of the catalytic systems have been discussed in the Catalysis sections along with catalytic properties. Moreover, one of the main criteria for the choice of catalytic systems presented in this chapter was the presence of the well-documented studies on the stability issues in the original papers. In this summary section on stability the discussion will be focused on the general trends.

Several mechanisms responsible for the loss of the catalytic properties of supported metal complexes preventing their efficient reuse can be listed. Metal complexes fixed onto supports by noncovalent interaction are often susceptible to leaching in the reaction solution. In general, strong covalent anchoring of the complex should prevent metal leaching, provided that the complex is stable under catalytic conditions. However, this issue should be surveyed by hot filtration tests and determination of the concentration of the metal in the solution after reaction because even in this case some leaching of the metal complex can occur.

The second reason for the catalyst inactivation is the destruction of the complex under oxidative conditions. In enzymes responsible for bio-oxidation, active sites containing reactive metal species are protected by surrounding protein. In addition, these enzyme systems are organized in such a way that limits or even avoids a nonproductive and nonselective generation of the strong oxidizing species [2, 123]. For example, cytochrome P-450 has a hydrophobic pocket in the vicinity of the iron porphyrin active site. When no substrate is present in the hydrophobic cavity, the low spin Fe(III) state ($S = 1/2$) with coordinated water molecule is favoured and no activation of O_2 occurs. Thus, cytochrome P-450 is in the resting state. Upon binding a hydrocarbon substrate in the hydrophobic cavity near the active site, the water molecule is removed and the iron(III) site adapts a high spin state ($S = 5/2$). These modifications induce a change in the redox potential of the iron which facilitates the reduction of Fe(III) to Fe(II) followed by binding and activation of O_2. Thus, the strong oxidizing species is generated only when the substrate to be oxidized is present in the active site. Such a perfect organization of the active site provides "protection by substrate" and prevents the organic surrounding of the enzyme active site from oxidative degradation. The development of a similar approach for bioinspired supported catalysts is highly challenging. Consequently, in order to achieve a reasonable stability of the supported metal complexes under strong oxidizing conditions, robust ligands, e.g. containing electron-withdrawing halogen substituents or phthalocyanine cores, should be preferred. Another important requirement is the selective generation of the metal-centered oxidizing species and avoiding the activation of the terminal oxidants *via* pathways generating free radicals that destroy the organic ligand of the metal complex.

Another reason for the loss of the catalytic activity upon reuse is the adsorption of the products on the surface leading to the blockage of the active sites. In principal, the catalyst can be regenerated by washing or by heating though the latter approach is less suitable for supported complexes owing to their limited thermal stability. The activation of TEOS/PDMS membranes is complicated since polar solvents used to avoid the complex leaching cannot enter into the hydrophobic membrane thus making the washing inefficient.

In some original studies the authors claim that their supported catalysts do not suffer from the catalyst leaching and can be used in several successive uses with no loss of the catalytic activity. However, the recycling number is often limited by 3 reuses. The examples when the supported catalyst can be reused at least 10 times while keeping catalytic performance are still rare. Continuous-flow oxidation with very high turnover numbers is still an open challenge. The importance of careful studies of all aspects of the catalyst stability and recycling is still underestimated.

7.5 CONCLUSION AND PERSPECTIVES

The appropriate choice of the oxidant and the change of the catalysts structure (metal, ligand type, electron-withdrawing or donating substituents, support, etc.) allow tuning the catalytic properties of the systems. The support should not be considered just as inert phase to facilitate the catalyst separation. It is highly desirable to take advantage of the hydrophilic/hydrophobic properties of support, its structural organization to improve the catalytic properties of the supported catalyst. There is no single approach that would be generally applicable. The elaboration of the catalyst depends on the particular system and reaction.

Recent progress in the preparation of organized porous solids constructed from porphyrin and phthalocyanine molecules has provided an access to materials with controlled porosity and very high concentration of active site. These materials are believed to be very useful in the catalytic applications [124]. However, the successful use of these materials in oxidation catalysis is still to be demonstrated. One of the future perspective directions with high potential is the development of chiral supports, in particular chiral MOFs.

Supported bioinspired complexes emerge as a prospective class of catalysts for clean oxidation under mild conditions. Many examples of efficient catalytic processes in terms of high activity and selectivity, high turnover numbers and catalyst stability allowing recycling are available. Such selective catalytic oxidations using clean oxidants might lead to significant reduction in problems of waste disposal. However, except for supported metal phthalocyanines for the Merox process and chiral salen complexes for asymmetric epoxidation of olefins, these catalysts have not yet became industrially attractive, even for the synthesis of special and pharmaceutical products. This situation can be explained by the limited availability of elaborated metal complexes, especially in a large scale, attributed to its multistep complex preparation. In this context, particular attention should be paid to the development of the complexes with simple preparation and readily available on a large scale. Stability and recycling issues have also to be improved.

ACKNOWLEDGMENTS

The author is grateful to coworkers and collaborators the names of which are given in references for their valuable contribution in the development of metallophthalocyanine

oxidation catalysts and Agence National de la Recherche (ANR, France, grant ANR-08-BLANC-0183-01) for the support of this research.

REFERENCES

1. Sheldon R.A. (2008). *Chem. Commun.*, 3352–3365.
2. Ortiz de Montellano P.R. (2010). *Chem. Rev.* 110, 932–948.
3. Baik M.-H., Newcomb M., Friesner R.A., Lippard S.J. (2003). *Chem. Rev.* 103, 2385–2419.
4. Meunier B. (1992). *Chem. Rev.* 92, 1411–1456.
5. Sorokin A.B., Kudrik E.V. (2011). *Catal. Today* 159, 37–46.
6. Tshuva E.Y., Lippard S.J. (2004). *Chem. Rev.* 104, 987–1012.
7. Centi G., Cavani F., Trifirò F. *Selective Oxidation by Heterogeneous Catalysis. Recent Developments*. Plenum, New York, 2001.
8. Averseng F., Vennat M., Che M. *Grafting and Anchoring of Transition Metal Complexes to Inorganic Oxides*. Wiley-VCH Verlag, Weinheim, 2008.
9. Alaerts L., Wahlen J., Jacobs P. A., De Vos D.E. (2008). *Chem. Commun.*, 1727–1737.
10. Hintermair U., Francio G., Leitner W. (2011). *Chem. Commun.* 47, 3691–3701.
11. Seki T., Baiker A. (2009). *Chem. Rev.* 109, 2409–2454.
12. Zhang W. (2009). *Green Chem.* 11, 911–920.
13. Muzart J. (2006). *Adv. Synth. Catal.* 348, 275–295.
14. Behr A., Henze G., Schomäcker R. (2006). *Adv. Synth. Catal.* 348, 1485–1495 and references therein.
15. Collis A.E.C., Horváth I.T. (2011). *Catal. Sci. Technol.* 1, 912–919.
16. Hunger M., Weitkamp J. (2001). *Angew. Chem. Int. Ed.* 40, 2954–2971.
17. Glatzel P., Bergmann U. (2005). *Coord. Chem. Rev.* 249, 65–95.
18. Taguchi A., Schüth F. (2005). *Micropor. Mesopor. Mater.* 77, 1–45.
19. Hoffmann F., Cornelius M., Morell J., Fröba M. (2006). *Angew. Chem. Int. Ed.* 45, 3216–3251.
20. Corma A., Garcia H. (2006). *Adv. Synth. Catal.* 348, 1391–1412.
21. Basset J.M., Ugo R. In: *Modern Surface Organometallic Chemistry*, Basset J.M., Psaro R., Roberto D., Ugo R., eds. Wiley-VCH, Weinheim, 2009, pp. 1–29.
22. Kholdeeva O.A. Chapter 4 in this book.
23. Clark J.H., Macquarrie D.J., Tavener S.J. (2006). *Dalton. Trans.*, 4297–4309.
24. Linares N., Serrano E., Rico M., Balu A.M., Losada E., Luque R., Garcia-Martinez J. (2011). *Chem. Commun.* 47, 9024–9035.
25. Corriu R.J.P., Mehdi A., Reyé C., Thieuleux C. (2004). *Chem. Mater.* 16, 159–166.
26. Sorokin A.B., Tuel A. (2000). *Catal. Today* 57, 45–59.
27. Sorokin A.B., Mangematin S., Pergrale C. (2002). *J. Mol. Catal. A: Chemical* 182–183, 267–281.
28. Zakharov V.Y., Zakharova O.M., Romanovsky B.V., Mardaleishvili R.E. (1977). *React. Kinet. Catal. Lett.* 6, 133–137.

29. Bedioui F. (1995). *Coord. Chem. Rev.* 144, 39–68.
30. Yang H., Zhang L., Su W., Yang Q., Li C. (2007). *J. Catal.* 248, 204–212.
31. Yang H., Li J., Yang J., Liu Z., Yang Q., Li C. (2007). *Chem. Commun.*, 1086–1088.
32. Fraile J.M., Garcia J.I., Herrerias C.I. Mayoral J.A., Rires E. (2009). *Chem. Soc. Rev.* 38, 695–706.
33. Yang H., Zhang L., Zhong L., Yang Q., Li C. (2007). *Angew. Chem. Int. Ed.* 46, 6861–6865.
34. Algarra F., Esteves M.A., Fornés V., Garcia H., Primo J. (1998). *New J. Chem.* 22, 333–338.
35. Sabater M.J., Corma A., Domenech A., Fornés V., Garcia H. (1997). *Chem. Commun.*, 1285–1286.
36. Balkus K.J., Jr., Gabrielov A.G., Bell S.L., Bedioui F., Roué L., Devynck J. (1994). *Inorg. Chem.* 33, 67–72.
37. Dhakshinamoorthy A., Alvaro M., Garcia H. (2011). *Catal. Sci. Technol.* 1, 856–867.
38. Farrusseng D., Aguado S., Pinel C. (2009). *Angew. Chem. Int. Ed.* 48, 7502–7513.
39. Hwang Y.K., Férey G., Lee U.-H., Chang J.-S., Chapter 8 in this book.
40. Zalomaeva O.V., Kovalenko K.A., Chesalov Y.A., Mel'gunov M.S., Zaikovskii V.I., Kaichev V.V., Sorokin A.B., Kholdeeva O.A., Fedin V.P. (2011). *Dalton Trans*. 40, 1441–1444.
41. Kockrick E., Lescouet T., Kudrik E.V., Sorokin A.B., Farrusseng D. (2011). *Chem. Commun.* 47, 1562–1564.
42. Farla O.K., Shultz A.M., Sarjeant A.A., Nguyen S.T., Hupp J.T. (2011). *J. Am. Chem. Soc.* 133, 5652–5655.
43. Xie M.-H., Yang X.-L., Wu C.-D. (2011). *Chem. Commun.* 47, 5521–5523.
44. Yoon M., Srirambalaji R., Kim K. (2012). *Chem. Rev.* 112, 1196–1231.
45. Groves J.T., Nemo T.E., Myers R.S. (1979). *J. Am. Chem. Soc.* 101, 1032–1033.
46. Nam W. (2007). *Acc. Chem. Res.* 40, 522–531.
47. Costas M. (2011). *Coord. Chem. Rev.* 255, 2912–2932.
48. Che C.-M., Kar-Yan Lo V., Zhou C.Y., Huang J.-S. (2011). *Chem. Soc. Rev.* 40, 1950–1975.
49. Lu H., Zhang X. P. (2011). *Chem. Soc. Rev.* 40, 1899–1909.
50. Cooke P.R., Lindsay Smith J.R. (1994). *J. Chem. Soc. Perkin Trans.* 1, 1913–1923.
51. Gilmartin C., Lindsay Smith J.R. (1995). *J. Chem. Soc. Perkin Trans.* 2, 243–251.
52. Battioni P., Lallier J.P., Barloy L., Mansuy D. (1989). *J. Chem. Soc. Chem. Commun.*, 1149–1151.
53. Battioni P., Cardin E., Louloudi M., Schöllhorn B., Spyroulias G.A., Mansuy D., Traylor T.G. (1996). *Chem. Commun.*, 2037–2038.
54. Che C.-M., Huang J.-S. (2009). *Chem. Commun.*, 3996–4015.
55. Franke A., Fertinger C., van Eldik R. (2011). *Bioinorg. React. Mech.* 7, 5–26.
56. Lyons J.E., Ellis, P.E., Jr., Myers H.K., Jr. (1995). *J. Catal.* 155, 59–73.
57. Basu B., Satapathy S., Bhatnagar A.K. (1993). *Catal. Rev.-Sci. Eng.* 35, 571–609.
58. Sorokin A., Meunier B. (1994). *J. Chem. Soc. Chem. Commun.*, 1799–1800.
59. Sanchez M., Chap N., Cazaux J.P., Meunier B. (2001). *Eur. J. Inorg. Chem.*, 1775–1783.

60. Sorokin A.B., Quignard F., Valentin R., Mangematin S. (2006). *Appl. Catal. A: General* 309, 162–168.
61. Zalomaeva O.V., Sorokin A.B. (2006). *New J. Chem.* 30, 1768–1773.
62. Beyrhouty M., Sorokin A.B., Daniele S., Hubert-Pfalzgraf L.G. (2005). *New J. Chem.* 29, 1245–1248.
63. Sorokin A.B., Buisson P., Pierre A.C. (2001). *Micropor. Mesopor. Mater.* 46, 87–98.
64. Tanamura Y., Uchida T., Teramae N., Kikuchi M., Kusaba K., Onodera Y. (2001). *Nano Lett*. 1, 387–390.
65. Pirouzmand M., Amini M.M., Safari N. (2007). *J. Porphyrins Phthalocyanines* 11, 118–124.
66. De Vos D.E., Jacobs P.A. (2000). *Catal Today* 57, 105–114.
67. Huybrechts D.R.C., Parton R.F., Jacobs P.A. (1991). *Stud. Surf. Sci. Catal.* 60, 225–254.
68. Balkus K.J., Jr., Eissa, M., Levado R. (1995). *J. Am. Chem. Soc.* 117, 10753–10754.
69. Paez-Mozo E., Gabriunas N., Lucaccioni F., Acosta D.D., Patrono P., La Ginestra A., Ruiz P., Delmon B. (1993). *J. Phys. Chem.* 97, 12819–12827.
70. Parton R.F., Bezoukhanova C.P., Grobet J., Grobet P.J., Jacobs P.A. (1994). *Stud. Surf. Sci. Catal.* 60, 371–378.
71. Parton R.F., Vankelecom I.F.J., Casselman M.J.A., Bezoukhanova C.P., Uytterhoeven J.B., Jacobs P.A. (1994). *Nature* 370, 541–544.
72. Kudrik E.V., Afanasiev P., Bouchu D., Millet J.M.M., Sorokin A.B. (2008). *J. Porphyrins Phthalocyanines* 12, 1078–1089.
73. Costas M., Mehn M.P., Jensen M.P., Que, L., Jr. (2004). *Chem. Rev.* 104, 939–986.
74. Lippard S.J. (2005). *Philos. Trans. R. Soc. A*, 363, 861–877.
75. Katsuki T. (2004). *Chem. Soc. Rev.* 33, 437–444.
76. Matsumoto K., Saito B., Katsuki T. (2007). *Chem. Commun.*, 3619–3627.
77. Larrow J.F., Jacobsen E.N. (2004). *Topics Organomet. Chem.* 6, 123–152.
78. Cozzi P.G. (2004). *Chem. Soc. Rev.* 33, 410–421.
79. Baleizao C., Garcia H. (2006). *Chem. Rev.* 106, 3987–4043.
80. Gupta K.C., Sutar A.K., Lin C.-C. (2009). *Coord. Chem. Rev.* 253, 1926–1946.
81. Corma A., Garcia H. (2008). *Top. Catal.* 48, 8–31.
82. De Vos D.E., Sels B.F., Jacobs P.A. (2002). *CATTECH* 6, 14–29.
83. Schoenfeldt N.J., Korinda A.W., Notestein J.M. (2010). *Chem. Commun.* 46, 1640–1642.
84. *Chiral Catalyst Immobilization and Recycling*. De Vos D.E., Varkelecom I.F.J., Jacobs P.A., eds. Wiley-VCH, Weinheim, 2000.
85. Jones C.W. (2010). *Top. Catal.* 53, 942–952.
86. Armengol E., Corma A., Fornés V., Garsia H., Primo J. (1999). *Appl. Catal. A: General* 181, 305–312.
87. Parton R.F., Neys P.E., Jacobs P.A., Sosa R.C., Rouxhet P.G. (1996). *J. Catal.* 164, 341–346.
88. Dioos B.M.L., Vankelecom I.F.J., Jacobs P.A. (2006). *Adv. Synth. Catal.* 348, 1413–1446.

89. Parton R.F., Vankelecom I.F.J., Tas D., Janssen K.B.M., Knops-Gerrits P.-P., Jacobs P.A. (1996). *J. Mol. Catal. A: Chemical* 113, 283–292.
90. Mac Leod T.C.O., Kirillova M.V., Pombeiro A.J.L., Schiavon M.A., Assis M.D. (2010). *Appl. Catal. A: General* 372, 191–198.
91. Shilov A.E., Shul'pin G.B. (1997). *Chem. Rev.* 97, 2879–2932.
92. Periana R.A., Taube D.J., Gamble S., Taube H., Satoh T., Fujii H. (1998). *Science* 280, 560–564.
93. Palkovits R., Antonietti M., Kuhn P., Thomas A., Schüth F. (2009). *Angew. Chem. Int. Ed.* 48, 6909–6912.
94. Sorokin A.B., Kudrik E.V., Bouchu D. (2008). *Chem. Commun.*, 2562–2564.
95. Afanasiev P., Kudrik E.V., Millet J.M.M., Bouchu D., Sorokin A.B. (2011). *Dalton Trans.* 40, 701–710.
96. Sorokin A.B., Kudrik E.V., Alvarez L.X., Afanasiev P., Millet J.M.M., Bouchu D. (2010). *Catal. Today* 157, 149–154.
97. Liu C.-J., Li S.-G., Pang W.-Q., Che C.-M. (1997). *Chem. Commun.*, 65–66.
98. Liu C.-J., Yu W.-Y., Li S.-G., Che C.-M. (1998). *J. Org. Chem.* 63, 7364–7369.
99. Yu X.-Q., Huang J.-S., Yu W.-Y., Che C.-M. (2000). *J. Am. Chem. Soc.* 122, 5337–5342.
100. Zhang R., Yu W.-Y., Wong K.-Y., Che C.-M. (2001). *J. Org. Chem.* 66, 8145–8153.
101. Zhang J.-L., Liu Y.-L., Che C.-M. (2002). *Chem. Commun.*, 2906–2907.
102. De Vos D.E., Mams M., Sels B.F., Jacobs P.A. (2002). *Chem. Rev.* 102, 3615–3640.
103. Jacobsen E.N. In: *Comprehensive Organometallic Chemistry II*, Vol. 12. Abel E.W., Stone F.G.A., Wilkinson E., eds. Pergamon, New York, 1995, p. 1097.
104. Katsuki T. (2000). In: *Catalytic Asymmetric Synthesis*, 2nd edn, Ojima I., ed. Wiley-VCH, New York, p. 287.
105. Zhang H., Xiang S., Li C. (2005). *Chem. Commun.*, 1209–1211.
106. Zhang H., Xiang S., Xiao J., Li C. (2005). *J. Mol. Catal. A: Chemical* 238, 175–184.
107. Wienhöfer G., Schröder K., Möller K., Junge K., Beller M. (2010). *Adv. Synth. Catal.* 352, 1615–1620 and references therein.
108. Brutchey R.L., Drake I.J., Bell A.T., Tilley T.D. (2005). *Chem. Commun.*, 3736–3738.
109. Meunier B., Sorokin A. (1997). *Acc. Chem. Res.* 30, 470–476.
110. Zalomaeva O.V., Kholdeeva O.A., Sorokin A.B. (2007). *C. R. Chimie* 10, 598–603.
111. Kholdeeva O.A., Zalomaeva O.V., Sorokin A.B., Ivanchikova I.D., Della Pina C., Rossi, M. (2007). *Catal. Today* 121, 58–64.
112. Zalomaeva O.V., Sorokin A.B., Kholdeeva O.A. (2010). *Green Chem.* 12, 1076–1082.
113. Zalomaeva O.V., Ivanchikova I.D., Kholdeeva O.A., Sorokin A.B. (2009). *New J. Chem.* 33, 1031–1037.
114. Besson M., Gallezot P. (2000). *Catal. Today* 57, 127–141.
115. Cheung W.-H., Yu W.-Y., Yip W.-P., Zhu N.-Y., Che C.-M. (2002). *J. Org. Chem.* 67, 7716–7723.
116. Sheldon R.A., Arends I.W.C.E., Brink G.-J.T., Dijksman A. (2002). *Acc. Chem. Res.* 35, 774–781.

117. Pagliaro M., Ciriminna R., Kimura H., Rossi M., Della Pina C. (2007). *Angew. Chem. Int. Ed.* 46, 4434–4440.
118. Katryniok B., Kimura H., Skrzynska E., Girardon J.-S., Fongarland P., Capron M., Ducoulombier R., Mimura N., Paul S., Dumeignil F. (2011). *Green Chem*. 13, 1960–1979.
119. Painter R.M., Pearson D.M., Waymouth R.M. (2010). *Angew. Chem. Int. Ed.* 49, 9456–9459.
120. Pérollier C., Sorokin A.B. (2002). *Chem. Commun.*, 1548–1549.
121. Belaroui L.S., Sorokin A.B., Figueras F., Bengueddach A., Millet J.M.M. (2010). *C. R. Chimie* 13, 466–472.
122. Li B., Bai S., Wang P., Yang H., Yang Q., Li C. (2011). *Phys. Chem. Chem. Phys.* 13, 2504–2511.
123. Klinman J.P. (2007). *Acc. Chem. Res.* 40, 325–333.
124. Bezzi G., Helliwell M., Warren J.E., Allan D.R., McKeown N.B. (2010). *Science* 327, 1627–1630.

8

LIQUID PHASE OXIDATION OF ORGANIC COMPOUNDS BY METAL-ORGANIC FRAMEWORKS

YOUNG KYU HWANG, GÉRARD FÉREY, U-HWANG LEE, AND JONG-SAN CHANG*

8.1 INTRODUCTION

Catalytic oxidation is widely used in the manufacture of bulk and fine chemicals from organic hydrocarbons in liquid phase as well as gas phase [1–3]. Liquid phase oxidations generally employ soluble metal salts or complexes in combination with oxidants such as O_2 (or air), H_2O_2, or organic hydroperoxides (RO_2H). However, heterogeneous solid catalysts have also been given some attention in liquid phase oxidations since they have advantages such as facile recovery and recycling, and amenability to continuous operation as compared to their homogeneous counterparts [2]. Incorporation of redox metal ions or complexes into the framework or cavities of zeolites and mesoporous materials can endow a regular microenvironment with uniform pore structures consisting of well-defined cavities and channels of molecular dimensions [3]. Since the success of titanium silicate (TS-1) as a commercial catalyst for versatile oxidations with 30% H_2O_2 in the mid-1980s, very extensive studies have been focused on the development of redox molecular sieves and their catalytic applications in liquid phase oxidations [4]. The rational design of tailor-made nanoporous catalysts that have a resemblance to redox enzymes could be a dream in the field of oxidation catalysis.

*Corresponding author

Liquid Phase Oxidation via Heterogeneous Catalysis: Organic Synthesis and Industrial Applications, First Edition. Edited by Mario G. Clerici and Oxana A. Kholdeeva.
© 2013 John Wiley & Sons, Inc. Published 2013 by John Wiley & Sons, Inc.

Porous Metal-Organic Frameworks (MOFs) are currently an important class of advanced functional materials due to their novel coordination structures, diverse topologies, and potential applications such as gas or liquid adsorption and separation, molecular recognition, drug storage and delivery, and catalysis [5–8]. These MOF solids result from the reaction between organic and inorganic species in order to build up three-dimensional frameworks whose skeleton contains both organic and inorganic moieties only linked by strong bonds, at variance to supramolecular chemistry. The structural nanoporosity and coordination environments of MOF materials place them at the frontier between zeolites and homogeneous organometallic complexes [5, 9]. Moreover, MOFs appear to be excellent candidates for oxidation catalysis because some of their frameworks contain a larger content of reducible metal ions than zeolite frameworks that have typically the low metal content. Although liquid phase oxidation in catalysis is potentially one of the most important applications of MOFs, as was the case in metal-containing microporous zeolites and mesoporous materials, the number of publications is not so large compared with those reported for other sorption applications with MOFs. Many reviews [10–22] have dealt with their unique and outstanding properties including catalytic properties, but some of them have been given to oxidation catalysis with MOFs [14–22]. In this review, we describe the use of MOFs as heterogeneous catalysts for liquid phase oxidations of organic compounds with conventional oxidants such as peroxides and molecular oxygen in most cases and special oxidants such as N-hydroxyphthalimide (NHPI)/oxygen and NaClO in certain cases. We also summarize catalytic properties of MOFs with the aim to understand possible approaches to oxidation catalysis with these materials.

8.2 CHARACTERISTICS AND STRUCTURES

8.2.1 Characteristics

MOFs are solid materials formed by an extended network of metal ions or clusters coordinated to multidentate organic molecules. These solids were first labelled as coordination polymers, but *Metal-Organic Frameworks* has now become the more general term to express such inorganic–organic hybrid framework materials. This definition covers a large variety of materials containing metals and organic molecules having very different characteristics, such as for instance crystalline and amorphous, as well as porous and nonporous solids [5, 9, 23]. Conceptually, there is no difference between classical inorganic porous solids including zeolites and hybrid ones, MOFs. The three-dimensional skeleton of MOF can also be described by the association of secondary building units (SBUs). In the hybrid SBU of MOF, the anionic species of zeolites are replaced by organic linkers, creating the difference of the bonds in the MOF framework from zeolite frameworks: mainly covalent for the organic parts and ionocovalent for the inorganic.

Zeolites are benchmarking materials for the development of MOFs since these are the most successful porous solids in academic research as well as the chemical industry [24]. Due to their high thermal and chemical stability, zeolites have

TABLE 8.1 Comparison Between Structural and Physicochemical Properties of MOFs and Zeolites [15, 22]

Properties	Zeolite	MOFs
Crystallinity	Very good	Very good
Surface area	200–700 m^2/g	500–10 000 m^2/g
Pore volume	0.1–0.5 cm^3/g	0.3–3.0 cm^3/g
Pore diameter	< 2 nm	< 10 nm
Thermal stability	Mostly stable above 400 °C	Unstable above 400 °C
Chemical stability	Strong in acid and solvents	Sensitive in moisture and chemicals
Metal site density	Few%	Dozens of percent of metal sites
Type of active site	Limited	Not limited
Lewis acidity	Metal sites in framework	Coordinatively unsaturated metal sites
Diffusivity	Low	Low to medium

become a good candidate of materials that can be used in catalysis under harsh conditions. These are crystalline aluminosilicates with an ordered framework structure built by corner sharing SiO_4 and AlO_4 units in different fractions, but with a Si/Al ratio greater than one. Zeolites are unique compared to other crystalline inorganic oxide materials because they have the following properties: the microporous character with uniform pore dimensions, molecular sieve character or shape selective control allowing certain molecules to enter the crystals while rejecting others based on too large a molecular size, the ion-exchange properties, internal acidity, and high thermal stability [25, 26]. However, their pore opening, usually below 1 nm, provides distinct limits in their catalytic applications where the substrates are relatively large such as in liquid phase transformations [26].

Table 8.1 summarizes similarity and difference in structural and physicochemical properties of MOFs and zeolites. Zeolites and MOFs have an inherent geometric regularity in their structures, different from mesoporous silicates and aluminosilicates that are usually not crystalline [27]. The regularity of their structures can lead to a homogeneous distribution of the active sites in both MOFs and zeolites. Aluminosilicate zeolites generally require the use of inorganic or organic templates (amines, quaternary ammoniums, etc.) beside the components of the skeleton and the solvent during the crystallization. In the crystallization of MOFs, the solvent itself acts as the main template, so that the skeleton of most of the MOFs is neutral [5, 22]. In MOFs, the solvents have weaker interactions with the framework and therefore easily evolve the pore structure at low temperature, often keeping the framework intact and providing very quickly an important and readily accessible porosity. Moreover, the existence of inorganic and organic moieties in the structure allows hydrophilic and hydrophobic parts to coexist within the pores and may have some influence on the adsorption properties.

MOFs actually bridge the gap between zeolites and mesoporous materials, because MOF pore systems range from ultramicropore to mesopore. Unique features of MOFs also include exceptionally high porosities, with regular pores and world-record surface areas, well-defined crystalline structures, the lack of

nonaccessible bulk volume, designable channel surface functionalities, framework flexibility, and flexible dynamic behaviors in response to guest molecules. The wide abundant choice of structure that facilitates pore-size tunability would be a great opportunity for the design of MOFs with pore openings suitable for generating size and shape selectivity. However, MOFs still have several issues to be solved, for example, thermal, hydrothermal and chemical stability as well as high material costs due to the use of organic linkers that are not commercially available from industry.

8.2.2 Structures

In this section, we describe briefly the structural characteristics of selected MOFs that have been mainly utilized for liquid phase oxidations (Table 8.2, Figures 8.1 to 8.5).

The present authors have developed the trivalent metal carboxylate systems [28–32] including the chromium(III) terephthalate and iron(III) trimesate with giant pores labeled MIL-101(Cr) and MIL-100(Fe), respectively (MIL for Materials of Institut Lavoisier). In the usual classification of porous solids, MIL-100 and MIL-101 structures represented the first examples of perfectly crystallized mesoporous solids, which are the two largest nonproteinic structures ever devised [28–32]. These materials are very useful for catalyst and catalyst support in liquid phase oxidations, as illustrated at the next section. These two solids are basically built up from trimers of trivalent metal(III) octahedra with terminal (H_2O and F^-/OH^-) ligands. Their linkages to the rigid carboxylate ligands (terephthalate or trimesate) generate microporous supertetrahedral units (Figure 8.1). The connection of these

TABLE 8.2 Selected MOF Candidates Used as Catalysts or Catalyst Supports for Liquid Phase Oxidation Reactions [14]

MOF[a]	Material name	Metal coordination	Dimension[b] (Pore/Inorg.)	Cavity size [Å]	BET Surface area [m^2/g]	Ref.
$[Cu_3(BTC)_2]$	HKUST-1	$\{Cu_2O_4\}$	3D/0D	9, 5, 3.5 (pore size)	692–1600	33
[V(OH)(BDC)]	MIL-47	$\{VO_6\}$	1D/1D	10.5×11	930	36
$[M_2(DHTP)]$ (M=Zn, Ni, Co)	CPO-27	$\{MO_6\}$	1D/1D	11	1083 (Langmuir)	34
$[Zr_6O_4(OH)_4(CO_2)_{12}]$	UiO-66	$\{Zr_6O_6O_{24}\}$	3D/0D	6	1187 (Langmuir)	37
$[Fe_3XO(BTC)_2]$ X=F, OH	MIL-100	$\{FeO_7X\}$	3D/0D	25, 29	2100 ±200	32
$[Cr_3XO(BDC)_3]$ X=F, OH	MIL-101	$\{CrO_7X\}$	3D/0D	29, 34	4100 ±200	31
$[Zn_2(DHBDC)]$	MOF-74	$\{ZnO_6\}$	1D/1D	5.5×10.3	264	35

[a]Coordinated solvent or H_2O molecules are omitted. BTC = 1,3,5-benzenetricarboxylate, BDC: 1,4-bezenedicarboxylate, DHTP: 2,5-dihydroxyterephthalate, DHBDC: 2,5-dihydroxybenzenedicarboxylate.
[b]Dimensionality of the porous structure and of the inorganic part (following Férey's classification [5]).

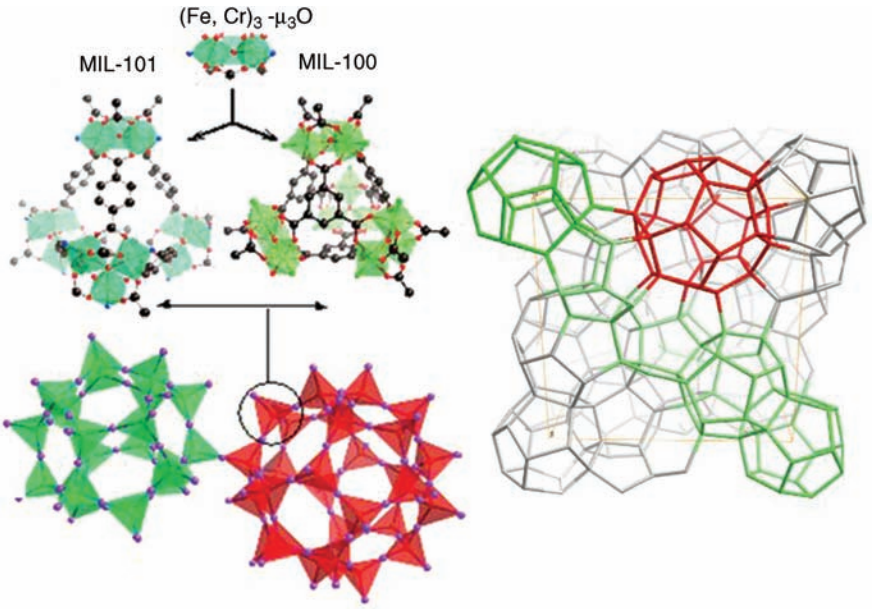


FIGURE 8.1 Evolution of supercages of mesoporous MIL-100(Fe) and MIL-101(Cr) from μ-oxo-bridged octahedral metal(III) trimer and ligands [28, 32].

motifs provides an augmented version of the 3D MTN zeolite topology. The resulting cubic cell volumes are huge (380 000 Å^3 and 702 000 Å^3), with two types of mesoporous cages limited by pentagonal faces for the smaller and by pentagonal and hexagonal faces for the larger. The free internal diameters are close to 25 and 29 Å (MIL-100) and 29 and 34 Å (MIL-101). The cages are accessible through microporous windows of 5.5 and 8.6 Å (MIL-100) and 12 and 16 Å (MIL-101). These MOF solids exhibit several unprecedented features: a mesoporous zeotype architecture with a MTN topology, a giant cell volume (702 000 Å^3 for MIL-101 and 380 000 Å^3 for MIL-100), a large free aperture (*ca.* 12 Å and *ca.* 16 Å $\times$ 14.5 Å for MIL-101; *ca.* 4.7 $\times$ 5.5 Å and *ca.* 8.6 Å for MIL-100), mesoporous cages (29 Å and 34 Å for MIL-101; 25 Å and 29 Å for MIL-100), huge BET surface areas ($4100 \pm 200\,m^2\,g^{-1}$ for MIL-101 and $2100 \pm 200\,m^2\,g^{-1}$ for MIL-100), and numerous unsaturated chromium or iron sites (up to theoretically *ca.* 3.0 mmol/g) [28–32].

HKUST-1 (or Cu-BTC) is one of the most studied MOFs to date. The structure is built up from $Cu_2(COO)_4$ paddle wheels with copper dimers as four connectors bound to the oxygen of four BTC linkers as three connectors to create the assembly of $[Cu_3(BTC)_2(H_2O)_3]$ [33] (Figure 8.2). This material presents a bimodal distribution of pores: a large central pore from a square cross section with a diameter of 9.0 Å surrounded by tetrahedral side pockets with a diameter of 5.0 Å. Pores and pockets are interconnected by triangular windows with a diameter of 3.5 Å [33].

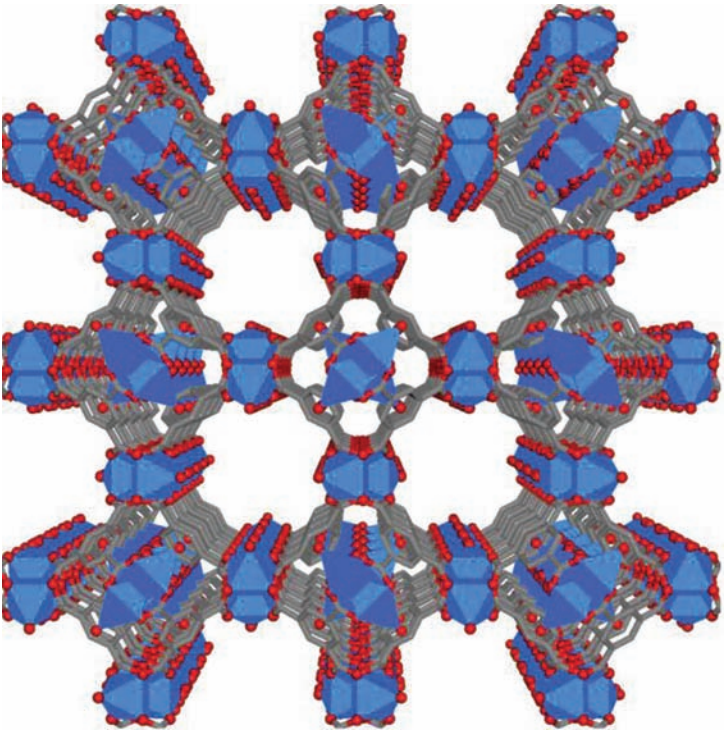


FIGURE 8.2 A polyhedral view of HKUST-1, $[Cu_3(BTC)_2(H_2O)_3]$ down the [100] direction, showing pore decorated with unsaturated copper sites. Reprinted with permission from Shoaee M., Anderson M.W., Attfield M.P. *Angew. Chem. Int. Ed.* 2008, *47*, 8525–8528. Copyright 2008 Wiley-VCH Verlag GmbH & Co. KGaA, Weinheim.

The crystal structures of $[M_2(DHTP)(H_2O)_2]\cdot 8H_2O$ (DHTP = 2,5-dihydroxyterephthalate), CPO-27(M) (M = Zn^{2+}, Ni^{2+}, Co^{2+}) and $Zn_2(DHBDC)(H_2O)_2(H_2O)_{0.5}(C_2H_5OH)_{1.5}$ (DHBDC = 2,5-dihydroxybenzenedicarboxylate), MOF-74(Zn) resemble a honeycomb, as illustrated in Figure 8.3 [34, 35]. All of these MOFs contain the same microporous honeycomb analogous framework [34], which contains solvent molecules coordinating the metal. However, the CPO-27(M) differs from MOF-74 in the type of solvent included in the pores. The intersections of the honeycomb are formed by one-dimensional helical chains of *cis*-edge-connected metal-oxygen coordination octahedra. Adjacent chains are linked by the organic ligand forming the honeycomb, the channels of which have an effective diameter of approximately 11 Å. The inversion center present in the organic linker results in opposite handedness of the neighboring metal-oxygen chains. In the solvated state, the metal atom is coordinated by one water molecule, with the remaining coordination sites being occupied by oxygen atoms belonging to the organic linker. The solutions of the structure at 100 and 150 °C confirmed the presence of a coordinatively unsaturated metal site in the dehydrated structure in analogy to CPO-27(Co) and CPO-27(Ni).

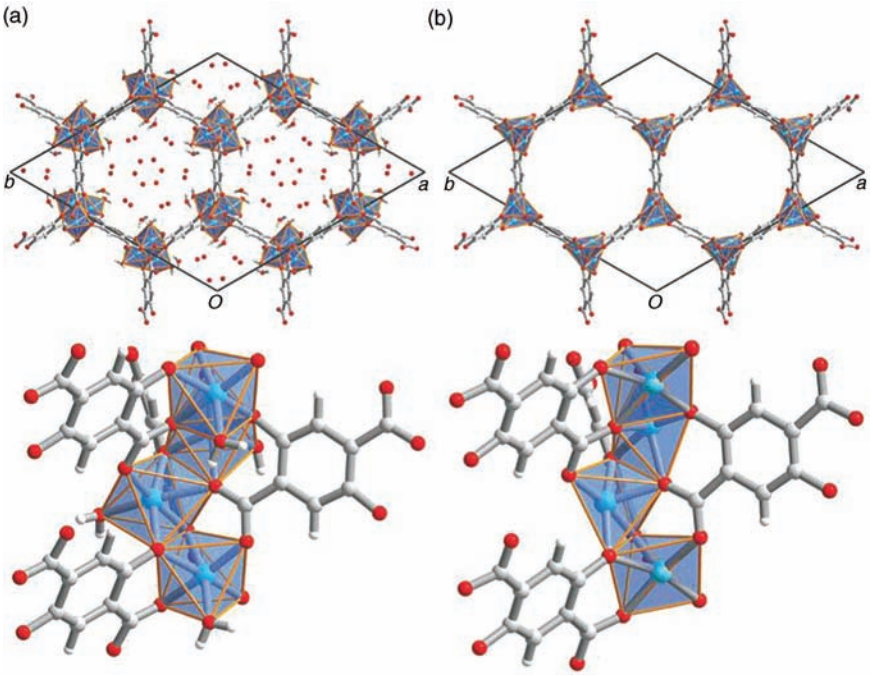


FIGURE 8.3 (a) Unit cell of the crystal structure of the hydrated CPO-27(Zn) (CPO-27 (Co) is isostructural) along [001] showing the honeycomb topology and one-dimensional solvent-filled channels (top) [34]. Three-fold helical chain of *cis*-edge-connected metal–oxygen octahedra in the hydrated structure (bottom). (b) Unit cell of the crystal structure of the dehydrated framework at 150 °C along [001] (top) and square pyramidal coordination of the zinc cation in the chains with an unoccupied sixth coordination site pointing towards the cavity (bottom). Reprinted with permission from *Chemistry - A European Journal.* Copyright 2008 Wiley-VCH Verlag GmbH & Co. KGaA, Weinheim.

The structure of MIL-47 with a framework of stoichiometry VO(BDC) has a 3D metal-organic framework with a 1D diamond-shape channels of around 0.85 nm [35, 36]. The SBU of MIL-47 consists of infinite $(\text{-O-V-})_\infty$ rods (Figure 8.4) with carboxylate O atoms completing octahedral coordination around V to result in an infinite rod of VO_6 octahedra sharing opposite corners. The carboxylate C atoms are at the vertices of a zigzag ladder SBU.

UiO-66(Zr), $Zr_6O_4(OH)_4(CO_2)_{12}$, with 12 coordination is the highest coordination MOF [37] so far reported in the literature. The structure of UiO-66(Zr) consists of an inner $Zr_6O_4(OH)_4$ core in which the triangular faces of the Zr_6-octahedron are alternatively capped by μ_3-O and μ_3-OH groups (Figure 8.5). All of the polyhedron edges are bridged by carboxylates ($\text{-}CO_2$) originating from the dicarboxylic acids forming a $Zr_6O_4(OH)_4(CO_2)_{12}$ cluster. Each zirconium atom is eight-coordinated forming a square-antiprismatic coordination consisting of eight oxygen atoms. One square face is formed by oxygen atoms supplied by carboxylates, while the second square face is formed by oxygen atoms coming from the μ_3-O and μ_3-OH groups.

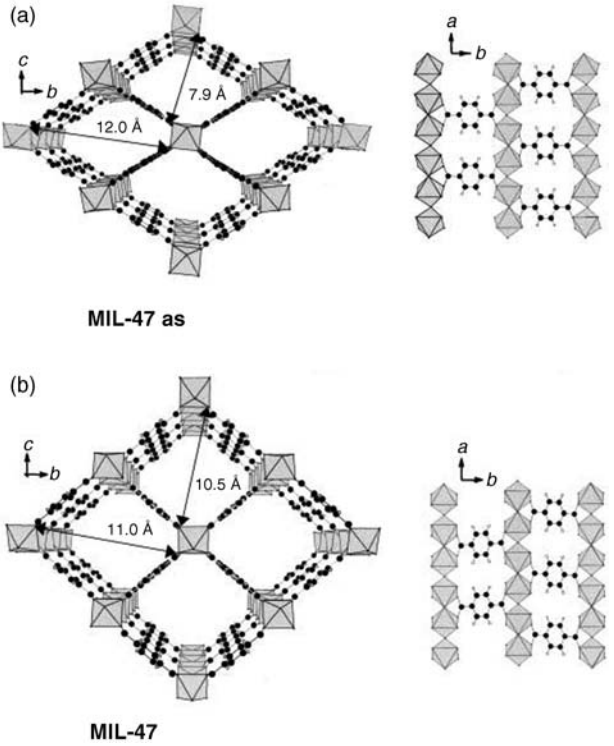


FIGURE 8.4 Projections of the structures of MIL-47 as-synthesized (a) and of MIL-47 desolvated (b) Guest atoms in MIL-47as are omitted for clarity [36]. Reprinted with permission from *Angewandte Chemie International Edition.* Copyright 2002 Wiley-VCH Verlag GmbH & Co. KGaA, Weinheim.

8.2.3 Syntheses

Most syntheses of MOFs are generally performed by solvothermal or hydrothermal process at relatively low temperature ($< 250\,^{\circ}C$) under autogeneous pressure *via* a cooperative ionic interaction between organic linkers containing polycarboxylate anions and inorganic cations constructing the skeleton of crystalline frameworks together with solvent as a template [5, 22]. In a typical synthesis of MOF, almost all of the di-, tri- or tetravalent cations can be used as inorganic metal precursors. The metal source is usually a salt selected from halides, nitrates, perchlorates or hydroxides but can also be a metal itself that is further oxidized by oxidizing agent such as nitric or perchloric acid. As an organic linker, organic components such as mono, di-, tri- and tetracarboxylic acids can be used in solvents. The main solvents include an amine (typically trialkylamine or pyridine) or amide (dimethylformamide and diethylformamide) in solvothermal synthesis beside water in hydrothermal synthesis. Their syntheses can be performed in an open vessel including

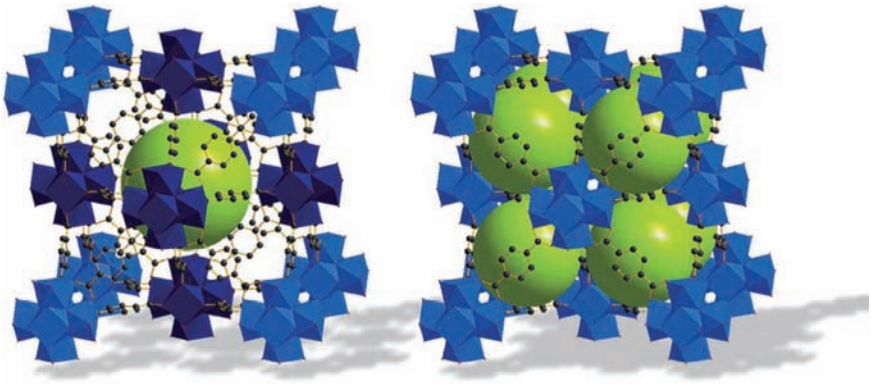


FIGURE 8.5 Schematic illustration of the UiO-66 structure that is based on Zr-MOF with 1,4-benzene-dicarboxylate as linker: left octahedral cages, right tetrahedral cages. Reprinted with permission from Wiersum A.D., Soubeyrand-Lenoir E., Yang Q., Moulin B., Guillerm V., Yahia M.B., Bourrelly S., Vimont A., Miller S., Vagner C., Daturi M., Clet G., Serre C., Maurin G., Llewellyn P.L. *Chem. Asian J.* 2011, *6,* 3270–3280. Copyright 2011 Wiley-VCH Verlag GmbH & Co. KGaA, Weinheim.

reflux condition or in a closed vessel above the boiling temperature of the selected solvent(s). The main parameters of the MOF synthesis are pH, concentrations and temperature.

Solvothermal synthesis is the most popular and classical method in the synthesis of MOFs. BASF SE has also utilized the solvothermal method for the large scale production of MOFs such as aluminum terephthalate MIL-53, copper trimesate HKUST-1 and magnesium formate [7, 28] In their solvothermal syntheses, well-soluble metal salts, benzene di- or tricarboxylic acids are mixed in a polar organic solvent such as dimethylformamide (DMF) or diethylformamide (DEF). Then, the metal-organic structures of MOFs are formed by a self-assembly pathway at temperatures starting at room temperature and up to solvothermal conditions at 200 °C within a few hours.

Hydrothermal syntheses of MOFs have been well applied to the syntheses of MILs such as MIL-101, MIL-100, and MIL-53 [31, 32, 39]. Mesoporous chromium (III) terephthalate MIL-101(Cr) was initially prepared from hydrothermal reaction of terephthalic acid with $Cr(NO_3)_3{\cdot}9H_2O$, HF, and H_2O at 220 °C for 8 h. This reaction produced a highly crystallized green powder of the chromium terephthalate with formula $Cr_3F(H_2O)_2O[(O_2C)\text{-}C_6H_4\text{-}(CO_2)]_3{\cdot}nH_2O$ (where n is < 25), based on chemical analysis. Mesoporous iron(III) trimesate MIL-100(Fe) was prepared from hydrothermal reaction of trimesic acid with metallic iron, HF, nitric acid and H_2O. The typical composition of a reaction mixture is 1.0 Fe : 0.67 1,3,5-BTC : 2.0 HF : 0.6 HNO_3 : 277 H_2O (1,3,5-BTC = 1,3,5-benzenetricarboxylic acid or trimesic acid). The reactant mixture was loaded in a Teflon autoclave. The autoclave was heated up to the reaction temperature and kept at 150 °C for 12 h.

Besides these classical methods mentioned above, new routes are currently being developed for the synthesis of MOFs. The BASF SE has recently succeeded in the large scale production of several selected MOFs by an electrochemical method as an alternative salt-free procedure [10, 38]. Bulk metal sacrificial plates as the anodes are oxidized in an electrochemical cell in the presence of carboxylates dissolved in solvent (methanol for copper trimesate HKUST-1), as proposed in the literature reported by BASF researchers [38]. After a certain period of time, colorful precipitates with crystalline MOF structures are formed. This method yields final MOF powder by simple recovery of the as-synthesized solid by filtration and subsequent drying. The formation of copper trimesate, iron trimesate (Basolite F300, Fe-EMOF), and zinc 2-methylimidazolite (Basolite Z1200, Zn-EZIF) has been proved by this method [10].

The microwave method has already attracted growing attention for the synthesis of nanoporous inorganic materials that normally require several days for their hydrothermal crystallization. It provides an efficient way to synthesize them with short crystallization times, narrow particle-size distributions, facile morphology control, and efficient evaluation of process parameters, etc. The present authors have first shown that the microwave syntheses offer several advantages such as fast crystallization as well as phase-selective synthesis. MOF solids with giant pores, chromium trimesate and terephthalate (MIL-100 and MIL-101), have been formed under microwave irradiation after less than 1 h at 220 °C, instead of 96 h using the conventional route [40, 41].

Another important point in the synthesis of MOFs is purification or activation. Pure crystalline materials with high porosity and surface areas are critically essential in terms of chemical and physical properties and of applications such as separation and catalysis [31, 42]. During the filtering and drying of MOFs in wet processing techniques, there are many unreacted precursors and ligands remaining in the pores of MOFs. Therefore, careful activation processes are needed for formation of high purity and high surface area MOFs. Several purification and activation methods in MOFs have been reported [31, 42–44], but the effect of the product quality of MOFs on catalytic activities and selectivities in oxidation catalysis has not been systematically studied yet.

8.2.4 Active Sites

Table 8.2 lists selected MOFs that are potential candidates of catalyst or catalyst support, along with a description of their porous structures, dimensionality and pore sizes. These MOFs have been reported to be active and selective for a wide range of reactions such as acid–base catalysis, hydrogenation, alcoholysis, alkoxylation, and C−C coupling reaction [10, 11, 15, 16]. Besides these reactions, they could also be utilized for several types of liquid phase oxidations, as illustrated in Tables 8.3 to 8.7.

For liquid phase oxidations, we could categorize four classes of MOF catalysts: (a) catalytic metal centers at the inorganic nodes of the SBUs (for framework catalysis), (b) homochiral MOFs, (c) metal complexes incorporated into

supramolecular porous frameworks, and (d) active components (metal complexes, highly dispersed metal or metal oxide nanoparticles) encapsulated in pores of MOFs. The inorganic nodes in the catalyst type (a) include metal ions, metal clusters or coordinatively unsaturated metal (CUM) centers from SBUs. The types of catalytically active sites in MOFs have already been proposed by several groups [5, 11, 15, 16]. The present classification is not so different from these categories.

Many examples for heterogeneous catalysis of oxidations with MOFs belong to framework catalysis by the use of CUM sites from SBUs that can be classified into the catalyst type (a) even though the metal ion and the ligand are usually selected as the building blocks rather than as catalysts. Several examples in framework catalysis may have been achieved by CUM centers in MOFs although they have not been clearly mentioned in many cases. As mentioned above, the crystalline chromium terephthalate MIL-101(Cr) and iron(III) trimesate MIL-100(Fe) are commonly built up from hybrid supertetrahedral units, made from μ_3-oxo-centered trimers of metal (III) octahedral clusters and rigid carboxylate ligands, terephthalate ligands for MIL-101(Cr) and trimesate ligands for MIL-100(Fe). In the as-synthesized forms (Figure 8.6), the oxo-centered octahedral metal trimers possess three terminal molecules with two neutral ligands (H_2O) and one anionic ligand (F^- or OH^-). As shown from IR studies on MIL-100 and MIL-101 [32, 45], terminal water molecules are removable from the framework by heating above 100 °C under vacuum or a gas stream, leading to a large number of CUM Cr(III) or Fe(III) sites [30–32, 46, 47]. These CUM can provide accessible sites for guest molecules, therefore acting as Lewis acid sites or catalytically active sites in the pores. For example, the CUM Cr(III) sites in MIL-101(Cr) have been used as the catalyst type (a) for oxidation of tetralin [48, 49], α-pinene and limonene [50, 51], and selective sulfoxidation of aromatic sulfides [46]. In copper trimesate HKUST-1, copper dimers as $Cu_2(COO)_4$ paddle wheels play a role as coordinatively unsaturated redox Cu(II) sites after dehydration. These Cu(II) sites were also used as the active catalyst for the

TABLE 8.3 Summary on Oxidation of Cycloalkanes with MOFs

Catalyst	Active Site	Substrate	Products	Oxidant	Ref.
$[Cu_3(H_2tea)_2(4\text{-}OC_6H_4COO)_2(H_2O)]\cdot 4H_2O$	Cu_3 trimer	Cyclohexane	Cyclohexanol/one	H_2O_2	64
$[Cu_3(\mu_3\text{-}OH)(\mu\text{-}PZ)_3(EtCO_2)_2(H_2O)]$	Cu_3 trimer	Cyclohexane	Cyclohexanol/one	H_2O_2	62
		Cyclopentane	Cyclopentanol/one	H_2O_2	
$[InN_4(CO_2)_4][H_2TMPyP]$	Mn-porphyrin	Cyclohexane	Cyclohexanol/one	TBHP	63
$[Cu_6(H_2tea)_6Fe(CN)_6]_n(NO_3)_2]_n$ and $[Cu_6(Hmdea)_6Fe(CN)_6]_n(NO_3)_2]_n$	Cu + Fe	Cyclohexane	Cyclohexanol/one	H_2O_2	65
FeBTC	Fe	Cyclooctane	Cyclooctanol/one	O_2/NHPI	61

H_2tea: triethanolamine, PZ: pyrazole, Hmdea: N-methyldiethanolamine, H_2TMPyP: 5,10,15,20-tetrakis(1-methyl-4-pyridinio)porphyrin, TBHP: *tert*-butyl hydroperoxide, NHPI: N-hydroxyphthalimide.

TABLE 8.4 Summary on Oxidation of Aromatics with MOFs

Catalyst	Active Site	Substrate	Products	Oxidant	Ref.
$[Fe_3F(H_2O)_2O(BTC)_2]$ (MIL-100)	Fe_3 trimer	Diphenylmethane Triphenylmethane	Benzophenone Triphenylmethanol	TBHP	69
FeBTC or $[Cu_3(BTC)_2]$ (HKUST-1)	Fe or Cu_2 dimer	Xanthene	Xanthone	TBHP	52
$[Cu^{II}(BPED)_2(H_2O)_2(SiF_6)]$ and $[Cu^{II}(BPED)_2(H_2O)_2(NO_3)]$	Cu	Tetralin	1-Tetralone 1,4-Naphthoquinone	TBHP	68
$\{[Cu_2(4,4\text{-BIPY})_4(H_2O)_4]\text{-}(SiW_{12}O_{40})(H_2O)_{18}\}_n$	$Cu + SiW_{12}O_{40}$	Ethylbenzene 1-Phenylethanol	Acetophenone	TBHP	71
$[Cr_3F(H_2O)_2O(BDC)_3]$ (MIL-101-Monolith)	Cr_3 trimer	Tetralin	Tetralone	TBHP	49
$[Cr_3F(H_2O)_2O(BDC)_3]$ (MIL-101)	Cr_3 trimer	Tetralin	1-Tetralone	TBHP	48
FDMS@$[Al(OH)BDC]_n$ (MIL-53)	FeCp	Benzene	Phenol	H_2O_2	72
[Cu(2-hydroxypyrimidinolate)$_2$] [Co(phenylimidazolate)$_2$]	Cu Co	Tetralin	Tetralone Tetralol	Air	73
$MPcF_{16}$@$[Cr_3F(H_2O)_2O(BDC)_3]$ (MIL-101)	$MPcF_{16}$	Tetralin	Tetralone	O_2	70

BPED: meso-1,2-bis(4-pyridyl)-1,2-ethanediol, BIPY: 2,2-bipyridine, FDMS: 1,1′-ferrocenediyl-dimethylsilane, $MPcF_{16}$: metal phthalocyanine perflorinated complexes (M = Fe, Ru).

TABLE 8.5 Summary on Oxidation of Olefins with MOFs

Catalyst	Active Site	Reactant	Products	Oxidant	Ref.
[VO(BDC)] (MIL-47)	V	Cyclohexene	Cyclohexene oxide	TBHP	79
$NH_4[Cu_3\text{-}(\mu_3\text{-}4\text{-carboxypyrazolato})_3]$	Cu	Cyclohexene	Cyclohexenone	TBHP	80
$[Co_4O(BDPB)_3]$ (MFU-1)	Co_4O	Cyclohexene	*tert*-butyl-2-cyclohexenyl -1-peroxide	TBHP	74
$[Cu(H_2BTEC)(BIPY)]$	Cu	Cyclohexene Styrene	Cyclohexene oxide Styrene oxide	TBHP	81
$[Cr_3F(H_2O)_2O(BDC)_3]$ (MIL-101)	Cr_3 trimer	Cyclohexene α-Pinene Limonene	Cyclohexenone Verbenone Carvone	TBHP	51
M-POM/$[Cr_3F(H_2O)_2O(BDC)_3]$, (M-POM/MIL-101, M = Ti, Co)	Co-POM Ti-POM	α-Pinene	Verbenol, verbenone	O_2 H_2O_2	60
$PW_x/[Cr_3F(H_2O)_2O(BDC)_3]$ (PW_x/MIL-101, $x = 4$ or 12)	PW_x	Cyclohexene	Cyclohexene oxide	H_2O_2	59
$[Ni_2(DHTP)(H_2O)_2]$ (CPO-27)	Ni_2	Cyclohexene	Cyclohexene oxide Cyclohexenol	H_2O_2	82
$[Cd_{1.25}Pd\text{-}H_{1.5}TCPP(H_2O)]$	Pd-porphyrin	Styrene	Acetophenone	$H_2O_2/HClO_4$	57
FeBTC	Fe	Styrene	Styrene epoxide Benzaldehyde	O_2/NHPI	83
$[Cu(BPY)(H_2O)_2(BF_4)_2(BPY)]$	Cu	Cyclohexene	Cyclohexene epoxide Hydroperoxide	O_2	84

(*continued*)

TABLE 8.5 (Continued)

Catalyst	Active Site	Reactant	Products	Oxidant	Ref.
$[Ni_3(bpdc)(RR\text{-}L)_2\cdot(DMF)]_n$	Metallocomplex (salen)Ni	Styrene	Syrene epoxide	NaClO TBHP	55
$Zn_2(bpdc)_2\mathbf{L}\cdot 10DMF\cdot 8H_2O$	(salen)Mn	2,2-dimethyl-2*H*-chromene	2,2-dimethyl-2*H*-chromene epoxide	TBSIB	76
[bis(catechol)salen]$Mn^{III}Cl$] (Poly(Cu-1))	(salen)Mn	2,2-dimethyl-2*H*-chromene	2,2-dimethyl-2*H*-chromene epoxide	TBSIB	77
Mn(acac)@IRMOF-3	Mn(acac)	Cyclohexene Cyclooctene Styrene	Cyclohexene epoxide Cyclooctene epoxide Styrene epoxide	O_2/TMA	75

BDPB: 1,4-bis[(3,5-dimethyl)pyrazol-4-yl]-benzene, BTEC:1,2,4,5-benzenetetracarboxylic acid, BIPY: 2,2-bipyridine, POM: polyoxometalates, DHTP: dihydroxyterephtalate, TCPP:5,10,15,20-tetra(carboxyphenyl)metalporphyrin, bpy: 4,4′-bipyridine, RR-L:(R,R)-(-)-1,2-cyclohexanediamino-N,N0-bis(3-tert-butyl-5-(4-pyridyl) salicylidene), bpdc: 2,2′-Bipyridyl-3,3′-dicarboxylate, DMF: N,N-Dimethylformamide, L1 and L2: 1,2,4,5-tetrakis(4-carboxyphenyl) benzene and 5,15-dipyridyl-10,20-bis(pentafluorophenyl)-Porphyrin, Mn(acac): Mn(II) acetylacetonate, TBSIB: 2-(*tert*-butylsulfonyl)iodosylbenzene, TMA: trimethylacetaldehyde.

TABLE 8.6 Summary on Oxidation of Alcohols and Phenols with MOFs

Catalyst	Active Site	Substrate	Products	Oxidant	Ref.
FePcS/$[Cr_3F(H_2O)_2O(BDC)_3]$	FePcS	Benzyl alcohol 2,3,6-trimethylphenol 8-Hydroxyquinoline	Benzaldehyde trimethyl-*p*-benzoquinone Quinoline-5,8-dione	TBHP	58
$[Fe_2(dhtp)(H_2O)_2]$ (MOF-74)	Fe	Phenol	Catechol Hydroquinone	H_2O_2	89
Cu_2(*trans*-1,4-Cy)	Cu_2 dimer	2-Propanol Cyclohexanol Benzyl alcohol 1-Octanol	Acetone Cyclohexanone Benzaldehyde 1-Octanal	H_2O_2	90
Pt/$[Zn_4O(BDC)_3]$ (MOF-5)	Pt	Vanillyl alcohol Piperonyl alcohol	Vanillin Piperonal	O_2	91
Au or Au/ZnO@$[Zn_4O(BDC)_3]$	Au	Benzyl alcohol	Methyl benzoate	O_2/base	92
$[Cu_3(BTC)_2]$ (HKUST-1)	Cu_2 dimer	Benzylic alcohols	Benzylic aldehydes	O_2/TEMPO	53
Au/$[Cr_3F(H_2O)_2O$ $(BDC)_3]$ (Au/MIL-101)	Au	Benzylic alcohols	Benzylic aldehydes Benzylic ketones	O_2	85
$Pd(O_2CCF_3)_2[O_2C–C_5H_3N–C_5H_3N–CO_2]Cu$	Pd complex	1-Phenylethanol	Acetophenone	O_2	88
$[M_3(BTC)_2]$, M=Cu,Co, Ni	Cu, Co, Ni	Hydroquinone	*p*-benzoquinone	O_2/H_2O_2	93
Pt@$[Zn_4O(btb)_2]_8$ (Pt@MOF-177)	Pt	Benzylic alcohols	Benzylic aldehydes	O_2	94
Au/$[Zn_4O(BDC)_3]$ (Au/MOF-5) Au//$[Cu_2(PZDC)_2(PYZ)]$ (Au/CPL-2)	Au	Benzyl alcohol	Benzaldehyde	O_2	95
$[Pd(2\text{-pymo})_2]_n$	Pd	Cinnamyl alcohol	Cinnamylaldehyde	Air	96

FePcS: iron tetrasulfophthalocyanine, dhtp: dihydroxyterephtalate, btb: 1,3,5-benzene-tri-benzoic acid, PZDC: pyrazine-2,3-dicarboxylate, PYZ: pyrazine, 2-pymo: 2-hydroxypyrimidinolate.

TABLE 8.7 Summary on Oxidation of S- or N-containing Compounds with MOFs

Catalyst	Active Site	Substrate	Products	Oxidant	Ref.
$[Zn_2(BDC)(L\text{-lac})(DMF)]$	Zn	Thioethers	Sulfoxides	H_2O_2/UHP	97
$[Sc_2(C_8H_4O_4)_3]$	Sc	Methyl phenyl sulfide	Methyl phenyl sulfoxide	H_2O_2	98
$Sc_2(NDS)(OH)_4$	Sc	Methyl phenyl sulfide	Methyl phenyl sulfoxide	H_2O_2	99
$[Cr_3F(H_2O)_2O(BDC)_3]$, (MIL-101)	Cr	Diphenyl sulfide	Diphenyl sulfoxide	H_2O_2	46
[Yb(OH)(2,6-AQDS)(H_2O)]	Yb	Methyl phenyl sulfide	Methyl phenyl sulfoxide	H_2O_2	100
$In_2(OH)_3(BDC)_{1.5}$	In	Methyl phenyl sulfide (2-Ethylbutyl)phenyl sulfide	Methyl phenyl sulfoxide (2-Ethylbutyl)phenyl sulfoxide	H_2O_2	101
FeBTC	Fe	Thiophenol 1,5-Pentanedithiol	Diphenyldisulfide Cyclic sulfide and disulfide	O_2	102
FeBTC	Fe	Benzylamine	Benzyl imines	O_2/NHPI	103
$[Fe_3F(H_2O)_2O(BTC)_2]$ (MIL-100)	Fe_3 trimer	Thiophenol	Diphenyldisulfide	O_2	104

L-lac: L-lactic acid, NDS: naphthalene disulfonate, UHP: urea hydroperoxide, NDS: naphthalenedisulfonate, 2,6-AQDS: anthraquinone-2,6-disulfonate, NHPI: N-hydroxyphthalimide.

oxidation of xanthene to xanthone and benzyl alcohol to benzaldehyde with good selectivity [52, 53].

Homochiral MOFs could behave as heterogeneous enzymatic catalysts, which are attractive candidates as heterogeneous asymmetric catalysts in liquid phase oxidations. To date, only a few groups have provided preliminary

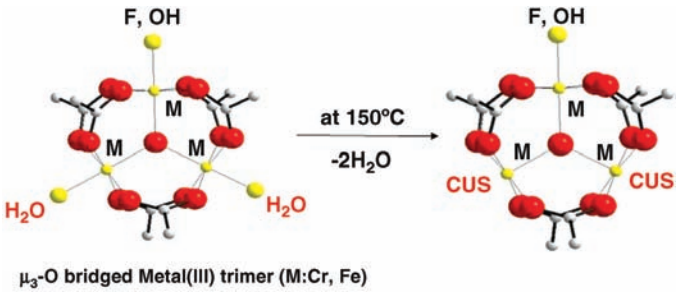


FIGURE 8.6 Formation of coordinatively unsaturated metal sites (CUS) as active sites in mesoporous MIL-100(Fe) and MIL-101(Cr) [31, 32].

evidence for the potential utility of homochiral MOFs in asymmetric catalysis, especially epoxidation of olefins [54, 55]. As the earliest example, it has been reported for Mn(III) phorphyrincarboxylate framework, which catalyzes the asymmetric epoxidation of olefins [54]. A recent example is one-dimensional (1D) homochiral nickel-based MOF $[Ni_3(bpdc)(RR\text{-}L)_2\cdot(DMF)]_n$ (2R, RR-L = (R,R)-(−)-1,2-cyclohexanediamino-N,N′-bis(3-tert-butyl-5-(4-pyridyl)salicylidene), bpdc = 4,4′-biphenyldicarboxylic acid) and $[Ni_3(bpdc)(SS\text{-}L)_2\cdot(DMF)]_n$ (2S, SS-L = (S,S)-(−)-1,2-cyclohexanediamino-N,N′-bis(3-tert-butyl-5-(4-pyridyl)salicylidene)) based on enantiopure pyridyl-functionalized salen (Ni) metalloligand units NiL [55]. Another good example of the homochiral MOF is a family of isoreticular chiral metal-organic frameworks (CMOFs) with the primitive cubic network topology, constructed from $[Zn_4(\mu_4\text{-}O)(O_2CR)_3]$ secondary building units and systematically elongated dicarboxylate struts that are derived from chiral Mn-Salen catalytic subunits (R) [54].

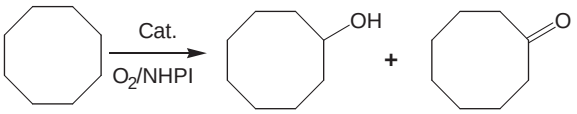
Given that inorganic porous materials that contain metal complexes introduced in their porous cavities take advantage of heterogeneous catalysts, there are two ways to include metal complexes in MOFs; one is the insertion into the framework and the other is the encapsulation inside pores. The catalyst type (c) includes an approach to encapsulate metal complexes into MOFs through supramolecular self-assembly [5, 22]. A few authors have recently illustrated this strategy [5, 11]. For instance, Qiu et al. [56] have tried to immobilize the metal complex $[Mn(phen)_2(H_2O)_2]^{2+}$ into supramolecular frameworks through hydrogen bonding and π–π interactions. The resulting supramolecular frameworks showed size- and shape-selective catalytic activity in the oxidation of phenols with H_2O_2 to form dihydroxybenzenes. A functional MOF $[Cd_{1.25}Pd\text{-}H_{1.5}TCPP(H_2O)]$ assembled from Pd-porphyrin (TCPP = tetra(4-carboxyphenyl)porphyrin) building blocks and Cd(II) connecting nodes also presented an interesting catalytic property for the selective oxidation of styrene [57].

Encapsulation of active components inside porous MOF host lattices by noncovalent interaction is another way of integration of dual functions derived from encapsulated components and MOFs. This approach has already been widely utilized for the heterogenization of metal complexes using zeolites and mesoporous materials as porous hosts [23, 24]. Kholdeeva and coworkers proposed a hybrid material FePcS (iron tetrasulfophthalocyanine)/MIL-101 that has been prepared by irreversible insertion of FePcS to mesoporous cages of MIL-101 [58]. This catalyst showed a superior catalytic performance in the selective oxidation of aromatic substrates with TBHP than homogeneous FePcS. Another interesting example is hybrid materials that have been prepared by encapsulation of polyoxometalates inside pores of MOFs. These hybrid materials have been prepared by the absorption of polyoxometalates, e.g. salts or acids of $[PW_4O_{24}]^{3-}$, $[PW_{12}O_{40}]^{3-}$, $[PW_{11}TiO_{40}]^{5-}$ and $[PW_{11}CoO_{39}]^{5-}$ dissolved in acetonitrile or water into pores of MIL-101 [59, 60]. Their catalytic performances have been addressed in the selective oxidation of alkenes with aqueous H_2O_2 under mild conditions.

8.3 CATALYTIC PROPERTIES

8.3.1 Oxidation of Cycloalkanes

Aerobic oxidation of cyclooctane to its corresponding ol/one mixture at atmospheric pressure and in the liquid phase has been promoted by the commercial MOF, Fe(BTC), incorporating NHPI (Eq. 8.1) [61]. Control experiments treating cyclooctane with oxygen alone or Fe(BTC) under nitrogen resulted in negligible conversion.



(8.1)

In contrast, very good selectivity to cyclohexanol/cyclohexanone (89%) at reasonably high conversion (40%) has been achieved with the presence of Fe(BTC)/NHPI and oxygen. Several evidences supported the view that the aerobic oxidation is a heterogeneous process. Chemical analysis of the liquid phase showed that the iron concentration in the liquid phase was below the 0.1 ppm detection limit. The hot filtration test and the available data indicated that the oxidation takes place in the solid phase. Concerning the reaction mechanism, it was assumed that a phthalimide N-oxy radical intermediate acts as a precursor for C-centered radicals that would undergo autoxidation.

Di Nicola et al. [62] reported the synthesis of a 3D Cu-MOF that is the trinuclear triangular copper derivative $[Cu_3(\mu_3\text{-}OH)(\mu\text{-}pz)_3(EtCOO)_2(H_2O)]$ (where Hpz = pyrazole) by addition of Hpz to a water solution of $Cu(EtCOO)_2H_2O$ and subsequent crystallization at 18–22 °C. This Cu-MOF acted as a remarkably active and selective catalyst or catalyst precursor for peroxidation of cyclohexane and cyclopentane in a solvent mixture of acetonitrile and water to the corresponding alcohols and ketones by aqueous H_2O_2 in a slight acidic medium at room temperature. This led to overall yields up to 32% and turnover numbers (TONs) up to 44 mole of products per mole of catalyst. Notably, the presence of nitric acid in the reaction medium was essential for high activity. Thus, no activity for the cyclohexane oxidation has been achieved in the absence of nitric acid. The effect of nitric acid was ascribed to a role toward the activation of catalyst by promoting the unsaturation of the copper center and the enhancement of its oxidative properties, the prevention of the decomposition of H_2O_2, and the stabilization of intermediate peroxo species. As a reaction mechanism, a main radical pathway involving both C- and O-centered radicals was proposed since the oxidation of cyclohexane is essentially suppressed in the presence of either a carbon-radical trap like bromotrichloromethane or an oxygen-radical trap such as diphenylamine or 2,6-di-*tert*-butyl-4-methylphenol.

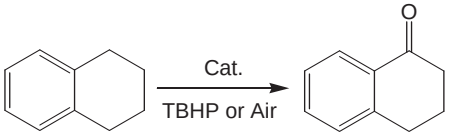
The extralarge cavities of zeolite-like metal-organic frameworks (ZMOFs) offer great potential for use as support to larger molecules, e.g., porphyrins. ZMOFs are

based on the assembly of rigid and directional InN_4 tetrahedral building units (TBUs) [63]. ZMOFs are topologically analogous to pure inorganic zeolites and, similarly, are anionic and chemically stable in aqueous media. The anionic nature of the framework allowed for facile *in situ* encapsulation of a cationic free-base porphyrin [63]. Metalation of the encapsulated *rho*-ZMOF by various transition-metal cations was accomplished *via* incubation of the encapsulated in a 0.1 M methanol solution of the corresponding metal nitrate at room temperature for up to 24 h. The Mn-metallated porphyrin encapsulated in *rho*-ZMOF was explored as a catalyst for cyclohexane oxidation, which was performed at 65 °C in the presence of TBHP as the oxidant, chlorobenzene as an internal standard. This material showed catalytic activity toward the oxidation with turnover number higher than those reported for similar heterogeneous systems [63]. The system can be recycled up to 11 cycles, which represents a longer lifetime than that reported for any other system. After 24 h, based on the amount of oxidant present in the initial reaction mixture, a total yield (from cyclohexane to cyclohexanol/cyclohexanone) of 91.5% and a corresponding turnover number (TON) of 23.5 (catalyst loading of 3.8%) were observed. It was a noticeably higher yield compared to metalloporphyrins supported on zeolites or mesoporous silicates.

8.3.2 Oxidation of Aromatic Compounds

Aerobic oxidation of alkyl aromatics is one of the most important processes in the petrochemical industry because aromatic carboxylic acids including terephthalic acid have widely been utilized as raw materials of polyesters. They are commercially produced by oxidation of aromatic hydrocarbons with air using Co/Mn/Br catalyst systems in acetic acid at 150–250 °C [66]. However, there has been no attempt for the oxidation of aromatic hydrocarbons to produce the corresponding carboxylic acids over MOFs because chemical stability of MOFs at harsh reaction conditions using strong acid media may pose a limitation to their utilization as heterogenenous catalysts together with a separation problem of solid carboxylic acid production from the catalysts.

To date, benzylic oxidation of tetralin, xanthene, diphenylmethane and triphenylmethane with MOFs have been used for model reactions to evaluate their catalytic activities and selectivities. The oxidation of tetralin (Eq. 8.2) has been used to synthesize 1-tetralone that is an intermediate for the production of various products such as dyes, pharmaceuticals and agrochemicals [67].



(8.2)

Ahn and coworkers have reported that MIL-101(Cr) is selectively used in the oxidation of benzylic compounds such as tetralin with TBHP or O_2 (Eq. 8.2) [48].

MIL-101(Cr) with a high content of Cr(III) active centers and mesoporosity exhibited excellent catalytic performance as compared with that obtained for microporous CrAlPO-5 catalyst. For MIL-101(Cr), tetralin conversion gradually increased from 55% to 73% as the reaction temperature was increased from 60 °C to 100 °C, while the selectivity to 1-tetralone remained almost constant (*ca.* 86%). Additional results indicated that tetralin oxidation with TBHP proceeds much better in the presence of a noncoordinating solvent, which means that the unsaturated Cr(III) in the framework plays a role as the active site. This conclusion was further supported by observation that dry MIL-101 showed significantly higher activity and selectivity than those with the water-entrapped sample.

Another interesting work on the use of MIL-101(Cr) has been reported by Ramos-Fernandez et al. MIL-101(Cr) immobilized on a monolithic structure was used for exploring the reactivation procedures of MIL-101(Cr) in the selective oxidation of tetralin in the liquid phase [49]. As illustrated in Figure 8.7, the MIL-101(Cr)-coated cordierite monolith showed a slightly higher activity than the crystals in the slurry, even though the MIL-101 crystals on the monolith were 10 times larger. The catalytic behavior of both crystals and monolith was exactly the same. The short internal diffusion distances in the washcoat layer in comparison with pellets and the large external surface area of the crystals were retained. Many of the problems of handling a suspension of the finely divided catalyst were eliminated. For example, the monoliths were easily recovered from the reaction mixture, while 20% of the slurry powder was lost in filtration. The results confirmed the long-term stability of the catalyst, and the absence of any transport limitations in this reaction.

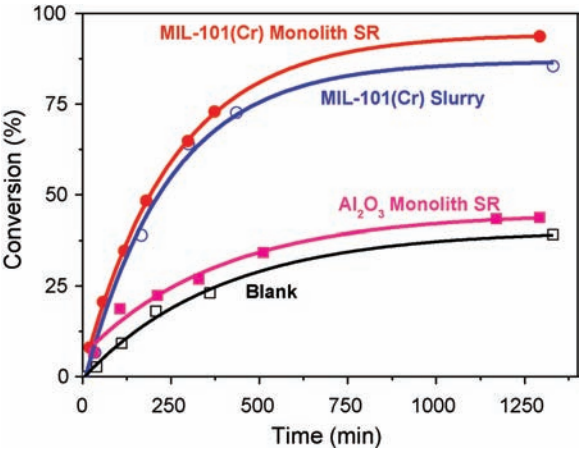
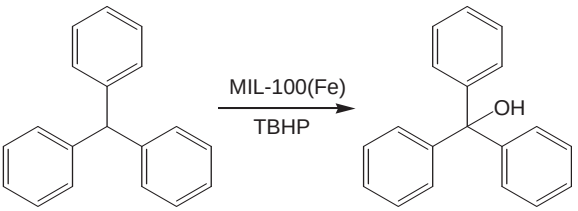


FIGURE 8.7 Oxidation of tetralin with MIL-101(Cr) as a function of time [49]. Comparison of the performance of MIL-101(Cr) in powder form (◯) and coated on monolith (●), and of the monolith support itself (■). Blank experiment without catalyst (□). Reaction conditions: 8 mmol tetralin, 16 mmol TBHP, 5 ml chlorobenzene, T = 80 °C, catalyst 50 mg. Reprinted with permission from *Applied Catalysis A: General.* Copyright 2011 Elsevier.

Two isomorphous Cu-MOFs have recently been applied to the oxidation of benzylic compounds [68]. The host material is a structurally flexible porous MOF, $[Cu^{II}(bped)_2(H_2O)_2(SiF_6)]\cdot 4H_2O$ (Cu-MOF-SiF_6) (bped = meso-1,2-bis(4-pyridyl)-1,2-ethanediol) that is a three-dimensional (3D) polycatenated framework consisting of two-dimensional (2D) (4,4) topolology grid networks. Cu-MOF-SiF_6 efficiently oxidized benzylic compounds to the corresponding ketones and aldehydes using TBHP with good selectivities under mild and convenient reaction conditions. When fluorene and indane were employed as the substrates, the corresponding ketones were obtained selectively in satisfying yields (selectivity: 85% and 88%, yield: 84% and 89%, respectively). The sole product obtained by oxidation of diphenylmethane is benzophenone with a low yield of 28%. The conversion of ethylbenzene to acetophenone was achieved in 93% selectivity and 38% yield. Cu-MOF-SiF_6 was also found to be active in the conversion of benzyl alcohol to benzaldehyde with 44% yield and 100% selectivity. This Cu-MOF as a self-supported heterogeneous catalyst appeared to have more effective individual centers in contrast to the homogeneous analog ($CuSiF_6$ and 4 equivalents pyridine) due to the presence of favorable host–guest interactions and potential CUM Cu(II) sites formed by the loss of the weakly bound axial water molecules. Interestingly, the SiF_6^{2-} anions hosted in the one-dimensional channels of Cu-MOF-SiF_6 can be readily exchanged with NO_3^- anions while keeping the framework intact, leading to isomorphous Cu-MOF-NO_3. The conversion of diphenylmethane to benzophenone was higher for Cu-MOF-NO_3 than Cu-MOF-SiF_6 under similar conditions (47% vs. 28% after 24 h). The results suggested that their catalytic activities are anion tunable. From the reusability of Cu-MOF-SiF_6, it was confirmed that the catalyst can be reused with the framework left intact at least three times without losing any activity. A trace amount of Cu (0.3% of Cu added) was found in the filtrate.

Garcia and coworkers [69] have recently attempted the oxidation of diphenyl- (DPM) and triphenylmethane (TPM) (Eq. 8.3) with mesoporous MIL-100(Fe) samples, with differing average crystal size (from 60–70 to >400 nm).



(8.3)

The results obtained have shown that all of the samples were highly selective catalysts for the oxidation, but a remarkable effect of diffusion control on the catalytic activity arises when bulky molecules are used as substrates for the oxidation. These samples showed similar reaction rates in the oxidation of DPM to benzophenone with TBHP regardless of its average particle size. In contrast, the activity of the three MIL-100 (Fe) samples for the oxidation of bulky TPM by TBHP largely depends on the average crystal size of the sample: the smaller the average particle size, the larger the initial reaction rate of TPM oxidation (Figure 8.8). It was

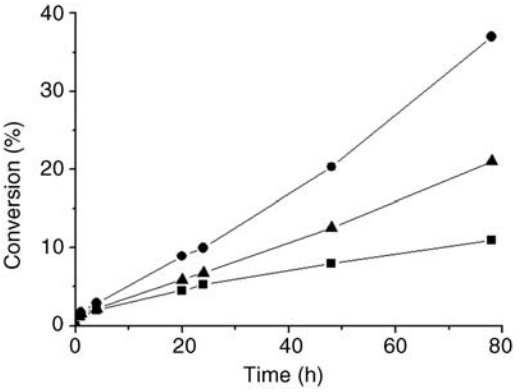


FIGURE 8.8 Oxidation of TPM to triphenylmethanol using MIL-100(Fe) with different HF/Fe ratio as catalyst and TBHP as oxidant [69]. Circles, triangles and squares represent MIL-100 (Fe) prepared using HF/Fe ratios of 0.125 (60–70 nm), 0.5 (120–130 nm) and 1.5 (400 nm), respectively. Reaction conditions: TPM (0.1 g), MIL-100 (Fe) (25 mg) preactivated at 150 °C for 3 h under vacuum, acetonitrile (4 mL), TBHP in decane (0.1 mL).

concluded that the oxidation of DPM with TBHP is not controlled by intracrystalline diffusion, while the oxidation of TPM may occur mainly at the external surface of the catalyst and near pore mouths.

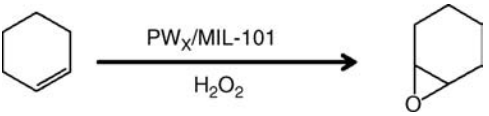
The commercially available iron trimesate BASF Basolite F300, Fe(BTC), has been used as a heterogeneous catalyst for the liquid phase oxidations of various organic compounds. This catalytic system was active for the oxidation of ethylbenzene and tetralin, with high selectivity (>85%) [52, 61]. The system can be reused, although there is a gradual decrease in turnover frequency, caused by minor changes in the crystal structure due to the formation of iron-oxide nanoparticles. The combination of Fe(BTC) as catalyst and TBHP as oxidant led to the transformation of xanthene to xanthone. Under the optimized conditions, above 90% yield of xanthone was achieved with 1.5 equivalents of TBHP [52]. However, the crystal structure of Fe(BTC) has been so far unknown because it is considered an amorphous-like phase [47]. BET surface area and micropore volume of Fe(BTC) are 950 m^2/g and 0.44 cm^3/g, respectively, which were half of those of the MIL-100 (Fe). Further studies to elucidate catalytic properties of two iron trimesates in more detail would be necessary.

Farrusseng and coworkers have recently reported outstanding results for the aerobic oxidation of tetralin over "ship-in-a-bottle"-type catalysts, metal phthalocyanine perfluorinated complexes ($MPcF_{16}$) encapsulated in MIL-101 [70]. The $MPcF_{16}$@MIL-101 catalysts were prepared by wet infiltration of the deep blue-colored $MPcF_{16}$ solutions into MIL-101 with a maximal theoretical complex loading inside the MOF of 9 wt%. In this work, two $MPcF_{16}$ (M = Fe, Ru) were used for the encapsulation and a bulky N-bridged di-iron phthalocyanine complex, $(FePctBu_4)_2N$, was used for comparison. After slow evaporation of the solvent (acetone for $MPcF_{16}$ and CH_2Cl_2 for $(FePctBu_4)_2N$), any complexes not strongly bound to the host MOFs

were removed by intensive washing until the filtrate remained colorless. The actual complex loading for the perfluorinated complexes inside the MIL-101 determined by ICP-OES measurements was 2.1 wt% and 3.6 wt% for $FePcF_{16}$ and $RuPcF_{16}$, corresponding to approximately 0.8 and 1.2 complexes per large pore, respectively. For the $(FePctBu_4)_2N$ dimeric complex, a higher encapsulation loading of 5.2 wt% was obtained, but it was assumed that the bulky dimer complex (*ca.* 2.0 × 2.0 nm) is not incorporated into the mesoporous structure of the MIL-101. The aerobic oxidation of tetralin was performed in parallel batch reactors at 8 bar of O_2 at 90 °C. The turnover numbers (TONs) of the homogeneous catalysts follow the order $(FePctBu_4)_2N > RuPcF_{16} > FePcF_{16}$. It has been highlighted that the encapsulated $MPcF_{16}$@MIL-101 catalysts allow an activity increase of approximately one order of magnitude in the oxidation reaction. The TON of $FePcF_{16}$@MIL-101 was 48 200 after 24 h, almost eight times higher than for the homogeneous $FePcF_{16}$ catalyst (TON = 6300). Similarly, the TON of $RuPcF_{16}$@MIL-101 was 46 300 after 24 h. Moreover, the $FePcF_{16}$@MIL-101 catalyst provided a higher selectivity (up to 80%) toward the desired 1-tetralone compared to the homogeneous $FePcF_{16}$ (68%) at similar conversion. The higher activity for encapsulated complexes has been explained by the preclusion of the dimerization process by π-stacking that is typically observed for homogeneous catalysts. In contrast, a limited conversion of up to 4% was obtained for the $(FePctBu_4)_2N$@MIL-101 catalyst, indicating that the synergistic effects arising from the confinement in the pore do not take place.

8.3.3 Oxidation of Olefins

Kholdeeva and coworkers [51] have studied the selective allylic oxidation of alkenes such as cyclohexene, α-pinene and limonene with TBHP over MIL-101(Cr). The selectivity towards unsaturated ketones reaches 86–93% at 70–92% conversions of olefins. The temperature of the catalyst activation strongly affected the ketone yields. MIL-101(Cr) was stable to chromium leaching and behaved as a true heterogeneous catalyst. This group has tried the encapsulation of polyoxometalates, $[PW_4O_{24}]^{3-}$ (PW_4) and $[PW_{12}O_{40}]^{3-}$ (PW_{12}), inside mesoporous cages of MIL-101 (Cr) to produce hybrid materials PW*x*/MIL-101 ($x = 4$ or 12) with 5–14 wt% polyoxotungstate [59]. Their catalytic performance was assessed in the selective oxidation of alkenes in acetonitrile with aqueous H_2O_2 under mild reaction conditions at 50 °C. Composite 5% PW*x*/MIL-101 exhibited fairly good catalytic activities in the epoxidation of various alkenes such as 3-carene, limonene, α-pinene, cyclohexene (Eq. 8.4), cyclooctene, 1-octene.



(8.4)

The turnover frequencies (TOF) and alkene conversions were close to the corresponding activities achieved with homogeneous PW_{12}. For the oxidation of the natural terpenes, PW_{12}/MIL-101 showed high olefin conversions (up to 76%) and high

epoxide selectivities (up to 96%). Siginificantly, the selectivity of epoxidation and the substrate conversion increased with increasing the molar ratio of $[H_2O_2]$/[alkene]. An opposite trend is typically observed with most homogeneous and heterogeneous epoxidation catalysts, i.e. the selectivity of epoxidation normally decreases with increasing alkene conversion [59]. Two hybrid materials PW*x*/MIL-101 ($x = 4$ or 12) behaved as true heterogeneous catalysts and could be recycled several times. Immobilization of PW_{12} within the MIL-101 matrix allowed the stability of PW_{12} toward solvolytic destruction in the presence of H_2O_2 to be increased.

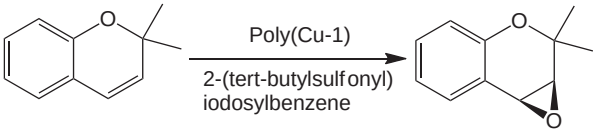
Volkmer and coworkers [74] have studied reaction pathways for the oxidation of cyclohexene with TBHP over Co-MOF, MFU-1. Single crystals of MFU-1 were grown under solvothermal conditions from solutions of the ligand 1,4-bis[3,5-dimethyl]-pyrazol-4-yl)benzene (H_2bdpb) and cobalt(II) chloride in DMF at 120 °C. The structure of MFU-1 is similar to MOF-5, which has a CaB_6-type framework topology. As a test reaction for catalytic activity, the liquid phase oxidation of cyclohexene in the presence of MFU-1 was examined using TBHP as oxidant. The catalytic results demonstrated that oxidation of cyclohexene is fast in the presence of MFU-1, whereas the reaction occurring in the absence of catalyst under the same conditions is almost negligible. The maximum cyclohexene conversion achieved after 22 h was 27.5%, and the main reaction products were *tert*-butyl-2-cyclohexenyl-1-peroxide, followed by 2-cyclohexene-1-one and cyclohexene oxide. MFU-1 was almost completely recovered from the reaction vessel after a catalytic test run. In the reaction of the filtrate after removal of solid catalyst, no significant catalytic conversion was observed, indicating that cobalt ions leaching from the catalyst is not responsible for the observed activity.

Ahn and coworkers have performed the immobilization of a Mn(II) acetylacetonate complex ($Mn(acac)_2$) to the IRMOF-3 through a one-step postsynthetic route by dissolving $Mn(acac)_2$ in toluene at 55 °C for 20 h, providing an effective and recyclable heterogeneous catalyst for epoxidation of alkenes [75]. The epoxidation of cyclohexene over $Mn(acac)_2$-immobilized IRMOF-3 ($Mn(acac)_2$@IRMOF-3) using O_2 (1 atm) with trimethylacetaldehyde as an oxidant precursor at 40 °C formed cyclohexene oxide with excellent selectivity (92%) and conversion (68%). Cyclooctene was converted to cyclooctene oxide with lower conversion (60%) and slightly higher selectivity (96%) than cyclohexene under identical reaction conditions. In addition, styrene was converted to the corresponding epoxide with 52% conversion and 81% selectivity. The reactivity of the double bond attached to benzylic rings showed lower conversion and selectivity to epoxide than in the other two cyclic alkenes, cyclohexene and cyclooctene.

As illustrated below, asymmetric epoxidation of olefins has been performed by homochiral MOFs formed by the incorporation of metalloligands into the frameworks. Hupp and coworkers [76] proposed a microporous homochiral MOF compound featuring chiral (salen)Mn struts that is highly effective as an asymmetric catalyst for olefin epoxidation, yielding enantiomeric excesses that rival those of the free molecular analog. The chiral (salen)Mn strut, (R,R)-(2)-1, 2-cyclohexanediamino-N,N′-bis(3-tert-butyl-5-(4-pyridyl)salicylidene) $Mn^{III}Cl$ (**L**) was incorporated instead in a more robust pillared paddlewheel structure containing

pairs of zinc ions together with biphenyldicarboxylate (bpdc) as the second ligand. The resulting MOF has the formula $Zn_2(bpdc)_2\mathbf{L}\cdot 10DMF\cdot 8H_2O$ and crystallizes in the triclinic P1 space group as an interpenetrating pair of networks. It has distorted-rectangular and rhombic channels in the *c* and *a* directions with dimensions of 6.2×15.7 Å and 6.2×6.2 Å, respectively. Diagonal displacement of the networks leaves all Mn^{III} sites accessible to the channels. The catalytic activity of the material toward asymmetric epoxidation was examined with 2,2-dimethyl-2*H*-chromene as substrate and 2-(*tert*-butylsulfonyl) iodosylbenzene (TBSIB, a soluble compound) as oxidant. The chiral (salen)Mn complex **L** was initially highly effective, but lost much of its activity after the first few minutes. After a few hours, essentially all activity was lost. In contrast, the homochrial MOF exhibited close to constant reactivity, culminating in nearly four times the number of turnovers seen for **L** by the time the experiment was terminated at 3.4 h. For (salen) Mn complexes, loss of catalytic activity typically was known to be associated with oxidation of the salen ligand.

Hupp and coworkers [77] proposed homochiral MOFs formed by the reaction of [bis(catechol)-salen]Mn^{III} with a wide range of di- and trivalent metal ions including Cr^{III}, Fe^{III}, Mn^{II}, Co^{II}, Ni^{II}, Cu^{II}, Zn^{II}, Cd^{II}, and Mg^{II}. Coordination polymerization of the above (salen)Mn compound with Cu(II) was accomplished under a N_2 atmosphere by adding $CuCl_2$ to a 1:4 mixture of the (salen)Mn compound and triethylamine dissolved in deoxygenated DMF. After filtration and washing with DMF, the Cu-linked (salen)Mn polymer, poly(Cu-1), was obtained as a brown solid. This homochiral MOF is insoluble in a wide range of organic solvents and water but could be dissolved upon addition of excess of pyrocatechol. These homochiral MOFs, particularly the (salen)Mn unit, were active for enantioselective heterogeneous epoxidation and exhibited catalytic activity comparable to that of the homogeneous [bis(catechol)-salen]Mn^{III} building blocks when used for the reaction of 2,2-dimethyl-2*H*-chromene with TBSIB, i.e. 79% yield and 76% *ee* for a homochiral Cu (II)-MOF with [bis(catechol)-salen]Mn^{III} vs. 87% yield and 86% *ee* for the homogeneous complex (Eq. 8.5). An important point for the use of the homochiral Cu(II)-MOF is that the insoluble MOF has a longer lifetime than the homogeneous catalyst during the reaction. The homogeneous epoxidation catalyst was initially effective, but it lost much of its activity after the first few minutes and showed complete deactivation after 0.5 h. In contrast, the homochiral Cu(II)-MOF had a total turnover number greater than 2000 within 3 h. After catalysis, catalyst isolation from the reaction mixture was able to be readily achieved by centrifugation and decantation without leaching of Mn and framework metal cations. Under practical oxidant concentrations, the catalyst can be recycled up to ten times with little loss of activity and no loss of enantioselectivity.



(8.5)

One-dimensional homochiral Ni-MOFs based on enantiopure pyridyl-functionalized nickel salen metalloligand units have been used as self-supported catalysts for alkene epoxidation [55]. These homochiral materials are based on a pyridyl-substituted metalloligand salen(Ni) unit *via* two self-assembly methods, in which only one pyridyl group of the NiL unit as unbridging pendant metalloligands coordinated to polymeric chains. Among them, the homochiral nickel-based MOF, $[Ni_3(bpdc)(RR\text{-}L)_2\cdot(DMF)]_n$, is prepared directly using chiral ligand (RR-H_2L, (R, R)-(-)-1,2-cyclohexanediamino-N,N′-bis(3-*tert*-butyl-5-(4-pyridyl)salicylidene), Ni$(NO_3)_2\cdot 6H_2O$, and bpdc (4,4′-biphenyldicarboxylic acid) (2:1:1) in a solvent mixture (DMF 10 ml and ethanol 1 ml) at 80 °C for 24 h. This homochiral MOF contains unsaturated active nickel center in metalloligand showing catalytic activity (62% styrene conversion and 61% selectivity to styrene oxide) comparable with their homogeneous counterpart in alkene epoxidation and exhibit potential as recyclable catalysts. When NaClO, TBHP, H_2O_2, and O_2 were tested as the oxygen source in dichloromethane for the oxidation of styrene, NaClO as the best oxidant gave higher conversion and selectivity. The choice of solvent is crucial for the catalytic epoxidation of alkenes. The weak donor solvent dichloromethane gave the highest epoxide yield among tested solvents. The use of strong coordinating solvents gave the lower catalytic activities because the axially coordinated solvents may prevent the oxidant NaOCl from forming nickel(IV)-oxo species and the assessment of substrates to active centers. However, the homochiral Ni-MOF did not provide enantioselectivities in the epoxidation reactions.

The isoreticular chiral metal-organic frameworks (CMOFs) with the primitive cubic network topology have been constructed from $[Zn_4(\mu_4\text{-}O)(O_2CR)_3]$ secondary building units and systematically elongated dicarboxylate struts that are derived from chiral Mn-Salen catalytic subunits (R) [54]. Chiral Mn-salen-derived dicarboxylate ligands were synthesized by Schiff base condensation reactions between (*R*,*R*)-cyclohexanediamine and corresponding 2-hydroxybenzaldehyde derivatives with pendant carboxylic acid groups. Reactions of $Zn(NO_3)_2\cdot 6H_2O$ with the Mn-salen complex in DMF/EtOH and DEF/EtOH at 60 °C for 12 days resulted in single crystals of CMOFs. Among CMOFs, the two-fold interpenetrated CMOF-3 possesses channel sizes of $1.5 \times 0.7\,nm^2$ and an open cavity of 2.0 nm in diameter, with 76.8% of void space, while the noninterpenetrated CMOF-4 exhibits the largest channel dimensions of $2.5 \times 2.3\,nm^2$ and a cavity diameter of 3.2 nm, reaching 88.4% of void space as calculated by PLATON. CMOFs have been shown to be highly effective catalysts for asymmetric epoxidation of a variety of unfunctionalized olefins with up to 92% *ee*. CMOFs 1, 3, and 5 are highly effective catalysts for asymmetric epoxidation of 1*H*-indene as substrate with 2-(*tert*-butylsulfonyl) iodosylbenzene as oxidant to generate (1*R*,2*S*)-indene oxide in 47–64% *ee*. The level of enantioselectivity observed for CMOF catalyzed alkene epoxidation is comparable to that of the homogeneous control catalyst. Asymmetric epoxidation of 2,2-dimethyl-2*H*-chromene by CMOF-5, for example, gave the (*R*,*R*)-chromene oxide in 92% *ee*, a value that is the same as the result of a homogeneous control catalyst. The rates of epoxidation reactions strongly depended on the CMOF open-channel sizes, providing solid evidence that larger open channel dimensions

can increase reaction rate by facilitating the diffusion of reactant and product molecules. These CMOF catalysts were recyclable and reusable and retain their framework structures after epoxidation reactions.

Metalloporphyrins have structural similarity to cofactors found in many metalloenzymes, so that they could be potential building blocks for catalytically active MOF materials. Recently, a few successful cases of porphyrin-based MOFs have been observed. Hupp and coworkers [78] have recently succeeded in the synthesis of an extended family of unique MOFs that directly incorporate a variety of metalloporphyrins that are composed of Al^{3+}, Zn^{2+}, Pd^{2+}, Mn^{3+}, and Fe^{3+} complexes. These robust porphyrinic materials (RPMs) feature large channels with high surface areas up to around $1000\,m^2/g$ and potentially accessible active sites. Structures of RPMs contain the paddlewheel-coordinated zinc nodes. A generic RPM unit cell is based on sheet formation by the tetraacid ligand (L^1) pillaring by a dipyridyl strut (L^2). These RPMs have been prepared by static heating of L^1 and $Zn(NO_3)_2{\cdot}6H_2O$ in DMF at 80 °C for 2 h, followed by addition of 30 mM HNO_3 in ethanol and L^2 and heating of the resulting suspension at 80 °C for 20 h. L^1 was employed as an Al^{3+}, Pd^{2+}, or Fe^{3+} complex, or simply as a free-base porphyrin, while L^2 was used as either the Mn^{3+} complex or the free base. For both kinds of struts, use of a free-base porphyrin in the synthesis resulted in Zn^{2+} complexes in the RPM. Analysis of single crystal data revealed noncatenated frameworks with formula of $Zn_2(L^1)(L^2)$. Among M^1M^2-RPMs (M^1 designates the metal in L^1 and M^2 designates the metal in L^2), ZnMn-RPM was found to be an active catalyst for the epoxidation of styrene using a soluble analog of iodosylbenzene. The RPM material showed much greater stability than an analogous homogeneous catalyst. While the homogeneous Mn complex of 5,10,15,20-tetrakis-(pentafluorophenyl)porphyrin showed complete catalyst deactivation after 780 epoxidation turnovers, ZnMn-RPM functioned for 2150 turnovers, stopping only because of depletion of oxidant. An induction period was observed for catalysis by ZnMn-RPM. This behavior was attributed to slow diffusion of reactants and/or oxidants into the MOF. No catalytic activity was observed in the reaction solution after removal of the MOF by filtration.

A functional MOF [$Cd_{1.25}$Pd-$H_{1.5}$TCPP(H_2O)] assembled from Pd-porphyrin (TCPP = tetra(4-carboxyphenyl)porphyrin) building blocks and Cd(II) connecting nodes have been successfully synthesized and used for the selective oxidation of styrene [57]. The functional MOF was synthesized by heating a mixture of Pd-H_4TCPP and $Cd(NO_3)_2{\cdot}4H_2O$ in a mixed solvent of DMF, methanol and acetic acid at 80 °C for 10 days. The resulting framework contains two kinds of channels with dimensions of $4.61 \times 12.55\,Å^2$ and $8.27 \times 9.32\,Å^2$ along the *a*-axis. When the reaction was performed over the functional MOF in CH_3CN using H_2O_2 as oxidant in the presence of $HClO_4$ at 55 °C for 12 h, styrene was completely oxidized into a mixture of 91% acetophenone and 9% benzaldehyde. The catalytic results are very sensitive to the quantity and acidity of the additive acids. When the addition of $HClO_4$ was increased, the styrene conversion increased gradually. Considering the catalytic results on a series of control catalysts, the catalytic activity of the material was superior to its corresponding components.

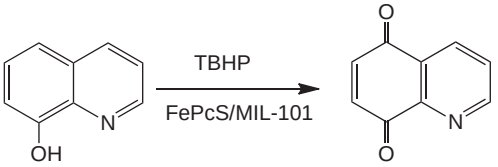
8.3.4 Oxidation of Alcohols and Phenols

Active gold nanoparticles (Au NPs) deposited onto MOFs in solution are good candidates for potential catalysts for a variety of catalytic reactions. Liu et al. [85] reported a highly efficient heterogeneous gold catalyst, which was deposited on MIL-101(Cr) by a simple colloidal dispersion (CD) method with polyvinylpyrrolidone (PVP) as a protecting agent using $HAuCl_4$ as an Au precursor. After the Au:PVP colloids (PVP monomer/Au = 80:1 molar ratio) were formed and reduced by an aqueous solution of $NaBH_4$, these colloids were immediately deposited onto the MIL-101(Cr) support to prepare the active Au NPs/MIL-101(Cr). The resulting Au loading was 0.48 wt%. Au NPs were highly dispersed on the Au/MIL-101 (CD/PVP) with a mean diameter of 2.3 ± 1.1 nm, which were in good agreement with the cage diameters of MIL-101 (Cr). The resulting Au/MIL-101 (CD/PVP) catalyst exhibited unbelievably high catalytic activities and selectivities to the corresponding aldehydes or ketones in liquid phase aerobic oxidation of a wide range of alcohols. It is noted that this catalyst could efficiently catalyze the oxidation under ambient conditions in the absence of water or base. Benzylic alcohols, either primary or secondary, were converted to the corresponding benzylic aldehydes or ketones in 99% yield. Substituted benzyl alcohols containing electron-donating groups such as $-CH_3$, $-OCH_3$ or -OH are more easily oxidized than those containing electron-withdrawing groups. The catalyst also displayed a very high activity for the oxidation of allylic alcohols such as cinnamyl alcohol. Under solvent- and base-free conditions, the Au/MIL-101 (CD/PVP) catalyst afforded an exceptionally high turnover frequency (TOF) of 29 300 h^{-1} with 99% selectivity to acetophenone at 160 °C. This TOF was larger than even that (25 000 h^{-1}) over $Au/Ga_3Al_3O_9$, which represents the most active Au catalyst in the current literature [86]. Moreover, the catalyst was easily recoverable and could be reused several times without leaching of metals. The observed high activities of the Au/MIL-101 catalyst were attributed to the high dispersion of Au NPs and the electron-donation effects of aryl rings to the Au NPs within the large cages of MIL-101 [85].

As another illustrative example, Haruta and coworkers have made Au clusters deposited on several MOFs such as MOF-5 and MIL-53(Al) by solid grinding. In a typical catalyst preparation, volatile organogold complex, $Me_2Au(acac)$ (acac = acetylacetonate) and MOF substrates were ground in an agate mortar in air. Then, the mixture was treated in a stream of 10 vol% H_2 in N_2 at 120 °C for 2 h to obtain the Au clusters-deposited MOFs. These Au catalysts showed good catalytic activities for the liquid phase aerobic oxidation of benzyl alcohol and 1-phenylethanol in methanol [87]. Au NPs supported on MOF-5 (0.5 wt% Au) had a particle size of 4.8 ± 2.2 nm as a mean diameter that is larger than the pore size of MOF-5, indicating that most of the Au NPs are present outside the pores. This type of catalyst exhibited 79% acetophenone yield in the oxidation of 1-phenylethanol in the presence of base. However, the catalyst gave about 31% selectivity to benzaldehyde at about 69% conversion of benzyl alcohol under base-free condition. Regarding catalytic activities of Au NPs in the absence of base, this result was not consistent with those reported by Liu et al. [85]. In this study, it should be noted that some problems may have

occurred during the preparation of the Au clusters-deposited MOFs with solid grinding in air because some of the MOFs such as MOF-5 and CPL-2 have weak mechanical stability as well as poor moisture stability. Additional work to elucidate the effect of base on the oxidation reaction more correctly would be necessary.

The hybrid material FePcS/MIL-101 (FePcS: iron tetrasulfophthalocyanine) has been applied to selective oxidation of aromatic compounds [58]. The FePcS/MIL-101 material was prepared by adsorption of FePcS from water at 25 °C. The hybrid material exhibited a superior catalytic performance in the selective oxidation of aromatic substrates such as benzyl alcohol, 2,3,6-trimethylphenol (TMP) and 8-hydroxyquinoline (Eq. 8.6) with TBHP as compared with the performance of homogeneous $FePcS(Bu_4N)_4$.



(8.6)

Almost complete conversion of the phenolic substrates at 60 °C was achieved within 15 min with 0.8–1 mol% of the catalyst, indicating no diffusion limitation. The higher activity of FePcS/MIL-101 compared to homogeneous FePcS has been rationalized assuming fast penetration and concentration of the aromatic substrates within MIL-101 cages, similarly to the fast encapsulation of FePcS molecules. The oxidation of TMP to 2,3,6-trimethylbenzoquinone with TBHP was faster but less selective in the presence of FePcS/MIL-101 as compared with $FePcS/SiO_2$, i.e. 55% yield after 15 min for FePcS/MIL-101 vs. 84% yield after 2 h for $FePcS/SiO_2$. For three substrates, the oxidation rates decreased on increasing the FePcS content in the hybrid material. A hot catalyst filtration test revealed no further conversion of substrates in the filtrate without leaching of iron or chromium, indicating the true heterogeneous nature of catalysis over FePcS/MIL-101.

Osako and Uozmi [88] proposed a new Cu-MOF, $Pd(TFA)_2BPy$-Cu, constructed from a bipyridyl–palladium complex bearing carboxylic groups and a copper(II) linker. The Cu-MOF was used for the aerobic oxidation of various benzylic alcohols including 1-phenylethanol in water under atmospheric molecular oxygen. The Cu-MOF exhibited high catalytic activity in the aerobic oxidation of 1-phenylethanol to acetophenone (82% yield) in the presence of Na_2CO_3 in H_2O at 100 °C for 24 h. Interestingly, the material was not actually active for this reaction in organic solvents. When the counterion was replaced with acetate and chloride, the catalytic activity decreased significantly. It was concluded that the self-supporting structure formed *via* the ionic assembly of $Pd(TFA)_2BPy$ with Cu^{II} or Zn^{II} is essential in bringing about high activity toward aerobic alcohol oxidations in water.

8.3.5 Oxidation of Sulfides

The oxidation of aryl sulfides using 35% hydrogen peroxide at 25 °C has been successfully carried out over MIL-101(Cr) [46]. MIL-101(Cr) was able to effectively

and selectively catalyze the oxidation of aryl sulfides to the corresponding sulfoxides by H_2O_2. The CUS Cr(III) center in dehydrated MIL-101(Cr) was the main active site. Product yield to methyl phenyl sulfoxide was increased with the increasing the number of CUS sites in MIL-101 by the activation treatment. Yields based on the substrate after 15 h of reaction at 25 °C ranged from 88 to 99%. No oxidation could be observed in the absence of MIL-101(Cr). Moreover, only the sulfide to sulfoxide conversion was catalyzed by MIL-101(Cr) under the reaction conditions, whereas the sulfoxide to sulfone conversion was not. As mentioned in oxidations with MIL-101(Cr), this catalyst also had no catalyst deactivation or leaching problem of chromium species from the MOF during five consecutive measurements without exchange of catalyst.

Kim and coworkers [89] have proposed a new synthetic approach starting from readily available chemicals such as zinc dinitrate hexahydrate, L-lactic acid, 1,4-benzenedicarboxylic acid to produce a robust and porous homochiral Zn-MOF, $[Zn_2(BDC)(L\text{-}Lac)(DMF)]\cdot DMF$, possessing the intrinsic chirality due to the chiral L-lactic acid (L-Lac). In the as-synthesized material, the pores are occupied by coordinated DMF ligands, as well as guest DMF molecules that can be readily removed at elevated temperatures. The permanent porosity of the partially evacuated material was established by reversible gas sorption experiments. This material exhibited size-selective and enantioselective guest sorption properties on several substituted thioether oxides. For example, the enantiomeric excess (*ee*) values for the adsorbed guests were found to be 20–27% for aromatic sulfoxides containing smaller substituents with the *S* enantiomer in excess. The porous homochiral Zn-MOF was shown to be capable of mediating highly size- and chemoselective catalytic oxidation of thioethers to sulfoxides by urea hydroperoxide (UHP) or H_2O_2. Among several thioethers, thioethers with smaller substituents exhibited reasonable conversion (58–64%) and high chemoselectivity (83–92%) after 16 h of catalytic reaction, whereas thioethers with bulkier substituents exhibited very poor conversion (3–7%). The remarkable size selectivity in the catalytic reaction implied that the reaction primarily occurs inside the uniform micropores of the MOF solid through the heterogeneous nature of the catalysis. This material was active for at least 30 catalytic cycles without loss of oxidation selectivity.

8.4 MECHANISTIC ASPECTS

It is known that liquid phase oxidations with O_2, H_2O_2 or RO_2H catalyzed by redox molecular sieves generally follow three reaction pathways: (a) one-electron homolytic pathways *via* free radical ($HO^{\bullet}$, $HO_2^{\bullet}$, $RO^{\bullet}$, $RO_2^{\bullet}$) intermediates, heterolytic oxygen-transfer processes involving (b) a peroxometal species, and (c) an oxometal species [3]. These pathways are actually similar to those of homogeneous metal-catalyzed oxidations. It is believed that the oxidation processes over transition-metal-containing MOFs may not be very different from the above-mentioned pathways although the mechanistic aspects in MOFs have not been established yet.

For the homolytic pathways, a metal ion selected from mainly the first-row transition-metal elements, e.g. Co^{3+}, Mn^{3+}, Fe^{3+}, and Cu^{2+}, acts as an initiator of free-radical autoxidation rather than a catalyst [2]. The one-electron metal oxidants can catalyze free-radical autoxidation processes, e.g. hydrocarbon oxidation, by promoting the decomposition of alkyl hydroperoxide into chain initiating alkoxy and alkyl peroxy radicals in one-electron transfer processes.

In oxygen-transfer pathways, the oxygen atom is provided heterolytically by an oxygen donor (H_2O_2 or RO_2H) that can generate either a oxometal or peroxometal species as the active oxidant [2]. Heterolytic peroxometal pathways are favored when the metal in its highest oxidation state is both a Lewis acid and a weak oxidant, e.g. early transition-metal ions with d^0 configurations such as Ti^{IV}, Zr^{IV}, Mo^{VI}, and W^{VI}. In the heterolytic peroxometal route, its oxidation state does not change during the catalytic cycle.

In the oxidation of cyclohexene with TBHP over MFU-1 [74], the main reaction product was *tert*-butyl-2-cyclohexenyl-1-peroxide, but not 2-cyclohexene-1-one and cyclohexene oxide. Radical trap experiments also confirm the formation of *tert*-butyl peroxy radicals and cyclohexenyl radicals throughout the course of the catalytic reaction. They proposed a reaction pathway in which freely diffusing peroxy radicals generated by cleavage of TBHP following the route of a Haber–Weiss-type decomposition at the Co^{II} centers. The net reaction equation could be formulated as the following equation (Eq. 8.7):

$$C_6H_{10} + 2(CH_3)_3COOH \rightarrow C_6H_9\text{-}OOC(CH_3)_3 + (CH_3)_3COH + H_2O \qquad (8.7)$$

Ahn and coworkers [48] compared the effect of oxidant (TBHP vs. trimethylacetaldehyde/O_2) and solvent used on catalytic activities of MIL-101(Cr) in the oxidation of tetralin. Tetralin oxidation with TBHP afforded higher conversion than the trimethylacetaldehyde/O_2 system, while higher selectivity to 1-tetralone was obtained with the latter oxidant system (*ca.* 93% vs. 86%). The activity using TBHP was high in chlorobenzene as a solvent but poor in acetonitrile. However, the use of acetonitrile resulted in the highest activity in the aerobic oxidation in the presence of trimethylacetaldehyde. They proposed that trimethylacetaldehyde formed in the oxidation using acetonitrile produces an acylperoxy radical in the presence of O_2 and this radical may attack the nitrile to form an active oxidant that is responsible for the higher conversion. In contrast, the use of THF showed very poor activity in both oxidant systems due to the strong coordination of THF though the O donor to the CUM Cr(III) site. This might indicate that the coordination of *tert*-butyl peroxo radical and/or acylperoxy radical to the Cr(III) site is essential for the oxidation of tetralin.

In Section 8.3.2, the encapsulated $MPcF_{16}$@MIL-101 catalysts have been shown to allow an activity increase of approximately one order of magnitude in the aerobic oxidation of tetralin [70]. Farresseng and coworkers also studied the kinetic isotope effect (KIE) in the oxidation of adamantane-1,3-d_2. This substrate has been used as a probe to determine an intramolecular KIE since it contains two equal tertiary C−H and two C−D bonds in the same molecule. Significantly, the reactivity

of adamantane was much lower compared to tetralin. The analysis of the isotopic composition of the adamantanol-1 product directly provided an intrinsic KIE. The KIE values were determined to be around 1.99 and 1.76 for $FePcF_{16}$@MIL-101 and $RuPcF_{16}$@MIL-101, respectively. The KIE measured using $FePcF_{16}$ and $RuPcF_{16}$ in homogeneous solutions were similar: around 1.94 and 1.68, respectively, suggesting that the same mechanism has been operated in both homogeneous and heterogeneous systems. These low KIE values also indicated the involvement of a radical mechanism in this reaction.

As mentioned above, MIL-101(Cr) was active and very selective in the sulfoxidation of aryl sulfides to the corresponding sulfoxides [46]. A linear free-energy correlation through the change of substituents in the sulfoxidation gave a large negative ρ value ($\rho = -1.8$), indicating that electron-releasing groups enhance the oxidation reactivity. Interestingly, the catalytic activities of MIL-101 in the sulfoxidation were very dependent on the type of oxidant. The high yields of sulfoxides were obtained with H_2O_2, while TBHP could not be used as an oxidant under the same conditions because it gave no yield in the reaction of phenyl methyl sulfide. It was assumed that Cr-oxo species could be generated and become responsible for transferring their oxygen to sulfide considering the Hammett ρ value obtained with MIL-101. In addition, ^{18}O-labeled experiments have been used to understand the source of oxygen found in sulfoxide. The oxygen atom in the sulfoxide product was entirely derived from H_2O_2 and not from water, as shown from labelling experiments in which the oxidation of methyl phenyl sulfide was performed in the presence of $H_2{}^{18}O$.

8.5 STABILITY

8.5.1 Thermal and Chemical Stability

Porous MOFs have less thermal stability than zeolites. Their thermal stability is generally limited to 350–400 °C, but in a few cases they are stable up to 500 °C [37, 105, 106]. However, the principally weak hydrothermal stability of porous MOFs may generally rule out applications at high temperatures in the presence of an oxidizing agent or water.

Hydrothermal stability is a pertinent issue to address for many applications where percent levels of water can be present at elevated temperatures. Most MOFs actually suffer from a lack of hydrothermal stability, but some of them are sufficiently stable to be utilized for applications in the presence of water. The reaction of water with the metal-oxide clusters (hydration) in metal-organic frameworks could involve ligand displacement and/or hydrolysis. The ligand displacement reaction involves inserting a water molecule into a metal–ligand bond of the MOF. During the hydrolysis reaction, the metal–ligand bond is broken and water dissociates into a hydroxide anion and proton. Structural damage to a MOF caused by moisture at operating conditions or during catalyst regeneration will strongly limit the utilization of the MOF as a catalyst. This limitation indicates that TBHP would be more suitable than H_2O_2 for liquid phase oxidations with MOFs.

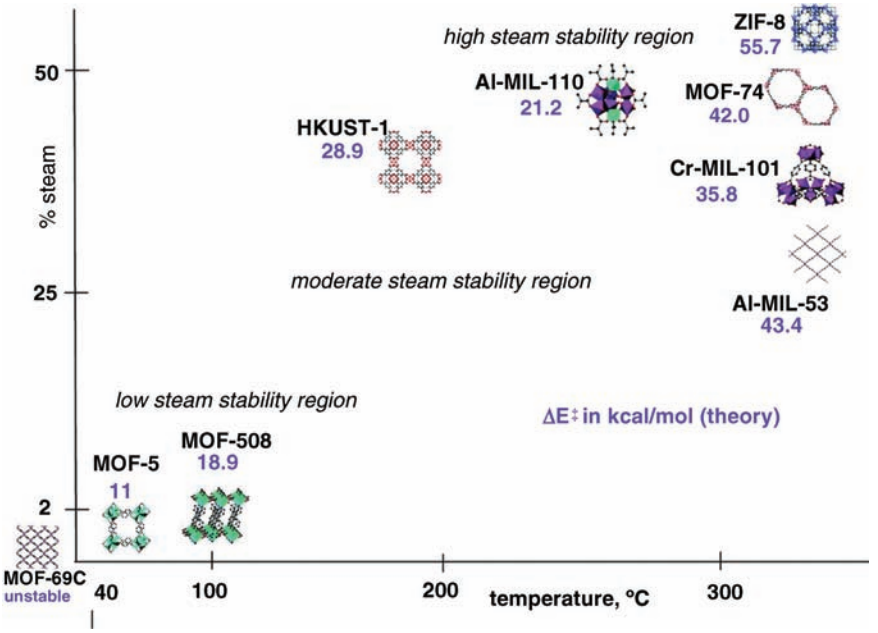


FIGURE 8.9 Steam stability map of selected MOFs [107]. Reprinted with permission from *Journal of American Chemical Society.* Copyright 2009 American Chemical Society.

Willis and coworkers [107] studied the hydrothermal stability of various MOFs with high-throughput experiments and quantum-mechanical calculations. Important parameters that affect the stability of MOFs include metal compositions, coordination, chemical functionality of a linker, interpenetration, flexibility, and framework dimensionality. The strength of the bond between the metal oxide cluster and the linker has been suggested to be important in determining the stability. As illustrated in Figure 8.9, they proposed a steam stability map that was formulated according to the relative stability of different MOF materials. According to this map, MIL-101(Cr), MIL-53(Al) and Zn-MOF-74 are hydrothermally stable, while MOF-5 and MOF-508 are definitely unstable under steaming conditions.

Cychosz and Matzger [108] have also studied the stability of a variety of MOFs to water-containing solutions by using powder X-ray diffraction. It was concluded that the stability of the MOF is related to the metal cluster present in the structure with trinuclear chromium clusters (in MIL-101(Cr) and MIL-53(Cr)) more stable than copper paddle-wheel clusters (in HKUST-1 or Cu-BTC) that are more stable than basic zinc acetate clusters. MIL-100(Fe) and MIL-100(Cr) were also found to be completely water stable.

Chemical stability of MOFs under organic solvents may not be crucial if they are not exposed to highly acidic or basic conditions because most MOFs are synthesized under solvothermal conditions using organic solvents. Chemical stability of

MOFs in the presence of the oxidant (H_2O_2, RO_2H) at elevated temperatures is questionable, but there have been no systematic studies on this issue yet. However, this stability may be dependent on the concentrations of oxidant or reaction mixture and temperature [60].

Very recently, Jhung and coworkers [109] have studied chemical and thermal stabilities of metal terephthalates with an isotypic structure such as MIL-53(Al), MIL-53(Cr) and MIL-47(V). Chemical stability to acids, bases, and water decreases in the order of MIL-53(Cr) > MIL-53(Al) > MIL-47(V), suggesting the stability increases with decreasing lability of the central metal ions. MIL-53(Cr) is very stable without any loss of crystallinity and surface area towards aqueous solutions of NaOH (70 mM) and HCl (70 mM) at room temperature for more than 6 h. However, MIL-47(V) degrades very rapidly with increasing treatment time under the same conditions. MIL-53(Al) showed the intermediate stability towards the acidic and basic conditions. However, the thermal stability decreases in the order of MIL-53 (Al) > MIL-53(Cr) > MIL-47(V), reflecting the strength of the metal–oxygen bond in common oxides like Al_2O_3, Cr_2O_3, and V_2O_5.

8.5.2 Leaching of Active Metal Components

In liquid phase oxidation, leaching of active metal components in redox molecular sieve catalysts has always been a debated issue. To have industrial utility a heterogeneous catalyst should be very robust without leaching of the active metal into the liquid phase under operating conditions. Arends and Sheldon [2] have well documented leaching problems in selective liquid phase oxidations performed by porous solid catalysts. The strong complexing and solvolytic properties of oxidants (e.g. H_2O_2, RO_2H) and/or products (e.g. H_2O, ROH, RCO_2H) tend to cause leaching of active components in the liquid phase oxidation catalysis. This means that leaching of active metal components is generally a result of solvolysis of metal–oxygen bonds that anchor the metal to catalyst surfaces.

The metal leaching might also be a crucial point in oxidation catalysis with MOFs, but systematic studies on the leaching have not been done yet. The metal leaching has not been mentioned clearly in most cases, but it is suspected that many of MOFs may have suffered from the metal leaching problem in liquid phase oxidations. However, some MOFs have been shown to be robust without serious metal leaching during oxidation reactions. Hot filtration experiments have often been used to confirm the heterogeneous nature of the catalytic test reactions in MOFs. For example, mesoporous MIL-101 has been reported as an efficient heterogeneous catalyst for the selective allylic oxidation of alkenes with TBHP [51]. This material was stable to chromium leaching. For the oxidation of tetralin over MIL-101, only a negligible amount of chromium was leached from the framework and found in the filtrate after removal of the catalyst by hot filtration. For the aerobic oxidation of thiophenol, MIL-100(Fe) showed high activity to form diphenyldisulfide very selectively [69]. This catalyst remained stable after recycling and no deactivation was observed after reuse three times. The crystallinity remained very high without significant variations upon recycling and reactivation, probably indicating the resistance to iron leaching.

8.6 CONCLUSION

This review has shown that many interesting examples are emerging in the design of heterogenenous oxidation catalysts containing the several types of active centers in constrained environments of MOFs. As mentioned earlier, the tunability of pore size, chemical versatility of pore structure and metal environment, and flexibility of frameworks in MOFs could be unique for the development of a new type of oxidation catalysis. In particular, the tailor-made catalysts based on MOFs can be designed which have a distinct resemblance to redox metalloenzymes. In this respect, it is highlighted that homochiral MOFs may offer new opportunities for enantioselective catalysis in liquid phase oxidations where zeolites have met with only limited success due to their limited pore dimensions. However, the success of MOFs as heterogeneous catalysts for liquid phase oxidations may greatly depend on whether the problem of catalyst stability can be overcome. Provided that the problems of activity and stability can be solved as the success of TS-1, this will lead to the development of potentially powerful catalysts for selective oxidations in the liquid phase.

ACKNOWLEDGMENTS

This work was supported by the General Research Program (ISTK, SI-1109) and partly by the international collaboration program (KICOS, KN-1228). We also thank You-Kyong Seo and other CCME members for their helpful discussion and contribution.

REFERENCES

1. Sheldon R.A., Kochi J.K. *Metal Catalyzed Oxidation of Organic Compounds*. Academic Press, New York, 1981.
2. Arends I.W.C.E., Sheldon R.A. (2001). *Appl. Catal. A.: Gen.*, *212*, 175–187.
3. Sheldon R.A., Arends I.W.C.E., Lempers H.E.B. (1998). *Catal. Today 41*, 387–407.
4. Arends I.W.C.E., Sheldon R.A., Wallau M., Schuchardt U. (1997). *Angew. Chem. Int. Ed. 36*, 1144–1146.
5. Férey G. (2008). *Chem. Soc. Rev. 37*, 191–214.
6. Yaghi O.M., O'Keeffe M., Ockwig N.W., Chae H.K., Eddaoudi M., Kim J. (2003). *Nature 423*, 705–714.
7. Kitagawa S., Kitaura R., Noro S.-I. (2004). *Angew. Chem. Int. Ed. 43*, 2334–2375.
8. Horcajada P., Chalati T., Serre C., Gillet B., Sebrie C., Baati T., Eubank J.F., Heurtaux D., Clayette P., Kreuz C., Chang J.-S., Hwang Y. K., Marsaud V., Bories P.-N., Cynober L., Gil S., Férey G., Couvreur P., Gref R. (2010). *Nat. Mater*. *9*, 172–178.
9. Perry IV. J.J., Perman J.A., Zaworotko M.J. (2009). *Chem. Soc. Rev. 38*, 1400–1417.
10. Czaja A.U., Trukhan N., Müller U. (2009). *Chem. Soc. Rev. 38*, 1284–1293.

11. Corma A., Garcia H., Llabres i Xamena F.X. (2010). *Chem. Rev. 110*, 4606–4655.
12. Lin W. (2007). *MRS Bull. 32*, 544–548.
13. Yoon M., Srirambalaji R., Kim K. (2011). *Chem. Rev. 112*, 1196–1231.
14. Farrusseng D., Aguado S., Pinel C. (2009). *Angew. Chem. Int. Ed. 48*, 2–14.
15. Dhakshinamoorthy A., Alvaro M., Garcia H. (2011). *Catal. Sci. Tech. 1*, 856–867.
16. Lee J.Y., Farha O.K., Roberts J., Scheidt K.A., Ngyen S.T., Hupp J.T. (2009). *Chem. Soc. Rev. 38*, 1450–1459.
17. Meek S.T., Greathouse J.A., Allendorf M.D. (2011). *Adv. Mater. 23*, 249–267.
18. Janiak C. (2003). *Dalton. Trans.*, 781–2804.
19. Jiang H.-L., Xu Q. (2011). *Chem. Commun. 47*, 3351–3370.
20. Maksimchuk N.V., Kovalenko K.A., Fedin V.P., Kholdeeva O.A. (2011). *Israel J. Chem. 51*, 281–289.
21. Maksimchuk N.V., Zalomaeva O.V., Skobelev I.Y., Kovalenko K.A., Fedin V.P., Kholdeeva O.A. (2012). *Proc. R. Soc. A 468*, 2017–2034.
22. Ranocchiari M., van Bokhoven J.A. (2011). *Phys. Chem. Chem. Phys. 13*, 6388–6396.
23. Devic T., Serre C. In: *Ordered Porous Solid. Recent Advances and Prospects*. Valtechev V., Mintova S., Tsapatsis M., eds. Elsevier B. V., Oxford, Amsterdam, 2009, pp. 77–99.
24. Cundy C.S., Cox P.A. (2003). *Chem. Rev. 103*, 663–701.
25. Corma A. (1997). *Chem. Rev. 97*, 2373–2419.
26. Choi M., Cho H.S., Srivastava R., Venkatesan C., Choi D.-H., Ryoo R. (2006). *Nat. Mater. 5*, 718–723.
27. Taguchi A., Schuth F. (2004). *Micropor. Mesopor. Mater. 77*, 1–45.
28. Férey G., Mellot-Draznieks C., Serre C., Millange F., Dutour J., Surblé S., Margiolaki I. (2005). *Science 23*, 2040–2042.
29. Férey G., Serre C., Mellot-Draznieks C., Millange F., Surblé S., Dutour J. Margiolaki I. (2004). *Angew. Chem. Int. Ed. 43*, 6296–6301.
30. Hwang Y.K., Hong D.-Y., Chang J.-S., Jhung S.H., Seo Y.-K., Kim J., Vimont A., Daturi M., Serre C., Férey G. (2008). *Angew Chem. Int. Ed. 47*, 4144–4148.
31. Hong D.-Y., Hwang Y.K., Serre C., Férey G., Chang J.-C. (2009). *Adv. Funct. Mater. 19*, 1537–1552.
32. Horcajada P., Surblé S., Serre C., Hong D.-Y., Seo Y.-K., Chang J.-S., Greneche J.-M., Margiolaki I., Férey G. (2007). *Chem. Commun.*, 2820–2822.
33. Chui S.S.-Y., Lo S.M.-F., Charmant J.P.H., Prpen A.G., Williams I.D. (1999). *Science 283*, 1148–1150.
34. Dietzel P.D.C., Johnsen R.E., Blom R., Fjellvag H. (2008). *Chem. Eur. J. 14*, 2389–2397.
35. Rosi N.L., Kim J., Eddaoudi M., Chen B.L., O'Keeffe M.O., Yaghi O.M. (2005). *J. Am. Chem. Soc. 127*, 1504–1518.
36. Barthelet K., Marrot J., Riou D., Férey G. (2002). *Angew. Chem. Int. Ed. 41*, 281–284.
37. Cavka, J., Jakobsen S., Olsbye U., Guillou N., Lamberti C., Bordiga S., Lillerud K. (2008). *J. Am. Chem. Soc. 130*, 13850–13851.
38. Mueller U., Schubert M., Teich F., Puetter H., Schierle-Arndt K., Pastre J.J. (2006). *J. Chem. Mater. 16*, 626–636.

39. Serre C., Millange F., Thouvenot C. Noguès M., Marsolier G., Louër D., Férey G. (2002). *J. Am. Chem. Soc. 124*, 13519–13526.
40. Jhung S.H., Lee J.-H., Chang J.-S. (2005). *Bull. Kor. Chem. Soc. 26*, 880–881.
41. Jhung S.H., Lee J.-H., Yoon J.W., Serre C., Férey G., Chang J.-S. (2007). *Adv. Mater. 19*, 121–124.
42. Farha O.K., Hupp J.T. (2010). *Acc. Chem. Res. 43*, 1166–1175.
43. Farha O.K., Mulfort K.L., Thorsness A.M., Hupp J.T. (2008). *J. Am. Chem. Soc. 130*, 8598–8599.
44. Cooper A.I., Rosseinsky M.J. (2009). *Nature Chem. 1*, 26–27.
45. Vimont A., Leclerc H., Mauge F., Daturi M., Lavalley J.-M., Surblé S., Serre C., Ferey G. (2007). *J. Phys. Chem. 111*, 383–388.
46. Hwang Y.K., Hong D.-Y., Chang J.-S., Seo H., Yoon M., Kim J., Jhung S.H., Serre C., Ferey G. (2009). *Appl. Catal. A: General 358*, 249–253.
47. Seo Y.K., Yoon J.-W., Lee J.S. Lee U-W., Hwang Y.K., Jun C.H., Horcajada P., Serre C., Chang J.-S. (2012). *Micropor. Mesopor. Mater. 157*, 137–145.
48. Kim J., Bhattacharjee S., Jeong K.-E., Jeong S.-Y., Ahn W.-S. (2009). *Chem. Commun.*, 3904–3906.
49. Ramos-Fernandez E.V., Garcia-Domingos M., Juan-Alcaniz J., Gascon J., Kapteijn F. (2011). *Appl. Catal. A: General 391*, 261–267.
50. Kholdeeva O.A., Maksimchuk N.V., Maksimov G.M. (2010). *Catal. Today 157*, 107–113.
51. Maksimchuk N.V., Kovalenko K.A., Fedin V.P., Kholdeeva O.A. (2010). *Adv. Synth. Catal. 352*, 2943–2948.
52. Dhakshinamoorthy A., Alvaro M., Garcia H. (2009). *J. Catal. 267*, 1–4.
53. Dhakshinamoorthy A., Alvaro M., Garcia H. (2011). *ACS Catal. 1*, 48–53.
54. Song F., Wang C., Falkowski J.M., Ma L., Lin W. (2010). *J. Am. Chem. Soc. 132*, 15390–15398.
55. Huang Y., Liu T., Lin J., Lu J., Lin Z., Cao R. (2011). *Inorg. Chem. 50*, 2191–2198.
56. Qiu L.-G., Xie A.-J., Zhang L.-D. (2005). *Adv. Mater. 17*, 689–692.
57. Xie M.-H., Yang X.-L., Wu C.-D. (2011). *Chem. Commun.*, 5521–5523.
58. Zalomaeva O.V., Kovalenko K.A., Chesalov Y.A., Melgunov M.S., Zaikovskii V.I., Kaichev V.V., Sorokin A.B., Kholdeeva O.A., Fedin V.P. (2011). *Dalton Trans. 40*, 1441–1444.
59. Maksimchuk N.V., Kovalenko K.A., Arzumanov S.S., Chesalov Y.A., Melgunov M.S., Stepanov A.G., Fedin V.P., Kholdeeva O.A. (2010). *Inorg. Chem. 49*, 2920–2930.
60. Maksimchuk N.V., Timofeeva M.N., Melgunov M.S., Shmakov A.N., Chesalov Yu.A., Dybtsev D.N., Fedin V.P., Kholdeeva O.A. (2008). *J. Catal. 257*, 315–323.
61. Dhakshinamoorthy A., Alvaro M., Garcia H. (2011). *Chem. Eur. J. 17*, 6256–6262.
62. Di Nicola C., Karabach Y.Y., Kirillov A.M., Monari M., Pandolfo L., Pettinari C., Pombeiro A.J.L (2007). *Inorg. Chem. 46*, 221–230.
63. Alkordi M.H., Liu Y., Larsen R.W., Eubank J.F., Eddaoudi M. (2008). *J. Am. Chem. Soc. 130*, 12639–12641.
64. Kirillov A.M., Kopylovich M.N., Kirillova M.V., Haukka M., Guedes da Silva M.F.C., Pombeiro A.J.L. (2005). *Angew. Chem. Int. Ed. 44*, 4345–4349.

65. Karabach Y.Y., Guedes da Silva M.F.C., Kopylovich M.N., Gil-Hernandez B., Sanchiz J., Kirillov A.M., Pombeiro A.J.L. (2010). *Inorg. Chem. 49*, 11096–11105.
66. Burri D.R., Jun K.-W., Yoo J.S., Lee C.W., Park S.-E. (2002). *Catal. Lett. 81*, 16–173.
67. Laitinen I.inventor; Orion Corporation Fermion, assignee, US Patent 6,723,878. 2004.
68. Wang S., Li L., Zhang J., Yuan X., Su C.-Y. (2011). *J. Mater. Chem. 21*, 7098–7104.
69. Dhakshinamoorthy A., Alvaro M., Hwang Y.K., Seo Y.-K., Corma A., Garcia H. (2011). *Dalton Trans. 40*, 10719–10724.
70. Kockrick E., Lescouet T., Kudrik E.V., Sorokin A.B., Farrusseng D. (2011). *Chem. Commun. 47*, 1562–1564.
71. Yu F., Zheng P.-Q., Long Y.-X., Ren Y.-P., Kong X.-J., Long L.-S., Yuan Y.-Z., Huang R.-B., Zheng, L.-S. (2010). *Eur. J. Inorg. Chem. 28*, 4526–4531.
72. Meilikhov M., Yusenko K., Fischer R.A. (2009). *J. Am. Chem. Soc. 131*, 9644–9645.
73. Llabres i Xamena F.X., Casanova O., Galiasso Tailleur R., Garcia H., Corma A. (2008). *J. Catal. 255*, 220–227.
74. Tonigold M., Lu Y., Bredenkoetter B., Rieger B., Bahnmueller S., Hitzbleck J., Langstein G., Volkmer D. (2009). *Angew. Chem. Int. Ed. 48*, 7546–7550.
75. Bhattacharjee S., Yang D.-A., Ahn W.-S. (2011) *Chem. Commun. 47*, 3637–3639.
76. Cho S.-H., Ma B., Nguyen S.T., Hupp J.T., Albrecht-Schmitt T.E. (2006). *Chem. Commun.*, 2563–2565.
77. Cho S.-H., Gadzikwa T., Afshari M., Nguyen S.T., Hupp J.T. (2007). *Eur. J. Inorg. Chem.*, 4863–4867.
78. Farha O.K., Shultz A.M., Sarjeant A.A., Nguyen S. T., Hupp J.T. (2011). *J. Am. Chem. Soc. 133*, 5652–5655.
79. Leus K., Muylaert I., Vandichel M., Marin G.B., Waroquier M., Van Speybroeck V., Van Der Voort P. (2010). *Chem. Commun.*, 5085–5087.
80. Quartapelle Procopio E., Linares F., Montoro C., Colombo V., Maspero A., Barea E., Navarro J.R. (2010). *Angew. Chem. Int. Ed.*, *49*, 7308–7311.
81. Brown K., Zolezzi S., Aguirre P., Venegas-Yazigi D., Paredes-Garcia V., Baggio R., Novak M.A., Spodine E. (2009). *Dalton Trans*. 1422–1427.
82. Lee J.S., Halligudi S.B., Jang N.H., Hwang D.W., Chang J.-S., Hwang Y.K. (2010). *Bull. Kor. Chem. Soc. 31*, 1489–1495.
83. Dhakshinamoorthy A., Alvaro M., Garcia H. (2011). *ACS Catal. 1*, 836–840.
84. Jiang D., Mallat T., Meier D.M., Urakawa A., Baiker A. (2010). *J. Catal. 270*, 26–33.
85. Liu H., Liu Y., Li Y., Tang Z., Jiang H. (2010). *J. Phys. Chem. C. 114*, 13362–13369.
86. Su F.Z., Liu Y.M., Wang L.C., Cao Y., He H.Y., Fan K.N. (2008). *Angew. Chem., Int. Ed. 47*, 334–337.
87. Ishida T., Nagaoka M., Akita T., Haruta M. (2008). *Chem. Eur. J. 14*, 8456–8460.
88. Osako T., Uozumi Y. (2009). *Chem. Lett.*, 902–903.
89. Bhattacharjee S., Choi J.-S., Yang S.-T., Choi S.B., Kim J., Ahn W.-S. (2010). *J. Nanosci. Nanotechnol. 10*, 135–141.
90. Kato C.N., Mori W. (2007). *C. R. Chimie 10*, 284–294.
91. Tarasov A.L., Kustov L.M., Isaeva V.I., Kalenchuk A.N., Mishin I.V., Kapustin G.I., Bogdan V.I. (2011). *Kinet. Catal. 52*, 273–276.

92. Mueller M., Turner S., Lebedev O.I., Wang Y., van Tendeloo G., Fischer R.A. (2011). *Eur. J. Inorg. Chem.*, 1876–1887.
93. Wu Y., Qiu L.-G., Wang W., Li Z.-Q., Xu T., Wu Z.-Y., Jiang X. (2009). *Trans. Metal Chem. 34*, 263–268.
94. Proch S., Herrmannsdörfer J., Kempe R., Kern C., Jess A., Seyfarth L., Senker J. (2008). *Chem. Eur. J. 14*, 8204–8212.
95. Ishida T., Nagaoka M., Akita T., Haruta M. (2008). *Chem. Eur. J. 14*, 8456–8460.
96. Llabres i Xamena F.X., Abad A., Corma A., Garcia H. (2007). *J. Catal. 250*, 294–298.
97. Dybtsev D.N., Nuzhdin A.L., Chun H., Bryliakov K.P., Talsi E.P., Fedin V.P., Kim K. (2006). *Angew. Chem. Int. Ed. 45*, 916–920.
98. Perles J., Iglesias M., Martin-Luengo M.-A., Monge M. A., Ruiz-Valero C., Snejko N. (2005). *Chem. Mater. 17*, 5837–5842.
99. Perles J., Snejko N., Iglesias M., Monge M.A. (2009). *J. Mater. Chem. 19*, 6504–6511.
100. Gandara F., Gutierrez Puebla E., Iglesias M., Proserpio D.M., Snejko N., Angeles M.M. (2009). *Chem. Mater. 21*, 655–661.
101. Gomez-Lor B., Gutiérrez-Puebla E., Iglesias M., Monge M. A., Ruiz-Valero C., Snejko N. (2002). *Inorg. Chem. 41*, 2428–2432.
102. Dhakshinamoorthy A., Alvaro M., Garcia H. (2010). *Chem. Commun.*, 6476–6478.
103. Dhakshinamoorthy A., Alvaro M., Garcia H. (2010). *ChemCatChem. 2*, 1438–1443.
104. Kirillov A.M., Kopylovich M.N., Kirillova M.V., Haukka M., Guedes da Silva M.F.C., Pombeiro A.J.L. (2005). *Angew. Chem. Int. Ed. 44*, 4345–4349.
105. Loiseau T., Serre C., Huguenard C., Fink G., Taulelle F., Henry M., Bataille T., Férey G. (2004). *Chem. Eur. J. 10*, 1373–1382.
106. Park K.S., Ni Z., Côte A.P., Cho J.Y., Huang R., Uribe-Romo E.J., Chae H.K., O'Keeffe M., Yaghi O.M. (2006). *PNAS 103*, 10186–10191.
107. Low J.J., Benin A.I., Jakubczak P., Abrahamian J.F., Faheem S.A., Willis R.R. (2009). *J. Am. Chem. Soc. 131*, 15834–15842.
108. Cychosz K.A., Matzger A.J. (2010). *Langmuir 26*, 17198–17202.
109. Kang I.J., Khan N.A., Haque E., Jhung S.H. (2011). *Chem. Eur. J. 17*, 6437–6442.

9

HETEROGENEOUS PHOTOCATALYSIS FOR SELECTIVE OXIDATIONS WITH MOLECULAR OXYGEN

ANDREA MALDOTTI,* ROSSANO AMADELLI, AND ALESSANDRA MOLINARI

9.1 INTRODUCTION

Photocatalysis, in its broader meaning, indicates catalytic processes initiated by light. The term is now largely used with reference to heterogeneous catalysis on semiconductor materials, due to the enormous development of this discipline in wastewater decontamination or water splitting for the generation of hydrogen as a fuel. Related applications in organic syntheses have equally attracted much interest [1–14] already from the infancy of the studies on photoelectrocatalysis, thirty years ago [15]. Photocatalysis for synthetic purposes concerns the light-induced chemical transformations of organic or inorganic substrates that are transparent in the wavelength range examined. Radiation absorbed by a photocatalyst leads to electronically excited states that, if sufficiently long-lived, can cause chemical reactions to take place. The overall process can be considered photocatalytic when (i) the photoactive species is regenerated in its initial state at the end of a reaction cycle, as happens in thermal catalysis; (ii) the photocatalyst is consumed less than in stoichiometric amounts, while light is a stoichiometric reagent. Albini and coworkers report that the reaction path in photocatalysis involves the lowest potential energy surface at any configuration of the reagent, as occurs in thermal reactions

*Corresponding author

Liquid Phase Oxidation via Heterogeneous Catalysis: Organic Synthesis and Industrial Applications, First Edition. Edited by Mario G. Clerici and Oxana A. Kholdeeva.
© 2013 John Wiley & Sons, Inc. Published 2013 by John Wiley & Sons, Inc.

and contrary to direct irradiation or photoinduced energy-transfer processes where part of the path occurs through excited-state surface [8].

Photocatalysis is particularly relevant to "sustainable and green chemistry" by virtue of the possibility to obtain fine chemicals with a low environmental impact. In fact, photochemical reactions require milder conditions than thermal processes as they involve sunlight as a completely renewable energy source. Additionally, side processes are often minimal because of mechanistic pathways involving short and efficient reaction sequences.

Selectivity is a key issue in fine chemicals production through photocatalysis, as in conventional catalysis. In order to pursue this objective, all steps of the catalytic process must be optimized. In particular, for heterogeneous systems, the efficiency and selectivity of photocatalytic processes can be maximized through tailoring the nature of the catalytic center and/or its microscopic environment, for example through control of the nature of the solid/liquid interface and catalyst porosity. In particular, the type and textural characteristics of the employed material have been shown to affect important parameters such as absorption of light, adsorption–desorption equilibria of reaction intermediates, control of reactants and products diffusion in or out of catalytic sites located inside of a porous network. It is in this context that recent developments in the discovery of strategies for the preparation of materials with well-defined structures at the nanometer scale may afford better design of active sites for selective catalytic processes, including photocatalytic processes [16]. Such goal is well described by the concept of *Site Isolation* introduced by Callahan and Grasselli [17]. The term indicates that a selective reaction to partial oxidation product requires a surface arrangement that limits the attack on the adsorbed intermediate, so that desorption of partially oxidized species is faster than its consecutive oxidation and degradation. One example of such approach is described in our earlier work on TiO_2 modified with Fe-porphyrins [9].

Of course, from the practical point of view, an important role of a solid support is that the photocatalysts become more easily handled and recycled.

Oxidation of organic molecules with an environmentally friendly and cheap species such as O_2 represents a major target from the synthetic and industrial points of view [18–20] and, in this context, this contribution describes results obtained on the selective oxidation of alcohols and the mono-oxygenation of hydrocarbons in the presence of molecular oxygen. We classify the significant features of widely used heterogeneous photocatalysts with a focus on titanium dioxide, highly dispersed oxides and polyoxotungstates. These compounds share similar primary photoreactions: light absorption induces a charge-separation process with formation of positive holes able to oxidize organic substrates. We emphasize that the optimal tailoring of the photoactive materials for synthetic purposes can be achieved by combining recent advances in the preparation of nanostructured materials with mechanistic knowledge derived from surface science and molecular-level investigations.

In the first part of this contribution, starting with the very basic principles that govern the primary photochemical steps, we proceed to examine the mechanisms of subsequent activation processes of both the substrate and molecular oxygen.

The second part mainly aims to present representative synthetic applications of photocatalysis. Some of the articles considered for this purpose are also mentioned in the first part that focuses on mechanistic aspects. We show that organized assemblies can drive the photochemical processes as well as the subsequent thermal reactions in order to control the efficiency and selectivity of the oxidation process. The more significant data on conversion and productivity are reported in tables or mentioned in the text.

9.2 CATALYSTS PREPARATION AND MECHANISTIC ASPECTS

All the photoactive compounds considered here are characterized by analogous primary photoprocesses. Absorption of light by their ground states (P, Eq. 1 of Figure 9.1) produces an excited state (P^*) from which oxidation of molecular or anionic species (S) and reduction of O_2 simultaneously occur (Eq. 2 of Figure 9.1), with an efficiency that depends on the possibility that the excited photocatalyst reacts successfully before its deactivation (Eq. 3 of Figure 9.1). The process occurs in a cyclic way and leads to the formation of the intermediates $S^{\cdot +}$ and the O_2-reduction species, which take part effectively in the subsequent oxofunctionalization of S.

9.2.1 Titanium Dioxide

Titanium dioxide is certainly the most investigated semiconductor in photocatalysis since it combines unique and attractive characteristics, such as high photocatalytic activity and chemical stability. There is an ever-increasing attention to tailoring the reactivity of TiO_2-based photocatalysts to drive reactions of interest from the synthetic point of view [1–12]. It is generally accepted [1–12, 21–25] that excitation of TiO_2 with suprabandgap photons of wavelength lower than 400 nm causes a charge separation in the semiconductor solid: electrons are promoted to the conduction band (e^-) and holes are left in the valence band (h^+) (Figure 9.2). Subsequently, the photogenerated charges can either recombine or undergo interfacial electron-transfer processes with adsorbed substrates. While in a n-type photoelectrode electrons can be conveyed through an external circuit, in a suspension of the same semiconductor both charges have to be transferred through the interface to independent (acceptor and donor) species. This means that, for charge transfer to compete with

$$P + h\nu \longrightarrow P^* \qquad (1)$$

$$P^* + S + O_2 \longrightarrow S^{\cdot +} + P + \text{reduction product of } O_2 \qquad (2)$$

$$P^* \longrightarrow P + h\nu'/\Delta T \qquad (3)$$

FIGURE 9.1 Common primary photochemical process.

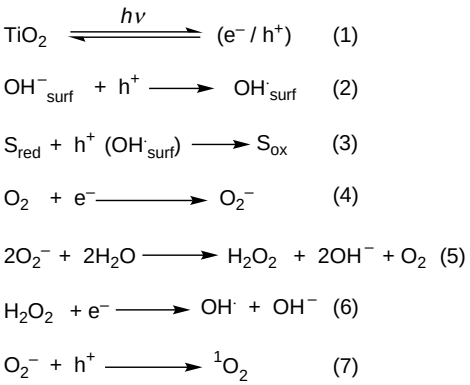


FIGURE 9.2 Possible reactions occurring after photoinduced charge separation on TiO_2.

recombination, reaction of at least one of the photogenerated charges with species in solution or at the surface must be a fast process.

Photo-oxidation of an organic substrate (S_{red}) can, in principle, take place according to Eqs. 1–3 of Figure 9.2 directly by hole capture or indirectly by primarily formed $OH^{\bullet}$ radicals. Because of its considerable oxidizing capability, TiO_2 is able to further photo-oxidize partially oxygenated products up to full mineralization of the starting organic substrate. This overoxidation process, which has contributed to the development of many studies focusing on environmental clean up, may be a problem when photoexcited TiO_2 must be employed for synthetic purposes.

Due to its unlimited availability, O_2 is a commonly employed electron acceptor independently of whether the target is mineralization or photosynthesis. Consequently, its reduction according to the commonly accepted pathway (Eqs. 4–6 of Figure 9.2) has been the focus of intense research and has been examined, in particular, in a number of seminal publications [26–28]. Analysis of photocatalytic oxidations revealed that the role of O_2 is not only that of scavenging the photogenerated electrons but, rather, its reductive activation contributes fundamentally to the overall photocatalytic process: organic radical intermediates can react with O_2 or the products of its reduction in a series of cross reactions leading to partial or total oxidation, depending on experimental conditions [29–31].

From a macroscopic point of view, it is accepted that the rates of reduction and oxidation must be equal at steady state to conform with electroneutrality requirements. Then, a different approach also named "O_2 flux-matching conditions" is described in the literature [32, 33]. This originates from the so-called "local cell mechanism" widely used in electrochemistry and is based on the fact that the anodic (i_{ox}) and cathodic (i_{red}) currents must be equal at steady state under no bias conditions. The anodic and cathodic curves, recorded separately on a photoelectrode of the same material, define a unique point (I_{mix}) which also corresponds to the working conditions of particles in suspensions (Figure 9.3). For the case where

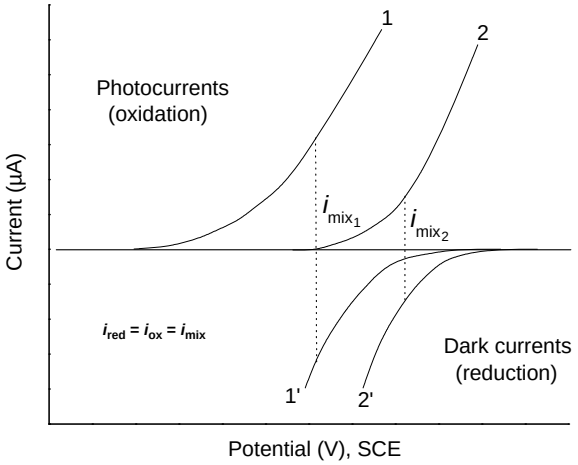


FIGURE 9.3 Local cell model of the photocurrents and dark currents for an illuminated TiO_2 electrode near open-circuit conditions.

I_{mix} is maximum, one observes the higher photocatalytic activity. This model is quite general and has been verified for a number of photocatalytic systems consisting of particles suspensions [34].

Superoxide is an important product of oxygen activation (Eq. 4 of Figure 9.2) and its role increases in nonaqueous solvents where it is considerably stable. It is, however, quite stable in aqueous solution too, where its lifetime is reported to be as much as 10 s [35]. Research on the role of O_2^- in photocatalytic systems and on TiO_2, in particular, is very intense [36]. Due to its stability and to the fact that its concentration reaches appreciable values [37], O_2^- can dismutate (Eq. 5 of Figure 9.2) to give peroxide but can also give singlet oxygen. Indeed, evidence of the presence of $^1O_2$ has been reported and its formation mechanism seemingly involves reaction of superoxide with holes rather than the energy-transfer route (Eq. 7 of Figure 9.2) [38]. The reaction is inhibited by adsorbed hole scavengers such as halides or ethanol.

There is now a number of studies indicating that it is possible to control the activity and selectivity of TiO_2-based photocatalysts by designing nanostructured materials with specific morphology and surface properties. In this context, TiO_2 particles, embedded in mesoporous silica, have been prepared by a surfactant-templating method or aggregation of nanosized TiO_2 particles [39–41]. Other TiO_2-based mesoporous photocatalysts have been obtained by templating preformed TiO_2 nanoparticles [42]. The preparation of these materials differs from conventional methods based on the use of relevant metal precursor in that the building blocks are preformed nanoparticles adequately stabilized by ligands that, after templation with surfactants, will form part of the pore walls [43, 44]. Synthesis and calcination finally produce very robust photocatalysts (Figure 9.4).

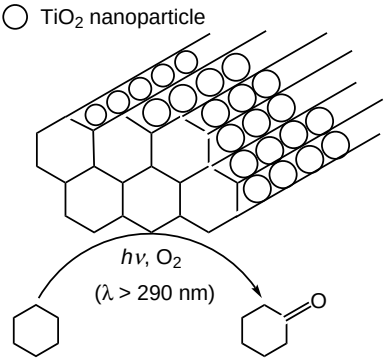


FIGURE 9.4 MCM-organized TiO_2 materials employed in the photo-oxygenation of cyclohexane to cyclohexanone with O_2.

Pillared clays are two-dimensional zeolite-like materials in which the original charge-compensating cations of the clay are exchanged by inorganic metal cations such as titanium. After calcination of the material, TiO_2 pillars are formed and interlayer and interpillar spaces are generated. These TiO_2-pillared clays have been employed for the photocatalytic oxidation of organic substrates [45, 46]. Selective organic oxidation can also be photocatalyzed by Y, beta, mordenite and ZSM-5 zeolites containing TiO_2 [47, 48]. In these systems, nanosized TiO_2 clusters can be obtained by ionic exchange between Na^+ and titanyl cations ($Ti{=}O^{2+}$) followed by condensation. The maximum loading of TiO_2 is determined by the cavity size and by the number of exchangeable cations [48].

Cristallinity is another important parameter affecting the photocatalytic activity of TiO_2. Anatase, rutile and brookite TiO_2 can be prepared with a simple sol-gel procedure that allows any calcination treatment to be avoided. These materials have been extensively studied as oxidation photocatalysts in aqueous medium [49–55]. Very recently, novel insights into the effect of crystallinity, availability of holes and electrons and the amount of surface OH-groups of anatase TiO_2 have been reported [56, 57].

9.2.2 Highly Dispersed Oxides

Highly dispersed metal-oxide species loaded on inorganic supports, such as micro- and mesoporous silica and aluminum oxide, exhibit interesting photocatalytic activities for synthetic purposes. These photocatalysts, containing spatially isolated catalytic active sites and called for this feature "single-site" photocatalysts, can often promote more selective organic transformations as compared to the bulk metal oxides [6]. TiO_2–SiO_2 binary oxides presenting isolated tetrahedral Ti species have been prepared by a sol-gel method consisting of a two-stage hydrolysis procedure

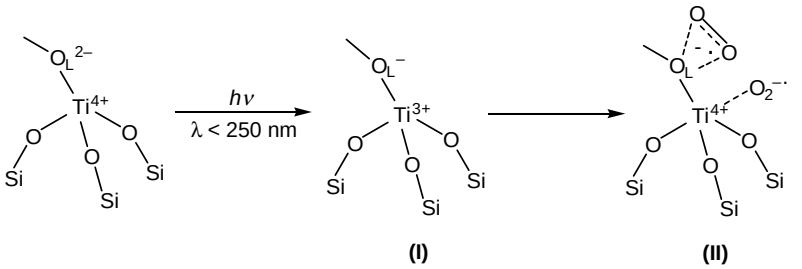


FIGURE 9.5 Photoinduced redox process on isolated Ti-oxide species and subsequent reaction with molecular oxygen.

[58–60]. In the first step, partial hydrolysis of tetraethylorthosilicate (TEOS) is obtained by mixing it with ethanol, distilled water and nitric acid. Then, gelation is completed by addition of an alcoholic solution of titanium isopropoxide. Finally, the gel is dried and calcined. Ti-containing mesoporous silica with hexagonal MCM-41 structure is prepared by adding a mixture of TEOS and tetramethylammonium hydroxide to an aqueous solution of cetyltrimethylammonium bromide as surfactant. Then, tetrabutyl orthotitanate is added to the mixture. The resulting solid is recovered after some days, washed, dried and calcined [61, 62]. Following an analogous synthetic procedure and aiming to control the hydrophobicity of the matrix, Ti-containing mesoporous organosilicas have been prepared by introducing 1,2-bis (triethoxysilyl)ethane together with TEOS and the surfactant [63]. Microporous titanosilicate ETS-10, containing one-dimensional linear chains of TiO_6 octahedra, has been obtained starting from an aqueous basic sodium silicate solution to which a $TiCl_3$ solution was added. After treatment at high temperature in an autoclave, the resulted crystalline product was recovered, washed and dried in vacuo [64, 65].

Upon photoexcitation of isolated Ti-oxide species, a localized excited state is produced (Figure 9.5, **I**). Deep studies concerning the mechanism of this photocatalytic process have been reported [59, 60]. The photoactive materials T-S(0.34) and T-S(0.1), with $Ti/(Ti + Si) = 0.34$ mol% and $Ti/(Ti + Si) = 0.1$ respectively, show a narrow absorption band centered at 210 nm that is assigned to a ligand-to-metal charge transfer between lattice oxygen and highly dispersed tetrahedral Ti^{4+}. So, when isolated [Ti^{4+}-$O_L{}^{2-}$] absorbs UV light ($\lambda < 250$ nm), a charge transfer from $O_L{}^{2-}$ to Ti^{4+} occurs and the excited state [Ti^{3+}-$O_L{}^{-}$]* is formed (Figure 9.5, **I**). Then, both $O_L{}^-$ and Ti^{3+} react with O_2 to produce two types of oxygen radicals, $O_3{}^{-\cdot}$ and $O_2{}^{-\cdot}$ (**II** in Figure 9.5). $O_3{}^{-\cdot}$ formed on $O_L{}^-$ has an electrophilic nature and adds directly to electron-rich bonds, while $O_2{}^{-\cdot}$ attracts the electron on Ti^{3+}, so preventing the otherwise very fast charge recombination with the hole on the lattice oxygen and stabilizing $O_3{}^{-\cdot}$. The samples containing more than 1 mol% Ti show additional absorption bands above 250 nm, which are assigned to the LMCT from O to Ti of aggregated titanium oxide species. The absorption edge is shifted to longer wavelengths with increasing Ti content and becomes close to that of bulk TiO_2.

Highly dispersed Cr-oxide species have been prepared following procedures similar to those described above for titanium [66–69]. Cr-SiO_2 is obtained by a sol-gel method using TEOS and $Cr(NO_3)_3{\cdot}9H_2O$ as starting materials [66, 68, 69]. Cr/MCM-41 is prepared by mixing MCM-41 and $Cr(NO_3)_3{\cdot}9H_2O$ and heating until evaporation of water. The yellowish powder is then calcined [68, 69]. An analogous procedure is also followed for the preparation of a catalyst where Cr is put on a mesoporous organo-modified silica, which is prepared starting from TEOS and 1,2-bis(triethoxysilyl)ethane [67, 70]. CrO_x-SiO_2 binary oxide shows three absorption bands centered at 245,330 and 460 nm, which are assigned to the LMCT (from O^{2-} to Cr^{6+}) transitions of monochromate species that are highly dispersed on silica matrix [68]. Increasing of Cr loading leads to an additional absorption band in the 580–800 nm region that is assigned to the d–d transition of octahedral Cr^{3+} in Cr_2O_3 clusters.

Vanadium oxide has been supported on alumina by impregnating the support with an aqueous solution of ammonium metavanadate and evaporating to dryness [71–73]. Vanadium has been loaded into siliceous mesoporous SBA-15 by different impregnation methods that use aqueous or methanolic solutions of ammonium metavanadate [74]. V-containing mesoporous silica with tetrahedrally coordinated V-oxide species ($V^{V}O_4$) has been prepared by a modified surfactant-templating method, consisting of an addition of surfactant to a mixture of water, alcohol, and Si and V precursors followed by calcination [75]. Vanadium-containing silicas show an absorption band below 400 nm, that is attributed to the LMCT transition from a terminal oxygen O^{2-} to V^{5+} to produce the couple V^{4+}-O^{-} [75]. The electrophilic character of O^{-} is responsible for the subsequent reaction with an organic substrate.

9.2.3 Polyoxotungstates

Iso- and heteropolyoxotungstates (POT) are tungsten-oxygen anionic clusters that can be considered soluble models of semiconductor metal oxide surfaces. They are prepared by condensation reactions starting from acidic solutions of $WO_4{}^{2-}$. When the reaction is carried out in the presence of a heteroatom, such as P or Si, a heteropolyoxotungstate can be obtained [76, 77]. These oxides have been intensively studied over the past 20 years because they exhibit interesting properties as catalysts and photocatalysts [9, 78–85]. In particular, the ability to undergo photoinduced multielectron transfers, without any change in structure, renders polyoxotungstates a very attractive class of photocatalysts. Among them, the polyoxotungstate $W_{10}O_{32}{}^{4-}$ (Figure 9.6) presents an absorption spectrum in the near-UV region ($\lambda_{max} = 323$ nm) that partially overlaps the UV solar emission spectrum, opening up the possibility to carry out benign solar-photoassisted applications [9, 77, 78, 83–85].

The cascade of events that follows light absorption by $W_{10}O_{32}{}^{4-}$ has been deeply investigated and is described in the following (Figure 9.7) [86–89]. Excitation of $W_{10}O_{32}{}^{4-}$ ($\lambda = 323$ nm) leads to an oxygen to metal [O^{2-}–W^{6+}] charge transfer excited state ($W_{10}O_{32}{}^{4-*}$, Figure 9.7**a**), in analogy to the photoinduced charge separation processes that occur in TiO_2 and highly dispersed oxides [85, 90]. Then, $W_{10}O_{32}{}^{4-*}$ decays in less than 30 ps to a very reactive nonemissive transient,

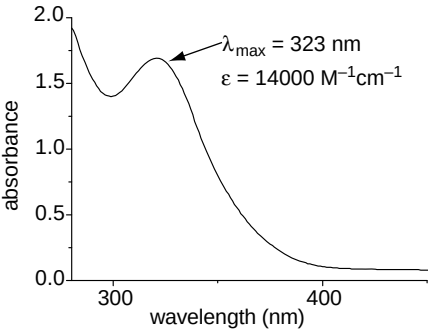


FIGURE 9.6 Absorption spectrum of $W_{10}O_{32}^{4-}$.

indicated as wO (step **b**). This species has an oxyradical-like character due to the presence of an electron-deficient oxygen center and has a lifetime of 65 ±5 ns and a quantum yield of formation of 0.57. wO possesses a very high reactivity towards any organic substrate RH: quenching of wO may occur either by hydrogen-atom abstraction or an electron-transfer mechanism, depending on the chemical nature of RH. In any case, both mechanisms lead to the one-electron-reduced form of decatungstate ($HW_{10}O_{32}^{4-}$) and to the substrate-derived radical (R•) (step **c**). At this stage, O_2 can regenerate the starting $W_{10}O_{32}^{4-}$ with parallel formation of peroxy compounds (step **d**).

The first examples of polyoxotungstates heterogenized on solid supports go back to about fifteen years ago [80, 91]. The main features of these materials are that they are easily handled and recyclable and that they can be employed in reaction media where the polyoxotungstates are insoluble. Different preparation procedures have been explored with the aim of controlling the microenvironment surrounding the photoactive species. The simplest is impregnation: it consists in the dissolution of polyoxotungstate in a suitable solvent, addition of a solid support and slow evaporation of the solvent until dryness. Among the available supports, the most

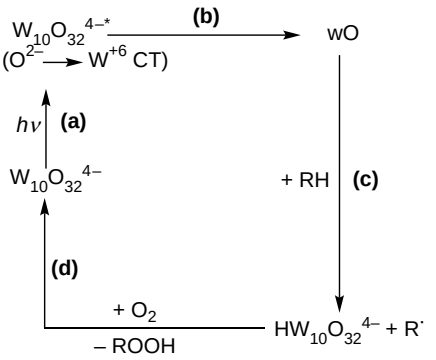


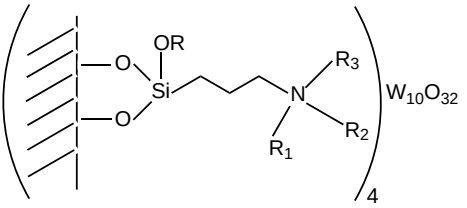
FIGURE 9.7 Reaction mechanism of photoexcited $W_{10}O_{32}^{4-}$.

frequently employed have been amorphous silica [92–96], mesoporous silica such as MCM-41 [97, 98], γ-alumina [96] and zeolite Y [99].

A new heterogenization procedure, proposed by Guo and coworkers some years go, allows the encapsulation of POTs inside a silica network *via* a sol-gel technique [100–102]. A CH_3CN/H_2O solution of the chosen polyoxotungstate, adjusted at pH 2, is added dropwise to a solution of tetraethylortho silicate (TEOS) and 1-butanol. After some hours of stirring and gentle warming, the hydrogel is dried and calcined to increase the rate of formation of silica network. Following this procedure, $Na_4W_{10}O_{32}$, $(n\text{-}Bu_4N)_4W_{10}O_{32}$, $H_3PW_{12}O_{40}$ and $H_4SiW_{12}O_{40}$ have been entrapped into the silica network during hydrolysis of TEOS [103–105]. Moreover, when TEOS has been replaced by zirconium (IV) *n*-butoxide, new analogous materials have been prepared where $Na_4W_{10}O_{32}$ and $H_3PW_{12}O_{40}$ are supported on zirconia [106, 107]. In all these materials the polyoxotungstate is firmly entrapped in the solid matrix *via* both electrostatic interactions and hydrogen bonding. In fact, protonated silanol groups act as positive counterions for the polyoxoanions and hydrogen bonds take place between the oxygen atoms of the polyoxotungstate and the hydroxy groups of the silica or zirconia networks. In the case of $W_{10}O_{32}{}^{4-}/SiO_2$ systems, the preservation of the absorption band at 323 nm and the maintenance of the fingerprint in the region from 1000 to 450 cm^{-1} after heterogenization is easily established by UV and IR spectroscopies and allowed the authors to conclude that the integrity of the photoactive polyoxoanion structure is retained [105].

As an alternative to the conventional impregnation or sol-gel entrapment procedures, it has been reported that $W_{10}O_{32}{}^{4-}$ can be supported on a solid matrix by ionic exchange [108–111]. Amberlite IRA-900 in the chloride form has been employed as support for $(n\text{-}Bu_4N)_4W_{10}O_{32}$ by our research group; the ion exchange of Cl^- with $W_{10}O_{32}{}^{4-}$ is favored by the soft character of $\text{-}N(CH_3)_3{}^+$ cations [108]. In a very similar way, $W_{10}O_{32}{}^{4-}$ has been successfully immobilized on poly (4-vinylpyridine) crosslinked methyl chloride quaternary salt [109]. In both cases the ionic interaction is strong enough to prevent the release of the polyoxoanion into the solution.

An ion-exchange procedure has been also employed to support $W_{10}O_{32}{}^{4-}$ on a silica matrix previously functionalized [110, 111]. The preparation of anchored primary and tertiary ammonium salts has been performed by reacting silica and the suitable (alkyl-aminopropyl)trialkoxysilane followed by acidification with trifluoromethane sulfonic acid. The preparation of supported quaternary ammonium salts has been carried out by condensation of (bromopropyl)trimethoxysilane with silica silanols and a subsequent reaction with triethylamine. Then, immobilization of $W_{10}O_{32}{}^{4-}$ has been realized by stirring a mixture of the selected surface-bound alkylammonium salt and an aqueous solution of sodium decatungstate (Figure 9.8) [110]. The polyoxoanion is firmly held on the support by ionic bonds with tetraalkylammonium cations in $Si\text{-}(alkyl)_4NW$, with trialkylammonium cations in $Si\text{-}(alkyl)_3NHW$ and with monoalkylammonium cations in $Si\text{-}alkylNH_3W$. Mesoporous silica SBA-15 has been modified by initial insertion of alkyl groups of chosen length using $C_n\text{-}Si(OEt)_3$ ($n = 2$, 4, 8, 16) followed by grafting of 3-aminopropyl groups [111]. The resulting material is acidified and then the ion exchange by



R_1, R_2, R_3 = H, H, H Si-alkylNH_3W
= Et, Et, H Si-(alkyl)$_3$NHW
= Et, Et, Et Si-(alkyl)$_4$NW

FIGURE 9.8 Structure of photocatalysts obtained upon heterogenization of $W_{10}O_{32}^{4-}$ by ionic exchange on silica functionalized with various ammonium cations.

decatungstate is carried out. 3-Ammoniumpropyl groups ($-(CH_2)_3NH_3^+$) immobilize $W_{10}O_{32}^{4-}$ on the pore walls, while the alkyl chains form hydrophobic regions around the decatungstate.

Among the different techniques for the immobilization of decatungstate, the occlusion in polymeric membranes offers new developments in aqueous photocatalysis. In fact, in water, the choice of an appropriate hydrophobic support may be the key to discriminate among reactants. In this context, Bonchio and coworkers have embedded $W_{10}O_{32}^{4-}$ in several polymeric membranes, such as polyvinylidene fluoride (PVDF) and polydimethylsiloxane (PDMS), using a phase inversion technique or a hydrosilylation reaction [112, 113]. Moreover, they have also prepared a new hybrid photocatalyst by embedding the fluorous-tagged decatungstate $(R_fN)_4W_{10}O_{32}$ ($R_fN = [CF_3(CF_2)_7(CH_2)_3]_3CH_3N^+$) within fluoropolymeric films, like Hyflon (Figure 9.9) [113, 114]. The peculiar aspect of this film is its high permeability for O_2 that renders this system of particular interest in oxidative photocatalysis.

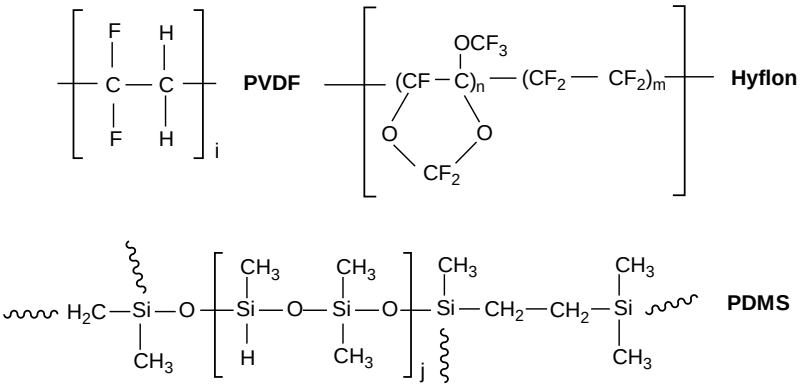


FIGURE 9.9 Polymeric and fluoropolymeric membranes used for the immobilization of decatungstate anion.

A very new generation of catalytically active membranes has been developed by using a low temperature plasma surface-modification technique that allows modification or functionalization by grafting, in a controlled way, only the topmost few layers of membranes while retaining their mechanical, physical and bulk properties. For instance, a PVDF membrane has been modified by plasma treatment to graft amino groups at its surface, which, in turn, have been used to anchor $W_{10}O_{32}^{4-}$ and $PW_{12}O_{40}^{3-}$ in a highly precise way [115, 116]. Although no applications for partial photocatalytic oxidations are present in the literature up to now, we cite here these results as a first successful example of plasma treatments applied for the heterogenization of polyoxotungstates on polymeric membranes.

9.3 CATALYTIC PROPERTIES

9.3.1 Oxidation of Alkanes

Catalytic oxidation of alkanes represents a fundamental process for the production of important chemicals [117–119]. In this context, there is a strong demand for the development of robust heterogeneous catalysts that can promote selective oxygenation of C−H bonds by O_2 under mild temperature and pressure conditions.

9.3.1.1 With Titanium Dioxide The liquid phase oxygenation of cyclohexane by photoexcited semiconductors such as TiO_2 continues to be the object of intense research for two main reasons. On the one hand, the study of this representative key reaction can provide insights on the oxygenation mechanism of nonactivated C−H bonds; on the other hand, the conversion of cyclohexane to cyclohexanone is important since this ketone is a precursor in the synthesis of adipic acid and caprolactam, which are ultimately used in the production of nylon 66 and nylon 6.

A number of articles indicate that the oxidation of cyclohexane by photoexcited TiO_2 at room temperature and atmospheric pressure yields cyclohexanone as the main product (selectivity higher than 80%) and minor amounts of cyclohexanol and carbon dioxide [42, 56, 57, 120–129]. Figure 9.10 summarizes the main steps of the

$$TiO_2 \xrightarrow{h\nu} e^-/h^+ \quad (1)$$

$$h^+ + C_6H_{12} \longrightarrow C_6H_{11}^{\cdot} \quad (2)$$

$$C_6H_{11}^{\cdot} + O_2 \longrightarrow C_6H_{11}OO^{\cdot} \quad (3)$$

$$C_6H_{11}OO^{\cdot} + e^- + H^+ \longrightarrow C_6H_{10}O + H_2O \quad (4)$$

$$2C_6H_{11}OO^{\cdot} \longrightarrow C_6H_{10}O + C_6H_{11}OH + O_2 \quad (5)$$

$$C_6H_{11}^{\cdot} + OH^{\cdot}_{surf} \longrightarrow C_6H_{11}OH_{surf} \quad (6)$$

$$C_6H_{11}OH_{surf} + 2OH^{\cdot}_{surf} \longrightarrow C_6H_{10}O + 2H_2O \quad (7)$$

FIGURE 9.10 Main steps of the reaction mechanism of cyclohexane oxidation by photoexcited TiO_2.

reaction mechanism. The cyclohexyl radicals, photogenerated as in Eqs. 1 and 2 of the figure, are able to react with O_2 under a diffusion-controlled rate to give peroxy radicals. Since hydrogen-atom abstraction by cyclohexyl-peroxy radicals is energetically unfavorable due to the high C−H bond dissociation energy in cyclohexane, the fate of these radicals is strongly determined by the competition between their reaction with the photogenerated electrons (Eq. 4) and their bimolecular radical disproportionation (Eq. 5). This competition affects the final yields to cyclohexanone and cyclohexanol [42, 57, 124, 126]. Cyclohexanol may also be formed on the surface of the semiconductor as a consequence of the reaction between cyclohexyl radical and $OH^{\bullet}$ radicals (Eq. 6). Consecutive photocatalytic oxidation of adsorbed cyclohexanol is a likely additional source of cyclohexanone (Eq. 7) [121]. Further overoxidation processes may yield strongly adsorbed carboxylates and carbonates that, likely, are a main cause of TiO_2 deactivation [125, 130] and that, finally, lead to the formation of carbon dioxide.

Several investigations report that adsorption equilibria of cyclohexanol and cyclohexanone strongly affect the final product distribution of the photocatalytic process [120–122, 125, 127, 131–133]. More specifically, it has been demonstrated [122, 125] that cyclohexanol is preferentially adsorbed onto the hydrophilic surface of TiO_2 with respect to both cyclohexane and cyclohexanone and, therefore, it undergoes facile overoxidation ultimately to CO_2. On the other hand, cyclohexanone is less adsorbed than cyclohexanol thus explaining, at least in part, its accumulation in the solution bulk. Dynamic step-response and pulse-response experiments have been carried out together with ATR FTIR spectroscopic measurements on the interaction of cyclohexanone with a TiO_2 surface [132]. It has been found that cyclohexanone desorbs readily from unexposed surfaces and desorbs an order of magnitude slower from UV-illuminated TiO_2. In particular, the spectroscopic results indicate that cyclohexanone binds to Ti–OH groups formed upon irradiation and, consequently, desorbs much slower. The rate of desorption can be improved through surface silylation of TiO_2 [133]. In particular, ATR-FTIR results show a linear increase in the rate of cyclohexanone desorption as a function of increasing silane content of the TiO_2 surface. Because of the enhanced desorption rates, silylation also results in a minor accumulation of surface-deactivating carbonate and carboxylate species on TiO_2.

The competitive interaction of the oxygenated intermediates on the semiconductor is also affected by the nature of the dispersing medium. Research in our laboratories [121] shows that the presence of CH_2Cl_2 as cosolvent inhibits cyclohexanol interaction with TiO_2 so improving the final yield to this photoproduct. Other authors provide evidence that the effect of CH_2Cl_2 may also be ascribed to its direct participation in the photocatalytic redox process [122, 131]. The influence of other dispersing media on the photocatalytic oxidation of cyclohexane by TiO_2 has also been investigated [122]. It has been found that isopropanol and chloroform are preferentially adsorbed in comparison to cyclohexane and that they form radicals that react with other solvent molecules more readily than with cyclohexane.

In addition to adsorption phenomena, the photoreactivity of TiO_2 towards cyclohexane can be controlled by textural effects. We have recently reported that a

TiO_2-based mesoporous material, prepared by templating preformed TiO_2 nanoparticles (Figure 9.4), is a robust photocatalyst for inducing cyclohexane photooxidation to cyclohexanone with only traces of cyclohexanol [42]. In particular, two hours of photoexcitation of $6\,g\,L^{-1}$of this material in pure cyclohexane leads to the formation of cyclohexanone $0.01\,mol\,L^{-1}$. This high selectivity has been ascribed to a different reactivity of O_2 and $C_6H_{11}OO^{\cdot}$ towards trapped and free conduction-band electrons of the semiconductor: the structure of this material, constituted exclusively of arrays of sintered TiO_2 particles, favors an interparticle electron connection that would entail a better utilization of electron traps. According to a previous investigation [124], once trapped, electrons are removed by $C_6H_{11}OO^{\cdot}$ radicals to yield cyclohexanone (Eq. 4 of Figure 9.10) rather than being scavenged by O_2. This statement is confirmed by the observation that the selectivity to cyclohexanone decreases significantly when the mesoporous material contains silica domains able to inhibit the interparticle electron mobility.

It has been reported [56, 127] that, upon increasing the crystallite size, the productivity decreases, due to the smaller OH-group concentration and the cyclohexanol/cyclohexanone ratio increases. The influence of particle size and crystallinity on this ratio is explained in terms of lifetime of the photogenerated conduction-band electrons. In particular, relatively large TiO_2 crystals (10–25 nm) are characterized by high effective hole concentration and, consequently, by accumulation of cyclohexyl peroxy radicals, which, in turn, undergo disproportionation to both cyclohexanone and cyclohexanol. The presence of Au on the TiO_2 surface gives similar effects [127]: the enhanced lifetime of the photogenerated electrons stabilized by Au particles allows a higher effective hole concentration and, consequently, a higher cyclohexanol formation rate as compared to unmodified TiO_2.

9.3.1.2 With Highly Dispersed Oxides Different types of Cr-Si binary oxides are able to induce the partial photo-oxidation of cyclohexane by O_2 under visible light ($\lambda > 400\,nm$) [66, 69, 70]. A series of photocatalysts, with the same Cr content but prepared by different procedures, has been studied: (i) sol-gel method (Cr-SiO_2), (ii) impregnation method on amorphous silica (Cr/SiO_2) and (iii) templating method (Cr/MCM-41). All the catalysts are active in the partial photo-oxidation of hydrocarbons by visible light, and, contrary to TiO_2, they do not produce significant amounts of CO_2. Among them, Cr-SiO_2 shows the highest activity yielding, after five hours of irradiation, cyclohexanone with 70% selectivity and with a TON value (moles of cyclohexanone/moles of Cr) of about four [66]. ESR analysis reveals that photoirradiation of the chromate species with tetrahedral coordination on Cr/SiO_2 and Cr/MCM-41 leads to the formation of an excited state (Cr^{5+*}) that is different from that produced in the case of Cr-SiO_2 (Cr^{4+*}) [66, 67]. The terminal oxygen (O_T^-) formed by photoinduced charge transfer has an electrophilic character and thus acts as a positive hole. In particular, it is proposed that the O_T^- adjacent to the highly reduced Cr^{4+} has a greater electrophilicity than the O_T^- close to Cr^{5+}. This produces an enhanced attraction with the proton of cyclohexane, resulting in higher oxidation activity. The rate of cyclohexane oxidation by Cr/MCM-41 photocatalyst is improved by introducing, during the synthesis of the material, 10% of 1,2-bis

(triethoxysilyl)ethane (BTESE), whose role is that of making the surface of the mesoporous silica more hydrophobic thanks to the presence of organic fragments [67, 70]. Access of cyclohexane to the photoactive chromate species is favored leading to improved yields. The selectivity to cyclohexanol and cyclohexanone with respect to CO_2 is maintained around 90%.

V_2O_5-Al_2O_3, containing orthovanadate-like species, is a quite selective photocatalyst for the oxidation of hydrocarbons to ketones [73]. The proposed mechanism consists of five elementary steps: (i) photoactivation of $(V{=}O)O_3$ species, (ii) adsorption of hydrocarbon, (iii) formation of an alkoxide intermediate, (iv) evolution of ketone and water, and (v) desorption of ketone.

Vanadium-containing mesoporous silicas, prepared following different procedures, show photocatalytic activity ($\lambda > 300$ nm) when suspended in a mixture of acetonitrile and cyclohexane [75]. Cyclohexanol and cyclohexanone are the main oxidation products obtained, with only a minor amount of CO_2 and with a TON value after five hours of irradiation of about two. Rubidium-ion-modified V_2O_5/SiO_2 is a good catalyst for the selective photo-oxidation of propane to acetone [134]. The presence of the alkali ion leads to an improvement of the photocatalytic activity. The rate-determining step is the reaction of propane on the lattice oxygen of the photoexcited VO_4Rb species to yield the vanadium isopropoxide species. Vanadium supported on mesoporous silica SBA-15 is used for the selective oxidation of methane to formaldehyde under UV irradiation [74]. Selectivity to formaldehyde is very high (about 90%) whereas methanol is formed in very small amounts. Moreover, a strong dependence of the selectivity to formaldehyde on the vanadium content is clearly observed. Selectivity is high (> 90%) when V loading is below 2.65 wt% and decreases for higher vanadium loadings in favor of carbon oxides formed by overoxidation of the aldehyde. Photoexcited V-MCM-41 is able to catalyze the photo-oxidation of methane to methanol (80% selectivity) by nitric oxide ($\lambda < 300$ nm) [135]. Methanol and N_2 are the main products, while small amounts of CO_2, CO, C_2H_4 and N_2O are observed. Interestingly, when O_2 is employed in place of NO, the complete oxidation of methane to CO_2 and H_2O is obtained. A charge-transfer excited triplet state of the tetrahedrally coordinated V-oxide species is the active site.

9.3.1.3 With Polyoxotungstates It has been reported that photoexcitation of heterogenized $(n\text{-}Bu_4N)_4W_{10}O_{32}$ and $H_3PW_{12}O_{40}$ dispersed in neat cyclohexane leads to the formation of cyclohexanol and cyclohexanone [92]. Further research developments have been devoted to improve the selective conversion of cyclohexane to cyclohexanone. It has been found that, depending on the nature of the cation, the heterogeneous photocatalysts show different and tunable photoreactivities (Table 9.1) [93]: $n\text{-}Bu_4N^+$ cations enhance the efficiency of cyclohexane photo-oxidation, likely because they create a hydrophobic environment around the photoactive species, favoring the approach and the subsequent oxidation of the cycloalkane. NH_4^+ and Na^+ cations improve the chemoselectivity, since the concentration ratios of cyclohexanone/cyclohexanol are 1.8 and 2.3, respectively. Likely, cyclohexanol, remaining close to the polar surface, is easily oxidized to cyclohexanone by the photoexcited decatungstate.

TABLE 9.1 Photocatalytic Properties of $(n\text{-}Bu_4N)_4W_{10}O_{32}/SiO_2$, $(NH_4)_4W_{10}O_{32}$ and of $Na_4W_{10}O_{32}$

Material	Cyclohexanol + cyclohexanone ($mol\,L^{-1}$)	Cyclohexanone to cyclohexanol ratio
$Na_4W_{10}O_{32}/SiO_2$	0.3×10^{-3}	2.3
$(NH_4)_4W_{10}O_{32}/SiO_2$	0.6×10^{-3}	1.8
$(n\text{-}Bu_4N)_4W_{10}O_{32}/SiO_2$	1.7×10^{-3}	1.0

In 2002, we reported on the immobilization of $(n\text{-}Bu_4N)_4W_{10}O_{32}$ on the mesoporous silica MCM-41, (mesopores ranging from 20 to 100 Å and surface area of $\sim 1000\,m^2\,g^{-1}$) [97]. Thanks to the large surface area of MCM-41, decatungstate is well dispersed, providing a large number of photocatalytic sites that leads to an enhancement of photochemical efficiency. In particular, about 20% of cyclohexane (initial concentration $10^{-2}\,mol\,L^{-1}$ in CH_2Cl_2) can be converted to cyclohexanone and cyclohexanol after two hours irradiation. Concerning the chemoselectivity in the photocatalytic oxidation of cyclohexane, the maximum value of the ketone to alcohol ratio is 2.6. We report that the polar surface of MCM-41 favors the accumulation of formed cyclohexanol at the interfaces and, consequently, its subsequent oxidation to ketone by the photoexcited decatungstate.

The decatungstate $W_{10}O_{32}{}^{4-}$ has been immobilized on a hydrophobically organomodified mesoporous silica SBA-15 by Cao's group [111]. Introduction of hydrophobic organic fragments of chosen length onto the silica surface, which is intrinsically hydrophilic, produces a series of photocatalysts where the active sites are more easily accessible to hydrocarbon molecules. These novel photocatalysts have been investigated in the oxidation of some aryl alkanes to the corresponding phenones by O_2 (in the best case, 60% conversion and selectivity of 90%). The length of alkyl chains affects the photocatalytic efficiency, with the octyl-grafted one showing the best performance. Interestingly, this photocatalyst is also able to oxidize cyclohexane with 100% chemoselectivity in terms of cyclohexanone production.

A simple ion-exchange procedure allowed Fornal and Giannotti to firmly immobilize $W_{10}O_{32}{}^{4-}$ on poly(4-vinylpyridine), crosslinked methyl chloride quaternary salt [109]. This material has been investigated in the photo-oxidation of cyclohexane in the presence of O_2. Cyclohexyl hydroperoxide is the main product but cyclohexanol and cyclohexanone are also formed. The selectivity depends on the decatungstate loading: cyclohexanone production is promoted by lower loadings, whereas cyclohexyl hydroperoxide formation is favored by higher loadings. A new hybrid photocatalyst has been obtained by embedding the fluorous-tagged decatungstate $(R_fN)_4W_{10}O_{32}$ ($R_fN = [CF_3(CF_2)_7(CH_2)_3]_3CH_3N^+$) within fluoropolymeric films, like Hyflon® [114]. The perfluoropolymer has thermal and oxidative resistance and high permeability of O_2. The photocatalytic membrane shows an optimized distribution of the catalyst domains and turnover frequency as high as $1500\,h^{-1}$ in the solvent-free oxygenation of benzylic hydrocarbons.

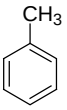
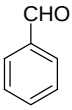
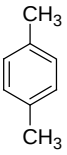
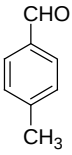
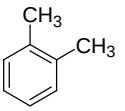
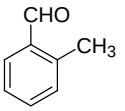
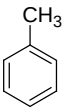
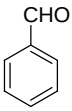
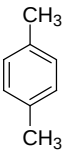
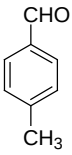
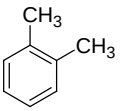
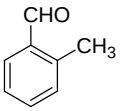
9.3.2 Oxidation of Aromatic Compounds

The search for new reaction pathways for the selective oxidation of aromatics continues to be of great interest in applied synthesis, since the main routes followed present several drawbacks in terms of cost and environmental impact.

9.3.2.1 With Titanium Dioxide The ability of photoexcited TiO_2 to induce oxidation of aromatic substrates has been well recognized [136–140]. Alkylaromatics mainly undergo oxidation of their alkyl chain by photoexcited TiO_2, according to the mechanism reported in Figure 9.10 for cyclohexane. Direct hydroxylation of the aromatic ring *via* electrophilic addition of the photogenerated $OH^{\bullet}$ is possible when the substrate is benzene [140]. This process occurs with a relatively low selectivity (about 15%) since phenol is easily decomposed through its subsequent reaction with $OH^{\bullet}$ radicals. Hydroxylation of monosubstituted benzene derivatives by photoexcited TiO_2 depends on the electron-withdrawing properties of the substituents [141, 142]. In particular, photoexcitation of TiO_2 suspended in water containing benzene derivatives with an electron-donating group leads to the formation of *ortho* and *para* hydroxylated isomers, in agreement with the directing properties of the substituent. On the contrary, with substrates containing an electron withdrawing group, the $OH^{\bullet}$ radical attack is non selective. Surface modifications of TiO_2 have significant influence on the synthesis of phenol from benzene [143]. In particular, platinum deposition and surface fluorination of TiO_2 enhances the phenol yield, indicating that the photoexcited surface plays a fundamental role in the hydroxylation of benzene. Other investigations show that photocatalysis with TiO_2 can be employed to induce the oxidation of naphthalene [144]. Irradiation of TiO_2 suspended in water containing O_2 and 1% acetonitrile leads to the conversion of naphthalene to the corresponding 2-formylcinnamaldehyde and 1,4-naphthoquinone with 16% yield at about 50% naphthalene conversion. TiO_2 has been also employed for the photo-oxidation of phenanthrene [145]. A coumarin derivative is obtained as the main product (45% yield) when the dispersing medium is an acetonitrile solution containing 8% of water. The production of a coumarin derivative is attractive since its formation from phenanthrene opens up new synthetic routes by a one-pot process.

Yield and selectivity of photocatalytic oxygenation of aromatics can be improved by designing TiO_2-based materials with specific textural and surface properties [44–48]. TiO_2 particles embedded in mesoporous silica show high efficiency in phenol oxidation [44]. In particular, the ratio between the initial oxidation rate of phenol and titanium amount of these materials is significantly higher (about twenty times) than that typical of commercial TiO_2-P25. This fact is ascribed to the large surface area of the mesoporous material, which favors the interaction of photoexcited TiO_2 with adsorbed phenol. Other works give evidence that the hydrophobic nature of the photoactive surface is beneficial for the selective oxidation of aromatic compounds. It has been shown that the high affinity of benzene for the surface of TiO_2-loaded ZSM-5 zeolites [47] contributes to increasing its conversion rate to phenol when the photocatalytic experiment is carried out in aqueous solution. An analogous result has been obtained with organophilic TiO_2-pillared clays [45]. It has been proposed that

TABLE 9.2 Photocatalytic Oxidation of Alkyl Aromatics by TiO_2 Pillared Montmorillonite Clay (Ti-PILC) and TiO_2-P25[a]

Photocatalyst	Substrate	Product	μmoles of product[b]	μmoles of CO_2[c]
Ti-PILC			3.0 *(2.7)*	< 0.4
			7.1 *(6.4)*	< 0.4
			2.4 *(2.2)*	< 0.4
TiO_2-P25			3.6 *(3.6)*	4.5 *(4.5)*
			24.2 *(4.8)*	6.5 *(1.3)*
			11.6 *(2.3)*	12.7 *(2.5)*

[a]Each photocatalyst (Ti-PILC and TiO_2-P25 4 g L^{-1}) was suspended in 3 mL of neat hydrocarbon and irradiated (60 min) at $\lambda > 290$ nm, at 26 ± 1 °C and 760 Torr of O_2. Reported values are the mean of three repeated experiments and are ±5%.
[b]In parentheses, *μmoles of oxidation product per gram of TiO_2*.
[c]In parentheses, *μmoles of CO_2 per gram of TiO_2*.

the hydrophobicity of these materials is related to a decrease in polarity of the clay surface by exchange of cations in the interlayer with metal-oxide pillars [45]. A TiO_2 pillared montmorillonite clay (Ti-PILC) has been recently investigated as photocatalyst for the selective oxygenation of several alkylaromatics [46]. As shown in Table 9.2, accumulation of valuable carbonyl derivatives is possible since their overoxidation to CO_2 is negligible. In particular, proper reaction conditions are found for obtaining carbonyl compounds with about 90% selectivity, a value significantly higher than that obtained with commercial TiO_2 Degussa P25. The chemical-physical characterization of the photoactive material indicates that its large and hydrophobic surface is beneficial for the alkylaromatics to reach the photoexcited TiO_2 inside the micropores of the sheet. The same surface characteristics inhibit the adsorption of the

more polar carbonyl photoproducts, which, therefore, are free to diffuse in the solution bulk, so preventing their further overoxidation to CO_2.

A series of Y, beta, mordenite and ZSM-5 zeolites containing nanosized TiO_2 clusters has been prepared by ionic exchange of Na^+ with titanyl cations ($Ti{=}O^{2+}$) followed by condensation [48]. TiO_2/Y and TiO_2/mordenite show higher photoactivity than commercial anatase for the photo-oxygenation of thianthrene to thianthrene oxide ($\lambda = 254$ nm).

A microporous titanosilicate ETS-10 has been recently used for selective organic transformations [65]. This photocatalyst has Ti–OH groups at the defect sites exposed on the external surface, whereas these groups are scarcely present on the channel walls. When the material is illuminated, $OH^{\bullet}$ radicals, formed at the titanol groups on the external surface, behave as active species. As a consequence, small substrates that can diffuse inside the pore system are protected from the photocatalytic reaction and, on the contrary, large substrates that cannot enter the pores react efficiently at the defect sites on the external surface. Moreover, since the inner pore environment is highly polarized, the material is able to discriminate among small molecules on the basis of their polarity. This peculiar ability of ETS-10 to control the photocatalytic activity by size and polarity of substrates is employed for the hydroxylation of benzene to phenol. The reactant is a non polar molecule that can efficiently react with $OH^{\bullet}$ radicals on the external surface to give phenol, which is by contrast a polar product. This can enter into the pores of ETS-10 where it is protected from reaction with $OH^{\bullet}$. The sequential oxidation of phenol is therefore suppressed and it can be accumulated with a high selectivity (65%, at benzene conversion of 40%).

9.3.2.2 With Highly Dispersed Metal Oxides An interesting example of "size-screening" photocatalytic activity has been reported by Shiraishi et al. [41]. The photocatalysts consist of titanosilicate molecular sieve zeolites containing isolated Ti-oxide species, such as titanium silicalites TS-1 and TS-2. They promote the selective conversion of "appropriate size" molecules, i.e. with a size close to the pore of the catalyst. A too small molecule diffuses smoothly inside the pore and is scarcely trapped by $[Ti^{3+}\text{-}O_L{}^-]^*$. A molecule that is too large cannot enter the pore, thus showing zero conversion. On the contrary, diffusion of a molecule with size close to the pore is restricted by the pore wall, trapped by $[Ti^{3+}\text{-}O_L{}^-]^*$ and converted. The authors highlight a successful application of this activity to a selective transformation of molecules that is associated with a size reduction, the so-labeled "molecular shave" transformation. Photoirradiation of TS-1 or TS-2 in aqueous solutions containing chlorohydroquinone gives rise to the corresponding 1,2,4-trihydroxybenzene derivative with high selectivity at about 70% substrate conversion (Table 9.3). This reaction is particularly interesting since the product is non toxic and valuable. The size of chlorohydroquinone is similar to the catalyst pore, thus allowing effective conversion. On the contrary, the size of 1,2,4-trihydroxybenzene is smaller than the pore, leading to smooth diffusion inside the pores and avoiding subsequent reactions of this molecule. When bulk TiO_2 is used, 1,2,4-trihydroxybenzene is initially formed but it is further completely decomposed (Table 9.3).

TABLE 9.3 Photocatalytic Properties of TS-1, TS-2 and of Bulk TiO_2 in the Transformation of Chlorohydroquinone to 1,2,4-trihydroxybenzene

System	Substrate conversion (%)	Product selectivity (%)
TS-1	67	85
TS-2	74	99
TiO_2	99	1

9.3.2.3 With Polyoxotungstates Zeolite Y (in the Na^+ form) has been used as a solid support for $H_2NaPW_{12}O_{40}$, $H_4SiW_{12}O_{40}$ and $H_3PMo_{12}O_{40}$ [99]. The photocatalytic activities of these systems have been investigated choosing 1,2-dichlorobenzene as the oxidizable probe. The constrained environment is responsible for a rate enhancement of the reaction, since it increases the encounter probability between photoexcited polyoxometalate and 1,2-dichlorobenzene, suppressing the back electron-transfer reaction.

9.3.3 Oxidation of Alcohols

The partial oxidation of alcohols to carbonylic derivatives is another important chemical transformation for the production of fine and specialty chemicals. In particular, the oxidation of primary aliphatic alcohols to the corresponding aldehydes is the most demanding chemical transformation since it is usually difficult to stop the oxidation at this stage, preventing the formation of carboxylic acids [146].

9.3.3.1 With Titanium Dioxide A vast number of studies has been devoted to the selective oxidation of alcohols catalyzed by photoexcited semiconductors and by TiO_2 in particular [49–55, 147–159]. It is generally accepted that direct adsorption of the alcohol onto the TiO_2 surface is a compulsory requirement for its oxidation; in particular, a dissociative adsorption of the alcohol as an alkoxide intermediate is proposed by many authors [152, 157, 158, 160]. Two different oxidation pathways have been proposed: oxidation of the adsorbed alkoxide by direct electron transfer to the positive holes [152, 158, 159] or oxidation of the adsorbed alkoxide mediated by $OH^{\bullet}$ radicals formed by the reaction between holes and superficial OH^- [161]. Subsequent coupling reactions may lead to the formation of partial oxidation products or to total combustion. Through current-efficiency measurements, obtained from the photoelectrochemical oxidation at TiO_2/Ti anodes, it has been established that, in a deaerated medium, two electrons are captured by the semiconductor from the considered alcohols. On the contrary, in aerated conditions, the number of TiO_2-captured electrons can be reduced to one because the alcoholic radical can be competitively captured by oxygen [155]. Very recent oxygen isotope studies show that, when the photocatalytic oxidation of labeled alcohols is carried out with anatase TiO_2 in benzotrifluoride, the oxygen atom of the substrate alcohol is completely replaced by one of the oxygen atoms of dioxygen [159]. It is proposed that both the photogenerated alcoholic radical and Ti(III) react with O_2 to form a Ti-peroxide

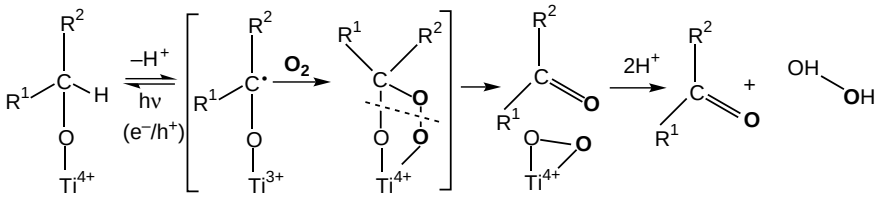


FIGURE 9.11 Proposed oxygen-transfer process in the TiO_2 photocatalytic oxidation of alcohols in the presence of O_2.

intermediate, whose cleavage gives rise to a carbonylic species containing one oxygen atom coming from O_2 (Figure 9.11).

It has been demonstrated that the oxidation mechanism, efficiency and selectivity of the photocatalytic oxidation of alcohols by TiO_2 Degussa P25 strongly depend on the nature of the dispersing medium. Indeed, as evidenced by ESR-spin trapping investigations, addition of small amounts of water to CH_3CN strongly inhibits alcohol adsorption and its subsequent oxidation [152]. The reactivity of alcohols on the surface of photoexcited TiO_2 is also affected by the nature of their hydrophobic aliphatic chain [152]: geraniol and citronellol are more susceptible to the water content than their short analogs *trans*-2-penten-1-ol and 1-pentanol. Proper reaction conditions have been found for the photocatalytic oxidation of geraniol, citronellol, *trans*-2-penten-1-ol and 1-pentanol to the corresponding aldehydes with a selectivity higher than 70% after 30% alcohol conversion (two hours of irradiation). These results are potentially important in applied synthesis considering that citral, obtained through the partial oxidation of geraniol, is widely used in perfumes and flavorings.

In another study, it has been reported that the polar surface of TiO_2 favors the preferential adsorption of the primary OH group of diols such as 1,2-propanediol, 1,3-butanediol and 1,4-pentanediol, thus favoring the subsequent oxidation of this alcoholic functionality [153]. In particular, it has been found that more than 75% of 4-hydroxypentanal from 1,4 pentanediol can be obtained with very low mineralization to CO_2 also under high conversion conditions. The regioselective oxidation of diols can be also achieved in water by photoexcitation of a composite system in which the natural enzyme glucose oxidase is adsorbed on the surface of TiO_2 Degussa P25 [154, 162]. Electrochemical measurements show that the enzyme is adsorbed on TiO_2 without changing the flat-band potential [154]. The main role of glucose oxidase is to mediate the electron-transfer process from photoexcited TiO_2 to O_2 leading to the formation of H_2O_2 [162]. ESR spin trapping investigations indicate that the enzyme favors the formation of $OH^{\cdot}$ radicals due to inhibition of electron–hole recombination and H_2O_2 reduction by conduction-band electrons. The photo-oxidation of 1,2-propandiol with this photocatalytic system is regioselective, in that, partial oxidation to hydroxyacetone is observed and no mineralization to CO_2 occurs [154].

Photocatalysis is a possible way to obtain value-added chemicals from glycerol, which is a 10% byproduct of biodiesel manufacture. The photocatalytic oxidation

of glycerol leads to relevant quantities of 1,3-dihydroxyacetone and glyceraldehyde [163]. The authors report that the highest conversion to these products has been obtained over TiO_2 Degussa P25 at pH 7 and over fluorinated photocatalysts at pH 3, with about 100% selectivity with glycerol conversion under 30%. The photooxidation of glycerol in aqueous suspensions containing TiO_2 in the anatase, rutile or anatase–rutile polymorphic phases has been investigated using two different batch photoreactors, an annular photoreactor and cylindrical photoreactor [164]. About 45% of glycerol is converted to 1,3-dihydroxyacetone, glyceraldehyde, formic acid and carbon dioxide. In both the photoreactors the commercial samples show the best activity for the oxidation of glycerol.

Anatase, rutile and brookite TiO_2 have been prepared with a sol-gel procedure that allows any calcination treatment to be avoided. These materials have been extensively studied in the partial oxidation of aromatic alcohols in an aqueous medium [50–55]. Their electronic properties have been investigated by diffuse reflectance spectroscopy and quasi-Fermi-level measurements [55]: the values of bandgap, valence-band and conduction-band edges are almost identical for all the samples in which anatase phase is predominant, whereas appreciable differences can be noticed in the presence of high amounts of rutile. ATR-FTIR results indicate that these TiO_2-based materials show a very dissimilar hydrophilicity and different ability for adsorbing reaction intermediates in comparison to commercial TiO_2 Degussa P25 [55]. The anatase samples are significantly more selective than commercial TiO_2 in the oxidation of 4-methoxybenzyl alcohol to the corresponding aldehyde [53], which is a fragrance and an intermediate in many industrial processes. CO_2 is the other main oxidation product together with traces of 4-methoxybenzoic acid and open-ring compounds. Subsequent investigations give evidence that the rutile samples are also able to photocatalyze the partial oxidation of benzylic alcohols [52, 54]. More specifically, with this material, the selectivity of the conversion of benzyl and 4-methoxybenzyl alcohols to the corresponding aldehydes maintains a value not less than 40%, even when the conversion reaches 50%, with a carbon balance better than 95% [54]. The physical chemical characterization of rutile samples points to a primary influence of crystallinity on selectivity. The photocatalytic properties of anatase, rutile and brookite TiO_2 have been compared in the oxidation of 4-methoxybenzyl alcohol in water [50]. Rutile exhibits the highest yield to aldehyde at a rate of the same order of magnitude of that shown by the other materials. In another study, the photocatalytic oxidation of benzyl, 4-methylbenzyl and 4-nitrobenzyl alcohols has been carried out in order to investigate the influence of -OCH_3 and -NO_2 substituents on oxidation rate and selectivity [50].

Visible-light illumination of nitrogen-doped TiO_2 (N-TiO_2) prepared by a sol-gel method brings about the selective oxidation of benzyl and cinnamyl alcohols to the corresponding aldehydes [151]. In particular, three hours photoexcitation ($\lambda > 450$ nm) of benzyl alcohol $10^{-3}\,\mathrm{mol\,L^{-1}}$ in acetonitrile suspensions of N-TiO_2 ($4\,\mathrm{g\,L^{-1}}$) leads to the selective formation of benzaldehyde with a yield higher than 90%. The reaction takes place in oxygenated dry nitrile solvents and is totally inhibited in the presence of more than 1% water. Benzyl alcohol adsorption follows Langmuir conditions with a K_{ads} of $3740\,\mathrm{mol^{-1}\,L}$, in agreement with previous data

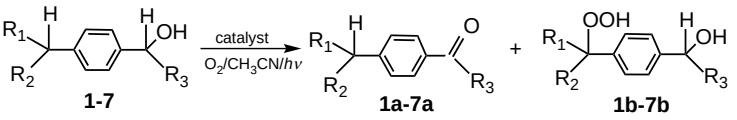
on commercial TiO_2 (Degussa P-25) [151]. The maximum coverage by adsorbed benzyl alcohol on N-TiO_2 is 0.4 molecules nm^{-2}. It is proposed that the presence of nitrogen-stabilized oxygen vacancies, their interaction with acetonitrile and active oxygen species have an important role in the visible-light-induced formation of aldehydes. Concerning the latter point, it has been communicated that superoxide can oxidize benzyl alcohol in ionic liquids, where O_2^- is highly stable [165], and a recent study assumes an involvement of singlet oxygen in N-TiO_2 visible-light photocatalysis [166].

Confirming that visible-light photoactivity is an important issue, Higashimoto et al. showed that visible-light photocatalytic conversion of benzyl alcohols to the corresponding aldehydes on undoped commercial TiO_2 proceeds with high selectivity [167, 168]. The authors claim that the OH groups of the semiconductor surface interact with the -CH_2OH group or possibly with the phenyl ring of benzyl alcohol, leading to surface complexes that exhibit strong absorption in the visible region by ligand-to-metal charge transfer. Actually, our ongoing work in this field underpins the role of vacancies and defects since, significantly, among several commercial TiO_2 samples, those characterized by a small particle size (higher number of defects) feature the higher visible photoactivity in visible-light oxidation of benzyl alcohols [169].

Mesoporous RuO_2-TiO_2 nanocomposites at different RuO_2 concentrations (0–10 wt%) have been investigated in the photocatalytic CH_3OH oxidation to HCHO under UV and visible light. The photo-oxidation of CH_3OH is affected by the loading amount and the degree of dispersion of RuO_2 particles under visible light. The cause of the visible-light photocatalytic behavior is the incorporation of small amounts of Ru^{4+} into the anatase lattice [170].

9.3.3.2 With Highly Dispersed Oxides The design of visible-light-responsive Ti/SiO_2 has been accomplished by applying an advanced metal ion implantation method [171–174]. Introduction of Cu(I) or Sn(II) centers in Ti-MCM-41 leads to metal-to-metal charge-transfer moieties (Ti^{IV}-O-Cu^{I} and Ti^{IV}-O-Sn^{II}) that absorb in the visible region (around 620 nm) [171]. Irradiation at these wavelengths allows the formation of Ti^{III}, showing that the assembly of metal-to-metal charge-transfer sites inside mesoporous silicas, with each metal in a preselected oxidation state, opens up the possibility of initiating photocatalytic processes by visible light. More recently, Ti^{IV}-O-Ce^{III} bimetallic assembly on mesoporous silica is employed for the photo-oxidation of 2-propanol to acetone by O_2 under $\lambda = 460$ nm [173] and V-containing Ti-MCM-41 shows an enhanced photoactivity in the conversion of propane to acetone with respect to Ti-MCM-41 [172].

Photocatalytic oxidation of methanol has been recently carried out in a continuous gas–solid reactor in the presence of commercial anatase TiO_2 [150]. Methyl formate can be obtained with a selectivity of about 90%. The authors report that high flow rates reduce the contact time of the gas mixture with the photocatalyst, so avoiding unwanted overoxidation processes of the desired product. Another factor affecting the selectivity is the reaction temperature: at 573 K the yield is three times higher than at room temperature at the expense, however, of selectivity.



R_1	R_2	R_3	
H	H	CH_3	**1**
CH_3	H	CH_3	**2**
CH_3	CH_3	CH_3	**3**
Ph	H	CH_3	**4**
Ph	Ph	CH_3	**5**
CH_3	H	Ph	**6**
CH_3	CH_3	Ph	**7**

FIGURE 9.12 Photocatalytic oxidation of *p*-substituted secondary benzyl alcohols by decatungstate supported on silica and γ-alumina.

9.3.3.3 With Polyoxotungstates Photo-oxidation of benzyl alcohols by $W_{10}O_{32}^{4-}$ impregnated on silica and on γ-alumina has been studied by Orfanopoulos and coworkers [96]. These photocatalysts have been investigated in the oxidation of a series of *p*-alkyl-substituted benzyl alcohols, **1–7** (Figure 9.12). These substrates bear two distinguishable benzylic hydrogen atoms, one on the alcohol carbon and one on the *p*-alkyl substituent, both of which potentially can be cleaved under photo-oxidation conditions to give aryl ketones **1a–7a** or dioxygenated products **1b–7b**, respectively. A strong preference for the hydrogen atom abstraction from the alcohol carbon is observed: selectivity for **1a–7a** compounds is, in most cases, higher than 80% at a conversion higher than 90% (90 min irradiation). This is ascribed to the surface polarity of the supports that probably favors adsorption of the polar alcohol moiety.

Shen and coworkers report that $H_3PW_{12}O_{40}$ impregnated on MCM-41 is able to photo-oxidize several alcohols to the corresponding carbonylic derivatives in the presence of O_2 [98]. In particular, an enhancement in activity is observed if an ionic liquid is used as dispersing medium instead of CH_3CN. Although this work has some interest from the synthetic point of view, a deeper investigation is needed in order to establish which is the photoactive species and the role of the ionic liquid in the reaction mechanism.

The polyoxotungstates $(n\text{-}Bu_4N)_4W_{10}O_{32}$ and $H_3PW_{12}O_{40}$ encapsulated inside a silica network (via a sol-gel technique) have been used in the oxidation of benzylic alcohols in the presence of O_2 [103, 104]. The authors performed a screening study choosing a variety of ring-substituted primary and secondary benzylic alcohols. These substrates are efficiently oxidized to the corresponding carbonylic compounds, without overoxidation of benzaldehydes to carboxylic acids (yields higher than 70% after two hours irradiation). This result is in contrast to that reported by Orfanopoulos with decatungstate immobilized on silica by impregnation [96], thus indicating that different preparation methods lead to a completely dissimilar morphology of the photocatalyst and, consequently, to a different photoreactivity.

In 2010 we reported on the photochemical characterization of two heterogeneous photocatalysts prepared by entrapment of $(n\text{-}Bu_4N)_4W_{10}O_{32}$ in a silica matrix through a sol-gel procedure: SiO_2/W30%, with 30% (w/w) of decatungstate, and SiO_2/W10%, obtained after removal of the decatungstate not firmly incorporated inside the silica network and weakly adsorbed on the external surface [105]. These two heterogeneous photocatalysts are characterized by the presence of both micropores (7 Å and 15 Å) and mesopores (25 Å), but, due to different preparation procedures, SiO_2/W10% presents a more remarkable porous network than SiO_2/W30%. Moreover, morphological features of SiO_2/W30% and of SiO_2/W10% differ from those of their parent material SiO_2/W0%, indicating that incorporation of decatungstate induces a significant modification of the porous texture of the siliceous material. Both photocatalysts are robust and able to induce the O_2-assisted oxidation of 1-pentanol and 3-pentanol to pentanal and 3-pentanone, respectively (10% conversion of 1-pentanol after 60 min irradiation). A very strong effect of the solid support on the relative reactivity of the two alcoholic substrates is observed. In fact, the molar concentration ratio between aldehyde and ketone, which is one in homogeneous solutions, increases to as high as four with SiO_2/W10%. Preferential adsorption effects are of great importance in controlling the nature of the products and yields of the photocatalytic process. It has been also observed that other textural parameters, related to the microporous structure of the heterogeneous photocatalysts, differentiate the relative reactivity of the two alcohols investigated, favoring the approach to the surface of the less hindered primary OH group of 1-pentanol. These findings are of particular importance since the selective oxidation of aliphatic primary alcohols at the aldehyde stage without further oxidation still remains a challenging transformation.

Zirconia-supported $Na_4W_{10}O_{32}$ and $H_3PW_{12}O_{40}$ have been prepared *via* sol-gel procedure by Farhadi's group [106, 107]. $Na_4W_{10}O_{32}/ZrO_2$ is more active than the homogeneous $Na_4W_{10}O_{32}$ in the photo-oxidation of primary and secondary benzylic alcohols. This is tentatively attributed to a synergistic effect between the polyoxoanion and the support that is a semiconductor. Interestingly, in the $H_3PW_{12}O_{40}/ZrO_2$ system, the absorption band typical of $H_3PW_{12}O_{40}$ at 270 nm is not present and a new broad band, shifted to the visible region, is observable. The authors attribute the photocatalytic activity of the nanocomposite system to the existence of this broad band. Colloidal $Cs_3PW_{12}O_{40}$, synthesized by metathesis of $H_3PW_{12}O_{40}$ and CsCl in water, has been supported on silica *via* a sol-gel procedure using tetraethoxy ortho-silane (TEOS) [175]. The obtained material is extremely porous (pore size centered at 23 Å) and with a very large surface area. It is effective in the photo-oxidation of aqueous solutions of 2-propanol to acetone. A deep investigation on the factors influencing the efficiency of this heterogeneous photocatalyst, such as events that follow the absorption of light and substrate adsorption, was published by the same authors in 2000 [176].

$W_{10}O_{32}^{4-}$, supported on a previously functionalized silica matrix (Figure 9.8), has been employed as photocatalyst for the O_2-assisted oxidation of 1,3-butanediol and 1,4-pentanediol [110]. For both the investigated diols, the only products obtained are the corresponding hydroxy-aldehyde and the hydroxy-ketone. The

ratio between aldehyde and ketone depends on the nature of the alkyl-ammonium cations; in particular, it increases markedly (from 0.06 to 0.63 for 1,3-butanediol and from 3.0 to 7.5 for 1,4-pentanediol) as the alkyl chains are substituted by hydrogen atoms. This substitution enhances the polarity of the environment surrounding $W_{10}O_{32}^{4-}$, favoring the preferential adsorption of primary OH group of the more hydrophilic head of diol molecule with respect to the secondary OH group placed in the more hydrophobic tail.

The decatungstate, immobilized inside polymeric membranes, has been studied in the photo-oxidation of several water-soluble alcohols (*n*-pentanol, cyclohexanol, cyclopentanol) [112, 113]. Carbonyl products accumulate in solution up to a substrate conversion in the range 10–30% and then they undergo consecutive oxidation. In comparison with homogeneous $Na_4W_{10}O_{32}$, the heterogeneous photo-oxidation is slower but proceeds to completion in a few hours. Interestingly, a heterogeneous matrix exerts a specific substrate recognition, a key factor to achieve selective processes: the preferential interaction with the polymeric membrane promotes the oxidation, favoring adsorption equilibrium and leading to a substrate enrichment on the surface close to the photoactive sites.

9.3.4 Oxidation of Olefins

9.3.4.1 With Highly Dispersed Metal Oxides Yoshida and coworkers report that silica containing isolated Ti-oxide species (Figure 9.5) is able to perform the photocatalytic epoxidation of light alkenes [58]. Irradiation of the catalyst T-S(0.34), with $Ti/(Ti + Si) = 0.34$ mol% in the presence of propene and O_2, leads to the corresponding epoxide with 57.5% selectivity, CO_2 6.6% and other products such as acrolein and acetaldehyde. Increasing the Ti content causes important variations in the UV spectra indicating the formation of aggregated titanium dioxide species. As a consequence, (i) conversion of olefin increases, (ii) yield to propene oxide decreases, (iii) side reactions for production of other products and CO_2 are favored. It is of note that the use of bulk TiO_2 does not produce epoxide and the main product is CO_2 with 96.2% yield. Another catalyst containing isolated Ti-oxide species has been employed for gas phase photocatalytic epoxidation of styrene with O_2 [177]. The obtained products are styrene oxide (62%), benzaldehyde (23%) and CO_2 (15%) at 18% styrene conversion. In contrast, when TiO_2 Degussa P-25 is used, no styrene oxide is accumulated, benzaldehyde selectivity is only 2% and the main product is carbon dioxide.

Shiraishi and coworkers report that addition of CH_3CN during the irradiation of a Ti-containing mesoporous silica in the presence of an olefin remarkably improves epoxide selectivity (> 98%) [62, 63]. As previously discussed in Section 9.2.2, irradiation in the presence of O_2 leads to the formation of the intermediate **II** of Figure 9.5 where $O_3^{-\bullet}$ is the active oxidant for the olefin epoxidation. The authors observe that the nature of the dispersing medium can control the selectivity of the process, likely through a suppression of side reactions. Moreover, highly stereoretentive (> 99%) epoxidation is also achieved in these conditions: in fact, reaction of *cis*- and *trans*-2-hexene gives the corresponding epoxides retaining the C=C

configuration of the olefin. Unfortunately, conversion is low (< 12%) and an attempt to improve them is performed by using Ti-containing mesoporous organosilicas, synthesized by a surfactant-templating method using an organosilane precursor [63]. The idea is that the hydrophobicity of these materials can enhance the access of hydrophobic alkenes to the photoexcited Ti-oxide species, but a destabilization of the species $O_3^{-\bullet}$ that is active in the olefin epoxidation is observed. The conclusion is that this destabilization counteracts the enhanced olefin access to the excited species, resulting in almost no improvement in olefin conversion.

Cr-containing silicas are able to promote partial oxidation of various aliphatic and aromatic olefins by visible light ($\lambda > 400$ nm) irradiation [68, 69]. Selectivity towards oxidation products is higher than 90% for all the investigated olefins, while TiO_2 promotes complete decomposition with CO_2 formation. Proper reaction conditions have been found to obtain a quite high selectivity (44%) to propene oxide [68].

Hydroxylated vanadyl centers incorporated in the mesoporous material TUD-1 can be activated with visible light catalyzing the selective photo-oxidation of cyclohexene to cyclohexenone [178]. The reaction has been studied by *in situ* time-resolved ATR-FTIR spectroscopy. It is observed that the extent of hydration is a crucial factor in determining the activity, since it shifts the absorption spectrum to the visible region. Cyclohexenyl hydroperoxide is the intermediate formed that, after rearrangement, leads to ketone and water. Progressive accumulation of water on the catalyst surface decreases the activity.

9.3.4.2 With Polyoxotungstates The photocatalytic properties of $(n\text{-}Bu_4N)_4W_{10}O_{32}$ impregnated on amorphous silica have been investigated in the oxidation of cycloalkenes, such as cyclohexene and cyclooctene. The study has been carried out in the presence of Fe^{III}[*meso*-tetrakis(2,6-dichlorophenyl)porphyrin] chloride (Fe(TDCPP)Cl) as a cocatalyst [94]. Cycloalkenes are mainly oxidized to the corresponding hydroperoxides by the photoexcited decatungstate according to Figure 9.7. The iron porphyrin reacts with the allylic hydroperoxides to give the corresponding alcohols as main products. The photocatalytic process occurs with a total turnover (moles of oxidized alkene per moles of decatungstate) of 52 after three hours of irradiation.

Amberlite IRA-900 in the chloride form has been employed as support for $(n\text{-}Bu_4N)_4W_{10}O_{32}$ by our research group [108]. The ion exchange of Cl^- with $W_{10}O_{32}{}^{4-}$ is favored by the soft character of -$N(CH_3)_3{}^+$ cations. This photocatalytic system promotes the conversion of olefins to the corresponding bromohydrins and dibromoalkanes in the presence of NaBr. By simply adjusting the pH value, bromohydrins can be quantitatively transformed into epoxides, which are important intermediates in organic synthesis. Photoexcited $(n\text{-}Bu_4N)_4W_{10}O_{32}$ causes the reductive activation of O_2 to alkyl hydroperoxides (Figure 9.7). These, in turn, reacting with bromide ions, give a brominating species that attacks the C=C double bond of olefins. A nucleophile such as H_2O or Br^- leads to bromohydrin and dibromo-derivative, respectively. Under analogous experimental conditions, phenol and anisole are converted to their monobrominated derivatives, a transformation of particular interest if one considers the otherwise difficult monobromination

TABLE 9.4 Photocatalytic Properties of Amb/$W_{10}O_{32}^{4-}$ and $W_{10}O_{32}^{4-}$ in the Bromide-assisted Functionalization of Cycloalkenes[a]

Alkene	System	Alkene product distribution (%)			
		Epoxide	Bromo-hydrin	Dibromo-alkane	Mono-oxygenated products
	Amb/$W_{10}O_{32}^{4-}$	13	23	42	22
	$W_{10}O_{32}^{4-}$	12	12	7	69
	Amb/$W_{10}O_{32}^{4-}$	56	13	5	26
	$W_{10}O_{32}^{4-}$	37	1	4	58

[a]In a typical experiment, Amb/$W_{10}O_{32}^{4-}$ (0.1 g) or $W_{10}O_{32}^{4-}$ (2×10^{-4} mol L^{-1}) were suspended/dissolved in a CH_3CN/H_2O 1/1 mixture (3 ml) containing the cycloalkene (3×10^{-2} mol L^{-1}) and NaBr (2×10^{-1} mol L^{-1}) and irradiated (4 h, $\lambda > 300$ nm) under aerobic conditions at 298 ± 1 K. Reported values are the mean of three repeated experiments.

of activated arenes. As shown in Table 9.4 for the case of cyclohexene and 1-methylcyclohexene, the polymeric matrix increases the yields to epoxides and bromohydrins and inhibits undesirable autooxidation processes leading to mono-oxygenated products. The crucial role of the resin in fostering the enrichment of Br^- ions close to the surface is evident, promoting their reaction with photo-generated alkyl hydroperoxides, before their diffusion in the solution bulk.

9.4 STABILITY

Evalutation of the performance of a heterogeneous photocatalyst is complete only when its stability under irradiation and under the reaction conditions is considered. Since a heterogeneous system is usually easier to handle and recover, it would also be desirable to recycle the photocatalyst in subsequent experiments without a significant loss of photocatalytic activity, especially when it is obtained after an expensive and time-consuming synthetic procedure. Efficient recycling is feasible only if the integrity of the photoactive species is maintained, if surfaces do not undergo poisoning processes and if leaching phenomena of the photoactive unit from the support to the solution bulk do not occur. Most of the studies concerning the use of titania for synthetic purposes have been carried out in organic solvent and only in a few of them do researchers deal with the important issue of stability. While it is generally accepted that unmodified TiO_2 is robust and recyclable, surface derivatized or doped titanium dioxide can present stability problems due to photodegradation and leaching of the molecular or metallic species that modify TiO_2.

Doping of TiO_2 can be either anionic or cationic. In the first, more recent, direction of research, the use of nitrogen and sulfur dopants has attracted much attention in the

last ten years, following a publication by Asahi et al. [179]. There is seemingly no systematic investigation on the stability of these photocatalysts. Information is likewise fragmentary in the case of metal (cationic) doping too but there are, comparatively, more examples in which the problem is tackled. Anpo has discussed the difference between TiO_2 doped by ion implantation and by chemical methods [180]. For the specific case of Cr-doped TiO_2, he underlines the advantages of the first approach since the resulting material maintains a high photoactivity under UV light irradiation. Conversely, when metal ions are chemically doped into TiO_2, the photocatalytic activity decreases dramatically as the catalyst is reused. It is sometimes stated that, among the metal-doped-TiO_2 materials, those that feature the higher photoactivity are characterized by surface rather than bulk doping. This is the case, for example, of Co-TiO_2 prepared by TiO_2 impregnation [9, 181]. This photocatalyst is not stable in aqueous acid solutions where leaching of cobalt is appreciably high.

A systematic study carried out on commercially available TiO_2 has pointed out that the amount of surface OH groups has a significant influence on TiO_2 stability [57]. In particular, it is seen that the quantity of surface OH groups and surface-bound water, that, in turn, depend on particle size and crystallinity, unfavorably affects the desorption rate of cyclohexanone. This fact enhances the probability of consecutive oxidation to carboxylates and carbonates that, likely, are the main cause of deactivation of TiO_2 in the photo-oxidation of cyclohexane. These considerations are of interest since they indicate the existing relationship between stability of the photocatalyst and its morphological and textural properties and the way to develop a pretreatment strategy in order to obtain a material with predictable characteristics.

The photocatalytic activity of Ti-pillared clays (Ti-PILC) has been evaluated in the photo-oxidation of alkylaromatics under prolonged irradiation [46]. Figure 9.13 gives evidence that the concentrations of carbonylic products increase quite linearly during the first 3 h of irradiation, thus indicating that these photocatalysts are rather robust. Its stability has been confirmed by repeating photocatalytic experiments after simple drying of the photocatalyst at 75 °C for 10 min. Figure 9.13 shows that the photo-oxidation rate of toluene did not change when the experiment was carried out with recycled samples of Ti-PILC (empty circles). The stability of the mesoporous TiO_2 materials prepared using colloidal nanoparticles as building blocks has been evaluated in the following way [42]: the same amount of photocatalyst has been used in repeated experiments suspending it in fresh aliquots of cyclohexane and evaluating the yields of cyclohexanone and cyclohexanol after a fixed irradiation time. The results show that these materials are rather robust and could withstand at least up to five cycles without appreciable loss of their activity.

It is often reported that Ti and Cr oxides highly dispersed on micro- and mesoporous supports, such as silica, are free of durability problems since they are completely inorganic in nature [6]. The issue of stability has been considered in the case of Ti-containing mesoporous organosilica photocatalyst, synthesized using an organosilane precursor [63]. The integrity of organic fragments during photoirradiation has been demonstrated by comparison of IR and XRD patterns before and after irradiation. Moreover, the photocatalyst recovered and reused for further cyclohexene oxidation leads to almost unchanged alkene conversion and epoxide selectivity.

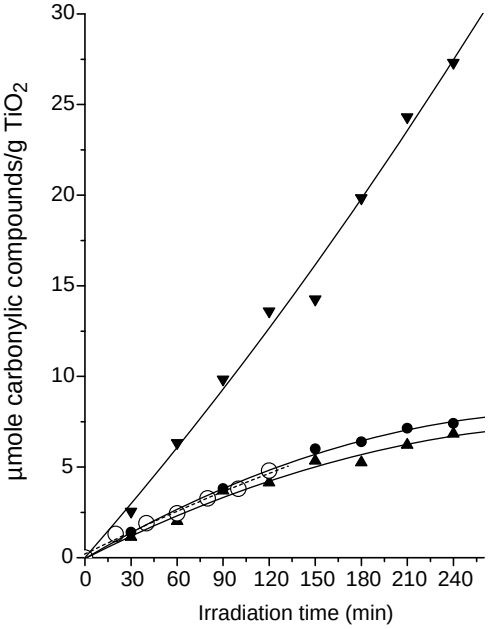


FIGURE 9.13 μmoles of carbonylic compounds formed per gram of TiO_2 as a function of time upon irradiation of Ti-PILC. (▲) Ortho-tolualdehyde, (●) benzaldehyde, (○) benzaldehyde after recycling and (▼) para-tolualdehyde.

In addition, no Ti leaching during the reaction is detected by ICP analysis. Chromium-containing mesoporous organosilica and hydrophobic Cr–Si mixed oxides employed in the photo-oxidation of cyclohexane with visible light have been recovered by filtration after the reaction, washed and reused in successive photocatalytic cycles. The same selectivity and almost the same activity as the initial catalyst are obtained. Moreover, no leaching of impregnated Cr is detected during the reaction [67, 70].

A surfactant-templating method leads to the synthesis of a mesoporous molecular sieve containing isolated V^VO_4 species confined within a silica layer and not exposed on the silica surface. The confinement strongly increases the stability of V^VO_4 even in the presence of water as reaction medium. In fact, hydrolysis of V^VO_4 is suppressed and the leaching of vanadium is negligible, allowing the possibility to recycle this kind of photocatalyst also in an aqueous reaction medium [75].

Evaluation of stability of photocatalytic systems obtained upon heterogenization of polyoxotungstate is of fundamental importance. In particular, two aspects must be considered: (i) the photochemical stability of the polyoxoanion during the experiment and (ii) leaching of the photoactive species into the dispersing medium. This last parameter is critical and depends on the nature and strength of the interaction/bond between the polyoxoanion and the support. When a polyoxotungstate is immobilized on a solid support by impregnation, interactions existing between the

two components are weak. For this reason these heterogeneous photocatalytic systems must be employed in dispersing media where the polyoxotungstate is insoluble. For instance, $(n\text{-}Bu_4N)_4W_{10}O_{32}$ supported on amorphous silica or on MCM-41 has been recycled up to three times without any loss of efficiency in CH_2Cl_2 and in neat cyclohexane [92–95, 97]. Some attempts to decrease the leaching have been carried out by studying the influence of pH during the preparation of $W_{10}O_{32}^{4-}/SiO_2$ and $W_{10}O_{32}^{4-}/\gamma\text{-}Al_2O_3$ [96]. Better dispersion of $W_{10}O_{32}^{4-}$ is achieved when the support surfaces are positively charged. However, the photocatalysts prepared by impregnation at low pH values show a relatively low activity. Among these catalysts, it has been demonstrated by UV spectra of the supernatant solutions that 3% of $(n\text{-}Bu_4N)_4W_{10}O_{32}$ is lost from the support. Homogeneous experiments containing this amount of decatungstate show that the contribution of the homogeneous reaction to the heterogeneously catalyzed reaction is around 5%. Concerning the recycling, these photocatalysts can be used at least twice without a significant loss of activity, but in the third run their efficiency is reduced by 75%.

Immobilization of $W_{10}O_{32}^{4-}$ on organic ion-exchange resins and on Amberlite IRA 900 leads to robust heterogeneous photocatalysts [108, 109]. No leaching is observed and recycle is very good since a decrease of less than 5% in terms of detected products is obtained after three repeated cycles. On the contrary, the use of a carbon material, such as Ambersorb, for supporting $W_{10}O_{32}^{4-}$ gives an unstable catalyst. In fact, significant leaching (about 30%) is observed during irradiation and also during washing steps. Furthermore, under prolonged irradiation the material undergoes complete destruction. Ionic interaction between $W_{10}O_{32}^{4-}$ and different ammonium cations covalently linked to the surface of silica is strong enough to lead to robust heterogeneous photocatalysts [110]. UV-vis spectra demonstrate that the decatungstate anion is not released in detectable amounts into the solution during the photocatalytic experiments. Loss of activity, in terms of detected end products, is less than 15% after five repeated cycles. This slow deactivation has been tentatively attributed to the degradation of $W_{10}O_{32}^{4-}$ to form smaller undetectable fragments. Decatungstate anion heterogenized on a hydrophobically modified mesoporous silica SBA-15 is stable and can be reused in five successive cycles in the photo-oxidation of ethylbenzene [111]. The acetophenone yield remains constant in each cycle and TEM and IR results of the recycled material show no changes both in the nanostructure of SBA-15 and in decatungstate. Moreover, the W content is the same as that of the fresh catalyst since no W is found in the filtrate by ICP analysis after the recycling.

Encapsulation inside a silica network *via* a sol-gel technique is a successful procedure for obtaining robust heterogeneous photocatalysts [105]. For instance, in the prolonged irradiation of $(n\text{-}Bu_4N)_4W_{10}O_{32}/SiO_2$ (10% w/w) in the presence of 1-pentanol, it is seen that the amount of pentanal increases quite linearly. Moreover, when the reaction filtrate is further irradiated under O_2, no additional formation of carbonylic product is observed, confirming that the photoreaction is heterogeneous in nature. The stability of this photocatalyst has also been assessed in repeated photocatalytic experiments after washing and drying the material. Figure 9.14 shows that the loss of activity is less than 15% after the first cycle. Interestingly, the

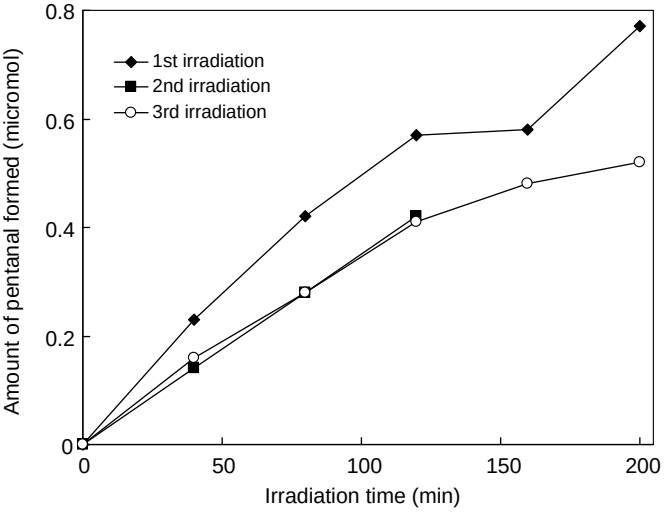


FIGURE 9.14 μMoles of pentanal formed as function of time upon irradiation of $(n\text{-}Bu_4N)_4W_{10}O_{32}/SiO_2$ (10% w/w).

photocatalytic system maintains the same level of activity after the first recycle [105]. Recycle and maintenance of the W content is also observed in zirconia-supported sodium decatungstate [106].

Occlusion of decatungstate in polymeric membranes gives heterogeneous photocatalysts whose stability has been carefully studied. First, the membranes resistance has been evaluated by means of total organic carbon (TOC) release determination under the employed photo-oxidation conditions. Minor oxidative damages are found for polyvinylidene fluoride (PVDF) and polydimethylsiloxane (PDMS), which undergo a TOC release of 5.6 and 2.4 mg L^{-1} respectively after 2 h irradiation at 25 °C. The performance of the heterogeneous photocatalysts has been assessed in the photo-oxidation of *n*-pentanol on the basis of recycling. After each run the membrane containing decatungstate is recovered, washed and reused. Table 9.5 shows that a poor recycling

TABLE 9.5 Photo-oxidation of *n*-pentanol with Membranes Incorporating Decatungstate

Photocatalyst	Run[a]	Conversion (%)	TON[b]
$PVDF/W_{10}O_{32}^{4-}$	I	100	67
	II	61	41
	III	39	26
$PDMS/W_{10}O_{32}^{4-}$	I	88	100
	II	67	77
	III	74	84

[a]Recycling experiments, 4 h irradiation each.
[b]Total turnover number (TON) = moles of substrate converted per mole of catalyst.

performance is obtained for PVDF/$W_{10}O_{32}^{4-}$, with the photocatalyst that loses activity in progressive runs. This drop is not due to a leaching problem but can be ascribed to the incomplete extraction of residual products that prevents an efficient supply of fresh reagents. The PDMS/$W_{10}O_{32}^{4-}$ photocatalyst appears to be the most stable and effective in multiple reaction runs, probably thanks to a good surface dispersion of the active decatungstate that leads both to a maximum photoactivity and to a better substrate supply [112].

9.5 CONCLUSIONS

Heterogeneous photocatalysis is an emerging, innovative and green method for the synthesis of fine chemicals. From a general point of view, an important advantage of heterogeneous over homogeneous catalysis is that solid catalysts can be easily removed from the reaction vessel and, in many cases, they can be reused without significant loss of activity. Research directed at tailoring the surface of heterogeneous systems so as to meet the need of a high selectivity is of paramount importance. Examples reported concern organized assemblies on matrix surfaces, adsorption-controlled reactions and molecular modification of surfaces by grafting. Studies benefit from analysis of the behavior of nanostructured photoactive materials with well-defined sizes and shapes.

The performance of semiconductor photocatalysts is illustrated by the particular case of the stable, widely employed TiO_2. It is a rather strong oxidant under illumination and applications in photocatalysis for synthetic purposes makes it necessary to optimize the photoactivity, which has provided a big stimulus to studies in this direction. In particular, control of the crystallographic and morphological characteristics, use of constrained systems, surface modification and loading with inorganic elements are successful strategies to obtain TiO_2-based photocatalysts with predictable properties.

The photochemical reactivity of metal oxides is influenced by their degree of dispersion on inorganic supports. Highly isolated metal oxides loaded on silica, mixed oxides and zeolites induce the occurrence of organic transformations that are not observed with the bulk metal oxides. Photocatalytic efficiencies that are comparable to that of TiO_2 and good selectivity are achieved with polyoxotungstates heterogenized with polymeric membranes or micro- and mesoporous inorganic materials. These systems do not cause mineralization of the substrate to carbon dioxide.

The organic substrates considered in this survey are important starting materials for producing a variety of chemicals. In particular, the selective oxidation of alcohols and the mono-oxygenation of C−H bonds with molecular oxygen at room temperature and atmospheric pressure represent attractive synthetic routes. The combination of the advances in the preparation of nanostructured materials with mechanistic knowledge, derived from surface science and molecular-level investigations, is the way to achieve optimal tailoring of photoactive materials for high selectivity in fine chemicals production.

REFERENCES

1. Fox M.A. In: *Electron Transfer in Chemistry. Principles and Theories*, Vol. I. Balzani V., ed. Wiley-VCH, Weinheim, 2001, pp. 271–311.
2. Li Y., Wang L. (1997). *Stud. Surf. Sci. Catal. 103*, 391–415.
3. Pichat P. (1994). *Catal. Today 19*, 313–333.
4. Ohtani B. (1994). *Trends Photochem. Photobiol. 3*, 531–539.
5. Fujishima A., Rao T.N., Tryk D.A. (2000). *J. Photochem. Photobiol. C: Photochem. Rev. 1*, 1–21.
6. Shiraishi Y., Hirai T. (2008). *J. Photochem. Photobiol. C: Photochem. Rev. 9*, 157–170.
7. Palmisano G., Augugliaro V., Pagliaro M., Palmisano L. (2007). *Chem. Commun.*, 3425–3437.
8. Fagnoni M., Dondi D., Ravelli D., Albini A. (2007). *Chem. Rev. 107*, 2725–2756.
9. Maldotti A., Molinari A., Amadelli R. (2002). *Chem. Rev. 102*, 3811–3836.
10. Tzirakis M.D., Lykakis I.N., Orfanopoulos M. (2009). *Chem. Soc. Rev. 38*, 2609–2621.
11. Kisch H. (2001). *Adv. Photochem. 26*, 93–143.
12. Griesbeck A.G., Mattay J., eds. *Synthetic Organic Photochemistry*. Marcel Dekker, New York, 2005.
13. Gambarotti C., Punta C., Recupero F., Caronna T., Palmisano L. (2010). *Curr. Org. Chem. 14*, 1153–1169.
14. Palmisano G., Garcia-Lopez E., Marcì G., Loddo V., Yurdakal S., Augugliaro V., Palmisano L. (2010). *Chem. Commun. 46*, 7074–7089.
15. Fox M.A. (1983). *Acc. Chem. Res. 16*, 314–321.
16. Zaera F.J. (2010). *J. Phys. Chem. Lett. 1*, 621–627.
17. Grasselli R.K. (2001). *Top. Catal. 15*, 83–83.
18. Sheldon R.A., Kochi J.K. *Metal-Catalyzed Oxidation of Organic Compounds*. Academic Press, New York, 1981.
19. Foote C.S. *Active Oxygen in Chemistry*. Chapman and Hall, New York, 1995.
20. Bielanski A., Haber J. *Oxygen in Catalysis*. Marcel Dekker, New York, 1991.
21. Hoffmann M.L., Martin S.T., Choi W., Bahnemann D.W. (1995). *Chem. Rev. 95*, 69–96.
22. Linsebligher A.L., Lu G., Yates Jr. J.T. (1995). *Chem. Rev. 95*, 735–758.
23. Herrmann J.M. (1999). *Catal. Today 53*, 115–129.
24. Fox M.A., Dulay M.T. (1993). *Chem. Rev. 93*, 341–357.
25. Augugliaro V., Loddo V., Marcì G., Palmisano L., Lopez-Munoz M.J. (1997). *J. Catal. 166*, 272–283.
26. Gerischer H., Heller A. (1991). *J. Phys. Chem. 95*, 5261–5267.
27. Gerischer H. (1993). *Electrochim Acta. 38*, 3–9.
28. Gerischer H., Heller A. (1995). *Electrochim Acta. 40*, 1277–1281.
29. Pichat P., Fox M.A. In: *Photoinduced Electron Transfer*, Part D. Fox M.A., Chanon M., eds. Elsevier, Amsterdam, 1988, pp. 241–302.
30. Wang Y., Hung C.-S. (2000). *Wat. Res. 34*, 2791–2797.
31. Pichat P., Guillard C., Amalric L., Renard A.C., Paidy O. (1995). *Sol. Energy Mater. Solar Cells 38*, 391–399.

32. Kesselman J.M., Shreve G.A., Hoffmann M.R., Lewis N.S. (1994). *J. Phys. Chem. 98*, 13385–13395.
33. Ahmed S., Fonseca S.M., Kemp T.J., Unwin P.R. (2003). *J. Phys. Chem. B 107*, 5892–5900.
34. Amadelli R., Maldotti A., Sostero S., Carassiti V. (1991). *J. Chem. Soc. Faraday Trans. 87*, 3267–3273 and refs therein.
35. Nosaka Y., Yamashita Y., Fukuyama H. (1997). *J. Phys. Chem. B 101*, 5822–5827.
36. Hirakawa T., Nosaka Y. (2002). *Langmuir 18*, 3247–3254.
37. Ishibashi K., Fujishima A., Watanabe T., Hashimoto K. (2000). *J. Phys. Chem. B 104*, 4934–4938.
38. Daimon T., Hirakawa T., Suetake J., Nosaka Y. (2008). *Appl. Catal. A: General 340*, 169–175.
39. Inumaru K., Kasahara T., Yasui M., Yamanaka S. (2005). *Chem. Commun.*, 2131–2133.
40. Shiraishi Y., Sugano Y., Inoue D., Hirai T. (2009). *J. Catal. 264*, 175–182.
41. Shiraishi Y., Saito N., Hirai T. (2005). *J. Am. Chem. Soc. 127*, 8304–8306.
42. Maldotti A., Molinari A., Amadelli R., Carbonell E., Garcia H. (2008). *Photochem Photobiol Sci. 7*, 819–825.
43. Bartl M.H., Puls S.P., Tang J., Lichtenegger H.C., Stucky G.D. (2004). *Angew. Chemie. Int. Ed. 43*, 3037–3040.
44. Alvaro M., Aprile C., Benitez E., Carbonell E., Garcia H. (2006). *J. Phys. Chem. B 110*, 6661–6665.
45. Shimizu K.-I., Kaneko T., Fujishima T., Kodama T., Yoshida H., Kitayama Y. (2002). *Appl. Catal. A: General 225*, 185–191.
46. Rezala H., Khalaf H., Valverde J.L., Romero A., Molinari A., Maldotti A. (2009). *Appl. Catal. A: General 352*, 234–242.
47. Chen J., Eberlein L., Langford C.H. (2002). *J. Photochem. Photobiol. A: Chem. 148*, 183–189.
48. Cosa G., Galletero M.S., Fernandez L., Marquez F, Garcia H., Scaiano J.C. (2002). *New J. Chem. 26*, 1448–1455.
49. Augugliaro V., Loddo V., Lopez-Munoz M.J., Marquez-Alvarez C., Palmisano G., Palmisano L., Yurdakal S. (2009). *Photochem. Photobiol. Sci. 8*, 663–669.
50. Yurdakal S., Palmisano G., Loddo V., Alagoez O., Augugliaro V., Palmisano L. (2009). *Green Chem. 11*, 510–516.
51. Addamo M., Augugliaro V., Bellardita M., Di Paola A., Loddo V., Palmisano G., Palmisano L., Yurdakal S. (2008). *Catal. Lett. 126*, 58–62.
52. Augugliaro V., Caronna T., Loddo V., Marcì G., Palmisano G., Palmisano L., Yurkadal S. (2008). *Chem. Eur. J. 14*, 4640–4646.
53. Palmisano G., Yurkadal S., Augugliaro V., Loddo V., Palmisano L. (2007). *Adv. Synth. Catal. 349*, 964–970.
54. Yurdakal S., Palmisano G., Loddo V., Augugliaro V., Palmisano L. (2008). *J. Am. Chem. Soc. 130*, 1568–1569.
55. Augugliaro V., Kisch H., Loddo V., Lopez-Munoz M.J., Marquez-Alvarez C., Palmisano L., Palmisano L., Parrino F., Yurdakal S. (2008). *Appl. Catal. A: General 349*, 182–188.

56. Carneiro J.T., Savenije T.J., Moulijn J.A., Mul G. (2010). *J. Phys. Chem. B 114*, 327–332.
57. Carneiro J.T., Almeida A.R., Moulijn J.A., Mul G. (2010). *Phys. Chem. Chem. Phys. 12*, 2744–2750.
58. Yoshida H., Murata C., Hattori T. (1999). *Chem. Commun.*, 1551–1552.
59. Murata C., Yoshida H., Kumagai J., Hattori T (2003). *J. Phys. Chem. B 107*, 4364–4373.
60. Murata C., Hattori T., Yoshida H. (2005). *J. Catal. 231*, 292–299.
61. Koyano K.A., Tatsumi T. (1997). *Microporous Mater. 10*, 259–271.
62. Shiraishi Y., Morishita M., Hirai T. (2005). *Chem. Commun.*, 5977–5979.
63. Morishita M., Shiraishi Y., Hirai T. (2006). *J. Phys. Chem. B 110*, 17898–17905.
64. Anderson M.W., Terasaki O., Ohsuna T., Philippou A., Mackay S.P., Ferreira A., Rocha J., Lidin S. (1994). *Nature 367*, 347–351.
65. Shiraishi Y., Tsukamoto D., Hirai T. (2008). *Langmuir 24*, 12658–12663.
66. Shiraishi Y., Teshima Y., Hirai T. (2005). *Chem. Commun.*, 4569–4571.
67. Shiraishi Y., Ohara H., Hirai T. (2008). *J. Catal. 254*, 365–373.
68. Murata C., Yoshida H., Hattori T. (2001). *Chem. Commun.*, 2412–2413.
69. Shiraishi Y., Teshima Y., Hirai T. (2006). *J. Phys. Chem. B 110*, 6257–6263.
70. Shiraishi Y., Ohara H., Hirai T. (2010). *New J. Chem. 34*, 2841–2846.
71. Teramura K., Tanaka T., Yamamoto T., Funabiki T. (2001). *J. Mol. Catal. A: Chemical 165*, 299–301.
72. Teramura K., Tanaka T., Kani M., Hosokawa T., Funabiki T. (2004). *J. Mol. Catal. A: Chemical 208*, 299–305.
73. Teramura K., Ohuchi T., Shishido T., Tanaka T. (2009). *J. Phys. Chem. C 113*, 17018–17024.
74. Lopez H.H., Martinez A. (2002). *Catal. Lett. 83*, 37–41.
75. Shiraishi Y., Morishita M., Teshima Y., and Hirai T. (2006). *J. Phys. Chem. B 110*, 6587–6594.
76. Filowitz M., Ho R.K.C., Klemperer W.G., Shun W. (1979). *Inorg. Chem. 18*, 93–103.
77. Chemseddine A., Sanchez C., Livage J., Launay J.P., Fournier M. (1984). *Inorg. Chem. 23*, 2609–2613.
78. Pope M.T. *Heteropoly and Isopoly Oxometalates. Inorganic Chemistry Concepts 8*. Springer-Verlag, Heidelberg, New York, Tokyo, 1983.
79. Hill C.L., Prosser-McCartha C.M. (1995). *Coord. Chem. Rev. 143*, 407–455.
80. Mizuno N., Misono M. (1998). *Chem. Rev. 98*, 199–218.
81. Palmisano G., Augugliaro V., Magliaro M., Palmisano L. (2007). *Chem. Commun.*, 3425–3437.
82. Khenkin A.M., Ben-Daniel R., Rosenberger A., Vigdergauz I., Neumann R. In: *Polyoxometalate Chemistry. From Topology via Self-Assembly to Applications*. Pope M.T., Müller A., eds. Kluwer Academic Publishers, Dordrecht, 2001, pp. 347–362.
83. Tzirakis M.D., Likakis I.N., Orfanopoulos M. (2009). *Chem. Soc. Rev. 38*, 2609–2621.
84. Maldotti A., Molinari A. In: *Progress in Heterogeneous Catalysis*. Marmaduke D.L., ed. Nova Science Publishers, New York, 2008, pp. 1–15.

85. Hiskia A., Mylonas A., Papaconstantinou E. (2001). *Chem. Soc. Rev. 30*, 62–69.
86. Duncan D.C., Netzel T.L., Hill C.L. (1995). *Inorg. Chem. 34*, 4640–4646.
87. Tanielian C., Duffy K., Jones A. (1997). *J. Phys. Chem. B 101*, 4276–4282.
88. Duncan D.C., Fox M.A. (1998). *J. Phys. Chem. A 102*, 4559–4567.
89. Tanielian C. (1998). *Coord. Chem. Rev. 178–180*, 1165–1181.
90. Maldotti A., Amadelli R., Varani G., Tollari S., Porta F. (1994). *Inorg. Chem. 33*, 2968–2973.
91. Wu Y., Ye X., Yang X., Wang X., Chu W., Hu Y. (1996). *Ind. Eng. Chem. Res. 35*, 2546–2560.
92. Molinari A., Amadelli R., Andreotti L., Maldotti A. (1999). *Dalton Commun*. 1203–1204.
93. Molinari A., Amadelli R., Mazzacani A., Sartori G., Maldotti A. (2002). *Langmuir 18*, 5400–5405.
94. Molinari A., Amadelli R., Carassiti V., and Maldotti A. (2000). *Eur. J. Inorg. Chem.*, 91–96.
95. Maldotti A., Amadelli R., Vitali I., Borgatti L., Molinari A. (2003). *J. Mol. Catal. A: Chemical 204–205*, 703–711.
96. Tzirakis M.D., Lykakis I.N., Panagiotou G.D., Bourikas K., Lycourghiotis A., Kordulis C., Orfanopoulos M. (2007). *J. Catal. 252*, 178–189.
97. Maldotti A., Molinari A., Varani G., Lenarda M., Storaro L., Bigi F., Maggi R, Mazzacani A., Sartori G. (2002). *J. Catal. 209*, 210–216.
98. Shen H.Y., Mao H.L., Ying L.Y., Xia Q.H. (2007). *J. Mol. Catal. A: Chemical 276*, 73–79.
99. Ozer R.R., Ferry J.L. (2002). *J. Phys. Chem. B 106*, 4336–4342.
100. Guo Y., Wang Y., Hu C., Wang E. (2000). *Chem. Mater. 12*, 3501–3508.
101. Guo Y., Hu C., Wang X., Wang Y., Wang E., Zou Y., Ding H., Feng S. (2001). *Chem. Mater. 13*, 4058–4064.
102. Guo Y., Hu C., Jiang S., Guo C., Yang Y., Wang E. (2002). *Appl. Catal. B: Environ. 36*, 9–17.
103. Farhadi S., Afshari M. (2006). *J. Chem. Res.*, 188–191.
104. Farhadi S., Afshari M., Malesi M., Babazadeh Z. (2005). *Tetrahedron Lett. 46*, 8483–8486.
105. Molinari A., Bratovcic A., Magnacca G., Maldotti A. (2010). *Dalton Trans. 39*, 7826–7833.
106. Farhadi S., Momeni Z. (2007). *J. Mol. Catal. A: Chemical 277*, 47–52.
107. Farhadi S., Zaidi M. (2009). *Appl. Catal. A: General 354*, 119–126.
108. Molinari A., Varani G., Polo E., Vaccari S., Maldotti A. (2007). *J. Mol. Catal. A: Chemical 262*, 156–163.
109. Fornal E., Giannotti C. (2007). *J. Photochem. Photobiol. A: Chem. 188*, 279–286.
110. Maldotti A., Molinari A., Bigi F. (2008). *J. Catal. 253*, 312–317.
111. Ni L., Ni J., Lv Y., Yang P., Cao Y. (2009). *Chem. Commun.*, 2171–2173.
112. Bonchio M., Carraro M., Scorrano G., Fontananova E., Drioli E. (2003). *Adv. Synth. Catal. 345*, 1119–1126.

113. Bonchio M., Carraro M., Gardan M., Scorrano G., Drioli E., Fontananova E. (2006). *Top. Catal. 40*, 133–140.
114. Carraro M., Gardan M., Scorrano G., Drioli E., Fontananova E., Bonchio M. (2006). *Chem. Commun.*, 4533–4535.
115. Lopez L.C., Buonomenna M.G., Fontananova E., Iacoviello G., Drioli E., d'Agostino R., Favia P. (2006). *Adv. Funct. Mater. 16*, 1417–1424.
116. Fontananova E., Donato L., Drioli E., Lopez L.C., Favia P., d'Agostino R. (2006). *Chem. Mater. 18*, 1561–1568.
117. Albonetti S., Cavani F., Trifirò F. (1996). *Catal. Rev.-Sci. Eng. 38*, 413–438.
118. Arends I.W.C.E., Sheldon R.A., Wallau M., Schuchardt U. (1997). *Angew. Chem. Int. Ed. Engl. 36*, 1144–1163.
119. Tryk D.A., Fujishima A., Honda K. (2000). *Electrochim. Acta 45*, 2363–2376.
120. Lu G., Gao H., Suo J., Li S.J. (1994). *J. Chem. Soc., Chem. Commun.*, 2423–2424.
121. Boarini P., Carassiti V., Maldotti A., Amadelli R. (1998). *Langmuir 14*, 2080–2085.
122. Almquist C.B., Biswas P. (2001). *Appl. Catal. A: General 214*, 259–271.
123. Li X., Quan X., Kutal C. (2004). *Scr. Mater. 50*, 499–505.
124. Brusa M.A., Grela M.A. (2005). *J. Phys. Chem. B 109*, 1914–1918.
125. Du P., Moulijn J.A., Mul G. (2006). *J. Catal. 238*, 342–352.
126. Goldstein S., Meyerstein D. (1999). *Acc. Chem. Res. 32*, 547–550.
127. Carneiro J.T., Yang C.C., Moma J.A., Moulijn J.A., Mul G. (2009). *Catal. Lett. 129*, 12–19.
128. Herrman J.M., Pichat P., Mu W. (1989). *Catal. Lett. 3*, 73–84.
129. Gonzalez M.A., Howell S.G., Sikdar S.K. (1999). *J. Catal. 183*, 159–162.
130. Almeida A.R., Moulijn J.A., Mul G. (2008). *J. Phys. Chem. C. 112*, 1552–1561.
131. Brusa M.A., Di Iorio Y., Churio M.S., Grela M. A. (2007). *J. Mol. Catal. A: Chemical 268*, 29–35.
132. Renckens T.J.A., Almedia A.R., Damen M.R., Kreutzer M.T., Mul G. (2010). *Catal. Today 155*, 302–310.
133. Almeida A.R., Carneiro J.T., Moulijn J.A., Mul G. (2010). *J. Catal. 273*, 116–124.
134. Amano F., Ito T., Takenaka S., Tanaka T. (2005). *J. Phys. Chem. B 109*, 10973–10977.
135. Hu Y., Higashimoto S., Takahashi S., Nagai Y., Anpo M. (2005). *Catal. Lett. 100*, 35–37.
136. Navio J.A., Garcia Gomez M., Pradera Adrian M.A., Fuentes Mota J. (1996). *J. Mol. Catal. A: Chemical 104*, 329–339.
137. Augugliaro V., Coluccia S., Loddo V. (1999). *Appl. Catal. B: Environ. 20*, 15–17.
138. Cao L.X., Gao Z., Suib S.L., Obee T.N., Hay S.O., Freihaut J.D. (2000). *J. Catal. 196*, 253–261.
139. Fujihira M., Satoh Y., Osa T. (1981). *Nature 293*, 206–208.
140. Shimizu K.I., Kaneko T., Fujishima T., Kodama T., Yoshida H., Kitayama Y. (2002). *Appl. Catal. A: General 225*, 185–191.
141. Palmisano G., Addamo M., Augugliaro V., Caronna T., Di Paola A., Garcia-Lopez E., Loddo V., Palmisano L. (2006). *Chem. Commun.*, 1012–1014.
142. Palmisano G., Addamo M., Augugliaro V., Caronna T., Di Paola A., Garcia-Lopez E., Loddo V., Marcì G., Palmisano L., Schiavello M. (2007). *Catal. Today 122*, 118–127.

143. Park H., and Choi W. (2005). *Catal. Today 101*, 291–297.
144. Soana F., Sturini M., Cermenati L., Albini A. (2000). *J. Chem. Soc. Perkin Trans. 2*, 699–704.
145. Higashida S., Harada A., Kawakatsu R., Fujiwara N., Matsumura M. (2006). *Chem. Commun.*, 2804–2806.
146. Mallat T., Baiker A. (2004). *Chem. Rev. 104*, 3037–3058.
147. Pichat P., Mozzanega M., Courbon H. (1987). *J. Chem. Soc. Faraday Trans. 183*, 697–704.
148. Muggli D.S., Falconer J.L. (1998). *J. Catal. 175*, 213–219.
149. Pillai U.R., and Sahle-Demessie E. (2002). *J. Catal. 211*, 434–444.
150. Kominami H., Sugahara H., Hashimoto K. (2010). *Catal. Commun. 11*, 426–429.
151. Samiolo L., Valigi M., Gazzoli D., Amadelli R. (2010). *Electrochim. Acta 55*, 7788–7795.
152. Molinari A., Montoncello M., Houria R., Maldotti A. (2009). *Photochem. Photobiol. Sci. 8*, 613–619.
153. Molinari A., Bruni M., Maldotti A. (2008). *J. Adv. Oxid. Techn. 11*, 143–148.
154. Amadelli R., Molinari A., Vitali I., Samiolo L., Mura G.M., Maldotti A. (2005). *Catal. Today 101*, 397–405.
155. Bettoni M., Rol C., Sebastiani G.V. (2008). *J. Phys. Org. Chem. 21*, 219–224.
156. Blake N.R., Griffin G.L. (1988). *J. Phys. Chem. 92*, 5697–5701.
157. Mohamed O.S., Gaber A.M., Abdel-Wahab A.A. (2002). *J. Photochem. Photobiol. A: Chem. 148*, 205–210.
158. Chen J., Ollis D.F., Rulkens W.H., Bruning H. (1999). *Wat. Res. 33*, 669–676.
159. Zhang M., Wang Q., Chen C., Zhang L., Ma W., Zhao J. (2009). *Angew. Chem. Int. Ed. 48*, 6081–6084.
160. Zhang Z.R., Bondarchuk O., White J.M., Kay B.D., Dohnalek Z. (2006). *J. Am. Chem. Soc. 128*, 4198–4199.
161. Mandelbaum P.A., Regazzoni A.E., Blesa M.A., Bilmes S.A. (1999). *J. Phys. Chem. B 103*, 5505–5511.
162. Ganadu M.L., Andreotti L., Vitali I., Maldotti A., Molinari A., Mura G.M. (2002). *Photochem. Photobiol. Sci. 1*, 951–954.
163. Maurino V., Bedini A., Minella M., Rubertelli F., Pelizzetti E., Minero C. (2008). *J. Adv. Oxid. Technol. 11*, 184–192.
164. Augugliaro V., Hamed E., Nazer H.A., Loddo V., Mele A., Palmisano G., Palmisano L., Yurdakal S. (2010). *Catal. Today 151*, 21–28.
165. Al Nashef I.M., Matthews M.A., Weidner J.W. (2003). In: *Ionic Liquids as Green Solvents*. Rogers R.D., Seddon K.R., eds. ACS Symposium Series 856, American Chemical Society, Washington, DC, 2003, pp. 509–525.
166. Cantau C., Pigot T., Dupin J.C., Lacombe S. (2010). *J. Photochem. Photobiol. A: Chem. 216*, 201–208.
167. Higashimoto S., Kitao N., Yoshida N., Sakura T., Azuma M., Ohue H., Sakata Y. (2009). *J. Catal. 266*, 279–285.
168. Higashimoto S., Suetsung N., Azuma M., Ohue H., Sakata Y. (2010). *J. Catal. 274*, 76–83.

169. Amadelli R., Samiolo L., Pichat P. Manuscript in preparation.
170. Ismail A.A., Robben L., Bahnemann D.W. (2011). *Chem. Phys. Chem. 59*, 982–991.
171. Lin W., Frei H. (2005). *J. Phys. Chem. B 109*, 4929–4935.
172. Hu Y., Wada N., Tsujimaru K., Anpo M. (2007). *Catal. Today 120*, 139–144.
173. Nakamura R., Okamoto A., Osawa H., Irie H., Hashimoto K. (2007). *J. Am. Chem. Soc. 129*, 9596–9598.
174. Anpo M., Kim T., Matsuoka M. (2009). *Catal. Today 142*, 114–124.
175. Friesen D.A., Gibson D.B., Langford C.H. (1998). *Chem. Commun.*, 543–544.
176. Friesen D.A., Morello L., Headley J.V., Langford C.H. (2000). *J. Photochem. Photobiol. A: Chem. 133*, 213–220.
177. Li X., Kutal C. (2002). *J. Mater. Sci. Lett. 21*, 1525–1527.
178. Mul G., Wasylenko W., Sameh Hamdy M., Frei H. (2008). *Phys. Chem. Chem. Phys. 10*, 3131–3137.
179. Asahi R., Morikawa T., Ohwaki T., Aoki K., Taga Y. (2001). *Science 293*, 269–271.
180. Anpo M. (2000). *Pure Appl. Chem. 72*, 1787–1792.
181. Amadelli R., Samiolo L., Maldotti A., Molinari A., Valigi M., Gazzoli D. (2008). *Int. J. Photoenergy*, Art. ID 853753, 9 pages.

10

INDUSTRIAL APPLICATIONS

10.1 THE HYDROXYLATION OF PHENOL TO HYDROQUINONE AND CATECHOL

UGO ROMANO* AND MARCO RICCI*

At the end of the 1940s, chemists of the Linde division of Union Carbide discovered the synthetic zeolites A, B, and X and, in the following years, their commercialization as adsorbents for gas separation was started. In the meantime, researchers of both Union Carbide and Mobil realized that selective catalytic processes could occur within the pores of zeolites and a hydrocracking catalyst based on zeolite Y was launched [1]. At the end of the 1960s, Mobil researchers discovered and then patented ZSM5, a new synthetic, crystalline, microporous aluminosilicate that found widespread application in different petrochemical and refinery processes [2]. At the time, it was generally accepted that a high dispersion of the active sites on amorphous supports with high surface area was needed to get good catalytic activities. So, discoveries at Mobil marked the start of a true revolution in the industrial application of heterogeneous catalysis, focused on the use of zeolites and other microporous materials.

10.1.1 The Discovery of TS-1

The research company of the Eni group (at the time Assoreni) entered the field of synthetic zeolites in the late 1970s, mainly focusing its studies on aluminosilicates with low Al content. It was shown that the content could be continuously decreased to the point that a new material could be prepared while still retaining the ZSM5 structure but composed by just silicon and oxygen. This new material, discovered at

*Corresponding authors

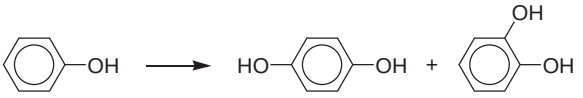
Liquid Phase Oxidation via Heterogeneous Catalysis: Organic Synthesis and Industrial Applications, First Edition. Edited by Mario G. Clerici and Oxana A. Kholdeeva.
© 2013 John Wiley & Sons, Inc. Published 2013 by John Wiley & Sons, Inc.

the same time at Union Carbide, is today referred to as silicalite-1. Eni's research went on attempting to prepare silica-based materials containing different elements (e.g., boron, aluminum, titanium, zirconium, vanadium, chromium, manganese, and iron), possibly substituting for silicon in the structure. During these attempts, a material was obtained with significant amounts of titanium that was shown to substitute for silicon in the crystal structure: titanium-silicalite, TS-1, was born [3, 4].

Soon after, the search started for catalytic applications of the new material. At the time, zeolites had only been applied, with significant success, to a number of acid-catalyzed reactions. Accordingly, the first patent describing synthesis and applications of TS-1 claims a number of such reactions including aromatics alkylation, olefins oligomerization, and hydrocarbon isomerization [3]. At the same time, however, an example dealt with the dihydroxylation of allyl alcohol by hydrogen peroxide to get 86% yield of glycerin.

10.1.2 The Hydroxylation of Phenol

In the late 1970s, ANIC, the chemical company of the Eni group, decided to diversify its activity, entering the fine chemistry business and bought a medium sized company involved in carbochemistry and, particularly, in the synthesis of phenol derivatives. The company ran a proprietary process for phenol hydroxylation with hydrogen peroxide to get a mixture of hydroquinone and catechol (Eq. 10.1).



(10.1)

These diphenols are widely used in industry with global capacities around 55 kt/a for hydroquinone and 30 kt/a for catechol. The former is mainly required for producing antioxidants and polymerization inhibitors and still finds use in the photographic processing. Catechol, in its turn, is mostly used in the production of the insecticide carbofuran and of synthetic vanillin and other fragrances.

The oxidation of phenol by hydrogen peroxide, developed together with prof. Francesco Minisci of the Politecnico di Milano, occurred through a radical mechanism catalyzed by a mixture of iron(II) and cobalt(II) salts and was not fully satisfactory due to low phenol conversion, moderate selectivity and significant tar formation [5]. Furthermore, the catechol to hydroquinone ratio was quite high, ranging from 2 to 2.3, close to the statistical value of 2 moles of catechol per mol of hydroquinone, whereas the market required more hydroquinone than catechol. So, Eni decided to start, in its corporate research center, a project aimed at solving the process problems.

Initially, the problem was addressed by a group with a strong experience on coordination chemistry and homogeneous catalysis, but it found it very difficult to identify solutions different from both the iron/cobalt catalysis already in use and the acid catalysis that had been developed by Rhône-Poulenc [6]. So, a collaboration started with the heterogeneous catalysis group that, at the time, was mainly involved in the study of classic acidic silicoaluminates catalysts, but also of new catalysts for

the selective gas phase oxidation of hydrocarbons to get, e.g., ethylene and propylene oxides, acrylonitrile, and maleic anhydride. From this collaboration, the idea arose that a metal-substituted zeolite could allow exploitation of both the capability of metal ions to activate hydrogen peroxide and that of the zeolites to provide the shape selectivity that would have helped to decrease the *ortho* to *para* ratio, i.e. to increase the hydroquinone production to the expenses of the less valuable catechol.

An extensive testing of catalysts was started, running batch reactions in liquid phase and feeding the hydrogen peroxide into a catalyst/phenol slurry, in the presence of suitable solvents able to dissolve both the phenol and the water. For the first time, people attempted to develop an industrial process based on the use of zeolites in liquid phase and at low temperature, both conditions that could greatly reduce reagents diffusivity within the catalyst.

The catalytic properties of several materials were tested, including those of acidic silicoaluminates that had previously been exchanged with transition metals (iron, cobalt), but also those of gels based on silicon, aluminum, titanium, zirconium, etc. TS-1 was also tested; quite soon it showed outstanding properties as a catalyst for hydrogen-peroxide-based oxidations including not only the phenol hydroxylation but also olefins epoxidation and alcohols and amines oxidation [7–9].

Very soon, a most critical issue had to be faced: the poor reproducibility of the catalytic performances of TS-1. This poor reproducibility was immediately attributed to some variability of the TS-1 composition and, particularly, to its small content of alkaline (sodium and potassium) or transition (vanadium, iron and nickel) metals and to the presence of small domains of extraframework titanium oxide, TiO_2. A careful re-examination of the TS-1 synthesis was undertaken, paying attention to the impurities of the raw materials. In particular, the quality of commercial tetrapropylammonium hydroxide, used as the templating agent during the TS-1 production, turned out to be relatively poor, with some contamination by potassium and bromide ions. Eventually, a new process for the production of tetrapropylammonium hydroxide was developed and industrialized, based on tetrapropylammonium bromide electrodialysis.

There were two reasons why alkalis affected the catalytic performances of the TS-1. The first one was that they favored the segregation of extraframework titanium as small TiO_2 (anatase) domains, which enhanced hydrogen peroxide decomposition and also promoted some side reactions of phenol. In this respect, it can be mentioned that, in the absence of any extraframework titanium, the TS-1 catalyst was very stable and remained white even under strongly reducing conditions (600 °C under hydrogen atmosphere). On the contrary, in the presence of TiO_2 domains, Ti(IV) was reduced to Ti(III) and the catalyst turned gray.

The second reason why alkalis affected the catalytic performances of the TS-1 was that only in their absence did the catalyst synthesis afford very small (i.e. submicrometric) crystals needed to get high yield and selectivity in the phenol hydroxylation. In fact, crystals larger than 1 μm invariably led to unsatisfactory catalytic performances, with high hydrogen peroxide consumption and tar formation. In particular, the tar formation was due to two different factors. On the one hand, product diffusion within the crystals was inevitably limited, so preventing them from being

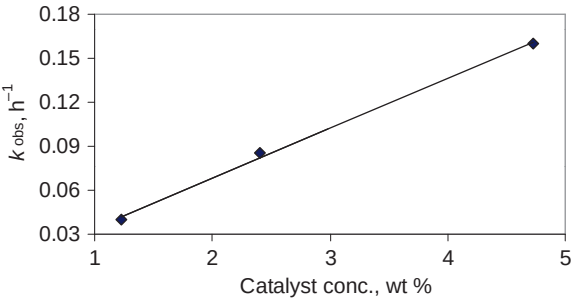


FIGURE 10.1 Effect of catalyst concentration on hydrogen peroxide decomposition. 30% aqueous H_2O_2/acetone 17/13; 50 °C; 1 h; optimized catalyst (submicrometric crystals prepared in the absence of alkalis) [7].

promptly released far away from the catalytic centers and enhancing, instead, the occurrence of consecutive oxidations after the first hydroxylation, eventually resulting in the cleavage of the aromatic ring with formation of acidic byproducts. On the other hand, the limited diffusion also enhanced radical coupling reactions, favored by some radical decomposition of hydrogen peroxide that always occurs (Figure 10.1).

Even when using TS-1 in very small crystals, however, the tar formation could be reduced but not completely suppressed. As a consequence, at high time onstream, the catalytic performances of TS-1 invariably broke down. So, it became mandatory to design a regeneration procedure that could allow restoration of the catalyst performances without affecting its morphology. Two procedures were actually developed. The first one was based on the gradual heating and calcination of the catalyst up to 600–610 °C, under a reducing (hydrogen) atmosphere. The second procedure again envisaged a gradual heating, carefully avoiding hot spots, initially under an inert atmosphere (nitrogen) that, starting at 400 °C, progressively became more and more oxidizing (nitrogen/air mixtures) up to 540–550 °C.

Both procedures required 2–3 h and recovered a catalyst with good performances without substantial morphological modifications. However, before regeneration, it was necessary to recover the catalyst from the reaction mixture, an operation made difficult by the submicrometric dimensions of the TS-1 crystals. Again, two routes were identified to solve the problem: (i) to support the TS-1 crystals on an inert material with high surface area, or (ii) to aggregate the crystals up to dimensions large enough to allow easy filtration. Both the solutions were developed and, to some extent, both were satisfactory. However, supporting the catalyst over, e.g., inert alumina, did not produce contents of the active phase higher than 25–30%. On the other hand, binding the catalyst crystals with some silica, stable catalysts particles of 20–30 μm containing 80–90% of active phase were obtained. The latter approach reduced the catalyst slurry used and, at the same time, gave very good performances of the catalyst due to the high concentration of the active phase. So, eventually, to develop the process, binding the catalyst with silica was preferred to supporting it on alumina.

It should be noted, however, that the supported catalyst could be used in another oxidation reaction: the epoxidation of propene. In this case, the process was run, on a micropilot scale, over a catalytic fixed bed. There was no need to filter the catalyst, and its rejuvenation did not require burning any tar but just washing out, with methanol at 120 °C, the reaction byproducts (polyglycols) that occluded the zeolite channels [10, 11].

The process performances, however, did not depend just on the catalyst quality. Another critical issue was the choice of the solvent. The best performances were obtained in a 60/40 acetone/water mixture: in particular, under the best reaction conditions, this mixture performed better than water alone. With pure acetone, excellent results were obtained, but dangerous acetone peroxides were also found in the reaction mixture. Good results were also obtained in methanol that, however, was discharged due to its high vaporization enthalpy and to the formation of few byproducts arising from its oxidation at relatively high temperatures. However, even under the best conditions, i.e. in the acetone/water mixture, formation of few byproducts cannot be avoided due to the occurrence of both parallel and consecutive side reactions: deep oxidation, radical coupling, and decomposition. Thus, small amounts of oxygen, carbon dioxide, carboxylic acids, and tars are usually found at the end of the reaction. The catalyst concentration was a key issue to get high selectivity: in particular, the amount of tars was greatly reduced at relatively high catalyst loading (Figure 10.2).

The temperature was also important: best performances were achieved around 90 °C. At lower temperatures, hydrogen peroxide is not so quickly converted and holds up in the reactor to undergo, eventually, to some decomposition. Above 90–100 °C, further oxidations of catechol and hydroquinone occur, together with some radical coupling (Figure 10.3).

Under the best conditions, in comparison to existing processes based either on acid catalysis or on radical chemistry, the process using TS-1 catalyst produced higher phenol conversions with a lower *ortho* to *para* ratio, more aligned to the market requirements (Table 10.1).

Sometimes, even lower *ortho* to *para* ratios, down to 0.35, have been observed. Usually, however, these high selectivities to hydroquinone are only apparent,

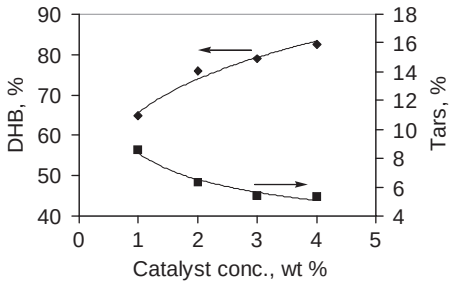


FIGURE 10.2 Phenol hydroxylation: effect of catalyst concentration (phenol/water/acetone 70/17/13; H_2O_2/phenol 0.25 mol/mol; 1 h). DHB (dihydroxybenzenes: hydroquinone + catechol) selectivity based on H_2O_2; tars selectivity based on phenol [7].

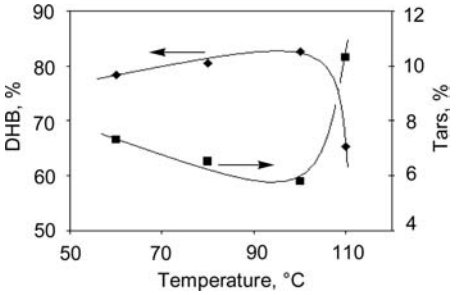


FIGURE 10.3 Phenol hydroxylation: effect of the temperature (phenol/water/acetone 70/17/13; H_2O_2/phenol 0.25 mol/mol; 1 h). DHB (dihydroxybenzenes: hydroquinone + catechol) selectivity based on H_2O_2; tars selectivity based on phenol [7].

actually, due to the occurrence of already mentioned decomposition reactions that preferentially affect catechol with cleavage of the aromatic ring and formation of acid byproducts with six carbon atoms (e.g., muconic acid) or less.

10.1.3 The Industrial Process

The results obtained during the initial development of phenol hydroxylation by TS-1 were clearly better than the performances of the competitors' processes. However, the development of a new industrial process for the production of hydroquinone and catechol needed the availability of commercial amounts of a catalyst, stable from both the chemical and structural point of views, with reproducible performances and easy to handle in all the process steps: reaction, separation, recycling and regeneration. So, a process for the production of TS-1 on an industrial scale was gradually defined (Figure 10.4).

The first step was the synthesis of TS-1 starting with the hydrolysis of tetraethyl orthosilicate (TEOS) and tetraethyl orthotitanate (TEOT) in the presence of a

TABLE 10.1 Comparison of Catalysts Performances for the Phenol Hydroxylation Process

Catalyst	Phenol conversion (%)	Selectivity (%) based on H_2O_2	Selectivity (%) based on phenol	Catechol to hydroquinone ratio	Ref.
$HClO_4$ [a]	5	85–90	90[b]	1.5	[6]
Fe^{2+} and Co^{2+} salts	20	50[b]	> 90	1.5–4	[5]
TS-1	20–30	80–90	90–95	1.1–1.2	this work

[a] Phosphoric acid, H_3PO_4, was also required to sequester metal ions that could promote undesired side reactions.
[b] From reference [12].

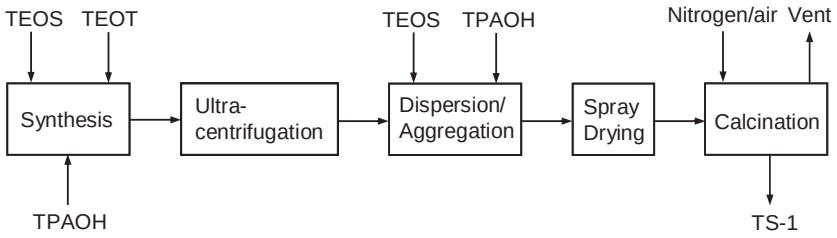


FIGURE 10.4 The industrial production of TS-1.

templating agent, tetrapropylammonium hydroxide (TPAOH), carefully avoiding any excess of TEOT with respect to the maximum amount of titanium that can substitute silicon in the silicalite structure (*ca.* 2.5% as TiO_2) [13]. The tiny crystals were then recovered by ultracentrifugation and again dispersed in water under high shearing stress, so as to produce complete disaggregation. Further TEOS and TPAOH were then added in order to form some binding silica with low molecular weight, without damaging the crystal structure of TS-1. Then, the resulting slurry was fed in a spray dryer that produced stable spherical aggregates with as high as 80–90% content of the active phase. The aggregates were finally calcined in two different consecutive steps, under nitrogen and nitrogen/air atmosphere, respectively. This calcination allowed removal of the water caged in the zeolite, thermal decomposition of the templating agent, and strengthening of the binding between the TS-1 crystals and the silica.

Both the spray drying and the calcination turned out to be quite critical for the catalyst stability. A too diluted slurry or a too fast heating often produced hollow spheres that, in turn, are quite brittle. Another critical point was the material in contact with the catalyst during the last phase of the calcination, beyond 400 °C. To avoid any contamination with metal traces from steel (iron, vanadium, molybdenum), the catalyst was layered on silicon carbide trays inside a column furnace. Silicon carbide was completely inert from a chemical point of view and, at the same time, its porosity allowed a suitable gas flow (nitrogen/air mixture) needed to get the removal of water and of the products arising from the thermal decomposition of TPAOH to be maintained.

The catalyst prepared by the described process proved to be fully suitable for the commercial production of hydroquinone and catechol.

For the industrial plant, both the slurry and the fixed-bed catalytic reactors were evaluated. However, a fixed bed of TS-1 on alumina arranged in external recirculation of the reaction mixture was quickly discarded due to the difficult *in situ* regeneration of the catalyst at 550 °C. So, eventually, a process was defined (Figure 10.5) in which the hydroxylation reaction was run batchwise in several parallel glass-lined reactors, fed alternately. Catalyst filtration and recycling were also discontinuous, whereas the distillation and recovery of the solvent, of the unreacted phenol and of the reaction products were continuous.

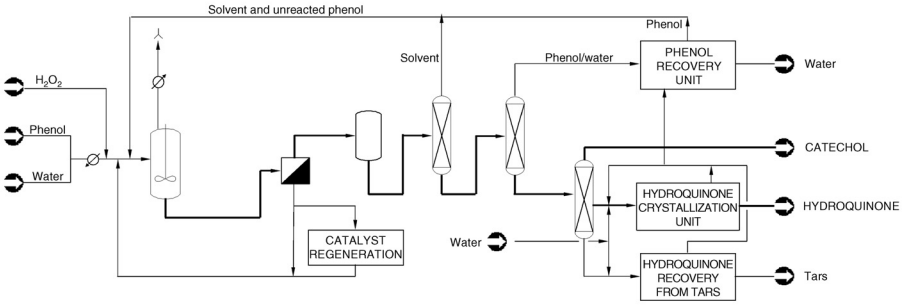


FIGURE 10.5 The EniChem process for the production of hydroquinone and catechol [14].

Both the fresh and the recycled phenol were fed through beds of strongly acidic (sulfonic) cation-exchange resins in order to sequester metals, either already present in the feed or arising from plant corrosion. Even trace amounts of these metals proved to be deleterious for the process performances: 0.5 ppm of iron was enough to lower selectivity by 30–40% due to the occurrence of radical chain reactions resulting in hydrogen-peroxide decomposition and increased tar formation. Furthermore, metal ions readily adsorbed on the catalyst surface, dramatically affecting its performances.

For the same reasons, great attention was also paid to the hydrogen peroxide supply. Hydrogen peroxide industrial production is based on the capability of alkyl derivatives of anthrahydroquinone to afford the corresponding anthraquinones and hydrogen peroxide under typical autoxidation conditions. The anthraquinones are then reduced back to the anthrahydroquinones by a metal-catalyzed hydrogenation (Chapter 1).

In the first generation plants, the hydrogenation catalysts was usually nickel and traces of this metal contaminated the hydrogen peroxide produced, making it unsuitable for the phenol hydroxylation. Only hydrogen peroxide produced with more recent palladium-based catalysts could be satisfactorily used. Furthermore, a special grade of hydrogen peroxide was required, without the tin derivatives usually added as stabilizers.

At the end of the reaction, the solvent and the unreacted phenol were recovered by distillation and recycled. Then, catechol and hydroquinone were separated by a further, more careful distillation and, finally, hydroquinone was crystallized. The tars, in their turn, were fluidified with some methanol and burnt.

Some of the catalyst (4–8% per batch) was continuously removed by a drum filter, washed, fed into a zirconium-lined rotary furnace to be dried under a nitrogen atmosphere, and finally regenerated by batchwise calcination in a silicon carbide kiln in which a nitrogen/air flow was also fed (Figure 10.6).

The main features of the process turned out to be as follows:

- Solvent: acetone/water, methanol, water.
- Temperature: 80–100 °C.
- Hydrogen peroxide to phenol molar ratio: 0.2–0.3.
- Hydrogen peroxide conversion: 100%.

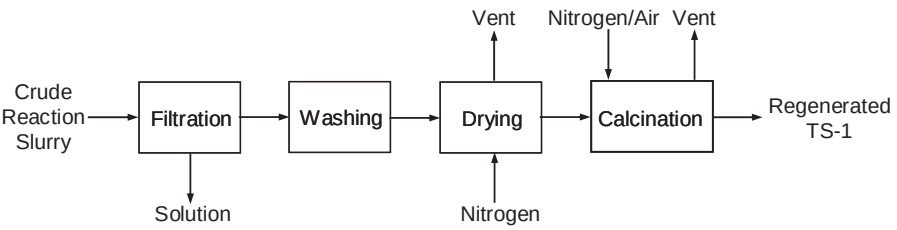


FIGURE 10.6 Scheme of TS-1 regeneration.

- Phenol conversion: 20–30%.
- Selectivity, based on hydrogen peroxide: 80–90%.
- Selectivity, based on phenol: 90–95%.
- *Ortho* to *para* ratio: 1.1–1.2 under the most profitable conditions (high phenol conversion).

The industrial plant for hydroquinone and catechol production (10 000 t/a altogether) was started up in 1986 in the EniChem Synthesis facilities in Ravenna, Italy. Plants for the production of TPAOH and of the TS-1 catalyst were also built by the main plant side. Catalyst regeneration was part of the process. After its realization, the industrial plant underwent very few changes with respect to the original design. The main one was the elimination of the column furnace used during the last phase of the fresh catalyst calcination: as a matter of fact, the silicon carbide kiln of the catalyst regeneration section proved to be perfectly suitable for both operations.

Several years after its realization, the plant was sold to Borregaard (Norway) and then, in December 2010, to Camlin Fine Chemicals (India) that requires hydroquinone as the starting material for its major product range of food antioxidant and products like tert-butylhydroquinone (TBHQ) and butylated hydroxyanisole (BHA).

10.1.4 Other Processes Exploiting TS-1

After the commercialization of the phenol hydroxylation, EniChem focused its research on selective oxidations by hydrogen peroxide on two other important technologies: propylene epoxidation and cyclohexanone ammoximation.

Propylene epoxidation was initially studied on micropilot plants and eventually demonstrated, starting from January 2001, on a 2000 t/a semiscale plant built at the EniChem premises in Ferrara, Italy [11]. The core of the plant was a slurry CSTR with the same catalyst used for phenol hydroxylation, confined in the reactor under propylene pressure, with continuous filtration of the reaction solution [11]. A few months after the start-up of the Ferrara plant, however, Dow Chemical bought the whole EniChem's polyurethanes business including the propylene oxide plant.

The first commercial-scale production of propylene oxide based on propylene epoxidation with hydrogen peroxide was successfully started up in 2008 by Dow and BASF at BASF's facilities in Antwerp, Belgium. The plant exploits the novel BASF/Dow HPPO (Hydrogen Peroxide for Propylene Oxide) technology [15]. A second plant based on this technology was scheduled to begin production in Map Ta Phut, Thailand, in 2011 [15].

Cyclohexanone ammoximation [16, 17], in its turn, was developed, after significant optimization work, basically relying upon the industrial catalyst produced in Ravenna for phenol hydroxylation. The reaction was run in a slurry reactor. Catalyst rejuvenation was not necessary and only a small catalyst integration was needed in order to compensate for a few mechanical losses. Again, the process was demonstrated on a semiscale plant (12 000 t/a) in Porto Marghera (Venezia, Italy) which started operations in 1994. The cyclohexanone oxime produced was cofed to an

existing plant for the conventional, oleum-catalyzed, Beckmann rearrangement to caprolactam. At the same time, Sumitomo Chemical was developing a solid catalyst avoiding the use of sulfuric acid in the Beckmann rearrangement. In order to completely avoid ammonium sulfate coproduction, Sumitomo acquired a license for the EniChem's technology for the ammoximation step and, in April 2003, it integrated its caprolactam production at the Niihama factory (Ehime, Japan) starting up a new line (*ca*. 60 kt/a) exploiting both the TS-1-catalyzed ammoximation of cyclohexanone and the catalytic Beckmann rearrangement, without any coproduction of ammonium sulfate.

Finally, at the same time, the direct oxidation of benzene to phenol was also studied, although just on a bench-scale microplant [18, 19].

REFERENCES

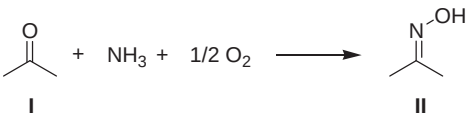
1. Rabo J.A., Schoonover M.W. (2001). *Appl. Catal. A: General 222*, 261–275.
2. Argauer R.J., Landolt G.R., inventors; Mobil Oil Corporation, assignee. US Patent 3,702,886. 1972.
3. Taramasso M., Perego G., Notari B., inventors; Snamprogetti, assignee. US Patent 4,410,501. 1983.
4. Bellussi G., Fattore V. (2003). *Chim. Ind. (Milan) 85*, 15–17.
5. Maggioni P., Minisci F. (1977). *Chim. Ind. (Milan) 59*, 239–242.
6. Varagnat J. (1976). *Ind. Eng. Chem., Prod. Res. Dev. 15*, 212–215.
7. Romano U., Esposito A., Maspero F., Neri C., Clerici M.G. (1990). *Chim. Ind. (Milan) 72*, 610–616.
8. Maspero F. (1993). *Chim. Ind. (Milan) 75*, 291–296.
9. Clerici M.G. (2003). *Chim. Ind. (Milan) 85*, 55–56.
10. Clerici M.G., Bellussi G., Romano U. (1991). *J. Catal. 129*, 159–167.
11. Romano U. (2001). *Chim. Ind. (Milan) 83*, 30–31.
12. Bellussi G., Perego C. In: *Handbook of Heterogeneous Catalysis*, Vol. *7*, 2nd edn, Ertl G., Knözinger H., Schüth F., Weitkamp. J., eds. Wiley-VCH, Weinheim, 2008, pp. 3538–3547.
13. Millini R., Previde Massara E., Perego G., Bellussi G. (1992). *J. Catal. 137*, 497–503.
14. Romano U. (2008). *The impact of zeolite catalysis on the development of new technologies and industrial processes*. 235th American Chemical Society National Meeting, New Orleans.
15. Dow and BASF win IChemE Award for jointly developed HPPO Technology. Available at http://www.dow.com/propyleneoxide/news/20091105a.htm (last accessed, 15 July 2011).
16. Roffia P., Leofanti G., Cesana A., Mantegazza M., Padovan M., Petrini G., Tonti S., Gervasutti P. (1990). *Stud. Surf. Sci. Catal. 55*, 43–52.
17. Petrini G., Leofanti G., Mantegazza M.A., Pignataro F. In: *Green Chemistry. Designing Chemistry for the Environment*. Anastas P.T., Williamson T.C., eds. ACS Symp. Series 626. American Chemical Society, Washington, DC, 1996, pp. 33–48.

18. Balducci L., Bianchi D., Bortolo R., D'Aloisio R., Ricci M., Tassinari R., Ungarelli R. (2003). *Angew. Chem. Int. Ed. 42*, 4937–4940.
19. Bianchi D., Balducci L., Bortolo R., D'Aloisio R., Ricci M., Spanò G., Tassinari R., Tonini C., Ungarelli R. (2007). *Adv. Synth. Catal. 349*, 979–986.

10.2 THE GREENING OF NYLON: THE AMMOXIMATION PROCESS

FRANCO RIVETTI* AND ROBERTO BUZZONI*

The term *ammoximation* dates back to 1980, when Armor and coworkers at Allied Chemical used it for the first time in a series of papers and patents [1, 2] to indicate "the conversion of a ketone to an oxime by treatment with ammonia and oxygen" (Eq. 10.2). Armor's work referred to a gas phase reaction using molecular oxygen as oxidant on heterogeneous catalysts such as xerogels derived from silica-alumina:



I II (10.2)

Actually, Lebedev et al. had reported earlier the formation of cyclohexanone oxime by reaction of cyclohexanone, ammonia and hydrogen peroxide in liquid phase using sodium tungstate as a catalyst [3]. In the following years a process based on a similar chemistry, and referred to as *ammoxidation*, was patented by Toa Gosei [4]. The term ammoxidation is also widely used for reactions generically involving oxidations in the presence of ammonia (like the well-known ammoxidation of light olefins and paraffins) [5]. Mueller and Hoelderich described the reaction of cyclohexanone to cyclohexanone oxime, by using solutions of ammonia and hydrogen peroxide with titanium-containing zeolite catalysts, as *ammonoximation* reaction [6].

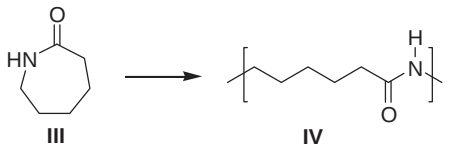
Regardless of the historical development, and without going into deeper details (which are not the object of this review), in its broadest form and in the current context, a catalytic process for the manufacture of oximes by reacting in the liquid phase the corresponding carbonyl compounds with ammonia and hydrogen peroxide, in the presence of heterogeneous catalysts, is generally named ammoximation [7, 8]. This newly discovered chemistry was, and still is, thoroughly studied and applied mainly to develop a direct route to cyclohexanone oxime and ε-caprolactam from cyclohexanone in view of their key role in the industrial production of Nylon-6.

10.2.1 Nylon-6 and ε-Caprolactam, Outlook and Industrial Production

Nylon-6 was industrially developed in Germany by P. Schlack at I.G. Farben in the late 1930s and commercialized under the trade name Perlon. As the naming "6"

*Corresponding authors

suggests, it was obtained starting from a single monomer through ring opening of ε-caprolactam, a cyclic amide that contains 6 carbon atoms in the ring (Eq. 10.3).



III IV (10.3)

Current (2010) worldwide production of ε-caprolactam amounts to approximately 4 million metric tons per year (Mt/a), with a capacity of about 4.7 Mt/a [9].

Caprolactam is used primarily in the production of Nylon-6 fibers, resins and films. Around 70% of world caprolactam production is consumed in the production of Nylon fibers for textiles (it can be combined with other fibers to give good stretch-fit properties for applications like hosiery, sportswear and so on), carpets and industrial yarns; around 30% is used in resins, films and engineering plastics (automotive, film packaging for food, wires, cables, etc.) [10]. Demand for Nylon resins has increased in recent years because of their increasing use in automobile production. Nylon-6 is less likely to crystallize and can be recycled many more times than Nylon-66, a significant amount of resin sold in the merchant market may be a blend of virgin and reprocessed resin.

Caprolactam is widely traded. Western Europe, Central and Eastern Europe, Japan and the United States send significant quantities to China, Taiwan and the Republic of Korea. Asia is the largest caprolactam consuming region in the world, mainly because of Nylon-6 fiber production, which has largely moved away from North America and Western Europe.

China is seeing a high average annual consumption growth rate (around 6–8%) because of the significant increase of domestic demand and also because many outside producers are establishing production facilities in China. Production of caprolactam in China was around 0.3 Mt in 2006 and consumption was around 0.7 Mt but Chinese demand for caprolactam is forecast to rise to over 1.0 Mt/a before 2015. Overall long-term growth for caprolactam is estimated to be around 2–3% per year: growth in Europe and North America will be lower than Asia, particularly China [11].

Industrially, ε-caprolactam is mainly obtained starting from cyclohexanone, a benzene derivative. Traditionally, in this technology, known as the Raschig process, cyclohexanone is transformed to cyclohexanone oxime by means of hydroxylamine sulfate and the latter to ε-caprolactam by Beckmann rearrangement [12–15]. According to the Raschig process, the intermediate production of hydroxylamine sulfate is carried out from NH_3, CO_2 and SO_2 (Eqs. 10.4 to 10.7):

$$2NH_3 + 3O_2 \rightarrow N_2O_3 + 3H_2O \tag{10.4}$$

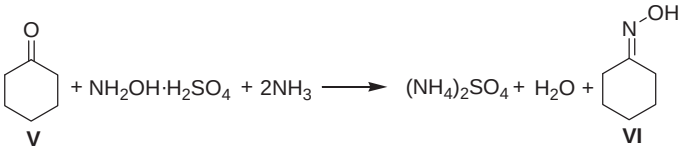
$$2NH_3 + CO_2 + H_2O \rightarrow (NH_4)_2CO_3 \tag{10.5}$$

$$(NH_4)_2CO_3 + N_2O_3 \rightarrow 2(NH_4)NO_2 + CO_2 \tag{10.6}$$

$$(NH_4)NO_2 + NH_3 + 2SO_2 + 3H_2O \rightarrow NH_2OH \cdot H_2SO_4 + (NH_4)_2SO_4 \tag{10.7}$$

In this approach, hydroxylamine sulfate is carried out through a complex series of reactions that include: (i) NO_x synthesis by ammonia combustion in air (Eq. 10.4), (ii) ammonium carbonate preparation by ammonia and carbon dioxide (Eq. 10.5), (iii) combination of nitric oxide and ammonium carbonate to ammonium nitrite and its reduction by SO_2 (Eqs. 10.6 and 10.7).

The overall hydroxylamine synthesis is penalized by its complexity, by the necessity of avoiding emissions of nitrogen oxides (NO_x) and sulfur oxides (SO_x) and by the coproduction of ammonium sulfate. Also, the following steps, i.e. the formation of cyclohexanone oxime by means of hydroxylamine sulfate (Eq. 10.8) and the successive production of ε-caprolactam by Beckmann rearrangement (Eq. 10.9), suffer from ammonium sulfate byproduction.



V **VI** (10.8)

$$\mathbf{VI} + H_2SO_4 + 2NH_3 \rightarrow \mathbf{III} + (NH_4)_2SO_4 \tag{10.9}$$

As a final result, a large coproduction of a salt, namely, ammonium sulfate, whose commercial value has become lower and lower in the past years, takes place (this lack of value is currently mitigated by its use as a fertilizer for agricultural feedstocks destined to biofuels manufacture). The overall coproduction of ammonium sulfate in hydroxylamine sulfate and cyclohexanone oxime synthesis amounts to about 2.8 kg/kg. In the following step, the Beckmann rearrangement of the oxime to caprolactam carried out in the presence of oleum, a further 1.6 kg/kg is produced, raising the total amount to approximately 4.4 kg/kg caprolactam. In addition, the process has to face the emission of nitrogen oxides (NO_x) and sulfur oxides (SO_x) related to the inorganic raw materials involved in hydroxylamine synthesis. Therefore, lowering or avoiding ammonium sulfate coproduction, as well as reducing the complexity of the process, has been a long sought target for many chemists.

Well-known alternative methods to cyclohexanone oxime synthesis from cyclohexanone are the BASF and DSM processes [16, 17]. In BASF-Inventa process, NO_x are reduced to hydroxylamine sulfate through catalytic hydrogenation on a Pt/Pd catalyst in the presence of H_2SO_4 (Eq. 10.10).

$$N_2O_3 + 4H_2 + 2H_2SO_4 \rightarrow 2NH_2OH \cdot H_2SO_4 + H_2O \tag{10.10}$$

The oxime production step follows as in Eq. 10.8. Ammonium sulfate coproduction is reduced to about 0.7 kg/kg cyclohexanone oxime. However, very pure raw materials and complex catalyst recovery procedures are required.

In the BASF acidic oximation process, NO is reduced to ammonium hydroxylammonium sulfate by catalytic hydrogenation on a Pt catalyst, in the presence of an ammonium hydrogen sulfate solution (Eq. 10.11).

$$NO + 3/2H_2 + (NH_4)HSO_4 \rightarrow NH_2OH \cdot (NH_4)HSO_4 \tag{10.11}$$

The resulting ammonium hydrogen sulfate coproduced during ammoximation (Eq. 10.12) can be recycled to hydroxylamine production.

$$\mathbf{V} + NH_2OH \cdot (NH_4)HSO_4 \rightarrow \mathbf{VI} + (NH_4)HSO_4 + H_2O \qquad (10.12)$$

Thus, salt production in the hydroxylamine/ammoximation production steps is nearly zeroed, to only 0.1 kg ammonium sulfate/kg cyclohexanone oxime.

The DSM hydroxylamine phosphate-oxime (HPO) process completely eliminates byproduction of ammonium sulfate during oxime production. Nitrate ions are reduced by hydrogen over palladium catalyst in a buffered aqueous phosphoric acid solution (Eq. 10.13).

$$NH_4NO_3 + 2H_3PO_4 + 3H_2 \rightarrow NH_2OH \cdot H_3PO_4 + (NH_4)H_2PO_4 + 2H_2O \qquad (10.13)$$

The obtained hydroxylamine-phosphate solution is directly reacted, in a two-phase medium, with cyclohexanone dissolved in toluene (Eq. 10.14) to yield an oxime–toluene phase and an aqueous solution to be recycled to the hydroxylamine step, where the nitrate ions consumed are replaced by the addition of nitric acid to restore the buffer solution (Eq. 10.15).

$$\mathbf{V} + NH_2OH \cdot H_3PO_4 + \rightarrow \mathbf{VI} + H_3PO_4 + H_2O \qquad (10.14)$$

$$(NH_4)H_2PO_4 + HNO_3 \rightarrow H_3PO_4 + NH_4NO_3 \qquad (10.15)$$

Formally, NO_3^- is a product of ammonia oxidation so the process can be written as oxidation of ammonia to hydroxylamine, with only a very low quantity of salt production if compared to the Raschig process: the excess ammonium formed as a byproduct in the reduction can be removed with nitrous gases (e.g., from ammonia combustion) (Eq. 10.16):

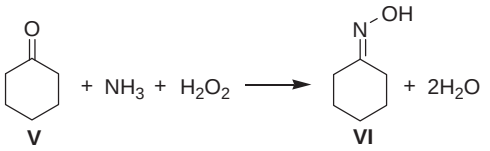
$$2NH_4H_2PO_4 + NO + NO_2 \rightarrow 2N_2 + 3H_2O + 2H_3PO_4 \qquad (10.16)$$

Other processes, with the aim to bypass the coproduction of ammonium sulfate, have made use of radically different routes and raw materials. In the SNIA Viscosa process, cyclohexanecarboxylic acid (from toluene *via* benzoic acid and hydrogen) is reacted with nitrosylsulfuric acid to caprolactam and CO_2. In Toray's PNC process, cyclohexane is photochemically converted into cyclohexanone oxime in the presence of nitrosyl chloride and hydrogen chloride ("photonitrosation"). More recently, a number of companies, among them BASF, DuPont, Rhodia, DSM and Shell, developed caprolactam manufacture from butadiene or adiponitrile. However, over 90% of the worldwide caprolactam production capacity is still based on the oxime route followed by Beckmann rearrangement (classical, oleum based). Therefore, not surprisingly, many efforts have also been devoted to the following step transforming cyclohexanone oxime into caprolactam without using oleum and fatally coproducing ammonium sulfate as well.

As a result of a long R&D activity independently carried out by the Eni group and Sumitomo dating back to the 1980s, the new Eni TS-1-based ammoximation process and the new Sumitomo zeolite-based vapor phase catalytic Beckmann rearrangement have been, respectively, industrially developed [18]. Such processes, when coupled together, are able to completely avoid ammonium sulfate coproduction in caprolactam industrial preparation.

10.2.2 TS-1 Catalyzed Ammoximation

The discovery of ammoximation reaction catalyzed by titanium-silicalite (TS-1) and the derived industrial process for cyclohexanonoxime production, represented a breakthrough in the above-depicted scenario of unresolved criticalities and sought answers (Eq. 10.17) [15, 19]. As already outlined, *ammoximation* means that the oxime production is carried out directly with ammonia (in the presence of an oxidant, namely hydrogen peroxide) avoiding the troublesome requirement of synthesizing and reacting hydroxylamine and the fatal inorganic salt coproduction:



(10.17)

A distinctive peculiarity of ammoximation vs. previous chemistry deserves to be emphasized: during ammoximation, ammonia is brought directly to the required oxidation state of hydroxylamine, whereas older processes were characterized by an overoxidation of ammonia to nitrogen oxides, followed by reduction with SO_2 (Raschig) or H_2 (BASF, DSM).

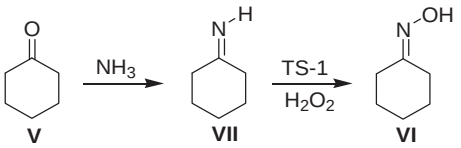
As said earlier, ammoximation was a fairly well-known reaction at the time TS-1-catalyzed ammoximation was devised. However, the Allied process was plagued by a modest yield, *ca.* 35–40%, as a result of 60–70% molar selectivity at 60% conversion based on cyclohexanone, and a fast decay of the catalyst [2]. On the other hand, the Toa Gosei process [4], although performing well in terms of oxime yield based on cyclohexanone (with molar selectivity and conversion both up to 96%), was characterized by a low yield on hydrogen peroxide (about 45% of hydrogen peroxide was lost), a low reaction temperature (18 °C) unattractive for an industrial development, and burdening catalyst recovery due to catalyst instability.

The use of TS-1 as catalyst for ammoximation was an outstanding innovation brought about by Eni researchers, dramatically enhancing reaction performances and paving the way to a successful industrial development of cyclohexanone ammoximation process *via* a greener route. TS-1 had been first synthesized in the Eni group R&D center in the late 1970s [20] and then applied to a series of other green oxidation processes based on the use of hydrogen peroxide as oxidant, as for the production of diphenols (catechol, hydroquinone) from phenol [21], phenol from benzene [22] and propylene oxide from propylene (see Chapter 2 for details)

[23]. In fact, in the last two decades new processes were installed on an industrial scale using TS-1 as the catalyst [24, 25].

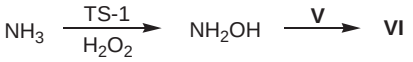
TS-1-catalyzed ammoximation was first devised and described in 1987 by Roffia and coworkers, while still in Montedipe before the merger with Enichem, followed by development of the industrial process in Eni group (*vide infra*) [7]. A study carried out on cyclohexanone at the laboratory scale clearly showed superior performances for a well-prepared TS-1, when compared to different catalytic materials, either containing or not containing titanium [19]. The afforded yield to oxime was very high, based both on cyclohexanone (>98%) and H_2O_2 (*ca.* 94%). *tert*-Butanol proved to be the best solvent for the reaction, at an optimum reaction temperature between 80 and 95 °C.

Two reaction routes have been proposed in the literature for ammoximation [26]. The first one involves the formation of imine as an intermediate, by reaction of cyclohexanone with ammonia (Eq. 10.18). Then the imine is oxidized to the oxime by hydrogen peroxide through a TS-1-catalyzed reaction [27]:



(10.18)

As alternative pathway, formation of hydroxylamine by TS-1-catalyzed reaction of hydrogen peroxide on ammonia, followed by the oximation of cyclohexanone is foreseen (Eq. 10.19):



(10.19)

This latter route is favored, since it has been proved that TS-1 does catalyze hydroxylamine formation from ammonia and hydrogen peroxide in the absence of cyclohexanone [28–31]. Moreover, it has been observed that sterically hindered ketones, like 4-*tert*-butylcyclohexanone and cyclododecanone, even if unable to diffuse into the catalyst channels, undergo ammoximation with fair yields, with implications also for the production of bulky oximes of commercial interest (*vide infra*). This is a specific feature that distinguishes ammoximation from other oxidation processes in which the organic products have to fit the pores of TS-1.

10.2.3 Eni Cyclohexanone Ammoximation Process

The discovery of TS-1-catalyzed ammoximation of cyclohexanone was the basis of the development of an industrial process at Eni. A demonstration unit of 12 000 t/a capacity was built in Porto Marghera, Venezia, Italy and started operation in 1994 [15, 24, 25]. The process is now licensed by Versalis (formerly Polimeri Europa), the petrochemical branch of Eni group.

According to the Eni process, the reaction takes place in liquid phase, in a continuous stirred tank reactor (CSTR) [32]. The TS-1-based catalyst is dispersed in the reaction medium as a slurry at a concentration of 2–3% by weight. The reactants,

i.e. cyclohexanone, ammonia and hydrogen peroxide (as concentrated aqueous hydrogen peroxide solution) are continuously fed to the reactor at molar ratios of about 1.0 : 2.0 : 1.1. The reaction is typically carried out in the range 80–90 °C under slight overpressure with a residence time of about 1.5 h. The reaction solvent is a mixture of *tert*-butanol and water. In these conditions cyclohexanone is nearly completely (99.9%) converted to the oxime with a selectivity, on a molar basis, >98%. The molar yield to oxime, based on hydrogen peroxide, is about 94%. Due to the high selectivity, only minor amounts of reaction byproducts (a critical factor for the quality of caprolactam) are observed [33, 34]. Inorganic byproducts such as N_2, N_2O, O_2, ammonium nitrite and nitrate originate from ammonia oxidation and hydrogen peroxide decomposition. Organic byproducts deriving from cyclohexanone are cyclohexanone azine, cyclohexenylcyclohexanone (produced from cyclohexanone by aldolic condensation), nitrocyclohexane and cyclohexenone oxime, as a result of consecutive reactions on the oxime. All these byproducts are considered to be formed through homogeneous noncatalytic competitive reactions, so that titanium active sites in TS-1 are not involved in their formation.

A schematic flow chart of the process, based on a recent patent disclosure [35], is depicted in Figure 10.7.

The reaction products are separated from the catalyst slurry by means of filters and taken out of the reactor. A rectification column removes from the top the non converted excess ammonia and the solvent (an azeotropic mixture of water and *tert*-butanol), to be recycled to the reactor. As a bottom stream, an aqueous solution of raw cyclohexanone oxime is released, which is sent to a purification section. The purification section may consist of an extraction step wherein cyclohexanone oxime is extracted with an organic solvent, e.g., toluene, from the water solution, a washing step wherein the extract containing cyclohexanone oxime is washed with water or an alkaline solution (in the latter case a further washing step with only water is

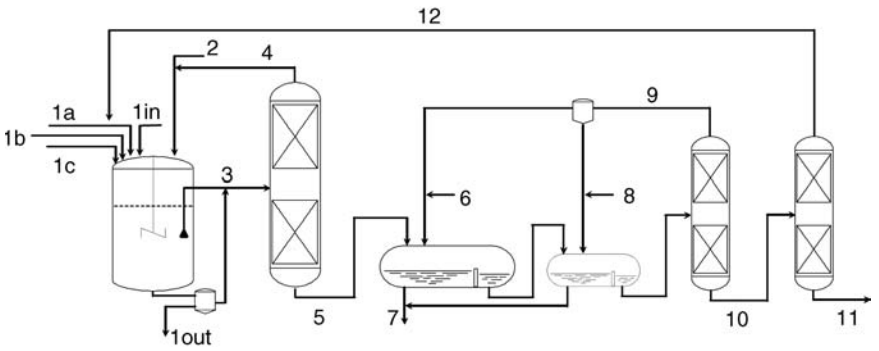


FIGURE 10.7 Schematic flow chart of TS-1-catalyzed cyclohexanone ammoximation process: (1 in) TS-1 based catalyst fed to reaction vessel; (1 out) exhausted catalyst purge; (1a) cyclohexanone; (1 b) NH_3; (1 c) H_2O_2; (2) *tert*-butanol; (3) reaction solution; (4) *tert*-butanol/ H_2O/NH_3 recycle; (5) aqueous oxime to extraction; (6) toluene; (7) water to treatment; (8) H_2O; (9) toluene/H_2O recycle; (10) crude oxime; (11) product; (12) cyclohexanone recycle. Adapted from Trivellone et al. [35].

required), and a distillation step wherein the organic solvent (and some accompanying water) is distilled off. The crude cyclohexanone oxime obtained as a bottom product undergoes a further distillation step under reduced pressure wherein residual cyclohexanone is distilled off to obtain pure cyclohexanone oxime. Residual cyclohexanone from the top is recycled to the reaction. The purified oxime showing "superior" [35] thermal stability is suitable for the next step of vapor phase rearrangement to caprolactam.

The TS-1-based catalyst can be used, for the sake of reliable operation in the slurry stirred reactor and easy separation from the reaction mixture by filtration, in the form of TS-1 zeolite crystals bound by silica into microspheres, with high mechanical resistance, having an average diameter of *ca.* 20–30 μm [36] (Figures 10.8 a–c).

During the industrial run the TS-1 catalyst must be periodically purged and made up. It has been observed that a slow dissolution of the silica framework takes place in the alkaline reaction medium due to the presence of excess ammonia [38]. The

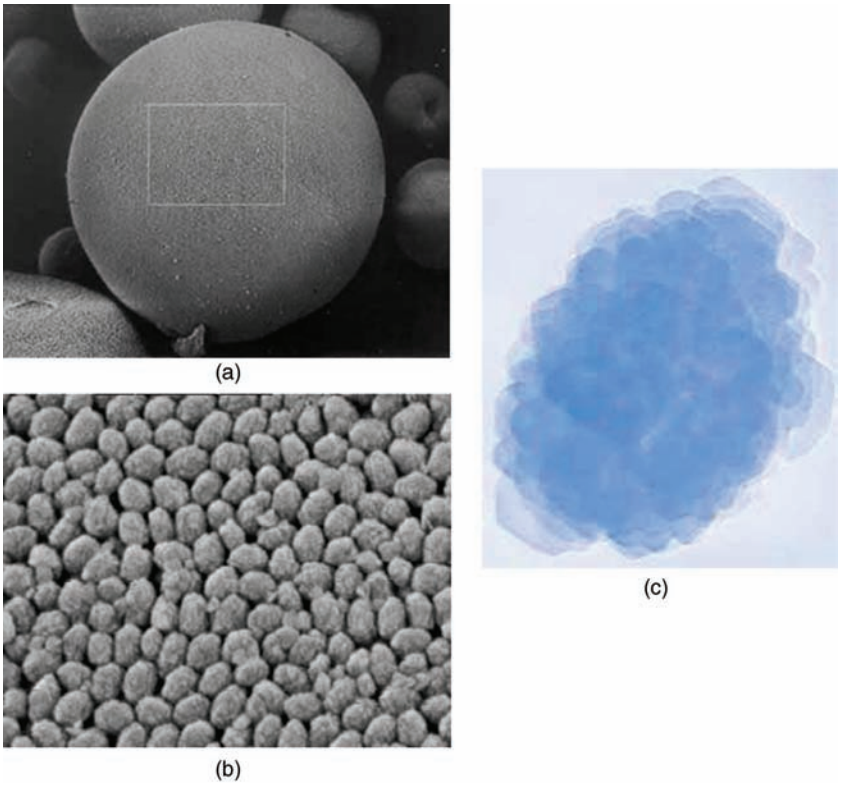


FIGURE 10.8 (a) Microsphere of TS-1 based catalyst. (b) TS-1 zeolite crystals bound on the microsphere surface. (c) Typical "blackberry" morphology of a TS-1 zeolite crystal. From Polimeri Europa Licensing Technology Brochure [37].

weight loss of the catalyst is accompanied by titanium migration from the zeolite framework onto the external surface and by a change of the coordination number, namely, from 4 to 6, suggesting the formation of anatase-like species. Therefore, a continuous decrease in the amount of the true titanium-silicalite in the reaction system takes place, bringing about a lower conversion of cyclohexanone and/or a lower selectivity to cyclohexanone oxime. Moreover, during operation the catalyst can also irreversibly adsorb some byproducts of the reaction that block the active sites. As an overall consequence, a slow loss of catalytic activity is experienced, to be controlled and counteracted in continuous industrial operation by purging and make up. This operation has been disclosed in some detail in the patent literature [39]. An expected catalyst consumption of 0.3 kg catalyst/t oxime can be estimated.

10.2.4 Salt-Free Caprolactam Production

As outlined before, the industrial development by Eni of the cyclohexanone ammoximation process catalyzed by TS-1 allowed complete elimination of ammonium sulfate coproduction as well as SO_x and NO_x emissions in the hydroxylamine-cyclohexanone oxime production step, while substituting at the same time quite complex operation units with an outstandingly simple technology. By coupling the Eni TS-1-catalyzed cyclohexanone ammoximation process to vapor phase Beckmann catalytic rearrangement of the oxime to caprolactam, which allows in turn avoiding ammonium sulfate coproduction in the rearrangement step, a new industrial route toward a salt-free production of caprolactam resulted.

The vapor phase catalytic Beckmann rearrangement of the oxime to caprolactam has been industrially developed by Sumitomo in Japan [25, 40]. According to the process, a methanol solution of the oxime is reacted in vapor phase at 300–400 °C and atmospheric pressure in a fluidized-bed reactor, on silicalite-1, an all-silica MFI zeolite containing tiny amounts of aluminum and other heteroelements. The choice of fluidized bed allows frequent catalyst regeneration by combustion, because the catalyst is quite rapidly deactivated, in a reversible way, due to organic tar deposition. Due to a combination of the selected catalyst and solvent, which actually acts as a reaction promoter, over 95% molar selectivity to caprolactam at nearly complete oxime conversion is obtained.

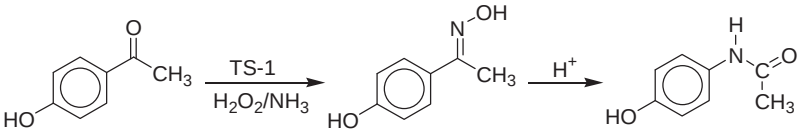
Sumitomo set up industrially a combined caprolactam process based on licensed Eni TS-1 ammoximation technology and its own catalytic rearrangement technology with a caprolactam capacity of 65 kt/a at its Niihama factory, Ehime, Japan, in 2003 [41–43]. This new process is extremely ecofriendly and, also, requires far fewer raw materials if compared with conventional route.

10.2.5 Other TS-1-Catalyzed Ammoximation Reactions and Related Processes of Industrial Relevance

Following the development of the Eni cyclohexanone ammoximation process, a similar technology was independently developed by SINOPEC Research Institute of Petroleum Processing in China and applied in the last decade to a 70 kt/a

"commercial test unit" [44]. Although very few details have been disclosed, the addition of a silicon additive to suppress the solubilization-induced loss of silicon in catalyst seems to take place in the SINOPEC process [25, 44].

As outlined before, it is mostly accepted that the ammoximation route involves *in situ* formation of hydroxylamine *via* TS-1-catalyzed oxidation of ammonia with hydrogen peroxide. It appears that in the absence of ketone, the production of hydroxylamines by direct ammonia or amine oxidation can be envisaged [31, 45]. The subsequent hydroxylamine–ketone reaction may take place outside the catalyst pores in the bulk reaction medium. So, different substrates with different sizes are expected to undergo fair reaction, to products with possible relevance to the chemical market. An example is the ammoximation of *p*-hydroxyacetophenone (Eq. 10.20) [46, 47]. The corresponding oxime is a precursor of the analgesic Paracetamol (4-acetaminophenol). TS-1 affords the oxime in 100% selectivity at 50% conversion:



(10.20)

A further example is the production of laurolactam, which is the Nylon-12 monomer also used as comonomer in Nylon-6. Laurolactam can be manufactured by oxime synthesis from cyclododecanone, ammonia and hydrogen peroxide using TS-1 as catalyst [48, 49], followed by oxime rearrangement, in a quite similar way to caprolactam.

10.2.6 Conclusion

Eliminating or reducing as much as possible the quantity and hazard of emissions and waste products from production processes is a fundamental strategy of Green Chemistry. Caprolactam, an important base chemical as a key intermediate in the production of Nylon-6, is mainly produced in the C6 route through cyclohexanone oxime and Beckmann rearrangement, involving formation of NO_x (and SO_x) and coproduction of substantial amounts of ammonium sulfate whose commercial exploitation or disposal is becoming increasingly difficult. In the Eni/Polimeri Europa TS-1-catalyzed cyclohexanone ammoximation process, direct ammonia oxidation to hydroxylamine with hydrogen peroxide on titanium-silicalite takes place, so that cyclohexanone oxime is obtained without involvement of NO_x and without formation of any ammonium sulfate coproduct. Furthermore, coupling the Eni ammoximation process to Sumitomo's vapor phase Beckmann catalytic rearrangement of the oxime to caprolactam, which allows in turn ammonium sulfate coproduction in the rearrangement step to be avoided a new industrial route to caprolactam completely free of salt coproduction has been established.

REFERENCES

1. Armor J.N. (1980). *J. Am. Chem. Soc. 102*, 1453–1454.
2. Armor J.N., Carlson E.J., inventors; Allied Chemical Corporation, assignee. US Patent 4,281,194. 1981.
3. Lebedev O.L., Kazarnovskii, S.N. (1960). *Zhur. Obshch. Khim. 30*, 1631–1635. Chem. Abstr. 1961, *55*, 1473a.
4. Yasui E., Kawaguchi T., Matsubara T., inventors; Toa Gosei Chemical Industry, assignee. US Patent 3,574,750. 1971.
5. Grasselli R.K. (2005). *Catal. Today 99*, 23–31.
6. Mueller U., Hoelderich W., inventors; BASF AG, assignee. US Patent 5,401,486. 1995.
7. Roffia P., Padovan M., Moretti E., De Alberti G., inventors; Montedipe, assignee. Eur. Patent 208311. 1987.
8. Padovan M., Genoni F., Leofanti G., Petrini G., Roffia P., Cesana A., inventors; Montedipe, assignee. Eur. Patent 347926. 1989.
9. Caprolactam. *SRI WP Report, Abstract*. January 2011. Available at (last accessed, 2011 Jun 27): http://www.sriconsulting.com/WP/Public/Reports/caprolactam/
10. Caprolactam Chemical Profile. *ICIS Chemical Business* Nov. 22–Dec. 5, 2010, p. 43.
11. Caprolactam Uses and Market Data. *ICB Chemical Profile*, May 12 2008. Available at (last accessed, 2011 Mar 29): http://www.icis.com/v2/chemicals/9075185/caprolactam/uses.html
12. Bellussi G., Perego C. (2000). *CATTECH 4*, 4–16.
13. Chauvel A., Lefebvre G. *Petrochemical Processes*, Vol. *2*. Editions Technip, Paris, 1989, pp. 258–274.
14. Maxwell G.R. *Synthetic Nitrogen Products: a Practical Guide to the Products and Processes*. Kluwer Academic Publishers, New York, 2004, pp. 373–390.
15. Petrini G., Leofanti G.A., Mantegazza M.A., Pignataro F. In: *Green Chemistry. Designing Chemistry for the Environment*. Anastas P.T., Williamson T.C., eds. ACS Symp. Series 626. American Chemical Society, Washington, DC, 1996, pp. 33–48.
16. Ritz J., Fuchs H., Kieczka H., Moran W.C. In: *Ullmann's Encyclopaedia of Industrial Chemistry*, Vol. *6*, 6th edn, Wiley-VCH, Weinheim, 2002, pp. 185–205.
17. Dahlhoff G., Niederer J.P.M., Hoelderich W.F. (2001). *Catal. Rev.-Sci. Eng. 43*, 381–441.
18. Ichihashi H., Sato H. (2001). *Appl. Catal. A: General 221*, 359–366.
19. Roffia P., Leofanti G., Cesana A., Mantegazza M.A., Padovan M., Petrini G., Tonti S., Gervasutti P. (1990). *Stud. Surf. Sci. Catal. 55*, 43–52.
20. Taramasso M., Perego G., Notari B., inventors; SnamProgetti, assignee. US Patent 4,410,501. 1983.
21. Romano U., Esposito A., Maspero F., Neri C., Clerici M.G. (1990). *Chim. Ind. (Milan) 72*, 610–616.
22. Bianchi D., Balducci L., Bortolo R., D'Aloisio R., Ricci M., Spanò G., Tassinari R., Tonini C., Ungarelli R. (2007). *Adv. Synth. Catal. 349*, 979–986.
23. Clerici M.G., Bellussi G., Romano U. (1991). *J. Catal. 129*, 159–167.
24. Clerici M.G. In: *Metal Oxide Catalysis*. Jackson S.D., Hargreaves S.J., eds. Wiley-VCH, Weinheim, 2009, pp. 705–754.

25. Schmidt W. In: *Ordered Porous Solids*. Valtchev V., Mintova S., Tsapatis M., eds. Elsevier, Amsterdam, 2009, pp. 52–73.
26. Mantegazza M.A., Paparatto G., Petrini G., Fornasari G., Trifirò F. In: *Catalysis of Organic Reactions*. Scaros M.G., Prunier M.L., eds. Dekker, New York, 1995, pp. 353–362.
27. Thangaraj A., Sivasanker S., Ratnasamy P. (1991). *J. Catal. 131*, 394–400.
28. Zecchina A., Spoto G., Bordiga S., Geobaldo F., Petrini G., Leofanti G., Padovan M., Mantegazza M.A., Roffia P (1993). *Stud. Surf. Sci. Catal. 75*, 719–728.
29. Dal Pozzo L., Fornasari G., Monti T. (2002). *Catal. Commun. 3*, 369–375.
30. Mantegazza M.A., Leofanti G., Petrini G., Padovan M., Zecchina A., Bordiga S. (1994). *Stud. Surf. Sci. Catal. 82*, 541–550.
31. Mantegazza M.A., Padovan M., Petrini G., Roffia P., inventors; Enichem Anic, assignee. Eur. Patent 522634. 1993.
32. Clerici M.G., Ricci M., Rivetti F. In: *Encyclopaedia of Hydrocarbons*, Vol. *2*. Beccari M., Romano U., eds. Eni & Istituto dell'Enciclopedia Italiana G. Treccani, Roma, 2006, pp. 661–686. Available at (last accessed, 2011 Apr 08): http://www.treccani.it/export/sites/default/Portale/sito/altre_aree/Tecnologia_e_Scienze_applicate/enciclopedia/inglese/inglese_vol_2/615-686_ING3.pdf.
33. Mantegazza M.A., Cesana A., Pastori M. (1996). *Top. Catal. 3*, 327–335.
34. Cesana A., Mantegazza M.A., Pastori M. (1997). *J. Mol. Catal. A: Chemical 117*, 367–373.
35. Trivellone F., Furlan P., Fukao M., inventors; Sumitomo Chemical, assignee. Eur. Patent 1674448. 2006.
36. Carati A., Bellussi G., Mantegazza M.A., Petrini G., inventors; Polimeri Europa, assignee. Eur. Patent 906784. 1999.
37. Titanium silicalite (TS-1) zeolite based proprietary catalyst. *Polimeri Europa Licensing Technology Brochure*. Available at (last accessed, 2011 Apr 08): http://www.eni.com/it_IT/attachments/azienda/attivita-strategie/petrolchimica/licensing/TS1-flyer-lug09.pdf.
38. Petrini G., Cesana A., De Alberti G., Genoni F., Leofanti G., Padovan M., Paparatto G., Roffia P. (1991). *Stud. Surf. Sci. Catal. 68*, 761–766.
39. Trivellone F., Furlan P., Oikawa M., inventors; Sumitomo Chemical, assignee. Eur. Patent 1674450. 2006.
40. Izumi Y., Ichihashi H., Shimazu Y., Kitamura M., Sato H. (2007). *Bull. Chem. Soc. Jpn. 80*, 1280–1287.
41. Ichihashi H., Ishida M., Shiga A., Kitamura M., Suzuki T., Suenobu K., Sugita K. (2003). *Catal. Surv. Asia 7*, 261–270.
42. Sumitomo Annual Report 2004. Available at (last accessed, 2011 Apr. 8): http://www.sumitomo-chem.co.jp/english/ir/library/annual_report/docs/ar2004_e.pdf
43. Sumitomo CSR Report 2004. Available at (last accessed, 2011 Jun. 21): http://www.sumitomo-chem.co.jp/english/csr/report/docs/2004csre.pdf.
44. Bin S., Wei W., Enze M., Ye X. (2007). *China Pet. Process Pe. 7*, 25–30.
45. Roffia P., Tonti S., Cesana A., Mantegazza M.A., Padovan M., inventors; Montedipe, assignee. Eur. Patent 314147. 1989.
46. Davenport K.G., Sheldon R.A., Le Bars J., Mueller W.H., inventors; Hoechst Celanese Corporation, assignee. US Patent 5,466,869. 1995.

47. Le Bars J., Dakka J., Sheldon R.A. (1996). *Appl. Catal. A: General 136*, 69–80.
48. Mantegazza M.A., Petrini G., inventors; Enichem, assignee. US Patent 5,498,793. 1996.
49. Herwig J., Roos M., Oenbrink G., Guenzel B., Kuppert D., inventors; Degussa, assignee. US Patent 7,608,738. 2008.

10.3 PRODUCTION OF PROPYLENE OXIDE

ANNA FORLIN,* MASSIMO BERGAMO, AND JOERG LINDNER

Propylene oxide (PO) is a colorless, volatile and liquid organic compound with the molecular formula CH_3CHCH_2O. It is produced on a large scale industrially and is mainly used for the production of polyether polyols that are intermediates for polyurethane plastics and in many other applications. In Table 10.2 is shown a short history of the propylene oxide process technology development.

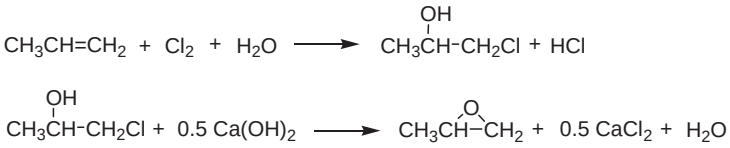
For a long period of time, the chlorohydrin process (CHPO) was the only technically practiced route to industrially used epoxides, primarily ethylene oxide and propylene oxide [1]. In Scheme 10.1 is shown the conventional chlorohydrin process using lime.

The situation changed dramatically with the discovery of the catalytic direct oxidation route to ethylene oxide (DOEO) by Le Fort in 1931, using a silver-based catalyst on a support, which is additionally activated with traces of other metals [2]. Since 1937, traditional chlorohydrins-based ethylene oxide plants were taken out of service and replaced by new advantaged direct oxidation plants. Over several years, attempts have been undertaken to adapt this new, very successful catalytic ethylene oxide process to the production of propylene oxide. Up to now, these efforts have not resulted in an ethylene oxide analog commercially feasible, viz. in a propylene oxide process by the direct gas phase oxidation of propylene. Difficult to control

TABLE 10.2 Propylene Oxide Process, Technology Development

Start-up of Industrial Production	Technology	Process characteristics
1910	PO *via* Chlorohydrin route (CHPO)	Noncatalytic reaction in the liquid phase
1969	PO/Coproduct	Catalytic oxidation to propylene oxide with an organic hydroperoxide in the liquid phase
2003	PO/Cumene	Catalytic oxidation to propylene oxide with cumene hydroperoxide in the liquid phase (coproduct free)
2008	HPPO	Catalytic oxidation to propylene oxide with hydrogen peroxide in the liquid phase (coproduct free)

*Corresponding author



SCHEME 10.1 Propylene oxide production *via* conventional chlorohydrin route.

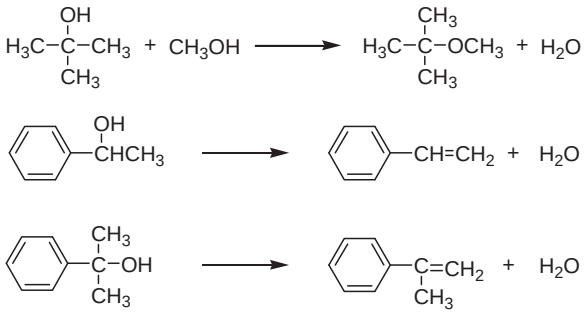
reaction conditions, side reactions, and coking of the catalyst shifted the interest to carrying out this chemistry in the liquid phase.

The initial work on liquid phase direct oxidation was done without a catalyst and based on free-radical chemistry. While this chemistry can achieve propylene oxide selectivity above 50%, many coproducts are formed at the same time. Attempts to improve the selectivity by applying catalysts did not change the product distribution to the degree that a technical application was implemented [3]. To resolve the problem of the plurality of byproducts, researchers selected a different approach. Instead of letting peroxidic radicals direct the epoxidation reaction in an uncontrolled autoxidation process, they discovered around 1963 that more stable organic hydroperoxides, like *t*-butyl hydroperoxide, ethylbenzene hydroperoxide, or cumene hydroperoxide can be produced with good selectivity and epoxidize propylene to propylene oxide selectively, in the presence of a suitable catalyst (Eq. 10.21) [4]. In addition to propylene oxide only one coproduct is formed in significant amounts.



(10.21)

Choosing the right peroxide leads to a coproduct that is of industrial use, as is PO. Such coproducts are *t*-butanol, which is further processed to methyl *t*-butyl ether (MTBE), ethylbenzene alcohol, which is further converted to styrene and cumene alcohol, which is further converted to α-methyl styrene (Scheme 10.2). However, the latter process (PO/α-methyl styrene) was never established as the market for α-methyl styrene is not large enough. While these coproduct processes in the development history of catalytic propylene oxide process technology were a significant progress, as only one coproduct was coupled to propylene oxide, there



SCHEME 10.2 Coproducts in propylene oxide production *via* organic hydroperoxides.

was still the limiting factor that the market for the coproduct had to be available and that the market size had to fit the stoichiometry. This limit was overcome when Sumitomo developed and later built a propylene oxide cumene plant. The key difference between this process and the propylene oxide/styrene and propylene oxide/MTBE is that the cumene alcohol, formed in the course of the epoxidation step, can be conveniently hydrogenated back to cumene. In this way there is no need for a coproduct outlet.

In 1983, a discovery was disclosed by Snamprogetti that would later lead to a dramatic innovation of PO technology. This was the catalytic effect of the zeolitic, heterogeneous TS-1 catalyst [5–9]. For the first time it was now possible to make propylene oxide conveniently from hydrogen peroxide and propylene. The "coproduct" of this process is water. In the timeframe 1987–2002 Enichem/Dow developed this technology from lab to pilot scale (2000 tons/year) and in the 1990s BASF, Evonik, Uhde and Solvay worked to develop their own process technology. In 2003, Dow and BASF together scaled up to industrial scale the HPPO process that is the newest technology, practiced meanwhile commercially and at large scale.

Potential future technology solutions may be based on interesting concepts under evaluation in industry and academia:

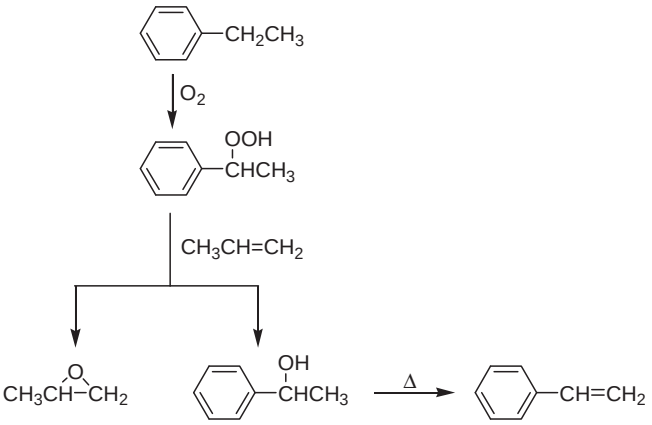
- Direct oxidation of propylene with oxygen (DOPO).
- Hydro-oxidation of propylene with oxygen and hydrogen in a single reaction step (HOPO). This concept was reported by Haruta and coworkers in 1996 [10]. According to the patent literature, Lyondell and more recently Sumitomo are very active in the development of such a process [11, 12].
- HPPO technology combined with direct catalytic oxidation of hydrogen and oxygen to H_2O_2 (HP/HPPO) [13]. The main potential advantages of HOPO and HPPO technology combined with direct catalytic synthesis of H_2O_2 against the conventional HPPO process would be that a separate hydrogen peroxide plant using the conventional technology would not be needed.

In the next sections the attention will be focused on those technologies that use heterogeneous catalysis:

- PO production *via* ethylbenzene hydroperoxide;
- PO production *via* cumene hydroperoxide;
- PO production *via* hydrogen peroxide.

10.3.1 Propylene Oxide Production *via* Ethylbenzene Hydroperoxide Route

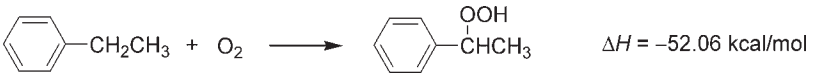
Commercially, styrene and propylene oxide are coproducts in a process known as POSM, operated by Lyondell Chemical Company and Shell. The overall chemistry for this process is shown in Scheme 10.3. In the first process step, ethylbenzene is treated with air and oxidized to form ethylbenzene hydroperoxide. In the second process step, the ethylbenzene hydroperoxide is used to oxidize propylene to



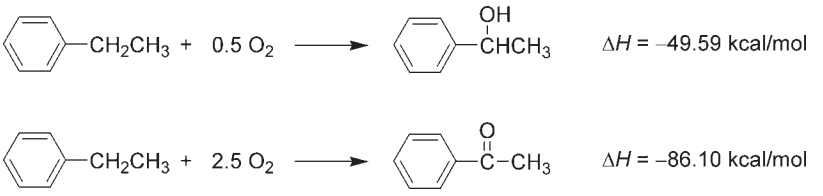
SCHEME 10.3 PO production *via* EB hydroperoxide route.

propylene oxide and α-phenylethanol. The epoxidation reaction occurs in the presence of a catalyst. The Lyondell technology uses a homogeneous molybdenum catalyst (Halcon), while in the Shell technology a heterogeneous titanium-based catalyst is used. The propylene oxide produced according to the second process step is recovered and purified by distillation. The separated coproduct (α-phenylethanol) is thermally dehydrated to styrene monomer.

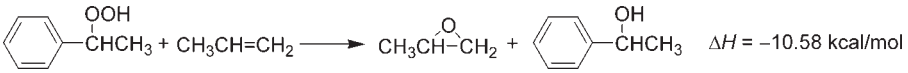
10.3.1.1 Chemistry In the first process step, ethylbenzene (EB) is oxidized to ethylbenzene hydroperoxide (EBHP) according to the exothermic reaction illustrated by Scheme 10.4. The main byproducts are methylbenzylalcohol (MBA) and acetophenone (ACP) (Scheme 10.5) [14].



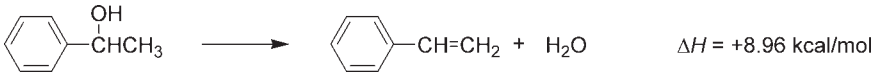
SCHEME 10.4 Ethylbenzene oxidation to EB hydroperoxide.



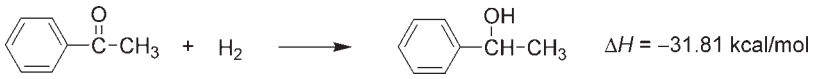
SCHEME 10.5 Secondary reactions in EB oxidation.



SCHEME 10.6 Propylene epoxidation *via* EBHP.



SCHEME 10.7 Styrene monomer formation *via* MBA thermal dehydration.



SCHEME 10.8 ACP hydrogenation to MBA.

The ethylbenzene oxidation involves a free-radical mechanism and many other byproducts like aldehydes, ketones, acids and alcohols are formed. It usually occurs at temperatures in the range 100–165 °C and 0.07–70 bar without using any catalyst [14]. According to the literature this reaction can be performed at lower temperatures in the presence of a catalyst but this route was never implemented at a commercial scale [15]. In the second process step, the ethylbenzene hydroperoxide intermediate reacts with propylene to propylene oxide and methylbenzylalcohol according to the exothermic reaction shown in Scheme 10.6. Also in this second step, acetophenone, aldehydes and ketones are formed as byproducts. Additional byproducts and impurities are phenols and hydrocarbons.

The epoxidation reaction is performed in the presence of a catalyst and a solvent (usually ethylbenzene) [16]. After propylene oxide separation and purification by distillation, the coproduct methylbenzylalcohol is thermally dehydrated to styrene monomer according to the endothermic reaction shown in Scheme 10.7. The dehydration is performed in the vapor phase at high temperatures (70–300 °C), under vacuum (0.13–0.53 bar) and in the presence of a suitable acid catalyst [17]. The chemical selectivities in this second step (EBHP-to-PO, EBHP-to-MBA and propylene-to-PO) are between 95 and 98% [18].

Acetophenone can be hydrogenated to MBA in the presence of a catalyst (Scheme 10.8). The reaction can be performed in the presence of a typical hydrogenation catalyst like palladium supported on carbon or alumina, at hydrogenation conditions of 20 to 50 °C and at least 0.34 bar hydrogen pressure [19].

10.3.1.2 Process Technology A general process flow diagram is shown in Figure 10.9 and both Shell and Lyondell technologies consist of five main sections:

1. Ethylbenzene oxidation;
2. Propylene epoxidation;

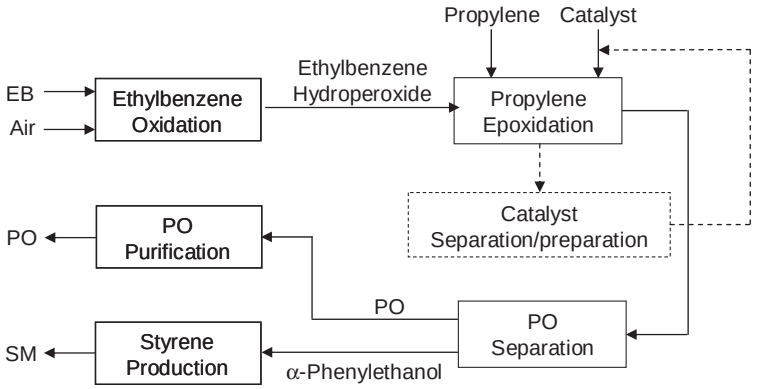


FIGURE 10.9 PO *via* EB hydroperoxide process: block diagram.

3. Propylene oxide separation;
4. Propylene oxide purification;
5. Styrene production.

In Lyondell technology where a homogeneous molybdenum catalyst is employed, an additional section for catalyst recovery and preparation is required. In Appendixes 10.3A and 10.3B are shown the Shell process flow diagrams related to EB oxidation/Propylene epoxidation/Product separation and PO Purification/Styrene production, respectively, as proposed by SRI Consulting (now part of IHS Inc.) [20].

Our attention will be now focused on this technology where a heterogeneous titanium-based catalyst is used. A more detailed description can be found in the report issued by SRI Consulting (now part of IHS Inc.) [20].

The epoxidation of propylene is an exothermic reaction conducted in a fixed-bed catalytic reactor under substantially isothermal conditions [16]. The reaction between propylene and ethylbenzene hydroperoxide occurs in the reactor filled with a titanium catalyst and using an excess of ethylbenzene. Typical operating temperatures are in the range 60–150 °C and the pressures are in the range 13–50 bar. The epoxidation catalyst used in the POSM process consists of dispersed titanium-on-silica and is made in four steps *via* a gas phase process. In the first step a silicon compound is impregnated with a stream of gaseous titanium tetrachloride diluted with nitrogen and in the second step the resulting product is calcined. The third step is the hydrolysis of the product of step two and the final step is silylation of the product of step 3 [18, 21].

The reaction mixture generated in the propylene epoxidation section is treated in a distillation train to separate the different components [22]. In the first step, the unreacted propylene is recovered from the epoxidation product as an overhead stream and recycled back to the epoxidation reaction. The bottom product

("crude PO") requires additional distillation operations to recover the propylene oxide from EB and byproducts. The EB recovered is recycled back to the ethylbenzene oxidation section.

The PO purification section has the main purpose to produce a final product with high purity. This step is critical to enhance the quality of PO derivatives like polyether polyols. One of the most critical impurities that can have a negative impact on PO derivatives is methyl formate and its separation from PO is complicated by its boiling point that is very close to propylene oxide. One potential option is to perform the separation with a basic ion-exchange resin, which converts methyl formate to methanol and formate ion. The latter is retained in the resin while methanol can be easily separated from propylene oxide [23].

10.3.1.3 POSM Technology Summary POSM technology is universally considered a reliable technology for the production of PO and is widely known as a process that has relatively low operating costs. For this process, the propylene oxide economics are strongly impacted by both styrene market demand and price. Geography is a key aspect for the POSM technology selection and recently most of the new plants based on POSM technology are being built in Asia where styrene still has a growing demand.

10.3.1.4 Existing Plants Existing plants that use Shell's POSM technology based on heterogeneous catalysis are listed in Table 10.3 (2009 data).

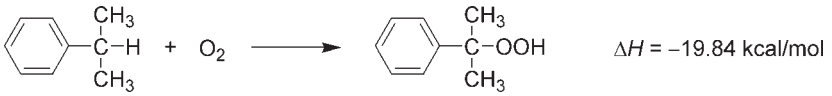
10.3.2 Propylene Oxide Production *via* Cumene Hydroperoxide Route

Cumene hydroperoxide is an important intermediate in the chemical process industry. For a long time, cumene hydroperoxide has been used as the starting material for the synthesis of acetone and phenol *via* the cumene process (Hock rearrangement) [24]. In analogy to ethylbenzene hydroperoxide, cumene hydroperoxide can also be employed as an epoxidation reagent for making propylene oxide in the presence of a suitable catalyst [25]. While this chemistry has been known for at least 45 years, the first industrial application was realized only recently.

TABLE 10.3 Plants Using Shell's POSM Technology

Location	Company	Capacity (kt/a)
Moerdijk - Netherlands	Ellba CV[a]	250
Moerdijk - Netherlands	Shell	220
Huizhou, Guandong - China	CSPC[b]	250
Ulsan - South Korea	SKC Chemical	180
Jurong Island - Singapore	Ellba Eastern[c]	250
Jurong Island - Singapore	Shell	175

[a]JV between Shell Chemicals Netherland (50%) and BASF (50%).
[b]JV between China National Offshore Oil Corporation (CNOOC) and Shell Company.
[c]JV between Shell Eastern Petroleum (50%) and BASF South East Asia (50%).

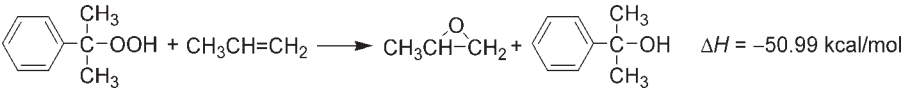


SCHEME 10.9 Cumene oxidation to cumene hydroperoxide.

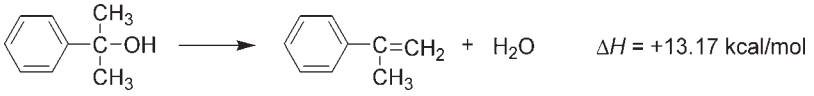
While the PO/Styrene process yields propylene oxide and styrene after dehydration of the coproduct methylbenzylalcohol, the cumene PO chemistry yields propylene oxide and cumene alcohol. Cumene alcohol can then be dehydrated to α-methylstyrene. As the market for α-methyl styrene is much smaller than for styrene, it is not easily possible to balance product and coproduct volume in an economically feasible way. With a nearly saturated styrene market and a continuously growing demand for propylene oxide, it is attractive to have a coproduct-free route to PO. Such a coproduct-free concept was demonstrated with the cumene hydroperoxide route: cumene alcohol is dehydrated and successively hydrogenated. The resulting cumene is recycled to the front end of the process. The propylene selectivity of this process is reported as high as 99% at a cumene hydroperoxide conversion of 95%. The cumene selectivity to cumene hydroperoxide should be in the range of 95–98% [26].

10.3.2.1 Chemistry Cumene is oxidized by air in a free-radical reaction to cumene hydroperoxide (Scheme 10.9). Typical byproducts are alcohols and ketones, such as acetophenone.

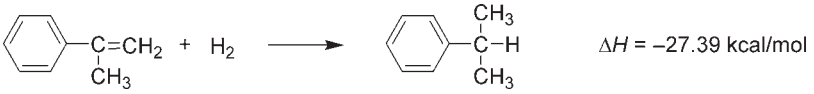
Cumene hydroperoxide is reacted with propylene to form propylene oxide and cumene alcohol in the presence of a heterogeneous catalyst, consisting of titanium-silica (Scheme 10.10). Cumene alcohol is dehydrated to α-methyl styrene (Scheme 10.11). α-Methyl styrene can be hydrogenated back to the starting material cumene (Scheme 10.12).



SCHEME 10.10 Propylene epoxidation *via* cumene hydroperoxide.



SCHEME 10.11 Cumene alcohol dehydration to α-methyl styrene.



SCHEME 10.12 α-Methyl styrene hydrogenation to cumene.

10.3.2.2 Process Technology Since 2003 Sumitomo has operated a cumene hydroperoxide PO process in Japan. The process is completely integrated, which means that the main feed materials to the process are propylene, oxygen and hydrogen. Cumene is re-established from the coproduct cumene alcohol and recycled in a loop to the front-end of the process. Only smaller cumene losses to byproducts have to be replaced. In Appendix 10.3C is shown a block-flow diagram of the process concept as proposed by Nexant [27]. In the following, a short description of the key process steps is provided. An excellent in depth survey of the Sumitomo cumene PO process can be found in the Nexant report [27].

The formation of the cumene hydroperoxide is a liquid phase autoxidation process of cumene with air. The reaction temperature is between 50 and 200 °C. The pressure can be between 0 and 50 bar. Due to the relatively high stability of the peroxide, good conversion rates and selectivities can be achieved. The produced peroxide solution is contacted with an aqueous solution of an alkali-metal compound (NaOH, KOH) to remove acids. After separation of oil and water phases, the target concentration for the successive epoxidation step is finally reached by a peroxide concentration step [28].

The epoxidation reaction of the Sumitomo process is carried out in a fixed-bed reactor and, according to a Sumitomo patent [29], at a temperature of 80 °C and 42 bar. A 25 wt% solution of cumene hydroperoxide in cumene is reacted with propylene, at a weight ratio of 1 : 1 (solution to propylene) over a proprietary catalyst (titanium silicate with a specific mesoporous texture) [30].

The reaction mixture leaving the epoxidation reactor is distilled to separate lights and heavies. Unconverted propylene is recycled to the epoxidation reactor. The remaining lights fraction consists mainly of crude propylene oxide and requires further purification. High-purity propylene oxide is obtained by extraction of alcohols and aldehydes with water [31] and extractive distillation with *n*-heptane to remove methyl formate [32].

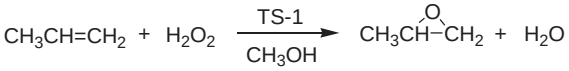
The coproduct of the epoxidation reaction, cumene alcohol, can be dehydrated to α-methylstyrene with activated alumina as dehydration catalyst. α-Methylstyrene can be hydrogenated to cumene over a palladium- or copper-containing hydrogenation catalyst. According to a Sumitomo patent disclosure [33], it is feasible to pack the dehydration and hydrogenation catalysts one after the other in a single fixed-bed flow reactor to increase the efficiency of the reaction steps. Accordingly, a 25% cumene alcohol solution was passed through the dehydration/hydrogenation reactor at 14 bar and 205 °C.

10.3.2.3 Cumene/PO Technology Summary Like the HPPO process, the Cumene/PO Process is independent from a coproduct and produces propylene oxide exclusively. As cumene, *via* dehydration and hydrogenation of cumene alcohol, is recovered and recycled to the front end of the process, it functions as an active oxygen carrier, like anthraquinone in the Anthraquinone process for hydrogen peroxide.

10.3.2.4 Existing Plants Currently, two cumene/propylene oxide plants are in operation: a 200 kt/a plant at Chiba, Japan, that was started up in 2003 by Sumitomo and another 200 kt/a plant, built in Saudi Arabia in a joint venture between Sumitomo and Saudi Aramco, that was started in 2009.

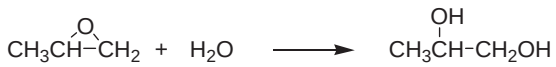
10.3.3 Propylene Oxide Production *via* Hydrogen Peroxide Route

Commercially, propylene oxide is produced *via* hydrogen peroxide route in a process known as HPPO. Presently, producers are Dow/BASF in Antwerp with jointly developed technology, SGC-Dow (Dow-Siam Cement Group Joint Venture) at Map Ta Phut, Thailand, and SKC Co., Ltd (leading PO producer in Korea) with technology licensed by Evonik (former Degussa)/Uhde Companies. In this process hydrogen peroxide in aqueous solution is used to oxidize propylene to propylene oxide. The epoxidation occurs in the liquid phase, in the presence of a heterogeneous catalyst (TS-1) and a solvent (methanol) (Eq. 10.22). The product propylene oxide is recovered and purified by distillation.

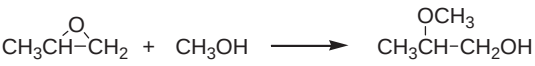


(10.22)

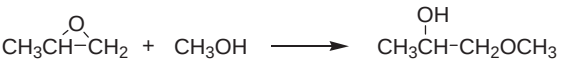
10.3.3.1 Chemistry In the HPPO process, propylene oxide (PO) is formed by the oxidation of propylene with hydrogen peroxide using titanium silicalite-1 zeolite (TS-1) as the catalyst, in the presence of methanol and water as solvents (water introduced together with H_2O_2). The major process steps are the synthesis of PO, the recovery of the solvent and propylene, and the separation/purification of PO. The main byproducts are 1,2-propandiol (propylene glycol) and glycol ethers (1-methoxy-2-propanol and 2-methoxy-1-propanol) produced by the consecutive reaction of propylene oxide with water and methanol, respectively (Eqs. 10.23–10.25). Both glycol and glycol ethers can further react with PO to form longer chain, high boiling oligomers. Small portions of methanol can be oxidized to formic acid by hydrogen peroxide. These can form esters with the remaining methanol (methyl formate). Acetaldehyde can also be formed through the oxidation of ethanol, an impurity of methanol.



(10.23)



(10.24)



(10.25)

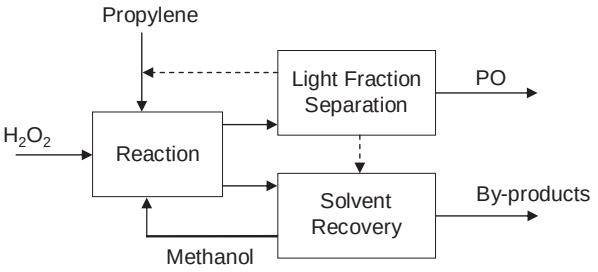


FIGURE 10.10 PO *via* H_2O_2 process: block diagram.

10.3.3.2 Process Technology A simplified process flow diagram is shown in Figure 10.10. In the known HPPO technologies (Dow/Enichem, Dow/Basf, Evonik/Uhde) the process consists of three main sections:

1. Propylene epoxidation;
2. Light fraction separation and purification;
3. Solvent recovery.

Hydrogen peroxide is an oxidizer commonly used as bleach. It is the simplest peroxide and is a clear liquid, slightly more viscous than water, that appears colorless in dilute solution. H_2O_2 is a neat and flexible oxidant that has a mild effect on the environment and represents a very good alternative for chlorinated oxidants or organic peroxides, which can present environmental challenges in many manufacturing operations [26, 34–38]. The hydrogen peroxide (HP) for the HPPO process is an aqueous solution produced in a plant located in the same site of HPPO plant, which eliminates the need for costly transport of large volumes of hydrogen peroxide and reduces the amount of added stabilizers. The catalyst used is a titanium silicalite heterogeneous catalyst (Chapter 2). To reduce catalyst deactivation occurring during its use in the epoxidation step, there is the option to add specific additives (basic or mildly basic) which can slow down the formation of propylene oxide oligomers within the zeolite micropores [39–42]. Efficient methods for a complete regeneration of catalytic activity are required to develop an economic propylene oxide manufacturing process based on TS-1. Different methods for regenerating titanium silicalite-1 are available: calcination at 550 °C, which brought back full catalytic activity [37, 43], or refluxing the catalyst with dilute aqueous hydrogen peroxide, which gradually regenerated the activity up to its initial value [37, 44]. The reaction takes place in methanol as a solvent and is assumed to proceed *via* a transition state, which is formed from titanium, methanol, hydrogen peroxide, and propylene [38]. Propylene oxide and water are the only products released from this transition state. Hydrogen peroxide is completely converted without the need for recycle. A propylene excess is required to obtain a PO yield of about 95% referred to propylene [26]. The reaction conditions are relatively mild: single liquid phase, temperature range between 30 and 80 °C, pressure range

between 10 and 30 bar [45]. Early efforts to develop hydrogen-peroxide-based PO processes used suspension processes (TS-1 powder catalyst) in stirred (CSTR), trickle-bed and fluid-bed reactors [46–48]. The titanium zeolite catalyst has also been formulated so that it can be used in a fixed-bed reactor system, enabling good conversion and selectivity characteristics, along with a suitable catalyst lifetime. The most recent applications of HPPO technology use fixed-bed reactors [45, 48]. There are different approaches described in patents for the treatment of unreacted H_2O_2: thermocatalytic decomposition [46] and hydrogenation [49]. There are also patents teaching the use of bases to reduce the complexity and number of byproducts [45, 46].

In Appendix 10.3D is reported the original PO-*via*-H_2O_2 Dow process scheme as proposed by Nexant [50]. According to this publication, it is based on stirred reactors in series, with a staged addition of H_2O_2 and propylene; the TS-1 catalyst used is in the form of a powder. In Appendix 10.3E is reported the Dow-Basf HPPO process scheme, again as proposed by Nexant [51]. According to this publication, it is based on fixed-bed reactors. The TS-1 catalyst used is in the form of pellets.

High-quality PO product is removed from the reaction mixture by distillation. The reaction mixture is made up of methanol, water, residual propylene, propylene oxide and byproducts (low boilers and high boilers). The first separation is related to the removal of lights like residual propylene and inerts. In the original Dow/Enichem process, propylene is recovered and recycled back to reaction. The crude PO is afterward separated as a top stream from water, methanol and high boilers. The purification of PO requires a dedicated column where the product is recovered as a side stream. Improved PO separation and purification are reported in patents that describe the use of reactive distillation [52, 53].

Water and a small quantity of glycols formed as byproducts are separated from methanol solvent. The glycols are a useful product and are separated from water before final treatment of the aqueous stream. The methanol solvent is recycled to the reactor after a further purification to remove low boilers, which otherwise can accumulate in the methanol recycle stream.

On the subject of methanol separation/purification there is a list of patents related to a complex heat-integration scheme and to the recycle of a part of methanol before its complete purification [45, 52]. A very detailed process description and economic evaluation can be found in Chemsystem PERP Program Reports [54, 55].

10.3.3.3 HPPO Technology Summary The new HPPO technology brings environmental improvements to the PO industry by reducing wastewater by 70 to 80%, compared with existing chlorohydrin PO technology. Energy usage is reduced by approximately 35%, also compared with existing CHPO technology. HPPO enables construction of a process with reduced infrastructure and physical footprint, with simpler raw material integration and avoidance of coproducts. New PO plants built using the HPPO technology are more economical because they require up to 25% less capital to build than conventional technologies. Being water the only coproduct, the adoption of this process avoids the need for additional infrastructure required for handling byproducts or coproducts, which must be marketed.

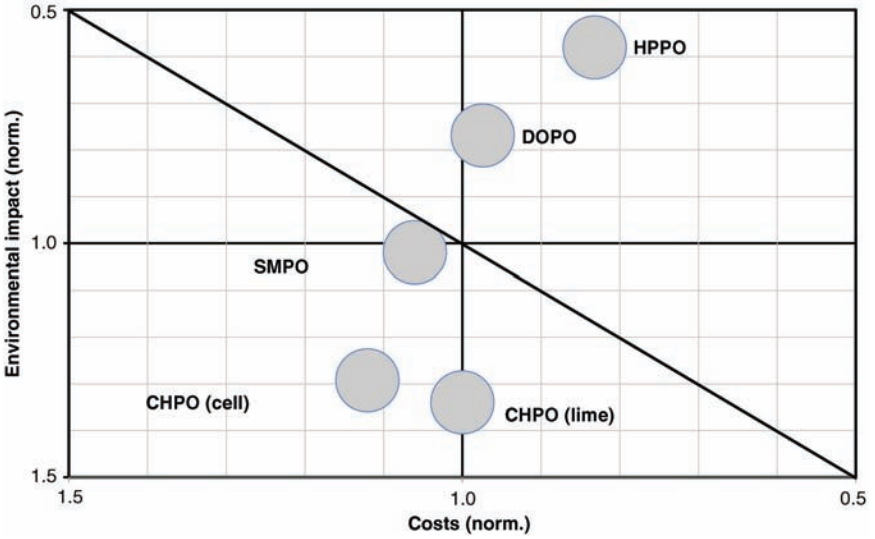


FIGURE 10.11 Ecoefficiency of PO processes.

Coproducts, such as styrene monomer, or byproducts, such as propylene dichloride, require conventional PO plants to be located in large, integrated chemical complexes. Raw material integration for the HPPO process is simple: just hydrogen peroxide and propylene are needed as raw materials. Compared with conventional PO process technologies, HPPO offers unique benefits in the areas of economics and environmental stewardship. These benefits create opportunities for future growth. A joint ecoefficient study conducted by BASF and Dow in 2007 illustrates the environmental benefits of the HPPO process; its results are summarized in Figure 10.11 [56, 57]. The chart compares the ecoefficiency of the HPPO process with the POSM process (called also SMPO), two versions of the CHPO process (use of lime and use of cell effluent), and the hypothetical direct oxidation process to propylene oxide. In theory, it should be possible to obtain propylene oxide through direct oxidation of propylene with oxygen, similarly to the industrial production of ethylene oxide. The analysis measures the cost competitiveness and environmental impact of each process. The upper-right quadrant is the region of highest ecoefficiency. The HPPO process is not dependent on the large volumes of hydrocarbons needed for the coproducts in the PO/TBA or POSM processes, or the presence of world-scale chlorine and caustic capacity required in the Chlorohydrin process. As a result, HPPO allows a high degree of flexibility in plant location and offers significantly reduced specific investments compared to the established POSM processes.

10.3.3.4 Existing Plants As a result of the environmental and economical aspects of the newly developed technology, in 2006, BASF and the Dow Chemical Company signed a joint venture agreement to construct a new commercial-scale PO

TABLE 10.4 Existing Technologies for PO Production *via* Heterogeneous Catalysis

Technology	Catalyst	Reagent(s)	Coproduct[a]	Yield to PO[b] [27]	Tons of coproduct/ ton PO
CHPO	–	$Ca(OH)_2/Cl_2$ or $NaOH/Cl_2$	Brine ($CaCl_2$ or NaCl)	89%	2
POSM	Ti/SiO_2	Ethylbenzene hydroperoxide	Styrene	≥90%	2.5
PO Cumene	Ti silicate	Cumene hydroperoxide	Water	≥90%	–
HPPO	TS-1	H_2O_2	Water	≥90%	–

[a]Waste water treatment is required for water and brine.
[b]Calculated with respect to the reagent.

manufacturing facility based on HPPO technology. Located in Antwerp, Belgium, the plant with a capacity of 300 kt/a PO achieved stable commercial production in 2008. This unit is operated jointly by BASF and Dow and represents the first commercial application of the BASF-Dow novel technology. On June 9, 2008, SGC-Dow (Dow-Siam Cement Group Joint Venture) broke ground on a world-scale HPPO plant with a capacity of 390 kt/a PO and production began in October 2011 at Map Ta Phut, Thailand. Evonik (former Degussa) together with Uhde GmbH, have developed a similar process for producing propylene oxide from H_2O_2, referred to as the Evonik-Uhde HPPO process. SKC has acquired a license and has started up a 100 kt/a plant at Ulsan, South Korea in July 2008.

10.3.4 Conclusions

Table 10.4 summarizes the key characteristics of the main existing technologies for the production of propylene oxide *via* heterogeneous catalysis (CHPO is added as reference of noncatalytic route). Today, all routes to propylene oxide shown in Table 10.4 are in use for commercial production. Availability of raw materials, site-integration aspects and market demand clearly influence the selection of the respective process technology. A coproduct process can be very attractive if a market, balanced with respect to volume and stoichiometric ratios, can absorb both products. If such a balance is not available, the coproduct-free routes are certainly the preferred ones.

Table 10.5 summarizes the key characteristics of the most attractive technologies still under development and not commercialized yet. Looking at the numerous and

TABLE 10.5 Technologies not Commercialized and Still under Development

Technology	Catalyst	Reagent(s)	Reaction steps	Coproduct	Selectivity to PO [34]
DOPO	Ag/SiO_2	O_2	1	–	≤55%
HOPO	Au/TS-1	O_2/H_2	1	H_2O	≥90%
Direct HP/HPPO[a]	Pd, TS-1	O_2/H_2	2	H_2O	≥90%

[a]HPPO technology combined with direct catalytic oxidation of H_2 and O_2 to hydrogen peroxide (HP).

moderately successful attempts that have been made during the past decades to achieve a technological break-through for DOPO in analogy to the direct oxidation process for ethylene oxide, it does not appear very probable that this technology will be able to compete short term with what is already there (Table 10.4) and the two other technologies under development (Table 10.5), respectively.

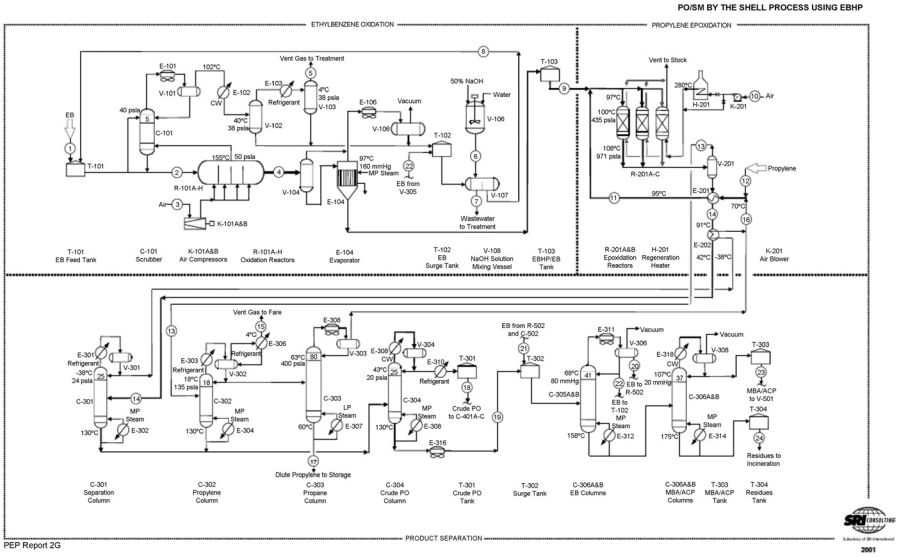
In contrast to DOPO, HOPO technology leads to attractive PO selectivities. The advantage over conventional HPPO would be that no separate conventional H_2O_2 plant is needed. On the other hand, the direct contact of hydrogen and propylene on the metal-doped TS-1 catalyst can lead to an undesirable partial hydrogenation to propane. This can represent a considerable yield loss, negatively affecting the process economics. This issue of HOPO could be overcome if the direct synthesis of H_2O_2 were to be separated from the epoxidation step and a direct catalytic synthesis of H_2O_2 with successive epoxidation were to be done (HP/HPPO). In this case, there would be no direct contact between hydrogen and propylene. However, the direct oxidation of hydrogen with oxygen leads to a lower concentrated H_2O_2 product solution than the conventional H_2O_2 process. Higher concentration would be desirable to achieve a more cost-effective process. In addition, it appears that process safety aspects for the direct synthesis of H_2O_2 might require another breakthrough in reactor-design or process chemistry. To close the gap to existing technologies and make these two process options competitive with conventional HPPO and PO/cumene, respectively, the following would be required:

- HOPO: suppress the propylene hydrogenation;
- Direct HP/HPPO: resolve the process safety aspects and achieve sufficiently high H_2O_2 concentrations.

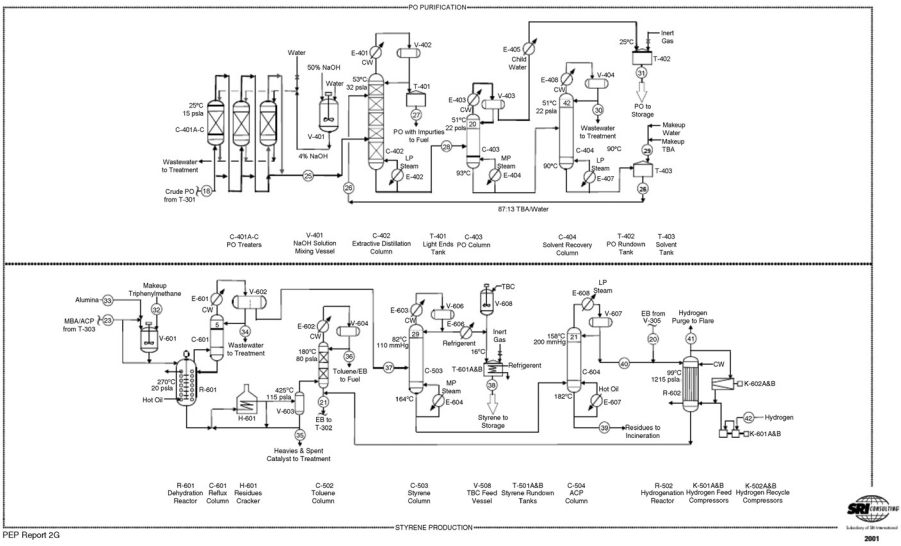
Whereas the earlier developments for catalytic propylene epoxidation chemistry, especially for the coproduct technologies like POSM, were based on homogeneous oxidation catalysts, the more recent and here described developments like POSM by Shell and PO Cumene by Sumitomo are based on the discovery and development of novel, tailor-made heterogeneous catalysts. Among the currently practiced epoxidation technologies based on discoveries in modern heterogeneous catalysis science, HPPO using the zeolitic TS-1 catalyst is the latest commercial technology available. As there is a clear advantage of heterogeneous catalysts, especially with respect to environmentally friendly recovery and regeneration, it can be expected that also in the future heterogeneous catalysts will be a central element for success in chemical process technologies.

ACKNOWLEDGMENTS

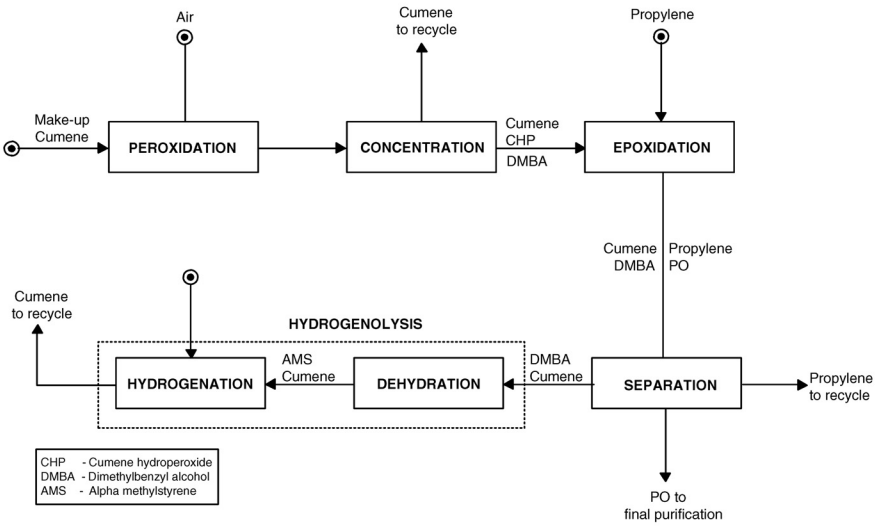
The authors of this section would like to thank Nexant and IHS Inc. for granting the permission to use the information from references [27, 50, 51, 54, 55] and the flow diagrams of their reports shown in Appendices A, B, C, D and E.



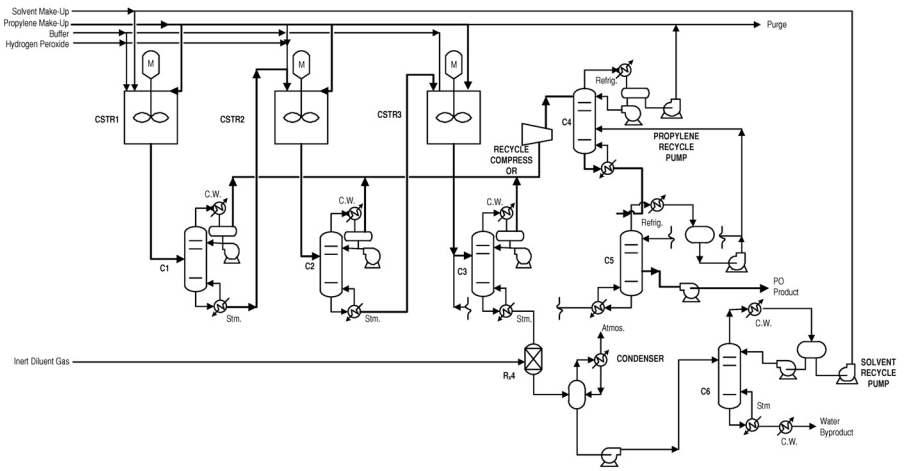
APPENDIX 10.3A POSM by the Shell Process using EBHP. Ethylbenzene oxidation/Propylene epoxidation (used with permission, copyright IHS Inc., December 2001).



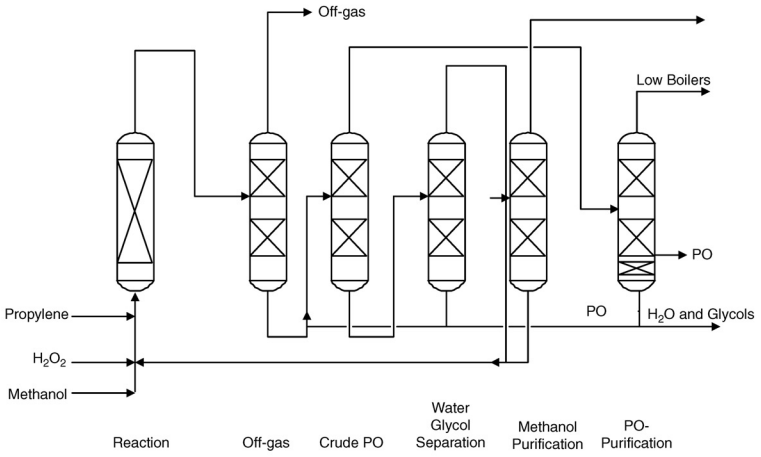
APPENDIX 10.3B POSM by the Shell Process using EBHP. PO purification/Styrene production (used with permission, copyright IHS Inc., December 2001).



APPENDIX 10.3C PO *via* cumene hydroperoxide process: block diagram (used with permission, copyright Nexant Inc., December 2007).



APPENDIX 10.3D PO Stirred reactors process (Hyprox-Dow) (used with permission, copyright Nexant Inc., December 2007).



APPENDIX 10.3E PO Fixed-bed reactors process (HPPO - Dow/Basf) (used with permission, copyright Nexant Inc., December 2007).

REFERENCES

1. Kahlich D., Wiechern U., Lindner J. In: *Ullmann's Encyclopedia of Industrial Chemistry*, Vol. *A22*. Wiley-VCH, Weinheim, 1993, pp. 313–335.
2. Lefort T.E., inventor; FR DE Catalyse Generalisée SA, assignee. US Patent 1,998,878. 1935.
3. National Research Corporation, inventor; National Research Corporation, assignee. GB Patent 786,301. 1957.
4. Halcon International Inc., inventor; Halcon International Inc., assignee. GB Patent 1,060,122. 1967.
5. Taramasso M., Perego G., Notari B., inventors; SnamProgetti, assignee. US Patent 4,410,501. 1983.
6. Neri C., Esposito A., Buonomo F., inventors; Enichem Anic SPA, assignee. Eur. Patent 100119. 1986.
7. Neri C., Buonomo F., Anfossi B., inventors; Anic SPA, assignee. Eur. Patent 100118. 1985.
8. Neri C., Buonomo F., inventors; Anic SPA, assignee. Eur. Patent 102097. 1986.
9. Padovan M., Leofanti G., Roffia P., inventors; Montedipe SPA, assignee. IT Patent 198722220. 1987.
10. Hayashi T., Tanaka K., Haruta M. (1996). *Preprints - American Chemical Society, Division of Petroleum Chemistry 41 (1)*, 71–74.
11. Jubin J.C., Grey R.A., inventors; Lyondell Chemical Tech LP, assignee. Eur. Patent 1742928. 2007.
12. Kawabata T., Abekawa H., Kawashita Y., inventors; Sumitomo Chemical Co, assignee. Eur. Patent 2125763. 2009.
13. Clerici M.G., Ingallina P. In: *Green Chemistry. Designing Chemistry for the Environment*. Anastas P.T., Williamson T.C., eds. ACS Symp. Series 626. American Chemical Society, Washington, DC, 1996, pp. 59–68.
14. Schmidt J.P., inventor; Halcon International Inc., assignee. US Patent 4,066,706. 1978.
15. Toribio P.P., Campos-Martin J.M., Fierro J.L.G. (2005). *J. Mol. Catal. A: Chemical 227*, 101–105.
16. Terlouw T., van Os G., Bakker A.G., inventors; Shell Int Research, assignee. Eur. Patent 323663. 1989.
17. Dubner W.S., Cochran R.N., inventors; Arco Chem Tech, assignee. US Patent 5,210,354. 1993.
18. Buijink J.K.F., Lange J.P., Bos A.N.R., Horton A.D., Niele F.G.M. In: *Mechanisms in Homogeneous and Heterogeneous Epoxidation Catalysis*. Oyama S.T., ed. Elsevier, Amsterdam, 2008, pp. 355–371.
19. Chan L.S., Cochran R.N., inventors; Arco Chem Tech, assignee. US Patent 4,996,374. 1991.
20. SRI Consulting (now part of IHS Inc.). Propylene Oxide. *Process Economics Program Report 2G*, December 2001, by S. Hao-Hwa Wang.
21. Buijink J.K.F., Vlaanderen J.J.M., Crocker M., Niele F.G.M. (2004). *Catal. Today 93–95*, 199–204.

22. Stein T.W., Gilman H., Bobeck R.L., inventors; Halcon International Inc., assignee. US Patent 3,849,451. 1974.
23. Shih T., inventor; Arco Chem Tech, assignee. US Patent 5,107,002. 1992.
24. Jordan W., van Barneveld H., Gerlich O., Boymann M.K., Ullrich J. In: *Ullmann's Encyclopedia of Industrial Organic Chemicals*, Vol. *A9*. Wiley-VCH, Weinheim, 1985, pp. 299–311.
25. Halcon International Inc., inventor; Halcon International Inc., assignee. GB Patent 1,060,122. 1967.
26. Cavani F., Teles H. (2009). *ChemSusChem 2*, 508–534.
27. Nexant. Hydrogen Peroxide-based Propylene Oxide. *ChemSystems PERP Report, 06/07S2* (December 2007). Section 3, p. 54.
28. Tetsuo S., Masaru I., Toshio N., inventors; Sumitomo Chemical Company Limited, assignee. US Patent 7,442,843. 2008.
29. Tsuji J., inventor; Sumitomo Chemical Company, Limited, assignee. Eur. Patent 1837334. 2007.
30. Jun Y., Shigeru G., inventors; Sumitomo Chemical Company Limited, assignee. US Patent Appl. 2010/0048925. 2010.
31. Koji S., Nakayama N., inventors; Sumitomo Chemical Company, Limited, assignee. US Patent 7,705,167. 2010.
32. Toshio N., Junpei T., Noriaki O., Koji S., inventors; Sumitomo Chemical Company, Limited, assignee. US Patent Appl. 2008/0035468. 2008.
33. Tsuji J., Junpei I., Ishino M., inventors; Sumitomo Chemical Company Limited, assignee. Eur. Patent 1598330. 2005.
34. Cavani F., Gaffney A.M. In: *Sustainable Industrial Processes*. Cavani F., Centi G., Perathoner S., Trifiro F., eds. Wiley-VCH, Weinheim, 2009, pp. 319–365.
35. Clerici M.G., Romano U., inventors; Eniricerche SpA, Enichem Sintesi SpA assignees. US Patent 4,824,976. 1989.
36. Clerici M.G., Romano U., inventors; Eniricerche SpA, Enichem Sintesi SpA assignees. US Patent 4,937,216. 1990.
37. Clerici M.G., Bellussi G., Romano U. (1991). *J. Catal. 129*, 159–167.
38. Clerici M.G., Ingallina P. (1993). *J. Catal. 140*, 71–83.
39. Haas T., inventor; Degussa AG, Uhde GMBH, assignees. Eur. Patent 1403259. 2002.
40. Paparatto G., Forlin A., Tegon P., inventors; Dow Global Technologies Inc., assignee. Eur. Patent 1072600. 2000.
41. Teles J.Q., Rehfinger A., Müller U., Wenzel A., Peter R., Harder W., Rieber N., Bassler P., inventors; BASF AG, assignee. WO 2002/020503. 2001.
42. Catinat J.P., Strebelle M., inventors; Solvay, assignee. WO 99/48882. 1999.
43. Müller U., Teles J.Q., Wenzel A., Harder W., Peter R., Rehfinger A., Bassler P., Rieber N., inventors; Basf AG, assignee. WO 2002/022260. 2001.
44. Thiele G.F., Roland E. (1997). *J. Mol. Catal. A: Chemical 117*, 351–356.
45. Göbbel H.G., Bassler P., Teles J.Q., Rudolf P., Müller U., Forlin A., Schulz M., Weidenbach M., inventors; Basf AG, The Dow Chemical Company, assignees. WO 2007/074101. 2006.

46. Forlin A., Paparatto G., Tegon P., inventors; Dow Global Technologies Inc., assignee. US Patent 7,138,534. 2001.
47. Balthasart D., Strebelle M., Catinat J.P., inventors; Solvay, assignee. US Patent Appl. 2003/0158431. 2001.
48. Hofen W., Thiele G., inventors; Degussa AG, assignee. US Patent Appl. 003/0092920. 2001.
49. Haas T., Thiele G., Moroff G., Ullrich N., Hofen W., Stochniol G., Eickhoff H., Pohl W., Wöll W., Brasse C., Berges J., Kampeis P., inventors; Degussa AG, Uhde GMBH, assignees. US Patent 7,141,683. 2003.
50. Nexant. Hydrogen Peroxide-based Propylene Oxide. *ChemSystems PERP report, 06/07S2* (December 2007). Section 2, p. 22.
51. Nexant. Hydrogen Peroxide-based Propylene Oxide. *ChemSystems PERP report, 06/07S2* (December 2007). Section 1, p. 4.
52. Göbbel H.G., Schultz H., Schultz P., Patrascu R., Schultz M., Weidenbach M., inventors; Basf AG, The Dow Chemical Company, assignees. US Patent 7,323,579. 2004.
53. Hofen W., Haas T., Wöll W., Thiele G., inventors; Degussa AG, Uhde GMBH, assignees. US Patent 7,049,450. 2003.
54. Nexant. Hydrogen Peroxide-based Propylene Oxide. *ChemSystems PERP Report, 06/07S2* (December 2007).
55. Nexant. Propylene Oxide. *ChemSystems PERP Report*, 07/08-6 (November 2008).
56. http://www.basf.com/group/corporate/en/news-and-media-relations/news-releases/P-10-327.
57. http://www.dow.com/news/corporate/2010/20100622a.htm.

10.4 ENGINEERING ASPECTS OF LIQUID PHASE OXIDATIONS

BRUCE D. HOOK

The chemistry and catalysis of liquid phase oxidation of organic chemicals is challenging enough. The oxidant feed may be gaseous oxygen (pure or diluted with nitrogen or other inerts), hydrogen peroxide in an aqueous solution, or perhaps an organic peroxide. The choice of oxidant, along with the choice of catalyst defines the reaction system: the number of phases, type of reactor, mobile or immobile catalyst. As a result, the remainder of this chapter will be divided into discussing the engineering aspects of scaling up these different systems. Several systems will be specifically addressed: stirred systems with suspended solids, including those with homogeneous and multiple fluid phases, stirred gas–liquid or liquid–liquid systems, bubble-flow packed-bed columns and trickle-flow packed-bed columns.

10.4.1 Heterogeneous Liquid Phase Systems

For liquid phase oxidation reactions, heterogeneous systems are quite common. Whether the secondary phase(s) are gas, liquid, or solid, the key to reactor

productivity is a sufficiently high dispersion of the secondary phase so that mass transfer of the oxidant to the organic reactant in the presence of the catalyst is fast enough that the rate-limiting steps for the reaction system become other constraints such as heat removal, reactor stability or kinetic control.

10.4.1.1 Stirred Reactors with Suspended Solids For a stirred reactor with suspended solids and an otherwise homogeneous liquid phase, the agitation system must be designed with sufficient power and downdraft to keep the solid phase suspended and dispersed within the liquid phase. Atiemo-Obeng et al. give several criteria for solid–liquid mixing design and recommend using Zwietering's equation for determining the minimum agitation rate required to keep solid particles suspended (Eq. 10.26) [1].

$$N_{\mathrm{js}} = Z\nu^{0.1}\left[\frac{g_c(\rho_{\mathrm{p}} - \rho_{\mathrm{f}})}{\rho_{\mathrm{f}}}\right]^{0.45} X^{0.13} d_{\mathrm{p}}{}^{0.2} D^{-0.85} \tag{10.26}$$

where N_{js} is the just suspended impeller speed, ν the kinematic viscosity of the liquid, g_{c} the acceleration of gravity, ρ_{p} and ρ_{f} are the particle and liquid densities, and Z is the Zwietering constant defined by tank and agitator placement and geometry. D is the impeller diameter, d_{p} is the mass-mean particle diameter, and X is the mass ratio of solids to liquids. Details on units and a compilation of Zwietering constants are found in Atiemo-Obeng et al. [1].

Unfortunately, however, the amount of shear required to impart sufficient suspension velocity to the liquid by a conventional impeller is often greater than the shear required to significantly attrit the catalyst particles. Alternatively, some new impeller designs have been developed that provide good solids suspension while significantly reducing the agitator velocity and resulting shear forces imparted to the particles. Two examples of such impeller designs are the anchor impeller and the newer spatula style such as the Maxblend™ impeller. These are shown in Figure 10.12. Unfortunately, scale-up data on these types of impellers are not as

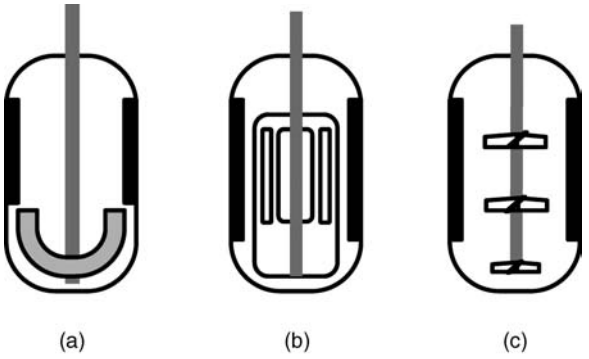


FIGURE 10.12 Impeller systems used for particle suspension in liquid systems: (a) anchor; (b) Maxblend™; (c) multiple impellers.

prevalent as for the typical axial-flow or radial-flow impellers used for liquid only or gas–liquid agitated systems. The work of Dohi and coworkers on the Maxblend™ impeller in comparison with other impeller types showed ~50 percent reduction in agitator rate to achieve solids suspension compared with a triple agitator system using two four-pitched blade downflow disk turbines and one Pfaudler-type impeller at the bottom [2].

Another way to inhibit particle attrition is to choose either small particles that are not as susceptible to high shear, or catalysts that are tougher and less susceptible to breakage. In either case, once the reaction has occurred, the particles must be separated from the liquid phase effluent prior to product purification in order to avoid undesirable secondary reactions promoted in the separation system if the solid catalyst is present, including potential deactivation of the catalyst. More detail is given on solid separation in another section below.

Stirred reaction systems with a homogeneous liquid phase may be among the simplest from a reactor modeling perspective, but perhaps the most difficult to achieve high efficiency with. In order to have a homogeneous liquid phase, the oxidant, organic reactant and reaction product must all be soluble in the same medium. For most organic molecules this is difficult to achieve, requiring large amounts of cosolvents to solubilize hydrogen peroxide as the oxidant, or requiring preformation of an organic peracid or peroxide to act as oxidant. Due to the instability of organic peroxides, and the care required in handling and processing them, this route is not recommended unless all other routes have been eliminated.

While the addition of cosolvents can often overcome the insolubility of the organic reactants in contact with aqueous H_2O_2, the amount of cosolvent required often burdens the overall process with high recycle rates and high separation-energy requirements. Examples of this are the epoxidation of olefins using titanium-silicalite [3, 4], which are described in more detail elsewhere.

10.4.1.2 Separation of Solids from Reactor Effluent and Recycle Back to Reactor

Whenever suspended solids are used as catalysts for liquid oxidation systems, inevitably the solid catalyst must be separated from the liquid reactor effluent. This chapter is much too short to get into a definitive discussion about solid–liquid separation, but some concepts particular to liquid oxidation reactors can be described.

For larger diameter catalyst particles ($>100\,\mu m$), settling or centrifugation of the particulates is typically simple as long as the liquid full particle density is greater than the liquid phase density by at least $0.05\,g/cm^3$. A cyclone, centrifuge or even a settling tank can be used to separate the particles. Depending on the process, the particulate cake or concentrate can be recycled directly back to the reactor, or it can be washed to remove residual reactor effluent from the voids between particles. For particles smaller than $100\,\mu m$, separation becomes progressively more difficult as the particles get smaller. Down to 10–30 μm (depending on liquid viscosity and density), a cyclone can effectively be used to clarify a reactor effluent stream and return a concentrated particle stream back to the reactor. For particles smaller than 10–30 micrometers centrifugation or filtering are recommended. Both filtration and centrifugal separation, however, suffer from

a linear scaling factor above a certain size. Filter elements, cyclones and centrifuges can be built only so large prior to requiring parallel unit installation. Thus, for very large scale operations it is often much more economical to concentrate and recycle the catalyst particles in a system, working only to clarify the reactor effluent that you desire, rather than trying to concentrate the catalyst into a cake or paste prior to recycling.

Catalyst particle-size degradation and metal leaching from the catalysts are other complications that can arise in many oxidative systems, including ammoximation. Catalyst particle-size degradation occurs due to the shear forces of agitation breaking up suspended catalyst particles to their nascent submicrometer size. While solvent and catalyst choice are the first lines of defense to minimize the dissolution of catalyst metals into the reactor fluids, leaching sometimes still occurs. Whether as ultrafines or dissolved specie, the catalyst metals leave with the reactor effluent, often depositing or plating out on downstream equipment. Recent work by Weihong Xing's group on fouling of membrane reactors shows that addition of noncatalytic particulates such as silica may be added to the reaction system to "scrub" reactor internal surfaces to reduce deposition and keep the active catalyst in circulation with the reaction medium [5–8].

10.4.2 Temperature-Control Requirements

For many, if not most, liquid phase oxidation reactions, temperature control and stability become constraints to productivity in a reaction system. For these cases, understanding and controlling the rate of reaction by cooling or by rate of reactant addition is imperative for reactor safety.

If a homogeneous liquid phase is both achievable and desirable, then the reaction engineering most often reduces to a heat transfer and mixing problem. Stirred-tank reactors are often used when the catalyst particles need to be kept small in order to avoid very large intraparticle diffusion times. However, as these reactors increase in size, they become more difficult to remove the necessary heat of reaction with a cooling jacket alone. For larger scale oxidative systems, a recirculation loop through an external cooling exchanger is often set up (see Figures 10.13 and 10.14c) since oxidation reactions are nearly always exothermic.

Another approach for removing heat from exothermic oxidation reactions is to use evaporative boiling. A solvent chosen for its reaction compatibility and sufficiently low boiling point can act as the boiling component whose energy of evaporation removes heat from the reaction mixture by evaporating, moving to a condenser where the energy of evaporation is removed and the vapor is condensed, and the condensed solvent is returned to the reactor to provide further cooling. Evaporative cooling systems, however, may be challenging to design and control due to multiplicity behavior in some regimes [9].

The simplest case is a packed-bed reactor, but heat-removal requirements often then dictate a shell and tube reactor design or a recirculated reactor with an external heat exchanger, or intermediate injections of cold feed to cool the reaction mixture. These are illustrated in Figure 10.14.

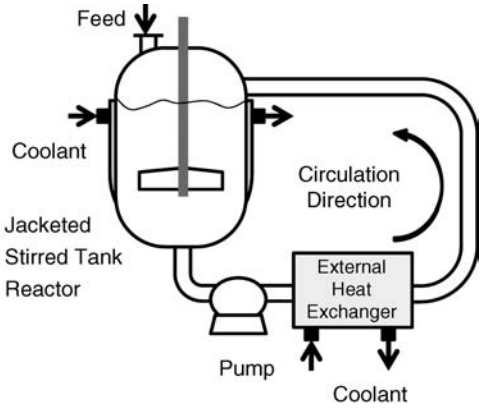


FIGURE 10.13 Typical stirred reactor with external cooling loop.

10.4.3 Packed-Bed Reactors

Often for homogeneous liquid systems with a solid catalyst, a packed-bed reactor is used to eliminate the high agitation power requirements as well as the downstream solid–liquid separation requirements of a stirred reactor with suspended solids. For these systems the internal diffusional resistance of the larger solid particles of a packed-bed catalyst, and the larger reactor size that requires, must be balanced against the cost of solids separation equipment and catalyst degradation effects in an agitated stirred reactor with suspended solids. For oxidation reactions, the liquid phase oxygen concentration often controls the rate of reaction as the rate-limiting

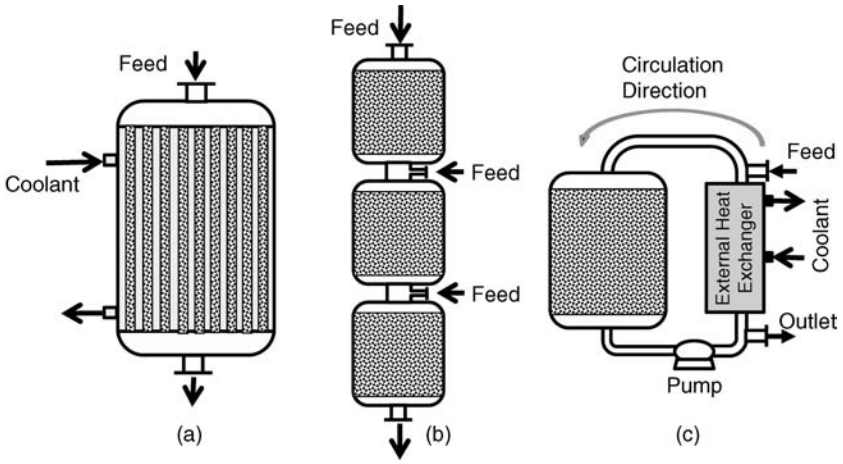


FIGURE 10.14 Three packed-bed reactor cooling configurations: (a) shell and tube reactor; (b) adiabatic reactor beds with periodic cold shots of feed; (c) adiabatic bed with an external heat exchanger.

reactant, either as dissolved oxygen or as soluble hydrogen peroxide. For such reactions, the oxidative reactant may be injected in stages along the packed bed, or between a series of packed beds. Heat exchangers may be used between the packed beds to remove the heat of reaction, or may be used in a recirculation loop around a single packed bed. The disadvantage of the recirculation loop is that when the recycle rate back to the reactor is more that twice the net fresh feed to the reactor, then the higher recirculation rates turns a packed-bed "plug-flow" reactor into what progressively approaches a Perfectly Mixed Flow Reactor.

10.4.4 Three-Phase Systems – Gas, Liquid, Solid

For systems where both a solid catalyst and a gas feed for oxygen supply are used, then both gas dispersion and good liquid–solid catalyst contact are important. Four typical systems are used for this type of application: trickle-flow reactors, bubble-flow reactors, stirred tanks and airlift systems. The trickle-flow and bubble-flow systems will be described later, while the stirred-tank and airlift systems are described below.

For stirred tank systems requiring both dispersed gas and solid phases, often more than one agitator is required to provide both the high dispersion of gas bubbles needed to overcome gas–liquid mass-transfer resistances, and also to keep the solids suspended throughout the reactor instead of having settled on the reactor bottom, as seen in Figure 10.12c. While axial-flow impellers, anchors and other impellers are useful for solids suspension, these are not typically as good at dispersing gas into small bubbles throughout the liquid.

Gas dispersion depends on two things, where the gas is fed into the system (into the liquid phase or into the headspace above the liquid) and how quickly the bubbles coalesce and rise to the surface of the liquid. Clearly, the smaller the bubbles are that are dispersed, the longer the coalescence time and the greater the gas holdup within the reaction mixture. Whether or not the gas is fed into the headspace or below the liquid level, it is nearly always beneficial to use a gas-inducing impeller (often a Rushton turbine) to pull headspace gas down into the liquid phase and disperse it at the impeller level. Such impellers use the vacuum created by their radial-flow action, combined with a hollow shaft, and vents near the impeller, to suck vapor from the headspace and force it into the high-shear radial flow typical of these systems.

For systems with gas phase feeds, Krishna and Sie have shown that by appropriate choice of the contacting mode between the gas, liquid and solid phases, then β, the ratio of liquid volume fraction (ε_i) to the volume of the diffusion layer within the liquid phase ($\delta_i a$) may be fixed ($\beta = \varepsilon_i/\delta_i a$) [10, 11]. For chemical systems with a high Hatta number ($\mathrm{Ha} = [k_1 D_L]^{1/2}/k_L > 10$), then systems with $\beta \sim 10$–50, such as film reactors or spray columns should be chosen. For systems with $\mathrm{Ha} < 1$, then systems with $\beta > 1000$, such as bubble columns or gas-dispersed stirred tank reactors should be used for greatest effect (k_1 is the reaction rate constant, D_L is the liquid diffusivity, and k_L is the liquid phase mass-transfer coefficient).

10.4.4.1 Airlift Systems Airlift systems are those in which the circulation of the liquid phase, as well as that of any suspended solids or secondary phase, is induced

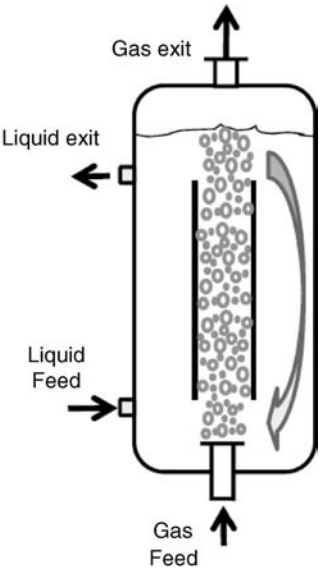


FIGURE 10.15 Typical airlift reactor showing the induced liquid circulation pattern.

by the injection of gas bubbles (typically air) at the bottom of a tank. As shown in Figure 10.15, a draft tube in the center of the airlift reactor can often help induce the overall circulation patterns desired for airlift systems. The liquid circulates upward through the draft tube, induced by the buoyancy of the gas bubbles, and then downward along the annulus of the reactor. The liquid may be loaded batchwise, or fed (and withdrawn) continuously as with a continuous stirred tank reactor. Originally developed for biological systems such as growing microbes, airlift systems have application for liquid oxidation systems where the catalyst is homogeneous or a fine suspended solid. Where the catalyst is a fine suspended solid, the increase in liquid density and viscosity caused by the suspended solids must be taken into account with respect to the flow that can be induced by the buoyancy of the gas. The downside to airlift systems is that the circulation rates that can be achieved with gas buoyancy alone are limited and therefore may need to be augmented with an agitator inside of or at the base of the draft tube in order to keep the solids suspended off the bottom of the reactor. Annular liquid flows or tangential liquid jets at the bottom of the annulus may also be used to aid in solids suspension.

10.4.4.2 Gas–Liquid Flows in a Packed Bed For reactions where the rate of oxygen mass transfer is rate controlling, and the liquid rate is also low because of long reaction times, then a trickle-flow reactor is often used [12]. In a trickle-flow reactor, the liquid flows down in a film or rivulets over a stationary packed bed while the gas phase, the continuous phase, flows downward past the liquid. This type of reactor has very high gas liquid interfacial area, approaching the outer

surface area of the packing as the catalyst bed becomes completely wetted. The low pressure drop of a trickle bed, compared with a bubble column, allows for nearly uniform vapor pressure along the length of the reactor, allowing for higher oxygen concentrations at the end of the reactor, if desired. The high solid/liquid ratio (relative to other reactors) also minimizes the relative amount of homogeneous noncatalytic (and typically undesired) oxidation reactions. Upward gas flows may also be used, in a countercurrent fashion, but this significantly reduces the hydrodynamic window for trickle-flow operation, which is limited when liquid rates become high enough that liquid pulses form, indicating flooding for a counterflow system. Shah, Dudukovic and Mills, and Al-Dahhan et al. provide excellent reviews of trickle-flow reactor hydrodynamics and their impact on mass transfer and reaction rates [12–14]. Dankworth et al. and Larachi et al. review the boundaries of trickle flow and the onset of pulsing flow in gas–liquid coflowing packed beds [15, 16].

10.4.4.3 Bubble Columns At the other end of the gas–liquid holdup spectrum, bubble columns provide either cocurrent or countercurrent contacting of gas and liquid so that the oxygen can be more fully depleted from the gas phase before exiting the reactor. Bubble columns typically have the gas flow moving in an upward direction (due to the buoyancy of the bubbles) and the liquid either moving upward or downward depending on the desire for coflow or counterflow. Bubble columns may be packed with catalyst, or inert packing or trays when a solid catalyst is not required. Some newer designs use monolithic catalyst structures similar to the structured packing used in distillation and other gas–liquid contacting systems. These are still uncommon and particular to the chemical systems they have been developed for, however. Shah also provides an excellent overview of bubble column systems [12].

10.4.5 Oxidant Selection

The choice of oxidizing agent is typically driven by the chemistry of the process, and is not a typical "engineering" variable. On the other hand, which oxidant is required by the chemistry has a very strong impact on the reactor engineering design of the process to be used.

10.4.5.1 Diatomic Oxygen If gas phase O_2 is used as the oxidant, then gas dispersion is critical. For such systems, mass transfer of oxygen molecules from the gas phase to the liquid phase is often rate controlling. While this may sometimes be desirable as a means of controlling the rate of reaction and managing the heat released from the reaction, or for selectivity reasons, it is more often desirable for the mass transfer of the oxygen to be faster than the reaction rate of that component. The mass-transfer rate of oxygen can be increased by a couple of means: increasing the specific contact surface area for mass transfer, increasing the turbulence in the regime near the gas/liquid interface, increasing the concentration of oxygen in the gas feed (e.g., use purified O_2 instead of air), or using a solvent or additive to make the oxygen more soluble in the liquid phase. Increasing the interfacial area can be accomplished by using a trickle flow or a bubble column system, or by increasing

the dispersion and holdup of gas in an agitated tank reactor. Increasing the turbulence near the interface can often be achieved by use of a static inline mixer, a jet eductor or increasing the shear in an agitated reactor. Middleton and Smith give an excellent overview of gas–liquid mixing in agitated vessels and how it is impacted by equipment selection [17]. One additional aspect of using diatomic oxygen as an oxidant is to make sure that one operates outside of any flammable or explosive regime when using combustible or flammable materials. Likewise, the use of purified oxygen substantially changes the flammability and explosivity envelope for most substances and should be handled with extreme care and understanding of the safety requirements for using purified oxygen.

10.4.5.2 Liquid Oxidants Liquid oxidants run the range from hydrogen peroxide (one of the most commonly used) to peracids such as peracetic acid (CH_3CO_3H) or persulfonic acid (H_2SO_5), to organic peroxides such as *tert*-butyl hydroperoxide ($(CH_3)_3COOH$) or ethylbenzene hydroperoxide ($C_6H_5CH(OOH)CH_3$), to aqueous solutions of peracid salts (e.g., $NaMnO_4$). The chlorine series of oxidants is not included in this discussion as they are generally out of scope for most of the articles in this text. For most of these liquid oxidants, their ability to release oxygen is inherent in their oxidative nature, but it is also a tendency to be mitigated so that oxygen is released in the desired portion of the reaction system, and not elsewhere such that a flammable or explosive atmosphere can be generated. Liquid organic peroxides and organic peracids, especially, should be kept under refrigerated conditions to enhance their stability (check Material Safety Data Sheet for appropriate temperatures), and stored quantities should be minimized. Many peroxides are autothermally unstable at room temperature. If possible, practitioners should create the peroxide or peracid *in situ* or just prior to use, and then consume it soon afterward.

If H_2O_2 is used, then traces of free iron need to be removed from piping (pickling with nitric acid often satisfies this requirement), along with appropriate metallurgy (stainless steel or better) and venting to account for peroxide degradation. Likewise, downstream of the reactor, residual peroxides and peracids need to be destroyed or captured in order to prevent undesired degradation and oxygen accumulation in downstream equipment that can cause a deflagration or explosion. For H_2O_2, several options for decomposition are available. Thiosulfate salts are commonly used for peroxide decomposition due to the natural reducing capability of the thiosulfate ion. In larger scale commercial use, however, this then leads to a wastewater stream contaminated with thiosulfate and sulfite salts that must then be removed or disposed of. Alternate treatments are using caustic, heat or iron-oxide catalysts to decompose the residual peroxide to oxygen and water (in the case of H_2O_2). Purging and venting of the produced oxygen from the organic mixture is necessary to prevent formation of flammable or explosive atmospheres in equipment.

10.4.5.3 Two Liquid Phases Arising from Liquid Oxidant Use One complication of using liquid oxidants such as hydrogen peroxide, permanganate or persulfate is that at some point in during the progression of the reaction the reaction mixture becomes two liquid phases. Ammoximation of cyclohexanone is one example

process. For some reactions, where the reactants are soluble in the aqueous phase and the products are more soluble in the organic phase, this can actually be advantageous since further reaction of the product by oxidation or hydrolysis is limited. More commonly, however, the product is more soluble in the aqueous phase after oxidation than the reactant is. When two liquid phases exist, then transport of the reactants to the catalyst is often the rate-limiting step for the reaction system. Thus, phase-transfer agents such as surfactants or charged organic species that can enhance the transport of the reactant to the catalyst, or enhance the ability of the catalyst to concentrate near the interfacial film between the phases may be used. Likewise, if the catalyst is a solid, and the particle size is small ($<200\,\mu m$) the inherent tendency of small particles to locate near interfaces (gas or liquid) may be used to advantage. In either case, mixing should be increased to fully disperse the noncontinuous phase and increase the interfacial area as much as possible without unacceptably atritting the catalyst (if a solid particle).

10.4.5.4 Using Cosolvents to Overcome Multiphase Complications Homogeneous liquid phase systems are the simplest of the reaction systems from a reactor modeling perspective, but perhaps the most difficult to achieve high efficiency with. In order to have a homogeneous liquid phase system, then the oxidant, organic reactant and reaction product must all be soluble in the same medium. For most organic molecules this is difficult to achieve, requiring large amounts of cosolvents to solubilize hydrogen peroxide or other inorganic oxidant, or requiring preformation of an organic peracid or peroxide to act as oxidant. Due to the instability of organic peroxides, and the care required in handling and processing them, this route is not recommended unless all other routes have been eliminated.

While the addition of cosolvents can often overcome the insolubility of the organic reactants in contact with aqueous H_2O_2, the amount of cosolvent required often burdens the overall process with high recycle rates and high separation energy requirements. Examples of this are the epoxidation of olefins using Payne chemistry or peracids such as peracetic or perbenzoic acid [18–20].

The advantage of homogeneous oxidation systems is the ease of mixing and reacting the reactants. Standard axial mixing impellers provide good mixing in a stirred tank, or the reagents can be premixed and then reacted in a plug-flow reactor. For such systems, temperature control and stability often become the operational constraints on the productivity of the reactor.

10.4.6 Summary

No brief review of such a complex topic is complete in such a short space. The interaction of mass transfer with reaction, with or without solids handling or gas dispersion, means that there is no *a priori* answer to every case [11]. As described in Krishna and Sie, the first level is to understand one's chemistry and catalyst and what makes that chemistry most productive [10]. The second level is to understand the interphase contacting mode and how the multiple phases are to be introduced (batch, continuous, pulsed, or staged) and how mixing will enhance the

interphase contacting after introduction. The third level is to assess the best hydrodynamic flow regimes based on the results of levels one and two.

REFERENCES

1. Atiemo-Obeng V.A., Penney W.R., Armenante P. In: *Handbook of Industrial Mixing: Science and Practice*. Paul E.L., Atiemo-Obeng V.A., Kresta S.M., eds. Wiley-Interscience, Hoboken, NJ, 2003, pp. 543–584.
2. Dohi N., Takahashi T., Minekawa K., Kawase Y. (2004). *Chem. Eng. J. 97*, 103–114.
3. Clerici M.G., Romano, U., inventors; Eniricerche and Enichem Synthesis, assignees. US Patent 4,937,216. 1990.
4. Strebelle M., Gilbeau P., Catinat J.P., inventors; Solvay (Societé Anonyme) assignee. US Patent 6,288,248. 2001.
5. Zhong Z., Xing W., Liu X, Jin W., Xu N. (2007). *J. Membr. Sci. 301*, 67–75.
6. Zhong Z., Li D., Liu X, Xing W., Xu N. (2009). *Chin. J. Chem. Eng. 17*, 53–57.
7. Zhong Z., Liu X, Chen R., Xing W., Xu N. (2009). *Ind. Eng. Chem. Res. 48*, 4933–4938.
8. Li Z., Chen R., Xing W., Liu X, Jin W., Xu N. (2010). *Ind. Eng. Chem. Res. 49*, 6309–6316.
9. Solorzano M.Z., Ray W.H. (2008). *Ind. Eng. Chem. Res. 47*, 9025–9039.
10. Krishna R., Sie S.T. (1994). *Chem. Eng. Sci. 49 (24A)*, 4029–4065.
11. Suresh A.K., Sharma M.M., Sridhar T. (2000). *Ind. Eng. Chem. Res. 39*, 3958–3997.
12. Shah, Y.T. *Gas-Liquid-Solid Reactor Design*. McGraw Hill, New York, 1979.
13. Dudukovic M.P., Mills P.L. (1978). *AIChE J. 65*, 387.
14. Al-Dahhan M.H., Larachi F., Dudukovic M.P., Laurent A. (1997). *Ind. Eng. Chem. Res. 36*, 3292–3314.
15. Dankworth D.C., Kevrekidis I.G., Sundaresan S. (1990). *AIChE J. 36*, 605–521.
16. Larachi F., Illuta I., Chen M., Grandjean B.P.A. (1999). *Can. J. Chem. Eng. 77*, 751–758.
17. Middleton J.C., Smith J.M. In: *Handbook of Industrial Mixing: Science and Practice*. Paul E.L., Atiemo-Obeng V.A., Kresta S.M., eds. Wiley-Interscience, Hoboken, NJ, 2003, pp. 585–635.
18. Payne G.B., Deming P.H., Williams P.H. (1961). *J. Org. Chem. 26*, 659–663.
19. Findley T.W., Swern D., Scanlan J.T. (1945). *J. Am. Chem. Soc. 67*, 412–414.
20. Garcia-Bosch I., Company A., Fontrodona X., Ribas X., Costas M. (2008). *Org. Lett. 10*, 2095–2098.

INDEX

4-acetaminophenol (Paracetamol), 61, 471
acetone peroxides, 456
acetophenone, 8, 47, 61, 63, 109, 169, 228, 382, 383, 385, 391, 397, 398, 441, 477, 478
acetylacetone, 133, 134, 143
α,β-acetylenic ketones, 359
acetylperoxyborate, 107
acid activity
  basic additives, neutralization with, 50, 51, 53, 55, 68, 75, 77
  of large pore Ti zeolites, 51
  of $M^{(III)}$-Ti zeolites (M = Al, Ga, B, Fe), 57
  of S-1, TS-1 and TS-1·H_2O_2 systems, 50
acid promoters (TS-1), 37
acid sites. *See also* Al-TS-1, Ti,Al-β, Ti-MOR
  Al impurities in TS-1, 50, 53
  Ti-OOH active species, 50
acrylic acid, 57
acylperoxy radical, 300, 401
adamantane, 287, 340, 401
adamantanone, 116, 183
adipic acid, 4, 107, 110, 117, 119, 138, 164, 166, 179, 200, 224
adiponitrile, 465
adsorption and catalytic activity, 37, 39, 42, 48, 66, 76, 189
aerogel, 128, 129, 132, 133, 134, 135, 170, 174, 199, 332, 343
  mechanical stability, 195
Aerosil, 147, 172, 308, 354
Ag/SiO_2, 488
agostic bond, 69
air (oxidant), 2, 3, 8, 503
$Al(i\text{-}C_3H_7O)_3$, 101
$Al(NO_3)_3$, 30
$Al(OC_4H_9)_3$, 103
$AlCl_3$, 103
alcohols, oxidation, 59–60, 112, 182, 228–33, 234–41, 297–98, 356–59, 385, 398–99
  basic promoters, 229, 230, 232
  kinetics (TS-1, Ti,Al-β), 60
  proposed mechanism (TS-1, Ti,Al-β), 60, 72
alcohols, photo-oxidation, 430–36
  proposed mechanisms (TiO_2), 430
aldehydes, oxidation, 241, 298–99. *See also* carbonyl compounds
  aromatic to phenols, 63, 183
Al-HMS, oxidation of cyclohexane, 164, 165
alkali metal ions, in
  synthesis of Ti-Beta, 30
  synthesis of TS-1, 24, 453
alkanes, hydroxylation, 35–40
  dihydroxylation, 37
  mechanistic aspects, 37–39, 69–71
  Ti^{IV}-$O^{\bullet}$ active species, 70
alkanes, oxidation, 106–08, 163–67, 224–25, 287, 339–44, 388–89

Liquid Phase Oxidation via Heterogeneous Catalysis: Organic Synthesis and Industrial Applications, First Edition. Edited by Mario G. Clerici and Oxana A. Kholdeeva.

© 2013 John Wiley & Sons, Inc. Published 2013 by John Wiley & Sons, Inc.

alkanes, photo-oxidation, 422–26
  mechanism, 425
3-, 4-alkenols, epoxidation/cyclization, 59
alkyl hydroperoxides, 5–9
  epoxidation with, 7, 172–73, 174–76, 475–76
    mechanism (Ti-silicates), 191
  metal-catalyzed activation, 6
2-alkylanthrahydroquinone, 54
alkylaromatics, oxidation, 46–47, 109–10, 168–69, 353
alkylaromatics, photo-oxidation, 426, 427, 428
alkylphenols, oxidation, 169, 288
  mechanism, 192
alkynes, oxidation, 359
Allied Chemical, 463, 467
allyl acetate, 57
allyl alcohol, oxidation, 48, 239–41
  to 3-hydroxypropionic acid, 240
  to glyceric acid, 252
allyl alcohols, epoxidation, 48, 55–56, 290
  OH-assistance, 56
  protic solvent, inhibition, 56
  regio-, stereo-, diastereoselectivity, 56
  Ti leaching, 56
  to triols in one step, 55, 452
allyl alcohols, OH-oxidation, 232, 239, 358
allyl carbonate, 57
allyl chlorides, epoxidation, 48, 56–57
  epichlorohydrin, reactor modeling, 57
  epichlorohydrin, synthesis, 56
  in situ H_2O_2 generation, 57
  kinetics (allyl chloride), 57
allyl esters, epoxidation, 57
allyl ethers, epoxidation, 57
allyl methacrylate, 57
allyl thioethers, S-oxidation, 65
allylic C-H oxidation, 180–82, 294–97
allylic oxidation/epoxidation competition, 47, 51, 75, 76, 173, 190
2-allylphenol, 172
AlPO-*n*. *See* aluminophosphate
aluminophosphates
  characterization, 103–6
  framework structures, 96, 101
  stability, 118–19
  synthesis of
    mesoporous, 102–3
    microporous, 100–2
aluminophosphates, mesoporous
  CoHMA, 108, 109, 119
  CrHMA, 107, 109, 119
  FeHMA, 108, 109, 114, 119
  TiHMA, 113, 119
  VHMA, 107, 109, 111, 119
aluminophosphates, microporous
  CoAPO-11, 109, 113, 118
  CoAPO-18, 107
  CoAPO-31, 109
  CoAPO-36, 110, 113, 116
  CoAPO-5, 107, 108, 109, 110, 111, 113, 116
  CoAPO-50, 113
  Co^{II}APO-36, 114
  $Co^{II}Co^{III}$APO-36, 114
  Co^{III}APO-18, 114
  CrAPO-11, 111
  CrAPO-5, 107, 109, 110, 111, 112, 181, 390
  CrAPO-VFI, 107
  CuAPO-11, 108, 117
  CuAPO-5, 117
  FeAPO-11, 113
  FeAPO-31, 107
  FeAPO-5, 107, 108, 110
  $Mg^{II}Co^{II}$APO-36, 114
  $Mg^{II}Co^{III}$APO-18, 114
  $Mg^{II}Co^{III}$APO-36, 114
  $Mg^{II}Mn^{III}$APO-36, 114
  MnAPO-36, 110, 116
  MnAPO-5, 107, 110, 111;112, 114, 117
  $Mn^{II}Mn^{III}$APO-36, 114
  TiAPO-11, 110
  TiAPO-36, 110
  TiAPO-5, 110, 111, 113, 114, 117
  TiCoAPO-5, 110, 111
  VAPO-11, 111
  VAPO-5, 111
  VAPO-VFI, 107
aluminophosphates, oxidations
  mechanistic aspects, 116–18
  of alcohols, 111–13
  of alkanes, 106–8
  of alkylaromatics, 109–10
  of ketones (Baeyer-Villiger), 116
  of ketones/NH_3 (ammoximation), 114–15
  of N-heterocycles, 116
  of olefins, 110–11
  of phenols, 113–14
Amano Enzyme Co, 242
Amberlist-15, 273
Amberlite IRA-900, 288, 332, 420, 437, 441
Ambersorb, 272, 302, 309, 441
amine-modified silica, 274, 298, 308
amines, oxidation, 63–64, 188–89, 244–45
  primary, to amides, 245
sec-amines, oxidative dehydrogenation, 245
α-amino alkenes, oxidation; 345
aminoalcohols, oxidation, 244–45
ammonia
  consecutive oxidation, 61
  oxidation to hydrazine, 65
  oxidation to hydroxylamine, 62, 74
ammoximation, 61–63, 114–15, 185, 466–67, 505
  alternative pathways, 62, 467
  proposed mechanism, 73
ammoximation of cyclohexanone
  continuous flow reaction, 62
  EniChem process, 467–70
  process integration, 63
  structural instability (Ti zeolites), 61, 63, 469

anchoring, 156, 277, 278, 283, 325, 333, 344, 353, 363, 420
aniline, 64, 188, 245
  oxidative polymerization, 245–49
anisole, 42, 47, 437
anthracene, 168, 288, 353
9,10-anthraquinone, 168, 288, 353
anthraquinone process (AO), 10–11, 54, 459
APO-*n*. *See* aluminophosphate
arenes, oxidation, 167–69, 352–53
aromatic aldehydes, oxidation to phenols, 63
aromatic compounds, oxidation, 167–72, 288, 389–93
  on photocatalysts, 427–30
aromatic ethers
  bromination (photo), 438
  oxidation, 47
aryl alkanes. *See* alkylaromatics
aspergillus niger, glucose oxidation, 241
Assoreni (Eni group), 451
asymmetric
  epoxidation of olefins, 346, 348, 351, 352, 387, 394–97
  oxidation of thioethers, 186, 362, 400
atom efficiency, 2
$Au_{55}(PPh_3)_{12}C_{l6}$, 228
Au-$O_2^{\bullet}$, 253
autoxidation, 7, 60, 107, 197, 294, 301, 388, 401, 475
  of cumene, 8, 482
  of ethylbenzene, 8, 478
  of isobutane, 8
autoxidation, for H_2O_2 production, 57
  of alkylanthrahydroquinones, 10, 54, 57, 63
  of isopropyl alcohol, 63
  of *sec*-alcohols, 54
azobenzene, 188
azoxybenzene, 64, 188

Baeyer-Villiger oxidation, 15, 33, 60, 63, 116, 183–84, 193, 360
  mechanism, 16, 63
Barrett–Joyner–Halenda (BJH) method, 130
BASF, 9, 379, 460, 464, 476, 483, 486
BASF/Dow process (HPPO), 460, 484, 487, 493
basic compounds
  oxidation inhibitors, 37, 69, 70
  selectivity enhancers, 50, 51, 53, 55, 68, 75, 77
Beckmann rearrangement, 114
  oleum-based, 461, 464, 471
  on Silicalite-1 (vapor-phase), 466, 470, 471
benign oxidants, 2
benzaldehyde, 47, 58, 109, 112, 168, 178, 182, 228, 238, 239, 292, 297, 298, 345, 353, 383, 385, 391, 398, 432, 436, 440
benzene, hydroxylation, 37, 40–41, 47, 70, 167, 427, 429
  continuous flow (CSTR), 41
  mechanistic studies, 42–43
  photocatalytic (TiO_2), 427
  post-treatement of TS-1 (TS-1B), 41
benzenedisulfonic acid, 138
benzil, 182
1,3-benzodioxole, 47
benzoin, 182
benzonorbornadiene, 290
benzophenone, 169, 382, 391
benzoquinone, 40, 42, 43, 44, 169, 234
benzothiophene, 66, 187
benzyl alcohol, 47, 109, 112, 182, 223, 230, 232, 238–39, 255, 298, 359, 385, 386, 391, 398, 432, 434
  kinetics (oxidation on Au), 239
benzyl alcohols, substituted, 239, 254, 297, 398, 434, 452
benzyl chloride, 47
benzyl imines, 386
benzylamine, 245, 386
benzylidene amines, 245
biomimetic metal complexes, 35, 70, 336–38
biphenyl ether, 47
bis(pentamethylcyclopentadienyl)cobalt(III) hydroxide, 33
Borregaard, 460
Brij56, 143
bromination, photo oxidative, 438
4-bromoethylbenzene, 353
Brønsted acid sites, 50, 51, 68, 97, 101, 114, 131
Brønsted acidity, 50, 51, 53, 57, 190
Brunauer–Emmett–Teller (BET), 130
butadiene, 57, 466
butan-1,2-dione, 60
n-butane, 37
1,3-butanediol, 431, 435
1,4-butanediol, 231
2,3-butanediol, 60
1,2,3-butanetriol, 77, 197
n-butanol, 231
butanone, 35, 37, 43, 49, 61
1-butene, 48
n-butyl hydroperoxide, 60
t-butyl hydroperoxide, 2, 7, 56, 59, 64, 174, 286, 475, 504
  market, uses, 9
  preparation (Halcon/ARCO process), 8
n-butylamine, 25
4-*tert*-butylbenzaldehyde, 168
4-*tert*-butylcyclohexanone, 61, 62, 467
p-*tert*-butylphenylallyl ether, 176, 190
butylproxitol, 359
4-*tert*-butyltoluene, 168
n-butyraldehyde, 60
γ-butyrolactone, 60, 231

Camlin Fine Chemicals, 460
camphene, 51, 182, 295
campholenic aldehyde, 110, 182, 295
ε-caprolactam, 114, 185, 245, 462–66, 469
  EniChem/Sumitomo process, 470
  global production, market, uses, 463

ε-caprolactone, 112, 183, 360
carbodiimides, 244
carbofuran, 452
carbohydrates, oxidation, 241–44
carbonyl compounds
  ammoximation, 61–63, 185
  Baeyer-Villiger oxidation, 15, 63, 116, 183–84, 360
  α,β-unsaturated, epoxidation, 57
carboxylic acid-modified silica, 350
carboxylic acids, 57, 59, 63, 116, 197, 229, 239, 245, 308, 378
carboxymethyl cellulose, 26
3-carene, 288, 292, 393
carveol, 175, 177, 297
carvone, 176, 383
carvotanacetol, 175
caryophyllene, 174, 190, 293
catechol, 42, 43, 46, 169, 385, 453, 461
  global capacity, 453
cationic silica nanoparticles, 278, 299, 302
Ce-SBA-15
  oxidative cleavage of cyclohexene, 179
cetyltrimethylammonium bromide. *See* CTAB
C-H activation, 34
  acid promoters, 37
  basic inhibitors, 37
  probe molecules, 38
charge transfer absorption (CT), 28, 106, 131, 413, 417, 424, 433
cheap TS-1, 25, 44, 53. *See also* Ti silicalite-1 synthesis
chemical vapor deposition (CVD), 158, 334
2-chloroethyl ethyl sulfide, 301
1-chlorohexane, 37
chlorohydroquinone, 429
choline chloride, 102
CHP. *See* cumyl hydroperoxide
cinnamyl alcohol, 231, 385, 398, 432
cinnamylaldehyde, 385
citral (3,7-dimethyl-6-octen-1-al), 184, 431
citronellol, 56, 431
Co/MCM-41
  oxidation of benzoin, 182
Co/SiO_2
  oxidation of cyclohexane, 108, 164
Co-HMS
  oxidation of cyclohexane, 164
colloidal silica, 24, 25, 53, 137, 141, 195
Co-MCM-41
  oxidation of isolongifolene, 181
composite micro/mesoporous materials, 198
conducting polymers, 245–46
co-oxidation of olefins and aldehydes, 299–301
core-shell morphology, 143
Co-TUD-1, 155
  alkene epoxidation, 178
  oxidation of cyclohexane, 164, 165
coumarin product, 427
Cr zeolites, 33, 64
o-cresol, 47, 168
p-cresol, 109, 117, 118, 168
Criegee intermediate, 63, 193
Cr-MCM-41, 150
  allylic oxidation, 181
  benzylic oxidations, 169
  oxidation of aniline, 189
  oxidation of anthracene, 168
  oxidation of cyclohexane, 165
  oxidation of cyclohexene, 180
Cr-MCM-48, 150
  oxidation of cyclohexane, 164
  oxidation of cyclohexene, 180
  stability, 198
crotyl alcohol, 56, 77, 197
Cr-PMO
  oxidation of cyclohexane, 164, 165
Cr-SBA-15
  allylic oxidation, 180
CTAB, 138, 143, 148, 151, 152, 153, 155, 162, 270
Cu/TiO_2, 226
cumene, 8, 46, 353, 474, 482, 488
cumene process (phenol), 41
cumyl alcohol, 8, 475, 481, 482
cumyl hydroperoxide, 2, 7, 8, 41, 174, 474, 487, 491
  production (PO process), 480–82
cyclocitral, 184
cyclododecane, 108, 167, 340
cyclododecanol, 182
cyclododecanone, 167
  ammoximation, 61, 62, 185, 467, 471
cyclododecene, 51, 173, 190
cycloheptane, 39
trans-1,2-cyclohexandiol, 179
cyclohexane, 37, 39, 107, 108, 117, 163, 165, 167, 197, 224, 287, 335, 339, 340, 381, 388
cyclohexane, photo-oxidation, 416, 422–24, 425, 426, 427, 439, 441, 465
  mechanism (TiO_2), 422
cyclohexanol, 37, 59, 68, 73, 107, 112, 163, 166, 225, 287, 297, 298, 306, 339, 381, 388, 422–27, 436, 439
cyclohexanone, 16, 37, 61, 107, 112, 114, 183, 225, 287, 298, 339, 360, 385, 388, 416, 422–26, 439
cyclohexanone oxime, synthesis, 61, 466–67, 468
  BASF acid process, 464
  BASF-Inventa process, 464
  DSM process, 465
  EniChem process, 461, 467–70
cyclohexene, 48, 51, 58, 110, 117, 173, 174, 176, 178, 180, 190, 200, 228, 288, 290, 292, 294, 300, 307, 345, 348, 351, 383, 393, 394, 437, 438
2-cyclohexene-1-ol, 173
2-cyclohexene-1-one, 173, 180, 394, 401, 437
cyclohexyl hydroperoxide, 107, 164, 426
cyclometalation, 34, 69

cycloocta-1,5-diene, 178
cyclooctane, 39, 108, 165, 167, 287, 381, 388
cyclooctanol, 287, 359, 381
cyclooctene, 178, 228, 288, 292, 330, 344, 348, 350, 384, 393, 394, 437
cis-cyclooctene, 176, 190, 228, 289, 345, 351
cycloolefins, allylic oxidation, 180
cycloolefins, epoxidation, 345
cyclopentane, 381, 388
cyclopentanol, 381, 436
cyclopentene, 49, 58, 111, 173, 179

DBT. *See* dibenzothiophene
Degussa/Uhde process (HPPO), 483, 484, 487
delamination, 33, 51, 52
desulfurization, oxidative (ODS), 65, 66, 187
diallyl ether, 57
diastereoselectivity, 56, 175, 291
dibenzothiophene, 66, 187, 304
dibenzyl sulfide, 302
dibenzylamine, 245
dibutylsulfoxide, 65
2,6-dichloropyridine-N-oxide, 330, 338, 345, 346
diethylamine, 25
1,4-diethylbenzene, 353
diffuse reflectance UV–vis, 28–29, 105, 131, 134
diffusion limitations
  in alkane hydroxylation, 37
  in epoxidation, 50
  in phenol hydroxylation, 44, 453
  of large crystals, 26, 44
diffusion measurements
  of 1-hexene in TS-1, 49
  of aromatics in TS-1 and Ti-MOR, 49
dihydroanthracene, 288
2,3-dihydrobenzofuran, 47
dihydrocarvone, 184
1,3-dihydroxyacetone, 236, 237, 359, 432
dihydroxybenzenes (diphenols), 40, 43–6, 387, 452, 455, 457
dihydroxylation
  of alkanes, 37
  of allyl alcohols to triols, 55, 452
  of olefins (*cis*-), 350
1,4-dimethoxybenzene, 47
3-dimethylamino-1-propanol, 244
2,2-dimethyl-2*H*-chromene, 383, 384, 395, 396
1,2-dimethylcyclohexanes, 39, 167, 190
dimethylcyclohexanones, 61
2,6-di-*tert*-butylphenol, 114, 169, 234
4,6-dimethyl-2-methylthiopyrimidine, 186
1,3-dimethylcyclopentanes, 38
1,3-dimethylcyclopentanol, 38
4,6-dimethyldibenzothiophene, 187
2,6-dimethylphenol, 288
di-*n*-propylamine, 101
diols, oxidation, 60, 230, 231, 235, 431, 435
diphenoquinone, 169
diphenyl sulfide, 386
diphenyl sulfoxide, 386
diphenylmethane, 169, 382, 389, 391
direct synthesis (H_2O_2). *See* hydrogen peroxide
direct synthesis (zeolites). *See* hydrothermal synthesis
Dow Chemical, 9, 460, 476, 484
dry gel synthesis, 25, 30, 102
DSM, 464, 465, 466
DuPont, 465

EBHP. *See* ethylbenzene hydroperoxide
ecoefficiency of PO technologies, 486
E-factor, 2, 8, 16
electron diffraction (ED), 130
electron spin resonance (ESR), 106, 424, 431
electron-transfer-oxygen transfer, 307
electrophilic oxygen transfer mechanism, 306
electrostatic interaction, 102, 137, 282, 303, 308, 324, 330, 420
Eley-Rideal, rate law, 45, 50, 57, 239
emeraldine (polyaniline), 246, 248
enamines, from diazoalkanes, 245
enantioselective adsorption, 400
enantioselectivity, 186, 337, 338, 351, 352, 362
encapsulation, 326
  in MOFs, 328
  in molecular sieves, 326–28
  in polymeric membranes, 328
EniChem process
  ammoximation, 460, 462, 467–70
  HPPO, 460
  hydroxylation of phenol, 456–60
EniChem Synthesis (ENI group), 460
EniChem/Dow process (HPPO), 476, 484, 485, 492
EniChem/Sumitomo process (ε-caprolactam), 470
enynes (conjugated), oxidation, 345
$EO_{20}PO_{70}EO_{20}$, 104, 139, 141, 142, 270. *See also* Pluronic
epichlorohydrin, 56
epimerization, 38
epoxidation of
  allyl alcohol, allyl chloride, 55–57
  olefins, 47–52, 57, 111, 172–78, 288–94, 344–52
  propylene, 52–55
  α,β-unsaturated compounds, 57
epoxidation/cyclization of alkenols, 59
epoxidation/hydrolysis to glycols, 58
3,4-epoxy-1-butene, 57
2,3-epoxybutane, 50
6,7-epoxygeraniol, 177
ES-40, 133
Esomeprazole, 6
esters, by alcohol oxidation, 231
ETBE (ethyl *t*-butyl ether), 7
ethandiol, 231
ethanol, 225, 233
ethers (cyclic), oxidation, 60
ethyl acrylate, 57
ethyl silicate 40 (ES-40), 133
ethylbenzene, 7, 8, 46, 109, 169, 353, 382, 291, 392, 441, 476, 479

ethylbenzene hydroperoxide, 7, 172, 475, 476, 478, 479, 504
  preparation (POSM process), 8, 477
(2-ethylbutyl)phenyl sulfide, 386
(2-ethylbutyl)phenyl sulfoxide, 386
2-ethylcyclopropane, 37
ethylene, 48, 226
ethylenediamine, 25
ethylenediaminetetraacetate, 138
4-ethylmethoxybenzene, 353
4-ethylnitrobenzene, 353
Evonik, 11, 476, 483, 488. *See also* Degussa
explosive regime, 5, 12, 504

fabric catalysts, 299
fatty acid methyl esters, unsaturated, 175
Fe zeolites, 33
  Fe-Beta, 47
  Fe-ZSM-5, 33
Fe/SBA-15
  hydroxylation of benzene, 167
  oxidation of benzyl alcohol, 182
  oxidation of toluene, 168
Fe^{III}-$O^{\bullet}$, 70
Fe^{IV}-$O^{\bullet}$, 70
Fe-MCM-41, 153
  Baeyer–Villiger oxidation, 183
Fe-MCM-48
  Baeyer-Villiger oxidation, 183
Fermi level, 432
flavor and fragrances, 180, 181, 184, 225, 226, 349, 431, 432, 452
fluorene, 391
fluoride medium, 22, 31, 33, 52, 101, 102, 133
formaldehyde, 299, 342, 425
2-formylcinnamaldehyde, 427
fouling, 46, 194, 234, 254, 499
FT–IR spectroscopy, 27–28, 32, 105
  probe molecules, 106, 132, 193
furfuryl alcohol, 42

geraniol, 56, 177, 178, 290, 291, 431
gluconic acid, 222, 241, 243
glucose oxidase, 242
glucose, oxidation, 241–43
  H_2O_2 byproduct, 243
  kinetic studies, 243
glutaraldehyde, 179
glutaric acid, 298
glycal, 345
glyceraldehyde, 237, 432
glyceric acid, 235, 236, 237, 238, 241, 252, 359
glycerol, oxidation, 113, 234–38, 359
  H_2O_2 byproduct, 236, 237
glycidol, 55, 252
glycolic acid, 60, 236
glycols. *See* diols
gold catalysis, base-assisted
  alcohol oxidation, 229, 230, 232
  aminoalcohol oxidation, 244
  glycerol oxidation, 236

gold catalysts
  Au/Al_2O_3, 228, 231, 244
  Au/Beta, 232
  Au/C, 226, 228, 231, 234, 236, 240, 242, 244, 247, 251, 253, 256
  Au/CeO_2, 232, 239
  Au/CPL-2, 385
  $Au/CuMg_xAl_yO_z$, 232
  Au/Fe_2O_3, 233
  $Au/Ga_3Al_3O_9$, 398
  Au/graphite, 225, 228, 235
  Au/MCM-41, 224
  $Au/MgAl_2O_4$, 233
  Au/MIL-101, 385, 398
  Au/MIL-53, 398
  Au/MOF-5, 385, 398
  Au/polymer beads, 243
  $Au^{(I)}$(rutin) complexes, 225
  Au/TiO_2, 226, 227, 231, 232, 233, 240, 244, 247, 248, 249
  Au/TS-1, 232, 487
  Au/U_2O_3, 232
  Au/Y, 232
  Au/ZMS-5, 224, 232
  $Au/[Zn_4O(BDC)_3]$, 385
  Au/ZrO_2, 231, 242
  Au_6-Au_{10} clusters, 227
  Au-Ag leached alloy, 243
  Au-Ag/C, 241
  $Au\text{-}Co/TiO_2$, 226
  Au-Cu/C, 241
  $Au\text{-}Cu/TiO_2$, 226
  $Au\text{-}Pd/Al_2O_3$, 228, 232
  Au-Pd/C, 225, 236, 241, 255, 238
  Au-Pd/carbon nanofibers, 238
  Au-Pd/carbon nanotubes, 238
  $Au\text{-}Pd/CeO_2$, 232, 239
  $Au\text{-}Pd/Fe_2O_3$, 232
  Au-Pd/graphite, 235, 236
  Au-Pd/polyvinylpyrrolidone, 239
  $Au\text{-}Pd/SiO_2$, 226, 236
  $Au\text{-}Pd/TiO_2$, 225, 232, 236
  $Au\text{-}Pd/TiSiO_2$, 236
  Au-Pt/C, 241, 244
  Au-Rh/C, 244
  $Au\text{-}Ru/TiO_2$, 226
  colloidal Au, 222, 223, 230, 242, 243, 247, 249, 253, 285, 294, 439
gold catalysts, activity
  improvement by metal alloying, 224
  mechanistic aspects, 250–54
  oxygen activation, 251
  particle size effect, 222, 228, 243, 244, 250
gold catalysts, characterization, 224
gold catalysts, oxidation of
  alcohol compounds, 228–41
  alkanes, 224–25
  alkylaromatics, 225–26
  amines, aminoalcohols, 244–45
  aniline, pyrrole (polymerization), 245–50

glucose, 241–43
olefins, 226–28
gold catalysts, stability, 254–56
improvement by metal alloying, 255
improvement by pretreatment, 254
on recycling (Au/C), 241
gold catalysts, synthesis, 222–24
colloidal Au, protected, 223
colloidal Au, supported, 223, 231, 235
deposition-precipitation (DP), 222
DP, NaOH, 223
DP, urea, 223
impregnation, 222, 235
in situ supporting, 245
solid grinding method, 242
gold catalysts, oxidation mechanisms 250–54
of alcohols, role of bases, 251
of allyl alcohol, 252
of benzyl alcohol, 253
of glucose, 253
gold sols, protected, 223
grafted catalysts, 161, 169, 171, 173, 178
Ta/SBA-15, 178
Ti/MCM-41, 159, 160, 172, 177
Ti/SiO_2, 159, 160, 172, 187
grafting, 156, 158, 159, 325

H_2O_2. *See* hydrogen peroxide
H_3BO_3, 32
Haber-Weiss mechanism, 4, 6, 401
Halcon/ARCO process (PO), 8, 477, 478
Hampson-Linde process, 3
hard template, 26, 44
n-heptane, 37, 167, 187, 190, 239, 341
n-hexane, 36, 37, 39, 66, 76, 107, 119, 164, 166, 341, 359
n-hexanol, 231
n-hexyl amine, 245
heteropoly acid, 269, 272, 308
$H_3PMo_{12}O_{40}$, 269, 279, 292, 430
$H_{3+n}PMo_{12-n}V_nO_{40}$, 287
$H_5PMo_{10}V_2O_{40}$ ($H_5PV_2Mo_{10}O_{40}$), 272, 278, 284, 294, 297
$H_6PMo_9V_3O_{40}$, 287, 288
$H_3PW_{12}O_{40}$, 269, 272, 273, 279, 420, 425, 434, 435
$H_5PW_{11}TiO_{40}$, 268, 269, 295, 296
heteropoly anion, 266, 266, 270, 277, 308. *See also* polyoxometalate
heteropolytungstate, 281
2,2′,3,3′,5,5′-hexamethyl-4,4′-biphenol, 170
hexamethyleneimine, 32
1,6-hexanediamine, 25, 245
2-hexanol, 36
3-hexanol, 36, 60
1-hexene, 49, 50, 52, 66, 68
2-hexene, 49, 436
hierarchical porosity
meso-Ti-MOR, 47, 63
meso-TS-1, 26, 37, 47, 50, 66
hierarchical structure, 26, 127, 139, 198, 335
hierarchical zeolites. *See* Ti zeolites, mesoporous
high resolution transmission electron microscopy (HR TEM), 129
Hock rearrangement, 480
homolytic pathway, 37, 43, 69, 71, 116, 192, 306
hot filtration test, 78, 164, 166, 167, 168, 176, 180, 182, 188, 197, 287, 288, 292, 295, 302, 348, 363, 404
HPA. *See* heteropoly anion
HPPO process, 9, 460, 476, 483–87, 488
industrial plants, 486
hybrid materials, organosilicas, 325–26
hybrid mesostructured materials, 162
hybrid organic–inorganic materials, 162
hydrazine, 65
hydrazones (tosyl-), oxidation, 65
hydrodesulfurization (HDS), 65, 186
hydrogen bonding, H_2O_2 activation, 68, 71, 192
hydrogen peroxide, 2, 9–14, 504
anthraquinone process (AO), 9–11
direct synthesis, 11–14, 55
in situ generation, 53, 54, 57
industrial uses, 9
world production, 9
hydrogen peroxide, activation
by hydrogen bonding, 192
by lattice Ti, 66–68
metal-catalyzed, 14
hydrogen peroxide, decomposition, 53, 61, 75, 76, 169, 307
by extralattice Ti, 43, 453
by lattice Ti sites, 74
by metal impurities (soluble), 459
in HPPO effluent, 485
hydrogen peroxide, oxidation byproduct, 236, 237, 243, 431
hydrogen-bonding interactions, 137
hydroquinone, 41, 42, 44, 46, 169, 307, 385, 430
global capacity, 452
hydrotalcites. *See* layered double hydroxides
hydrothermal stability, 22, 119, 133, 139, 140, 143, 185, 197–200, 280, 309, 402–3
hydrothermal synthesis, 22, 23, 101, 138, 150, 153, 549 102, 138, 146, 150, 153, 378
alkaline conditions (OH^-), 22, 30
fluoride conditions (F^-), 22, 31, 101, 102
microwave (MW) assisted, 146
hydroxyacetone, 60, 61, 431, 471
p-hydroxyacetophenone, 61, 472
p-hydroxybenzaldehyde, 109, 112, 117
2-hydroxybenzyl alcohol, 172, 233
hydroxyl radicals, 39, 43, 109, 117, 189, 190, 330, 414, 423, 427, 429, 430
hydroxylamine, 62, 73 114, 463, 467, 471
hydroxylation of
alkanes, 34–40, 69–71
benzene, 40–43, 382, 427
phenol, 43–46
3-hydroxypropionic acid, from allyl alcohol, 239, 241, 252, 255, 256
proposed mechanism, 240

8-hydroxyquinoline, 356, 385, 399
4-hydroxytoluene, 112

I.G. Farben, 462
IBA. *See* isobutyraldehyde
IHS Inc, 479, 488
imines, 64, 245, 386
impregnation, 25, 158, 173, 178, 180, 198, 222, 223, 231, 235, 251, 265, 271, 283, 292, 298, 308, 335, 339, 343, 356, 400, 418, 424, 434, 439, 441
indane, 225, 391
Indinavir, 6
indoline, 245
International Zeolite Association (IZA), 22
iodoso benzene, 2
ion-beam implantation, 158
ionic liquid-modified SiO_2, 278, 290, 297, 302
ionic liquids, 102, 186, 278, 323, 433, 434
ionothermal synthesis, 102
isoamyl butyrate, 60
isobutyraldehyde, 298
isolongifolen-9-one, 181
isolongifolene, 181
isomorphous substitution, 23, 78, 97
  Pauling criterion, 23
  unit cell variation, 23, 103
isonicotinic acid, 116
isopentyl phenyl sulfide, 185
β-isophorone, 334, 349
isopulegol, 59, 175
isopulegol epoxide, 177

Joule-Thomson effect, 3

K-A oil, 163, 224
ketones. *See also* carbonyl compounds
  ammoximation, 61–63, 185
  Baeyer-Villiger oxidation, 183–84, 360
kinetic isotope effect, 39, 70, 254, 340, 341, 401
kinetic resolution 186, 362
kinetic studies
  ammoximation, 62
  epoxidation of allyl choride, 57
  epoxidation of olefins, 50
  hydroxylation of alkanes, 39
  hydroxylation of phenol, 44
  oxidation of alcohols, 60, 239
  oxidation of glucose, 243
  oxidation of S-compounds, 65, 66

lactic acid, from glycerol, 235
Langmuir-Hinshelwood approach, single site catalysts, 45, 50
Langmuir-Hinshelwood, rate law, 44, 46, 50, 60, 239
lattice Ti content
  efforts to increase it, 24
  upper limit in TS-1 and Ti-Beta, 24, 31
laurolactam, 471
layered double hydroxides, 267, 279, 290
LDHs. *See* layered double hydroxides
Lewis acid sites, 28, 97, 131, 193
Lewis acidity, 116, 158
limonene, 51, 110, 173, 174, 177, 181, 288, 292, 345, 381, 383, 393
linalool, 56, 59
Linde division, 451
lithium acetate, 37
lithium chloride, 37
local cell mechanism, 414
Löwenstein's rule, 99
Lyondell, 476. *See* Halcon/ARCO for PO process
Lyondell-Basell, 9

M41S family, 128, 137, 139
magnetic core, 146, 185
maleic acid, 234
malonic acid, 234
MAPO-*n*. *See* aluminophosphates
Mars-van Krevelen mechanism, 4, 307
mechanical stability, 157, 195, 469, 499
melonal, 184
trans-p-menth-6-ene-2,8-diol, 59
Merox process, 331
mesophase, 129, 138
mesoporous metal silicates, characterization, 129–32
  bulk techniques, 131
  surface techniques, 131
mesoporous metal silicates, mechanistic aspects, 189–94
  Sn-, Baeyer-Villiger oxidation, 193
  surface role, 189
  Ti-, epoxidation, 190–92
  Ti-, model compounds, 191–92
mesoporous metal silicates, oxidations
  allylic C-H oxidation, 180–82
  ammoximation, 185
  Baeyer-Villiger oxidation, 183–184
  epoxidation of olefins, 172–78
  oxidation of alcohols, 182
  oxidation of alkanes, 163–67
  oxidation of alkylaromatics, 168–69
  oxidation of amines, 188–89
  oxidation of arenes, 167–68
  oxidation of phenols and naphthols, 169–72
  oxidation of S-compounds, 185–88
  oxidative cleavage of olefins, 178–79
mesoporous metal silicates, stability, 194–200
  deactivation mechanisms, 194–97
mesoporous metal silicates, synthesis
  general approaches, 128–29
  post-synthesis modifications, 156–61
  sol-gel, amorphous mixed oxides, 132–36
    other mixed oxides, 135
    titania-silica, 133–35
  templated method, 136–56, 162–63. *See also* mesostructured materials
  thermolytic method, 136

mesoporous region, 127
mesoporous silica, supports, 156–57
mesostructure, 129, 130, 137, 139
mesostructured cellular foam (MCF), 140
mesostructured metal silicates, 140, 143–56
  cerium silicates, 147, 179
  chromium silicates, 110, 150–51, 164–66, 168–69, 180–81, 189, 418, 424
  cobalt silicates, 108, 155–56, 164–65, 178, 181, 182
  copper silicates, 156,
  iron silicates, 153–54, 164, 167, 168, 182, 183
  manganese silicates, 154–55, 167, 178
  molibdenum silicates, 151–52
  niobium silicates, 149–50, 177
  tin silicates, 147, 169, 183–84
  titanium silicates, 143–46, 166–77, 179, 182, 185–89, 199
  tungsten silicates, 152, 178–79
  vanadium silicates, 148–49, 167–70, 182, 189, 425, 437
  zirconium silicates, 146–47, 169, 182, 188
mesostructured silicates, 136–42. *See also* ordered mesoporous silica
  hydrothermal stability, 195–99
  mechanical stability, 194
  thermal stability, 195
mesostructured titanium silicates, 143–46
  MTS-9, 143, 144, 169
  Ti-HMS, 110, 143, 144, 168–170, 186
  Ti-MCM-41, 76, 143, 144, 162, 164, 166, 167–169, 172–177, 185, 187, 188, 190, 195, 199, 433
  Ti-MCM-48, 143, 144, 166, 173, 174, 199
  Ti-MMM, 143, 144, 170, 174, 185–86, 199
  Ti-MMM-1, 143, 145, 166, 167
  Ti-MMM-2, 143, 145, 153, 167, 172, 174, 179, 182, 185–86, 190, 199, 200, 233–34
  Ti-MMS, 143, 144, 169
  Ti-MSU-1(2), 143, 144
  Ti-MSU-G, 143, 144, 198, 199
  Ti-SBA-1, 143, 144
  Ti-SBA-15, 74, 143, 145, 162, 172, 176, 186, 188, 199
  Ti-TUD-1, 143, 144, 174, 176
metal alkoxides, 132
metal complexes (supported)
  Co(bipy)/SBA-15, 353
  Co(salen)/SBA-16, 362
  CoPc/MCM-41, 339
  CoPc/zeolite Y, 339
  $CoPcF_{16}$/MCM-41, 339
  $CoPcF_{16}$/zeolite X, 327
  $CoPcF_{16}$/zeolite Y, 339
  CoPcS/chitosan, 350
  CuPc/MCM-41, 339
  CuPc/zeolite Y, 339
  $CuPcF_{16}$/zeolite X, 327
  FDMS/MIL-53, 382
  FePc/C, 339
  $FePcCl_{16}/SiO_2$, 359
  $FePcF_{16}$/MIL-101, 328, 340, 382, 392
  $FePcF_{16}$/zeolite X, 340
  $FePc(NO_2)_4$/zeolite Y, 339
  $(FePc)_2N/SiO_2$, 343
  FePc/PDMS, 340
  FePcS/chitosan, 350
  FePcS/MIL-101, 328, 387, 399
  FePcS/MCM-41, 352, 353
  $FePcS/SiO_2$, 359, 350, 352–354, 359, 399
  $FePcS/TiO_2$, 350
  $(FePctBu_4)_2N$/MIL-101, 392, 393
  FePc/Y-PDMS, 340
  FePc/zeolite Y, 339
  Fe(salan)/SBA-16, 360
  $Fe(TDCPP)/SiO_2$-Im, 344
  $Fe(TDCPP)/SiO_2$-Py, 344
  $Mn(acac)_2$/IRMOF-3, 394, 384
  MnPcS/MCM-41, 353
  $MnPcS/SiO_2$, 353
  Mn-porphyrin/*rho*-ZMOF, 337
  Mn(salen)/PDMS, 508, 353
  $Mn(TDCPP)/SiO_2$-Im, 344
  $Mn(TDCPP)/SiO_2$-Py, 344
  MnTMPyP/montmorillonite, 330
  $Mn(tmtacn)/SiO_2$, 350
  $Mn(tmtacn)/SiO_2$-COOH, 337, 350
  MnT(4-carboxy)PP/ MgO, 330
  $MnT(4\text{-carboxy})PP/Al_2O_3$, 330
  $MnT(4\text{-sulfonato})PP/Al_2O_3$, 330
  MnT(4-sulfonato)PP/MgO, 330
  M-POM/MIL-101 (M = Ti, Co), 282, 296, 309, 383
  Pd porphyrin/MOF, 348
  PW*x*/MIL-101 (x = 4 or 12), 293, 383, 393
  Ru(II) 5,10,17-(tris(4-R-phenyl)-20-(4-hydroxyphenyl)porphyrins (R = Cl, Me)/ Merrifield resin, 345
  $Ru(III)(tmtacn)/SiO_2$, 356
  $RuPcF_{16}$/MIL-101, 328, 340, 382, 392
  $RuPcF_{16}$/zeolite X, 340
  RuT(4-chloro)PP /MCM-41, 344
  RuTDCPP/MCM-41-amine, 345
metal complexes (supported), chiral
  Co(salen), encapsulated, 327
  D_4-symmetric Ru porphyrin/MCM-41, 346
  D_4-symmetric Ru porphyrin/MCM-48, 346
  D_4-symmetric Ru porphyrin/SiO_2, 346
  Mn(salen)/MCM-41, 351
  Mn(salen)/SBA-15, 351
  $Mn(salen)/SiO_2$, 351
metal complexes (supported), oxidation of
  alcohols, 356–59
  alkanes, 339–44
  aromatic hydrocarbons, 352–53
  miscellanea, 359–62
  olefins, 344–52
  phenol compounds, 353–56
metal complexes (supported), stability, 362–64

metal complexes (supported), synthesis
chiral complexes, 337–38
metal phthalocyanines, 326, 331–36
metal porphyrins, 329–31
metal salen, 327, 336
metal tmtacn, 327, 337
synthetic strategies, 324–29
metal complexes, characterization, 324
metal complexes, immobilization, 323–24
metal ion implantation, 433
metal leaching, 47, 56, 77–78, 107, 109, 110, 113, 119, 129, 149, 152, 161, 163, 164, 165, 168, 170, 180, 182, 194, 196, 200, 254, 350, 363, 404, 439, 438, 443, 499
Cr zeolites, 77
Ti zeolites, 51, 56, 77
V zeolites, 40, 46, 47, 77
metal nanoparticles (NP), 230
Au(NP), D-glucose-stabilized, 223
Au(NP), polyvinylalcohol-stabilized, 223, 231
Au(NP), polyvinylpyrrolidone-stabilized, 223, 230
Au(NP), supported, 231
Pd(NP), 230
metal zeolites, stability, 77–78, 118–19
metal-organic framework. *See* MOF
metal-substituted APO-*n*, 97–99
metal-substituted SAPO-*n*, 98
methallyl chloride, 56
methane, 425
oxidation on $(FePc)_2N$, 341–44
1-methoxy-2-propanol, 483
2-methoxy-1-propanol, 484
4-methoxybenzyl alcohol, 432
o-methoxyphenol, 47
p-methoxyphenol, 47
methyl benzoate, 385
methyl diepoxystearate, 177
methyl elaidate, 175
methyl heptanoate, 37
methyl linoleate, 175
methyl oleate, 175
methyl phenyl sulfide, 185, 303, 386
methyl phenyl sulfoxide, 386, 400
methylamine, 25
4-methylbenzyl alcohol, 432
methylcyclohexane, 167, 190
methylcyclohexanones, 61
2-methyl-1-butene, 48
2-methyl-2-butene, 48
3-methyl-1-butene, 48
1-methyl-3-ethyl imidazolium bromide, 102
2-methyl-1-naphthol, 172, 233
2-methyl-1,4-naphthoquinone, 47, 168, 233, 352. *See also* vitamin K_3
2-methyl-2-pentene, 49
1-methylcyclohexene, 49, 110
1-methylcyclopentene, 51
p-methylethylbenzene, 46
2-methylnaphthalene, 47, 172, 352
methylphenylketone, 348
α-methylstyrene, 351, 352, 482
cis-β-methylstyrene, 351, 352
trans-β-methylstyrene, 350
microcalorimetry, 32
microwave heating, 102, 137, 146, 178, 334, 380
mixed alkoxide method, 24
mixed oxides, 128, 197
ceria–silica, 165
niobia–silica, 135, 172, 178
silica–chromia, 181
tantala–silica, 178
titania–silica, 133, 174, 188
vanadia–silica, 135
WO_3–SiO_2, 136, 178
zirconia–silica, 135
Mn-TUD-1, 155
alkene epoxidation, 178
Mobil Oil, 128, 136, 451
MOF-immobilized complexes
FePcS/MIL-101, 328, 387, 399
$(FePctBu_4)_2N$/MIL-101, 393
$Mn(acac)_2$/IRMOF-3, 384, 394
Mn-porphyrin/*rho*-ZMOF, 389
$MPcF_{16}$/MIL-101 (M = Fe, Ru), 341, 393, 402
MOF-immobilized POMs
M-POM/MIL-101 (M = Ti, Co), 282, 296, 309, 383
$PMo_{10}V_2$/MIL-101, 297
$PW_{11}Co$/MIL-101, 295
$PW_{11}Ti$/MIL-101, 293, 295
PW_{12}/MIL-101, 292, 293
PW*x*/MIL-101 (*x* = 4 or 12), 292, 293, 383, 393
MOFs, 280, 328, 371
Basolite F300, 380, 392
Basolite Z1200, 380
$[Cd_{1.25}Pd\text{-}H_{1.5}TCPP(H_2O)]$, 383, 387, 397
CPO-27, 374, 376, 377, 383
[Cu(2-hydroxypyrimidinolate)$_2$] [Co(phenylimidazolate)$_2$], 382
$[Cu(BPY)(H_2O)_2(BF_4)_2(BPY)]$, 383
$[Cu(H_2BTEC)(BIPY)]$, 383
$\{[Cu_2(4,4\text{-}BIPY)_4(H_2O)_4]\text{-}(SiW_{12}O_{40})(H_2O)_{18}\}_n$, 382
$\{[Cu_3(C_9H_3O_6)_2]_4\}_n$, 303
$[Cu_6(H_2tea)_6Fe(CN)_6]_n(NO_3)_2]_n$, 381
$[Cu_6(Hmdea)_6Fe(CN)_6]_n(NO_3)_2]_n$, 381
$[Cu^{II}(BPED)_2(H_2O)_2(X)]$ (X = SiF_6, NO_3), 382, 391
Cu_2(*trans*-1,4-Cy), 385
$Cu_3(H_2tea)_2(4\text{-}OC_6H_4COO)_2(H_2O)]\cdot 4H_2O$, 381
$[Cu_3(\mu_3\text{-}OH)(\mu\text{-}pz)_3(EtCO_2)_2(H_2O)]$, 381, 388
Fe(BTC), 388, 392
Fe-EMOF, 380
HKUST-1, 282, 374–75, 376, 379–81, 382, 385, 403
$In_2(OH)_3(BDC)_{1.5}$, 386
$[InN_4(CO_2)_4][H_2TMPyP]$, 381
IRMOF-3, 384, 394
magnesium formate, 379

$[M_3(BTC)_2]$ (M=Cu,Co, Ni), 385
MFU-1, 383, 394, 401
MIL-100, 374, 375, 379–82, 386, 391, 392, 403, 404
MIL-101, 281, 282, 292–97, 307, 328, 341, 374, 375, 379, 380–83, 385–387, 389, 390, 392–94, 398, 399–404
MIL-47, 374, 377, 378, 383, 403
MIL-53, 379, 382, 398, 403
MOF-5, 385, 394, 398, 399, 403
MOF-74, 374, 376, 385, 403
MOF-199, 282
$NH_4[Cu_3\text{-}(\mu_3\text{-}4\text{-carboxypyrazolato})_3]$, 383
$Pd(O_2CCF_3)_2[O_2C–C_5H_3N–C_5H_3N–CO_2]$ Cu, 385
$[Pd(2\text{-pymo})_2]_n$, 385
$Pd(TFA)_2BPy\text{-}Cu$, 399
rho-ZMOF, 389
$[Sc_2(C_8H_4O_4)_3]$, 386
$Sc_2(NDS)(OH)_4$, 386
UiO-66, 374, 377, 379
[Yb(OH)(2,6-AQDS)(H_2O)], 386
Zn-EZIF, 380
MOFs, active sites, 380–88
encapsulated metal complexes, 381
encapsulated nanoparticles, 381
framework metal centers, 380–87
framework-bonded metal complexes, 387
MOFs, general features, 371–73
MOFs, homochiral
[bis(catechol)salen]$Mn^{III}Cl$] (Poly(Cu-1)), 384, 395
CMOFs (chiral metal-organic frameworks), 387, 396
Mn(III) phorphyrincarboxylate, 387
$[Ni_3(bpdc)(RR\text{-}L)_2\cdot(DMF)]_n$, 383, 387, 396
$[Ni_3(bpdc)(SS\text{-}L)_2\cdot(DMF)]_n$, 387
$Zn_2(BDC)(L\text{-}Lac)(DMF)]\cdot DMF$, 386, 400
$Zn_2(bpdc)_2L\cdot 10DMF\cdot 8H_2O$, 383, 395
ZnMn-RPM, 397
MOFs, oxidation
mechanistic aspects, 400–402
of alcohols and phenols, 398–99
of alkanes, 388–89
of aromatic compounds, 389–93
of olefins, 393–97
of sulfides, 399–400
MOFs, stability, 402–404
hydrothermal, 402–404
thermal, 402, 404
to metal leaching, 404
MOFs, structures, 374–78
CPO-27, 374, 377
HKUST-1, 374, 376
MIL-100, 374, 375
MIL-101, 374, 375
MIL-47, 374, 378
MOF-74, 374, 376
UiO-66, 374, 379
MOFs, supported
MIL-101 on monolith, 382, 390
MOFs, synthesis, 378–80
electrochemical, 380
hydrothermal, 378–79
microwave, 380
solvothermal, 378–79
MOF-supported metals
Au/CPL-2, 385
Au/MIL-101, 385, 398
Au/MIL-53(Al), 398
Au/MOF-5, 385, 398
$Au/[Zn_4O(BDC)_3]$, 385
Pt/MOF-177, 385
Pt/MOF-5, 385
molecular adsorbates, 131
molecular convolution, 273
molecular designed dispersion (MDD), 158
molecular models, 191
molecular precursors, 136, 196
monooxygenase enzymes, 70, 322
MMO, 34, 35, 70, 335, 341, 342
P450 type, 34, 70, 322, 329, 335, 363
Montedipe, 467
MSAPO-*n*. *See* metal-substituted SAPO-*n*
MTBE (methyl *tert*-butyl ether), 7, 475
MTS-9, 143
oxidation of phenol, 169
mustard gas simulant, 301

N-(4-aminophenyl)aniline, oxidative polymerization, 246
N,N′-diethyl hydroxylamine, 64
nanocomposite, 269, 271, 291, 292, 433, 435
nanosized Au, 222
nanosized CeO_2, 232
nanosized TiO_2 415, 416, 429
NaOCl (oxidant), 352, 359, 396
naphthalene, 47, 168, 427
1-naphthol, 169
1,4-naphthoquinone, 47, 169, 382, 427
1-naphtylamine, 64
Nb-MSU-X
alkene epoxidation, 177
nerol, 56
neutron powder diffraction, 27, 45, 130
Nexant, 482, 486
NH_2-modified silica, 267, 276, 283, 300
$(NH_4)_2SO_4$; 25; 461; 464; 470
N-heterocycles, oxidation, 65
N-hydroxyphthalimide (NHPI), 372, 381, 386
4-nitrobenzyl alcohol, 432
nitrogen adsorption isotherms, 30, 129, 199, 324
nitrosobenzene, 64, 188
NMR. *See* nuclear magnetic resonance spectroscopy
2-nonanol, 119
norbornadiene, 290
norbornene, 51, 111, 173, 288, 345, 351
exo-norbornene oxide, 111

nuclear magnetic resonance spectroscopy
^{27}Al MAS NMR, 105, 156
^{1}H→^{29}Si CP MAS NMR, 32, 286
^{17}O MAS NMR, 66, 134
^{31}P MAS NMR, 105, 298
^{29}Si MAS NMR, 30, 32, 130, 133, 134, 142, 147, 148, 150, 155, 162: 196, 198, 199
^{119}Sn MAS NMR, 33, 147
^{51}V MAS NMR, 148
Nylon-6, 163, 462, 463, 471
Nylon-6,6, 163

O_2/aldehyde (oxidant), 110, 116, 183, 299, 300, 299–301, 348, 360, 394
octanal, 112, 385
n-octane, 37, 166, 167, 190, 341
1-octanol, 112, 231, 269, 385
2-octanol, 112, 359
1-octene, 176, 292, 294, 345, 351, 393
2-octene, 291
olefins, co-oxidation with aldehydes on supported POMs, 299–301
olefins, epoxidation. *See also* propylene
asymmetric, 387, 394–97
continuous flow, 51
on large pore zeolites, 51–52
Ti-MWW specificity, 52
on metal complexes, 344–52
on metal-silicates, 172–78
on supported POMs, 288–94
on TS-1, TS-2, 48–51
proposed mechanisms, 71–72
side reactions, 47, 49, 51, 75
surface hydrophobicity, 51, 76, 176
olefins, epoxidation (photo), 437
mechanism of Ti catalysts, 436
olefins, oxidation
allylic, 180–2
cis-dihydroxylation, 350
on Au catalysts, 226–28
on metal complexes, 344–52
on metal-organic frameworks, 393–97
on supported POMs (allylic), 294–97
oxidative cleavage, 178–79
to glycols, 58
olefins, oxidative bromination, 437
O-O peroxide bond, 3, 5
ordered mesoporous silica, 136, 141–42, 269, 308
COK-11, 196
COK-12, 141, 196
FDU-5, 142
FSM-16, 137, 141
HMS, 138, 141, 195, 248, 294,
KIT-1, 138, 141, 158, 169, 195, 198
MCF, 140, 142, 178, 194, 274, 275, 294, 300, 310
MCM-41, 138, 141, 274, 277, 284, 287, 288, 289, 300, 308, 309, 351, 359, 426
MCM-48, 138, 141, 277, 303
MCM-50, 138
MSU-F, 139
MSU-G, 139, 141, 198
MSU-H, 139, 141
MSU-X, 139, 141, 194
PHC, 137, 141
SBA-1, 141
SBA-15, 139, 142, 198, 259, 270, 274, 275, 277, 278, 286, 287, 288, 294, 297, 298, 300, 303, 308, 310, 351;353, 420, 426, 441
SBA-16, 142
SBA-3, 142, 277, 303
TUD-1, 139, 141;199
organic linkers for MOFs, 372, 374, 376, 377
1,4-benzenedicarboxylate (BDC), 374, 376, 379
1,3,5-benzenetricarboxylate (BTC), 374, 375, 379
1,4-bis[3,5-dimethyl]-pyrazol-4-yl) benzene, 394
2,5-dihydroxybenzenedicarboxylate (DHBDC), 374, 376
dicarboxylic acids, 377
2,5-dihydroxyterephthalate (DHTP), 374, 376
organic-inorganic ionic hybrid materials, 280
organometallic precursors, 159
organosilicas, synthesis, 325–26
oxidants
engineering issues, 503–6
general features, 2
oxidation
heterolytic mechanism, 4, 6
homolytic mechanism, 3
oxidation of (*See also* epoxidation, hydroxylation)
alcohols, 59–60, 72, 182, 228–41, 297–98, 356–59, 398–99, 430–6
aldehydes, 298–99
alkanes, 106–8, 163–67, 224–45, 287–88, 339–44, 388–89, 422–26
alkylaromatics, 47, 109, 168, 353
alkynes, 359
aromatic compounds, 167–72, 288, 352–53, 427–30
benzene, 108, 117
carbohydrates, 241–3
carbonyl compounds (Baeyer-Villiger), 15, 63, 116, 183–84, 360
carbonyl compounds/NH_3 (ammoximation), 61–63, 114–15, 185
N-compounds, 63–65, 116, 188–89, 244–45
olefins, 110–1, 226–28, 344–52, 393–97, 436–38
olefins (allylic), 294–97
phenol and phenolic compounds, 113–14, 169–72, 353–56, 399
S-compounds, 65–66, 185–88, 301–4, 399–400
oxidative cleavage, 60, 178–79
oximes
in situ formation, 62
oxidation, 65

oxydehydrogenation, 288, 306
oxygen (oxidant), 2, 3–5, 233, 243, 503
  explosive gas mixtures, 5
  metal-catalyzed activation, 4
  photoactivation, 414
oxygen rebound mechanism, 70

P123. *See* Pluronic 123
palladium catalysts
  Pd leaching and sintering, 238
  Pd/C, 226, 236, 238
  Pd/carbon nanotubes, 238
  Pd/CeO_2, 232, 239
  Pd/TS-1, 40, 53, 57, 487
palladium catalysts, oxidation
  of alcohols, 230, 231
  of glycerol, 236
Paracetamol (4-acetaminophenol), 61, 471
particle size degradation, 499
partition coefficients, 44, 49, 66, 76
Pauling criterion, 23
PCl_3, 103
pentanal, 435, 441
n-pentane, 37, 341
1,4-pentanediol, 431
1,5-pentanedithiol, 386
1-pentanol, 166, 431, 435, 436, 441, 442
3-pentanol, 435
3-pentanone, 435
trans-2-penten-1-ol, 431
1-pentene, 51
peracetic acid, 504
periodic mesoporous organosilica (PMO), 163, 164, 199
pernigraniline (polyaniline), 246
peroxotungstate, 278, 284
peroxytitanates method, 24
PFe^{IV}=O, (P = Porphyrin), 330
"pH-adjusting" method, 140
phenanthrene, 427
phenol, deep oxidation, 234
phenol, hydroxylation, 43–46, 113, 385
  continuous flow, 44
  o- and *p*-attack, competition, 45
  proposed mechanisms, 71
phenol, hydroxylation (industrial)
  Brichima process, 452
  commercial processes features, 456
  EniChem process, 456–60
    process development, 453–5
    TS-1 development, 453–54
  Rhône-Poulenc process, 456
phenol, photo-oxidation, 427
  photobromination, 437
phenolic compounds, oxidation, 169–72, 353–56, 387
phenols (substituted), oxidation to quinones, 354
phenols (substituted), oxidative coupling, 234
phenyl acetylene, 42
1-phenyl-1-butyne, 359
1-phenyl-1-propanol, 359
3-phenyl-1-propanol, 231
1-phenyl-1-propanone, 359
β-phenylacetaldehyde, 58
2-phenylethane-1,2-diol, 60
1-phenylethanol, 8, 54, 239, 359, 382, 385, 398, 399
PhIO (oxidant), 2, 330, 344
photoactivation
  polyoxotungstates, 418
  single site Ti oxides, 417
  tetrahedral chromate species, 424
photoactivation of oxygen, 414
photocatalysis
  molecular shave selectivity, 429
  photoexcitation of Ti catalysts, 417
  primary photoprocesses, 413, 418
  size screening, 429
  surface effects, 423, 426, 427, 428, 431, 434, 435, 437
  texture and composition of catalysts, 412
photocatalysts
  Cr-MCM-41, 424, 425
  CrO_x-SiO_2 mixed oxide, 417, 424, 437
  ETS-10, 429
  $PW_{12}O_{40}^{3-}$/MCM-41, 434
  $PW_{12}O_{40}^{3-}$/SiO_2, 420, 434, 435
  $PW_{12}O_{40}^{3-}$/ZrO_2, 420, 435
  $SiW_{12}O_{40}^{4-}$/SiO_2, 420
  Ti-MCM-41, 417, 433
  TiO_2, 427, 429, 430, 433, 436, 437
    anatase, 416, 429, 430, 432, 433
    brookite, 416, 432
    Degussa P25, 427, 428, 431, 432, 433, 436
    rutile, 599, 432
  TiO_2, fluorinated, 427
  TiO_2, mesoporous, 415, 424
  TiO_2, metal-modified, 424, 427, 433, 439
  TiO_2, N-, S-doped, 432, 439
  TiO_2, pillared clays, 416, 427
  TiO_2/zeolites, 416, 427, 429
  TiO_2-SiO_2 mixed oxides, 415, 416, 427, 436
  TS-1, 430
  TS-2, 430
  V_2O_5/SBA-15, 418, 425
  V_2O_5-Al_2O_3, 425
  V_2O_5-SiO_2 mixed oxides, 418, 425
  V-MCM-41, 425
  V-TUD-1, 437
  $W_{10}O_{32}^{4-}$/Amberlite, 420, 437, 441
  $W_{10}O_{32}^{4-}$/Ambersorb, 441
  $W_{10}O_{32}^{4-}$/Hyflon, 421, 426
  $W_{10}O_{32}^{4-}$/MCM-41, 426, 441
  $W_{10}O_{32}^{4-}$/organosilica, 420, 435
  $W_{10}O_{32}^{4-}$/organosilica (SBA-15), 420
  $W_{10}O_{32}^{4-}$/PDMS, 421, 442
  $W_{10}O_{32}^{4-}$/PVDF, 421, 422, 442
  $W_{10}O_{32}^{4-}$/polyvinyl pyridine, 426
  $W_{10}O_{32}^{4-}$/SBA-15, 426, 441
  $W_{10}O_{32}^{4-}$/SiO_2, 420, 426, 434, 435, 437, 441
  $W_{10}O_{32}^{4-}$/ZrO_2, 420, 435, 442
  $W_{10}O_{32}^{4-}$/γ-Al_2O_3, 434, 441

photocatalysts, preparation
highly dispersed metal oxides, 416–18
polyoxotungstates, supported, 418–22
TiO_2, 413–16
photocatalysts, stability, 438–43
photocatalysts, UV-vis
CrO_x-SiO_2, 418
TiO_2, 432
V_2O_5-SiO_2, 418
$W_{10}O_{32}^{4-}$, 418
$W_{10}O_{32}^{4-}/ZrO_2$, 435
photo-oxidation of
alcohols, 430–36
alkanes, 422–26
aromatic compounds, 427–30
glycerol, 432
olefins, 436–38
phthalan, 47
physisorption and activty, 49, 66, 76
3-picoline, 65
4-picoline, 65, 116
pillaring, 33, 52, 279, 298, 325, 360, 395, 397, 416, 427, 439
pinacols, 58
α-pinene, 110, 174, 176, 182, 292, 300, 381, 383, 393
allylic oxidation, 111, 173, 180, 181, 226, 294–97
α-pinene oxide, 111, 226
β-pinene, 181
piperidine, 32, 52, 78
piperonal, 385
piperonyl alcohol, 385
platinum catalysts
Pt/Al_2O_3, 234
Pt/C, 223, 234, 237, 244
Pt/graphite, 234
Pt/MOF-177, 385
Pt/MOF-5, 385
Pt/TiO_2, 234
Pt/ZrO_2, 239
platinum catalysts, oxidation
of benzyl alcohol, 239
of glucose, 242
of glycerol, 237
Pluronic 123, 103, 143, 148, 156, 162, 163, 270, 286
Pluronic F127, 103, 271
Pluronics, 139
PO. *See* propylene oxide
$PO(OCH_3)_3$, 103
PO/Styrene. *See* POSM process
poisoning, 55, 194, 228, 234, 242, 254, 438
polyaniline, synthesis and properties, 246–49
polyethylene oxide (PEO), 139
polyhedral oligomeric silsesquioxane derivatives (POSS), 191
polyoxometalates, 192, 264
Ce-POM, 275, 299
Co-POM, 267–69, 273–77, 295, 296, 298–301, 383
$[Co^{II}M_{11}Co^{II}(H_2O)O_{39}]^{8-}$, 279, 287
$[CuPW_{11}O_{39}]^{5-}$, 282, 303
$[Fe_4(H_2O)_{10}(\beta\text{-}XW_9O_{33})_2]^{n-}$, 277, 287
$[(Fe^{III}(OH_2)_2)_3(A\text{-}\alpha\text{-}PW_9O_{34})_2]^{9-}$, 278, 299
HPA-*n*, 266, 297. *See also* $[PV_nMo_{12-n}O_{40}]^{(3+n)-}$
M-POM, 266, 268, 269, 274, 296, 383. *See also* $[XW_{11}M(L)O_{39}]^{n-}$
$\{PO_4[WO(O_2)_2]\}^{3-}$ (or PW_4), 266, 273, 277, 280, 281, 289, 294, 304, 305, 387, 393. *See also* Venturello complex
$[PV_2Mo_{10}O_{40}]^{5-}$ (PV_2Mo_{10} or $PMo_{10}V_2$), 272, 278, 281, 284, 288, 294, 297, 299–302, 309
$[PV_nMo_{12-n}O_{40}]^{(3+n)-}$ (PV_nMo_{12-n}), 266, 288, 306
$[(PW_9O_{34})_2Co_4^{II}(H_2O)_2]^{10-}$, 283
$[PW_{11}O_{39}]^{7-}$, 280, 304
$[PW_{11}CoO_{39}]^{5-}$ ($PW_{11}Co$), 268, 269, 274–77, 281, 283, 295, 298, 387
$[PW_{11}Fe^{III}(H_2O)O_{39}]^{4-}$, 269
$[PW_{11}TiO_{40}]^{5-}$ ($PW_{11}Ti$), 268, 269, 281, 293–96, 387
$[PW_{12}O_{40}]^{3-}$ (PW_{12}), 266, 268–74, 278, 279, 281, 282, 286, 289, 292, 293, 298, 304, 305, 307, 308, 311
$[\gamma\text{-}SiW_{10}\{Fe(OH_2)\}_2O_{38}]^{6-}$, 267
$[\gamma\text{-}SiW_{10}O_{36}]^{8-}$, 267, 285
$[SiW_{10}O_{38}V_2(\mu\text{-}OH)_2]^{4-}$, 267
$[SiW_{11}CeO_{39}]^{4-}$, 274, 275
$[SiW_{11}Co^{II}(H_2O)O_{39}]^{6-}$, 283
$[SiW_9O_{37}\{Co^{II}(H_2O)\}_3]^{10-}$, 279
$[SiW_{12}O_{40}]^{4-}$, 305
Ti-POM, 192, 268, 269, 293, 295, 297, 306, 383
$[V_{10}O_{28}]^{6-}$, 278, 299
$[XW_{11}M(L)O_{39}]^{n-}$ *(XW$_{11}$M), 267*. See also *M-POM*
$\{[(WZnM_2(H_2O)_2][(ZnW_9O_{34})_2]\}^{q-}$, 267
$[ZnWM_{n2}(ZnW_9O_{34})_2]^{12-}$, 277, 289
Zr-POM, 192
polyoxometalates (supported)
leaching, 265, 271, 287, 288, 289, 297–303, 307
stability, 307–09
polyoxometalates, heterogenization
coordination polymer, 280
insoluble salts, 265
polyoxometalates, immobilization, 265
adsorption on active carbon, 271–273
anchoring, 283
anion exchange, 273, 274, 278, 279, 282
covalent binding, 283–86
dative binding, 283–84
electrostatic attachment, 273–282
embedding into silica, 267–271
impregnation, 265, 271, 298, 308
ion pairing, 273, 274
polyoxometalates, mechanistic aspects, 304–307
polyoxometalates, oxidation of
alcohols, 297–98
aldehydes, 298–99
alkanes, 287

aromatic compounds, 288
olefins
allylic, 294–97
co-oxidation with aldehydes, 299–301
epoxidation, 288–94
S-compounds, 301–304
polyoxometalates, protonation state, 192
polyoxometalates, stability, 307
solvolytic destruction by H_2O_2, 304, 307, 394
thermal, 264
polyoxometalates, structure
Dawson, 264, 266, 303
Keggin, 264, 266, 267, 269, 305
lacunary, 266, 280, 285
Linquist, 285
Preyssler, 264, 277, 303
sandwich, 264, 267, 273, 280, 289, 299, 305
Wells–Dawson, 277. *See also* Dawson
polypyrrole, synthesis and properties, 249–50
polyvinylsiloxane, 162, 176
POM. *See* polyoxometalates
pore size distribution, 30, 130, 135, 157, 199, 351
POSM process, 8, 157, 172, 476, 480
existing plants, 480
postsynthesis, 26, 31, 32, 129, 156–61, 179, 198, 286
post-treatment, 26, 37, 41, 50, 52, 63
prehydrolysis, 135
of TEOS, 132, 143
of TMOS, 132
probe molecules, C-H hydroxylation, 37, 70
process engineering
gas, liquid, solid systems, 501–503
liquid-solid separation, 498
oxidant selection, 503–505
stirred reactors with suspended solids, 497–99
temperature control, 499
process integration, 53, 54, 63
propane, 37, 71, 74, 225, 425, 433
1,2-propanediol. *See* propylene glycol
1,3-propanediol, 235
1-propanethiol, 299, 303
1-propanol, 235
2-propanol, 25, 49, 54, 225, 235, 385, 433, 435
propargyl alcohols, oxidation, 356, 359
propionaldehyde oxime, 188
propylamine, 188, 245
2-propylcyclopropane, 37
propylene glycol, 60, 235, 431, 484
propylene oxide, production
chlorohydrin route, 474, 485
cumene hydroperoxide route, 480–83
HPPO route, 483–87
extruded catalyst, 455
POSM route, 476–80
propylene oxide, routes studied
direct oxidation (DOPO), 476, 487, 488
direct synthesis of H_2O_2 + HPPO (HP/HPPO), 476, 488
hydro-oxidation (HOPO), 227, 476, 488
propylene, epoxidation, 52–55, 294, 474–76
continuous flow, 53
photocatalysis, 436
process integration, 54
TS-1 from cheaper reagents, 53
TS-1 regeneration, 98, 77, 484
TS-1 with Ti and Al impurities, 53
with *in situ* H_2O_2, 53–55
propylene, photo-oxidation, 437
pseudo-boehmite, 101
pyrazines, 116
pyridazines, 116
pyridine, 28, 65, 131, 182, 244, 330
pyrrole, oxidative polymerization, 249–50

quenching tests, 166
quinoline-5,8-dione, 356, 385
quinones, 288

$[R(CH_3)_2N^+\text{-}C_6H_{12}\text{-}N^+(CH_3)_2C_6H_{13}](OH^-)_2$ template, 26
R-(–)-carvone, 176
radical clocks, C-H hydroxylation, 38
radical quenchers, 38, 70, 109, 117
Raman spectroscopy, 28, 34, 130, 134
Raschig process, 463
reactor
CSTR, 41, 44, 53, 62, 234, 460, 467, 485
fixed bed, 457
gas-lift recirculated, 54, 501
membrane microreactor, 62, 64, 243, 340
microstructured, 44, 51, 229
packed bed, 44, 53, 54, 57, 479, 482, 485, 500
photoreactor, 432, 433
regioselectivity, 35, 36, 39, 40, 51, 56, 107, 290, 291, 341, 431
Rh/C, 244
Rhône-Poulenc, 452, 465
R_T/R_O ratio, 23
ruthenium catalysts
oxidation of alcohols, 231
Ru/Al_2O_3, 231

SAPO-*n*. *See* silicoaluminophosphate
Saudi Aramco, 483
scanning electron microscopy (SEM), 30, 129
S-compounds, oxidation, 65–66, 185–88, 301–304, 381, 399–400
secondary synthesis of metal zeolites, 23, 198
self-assembly, 136
semiconductor oxides, 4, 411, 413, 418, 422, 423, 430, 433, 435, 443
sesquiterpenes, 181
SGC (Siam Cement Group), 483
shape selectivity, 48, 59, 61, 97, 189, 290, 303, 373, 387, 453
Shell, 8, 157, 465, 476, 478, 480, 488
Shell catalyst. *See* Ti/SiO_2 catalyst (POSM)
Shell process. *See* POSM process
ship-in-a-bottle complexes, 326
$Si(OC_2H_5)_4$, 24. *See also* TEOS
Siam Cement Group, 483

Sibunit, 272, 273, 292, 301, 309
silanol nest, 27, 68, 72
silica wall thickness, 138, 197
silica, amorphous, 28, 30, 157, 160, 325, 348, 420
silica, colloidal, 53, 141, 144, 195, 196
silica, fumed, 32, 137, 141, 144, 147, 195, 196, 283
silica–titania EP350, 180
silicoaluminophosphates, 95, 96, 100, 101, 102, 105
silylating reagents, 162, 163, 169, 173, 176, 199
silylation, 26, 33, 133, 157, 162, 166, 168, 171, 176, 187, 195, 199, 325, 327, 360, 362, 423, 479
single-site heterogeneous catalysts, 45, 50, 129, 156, 161, 264, 266, 416
singlet oxygen, 415, 433
SINOPEC, 470
site isolation, 129, 157, 160, 192, 327, 339, 412
SKC Co., 480, 483, 487
small-angle X-ray/neutron scattering (SAXS/SANS), 103, 130, 274
Sn zeolites
  Sn-Beta, 15, 33, 63, 183
  SnS-1, 33, 42, 47
  SnS-2, 33
  SnTS-1, 45, 42
  Sn-ZSM-12, 33
Sn zeolites, oxidations
  Baeyer-Villiger oxidation, 63
  hydroxylation of phenol, 45, 42
Sn/MCM-41
  Baeyer-Villiger oxidation, 183
Snamprogetti, 461
$SnCl_4$, 63, 147
SNIA Viscosa, 465
Sn^{IV} centers, 193
Sn-MCM-41, 147
  Baeyer-Villiger oxidation, 183–84
  oxidation of phenol, 169
Sn-SBA-15
  Baeyer-Villiger oxidation, 183
sodium silicate, 137, 140, 143, 147, 149, 154, 417
sol-gel, 127, 129, 133, 135, 146, 181, 268, 269, 271, 277, 283, 286, 295, 308, 328, 330, 334, 346, 348, 416, 420, 432, 434, 435, 441
  non-hydrolytic synthesis, 132, 134, 162, 176, 188
solvent effects, 66, 76
  alcohol oxidation on Au, 232
  epoxidation, 49, 52, 55
  epoxide solvolysis, 50
  hydroxylation of alkanes, 35–36
  hydroxylation of benzene, 40
  hydroxylation of phenol, 43, 455
solvent, as template, 378
solvent-anchored catalyst, 289
solvent-anchored supported liquid phase catalysis, 283
solvolysis of epoxides, 49–50, 51, 55
  as probe of TS-1 acidity, 50
  uncatalyzed, 50
solvothermal synthesis, 101, 134, 378, 378, 379, 403
spectroscopic and structural properties of
  Sn-Beta, 34
  Ti-Beta, 34
  Ti-MOR, 34
  Ti-MWW, 34
  TS-1, 34
  TS-2, 34
  VS-1, 34
  VS-2, 34
spectroscopic characteristics of
  anatase, 189
  Ti/MCM-41, 189
  Ti-MCM-41, 189
  Ti-MMM-2, 189
  TiO_2–SiO_2 aerogels, 189
  TS-1, 189
spray drying, 53, 457
SRI Consulting, 479
stability of
  aerogels and xerogels, 195
  gold catalysts, 254–56
  mesostructured silicates, 195
  metal aluminophosphates, 118–19
  metal complexes (supported), 362–64
  metal substituted zeolites, 77–78
  metal-organic frameworks, 402–4
  metal-silicates, 194–200
  photocatalysts, 438–43
  polyoxometalates (supported), 307–9
steaming, regeneration of TS-1, 77
stereoselectivity, 38, 39, 61
  cis-, *trans*-epoxidation, 48, 52, 55, 291, 436
cis-stilbene, 228, 345, 351, 393
trans-stilbene, 178, 292, 345, 393
structure-directing agents, 26, 30, 31, 32, 136
styrene, 49, 58, 110, 178, 288, 292, 344, 346, 348, 351, 383, 387, 393, 394, 396, 436: 475, 477, 478, 480, 486
  oxidation on TS-1, 58
styrene, asymmetric epoxidation, 397
styrenes (substituted), oxidation, 228
sulfolane, 41
Sumitomo process (Beckmann), 461, 470
Sumitomo process (PO), 8, 173, 480–83, 488
supercritical CO_2, solvent, 54, 228, 229, 233, 239
supercritical drying (SCD), 132
superoxide species
  Au-$O_2^{\bullet}$, 253
  $O_2^{\bullet-}$, 5, 415, 433
  Ti-$O_2^{\bullet}$, 58, 71, 74
supports for POMs, 265
  active carbon, 265, 271, 272, 301, 307, 309
  Al_2O_3, 265, 273, 294
  MgO, 265
  MIL-101, 281
  silica, 265, 267, 274
  ZrO_2, 271, 278, 292
surface acidity, 58, 131, 190

surface hydrophobization, 162, 177, 306. *See also* silylation
surface organometallic chemistry, 159
surface-solvent-activity, relationship, 76
surfactant-encapsulated polyoxometalate, 286, 303
surfactants, 136
  gemini, 138, 139
  nonionic, 138

T atom, 23
T sites, 23, 27, 45, 68
TAPO-5
  oxidative cleavage of cyclohexene, 179
tartronic acid, 236, 237, 238,
TBAOH, 25
TBHP. *See t*-butyl hydroperoxide
TBOT, 25
TEAOH, 25, 30, 31, 155
template ion exchange. *See* TIE method
templated synthesis, 129, 136, 140
templates, 24, 25, 26, 44, 46, 52, 101, 102, 103, 119, 128, 136, 137, 138, 143, 162, 269, 378
TEMPO (oligomeric), 359, 385
TEOS, 24, 52, 132, 133, 135, 139, 141, 143, 144, 146, 147, 149, 159, 151, 152, 153, 154, 155, 156, 162, 163, 195, 196, 268, 269, 270, 271, 286, 417, 418, 420, 435, 456, 457
TEOT, 24, 25, 456, 457
terpenes, 51, 177, 288
  allylic oxidation, 180
terpenoids, 175, 177, 181
terpinen-4-ol, 175,
α-terpineol, 59, 173, 175, 177
α-terpinylacetate, 175
tethering, 128, 156, 264, 325
tetrabutylammonium hydroxide. *See* TBAOH
tetraethyl orthosilicate. *See* TEOS
tetrahethylammonium hydroxide. *See* TEAOH
tetrahydrofuran, 60
tetrahydropyran, 60
tetrahydrothiophene, 302, 309
tetralin, 109, 169, 340, 341, 381, 382, 389, 390, 392, 393, 401, 404
1-tetralone, 169, 341, 382, 389, 393, 401
tetramethyl orthosilicate. *See* TMOS
tetrapropylammonium bromide. *See* TPABr
theoretical studies, 15, 67, 68, 71, 191, 193
thermal degradation, 195, 254, 264
thermolytic molecular precursor method, 136, 161, 167, 178
thianthrene, 429
thioanisole, 360
thioethers. *See* S-compounds
thiophene, 66, 187, 188, 272
thiophenol, 386, 404
thiosulfate salts, 504
Ti molecular sieves, activity
  network of oxidations, 74
  relationship with adsorption, 76
  surface-solvent synergism, 74–76
Ti peroxo species, 28
  anionic, 50, 68, 73
  in oxidation mechanisms, 69–74, 191
  structures, 66–68
  theoretical studies, 67, 191, 193
Ti silicalite-1, 167, 168, 169, 172
  ammoximation, 61–63, 73, 467–70
    structural instability, 62, 78, 469
  Baeyer-Villiger oxidation, 63
  decomposition of H_2O_2, 74
  epoxidation of allyl alcohols, 55–56
  epoxidation of allyl chlorides, 56–57
  epoxidation of olefins, 48–51, 57–58, 71–72
  epoxidation of propylene, 52–53, 190
  hydroxylation of alkanes, 34–39, 69–71, 166, 190
  hydroxylation of benzene, 40–43
  hydroxylation of phenol, 43–46, 71
  network of competing oxidations, 74
  oxidation of alcohols and ethers, 59–60, 72
  oxidation of alkylaromatics, 47
  oxidation of amines and N-heterocycles, 63–65
  oxidation of S-compounds, 65–66
Ti silicalite-1, bifunctional
  Au/TS-1, 487
  Pd/TS-1, 40, 53, 57, 487
Ti silicalite-1, characterization, 26–30
  EXAFS, XANES, 29–30
  FT-IR, Raman spectroscopy, 27–28
  neutron powder diffraction, 27
  NMR, SEM, TEM, XPS, 30
  UV-Vis., 28–29
  XRD, 26–27
Ti silicalite-1, regeneration, 53, 77, 454, 484
Ti silicalite-1, synthesis, 24–26, 453
  hydrothermal, 24–25
  industrial scale, 456
  mesoporous TS-1, 26
  post-treatment of MFI zeolites, 26, 53
  reproducibility, 453
  shaped catalysts, 53, 57, 62, 454, 469
  with cheaper reagents, 25–26
Ti silicalite-2
  epoxidation of allyl alcohols, 55
  epoxidation of allyl chlorides, 56
  epoxidation of olefins, 48, 52
  hydroxylation of *n*-hexane, 35, 36
  hydroxylation of phenol, 43–46
  oxidation of amines, 64
Ti silicates with MFI structure, 39, 41
Ti sites, 158, 169, 191, 192
  dimeric, 25, 134, 192
  extra lattice, 24, 43, 453
  isolated, 29, 134, 191
  non-random distribution in TS-1, 27, 45
  oligomeric, 29, 196, 200
  Ti coordination, 29, 32, 191
  $Ti(OSi)_3OH$ species, 30, 67, 191
  $Ti(OSi)_4$ species, 30
  Ti-O bond length, 29, 31

Ti zeolites. *See also* Ti zeolites, mesoporous
Al-TS-1, 35, 40, 50, 58
B-TS-1, 58, 65
B-TS-2, 58
ETS-10, 417, 429
SnTS-1, 45, 46
Ti-β, 31, 46, 47, 51, 52, 55, 56, 57, 59, 63, 65, 66, 76
Ti,Al-β, 30, 39, 46, 51, 52, 56, 57, 58, 59, 60, 61, 64, 66, 68, 76, 78, 185, 187, 188
Ti-CHA, 32
Ti-FAU. *See* Ti-Y
Ti-FER, 32, 33, 51
Ti-ITQ-7, 33
Ti-LTL, 32
Ti-MAZ, 32
Ti-MCM-22. *See* Ti-MWW
Ti-MCM-68, 32, 46
Ti-MOR, 32, 34, 40, 46, 47, 56, 57, 61, 62, 63, 65, 68, 73, 78
Ti-MWW, 32, 33, 34, 46, 51, 52, 55, 56, 57, 61, 62, 65, 73, 76, 78, 79
Ti-NCL-1, 47
Ti-SSZ-33, 32, 51
Ti-SSZ-42, 32, 46
Ti-STT, 32
Ti-UTD-1, 33
Ti-Y, 32, 51
Ti-ZSM-12, 33
Ti-ZSM-48, 32, 61, 64
TS-1, 185, 188, 429
TS-2, 26, 32, 34, 35, 36, 43, 46, 48, 52, 55, 56, 61, 64, 65, 188, 429, 430
Ti zeolites, delaminated
del-Ti-MWW, 33
IEZ-Ti-MWW, 33, 51
Ti-ITQ-2, 33, 51
Ti-ITQ-6, 33, 51
Ti-MCM-36, 33, 51
Ti-MCM-56, 33, 51
Ti-YNU-1, 33, 51, 57
Ti zeolites, mesoporous
meso-Ti-MOR, 47, 63
meso-TS-1, 26, 37, 47, 50, 56
epoxidation with TBHP, 51
nanosheet TS-1, 26
$Ti(OC_2H_5)_4$, 24
$Ti(OC_4H_9)_4$, 25
Ti/(Ti+Si) ratio, upper limit, 24, 27, 31
Ti/MCF
allylic oxidation, 182
Ti/MCM-41, 159
alkene epoxidation, 174
functionalized alkene epoxidation, 175
Ti/MCM-48
alkene epoxidation, 175
Ti/SBA-15
alkene epoxidation, 173, 174
Ti/SiO_2, 61
epoxidation of alkenes, 175
oxidation of phenols, 170–72
Ti/SiO_2, POSM process, 8, 157, 172, 192, 196
preparation, 479
Ti-Beta
ammoximation, 61
epoxidation of allyl alcohols, 55
epoxidation of allyl chlorides, 56
epoxidation of olefins, 49, 51–52, 58, 60, 190
hydroxylation of phenol, 46
oxidation of alcohols, 59
oxidation of alkanes, 39
oxidation of N-compounds, 64, 65
oxidation of S-compounds, 65
Ti-Beta, characterization, 31–32
polymorph A, 31
structural instability, 78
Ti-Beta, synthesis, 30–31
F^- method, 31
OH^- method, 30
polymorphs, 30
post-treatment of BEA zeolites, 31
$TiCl_3$, 25, 145, 163, 417
$TiCl_4$, 23, 26, 53, 134, 145, 157, 158, 162
TIE method, 150, 153, 157
Ti-HMM
ammoximation, 185
Ti-HMS, 143, 169
oxidation of aniline, 188
oxidation of anthracene, 168
oxidation of benzene, 167
oxidation of benzothiophenes, 187
oxidation of phenols, 169
oxidation of thioethers, 186
Ti^{IV}-$O^{\bullet}$ active species, 70, 71, 74, 76, 193
Ti-MCM-41
alkene epoxidation, 172, 173, 175, 176, 177
ammoximation, 185
oxidation of 2-methylnaphtalene, 168
oxidation of aniline, 188
oxidation of benzene, 167
oxidation of cyclohexane, 164
oxidation of *n*-hexane, 166
oxidation of propylene, 190
oxidation of thioethers, 185
oxidative desulfurization, 187
stability, 195, 199
Ti-MCM-48
alkene epoxidation, 174
oxidation of *n*-hexane, 166
stability, 199
Ti-MMM
oxidation of phenols, 170
Ti-MMM-1
oxidation of alkanes, 166
Ti-MMM-2
allylic oxidation, 167
oxidation of 2-methylnaphthol, 172
oxidation of alkanes, 167, 190
oxidation of caryophyllene, 174
oxidation of functionalized phenols, 172
oxidation of thioethers, 185

oxidative cleavage of cyclohexene, 179
stability, 199
Ti-MOR
ammoximation, 61, 63, 73
epoxidation of allyl chlorides, 56
oxidation of alkanes, 39
oxidation of alkylaromatics, 47
oxidation of benzene, 40
oxidation of N-heterocycles, 65
Ti-MSF
stability, 199
Ti-MSU-G
stability, 198, 199
Ti-MWW
ammoximation, 61, 63, 73
epoxidation of allyl alcohols, 55
epoxidation of allyl chlorides, 56
epoxidation of olefins, 51–52
hydroxylation of phenol, 46
TiO_2 (anatase), 24, 25, 28, 31, 43, 44, 53, 61, 78, 134, 135, 190, 247, 453, 471. *See also* photocatalysts
H_2O_2 decomposition, 453
Raman detection, 28, 31
UV-Vis detection, 29
Ti-O_2^-, anionic η^2-peroxide, 68, 73
Ti-$O_2^\bullet$ superoxide, 58, 71, 74
TiO_2–SiO_2 aerogels
alkene epoxidation, 174
oxidation of phenols, 170
Ti-OOH, active species, 37, 50, 51, 53, 60, 65, 67, 68, 71, 74, 75, 189, 192, 234
Ti-OOH, η^1-hydroperoxide (cyclic), 68, 71
Ti-OOH, η^2-hydroperoxide, 67, 72
Ti-OOR, alkyl-η^2-hydroperoxide, 191
TiOOSi peroxide, 68
Ti-OSi bond, hydrolysis, 66
Ti-POM, as molecular models, 192
Ti-POSS
model studies, 192
Ti-SBA-15
alkene epoxidation, 176
oxidation of aniline, 188
stability
sulfoxidation, 186
titanocene dichloride, 33, 159
Ti-TUD-1
alkene epoxidation, 176
Ti-MMM
oxidation of thioethers, 185
TMBQ. *See* trimethyl-*p*-benzoquinone
TMOS, 132, 133, 147, 152, 162, 268
Toa Gosei, 462, 466
tolualdehyde, 440
toluene, 46, 47, 168, 189, 225, 228, 255, 353, 439, 465
Toray, 465
TPABr, 25, 44, 52, 53, 143
electrodialysis to TPAOH, 453
TPAOH, 24, 25, 26, 37, 52, 198, 453, 457, 460
transmission electron microscopy (TEM), 30, 129, 224, 248, 267
triblock copolymer(s). *See* Pluronic(s)
2,4,6-trichlorophenol, 353
triethanolamine, 25, 26, 139, 143
triethylamine, 244, 277, 295, 420
trifluoroacetic acid, 37
1,2,4-trihydroxybenzene, 429, 430
trimethylbenzenes, 40, 47
trimethyl-*p*-benzoquinone, 47, 113, 170, 171, 288, 353, 385
2,2,4-trimetylpentane, 190
2,3,5-trimethylphenol, 113
2,3,6-trimethylphenol, 47, 170, 234, 288, 353, 385, 399
triphase conditions, 36, 39, 41, 58, 63
triphenylmethane, 382, 389, 391
triphenylmethanol, 382, 392
TS-1. *See* Ti silicalite-1
TS-1/MCF, 169
TS-1B (hydroxylation), 41, 42, 44, 47

Union Carbide, 451
unit cell parameters, 23, 25, 27, 31, 45, 103, 130, 148, 150
α,β-unsaturated ketones, oxidation, 57, 180, 330, 345
urea·H_2O_2, 58, 59, 386, 400
ureas, from CO and primary amines, 244

V sites, "framework satellite", 33
V zeolites
V-Beta, 33, 46
V-NCL-1, 33, 40, 47
VS-1, 33, 34, 46, 65, 77
VS-2, 33, 34, 40, 47, 77, 168
V-ZSM-48, 33, 46
V zeolites, oxidation of
alkanes, 40
alkylaromatics, 47
phenol, 46
δ-valerolactone, 60
vanillin, 385, 452
vanillyl alcohol, 385
Venturello complex, 266, 273, 288, 304, 305, 311
verbenol, 182, 226, 295, 383
verbenone, 111, 180, 182, 226, 295, 383
Versalis (ENI Group), 467
V-HMS
oxidation of aniline, 188
oxidation of cyclododecanol, 182
oxidation of phenol, 169
vinyl acetate, 57, 226
vinyl esters, oxidation, 57
vitamin E, 47, 170, 353
vitamin K_3, 47, 168, 353
V-MCM-41
hydroxylation of benzene, 167
oxidation of alkylaromatics, 168
oxidation of cyclododecane, 167

V-MMM
  oxidation of 2,3,6-trimethylphenol, 170
$VO(\eta^2\text{-}O_2)(H_2O)_2L$, (L = picolinic acid), 70
VS-1. *See* V zeolites
VS-2. *See* V zeolites
V-SBA-15
  oxidation of cyclododecane, 167
$V^V\text{-}O^\bullet$, benzene hydroxylation, 70

Weisz theory, 44, 49
W-MCF
  alkene epoxidation, 178
working solution, 54, 57
wormhole-like structure, 139
W-SBA-15, 152
  oxidation of cyclopentene, 179
  oxidative cleavage of cyclohexene, 179

xanthene, 353, 382, 386, 389, 392
xanthone, 353, 382, 386, 392
xerogel, 129, 132
  mechanical stability, 195
X-ray absorption spectroscopy (EXAFS/XANES), 29–30, 29, 31, 103, 130, 134, 324
X-ray diffraction (XRD), 26–27, 103, 130, 324
X-ray photoelectron spectroscopy (XPS), 30, 130, 224
X-ray structural modeling, 138

p-xylene, 46, 47, 232
xylenes, 47, 428

zeolite
  A, 22, 451
  B, 451
  Beta, 22
  B-MWW, 32
  Mordenite, 22, 42
  S-1, 22, 451
  X, 22, 451
  Y, 22, 42, 451
  ZSM-11, 22
  ZSM-5, 22, 58, 451
zeolite-like metal-organic frameworks (ZMOFs), 388
zeolites
  isomorphous substitution, 23
  nomenclature, 22
  syntheses, 22–23
zeolitic structure type
  BEA, 30
  FER, 32
  MEL, 32
  MFI, 24
  MTN, 281
  MWW, 52
zeolitization of silica walls, 198
Zr-HMS
  oxidation of aniline, 188
Zr-POM, as molecular models, 192